Advances in Volcanology

Dmitri Rouwet
Bruce Christenson
Franco Tassi
Jean Vandemeulebrouck
Editors

Volcanic Lakes

Springer

Advances in Volcanology

Series editor

Karoly Nemeth, Palmerston North, New Zealand

Editor-in-Chief

IAVCEI, Barcelona, Spain

For further volumes:
http://www.springer.com/series/11157

Dmitri Rouwet · Bruce Christenson
Franco Tassi · Jean Vandemeulebrouck
Editors

Volcanic Lakes

Springer

Editors
Dmitri Rouwet
Sezione di Bologna
Istituto Nazionale di Geofisica e Vulcanologia
Bologna
Italy

Bruce Christenson
GNS Science
Lower Hutt
New Zealand

Franco Tassi
Earth Sciences
University of Florence
Florence
Italy

Jean Vandemeulebrouck
Institut des Sciences de la Terre
Université de Savoie
Le Bourget du Lac
France

Videos to this book can be accessed at http://www.springerimages.com/videos/978-3-642-36833-2.

Advances in Volcanology
ISBN 978-3-642-36832-5 ISBN 978-3-642-36833-2 (eBook)
DOI 10.1007/978-3-642-36833-2

Library of Congress Control Number: 2014957163

Springer Heidelberg New York Dordrecht London
© Springer-Verlag Berlin Heidelberg 2015
This work is subject to copyright. All rights are reserved by the Publisher, whether the whole or part of the material is concerned, specifically the rights of translation, reprinting, reuse of illustrations, recitation, broadcasting, reproduction on microfilms or in any other physical way, and transmission or information storage and retrieval, electronic adaptation, computer software, or by similar or dissimilar methodology now known or hereafter developed.
The use of general descriptive names, registered names, trademarks, service marks, etc. in this publication does not imply, even in the absence of a specific statement, that such names are exempt from the relevant protective laws and regulations and therefore free for general use.
The publisher, the authors and the editors are safe to assume that the advice and information in this book are believed to be true and accurate at the date of publication. Neither the publisher nor the authors or the editors give a warranty, express or implied, with respect to the material contained herein or for any errors or omissions that may have been made.

Printed on acid-free paper

Springer-Verlag GmbH Berlin Heidelberg is part of Springer Science+Business Media (www.springer.com)

Foreword

Volcanic Lakes are fascinating. And useful. They trap. They integrate. They evaporate. They are dynamic balances of input, both volcanic and meteoric, and output (gas through-flux, evaporation, seepage and spillover). Changes in lake temperature or chemistry often, though not always, indicate changes in magma degassing; changes in lake level can indicate strain of the edifice; and bubbling in lakes can be recorded acoustically—all helpful in eruption forecasting. Lakes are windows into groundwater and many are windows into hydrothermal systems with a myriad of processes including chemical transport and deposition, self-sealing, transient pressurization, and explosive disruption. Seepage of acidic hydrothermal fluid weakens rock of volcanic edifices, making them prone to collapse. Accumulation of CO_2 and/or CH_4 deep within lakes creates the potential for overturn. Volcanic lakes that are suddenly breached or expelled scour channels to form sediment-rich lahars.

Volcanic lakes also record history. They preserve thin ash layers that are unlikely to survive erosion and bioturbation outside the lakes. Such ash can be from the host volcano or from afar, giving valuable information about eruptive histories in both instances. They preserve environmental indicators such as pollen, diatoms, and inorganic indicators. And, in some cases, they capture a history of unrest of the volcano itself—precious data that predate modern monitoring.

Some lakes are extreme environments—in acidity, sulfur, trace metals, and a primordial soup of extremophile organisms. Every volcanic lake, from acidic to alkaline, has its own story to tell about its host volcano and its surroundings. The chapters in this monograph tell some of those stories, but focus mainly on reviewing tools with which future workers can decipher stories by themselves. Enjoy the vast experience represented by these authors! Just as volcanic lakes are enriched by multiple inputs, so too will your enjoyment of the lakes be enriched by these chapters!

Chris Newhall

Contents

Volcanic Lakes

Bruce Christenson, Karoly Németh, Dmitri Rouwet, Franco Tassi, Jean Vandemeulebrouck, and Johan C. Varekamp

Abstract

Volcanic lakes are amongst the most spectacular natural features on the planet. These intersections of magmatic-hydrothermal systems and the Earth's surface are, poetically speaking, "blue windows" into the depth of a volcano (Fig. 1). The changing water compositions and colors of these lakes over time provide insights into the volcanic, hydrothermal and degassing processes of the underlying volcano.

Keywords

Volcanic lakes · Genetic classification · Chemical classification · Limnology · Volcanic lake color · Statement

B. Christenson
GNS, Lower Hutt, New Zealand

K. Németh
CS-INR, Volcanic Risk Solutions,
Massey University, Palmerston North, New Zealand

D. Rouwet (✉)
Istituto Nazionale di Geofisica e Vulcanologia,
Sezione di Bologna, Via Donato Creti 12 CAP,
40128 Bologna, Italy
e-mail: dmitri.rouwet@ingv.it

F. Tassi
Department of Earth Sciences, University of
Florence, Florence, Italy

F. Tassi
CNR-IGG, Florence, Italy

J. Vandemeulebrouck
Laboratoire de Géophysique Interne et
Tectonophysique, CNRS, Université de Savoie,
Chambéry, France

J.C. Varekamp
Department of Earth and Environmental Sciences,
Wesleyan University, Middletown, CT, USA

1 Introduction

Volcanic lakes are amongst the most spectacular natural features on the planet. These intersections of magmatic-hydrothermal systems and the Earth's surface are, poetically speaking, "blue windows" into the depth of a volcano (Fig. 1). The changing water compositions and colors of these lakes over time provide insights into the volcanic, hydrothermal and degassing processes of the underlying volcano. Volcanic lakes can be highly dynamic systems or pass through stages of relatively slow fluid exchanges, depending on the lake water residence time (RT), which is defined by the lake volume and the input (or output) fluxes ($RT = V/Q_{input}$); the larger the lake volume and the lower the input fluxes, the longer the RT will be (months to years), while smaller lakes affected by high fluid input will result in a short RT (weeks to months) (Varekamp 2003;

D. Rouwet et al. (eds.), *Volcanic Lakes*, Advances in Volcanology,
DOI 10.1007/978-3-642-36833-2_1,
© Springer-Verlag Berlin Heidelberg 2015

Fig. 1 Yugama lake, Kusatsu-Shirane volcano, Honshu, Japan (26 June 2012) (picture by T. Ohba). Yugama lake is probably the most monitored crater lake in the world, with the record starting in the 1960s. Currently many small earthquakes happen under the Yugama crater. The area 1 km from the center of the crater is restricted to approach

Taran and Rouwet 2008; Taran et al. 2013; Rouwet et al. 2014). The RT thus controls (i) the lake's sensitivity to potential changes caused by processes external to the lake (e.g., fluid input from the volcano), and (ii) the frequency needed to effectively monitor the lake (Rouwet et al. 2014).

Many studies dealt with mass, energy, chemical or isotopic budget analyses, with the aim to combine the thermal and chemical behavior of lakes, often useful in volcanic monitoring setups (Hurst et al. 1991, 2012, this issue; Rowe et al. 1992a; Ohba et al. 1994, 1994; Pasternack and Varekamp 1997; Rouwet et al. 2004, 2008; Taran and Rouwet 2008; Rouwet and Tassi 2011; Varekamp, this issue). Lakes are approximated by a box of which the volume and temperature variations depend on heat and water entering (meteoric recharge, surface runoff, fluid input from the volcano) or exiting (evaporation, seepage, overflow) the lake. Fluid geochemistry is a common tool to study volcanic lakes, whereas subsurface processes may also be investigated by geophysical surveys (Rymer et al. 2000, 2009; Vandemeulebrouck et al. 2005; Fournier et al. 2009; Caudron et al. 2012), numerical modeling (Christenson et al. 2010; Todesco et al. 2012, this issue; Christenson and Tassi, this issue), and hydrogeology (Mazza et al., this issue).

Volcanic lake research was boosted after the August 1986 Lake Nyos limnic gas burst (Kling et al. 1987; Costa and Chiodini, this issue). This unfortunate event led to the foundation of the International Working Group on Crater Lakes (IWGCL), in the early 1990s re-baptized into the IAVCEI Commission on Volcanic Lakes (CVL). Former CVL-Leader JC Varekamp stated the multi-disciplinary character of CVL as follows: "the CVL has an important role to play within IAVCEI and a significant scientific mission in volcanology. Volcanic lakes are used to monitor volcanic activity, they harbor their own volcanic dangers (CO_2 explosions, lahars, phreatic explosions; Mastin and Witter 2000; Delmelle et al., this issue; Manville, this issue; Kusakabe, this issue; Rouwet and Morrissey, this issue), and may leak toxic fluids into the surface environment. In addition, they provide "deep blue" windows into the interior of volcanoes and even deeper into the magma source regions, with topical linkages towards ore deposition and geothermal energy development, all of which are reasons to pay substantial attention to volcanic lakes. In addition, many global change researchers use volcanic lakes for the study of environmental change. The sedimentary records are influenced both by climatic/hydrological parameters and volcanic

inputs, and the expertise of CVL members can contribute to decipher these records. The CVL originators recognized that volcanic lakes provide a special field of endeavor, with intertwined aspects of volcanology, limnology, geochemistry, biology and toxicology."

This monograph on volcanic lakes touches on many of the above topics and aims to give an overview of the current state of volcanic lake research. We aim at offering an up-to-date manual on volcanic lake research, providing classic research methods as well as more high-tech approaches of future volcanic lake investigation and continuous monitoring. This chapter stresses the need to better define the various types of volcanic lakes, and provides a broad conceptual classification system based on the formation processes of lakes with respect to why, where, and how volcanic lakes form. Basic limnological aspects of lakes are reviewed, and color changes are explained, as not all volcanic lakes are just blue windows.

2 A Genetic Classification of Volcanic Lakes

For historical reasons, the nomenclature of volcanic lakes is thoroughly embedded in our geological vernacular, but may need some revisions. Tectonic, geomorphic and volcanologic processes all contribute to the formation of volcanic lakes as detailed below.

Classifying volcanic lakes can be based on the timing and status of volcanism of the region that hosts the volcanic lake. The temporal link between a volcanic event and lake formation provides one defining parameter for volcanic lake classification. A lake may develop inside the main active crater on a volcano or in a satellite vent that has only a minor role in the main volcanic structure. Alternatively, volcano/geomorphic processes (e.g., mudslides, lava flows, ash fall) may divert or block surface waters, or interfere gradually with drainage patterns far from an active vent. The latter may happen during volcanic activity or in a period following it. Areas with dispersed vents (e.g., cinder cone fields) can host maar lakes in active or long extinct craters, some with minor, other with major volcanic fluids inputs (Connor and Conway 2000; Németh 2010).

Before establishing an easy to follow matrix for volcanic lake genesis, some key questions should be addressed:

1. What is the status of the volcanic system associated with the lake?
2. Does magma reside close to the surface, and is eruption imminent?
3. How long after the last eruption did the volcanic lake form?
4. How strong is the genetic relationship between volcanic activity and the presence of a lake?
5. What is the role of the volcanic landform in providing the adequate basin for the volcanic lake?

So far, within this geotectonic perspective, there is no universal guideline on how such questions should be answered and, consequently, how lakes should be classified in relation to volcanic terrains. We suggest that the classification of volcanic lakes could follow a few main rules, based on four major variables:

1. the geotectonic assessment in which the lake is found (G), that can be expressed as monogenetic (0) or polygenetic (1) volcanic systems;
2. the relationship between the volcanism and the lake formation (R), that can be expressed as weak (0) or strong (1);
3. the timing of the volcanic lake formation in relationship to the volcanism (T), that can be expressed as long (0) or shortly (1) after the volcanic eruption;
4. the location of the volcanic lake in relationship to the volcanic center (L), that can be expressed as off (0) or over (1) the vent.

Such alpha-numerical expressions of lake types lead to a coding of volcanic lakes. The above suggested scheme can be combined with other aspects of the lakes that are more relevant to their chemical maturity (see below) and, eventually, biological status (Mapelli et al., this issue). Overall, we can say that deciphering the genetic background of volcanic lakes is often difficult, as the lake might literally cover part of the story to backtrack the

formation history of some lakes (Marchetto et al., this issue). In the following sections some historically defined volcanic lake types are discussed in terms of the genetic classification issues outlined above.

2.1 Crater Lake (Code: G1, R1, T1, L1)

Volcanic lakes are often erroneously called crater lakes. Crater lakes are volcanic lakes typically associated with volcanoes that are classified as polygenetic from the genetic point of view (G1). Such volcanoes can form summit or central craters from explosive eruptive processes (e.g., Plinian eruptions, R1) that opened up deep and fairly large craters (Fig. 2). Soon after the crater forming eruptions (T1), due to climatic influences, local hydrogeology, and permanent degassing such craters can host deep and confined lakes that are eventually heated by the underlying magmatic-hydrothermal systems.

Crater lakes can be grouped into active versus inactive types as an expression whether the underlying vent is still considered to be connected with a magma reservoir or not. An active crater lake is located above an active vent (L1) producing continuous degassing during inter-eruptive periods. During eruptive periods such lakes can be totally or partially expelled and become the main water source of mass flow processes (e.g., lahars, Manville this issue) (Fig. 2).

Inactive crater lakes are associated with volcanic vents that are no longer attached to magma reservoirs. As a consequence such crater lakes are not influenced by degassing processes, nor significant hydrothermal activity. Beyond the scope of the genetic classification system, lake chemistry is the best means to provide information about the state of activity of the underlying vent (see below).

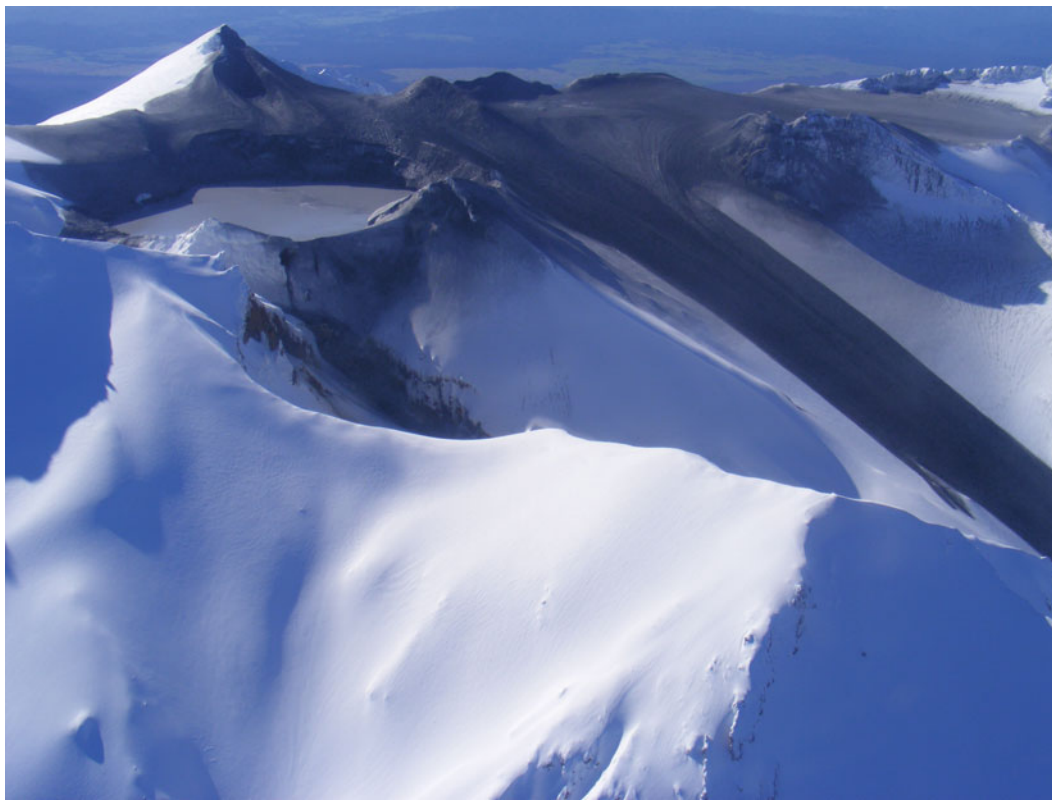

Fig. 2 Ruapehu Crater Lake after the September 2007 phreatomagmatic eruption and lahar (picture by K.N.)

Fig. 3 Crater Lake, Oregon, nearly 10 km in diameter, is actually a caldera lake formed after the 7700 y BP Mt Mazama eruption (Mandeville et al. 2009). In the front is Wizard Island (picture by D.R., August 2010)

2.2 Caldera Lake (Code: G1, R1, T0, L1)

Calderas are formed by collapse of the magma chamber after voluminous, often explosive eruptions in silicic volcanism (G1, R1) (e.g., Mt Masama-Crater Lake, Oregon, Fig. 3; Cosigüina lake, Nicaragua; Bolsena lake, Italy). They can have dimensions from kilometers to even tens of kilometers. The duration of the lake water fill after the eruption is unsure, but can be considerably long after (T0). Caldera lakes fill up these large calderas, most of the time entirely (L1).

2.3 Maar-Diatreme Lakes (Code: G0, R1, T1, L1)

Maar volcanoes are typically formed by diatremes, and consist of maar craters surrounded by a relatively thin (few meters to over hundred meters) tephra rim. They are commonly associated with alkaline basaltic intra-continental volcanism (Lorenz 1986; White and Ross 2011; Kereszturi and Németh 2012; Aka, this issue). In such a scenario however, the erodible scoria deposits can be weathered significantly providing low permeable sediments, a necessary constraint to form a lake (Pasternack and Varekamp 1997). The lake can fill the gaps between the intra-crater scoria and lava spatter cone edifices and their remnants and the inner crater wall of the maar (Fig. 4).

2.4 Geothermal Lake (Code: G0-1, R1, T1, L0-1)

Geothermal lakes are formed in volcanic areas within explosion craters, but are not necessarily formed within a volcanic edifice as such (G0-1). A vent or crater formed during a phreatic eruption (R1), is filled by the geothermal aquifer fluid which gave rise to the eruption (T1). A clear example of a geothermal lake is Oyunama Lake, Noboribetsu geothermal area, Hokkaido, Japan (Fig. 5) (Delmelle and Bernard, this issue).

2.5 Lake in a Volcanic Environment (Code: G1, R0, T0, L0)

Lakes can form in depressions caused by active tectonics in volcanic areas (G1). The tectonics has a regional character, rather than being related to the volcano itself. The graben lakes of the East African Rift system, surrounded by volcanoes, are probably the best examples (e.g., Kivu lake, Vaselli et al.,

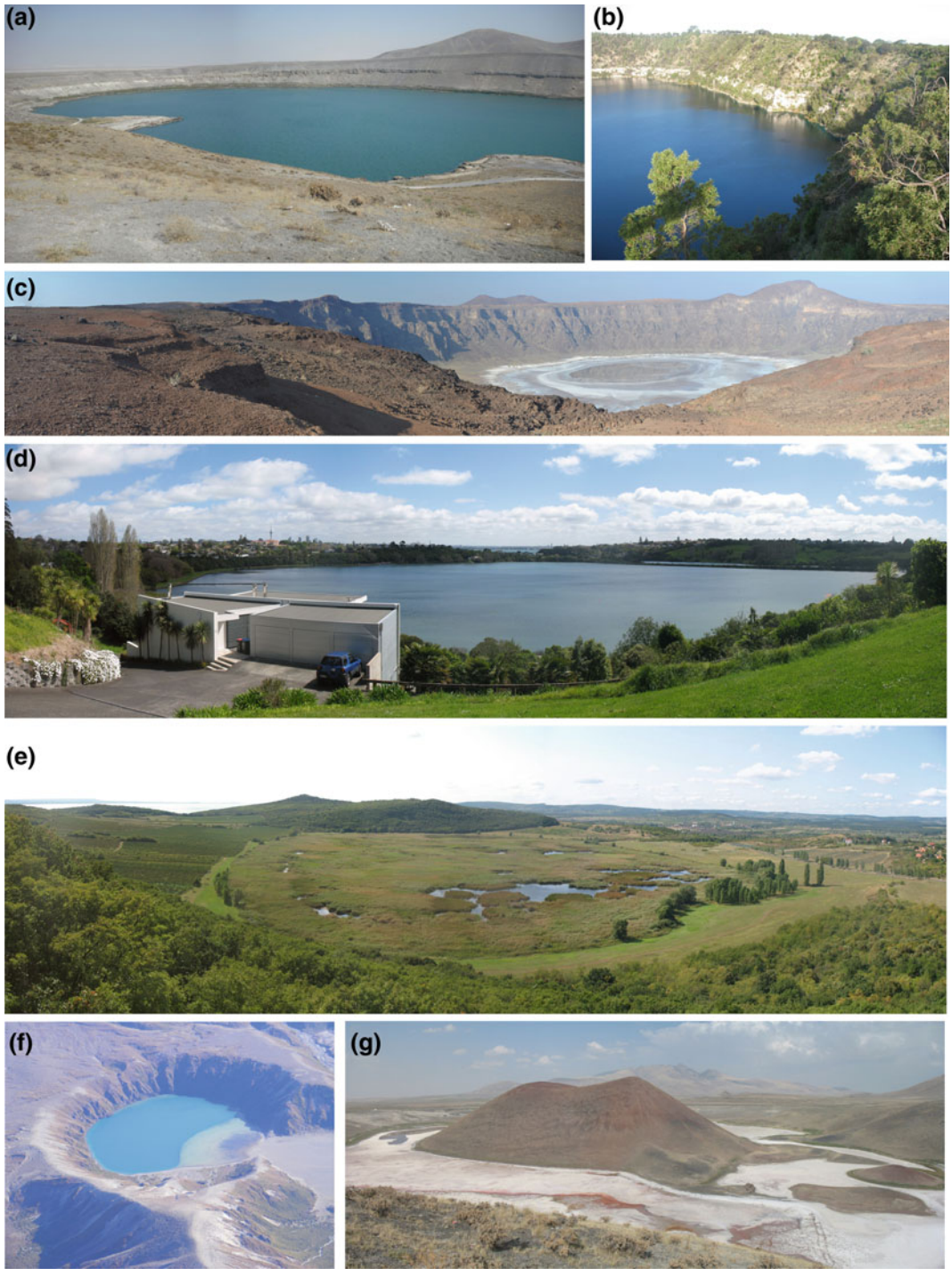
(a)
(b)
(c)
(d)
(e)
(f)
(g)

◀**Fig. 4** Volcanic lakes associated with maar-diatreme volcanoes such as in the case of the **a** Aci Gölü (Aci Lake) near Karapınar in Turkey (Keller 1975) represents a near perfect circular maar crater filled with deep water. The maar crater wall today represents the structural boundary of the maar-diatreme itself; **b** Blue Lake at Mt Gambier in South Australia (van Otterloo and Cas 2013) is a maar lake cut deeply into a limestone country rock. The lake level is controlled by karstic water systems of the limestone country rocks keeping the lake deep; **c** Al Wahbah crater is a maar volcano in Saudi Arabia that cut into a Proterozoic crystalline basement rock (Moufti et al. 2013). It hosts a temporal shallow lake that changes its level according to climatic conditions; **d** Orakei maar in Auckland, New Zealand (Németh et al. 2012) hosts a maar lake formed over alluvial, coastal deposits and it occupies the space between the erosionally retreated maar crater wall today. This means that the volcanic lake today has a larger surface area and shallower water depth than the original maar lake; **e** Külsö-tó in Tihany, Hungary (Németh et al. 2001) is a volcanic lake that is inferred to be formed more or less in the same area where a former volcano was located that was eroded later on and the created depression subsequently filled with water; **f** Tama Lakes near the Ruapehu volcano in New Zealand is another fine example for erosional enlargement of a maar crater lakes where the tuff ring has been eroded away completely; **g** Meke Gölü (Meke Lake) Konya near Karapınar in Turkey (Keller 1975) is a complex maar volcano. Its crater is partially filled with a large scoria cone (pictures by K.N.)

this issue). Volcanic activity does not play a role in the formation of the lake basin (R0), and the timing (T0) and spacing (L0) of the lake formation is unrelated to activity of a volcanic vent.

2.6 Lakes Dammed by Volcanic Deposits (Code: G0-1, R0-1, T0-1, L0)

Dammed lakes with a volcanic origin can be very diverse. Here we distinguish three types of such lakes:

1. when a volcanic edifice (Müller and Veyl 1956; Weinstein 2007) and/or associated lava field grow in a pre-existing fluvial network, water can be dammed creating lakes (e.g., Snag and Butte Lakes, California; Heiken 1978; Weinstein 2007) (G0-1, R1, T0-1, L0);
2. when active volcanic processes lead to failure of a volcanic edifice that dams or alters the pre-existing drainage network and forms or enlarges lakes (e.g., Spirit Lake near Mt St Helens, Washington; Zheng et al. 2014) (G1, R1, T0-1, L0);

Fig. 5 Oyunama lake, Noboribetsu geothermal area, Hokkaido, Japan, is a geothermal lake filling vents of previous phreatic eruptions (picture by D.R., July 2013)

3. when long-term geomorphological processes (e.g., landslides) lead to a change of the physiography of a volcanic terrain to cause damming of existing drainage patterns by non-volcanic surficial processes (G0-1, R0, T0, L0).

2.7 Volcanic Lakes After Snowmelting (Code: G0-1, R1, T1, L1)

Glaciers or snow caps topping volcanic craters can melt upon reactivation and form volcanic lakes. Such volcanic lakes can be the direct result of meltwater accumulation in the former crater of the volcano (G1), or fill other depressions of the volcanic system (G0). The relation with volcanic activity is clear as renewed heating is a must to melt the ice (R1), but eruptive activity is not necessarily involved. The lake formation is immediately after the ice melting phase, so T1. The lake forms on the vent (L1), the place where the heating phase starts. A clear example of the formation of a volcanic lake after snowmelting is Chiginagak lake, Alaska (Fig. 6), where a lake was formed in 2005, followed by snow dam breakage and a lahar (Schaefer et al. 2008). Many snow-capped volcanoes can potentially become the hosts of volcanic lakes after snow melting, when volcanic unrest resumes.

2.8 Volcanic Lake (Code: G0-1, R0-1, T0-1, L0-1)

A volcanic lake is a generic term incorporating all the above defined lake types. This explains the title of the here presented book issue: Volcanic Lakes.

Fig. 6 Chiginagak lake formed after snowmelting, Alaska (picture by G. Mc Gimsey, 21 August 2006, picture courtesy USGS, http://www.avo.alaska.edu/images/image.php?id=10973) (Schaefer et al. 2008). The depression in the crater rim on the *left* is filled by a snow dam

3 Classifying Volcanic Lakes from the Water Chemistry Perspective

As noted above, throughout history there has been some confusion and informal use of terms to describe the study objects of this monograph. Previously, volcanic lake classifications were based on water composition, especially lowered pH as a result of volcanic acid inputs (Delmelle and Bernard 2000a; Varekamp et al. 2000). A survey of the pH of volcanic lakes shows that many acid lakes have pH values below 3 and another suite has pH values between 5 and 8, whereas there is a paucity of lakes with pH values between 3 and 5. This duality in pH is most likely caused by the pH buffers of HSO_4^-/SO_4^{2-} and H_2CO_3/HCO_3^- (Marini et al. 2003). The lake classifications can be based on the character of the acidifying component (CO_2 versus the strong acids of S, Cl and F) or on general pH levels. Some volcanic lakes with carbonate inputs may have pH values >8, and evaporation processes may also lead to high pH values in some volcanic lakes (e.g., Farias et al. 2013; Pecoraino et al., this issue). As pointed out by Christenson and Tassi (this issue), lake compositional signatures are largely attributable to the age and depth of the degassing magma feeding the system.

A simple physical classification distinguishes volcanic lakes based on their water balance: those positioned inside a volcanic crater or caldera depression may have no surface outlets (Crater Lake, Oregon, Fig. 3; El Chichón lake, Mexico, Fig. 7) and are then terminal lakes where evaporation and eventually seepage has an important role in the water balance. Other lakes have subaqueous or surface geothermal or volcanic inputs but also an overflow or outlet system (Ruapehu, New Zealand, Christenson and Wood 1993; Kawah Ijen lake, Indonesia, Delmelle and Bernard 2000b; Caviahue lake, Argentina, Varekamp 2008). The lake water dynamics in these two types of lakes are fundamentally different: open lakes with an outlet experience only small variations in lake volume or mass, because the outflow term is constrained by the lake level. If, however, the lake level drops below the outlet, the lake then can shrink and become a closed, 'non-surface outlet' lake. Closed lakes have water outputs through seepage and evaporation and the seepage flux may vary with water level (hydraulic head, see e.g., Rouwet and Tassi 2011; Todesco et al. 2012, this issue).

Volcanic lakes can also be subdivided into several end member classes that reflect their origin, setting and the chemical composition of their waters. Lakes that occupy active volcanic craters or craters of recently active volcanoes will intercept the emitted volcanic gases directly in the lake environment, leading to very acid and sulfur-rich fluids. In many cases, the volcanic gases are intercepted in an underlying magmatic-hydrothermal system (Henley, this issue), where magma at several km depth is venting gases into a local groundwater layer of meteoric water. These acidified and mineralized waters may then enter the lake waters, creating a suite of lakes with different properties. The anion concentrations reflect the composition of the volcanic gas (Christenson and Tassi, this issue; Fig. 8a). Chloride loss as HCl vapor in hot concentrated lakes (e.g., Poás and Copahue lakes) is common (Rowe et al. 1992b; Rouwet and Ohba, this issue; Shinohara et al., this issue; Varekamp, this issue), leading to Cl depletion. Precipitation in the lakes of native sulfur, gypsum, anhydrite or jarosite, all common minerals in volcanic lakes, may deplete the waters in S (Delmelle and Bernard, this issue; de Ronde et al., this issue; Henley, this issue). The S–Cl–C diagram shows the clear partition in the acid S–Cl lakes with low pH values and the carbonate rich lakes with much higher pH values (Fig. 8b). Intermediate lakes are rare, which have an input of a mixed volcanic fluid but do not reach a pH low enough to let CO_2 escape. Concentrated pools of exotic S–Cl-rich water are found where the lake absorbs largely unprocessed raw volcanic gases, such as in the Keli Mutu lakes (Pasternack and Varekamp 1994) and Kawah Putih lake, both in Indonesia (Sriwana et al. 2000), and Poás and Rincón de la Vieja lakes in Costa Rica (Tassi et al. 2005, 2009).

Fig. 7 El Chichón crater lake, Chiapas, Mexico, was formed immediately after the March–April 1982 Plinian eruptions (picture by D.R., March 2004) (Rouwet et al. 2008; Taran and Rouwet 2008)

A second class of volcanic lakes receives hydrothermal fluids from underlying systems on active volcanoes, but here the fluids have already been processed extensively. These acid hydrothermal fluids may be strongly mineralized, but tend to be less rich in the volcanogenic volatile components (S+halogens). Examples are Taal lake, Phillipines (Delmelle et al. 1998; Zlotnicki et al. 2009; Gordon et al. 2009), the pre-2007 Kelut lake (Indonesia, Bernard and Mazot 2004; Mazot and Bernard, this issue), and El Chichón lake (1990–2013; Armienta et al. 2000; Rouwet et al. 2004, 2008; Peiffer et al. 2011).

The third class of volcanic lakes is contaminated with volcanic fluids that have largely lost their most reactive components such as the halogens and sulfur, and are CO_2 and/or carbonate rich. Their pH hovers from neutral to >7, tend to foster productive ecosystems, but their bottom waters may be charged with CO_2 that could lead to limnic eruptions (Nyos-type lakes, Tassi and Rouwet 2014; Costa and Chiodini, this issue; Kling et al., this issue; Kusakabe, this issue). Many of these lakes have a substantial diffusive CO_2 flux to the ambient atmosphere (Pérez et al. 2011; Mazot and Bernard, this issue) and some have direct bubble transport of CO_2 to the surface (Caudron et al. 2012). Examples are the African lakes Monoun, Nyos and Kivu, the carbonate lakes in Italy (Carapezza et al. 2008; Chiodini et al. 2012), Kelut lake on Java (Bernard and Mazot 2004; Caudron et al. 2012; Mazot and Bernard, this issue) and Quilotoa and Cuicocha lakes in Ecuador (Fig. 9, Aguilera et al. 2000; Gunkel et al. 2008; Gunkel and Beulker 2009).

The last class of lakes are dominated by meteoric fluids, either as a result of their sheer size (Toba lake, Indonesia; Bolsena lake, Italy; Crater Lake, Oregon) or because the volcanic/geothermal inputs are indeed very small (maar

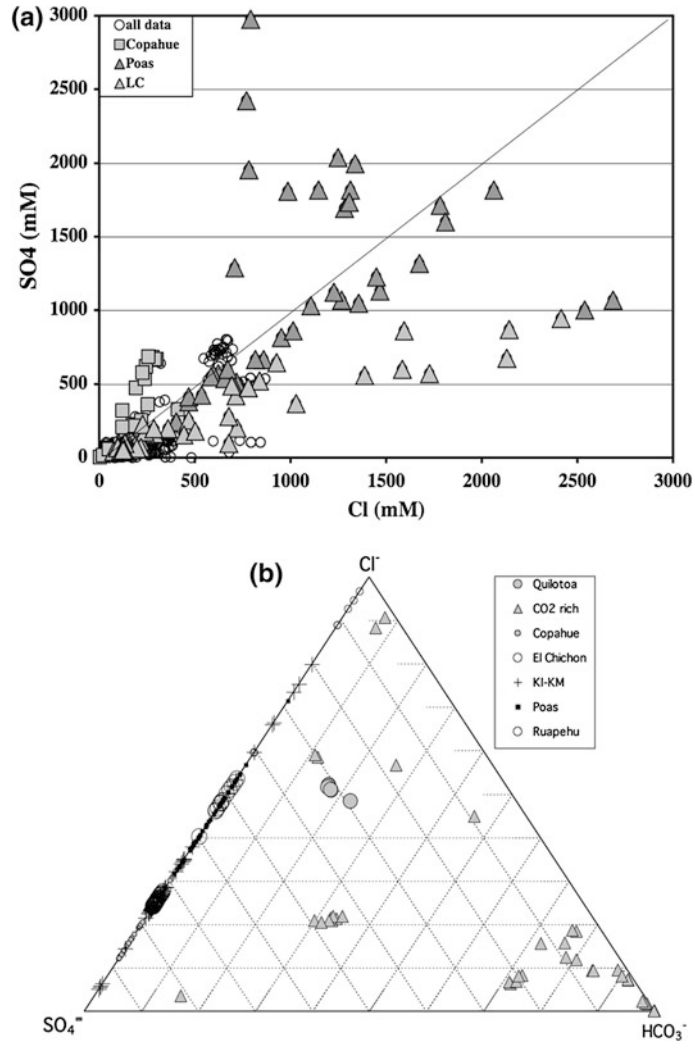

Fig. 8 **a**. Molar S/Cl is on average ~1, but both S excess and deficits are common. The Poás crater lake samples (LC) probably suffered from sulfur loss through liquid sulfur formation and anhydrite crystallization. The Poás samples with excess sulfur (Poás lake) probably suffered from HCl loss through HCl vapor loss. **b**. The S–Cl–C diagram shows the acid lakes on the S–Cl axis, and the very CO_2 rich samples near the HCO_3 corner. Very few lakes have mixed S–Cl–HCO_3 compositions, and most of these have a relatively high pH values

lakes in the Eifel, FRG, Aeschbach-Hertig et al. 1996). Lakes that are non-volcanic in origin (e.g., some glacial lakes) may become contaminated through surface inflow of volcanically-contaminated rivers, with Caviahue lake in Argentina as an example (Varekamp 2008). An alternative volcanic lake classification based on lake water chemistry is proposed in a later chapter (Varekamp, this issue) grouping into active lakes, quiescent lakes and CO_2-rich lakes.

4 Limnology

The chemistry of lake water, including that of volcanic lakes, changes along the vertical profile when the heat budget results in a thermal gradient between the cooler surface waters and generally hotter bottom waters when affected by fluid input of volcanic origin (Boehrer and Schultze 2008; Kling et al., this issue). The thermal and chemical

Fig. 9 Laguna Cuicocha is a volcanic lake in the Andes of Ecuador, about 100 km north of Quito (the capital city) (picture by J. Ratner, University of Oxford)

stratification leads to the formation of different zones within a lake, characterized by distinct chemical-physical features and behavior (Fig. 10), as follows:

1. The epilimnion: the surface water layer sensitive to external temperature and solar radiation. Epilimnitic water exchanges heat and volatile substances (gases) with the atmosphere. The epilimnions recirculate episodically by wind and/or by changes of external temperatures.
2. The hypolimnion: the deep water layer showing the lowest temperature along the vertical lake profile, generally determined by the final water temperature during the spring

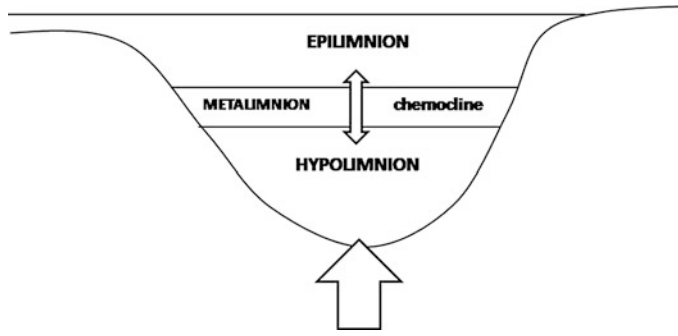

Fig. 10 Sketch of the lake stratification, simplified from Tassi and Rouwet (2014). The *lower arrow* indicates eventual heat and fluid input from the aquifer, the *double-arrow* indicates mixing processes (see text for further details)

lake turnover. Colder water is denser and tends to sink to the lake bottom.
3. The metalimnion: the water layer between the epilimnion and the hypolimnion, showing a marked thermal gradient. It basically corresponds to the thermocline which refers to the plane of maximum rate of temperature decrease with depth.

Different types of lakes can be recognized on the basis of thermal and water circulation features, basically depending on the lake's longitude and altitude.

Amictic lakes are lakes sealed off perennially by ice from annual variations in temperature. No vertical stratification occurs in these lakes. They are typical in the Antarctic.

Cold monomictic lakes are ice-covered lakes most of the year and experience complete mixing once a year during the summer. These lakes are found in the Arctic and high mountains.

Warm monomictic lakes show complete water circulation in winter and most stable stratification in summer. These lakes are common in warm regions of temperate zones.

Dimictic lakes experience complete mixing twice a year. These lakes are typical for cool temperate regions. Thermal stratification always has the 4 °C waters at the bottom and warmer waters higher up.

Oligomictic lakes mix completely irregularly, i.e., less than once a year. They can be found at low altitude in tropical regions (e.g., Hule and Río Cuarto lakes, Costa Rica; Cabassi et al. 2014).

Cold polymictic lakes a covered by lakes part of the year, and experience frequent or continuous complete mixing during the ice-free period. This behavior is typical for temperate lakes.

Warm polymictic lakes are never covered by ice, and show continuous complete mixing except for short (few hours) stratification periods. They are shallow lakes in tropical areas.

Meromictic lakes are those that do not undergo complete mixing, and are characterized by a permanent stratification (e.g., Lake Nyos, Kling et al., this issue). In meromictic lakes the monimolimnion is the deeper lake layer perennially isolated from the surface. Water chemistry in the monimolimnion is different with respect to the one of the shallower water layers.

The mixolimnion is the layer overlying the monimolimnion, where lake waters periodically circulate and mix. The chemolimnion is the layer separating the monimolimnion and the mixolimnion, characterized by a steep salinity gradient. The chemocline (Fig. 9) is the plane of density change; the pycnocline is the plane of density change which may be thermal or chemical in origin. The chemocline is a plane where a significant transition in composition occurs and may thus be also the pycnocline.

5 Volcanic Lake Colors

Lakes have a range of colors, dependent on their chemical composition or particular ecosystem. In general, oligotrophic lakes, i.e., those that are biologically unproductive, have a deep blue color (absorption of longer wavelengths, scattering of short wavelengths of the visible spectrum), somewhat similar to marine environments with limited productivity. Eutrophic lakes are rich in nutrients, carried in from local catchments, geothermal inputs or human contamination, and have a more greenish blue color, and in extreme cases may become truly green from algae in the water column. Brown lakes have high concentrations of dissolved organic matter, leading to brownish organic acids in the water. Some extreme lakes have a deep red color because of the presence of red algae in the water column.

Volcanic lakes may deviate from this four-color scheme of common lakes because of their sometimes unusual chemical inputs. Volcanic lakes dominated by meteoric waters are also often deep blue, because they tend to be oligotrophic with their very small catchment areas (e.g., Crater Lake, Oregon, Fig. 3). Three other 'color groups' of volcanic lakes exist:
1. Lakes with a geothermal or volcanic nutrient input, usually phosphorous;
2. Lakes with a colored dissolved substance, usually Fe or sulfur;
3. Lakes with a suspended substance or chemical precipitate with a specific color.

Some volcanic lakes have a P-rich input, which are usually relatively low pH systems, where the P is derived from the dissolution of volcanic rocks. Phosphorous is removed once a phosphate mineral becomes saturated or the P-oxyanion is removed by adsorption onto a host phase that precipitates (usually an Fe-rich phase). If the P enters a volcanic lake, it may stimulate the biotic productivity, which could create a green lake. Geothermal nitrogen fluxes tend to be relatively small, although traces of ammonia and nitrate occur in geothermal systems and may provide the basis of the local food chains (Pedrozo et al. 2001, 2008). These lake colors are common compared to non-volcanic lakes, except that the source of the nutrients is here geothermal or volcanic and not anthropogenic.

Fundamentally different are volcanic lakes that contain a dissolved substance that lends a color to the water. Waters rich in Fe^{2+} may be deep green, whereas Fe^{3+} in water may produce a violet to brownish water color, depending on speciation and complexation.

The third group of volcanic lakes may have colors that reflect the presence of a suspended solid, be it a colloid or a fine mineral precipitate. Some acid volcanic lakes are deep gray (e.g., Poás lake, Costa Rica, Fig. 11) when the grey bottom sediments are stirred up by convection currents. Other acid lakes are saturated in elemental sulfur, which in hot lakes may form a pool of liquid sulfur at the bottom (e.g., Poás lake; Oppenheimer and Stevenson 1989; Yugama lake, Kusatsu Shirane, Japan; Takano et al. 1994). Gas percolation through this liquid layer may bring up small spheres of molten sulfur that chills in the cooler surface waters and may float as small suspended masses partly due to its hydrophobic nature. Small colloids of sulfur may form as well, which will give the water a blue white tinge, which together with the other constituents (green from ferrous ions) may create the turquoise colored lakes (e.g., middle Keli Mutu lake, Indonesia; Pasternack and Varekamp 1994) (Fig. 12). The crater lake of Aso volcano, Japan (Yudamari lake, Fig. 13, Shinohara et al., this issue) changes its color from blue-ish green to more deep green colors, the result of the disappearance of the blue color component (Ohsawa et al. 2010). The presence of the sulfur colloids creates the blue color, and with diminishing concentrations of colloidal sulfur, the lake turns greener. In the case of Yudamari lake, the disappearance of colloidal sulfur is caused by enhanced SO_2 inputs into the system (Delmelle and Bernard, this issue), and

Fig. 11 Laguna Caliente, Poás, Costa Rica (picture by R. Mora-Amador, 11 April 2007). The *grey color* of the lake is due to strong lake water convection, mixing lake bottom sediments with the water. Note the *yellow mats* of floating sulphur spherules

Fig. 12 Keli Mutu volcano, Flores, Indonesia (picture by R. Campion, 22 August 2011), with its three colorful lakes. From *left* to *right*: Tiwu ata Polo, Tiwu Nuwa Muri Khoofai, and Tiwu ata Mbupu. The three lakes are known for their occasional changes in color, believed to be the result from the modification of the size and composition of mineral precipitates suspended in their waters

Fig. 13 Yudamari crater lake, Mt Nakadake, Aso volcano, Kyushu, Japan (picture by N. Vinet, 5 December 2011). Intense degassing from the turquoise lake and fumaroles (right of Yudamari lake). The stratified, steep cliffs of the crater well illustrate the sustained volcanic activity of Aso volcano. Lake-derived plume and fumarole gas measurements using a portable Multi-Gas station are conducted (Shinohara et al., this issue)

as such, color changes may have a role in eruption monitoring. Colloidal silica is found in silica-rich geothermal pools which tend to have a specific blue color as a result of the scattering of light on these tiny colloids (Ohsawa et al. 2010).

Changes in color of crater lakes are sometimes related to the precipitation of new mineral phases. A most striking example was Voui lake in 2005, which changed from a deep blue, rather dilute lake at the top of Ambae volcano (Vanuatu) into a pool of blood red, very acidic water, with a small new island volcano in the middle (Fig. 14). Water analyses and saturation calculations suggest that the red color of the lake was the result of the precipitation of jarosite and hematite (Bani et al. 2009). The three Keli Mutu lakes on Flores, Indonesia are also famous for their colors and color changes with the seasons (Fig. 12). The three lakes have pH values ranging from 3 to <1, with the smallest, and most dilute lake being black, and the center, most acidic lake being turquoise (and saturated with sulfur). The first lake is green in the dry season (with Fe contents dominated by Fe^{2+}) and red to brown during the wet season (November–April), possibly the result of a pH increase with rainwater dilution and oxidation of Fe^{2+} into Fe-oxide phases (hematite, Pasternack and Varekamp 1994).

6 Statement of This Monograph

This first monograph on volcanic lakes aims to give an overview on the present state of volcanic lake research, covering topics such as volcano monitoring, the chemistry, dynamics and degassing of acidic crater lakes, mass-energy-chemical-isotopic balance approaches, limnology and degassing of Nyos-type lakes, the impact on the human and natural environment, the eruption products and impact of crater lake breaching eruptions, numerical modeling of gas clouds and fluid migrations, CO_2 fluxes from lakes, biological activity, monitoring techniques, and some aspects more. We aim to offer an updated manual

Fig. 14 Voui lake, Ambae volcano, Vanuatu, before the 2005 eruptions (picture by K.N.) (Bani et al. 2009). The *darker blue* lake behind Voui lake is the inactive Manaro lake

on volcanic lake research, providing classic research methods, and point towards a more high-tech approach of future volcanic lake research and continuous monitoring.

The target audience of the book is strictly scientific, composed of volcanologists, limnologists, and biologists, among other volcano-phyles. Despite this scientific focus, we would like to leave a visually attractive, illustrated handbook to all people interested in one of the most extreme and spectacular features on the Earth's surface: volcanic lakes.

References

Aeschbach-Hertig W, Kipfer R, Hofer M, Imboden DM, Wieler R, Signer P (1996) Quantification of gas fluxes from the subcontinental mantle: the example of Laacher See, a maar lake in Germany. Geochim Cosmochim Acta 60:31–41

Aguilera E, Chiodini G, Cioni R, Guidi M, Marini L, Raco B (2000) Water chemistry of Lake Quilotoa (Ecuador) and assessment of natural hazards. J Volcanol Geotherm Res 97:271–285

Aka FT (this issue) Depth of melt segregation below the Nyos maar-diatreme volcano (Cameroon, West Africa): major-trace element evidence and their bearing on the origin of CO_2 in Lake Nyos. In: Rouwet D, Christenson BW, Tassi F, Vandemeulebrouck J (eds) Volcanic Lakes, Springer, Heidelberg

Armienta MA, De la Cruz-Reyna S, Macías JL (2000) Chemical characteristics of the crater lakes of Popocatépetl, El Chichón, and Nevado de Toluca volcanoes, Mexico. J Volcanol Geotherm Res 97:105–125

Bani P, Oppenheimer C, Varekamp JC, Quinou T, Lardy M, Carn S (2009) Remarkable geochemical changes and degassing at Voui crater lake, Ambae volcano, Vanuatu. J Volcanol Geotherm Res 188:347–357. doi:10.1016/j.jvolgeores.2009.09.018

Bernard A, Mazot A (2004) Geochemical evolution of the young crater lake of Kelud Volcano in Indonesia. In: Wanty and Seal II (eds) Water-Rock Interaction, pp 87–90

Boehrer B, Schultze M (2008) Stratification of lakes. Rev Geophysics 46, RG2005/2008. doi:10.1029/2006RG000210

Cabassi J, Tassi F, Mapelli F, Borin S, Calabrese S, Rouwet S, Chiodini G, Marasco R, Chouaia B, Avino R, Vaselli O, Pecoraino G, Capecchiacci F, Vicocchi G, Caliro S, Ramírez C, Mora-Amador R (2014) Geosphere-biosphere interactions in bio-activity volcanic lakes. Evidence from Hule and Río Cuarto (Costa Rica). PLoS one 7(9):e102456

Carapezza ML, Lelli M, Tarchini L (2008) Geochemistry of the Albano and Nemi crater lakes in the volcanic district of Alban Hills (Rome, Italy). J Volcanol Geotherm Res 178:297–304

Caudron C, Mazot A, Bernard A (2012) Carbon dioxide dynamics in Kelud volcanic lake. J Geophys Res 117: B05102. doi:10.1029/2011JB008806

Chiodini G, Tassi F, Caliro S, Chiarabba C, Vaselli O, Rouwet D (2012) Time-dependent CO_2 variations in Lake Albano associated with seismic activity. Bull Volcanol 74:861–871. doi:10.1007/s00445-011-0573-x

Christenson BW, Reyes AG, Young R, Moebis A, Sherburn S, Cole-Baker J, Britten K (2010) Cyclic processes and factors leading to phreatic eruption events: insights from the 25 Sept 2007 eruption through Ruapehu Crater Lake, New Zealand. J Volcanol Geotherm Res 191:15–32

Christenson BW, Tassi F (this issue) Gases in volcanic lake environments. In: Rouwet D, Christenson BW, Tassi F, Vandemeulebrouck J (eds) Volcanic Lakes. Springer, Heidelberg

Christenson BW, Wood CP (1993) Evolution of a vent-hosted hydrothermal system beneath Ruapehu Crater lake, New Zealand. Bull Volcanol 55:547–565

Connor CB, Conway FM (2000) Basaltic volcanic fields. In: Sigurdsson H (ed) Encyclopedia of volcanoes. Academic Press, San Diego, pp 331–343

Costa A, Chiodini G (this issue) Modelling air dispersion of CO_2 from limnic eruptions. In: Rouwet D, Christenson BW, Tassi F, Vandemeulebrouck J (eds) Volcanic lakes. Springer, Heidelberg

Delmelle P, Bernard A (2000a) Volcanic lakes. In: Sigurdsson H (ed) Encyclopedia of volcanoes. Academic Press, San Diego, pp 877–896

Delmelle P, Bernard A (2000b) Downstream composition changes of acidic volcanic waters discharged into the Banyupahit stream, Ijen caldera, Indonesia. J Volcanol Geotherm Res 97:55–75

Delmelle P, Bernard A (this issue) The remarkable chemistry of sulfur in volcanic acid crater lakes: a scientific tribute to Bokuichiro Takano and Minoru Kusakabe. In: Rouwet D, Christenson BW, Tassi F, Vandemeulebrouck J (eds) Volcanic lakes. Springer, Heidelberg

Delmelle P, Henley RW, Opfergelt S, Detienne M (this issue) Summit acid crater lakes and flank instability in composite volcanoes. In: Rouwet D, Christenson BW, Tassi F, Vandemeulebrouck J (eds) Volcanic lakes. Springer, Heidelberg

Delmelle P, Kusakabe M, Bernard A, Fischer T, de Brouwer S, del Mundo E (1998) Geochemical and isotopic evidence for seawater contamination of the hydrothermal system of Taal Volcano, Luzon, the Philippines. Bull Volcanol 59:562–576

de Ronde CEJ, Chadwick Jr WW, Ditchburn RG, Embley RW, Tunnicliffe V, Baker ET, Walker SL, Ferrini VL, Merle SM (this issue) Molten sulfur lakes of intra-oceanic arc volcanoes. In: Rouwet D, Christenson BW, Tassi F, Vandemeulebrouck J (eds) Volcanic lakes. Springer-Heidelberg

Farias ME, Rascovan N, Toneatti DM, Albarrac'n VH, Flores MR, Poire DG, Collavino MM, Aguilar OM,

Vazquez MP, Polerecky L (2013) The discovery of Stromatolites developing at 3570 m above sea level in a high-altitude volcanic lake Socompa. Argentinean Andes. PLOS one 8(1):e53497. doi:10.1371/journal.pone.0053497

Fournier N, Witham F, Moreau-Fournier M, Bardou L (2009) Boiling Lake of Dominica, West Indies: high-temperature volcanic crater lake dynamics. J Geophys Res 114:B02203. doi:10.1029/2008JB005773

Gordon E, Corpuz G, Harada M, Punongbayan JT (2009) Combined electromagnetic, geochemical and thermal surveys of Taal Volcano (Philippines) during the period 2005–2006. Bull Volcanol 71:29–47

Gunkel G, Beulker C, Grupe B, Viteri F (2008) Hazards of volcanic lakes: analysis of Lakes Quilotoa and Cuicocha, Ecuador. Adv Geosci 14:29–33

Gunkel G, Beulker C (2009) Limnology of the crater lake Cuicocha, Ecuador, a cold water tropical lake. Int Rev Hydrobiol 94(103):125

Heiken G (1978) Characteristics of tephra from Cinder Cone, Lassen volcanic National Park, California. Bull Volcanol 41(2):119–130

Henley RW (this issue) Hyperacidic Volcanic lakes. metal sinks and magmatic gas expansion in arc volcanoes. In: Rouwet D, Christenson BW, Tassi F, Vandemeulebrouck J (Eds) Volcanic lakes. Springer, Heidelberg

Hurst AW, Bibby HM, Scott BJ, McGuinness MJ (1991) The heat source of Ruapehu Crater Lake; deductions from the energy and mass balances. J Volcanol Geotherm Res 6:1–21

Hurst T, Christenson B, Cole-Baker J (2012) Use of a weather buoy to derive improved heat and mass balance parameters for Ruapehu Crater Lake. J Volcanol Geotherm Res 235–236:23–28

Hurst T, Hashimoto T, Terada A (this issue) Crater lake energy and mass balance. In: Rouwet D, Christenson BW, Tassi F, Vandemeulebrouck J (eds) Volcanic lakes. Springer, Heidelberg

Keller J (1975) Quaternary maar volcanism near Karapinar in central Anatolia. Bull Volcanol 38(2):378–396

Kereszturi G, Németh K (2012) Monogenetic basaltic volcanoes: genetic classification, growth, geomorphology and degradation. In: K Németh (ed) Updates in volcanology—new advances in understanding volcanic systems. inTech Open, Rijeka, Croatia, pp 3–88. doi:10.5772/51387

Kling GW, Clark MA, Compton HR, Devine JD, Evans WC, Humphrey AM, Koenigsberg EJ, Lockwood JP, Tuttle ML, Wagner GN (1987) The 1986 Lake Nyos gas disaster in Cameroon, West Africa. Science 236:169–175

Kling GW, Evans WC, Tanyileke GZ (this issue) The Comparative Limnology of Lakes Nyos and Monoun, Cameroon. In: Rouwet D, Christenson BW, Tassi F, Vandemeulebrouck J (eds) Volcanic lakes. Springer, Heidelberg

Kusakabe M (this issue) Evolution of CO_2 content in Lakes Nyos and Monoun, and sub-lacustrine CO_2-recharge system at Lake Nyos as envisaged from $C/^3He$ ratios in noble gas signatures. In: Rouwet D, Christenson BW, Tassi F, Vandemeulebrouck J (eds) Volcanic lakes. Springer, Heidelberg

Lorenz V (1986) On the growth of maars and diatremes and its relevance to the formation of tuff rings. Bull Volcanol 48:265–274

Mandeville CW, Webster JD, Tappen C, Taylor BE, Timbal A, Sasaki A, Hauri E, Bacon CR (2009) Stable isotope and petrologic evidence for open-system degassing during the climactic and pre-climactic eruptions of Mt. Mazama, Crater Lake. Oregon. Geochim Cosmochim Acta 73:2978–30123. doi:10.1016/j.gca.2009.01.019

Manville V (this issue) Volcano-hydrologic hazards from volcanic lakes. In: Rouwet D, Christenson BW, Tassi F, Vandemeulebrouck J (eds) Volcanic lakes. Springer, Heidelberg

Mapelli F, Marasco R, Rolli E, Daffonchi D, Donachie S, Borin S (this issue) Microbial life in volcanic lakes. In: Rouwet D, Christenson BW, Tassi F, Vandemeulebrouck J (eds) Volcanic lakes. Springer, Heidelberg

Marchetto A, Ariztegui D, Brauer A, Lami A, Mercuri AM, Sadori L, Vigliotti L, Wulf S, Guilizzoni P (this issue) Volcanic lake sediments as sensitive archives of climate and environmental change. In: Rouwet D, Christenson BW, Tassi F, Vandemeulebrouck J (eds) Volcanic lakes. Springer, Heidelberg

Marini L, Vetuschi Zuccolini M, Saldi G (2003) The bimodal pH distribution of volcanic lake waters. J Volcanol Geotherm Res 121:83–98

Mastin LG, Witter JB (2000) The hazards of eruptions through lakes and seawater. J Volcanol Geotherm Res 97:195–214

Mazot A, Bernard A (this issue) CO_2 Degassing from volcanic lakes. In: Rouwet D, Christenson BW, Tassi F, Vandemeulebrouck J (eds) Volcanic lakes. Springer, Heidelberg

Mazza R, Taviani S, Capelli G, De Benedetti AA, Giordano G (this issue) Quantitative hydrogeology of volcanic lakes: examples from the Central Italy Volcanic Lake District. In: Rouwet D, Christenson BW, Tassi F, Vandemeulebrouck J (eds) Volcanic lakes. Springer, Heidelberg

Moufti MR, Németh K, El-Masry N, Qaddah A (2013) Geoheritage values of one of the largest maar craters in the Arabian Peninsula: the Al Wahbah Crater and other volcanoes (Harrat Kishb, Saudi Arabia). Centr Europ J Geosci 5(2):254–271

Müller G, Veyl G (1956) The birth of Nilahue, a new maar type volcano at Rininahue, Chile. Congreso Geologico Internacional, Seccion I—Vulcanologia del Cenozoico:pp 375–396

Németh K (2010) Monogenetic volcanic fields: Origin, sedimentary record, and relationship with polygenetic volcanism. In: Canon-Tapia E, Szakacs A (eds) What is a volcano? Geological Society of America, Boulder, pp 43–66

Németh K, Cronin SJ, Smith IEM, Agustin Flores J (2012) Amplified hazard of small-volume monogenetic

eruptions due to environmental controls, Orakei Basin, Auckland volcanic field, New Zealand. Bull Volcanol 74(9):2121–2137

Németh K, Martin U, Harangi S (2001) Miocene phreatomagmatic volcanism at Tihany (Pannonian Basin, Hungary). J Volcanol Geotherm Res 111(1–4):111–135

Ohba T, Hirabayashi J, Nogami K (1994) Water, heat and chloride budgets of the crater lake, Yugama at Kusatsu-Shirane volcano, Japan. Geochem J 28:217–231

Ohba T, Hirabayashi J, Nogami K (2000) D/H and $^{18}O/^{16}O$ ratios of water in the crater lake at Kusatsu-Shirane volcano, Japan. J Volcanol Geotherm Res 97:329–346

Ohsawa S, Saito T, Yoshikawa S, Mawatari H, Yamada M, Amita K, Takamatsu N, Sudo Y, Kagiyama T (2010) Color change of lake water at the active crater lake of Aso volcano, Yudamari, Japan: is it in response to change in water quality induced by volcanic activity? Limnology 11:207–215

Oppenheimer C, Stevenson D (1989) Liquid sulphur lakes at Poás volcano. Nature 342:790–793

Pasternack GB, Varekamp JC (1994) The geochemistry of the Keli Mutu crater lake, Flores, Indonesia. Geochem J 28:43–262

Pasternack GB, Varekamp JC (1997) Volcanic lake systematics I. Physical constraints. Bull Volcanol 58:528–538

Pecoraino G, D'Alessandro W, Inguaggiato S (this issue) The other side of the coin: geochemistry of alkaline lakes in volcanic areas. In: Rouwet D, Christenson BW, Tassi F, Vandemeulebrouck J (eds) Volcanic lakes. Springer, Heidelberg

Pedrozo F, Kelly L, Diaz M, Temporetti P, Baffico G, Kringel R, Friese K, Mages M, Geller W, Woelfl S (2001) First results on the water chemistry, algae and trophic status of an Andean acidic lake system of volcanic origin in Patagonia (Lake Caviahue). Hydrobiologia 452:129–137

Pedrozo FL, Temporetti P, Beamud SG, Diaz MM (2008) Volcanic nutrient inputs and trophic state of Lake Caviahue, Patagonia, Argentina. J Volcanol Geotherm Res 178:205–212

Peiffer L, Taran Y, Lounejeva E, Solis-Pichardo G, Rouwet D, Bernard-Romero R (2011) Tracing thermal aquifers of El Chichón volcano-hydrothermal system (México) with $^{87}Sr/^{86}Sr$, Ca/Sr and REE. J Volcanol Geotherm Res 205:55–66

Pérez NM, Hernández PA, Padilla G, Nolasco D, Barrancos J, Melían G, Dionis S, Calvo D, Rodríguez F, Notsu K, Mori T, Kusakabe M, Arpa MC, Reniva P, Ibarra M (2011) Global CO_2 emission from volcanic lakes. Geology 39:235–238. doi:10.1130/G31586.1

Rouwet D, Morrissey MM (this issue) Mechanisms of crater lake breaching eruptions. In: Rouwet D, Christenson BW, Tassi F, Vandemeulebrouck J (eds) Volcanic lakes. Springer, Heidelberg

Rouwet D, Ohba T (this issue) Isotope fractionation and HCl partitioning during evaporative degassing from active crater lakes. In: Rouwet D, Christenson BW, Tassi F, Vandemeulebrouck J (eds) Volcanic lakes. Springer, Heidelberg

Rouwet D, Taran Y, Inguaggiato S, Varley N, Santiago SJA (2008) Hydrochemical dynamics of the "lake-spring" system in the crater of El Chichón volcano (Chiapas, Mexico). J Volcanol Geotherm Res 178:237–248

Rouwet D, Taran Y, Varley N (2004) Dynamics and mass balance of El Chichón crater lake, Mexico. Geofís Int 43:427–434

Rouwet D, Tassi F (2011) Geochemical monitoring of volcanic lakes. A generalized box model for active crater lake. Ann Geophys 54(2):161–173

Rouwet D, Tassi F, Mora-Amador R, Sandri L, Chiarini V (2014) Past, present and future of volcanic lake monitoring. J Volcanol Geotherm Res 272:78–97. doi:10.1016/j.jvolgeores.2013.12.009

Rowe GL, Brantley SL, Fernández M, Fernández JF, Borgia A, Barquero J (1992a) Fluid-volcano interaction in an active stratovolcano: the Crater Lake system of Poás Volcano, Costa Rica. J Volcanol Geotherm Res 64:233–267

Rowe GL, Ohsawa S, Takano B, Brantley SL, Fernández JF, Barquero J (1992b) Using Crater Lake chemistry to predict volcanic activity at Poás Volcano, Costa Rica. Bull Volcanol 54:494–503

Rymer H, Cassidy J, Locke CA, Barboza MV, Barquero J, Brenes J, van der Laat R (2000) Geophysical studies of the recent 15 year eruption cycle at Poás Volcano, Costa Rica. J Volcanol Geotherm Res 97:425–442

Rymer H, Locke CA, Borgia A, Martínez M, Brenes J, van der Laat R, Williams-Jones G (2009) Long-term fluctuations in volcanic activity: implications for future environmental impact. Terra Nova 21:304–309

Schaefer JR, Scott WE, Evans WC, Jorgenson J, McGimsey RG, Wang B (2008) The 2005 catastrophic acid lake drainage, lahar, and acidic aerosol formation at Mount Chiginagak volcano, Alaska, USA: Field observations and preliminary water and vegetation chemistry results. Geochem Geophys Geosyst 9(7): Q07018. doi:10.1029/2007GC001900

Shinohara H, Yoshikawa S, Miyabuchi Y (this issue) Degassing activity of a volcanic crater lake: Volcanic plume measurements at the Yudamari crater lake, Aso volcano, Japan. In: Rouwet D, Christenson BW, Tassi F, Vandemeulebrouck J (eds) Volcanic lakes. Springer, Heidelberg

Sriwana T, van Bergen MJ, Varekamp JC, Sumarti S, Takano B, van Os BJH, Leng MJ (2000) Geochemistry of the acid Kawah Putih lake, Patuha Volcano, West Java, Indonesia. J Volcanol Geotherm Res 97:77–104

Takano B, Saitoh H, Takano E (1994) Geochemical implications of subaqueous molten sulfur at Yugama crater lake, Kusatsu-Shirane volcano, Japan. Geochem J 28:199–216

Taran YA, Inguaggiato S, Cardellini C, Karpov G (2013) Posteruption chemical evolution of a volcanic caldera lake: Karymsky Lake, Kamchatka. Geophys Res Lett 40:5142–5146. doi:10.1002/grl.50961

Taran Y, Rouwet D (2008) Estimating thermal inflow to El Chichón crater lake using the energy-budget, chemical and isotope balance approaches. J Volcanol Geotherm Res 175:472–481

Tassi F, Rouwet D (2014) An overview of the structure, hazards, and methods of investigation of Nyos-type lake from the geochemical perspective. J Limnol 73(1). doi:10.4081/jlimnolo.2014.836

Tassi F, Vaselli O, Capaccioni B, Giolito C, Duarte E, Fernández E, Minissale A, Magro G (2005) The hydrothermal-volcanic system of Rincón de la Vieja volcano (Costa Rica): a combined (inorganic and organic) geochemical approach to understanding the origin of the fluid discharges and its possible application to volcanic surveillance. J Volcanol Geotherm Res 148:315–333

Tassi F, Vaselli O, Fernández E, Duarte E, Martínez M, Delgado-Huertas A, Bergamaschi F (2009) Morphological and geochemical features of crater lakes in Costa Rica: an overview. J Limnol 68 (2):193–205

Todesco M, Rouwet D, Nespoli M, Bonafede M (this issue) How steep is my seep? Seepage in Volcanic lakes. hints from numerical simulations. In: Rouwet D, Christenson BW, Tassi F, Vandemeulebrouck J (eds) Volcanic lakes. Springer, Heidelberg

Todesco M, Rouwet D, Nespoli M, Mora-Amador RA (2012) To seep or not to seep? Some considerations regarding water infiltration in volcanic lakes. In: Proceedings, TOUGH Symposium 2013

Vandemeulebrouck J, Stemmelen D, Hurst T, Grangeon J (2005) Analogue modeling of instabilities in crater lake hydrothermal systems. J Geophys Res 110: B02212. doi:10.1029/2003JB002794

van Otterloo J, Cas RAF (2013) Reconstructing the eruption magnitude and energy budgets for the prehistoric eruption of the monogenetic similar to 5 ka Mt. Gambier Volcanic Complex, south-eastern Australia. Bull Volcanol 75(12):769–786. doi:10.1007/s00445-13-0769-3

Varekamp JC (2003) Lake contamination models for evolution towards steady state. J Limnol 62:67–72

Varekamp JC (2008) The acidification of glacial Lake Caviahue, Province of Neuquen, Argentina. J Volcanol Geotherm Res 178:184–196. doi:10.1016/j.jvolgeores.2008.06.016

Varekamp JC (this issue) The chemical composition and evolution of volcanic lakes. In: Rouwet D, Christenson BW, Tassi F, Vandemeulebrouck J (eds) Volcanic lakes. Springer, Heidelberg

Varekamp JC, Pasternack GB, Rowe GL Jr (2000) Volcanic lake systematics II. Chemical constraints. J Volcanol Geotherm Res 97:161–179

Vaselli O, Tedesco D, Cuoco E, Tassi F (this issue) Are limnic eruptions in the CO2-CH4-rich gas reservoir of Lake Kivu (Democratic Republic of the Congo and Rwanda) possible? Insights from physico-chemical and isotopic data. In: Rouwet D, Christenson BW, Tassi F, Vandemeulebrouck J (eds) Volcanic lakes. Springer, Heidelberg

Weinstein Y (2007) A transition from strombolian to phreatomagmatic activity induced by a lava flow damming water in a valley. J Volcanol Geotherm Res 159(1–3):267–284

White JDL, Ross PS (2011) Maar-diatreme volcanoes: a review. J Volcanol Geotherm Res 201(1–4):1–29

Zlotnicki J, Sasai Y, Toutain JP, Villacorte EU, Bernard A, Sabit JP, Gordon JM, Corpuz EG, Harada M, Punongbayan JT (2009) Combined electromagnetic, geochemical and thermal surveys of Taal Volcano (Philippines) during the period 2005–2006. Bull Volcanol 71(29):47

Zheng S, Wu B, Thorne CR, Simon A (2014) Morphological evolution of the North Fork Toutle River following the eruption of Mount St. Helens. Washington. Geomorphology 208:102–116

Volcano-Hydrologic Hazards from Volcanic Lakes

V. Manville

Abstract

Volcanic regions typically host multiple lakes developed in explosion craters, volcano-tectonic collapse structures, and valley systems blocked as a result of eruptive activity, their boundaries and dimensions shifting in response to renewed activity and modification by background processes of erosion, sedimentation and tectonism. Such water bodies are a potent source of a wide range of complex and inter-related hydrologic hazards owing to their proximity to active volcanic vents, the consequent potential for violent mixing of magma with water, and the frequent fragility of their impoundments. These hazards arise as a result of water displacements within or from the lake basin and can be broadly sub-divided into 3 main types: (I) phenomena sourced within the lake basin as a direct or indirect consequence of subaqueous or subaerial volcanic activity; (II) floods from volcanic lakes triggered by volcanic activity, including induced breaching; and (III) floods from volcanic lakes with a non-volcanic cause. Type I hazards include subaqueous explosive volcanism and associated Surtseyan jets, base surges and tsunamis, which can impact lake shorelines and displace water over basin rims and through outlets. This results in Type II lahar and flooding hazards. Both types have been historically responsible for significant losses of life at many volcanoes worldwide. Other rapid phenomena such as pyroclastic flows, debris avalanches, and large lahars from intra- or extra-lake volcanoes are potentially tsunamigenic (Type I), and/or displacing, and can hence also lead to secondary (Type II) hazards, as can seismicity-producing volcano-tectonic movements. Slower processes including volcano-tectonic movements, subaqueous lava dome extrusion, cryptodome intrusion, and magmatic inflation can potentially produce Type II flooding through volumetric water displacement over the outlet. Erosion of the outlet can be catastrophic, magnifying the size of

V. Manville (✉)
School of Earth and Environment,
University of Leeds, Leeds LS2 9JT, UK
e-mail: v.r.manville@leeds.ac.uk

D. Rouwet et al. (eds.), *Volcanic Lakes*, Advances in Volcanology,
DOI 10.1007/978-3-642-36833-2_2,
© Springer-Verlag Berlin Heidelberg 2015

flood events. Damming of the outlet itself can result in backflooding of the basin. Type III hazards, i.e. volcanic lake break-out floods; result from breaching of the barrier constraining a volcanic lake as a result of passive overtopping, piping, mechanical failure, or headward erosion of the natural dam. Such events range in scale from relatively minor outflows triggered by failure of crater walls or the breaching of riverine dams composed of pyroclastic, volcaniclastic, or lava flow material to catastrophic floods generated by the breaching of caldera rims. Palaeohydraulic reconstructions of some of the latter indicate that they are amongst the largest post-glacial floods on Earth, being exceeded only by late Pleistocene deluges associated with breaching of ice-dammed lakes and pluvial basins.

Keywords
Volcanic lakes · Subaqueous explosive volcanism · Base surges · Tsunami · Floods · Lahars · Natural hazards

1 Introduction

Volcanic activity is a prolific producer of lakes due to the capacity of eruptions and volcano-tectonic activity to generate both positive and negative relief. In the strictest definition, a volcanic lake is a cap of meteoric water over the vent of an active volcano: according to this criterion 16 % of the 714 identified Holocene volcanoes world-wide host one or more, frequently ephemeral, lakes in explosion craters and subsidence calderas (Delmelle and Bernard 2000). Many typical crater lakes (Fig. 1a) contain 1–10 × 10^6 m^3 of water, often at elevations several km above the surrounding landscape (Casadevall et al. 1984; Rowe et al. 1992; Christenson and Wood 1993; Kempter and Rowe 2000). Hydrothermal and hydromagmatic (maar) eruption craters (Fig. 1b) are typically <2 km in diameter and comprise a central pit ringed by a raised ejecta rim (Lorenz 1973). The transition from purely magmatic explosion craters to volcano-tectonic depressions formed by a combination of explosive ejection of material and magma withdrawal occurs at c. 2.5 km diameter (Williams 1941). The largest volcanic impoundments comprise intracaldera lakes, either developed by collapse at the summit of shield or cone volcanoes such as Crater Lake in Oregon (Fig. 1c), which impounds 1.9 × 10^{10} m^3 at an elevation of 1,882 m (Nelson et al. 1994), or superimposed on regional tectonic depressions, like Lake Taupo in New Zealand (Fig. 1d), which contains 6 × 10^{10} m^3 (Lowe and Green 1992). Lake Toba in Indonesia is the world's largest caldera lake and holds 2.4 × 10^{11} m^3 of water (Chesner and Rose 1991). A review of c. 200 Late Pleistocene or younger terrestrial calderas found that around half held one or more intracaldera lakes (Manville 2010), either with or without a surface outlet (Larson 1989).

In addition, volcanism is the third most common dam-forming mechanism, accounting for 8 % of natural-dammed lakes globally (Costa and Schuster 1988). Volcanogenic dams include lava flows (Fenton et al. 2004), pyroclastic flows (Aramaki 1981; Macías et al. 2004), debris avalanches from the collapse of stratovolcanoes (Meyer et al. 1986; Capra and Macías 2002), and rapid aggradation by lahars (Umbal and Rodolfo 1996). These blockages may impound lakes in the source crater or caldera, adjacent ones, or local valley systems (Fig. 2). All such impoundments have the potential to generate catastrophic break-out floods through sudden failure of the volcanic barrier, in some cases triggered by the resumption volcanism. The resulting floods from large volcanic lakes rank

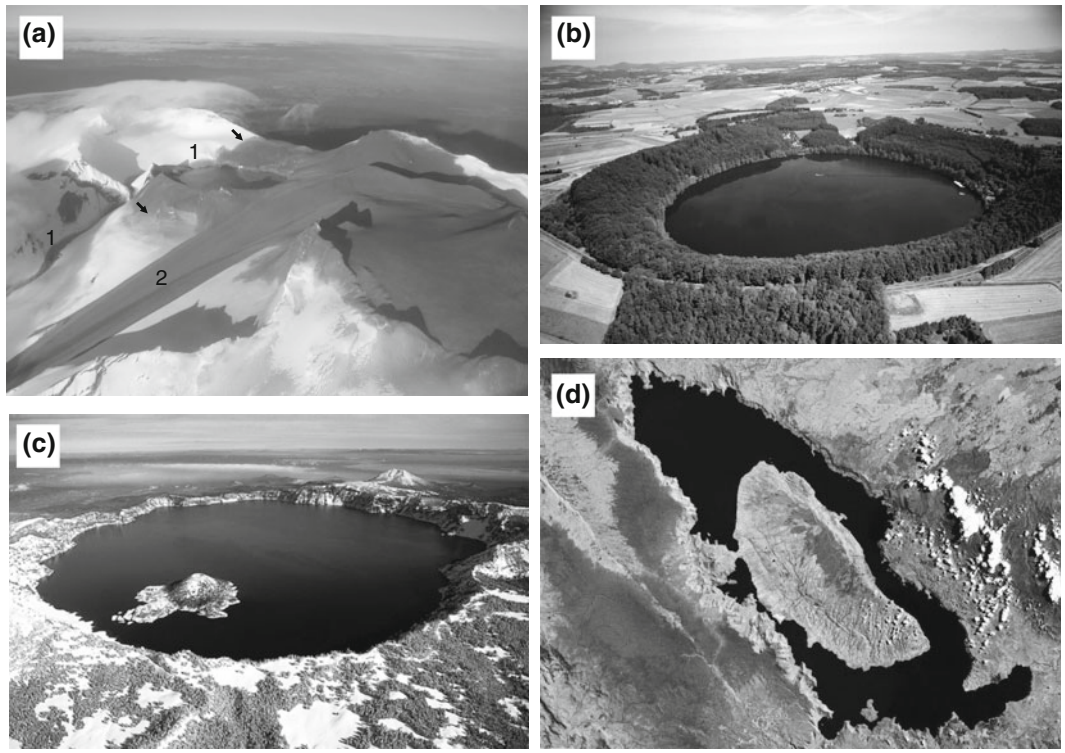

Fig. 1 A selection of volcanic lakes from around the world. **a** Crater Lake, Mt. Ruapehu, New Zealand. This c. 400 m diameter lake lies at a surface elevation of c. 2,530 mASL. Explosive volcanic activity has generated frequent hazards, including base surges (deposits arrowed) and eruption-triggered lahars by displacement waves over the outlet (1) or Surtseyan jetting over the crater rim (2). This photo was taken the day after the 25 September 2007 eruption. (Image B. Christenson, GNS Science). **b** Pulvermaar in the volcanic Eifel region of Germany. Diameter is c. 700 m. **c** Crater Lake, Oregon. Formed by caldera collapse during the 7.7 ka Mazama eruption, this 10 km diameter lake lies 1882 mASL and has no surface outlet. (Wikipedia commons). **d** Lake Toba, 87 km long, lies in a volcano-tectonic collapse structure last modified during the 74 ka Toba super-eruption. (Landsat Image)

amongst the largest post-glacial floods on Earth (O'Connor et al. 2013).

1.1 Classification of Hazards Associated with Volcanic Lakes

A wide range of hazards derive from volcanic lakes as a direct consequence of magma:water interactions at the vent, or through the interaction of volcanically generated mass-flows (pyroclastic flows, debris avalanches, lahars, and lava flows) with the water body (Fig. 3). Consequently, although only c. 3.5 % of recorded volcanic eruptions have occurred through lakes (Simkin and Siebert 1994), these have been responsible for approximately 15 % of recorded deaths (Table 1). In many cases, a primary hazardous phenomenon can trigger a series of other secondary effects in a process-chain (Fig. 3): for example, a subaqueous explosion that breaches the lake surface can generate tsunamis that overtop the lake outlet to form a lahar, which itself causes erosion of the spillway leading to further water release and downstream flooding (McGimsey et al. 1994; Waythomas et al. 1996). Under certain (poorly understood) conditions, magma:water interactions can increase the violence and explosivity of volcanic eruptions (Thorarinsson et al. 1964; Lorenz 1973; Sheridan

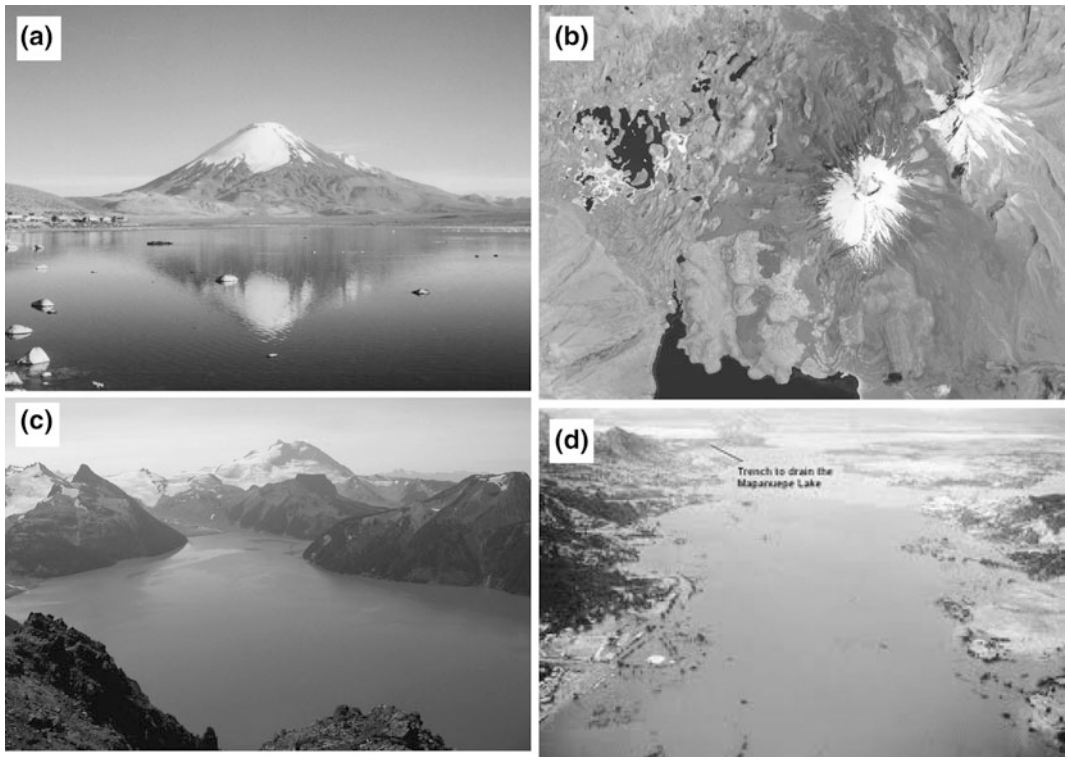

Fig. 2 Lakes impounded behind dams of volcanic material. **a** Lake Chungará, dammed at c. 6 ka by a debris avalanche from Parinacota stratovolcano, Chile. (Wikipedia commons). **b** Spaceborne view of the snow-capped cone of Parinacota: Lake Chunagará lies c. 8 km to the south. Numerous other lakes, including Cotacotani, are impounded by the irregular topography of the debris avalanche deposits to the west (NASA image ISS029-E-20003). **c** Lake Garibaldi (10 km^2, 1,500 m ASL, >250 m deep) dammed by lave flows from Mt. Price and Clinker peak, British Columbia, Canada. (Wikipedia commons). **d** Lake Mapanuepe, dammed by lahars in the Marella river, Pinatubo, Philippines 1991 (USGS image)

and Wohletz 1983; Wohletz 1986). Factors that influence the explosivity of the interaction likely include magma type, mass eruption rate, nature of magma pre-fragmentation, and water depth (Wohletz 1986; Mastin 1995; Koyaguchi and Woods 1996). The net effect can be to increase the area of the primary hazard by up an order of magnitude through the generation of base surges (Moore 1967) and even more with tsunamis (Latter 1981). A 0.01 km^3 monogenetic basaltic eruption in an arid environment would produce a localised scoria cone, the same magma volume erupted in wet environment can produce a 1 km diameter maar/tuff-ring with phreatomagmatic base surges extending to >3 km radius (Németh et al. 2012). The travel distance of tsunamis is effectively limited by the dimensions and bathymetry of the water body, in lakes this can be 10's of km. Alternatively, magma and water can mix relatively non-violently (Batiza and White 2000). A review of historical eruptions through volcanic lakes shows that c. 2 % involved relatively passive growth of subaqueous to emergent lava domes (Table 1). Other hazards reported during eruptions through water include tsunamis and seiches generated by volcano-tectonic displacements of the lake floor, Surtseyan jets, tephra and ballistic fall, lahars, lightning (associated with wet ash clouds), and torrential rainstorms (Mastin and Witter 2000). Growth in population and infrastructure, particularly in the developing world, has increased exposure to hazards from volcanic lakes and a number of major cities are vulnerable to volcano-lake

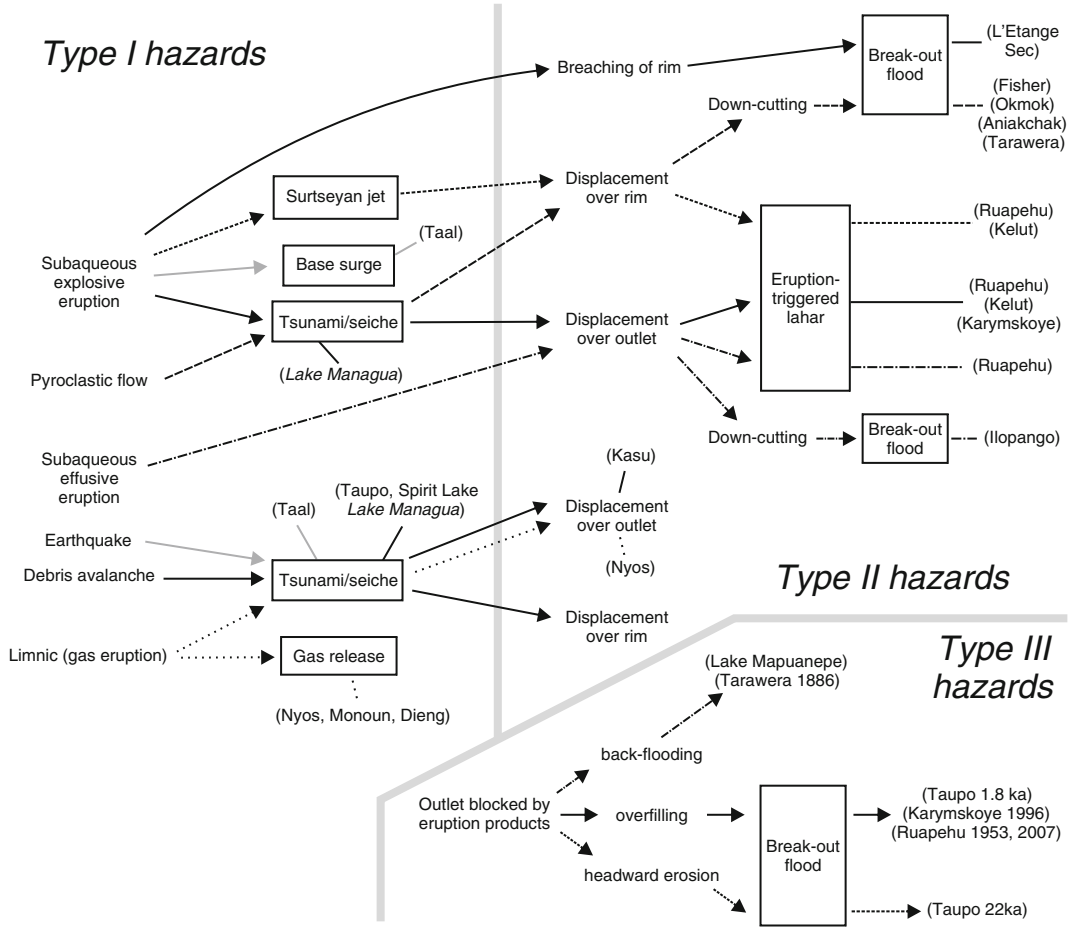

Fig. 3 Classification of the main hazards associated with volcanic lakes, including triggering mechanisms and process-chains. Examples of volcanoes where these hazards have been observed historically are shown in *brackets*; names are *italicized* where the hazard has been inferred

interactions including Managua, the capital of Nicaragua (population 2.2 million). Therefore, characterisation and understanding of the range of hazards is vital to their mitigation.

2 Subaqueous Explosive Volcanism

The rapid conversion of thermal to kinetic energy during the violent mixing of magma and water in a subaqueous eruption fuel-coolant reactions (Wohletz 1986; Frost et al. 1994; White 1996) produces an expanding and buoyantly rising bubble of water vapour, magmatic gas, and magma fragments whose interactions with the ambient water column can cause ballistic ejection of most of the volume of a crater lake from its basin (Nairn et al. 1979), as well as generating base surges (Moore 1967; Waters and Fisher 1971) and impulsive tsunami in larger water bodies (Watts and Waythomas 2003). Volcanic tsunamis (Latter 1981), including explosion generated waves, are treated separately in this discussion due to their range of potential triggering mechanisms.

Table 1 Compilation of historical Type I and II hazardous events at volcanic crater and caldera lakes, with a focus on the best characterised or most deadly

Volcano, Location	Date	Lake type	S	B	T	L	P	A	D	Other	Fatalities	Events	Notes, references
Ruapehu, New Zealand	25 Sep. 2007	Crater	X	x	x	x	–	–	–	–	–	53	More than 53 eruptions have occurred through Crater Lake in historic times, typically in the form of minor phreatic to larger phreatomagmatic explosions accompanied by Surtseyan jets, base surges, and tsunamis confined to the lake basin (Hackett and Houghton 1989; McClelland et al. 1989). Larger events have swept the summit area with base surges and ballistic fall-out in 1969 (Healy et al. 1978) and 1975 (Nairn et al. 1979). Magmatic eruption episodes occur every c. 50 years, including in 1945-46 when a lava dome was extruded (Beck 1950) and 1995-1996 (Cronin et al. 1996, 1997). Eruption-triggered lahars have entered areas now occupied by ski fields on 6 occasions, most recently in 2007 (Kilgour et al. 2010). Break-out lahars from Crater Lake happened in 1953 (O'Shea 1954) and 2007 (Massey et al. 2010)
	23 Sep. 1995		X	x	x	x	–	–	–	–	–		
	18 Sep. 1995		X	x	x	x	–	–	–	–	–		
	24 April 1975		X	X	X	X	–	x	–	–	–		
	22 June 1969		X	X	x	x	–	x	–	–	–		
	1945		X	–	–	X	–	X	X	–	–		
	1861–2012		–	–	–	–	–	–	–	–	–		
Tarawera, New Zealand	10 Jun. 1886	Valley/ crater	X	X	X	–	–	X	–	x	151	1	Basaltic fissure eruption through Lakes Rotomahana/Rotomakariri generates base surges that travelled up to 6 km, these and wet ash fall kill 151 (Nairn 1979; Simmons et al. 1993). Blockage of outlet to Lake Tarawera by primary and remobilised eruption products results in 12.8 m rise in lake level, inundating lake shore villages (White et al. 1997)
Taupo, New Zealand	1846	Caldera	–	–	x	–	–	–	–	–	–	1	Landslide from the Hipaua Cliffs geothermal area at the south end of Lake Taupo killed over 150 and generated a small tsunami when it entered the lake (Hegan et al. 2001)

(continued)

Table 1 (continued)

Volcano, Location	Date	Lake type	S	B	T	L	P	A	D	Other	Fatalities	Events	Notes, references
White Island, New Zealand	1826–2012	Crater	X	x	–	–	–	x	–	–	–	>>1	Intermittent moderate phreatomagmatic eruptions, sometimes occurring through ephemeral crater lakes have occurred through the historical period, most recently in July 2000 (BGVN 25:07) (Houghton and Nairn 1991)
Raoul Island, Kermadecs	17 Mar. 2006	Crater	x	x	–	–	–	x	–	–	1	1	Phreatomagmatic eruption through Green Lake (BGVN 31:03)
Aoba (Ambae), Vanuatu	Nov. 2005–Jan. 2006	Caldera	x	x	x	–	–	–	–	–	–	2	Growth of tuff ring in Lake Voui produced Surtseyan eruptions with hazards confined to lake basin (Németh et al. 2006; Bani et al. 2009) (BGVN 30:11). Phreatic eruptions also occurred in 1995 (BGVN 20:02)
Niuafo'ou, Tonga	1814–1985	Caldera	–	–	–	–	–	–	–	–	–	3	At least 3 eruptions have occurred through the central caldera lake during historical times (BGVN 28:04, SEAN 10:09)
Long Island, Papua New Guinea	Nov. 1993	Caldera	x	–	–	–	–	–	–	–	–	8	Phreatomagmatic eruptions and emissions discoloured 8 km diameter Lake Wisdom. Largest explosions broke lake surface in depths of 300–350 m. Similar eruptions beneath the lake or on Motmot Island have occurred in 1933, 1943, 1953, 1955 and 1968. (BGVN 18:12)
	1660	Caldera	–	x	X	X	?	x	–	X	>2,000		Explosive eruption deepened a pre-existing caldera lake (Pain et al. 1981)
Kasu, Papua New Guinea	20 Apr. 1999	Crater	–	–	X	–	–	–	–	–	1	1	A 150,000 m^3 landslide into the small crater lake generated a 15 m high wave that washed over the outlet, injuring 11 and killing one (Wagner et al. 2003)
Rabaul, Papua New Guinea	Mar. 1940	Crater	–	–	–	–	–	–	–	–	–	1	Small phreatic eruptions occurred through an ephemeral lake developed in the crater of Tavurvur (Simkin and Siebert 1994)

(continued)

Table 1 (continued)

Volcano, Location	Date	Lake type	S	B	T	L	P	A	D	Other	Fatalities	Events	Notes, references
Karkar, Papua New Guinea	1979–9180	Crater	x										Phreatomagmatic eruptions through small intermittent crater lake
Kerinci, Indonesia	Sep. 1937	Crater	–	–	–	–	–	–	–	–	–	1	Phreatic eruption through ephemeral lake developed in crater of Indonesia's highest volcano (Simkin and Siebert 1994)
Kaba, Indonesia	1833	Crater	–	–	–	X	–	–	–	–	126	1	Eruption ejected crater lake at Kan Vogelsang (van Padang 1951)
Dempo, Indonesia	1905–2006	Crater	x	x	–	x	–	–	–	–	–	8	Eruptions through the crater lake have occurred on 8 occasions, most severely in Dec. 1939, and most recently on 25 Sep. 2006 (BGVN 34:03)
Anak Krakatau, Indonesia	1931–1959	Crater	–	–	–	–	–	–	–	–	–	16	Eruptions through ephemeral crater lakes have occurred on at least 16 occasions since the growth of Anak Krakatau in the 1883 caldera, most recently in 1959 (Simkin and Siebert 1994)
Kelimutu, Indonesia	1968	Crater	–	–	–	–	–	–	–	–	–	1	Small eruption through Tiwu Nua Muri, one of 3 crater lakes at the summit of this stratovolcano.
Dieng Volcanic Complex, Indonesia	1766-2009	Crater	x	–	x	x	–	–	–	x	149	18	This region contains a caldera, two stratovolcanoes, 20 craters and geothermal areas. It has a history of producing lethal gas eruptions, phreatic explosions and other hazards. Since the 18th century 18 phreatic eruptions through 7 different crater lakes have caused lahars on 3 occasions and deaths on 8. On 20 Feb. 1979, a limnic eruption of CO_2 from Sinila killed 149 (SEAN 04:03) (Le Guern et al. 1982)

(continued)

Table 1 (continued)

Volcano, Location	Date	Lake type	S	B	T	L	P	A	D	Other	Fatalities	Events	Notes, references
Kelut, Indonesia	Nov. 2007	Crater	–	–	–	–	–	–	X	–	–	35	Passive extrusion of a lava dome displaced the crater lake (BGVN 37:03)
	10 Feb. 1990		–	x	x	x	–	–	–	–	36		Ganung Kelut is one of the most dangerous volcanoes in Indonesia. More than 30 eruptions have occurred since AD 1000, typically of VEI magnitude 2–4, on a c. 13 year cycle (8-18 year range). These have ejected the summit crater lake to form lethal lahars on 10 occasions, killing >15,000 in total (Thouret et al. 1998). Tunnels were constructed during 1923–1926 to artificially lower the lake level following the devastating 1919 eruption (Zen and Hadikusumo 1965; Smart 1981; Suryo and Clarke 1985). Following their destruction by the 1951 eruption (which produced no lahars because of the reduced crater lake volume) they were rebuilt
	26 Apr. 1966		–	–	–	X	–	–	–	–	282		
	31 Aug. 1951		–	–	–	–	–	–	–	–	7		
	19 May 1919		–	–	–	X	–	–	–	–	5,110		
	22 May 1901		–	–	–	X	–	–	–	–	Many		
	4 Jun. 1864		–	–	–	x	–	–	–	–	54		
	24 Jan. 1851		–	–	–	x	–	–	–	–	21		
	1826		–	–	–	x	–	–	–	–	–		
	1716		–	–	–	x	–	–	–	–	–		
	1586		–	–	–	X	–	–	–	–	>10,000		
	AD1000–1586		–	–	–	X	–	–	–	–	Many		13 other explosive eruptions through the crater lake of Kelut are known from this period
Tengger, Indonesia	24 Jan. 1842	Crater	–	–	–	–	–	–	–	–	–	1	Explosion through crater lake (Simkin and Siebert 1994)
Raung, Indonesia	1838	Crater	–	–	–	x	–	–	–	–	–	6	Eruptions through the summit crater lake of Raung produced eruption-triggered lahars until modification of the crater area by the 1838 eruptions prevented ponding of water (van Padang 1951)
	16 Jan. 1817		–	–	–	–	–	–	–	–	–		
	1730		–	–	–	X	–	–	–	–	Many		
	1638		–	–	–	X	–	–	–	–	>1,000		
	1597		–	–	–	–	–	–	–	–	–		
	1593		–	–	–	–	–	–	–	–	–		
Rinjani, Indonesia	1994	Crater	–	–	–	–	–	–	–	–	30	2	Phreatomgmatic eruptions from cone growing on lake shore. Fatalities resulted from cold lahar—possibly rain triggered (BGVN 20:05)
	1944		–	–	–	–	–	–	–	–	–		Eruption through crater lake.

(continued)

Table 1 (continued)

Volcano, Location	Date	Lake type	S	B	T	L	P	A	D	Other	Fatalities	Events	Notes, references
Kawah Ijen, Indonesia	28 Jun. 1999	Crater	–	–	–	–	–	–	–	–	–	8	Kawah Ijen hosts a c. 1 km diameter, hot, highly acidic crater lake at an elevation of 2,200 mASL, and is the focus of sulphur mining activity. 8 historical eruptions have occurred through the crater lake, producing lethal lahars on a number of occasions
	3 Feb. 1994		–	–	–	–	–	–	–	–	–		
	3 Jul. 1993		–	–	–	–	–	–	–	–	–		
	22 Apr. 1952		–	–	–	–	–	–	–	–	–		
	5 Nov. 1936		–	–	x	–	–	–	–	–	–		
	25 Feb. 1917		–	–	–	–	–	–	–	–	–		
	15 Jan. 1817		–	–	X	–	–	–	–	–	yes		
	1796		–	–	x	–	–	–	–	–	–		
Awu, Indonesia	1966	Crater	–	–	–	X	X	–	–	–	<39	7	Powerful explosive eruptions through the crater lake of this massive stratovolcano generated devastating lahars and pyroclastic flows. Smaller eruptions through crater lake also occurred in 1921, 1922 and 1930 (Delmelle and Bernard 2000; Simkin and Siebert 1994). 1966 eruption changed crater geometry and minimised size of lake.
	1892		–	–	–	X	X	–	–	–	1,530		
	1856		–	–	–	X	X	–	–	–	>3,000		
	1711		–	–	–	X	X	–	–	–	>3,200		
Galunggung, Indonesia	1982	Crater	–	–	–	x		–	–	–	8	2	Eruptions expelled half of c. 8.6×10^6 m^3 crater lake as hot lahar (SEAN 07:03). Since 1984 only a shallow wide lake has survived.
	1822		–	–	–	X	x	–	–	–	3,600		Eruptions through crater lake expelled massive lahars that destroyed 114 villages (Delmelle and Bernard 2000)
Lokon-Empung, Indonesia	22 Mar. 1986	Crater	–	–	x	–	–	–	–	–	–	2	Eruptions expelled a small (0.7×10^6 m^3) lake from the Tompaluan crater generating lahars (SEAN 11:03)
	27 Nov. 1969		–	–	–	–	–	–	–	–	–		
Mahawu, Indonesia	16 Nov. 1977	Crater	–	–	–	–	–	–	–	–	–	1	Phreatic explosion through intermittent small crater lake (SEAN 12:07)
Tongkoko, Indonesia	1801	Crater	–	–	–	–	–	–	–	–	–	1	Eruption through crater lake that no longer exists.

(continued)

Table 1 (continued)

Volcano, Location	Date	Lake type	S	B	T	L	P	A	D	Other	Fatalities	Events	Notes, references
Taal, Philippines	31 Jan. 1968	Caldera	–	–	–	–	–	–	–	–	–	9	Historical eruptions at Taal have been concentrated on volcano island, and involve small crater lakes and/or interactions with the larger caldera lake. Other eruptions involve lake water flooding volcanic fissures.
	5 Jul. 1966		–	–	–	–	–	–	–	–	–		
	28–30 Sep. 1965		x	X	x	–	x	x	–	–	>190		Initial magmatic eruption on volcano island evolved to phreatomagmatic when caldera lake waters gained access to vent. Base surges travelled over 6 km (Moore et al. 1966a, 1966b; Moore 1967)
	27 Jan. 1911		x	X	X	–	x	x	–	–	>1,335		Most fatalities occurred in boats capsized by tsunamis and seiches. Similar waves up to 2-5 m high and other phenomena accompanied eruptions in 1716, 1731, 1749 and 1754 (Latter 1981; Newhall and Dzurisin 1988)
Pinatubo, Philippines	Jul.–Oct. 1992	Caldera	–	–	–	–	–	–	X	–	–	1	Growth of a lava dome on the floor of the flooded 2.5 km diameter caldera created by the 1991 eruption (BGVN 17:06).
Aso, Japan	17 Feb. 2008	Crater	–	–	–	–	–	–	–	–	–	55	Historic activity at Aso caldera has been confined to the Naka-dake crater in the central resurgent dome and cone complex. Frequent VEI magnitude 0–2 eruptions have expelled an ephemeral crater lake on 55 recorded occasions, dating back to AD 769 and most recently in 2008
	1979		–	–	–	–	–	–	–	–	3		
	1872		–	–	–	–	–	–	–	–	4		
	1485		–	–	–	–	–	–	–	–	1		
Kusatsu-Shirane, Japan	6 Jan. 1989	Crater	–	–	–	x	–	–	–	–	2	5	Historic events have included at least 5 small phreatic/phreatomagmatic explosions through one or more of the three summit crater lakes and their margins. (SEAN 07:10)
Zao, Japan	1183-1940	Crater	–	–	–	x	–	–	–	–	3	17	Eruptions through the Okama crater lake of Goshiki-dake in the Zao volcanic complex have occurred 17 times since historic records began in AD1183, most recently in May 1940, with a larger event in 1895 (Miura et al. 2012)

(continued)

Table 1 (continued)

Volcano, Location	Date	Lake type	S	B	T	L	P	A	D	Other	Fatalities	Events	Notes, references
Towada, Japan	915	Caldera	–	–	–	–	–	–	X	–	–	1	Eruption of the Goshikiiwa lava dome on the flanks of an older intracaldera volcano
Haku-san, Japan	1579	Crater	–	–	–	x	–	–	–	–	–	1	Eruption through crater lake
Kirishima, Japan	1716-1959	Crater	–	–	–	–	–	–	–	–	–	3	Kirishima is a cluster of c. 20 Quaternary volcanoes. Historical eruptions have occurred through the crater lake of Shinmoe-dake, most recently in 1959, and also in 1822 and 1716
Karymskoye, Kamchtaka	2 Jan. 1996	Caldera	X	X	X	–	–	–	–	x	–	1	Surtseyan phreatomagmatic eruption constructed a tuff ring in the lake. Adjacent lake shores were swept with base surges and tsunamis up to 25 m above lake level. Outlet river was blocked by pyroclastic material causing temporary lake level rise of 2.6 m (Belousov et al. 2000; Belousov and Belousov 2001; Torsvik et al. 2010)
Tao-Rusyr, Kamchtaka	12 Nov. 1952	Caldera	–	–	–	–	–	–	X	–	–	1	Extrusion of a lava dome on the flank of Krenitzyn Peak interacted with the 7 km diameter caldera lake
Ebeko, Kamchtaka	1965–1989	Crater	–	–	–	–	–	–	–	–	–	5	5 small eruptions have occurred through minor crater lakes
Zavaritzki, Kamchtaka	1923?	Caldera	–	–	–	–	–	–	X	–	–	1	Lava dome extrusion.
Gorely, Kamchtaka	1984	Crater	–	–	–	–	–	–	–	–	–	1	Gorely caldera complex hosts 11 summit and 30 flank craters, some containing lakes. One historical eruption through a crater lake is known
Maly Semiachik, Kamchatka	1804–1952	Crater	–	–	–	–	–	–	–	–	–	5	A number of historic eruptions have occurred through Troitsky Crater
Ukinrek, Alaska	1977	Maar crater	–	–	–	–	–	–	X	–	–	1	A lava dome was extruded into one of the two maars formed by the 1977 eruption

(continued)

Table 1 (continued)

Volcano, Location	Date	Lake type	S	B	T	L	P	A	D	Other	Fatalities	Events	Notes, references
Kilauea, Hawai'i	1790	Caldera	–	X	–	–	–	–	–	–	80–300	1	Phreatomagmatic eruption through inferred caldera lake (Mastin 1997)
Lake Nyos, Cameroon	21 Aug. 1986	Maar crater	–	–	X	x	–	–	–	X	1,746	1	Catastrophic exsolution of magmatic CO_2 resulted in limnic eruption of c. 1 km^3 of gas that overspilled the lake basin to suffocate >1,700 people (Kling et al. 1987; Barberi et al. 1989; Tazieff 1989). Tsunami waves ran up to 25 m above lake level and a 6 m high surge was displaced over the outlet
Lake Monoun, Cameroon	15 Aug. 1984	Maar crater	–	–	–	–	–	–	–	X	37	1	Limnic eruption of CO_2 (Sigurdsson et al. 1987)
Nyamuragira, Zaire	1920	Crater	–	–	–	–	–	–	–	–	–	1	Reprted eruption through crater lake (Simkin and Siebert 1994)
Soufrière, St. Vincent (WI)	13 Apr. 1979	Crater	–	–	–	X	x	–	X	x	–	6	Historical explosive eruptions have ejected crater lakes and generated pyroclastic flows followed by lava domes. Most deaths resulted form pyroclastic flows. (Anderson and Flett 1903; Shepherd et al. 1979)
	6 May 1902		–	–	–	X	x	–	–	x	1,680		
	27 Apr. 1812		–	–	–	X	x	–	–	x	–		
Pelée, Martinique (WI)	23 Apr. 1902	Crater	–	–	–	X	–	–	–	–	23	1	Eruptions triggered breaching of L'Etang Sec causing a hot lahar that triggered a tsunami when it reached the coast. Shortly followed by the catastrophic pyroclastic flow that killed 29,000 (Fisher and Heiken 1982; Chrétien and Brousse 1989)
Santa Maria, Guatemala	1903	Crater	–	–	–	–	–	–	–	–	–	1	Eruption through lake developed in crater formed by VEI magnitude 6 eruption in AD 1902 (Rose 1972; Simkin and Siebert 1994)
San Salvador, El Salvador	7 Jun. 1917	Crater	–	–	–	–	–	–	–	–	–	1	Eruption permanently expelled crater lake.

(continued)

Table 1 (continued)

Volcano, Location	Date	Lake type	S	B	T	L	P	A	D	Other	Fatalities	Events	Notes, references
Santa Ana, El Salvador	1 Oct. 2005	Crater	–	–	–	x	–	–	–	x	2	1	Eruption through small crater lake coincided with heavy rain that also triggered lahars (BGVN 30:09) (Hernández et al. 2007)
Ilopango, El Salvador	1880	Caldera	X	X	X	–	–	–	X	x	–	1	Eruption of an intra-lake dacitic lava dome raised lake level by 1.2 m, triggering increased overflow and downcutting of the outlet by 9.2 m, releasing 1.2×10^9 m^3 of water at peak discharges of 3×10^3 m^3/s (Mann et al. 2004)
Rincón de la Vieja, Costa Rica	1922–1998	Crater	–	–	–	X	x	–	–	–	–	13	A small hyper-acidic crater lake 1750 m ASL has been the source of at least 13 historic eruptions at this remote volcano, most recently on 15 Feb. 2008 (BGVN 23:03)
Poás, Costa Rica	1828–2011	Crater	x	–	–	–	–	–	–	–	–	47	Poás hosts three craters and two crater lakes. The active Laguna Caliente has been the source of numerous small phreatic and phreatomagmatic eruptions since 1828, most recently in Feb. 2011 (BGVN 36:04)
Volcan Copahue, Chile/ Argentina	1 Jul. 2000	Crater	–	–	–	X	x	–	–	–	–	4	Eruptions through the Del Agrio crater lake have occurred 4 times since 1992 (BGVN 25:06)
Planchón-Peteroa, Chile	9 Feb. 1991	Crater	–	–	–	x	–	–	–	–	–	1	Phreatomagmatic eruption through small crater lake (BGVN 16:01)
Fernandina, Galapagos	14 Sep. 1988	Caldera	–	–	X	–	–	–	–	–	–	1	Approximately 1 km^3 of the caldera rim, oversteepened by collapse of the caldera floor in 1968, failed to form a debris avalanche that displaced the 2 km diameter caldera lake to the N and NW as a tsunami. (SEAN 13:10)
Askja, Iceland	Jul. 1926	Caldera	–	–	–	–	–	–	–	–	–	1	Explosive eruption created new island at S end of Öskjuvatn lake.

Data principally derived from Simkin and Siebert (1994), Mastin and Witter (2000), Neall (1996), and the Smithsonian Institution Global Volcano Programme (SEAN and BGVN reports). Hazard codes are: *S* Surtseyan jetting; *B* base surges; *T* tsunami; *L* lahars; *P* pyroclastic flows; A ash fall; *D* dome growth; and other as explained in the notes

2.1 Surtseyan Jets

Surtseyan jets, also known as "cock's (rooster) tail" or "cypressoid" jets (Fig. 4) are characteristic of subaqueous explosive volcanism (Thorarinsson et al. 1964), and have been observed in a number of lacustrine (Belousov et al. 2000; Belousov and Belousov 2001) and shallow marine settings (Morimoto 1948; Machado et al. 1962; Reynolds et al. 1980). They comprise black jets of tephra and water that are ejected on sub-ballistic trajectories to heights of up to 800 m at velocities exceeding c. 100 m/s, and are produced during discrete explosions in relatively shallow water (<200 m). As the jets cool, they become fringed with white clouds of condensing steam (Fig. 4).

By analogy with conventional (Cole 1948; Kedrinksii 2005) and nuclear (Glasstone and Dolan 1977) explosive tests, detailed observations and analysis of selected eruptions (Belousov et al. 2000; Kilgour et al. 2010), and numerical simulations (Morrissey et al. 2010) a subaqueous volcanic explosion forms a sub-spherical bubble filled with super-heated explosion products including water vapour, magmatic gases and pyroclastic material (Fig. 5). This rises buoyantly towards the surface, expanding as its internal pressure equilibrates with the confining hydrostatic pressure. Ahead of this, the explosion shock wave impinges on the water surface, typically forming a symmetrical spray dome by spallation and cavitation that may rise several hundred metres into the air but which contains a volumetrically insignificant volume of water. The ascending explosion bubble then deforms the water surface above it, forming a rapidly rising dome of water. When this breaches, the explosion bubble vents to the atmosphere. The sudden drop in internal pressure causes the water:gas interface at the bubble's base to rebound, rapidly collapsing the transient cavity and generating vertically- and radially-directed jets as it 'turns inside out' (Fig. 5).

2.2 Base Surges

Base surges are ring-shaped basal clouds (Figs. 4 and 5) that sweep outwards as a dilute density current from the base of a vertical explosion column (Moore 1967). They are produced during subaqueous explosive eruptions principally through disruption of the rim of the transient cavity (Fig. 5), and secondarily by collapse of Surtseyan jets, and move radially outwards as mixtures of pyroclasts, water droplets and steam at typical velocities of 20–65 m/s (Moore 1967;

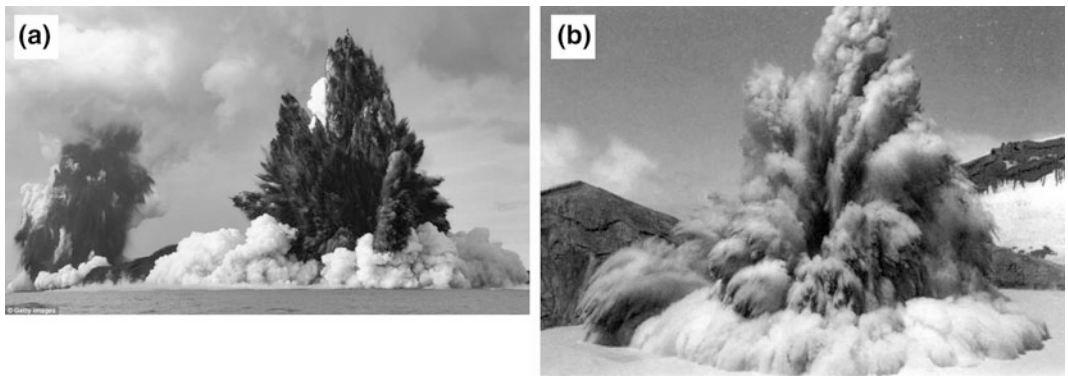

Fig. 4 **a** Surtseyan jets generated during the eruption of a submarine volcano north of Tongatapu in the Tonga Islands rising to >800 m. Darker 'cypressoid' or 'rooster-tail' jets are composed of mixtures of water droplets, gas and pyroclastic fragments, lighter clouds are steam and condensate. A toroidal base surge is propagating out from the base of one of the eruption columns (*Getty images*). **b** Small Surtseyan jet and base surge generated during a minor phreatic eruption, typical of activity during the late 1970s and early 1980s at Ruapehu volcano, New Zealand (Image GNS archive)

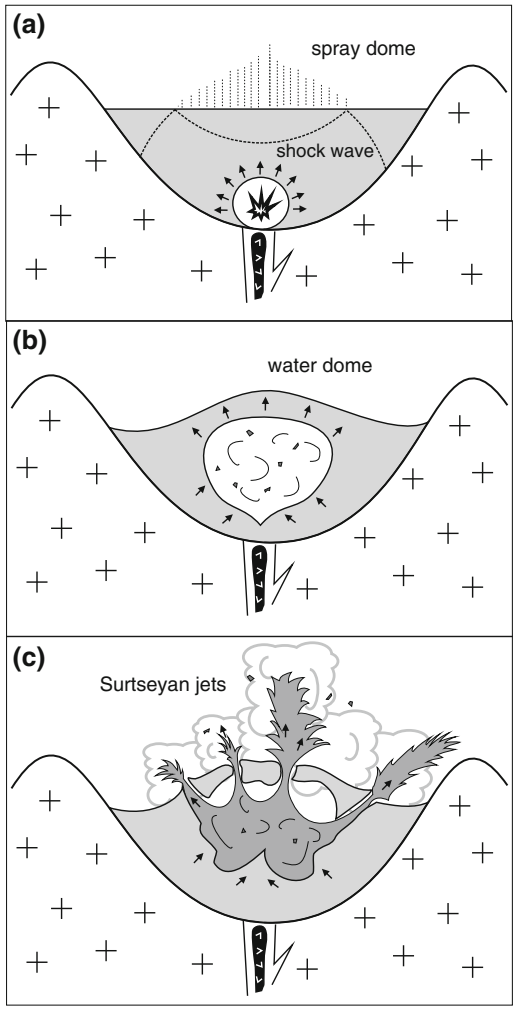

Fig. 5 Inferred sequence of events during a subaqueous explosive eruption. **a** Initial explosion during magma-water mixing: this fuel:coolant reaction generates a shock-wave whose energy is largely reflected off the air:water interface at the lake surface, but still manages to raise a dome of spray. **b** As the explosion bubble of eruption products and water vapour equilibrates with the ambient hydrostatic pressure it expands and rises buoyantly, lifting a semi-spherical dome of water above it. **c** The water dome breaches as it thins and stretches and as the explosion bubble breaches the surface, the sudden drop in internal pressure as the transient cavity vents to the atmosphere causes its base and sides to rebound, generating vertical and radial water jets that entrain the bubble contents and remnants of the water dome

Belousov et al. 2000). Base surges generated at Taal volcano in the Philippines are likely to have been responsible for most of the deaths on Volcano Island during the 1911 eruption, while in 1965 they reached up to 8 km from the vent, depositing surge-bedded dunes proximally and wet-mud aggregates and coatings distally (Moore et al. 1966a, b; Moore 1967). Base surges generated by explosive eruptions through a postulated caldera lake have been suggested as playing a role in the 1790 AD Kilauea eruption that killed 80–300 people (Mastin 1997).

2.3 Seiches

Seiches are standing waves produced in semi- or fully enclosed bodies of water due to resonant amplification of waves initiated by another mechanism (i.e. fluctuations in atmospheric pressure, earthquakes, or tsunami). Under certain circumstances they may be higher and more persistent than the original tsunami: studies at intermontane Lake Tahoe indicate potential seiche run-ups of up to 10 m in response to seismogenic fault offsets of the lake bed (Ichinose et al. 2000). Seiches are also a demonstrated hazard at volcanic lakes: a tectonic earthquake at Taal caldera lake in 1749 destroyed villages and caused fatalities (Newhall and Dzurisin 1988), while seiches of up to 0.5 m were reported at Lake Taupo in response to seismic faulting during earthquake swarms in 1922 and 1983 (Ward 1922; Otway 1986; Webb et al. 1986). Seiches set up by volcanic explosions during the 1965 Taal eruption capsized a number of boats, resulting in a number of fatalities (Moore et al. 1966b).

2.4 Atmospheric Effects—Rain and Lightning

Phreatomagmatic eruptions through volcanic lakes can result in torrential local rain due to steam condensation, potentially aided by nucleation on ash particles, sometimes in association with intense lightning activity (Mastin and Witter 2000). This can contribute to local flood hazards and syn-eruptive reworking of pyroclastic

deposits. Examples have been observed at Taal volcano (Moore et al. 1966a, b), and inferred at: (i) Lake Taupo during the Hatepe and Rotongaio phases of the 1800a Taupo eruption (Walker 1981; Smith and Houghton 1995); and (ii) deposition of the Rotomohana Ash during the 1886 eruption at Tarawera (Nairn 1979; Walker et al. 1984).

3 Volcanic Tsunamis

Tsunami triggered by volcanic processes account for 25 % of all volcano-related fatalities since 1783 (Witham 2005), mostly associated with the marine 1883 Krakatau eruption (Carey et al. 2001). A range of triggers have been implicated (Latter 1981), with wave generation typically accomplished by volumetric water displacement (Fig. 6), for example by: a gas-filled explosion bubble (Egorov 2007; Morrissey et al. 2010); pyroclastic flows (Waythomas and Neal 1998; McCoy and Heiken 2000; de Lange et al. 2001; Watts and Waythomas 2003); basin floor displacement; and subaerial and/or subaqueous mass flows including debris avalanches (Johnson 1987; Tinti et al. 2006a; Begét et al. 2008) and landslides (Ward 2001), and lahars (Chrétien and Brousse 1989; Walder et al. 2003). While the greater travel distance of such events is largely irrelevant in the context of confined lake basins, the generating mechanisms remain pertinent.

3.1 Explosion-Generated Tsunamis

During subaqueous volcanic explosions, tsunamis are principally generated during the phase of updoming of the water surface, including the period when the bubble breaches the surface and the uplifted rim of the transient cavity is pushed outwards by its expanding contents (Figs. 5 and 6). Smaller tsunamis are also generated by fallback of Surtseyan tephra jets and coupling of the water surface with atmospheric shock waves and base surges (Latter 1981; Mastin and Witter 2000;

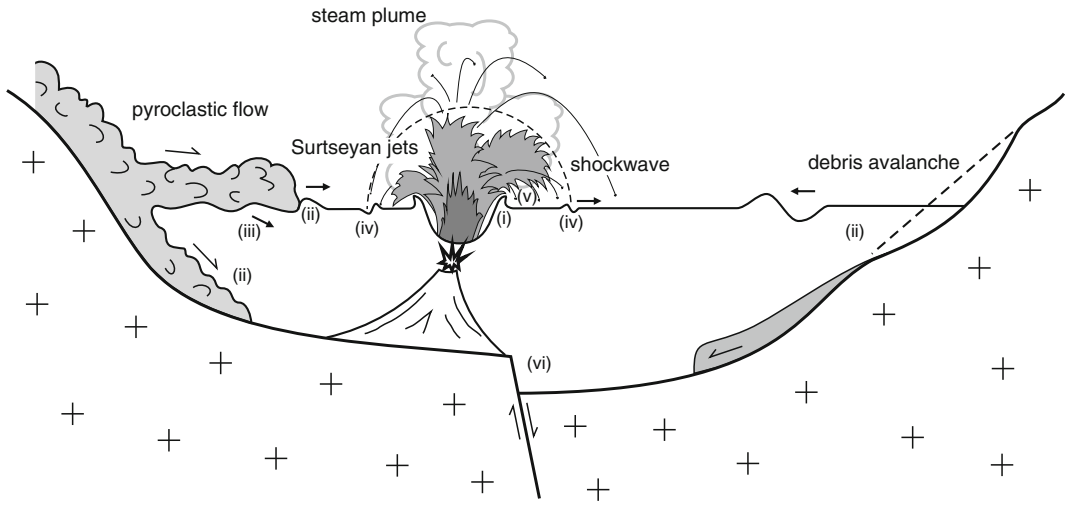

Fig. 6 Tsunami-generating mechanisms associated with volcanic lakes, including subaqueous explosive eruptions. Surface waves may be triggered by upward and lateral displacement of water due to: (*i*) an expanding explosion bubble; and (*ii*) entry, and continued subaqueous movement of an initially subaerial (or wholly subaqueous) gravitational mass flow (pyroclastic flow, landslide, debris avalanche, or major lahar). Other causes include downward and lateral displacement of water caused by: (*iii*) the sinking of material from a segregating pyroclastic flow travelling over the water surface; (*iv*) coupling with a base surge or atmospheric pressure wave; and (*v*) collapse of jetted material. Also, (*vi*) upward or downward displacements due to seismogenic (i.e. rapid) volcano-tectonic movements. Of these only (*i*), (*ii*) and (*vi*) are capable of generating large waves in the far field (Watts and Waythomas 2003)

Watts and Waythomas 2003). Observations of tsunami waves at volcanic lakes are limited to the 1996 Karymskoye Lake eruption (Belousov et al. 2000), minor phreatic events at Ruapehu during the 1970s and 1980s (McClelland et al. 1989), Taal volcano in 1911 and 1965 (Moore et al. 1966a, b), and a number of other crater lakes (Table 1) mainly known for their eruption-triggered lahar record (Mastin and Witter 2000). During the 1996 eruption at Karymskoye Lake "a light gray 'collar' [which] appeared around the focus (epicentre) of the explosion, representing a nearly axially-symmetric elevation of the water surface 130 m high that propagated radially at about 40–20 m/s to form the tsunami" (Belousov et al. 2000). Run-up from these surface gravity waves reached 30 m on adjacent shorelines 1.3 km away from the eruption centre (Belousov et al. 2000; Torsvik et al. 2010). Tsunami run-up deposits have been identified c. 20 m above the contemporaneous lake level at Lake Managua in Nicaragua in association with the 6.3 ka Mateare Tephra eruption (Freundt et al. 2006, 2007), and at Fisher caldera in Alaska (Stelling et al. 2005).

3.2 Pyroclastic Flow-Generated

Pyroclastic flows, comprising hot, gas-rich, debris-laden, ground-hugging free-surface gravity currents that travel laterally away from their sources (Sparks 1976; Druitt 1998), are a common phenomenon associated with explosive volcanic activity and are demonstrably tsunamigenic (Latter 1981; Carey et al. 1996, 2000; Hart et al. 2004).

Most studies of volcanic tsunamis are based on submarine and coastal volcanoes, including the 1883 AD Krakatau eruption in Indonesia (Self and Rampino 1981) which produced proximal tsunami waves up to 35 m high that caused c. 36,000 deaths in coastal areas of Java and Sumatra up to 100 km from the volcano, and were still lethal in Sri Lanka 2,500 km away (Latter 1981; Carey et al. 2000, 2001). Pre-historic tsunami generated by pyroclastic flows entering the sea are known from a number of other regions, including Alaska (Waythomas and Neal 1998) and the Mediterranean, where they are associated with the Minoan eruption of Santorini (McCoy and Heiken 2000).

Pyroclastic flow-triggered lacustrine tsunamis have not been observed in historical times. However, they have been inferred at Lake Managua in Nicaragua where the c. 24 ka Apoyo ignimbrite erupted from a caldera 20 km away is estimated to have entered the lake at volume fluxes of 3×10^6 m^3/s and velocities of 65 m/s (Freundt et al. 2006), and at Lake Tarawera in New Zealand during the c. 1315 AD Kaharoa eruption (Hodgson and Nairn 2005). They will certainly have occurred at many caldera lakes where voluminous explosive activity has produced pyroclastic flows from mid-lake vents, for example during several Holocene eruptions at Lake Taupo (Wilson 1993). Tsunamis with this source mechanism are also implicated in the triggering of break-out floods at a number of Alaskan calderas (Table 2). At Fisher, an eruption at c. 1.5 ka from an mid-lake vent apparently triggered breaching of the southern caldera wall by overtopping waves with run-ups exceeding 20 m (Stelling et al. 2005).

3.3 Debris Avalanches/Landslide-Triggered

Debris avalanches generated by the gravitational collapse of a volcanic edifice are a common phenomenon at stratovolcanoes around the world, occurring on average 4 times per century (Siebert 1984, 1996) due to a range of causes (McGuire 1996). Such failures are highly tsunamigenic (Keating and McGuire 2000), as has been demonstrated at a number of coastal (Siebert et al. 1995; Begét et al. 2008) and island volcanoes (Johnson 1987; Tinti et al. 2006b; Chiocci et al. 2008). For example, the tsunami generated by the 1792 AD collapse of the Mayuyama dome at Shimabara killed an estimated 15,000 people around the shores of the Sea of Japan (Neall 1996; Tanguy et al. 1998).

Table 2 Compilation of known break-out floods from volcanic lakes, including Type II and III events

Volcano	Location	Date	Lake type	Dam type	Hazard type	Dam height (lake depth) m	Lake volume m^3	Breach depth m	Volume released m^3	Peak discharge m^3/s	Notes, references
Ruapehu, New Zealand	Whangaehu River	18 Mar. 2007	Crater	Tephra	III	6.4	1.0×10^7	6.4	1×10^6	530	Followed 1995–1996 eruptions (Manville and Cronin 2007; Manville et al. 2007; Massey et al. 2010)
		24 Dec. 1953	Crater	Ice/tephra	III	20	1.0×10^7	8	1.8×10^6	350	Followed refilling of lake after 1945-46 eruptions. Lahar destroyed Tangiwai railway bridge with loss of 151 lives. (Healy 1954; O'Shea 1954; Manville 2004). Breakouts also inferred in 1925 and 1861 (Manville et al. 2007; Graettinger et al. 2010)
		January 1925	Crater	Ice?	III						Unexplained flood surge on Whangaehu River, the natural outlet to Crater Lake, no eruption observed (Manville et al. 2007)
		13 Feb. 1861	Crater	Ice/tephra	III				6×10^6		Largest lahar in historic sequence, possible break-out. No eruption observed (Manville et al. 2007). All prehistoric lahars post-dating 1800a have been much bigger (Hodgson et al. 2007)
Taupo, New Zealand	Waikato River	c. 1.78 ka	Caldera	Pyroclastic flow	III	34	8×10^{10}	32	2×10^{10}	3×10^4	Followed damming of the outlet gorge by ignimbrite erupted during the 1.8 ka Taupo eruption (Manville et al. 1999)
		c. 24 ka	Caldera	Pyroclastic flow	III	(330)	1.1×10^{11}	80	6×10^{10}	1×10^5	Triggered by headward erosion through ignimbrite shield. Permanently changed course of lower Waikato River. (Manville and Wilson 2004)

(continued)

Table 2 (continued)

Volcano	Location	Date	Lake type	Dam type	Hazard type	Dam height (lake depth) m	Lake volume m^3	Breach depth m	Volume released m^3	Peak discharge m^3/s	Notes, references
Tarawera, New Zealand	Tarawera River	1904	valley	lahar	III	12.8	2.3×10^9	3.3	1.3×10^8	780	Triggered by 3 days of heavy rain 18 years after 1886 eruption. (White et al. 1997; Hodgson and Nairn 2005)
		c. 1315	Valley	Pyroclastic flow/lahar	II	(118)	4×10^9	40	1.7×10^9	5×10^4	Syn-eruptive event breaching composite pyroclastic flow/lahar dam, possibly triggered by pyroclastic flow-generated tsunamis (Hodgson and Nairn 2005). Earlier break-outs are hypothesized on geological grounds (Manville et al. 2007)
Aoba (Ambae), Vanuatu		1916	Caldera	Rim	III						Report of a large flood on SE coast that killed c. 100 linked to possible break-out from Lake Manaro Lakua (Bani et al. 2009)
Kelut, Indonesia		1875	Crater	Rim					3.8×10^7		Cold lahar triggered by failure of crater rim (Schuster 2000)
Raung, Indonesia		1638	Crater	Rim							
Pinatubo, Philippines	Bucao River	10 Jul. 2002	Caldera	Rim	III	(175)	1.6×10^8	23	6.5×10^7	3×10^3	Caldera lake break-out following 1991 eruption generated largest single lahar of post-eruption sequence (Lagmay et al. 2007)

(continued)

Table 2 (continued)

Volcano	Location	Date	Lake type	Dam type	Hazard type	Dam height (lake depth) m	Lake volume m^3	Breach depth m	Volume released m^3	Peak discharge m^3/s	Notes, references
	Pasig-Potrero river	22 Sep. 1994	Valley	Lahar	III						Voluminous pyroclastic flows generated during the 1991 Pinatubo eruption dammed tributaries along multiple radial drainages surrounding the volcano. Break-outs from these ephemeral lakes, which were often re-dammed by secondary pyroclastic flows or lahars were a recurrent hazard in the years after the eruption. Peak discharges reached 1000–5000 m^3/s. In the Pasig-Portero River (east side of Pinatubo), break-outs in 1991 and 1994 killed 7 and 25 respectively and buried several villages including Bacalor. (Arboleda and Martinez 1996; Scott et al. 1996b)
		29 Aug. 1992	Valley	Secondary pyroclastic flow	III						
		7 Sep. 1991	Valley	Pyroclastic flow	III						
	Santo Tomas River	12 Oct. 1991	Valley	Lahar	III					400	The Marella-Mapanuepe junction of the Santa Tomas river system on the west side of Pinatubo was dammed on multiple occasions by lahars flowing down the Marella River. The resulting Lake Mapanuepe grew to a maximum size of 6.7 km^2, 7.5×10^7 m^3 volume, and 25 m depth, breaking out on multiple occasions, until its level was stabilised by construction of an artificial spillway in Nov. 1992 (Rodolfo et al. 1996; Umbal and Rodolfo 1996)
		21 Sep. 1991	Valley	Lahar	III					500	
		25 Aug. 1991	Valley	Lahar	III					650	

(continued)

Table 2 (continued)

Volcano	Location	Date	Lake type	Dam type	Hazard type	Dam height (lake depth) m	Lake volume m^3	Breach depth m	Volume released m^3	Peak discharge m^3/s	Notes, references
	Sacobia River	25 Jul. 1991	Valley	Pyroclastic flow	III						Break-out lahars in the Sacobia River were triggered by failure of primary and secondary pyroclastic flow dams (Scott et al. 1996b)
Parker, Philippines		2002		Landslide	III				2.7×10^7		Breach of the rim in 1995 caused a large flood that undercut and destabilised the outlet walls. An earthquake in 2002 caused further landsliding, blocking the gorge and resulting in another flood (Catane et al. 2005)
		1995		Rim	III				3×10^7		
Bandai, Japan		Apr. 1889	Valley	Debris avalanche	III						The 1888 collapse of Bandai volcano generated a debris avalanche that impounded 5 lakes: Lake Onagawa breached a year later (Schuster 2000)
Asama, Japan	Agatsuma River	5 Aug. 1783	Valley	Pyroclastic flow	III						Pyroclastic flow temporarily blocked river, breaching generated hot lahar that killed 919 people (Aramaki 1956, 1981; Simkin and Siebert 1994; Yasui and Koyaguchi 2004)
Numuzawa, Japan	Tadami River	5 ka	Valley	Pyroclastic flow	III	100	1.7×10^9	70	1.6×10^9	2.7×10^4	Pyroclastic flow from caldera-forming eruption dammed adjacent river valley (Kataoka et al. 2008)
Towada, Japan	Oirase River	12–15 ka	Caldera	Pyroclastic flow	III		1.3×10^{10}	76	6×10^9	2–30×10^5	First identified intracaldera lake break-out flood in Japan (Kataoka 2011; Gomez et al. 2012)

(continued)

Table 2 (continued)

Volcano	Location	Date	Lake type	Dam type	Hazard type	Dam height (lake depth) m	Lake volume m^3	Breach depth m	Volume released m^3	Peak discharge m^3/s	Notes, references
Karymskoye, Kamchatka	Karymskaya River	15 May 1996	caldera	tuff ring	III	2.6			3.25×10^7		Tuff cone produced by subaqueous eruption near outlet to Akademiya Nauk intracaldera lake temporarily blocked outlet to the 4 km diameter lake (Belousov and Belousov 2001)
Crater Peak, Alaska	Chakatchatna River	1992	Valley	Lahar	III	10	3.2×10^7	10		$1–8 \times 10^3$	Eruptions from Spurr volcanic complex, including Crater Peak have dammed Chakachatna River at least 5 times in last 10 ka with a combination of lahar and debris avalanche deposits (Waythomas 2001)
		1953	Valley	Lahar	III	20	1.2×10^8	20		$8–15 \times 10^3$	
Spurr Volcano, Alaska		Late Holocene	Valley	Lahar	III	60	4.5×10^8	61		1×10^4	
		Holocene	Valley	Debris avalanche	III	150	1.23×10^9	150		3×10^4	
Iliamna, Alaska	Johnson River	Late Holocene	Valley	Lahar	III						Waythomas (2001)
Novarupta, Alaska		1912	Valley	Pyroclastic flow	III						Tributary valleys blocked by Valley of Ten Thousand Smokes pyroclastic flow and secondary phreatic explosion crater rims. Breaching of a dam formed a pumiceous debris flow deposit with a volume of $3\text{-}6 \times 10^6$ m^3 (Hildreth 1983)
Wrangell Volcano, Alaska	Copper River	Pleistocene	Valley	Debris avalanche	III						Waythomas (2001)
Aniakchak, Alaska	Aniakchak River	c. 3.4 ka	Caldera	Pyroclastic flow		183	3.7×10^9	183	3.7×10^9	1×10^6	Caldera lake break-out flood (McGimsey et al. 1994; Waythomas et al. 1996)
Okmok, Alaska	Crater Creek	1817	Caldera	Scoria cone	III	8	8×10^6	–	–	2×10^3	Minor eruption dammed intracaldera lake. Break-out flood destroyed Aleut village (Wolfe and Begét 2002)

(continued)

Table 2 (continued)

Volcano	Location	Date	Lake type	Dam type	Hazard type	Dam height (lake depth) m	Lake volume m^3	Breach depth m	Volume released m^3	Peak discharge m^3/s	Notes, references
Okmok, Alaska		c. 1.5 ka	Caldera	Pyroclastic flow	II	150	5.8×10^9	150	5.8×10^9	1.9×10^6	Caldera lake break-out (Wolfe and Begét 2002; Begét et al. 2005)
Chiginagak, Alaska	Volcano Creek	May 2005	Crater	Glacier	II		5.4×10^6	45	3.8×10^6		Break-out from acidic crater lake following geothermal melting of ice-cap, sulphuric acid vapour damaged vegetation along flood path (Schaefer et al. 2008)
Fisher, Alaska		1.5 ka	Caldera	Pyroclastic flow	II	100			1×10^{10}		Triggered by overtopping waves generated by explosive eruption through intracaldera lake (Stelling et al. 2005)
Mount Meager, Canada	Lillooet River	2.35 ka	Valley	Pyroclastic flow	III	100	0.25–1×10^9				Block and ash flows and welded pyroclastic flow deposits dammed river valley resulting in staged break-out flood (Hickson et al. 1999)
Uinkaret Volcanic Field	Colorado River	104 ± 12 ka	Valley	Lava flow	III	180	–	–	2.7×10^9	1.7×10^5	Pleistocene eruptions have dammed Grand Canyon with basaltic lava flows on at least 5 occasions (Fenton et al. 2004; Fenton et al. 2006)
		165 ± 18 ka	Valley	Lava flow	III	280			9×10^9	3.8×10^5	
		Pleistocene	Valley	Lava flow	III	302	1.1×10^{10}	302	1.1×10^{10}	5.3×10^5	
Crater Lake, USA	Williamson River	7.7 ka	Valley	Pyroclastic flow	III	21	6.5×10^9	17	5.5×10^9	1.3×10^4	Valley dammed by pyroclastic flow from Mount Mazama eruption (Conaway 2000)
Mount St. Helens	North Fork Toutle River	18 May 1980	Valley	Debris avalanche	III	9.1	0.3×10^6			450	Break-out from Elk Rock Lake tributary dammed by Mount St. Helens debris avalanche (Jennings et al. 1981)

(continued)

Table 2 (continued)

Volcano	Location	Date	Lake type	Dam type	Hazard type	Dam height (lake depth) m	Lake volume m^3	Breach depth m	Volume released m^3	Peak discharge m^3/s	Notes, references
	North Fork Toutle River	19 Mar. 1982	Crater	Snow/ tephra	II		4×10^6			2.6–4.4 $\times 10^3$	Melting of snow and ice by lateral blast resulted in accumulation of an ephemeral lake that broke out to form a large lahar (Pierson 1997)
	North Fork Toutle River	2.5 ka	Valley	Debris avalanche	III						Break-out from ancestral Spirit Lake (Scott 1988)
Newberry Volcano	Paulina Creek	1860-1730	Caldera	?	III	78	3.2×10^8	2	1.24×10^7	200	Chitwood and Jensen (2000), O'Connor and Beebee (2009)
Medicine Lake Volcano		Late Pleistocene	Caldera	?	II						Possible eruption-triggered break-out from ice-covered caldera lake (Donnelly-Nolan and Nolan 1986)
El Chichón, Mexico	Rio Magdalena	27 May 1982	Valley	Pyroclastic flow	III	75	4.8×10^7	25	1.7×10^7	1.1×10^4	Breaching of pyroclastic flow dam triggered hot lahar 55 days after its emplacement. Flow temperatures reached: 82 °C 10 km downstream and 52 °C at 35 km where 1 person died (Macías et al. 2004). Lake developed in new eruption crater
Volcan de Colima, Mexico	Rio Armeria	3.6 ka	Valley	Debris avalanche	III		0.4×10^9				Córtes et al. (2010)
Colima, Mexico	Naranjo River	Pleistocene	Valley	Debris avalanche	III	150	1×10^9	150	1×10^9	5.7×10^5	Break-out bulked with material eroded from dam to form massive lahar with peak discharge of 3.5×10^6 m^3/s. (Capra and Macías 2002)
Santaguito (Santa Maria), Guatemala	Nimá I	Nov. 1983	Valley	Lahar	III						Lahars in Nimá II blocked Nimá I River, before a spillway could be completed the lake broke-out destroying several dozen houses (McClelland et al. 1989).

(continued)

Table 2 (continued)

Volcano	Location	Date	Lake type	Dam type	Hazard type	Dam height (lake depth) m	Lake volume m^3	Breach depth m	Volume released m^3	Peak discharge m^3/s	Notes, references
	Nimá I, Nimá II and Tambo Rivers	24 Jul. 1978	Valley	Pyroclastic flow	III						Block and ash flows erupted on 23 Jul dammed 3 rivers, break-outs the next day destroyed farms and damaged bridges. (McClelland et al. 1989)
Nevado del Huila, Colombia	Paèz River	Late Pleistocene	Valley	Debris avalanche	III	150	0.5×10^9				Breaching of dam generated a 100 m deep lahar that bulked by a factor of 3.2 and travelled more than 67 km downstream (Pulgarin et al. 2004)
Antuca, Chile	Rio Laja	9.7 ka	Valley	Debris avalanche	III						Thiele et al. (1998)
Mt Pelee, Martinique	Rivière Blanche	5 May 1902	Crater	Rim	II	–	–	–	5×10^6	–	Rim of l'Etang Sec crater failed due to eruption (or explosively ejected water). 23 fatalities (Chrétien and Brousse 1989)
Eyjafjallajökull, Iceland	Markarfljót River	15 April 2010	Englacial	Ice	II	–	–	–	4-8 × 10^6	5-15 × 10^3	Largest of a complex series of lake drainages Magnússon et al. (2012). Similar floods in 1612, 1821-23 Björnsson (2002)
Grimsvötn, Iceland	Gígjukvísl River, Skeidárasandur	4-5 Nov. 1996	Englacial	Ice	II	(175)			3.2×10^9	5.3×10^4	Triggered by subglacial Gjálp eruption (Gudmundsson et al. 1997; Tweed and Russell 1999)
	Skeidárasandur	1938	Englacial	Ice	II				4×10^9		Triggered by subglacial fissure eruption (Björnsson 2002).
Oraefajökull, Iceland		1727	Subglacial	Ice	III	–	X	–	–	–	
		1362	Subglacial	ice	II		X			1×10^5	Flood lasted < 1 day and destroyed several farmsteads.

(continued)

Table 2 (continued)

Volcano	Location	Date	Lake type	Dam type	Hazard type	Dam height (lake depth) m	Lake volume m^3	Breach depth m	Volume released m^3	Peak discharge m^3/s	Notes, references
Katla, Iceland	Mýrdalssandur	12 Oct. 1918	Subglacial	ice	II				5×10^9	2.8×10^5	Tómasson (1996). Similar events have occurred in 1179, 1311, 1660 and 1721.
Kverkfjöll/ Bárdarbunga, Iceland	Jökulsá á Fjöllum	Holocene	Subglacial	Ice	II					9×10^5	Alho et al. (2005), Howard et al. (2012)
Laacher See, Germany	Rhine River	12.9 ka	Valley	Pyroclastic flow	III	15			9×10^8	1×10^4	Neuwied Basin backflooded, break-out flood deposits can be traced 50 km downstream to Bonn (Park and Schmincke 1997; Schmincke et al. 1999; Baales et al. 2002)

Data principally derived from Simkin and Siebert (1994), Newhall and Dzurisin (1988), and Manville (2010)

Lacustrine tsunamis generated by landslides, rockfalls and icefalls are well known, and are often implicated in the failure of natural landslide and moraine dams (Lliboutry et al. 1977; Hermanns et al. 2004; Kershaw et al. 2005). Volcanogenic examples are less frequent (Table 1), but the most notable historic case is the 18 May 1980 debris avalanche at Mount St. Helens, which entered Spirit Lake (itself the product of valley-damming by a prehistoric flank collapse) to generate a wave with a run-up of 260 m (Voight et al. 1981). In 1999, a relatively small (150,000 m^3) landslide from the crater walls of the Quaternary Kasu tephra cone in the highlands of Papua New Guinea displaced 5–10 % of the lake's volume, triggering a 15 m high wave that overtopped a low point on the crater rim killing one person (Wagner et al. 2003). At Fernandina volcano in the Galapagos, c. 1 km^3 of the caldera rim collapsed forming a debris avalanche that displaced the existing 2 km wide shallow intracaldera lake to the N and NW as a tsunami in 1988 (SEAN 13:10). Collapse of a geothermally-weakened fault scarp at the southern end of Lake Taupo in 1846 AD generated a lethal debris avalanche that triggered a small tsunami when it entered the lake (Hegan et al. 2001).

Prehistoric tsunamis induced in volcanic lakes by mass movements are inferred at Lake Managua, Nicaragua, where two recent debris avalanche deposits from Volcán Mombacho penetrate up to 7 km into the lake to form small islands (Freundt et al. 2007).

3.4 Lahar-Triggered

Lahars entering volcanic lakes are also tsunamigenic if they are sufficiently rapid and voluminous (Walder et al. 2006): the 18 May 1980 Pine Creek lahar at Mount. St. Helens generated a 0.4 m high wave on Swift Reservoir 22.5 km away from its entry point (Pierson 1985). During the May 1902 eruption of Soufrière St. Vincent, a lahar triggered by collapse of the crater rim of L'Etang Sec generated a 3–4 m high tsunami when it reached the sea (Chrétien and Brousse 1989). Similarly, very large and fast jökulhlaups have produced waves in coastal waters around Iceland (Björnsson 2002).

3.5 Earthquake-Triggered

Tectonic movements on faults crossing volcanic lakes can cause displacements sufficient to generate tsunami or excite seiches, whether related to volcanic activity or not. Recorded examples include at Taal in 1749 AD, where villages were destroyed and lives lost (Newhall and Dzurisin 1988), and at Lake Taupo in association with historic earthquake swarms (Ward 1922; Otway 1986; Webb et al. 1986).

4 Limnic Gas Eruptions

A special hazard at volcanic lakes, and some other major volcanically-influenced water bodies such as Lake Kivu (Nayar 2009), is the explosive exsolution of dissolved magmatic gases, principally CO_2 and methane, which accumulate in the water column (Tazieff 1989). Eruptions can be driven by over-saturation, climatic conditions, landslides into the lake, or volcanic activity. In 1984 a gas burst from Lake Monoun killed 37 people (Sigurdsson et al. 1987), and was followed 2 years later by the Lake Nyos disaster in the same country (Kling et al. 1987; Barberi et al. 1989; Tazieff 1989). Lake Nyos is a small (1,925 × 1,180 m) water body hosted in a maar-diatreme crater. On 21 August 1986, a small landslide into the 208 m deep lake triggered overturn and the catastrophic release of 0.3–1 km^3 of CO_2 which overflowed the crater outlet and travelled over 10 km downstream as a dense, suffocating flow. Water surges triggered by the gas release caused waves that washed up to 25 m above the lake shoreline and 6 m deep over the outlet (Kling et al. 1987).

5 Volcanogenic Floods from Volcanic Lakes

Volcanic lakes are prone to sudden and catastrophic releases of water, either directly as a result of explosive volcanic activity (Table 1), or due to failure of their impoundments following active (i.e. eruption-triggered) or passive (i.e. overfilling) overtopping and runaway erosion (Table 2). In either case, the combination of large volumes of water, significant topographic elevation, and abundant pyroclastic material available for remobilisation makes such events particularly hazardous as they tend to travel down existing river valleys, which are frequently the locus of extensive populations.

Crater lakes, developed in pits excavated by explosions above volcanic vents, are prone to explosive (ballistic) ejection or displacement (including by waves) during eruptive activity. Consequently, primary eruption-triggered lahars from such water bodies have been one of the most lethal historic volcanic hazards (Table 1).

5.1 Eruption-Triggered Lahars

The summit of the stratovolcano of Mt. Kelut (1,731 m) on the Indonesian Island of Java is occupied by a crater lake that has been the source of multiple eruption-triggered lahars that have claimed tens of thousands of lives over the past millennium. Initial explosive phases of VEI-4 eruptions, occurring at mean intervals of 13 years (range 8–18) have ejected up to 40×10^6 m^3 of water in a matter of seconds, before progressing to Vulcanian eruptions, sometimes accompanied by pyroclastic flows. The resulting lahars have devastated the densely populated Plains of Blitar, destroying villages and killing tens of thousands since records began in c. AD 1000 (van Padang 1951; Zen and Hadikusumo 1965). In May 1848 an eruption caused partial breaching of the crater rim, releasing 48.7×10^6 m^3 of water (Neall 1996). Similar events (Table 1) are reported at Galunggung, Kaba, Raung, and Ijen (Mastin and Witter 2000).

The summit crater of Mt. Ruapehu, New Zealand's largest and most active onshore andesitic stratovolcano, hosts a hot acidic lake at an elevation of c. 2,530 m. Primary lahars have accompanied all large historic eruptions through the explosive ejection of Crater Lake water over the rim (Fig. 1a), and volumetric displacement (Healy et al. 1978; Nairn et al. 1979; Cronin et al. 1997), sometime forming unusual snow slurry lahars (Kilgour et al. 2010). Secondary lahars have been triggered by heavy rain on ash deposits (Cronin et al. 1997; Hodgson and Manville 1999), while break-out lahars have followed magmatic eruptions by a decade (Manville et al. 2007) (see below).

5.2 Floods Triggered by Tsunami

During the 1996 eruption of Karymskoye in Kamchatka, tsunamis triggered by subaqueous explosive eruptions caused water to surge over the outlet from the lake as a series of waves, triggering flooding along the Karymskaya River with a maximum discharge of 500 m^3/s (Belousov and Belousov 2001). Similar lahars have been observed at Ruapehu where explosions have also displaced water over the outlet area when the lake has been full during eruptions (Cronin et al. 1997; Kilgour et al. 2010).

5.3 Floods Triggered by Lake Floor Displacement

Volcano-tectonic uplift of basin floors has been implicated as a factor in the generation of a number of volcanic floods. This may occur through emplacement of a subaqueous lava dome or shallow intrusion, or through inflation of a shallow magma chamber, although it has been argued that even a significant magma intrusion event would produce negligible surface deformation at a caldera lake like Taupo (Ellis et al. 2007). Rates of water displacement by subaqueous intrusion of lava domes are limited by the effusion rate, which is typically 1–10 m^3/s.

Higher rates may be associated with inflation of a shallow magma chamber, either due to injection of a hot slug of basaltic magma or runaway vesiculation at its top, or thermal expansion of groundwater.

A historical flood of this type from an intracaldera lake occurred at Ilopango Caldera, El Salvador (Goodyear 1880; Newhall and Dzurisin 1988; Richer et al. 2004). The present lake occupies a nested rectangular caldera most recently modified by eruption of the Tierra Blanca Joven ignimbrite in AD 479 (Rose et al. 1999). In January 1880, subaqueous eruption of a dacitic lava dome raised the level of the 108 km^2 lake by 1.2 m (Goodyear 1880) over a period of 5 days. Increased overflow through the narrow outlet channel of the Río Desagüe caused rapid downcutting, with the lake level falling by 9.2 m between 12 and 20 January. Peak discharges are estimated at c. 3×10^3 m^3/s based on drawdown rates of c. 0.1 m/h, resulting in destruction of the downstream town of Atusulca (Newhall and Dzurisin 1988; Richer et al. 2004). By 8 February the lake had fallen by an additional 2.6 m, corresponding to a total water loss of 1.2×10^9 m^3.

Displacement of the floor of Crater Lake, Ruapehu, during the 1995 eruption sequence is recorded by a stage hydrograph on the single outlet channel 58 km downstream at Karioi. The data shows a complex series of transient, spiky, primary explosion-triggered lahars superimposed on a broad trend lasting c. 14 days with a peak discharge of c. 30 m^3/s that is inferred to represent steady uplift of the lake floor by rising magma (Cronin et al. 1997). Total displacement by this uplift is estimated at c. 6×10^6 m^3, representing half the volume of the pre-eruption lake, and a volume equivalent to that expelled by explosive ejection over the rim and outlet. An alternative explanation is that this represents superposition of the exponential waning limbs of individual eruption-triggered flows. Water displacements are also associated with the October 2006 (Kilgour et al. 2007) and September 2007 (Kilgour et al. 2010) phreatic events at Ruapehu, where increased lake level has also been associated with injection of water from the sub-lake hydrothermal system (Christenson and Wood 1993; Christenson et al. 2010).

5.4 Jökulhlaups

A special class of potentially hazardous volcanic lake comprises sub-glacial water bodies, breakouts from which, termed jökulhlaups, have been identified as the most frequently occurring volcanic hazard in Iceland where a number of large basaltic calderas filled with subglacial lakes lie beneath the Vatnajökull and Mýrdalsjökull icecaps (Björnsson 1975, 1992; Tómasson 1996; Björnsson 2002). Most such floods are relatively small, and result from semi-periodic accumulation and drainage of geothermally sustained subglacial lakes. However, larger, less frequent events with peak discharges in the range 10^3–10^5 m^3/s are associated with major subglacial volcanic eruptions that create transient lakes or overfill existing ones (Tómasson 1996; Gudmundsson et al. 1997; Tómasson 2002; Carrivick et al. 2004). Despite being functionally a class of glacier-lake breakout because the outflow hydrograph is controlled by the glacier not the volcano (Walder and Costa 1996; Clarke 2003), they are included here since the lake is the result of volcanic activity. Volcanogenic floods generated by the melting of snow and ice (Pierson et al. 1990) are however excluded unless a transient lake is developed (Waitt et al. 1983; Pierson 1997). In the latter case, a directed blast from the Mount St. Helens lava dome on 19 March 1982 dynamically mixed hot pyroclastic debris with snow and ice in the crater basin. A meltwater lake developed within tens of minutes to cover an area of 0.3 km^2 to a depth of 8–15 m, as indicated by rafted pumice blocks and mudlines, before simultaneously breaching through outlet channels on either side of the lava dome. The lake held c. 4×10^6 m^3 of water at its

highstand, but the total outflow was considerably more as contributions from snowmelt continued during lake drainage. Combined peak discharge for the two spillways is estimated at 2.6–4.4 × 10^3 m^3/s: bulking and transformation to debris flow increased this to 9 × 10^3 m^3/s by 6 km downstream.

6 Non-volcanogenic Floods from Volcanic Lakes

In addition to the volcanogenic triggering of break-out floods from volcanic lakes, these water bodies are also vulnerable to non-volcanic breaching of their impoundments, resulting in partial or total drainage of the whole basin. Newly created volcanic lakes are particularly vulnerable to breaching as they fill with meteoric water due to the inherent instability of their dams, which are typically constructed of unconsolidated, often low density material, and without the benefit of engineered spillways. Failure of the volcanic dam or basin rim can occur due to either overtopping or piping from within (Waythomas et al. 1996; Massey et al. 2010) or headward erosion of an external drainage (Karátson et al. 1999). A review of the geological literature reveals that such floods are a relatively common phenomena worldwide (Table 2).

6.1 Crater Lakes

The best characterised example of a passive break-out from a Crater Lake is at Mt. Ruapehu, New Zealand. Following the 1995–1996 sequence that emptied the Crater Lake during a series of initially phreatic, phreatomagmatic and then purely magmatic eruptions (Nakagawa et al. 1999), the lake basin refilled with precipitation run-off and fumarolic condensate over the following 11 years. On 18 March 2007, the rising Crater Lake breached the tephra dam following destabilisation of its downstream face by piping flow (Massey et al. 2010); releasing c. 1.3 million m^3 of water in less than 2 h (Manville and Cronin 2007). The flood bulked up through entrainment of snow, ice, colluvium, and older lahar deposits in the Whangaehu Gorge to form one of the largest lahars of the historical sequence (Carrivick et al. 2009; Graettinger et al. 2010; Procter et al. 2010; Lube et al. 2012). No lives were lost during this event owing to improvements in knowledge and monitoring, in contrast with the 1953 Tangiwai lahar that claimed 151 lives (Healy 1954; O'Shea 1954). This break-out was triggered by collapse of an unstable barrier composed of volcanic material deposited during the 1945 eruption and buttressed by the Crater Basin Glacier (O'Shea 1954; Manville 2004). Approximately 1.8 × 10^6 m^3 of 26 °C water was released into the headwaters of the Whangaehu River over a period of 1–2 h following piping failure of the tephra dam (Fig. 7a). The flow rapidly entrained snow, ice, and volcanic debris and alluvium to transform into a debris- to hyperconcentrated flow that critically damaged a railway bridge 39 km downstream at Tangiwai (Fig. 7b), resulting in the loss of 151 lives (O'Shea 1954; Stilwell et al. 1954). Palaeohydraulic analysis indicates that the peak discharge from Crater Lake was c. 350 m^3/s, bulking to 2,000 m^3/s by 10 km downstream (Manville 2004) and attenuating to c. 590–650 m^3/s at Tangiwai.

Other historic non-volcanic floods from crater lakes include the 1875 non-volcanic failure of 60 m of the western rim of Mt. Kelut (Table 2), which collapsed during heavy rain releasing a lethal cold lahar and changing the principle lahar path to the southwest (Suryo and Clarke 1985). Elsewhere in Indonesia, break-out of a crater lake has been correlated with a devastating flood in AD 1638 at Raung (van Padang 1951).

A mudflow and flood in 1541 AD that destroyed part of the former capital of Guatemala, Ciudad Vieja, claiming >1,300 lives has been attributed to collapse of the crater rim of Agua following a period of torrential rain (Mooser et al. 1958; Neall 1996). No lake was reported in the crater prior to this event, although it is possible that an ephemeral water body formed and failed due to the intense precipitation.

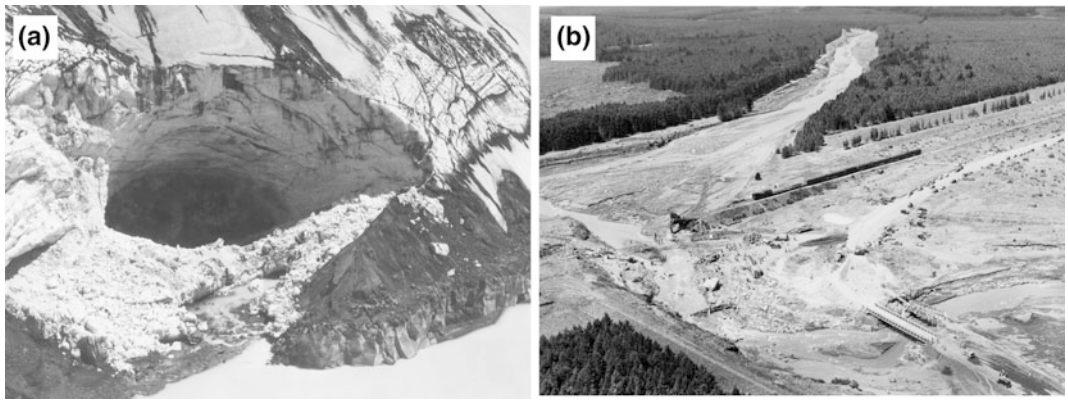

Fig. 7 **a** Breach in tephra dam/glacier ice resulting from the 24 December 1953 break-out of Ruapehu's Crater Lake. Mouth of ice tunnel is c. 50 m wide and 30 m high. Remnants of tephra dam visible to *left* of breach. (GNS archive). **b** Oblique aerial view of Tangiwai, 38 km downstream from Crater Lake. The lahar came from the *top* of the picture and partially destroyed the railway bridge just before the Wellington-Auckland express train arrived [Archives New Zealand, R5, W2279/13, 300/1607]

An unusual mechanism for generating a crater lake break-out has been inferred for the c. 2.5 km diameter Albano composite maar in Italy (Funiciello et al. 2003; De Benedetti et al. 2008). In Roman times, the lake stood some 70 m higher than its current surface elevation of 293 m, coincident with the low point of the topographic rim, which also forms the apex of a 60 km^2 outwash fan of laharic deposits. This fan indicates at least two catastrophic water releases from the lake during the Holocene (Funiciello et al. 2003), while Roman archives record an overspill event in 398 BC (De Benedetti et al. 2008). Both authors speculate that during climatic highstand periods, seismically-triggered injections of CO_2-rich hydrothermal fluid into the groundwater and lake bed triggered dramatic rises in lake level accompanied by overspill and partial failure of the crater rim.

6.2 Caldera Lakes

Historical examples of break-out floods from caldera lakes include Pinatubo, in the Philippines, in 2002. The 5–7 km^3 DRE eruption of Pinatubo in June 1991 formed a 2.5 km wide summit caldera that accumulated a lake over the following decade (Stimac et al. 2004). As the lake approached the low point on the rim (960 mASL) a crisis developed due to recognition of the potential for catastrophic breaching and the release of a huge lahar into the heavily populated Balin-Baquero catchment. During August-September 2001 a trench was dug by hand through the unconsolidated 1991 pyroclastic deposits forming the upper part of the rim in an attempt to trigger a controlled break-out, or at least prevent a further rise in lake level (Lagmay et al. 2007). However, outflow through the trench was too slow to produce a controlled breach. Failure of the caldera rim was delayed until 10 July 2002 when Typhoon Gloria delivered 740 mm of rain to the Pinatubo area (Bornas et al. 2003). Approximately 65×10^6 m^3 of water was released at up to 3,000 m^3/s, lowering the lake level by 23 m and eroding a V-shaped notch in the caldera rim. Downstream bulking of the flow with abundant pyroclastic debris from the 1991 eruption generated the largest lahar of the entire post-Pinatubo sequence, aggrading the Bucao River valley by 3–5 m and threatening the town of Botolan (population 40,000).

Subaqueous eruption of a tuff ring in Karymskoye lake, Kamchatka, on 3 January 1996 generated not only primary lahars through the explosive displacement of lake water, but also temporarily blocked the outlet to the 4 km

diameter Akademiya Nauk caldera (Belousov and Belousov 2001). After rising by 2.6 m, the 12.5 km^2 lake breached the pyroclastic barrier on 15 May 1996, triggering a flood that deposited a small fan downstream of the outlet gorge.

The c. 10 km diameter Aniakchak caldera was formed by a major ignimbrite emplacing eruption at c. 3.4 ka on the Alaskan peninsula (Miller and Smith 1977). Post-eruption, the closed topographic depression (Fig. 8) was partially filled by an intracaldera lake that rapidly drained following failure of the caldera rim, releasing c. 3.7×10^9 m^3 of water at a peak rate of 7.7×10^4 to 1.1×10^6 m^3/s and cutting a 183 m deep notch (McGimsey et al. 1994; Waythomas et al. 1996). Highstand terraces indicate that the lake was close to its maximum capacity before the breakout, suggesting failure was initiated by overtopping, possibly triggered by tsunamis or water displacement during an intracaldera eruption. Similar scenarios have been reconstructed at the Fisher (Stelling et al. 2005) and Okmok (Almberg et al. 2003) calderas in Alaska, and at Towada volcano in Japan (Kataoka 2011) on the basis of geological and geomorphic evidence (Table 2).

Lake Taupo, the largest lake in the central North Island of New Zealand partially occupies a volcano-tectonic collapse structure whose present configuration largely reflects caldera collapse during the 26.5 ka Oruanui eruption and faulting and downwarping on regional structures (Davy and Caldwell 1998; Wilson 2001). The 530 km^3 DRE Oruanui eruption destroyed a long-lived Pleistocene lake system and deposited hundreds of metres of unwelded pyroclastic deposits around the collapse caldera to produce a closed topographic depression (Wilson 2001; Manville and Wilson 2004). Following the eruption, water in Lake Taupo accumulated to reach a highstand elevation of c. 500 m, as marked by an irregularly preserved shoreline terrace (Grange 1937; Manville and Wilson 2003, 2004). Overtopping caused an initial overspill and 10–20 m drop to a level controlled by a resistant sill of welded ignimbrite, allowing development of another palaeoshorelines terrace. Some time before 22 ka, headward erosion through non-welded pyroclastic flow deposits 20 km to the east breached the caldera rim, releasing an estimated 60 km^3 of water in a break-out flood peaking at 3.5×10^5 m^3/s (Manville and Wilson 2004). During the 1800 a Taupo eruption, the outlet gorge from the lake was blocked by voluminous pyroclastic flow deposits (Wilson and Walker 1985) while much of the pre-eruption lake was expelled, evaporated, or drained into a subrectangular caldera collapse structure (Davy and Caldwell 1998). Over a period of several decades (Wilson and Walker 1985; Smith 1991a), the

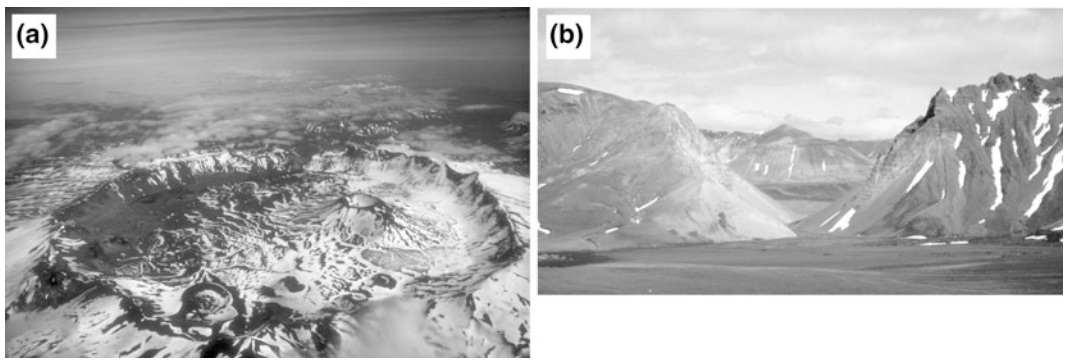

Fig. 8 Aniakchak caldera in Alaska formed at c. 3.4 ka: the intracaldera lake later breached to produce the largest known Holocene terrestrial flood, releasing 3.7×10^9 $m^3$of water at a peak discharge of up to 1×10^6 m^3/s (Waythomas et al. 1996). **a** Aniakchak caldera looking east, diameter c. 10 km (Image M. Williams, National Park Service 1977). **b** 'The Gates' the c. 200 m deep breach cut in the rim of the Aniakchak caldera by the break-out flood (*Image* C.A. Neal, USGS)

lake refilled to a mean highstand level of +34 m above the modern elevation of 357 m, as marked by a semi-continuous, tectonically warped and offset wave-cut bench and highstand shoreline deposit (Wilson et al. 1997; Riggs et al. 2001; Manville and Wilson 2003). Failure of the 12 km long unconsolidated pumiceous pyroclastic dam was initiated by overtopping, and is inferred to have been catastrophic based on the absence of intermediate shoreline terraces between the highstand and a wave-cut bench at +2–5 m (Manville et al. 1999), releasing c. 20 km^3 of water in a single phase. Flood deposits can be traced for over 220 km downstream from Lake Taupo (Manville et al. 1999; Manville 2002), and include: a 12-km-long vertical-walled spillway immediately downstream of the outlet floored with lithic gravel and boulder lags; streamlined landforms sculpted from older deposits and exhumed river terraces; bouldery fan deposits and expansion bars downstream of valley constrictions; fine-grained slackwater deposits in off-channel embayments and hydraulically ponded depressions; valley-wide erosional unconformities; and buried forests in distal areas.

6.3 Pyroclastic Dams

As well as impounding water bodies within the depressions of erupting volcanic centres, pyroclastic material emplaced laterally by pyroclastic flows and surges, or by vertical fallout from Plinian or ballistic eruptions can dam existing valley systems at varying distances from the active volcano.

The 1991 Pinatubo eruption in the Philippines generated proximal pyroclastic flow deposits up to 200 m thick that locally dammed numerous catchments (Scott et al. 1996a). Most lakes were shallow and short-lived, failing by overtopping during the 1991 wet season, but others filled and failed repeatedly as secondary pyroclastic flows and/or lahars rebuilt barriers at late as 1994 (Table 2).

Pyroclastic flows emplaced by the March-April 1982 eruption of El Chichón in southern Mexico partially filled the drainage network on and around the volcano, blocking the adjacent Río Magdalena with deposits up to 30 m thick and 300–400 m wide that extended for c. 1 km along the valley (Silva et al. 1982; Macías et al. 2004). By the time the dam failed by overtopping on 26 May it impounded a 5 km-long lake with a volume of 48×10^6 m^3 that reached boiling temperatures due to its contact with 650 °C pyroclastic material. Drainage is estimated to have taken c. 2 h, generating a scalding flood that cooled from 82 °C at 10 km downstream to 52 °C at a hydroelectric plant 35 km downstream where a worker was killed. Peak discharge was estimated at 1.1×10^4 m^3/s (Macías et al. 2004), while the break-out deposits covered 5 km^2 and thinned from 8.5 to 2 m distally. Deposit sedimentology indicates that the flow evolved from clear-water, through hyperconcentrated flow to debris flow (Costa 1988). This event resembles an oral legend of a hot flood in the same area centuries before (Duffield 2001).

In 1912, the largest pyroclastic eruption of the 20th Century occurred in the Valley of Ten Thousand Smokes in Katmai National Park in Alaska (Hildreth 1983). A chain of secondary phreatic explosion craters impounded a 1.5 km long supra-ignimbrite lake that failed in the summer of 1912 or 1913. The resulting flood scoured the surface of the pyroclastic flow deposit to a depth of 1–2 m, transported 0.5 m diameter blocks of welded tuff over 20 km, and aggraded the lower parts of the valley by 1–8 m (Hildreth 1983). The eruption at Katmai also created a small caldera, now occupied by a lake. As the rate of filling has slowed markedly since the 1950s a break-out is considered unlikely (Motyka 1977).

The eruption of Asama, Japan, in 1783 AD dammed the Agatuma-gawa River with a block-and-ash flow. Breaching of the dam resulted in a catastrophic flood that destroyed over 1,200 houses and killed an estimated 1,300 people (Aramaki 1981; Yasui and Koyaguchi 2004).

Emplacement of the 30 km^3 Taupo ignimbrite over an area of 20,000 km^2 radially disposed around the vent also blocked numerous other

catchments, leading to the development of multiple supra-ignimbrite lakes (Smith 1991b; Manville et al. 2005), the largest of which impounded c. 1.5×10^9 m^3 of water over an area of 190 km^2 in the Reporoa Basin (Manville 2001). Further lakes formed in areas where river valleys were dammed by distal pyroclastic flow lobes (Segschneider et al. 2002). Overtopping failure of these lakes likely generated break-out floods and is believed to have contributed to the re-establishment of drainage systems (Meyer and Martinson 1989; Manville 2002). In more distal areas, aggradation by lahars also dammed tributaries to form numerous shallow, ephemeral lakes.

The eruption of the Laacher See volcano at 12.9 ka, the largest late Quaternary eruption in central and western Europe, blocked the Rhine River to a depth of at least 15 m by a combination of primary pyroclastic flows that travelled down tributary valleys and reworked pyroclastic fall material from the lower Neuwied Basin (Park and Schmincke 1997; Baales et al. 2002). Six km upstream of the gorge blockage site an ephemeral lake developed in the Neuwied Basin proper, covering 80–140 km^2 at its maximum as marked by highstand rafts of floated pumice c. 15 m above the pre-eruption land surface. The lake is inferred to have failed catastrophically by earthquake shaking during late stage explosions from Laacher See (Park and Schmincke 1997), releasing an estimated 9×10^8 m^3 of impounded water in a flood that scoured channels floored by dense lag deposits in the Neuwied Basin as it drained and deposited fluvially-reworked pyroclasts for over 50 km downstream as far as Bonn.

6.4 Lava Flow Dams

Lava flows are eminently capable of blocking river valleys owing to their downslope flow and physical properties and dimensions. Lava flows emplaced during the 1846–1847 eruptions of Volcán Quizapu in Chile blocked a number of tributaries of the Rio Blanquillo (Hildreth and Drake 1992). In 1932 a pumiceous lahar accompanying an eruption triggered break-out and permanent drainage of the Lagunas del Blanquillo, causing much damage downstream on the Río Maule: concerns had been expressed about the dam-break hazard from these lakes as early as 1916.

Eruption of a rhyolitic lava flow at 23 ka dammed the 25 × 15 km Laguna del Maule intracaldera lake basin in Chile, raising the lake level by 160 m. A single sharp strandline suggests rapid break-out of the lake, while its catastrophic nature is indicated by a narrow gorge cut through the lava and boulder bars and scablands below the gorge outlet (Hildreth, pers. comm. 2004).

Basaltic lava flows have dammed a number of rivers in the western United States (Ely et al. 2012). As well as rivers in Arizona, Idaho, Oregon, and Washington, the Colorado River in the western Grand Canyon in Arizona has been dammed at least 13 times in the last 1.2 Ma (Hamblin 1994; Fenton et al. 2002). Evidence for catastrophic failure of some of these dams has been presented by Fenton et al. (2002, 2003), who argued that emplacement of basaltic lava erupted from the Uinkaret Volcanic Field adjacent to the canyon on unstable talus slopes and alluvium deposits, in addition to the hyaloclastic foundations of the flows formed through interaction of the lava with river water, made the blockages inherently unstable. At least 5 lava dams failed catastrophically between 100 and 525 ka, depositing flood gravels 20–110 m thick between 53 and 200 m above current river level and up to 53 km downstream from the inferred dam site (Fenton et al. 2003). Sedimentary evidence of large scale floods from these break-outs includes downward fining boulder deposits with maximum clast dimensions of up to 35 m, giant cross-beds (up to 45 m high foresets), slackwater deposits, and high-water markers that decline exponentially in elevation downstream of the dam site. The Qfd4 unit flood at 165 ± 18 ka resulted from failure of a 280 m high dam impounding an estimated 9 km^3 of water: peak outlet discharge is estimated as $2.8–4.8 \times 10^5$ m^3, declining to 1.6×10^5 m^3/s by 59 km downstream (Fenton

et al. 2003). The youngest flood event, Qfd5 at 104 ± 12 ka, resulted from failure of a 180 m high dam with a reservoir volume of 2.7 km^3 to give an estimate peak discharge of 1.4–2 x 10^5 m^3/s. Non-catastrophic breaching of many valley lava flow dams occurred over thousands of years following filling of the impoundment with sediment (Crow et al. 2008; Ely et al. 2012).

Late Pleistocene basaltic lava flows erupted from the Fort Selkirk area in Canada dammed the Yukon River to a depth of c. 30 m, representing the most recent volcanic blockage of this drainage: distinctive pillow lavas are interpreted as representing lava emplacement into standing water (Huscroft et al. 2004). A coarse unit composed of basalt boulders >1 m in diameter outcropping 6 km downstream of the inferred dam site are interpreted as the product of a catastrophic breaching of the barrier.

6.5 Debris Avalanche Dams

The growth of a volcanic edifice is typically limited by the gravitational stability of its cone, with periods of instability experienced as a consequence of both endogenous and exogenous factors (Siebert 1984; McGuire 1996). Structural failure can then be triggered by other factors such as tectonic or volcanic earthquakes (Vidal and Merle 2000) or pore fluid pressure changes induced by magma intrusion (Iverson 1995). Such failures typically generate massive landslides, or debris avalanches (Glicken 1998; Siebert 1996), with the largest terrestrial examples having volumes of c. 30 km^3 (Stoopes and Sheridan 1992).

The May 1980 eruption of Mount St. Helens in the western USA was accompanied by emplacement of a 2.3 km^3 debris avalanche deposit following gravitational collapse of the volcanic edifice (Lipman and Mullineaux 1981; Glicken 1998). The debris avalanche deposits impounded or modified three large lakes (Coldwater Creek, South Fork Castle Creek, and Spirit Lake) and several smaller ones (Jennings et al. 1981; Meier et al. 1981; Youd et al. 1981; Meyer et al. 1986; Glicken et al. 1989). Failure of the blockage to Maratta Creek on 19 August 1980 transferred water to the Elk Rock impoundment, which itself overtopped and breached on 27 August, releasing 0.3 × 10^6 m^3 of water into the North Fork Toutle River with a peak discharge of 450 m^3/s (Jennings et al. 1981; Costa 1985). Modelling of the potential peak discharges from failure of the three largest lakes (Jennings et al. 1981; Dunne and Fairchild 1983; Swift and Kresch 1983) suggested clear-water peaks > 7.5 × 10^4 m^3/s were possible, prompting intervention by the U.S. Army Corps of Engineers to artificially stabilise their levels (Costa 1985). A pre-historic break-out from an ancestral Spirit Lake similarly dammed by a debris avalanche occurred at c. 2.5 ka, generating a peak discharge estimated at 2.6 × 10^5 m^3/s (Scott 1989).

A number of prehistoric break-out floods from debris avalanche dammed lakes have been identified globally. In Alaska the upper Chakachatna valley was dammed to a depth of 150 m by a Holocene debris avalanche from the Spurr volcanic complex, impounding a lake estimated to have held 1.2 × 10^9 m^3 of water (Waythomas 2001). Other examples include a major debris avalanche from the Antuco volcano at c. 9.7 ka that dammed the outlet to the Río Laja in Chile, impounding a large lake that subsequently failed to generate an outwash fan covering an area of 50 × 60 km (Thiele et al. 1998), and collapse of the eastern flank of the Nevado de Colima Volcano in Mexico at 18.5 ka which produced a voluminous debris avalanche that dammed the Naranjo River 20 km away to a depth of 150 m. Obstruction of the drainage produced a temporary impoundment of c. 1 km^3 of water, which eventually breached the dam through overtopping, generating a peak discharge estimated at 5.7 × 10^5 m^3/s (Capra and Macías 2002). Bulking of the flow through entrainment of material from the dam and along the flood path increased the peak discharge by a factor of 6 and deposited c. 10 km^3 of debris.

6.6 Lahar Dams

Rapid sedimentation by lahars is capable of damming rivers at confluences where one stream aggrades its bed more rapidly than the other (Rodolfo et al. 1996). The dominant stream builds a steep-fronted delta, fed by sediment-laden underflows, which progrades into the subordinate channel as the stagnation zone at the flow confluence migrates. Damming occurs when the rate of aggradation is faster than the rate of water level rise in the impounded channel.

Remobilisation of voluminous pyroclastic flow deposits at Pinatubo in the Philippines following the June 1991 eruption led to multiple instances of lahar-dammed lakes and subsequent breakouts in a number of catchments (Pierson et al. 1992; Newhall and Punongbayan 1996). The largest such impoundment, Lake Mapanuepe (Fig. 2d), covered an area of 6.7 km^2 and held 75×10^6 m^3 of water at its maximum extent in 1991 (Umbal and Rodolfo 1996). Eighteen breakouts, peaking at 400–650 m^3/s, were recorded in 1991 alone as the lake repeatedly overtopped and partially breached the impounding lahar deposit, which was rapidly rebuilt by aggradation of 7–20 m/year (Rodolfo et al. 1996). In total, the dam reached a height of c. 25 m before engineering intervention stabilised the lake elevation at 111 m. Numerous other lakes filled and spilled between 1991 and 1994, generating large lahars and entrenching drainage routes that became conduits for subsequent damaging flows (Newhall and Punongbayan 1996; Rodolfo 2000). Similarly, the 1902 eruption of Santa Maria in Guatemala resulted in the creation of at least 16 lahar-dammed lakes large enough to be mapped in the decades after the eruption (Kuenzi et al. 1979). However, it is not recorded whether any of these failed catastrophically.

A number of small, short-lived lakes were impounded by lahar dams in the upper Chakachatna River valley, following historic eruptions in 1953 and 1992 of the Spurr volcanic complex in Alaska (Waythomas 2001). The 1953 lahar dam was c. 20 m high, 600 m long and 200 m wide; the 1992 lahar dam was approximately 10 m high, 200 m long and 50 m wide: lake volumes are estimated at 10^7–10^8 m^3 from modern topography. Lahar dams up to 60 m high have also formed at least twice in the late Holocene, impounding up to 4.5×10^8 m^3 of water.

In the aftermath of 1886 AD basaltic plinian eruption of Tarawera, New Zealand (Walker et al. 1984), the level of Lake Tarawera rose by 12.8 m, before a rain-triggered break-out in November 1904 reduced it by 3.3 m, producing a flood estimated to have peaked at c. 780 m^3/s 24 km downstream (White et al. 1997). The post-eruptive rise has been attributed to construction of a small alluvial fan across the outlet channel by flash-flood induced remobilisation of 1886 pyroclastic and older debris in the Tapahoro gully (Hodgson and Nairn 2000).

As well as multiple pyroclastic-flow dammed lakes, numerous temporary impoundments were created in the aftermath of the 1.8 ka Taupo eruption through volcaniclastic resedimentation and laharic aggradation of up to 10s of metres in distal areas (Kear and Schofield 1978; Manville 2002; Segschneider et al. 2002).

6.7 Composite Dams

Composite dams are those formed by a combination of mechanisms, most commonly primary and secondary pyroclastic flows and lahars (Table 2). One such example occurred at Lake Tarawera following the c. 1315 AD Kaharoa eruption (Nairn et al. 2001). Lake Tarawera lies within the 64 ka Haroharo caldera in the Okataina Volcanic Centre in New Zealand (Nairn 2002), and is bounded by the western rim of the caldera and the resurgent lava dome complexes of Haroharo and Tarawera to the east. The 5-7 km^3 DRE Kaharoa eruption formed much of the Tarawera dome complex and deposited widespread plinian falls (Nairn et al. 2001). Primary block-and-ash flows and pyroclastic debris remobilised by flash floods off the Tapahoro dome blocked the narrow lake outlet, infilling a narrow channel cut through a c. 5 ka pyroclastic/volcaniclastic fan

implicated in a previous highstand. Lake Tarawera rose by c. 30 m above its pre-eruption level before tsunami generated by late-stage pyroclastic flows overtopped the dam and triggered its catastrophic failure (Hodgson and Nairn 2005). Approximately 1.7×10^9 m^3 of water was released into the head of the Tarawera valley as the lake level fell by >40 m, excavating a 300 m wide and 3 km long spillway before overtopping the 70 m high Tarawera Falls. Flood deposits including boulders up to 13 m in diameter and giant bars extend c. 40 km from the lake; approximately 700 km^2 of the Rangitaiki Plains was resurfaced and the shoreline advanced by c. 2 km (Pullar and Selby 1971). Peak discharge at the outlet was estimated at 1.5×10^5 m^3/s assuming instantaneous breach formation, while boulder flow-competence relations further downstream indicate flows in the 10^4–10^5 m^3/s range (Hodgson and Nairn 2005).

7 Discussion

A review of hazards from volcanic lakes due to eruptive activity or other causes reveals a great deal of complexity in triggering mechanisms and hazardous phenomena. Well-studied historic examples such as the 1996 eruptions at Karymskoye (Belousov and Belousov 2001) and Taal (Moore et al. 1966a), the 1991 Pinatubo eruption and its aftermath (Newhall and Punongbayan 1996), and lahar events at Ruapehu (Cronin et al. 1997; Kilgour et al. 2010) and Kelut (Suryo and Clarke 1985) demonstrate this variety and complexity: in many cases individual hazards contribute to subsequent effects in a process-chain. Examination of the geological record reveals a fuller range of both hazards and event magnitudes.

Moderate-sized (10^7–10^8 m^3) crater lakes developed at the summits of andesitic-dacitic stratovolcanoes in relatively humid arc environments are potentially the most dangerous volcanic lakes due to their capacity for almost instantaneous expulsion of large water volumes during subaqueous explosive eruptions, which can occur with little or no effective warning (e.g. Mt. Kelut, Ruapehu). Smaller water bodies are either evaporated or the expelled water is too widely dispersed during eruptions to generate significant lahars. In larger diameter lakes the Surtseyan jets that are the main displacers of water cannot reach their rims, and water depths >100 m suppress the ability of subaqueous explosions to breach the surface (Mastin and Witter 2000; Morrissey et al. 2010).

At crater and caldera lakes more than 2 km in diameter, base surges and tsunamis generated by volcanic activity, or collapse of the caldera walls (Ramos 1986), are the most significant hazard. Examples with populated shorelines that fall into this category include Taal in the Philippines, where historic eruptions have resulted in major loss of life, Taupo and Rotorua in New Zealand, Ilopango in El Salvador, and Toya and Towada in Japan. Volcano-tectonic lakes facing similar hazards include Lakes Managua and Nicaragua in Nicaragua. Tianchi (Baitoushan) at the summit of Mount Paektu/Changnai on the North Korea/China border is vulnerable to both renewal of volcanic activity and collapse of the steep walls of this very young (c. 1 ka) 5 km diameter lake (Wei et al. 2003, 2004). Lakes Quilotoa and Cuicocha in Ecuador are also potentially hazardous (Gunkel et al. 2008).

Volcanic lakes have lifespans measured in minutes to thousands of years. Intervals between creation and failure are a function of the geometry and stability of the lake-forming blockage, and the rate of lake level rise, which is itself a function of the catchment area, the proportion occupied by the lake, climatic effects, and seepage losses (Capra 2007). Examination of Tables 1 and 2 shows that a number of hazardous volcanic lakes have been destroyed in the past few hundred years while new ones have been created. Natural dams composed of unconsolidated pyroclastic deposits are extremely vulnerable to break-outs triggered by non-volcanic processes, such as erosion following overtopping (El Chichón), internal piping (Ruapehu), or headward erosion. Where barriers are composed of indurated material such as lava flows or welded ignimbrites, lakes can persist for many thousands of years: some, such as Crater Lake,

Oregon, never reach overtopping level because seepage losses match water inflows as the lake level rises and hydrostatic pressures increase. Others, such as Aniakchak (McGimsey et al. 1994; Waythomas et al. 1996) and Fisher volcano (Stelling et al. 2005) in Alaska appear to have reached a stable highstand level controlled by a hard rock sill. Failure required active breaching of the rim by tsunamis generated during intra-lake eruptions, in the case of Fisher volcano this was 7.9 ka after caldera formation (Stelling et al. 2005).

The largest volcanic flood hazards derive from break-outs from intracaldera lakes (Taupo, Okmok, Aniakchak, Towada), and from valleys dammed by debris avalanches (Colima, Mount St. Helens) because of the potential volumes of water involved. Avalanche-dammed lakes are particularly hazardous not only because they can be voluminous but also because flood discharge can be amplified by the erosion and entrainment of unconsolidated material from the blockage (Capra and Macías 2002).

Other hazards can arise at crater lakes due to acid brine seepage, which can weaken the edifice (Reid et al. 2001), potentially leading to sector collapse debris avalanches and break-out lahars, e.g. at Rincon de la Vieja, Costa Rica (Kempter and Rowe 2000), and Copahue, Argentina (Varekamp et al. 2001). Acid brines can also contaminate drinking and irrigation water, while acid gas aerosols released from hyper-acidic crater lake waters are an unusual potential hazard along flow paths (Schaefer et al. 2008).

7.1 Mitigation

A variety of engineering interventions have been applied to prevent break-outs of unstable lakes and to mitigate lake break-out floods (Schuster 2000). Successfully applied techniques include: (i) reinforced spillways and check dams on weak blockages; (ii) drainage and diversion channels or tunnels across or through stable (bedrock) abutments; and (iii) pumps or siphons to lower lake level. These methods vary in expense and difficulty, and some are reliant on suitable topography or an adequate timeframe and success is not guaranteed. Diversion tunnels are probably the most long-term (and expensive solution), but despite their success at some volcanoes (e.g. Kelut and Mount St. Helens), they require maintenance and are vulnerable to destruction by renewed volcanic activity. There are also considerable eruption and other risks to workers during construction phases. Downstream mitigation measures against lahars and floods include construction of check dams, bunds and dykes, and raising and strengthening of bridges.

7.1.1 Engineering Interventions

Engineering interventions to reduce the hazard from volcanic lakes pre-date the Romans: at Albano maar, a tunnel dug by the Etruscans to drain the lake below its overspill level was rebuilt by the Romans in c. 396 BCE (Funiciello et al. 2003; De Benedetti et al. 2008). This 1.5 km long tunnel lowered the lake by 70 m and still functions today.

Mt. Kelut in Indonesia is probably the best example of a successful, although protracted, expensive, and technologically challenging intervention (Zen and Hadikusumo 1965; Suryo and Clarke 1985). The first attempt to control eruption-triggered lahars from the summit crater lake was construction of a diversion dam on the Badak ravine in 1905 following the 1901 eruption. This was overwhelmed by the 1919 lahars when all water was explosively expelled from the lake, triggering flows up to 58 m deep that travelled up to 38 km from source, inundating 131 km^2, destroying more than 100 villages and killing over 5,000 people. Following this disaster, an earlier plan to drain the lake was implemented in September 1919. This involved excavating a 955 m long tunnel with a 3 % gradient designed to intercept the bottom of the lake. Tunnelling was begun at both ends as the lake was dry following the eruption earlier in the year, but was stopped at the upstream end by lava ascent a year later. After tunnelling upwards for 735 m, volcanic debris in the inner crater wall

was encountered and the tunnel needed to be lined with concrete. Meanwhile, the crater lake had been refilling until by early April 1923 it held 22 × 10^6 m^3 of water: at this point leakage into the tunnel killed 5 workers. This led to modification of the plan to include a series of tunnels through which water would be siphoned at progressively lower levels (Fig. 9). The first tunnel was driven just above the then lake level of 1,185 m, preventing any further rise, and the lake was progressively lowered to 1,129 m. The volcano erupted again on 31 August 1951, but the small (<2 × 10^6 m^3) volume of lake water was largely evaporated rather than explosively expelled, leading to minimal lahars. Unfortunately the tunnels were blocked by the eruption and the crater deepened by c. 70 m (Zen and Hadikusumo 1965). In 1954, work was begun to reactivate the tunnels, with 3 being cleared by 1955 when the lake volume was limited to 23.5 × 10^6 m^3. A new tunnel was then driven 20 m below the lowest old tunnel, and two galleries and further adits were then driven from it towards the lake in the hope that seepage would drain the water. Unfortunately the desired drainage rate was never achieved and the project was abandoned in March 1963. On 26 April 1966 an eruption expelled the c. 20 × 10^6 m^3 of water in the lake, generating lahars that destroyed the rebuilt Badak diversion dam, killing 208, and again damaging the tunnel system. In June 1966 a new tunnel was dug linking the then empty crater to an older unfinished drive. Completion of this by the end of December 1967 limited the lake to a maximum volume of 4.3 × 10^6 m^3 with the result that the 1990 eruptions produced only minor primary lahars that killed only 32 (Thouret et al. 1998).

At Mount St. Helens, the levels of the three largest lakes impounded by the 1980 debris avalanche were stabilised by the U.S. Army Corps of Engineers by the construction of permanent spillways and bedrock drainage tunnels (Costa 1985). The greatest assessed risk was from Spirit Lake: numerical studies suggested that failure of the debris avalanche dam could generate a flood with a peak discharge of 7.5 × 10^4 m^3/s (Swift and Kresch 1983). To gain time, a 20-pump facility was installed to remove up to 5 m^3/s of water through a 1.5 m diameter pipe buried in the dam crest while a 2.59 km long, 3.4 m diameter tunnel was bored through the ridge to the west of the lake, ultimately stabilising the lake at 1,048 m (Schuster and Evans 2011). Meanwhile, Coldwater Lake was stabilised by construction of a permanent spillway across a resistant bedrock abutment, and Castle Lake was stabilised by construction of an armoured spillway.

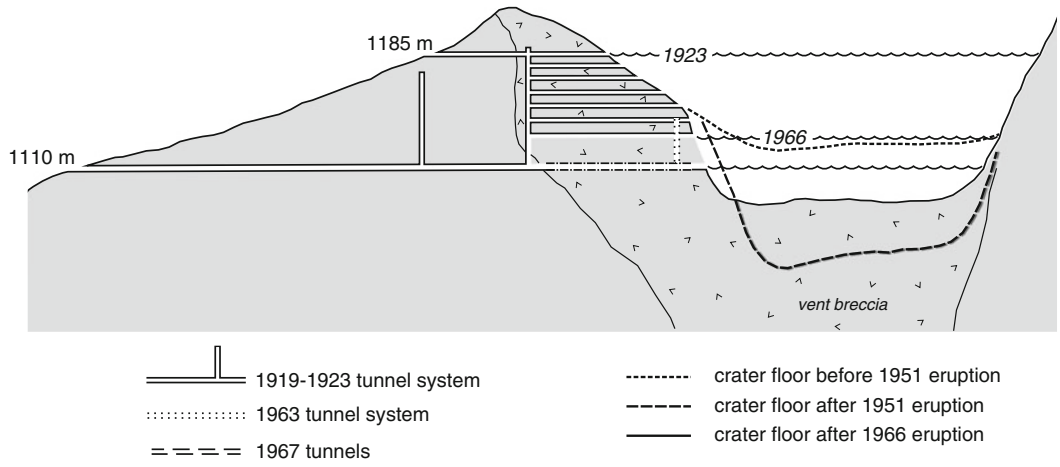

Fig. 9 Cross-section of the crater lake of Mt. Kelut in Indonesia showing the tunnel system used to lower the lake level and reduce the hazard from eruption-triggered lahars (after Zen and Hadikusumo 1965)

Repeated break-out floods from the lahar-dammed Mapanuepe Lake were a feature of the early years at Pinatubo in the Philippines following the 1991 eruption (Rodolfo et al. 1996; Umbal and Rodolfo 1996). Its level was stabilised in November 1992 by excavation of a bedrock spillway through an adjacent rock spur. Geological and anthropological data indicate that a similar lake occupied this site on two previous occasions (Rodolfo and Umbal 2008).

Emptying of the summit Crater lake of Mt. Ruapehu during the 1995–1996 eruptions (Johnston et al. 2000), coupled with deposition of a c. 8 m thick blanket of tephra over the former outlet area, raised the possibility of a future break-out lahar in a repeat of the 1953 Tangiwai lahar scenario, which resulted in New Zealand's worst volcanic disaster (Healy 1954; O'Shea 1954). Given the decade-long delay between formation of the tephra barrier and the subsequent breakout in March 2007 (Manville and Cronin 2007; Massey et al. 2010; Lube et al. 2012) there was adequate time to quantify the relative risks of intervention at the crater rim versus downstream mitigation efforts. The situation was complicated by the status of the summit of Ruapehu as a World Heritage Site, its location in a National Park, and not least Crater Lake's special spiritual significance to the local Maōri population. Numerical modelling of the potential magnitude of any lahar event (Hancox et al. 2001) and a residual analysis of the risks of intervention versus non-intervention (Taig 2002) resulted in the decision to install a real-time telemetered warning system on the tephra dam and downstream channel, a bund at the apex of the Whangaehu Fan to prevent overspill into vulnerable northern drainages, raising and strengthening of the State Highway 49 road bridge at Tangiwai, a system of automatic lights and gates to close roads close to or crossing the predicted lahar path, and a public education campaign (Keys 2007; Becker et al. 2008; Keys and Green 2008). In the event, the lahar occurred as predicted with no loss of life or injuries and minimal infrastructural damage.

7.1.2 Limnic Gas Eruptions

Following the gas eruptions from Lakes Monoun and Nyos, warning systems comprising CO_2 monitors, sirens and public education were implemented, as well as a pipe system designed to safely degas the lake water (Kusakabe et al. 2008). Reinforcement of the outlet to Lake Nyos to stabilise the natural dam is also currently underway (Aka and Yokoyama 2013), in response to the potential for breaching to catastrophically release the upper 40 m of lake water. This would not only cause flooding into Nigeria over 200 km downstream, but also release another burst of CO_2 due to depressurisation of the gas-saturated deep water (Lockwood et al. 1988).

8 Conclusions

Although hydrologic hazards from volcanic lakes are over-represented in terms of fatalities per eruption, improvements in volcano monitoring and increased awareness are mitigating the risk at many volcanoes around the world. Timely and appropriate engineering interventions have been effective in minimising deaths at a number of volcanoes (Kelut) and preventing disasters at others (Mount St. Helens, Lake Nyos). Although currently very few volcanic lakes are monitored on a regular basis, changes in a lake's appearance, thermal, and/or chemical characteristics could be diagnostic of impending volcanic activity (Oppenheimer 1993; Hurst and Vandemeulebrouck 1996; Christenson 2000; Christenson et al. 2010). Break-outs associated with collapse of blockages are less predictable, unless the lake level is approaching the overflow point, or seepage on the downstream face of the dam is obvious and sediment-laden (Turner et al. 2007; Massey et al. 2010).

Most fatalities due to volcanic activity occur between 10–30 km away from the vent (Auker et al. 2013). This reflects the combination of (i): this distance being within the range of the heaviest tephra falls; (ii) the typical travel distance of pyroclastic flows, lahars and intra-lake

tsunamis; and (iii) the tendency for populations to be concentrated on the gentler slopes and flat alluvial (often lahar) terraces and plains flanking and downstream of volcanoes, (volcanic) lakeshores, and along coastlines vulnerable to volcanogenic tsunamis. However, this is also far enough away for a combination of effective monitoring and warning systems, public education, land-use planning, and engineering interventions to mitigate many of the hazards presented by volcanic lakes. In the future, a combination of clearer understanding and better practice are likely to be most effective in alleviating the associated dangers.

Acknowledgments Research for this study began under the Catastrophic Flooding and Lahars programme founded by B.F. Houghton and funded by the Foundation for Research Science and Technology, New Zealand under contracts C05516 and C0005X6 to Manville. The manuscript benefited from reviews by TC Pierson and JE O'Connor.

References

Aka FT, Yokoyama T (2013) Current status of the debate about the age of Lake Nyos dam (Cameroon) and its bearing on potential flood hazards. Nat Hazards 65:875–885

Almberg LD, Beget JE, Larsen JF (2003) Magmatic production rate determined by volcaniclastic lithofacies variations in a rapidly fluctuating caldera lake, Okmok Volcano, Alaska. In: Proceedings and abstract volume of IUGG 2003 Congress, Sapporo, Japan: A. p 519

Anderson TR, Flett JS (1903) Report on the eruptions of the Soufriere, in St. Vincent in 1902, and on a visit to Montagne Pelee, Martinique—part 1. Philos Trans Roy Soc Ser A 200:353–553

Aramaki S (1956) The 1783 activity of Asama volcano, part 1. Jpn J Geol Geogr XXVII(2–4):189–229

Aramaki S (1981) The sequence and nature of 1783 eruption of Asama volcano. In: Abstracts of the symposium on Arc Volcanism, Tokyo and Hakone-Machi, Japan, pp 11–12

Arboleda RA, Martinez MML (1996) 1992 lahars in the Pasig-Potrero river system. In: Newhall CG, Punongbayan RS (eds) Fire and Mud, eruptions and lahars of Mount Pinatubo. University of Washington Press, Seattle, Philippines, pp 1045–1052

Auker MR, Sparks RSJ, Siebert L, Crossweller HS, Ewert J (2013) A statistical analysis of the global historical volcanic fatalities record. J Appl Volcanol 2. doi:10.1186/2191-5040-2-2

Baales M, Jöris O, Street M, Bittman F, Wninger B, Wiethold J (2002) Impact of the late glacial eruption of the Laacher See volcano, central Rhineland, Germany. Quatern Res 58:273–288

Bani P, Join J-L, Cronin SJ, Lardy M, Rouet I, Garaebiti E (2009) Characteristics of the summit lakes of Ambae volcano and their potential for generating lahars. Nat Hazards Earth Syst Sci 9:1471–1478

Barberi F, Chelini W, Marinelli G, Martini M (1989) The gas cloud of Lake Nyos (Cameroon, 1986): results of the Italian technical mission. J Volcanol Geoth Res 39:125–134

Batiza R, White JDL (2000) Submarine lavas and hyaloclastite. In: Sigurdsson H, Houghton B, McNutt S, Rymer H, Stix J (eds) Encyclopedia of volcanoes. Academic Press, New York, pp 361–381

Beck AC (1950) Volcanic activity at Mt. Ruapehu from August to December, 1945. NZ J Sci Technol B31:1–13

Becker J, Manville V, Leonard G, Saunders W (2008) Managing lahars the New Zealand way: a case study from Mount Ruapehu volcano. Natural Hazards Observer XXXII(5):4–6

Begét JE, Larsen JF, Neal CA, Nye CJ, Schaefer JR (2005) Preliminary volcano-hazard assessment of Okmok volcano, Umnak Island, Alaska. Alaska department of natural resources, division of geological and geophysical surveys, report of investigations 2004-3, 32 p

Begét JE, Gardner C, Davis K (2008) Volcanic tsunamis and prehistoric cultural transitions in Cook Inlet, Alaska. J Volcanol Geoth Res 176:377–386

Belousov A, Belousov M (2001) Eruptive process, effects and deposits of the 1996 and the ancient basaltic phreatomagmatic eruptions in Karymskoye lake, Kamchatka, Russia. In: White JDL, Riggs NR (eds) Volcanogenic sedimentation in lacustrine settings. International Association of Sedimentologists, Special Publication, vol 30, pp 35–60

Belousov A, Voight B, Belousova M, Muravyev Y (2000) Tsunamis generated by subaquatic volcanic explosions: unique data from 1996 eruption in Karymskoye Lake, Kamchatka, Russia. Pure Appl Geophys 157:1135–1143

Björnsson H (1975) Subglacial water reservoirs, jökulhlaups and volcanic eruptions. Jökull 25:1–14

Björnsson H (1992) Jökulhlaups in Iceland: prediction, characteristics and simulation. Ann Glaciol 16:95–106

Björnsson H (2002) Subglacial lakes and jökulhlaups in Iceland. Glob Planet Change 35:255–271

Bornas MA, Tungol N, Maximo RPR, Paladio-Melosantos ML, Mirabueno HT, Javier DV, Corpuz EG, Dela Cruz EG, Ramos AF, Marilla JD, Villacorte EU (2003) Caldera-rim breach and lahar from Mt. Pinatubo, Philippines: natural breaching and resulting lahar. In: Proceedings and abstract volume of IUGG 2003 Congress, Sapporo, Japan A, p 558

Capra L (2007) Volcanic natural dams: identification, stability, and secondary effects. Nat Hazards 43:45–61

Capra L, Macías JL (2002) The cohesive Naranjo debris-flow deposit (10 km^3): a dam breakout flow derived from the Pleistocene debris-avalanche deposit of Nevado de Colima Volcano (México). J Volcanol Geoth Res 117:213–235

Carey S, Sigurdsson H, Mandeville C, Bronto S (1996) Pyroclastic flows and surges over water: an example from the 1883 Krakatau eruption. Bull Volc 57:493–511

Carey S, Sigurdsson H, Mandeville C, Bronto S (2000) Volcanic hazards from pyroclastic flow discharge into the sea: examples from the 1883 eruption of Krakatau, Indonesia. In: McCoy FW, Heiken G (eds) Volcanic hazards and disasters in human antiquity. Geological Society of America, Special Publication, vol 345, pp 1–14

Carey S, Morelli D, Sigurdsson H, Bronto S (2001) Tsunami deposits from major explosive eruptions: an example from the 1883 eruption of Krakatau. Geology 29:347–350

Carrivick JL, Russell AJ, Tweed FS, Twigg D (2004) Palaeohydrology and sedimentary impacts of jökulhlaups from Kverkfjöll, Iceland. Sed Geol 172:19–40

Carrivick JL, Manville V, Cronin SJ (2009) A fluid dynamics approach to modelling the 18th March 2007 lahar at Mt. Ruapehu. NZ Bull Volcanol 71:153–169

Casadevall TJ, de la Cruz-Reyna S, Rose WI, Bagley S, Finngean DL, Zollwer WH (1984) Crater lake and post-eruption hydrothermal activity, El Chichón volcano, Mexico. J Volcanol Geoth Res 23:169–191

Catane SG, Taniguchi H, Goto A, Givero AP, Mandanas AA (2005) Explosive volcanism in the Philippines. CNEAS monograph series. Centre for Northeast Asian studies, Tohuku University, Tohuku, 146 p

Chesner CA, Rose WI (1991) Stratigraphy of the Toba tuffs and the evolution of the Toba caldera Complex, Sumatra, Indonesia. Bull Volcanol 53:343–356

Chiocci FL, Romagnoli C, Tomassi P, Bosman A (2008) The Stromboli 2002 tsunamigenic submarine slide: characteristics and possible failure mechanisms. J Geophys Res 113:B10102

Chitwood L, Jensen R (2000) Large prehistoric flood along Paulina Creek. In: Jensen R, Chitwood L (eds) What's new at Newberry volcano, Oregon. USDA Forest Services, Bend, Oregon, pp 31–40

Chrétien S, Brousse R (1989) Events preceding the great eruption of 8 May, 1902 at Mount Pelée, Martinique. J Volcanol Geoth Res 38:67–75

Christenson BW (2000) Geochemistry of fluids associated with the 1995–1996 eruption of Mt. Ruapehu, New Zealand: signatures and processes in the magmatic-hydrothermal system. J Volcanol Geoth Res 97:1–30

Christenson BW, Wood CP (1993) Evolution of a vent-hosted hydrothermal system beneath Ruapehu Crater Lake, New Zealand. Bull Volc 55:547–565

Christenson BW, Reyes AG, Young R, Moebis A, Sherburn S, Cole-Baker JC, Britten K (2010) Cyclic processes and factors leading to phreatic eruption events: insights from the 25 September 2007 eruption through Ruapehu Crater Lake, New Zealand. J Volcanol Geoth Res 191:15–32

Clarke GKC (2003) Hydraulics of subglacial outburst floods: new insights from the Spring-Hutter formulation. J Glaciol 49:299–313

Cole RH (1948) Underwater explosions. Princeton University Press, Princeton 437 p

Conaway J (2000) Hydrogeology and paleohydrology in the Williamson River Basin, Klamath County, Oregon. Unpublished M.Sc. thesis, department of geology. Portland State University, Portland, 117 p

Córtes A, Macías JL, Capra L, Garduño-Monroy VH (2010) Sector collapse of the SW flank of Volcán de Colima, México: the 3600 yr BP La Lumbre-Los Ganchos debris avalanche and associated debris flows. J Volcanol Geoth Res 197:52–66

Costa, J. E. 1985. Floods from dam failures. USGS Open-file report 85-560, 54 p

Costa JE (1988) Rheologic, geomorphic, and sedimentologic differentiation of water floods, hyperconcentrated flows and debris flows. In: Baker VR, Kochel RC, Patton PC (eds) Flood geomorphology. Wiley, New York, pp 113–122

Costa JE, Schuster RL (1988) The formation and failure of natural dams. Geol Soc Am Bull 100:1054–1068

Cronin SJ, Neall VE, Lecointre JA, Palmer AS (1996) Unusual "snow slurry" lahars from Ruapehu volcano, New Zealand, September 1995. Geology 24:1107–1110

Cronin SJ, Neall VE, Lecointre JA, Palmer AS (1997) Changes in Whangaehu River lahar characteristics during the 1995 eruption sequence, Ruapehu volcano, New Zealand. J Volcanol Geoth Res 76:47–61

Crow R, Karlstrom KE, McIntosh WC, Peters L, Dunbar NW (2008) History of Quaternary volcanism and lava dams in western Grand Canyon based on lidar analysis, $^{40}Ar/^{39}Ar$ dating, and field studies: implications for flow stratigraphy, timing of volcanic events, and lava dams. Geosphere 4:181–206

Davy BW, Caldwell TG (1998) Gravity, magnetic and seismic surveys of the caldera complex, Lake Taupo, North Island, New Zealand. J Volcanol Geoth Res 81:69–89

De Benedetti AA, Funiciello R, Giordano G, Diano G, Caprilli E, Paterne M (2008) Volcanology, history and myths of the Lake Albano maar (Colli Albani volcano, Italy). J Volcanol Geoth Res 176:387–406

de Lange WP, Prasetya GS, Healy TR (2001) Modelling of tsunamis generated by pyroclastic flows (ignimbrites). Nat Hazards 24:251–266

Delmelle P, Bernard A (2000) Volcanic lakes. In: Sigurdsson H, Houghton B, McNutt S, Rymer H, Stix J (eds) Encyclopedia of volcanoes. Academic Press, New York, pp 877–895

Donnelly-Nolan JM, Nolan KM (1986) Catastrophic flooding and eruption of ash-flow tuff at Medicine Lake volcano, California. Geology 14:875–878

Druitt TH (1998) The eruption, transport and sedimentation of pyroclastic flows. In: Gilbert J, Sparks RSJ (eds) The physics of explosive volcanic eruptions. Geological Society of London, Special Publication, vol 145, pp 145–182

Duffield WA (2001) At least Noah had some warning. EOS Trans AGU 82(28):305–309

Dunne T, Fairchild LH (1983) Estimation of flood and sedimentation hazards around Mt. St. Helens. Shin Sabo 36:12–22

Egorov Y (2007) Tsunami wave generation by the eruption of underwater volcano. Nat Hazards Earth Syst Sci 7:65–69

Ellis SM, Wilson CJN, Bannister S, Bibby H, Heise W, Wallace L, Patterson N (2007) A future magma inflation event under the rhyolitic Taupo volcano, New Zealand: numerical models based on constraints from geochemical, geological, and geophysical data. J Volcanol Geoth Res 168:1–27

Ely LL, Brossy CC, House PK, Safran EB, O'Connor JE, Champion DE, Fenton CR, Bondre NR, Orem CA, Grant GE, Henry CD, Turrin BD (2012) Owyhee Rover intracanyon lava flows: does the river give a dam? Geol Soc Am Bull 124:1667–1687

Fenton CR, Cerling TE, Nash BP, Webb RH, Poreda RJ (2002) Cosmogenic ^{3}He ages and geochemical discrimination of lava-dam outburst-flood deposits in western Grand Canyon, Arizona. In: House PK, Webb RH, Baker VR, Levish DR (eds) Ancient floods, modern hazards: principles and applications of paleoflood hydrology. Am Geophys Union, Washington, D. C., pp 191–215

Fenton CR, Webb RH, Cerling TE (2003) Peak discharge estimates of two Pleistocene lava-dam outburst floods, western Grand Canyon, Arizona, USA. In: Ely LL, O'Connor JE, House PK (eds) Abstract volume, Paleoflood III conference. Hood River, Oregon, p 18

Fenton CR, Poreda RJ, Nash BP, Webb RH, Cerling TE (2004) Geochemical discrimination of five Pleistocene lava-dam outburst flood deposits, western Grand Canyon, Arizona. J Geol 112:91–110

Fenton CR, Webb RH, Cerling TE (2006) Peak discharge of a Pleistocene lava-dam outburst flood in Grand Canyon, Arizona, USA. Quatern Res 65:324–335

Fisher RV, Heiken G (1982) Mt. Pelée, Martinique: May 8 and 20, 1902, pyroclastic flows and surges. J Volcanol Geoth Res 13:339–371

Freundt A, Kutterolf S, Wehrmann H, Schmincke H-U, Strauch W (2006) Eruption of the dacite to andesite zoned Mateare Tephra, and associated tsunamis in Lake Managua, Nicaragua. J Volcanol Geoth Res 149:103–123

Freundt A, Strauch W, Kutterolf S, Schmincke H-U (2007) Volcanogenic tsunamis in lakes: examples from Nicaragua and general implications. Pure appl Geophys 164:527–545

Frost DL, Lee JHS, Thibault P (1994) Numerical computation of underwater explosions due to fuel-coolant interactions. Nucl Eng Des 146:165–179

Funiciello R, Giordano G, De Rita D (2003) The Albano maar lake (Colli Albani Volcano, Italy): recent volcanic activity and evidence of pre-Roman Age catastrophic lahar events. J Volcanol Geoth Res 123:43–61

Glasstone S, Dolan PJ (1977) The effects of nuclear weapons. United States department of defence and the energy research and development administration, Washington D.C., 644 p

Glicken, H, Meyer, W, Sabol, M (1989) Geology and ground-water hydrology of Spirit Lake blockage, Mount St. Helens, Washington, with implications for lake retention. US Geol Surv Bulletin 1789:30

Glicken H (1998) Rockslide-debris avalanche of May 18, 1980, Mount St. Helens Volcano, Washington. Bull Geol Surv Jpn 49:55–106

Gomez C, Kataoka KS, Tanaka K (2012) Large-scale internal structure of the Sanbongi Fan—Towada volcano, Japan: putting the theory to the test, using GPR on volcaniclastic deposits. J Volcanol Geoth Res 229–230:44–49

Goodyear WA (1880) Earthquake and volcanic phenomena, December 1879 and January 1880, in the Republic of Salvador, Central America. Panama Star and Herald, p 56

Graettinger AH, Manville V, Briggs RM (2010) Depositional record of historic lahars in the Whangaehu valley, Ruapehu, New Zealand: implications for trigger mechanisms, flow dynamics, and lahar hazards. Bull Volc 72:279–296

Grange LI (1937) The geology of the Rotorua-Taupo subdivision. N Z Geol Surv Bull 37:138

Gudmundsson MT, Sigmundsson F, Björnsson H (1997) Ice-volcano interaction of the 1996 Gjálp subglacial eruption, Vatnajökull, Iceland. Nature 389:954–957

Gunkel G, Beulker C, Grupe B, Viteri F (2008) Hazards of volcanic lakes: analysis of Lakes Quilotoa and Cuicocha, Ecuador. Advances in Geosciences 14:29–33

Hackett WR, Houghton BF (1989) A facies model for a quaternary andesitic composite volcano: Ruapehu, New Zealand. Bull Volc 51:51–68

Hamblin WK (1994) Late Cenozoic lava dams in the western Grand Canyon. Geological Society of America, Memoir 183

Hancox GT, Keys H, Webby MG (2001) Assessment and mitigation of dam-break lahar hazards from Mt. Ruapehu Crater Lake following the 1995–1996 eruptions. In: McManus KJ (ed) Engineering and development in hazardous terrains. In: Proceedings of New Zealand Geotechnical Society/NZ Institute of Professional Engineers Conference, Christchurch, New Zealand, pp 385–409

Hart K, Carey S, Sigurdsson H, Sparks RSJ, Robertson REA (2004) Discharge of pyroclastic flows into the sea during the 1996–1998 eruptions of the Soufrière Hills volcano, Montserrat. Bull Volcanol 66:599–614

Healy J (1954) The Whangaehu lahar of 24th December 1953. New Zealand geological survey, T20/501 Ruapehu immediate reports, vol 1, no 587

Healy J, Lloyd EF, Rushworth DEH, Wood CP, Glover RB, Dibble RR (1978) The eruption of Ruapehu, New Zealand on 22 June 1969. NZ Depart Sci Ind Res Bull 224:1–80

Hegan BD, Johnson JD, Severne C (2001) Landslide risk from the Hipaua geothermal area near Waihi village at the southern end of Lake Taupo. In: McManus KJ (ed) Engineering and development in hazardous terrains. In: Proceedings of New Zealand Geotechnical Society/ NZ Institute of Professional Engineers Conference, Christchurch, New Zealand, pp 439–448

Hermanns R, Nierdermann S, Ivy-Ochs S, Kubik PW (2004) Rock avalanching into a landslide-dammed lake causing multiple dam failure in Las Conchas valley (NW Argentina)—evidence from surface dating and stratigraphic analyses. Landslides 2:113–122

Hernández PA, Pérez NM, Varekamp JC, Hernriquez B, Hernández A, Barrancos J, Padrón E, Calvo D, Melián G (2007) Crater lake temperature changes of the 2005 eruption of Santa Ana volcano, El Salvador, Central America. Pure appl Geophys 164:2507–2522

Hickson CJ, Russell JK, Stasiuk MV (1999) Volcanology of the 2350 B.P. eruption of Mount Meager volcanic complex, British Columbia, Canada: implications for hazards from eruptions in topographically complex terrain. Bull Volcanol 60:489–507

Hildreth W (1983) The compositionally zoned eruption of 1912 in the valley of ten thousand Smokes, Katmai National Park, Alaska. J Volcanol Geoth Res 18:1–56

Hildreth W, Drake RE (1992) Volcán Quizapu, Chilean Andes. Bull Volcanol 54:93–125

Hodgson KA, Manville V (1999) Sedimentology and flow behaviour of a rain-triggered lahar, Mangatoetoenui stream, Ruapehu volcano, New Zealand. Geol Soc Am Bull 111:743–754

Hodgson KA, Nairn IA (2000) The catastrophic—1350 AD post-eruption flood from Lake Tarawera, New Zealand. Bay of plenty regional council, resource planning report. 61 p

Hodgson KA, Nairn IA (2005) The—AD 1315 syn-eruption and AD 1904 post-eruption breakout floods from Lake Tarawera, Haroharo caldera, North Island, New Zealand. NZ J Geol Geophys 48:491–506

Hodgson KA, Lecointre J, Neall VE (2007) Onetapu formation: the last 2000 yr of laharic activity at Ruapehu volcano, New Zealand. NZ J Geol Geophys 50:81–99

Houghton BF, Nairn IA (1991) The 1976–1982 Strombolian and phreatomagmatic eruptions of White Island, New Zealand: eruptive and depositional mechanisms at a wet volcano. Bull Volcanol 54:25–49

Hurst AW, Vandemeulebrouck J (1996) Acoustic noise and temperature monitoring of the crater lake of Mount Ruapehu volcano. J Volcanol Geoth Res 71:45–51

Huscroft CA, Ward BC, Barendregt RW, Jackson LE Jr, Opdyke ND (2004) Pleistocene volcanic damming of Yukon river and the maximum age of the Reid glaciation, west-central Yukon. Can J Earth Sci 41:151–164

Ichinose G, Anderson JG, Satake K, Schwieckert RA, Lahren MM (2000) The potential hazard from tsunami and seiche waves generated by large earthquakes within Lake Tahoe, California-Nevada. Geophys Res Lett 27:1203–1206

Iverson RM (1995) Can magma-injection and groundwater forces cause massive landslides on Hawaiian volcanoes? J Volcanol Geoth Res 66:295–308

Jennings ME, Schneider VR, Smith PE (1981) Computer assessments of potential hazards from breaching of two debris dams, Toutle river and Cowlitz river systems. In: Lipman PW, Mullineaux DR (eds) The 1980 eruptions of Mount St. Helens, Washington. United States geological survey professional paper, vol 1250, pp 829–836

Johnson RW (1987) Large-scale volcanic cone collapse: the 1888 slope failure of Ritter volcano, and other examples from Papua New Guinea. Bull Volcanol 49:669–679

Johnston DM, Houghton BF, Neall VE, Ronan KR, Paton D (2000) Impacts of the 1945 and 1995–1996 Ruapehu eruptions, New Zealand: an example of increasing societal vulnerability. Geol Soc Am Bull 112:720–726

Karátson D, Thouret J-C, Moriya I, Lomoschitz A (1999) Erosion calderas: origins, processes, structural and climatic control. Bull Volcanol 61:174–193

Kataoka KS (2011) Geomorphic and sedimentary evidence of a gigantic outburst flood from Towada caldera after the 15 ka Towada-Hachinohe ignimbrite eruption, northeast Japan. Geomorphology 125:11–26

Kataoka KS, Urabe A, Manville V, Kajiyama A (2008) Large-scale breakout flood from an ignimbrite-dammed river: aftermath of the Numazawako eruption (BC 3400), northeast Japan. Geol Soc Am Bull 120:1233–1247

Kear D, Schofield JC (1978) Geology of the Ngaruawahia subdivision. NZ Geol Surv Bull 88:168

Keating BH, McGuire WJ (2000) Island edifice failures and associated tsunami hazards. Pure Appl Geophys 157:899–955

Kedrinksii VK (2005) Hydrodynamics of explosions: experiments and models. Springer, Berlin, 362 p

Kempter KA, Rowe GL (2000) Leakage of active crater lake brine through the north flank at Rincón de la Veja volcano, northwest Costa Rica, and implications for crater collapse. J Volcanol Geoth Res 97:143–159

Kershaw JA, Clague JJ, Evans SG (2005) Geomorphic and sedimentological signature of a two-phase outburst flood from moraine-dammed Queen Bess Lake, British Columbia. Earth Surf Proc Land 30:1–25

Keys HJR (2007) Lahars of Ruapehu volcano, New Zealand: risk mitigation. Ann Glaciol 45:155–162

Keys HJR, Green PM (2008) Ruapehu lahar New Zealand 18 March 2007: lessons for hazard assessment and risk mitigation 1995–2007. J Disaster Res 3:284–296

Kilgour G, Jolly AD, Sherburn S, Scott B, Miller C, Rae AJ (2007) The October 2006 eruption of Ruapehu Crater Lake. In: Mortimer N, Wallace L (eds) Proceedings, Joint GSNZ/NZGS annual conference, Tauranga

Kilgour G, Manville V, Della Pasqua F, Reyes AG, Graettinger AH, Hodgson KA, Jolly AD (2010) The 25 September 2007 eruption of Mt. Ruapehu, New Zealand: Directed ballistics, Surtseyan jets, and ice-slurry lahars. J Volcanol Geoth Res 191:1–14

Kling GW, Clark MA, Compton HR, Devine JD, Evans WC, Humphrey AM, Koenigsberg EJ, Lockwood JP, Tuttle ML, Wagner GN (1987) The 1986 Lake Nyos gas disaster in Cameroon, West Africa. Science 236:169–175

Koyaguchi T, Woods AW (1996) On the formation of eruption columns following explosive mixing of magma and surface water. J Geophys Res 101:5561–5574

Kuenzi WD, Horst OH, McGehee RV (1979) Effect of volcanic activity on fluvial-deltaic sedimentation in a modern arc-trench gap, southwestern Guatemala. Geol Soc Am Bull 90:827–838

Kusakabe M, Ohba T, Yoshida Y, Satake H, Ohizumi T, Evans WC, Tanyileke G, Kling GW (2008) Evolution of CO2 in Lakes Monoun and Nyos, Cameroon, before and during controlled degassing. Geochem J 42:93–118

Lagmay AMF, Rodolfo KS, Siringan FP, Uy H, Remotigue C, Zamora P, Lapus M, Rodolfo R, Ong J (2007) Geology and hazard implications of the Maraunot notch in the Pinatubo caldera, Philippines. Bull Volcanol 69:797–809

Larson GL (1989) Geographical distribution, morphology and water quality of caldera lakes: a review. Hydrobiologia 171:23–32

Latter JH (1981) Tsunamis of volcanic origin: summary of causes, with particular reference to Krakatoa, 1883. Bull Volcanol 44:467–490

Le Guern F, Tazieff H, Pierret RF (1982) An example of health hazard: people killed by gas during a phreatic eruption: Dieng Plateau (Java, Indonesia), February 20th 1979. Bull Volc 45:153–156

Lipman PW, Mullineaux DR (1981) The 1980 eruptions of Mount St. Helens, Washington. United Stated geological survey, Professional Paper, vol 1250, 844 p

Lliboutry L, Arnao BM, Pautre A, Schneider B (1977) Glaciological problems set by the control of dangerous lakes in Cordilerra Blanca, Peru 1. Historical failures of morainic dams, their causes and prevention. J Glaciol 18:239–254

Lockwood JP, Costa JE, Tuttle ML, Nni J, Tebor SG (1988) The potential for catastrophic dam failure at Lake Nyos maar, Cameroon. Bull Volcanol 50:340–349

Lorenz V (1973) On the formation of maars. Bull Volcanologique 37:183–204

Lowe DJ, Green JD (1992) Lakes. In: Soons JM, Selby MJ (eds) Landforms of New Zealand. Longman Paul Ltd., pp 107–143

Lube G, Cronin SJ, Manville V, Procter JN, Cole SE, Freundt A (2012) Energy growth in laharic mass flows. Geology 40:475–478

Machado F, Parsons WH, Richards AF, Mulford JW (1962) Capelinhos eruption of Fayal volcano, Azores, 1957–1958. J Geophys Res 67:3519–3529

Macías JL, Capra L, Scott KM, Espíndola JM, García-Palomo A, Costa JE (2004) The 26 May 1982 breakout flows derived from failure of a volcanic dam at El Chichón, Chiapas, Mexico. Geol Soc Am Bull 116:233–246

Magnússon E, Gudmundsson MT, Roberts MJ, Sigurðsson G, Höskuldsson F, Oddsson B (2012) Ice-volcano interactions during the 2010 Eyjafjallajökull eruption, as revealed by airborne imaging radar. J Geophys Res 117:B07405

Mann CP, Stix J, Vallance JW, Richer M (2004) Subaqueous intracaldera volcanism, Ilopango Caldera, El Salvador, Central America. In: Rose WI Jr, Bommer JJ, López DL, Carr MJ, Major JJ (eds) Natural hazards in El Salvador. Geological Society of America, Special Paper, vol 375, pp 159–174

Manville VR (2001) Sedimentology and history of Lake Reporoa: an ephemeral supra-ignimbrite lake, Taupo Volcanic Zone, New Zealand. In: White JDL, Riggs NR (eds) Volcanogenic sedimentation in lacustrine settings. International association of sedimentologists, Special Publication, vol 30, pp 109–140

Manville V (2002) Sedimentary and geomorphic responses to a large ignimbrite eruption: readjustment of the Waikato river in the aftermath of the A.D. 181 Taupo eruption, New Zealand. J Geol 110:519–542

Manville V (2004) Palaeohydraulic analysis of the 1953 Tangiwai lahar: New Zealand's worst volcanic disaster. Acta Vulcanol XVI(1/2):137–152

Manville V (2010) An overview of break-out floods from intracaldera lakes. Glob Planet Change 70:14–23

Manville V, Cronin SJ (2007) Break-out lahar from New Zealand's Crater Lake. EOS Trans AGU 88:441–442

Manville V, Wilson CJN (2003) Interactions between volcanism, rifting and subsidence: implications of intracaldera palaeoshorelines at Taupo volcano, New Zealand. J Geol Soc London 160:3–6

Manville V, Wilson CJN (2004) The 26.5 ka Oruanui eruption, New Zealand: a review of the roles of volcanism and climate in the post-eruptive sedimentary response. NZ J Geol Geophys 47:525–547

Manville VR, White JDL, Houghton BF, Wilson CJN (1999) Paleohydrology and sedimentology of a post-1800a breakout flood from intracaldera Lake Taupo, North Island, New Zealand. Geol Soc Am Bull 111:1435–1447

Manville V, Newton EH, White JDL (2005) Fluvial responses to volcanism: resedimentation of the 1800a Taupo ignimbrite in the Rangitaiki River catchment, North Island, New Zealand. Geomorphology 65:49–70

Manville V, Hodgson KA, Nairn IA (2007) A review of break-out floods from volcanogenic lakes in New Zealand. NZ J Geol Geophys 52:131–150

Massey C, Manville V, Hancox GT, Keys HJR, Lawrence C, McSaveney MJ (2010) Out-burst flood (lahar) triggered by retrogressive landsliding, 18 March 2007 at Mt. Ruapehu, New Zealand—a successful early warning. Landslides 7:303–315

Mastin LG (1995) Thermodynamics of gas and steam-blast eruptions. Bull Volcanol 57:85–98

Mastin LG (1997) Evidence for water influx from a caldera lake during the explosive hydromagmatic eruption of 1790, Kilauea volcano, Hawaii. J Geophys Res 102:20093–20109

Mastin LG, Witter JB (2000) The hazards of eruptions through lakes and seawater. J Volcanol Geoth Res 97:195–214

McClelland L, Simkin T, Summers M, Nielsen E, Stein TC (1989) Global volcanism, 1975–1985. Prentice-Hall, Englewood Cliffs, 655 p

McCoy FW, Heiken G (2000) The late-bronze age explosive eruption of Thera (Santorini), Greece: regional and local effects. In: McCoy FW, Heiken G (eds) Volcanic hazards and disasters in human antiquity. Geological Society of America, Special Publication, vol 345, pp 43–70

McGimsey RG, Waythomas CF, Neal CA (1994) High stand and catastrophic draining of intracaldera Surprise Lake, Aniakchak Volcano, Alaska. U.S. Geol Surv Bull 2107:59–71

McGuire WJ (1996) Volcano instability: a review of contemporary issues. In: McGuire WJ, Jones AP, Neuberg J (eds) Volcano instability on the Earth and other planets. Geological Society of London, Special Publication, vol 110, pp 1–23

Meier MF, Carpenter PJ, Janda RJ (1981) Hydrologic effects of Mount St. Helens' 1980 eruptions. EOS Trans AGU 62(33):625–626

Meyer DF, Martinson HA (1989) Rates and processes of channel development and recovery following the 1980 eruption of Mount St. Helens, Washington. J Hydrol Sci 34:115–127

Meyer W, Sabol MA, Schuster RL (1986) Landslide dammed lakes at Mount St. Helens, Washington. In: Schuster RL (ed) Landslide dams—process, risk, and mitigation. American society of civil engineers geotechnical Special Publication, vol 3, pp 21–41

Miller TP, Smith RL (1977) Spectacular mobility of ash flows around Aniakchak and Fisher calderas, Alaska. Geology 5:173–176

Miura K, Ban M, Ohba T, Fujinawa A (2012) Sequence of the 1895 eruption of the Zao volcano, Tohuku Japan. J Volcanol Geoth Res 247–248:139–157

Moore JG (1967) Base surge in recent volcanic eruptions. Bull Volcanol 30:337–363

Moore JG, Nakamura K, Alcarez A (1966a) The September 28–30, 1965 eruption of Taal Volcano, Philippines. Bull Volcanol 29:75–76

Moore JG, Nakamura K, Alcarez A (1966b) The 1965 eruption of Taal Volcano. Science 151:955–960

Mooser F, Meyer-Abich H, McBirney AR (1958) Central America. Catalogue of active volcanoes of the world including solfatara fields, Part VI, International Association of Volcanology and Chemistry of the Earth's Interior, Rome, Italy, 146 p

Morimoto R (1948) Submarine eruption of the Myôjin reef. Bull Volcanol 23:151–160

Morrissey M, Gisler G, Weaver R, Gittings ML (2010) Numerical model of crater lake eruptions. Bull Volcanol 72:1169–1178

Motyka RJ (1977) Katmai caldera: glacier growth, lake rise, and geothermal activity. Short Notes Alaskan Geol 55:17–21

Nairn IA (1979) Rotomahana-Waimangu eruption, 1886. base-surge and basalt magma. NZ J Geol Geophys 22:363–378

Nairn IA (2002) Geology of the Okataina volcanic centre. Institute of Geological and Nuclear Sciences, geological map no. 25 (1:50 000). Lower Hutt, New Zealand, 1 sheet + 156 p

Nairn IA, Wood CP, Hewson CAY (1979) Phreatic eruptions of Ruapehu: April 1975. NZ J Geol Geophys 22:155–173

Nairn IA, Self S, Cole JW, Leonard GS, Scutter C (2001) Distribution, stratigraphy and history of proximal deposits from the—AD 1305 Kaharoa eruption of Tarawera volcano, New Zealand. NZ J Geol Geophys 44:467–484

Nakagawa M, Wada K, Thordarson T, Wood CP, Gamble JA (1999) Petrological investigations of the 1995 and 1996 eruptions of Ruapehu volcano, New Zealand: formation of discrete and small magma pockets and their intermittent discharge. Bull Volcanol 61:15–31

Nayar A (2009) A lakeful of trouble. Nature 460:321–333

Neall VE (1996) Hydrological disasters associated with volcanoes. In: Singh VP (ed) Hydrology of disasters. Kluwer, Dordrecht, pp 395–425

Nelson CH, Bacon CR, Robinson SW, Adam DP, Bradbury JP, Barber JH Jr, Schwartz D, Vagenas G (1994) The volcanic, sedimentologic, and paleolimnologic history of the Crater Lake caldera floor, Oregon: evidence for small caldera evolution. Geol Soc Am bull 106:684–704

Németh K, Cronin SJ, Charley D, Harrison M, Garae E (2006) Exploding lakes in Vanuatu—"Surtseyan-style" eruptions witnessed on Ambae Island. Episodes 29:87–92

Németh K, Cronin SJ, Smith IEM, Flores JA (2012) Amplified hazard of small-volume monogenetic eruptions due to environmental conditions, Orakei Basin, Auckland Volcanic Field, New Zealand. Bull Volcanol 74:2121–2137

Newhall CG, Dzurisin D (1988) Historical unrest at large calderas of the world. US Geol Surv Bull 1855:1108 p

Newhall CG, Punongbayan RS (1996) Fire and mud: eruptions and lahars of Mount Pinatubo, Philippines. University of Washington Press, Seattle, 1126 p

O'Connor JE, Beebee RA (2009) Floods from natural rock-material dams. In: Burr DM, Carling PA, Baker VR (eds) Megaflooding on Earth and Mars. Cambridge University Press, Cambridge, pp 128–171

O'Connor JE, Clague JJ, Walder JS, Manville V, Beebee RA (2013) Outburst floods. In: Shroder JF (ed) Treatise on geomorphology. Academic Press, San Diego, pp 475–510

Oppenheimer C (1993) Infrared surveillance of crater lakes using satellite data. J Volcanol Geoth Res 55:117–128

O'Shea BE (1954) Ruapehu and the Tangiwai disaster. NZ J Sci Technol B36:174–189

Otway PM (1986) Vertical deformation associated with the Taupo earthquake swarm, June 1983. In: Reilly WI,

Harford BE (eds) Recent crustal movements. Royal Society of New Zealand Bulletin, vol 24, pp 187–200
Pain CF, Blong RJ, McKee CO, Polach HA (1981) Pyroclastic deposits and eruptive sequences of Long Island. In: Johnson RW (ed) Cooke-Ravian volume of volcanological papers. Geological Survey of Papua New Guinea, Port Moresby, Memoir, vol 10, pp 101–113
Park C, Schmincke H-U (1997) Lake formation and catastrophic dam burst during the Late Pleistocene Laacher See eruption (Germany). Naturwissenschaft 84:521–525
Pierson TC (1985) Initiation and flow behavior of the 1980 Pine Creek and Muddy River lahars, Mount St. Helens, Washington. Geol Soc Am Bull 96:1056–1069
Pierson TC (1997) Transformation of water flood to debris flow following the eruption-triggered transient-lake breakout from the crater on 19 March 1982. In: Pierson TC (ed) Hydrologic consequences of hot-rock/snowpack interactions at Mount St. Helens volcano, Washington, 1982–1984. United States geological survey open-file report, vol 96–179, pp 19–36
Pierson TC, Janda RJ, Thouret J-C, Borrero CA (1990) Perturbation and melting of snow and ice by the 13 November 1985 eruption of Nevado del Ruiz, Columbia, and consequent mobilization, flow and deposition of lahars. J Volcanol Geoth Res 41:17–66
Pierson TC, Janda RJ, Umbal JV, Daag AS (1992) Immediate and long-term hazards from lahars and excess sedimentation in rivers draining Mt. Pinatubo, Philippines. U.S. Geol Surv Water-Resour Invest Rep 92–4039:183–203
Procter JN, Cronin SJ, Fuller IC, Lube G, Manville V (2010) Quantifying the geomorphic impacts of a lake break-out flood, Mt. Ruapehu. NZ Geol 38:67–70
Pulgarin B, Macías JL, Cepeda H, Capra L (2004) Late Pleistocene deposits associated with a southern flank collapse of the Nevado del Huila volcanic complex (Colombia). Acta Vulcanolgica 16:37–58
Pullar WA, Selby MJ (1971) Coastal progradation of Rangitaiki Plains, New Zealand. NZ J Sci 14:419–434
Ramos EG (1986) Lakeshore landslides: unrecognised hazards around Taal volcano. Philippine J Volcanol 3:28–53
Reid ME, Sisson TW, Brien DL (2001) Volcano collapse promoted by hydrothermal alteration and edifice shape, Mount Rainier, Washington. Geology 29:779–782
Reynolds MA, Best JG, Johnson RW (1980) 1953–57 eruption of Tuluman volcano: rhyolitic volcanic activity in the northern Bismarck sea. Geol Surv P N G Mem 7:5–44
Richer M, Mann CP, Stix J (2004 Mafic magma injection triggers eruption at Ilopango Caldera, El Salvador, Central America. In: Rose WI Jr, Bommer JJ, López DL, Carr MJ, Major JJ (eds) Natural hazards in El salvador. Geological Society of America, Special Paper, vol 375, pp 175–189
Riggs NR, Ort M, White JDL, Wilson CJN, Clarkson R (2001) Post-1.8-ka marginal sedimentation in Lake Taupo, New Zealand: effects of wave energy and sediment supply in a rapidly rising lake. In: White JDL, Riggs NR (eds) Volcanogenic sedimentation in lacustrine settings. International Association of Sedimentologists, Special Publication, vol 30, pp 151–177
Rodolfo KS (2000) The hazard from lahars and jökulhlaups. In: Sigurdsson H, Houghton B, McNutt S, Rymer H, Stix J (eds) Encyclopedia of volcanoes. Academic Press, New York, pp 973–995
Rodolfo KS, Umbal JV (2008) A prehistoric lahar-dammed lake and eruption of Mount Pinatubo described in a Philippine aborigine legend. J Volcanol Geoth Res 176:432–437
Rodolfo KS, Umbal JV, Alonso RA, Remotigue CT, Paladio-Melosantos ML, Salvador JHG, Evangelista D, Miller Y (1996) Two years of lahars on the western flank of Mount Pinatubo: Initiation, flow processes, deposits, and attendant geomorphic and hydraulic changes. In: Newhall CG, Punongbayan RS (eds) Fire and Mud, eruptions and lahars of Mount Pinatubo. University of Washington Press, Seattle, Philippines, pp 989–1013
Rose WI (1972) Notes on the 1902 eruption of Santa María Volcano, Guatemala. Bull Volcanol 36:1–17
Rose WI, Conway FM, Pullinger CR, Deino CR, McIntosh WC (1999) An improved age framework for late quaternary silicic eruptions in northern Central America. Bull Volcanol 61:106–120
Rowe GLJ, Ohsawa S, Takano B, Brantley SL, Fernandez JF, Barquero J (1992) Using crater lake chemistry to predict volcanic activity at Poás volcano, Costa Rica. Bull Volcanol 54:494–503
Schaefer JR, Scott WE, Evans WC, Jorgenson J, McGimsey RG, Wang B (2008) The 2005 catastrophic acid crater lake drainage, lahar, and acidic aerosol formation at Mount Chiginagak volcano, Alaska, USA: field observations and preliminary water and vegetation chemistry results. Geochem Geophys Geosyst 9:Q07018
Schuster RL (2000) Outburst debris-flows from failure of natural dams. In: Wieczorek G, Naeser N (eds) Debris-flow hazards mitigation: mechanics, prediction, and assessment. Balkema, Rotterdam, pp 29–42
Schuster RL, Evans SG (2011) Engineering measures for the hazard reduction of landslide dams. In: Evans SG, Hermanns RL, Strom A, Scarascia-Mugnozza G (eds) Natural and artificial rockslide dams. Springer, Berlin, pp 77–100
Scott KM (1988) Origin, behavior, and sedimentology of prehistoric catastrophic lahars at Mt. St. Helens, Washington. Geological Society of America, Special Paper, vol 229, pp 23–36
Scott KM (1989) Magnitude and frequency of lahars and lahar-runout flows in the Toutle-Cowlitz River system. United States geological survey, Professional Paper, vol 1447-B, 33 p
Scott KM, Hoblitt RE, Torres RC, Self S, Martinez MML, Nillos T Jr (1996a) Pyroclastic flows of the June 15, 1991, climactic eruption of Mount Pinatubo. In: Newhall CG, Punongbayan RS (eds) Fire and Mud, eruptions and lahars of Mount Pinatubo, Philippines. University of Washington Press, Seattle, pp 545–570

Scott KM, Janda RJ, De La Cruz EG, Gabinete E, Eto I, Isada M, Sexon M, Hadley KC (1996b) Channel and sedimentation responses to large volumes of 1991 volcanic deposits on the east flank of Mount Pinatubo. In: Newhall CG, Punongbayan RS (eds) Fire and Mud, eruptions and lahars of Mount Pinatubo. University of Washington Press, Seattle, Philippines, pp 971–988

Segschneider B, Landis CA, Manville V, White JDL, Wilson CJN (2002) Environmental response to a large, explosive rhyolite eruption: Lithofacies and physical sedimentology of post-1.8 ka pumice-rich Taupo volcaniclastics in the Hawke's Bay region. NZ Sediment Geol 150:275–299

Self S, Rampino MR (1981) The 1883 eruption of Krakatau. Nature 294:699–704

Shepherd JB, Aspinall WP, Rowley KC, Pereira J, Sigurdsson H, Fiske RS, Tomblin JF (1979) The eruption of Soufrière volcano, St Vincent April–June 1979. Nature 282:24–28

Sheridan MF, Wohletz KH (1983) Hydrovolcanism: basic considerations and review. J Volcanol Geoth Res 17:1–29

Siebert L (1984) Large volcanic debris avalanches: characteristics of source areas, deposits, and associated eruptions. J Volcanol Geoth Res 22:163–197

Siebert L (1996) Hazards of large volcanic debris avalanches and associated eruptive phenomena. In: Scarpa R, Tilling RI (eds) Monitoring and mitigation of volcano hazards. Springer, Berlin, pp 541–572

Siebert L, Begét JE, Glicken H (1995) The 1883 and late-prehistoric eruptions of Augustine volcano, Alaska. J Volcanol Geoth Res 66:367–395

Sigurdsson H, Devine JD, Tchoua FM, Presser TS, Pringle MKW, Evans WC (1987) Origin of the lethal gas burst from Lake Monoun, Cameroon. J Volcanol Geoth Res 31:1–16

Silva L, Cochemé JJ, Canul R, Duffield W, Tilling R (1982) El Chichón Volcano. SEAN Bulletin, Smithsonian Institution 7(5):2–6

Simkin T, Siebert L (1994) Volcanoes of the world. Smithsonian institution, global volcanism program. Geoscience press, Tucson, Arizona, 349 p

Simmons SF, Keywood M, Scott BJ, Kearn RF (1993) Irreversible change of the Rotomahana-Waimangu hydrothermal system (New Zealand) as a consequence of a volcanic eruption. Geology 21:643–646

Smart GM (1981) Volcanic debris control, Gunung Kelud, East Java. In: Erosion and transport in Pacific Rim steeplands. International Association of Hydrological Sciences Publication, vol 134, pp 604–654

Smith RCM (1991a) Landscape response to a major ignimbrite eruption, Taupo Volcanic Center, New Zealand. In: Fisher RV, Smith GA (eds) Sedimentation in volcanic settings. Society of Economic Paleontologists and Mineralogists Special Publication, vol 45, 123–137

Smith RCM (1991b) Post-eruption sedimentation on the margin of a caldera lake, Taupo Volcanic Centre, New Zealand. Sed Geol 74:89–138

Smith RT, Houghton BF (1995) Vent migration and changing eruptive style during the 1800a Taupo eruption: new evidence from the Hatepe and Rotongaio phreatoplinian ashes. Bull Volcanol 57:432–440

Sparks RSJ (1976) Grain size variations in ignimbrites and implications for the transport of pyroclastic flows. Sedimentology 23:147–188

Stelling P, Gardner J, Begét JE (2005) Eruptive history of fisher Caldera, Alaska, USA. J Volcanol Geoth Res 139:163–183

Stilwell WF, Hopkins HJ, Appleton W (1954) Tangiwai railway disaster: report of board of inquiry, Wellington, NZ, 31 p

Stimac JA, Goff F, Counce D, Larocque ACL, Hilton DR, Morgenstern U (2004) The crater lake and hydrothermal system of Mount Pinatubo, Philippines: evolution in the decade after the eruption. Bull Volcanol 66:149–167

Stoopes GR, Sheridan MR (1992) Giant debris avalanches from the Colima volcanic complex, Mexico: implications for long runout landslides (>100 km) and hazard assessment. Geology 20:299–302

Suryo I, Clarke MCG (1985) The occurrence and mitigation of volcanic hazards in Indonesia as exemplified at the Mount Merapi, Mount Kelut and Mount Galunggung volcanoes. Q J Eng Geol 18:79–98

Swift CHI, Kresch DL (1983) Mudflow hazards along the Toutle and Cowlitz rivers from a hypothetical failure of Spirit Lake blockage. U.S. geological survey, water-resources investigation report, vol 82–4125. Tacoma, Washington, 10 p

Taig T (2002) Ruapehu lahar residual risk assessment. TTAC Limited, 77 p. and 8 appendices

Tanguy J-C, Ribière C, Scarth A, Tjetjep WS (1998) Victims from volcanic eruptions: a revised database. Bull Volcanol 60:137–144

Tazieff H (1989) Mechanisms of the Nyos carbon dioxide disaster and of co-called phreatic steam eruptions. J Volcanol Geoth Res 39:109–116

Thiele R, Moreno H, Elgueta S (1998) Quaternary geological-geomorphological evolution of the uppermost course of the Río Laja valley. Rev Geol Chile 25:229–253

Thorarinsson S, Einarsson T, Sigvaldason GE, Elisson G (1964) The submarine eruption off the Vestmann Islands 1963-64. Bull Volcanol 27:434–445

Thouret JC, Abdurachman KE, Bourdier J-L, Bronto S (1998) Origin, characteristics, and behaviour of lahars following the 1990 eruption of Kelud volcano, eastern Java (Indonesia). Bull Volcanol 59:460–480

Tinti S, Pagnoni G, Zaniboni F (2006a) The landslides and tsunamis of the 30th December 2002 in Stromboli analysed through numerical simulations. Bull Volcanol 68:462–479

Tinti S, Maramai A, Armigliato A, Graziani L, Manucci A, Pagnoni G, Zaniboni F (2006b) Observations of physical effects from tsunamis of December 30, 2002 at Stromboli volcano, southern Italy. Bull Volcanol 68:450–461

Tómasson H (1996) The jökulhlaup from Katla in 1918. Ann Glaciol 22:249–254

Tómasson H (2002) Catastrophic floods in Iceland. In: Snorrason Á, Finnsdóttir HP, Moss ME (eds) The extremes of the extremes: extraordinary floods. International Association of Hydrological Sciences publication, vol 271, pp 121–126

Torsvik T, Paris R, Didenkulova I, Pelinovsky E, Belousov A, Belousova M (2010) Numerical simulation of a tsunami event during the 1996 eruption in Karymskoye lake, Kamchatka, Russia. Nat Hazards Earth Syst Sci 10:2359–2369

Turner G, Ingham M, Bibby H (2007) Electrical resistivity monitoring of seepage and stability of the tephra barrier at Crater Lake, Mt Ruapehu, New Zealand. Geophys Res Abstr 9:11630

Tweed FS, Russell AJ (1999) Controls on the formation and sudden drainage of glacier-impounded lakes: implications for jökulhlaup characteristics. Prog Phys Geogr 23:79–110

Umbal JV, Rodolfo KS (1996) The 1991 lahars of southwestern Mount Pinatubo and evolution of the lahar-dammed Mapanuepe Lake. In: Newhall CG, Punongbayan RS (eds) Fire and Mud, eruptions and lahars of Mount Pinatubo. University of Washington Press, Seattle, Philippines, pp 951–970

van Padang MN (1951) Indonesia. Catalogue of active volcanoes of the world including solfatara fields, part I, International Association of Volcanology and Chemistry of the Earth's Interior, Rome, Italy, 271 p

Varekamp JC, Ouimette AP, Herman SW, Bermúdez A, Delpino D (2001) Hydrothermal element fluxes from Copahue, Argentina: a "beehive" volcano in turmoil. Geology 29:1059–1062

Vidal N, Merle O (2000) Reactivation of basement faults beneath volcanoes: a new model of flank collapse. J Volcanol Geoth Res 99:9–26

Voight B, Glicken H, Janda RJ, Douglass PM (1981) Catastrophic rockslide avalanche of May 18. In: Lipman PW, Mullineaux DR (eds) The 1980 eruptions of Mount St. Helens, Washington. United States geological survey professional paper, vol 1250, pp 347–377

Wagner TP, McKee CO, Kuduon J, Kombua R (2003) Landslide-induced wave in a small volcanic lake: Kasu Tephra Cone, Papua New Guinea. Int J Earth Sci 92:405–406

Waitt RB Jr, Pierson TC, MacLeod NS, Janda RJ, Voight B, Holcomb RT (1983) Eruption-triggered avalanche, flood, and lahar at Mount St. Helens—effects of winter snowpack. Science 221:1394–1397

Walder JS, Costa JE (1996) Outburst floods from glacier-dammed lakes: the effect of mode of drainage on flood magnitude. Earth Surf Proc Land 21:701–723

Walder JS, Watts P, Sorensen OE, Janssen K (2003) Tsunamis generated by subaerial mass flows. J Geophys Res 108:EPM 2.1–2.19

Walder JS, Watts P, Waythomas CF (2006) Case study: mapping tsunami hazards associated with debris flow into a reservoir. J Hydraul Eng 132:1–11

Walker GPL (1981) Characteristics of two phreatoplinian ashes, and their water-flushed origin. J Volcanol Geoth Res 9:395–407

Walker GPL, Self S, Wilson L (1984) Tarawera 1886—a basaltic plinian fissure eruption. J Volcanol Geoth Res 21:61–78

Ward RH (1922) A note on the significance of the recent subsidence of the shore of Lake Taupo. NZ J Sci Technol 5:280–281

Ward SN (2001) Landslide tsunami. J Geophys Res 106:11201–11215

Waters AC, Fisher RV (1971) Base surges and their deposits: Capelinhos and Taal volcanoes. J Geophys Res 76:5596–5614

Watts P, Waythomas CF (2003) Theoretical analysis of tsunami generation by pyroclastic flows. J Geophys Res 108(B12):EPM 4.1–4.4.21

Waythomas CF (2001) Formation and failure of volcanic debris dams in the Chakachatna river valley associated with eruptions of the Spurr volcanic complex, Alaska. Geomorphology 39:111–129

Waythomas CF, Neal CA (1998) Tsunami generation by pyroclastic flow during the 3500-year B.P. caldera-forming eruption of Aniakchak Volcano, Alaska. Bull Volcanol 60:110–124

Waythomas CF, Walder JS, McGimsey RG, Neal CA (1996) A catastrophic flood caused by drainage of a caldera lake at Aniakchak Volcano, Alaska, and implications for volcanic-hazards assessment. Geol Soc Am Bull 108:861–871

Webb TH, Ferris BG, Harris JS (1986) The Lake Taupo, New Zealand, earthquake swarms of 1983. NZ J Geol Geophys 33:377–389

Wei H, Sparks RSJ, Liu R, Fan Q, Wang Y, Hong H, Zhang HW, Chen H, Jiang C, Dong J, Zheng Y, Pan Y (2003) Three active volcanoes in China and their hazards. J Asian Earth Sci 21:515–526

Wei H, Hong H, Sparks RSJ, Walder JS, Han B (2004) Potential hazards of eruptions around the Tianchi caldera lake, China. Acta Geol Sinica 78:790–794

White JDL (1996) Impure coolants and interaction dynamics of phreatomagmatic eruptions. J Volcanol Geoth Res 74:155–170

White JDL, Houghton BF, Hodgson KA, Wilson CJN (1997) Delayed sedimentary response to the A.D. 1886 eruption of Tarawera, New Zealand. Geology 25:459–462

Williams H (1941) Calderas and their origins. Univ Calif Bull Geol Sci 25:239–346

Wilson CJN (1993) Stratigraphy, chronology, styles and dynamics of late Quaternary eruptions from Taupo volcano, New Zealand. Philos Trans R Soc Lond A343:205–306

Wilson CJN (2001) The 26.5 ka Oruanui eruption, New Zealand: an introduction and overview. J Volcanol Geoth Res 112:133–174

Wilson CJN, Walker GPL (1985) The Taupo eruption, New Zealand. I. General aspects. Philos Trans R Soc Lond A314:199–228

Wilson CJN, Riggs NR, Ort MH, White JDL, Houghton BF (1997) An annotated atlas of post-1.8 ka shoreline features at Lake Taupo, New Zealand. Institute of Geological and Nuclear Sciences, Science Report, vol 97, no 19, Lower Hutt, New Zealand, 35 p

Witham CS (2005) Volcanic disasters and incidents: a new database. J Volcanol Geoth Res 148:191–233

Wohletz KH (1986) Explosive magma-water interactions: thermodynamics, explosion mechanisms, and field studies. Bull Volcanol 48:245–264

Wolfe BA, Begét JE (2002) Destruction of an Aleut village by a catastrophic flood release from Okmok caldera, Umnak Island, Alaska. In: Proceedings of GSA Denver annual meeting. Division of Geological and Geophysical Surveys, Denver, CO

Yasui M, Koyaguchi T (2004) Sequence and eruptive style of the 1783 eruption of Asama Volcano, central Japan: a case study of an andesitic explosive eruption generating fountain-fed lava flow, pumice fall, scoria flow and forming a cone. Bull Volcanol 66:243–262

Youd TL, Wilson RC, Schuster RL (1981) Stability of blockage in North Fork Toutle river. In: Lipman PW, Mullineaus DR (eds) The 1980 eruptions of Mount St. Helens, Washington. United States Geological Survey Professional Paper 1250, pp 821–828

Zen MT, Hadikusumo D (1965) The future danger of Mt. Kelut (eastern Java—Indonesia). Bull Volcanol 28:275–282

Mechanisms of Crater Lake Breaching Eruptions

Dmitri Rouwet and Meghan M. Morrissey

Abstract

In this chapter we review physical models on phreatomagmatic, phreatic, hydrothermal, and geyser-like eruptions and, for the first time, place them in a crater lake context. Examples of known crater lake systems for the different eruption types are provided. Besides the direct injection of a fresh magma into a crater lake, leading to phreatomagmatic activity, a crater lake is a strong condensing medium, sensitive to sudden pressure changes when injected by gas-vapor batches, which can lead to non-magmatic, though violent eruptions. The implosive nature, the role of the heat pipe and molten sulfur pool at the lake bottom are central in the phreatic eruption model. Contrary to phreatic eruptions, hydrothermal eruptions are instigated by a sudden pressure drop, causing boiling and vapor release, rather than by the input of a gas-vapor phase of magmatic origin. Geyser-like activity beneath or near crater lakes is analog to classic geysering, and becomes more obvious when lake water level is low. Although not explosive, the peculiar lake drainage and refill cycles of two lakes are discussed. The first outcomes of numerical simulation approaches help to better quantify injection pressure and vapor/liquid proportions of the input fluid. We stress that the various manifestations of eruptive activity at crater lakes is not necessarily linked to changes in magmatic activity, which could lead to misleading interpretations regarding volcano monitoring.

Keywords

Crater lake eruptions · Phreatic eruptions · Phreatomagmatic eruptions · Hydrothermal eruptions · Geyser-like activity · Volcano monitoring

D. Rouwet (✉)
Istituto Nazionale di Geofisica e Vulcanologia,
Sezione di Bologna, Bologna, Italy
e-mail: dmitri.rouwet@ingv.it

M.M. Morrissey
Formerly Colorado School of Mines,
Golden, CO, USA

D. Rouwet et al. (eds.), *Volcanic Lakes*, Advances in Volcanology,
DOI 10.1007/978-3-642-36833-2_3,
© Springer-Verlag Berlin Heidelberg 2015

1 Introduction

Despite the fact that only 8 % of the reported volcanic eruptions occured in a subaqueous setting, they have caused 20 % of the fatalities (Mastin and Witter 2000). Even more than shallow sea water, a proto-type setting for such eruptive activity is an active crater lake. An active crater lake can be defined as a water body in a crater structure topping a volcano, affected by magma degassing and dynamical fluid circulation (Christenson et al. 2015). Active crater lakes are generally hot, acidic brines (Pasternack and Varekamp 1997; Varekamp et al. 2000; Rouwet et al. 2014; Varekamp 2015), which are thought to preserve physical and chemical markers related to the variations in activity of the underlying magmatic-hydrothermal system. The goal of most studies on active crater lakes is to find the key precursor for explosive eruptive activity. Notwithstanding thorough insights in crater lakes' dynamic behavior, it is honest to note that lake breaching eruptions were often "surprise events" (Christenson et al. 2007, 2010; Jolly et al. 2010), not necessarily due to the lack of monitoring information but rather due to the intrinsic complexity of crater lake systems and speed of fluid cycling.

Because of the high compressibility of gas, a gas reservoir buffers pressure changes by sudden inputs of new gas-vapor batches. On the other hand, a crater lake or liquid-dominated hydrothermal system, which are strong condensing media, are sensitive to sudden pressure drops when injected by gas-vapor batches, eventually leading to eruptions. When an eruption occurs at crater lakes, it is subaqueous and either phreatomagmatic, phreatic, hydrothermal or geyser-like. This chapter will review the various eruption mechanisms related to active crater lakes.

A phreatomagmatic eruption produces ejecta (fluids and juvenile solids) of magmatic origin (Belousov and Belousova 2001; Manville 2015). It has magmatic gases, lake sediments and water mixed in. In spite of many studies since the 1940s, an unambiguous nomenclature of what a "phreatic eruption" actually is does not exist (Stearns and McDonald 1949; Muffler et al. 1971; Nairn and Wiradiradja 1980; Hedenquist and Henley 1985; Barberi et al. 1992; Mastin 1995; Browne and Lawless 2001). Although phreatic eruptions do not expel large volumes of solid material, they are often more violent than magmatic or phreatomagmatic eruptions (>130 m/s eruption velocity, Mastin 1995; Kilgour et al. 2010). For an eruption to be phreatic, heated groundwater and the related vapor phase is the driving agent (Stearns and McDonald 1949), but the input of mass and energy derived from magma is thought to be the trigger (Browne and Lawless 2001). Hydrothermal eruptions specifically involve pre-existing hydrothermal systems (Mastin 1995), but are generated after the sudden generation of steam, probably due to pressure drop, rather than fluid input (Browne and Lawless 2001; Shanks et al. 2005; Morgan et al. 2009; Kiryukhin et al. 2012). More exotic names of non-juvenile eruptions, such as "hydroexplosions", "steam-blast eruptions", "boiling-point eruptions", "gas-driven eruptions" and "mixing eruptions", are introduced to detail specific eruption mechanisms (Barberi et al. 1992; Mastin 1995), but often create ambiguity.

The main focus of this chapter is to understand the physical processes behind crater lake eruptions by studying field observations, and by physical and numerical modeling investigations. We review existing literature on the four eruption types mentioned above and place them in a crater lake context. Some insights from numerical modeling can elucidate eruption physics in heterogeneous crater lake systems (Morrissey et al. 2010). A few tips on how to recognize key precursory signals of the different eruption types are provided.

2 Physical Mechanisms of Crater Lake Breaching Eruptions

2.1 Phreatomagmatic Eruptions

One of the first well-documented observations of phreatomagmatic eruptions is from the 1963 eruption of Surtsey off the coast of Iceland, near

the Westmann Islands (Thorarinsson 1967). Published accounts of the eruptions characterize them as short-lived, discrete explosions followed by an upward rush of black tephra-laden masses and ballistic material (Kokelaar and Durant 1983). Tephra jets have a variety of directions with some spreading into so-called cockscombs (Fig. 1a, b) and others are limited in spreading resulting in a cypress tree shape (Kokelaar 1983). Depending on frequency and duration of each eruption, sustained ash columns form by a continuous up-rush of material. All explosive activity occurr without noticeable sound (Thorarinsson 1967; Kokelaar 1983). Also noted are concentric waves emanating from the center of volcanic activity without the need of explosive activity.

Since the eruption at Surtsey, several subaqueous phreatomagmatic eruptions have been observed: the 1995–1996 and 2007 Ruapehu Crater Lake eruptions in New Zealand (Christenson 2000; Kilgour et al. 2010) (Fig. 1a), the 1996 eruption at Karymskoye Lake in Kamchatka (Belousov and Belousova 2001), the 2000 and 2012 Copahue eruptions in

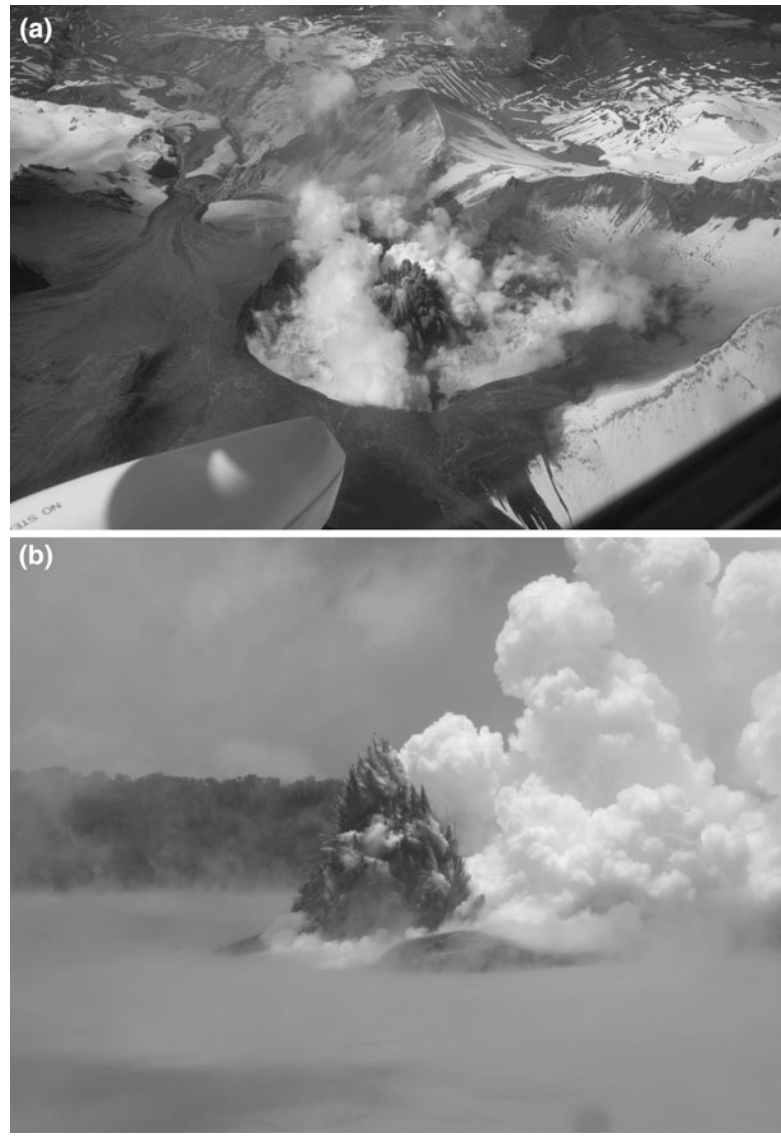

Fig. 1 Cockscomb of Surtseyan eruptions at **a** Ruapehu volcano, New Zealand, during the early stages of the 1995–1996 phreatic-phreatomagmatic eruption sequence (24 September 1995, picture by Tony Hurst), and **b** Lake Voui, Ambae Volcano, Vanuatu, during the November–December 2005 phreatomagmatic eruption (picture by Karoly Németh)

Argentina-Chile (Varekamp et al. 2001; Agusto et al. 2013), the 2000–2007 Kavachi eruptions in the Solomon Islands (Baker et al. 2002), the 2005 eruption at Lake Voui of Manaro Volcano (Ambae Island, Vanuatu; Németh et al. 2006; Bani et al. 2009), and very recently, the November 2013 Nishinoshima eruption (Japan) (Fig. 1b). The features of these subaqueous eruptions are similar to those observed during the eruption at Surtsey, such as the discrete, tephra laden jets that form surges from their collapse associated with expanding steam bubbles or copulas. Surtseyan eruptions that occur in a shallow subaqueous environment (<100–200 m depth) and involve basaltic magma produce characteristic monogenetic tephra rings or cones (Thorarinsson 1967; Belousov and Belousova 2001; White et al. 2003; Németh et al. 2006). These landforms are comprised of tephra fallout deposits and pyroclastic density current deposits and are frequently underlain by pillow lava (Jones 1970). During the eruptions at Lake Voui on Ambae Island in 2005, a tuff cone was constructed from material deposited from subaerial tephra jets commonly 200 m high (Fig. 1b). These produced the fall deposits whereas eruptions from the same underwater vent that did not breach the lake surface produced subaqueous pyroclastic density current deposits (Németh et al. 2006). Base surges were also common features that accompanied tephra jets and were observed to travel over 300–500 m from the vent (Németh et al. 2006).

The eruption at Karymskoye Lake in 1996 is one of the best-documented subaqueous eruptions since Surtsey that includes an hour-long video record 2 h into the eruption and excellent field data (Belousov and Belousova 2001). The Karymskoye Lake eruption lasted only 10–20 h and produced a tuff ring on the northern edge of the lake. Preliminary field studies demonstrate that the tuff ring is comprised of 100–200 lapilli tephra layers (Kokelaar 1986; Belousov and Belousova 2001; Németh et al. 2006). The tuff ring deposits comprise 95 % of the volume of material erupted during the 10–20 h long eruption with each layer produced from a single explosion (Belousov and Belousova 2001).

Figure 2, although based on recent Poás phreatic eruptions, does show the same features as the Surtseyan eruption model by Belousov and Belousova (2001). The basic ideas of the Belousov and Belousova (2001) model may be described in four steps. Step (1) assumes that basaltic magma ascends to the surface through a fissure that breaks the surface at the edge of the ice covered lake. The initial eruption is a vent clearing phreatic explosion that ejects blocks of ice and country rock. This phase is followed by a series of 100–200 Surtseyan explosions. The explosions are thought to occur in the vent and not deeper in the conduit based on the vesicularity of tephra. Step (1) of the eruption process involves vesiculation of basaltic magma in the conduit from which bubbles form that expand in the magma as it nears the surface. No external water interacts with magma until it reaches the vent. Rapid ascent, growth and coalescence of bubbles force magma into the vent where magma fragmentation (bubble burst) occurs similar to the fluid of a typical Strombolian eruption. During Step (2) fragmented magma is injected into the water and slurry filled vent at the bottom of the crater lake where it experiences a second stage of fragmentation due to water-magma interaction. Step (3) involves the ejection of the phreatomagmatic gas and tephra mixture through the lake creating a bulge at the lake surface. The gas-tephra mixture penetrates through the bulge and breaks the lake surface forming a cockscomb jet (Fig. 2a). Step (4) is the collapse of the jet on to the lake surface forming a water-rich, base surge that moves radially from the vent (Fig. 2b, c). Gravitational settling forms a density current that produces a layer of lapilli at the bottom of the lake while the fines material are transported by the surge. Each explosion produces another lapilli layer that gradually build-up the tuff ring.

Surtseyan is mostly used as a classifying term, now familiar to most volcanologists. Is this term all inclusive? As shown by the similarity of the physical manifestations (Fig. 2), can we exclude if a Surtseyan eruption is phreatomagmatic or rather only phreatic in nature?

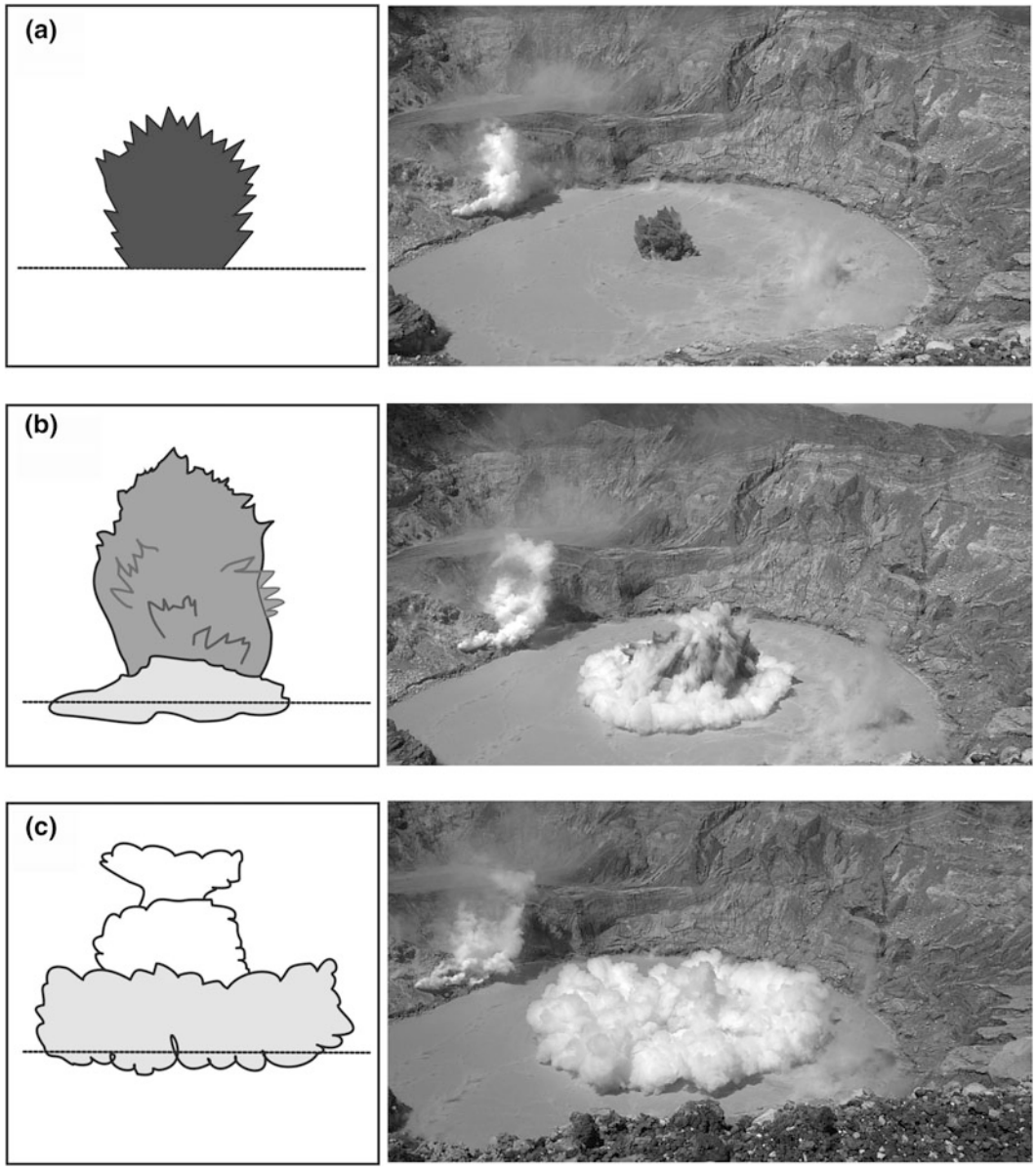

Fig. 2 Illustrative sketch and pictures of phreatic and phreatomagmatic eruption dynamics during the 2006–ongoing phreatic eruption cycle of Poás volcano, Costa Rica (pictures by Ana Belén Castro). The model is modified from Belousov and Belousova (2001). **a** Slurry filled vent masses, lake sediments and eventually fragmented magma (in case of a phreatomagmatic eruption) is injected into the water at the *bottom* of the crater lake and out of the lake at the surface as a bulge. **b** The gas-tephra/sediment mixture penetrates through the bulge and breaks the lake surface forming a cockscomb. **c** The collapse of the jet on to the lake surface forms a water-rich, base surge that moves radially from the crater lake

2.2 Phreatic Eruptions

Following Browne and Lawless (2001), a phreatic eruption is probably instigated by the direct input of mass and heat of magmatic origin, although without the magma itself being involved. Gas exsolved from a crystallizing magma during upward migration can already be sufficient to trigger a "gas eruption" (Burnham 1979; Mastin 1995). Such eruption mechanism can escalate into phreatomagmatic eruptions (Barberi et al. 1992), or can be paired with dome extrusion (e.g. Mount St. Helens post-1980 dome activity, Mastin 1994). Phreatic eruptions lack the above Step (2)—the injection of fragmented magma into the lake- of the phreatomagmatic eruption model, charged with non-juvenile material eruption columns though appear extremely similar in morphology (Fig. 2b).

Eruptions are often considered explosions, although counterintuitively, a decompression from hydrostatic to atmospheric pressure intrinsically implies an *implosion*. Moreover, for highly active and acidic crater lakes (e.g. Laguna Caliente, Poás in Costa Rica; Ruapehu in New Zealand, Copahue in Argentina-Chile; Aso in Japan) all entering gas species are physically or chemically "quenched" in the lake water, by condensation (vapor, the most abundant species) or hydrolysis of acidic gases (SO_2 and H_2S as SO_4^{2-}, HCl as Cl^-, and HF as F^-), or are released "peacefully" and unaffected at the lake surface by bubbling or diffusive degassing (Mazot et al. 2011; Mazot and Bernard 2015) (the second most abundant gas CO_2, and inert and poorly soluble gases such as N_2, CH_4, H_2, CO and the noble gases). This practically sudden complete loss of gas mass ($n.R.T \rightarrow 0$, as $n \rightarrow 0$, following the ideal gas law, with R the gas constant, 8.3145 J mol^{-1} K^{-1}, and T the temperature in K) reduces the volume or the pressure of the original gas-vapor pocket to 0 ($P.V = n.R.T \rightarrow 0$, so $V \rightarrow 0$, or $P \rightarrow 0$, considering T constant, at least initially), stating the implosive nature of phreatic "explosions".

Crater lakes and their underlying hydrothermal systems are heterogeneous physical entities, testified by: (1) fluid cycling of lake water in concomitant upward flow of steam and downward flow of liquid (heat pipe mechanism; White et al. 1971; Hurst et al. 1991; Christenson and Wood 1993), (2) the eventual presence of a molten sulfur pool at the lake bottom (Toraishi and Tominaga 1940; Hurst et al. 1991; Rowe et al. 1992; Delmelle and Bernard 1994, 2015; Pasternack and Varekamp 1994; Takano et al. 1994, 2008; Ohba et al. 2008), and (3) highly variable lake volumes, and thus variable hydrostatic loading, due to seasonal rainfall contributions or strong evaporation. The latter feature is visible and quantifiable (see Hurst et al. 2012 for a thorough review), and may eventually be used as a guideline: evaporation is the major process and only non-eruptive surface manifestation of heat and energy dissipation, resulting from the underlying fluid flushing.

Besides the "steam devils", evaporation clouds swirling over the lake surface (Hurst et al. 2012), the processes occurring at the crater lake surface largely depend on the input dynamics of fluid and heat at the lake bottom. Floating sulfur spherules at the lake surface are tiny testimonies of the presence of a molten sulfur pool at the lake bottom. Such sulfur pools are a lot less voluminous than the lake itself, nonetheless, they have demonstrated to play a major role in phreatic eruptive activity at crater lakes (Hurst et al. 1991; Takano et al. 1994). Subaqueous fumaroles vent sulfur species into the lake (i.e. SO_2 and H_2S); some of the species are absorbed into the lake water as sulfate or thiosulfates, while for temperatures >119 °C, elemental sulfur remains as a molten sulfur pool at the lake bottom (Delmelle and Bernard 2015) (Fig. 3a). The rising gases flush through the molten sulfur pool, transporting hollow tailed yellow S-spherules to the lake surface.

Yellow sulfur spherules on the lake surface suggest a preceding vent clearing event, to restore a more dynamic fluid circulation between the lake bottom and underlying hydrothermal system (Fig. 3a). During such open-vent situations, recycling of crater lake water is a fact, as suggested by Hurst et al. (1991) based on an energy and mass balance of Ruapehu Crater Lake. Only 50 % of the heating of the lake since

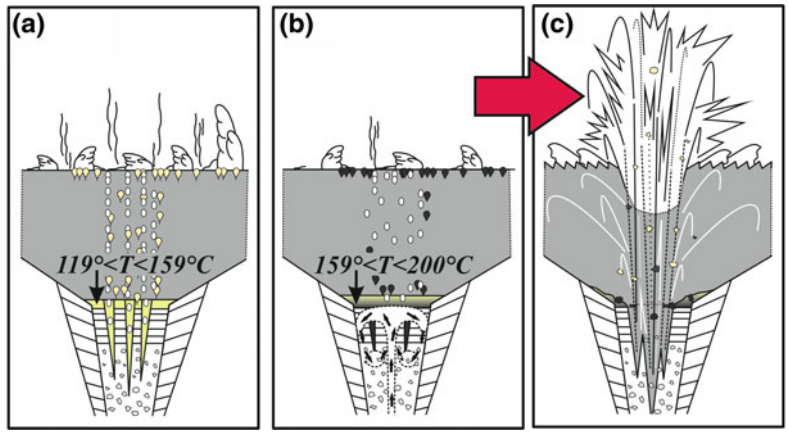

Fig. 3 Conceptual model of phreatic eruption dynamics (modified from Takano et al. 1994). **a** An "open-vent" system: SO_2–H_2S bearing gases with a temperature between the melting point of elemental sulfur (119 °C) and 159 °C enter the lake leaving a molten sulfur pool at the lake *bottom*, testified by tailed *yellow* sulfur spherules floating on the lake surface. **b** A "sealed-vent" system: if the temperature of the entering gases increases to above 159 °C the sulfur pool increases its viscosity, resulting in the sealing of the vent system. The higher temperature is proven by impurities (sulfites) in the molten sulfur pools, testified as *black* untailed sulfur slicks floating on the lake surface. **c** A sealed system inhibits the efficient energy (heat) and mass (vapor-liquids) dissipation through the crater lake, resulting in a pressure build-up beneath the vent sealing and eventually a phreatic eruption. The unsealed vent, breached by the eruption, restores its more efficient fluid circulation (back to **a**)

the 1980s results from the direct input of steam, the other 50 % is accounted for by the seepage-reheating-reinjection of the crater lake water itself (i.e. heat pipe mechanism, Fig. 5). Heating episodes (Werner et al. 2006) enhances evaporation from the lake and probably states an open-vent circulation of fluids, and thus a lower probability of occurrence of phreatic eruptions. During periods of lake unrest, cooling episodes and less evaporation indicate an inefficient heat and mass dissipation in a sealed-vent system, increasing the probability of a phreatic eruption. The presence of sulfur and related species in eruptive products (anhydrite, gypsum, natroalunite, pyrite, marcasite, jarosite; Hurst et al. 1991; Christenson et al. 2010; Delmelle and Bernard 2015; Henley 2015), and sulfur pools and "volcanoes" at a dried lake bottom (Oppenheimer and Stevenson 1989; Oppenheimer 1992) suggests its role as sealing agents in phreatic activity and heat dissipation.

When the molten sulfur pool is heated and "contaminated" with impurities of mainly pyrite, black sulfur spherules are observed at the lake surface (Delmelle and Bernard 1994; Takano et al. 1994; de Ronde et al. 2015). This process takes place when higher temperature gases (>150 °C) pass through the cooler molten sulfur pool (~120 °C) (Fig. 3b). Temperature can modify the physical properties of the sulfur pool: pure sulfur becomes 2,000 times more viscous at temperatures from 159° to ~200 °C (Hurst et al. 1991; Oppenheimer 1992; Takano et al. 1994). The presence of a higher viscosity body could thus imply vent sealing. Nevertheless, in reality sulfur pools are rather highly contaminated ore-bearing deposits rich in sulfites (Brantley et al. 1987; Delmelle and Bernard 1994; Hedenquist and Lowenstern 1994; Henley 2015), and the temperature-viscosity relation must be interpreted with caution. Fact is that the presence of black sulfur spherules indicate a higher temperature of entering fluids, higher metal content in the sulfur pool, and a higher possibility for gas to remain trapped inside or below the high-viscosity sulfur pool. This self-sealing of the vent stimulates pressure build up beneath the sulfur pool (Fig. 3b), eventually leading to phreatic eruptions (Fig. 3c).

During the 2006 ongoing phreatic eruption cycle at Poás volcano (Costa Rica), many, if not all these sulfur features have been observed. In May 2005, molten sulfur flowed out of a fumarole north of Laguna Caliente crater lake. A few months later, yellow sulfur spherules floated on the lake, which was steadily heated from 22° to 58 °C. Enhanced evaporation was observed. In March 2006, phreatic eruptions resumed after almost 12 years of quiescence. Black mats of sulfur spherules covered the lake surface following the eruptions (Fig. 4, April 2007). After the pre-eruptive heating the lake water temperature remained high (from ~40 to ~60 °C) throughout the entire period, and demonstrated a cyclic behavior. Until June 2010, periods of higher evaporation rates often coincided with eruptive quiescence; lower evaporation rates with phreatic eruptions (Fig. 3). A Mw 6.2 tectonic earthquake near Poás volcano (8 January 2009) triggered phreatic eruptions 4 days later, probably disturbing the already delicate system and leading to more violent phreatic eruptions since September 2009 (following Manga and Brodsky 2006). Eruption frequency strongly increased since June 2010. From 2005 until 2014, the lake level dropped continuously for a total of ~40 m. The lower hydrostatic loading of the lake in more recent years is probably a contributing factor and a reason why the eruptions have become more dynamic, and probably will become more frequent in the future. Despite the fact that the proposed theory above seems to fit the ongoing phreatic activity at Poás, as eruption frequency increases data gathering has to increase (sampling time ≪ inter-eruptive time, so, toward continuous monitoring; Rouwet et al. 2014) to be able to eventually forecast single phreatic eruptions at Poás.

Fig. 4 *Black* sulfur-sulfite mats floating on Poás' Laguna Caliente, probably indicating post eruptive venting from the lake *bottom* in the *middle* of the lake (April 2007, picture by Dmitri Rouwet)

2.3 Hydrothermal Eruptions

Contrary to phreatic eruptions, hydrothermal eruptions do not result from any direct input of mass or energy directly derived from magma (Browne and Lawless 2001). Hydrothermal eruptions in hot water or steam-dominated hydrothermal systems are generated near-surface due to the phase transition from liquid to steam following a sudden pressure drop. At temperatures below the critical point of water, a single liquid phase is able to provide more energy to a hydrothermal eruption than a steam-dominated phase does, making the boundary between a crater lake and the underlying system extremely prone to hydrothermal eruption activity (Browne and Lawless 2001).

A sealing cap rock is not needed to generate such triggering overpressure regimes, nor the pressure within the reservoir necessarily must exceed the hydrostatic pressure of the overlying water column (i.e. in active crater lakes). The erupted products never contain juvenile magmatic material, but rather are poorly sorted, matrix-supported breccias of hydrothermally altered material, pointing to fast settling rates. Hydrothermal eruption deposits are generally of low volume ($<10^5$ m^3), although large volume deposits have been recognized (Browne and Lawless 2011, and reference therein).

From the deposits, it is often hard to distinguish whether the non-magmatic eruptions breaching crater lakes are hydrothermal or phreatic in nature, as both eruption types imply the absence of juvenile material, and, for more energetic eruptions, the ejection of altered material from the underlying hydrothermal system (e.g. lake bottom sediments) (Shanks et al. 2005; Morgan et al. 2009). A possible means to distinguish between a hydrothermal and phreatic eruption from beneath a crater lake could be the chemical and isotopic composition of the post- or eventually pre-eruptive crater lake water (Truesdell et al. 1977; Rouwet et al., in prep.). Hydrothermal eruptions vent an isotopically light, Cl–SO_4-poor steam into the crater lake, while phreatic eruptions could rather be triggered by the input of an isotopically heavy, Cl–SO_4-rich liquid phase. At this moment, this is only a working hypothesis.

For hydrothermal systems topped by a crater lake, the hydrostatic pressure is determined by the weight of the crater lake itself. The necessary differential pressure decrease to trigger a hydrothermal eruption can be caused be sudden lake level drops, e.g., by enhanced evaporation, seepage, or the expulsion of lake water by previous eruptions. Hydrothermal systems related to active crater lakes are often in a near-disequilibrium and heterogeneous physical state; sudden minor confining pressure drops in this sensitive system at any depth or place can be enough to initiate subsurface boiling which eventually leads to a hydrothermal eruption. Moreover, hydrodynamic circulation near the lake bottom of colder and denser lake water infiltrating into the underlying heat pipe (Hurst et al. 1991) can lead to venting of hot fluids subject to a sudden pressure drop forced to boiling.

Bi-phase (liquid-vapor) and vapor-only regions underlay active crater lakes (Fig. 5). With a magma degassing at shallow depth, the abundant steam (the most abundant "gas" phase in magmatic gases) will easily condense when reaching the more liquid-dominated shallow parts of the hydrothermal system, while the incondensable gas phase will not, creating gas pockets beneath the lake. Besides direct "gas explosions", the sudden condensation of the vapor phase will lead to a drastic pressure drop, consequent boiling and eventually a hydrothermal explosion. This effect is most significant for highly active crater lakes (e.g. Laguna Caliente, Poás and Rincón de la Vieja, Costa Rica; Ruapehu, New Zealand; Copahue, Argentina-Chile) with extremely high acidities, making these systems "transparent" to CO_2, the most abundant species in a water-free magmatic gas, increasing the pressure drop effect. For less acidic crater lake systems (e.g. Pinatubo and Taal, Philippines; pre-2007 Kelud, Indonesia), increasing amounts of dissolved gases (mainly CO_2) in water causes the water to boil at lower temperatures, eventually speeding up the eruption dynamics, although fluid cycling at such

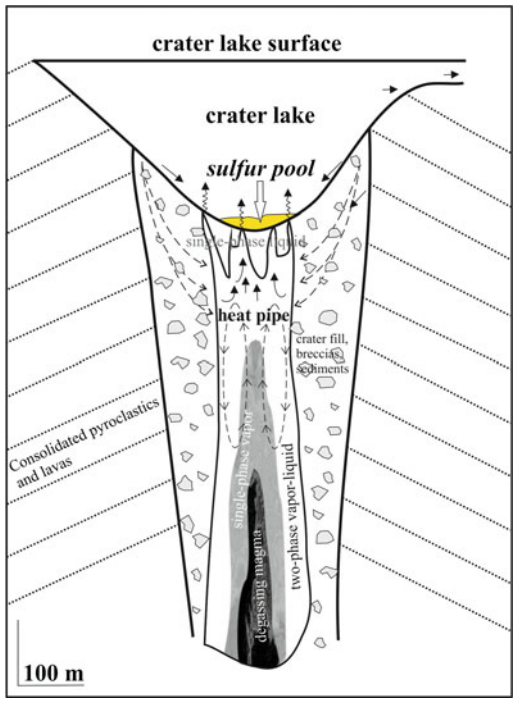

Fig. 5 Sketch of a hypothetical crater lake and underlying conduit system: the heat pipe model (simplified from Christenson and Wood 1993). At the base of the crater lake an impermeable layer is composed of a liquid sulfur pool (see Fig. 4) and mineralization of secondary minerals (Christenson et al. 2010). The top of the heat pipe is saturated with fluids (single-phase liquid, in grey), capable of scrubbing acidic magmatic gases and condensing rising vapor, while being transparent for CO_2 and low-soluble gases (e.g. He). The base of the heat pipe consists of a single-phase vapor region at the base and condensation front. Volatile storage likely occurs in this single-phase vapor region. The single-phase liquid region and single-phase vapor region is separated by a two-phase liquid/vapor region, where infiltrating lake water is reheated, mainly by vapor condensation. Magmatic volatiles and heat is released from a cooling and crystallizing magma at depth. Deep volatile storage possibly occurs below the brittle/plastic zone at the *top* of the magma

lakes is often too low to enter in eruption. CO_2-dominated volcanic lakes are less prone to a sudden change in thermal input into the lake, as their bottom waters become gas-rich by the regional input of CO_2-laden ground waters (i.e. Nyos-type lakes, Tassi and Rouwet 2014; Kusakabe 2015; Kling et al. 2015; Vaselli et al. 2015).

2.4 Geyser-like Eruptions

As for hydrothermal eruptions, geyser eruptions (from the Icelandic word "geysir") are boiling-point eruptions, but water expulsion is cyclic, and no solids are involved (Mastin 1995). These generally non-violent eruptions occur when a buried fluid near boiling conditions is depressurized leading to the creation of a bi-phase, liquid-vapor mixture, expansion and, finally, explosion (White 1967; Kieffer 1984). If we assume a constant water recharge and heating during intereruptive periods, what does actually change the pressure gradient to make the liquid boil, leading to cyclic geyser eruptions? An intrinsic property of the geyser plumbing system is its discontinuous geometry and/or permeability (Kieffer 1984; Ingebritsen and Rojstaczer 1993, 1996). This leads to a discontinuous rise in water level within the conduit, and thus a step-wise variation in hydrostatic pressure: resulting from Bernouilli's law, boiling will eventually occur when large cavities (or higher permeable zones, e.g. fractured zones) are filled slowly, while boiling will be suppressed when narrow conduit (or less permeable) parts are quickly filled (Steinberg et al. 1981, 1982a, b, c; Kieffer 1984; Ingebristen and Rojstaczer 1993). The initial water burst or steam flashing (i.e. "flash boiling"; Fournier 1969) during geyser preplay and unsteady flow regime will lead to sudden pressure drop of the near-surface water mass in the conduit, triggering a steady flow, high column geyser eruption (Kieffer 1984; Dowden et al. 1991). Classical geyser eruptions (e.g. Old Faithful, Yellowstone NP, Wyoming, USA; Kieffer 1984) have a duration of 1.5–5.5 min with intereruptive periods of ~50 to ~75 min.

Analog geyser-like geometries can exist in hydrothermal systems underneath crater lakes. Real geyser conduits are rather constricted, sintered vents, while vents at crater lakes are less well defined in time and space. Based on an energy balance of the 1985–1988 Laguna Caliente (Poás volcano, Costa Rica), Brown et al. (1989) and Dowden et al. (1991) concluded that frequent (every 10 min) and short (10 s) geyser-like

eruptions offered an efficient means to dissipate energy from the lake. Overlying liquid water will be disrupted when a submerged vent or fumarole, filled with vapor under pressure that will become unstable as steam accumulates, is followed by a pressure release paired with the water ejected upward (Dowden et al. 1991). It is noteworthy that Laguna Caliente passed a phase of lake level drop, due to enhanced evaporation that steadily decreased hydrostatic pressure, teasing the underlying system with near-boiling conditions. During complete dry-out of the lake in 1989, Poás exhibited nearly continuous geysering (Dowden et al. 1991). Since 2010, Laguna Caliente exhibits a similar behavior. It sounds reasonable that the ongoing periodical fluid injections in more peaceful manner into Laguna Caliente during intereruptive periods of more powerful phreatic or hydrothermal eruptions, are controlled in some way by this geyser-like mechanism. When crater lake level drops, geyser eruption height lowers (Dowden et al. 1991). Consequently, the more powerful eruptions observed at a crater lake, which can easily destroy geyser plumbing systems, are rather phreatic or hydrothermal. Strong enough ground shaking due to proximal or distal tectonic earthquakes can also considerably modify the geyser periodicity (Ingebritsen and Rojstaczer 1993, 1996; Brodsky et al. 1998, 2003; Manga and Brodsky 2006; Alvarado 2010).

A less intense geyser activity is observed north of the El Chichón crater lake (Chiapas, Mexico) (Fig. 6a). This "Soap Pool" geyser (Taran et al. 1998) is the main reason why the El Chichón crater lake actually exists (Rouwet et al. 2004, 2008). Several months of water discharge (10–30 kg/s, Fig. 6b) toward the lake alternate rather long periods (up to 2–3 years) of pure vapor exhalation from the same subaerial vent (Fig. 6c). It is not known if the reactivation of the water expulsion from the Soap Pool geyser occurs violently, or not. Nevertheless, the vent does not manifest any mechanical rupture, suggesting that the emission of water takes place gradually. The geyser probably taps a superficial aquifer with a presumed volume in the order of

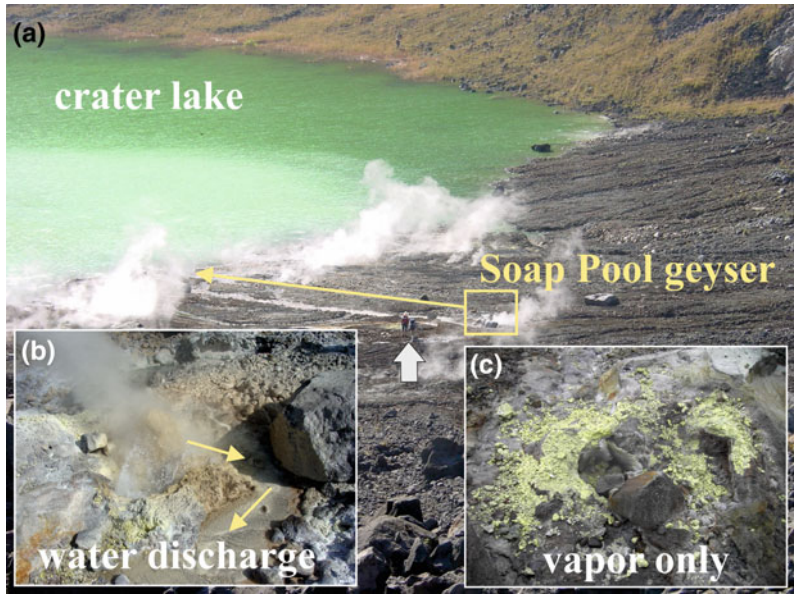

Fig. 6 **a** The Soap Pool geyser (*yellow square*) on the northern shore of El Chichón crater lake, Chiapas, Mexico. Note the persons for scale (*white arrow*) (March 2004, picture by Salvatore Inguaggiato). **b** Water discharge from the same Soap Pool geyser, discharging towards the crater lake (*yellow arrows*, such as in **a**) (November 2009, picture by Yuri Taran). **c** Exhalation of vapor only from the Soap Pool geyser (November 2006, picture by Mike Cassidy)

10^5 m^3, similar as the lake itself (Rouwet et al. 2008), and seems to be connected with the same aquifer feeding thermal springs on the volcano flanks, ~250 m lower (Peiffer et al. 2011). The "buried lake" of Rouwet et al. (2008) eventually is a fractured, heterogeneous porous medium (Fournier 1969), rather than a "U-shaped" cavity with a well-defined sealed steam cap. The extremely long periodicity of the Soap Pool geyser (years) probably states a larger reservoir volume, a longer meteoric recharge time, and a slower heating process to reach critical temperature and pressure, before eruption. Besides this geyser-like activity, El Chichón crater lake is not subject to any type of eruptions since the 1982 Plinian eruptions.

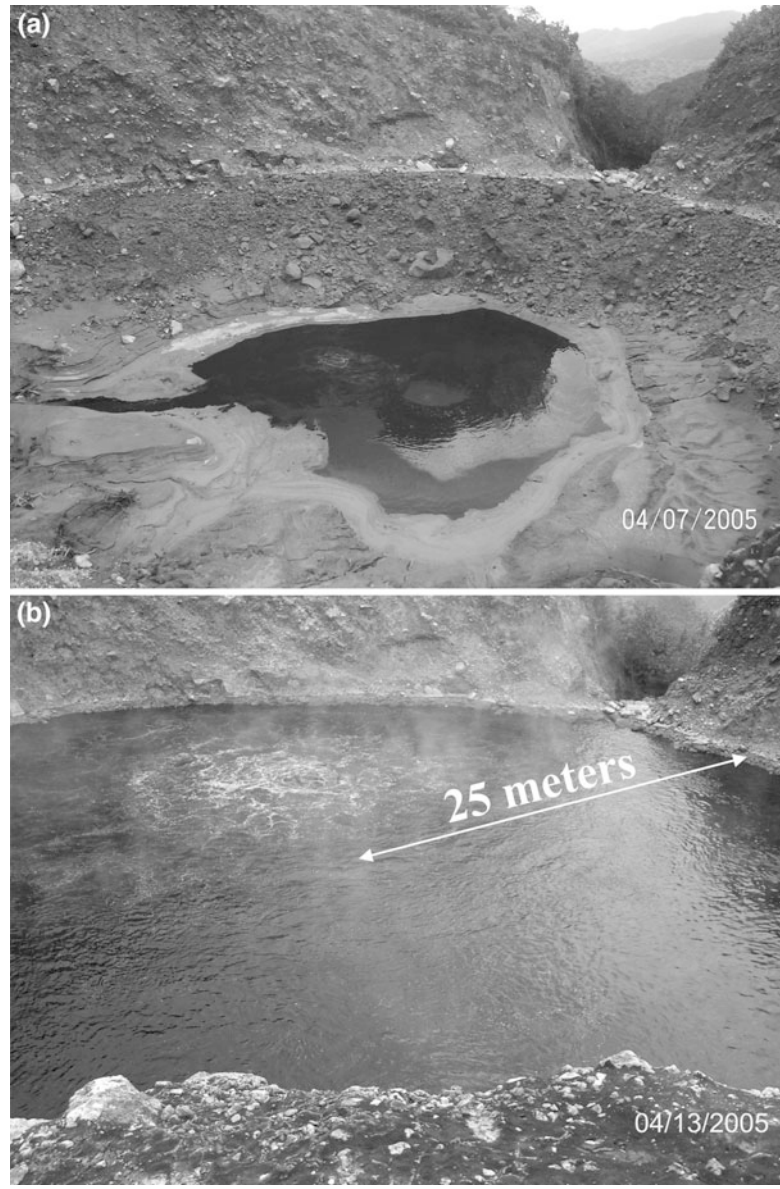

Fig. 7 Boiling Lake, Dominica, during a period of unusual activity at the lake where water levels and geothermal activity were rapidly fluctuating. **a** Rapid draining of the lake (7 April 2005), followed by **b** rapid refilling of the lake (13 April 2005). The volume difference between the empty and full lake is in the order of 10^5 m^3 (pictures by Arlington James, Forestry Officer, Forestry and Wildlife Division, Dominica, used with permission of Erouscilla Joseph)

3 Non-eruptive Unstable Draining Lakes

A spectacular, although less explosive demonstration of the delicate physical state beneath crater lakes is manifested when a denser liquid layer (a lake) is placed atop a gas-filled or multi-phase layer (vent system). The best examples are Boiling Lake (Dominica; Fournier et al. 2009, Fig. 7) and Inferno Crater Lake (Waimangu Geothermal area, New Zealand; Vandemeulebrouck et al. 2005, 2008; Legaz et al. 2009). Such an intrinsically gravitationally unstable system is manifested as a near-boiling lake that occasionally drains (Fig. 7a) and refills its water (Fig. 7b), without any clear cyclicity (contrary to geysers) (Vandemeulebrouck et al. 2005; Fournier et al. 2009). If such lakes are gravitationally unstable, why do they exist in the first place?

Lakes can be sustained above the regional aquifer by the drag force caused by a gas phase flowing through a liquid-filled permeable conduit. At the equilibrium, the drag stress for each bubble is exactly balanced by the hydrostatic pressure of the water raised above the water table. So, bubbles are needed to "carry" the lake. When bubbles are present, boiling and degassing is a fact. Moreover, cold water in the near surface (lake and surroundings) will be lifted by underlying hotter water, which needs to boil (and bubble) to keep the unstable lake suspended. A disruption in the bubbling behavior can literally lead to a collapse of the delicate equilibrium state and the consequent sudden draining of the lake (e.g. steam-bubble collapse in the lake, seismic triggers). Such draining can even occur when the heat power and thermal boundary conditions of the gravitationally unstable lake system are maintained constant. With the scope of volcano monitoring, crises of lake draining and refill of such lake systems can occur without any changes in their underlying magmatic systems (Vandemeulebrouck et al. 2005).

Other active gas-flushed crater lakes, which do not demonstrate this obvious draining-refill behavior can be subject to similar dynamics, e.g. shown by lake level variations generated by a pushing or retreating underlying vapor-gas front. As the lake functions as a "shock absorber" with gas bubbles as driving agent, it is crucial to be able to distinguish such hydrothermal instabilities of the lake from real changes in magmatic

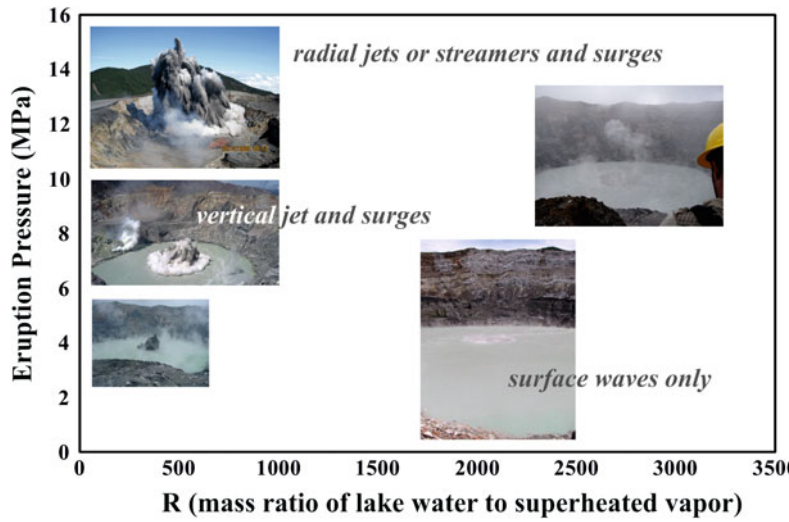

Fig. 8 The results of the numerical modeling are illustrated by real phreatic eruptions observed at Laguna Caliente, Poás, Costa Rica, during the 2006–2012 eruption cycle (modified from Morrissey et al. 2010). The eruption style reflects the mass ratio of lake water to superheated vapor and eruption pressure. Picture courtesy, clockwise from lower *left*, used with permission: Gino González-Ilama, Ana Belén Castro, Cindy and Jean-Michel Doire (URL: https://picasaweb.google.com/cjmdoire), Raúl Mora-Amador (2x)

activity (Vandemeulebrouck et al. 2005, 2008). The pre-eruption lake level rise of Poás' Laguna Caliente in 2005 can be interpreted as a rising steam pushing the lake up, a first "shock being absorbed" before liberating the increased energy release as an eruption (starting in March 2006).

4 Numerical Modeling of Crater Lake Breaching Eruptions

From the above review it is clear that unambiguous precursory signals of single eruptions breaching a crater lake are not well established. Due to the high frequency of eruptions within phreatic cycles, such as currently at Poás' Laguna Caliente, a continuous monitoring (geochemical, temperature logging, magnetometry, thermal and visual imaging, etc.; Rouwet et al. 2014) is needed to find the key to effective eruption forecasting. Especially for crater lake eruptions the physical processes are still not fully understood. As for any eruption, magmatic or not, the occurrence and violence of an eruption depends on how efficiently thermal energy is converted into mechanical energy (Newhall and Self 1982; Moyer and Swanson 1987; Mastin 1991; Marini et al. 1993). The initial amount of energy available to trigger an eruption depends on the initial pressure and temperature of the rock-gas-liquid-vapor mixture. As direct clues of these parameters are often masked by the presence of the lake

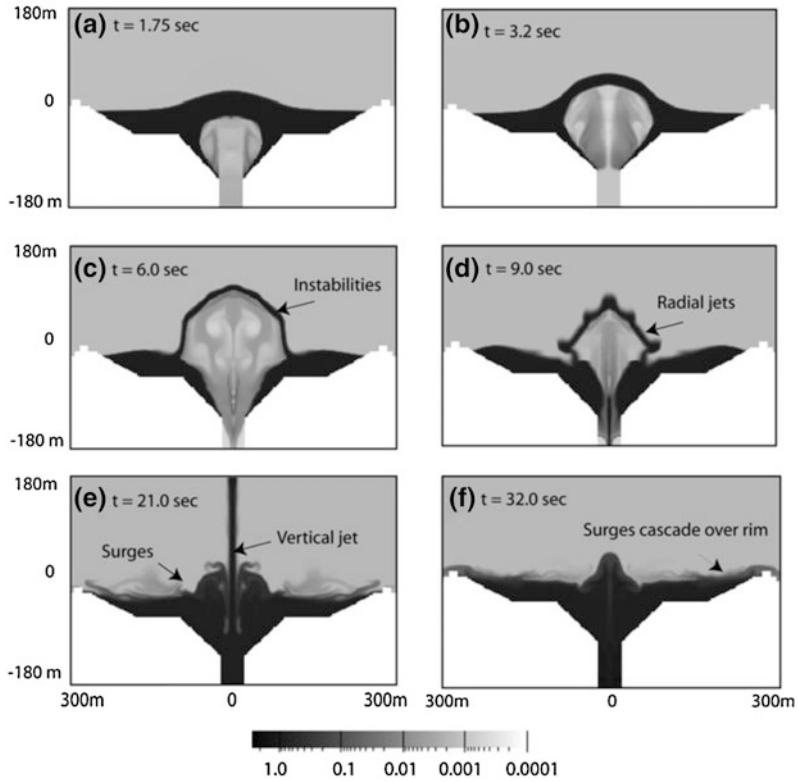

Fig. 9 Snapshots of the density field from preliminary simulations (Morrissey et al. 2010). **a–c** A gas cavity rapidly forms and expands raising the lake surface (surface bulge) 90 m before collapsing. **c–f** As the cavity collapses, instabilities form along the lake surface forming finger or radial jets that coincide with the development of the main vertical jet. Surges flows are observed to flow toward the crater rim where they eventually cascade over the rim and begin to flow down the crater walls. Grey scale values range from on the order of 1.0 kg/m^3 for *black* to 0.001 kg/m^3 for *light gray*. Wall rock (*white*) is not part of the *gray* scale value scheme

itself, physical modeling and numerical simulations can be of help to better understand the eruption mechanism (Brown et al. 1989; Dowden et al. 1991; Bercich and McKibbin 1992; Christenson et al. 2010; Morrissey et al. 2010).

Numerical simulations using the SAGE code (Gittings et al. 2008) that mimicked Ruapehu's Crater Lake, New Zealand, result in a spectrum of activities that range from small-scale surface-waves to a series of surges accompanying radial jets, and depend on eruption pressure, the initial mass ratio of lake water to supercritical vapor (=R) and lake level (Fig. 8) (Morrissey et al. 2010). Calculations involving R > 1,100, a full lake and supercritical vapor with an initial pressure between 0.5 and 5.0 MPa produces a vapor cavity that raises the lake surface (i.e. surface bulge) several meters before it collapses or cavitates causing small disturbances on the lake surface within <25 s. At higher eruption pressures between 5 and 10 MPa, and R between 1,100 and 1,600, the vapor cavity rises through the lake displacing the lake surface tens of meters before it begins to collapse (Fig. 9a, b). As the cavity collapses (Fig. 9c, d), a vertical jet forms reaching a height of 100–200 m above the crater-lake surface. The lake surface drops due to the collapse of the vapor cavity and surge waves form along the base of the jet (Fig. 9e, f). The surges are several meters high and move rapidly toward the rim of the crater-lake eventually cascading over the edge (Fig. 10). The surges are composed of saturated steam due to turbulence of the lake surface. At vapor pressures >10 MPa with R < 1,600 in a full lake, the vapor cavity rises rapidly through the lake, expanding the lake surface radially >100 m to a point where instabilities form producing fingers or streamers of

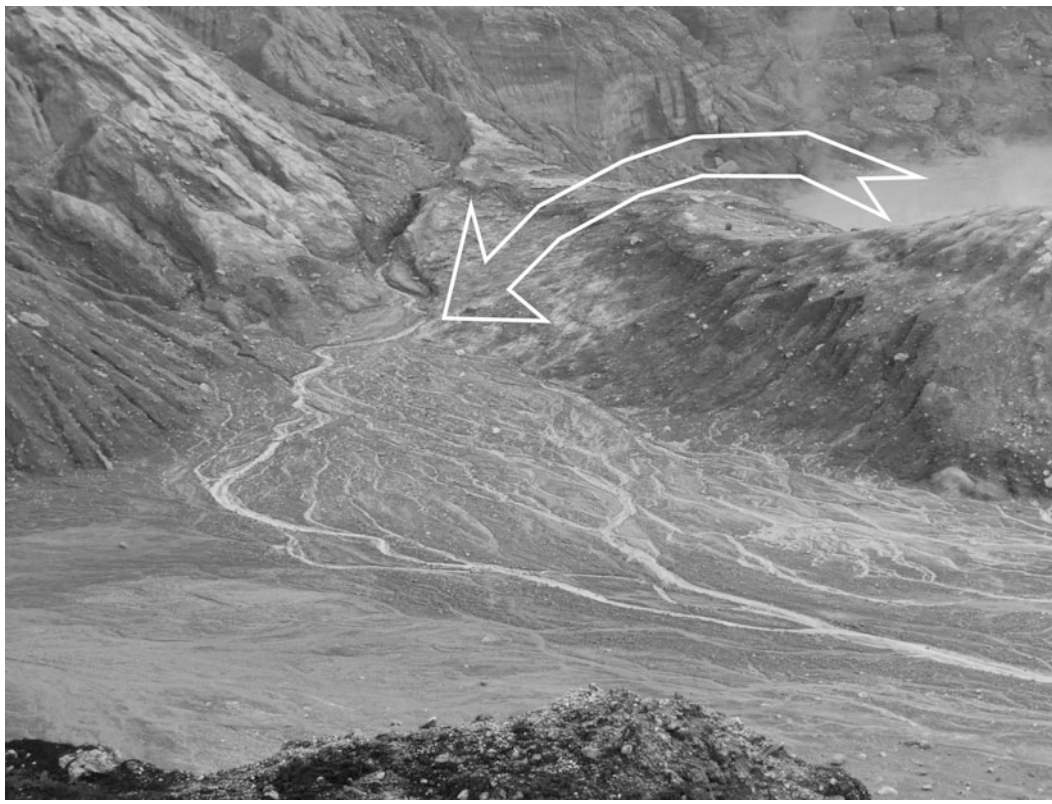

Fig. 10 Proof of lake cascading over the southern dome after the 16 April 2012 phreatic eruption of Poás Volcano, Costa Rica (picture by Raúl Mora-Amador). Surges of several tens of meters high (dome height ~30 m) throw the lake out beyond the lake rims

liquid. The numerical simulations confirm the implosive nature of phreatic eruptions, as suggested above by physical insights.

5 Conclusions

An active crater lake is potentially one of the most dangerous sites to be around due to the high compressibility of gases and inputs of gas-vapor batches. When an eruption occurs at crater lakes, it is subaqueous and either phreatomagmatic, phreatic, hydrothermal or geyser-like. Belousov and Belousova (2001) proposed a model for the phreatomagmatic Surtseyan eruptions at Karymskoye Lake based on video images, depositional characteristics and tephra morphology. The ejection of the gas and tephra mixture (fragmented magma) through the lake creates a bulge at the lake surface. The gas-tephra mixture penetrates through the bulge and breaks the lake surface forming a cockscomb jet followed by a base surge that moves radially from the eruptive center.

Before the 1940s, the term "phreatic eruption" did not exist in the literature. Phreatic eruptions do not expel juvenile magma but instead only fragments of non-juvenile rocks mixed with gas, steam or liquid water (non-magmatic). Visually, phreatic eruptions are very similar to phreatomagmatic Surtseyan eruptions, but are often more violent than their magmatic or phreatomagmatic counterparts. Examples include Laguna Caliente, Poás in Costa Rica; Ruapehu in New Zealand, (pre-2013) Copahue in Argentina-Chile; and Aso in Japan.

Hydrothermal eruptions in hot water or steam-dominated hydrothermal systems are generated near-surface due to the phase transition from liquid to steam following a sudden pressure drop. The hydrostatic pressure is determined by the weight of the crater lake itself, being variable by sudden lake level drops by enhanced evaporation or seepage, or the expulsion of lake water by previous phreatic or hydrothermal eruptions. Less hazardous geyser-like eruptions and draining-refill sequences of "boiling lakes" can also occur at active crater lakes.

A continuous monitoring system will be key to better understand crater lake eruptions. Unfortunately, this remains utopia for many lakes. As direct clues are often masked by the presence of the lake itself, physical modeling and numerical simulations can be of help to better understand the eruption mechanism. The first numerical simulations resulted in a spectrum of activity that ranges from small-scale surface-waves to a series of surges accompanying radial jets, and depends on eruption pressure, the initial mass ratio of lake water to supercritical vapor and lake level. This review has shed light on the various eruption mechanisms in a crater lake focussed perspective, but on the other hand, has demonstrated that it remains challenging to correctly recognize, understand and monitor eruptions, as the lake itself "hazes" our view into the depths where eruption-triggering pressures reign.

Acknowledgments DR wishes to thank his co-author MM for encouraging to write this review chapter. The chapter is "VUELCO inspired", and hopefully reaches multiple needs. The authors wish to thank Nico Fournier and an anonymous reviewer for constructive and insightful comments which largely enhanced the chapter. Jean Vandemeulebrouck is acknowledged for efficient editorial handling.

References

Agusto M, Tassi F, Caselli AT, Vaselli O, Rouwet D, Capaccioni B, Caliro S, Chiodini G, Darrah T (2013) Gas geochemistry of the magmatic-hydrothermal fluid reservoir in the Copahue-Caviahue Volcanic Complex (Argentina) J Volcanol Geotherm Res 257:44–56. doi:10.1016/j.volgeores.2013.3.03.003

Alvarado GE (2010) Hydrogeological and sedimentological aspects of the mud flows related to the Cinchona earthquake (Mw 6.2) of January 8, 2009, Costa Rica. Rev Geol Am Centr 43:67–96

Baker ET, Massoth GJ, de Ronde CEJ, Lupton JE, McInnes BIA (2002) Observations and sampling of an ongoing subsurface eruption of Kavachi volcano, Solomon Islands, May 2000. Geology 30:975–978

Bani P, Oppenheimer C, Varekamp JC, Quinou T, Lardy M, Carn S (2009) Remarkable geochemical changes and degassing at Voui crater lake, Ambae volcano, Vanuatu. J Volcanol Geotherm Res 188:347–357. doi:10.1016/j.jvolgeores.2009.09.018

Barberi F, Bertagnini A, Landi P, Principe C (1992) A review on phreatic eruptions and their precursors. J Volcanol Geotherm Res 52:231–246

Belousov A, Belousova M (2001) Eruptive process, effects and deposits of the 1996 and the ancient basaltic phreatomagmatic eruptions in Karymskoye lake, Kamchatka, Russia. In: White JDL, Riggs NR (eds) Volcaniclastic sedimentation in lacustrine settings. Blackwell Sciences, Oxford, pp 35–60

Bercich BJ, McKibbin R (1992) Modelling the development of natural hydrothermal eruptions. In: Proceedings 14th NZ geothermal workshop 1992, pp 305–312, and corrigendum, Proceedings of the 15th NZ geothermal workshop 1993, University of Auckland, Auckland, New Zealand, pp 345–346

Brantley SL, Borgia A, Rowe G, Fernández JF, Reynolds JR (1987) Poás volcano crater lake acts as a condenser for acid metal-rich brine. Nature 330:470–472

Brodsky EE, Roeloffs E, Woodcock D, Gall I, Manga M (2003) A mechanism for sustained ground water pressure changes induced by distant earthquakes. J Geophys Res 108. doi:10.1029/2002JB002321

Brodsky EE, Sturtevant B, Kanamori H (1998) Volcanoes, earthquakes and rectified diffusion. J Geophys Res 103:23827–23838

Brown G, Rymer H, Dowden J, Kapadia P, Stevenson D, Barquero J, Morales LD (1989) Energy budget analysis for Poás Crater lake: implications for predicting volcanic activity. Nature 339:370–373

Browne PRL, Lawless JV (2001) Characteristics of hydrothermal eruptions, with examples from New Zealand and elsewhere. Earth Sci Rev 52:299–331

Burnham CW (1979) Magmas and hydrothermal fluids. In: Barnes HL (ed) Geochemistry of hydrothermal ore deposits. Wiley, New York, pp 71–136

Christenson BW (2000) Geochemistry of fluids associated with the 1995–1996 eruption of Mt. Ruapehu, New Zealand: signatures and processes in the magmatic-hydrothermal system. J Volcanol Geotherm Res 97:1–30

Christenson BW, Németh K, Rouwet D, Tassi F, Vandemeulebrouck J, Varekamp JC (2015) Introduction chapter volcanic lakes. In: Rouwet D, Tassi F, Vandemeulebrouck J, Christenson B (eds) Volcanic Lakes. Springer, Berlin. doi:10.1007/978-3-642-36833-2_1

Christenson BW, Reyes AG, Young R, Moebis A, Sherburn S, Cole-Baker J, Britten K (2010) Cyclic processes and factors leading to phreatic eruption events: insights from the 25 September 2007 eruption through Ruapehu Crater Lake, New Zealand. J Volcanol Geotherm Res 191:15–32

Christenson BW, Wood CP (1993) Evolution of the vent-hosted hydrothermal system beneath Ruapehu Crater Lake, New Zealand. Bull Volcanol 55:547–565

Christenson BW, Werner CA, Reyes AG, Sherburn S, Scott BJ, Miller C, Rosenburg MJ, Hurst AW, Britten KA (2007) Hazards from hydrothermally sealed volcanic conduits. EOS 88(50):53–55

de Ronde CEJ, Chadwick WW Jr, Ditchburn RG, Embley RW, Tunnicliffe V, Baker ET, Walker SL, Ferrini VL, Merle SM (2015) Molten sulphur lakes of intraoceanic arc volcanoes. In: Rouwet D, Tassi F, Vandemeulebrouck J, Christenson B (eds) Volcanic Lakes. Springer, Berlin. doi:10.1007/978-3-642-36833-2_11

Delmelle P, Bernard A (1994) Geochemistry, mineralogy, and chemical modeling of the acid crater lake of Kawah Ijen volcano, Indonesia. Geochim Cosmochim Acta 58:2445–2460

Delmelle P, Bernard A (2015) The remarkable chemistry of sulfur in volcanic acid crater lakes: a scientific tribute to Bokuichiro Takano and Minoru Kusakabe. In: Rouwet D, Tassi F, Vandemeulebrouck J, Christenson B (eds) Volcanic Lakes. Springer, Berlin. doi:10.1007/978-3-642-36833-2_10

Dowden J, Kapadia P, Brown G, Rymer H (1991) Dynamics of a geyser eruption. J Geophys Res 96:18059–18071

Fournier N, Witham F, Moureau-Fournier M, Bardou L (2009) Boiling Lake of Dominica, West Indies: high-temperature volcanic crater lake dynamics. J Geophys Res 114:B02203. doi:10.1029/2008JB005773

Fournier RO (1969) Old faithful: a physical model. Science 163:304–305

Gittings ML, Weaver RP, Clover M, Betlach T, Byrne N, Coker R, Dendy E, Hueckstaedt R, New K, Oakes WR, Ranta D, Stefan R (2008) The RAGE radiation hydrodynamic code. Comput Sci Disc 1(015005):63

Hedenquist JW, Henley RW (1985) Hydrothermal eruptions in the Waiotapu geothermal system. Econ Geol 80:1640–1688

Hedenquist JW, Lowenstern JB (1994) The role of magmas in the formation of hydrothermal ore deposits. Nature 370:519–527

Henley RW (2015) Hyperacidic volcanic lakes, metal sinks and magmatic gas expansion in arc volcanoes. In: Rouwet D, Tassi F, Vandemeulebrouck J, Christenson B (eds) Volcanic Lakes. Springer, Berlin. doi:10.1007/978-3-642-36833-2_6

Hurst AW, Bibby HM, Scott BJ, McGuinness MJ (1991) The heat source of Ruapehu Crater Lake; deductions from the energy and mass balances. J Volcanol Geotherm Res 6:1–21

Hurst T, Christenson B, Cole-Baker J (2012) Use of a weather buoy to derive improved heat and mass balance parameters for Ruapehu Crater Lake. J Volcanol Geotherm Res 235–236:23–28

Ingebritsen SE, Rojstaczer SA (1993) Controls on geyser periodicity. Science 262:889–892

Ingebritsen SE, Rojstaczer SA (1996) Geyser periodicity and the response of geysers to deformation. J Geophys Res 101:21891–21905

Jolly AD, Sherburn S, Jousset P, Kilgour G (2010) Eruption source processes derived from seismic and acoustic observations of the 25 September 2007 Ruapehu eruption-North Island, New Zealand. J Volcanol Geotherm Res 191:33–45. doi:10.1016/j.volgeores.2010.01.009

Jones JG (1970) Intraglacial volcanoes of the Laugarvatn region, southwest Iceland, II. J Geol 78:127–140

Kling GW, Evans WC, Tanyileke GZ (2015) The comparative limnology of Lake Nyos and Monoun, Cameroon. In: Rouwet D, Tassi F, Vandemeulebrouck J, Christenson B (eds) Volcanic Lakes. Springer, Berlin. doi:10.1007/978-3-642-36833-2_18

Kieffer SW (1984) Seismicity at old faithful geyser: an isolated source of geothermal noise and possible analogue of volcanic seismicity. J Volcanol Geotherm Res 22:59–95

Kilgour G, Manville V, Della Pasqua F, Graettinger A, Hodgson KA, Jolly GE (2010) The 25 September 2007 eruption of Mount Ruapehu, New Zealand: directed ballistics, surtseyan jets, and ice-slurry lahars. J Volcanol Geotherm Res 191:1–14

Kiryukin AV, Rychkova TV, Dubrovskaya IK (2012) Formation of the hydrothermal system in Geysers Valley (Kronotsky Nature Reserve, Kamchatka) and triggers of the Giant Landslide. Appl Geochem 27:1753–1766

Kokelaar BP (1983) The mechanism of Surtseyan volcanism. J Geol Soc London 140:939–994

Kokelaar BP (1986) Magma-water interactions in subaqueous and emergent basaltic volcanism. Bull Volcanol 48:275–289

Kokelaar BP, Durant GP (1983) The submarine eruption of Surtla (Surtsey, Iceland). J Volcanol Geotherm Res 19:239–246

Kusakabe M (2015) Evolution of CO_2 content in Lakes Nyos and Monoun, and sub-lacustrine CO_2-recharge system at Lake Nyos as envisaged from C/^{3}He ratios in noble gas signatures. In: Rouwet D, Tassi F, Vandemeulebrouck J, Christenson B (eds) Volcanic Lakes. Springer, Berlin. doi:10.1007/978-3-642-36833-2_19

Legaz A, Revil A, Roux P, Vandemeulebrouck J, Gouédard P, Hurst T, Bolève (2009) Self-potential and passive seismic monitoring of hydrothermal activity: a case study at Iodine Pool, Waimangu geothermal valley, New Zealand. J Volcanol Geotherm Res 179:11–18

Manga M, Brodsky E (2006) Seismic triggering of eruptions in the far field: volcanoes and geysers. Annu Rev Earth Planet Sci 34:263–291

Manville V (2015) Volcano-hydrologic hazards from volcanic lakes. In: Rouwet D, Tassi F, Vandemeulebrouck J, Christenson B (eds) Volcanic Lakes. Springer, Berlin. doi:10.1007/978-3-642-36833-2_2

Marini L, Principe C, Chiodini G, Cioni R, Fytikas M, Marinelli G (1993) Hydrothermal eruptions of Nysiros (Dodecanese, Greece). Past events and present hazard. J Volcanol Geotherm Res 56:71–94

Mastin LG (1991) The roles of magma and groundwater in the phreatic eruptions at Inyo Craters, Long Valley Caldera, California. Bull Volcanol 53:579–596

Mastin LG (1994) Explosive tephra emissions at Mount St. Helens, 1989–1991: the violent escape of magmatic gas following storms? Geol Soc Am Bull 106:175–185

Mastin LG (1995) Thermodynamics of gas and steam-blast eruptions. Bull Volcanol 57:85–98

Mastin LG, Witter JB (2000) The hazards of eruptions through lakes and seawater. J Volcanol Geotherm Res 97:195–214

Mazot A, Bernard A (2015) CO_2 degassing from volcanic lakes. In: Rouwet D, Tassi F, Vandemeulebrouck J, Christenson B (eds) Volcanic Lakes. Springer, Berlin. doi:10.1007/978-3-642-36833-2_15

Mazot A, Rouwet D, Taran Y, Inguaggiato S, Varley N (2011) CO_2 and He degassing at El Chichón volcano, Chiapas, Mexico: gas flux, origin and relationship with local and regional tectonics. Bull Volcanol 73:423–441

Morgan LA, Shanks PWC, Pierce KL (2009) Hydrothermal processes above a large magma chamber: large hydrothermal systems and hydrothermal explosions in Yellowstone National Park. Geol Soc Am Spec Pap 459:95

Morrissey M, Gisler G, Weaver R, Gittings M (2010) Numerical model of crater lake eruptions. Bull Volcanol. doi:10.1007/s00445-010-0392-5

Moyer TC, Swanson DA (1987) Secondary hydroeruptions in pyroclastic-flow deposits: examples from Mount St. Helens J Volcanol Geotherm Res 32:299–319

Muffler LJP, White DE, Truesdell AH (1971) Hydrothermal explosion craters in yellowstone National Park. Geol Soc Am Bull 82:723–740

Nairn IA, Wiradiradja S (1980) Late quaternary hydrothermal explosion breccias at Kawerau Geothermal Field, New Zealand. Bull Volcanol 43:1–13

Németh K, Cronin SJ, Charley D, Harrison M, Garae E (2006) Exploding lakes in Vanuatu—Surtseyan-style eruptions witnessed on Ambae Island. Episodes 29:87–92

Newhall CG, Self S (1982) The volcanic explosivity index (VEI): an estimate of explosive magnitude for historical volcanism. J Geophys Res 87(C2):1231–1238

Ohba T, Hirabayashi J, Nogami K (2008) Temporal changes in the chemistry of lake water within Yugama Crater, Kusatsu-Shirane Volcano, Japan: implications for the evolution of the magmatic-hydrothermal system. J Volcanol Geotherm Res 178:131–144

Oppenheimer C (1992) Sulphur eruptions at Volcán Poás, Costa Rica. J Volcanol Geotherm Res 49:1–21

Oppenheimer C, Stevenson D (1989) Liquid sulphur lakes at Poás volcano. Nature 32:790–793

Pasternack GB, Varekamp JC (1994) The geochemistry of the Keli Mutu crater lake, flores, Indonesia. Geochem J 28:243–262

Pasternack GB, Varekamp JC (1997) Volcanic lake systematcis 1. Physical constraints. Bull Volcanol 58:528–538

Peiffer L, Taran Y, Lounejeva E, Solis-Pichardo G, Rouwet D, Bernard-Romero R (2011) Tracing thermal aquifers of El Chichón volcano-hydrothermal system (México) with $^{87}Sr/^{86}Sr$, Ca/Sr and REE. J Volcanol Geotherm Res 205:55–66

Rouwet D, Taran Y, Inguaggiato S, Varley N, Santiago SJA (2008) Hydrochemical dynamics of the "lake-spring" system in the crater of El Chichón volcano (Chiapas, Mexico). J Volcanol Geotherm Res 178:237–248

Rouwet D, Taran Y, Varley NR (2004) Dynamics and mass balance of El Chichón crater lake, Mexico. Geofís Int 43:427–434

Rouwet D, Tassi F, Mora-Amador RA, Sandri L, Chiarini V (2014) Past, present and future of volcanic lake monitoring. J Volcanol Geotherm Res 272:78–97. doi:10.1016/j.volgeores.2013.12.009

Rowe GL, Brantley SL, Fernández M, Fernández JF, Borgia A, Barquero J (1992) Fluid-volcano interaction in an active stratovolcano: the Crater Lake system of Poás Volcano, Costa Rica. J Volcanol Geotherm Res 64:233–267

Shanks PWC, Morgan LA, Balistrieri LA, Alt JC (2005) Hydrothermal vents, siliceous hydrothermal deposits, and hydrothermally altered sediments in Yellowstone Lake. In: Inskeep WP, McDermott TR (eds) Geothermal biology and geochemistry in yellowstone national park, pp 53–72

Stearns HA, McDonald GA (1949) Geology and groundwater resources of the island of Hawaii. Hawaii Div Hydrogr Bull 9:1–363

Steinberg GS, Merzhanov AG, Steinberg AS (1981) Geyser process: its theory, modeling and field experiment, 1, theory of the geyser process. Mod Geol 8:67–70

Steinberg GS, Merzhanov AG, Steinberg AS (1982a) Geyser process: its theory, modeling and field experiment, 3, on metastability of water in geysers. Mod Geol 8:75–78

Steinberg GS, Merzhanov AG, Steinberg AS (1982b) Geyser process: its theory, modeling and field experiment, 4, on seismic influence on geyser regime. Mod Geol 8:79–86

Steinberg GS, Merzhanov AG, Steinberg AS, Rasina AA (1982c) Geyser process: its theory, modeling and field experiment, 2, a laboratory model of a geyser. Mod Geol 8:71–74

Takano B, Kuno A, Ohsawa S, Kawakami H (2008) Aqueous sulfur speciation possibly linked to sublimnic volcanic-gas water interaction during a quiescent period at Yugama crater lake, Kusatsu-Shirane volcano, Central Japan. J Volcanol Geotherm Res 178:145–168. doi:10.1016/j.volgeores.2008.06.038

Takano B, Saitoh H, Takano E (1994) Geochemical implications of subaqueous molten sulfur at Yugama crater lake, Kusatsu-Shirane volcano, Japan. Geochem J 28:199–216

Taran Y, Fischer TP, Pokrovsky B, Sano Y, Armienta MA, Macías JL (1998) Geochemistry of the volcano–hydrothermal system of El Chichón Volcano, Chiapas, Mexico. Bull Volcanol 59:436–449

Tassi F, Rouwet D (2014) An overview of the structure, hazards, and methods of investigation of Nyos-type lakes from the geochemical perspective. J Limnol 73 (1). doi:10.4081/jlimnol.2014.836

Thorarinsson S (1967) Surtsey: the new Island in the North Atlantic. Viking Press, NY, p 47

Toraishi S, Tominaga H (1940) Sulfur spherules in crater lake, Okama, Zao Volcano. Kagaku (Science) 10:3–4 (in Japanese)

Truesdell AH, Nathenson M, Rye RO (1977) The effects of subsurface boiling and dilution on the isotopic compositions of yellowstone thermal waters. J Geophys Res 82:3694–3704

Vandemeulebrouck J, Hurst T, Scott BJ (2008) The effects of hydrothermal eruptions and a tectonic earthquake on a cycling crater lake (Inferno Crater Lake, Waimangu, New Zealand). J Volcanol Geotherm Res 178:271–275

Vandemeulebrouck J, Stemmelen D, Hurst T, Grangeon J (2005) Analogue modeling of instabilities in crater lake hydrothermal systems. J Geophys Res 110: B02212. doi:10.1029/2003JB002794

Varekamp JC (2015) The chemical composition and evolution of volcanic lakes. In: Rouwet D, Tassi F, Vandemeulebrouck J, Christenson B (eds) Volcanic Lakes. Springer, Berlin. doi:10.1007/978-3-642-36833-2_4

Varekamp JC, Ouimette AP, Herman SW, Bermúdez A, Delpino D (2001) Hydrothermal element fluxes from Copahue, Argentina: a "beehive" volcano in turmoil. Geology 29:1059–1062

Varekamp JC, Pasternack GB, Rowe GL Jr (2000) Volcanic lake systematics II. Chemical constraints. J Volcanol Geotherm Res 97:161–179

Vaselli O, Tedesco D, Cuoco E, Tassi F (2015) The CO_2-CH_4-rich gas reservoir of Lake Kivu (democratic republic of the Congo and Rwanda): a review of physical-chemical and isotopic data and triggers of limnic eruptions. In: Rouwet D, Tassi F, Vandemeulebrouck J, Christenson B (eds) Volcanic Lakes. Springer, Berlin. doi:10.1007/978-3-642-36833-2_22

Werner C, Christenson BW, Hagerty M, Britten K (2006) Variability of volcanic gas emissions during a crater lake heating cycle at Ruapehu Volcano, New Zealand. J Volcanol Geotherm Res 154:291–302

White DE (1967) Some principles of geyser activity, mainly from steamboat springs, Nevada. Am J Sci 265:641–684

White DE, Muffler LJP, Truesdell AH (1971) Vapor-dominated hydrothermal systems compared with hot-water systems. Econ Geol 66:75–97

White JDL, Smellie JL, Clague DA (2003) Introduction: a deductive outline and topical overview of subaqueous explosive volcanism. Explosive subaqueous volcanism. Geophys Mono 140:1–23

The Chemical Composition and Evolution of Volcanic Lakes

Johan C. Varekamp

Abstract

Volcanic lakes carry fluids that range from ultra acid, high TDS brines to largely meteoric fluids. Their water compositions are governed by volcanic fluid inputs, which range from almost raw, cooled volcanic gases (largely S–Cl–F–CO_2 rich fluid) to more mature solutions that result from interaction of these acid fluids with volcanic rocks. Volcanic inputs can have reacted with mature protoliths (low degrees of neutralization) or with freshly intruded magma (high degrees of water rock interaction), the latter often resulting in the precipitation of secondary minerals such as alunite. The detailed chemical lake water composition is a reflection of mineral precipitation, fractionation of trace elements in the precipitated phases (such as the rare earth elements and metals in sulfides) and element vapor phase transport by the volcanic gases. Variations in lake composition result from a changing volcanic input composition or magnitude and thus are important in volcano monitoring. The lake water dynamics also impact the lake water composition over time, and variations in evaporation rate, meteoric water input and dramatic changes in input may cause changes in element concentrations and ratios related to non steady state effects. The recovery time to steady state differs strongly between open and closed lake systems. The stable isotope compositions of volcanic lake waters reflect W/R interaction (higher $\delta^{18}O$), degree of volcanic gas input (higher $\delta^{18}O$ and δD), and evaporation at elevated temperatures (flat evaporation lines). Isotope ratios of other elements usually reflect the nature of the volcanic inputs or dissolved rock. Volcanic lakes can be charged with toxic elements that upon release may impact local ecosystems and agricultural land or drinking water downstream. Volcanic lakes charged with poorly soluble gases such as CO_2 and methane may represent hazards of limnic

J.C. Varekamp (✉)
Earth and Environmental Sciences, Wesleyan University, 265 Church Street, Middletown, CT 06459, USA
e-mail: jvarekamp@wesleyan.edu

D. Rouwet et al. (eds.), *Volcanic Lakes*, Advances in Volcanology,
DOI 10.1007/978-3-642-36833-2_4,
© Springer-Verlag Berlin Heidelberg 2015

eruptions. Failure of retaining walls or dams of acid lakes may cause acid floods with damage to land and livestock downstream.

Keywords
Volcanic lakes · Chemical composition · REE · Lake dynamics · Stable isotopes · Volcanic contaminants

1 Introduction

Volcanic lakes dot the landscape in many volcanic terrains (e.g., Delmelle and Bernard 2000a; Tassi et al. 2009a). They range in size from tiny maar lakes to giant caldera lakes. Volcanic lakes may have their origin in true volcanic processes that disturb the watershed: explosion craters, collapse calderas as well as streams and rivers that were cut off by volcanic products (lava flows, lahars, ash flows). Ancillary "volcanic lakes" are those that are impacted by volcanic processes but are not truly volcanic in origin. Some lakes may be receiving volcanic inputs in the form of hydrothermal fluids, which impacts their chemical composition and possibly their nutrient balance. In this review I will deal with all lakes that have a discernible volcanic component in their water composition.

Many volcanic lakes are known for their beauty and pristine surroundings (e.g., Crater Lake, Oregon, USA; Heavenly Lake, N-Korea), but in their waters or sediments many natural pollutants may lurk. They range in composition from largely meteoric water (e.g., Crater Lake, Oregon, Drake et al. 1990; McManus et al.1992; Bolsena Lake, Italy, Mosello et al. 2004; Azores lakes, Martini et al. 1994) to extreme fluids with high TDS and low pH values (e.g., Poás Lake, Costa Rica; Rowe et al. 1992a, b; Martínez et al. 2000). The composition of lake waters can be used for volcano monitoring purposes (e.g., Giggenbach 1974; Giggenbach and Glover 1975; Armienta et al. 2000; Tassi et al. 2005; Zlotnicki et al. 2009; Martini et al. 2010) and the water compositions may provide fundamental insights into the origin and evolution of hydrothermal fluids and associated ore deposits (e.g., Giggenbach 1988, 1992b). Some lakes contain hazardous low-pH fluids and failure of a retaining wall (Schaeffer et al. 2008) or leakage into the watershed can provide a natural hazard (e.g., Delmelle and Bernard 2000b; Löhr et al. 2005; van Rotterdam et al. 2008; Kempter and Rowe 2000; Delmelle et al. this issue). Some lakes accumulate volcanic or geothermal gases (CO_2 or methane) that can accumulate in the water column (e.g., Lake Nyos, Cameroon, Kling et al. 1987, this issue; Evans et al. 1993; Lake Kivu, Democratic Republic of Congo, Tietze et al. 1980; Tassi et al. 2009b; Tedesco et al. 2010; Lake Kelud, Indonesia, Bernard and Mazot 2004; Caudron et al. 2012; Lake Quilotoa Chiodini et al. 2000; Gunkel et al. 2008). Most lakes in moderate climate zones mix once or twice a year and then release their stored gases to the atmosphere. In the case of meromictic lakes, gas storage can occur over 100–1000s of years and catastrophic release of gases may take place during a forced overturn (seismic event, volcanic event, landslide) as occurred at Lake Monoun and Lake Nyos (Kling et al. this issue; Kusakabe this issue; Tassi and Rouwet 2014). Lake Kivu may have overturned during a gas eruption in the far past (Haberyan and Hecky 1987), although this is being debated.

The boundary conditions for volcanic lake existence are the degree of water input (precipitation, watershed size) and water loss (evaporation, seepage, outlets). Moreover, crater lakes have a limiting temperature of stability for a given location (Pasternack and Varekamp 1997). As a result, many crater lakes occur in wet tropical regions or on top of tall volcanoes with a glacier-fed water supply. Evidence for a volcanic component in lake waters may be a lowered pH value, usually associated with high concentrations of the

major cations, or high CO_2, Cl^- or SO_4^{2-} concentrations. In some cases, enrichments in trace elements like fluorine, arsenic or lithium or sediments with a geothermal component serve as indicators for a subaqueous volcanic input (e.g., López et al. 2009; Miyabuchi and Terada 2009). Of course, all common limnological and biological processes also occur in volcanic lakes, but the volcanic influence may overprint the usual state of a lake.

Geothermal inputs of dissolved silica or leaching of fresh volcanic ash may stimulate diatom productivity in volcanic lakes (Burwell 2003; Telford et al. 2004). Volcanic CO_2 may be used in biological productivity and the enhanced input of nutrients like dissolved P from volcanic/geothermal sources may stimulate primary productivity (Pedrozo et al. 2001, 2008; Lefkowitz 2012). In extreme cases, the water density may be influenced by the geothermal inputs (salinity, dissolved CO_2) and bottom waters may become stagnant as a result of the volcanic inputs. Some volcanic lakes have lake beds with a peculiar composition, like the varved beds of Lake Tateyama in Japan (Kusakabe et al. 1986) that consists of thin silica layers (diatoms) and thicker native sulfur layers that formed through oxidation of volcanic H_2S in the water. Other lakes with non-extreme water compositions have floating sulfur nodules at the surface during periods of turnover, a result of volcanic and/or bacterial processes in the lake (e.g., Lake Ilopango, El Salvador, López et al. 2004). So volcanic lakes are either formed through volcanic processes (mainly physical) or their water composition is impacted by direct volcanic inputs, be it subaqueous or through mineralized rivers. Volcanic ash or aerosol inputs into lakes usually do not make them part of the volcanic lakes clan. Acid volcanic lakes may be terrestrial analogs of early Mars environments (Varekamp 2004; Chapman 2007) and also have strong chemical similarities with acid mine drainage areas.

2 Chemical Composition of Volcanic Lakes

The chemical compositions of volcanic lakes cover a wide range, from dilute, largely meteoric water fluids to very concentrated hyper acidic fluids (Table 1). The source of the anions is ultimately a volcanic gas phase rich in SO_2, HCl and HF and possibly CO_2, which may have been absorbed at depth in a hydrothermal system and then subsequently is injected into the volcanic lake (Christenson and Tassi this issue). The anion concentrations reflect the composition of the volcanic gas, commonly with S/Cl $\sim$1, be it with many exceptions (Fig. 1a). Chloride loss as HCl vapor in hot concentrated lakes (e.g., Poás, Copahue) is common (Rowe et al. 1992a), leading to Cl depletion. Precipitation in the lakes of native sulfur, gypsum, anhydrite or jarosite, all common minerals in volcanic lakes, may deplete the waters in S. The S–Cl–C diagram shows the clear partition in the acid S–Cl lakes with low pH values and the carbonate rich lakes with much higher pH values (Fig. 1b). Some lakes have an input of a mixed volcanic fluid but do not reach low enough pH values to let CO_2 escape. Concentrated pools of exotic S–Cl-rich water are found where the lake absorbs largely unprocessed raw volcanic gases, such as in Keli Mutu in Indonesia (Pasternack and Varekamp 1994) and Kawah Putih on Java (Sriwana et al. 2000), and Poás and Turrialba in Costa Rica (Tassi et al. 2005, 2009a, b; Martini et al. 2010). Other volcanic lakes receive hydrothermal fluids that have already been processed extensively. These acid hydrothermal fluids may be strongly mineralized, but tend to be less rich in the volcanogenic elements (S+halogens). Examples are Taal, Phillipines (Gordon et al. 2009; Zlotnicki et al. 2009), Kelud (Indonesia, Bernard and Mazot 2004), and El Chichón (Mexico) during the period 1990–2014 (Armienta et al. 2000; Rouwet et al. 2004, 2008).

Table 1 Representative analyses of volcanic lake waters (references to original papers can be found in Varekamp et al. 2000)

Year	LAKE	Temp (°C)	pH	Cl (ppm)	SO_4 (ppm)	F (ppm)	B (ppm)	HCO_3 (ppm)	Na (ppm)	Mg (ppm)	Al (ppm)	SiO_2 (ppm)	K (ppm)	Ca (ppm)	Mn (ppm)	Fe (ppm)	Li (ppm)
1989	Poás 030389	82.0	−0.55	27,200	233,000	6,310			3,680	3,650	7,400		2,280			6,310	
1993	K. Ijen 091893		0.28	21,832	74,133		54.4		940	569	5,530	175	1,180	911	38	1,888	
1999	Copahue springs	83	0.3	9,800	65,400	700			910	500	3,250		880	770	23	1,860	
1999	Copahue crater lake	21	0.3	8,000	55,400	720			470	290	1,560		390	850	13	800	
1999	Caviahue lake	15	2.36	93	461	9.7			12	14	31		8	22	1	21	
1992	Keli Mutu TAP0921L	19.0	1.9	3,120	8,940	252	22.6		243	254	1,580	205	53	630	9	1,250	0.3
1989	Keli Mutu TAM89 J	22.0	2.9	90	1,475	10.0	0.6		43	32	68	95	4	434	1	10	0.03
1992	Keli Mutu TiN0923P	31.4	0.4	26,700	49,350	2,460	224		942	1,280	8,610	141	545	899	38	2,620	1.4
1983	El Chichón 83	56.0	0.56	24,030	3,550	0.2	433		607	424	745	232	232	2,110		914	0.76
1992	El Chichón may92	32.1	2.15	12,250	420	0.5	165		3,400	317		273	670	2,517			0.46
1995	Ruapehu RNZ 3/2/95	46.0	0.67	7,020	22,200	380	16.3		317	243	1,640	350	224	890		370	0.64
1975	Yugama 111975	11.0	1.1	3,040	2,560				25	11	130		15	112		139	
1982	Volcano - HIP0982	25.0	1.5	9,700	11,800				5,250	750			730	810			
	Lago Albano-160	9.0	5.55	21	3		0.2	262	32	17			48	40			0.001
	Nyos B090986-70	23.4	5.6	0	2			370	12	38		36	3	28	1	49	
	Lake Bannoe	16.0	5.7	10	133	0.1	0.7	0	20	5	0	105	6	21	0	0	
1995	Lake Monoun-95	23.0	5.9	3	0			1,660	22	23			7	19			
1993	Kelut 122093	41.6	6.0	1,358	657	7.0	11		674	56	0	244	92	106	2	0	
1995	Piccolo 95-20	12.3	6.35	22	9	0.1	19	916	40	13			25	34		45	0.01
	Quilotoa 200	13.6	6.35	4,120	2,480	0.2	156	1,910	2,400	768		115	192	614	4		3.7
	Bracciano-162	11.0	7.62	43	32		0.3	269	40	12			39	37			0.014
	Bolsena-140	8.0	8.25	30	20		0.4	270	41	15			45	24			0.018
	Nemi-0	17.0	8.35	17	3		0.3	186	22	11			22	21			0.001

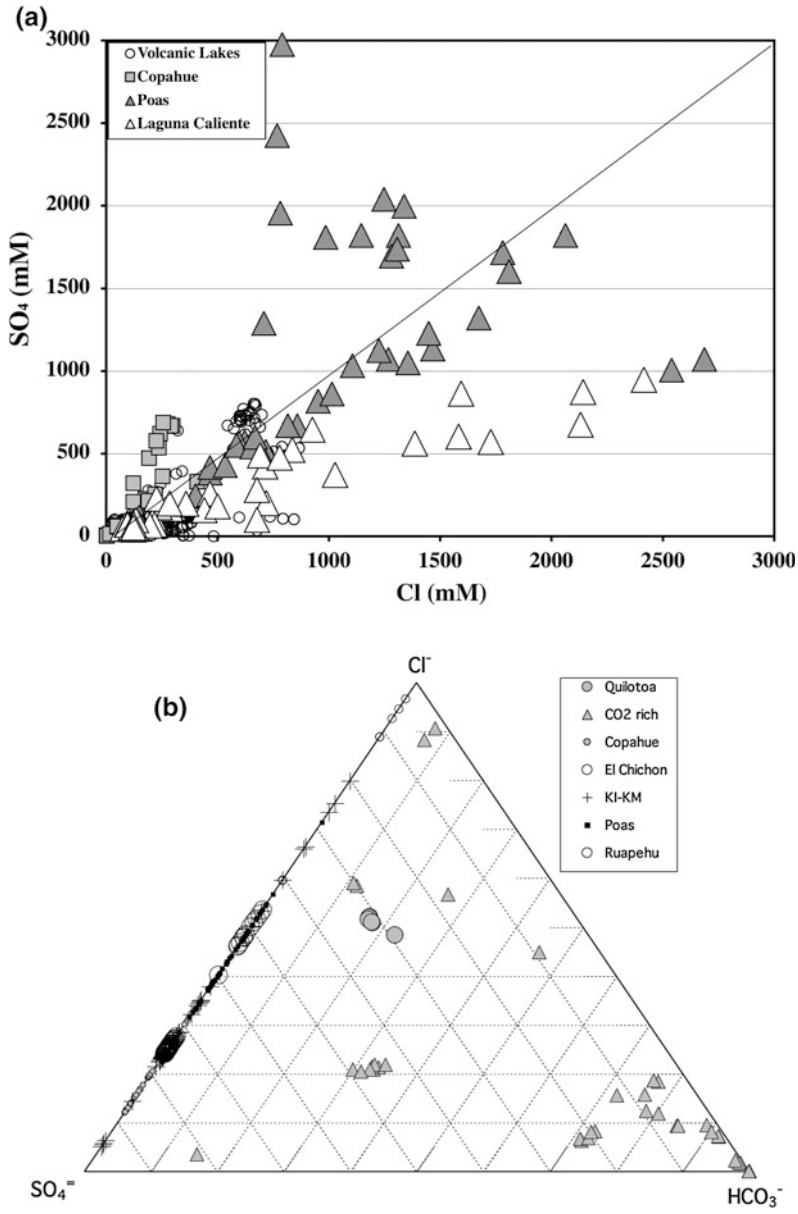

Fig. 1 **a** The molar S/Cl is on average ~1, but S excesses and deficits are common. Some Poás crater lake samples (Laguna Caliente) probably suffered from sulfur loss through liquid sulfur formation and anhydrite crystallization. Other Poás samples with excess sulfur (Poás) probably have undergone HCl vapor loss. **b** The S–Cl–C diagram shows the acid lakes on the S–Cl axis, and the very CO_2 rich samples near the HCO_3 corner. A few lakes have mixed S–Cl–HCO_3 compositions, and most of these have relatively high pH values

The sources of most cations in volcanic lakes are the local volcanic rocks that react with the volcanic fluids (e.g., Sriwana et al. 2000), either in the lake environment itself or in the underlying hydrothermal system down to some kilometers depth. The volcanic gases may have already interacted at high temperatures (>600 °C) at greater depths with intrusive rocks, possibly forming porphyry copper deposits (e.g., Reed et al. 2013; Henley this issue) before entering the shallower and cooler zones below volcanic lakes, where they may form alteration zones with high-sulfidation ore deposits (e.g., Brantley et al. 1987; Hedenquist and Lowenstern 1994; Arribas 1995; Henley this issue). The volcanic gases that are trapped in the lake or underlying hydrothermal system carry besides the CO_2–S–Cl–F also some volatile cation-forming elements such as Na, B, Rb and trace elements such as Pb, Zn, Hg, As, and Cd (Symonds et al. 1987; Taran et al. 1995). In highly

acid volcano-hydrothermal systems where wholesale (near-congruent) dissolution of rocks may occur at elevated temperatures, the chemical composition of the lake water is a direct reflection of the composition of the underlying rock matrix. Compositional differences may exist as a result of the preferential dissolution of certain minerals before the remainder of the rock dissolves or the precipitation of secondary minerals.

Three types of diagrams are commonly used to provide a genetic illustration of lake water compositions of the acid lake group (pH < 3): (1) the element transfer ratio (ETR) diagram, (2) the "isosol" diagram, and (3) ternary molar composition diagrams. The degree of congruent rock dissolution of lake waters can be assessed by plotting the element transfer ratios (Pasternack and Varekamp 1994; Aiuppa et al. 2000; Takano et al. 2004; Colvin et al. 2013), which is the lake water composition normalized to the rock composition, using a common index element for dilution scaling, usually Mg or Na because of their conservative nature in acid fluids. The ETR for Mg is than by definition 1, and elements with an ETR close to 1 behaved like Mg, whereas ETR >1 suggests either preferential mineral dissolution or addition of elements by a volcanic vapor phase. Elements with ETR <1 may have been retained in the rock matrix (e.g., Si, Ti, Nb, Zr) or precipitated in secondary minerals (e.g., barite precipitation creates a Ba depletion). Two examples of ETR diagrams are shown for water samples from Santa Ana and Poás crater lakes (Fig. 2a, b), showing the depletions in several elements, in this case because of alunite and anhydrite retention, and enrichments because of vapor transport of volatile elements (see also Delmelle and Bernard 1994). The depletions in Si and Ti are common to most fluids and discussed in more detail below.

The "isosol" diagram is a log-log compositional diagram (Fig. 3a, b), with the water composition along the vertical axis and the mean volcanic rock composition along the horizontal axis (e.g., Taran et al. 2008; Colvin et al. 2013). Sloping isosol lines ("isosols" equal amount of rock dissolved for the various elements) indicate the "grams of rock dissolved" per liter of hydrothermal water if congruent rock dissolution took place. If all elements from a given sample plot on a specific isosol, the fluid resulted from congruent rock dissolution at that W/R value, whereas deviations from an isosol show the amount of relative depletion or enrichment in a given element. Waters from Copahue crater lake (Varekamp et al. 2009) and Santa Ana crater lake (Bernard et al. 2004; Colvin et al. 2013) show both close to congruent dissolution with about 30 g of rock per liter of water, with slight dilution trends over time (Fig. 3a, b). The elements Si and Ti show strong negative deviations from the 30 g isosols, suggesting that those elements were either left behind in the dissolving rock matrix or precipitated in a secondary phase in the underlying system or lake. The high field strength elements (HFSE) like Ti and Nb are poorly soluble even in hot acids, and Ti and the other HFSE may remain behind during the dissolution process (Aja et al. 1995; Wood 2005; Varekamp et al. 2009). Alternatively, they were precipitated in the lake environment (Delmelle and Bernard 1994) after removal from the rock matrix. The solubility of silica (expressed here as ppm Si in the fluid instead of ppm SiO_2) is a strong function of temperature, but relatively modest even at high temperature ($\sim$320 ppm Si at $\sim$300 °C, Verma 2000), whereas fluids with 30 g of dissolved bulk andesite per liter would require $\sim$8,000 ppm Si in solution for congruent dissolution. The Si depletion as commonly found in the ETR and isosol diagrams is thus not necessarily the result of silica precipitation during late-stage cooling, but a direct result of incongruent dissolution of the rock matrix. This rock dissolution with contemporaneous precipitation of hydrothermal silica, produced probably the so-called "vuggy silica' as found in many ore deposits (e.g., Arribas 1995; Reed et al. 2013). The silica concentration in volcanic lakes is further influenced by precipitation of silica minerals during the cooling of the hydrothermal fluids as well as by the degree of dilution with meteoric water in the lake system. Enhanced silica concentrations in cool volcanic lakes are a certain indicator for hydrothermal fluid inputs, but have only limited geothermometric value.

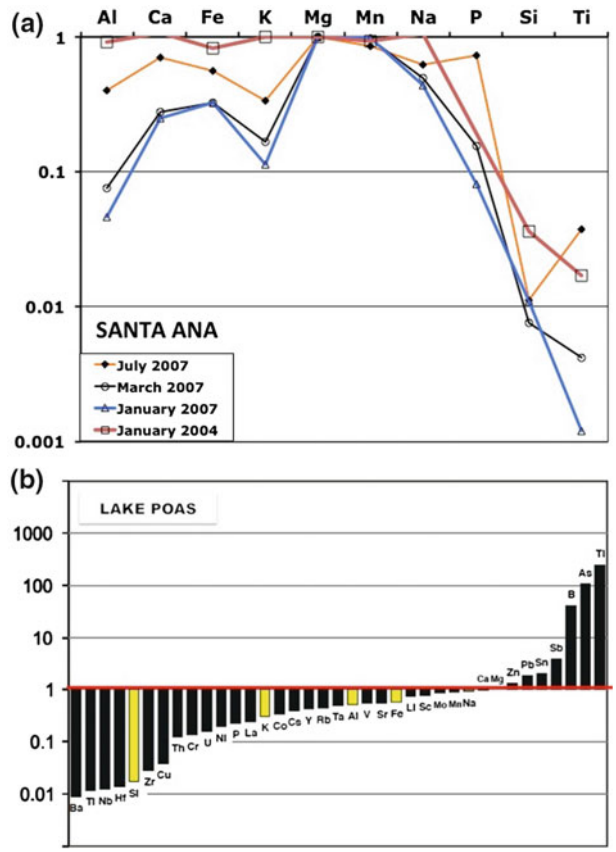

Fig. 2 **a** Element transfer ratio diagram for the 2004 crater lake fluids from Santa Ana volcano (El Salvador) showing near-congruent rock dissolution, with depletions in Si and Ti (Bernard et al. 2004). The 2007 samples show also depletions in K, Al, Na and Fe, suggesting alunite-jarosite saturation and Ca depletions suggesting anhydrite saturation. **b** Diagram with relative abundances for Poás Lake, with strong enrichments in the volatile trace elements such as arsenic, thallium and boron, and depletions in Ca (anhydrite), Ba (barite), Cu (sulfide) and Si in vuggy silica. The HFSE are all depleted either as a result of retention in the protolith or precipitation in the lake waters (Martínez 2008)

A combination of $\delta^{18}O$ and Si data of lake waters may narrow the Si contents of the parental hydrothermal input fluid, if the $\delta^{18}O$ value of the input fluids is known and corrections for evaporation can be made. Temperatures of last equilibration with a solid silica phase can then be estimated, which may approach the temperature of the hydrothermal input into the lake. It is important to realize this two-step process of silica depletion in the hydrothermal systems: the precipitation of silica minerals during the W/R interaction process, and the later cooling-precipitation and dilution steps.

The 2007 Santa Ana crater lake fluids also show depletions in K and Al in addition to the Si and Ti deficits, with possibly a minor depletion in Na. Precipitation of a K–Na–Al rich phase would explain this pattern, and saturation modeling of these fluids (Colvin et al. 2013) indicates alunite saturation ((Na, K) Al_3 $(SO_4)_2$ $(OH)_2$). From the expected and observed Al concentration (intercept Al*, Fig. 3a) and the stoichiometry of alunite, the amount of precipitated alunite per liter of water is estimated. For the July 2007 Santa Ana fluids, for every 30 g of rock dissolved, about 8 g of alunite were precipitated.

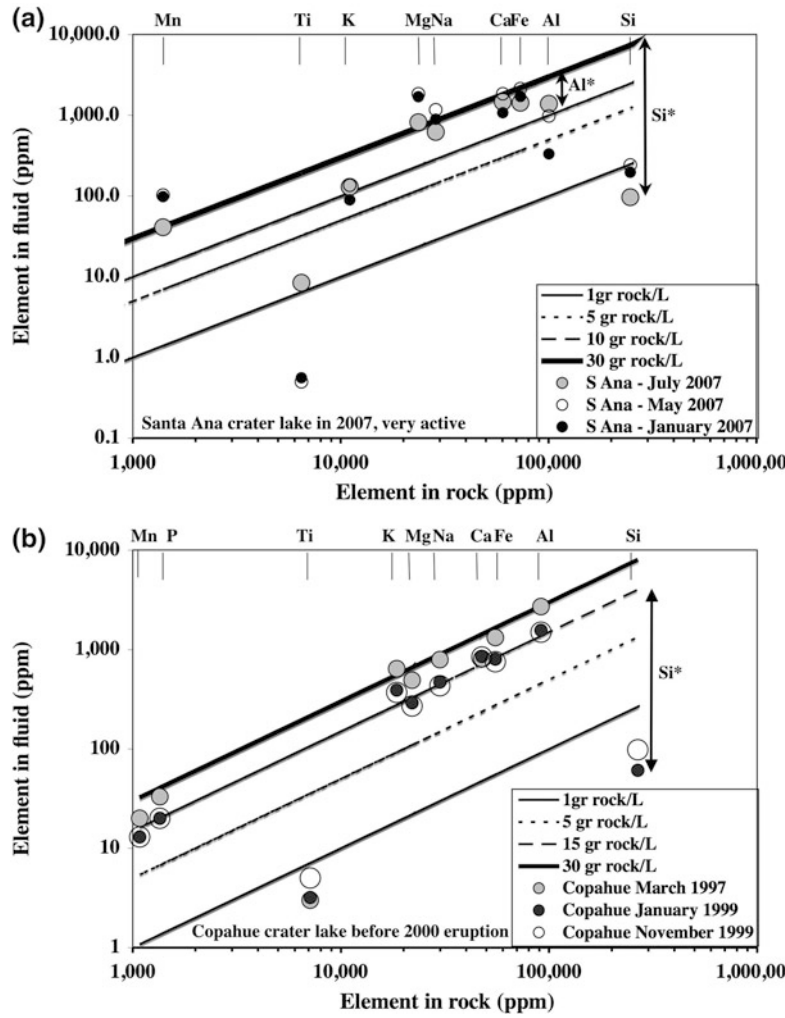

Fig. 3 Isosol diagrams for Santa Ana (**a**) and Copahue (**b**) crater lakes. **a** Santa Ana lake shows on average 30 g/L total dissolved solids and element depletions in Al and K due to alunite precipitation. **b** Copahue crater lake shows congruent dissolution at 30 g/L total dissolved solids in 1997, decreasing to 15 g/L in 1999. Only Si and Ti show strong depletions. The slight decrease in Si* in 1999 may herald the heating of the hydrothermal system prior to the 2000 eruption

These isosol diagrams thus show both the amount of rock dissolved in the fluids that feed a given volcanic lake (possibly corrected for dilution with meteoric water) as well as the reaction progress of the dissolution process with precipitation of specific secondary minerals. The example from Copahue crater lake shows near congruent dissolution for all major elements at close to 30 g rock/L, suggesting close to congruent rock dissolution, except for Si and Ti, with the two-step silica precipitation discussed above.

The Si depletion process can be further quantified with the Si* parameter (Fig. 4), which is here defined as the expected ppm Si from congruent rock dissolution based on a given isosol and the observed Si concentration (or Si* = Si(obs)/Si(isosol)). Plots of Si* versus W/R can be used to check if any late stage silica precipitation has taken place (Fig. 4) and what the approximate temperature of the input fluids was, if no major dilution has taken place. For example, a W/R value of 5 g rock/L as derived from the isosol diagram would produce a theoretical Si* of ~24 % at 300 °C as a result of incongruent rock dissolution; the temperature needs to be derived from other indicators such as sulfur isotope data, chemical thermometry, or drill hole data. If the Si*(observed) for the specific system equals 15 %, an additional amount

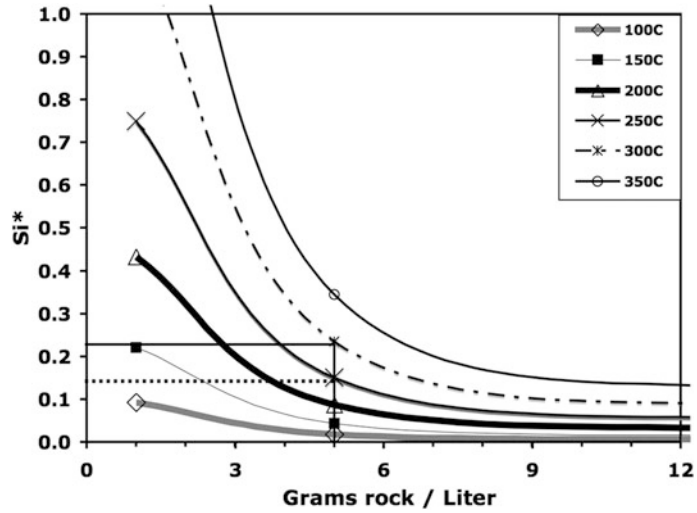

Fig. 4 The Si* versus W/R diagram shows isotherms for rock dissolution with associated Si* values. An example is shown for 5 g/L total dissolved rock, which would at 300 °C yield a Si* of 0.25. If the observed Si* = 0.15, the last equilibration with quartz then occurred at 250 °C (*dotted line*)

of Si has been removed from the fluid through cooling-precipitation after the initial rock dissolution step, and the last silica equilibration temperature is then given by the intersection of the lines as shown in Fig. 4 (~250 °C). Other variations on Si evolution in lake fluids and the relation to the feeding underlying hydrothermal system uses the Si/Cl in lakes (Varekamp et al. 2000), which can be related through the temperature of the hydrothermal system to dilution (~constant Si/Cl) or conductive cooling (decreasing Si/Cl).

The compositional variation in volcanic lakes can also be illustrated in ternary ion diagrams (e.g., Christenson 2000). The molar composition of three components is plotted (Fig. 5a–d), sometimes scaled to make better use of the plotting space, together with the compositions of primary rock-forming minerals in the andesitic protolith, secondary minerals that may precipitate from the fluids, and the volcanic bulk rock composition itself (VRIP = volcanic rock index point). These diagrams are projections of multi-dimensional compositional space and should be interpreted with care. Dilution by meteoric waters will not impact the plotted data points in the simple, non-scaled diagrams whereas the diagrams with components that have exponents will be distorted. Data from an extended version of the volcanic lakes data base (Varekamp et al. 2000) with a pH below 3 are plotted in four of these diagrams (Fig. 5a–d), which cover water analyses of some well-studied crater lakes such as Keli Mutu, Kawah Ijen, Copahue, Poás, El Chichón, Ruapehu, and Yugama. An andesitic rock protolith is the source of cations for all these lake waters, although in specific cases the protolith composition may vary from basaltic andesite to dacitic/rhyolitic rocks and can be plotted as such. If fluids plot close to the VRIP, a congruent process of dissolution probably took place for the three elements involved. Preferential dissolution of a specific mineral would create tails from VRIP towards that mineral point. If the fluid compositions form tails behind the VRIP opposite from a secondary mineral, precipitation of that mineral may have left its imprint on the chemical composition of the waters. Conversely, tails between the VRIP and secondary minerals may indicate re-dissolution of secondary minerals that precipitated during an earlier phase of hydrothermal activity.

The Al–Mg–(Na + K) diagram (Fig. 5a) shows the VRIP, alunite and alkalifeldspar (mainly albite) compositional points, and clay minerals at the Al corner. The compositional array lines up between alunite and the VRIP with a long tail down (Copahue, Poás, Ruapehu), suggesting extensive alunite precipitation from some of these waters. The Kawah Ijen samples

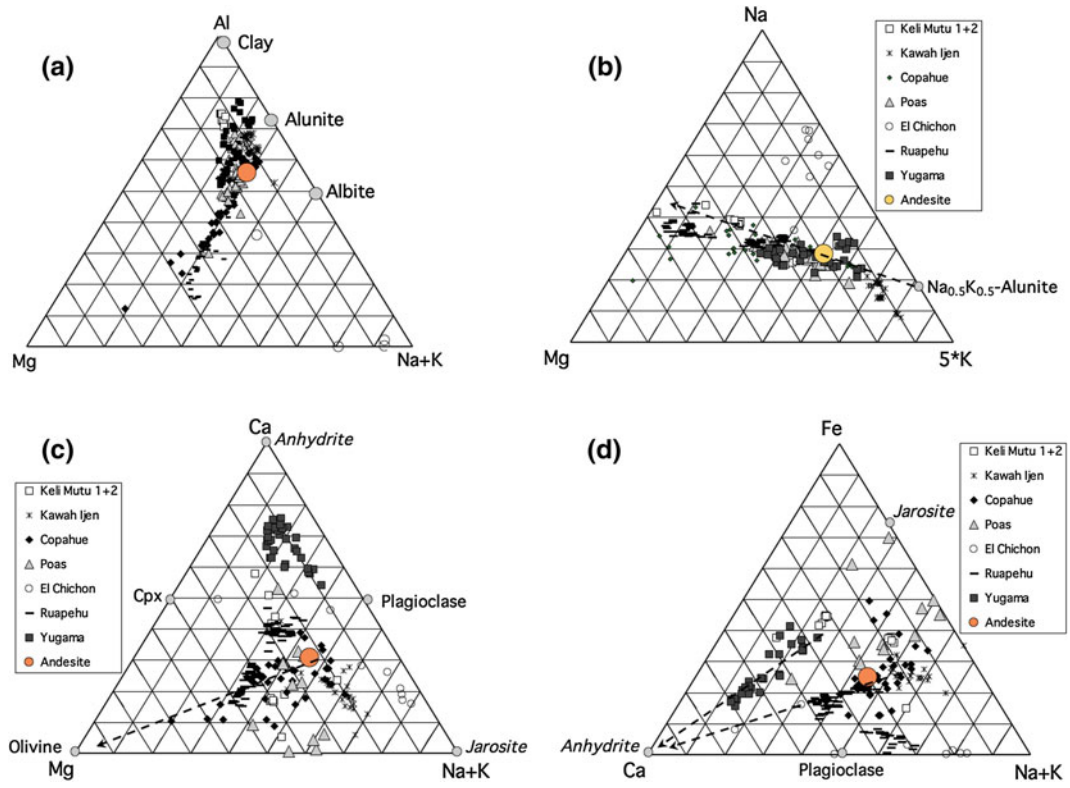

Fig. 5 Ternary molar compositional diagrams for several acid crater lakes with an average andesite composition (VRIP, Copahue rock, Varekamp et al. 2006). The data suggest a strong influence from precipitation of mixed Na–K alunite in most systems (**a**, **b**) and anhydrite precipitation and dissolution in **c** and **d**. See text for full discussion

plot above the VRIP, suggesting dissolution of earlier formed clays and/or alunite. The Yugama samples plot along and above the VRIP as do the two Keli Mutu lakes, suggesting re-equilibration of the fluids with clay minerals. The Na–Mg–5 K graph (Fig. 5b) shows a very narrow array of data for many of these lake waters that aligns with the VRIP—alunite trend. The data to the left of the VRIP may indicate evolving compositions because of alunite precipitation, whereas the few points to the right of the VRIP may indicate re-dissolution of earlier formed alunite in the reservoir. The El Chichón waters plot in a different field than the other acid lakes, indicating that the water chemistry of El Chichón lake results of multistep or separate processes (e.g., mixing of various fluids, Rouwet et al. 2008; Taran and Rouwet 2008). The Kawah Ijen waters form a separate array, possibly indicating dissolution of pure K-alunite. No strong evidence is present for preferential dissolution of albite or olivine relative to the bulk VRIP in these data plots, suggesting that differences in mineral solubility kinetics are largely overwhelmed by the sheer dissolution power of the hot acid fluids. The Ca–Mg–(Na + K) diagram (Fig. 5c) shows anhydrite as a common additional secondary mineral and the data show a more complex pattern. The Yugama samples are strongly displaced towards the anhydrite corner, whereas the tail towards the Mg corner may be best explained as the simultaneous precipitation of anhydrite, alunite and/or jarosite, leading to an apparent enrichment in Mg. Some of the Poás samples plot behind the VRIP and suggest precipitation of anhydrite. The Kawah Ijen samples may show

dissolution of alunite/jarosite, while precipitating anhydrite. The last diagram (Fe–Ca–(Na + K)) shows a more complex distribution of water compositions (Fig. 5d). The Yugama samples once more plot far away from the VRIP in an area lined-up between anhydrite and jarosite. The Ruapehu samples suggest dissolution of anhydrite with precipitation of jarosite during the rock dissolution process. These observations can be used as a first indicator for mineral saturation in the lake source fluids at specific temperature and fO_2 conditions.

The pH is an important water composition parameter, but the precision and accuracy of pH values below one are commonly difficult to assess (Nordstrom et al. 2000). The measurement of pH values below one requires purpose-made standard series for the specific acid involved (usually sulfuric acid, see Nordstrom and Alpers 1999), so any differentiation of pH values below one should be considered with caution. Some studies use charge balance on H^+ to obtain calculated pH values from speciation programs. Concentrated volcanic lake fluids are difficult to analyze, as shown by cross laboratory calibrations (Takano et al. 2000), which then provides more uncertainty. The characterization of lake fluids based on pH values at the low pH end is relatively coarse as well because of its logarithmic nature. The frequency of pH values in volcanic lakes is thought to be controlled by the SO_4^{2-}-HSO_4^- and the H_2CO_3–HCO_3^- buffers, leading to a bimodal distribution of pH values (Marini et al. 2003). An alternative way of considering the lake composition involves a measure of the amount of free H^+ ions versus the amount that was present while the waters became acidified by volcanic inputs (Varekamp et al. 2000). A simple example goes as follows: if volcanic lake water has 5,000 ppm SO_4^{2-} and 3,500 ppm Cl^-, the initial pH of the fluid is derived from 52 micromoles H^+ from HSO_4^- and 100 micromoles from Cl^- per gram of water, which translates into a $pH_{(initial)}$ of ~0.8. Obviously, this approach has its weaknesses in not considering ion pairing for HCl in concentrated Cl-brines, differences in activity and concentration (H^+ concentration is equated to pH), but nonetheless, the procedure provides a first order estimate of the original fluid prior to W/R interaction. Application of a speciation program such as phreeqc (Parkhurst and Appelo 1999) provides better solutions for the original pH, e.g., in the above example at 30 °C the pH would be 0.9 instead of 0.8 as based on charge balance only. I calculated "initial pH values" for the volcanic lakes water database (~800 entries), based on their SO_4^{2-}, Cl^-, F^-, and HCO_3^- contents at 25 °C using a speciation program. The difference between observed pH and "initial pH" is the amount of H^+ consumed during W/R interaction, which can be expressed as the (H^+ consumed)/(original amount of H^+) or the "degree of neutralization" factor (DON, expressed in %). The volcanic lakes database shows DON values ranging from 10 to 100 % (Fig. 6). The DON values approach 100 % for all fluids above pH ~4. The acid lake clan can both have low and high DON values, providing a means of distinction between them. Dilution of lake fluids has only a small impact on the DON values because of changes in the activity coefficients, but the general relationships are still valid. A high DON value is a reflection of a "mature water" in the sense of Giggenbach et al. (Giggenbach 1988), indicating advanced stages of reaction progress.

The DON parameter can also be used for an alternative classification diagram for volcanic lakes. The measured or calculated pH values show the H^+ activities after W/R interaction whereas the DON parameter approaches the amount of W/R interaction. In the low pH realms, this enables to separate between more mature and less mature hydrothermal fluids, here arbitrarily chosen at the 50 % DON value (Fig. 6). Fluids with pH >4 have DON values approaching 100 %, creating the most mature clan of waters. Many of the more mature fluids have still very low pH values, indicating that pH alone is not the most precise indicator of water evolution in these systems. The relations between the DON parameter and bulk fluid geochemistry are system specific and an example from Copahue crater lake is given here (Varekamp et al. 2009). Copahue volcano was in a quiet episode from 1997 to 2000, and erupted in July 2000. It remained active

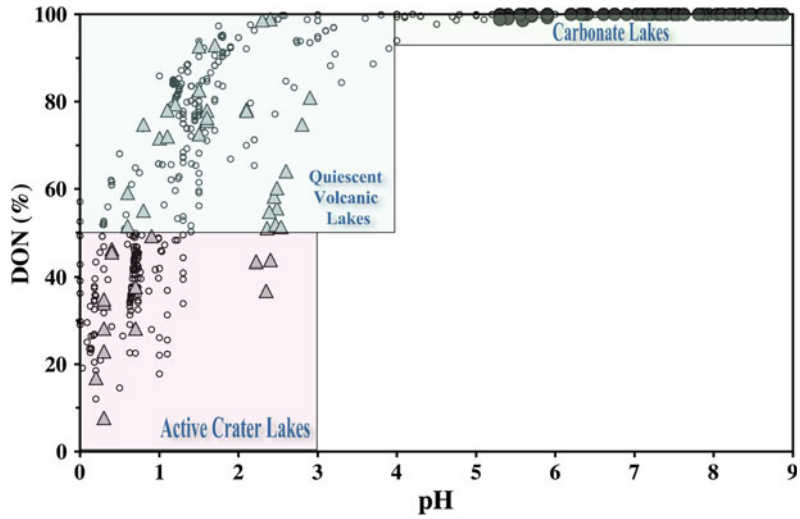

Fig. 6 DON—pH data for volcanic lakes. The lake waters are grouped according to pH and DON values into active crater lakes (DON < 50 %, pH < 3) and quiescent crater lakes (DON > 50 %, pH 0-4) and a group of CO_2 rich lakes (DON > 90 %, pH > 6)

for several months, then quieted down, and then had a period of 'anomalous hydrothermal fluid' emissions in 2004 (Varekamp 2008) which was associated with a freeze-over of the crater lake ('thermal anomaly'; Agusto et al. 2012). The DON and pH values were both low in 1997–1999 (Fig. 7a), suggesting that the volcanic fluids were interacting with a mature protolith. The eruption of July 2000 was probably preceded by a shallow magmatic intrusion into the hydrothermal system (Varekamp et al. 2001), and reaction between the acid fluids and the fresh, quenched volcanic rock led to enhanced rock dissolution, with enhanced element export through the springs and into the crater lake, with very high dissolved cation contents. The DON values (Fig. 7a) jumped from 20–40 % in 1997–1999 to 50–100 % in 2000–2001 and remained high also after the eruption (presumably reflecting ongoing W/R interaction with the newly emplaced volcanic rocks). The Mg/Cl values also were much higher during the 2000 eruptive and post-eruptive period (Fig. 7b). During the eruptive period with a higher DON value, the system became saturated with alunite, which reduced the permeability, limiting the export of hydrothermal fluids into the lake in the years following the eruption. The DON parameter thus may serve as an indicator of W/R interaction during an eruptive episode (Fig. 7).

The common island silicate mineral olivine is very soluble in hot concentrated sulfuric acid (e.g., Schuiling 1998), contrary to many other silicate minerals that need HF to dissolve rapidly. During attack of a mafic volcanic rock, we therefore expect that olivine will be one of the first minerals to dissolve, releasing Mg, Fe, Ni, Mn and Si to the waters. In low DON fluids, Mg can make up to 20 % of the cations, and we surmise that these fluids started to dissolve olivine before the whole rock was dissolving. In such fluids we also find a close positive correlation between Mg and Mn, probably reflecting the olivine dissolution process. Evidence for early release of Ca–Na from feldspar weathering in acid lake water compositions with low DON values is lacking. So in conclusion, the chemical composition of lake fluids is in many cases a reflection of the composition of the volcanic input and W/R interaction during residence in one or more "reservoirs" below the lake. Some lake systems may have a volcanic gas input directly into the lake with associated reactions with suspended sediment and wall rock, but most if not all have an underlying hydrothermal system.

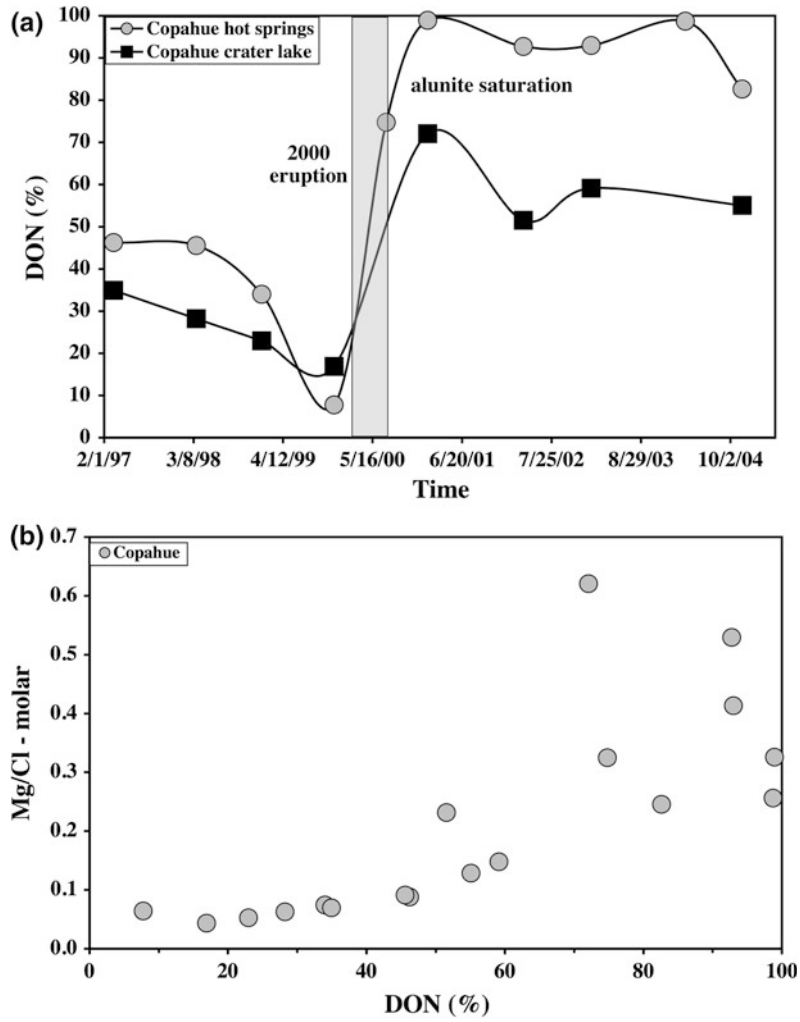

Fig. 7 **a** The DON parameter versus time for the crater lake and hot springs at Copahue volcano. The DON parameter decreased prior to the eruption (flushing with volcanic gases, mature protolith) followed by a strong increase in DON just prior to and during the eruption (intrusion of new magma). The DON value remains high after the 2000 eruption, supposedly because of the abundance of freshly intruded volcanic rock for W/R interaction. **b** The DON parameter versus Mg/Cl showing increasing amounts of dissolved rock in the waters at higher DON values (more mature fluids)

3 The REE in Volcanic Lakes

The REE and Y are a homogenous group of elements (Lanthanides) with similar valences and a decreasing ionic radius with increasing Z number (from La to Lu). As a result, the light REE (LREE) tend to be more incompatible than the heavy REE (HREE) and Y. The element Eu is commonly depleted relative to its direct neighbors because it may occur with 2^{+}valency (dependent on fO_2) and then behaves very similar to Sr and partitions into plagioclase. The Eu depletion is commonly referred to as the Eu anomaly (or Eu/Eu*), which tends to be positive in plagioclase crystals. Modern analytical techniques (ICP-MS) can detect the REE at ppb levels in waters and they make good tracers for W/R interaction. The geochemistry of the REE in geothermal fluids (and acid mine drainage fluids) was considered by Morgan and Wandless (1980), Michard (1989), Wood (2003, 2006a, b), Wood and Shannon (2003), Gammons et al. (2002, 2003), Bozau et al. (2004), Samson and Wood (2005), with papers more specific to volcanic lakes by Kikawada et al. (1993, 2001), Fulignati et al. (1999), Takano et al. (2004), Gammons et al. (2005), Varekamp et al. (2009), Morton-Bermea et al. (2010), Peiffer et al. (2011), and recently in a MSc thesis by Ayers (2012).

The solubility of the REE in geothermal fluids (Michard 1989) depends on the pH, the presence of ligands for complexing the REE, and the stability of solid phases that may incorporate the REE, adsorb them on active surfaces, or the formation of more or less pure REE phases (e.g., xenotime, monazite). The REE may co-precipitate with some Al-rich phases and phosphates (Gammons et al. 2005). To evaluate the abundance of the REE in volcanic lakes, rivers and springs, the data are usually normalized on their chondritic abundances. Because the REE in hydrothermal fluids are ultimately derived from the dissolution of the local volcanic rocks, normalization of the aqueous REE abundances on the REE in the local rocks is a useful alternative, where fully flat REE patterns suggest simple congruent dissolution of the REE from the hydrothermal rock matrix.

The fluid REE patterns may deviate from the rock patterns as a result of

1. Preferential LREE leaching from bulk fresh volcanic rock (Takano et al. 2004);
2. Preferential attack of specific minerals that are enriched in LREE (e.g., plagioclase, apatite, anhydrite) or have a positive Eu anomaly (plagioclase);
3. Leaching of REE from "mature reservoir rocks" that were already depleted in LREE through 1 and 2;
4. Precipitation of hydrothermal minerals that fractionate the LREE such as anhydrite, apatite, and jarosite-alunite;
5. Re-dissolution of hydrothermal reservoir minerals (see #4);
6. Presence of ligands that preferentially bond to a subgroup of the REE.

Primary chloride-rich volcano-magmatic fluids have LREE enriched patterns relative to the associated magma (Wood 2003). Interaction of geothermal fluids with fresh volcanic rock also will lead to LREE-enriched fluids, and this has been well established for submarine hydrothermal systems (e.g., Bao et al. 2008). These simple observations are complicated by the time progression of W/R interaction, with LREE depletion in the rock protoliths taking place over time. Systems with intense rock dissolution such as the acid volcano hydrothermal systems have the highest REE concentrations (Wood 2003), and as a result of earlier intense W/R interaction may show effects of protolith maturation. Most rock-forming minerals in andesitic rocks are LREE-enriched, but have lower REE concentrations than the remaining melt. In most mafic magmas, the REE act as mildly incompatible elements and largely end up in the glassy groundmass (Wood 2003). The preferential dissolution of one or more of the rock-forming minerals during W/R interaction will influence the REE pattern in the fluids, and is best traced by combining the water chemistry with REE patterns, e.g., enrichments in Al, Na, Ca and Sr in the fluids suggest plagioclase dissolution, and may be possibly associated with a positive Eu anomaly. Dissolution of important REE host minerals such as apatite would be accompanied by increases in P while a strong decrease in K concentration in time series suggests saturation with K-rich phases like alunite-jarosite and associated LREE fractionations (Ayers 2012).

The REE patterns in fluids at Copahue volcano show several trends over a 15 year record (Fig. 8a). The Eu anomaly in the fluids peaked during the 2000 eruption and then again during the 2004 period of anomalous activity (Varekamp et al. 2009; Agusto et al. 2012). The smaller negative Eu anomaly (higher Eu/Eu* values) may be correlated with the dissolution of plagioclase from the freshly intruded magma batch. The La/Sm varies more or less opposite from the Eu anomaly, and suggests that the REE contributions from plagioclase (low in REE) are not dominating the REE releases from the rocks, but provide an influence on the Eu anomaly. The La/Sm varies over time and shows a discrete low during the 2000 eruption, probably caused by the crystallization of alunite that strongly fractionates the LREE (Fig. 8b).

The Santa Ana (El Salvador) lake fluids (Colvin et al. 2013) show a trend over time in the first half of 2007 of LREE-depleted fluids to roughly "rock patterns" (REE/rock pattern flat, Fig. 8c). All element concentrations changed over the first six months in Santa Ana crater lake, as a result of intense evaporation, so only cation

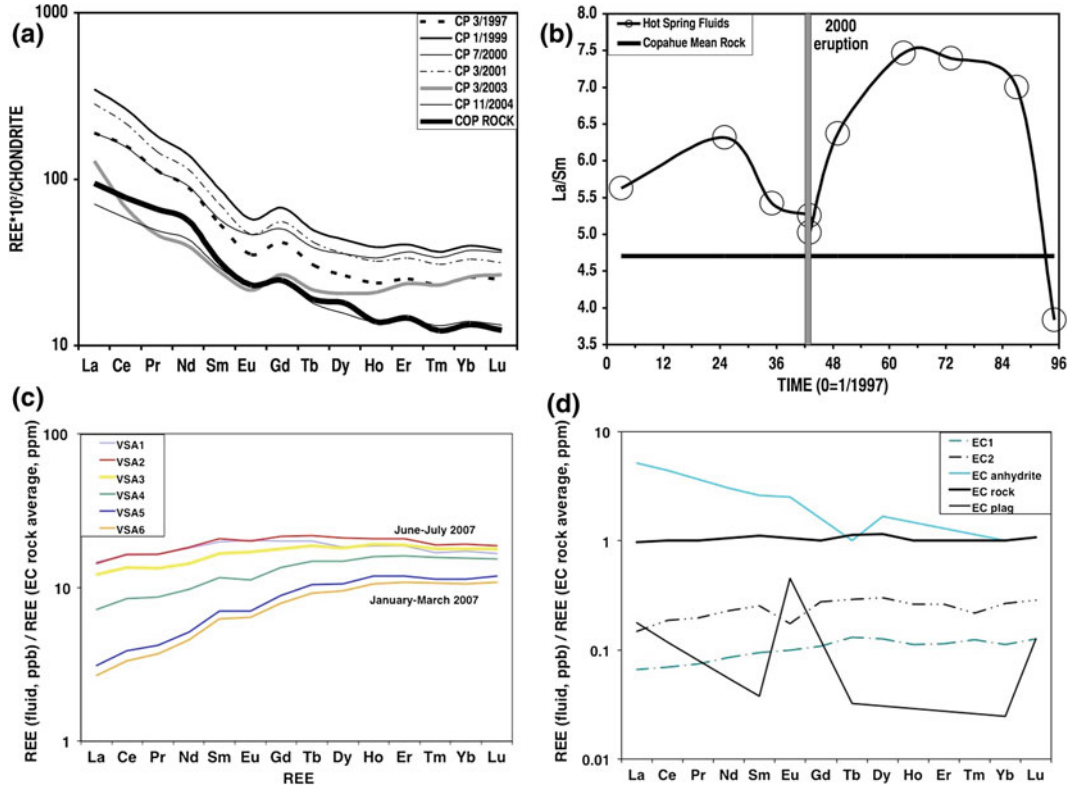

Fig. 8 **a** The REE patterns (normalized on chondritic values) show LREE enrichment in the Copahue rock but even more so in the Copahue fluids, with only minor variations over time. **b** The La/Sm values in Copahue hot spring fluids decreased strongly during the eruption; the alunite saturation at the time fractionated the LREE. **c** The REE patterns for Santa Ana Lake, normalized on local rock. The January 2007 fluids are strongly depleted in LREE (through LREE retention in precipitated alunite), which decreases in strength in the later water samples (July 2007), which show REE patterns close to those of the Santa Ana rock (values >1 because of dilution scaling). **d** The REE patterns for rock and mineral phases of the 1982 El Chichón eruption with two lake water REE patterns (EC1–EC2). The lake fluids resemble the rock pattern (flat to slightly LREE depleted), suggesting that the anhydrite (important LREE reservoir) was already dissolved away at this stage of the lake evolution

ratios are good indicators of relative element depletion. The La/Sm is negatively correlated with Mg/K and Na/K, indicating that La/Sm decreases when K decreases. The minerals alunite-jarosite are both REE-rich and strongly LREE-enriched, and their precipitation creates LREE-depleted patterns in the fluids, whereas dissolution of these minerals may have driven the patterns back to a flat shape or even LREE-enriched patterns in rock normalized REE plots (Fig. 8c).

The El Chichón fluids (Peiffer et al. 2011) show relatively flat to slightly depleted LREE patterns relative to local rocks (Fig. 8d), suggesting that near congruent dissolution of the rocks occurs. The REE patterns of the phenocrystic phases in the 1982 pumices of El Chichón are shown as well (Luhr et al. 1984) and all of these minerals are LREE enriched, with the magmatic anhydrite having the highest REE levels. Apparently, these phases were already dissolved in the protolith and a LREE-depleted rock remnant is being dissolved. Many mature lake fluids are LREE depleted with respect to the source rock as a result of protolith maturation and alunite precipitation in the deep hot reservoir underlying the lake, whereas immature fluids may be LREE enriched because of the

preferential removal of the LREE during incipient W/R interaction with fresh rocks (Takano et al. 2004). The review on the REE in the major acidic active crater lakes of Ayers (2012) concludes that both preferential dissolution and precipitation of alunite-jarosite are the main processes that influence the REE patterns in these acid lake fluids.

4 Long-Term Compositional Lake Water Trends and Lake Dynamics

Volcanic lakes are dynamic systems that may have secular changes in chemical composition at time scales of months to decades, reflecting changes in the inputs or outputs (e.g., enhanced evaporation). Trends in volcanic lake compositions may aid in monitoring volcanic and geothermal activity (Takano 1987; Takano and Watanuki 1990; Rowe et al. 1992a; Takano et al. 1994a; Vaselli et al. 2003; Ohba et al. 2008).The following processes change the chemical composition of volcanic lakes:

- Changes in the input composition and/or magnitude;
- Shifts in meteoric water inputs or evaporation, disturbing the hydrological balance of the lake;
- Lake water saturation with a new mineral;
- Changes in a lake ecosystem with changes in biological element drawdown;
- Changes in physical or chemical lake condition such as stratification, bottom water oxygenation, or temperature structure.

All of the above processes may impact the steady state condition of a lake for dissolved elements, and the effects of non-steady state dynamics should always be considered. The simplest reason for changes in lake water composition is a change in the volcanic input (1 above), which may reflect changes in the overall composition of the underlying volcano hydrothermal system. Time-composition histories of well studied volcanic lakes such as at Lake Ruapehu, Poás volcanic lake, Copahue crater lake, Lake Caviahue, Kawah Ijen and Yugama-Kusatsu Shirane serve as examples where the lake composition variations over time resulted from changes in input flux in terms of its mass flux and its chemical composition (Christenson and Wood 1993; Ohba et al. 1994, 2000; Delmelle and Bernard 1994; Delmelle et al. 2000; Martínez et al. 2000; Christenson 2000; Varekamp 2008; Agusto et al. 2012). With a change in input composition, element ratios in the lake waters will change and overall concentrations may increase or decrease. Input changes may induce other limnological shifts such as density stratification (Christenson 1994) or ecosystem impacts (e.g., enhanced productivity). Obviously, changes in the input will take the lake system out of compositional steady state and the composition will evolve over time towards a new steady state, as discussed below. Enhanced evaporation (with increased lake temperature or changes in climate) or decreases in meteoric water input may lead to a smaller lake volume with higher dissolved element concentrations for similar volcanic input (Rowe et al. 1992a, b; Rouwet et al. 2008).

Many carbonate-rich lakes are close to saturation with carbonate minerals and various organisms may precipitate carbonate shells (e.g., snails, ostracods) providing an in-lake sink for carbonate and cations. Many volcanic lakes are rich in dissolved silica, and diatoms precipitate silica frustules in large quantities. Chemically more extreme lakes may be saturated with gypsum, jarosite, and schwertmannite and one or more of the Fe-oxides (goethite, ferrihydrite, possibly hematite; e.g., Bani et al. 2009). Precipitation of one or more of these phases will change the lake water compositions.

Changes in nutrient dynamics may stimulate a lake ecosystem, resulting in enhanced drawdown of carbon, possibly Si and the common nutrients N and P (e.g., Pedrozo et al. 2008). The concentrated input of a volcanic river in a lake may either mix completely with the lake waters or may form a plume with a higher density that settles to the deeper regions of the lake or into the hypolimnion, the deep bottom water layer in thermally stratified lakes. Changes in element concentration or temperature thus may influence the chemical stratification of a lake with either a less concentrated epilimnion (top layer, less dense lake water) or building a more saline and

cold (dense) bottom water mass. Such a density stratification may impact the seasonal mixing characteristics of the lake and may lead to bottom water hypoxia or anoxia in case of a productive epilimnion or organic-rich bottom sediments.

Volcanic lake systems vary from very stable examples, with a long-term constant composition, to lakes with wildly variable compositions. These secular composition trends are both a function of the magnitude of the input fluctuations but just as much of the physical properties of the lake system. Box modeling of volcanic lakes was discussed among others by Varekamp (2003), Rouwet et al. (2004), Rouwet and Tassi (2011). The lake dynamics are best treated in terms of a "closed" and an "open" lake system:

I. Many crater lakes and caldera lakes occur in a "closed container", with a conical or broadly cylindrical volume. These lakes have substantial fluctuations in water level and volume with changes in lake temperature (evaporation) or shifts in hydrological inputs (e.g., Rouwet et al. 2008). Water loss occurs largely through seepage and evaporation (e.g., Hurst et al. 1991; Rowe et al. 1992a).
II. Open lakes have a surface outlet, and as a result a more stable lake volume. The outflow rate is impacted by lake level, because open channel flow is sensitive to water level. The enhanced outflow at a lake high stand will quickly lower the water level, with resulting slower outflow rates.

The water residence time (RT) in lakes is usually defined as the mass of water in the lake divided by the total input or output fluxes (Varekamp 2003; Taran and Rouwet 2008). The RT can only be formally defined at steady state (SS), when input equals output and lake volume is constant. In lakes with variable volume, the RT becomes a transient, but stabilizes once water steady state is restored. The dynamics of dissolved chemicals follow that of water for conservative elements but may differ for elements with additional sources or sinks in the lake. Changes in the hydrological balance of a lake will impact the dynamics of dissolved elements, even at a constant element input rate.

A main difference between the two types of lakes is the magnitude of the water outflux (Fig. 9a). In open lakes, the outflux of water adapts rapidly to changes in water input, and water steady state is maintained together with a close to constant lake volume. In closed lakes, the output (seepage) is in the simplest case a linear function of the hydrostatic pressure at the bottom of the lake, which depends on the water depth. As a simple example, consider a cylindrical lake with surface area A and initial volume V. The water outflux is a function of the height of the overlying water column (d_{max}) and described by Darcy's law (e.g., Todesco et al. 2012). We can phrase the seepage outflow of the lake when fully filled and at steady state for water as a constant K_1 (containing variables such as permeability, viscosity, length scale of seepage, etc.) multiplied by the water height (d_{max}, the hydraulic head). When we reduce the inflow (e.g., long term climate change or multiyear droughts), the outflow will remain initially roughly the same, whereas the input has been reduced. As a result, water level will fall, with then a diminished seepage outflow at the bottom when d_{max} becomes d_t. The seepage outflow can then be phrased as $(d_t/d_{max})*K_1$, where K_1 is determined from the original steady state flow condition. The parameter d_t can also be expressed as a function of V through the constant surface area A, leading to $dV/dt = INPUT—K_2\ V$ with K_2 a new assembled constant. Solution of this equation shows an exponential decrease in volume V over time reaching a new water steady state when input equals output again.

The responses in closed lake systems are identical to that of open lakes for changes in hydrothermal input only (volume of lake is constant, hydrothermal input small compared to meteoric water input) but quite diverse for changes in hydrology (changes in water input). Changes in output flux of a substance P are shown for both lakes (Fig. 9b) at constant volcanic input but changing the hydrology, in this case a fivefold decrease in meteoric water input. This leads to a fivefold decrease in the rate of outflow in the open lake system and ultimately a

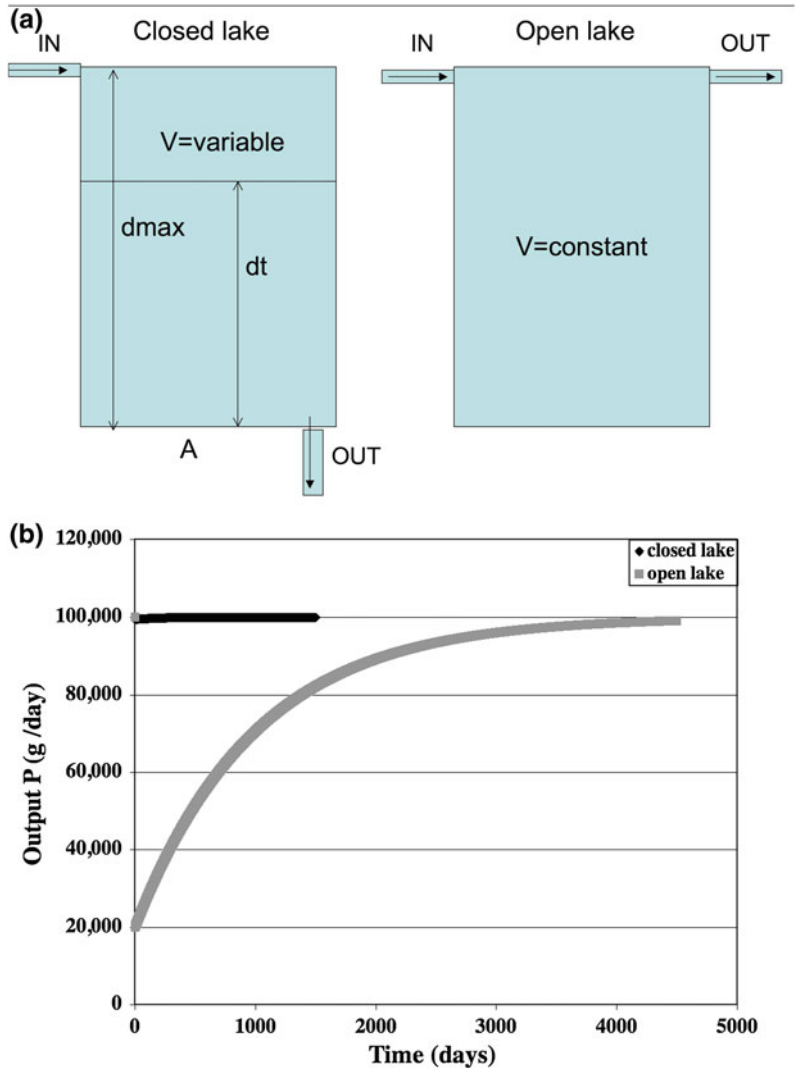

Fig. 9 **a** Closed and open lake systems with different water outlet dynamics. In the closed case, the outlet flux is a function of water depth (d_t) whereas the influx and outflux are equal in the open lake system. **b** Example of adjustment of the flux of an element P after a five-fold decrease in meteoric water input while the volcanic input remains constant. The element output in the seepage lake is constant (smaller volume, smaller water outflux with higher concentrations), whereas the open lake takes ~6 RT to reach close to steady state again

fivefold increase in concentration in both lakes after steady state has been restored. The element output in the closed lake remains constant (decreasing water flow with increasing concentrations) and steady state is restored fairly quickly. The open lake will take ~6 RT to restore to close to steady state (Varekamp 2003) when the element output flux equals the input flux again. The concentrations in the closed lake system also respond very quickly to the disturbance (smaller RT of water with smaller water volume in lake) whereas it takes longer to be implemented in the open lake system (Fig. 10).

Lake water compositional trends are commonly used as a tool in volcano monitoring, so a good understanding of the lake dynamics is essential. The principles of non-steady state lake water evolution in a perfectly mixed lake with a single surface outlet, evaporation, and multiple inlets has been treated by Albarede (1995), and specific cases for volcanic lakes were treated by Varekamp (1988, 2003, 2008) and Taran et al. (2013). The master equation for a dissolved element E is

$$dA_E/dt = IN - OUT \quad (1)$$

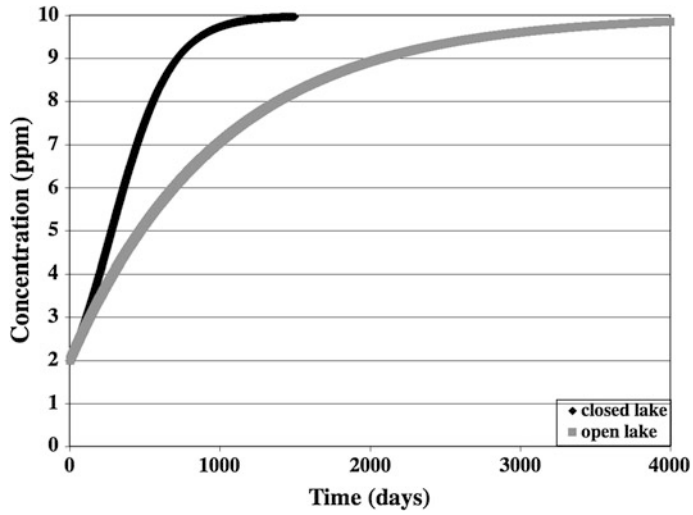

Fig. 10 Concentration-time curves for open and closed lake systems after a fivefold decrease in fresh water input. The closed lake reacts much quicker than the open system because the decreasing lake volume leads to a shorter RT with the initially still large outflux at d_{max}. The fivefold reduction in fresh water input leads to a fivefold increase in concentration at steady state

in which A_E is the total amount of an element E in a lake and IN and OUT represent the sum of the influxes and sum of the out fluxes of E. For a lake system with water in steady state, the lake volume is constant, and the IN term for E can be phrased as the Σinputs = $\Sigma\, Q_{in}{*}C_{in}$. The Q_{in} is the water influx, and C_{in} is the concentration of E in the inputs, which could be a river or subaqueous hydrothermal springs or both. For a conservative element, the output of E is $Q_{out}{*}C_t$, where C_t is the time dependent concentration of E in the lake water, and Q_{out} is the liquid water outflow of the lake. The lake has a volume (or mass) of V and the residence time of water (RT) is defined as V/Q_{out}, where Q_{out} equals ΣQ_{in} at water steady state (neglecting the evaporation term). The elemental output term can be rephrased as the fraction of A_E removed per time unit which translates into $Q_{out}{*}C_t = (Q_{out}/V){*}C_t{*}V = (1/RT){*}A_E = kA_E$, where $1/RT = k$, which is the renewal or flushing rate. In this case, the RT of water equals the RT of E if the evaporation term is negligible with respect to Q_{out}. Equation (1) for conservative elements can then be restated as

$$dA_E/dt = \sum Q_{in} * C_{in} - kA_E \qquad (2)$$

and the general solution to this equation is

$$C_t = C_{ss}\left(1 - e^{-kt}\right) + C_o e^{-kt} \qquad (3)$$

where C_o is the initial concentration and C_{ss} is the steady state concentration. The C_{ss} for conservative elements can be expressed as $\Sigma(Q_{in}{*}C_{in})/Q_{out}$ (Varekamp 1988, 2003). If the evaporative flux is significant, the RT(water) is unequal to the residence time of E which then equals $(V{*}C_t)/(Q_{out}{*}C_t) = V/Q_{out}$, whereas the RT(water) equals $V/(Q_{out} + Qe_{vap})$. For non-conservative elements, Eq. (2) is rewritten as

$$dA_E/dt = \sum Q_{in} * C_{in} - k_1 A_E - k_2 A_E - kA_E \qquad (4)$$

where the different k factors represent the rate factors for the various sink processes, including the flushing factor k as in Eq. (2). The various k terms can be assembled into a compound k_{tot} which then replaces the simple k factor in Eq. (3). The C_{ss} in that case is then rephrased as

$$C_{ss} = \sum (Q_{in} * C_{in})/(k_{tot} * V) \qquad (5)$$

which is the general form (Varekamp 2003). Equation (3) can be used for forward modeling of time series of lake water composition for conservative elements with k known from hydrologic studies. For non-conservative elements, the different k values are required for forward modeling, but a comparison between a conservative and a "suspect" non-conservative element will provide information on the strength (k value) of its in-lake sink (e.g., saturation with a mineral or adsorption onto another phase).

Empirical time series of lake water data can also be analyzed by plotting the lake water composition versus time in order to determine the input fluxes of a conservative element of interest. The time series may reflect dilution processes after a period of contamination of a lake with volcanic fluids, or progressive contamination with a volcanic input until the lake reaches steady state for that element. Equation (2) can be developed for 'backward looking' scenarios:

$$(C_t - C_{ss})/(C_o - C_{ss}) = e^{-kt} \quad (6)$$

which is rephrased for the general case as

$$\ln(\mathrm{ABS}(C_t - C_{ss})) = -k * t + \ln(\mathrm{ABS}(C_o - C_{ss})) \quad (7)$$

where the absolute values (ABS) are used in the logarithmic terms. Equation (7) is an expression of the form y = ax + b, so a plot of ln(ABS $(C_t - C_{ss})$) versus time t provides a straight line with a slope of -k and an intercept along the y axis of ln(ABS$(C_o - C_{ss})$), with at t = 0, $C_t = C_o$ and at t = ∞, Ct = C_{ss}. Measured data can be easily back-fitted by varying Css (e.g., in Excel) until the slope assumes the required −k value, which will constrain the mean input flux of the element E (Eq. 5). For a pure dilution scenario, $C_{ss} = 0$, and Eq. (6) then reduces to $C_t = C_o\, e^{-kt}$ and Eq. (7) reduces to ln(Ct) = −k * t + ln (C_o) with $C_t = C_o$ at t = 0 and $C_t = 0$ at t = ∞. When a variable input flux is suspected, linear segments of a composition-time curve can be fitted with the appropriately chosen C_o values.

These principles are applied here for Lake Caviahue at Copahue volcano in Argentina. This lake has a volume of ∼0.5 km^3 and a water RT of ∼42 month, giving a mean outflow rate of 4.3 m^3/s. The total amount of rock forming elements in the lake (RFE) has varied substantially over the years (Fig. 11) with an increase between 1997 and 2000, which is a non steady state effect at a constant input rate. During the 2000 eruption (month 43), the fluxes increased strongly, and then the hydrothermal system almost shut off as a result of reduced permeability through alunite crystallization in the reservoir (Varekamp et al. 2009). The lake input fluxes became very small and Lake Caviahue became more dilute between 2000 and 2003 (month 43–72). In late 2003, the fluxes increased again during the "thermal anomaly" (month 84), which created a blockage of the pathway of fluids into the Copahue crater lake (Agusto et al. 2012), but caused enhanced element export through the hot springs into the Upper Agrio River. After the thermal anomaly, the fluxes decreased and then increased again and non steady state effects governed the increase in concentrations over the next three years (till 2009 or month 147). The flux of volcanic elements (S, Cl) increased over the last three years and a summary of all the fluxes is shown in Fig. 12. The Cl-time curve for the lake (Fig. 13) from 1997 to 2009 shows a peak in 2000 (eruption) and a small bulge around the 2004 "thermal anomaly" (Agusto et al. 2012). I fitted the data from 1997–2000 according to Eq. (7), and obtained a mean flux of 1,174 tons Cl/month, whereas the mean of the measured fluxes from data on the inflow river was 1,192 tons Cl/month. The intercept on the graph was 3.1, whereas the calculated intercept from Eq. (7) was 3.0. The dilution over the period 2000–2003 with the strongly reduced influx was estimated at 475 tons Cl/month. The observed Cl inputs in 2001 and 2002 had a mean of 560 tons Cl/month. The period 2006–2009 gives a mean Cl flux of 1,100 tons Cl/month versus a measured value of 1,160 tons Cl in 2006, but higher measured fluxes (1,650–1,700 tons Cl/month) were found in 2008 and 2009 compared to the modeled fluxes.

The differences between measured and calculated values are the result of uncertainties in the measurements of water flux and concentrations

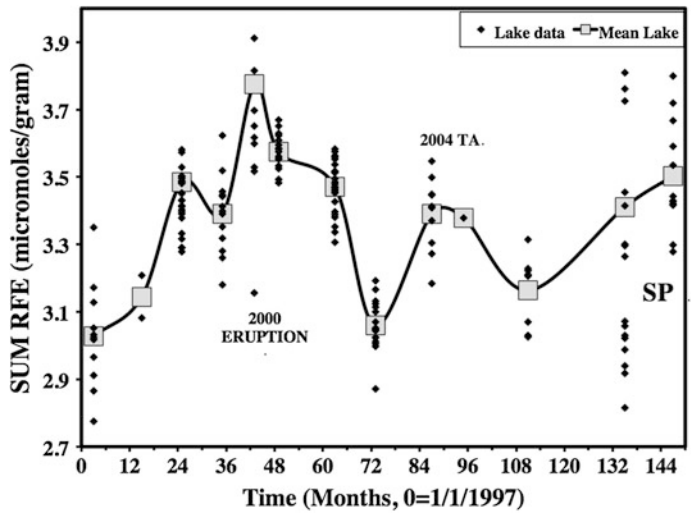

Fig. 11 Time versus total concentration of rock forming elements (RFE) for Lake Caviahue, with an increase prior to the 2000 eruption (non steady state effect), a peak during the 2000 eruption (enhanced flow and element concentrations from the hydrothermal system), with strongly diminished concentrations after the 2000 eruptions. During the 2004 thermal anomaly (TA), the fluxes increased again (intrusion into hydrothermal system, abundant alunite precipitation in upper part of system, no eruption). After the 2004 thermal anomaly, concentrations showed a steady rise, (non steady state effect) with Schwertmannite precipitation (SP) in 2009 (month 135), ultimately leading up to the next eruption in 2012

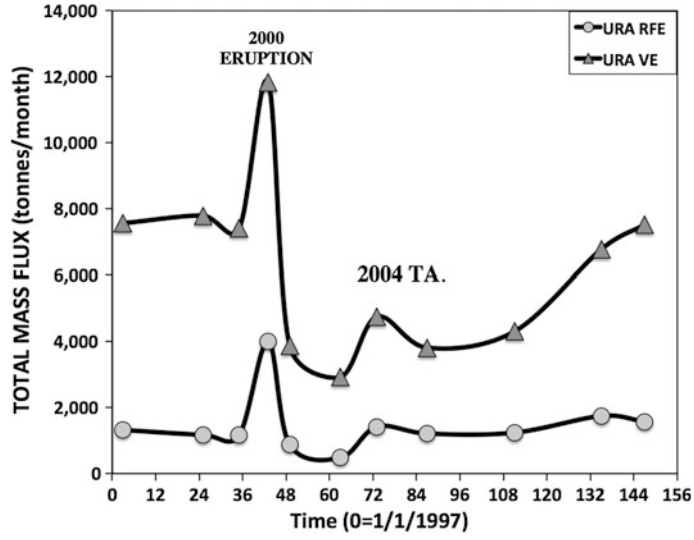

Fig. 12 Element mass fluxes as measured at the entrance of Lake Caviahue. Strong increase in fluxes during the 2000 eruption and during the 2004 thermal anomaly, with an increase in the volcanic gas elements (VE) towards 2010

(±15 %), whereas the lake concentration values are the average of full depth profiles, which in a stratified lake may not represent the fully-mixed concentration as related to a current input value. And of course, the true fluxes may have varied over time and a single annual measurement is only a crude approximation. This graphical approach of estimating mean input fluxes from a changing lake composition is a very useful tool in lake pollution in general and especially in volcano monitoring. Taran et al. (2013) applied a similar rationale to input changes in Karymsky

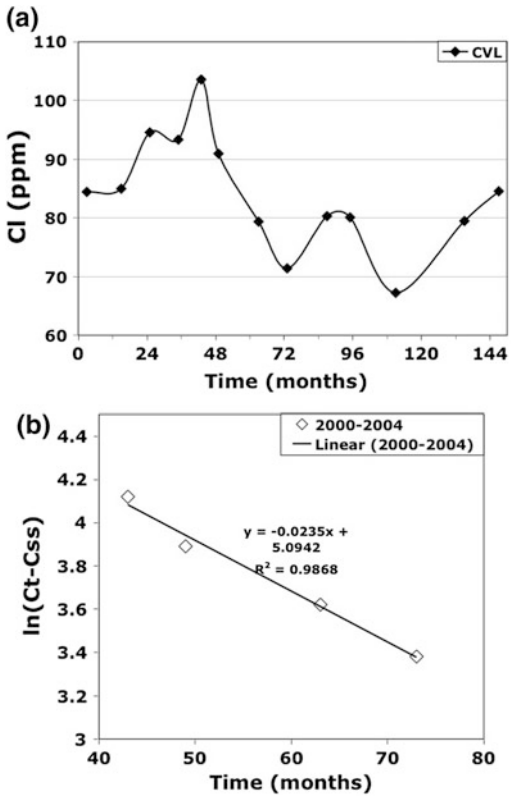

Fig. 13 **a** Concentration of Cl in Lake Caviahue over time. The interval from 2000 to 2003 (month 43–72) was a time of strong dilution. **b** Application of backward modeling for Cl, where the slope of the line equals the −k value when the appropriate Cl influx value (equates to the C_{ss} value) is selected

Lake (Kamchatka) after a volcanic eruption. Alternatively, if the inputs are known from river water measurements, the same set of equations can be used to get better estimates of the RT of an element in a lake system in search for possibly unknown element sinks.

The forward modeling approach is illustrated for aluminum in Lake Caviahue. The time-concentration graph for Al (Fig. 14a) shows slightly elevated concentrations during the 2000 eruption and then a dramatic drop off after the eruption. The forward modeling is done by varying the input fluxes over time, showing good agreement until 2008–2009, when the measured fluxes become substantially larger than the required fluxes according to the model (Fig. 14b, similar to Cl). The lake was theoretically saturated in schwertmannite, jarosite and Fe-oxides but not with Al-rich phases like alunite (Varekamp 2008). Thus variations in volcanic lake water composition should be interpreted within the context of both the water balance (e.g., evaporation rate, meteoric water fluxes) as well as changes in the volcanic input (magnitude or composition). Every change in parameter will be accompanied by a return to steady state and these non steady state dynamics need to be considered when interpreting lake water composition time trends.

5 Isotopes in Volcanic Lakes

Volcanic lakes may have unusual isotopic characteristics compared to non volcanic lakes because of their geothermal/volcanic inputs. A detailed chapter on the isotope geochemistry of volcanic lakes treats the main aspects of the isotopic abundances of the common elements (Rouwet and Ohba this issue). In terms of O and H isotopes, many volcanic lakes have a geothermal component that is heavy in $\delta^{18}O$ as a result of W/R interaction, whereas some lakes have a volcanic gas component that is very heavy in $\delta^{18}O$ and δD (Giggenbach 1992a). In addition, volcanic lakes may be slightly warmer than non-volcanic lakes, leading to higher evaporation rates and as a result, more evolved isotopic compositions. Evaporation of lake waters creates a straight line (evaporation line) in $\delta^{18}O$–δD diagrams, with a slope that depends on the relative ambient humidity but is less than the meteoric water line. Evaporation from lakes that are warmer than ambient creates flatter evaporation lines than similar cooler lakes (Varekamp and Kreulen 2000). The open and closed lakes discussed above also would have different isotopic characteristics because open lakes usually have a shorter water residence time for the same lake volume, creating less evolved isotopic compositions than closed lakes, be it on the same evaporation line if in geographically close proximity. An extreme example from the Copahue crater

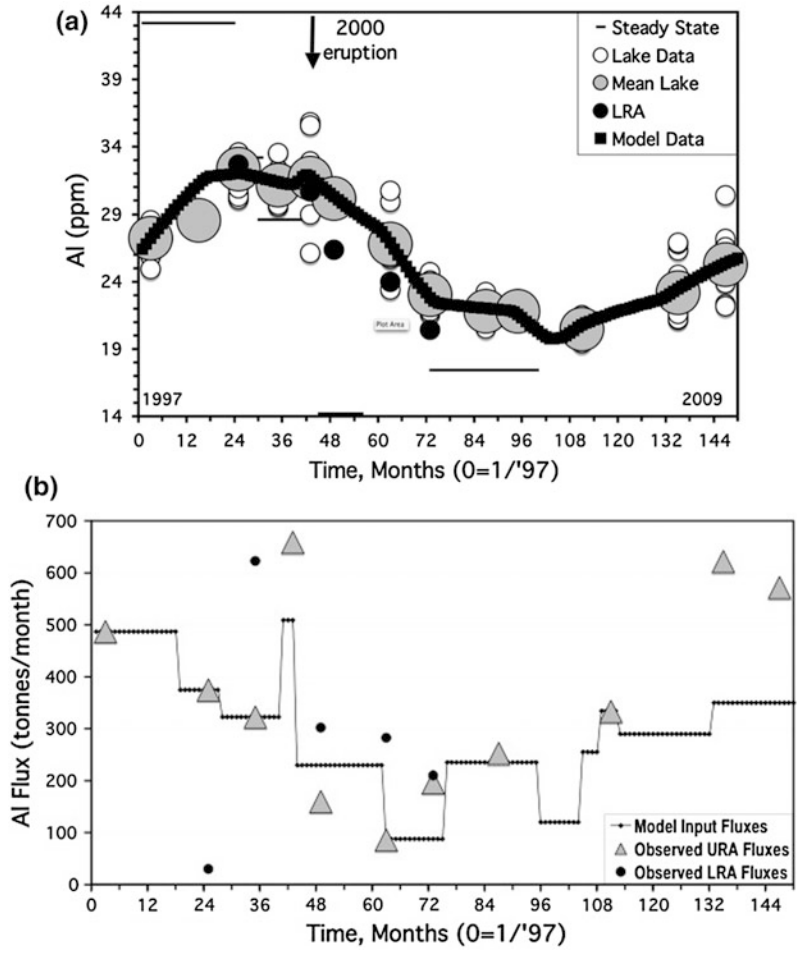

Fig. 14 **a** Time versus Aluminum concentration in Lake Caviahue. The general decrease in Al after the 2000 eruption is a reflection of Al retention in the hydrothermal system in alunite as well as a diminished flux magnitude into the lake. **b** The observed and modeled Al fluxes over time, showing good agreement between the annual data and modeled values, with a strong disagreement over the last two years (Al sink in lake?)

lake and hot spring system is shown in Fig. 15. The hot spring samples show pure mixing between meteoric waters and a volcanic brine, whereas the crater lake shows the added effects of evaporation through enrichment in $\delta^{18}O$. Close to 50 % of the hot spring fluids may be volcanic brine, the rest is glacial melt water. Lake Caviahue (Argentina) consists largely of meteoric water, and despite its long-term input of volcanic fluids, this open lake plots close to local meteoric waters in the $\delta^{18}O$ and δD diagram (Varekamp et al. 2004) with only a 0.5–1 ‰ offset for $\delta^{18}O$ as a result of evaporation.

The sulfur isotope values in the extremely acidic crater lakes (Delmelle and Bernard this issue) are determined by the disproportionation processes of SO_2 in the hydrothermal reservoir, and may reach up to +20 ‰ for dissolved sulfate species. The liquid sulfur that is the second component of the disproportionation process (Oppenheimer and Stevenson 1989; Takano et al. 1994b) can be as light as −10 ‰. The $\Delta\delta^{34}S$ ($S–SO_4$) is a function of the temperature of disproportionation and the kinetics of the process (Kusakabe et al. 2000). In addition, bacterial processes may modify the sulfur isotope ratios at lower temperatures in acidic lakes (Gyure et al. 1990).

Some cosmogenic isotopes survive the subduction process, e.g., ^{129}I, which forms from Xe in the upper atmosphere. Small amounts of ^{129}I have been detected in hydrothermal fluids and crater lakes, indicating the presence of recycled volatiles in these lakes that were originally

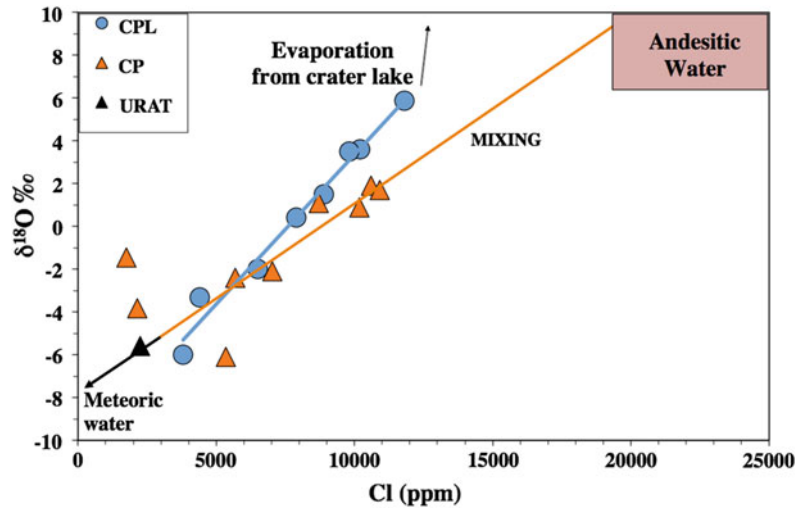

Fig. 15 The $\delta^{18}O$ in the Copahue hot spring system (CP and URAT) and in the crater lake fluids (CPL) is a mixture between local meteoric water and a volcanic brine (andesitic water). The crater lake water samples also show evidence of strong evaporation, leading to "heavier" $\delta^{18}O$ values

hosted in subducted sediments (Fehn et al. 2002). The isotopes of the noble gases are used to trace the origin of the magmas: mantle versus crustal gases (e.g., Aeschbach-Hertig et al. 1996; Agusto et al. 2013).

Many volcanic lakes with a geothermal/volcanic CO_2 input (Chiodini et al. 2000, 2012; Carapezza et al. 2008) have $\delta^{13}C$ compositions that deviate from atmosphere-derived carbon. The bulk $\delta^{13}C$ of dissolved carbonate in volcanic lakes is a function of the bulk $\delta^{13}C$ of the input term, and the fractionations that may occur in the lake as a result of photosynthetic activity. In addition, the various carbonate species each have their own $\delta^{13}C$ offset, with the dissolved CO_2-H_2CO_3 lighter than the HCO_3^-, which is usually the main component. Loss of CO_2 through diffusion processes at the lake surfaces may fractionate the bulk dissolved $\delta^{13}C$. To reconstruct the isotopic values of the CO_2 input in a volcanic lake, all other processes have to be quantified. The organic matter that is produced through primary productivity in these lakes may also be different from that in non-volcanic lakes. The $\delta^{13}C$ of most "magmatic" CO_2 (mantle) is in the range of −3.5 to −6 ‰ (e.g., Cartigny et al. 2001), which is not far from modern atmospheric values for CO_2 (Keeling et al. 1979; −7.5 to −8.5 ‰). The uptake of CO_2 from the atmosphere is an open system, with a shift of about 7 ‰ from CO_2(atm) to HCO_3^-(water), which would lead to dissolved bicarbonate close to 0 ‰ for non-volcanic lakes at neutral pH values. With subaqueous CO_2 inputs, most likely the CO_2 stream is completely absorbed and no isotope fractionation occurs between gas and fluid, and the bulk $\delta^{13}C$ is equal to that of the incoming gas. Surface degassing through diffusion will fractionate the remainder, leaving behind a heavier $\delta^{13}C$ signature in dissolved inorganic carbon. The CO_2 degassing from volcanic lakes may constitute a significant term in the terrestrial CO_2 degassing (Pérez et al. 2011).

Radiogenic isotope ratios in lake waters can be used to trace the sources of the fluids. Strontium isotope ratios were used in El Chichón lake to trace the incoming fluids and their origin (Peiffer et al. 2011). Stable lead isotope ratios in Copahue crater lake waters were identical to that of the rocks that make up the underlying volcano (Varekamp et al. 2006). The Pb in the lake waters thus was acquired during rock dissolution in the hydrothermal system below the lake, and subsequently injected into the surface environment, proving once more that the local volcanic rocks provide the source for most of the rock-derived cations.

6 Volcanic Contaminants in Lakes and Outlets

Volcanic emissions are rich in volatile metals such as Fe, Pb, Cu, Zn, Cd, Hg as well as the non-metals As, Li, Al, and B (Symonds et al. 1987; Taran et al. 1995). These elements, together with F, are among the more potent contaminants that form a health hazard for people or animals (Sriwana et al. 1998; Heikens et al. 2005a, b; Löhr et al. 2005; Hansell et al. 2006; López et al. 2009, 2012). Concentrations of these elements in volcanic emissions vary widely: this variability relates to the degree of maturity of the hydrothermal fluids, the original magmatic signature as well as the emission pH and temperature, which may have led to precipitation of sulfides in the shallow volcano superstructure. Volcanic hot springs and volcanic lakes show values in the ppm range for the base metals, much lower concentrations for Hg and up to 15 ppm for As (Kading 2011). The element Li can run up to several ppm and boron to >100 ppm (Table 1), whereas F concentrations may exceed 2,000 ppm (Table 1). Many of these fluids may create local surface waters that far exceed drinking water standards (WHO 1996). Crater lake water analyses often show high concentrations of these trace elements, but these waters are in general not for consumption, although some lake waters are used for therapeutic purposes in thermal health spas (e.g., Copahue). More dilute lakes usually have very low base metal concentrations but may have As concentrations well above the drinking water limit. East Lake and Paulina Lake in the Newberry caldera (OR, USA) are respectively enriched in Hg and As, with up to 15 ppb As in the water (Lefkowitz 2012). The Hg in East Lake resides largely in the sediment but all fish tend to have high Hg concentrations as well. Direct risks for human exposure to volcanic contaminants come from contaminated drinking water (most common are F, As) and use of volcanic lake waters in irrigation (near Kawah Ijen, Löhr et al. 2005). Other examples of large, largely meteoric water lakes contaminated by hydrothermal fluids of a volcanic origin are Clear Lake (California, USA), which has a strong Hg input from subaqueous and coastal hot springs (Suchanek et al. 2008). The Hg pollution of Clear Lake is often blamed on Hg mines present on the margin of the lake (e.g., the Sulphur Banks Hg mine), but many hot springs produce Hg-rich waters that drain into the lake and probably occur at the lake bottom as well. Most likely, the Hg contamination was enhanced through the mining activities, but the lake has a history of 1000s of years of Hg contamination from volcanic sources, and the Hg deposits on its rim are just an expression of the presence of these subterranean fluids (Varekamp and Waibel 1987). Northern Chile has a long history of As pollution from volcanic sources, and As-related disease among the local Mapuche Indians is common (Romero et al. 2003; Oyarzun et al. 2004).

The acid lakes and their outlets with high trace contaminant concentrations also tend to be rich in iron, which upon dilution (pH>) may precipitate as Fe-oxides or Fe sulfates. The mineral schwertmannite ($Fe_8O_8SO_4(OH)_6(H_20)$) is common in mineralized volcanic rivers and in many acid mine drainage environments, and is a strong absorbent for the oxyanions of P, V and As (e.g., Acero et al. 2006; Fernández-Remolar et al. 2005). The Lower Río Agrio that drains Lake Caviahue has been saturated from 2003 till recent in schwertmannite, and the mineral has up to 1,000 ppm As and 5,000 ppm P (Kading 2011). The concentrations of As and P in the water drop to levels close to 'below detection values' in the zones with the schwertmannite beds. However, with re-acidification of Lake Caviahue during renewed volcanic activity, as occurring in 2013, the schwertmannite is re-dissolved and the As, V and P are re-released and may present a health danger further downstream. Photochemical processes may influence the dissolved Fe contents of rivers at high altitude and influence the scavenging of oxyanions such as arsenic by Fe-oxides (e.g., McKnight et al. 2001; Parker et al. 2008).

7 Conclusions

Volcanic lakes show a wide variety of compositions, spanning the complete range of extreme fluids with ultra low pH to carbonate-rich fluids with pH >9. The origin of these lake waters is either in hydrothermal fluid reservoirs under the lake inside active volcanoes, or directly in the lake system itself. Variations in lake water composition are a function of fluctuations in hydrothermal inputs, variations in meteoric water fluxes, activity of ecosystems, and chemical processes in the lake itself, coupled with non-steady state dynamics. The long term compositional trends carry useful information on the activity of the underlying volcano, if corrected for dynamic effects of water recharge and non-steady state processes. The stable isotope characteristics of lake waters provide insights into the underlying hydrothermal reservoir and its temperature regime as well as lake processes like evaporation and magmatic gas supply. The chemical lake water composition has important environmental health implications, with special reference to acidity, and dispersal of fluorine, heavy metals and arsenic.

Acknowledgments The author has appreciated the input from his former students in our work on volcanic lakes over the years: Scott Herman, Gregory Pasternack, Andrew Ouimette, Conor Gately, Kathryn Flynn, Tristan Kading, and Jared Lefkowitz. Manfred van Bergen (Utrecht University, The Netherlands) has made unpublished papers, data, and ideas available for this summary, which is greatly appreciated. Discussions with many volcanic lake colleagues over the years have helped shape the ideas presented here. I thank NSF for their funding (Awards NSF EAR-0949376 and NSF RAPID-1331167) and the Wesleyan University Harold Stearns Endowed Chair fund for financial support.

References

Acero P, Ayora C, Torrento C, Nieto JM (2006) The behaviour of trace elements during schwertmannite precipitation and subsequent transformation into goethite and jarosite. Geochim Cosmochim Acta 70:4130–4139

Aeschbach-Hertig W, Kipfer R, Hofer M, Imboden DM, Wieler R, Signer P (1996) Quantification of gas fluxes from the subcontinental mantle; the example of Laacher See, a maar lake in Germany. Geochim Cosmochim Acta 60:31–41

Aiuppa A, Allard P, D'Alessandro W, Michel A, Parello F, Treuil M, Valenza M (2000) Mobility and fluxes of major, minor and trace metals during basalt weathering and groundwater transport at Mt. Etna volcano (Sicily). Geochim Cosmochim Acta 64(11):1827–1841

Aja SU, Wood SA, Williams-Jones AE (1995) The aqueous geochemistry of Zr and the solubility of some zirconium-bearing minerals. Appl Geochem 10:603–620

Agusto M, Caselli AT, Tassi F, Dos Santos Afonso M, Vaselli O (2012) Seguimiento geoquímico de las aguas ácidas del sistema volcán Copahue-Río Agrio: posible aplicación para la identificación de precursores eruptivos. Revista de la Asociación Geológica Argentina 69(4):481–495

Agusto M, Tassi F, Caselli AT, Vaselli O, Rouwet D, Capaccioni B, Caliro S (2013) Gas geochemistry of the magmatic-hydrothermal fluid reservoir in the Copahue-Caviahue volcanic complex (Argentina). J Volcanol Geotherm Res 257:44–56

Albarède F (1995) Introduction to geochemical modeling. Cambridge Univ Press, Cambridge, p 543

Armienta MA, De la Cruz Reyna S, Macías JL (2000) Chemical characteristics of the crater lakes of Popocatepetl, El Chichón, and Nevado de Toluca volcanoes, Mexico. J Volcanol Geotherm Res 97:105–125

Arribas A (1995) Characteristics of high-sulfidation epithermal deposits, and their relation to magmatic fluid in magmas, fluids, and ore deposits. In: Thompson JFM (ed), Mineralogical Association of Canada Short Course, vol 23(19), pp 419–454

Ayers G (2012) Behaviour of the REE during water rock interaction and alteration processes in volcanic lake systems. Ms thesis, Utrecht University, The Netherlands, pp 102

Bani P, Oppenheimer C, Varekamp JC, Quinou T, Lardy M, Carn S (2009) Remarkable geochemical changes and degassing at Voui crater lake, Ambae volcano, Vanuatu. J Volcanol Geotherm Res 213:47–357

Bao SX, Zhou HY, Peng XT, Ji FW, Yao HO (2008) Geochemistry of REE and yttrium in hydrothermal fluids from the endeavour segment, Juan de Fuca Ridge. Geochem J 42:359–370

Bernard A, Mazot A (2004) Geochemical evolution of the young crater lake of Kelud volcano in Indonesia. Water-Rock interaction (WRI-11). In: Wanty and Seal II (eds) Balkema AA Publishers vol 1 pp 87–90

Bernard A, Escobar CD, Mazot A, Guttiérez RE (2004) The acid volcanic lake of Santa Ana volcano, El Salvador. In: Rose WI, Bommer JJ, López, DL, Carr MJ, Major JJ (eds) Natural hazards in El Salvador: Boulder, Colorado, Geol Soc Am Special, Paper vol 375 pp 121–133

Bozau E, LeBlanc M, Seidel JL, Stark HJ (2004) Light rare earth element enrichments in an acidic mine lake (Lusatia, Germany). Appl Geochem 19:261–271

Brantley SL, Borgia A, Rowe G, Fernández JF, Reynolds JR (1987) Poás volcano crater lake acts as a condenser for acid metal-rich brine. Nature 330:470–472

Burwell IR (2003)The responses of diatoms to the influx of tephras into lacustrine environments. MSc thesis, Canterbury University, New Zealand, pp 170

Carapezza ML, Lelli M, Tarchini L (2008) Geochemistry of the Albani and Nemi crater lake in the volcanic district of Alban Hills. J Volcanol Geotherm Res 178:297–304

Cartigny P, Harris JW, Javoy M (2001) Diamond genesis, mantle fractionations and mantle nitrogen content: a study of $\delta^{13}C$–N concentrations in diamonds. Earth Plan Sci Lett 185:85–98

Caudron C, Mazot A, Bernard A (2012) Carbon dioxide dynamics in Kelud volcanic lake. J Geophys Res B5102. doi:10.1029/2011JB008806

Chapman M (2007) The geology of Mars—evidence from earth-based analogs. Cambridge University Press, Cambridge, p 484

Chiodini G, Cioni R, Guidi M, Marini L, Raco B (2000) Water chemistry of Lake Quilotoa (Ecuador) and assessment of natural hazards. J Volcanol Geotherm Res 97:271–285

Chiodini G, Tassi F, Caliro S, Chiarabba C, Vaselli O, Rouwet D (2012) Time-dependent CO_2 variations in Lake Albano associated with seismic activity. Bull Volcanol 74:861–871

Christenson BW (1994) Convection and stratification in Ruapehu Crater Lake, New Zealand: implications for Lake Nyos-type gas release eruptions. Geochem J 28:185–198

Christenson BW (2000) Geochemistry of fluids associated with the 1995–1996 eruption of Mt. Ruapehu, New Zealand: signatures and processes in the magmatic hydrothermal system. J Volcanol Geotherm Res 97:1–30

Christenson BW, Tassi F (this issue) Gases in volcanic lake environments. In: Rouwet D, Christenson BW, Tassi F, Vandemeulebrouck J (eds) Volcanic lakes. Springer, Heidelberg

Christenson BW, Wood CP (1993) Evolution of a vent-hosted hydrothermal system beneath Ruapehu Crater Lake, New Zealand. Bull Volcanol 55:547–565

Colvin A, Rose WI, Varekamp JC, Palma JL, Escobar D, Gutiérrez E, Montalvo F, Maclean A (2013) Crater lake evolution at Santa Ana volcano following the 2005 eruption. In: Rose WI, Palma JL, Delgado Granados H, and Varley N (eds) Understanding open vent volcanism and related hazards, Geol Soc America, Special Paper, vol 498(2), pp 23–44. doi:10.1130/2013.2498(00)

Delmelle P, Bernard A (1994) Geochemistry, mineralogy and chemical modeling of the acid crater lake of Kawah Ijen Volcano, Indonesia. Geochim Cosmochim Acta 58:2445–2460

Delmelle P, Bernard A (2000a) Volcanic Lakes. In: H Sigurdsson B Houghton S McNutt H Rymer and J Stix (eds) Encyclopedia of volcanoes. Academic Press San Diego: ISBN 012643140X, pp 877–895

Delmelle P, Bernard A (2000b) Downstream composition changes of acidic volcanic waters discharged into the Banyupahit stream, Ijen caldera, Indonesia. J Volcanol Geotherm Res 97:55–75

Delmelle P, Bernard A, Kusakabe M, Fischer T, Takano B (2000) Geochemistry of the magmatic-hydrothermal system of Kawah Ijen volcano, East Java, Indonesia. J Volcanol Geotherm Res 97:31–53

Delmelle and Bernard (this issue) The remarkable chemistry of sulfur in volcanic acid crater lakes: a scientific tribute to Bokuichiro Takano and Minoru Kusakabe. In: Rouwet D, Christenson BW, Tassi F, Vandemeulebrouck J (eds) Volcanic lakes. Springer, Heidelberg

Delmelle P, Henley RW, Opfergelt S, Detienne M (this issue) Summit acid crater lake and flank instability in composite volcanoes. In: Rouwet D, Christenson BW, Tassi F, Vandemeulebrouck J (eds) Volcanic lakes. Springer, Heidelberg

Drake ET, Larson GL, Dymond J, Collier R (eds) (1990) Crater Lake: an ecosystem study. AAAS-Pacific Division, pp 69–80

Evans WC, Kling GW, Tuttle ML, Tanyileke G, White LD (1993) Gas buildup in Lake Nyos, Cameroon: the recharge process and its consequences. Appl Geochem 8(3):207–221

Fehn U, Snijder G, Varekamp JC (2002) Detection of recycled marine sediment components in crater lake fluids using ^{129}I. J Volcanol Geotherm Res 115:451–460

Fernández-Remolar DC, Morris RV, Gruener JE, Amils R, Knoll AH (2005) The Río Tinto Basin, Spain: mineralogy, sedimentary geobiology, and implications for interpretation of outcrop rocks at Meridiani Planum, Mars. Earth Plan Sc Lett 240(1):149–167

Fulignato P, Gioncanda A, Sbrana A (1999) Rare earth element (REE) behaviour in the alteration facies of the active magmatic-hydrothermal system of Vulcano (Aeolian Islands, Italy). J Volcanol Geotherm Res 88:325–342

Gammons CH, Wood SA, Li Y (2002) Complexation of the rare earth elements with aqueous chloride at 200 and 300 °C and saturated water vapor pressure. In: Hellmann, R., Wood, S.A. (eds) Water–rock interaction, ore deposits, and environmental geochemistry: a tribute to David A. Crerar. Geochemical Society Special Publication No. 7, pp 191–207

Gammons CH, Wood SA, Jonas JP, Madison JP (2003) Geochemistry of the rare-earth elements and uranium in the acidic Berkeley Pit lake, Butte, Montana. Chem Geol 198:69–288

Gammons CH, Wood SA, Pedrozo F, Varekamp JC, Nelson BJ, Shope CL, Baffico G (2005) Hydrogeochemistry and rare earth element behavior in a volcanically acidified watershed in Patagonia, Argentina. Chem Geol 222:249–267

Giggenbach WF (1974) The chemistry of Crater Lake, Mt. Ruapehu (New Zealand) during and after the 1971 active period. NZ J Science 17:33–45

Giggenbach WF (1988) Geothermal solute equilibria. Geochim Cosmochim Acta 52:2749–2765

Giggenbach WF (1992a) Isotopic shifts in waters from geothermal and volcanic systems along convergent plate boundaries and their origin. Earth Plan Sc Lett 113:495–510

Giggenbach WF (1992b) Magma degassing and mineral deposition in hydrothermal systems along convergent plate boundaries. SEG distinguished lecture. Econ Geol 87:1927–1944

Giggenbach WF, Glover RB (1975) The use of chemical indicators in the surveillance of volcanic activity affecting the crater lake on Mt. Ruapehu. New Zealand. Bull Volcanol 39:70–81

Gordon E, Corpuz G, Harada M, Punongbayan JT (2009) Combined electromagnetic, geochemical and thermal surveys of Taal Volcano (Philippines) during the period 2005–2006. Bull Volcanol 71:29–47

Gunkel G, Beulker C, Grupe B, Viteri F (2008) Hazards of volcanic lakes: analysis of Lakes Quilotoa and Cuicocha, Ecuador. Adv Geosci 14:29–33

Gyure RA, Konopka A, Brooks A, Doemel W (1990) Microbial sulfate reduction in acidic (pH $\sim$ 3) strip mine lakes. FEMS Microbiol Ecol 73:193–202

Haberyan KA, Hecky RE (1987) The late Pleistocene and Holocene stratigraphy and paleolimnology of Lakes Kivu and Tanganyika. Palaeogeogr Palaeoclimat Palaeoecol 62:169–19

Hansell AL, Horwell CJ, Oppenheimer C (2006) The health hazards of volcanoes and geothermal areas. Occup Environ Med 63(2):149–156

Hedenquist JW, Lowenstern JB (1994) The role of magmas in the formation of hydrothermal ore deposits. Nature 370:519–527

Heikens A, Sumarti S, van Bergen MJ, Widianarko B, Fokkert L, van Leeuwen K, Seinen W (2005a) The impact of the hyperacid Ijen Crater Lake: risks of excess fluoride to human health. Sci Total Env 346(1–3):56–69

Heikens A, Widianarko B, Dewi IC, De Boer JL, Seinen W, van Leeuwen K (2005b) The impact of the hyperacid Ijen Crater Lake. Part I: concentrations of elements in crops and soil. Environ Geochem Health 27(5–6):409–418

Henley RW (this issue) Hyperacidic volcanic lakes, metal sinks and magmatic gas expansion in arc volcanoes. In: Rouwet D, Christenson BW, Tassi F, Vandemeulebrouck J (eds) Volcanic lakes. Springer, Heidelberg

Hurst AW, Bibby HM, Scott BJ, McGuinness MJ (1991) The heat source of Ruapehu Crater Lake; deductions from the energy and mass balances. J Volcanol Geotherm Res 46:1–20

Kading T (2011) Attenuation of pollutants in Caviahue Lake, Copahue, Argentina, Master thesis, Wesleyan University, Middletown CT USA p 304

Keeling CD, Mook WG, Tans PP (1979) Recent trends in the $^{13}C/^{12}C$ ratio of atmospheric carbon dioxide. Nature 277:121–123

Kempter KA, Rowe GL (2000) Leakage of active crater lake brine through the north flank at Rincon de la Vieja volcano, northwest Costa Rica, and implications for crater collapse. J Volcanol Geotherm Res 97:143–159

Kling GW, Clark M, Compton HR, Devine JD, Evans WC, Humphrey AM, Lockwood JP, Tuttle ML (1987) The 1986 Lake Nyos gas disaster, Cameroon, West Africa. Science 236:169–175

Kling GW, Evans WC, Tanyileke GZ (this issue) The comparative limnology of Lakes Nyos and Monoun, Cameroon. In: Rouwet D, Christenson BW, Tassi F, Vandemeulebrouck J (eds) Volcanic lakes. Springer, Heidelberg

KikawadaY Oi T, Honda T, Ossaka T, Kakihana H (1993) Lanthanoid abundances of acidic hot spring and crater lake waters in the Kusatsu—Shirane volcano region, Japan. Geochem J 27:19–33

Kikawada Y, Ossaka T, Oi T, Honda T (2001) Experimental studies on the mobility of lanthanides accompanying alteration of andesite by acidic hot spring water. Chem Geol 176:137–149

Kusakabe M (this issue) Evolution of CO_2 content in Lakes Nyos and Monoun, and sub-lacustrine CO_2-recharge system at Lake Nyos as envisaged from $C/^3He$ ratios in noble gas signatures. In: Rouwet D, Christenson BW, Tassi F, Vandemeulebrouck J (eds) Volcanic lakes. Springer, Heidelberg

Kusakabe M, Hayashi N, Kobayashi T (1986) Genetic environments of the banded sulfur sediments at the Tateyama Volcano, Japan. J Geophys Res (Solid Earth) 91(B12):12159–12166. doi:10.1029/JB091iB12p12159

Kusakabe M, Komoda Y, Takano B, Abiko T (2000) Sulfur isotope effects in the disproportionation reaction of sulfur dioxide in hydrothermal fluids: implications for the $\delta^{34}S$ variations of dissolved bisulfate and elemental sulfur from active crater lakes. J Volcanol Geotherm Res 97:287–308

Lefkowitz JL (2012) A tale of two lakes: the Newberry twin crater lakes, OR. BA thesis, Wesleyan University, Middletown CT, pp 203

López DL, Ransom L, Pérez N, Hernández P, Monterrosa J (2004) Dynamics of diffuse degassing at Ilopango Caldera, El Salvador. In: Rose WI, Bommer JJ, López DL, Carr MJ and Major JJ (eds) Natural hazards in El Salvador, Geol Soc of America Special Paper No. 375:191–202

López DL, Ransom L, Monterrosa J, Soriano T, Barahona F, Olmos R, Bundschuh J (2009) Volcanic arsenic and boron pollution of Ilopango Lake, El Salvador. In: Bundschuh J, Armienta M, Birkle P, Bhattacharya P, Matschullat J, Mukherjee AB (eds) Natural arsenic in groundwater of Latin America, Taylor and Francis, Cambridge, pp 129–143

López DL, Bundshuh J, Birkle P, Armienta MA, Cumbal L, Sracek O, Cornejo L, Ormachea M (2012) Arsenic in volcanic geothermal fluids of Latin America. Science Total Env 429:57–75

Löhr AJ, Bogaard TA, Heikens A, Hendriks MR, Sumarti S, Van Bergen MJ, Van Gestel CA, Van Straalen NM, Vroon PZ, Widianarko B (2005) Natural pollution caused by the extremely acidic crater lake Kawah Ijen, East Java. Indonesia. Environ Sci Pollut Res Int 12 (2):89–95

Luhr JF, Carmichael ISE, Varekamp JC (1984) The 1982 eruptions of El Chichón volcano, Chiapas, Mexico: mineralogy and petrology of the anhydrite-bearing pumices. J Volcanol Geotherm Res 23:69–108

Marini L, Vetuschi Zuccolini M, Saldi G (2003) The bimodal pH distribution of volcanic lake waters. J Volcanol Geotherm Res 121(1–2):83–98

Martínez M (2008) Geochemical evolution of the acid crater lake of Poás Volcano (Costa Rica): insights into volcanic-hydrothermal processes. PhD thesis, University of Utrecht, the Netherlands

Martínez M, Fernández E, Valdés J, Barboza V, Van der Laat R, Duarte E, Malavassi E, Sandoval L, Barquero J, Marino T (2000) Chemical evolution and activity of the active crater lake of Poás volcano, Costa Rica, 1993-1997. J Volcanol Geotherm Res 97:127–141

Martini M, Giannini L, Prati F, Tassi F, Capaccioni B, Iozzelli P (1994) Chemical characters of crater lakes in the Azores and Italy: the anomaly of Lake Albano. Geochem J 28(3):173–184

Martini F, Tassi F, Vaselli O, Del Potro R, Martínez M, Van der Laat R, Fernández E (2010) Geophysical, geochemical and geodetical signals of reawakening at Turrialba volcano (Costa Rica) after almost 150 years of quiescence. J Volcanol Geotherm Res 198(3):416–432

McKnight DM, Briant A, Kimball A, Runkel RL (2001) pH dependence of iron photo reduction in a rocky mountain stream affected by acid mine drainage. Hydrol Process 15:1979–1992. doi:10.1002/hyp.251

McManus J, Collier RW, Chen CTA, Dymond J (1992) Physical properties of Crater Lake, Oregon: a method for the determination of a conductivity- and temperature-dependent expression for salinity. Limnol Ocean 37(1):41–53

Michard A (1989) Rare earth element systematics in hydrothermal fluids. Geochim Cosmochim Acta 53:745–750

Miyabuchi Y, Terada A (2009) Subaqueous geothermal activity revealed by lacustrine sediments of the acidic Nakadake crater lake, Aso Volcano, Japan. J Volcanol Geotherm Res 187:140–145

Morgan JW, Wandless GA (1980) Rare earth element distribution in some hydrothermal minerals: evidence for crystallographic control. Geochim Cosmochim Acta 44:973–980

Morton-Bermea O, Armienta MA, Ramos S (2010) Rare-earth element distribution in water from El Chichón Volcano Crater Lake, Chiapas Mexico. Geofís Int 49:43–54

Mosello R, Arisci S, Bruni P (2004) Lake Bolsena (Central Italy): an updating study on its water chemistry. J Limnol 63(1):1–12

Nordstrom DK, Alpers CN (1999) Geochemistry of acid mine waters. In: Plumlee GS, Logsdon MJ (eds) The environmental geochemistry of mineral deposits: processes, techniques, and health issues, Soc Econom Geol Rev Econom Geol 6A:pp 133–160

Nordstrom DK, Alpers CN, Ptacek CJ, Blowes DW (2000) Negative pH and extremely acidic mine wastes from Iron Mountain, California. Environ Sci Technol 34:254–258

Ohba T, Hirabayashi J, Nogami K (1994) Water, heat, and chloride budgets of the crater lake, Yugama at Kusatsu-Shirane volcano, Japan. Geochem J 28:217–231

Ohba T, Hirabayashi J, Nogami K (2000) D/H and $^{18}O/^{16}O$ ratios of water in the crater lake at Kusatsu-Shirane volcano, Japan. J Volcanol Geotherm Res 97:329–346

Ohba T, Hirabayashi J, Nogami K (2008) Temporal changes in the chemistry of lake water within Yugama Crater, Kusatsu-Shirane Volcano, Japan: Implications for the evolution of the magmatic hydrothermal system. J Volcanol Geotherm Res 178:131–144

Oppenheimer C, Stevenson D (1989) Liquid sulphur lakes at Poás volcano. Nature 342:790–793

Oyarzun R, Lillo J, Higueras P, Oyarzœn J, Maturana H (2004) Strong arsenic enrichment in sediments from the Elqui watershed, Northern Chile: industrial (gold mining at El Indio-Tambo district) vs. geologic processes. J Geochem Explor 84:53–64

Parker SR, Gammons CH, Pedrozo FL, Wood SA (2008) Diel changes in metal concentrations in a geogenically acidic river: Río Agrio, Argentina. J Volcanol Geotherm Res 178:213–223. doi:0.1016/j.jvolgeores.2008.06.029

Parkhurst DL, Appelo CAJ(1999) User's guide to PHREEQC—a computer program for speciation, batch-reaction, one-dimensional transport, and inverse geochemical calculations. US Geol Surv Water-Res Inv Rep 99-4259:312

Pasternack GB, Varekamp JC (1994) The geochemistry of the Keli Mutu crater lakes, Flores, Indonesia. Geochem J 28:243–262

Pasternack GB, Varekamp JC (1997) Volcanic lake systematics I. Physical constraints. Bull Volcanol 58:528–538

Pedrozo FL, Kelly L, Díaz MM, Temporetti P, Baffico G, Kringel R, Friese K, Mages M, Geller W, Woelfl S (2001) First results on the water chemistry, algae and trophic status of Andean acidic lake system of volcanic origin in Patagonia (Lake Caviahue). Hydrobiologia 452:129–137

Pedrozo FL, Temporetti P, Beamud SG, Diaz MM (2008) Volcanic nutrient inputs and trophic state of Lake Caviahue, Patagonia, Argentina. J Volcanol Geotherm Res 178:205–212

Peiffer L, Taran YA, Lounejeva E, Solís-Pichardo G, Rouwet D, Bernard-Romero RA (2011) Tracing thermal aquifers of El Chichón volcano-hydrothermal system (Mexico) with $^{87}Sr/^{86}Sr$, Ca/Sr and REE. J Volcanol Geotherm Res 205:55–66

Pérez NM, Hernández PA, Padilla G, Nolasco D, Barrancos J, Melían G, Dionis S, Calvo D, Rodríguez F, Notsu K, Mori T, Kusakabe M, Arpa MC, Reniva P, Ibarra M (2011) Global CO_2 emission from volcanic lakes. Geology 39:235–238. doi:10.1130/G31586.1

Reed M, Rusk B, Palandri J (2013) The Butte magmatic-hydrothermal system: one fluid yields all alteration and veins. Econ Geol 108:1379–1396

Romero L, Alonso H, Campano P, Fanfani L, Cidu R, Dadea C, Keegan T, Thornton I, Farago M (2003) Arsenic enrichment in waters and sediments of the Río Loa (Second Region, Chile). Appl Geochem 18:1399–1416

Rouwet D, Ohba T (this issue) Isotope fractionation and HCl partitioning during evaporative degassing from active crater lakes. In: Rouwet D, Christenson BW, Tassi F, Vandemeulebrouck J (eds) Volcanic lakes. Springer, Heidelberg

Rouwet D, Tassi F (2011) Geochemical monitoring of volcanic lakes. A generalized box model for active crater lakes. Ann Geophys 54. doi: 10.4401/ag-5035

Rouwet D, Taran YA, Inguaggiato S, Varley N, Santiago JA (2008) Hydrochemical dynamics of the "lake-spring" system in the crater of El Chichón volcano (Chiapas, Mexico). J Volcanol Geotherm Res 178:237–248

Rouwet D, Taran Y, Varley N (2004) Dynamics and mass balance of El Chichón crater lake, Mexico. Geofís Int 43:427–434

Rowe GL, Ohsawa S, Takano B, Brantley SL, Fernández JF, Barquero J (1992a) Using crater lake chemistry to predict volcanic activity at Poás Volcano, Costa Rica. Bull Volcanol 54:494–503

Rowe GL, Brantley SL, Fernández M, Fernández JF, Borgia A, Barquero J (1992b) Fluid-volcano interaction in an active stratovolcano: the volcanic lake system of Poás Volcano, Costa Rica. J Volcanol Geotherm Res 49:23–51

Samson IM, Wood SA (2005) The rare earth elements: Behaviour in hydrothermal fluids and concentration in hydrothermal mineral deposits, exclusive of alkaline settings. In: Linnen RL, Samson IM (eds) Rare-element geochemistry and mineral deposits: Geological Association of Canada, GAC short course notes, vol 17, pp 269–297

Schaefer JR, Scott WE, Evans WC, Jorgenson J, McGimsey RG, Wang B (2008) The 2005 catastrophic acid crater lake drainage, lahar, and acidic aerosol formation at Mount Chiginagak volcano, Alaska, USA: field observations and preliminary water and vegetation chemistry results. Geochem Geophys Geosyst 9(7). doi:10.1029/2007GC001900

Schuiling RD (1998) Geochemical engineering-taking stock. J Geochem Explor 62:1–28

Sriwana T, van Bergen MJ, Sumarti S, de Hoog JCM, Van Os BJ, Wahyuningsih R, Dam MAC (1998) Volcanogenic pollution by acid water discharges along Ciwidey River, West Java (Indonesia). J Geochem Explor 62:161–182

Sriwana T, van Bergen MJ, Varekamp JC, Sumarti S, Takano B, Van Os BJH, Leng MJ (2000) Geochemistry of the acid Kawah Putih Lake, Patuha volcano, West Java, Indonesia. J Volcanol Geotherm Res 97:77–104

Suchanek TH, Eagles-Smith CA, Slotton DG, Harner EJ, Adam DP (2008) Mercury in abiotic matrices of Clear Lake, California: human health and ecotoxicological implications. Ecol Appl 18(8 Suppl):A128–A157

Symonds RB, Rose WI, Reed MH, Lichte FE, Finnegan DL (1987) Volatilization, transport and sublimation of metallic and non-metallic elements in high temperature gases at Merapi Volcano, Indonesia. Geochim Cosmochim Acta 51:083–2101

Takano B (1987) Correlation of volcanic activity with sulfur oxyanion speciation in a crater lake. Science 235:1633–1635

Takano B, Watanuki K (1990) Monitoring of volcanic eruptions at Yugama crater lake by aqueous sulfur oxyanions. J Volcanol Geotherm Res 40:71–87

Takano B, Ohsawa S, Glover RB (1994a) Surveillance of Ruapehu crater lake, New Zealand, by aqueous polythionates. J Volcanol Geotherm Res 60:29–57

Takano B, Saitoh H, Takano E (1994b) Geochemical implications of subaqueous molten sulfur at Yugama crater lake, Kusatsu-Shirane volcano, Japan. Geochem J 28:199–216

Takano B, Fazlullin SM, Delmelle P (2000) Analytical cross check of major and minor constituents in active crater lakes. J Volcanol Geotherm Res 97:497–508

Takano B, Suzuki K, Sugimori K, Ohba T, Fazlullin SM, Bernard A, Sumarti S, Sukhyar R, Hirabayashi M (2004) Bathymetric and geochemical investigation of Kawah Ijen Crater Lake, East Java, Indonesia. J Volcanol Geotherm Res 135:299–329

Taran YA, Rouwet D (2008) Estimating thermal inflow to El Chichón crater lake using the energy budget, chemical and isotope balance approaches. J Volcanol Geotherm Res 175:472–481

Taran Y, Rouwet D, Inguaggiato S, Aiuppa A (2008) Major and trace element geochemistry of neutral and acidic thermal springs at El Chichón volcano, Mexico. Implications for monitoring of the volcanic activity. J Volcanol Geotherm Res 178:224–236, doi:10.1016/j.volgeores.2008.06.030

Taran YA, Hedenquist JW, Korzhinsky MA, Tkachenko SI, Shmulovich KI (1995) Geochemistry of magmatic gases of Kudryavy volcano, Iturup, Kuril islands. Geochim Cosmochim Acta 59:1749–1761. doi:10.1016/0016-7037(95)00079-F

Taran YA, Inguaggiato S, Cardellini C, Karpov G (2013) Posteruption chemical evolution of a volcanic caldera lake: Karymsky Lake, Kamchatka. Geophys Res Lett 40:5142–5146. doi:10.1002/grl.50961

Tassi F, Rouwet D (2014) An overview of the structure, hazards, and methods of investigation of Nyos-type lakes from the geochemical perspective. J. Limnol 73 (1):39–54

Tassi F, Vaselli O, Capaccioni B, Giolito C, Duarte E, Fernandez E, Minisale A, Magro G (2005) The

hydrothermal-volcanic system of Rincon de la Vieja volcano (Costa Rica): a combined (inorganic and organic) geochemical approach to understanding the origin of the fluid discharges and its possible application to volcanic surveillance. J Volcanol Geotherm Res 148(3):315–333

Tassi F, Vaselli O, Fernández E, Duarte E, Martínez M, Delgado Huertas A, Bergamaschi F (2009a) Morphological and geochemical features of crater lakes in Costa Rica: an overview. J Limnol 68(2):193–205. doi:10.3274/JL09-68-2-04

Tassi F, Vaselli O, Tedesco D, Montegrossi G, Darrah T, Cuoco E (2009b) Water and gas chemistry at Lake Kivu (DRC): geochemical evidence of vertical and horizontal heterogeneities in a multi basin structure. Geochem Geophys Geosyst 10(2). doi:10.1029/2008GC002191

Tedesco D, Tassi F, Vaselli O, Poreda RJ, Darrah T, Cuoco E, Yalire MM (2010) Gas isotopic signatures (He, C, and Ar) in the Lake Kivu region (western branch of the East African rift system): Geodynamic and volcanological implications. J Geophys Res 115 (B01205)doi:10.1029/2008JB006227

Telford R, Barker P, Metcalfe S, Newton A (2004) Lacustrine responses to tephra deposition: examples from Mexico. Quat Sci Rev 23:2337–2353

Todesco M, Rouwet D, Nespoli M, Mora-Amador RA (2012) To seep or not to seep? Some considerations regarding water infiltration in volcanic lakes. In: Proceedings, TOUGH symposium 2012 Lawrence Berkeley National Laboratory, Berkeley, California, September pp 17–19

Tietze K, Geyh M, Muller H, Schröder L, Stahl W, Wehner H (1980) The genesis of the methane in Lake Kivu (Central Africa). Geol Rundschau 69:452–472

van Rotterdam-Los AMD, Vriend SP, van Bergen MJ, van Gaans PFM (2008) The effect of naturally acidified irrigation water on agricultural volcanic soils. The case of Asembagis, Java. Indonesia. J Geochem Explor 96:53–68

Varekamp JC (1988) Lake pollution modeling. J Geol Educat 36:4–9

Varekamp JC (2003) Lake contamination models: evolution towards steady state. J Limnol 62:67–72

Varekamp JC (2004) Copahue Volcano: a modern terrestrial analog for the opportunity landing site. Eos 85(41):401–407

Varekamp JC (2008) The acidification of glacial Lake Caviahue, province of Neuquen, Argentina. J Volcanol Geotherm Res 178:184–196. doi:10.1016/j.jvolgeores.2008.06.016

Varekamp JC, Waibel A (1987) Natural cause for mercury pollution at Clear Lake, California, and paleotectonic inferences. Geology 15:1018–1021

Varekamp JC, Kreulen R (2000) The stable isotope geochemistry of volcanic lakes: examples from Indonesia. J Volcanol Geotherm Res 97:309–327

Varekamp JC, Pasternack GB, Rowe GL (2000) Volcanic lake systematics II. Chemical constraints. J Volcanol Geotherm Res 97:161–180

Varekamp JC, Ouimette A, Herman S, Delpino D, Bermúdez A (2001) The 1990–2000 eruptions of Copahue, Argentina: a 'bee-hive volcano' in turmoil. Geology 29:1059–1062

Varekamp JC, Ouimette A, Kreulen R (2004) The magmato-hydrothermal system of Copahue volcano, Argentina. In: Wanty RB and Seal RR (eds) Proceeding of the 11th Water Rock Interaction Symposium, 1:215–218, Balkema Publishers, Leiden

Varekamp JC, de Moor JM, Merrill MD, Colvin AS, Goss AR, Vroon PZ, Hilton DR (2006) The geochemistry and isotopic characteristics of the Caviahue Copahue volcanic complex, province of Neuquen, Argentina. GSA Special Paper 407:317–342

Varekamp JC, Herman S, Ouimette A, Flynn K, Bermúdez A, Delpino D (2009) Naturally acid waters from Copahue volcano, Argentina. Appl Geochem 24:208–220

Vaselli O, Tassi F, Minissale A, Montegrossi G, Duarte E, Fernández E (2003) Fumarole migration and fluid geochemistry at Poás volcano (Costa Rica) from 1998 to 2001. Geological Society, London, Special Public 213(1):247–262

Verma MP (2000) Revised quartz solubility temperature dependence equation along the water-vapor saturation curve. In: Proceedings World Geothermal Congress 2000 Kyushu—Tohoku, Japan, May 28–June 10, pp. 1927–1932

WHO (1996) Guidelines for drinking-water quality, 2nd edn. Switzerland, Geneva

Wood SA (2003) The geochemistry of rare earth elements and yttrium in geothermal waters. In Simmons SF and Graham I (eds), Volcanic, geothermal, and ore-forming fluids: rulers and witnesses of processes within the earth. Soc Econ Geol Spec Publ, vol 10, 133–158

Wood SA (2005) The aqueous geochemistry of zirconium, hafnium, niobium and tantalum. In Linnen RL and Samson IM (eds) Rare-element geochemistry and mineral deposits. Geological Association of Canada, GAC Short Course Notes 17:217–268

Wood SA (2006a) The behavior of rare earth elements in naturally and anthropogenically acidified waters. J Alloys Comps 418:161–165

Wood SA (2006b) Rare earth element systematics of acidic geothermal waters from the Taupo Volcanic Zone, New Zealand. J Geochem Explor 89:424–427

Wood SA, Shannon WM (2003) Rare-earth elements in geothermal waters from Oregon, Nevada, and California. J Solid State Chem 171:246–253

Zlotnicki J, Sasai Y, Toutain IO, Villacorte EU, Bernard A, Sabit JP, Gordon JM, Corpuz EG, Harada M, Punongbayan JT (2009) Combined electromagnetic, geochemical and thermal surveys of Taal Volcano (Philippines) during the period 2005–2006. Bull Volcanol 71:29–47. doi:10.1007/s00445-008-0205-2

Gases in Volcanic Lake Environments

B. Christenson and F. Tassi

Abstract

Volcanic lake systems derive their gases from four distinct sources. Of greatest importance from a hazard perspective, and those which set these limnic systems apart from non-volcanic lakes, are gases derived directly from magmatic sources feeding the volcano, including CO_2, SO_2, H_2S, HCl, HF and a myriad of minor species. The major gases are acidic in nature, and when dissolved into ground water, lead to the development of aggressively acidic solutions. Hydrolysis reactions with enclosing rocks, systematically alter the magmatic gas compositions towards more benign hydrothermal signatures, and this process usually leads to precipitation of permeability-reducing mineral assemblages. Ground and lake waters carry dissolved atmospheric constituents into these environments, whereas lakes are well-known biotic environments, whose populations may also leave their mark on solute gas compositions through their normal metabolic processes. Apart from magmatic eruption events, at least two specific hazards are attributable to gases in volcanic lake environments, both of which have been responsible for loss of life near volcanic lakes. Physical and chemical processes extant in systems where magmas lie within 100s of metres of the surface have the propensity to form mineralogic seals beneath the lakes. Such sealing may foster over-pressuring and associated gas-driven phreatic eruptions of the type that has occurred recently at Ruapehu and Raoul Island, New Zealand, often with little or no precursory activity. On the other hand, where

B. Christenson (✉)
GNS Science, National Isotope Centre, Lower Hutt, New Zealand
e-mail: b.christenson@gns.cri.nz

F. Tassi
Department of Earth Sciences, University of Florence, Via G. La Pira, 4, 50121 Florence, Italy

F. Tassi
CNR-IGG, Institute of Geosciences and Earth Resources, Via G. La Pira, 4, 50121 Florence, Italy

D. Rouwet et al. (eds.), *Volcanic Lakes*, Advances in Volcanology,
DOI 10.1007/978-3-642-36833-2_5,
© Springer-Verlag Berlin Heidelberg 2015

magmatic gas sources are deeply-seated, to such an extent where heat decouples from the rising gas stream (principally CO_2), conditions are perfect for the formation of cold, gas-stratified lakes. Overturn of such lakes typically leads to violent release of the gas, as has occurred in the Cameroonian Lakes Nyos and Monoun, leading to the deaths of near-by inhabitants. Both situations are endmembers of a continuum of processes operating where volcanoes interact with Earth's hydrosphere.

Keywords
Dissolved gas composition · Hyperacidic lake · Lake monitoring · Nyos-type lake · Gas/water reaction

1 Introduction

Gases are the lifeblood of volcanic systems. From the onset of volatile exsolution from vapour-saturated host magmas, and from depths extending to deep crustal environments (e.g., Anderson 1975; Giggenbach 1996; Wallace 2005) through to their interaction with volcanic lakes at the Earth's surface, magmatic volatiles play a key role in the physical and chemical evolution of their enclosing magmatic-hydrothermal environment. Whereas exsolved magmatic gases not only augment density differences between the melt phase and enclosing crustal materials, thereby driving buoyant ascent of magma, in the words of Giggenbach, they also "rule, or at least witness", many of the chemical processes operating on both sides of the magma-hydrothermal interface during ascent.

Interaction between magmatic volatiles and the Earth's hydrosphere leads to complex physico-chemical processes, most of which are not observable to us on the surface, and many of which lead to potential hazards for those living near such volcanic systems. These hazards include, but are not limited to, the development of hydrothermal seals which typically lead to phreatic and/or phreatomagmatic eruptions, and the accumulation of gases in lakes (e.g., Nyos-type hazards).

In this chapter, we briefly explore the nature of magmatic volatiles which are released from active volcanoes, and some of the key physical and chemical consequences of their interaction with meteoric surface waters, including lakes. We also briefly discuss how these signatures are opportunistically altered by living organisms in lake environments. We will then look at two representative case histories where gases have contributed to hazardous natural events in volcanic lake settings, including a recent gas-driven phreatomagmatic eruption from the active andesitic massif of Mt Ruapehu (New Zealand), and an overview of the key processes associated with the accumulation and cataclysmic release of gases from Cameroonian lakes (e.g. Nyos), detailed discussions for which are found elsewhere in this volume.

2 Origins of Gases in Volcanic Lake Systems

Gases in volcanic lake systems can be described in terms of four endmember components, including two principle sources (magmatic and meteoric) and two derived sources (hydrothermal and biogenic), as shown schematically in Fig. 1. Of greatest interest to us from a hazard stand point, and those which will therefore receive most of our attention here, are gases derived from the magma, and its enveloping magmatic-hydrothermal environment. The hydrosphere accommodates the other two sources, including atmospheric gases dissolved in ground and lake water, and those derived from metabolic processes of living organisms (the biogenic fraction).

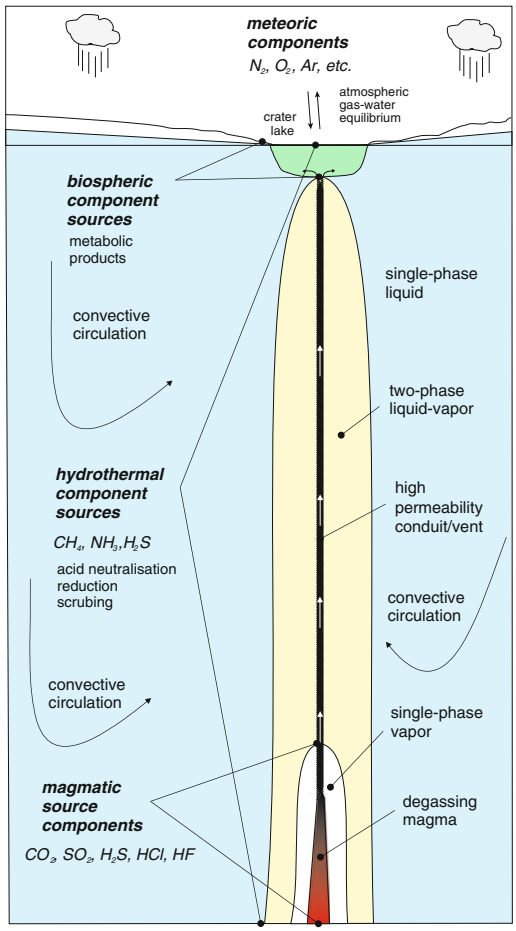

Fig. 1 Schematic model for component source gases in a typical volcanic lake plumbing system. The scale is purposefully not shown, as the configuration is generic to both deep and shallow magmatic sources, with only the topology of the two-phase liquid region adjusting vertically to P-T-X constraints

The degree to which a lake in a volcanic terrain will be chemically or physically influenced by a deeper magmatic system is dependent upon its proximity to the underlying magma, the rate of degassing, the permeability of the intervening rock mass, and the degree to which convective circulation (if any) is established between the two environments. Maximum magmatic gas emission rates will occur where gases transfer across an open, freely degassing lava surface within the magma conduit into a highly permeable vent system, as portrayed in Fig. 1. At relatively shallow depths (say 1–3 km), pressure-temperature and compositional (P-T-X) conditions are conducive to the development of a single-phase vapour envelope surrounding the magma, the size of which will be proportional to the magma body, and its heat/gas emission rate (Todesco et al. 2004, this issue; Christenson et al. 2010). Enclosing this zone of single-phase vapour will be a 2-phase vapour-liquid region, which in turn is surrounded by single-phase liquid (i.e., water). The vertical extent of this topology will again be controlled largely by heat and mass flow of volatiles from the magma, and permeability within the conduit. Heat and mass transport modelling of these systems indicates that convective circulation develops around the conduits, with hot, low density fluids rising within and adjacent the conduit, and drawing cooler marginal fluids into the flow regime.

The most extreme examples of this type of lake system are found where the volcanoes are active, with magma residing close to the surface, and where the *main* eruption vents are covered by the lake. Examples of such lakes are Aso (Shinohara et al. this issue), Poás (Rowe et al. 1992), Ruapehu (Christenson and Wood 1993), and Copahue (Varekamp et al. 2009).

A similar, but less expansive topology arises in systems with less vigorously degassing magma bodies at their core, or perhaps where both crystallisation and magmatic degassing are well advanced, and the remaining melt fraction is enclosed by a hot, ductile carapace. A model for gas release across quenched margins of magma bodies has been elegantly described by Fournier (1999), and a possible example of this type of lake system is located at Raoul Island (e.g., Weissberg and Sarbutt 1966; Christenson et al. 2007). Similarly, and for reasons which will be discussed below, systems where the magma body resides at great depth (such as Laacher See and Lake Nyos), have rather simpler gas compositions, consisting predominantly of CO_2.

Water-rock interaction, and the transition from the magmatic to the hydrothermal environment, initiates from the moment that condensation begins in the 2-phase liquid-vapour environment enveloping the conduit and single-phase vapour region, and proceeds across this zone and to the thermal margins of the single

phase liquid region (Fig. 1). Processes operating therein, and their impact on the gas composition, define the so-called hydrothermal source component in these systems, as discussed below. For modelling purposes (both conceptual and numeric), the hydrothermal region is bound hydrostatically on its outer margins by non-thermal groundwater, and the nature of this boundary is both dynamic and responsive to changes in volcanic activity. As a result of the convective processes operating in this zone, hydrothermal fluids are typically composite mixtures of meteoric and magmatic source fluids, with chemical processes operating to generate distinctly hydrothermal compositional signatures.

Another, potentially dominant component signature in volcanic lakes is that derived from biological activity in both lakes and sediments associated with them (i.e., gases of biogenic origins). A wide range of opportunistic microbial organisms gain metabolic energy from oxidation-reduction reactions involving principally magmatic-hydrothermal C, S and N, often leaving distinctive isotopic signatures (discussed by Mapelli et al. this volume), described briefly below.

The gases which derive from these sources are individually identified in this section, and therein the following sections.

2.1 Magmatic Gases and Processes

Gases released from active volcanoes owe their bulk compositions to a variety of complex processes and interactions, both chemical and physical, as they ascend from their source regions in the mantle to the surface. Excellent reviews of the compositional characteristics and evolution of magmatic volatiles are available from a number of sources, including Carrol and Webster (1994), Giggenbach (1996), Wallace (2005), Webster and Mandeville (2007), Aiuppa et al. (2009), Oppenheimer et al. (2011) and the many references therein. Only aspects most commonly affecting chemical signatures in volcanic lake systems are introduced here.

2.1.1 Major Component Species

The principle components of magmatic gases are H, O, C, S and Cl and these comprise >95 % of magmatic volatiles, regardless of tectonic source environment.

Hydrogen

Water is the most prevalent H-bearing volatile species in magmas, followed by comparatively minor amounts of H_2, NH_3, H_2S, and trace amounts of CH_4. Arc magmas tend to have higher water contents and larger ranges (0.2–6 wt %, Métrich and Wallace 2008) than their ridge counterparts (0.12–0.5 wt%, Sobolev and Chaussidon 1996; Saal et al. 2002). Water enrichment along arcs is the result of dehydration reactions in the subducting oceanic crust and sediments, whereas the large range of observed volatile contents in arc environments is attributable to heterogeneity of source materials, differentiation, and assimilation (e.g. Fischer 2008). Water partially dissociates in magma to OH, but Silver et al. (1990) have shown that maximum solubility is controlled by saturation equilibrium with its vapour phase. Isotopic signatures of magmatic water range from highly depleted values in ridge and intraplate settings ($\delta^2H = -100$; Taylor and Sheppard 1986) to ca. $\delta^2H = -20$ in subduction zone environments (Taran et al. 1989; Giggenbach 1992).

Carbon

CO_2 is the predominant carbon species in volcanic gases. It is the least soluble of the major constituents, and is probably already saturated with respect to a separate vapour phase at deep crustal depths (Anderson 1975; Wallace 2005). Primary basaltic MORB and hot spot melts are inferred to have rather similar CO_2 contents of 0.6 and 0.7 wt % respectively (Gerlach et al. 2002; Fischer et al. 2005), whereas arc basalts are comparatively CO_2 enriched, with contents ranging between 0.6 and 1.3 wt% CO_2 (Wallace 2005). As for water, this is attributed to the very efficient recycling of subducted C in arc systems (e.g., Fischer 2008). CO_2 is present in the melt phase as CO_3^-, and Fine and Stolper (1986) have suggested that CO_2 degassing

has an oxidising effect on the remaining melt phase, as described by the following reaction:

$$CO_3^- + H^+ + 0.5\ H_2 = CO_2 + H_2O. \quad (1)$$

CO is a comparatively minor species characterised by relatively fast reaction kinetics with CO_2. As such, it is particularly useful as both a redox and temperature geoindicator in magmatic-hydrothermal environments (e.g., Giggenbach 1987; Chiodini and Cioni 1989).

$\delta^{13}C$ signatures of volcanic C are variably influenced by three main source signatures, depending on tectonic setting. Mantle signatures of $\delta^{13}C = -6.5 \pm 2.5$ ‰ are typically encountered in rift margin and hot spot centres, whereas organic material ($\delta^{13}C \leq -20$ ‰) and carbonate signatures ($\delta^{13}C \sim 0$ ‰) typically contribute to subduction zone derived magmatic CO_2 (Sano and Marty 1995). In addition, $\delta^{13}C$ signatures are also affected by melt-vapour fractionation, where the heavier isotope systematically favours the vapour phase (Mattey 1991). While this process has the potential to mask original isotopic source signatures, such fractionation may also provide insights into the nature and extent of batch degassing processes, including potential recognition of new pulses of magmatic degassing (as at Mt Etna, Chiodini et al. 2011).

Sulfur

Sulfur is a particularly important component in volcanic lake systems, where it typically plays a major role in mediating the redox state of the proximal magmatic-hydrothermal environments (Giggenbach 1987), but its deposition in elemental form can also become an important control on permeability therein (Hurst et al. 1991; Oppenheimer 1992; Christenson 1994). Thorough reviews of S chemistry in magmatic environments have been provided by Wallace and Edmonds (2011) and Oppenheimer et al. (2011), for which only a few key aspects relevant to volcanic lake environments are presented here.

S behaviour in magmas is complicated by the fact that it may exist over a range of valence states (−2, 0, +4 and +6). In the melt phase, therefore, S may speciate across $S_2°$, SO_3^{2-} and SO_4^{2-}, according to the oxidation state imposed by Fe in the melt-mineral system (Carmichael and Ghiorso 1986). This variation is reflected in the range of S gas species which may coexist with the melt, including H_2S, S_2, SO_2, SO_3 and OCS.

S solubility in silicate melts is limited by the occurrence of non-volatile S phases, including Fe–S–O immiscible liquids and sulphide minerals under reducing conditions, and sulphate minerals under more oxidising conditions (Wallace and Edmonds 2011), with melt-phase solubility generally increasing with oxidation state. S solubility is also linked to total FeO content, ranging from 800 to 1,200 ppm in MORB basalts with 8–10 wt% total FeO, to 2,000–2,400 ppm at 15–16 wt% FeO (Wallace and Carmichael 1992). In more evolved arc magmas, however, S shows minor inverse solubility with silica contents (Scaillet and Pichavant 2003).

Thermodynamic modelling of primitive MORB melts at 1,280 °C shows that the total abundance of S gas species varies directly with redox state of the melt, with the sulphur content of the gas phase ranging from ca. 0.05 to over 40 % for NNO values of −3 to +1 respectively (Oppenheimer et al. 2011). These authors also found that SO_2 is the predominant S-bearing gas species in equilibrium with the melt above NNO = −2.5, with the next most prevalent species being S_2. H_2S becomes predominant only below NNO ∼−2.5.

The $\delta^{34}S$ signature of bulk mantle S is similar to that of the internationally accepted standard value derived from the Canyon Diablo Troilite meteorite. MORB sulfides, for example, cluster around −0.3 ± 2.3 ‰ VCTD, whereas OIB sulphides are +1.0 ± 1.9 ‰ VCTD (Marini et al. 2011). However, there is strong, temperature-dependent fractionation of ^{34}S between SO_2 and H_2S (+10 to +2 over the temperature range 300–1,000 °C; (Friedman and O'Neil 1977), making the $\delta^{34}S$ isotope systematics a powerful tool for understanding volcanic lake environments (e.g., Marini et al. 2011; Kusakabe et al. 2000; Delmelle and Bernard this volume).

Halogens

The halogens constitute the last major component group in volcanic emissions affecting volcanic lakes, and include in decreasing order of abundance, Cl, F, Br and I. While both Cl and F are relatively abundant in crustal rocks with mean concentrations of 550 and 240 ppm respectively, Br and I are typically present at levels less than 1 ppm. Cl is the dominant halogen in volcanic emissions and crater lakes, and it is an important conservative constituent in hydrothermal systems generally. As such, our very cursory discussion here will be limited to this single specie, although its general behaviour remains applicable to the halogens as a whole, and the reader is referred to the vast literature on halogen behaviour in magmatic systems (e.g., Aiuppa et al. 2009; Pyle and Mather 2009, and references therein).

Cl concentrations in magma show considerable variation between differing tectonic regimes and melt compositions. Cl in basalts from ridges and oceanic islands have Cl contents generally <800 ppm. However, Cl is essentially an incompatible component in silicate melts, tending to fractionate into the remaining melt fractions during crystallisation (e.g., Anderson 1975), as evident in the occurrence of melt inclusions in calc-alkaline volcanics with Cl contents exceeding 7,500 ppm, and high silica peralkaline magmas up to 1.2 wt% (Aiuppa et al. 2009). Once magmas become saturated with respect to H_2O, however, Cl is strongly fractionated into the fluid phase at supercritical conditions (Kilinc and Burnham 1972). With transition to sub-critical conditions, this fluid becomes immiscible, with Cl strongly fractionating into the liquid fraction to form NaCl-rich brine and a low-density vapour phase (Shinohara et al. 1989). Further pressure decline leads to the brine becoming increasingly hypersaline (see Henley this volume), ultimately entering the halite + vapour region in PTX space (e.g., Shinohara and Fujimoto 1994). It is typically this associated aqueous vapour, in conjunction with the aforementioned volatiles species, which constitutes the magmatic volatile phase on active volcanoes. The predominant Cl species in volcanic emissions is HCl (e.g., Symonds et al. 1988), with high temperature fumarolic emissions from andesitic volcanoes (>500 °C) typically ranging between 1,000 and 14,000 mmol/mol (Giggenbach 1996).

2.1.2 Minor and Trace Gases

In volcanic systems, N_2 is typically a non-reactive component (Giggenbach 1996) derived from one of three main component sources. These include: primordial mantle gas, N derived from subducted sedimentary/organic material along convergent margins (Hilton et al. 2002; Fischer 2008) and also that contained in meteoric waters convectively swept into volcanic hydrothermal environments (Giggenbach 1987, 1996). ^{15}N signatures of the upper mantle, as represented by MORB analyses, have $\delta^{15}N_2$ values uniformly in the vicinity of −5.0 (i.e., depleted in ^{15}N relative to air, Marty and Humbert 1997), whereas sediment-derived N_2 is distinctly heavier, ranging from +5 to +7 (Cartigny and Ader 2003). Interestingly, deep mantle signatures from mantle plumes have been shown to be quite variable (−5 to +5), raising questions about deep mantle convection and mixing of subducted sediments (Marty and Dauphas 2003), although others argue that N is efficiently recycled at subduction zones (i.e., volatilised) from subducted slabs and related sediments (Fischer et al. 2002).

Numerous other trace-level gases are found in volcanic emissions, including most notably, the noble gases which serve as useful tracers (Hilton and Porcelli 2013), metal species (e.g., Symonds et al. 1987, 1992; Henley this issue), and a multitude of trace and ultra-trace species derived from interactions between major component sources (e.g., Symonds and Reed 1993).

2.1.3 Gas Solubility in Magma

A general theoretical treatment relating solubility of the major gases to total confining pressure in andesitic melts was presented by Giggenbach (1996), and his summary diagram is reproduced in Fig. 2. In its formulation, Henry's constants

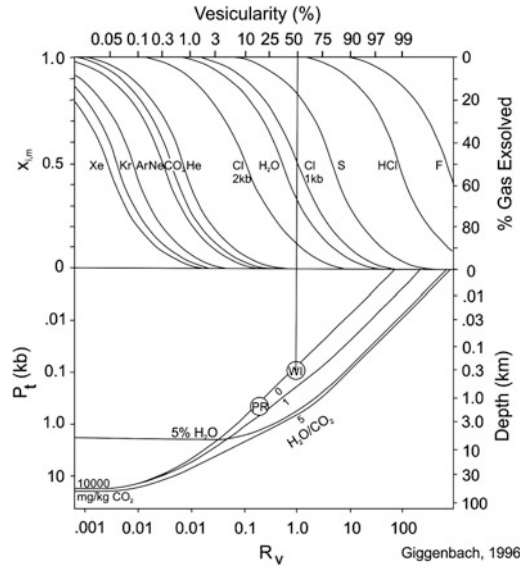

Fig. 2 Gas solubility in magma as a function of vesicularity (after Giggenbach 1996). CO_2 is relatively insoluble in melts, having a bulk solubility similar to that of the noble gases

were derived from Ostwald coefficients presented by Zhang and Zindler (1989), and were used to assess the solubility of the predominant gases in White Island (New Zealand) magmas. Total gas pressure is derived from summing the partial pressures of component species via:

$$P_t = \Sigma\left(c_{i,o}/R_v Q_{i,T} + 1\right)K_{i,T}, \qquad (2)$$

where $c_{i,o}$ is the initial concentration of species i, R_v is the vapour-melt volume ratio, $Q_{i,T}$ is the Ostwald coefficient for species i, and $K_{i,T}$ is the temperature dependent Henry's law constant. Solute gas contents are plotted in Fig. 2 as functions of vesicularity, V_v, (volume %) which is related to R_v by:

$$V_v = 100\,R_v/(1 + R_v). \qquad (3)$$

Assuming single step vapour separation, the curves in Fig. 2 show that CO_2 has low solubility in the melt phase, comparable to the noble gases, and is >90 % evolved by the time vesicularity approaches 1 %. At 50 % vesicularity, all of the noble gases, CO_2 and some 70 % of the water are exsolved, but just 20 % of total S and virtually none of the HCl has entered the vapour phase. From these relations it is clear that depth of degassing and decoupling of gas from magma are critically important controls on the composition of gases reaching volcanic lake environments. Distal magma sources will result in gases comprised predominantly of CO_2, as in the case of maar lake systems, whereas shallow degassing will provide the full complement of magmatic volatiles and heat in the lake systems.

Another interesting insight to be gained from Eq. 3 is also portrayed in Fig. 2. Here, considering CO_2 and H_2O to be the predominant pressure generating species in the melts allows the total vapour pressure to be calculated as a function of R_v, and thereby the depths at which vapour-melt separation may begin. For melts with CO_2 contents of 10,000 mg/kg, the calculated depth exceeds 80 km, suggesting that phase separation is probably already occurring close to the depths of magma generation. It is clear from Fig. 2 that the depth of gas-melt decoupling places a first order constraint on the relative compositions of the principle gas species reaching the surface, and thereby the chemical characteristics of volcanic lakes into which they discharge. Evidence suggests that vapour segregation readily occurs in the plumbing systems of erupting basaltic volcanoes (Aiuppa et al. 2010; Allard 2010), through the generation of volatile-rich foams (Vergniolle and Jaupart 1990; Sparks 2003), or through separation processes invoked by branching conduit geometries as proposed for Etna (Burton et al. 2003), or Mount Cameroon (Suh et al. 2003). What this means for volcanic lakes, is that deeply decoupled volatile streams will consist largely of CO_2 (plus noble gases), whereas shallow decoupling will contribute CO_2, S species and halogens directly into the lake environment.

It is well recognised that many volcanoes emit large quantities of gas in the absence of significant eruption activity, including Etna (Aiuppa et al. 2007); Popocatépetl (Delgado-Granados et al. 2001), Ambrym (Bani et al. 2009), Miyakejima (Shinohara et al. 2003) and a wide range of less prodigeous emitters, some including volcanic lakes (e.g., Aso, Shinohara et al. this issue), White

Island (Werner et al. 2008), Poás (Rowe et al. 1992), and Ruapehu (Christenson 2000, Christenson et al. 2010). In these cases, the amounts of emitted gas well exceed those which could be derived from associated erupted magmas, if any. So the question is, by what mechanism(s) do the gases reach the surface?

Bubble accumulation and coalescence to form foams, with subsequent shearing and collapse to form permeable channel-ways for gas migration, have been proposed to explain differential gas transfer and observed slug-flow and lava fountaining phenomena (Jaupart and Vergniolle 1988; Vergniolle and Jaupart 1990). Sparks (1978) modelled the diffusive transfer of water vapour through ascending basaltic melts and found that bubble diameters ranged between 0.1 and 1.0 cm, consistent with the majority of observed scoria bubble diameters. However, for a typical basalt melt viscosity range of between 30 and 3 Pa.s, bubble diameters of between 14.5 and 4 cm, respectively, are required for bubbles to move significantly faster than the magma (Sparks 2003), suggesting that other transfer mechanisms are at play in the formation of foams.

Carrigan (1983) proposed forced convection within magma conduits of radii as small as 5 m diameter, as a means of offsetting heat loss and attendant solidification of magma in feeder conduits for active volcanoes. The model incorporates buoyant rise of vesiculated melt to some level in the volcano conduit, where decoupling takes place and gases either accumulate, or are released into the surrounding hydrothermal environment, after which the denser, degassed magma convectively sinks back to the source. Since then, compelling evidence has emerged for magmatic convection being the principle driver for magmatic degassing at numerous volcanoes (e.g., Kazahaya et al. 1994; Allard 1997; Stevenson and Blake 1998; Shinohara et al. 2003; Oppenheimer et al. 2004). By this means, we have at least one mechanism for continuous, or near continuous delivery of magmatic volatiles to the hydrothermal environments associated with volcanic lakes.

2.2 Hydrothermal Gases and Processes

As previously described, the hydrothermal environment in magmatic-hydrothermal systems effectively begins at the transition from single phase vapour to the 2-phase vapour-liquid envelopes surrounding a magma conduit (Fig. 1). The gases involved in this environment consist of the aforementioned magmatic inputs, the meteoric gases (of atmospheric origin, primarily N_2, O_2, Ar), and gases formed through heterogeneous reaction of these species with the host rocks.

2.2.1 Redox State

A most remarkable feature of proximal magmatic-hydrothermal environments is the wide range of redox conditions found within, a variability which owes its existence to the interplay between the two principle redox buffers. A measure of redox state, as proposed by Giggenbach (1987), is the readily measurable ratio of f_{H_2}/f_{H_2O} (with parameter R_H defined = log (f_{H_2}/f_{H_2O})). Gases leaving magmas typically have their redox state buffered by the temperature- and pressure-dependent equilibrium between H_2S and SO_2, the so-called "magmatic gas buffer" of Giggenbach (1987):

$$H_2S + 2H_2O = SO_2 + 3H_2. \quad (4)$$

At temperatures close to 1,000 °C, this buffer closely approaches the FMQ (i.e., fayalite-magnetite-quartz) buffer, which is generally accepted as being the primary redox control in silicate melts Carmichael and Ghiorso (1986). At this temperature R_H is approximately −2.0. On departure from the magma, and with decreasing temperature, however, the gas buffer drives the redox state of the gas stream to ever higher oxidation potential (decreasing R_H), where at temperatures approaching ca. 300 °C, the redox potential of the gas stream is very close to that governed by magnetite-hematite equilibrium at 1 bar pressure.

As described by Giggenbach (1987), observed deviations of gas compositions away from the magmatic gas buffer (i.e., toward lower oxidation potentials with decreasing temperature) is normally attributable to interaction with Fe^{2+} and Fe^{3+} in silicate rocks, whose redox potential is well represented by the reaction between fayalite (a proxy for FeO) and hematite according to:

$$\text{Fayalite} + H_2O = \text{Hematite} + \text{Quartz} + H_2, \quad (5)$$

which has a nearly temperature independent R_H value of ~ -2.8. Buffering by rocks in this environment effectively converts SO_2 in the hydrothermal environment to H_2S.

As we shall see below, another reaction which indirectly affects the redox state of the magmatic-hydrothermal environment is that governing the formation of the elemental sulphur from the magmatic gas stream:

$$2H_2S + SO_2 = 3S_e + 2H_2O \quad (6)$$

Here, the forward reaction depletes the volatile stream of H_2S, driving Eq. (4) to the left, effectively lowering fH_2.

As in the magmatic realm, CO_2 is also the predominant C-gas in the hydrothermal environment. Here it enters into temperature- and redox-sensitive equilibria with both CO and CH_4 (Giggenbach 1980, 1987; Taran 1986; Chiodini et al. 1993). The reaction kinetics for:

$$CO + H_2O = CO_2 + H_2 \quad (7)$$

are demonstrably fast, and have been shown to carry the redox signature of either the gas or rock buffers within the magmatic-hydrothermal environment (Giggenbach 1987; Chiodini et al. 1993), and the reaction readily equilibrates in either the liquid or vapour phase. The reaction:

$$CH_4 + 2H_2O = CO_2 + 4H_2, \quad (8)$$

on the other hand, has much slower kinetics, and is typically buffered by the FeO–$FeO_{1.5}$ rock buffer within the liquid-phase environment marginal to high temperature conduits (Taran and Giggenbach 2003). As such, CH_4 may be regarded as both a tracer and component species of the hydrothermal equilibrium environment (Chiodini 2009).

A good example of the interplay between hydrothermal and magmatic source environments is found on White Island (Fig. 3) where the relative variations amongst N_2, CH_4 and CO_2 in a single fumarole show a progressive shift towards magmatic signatures since the late 1970s through to the present time. Three end-member components can be described in terms of their relative N_2/CH_4 ratios, including a N_2-rich meteoric component, a CH_4-rich hydrothermal gas and a relatively CH_4-depleted magmatic endmember. N_2/CH_4 ratios close to 0.5 in the late 1970s trend towards a CH_4-depleted signature of $N_2/CH_4 > 30$ by 2004, during the magmatically active period of the volcano.

Heavier hydrocarbons of thermogenic derivation are also typically present as either trace or ultra-trace species in hydrothermal environments associated with magmatic systems such as White Island (e.g., Taran and Giggenbach 2003), and Vulcano Island (Tassi et al. 2012), with alkanes

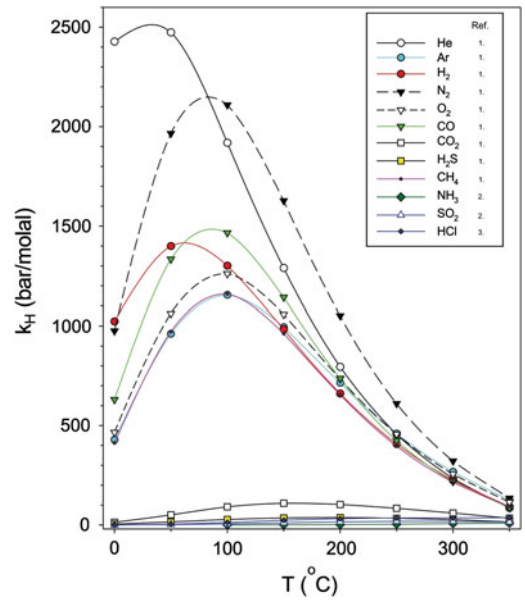

Fig. 3 Variability in hydrothermal and magmatic end-member components in a low temperature fumarole from White Island, New Zealand. CO_2/CH_4 ratios for the magmatic and hydrothermal endmembers are ca. 50 and >50,000 respectively

generally predominating in the rock-buffered environments, although varying mixtures of alkenes and alkanes typically occur in the more oxidising (i.e., H_2S–SO_2 gas-buffered) environments. The species are typically thermogenic in origin, derived from kerogen cracking in the hydrothermal environment (Taran and Giggenbach 2003).

NH_3 bears a similar equilibrium relationship to N_2 as CH_4 and CO have to CO_2 (Eq. 8) in hydrothermal environments, i.e. it is present in subordinate concentrations relative to the main species and therefore behaves more as an indicator rather than an iso-molar redox buffer Giggenbach (1980). The equilibrium reaction is:

$$2NH_3 = N_2 + 3H_2 \quad (9)$$

The two equilibria share other characteristics as well, including equilibration under reducing conditions, and similarity in their relative rates of equilibration which are relatively slow in comparison to H_2–H_2O, CO–CO_2 and H_2S–SO_2 (Giggenbach 1987).

2.2.2 Aqueous Solubility of Gases in the Hydrothermal Environment

All gases are soluble in water to varying degree. At relatively low gas pressures, the aqueous concentration of any gas are conveniently described by Henry's Law,

$$x_i = P_i / K_{H,i} \quad (10)$$

where x_i is the molality, P_i is the partial pressure (bar), and $K_{H,i}$ is the temperature dependent Henry's Law constant (with units of bar/molal) for species i. Where the total pressure of volatile species exceeds the confining pressure (typically hydrostatic in hydrothermal environments), gases will partition between vapour and liquid phases according to:

$$B_i = x_{i,v} / x_{i,l} = z_v * K_{H,i} / P_{H_2O} \quad (11)$$

where B_i is the vapour-liquid distribution coefficient, and z_v and P_{H_2O} are the compressibility and pressure of water vapour, respectively.

Henry's Law constants for the major gas species found in volcanic hydrothermal environments are shown as functions of temperature in Fig. 4 (as bar·molal^{-1}, using regressions of Fernandez-Prini et al. (2003), Naumov et al. (1974) and Truesdell et al. (1989). Two broad solubility groups are apparent in these data. The smaller, lighter and/or mono-atomic gas species (e.g., He, Ar, H_2, N_2, O_2, CO and CH_4) are less soluble than their larger and/or heavier molecular counterparts (CO_2, H_2S, HCl, SO_2 and NH_3), and the former typically shows aqueous solubility minima between 0 and 100 °C.

The more soluble protonated species typically exhibit dissociative solvent-ion interaction, leading to pH-dependent speciation, and this somewhat complicates their behaviour as volatiles in the magmatic-hydrothermal environment. For example, CO_2 undergoes temperature- and pH-dependent speciation across $H_2CO_3°$, HCO_3^- and CO_3^{2-}. At 20 °C and pH < 4, for example, it exists almost entirely as hydrated molecular CO_2 and H_2CO_3 (e.g., Stumm and Morgan 1981), and behaves effectively as an inert species. Where pH may be controlled by mineral buffers at levels >4, dissociation of H_2CO_3 provides a source of protons for hydrolysis reactions between fluid and rock Giggenbach (1981). H_2S is similar in behaviour, with a pK_1 of ca. 7.5, whereas

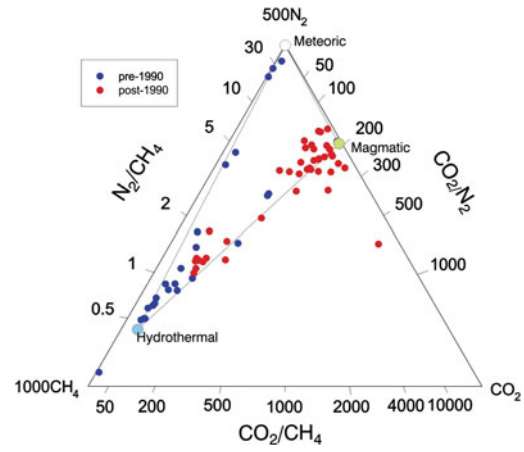

Fig. 4. Henry's law constants for typical gases in volcanic lakes. Units are bar/molal. Reference data are from: Fernandez-Prini et al. (2003), Naumov et al. (1974), and Truesdell et al. (1989)

ammonia predominates over ammonium only at pH levels > ca. 9.

HCl is a gas with bulk solubility similar to that of H_2S. It is, however, a strong electrolyte which becomes significantly associated only at very low pH and/or temperatures approaching the critical point Ruaya and Seward (1987). Therefore, contact between high temperature HCl-bearing vapours and liquid water generally leads to dissolution and dissociation of the HCl, potentially leading to the formation of highly acidic solutions (e.g., Truesdell et al. 1989). These processes are discussed further below.

2.3 Meteoric Gases

As already mentioned, the meteoric constituents are composed of atmospheric gases introduced into the hydrothermal environment by air saturated rain water entering into groundwater systems, or in the case of volcanic lakes, by direct equilibration with air which is in contact with the lake water. The principle components are, not surprisingly, those of highest partial pressure in the atmosphere (i.e., N_2, O_2 and Ar), and their equilibrium concentrations in groundwater are proportional to their temperature-dependent Henry's Law solubilities. As an example, two component mixing between atmospheric and magmatically derived end-members is clearly evident in solute N_2, Ar and CO_2 compositions from Ruapehu Crater Lake (Fig. 5; data from Christenson et al. submitted). Here fumarolic discharges from both Ruapehu and White Island represent the magmatic-hydrothermal end member, whereas the theoretical meteoric component signatures are calculated for temperature ranging between 0 and 40 °C using the Henry's constants of Fernandez-Prini et al. (2003). CO_2/N_2 ratios vary between ca. 40 and 3 over the 3 year-long period represented by the data, and reflect varying emissions from the magmatic system on the volcano. Interestingly, projection back to the N_2–Ar axis reveals a N_2/Ar ratio of ca. 55, well above the meteoric range of 36–40. This higher value most probably represents the N_2-enriched magmatic component which is prevalent on NZ arc-type hydrothermal environments (e.g., Christenson et al. 2002), with the N_2/Ar ratio of ~1,000 for Ruapehu (Christenson 2000).

2.4 Biogenic Gases

The distribution of biomass along the vertical water column of a lake is controlled by water chemical-physical conditions, i.e. temperature, pH and redox. Biomass is relatively abundant in the epilimnion, decreases to a minimum in the metalimnion and increases in the lower anoxic hypolimnion (Niewolak 1974; Jones 1978; Kato and Sakamoto 1981; Coveney and Wetzel 1995; Simon 1998). Irrespective of their primary origin, CO_2, CH_4, N_2, O_2, S gases and H_2 dissolved in volcanic lakes are involved in biogeochemical processes (Mapelli et al. this issue). As shown in the following sections, lakes hosted in quiescent volcanoes, characterized by relatively low temperature, almost-neutral pH and establishment of meromictic conditions (i.e., a permanent thermal and chemical stratification), the vertical distribution of these gases and that of microbial populations are intimately related.

2.4.1 CO_2

Although dissolved CO_2 in volcanic lakes are typically fed by sub-lacustrine gas discharges (Sigurdsson et al. 1987; Tazieff 1989; Aeschbach-Hertig et al. 1999; Tassi et al. 2009), the fate of dissolved CO_2 strongly depends on addition-consumption processes related to biotic respiration, anaerobic decomposition of organic matter and microbial oxidation of CH_4 (Rudd et al. 1974; Rich 1975, 1980), especially in lakes hosted in quiescent volcanoes. In an aerobic environment, i.e. in the shallower portions of crater lakes, microalgae and cyanobacteria along with higher plants, are capable of CO_2-consuming oxygenic photosynthesis Nelson and Ben-Shem (2004), which proceeds following two main pathways: light energy conversion to biochemical energy by a photochemical reaction, and CO_2 reduction to

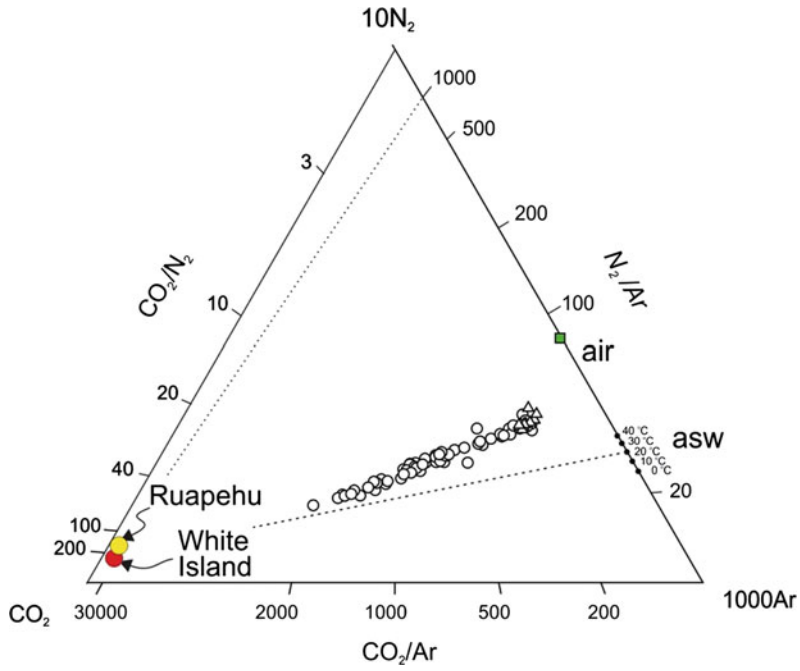

Fig. 5 Relative solute CO_2–N_2–Ar contents in Ruapehu Crater lake water, showing mixing relations between magmatic and meteoric lake water components. Ruapehu source gas composition is taken from Christenson (2000), and bears close similarities to gases to values observed from White Island (Giggenbach and Sheppard 1989), both having N_2/Ar ratios ≥1,000. The meteoric endmember component is N_2-enriched over the range of theoretical equilibrated air-saturated water compositions (calculated for temperatures of 0–40 °C), reflecting excess N_2 in the source gas. Open circles reflect time series data collected over the period 2007–2012, and open triangles represent multiple samples collected by boat over a single day in 2010

organic compounds such as sugar phosphates, through the use of this biochemical energy by Calvin-cycle enzymes. In the hypolimnion, CO_2 biogenic and geogenic inputs are counteracted by microbial reduction processes mainly by methanogens (Schoell 1988; Whiticar 1999), a group of microorganisms phylogenetically affiliated to the kingdom Euarchaeota of the domain Archaea Woese et al. (1990). Anaerobic methanotrophy coupled to Fe or Mn reduction Valentine (2002) and using nitrates as substrates Raghoebarsing et al. (2006) can also occur, although most of CH_4 oxidation is carried out in the epilimnion (Hanson and Hanson 1996; Lopes et al. 2011). The combination of loss and addition of CO_2 related to the various biogeochemical processes occurring at different depth along the water vertical column maintain stable CO_2-rich reservoirs typically characterizing Nyos-type meromictic volcanic lakes.

2.4.2 CH_4

Methanogenic processes are active within sediments of anoxic hypolimnia of meromictic lakes Rudd and Taylor (1980). In the presence of free oxygen, particularly at oxic/anoxic boundaries, CH_4 is easily consumed by methanotrophs phylogenetically affiliated to the *a*, *h* and *g* subdivisions of kindom Proteobacteria in the domain Eubacteria (Hanson and Hanson 1996). Methanogenic processes proceeds through carbonate-reduction and acetate fermentation pathways Schoell et al. (1988), which can be described by the following reactions:

$$CO_2 + 8H^+ + 8e^- \rightarrow CH_4 + H_2O \qquad (12)$$

and

$$^*CH_3COOH \rightarrow ^* CH_4 + CO_2 \qquad (13)$$

where the * indicates the intact transfer of the methyl position to CH_4. Reaction (12) prevalently

occurs in sulfate-free marine sediments, whereas in freshwater environments the two processes are competitive (e.g., Takai 1970; Winfrey et al. 1977). Methane produced by microbial methyl-type fermentation is typically ^{2}H-depleted ($\delta^{2}H$–$CH_4 < -250$ ‰ V-SMOW) and ^{13}C-enriched ($\delta^{13}C$–$CH_4 > -70$ ‰ V-PDB) with respect to that produced by bacterial CO_2 reduction Whiticar et al. (1986), although these boundary values may vary depending on the maturity and type of the organic source Whiticar (1999).

2.4.3 N_2

The triple–bounded N_2 molecule is involved in biological processes to produce reactive N_2-bearing compounds, such as NO_x and NH_x. Therefore, the distribution of N_2 concentrations in stratified lakes is controlled biological processes able to fix or produce N_2. Biological N_2 fixation, which depends on light (Tison et al. 1977), and presence of bioavailable trace metals (Hysenstrand et al. 1988) is carried out in water, on the sediment surface and in sediment pores by heterocyst-forming species such as cyanobacteria (Loeb and Reuter 1981; Valelia 1991) and methane-oxidizing bacteria (Rudd and Taylor 1980). Denitrification, i.e. the reduction of NO_3^- to NO_2^- and then to N_2 (Ahlgren et al. 1994) commonly occurs at anaerobic conditions. In this process, NO_3^- is used as an electron acceptor during respiration of bacterial species such as *Pseudomonas* and *Clostridium*. Bacterial N_2 production may also occur through NH_4 oxidation with NO_2^- as electron acceptor, a process termed as anammox (Anaerobic Ammonium Oxidation) that is carried out by the bacteria phylum *Planctomycetes* (Jetten et al. 1998).

2.4.4 O_2

Oxygen concentrations in permanently stratified volcanic lakes typically decrease with depth, since this gas is depleted rapidly by oxidative processes. This produces a vertical O_2 profile termed *clinograde*, where aerobic epilimnion and anaerobic hypolimnion can be clearly distinguished. Oxygen consumption, which is primarily due to biological oxidation of organic matter, intensively occurs at all the depths, but in the epilimnion is frequently offset by water circulation and photosynthesis, two O_2 renewal mechanisms that are not active in the hypolimnion. Pure chemical oxidation and photochemical oxidation induced by ultraviolet light may also significant contribute to oxygen depletion of deep lake waters (Laane et al. 1985; Wetzel et al. 1995).

2.4.5 H_2

Cyanobacteria produce molecular H_2 through both photosynthesis and anaerobic fermentation processes (Asada and Kawamura 1986; Asada and Miyake 1999). Hydrogen biogenesis and consumption is related to metabolic activity of several enzymes: nitrogenase catalyzes H_2 production concomitantly with the reduction of N_2 to NH_4, whereas hydrogenase is able to both take up and produce H_2 (Bergman et al. 1997; Tamagnini et al. 2002). At anaerobic conditions, H_2 is involved in mineralization processes of organic matter, being used as electron donor by methanogenic and sulfate-reducing bacteria (Zehnder 1978; Thaurer and Badziong 1980). These processes mainly occur at the water-sediment interface, thus H_2 slowly diffuses from the lake bottom sediment toward the surface is efficiently consumed before arriving at the lake surface.

3 Chemical and Physical Models of Sub-lake Environments

As the foregoing suggests, our understanding of the chemical interaction between ascending magmatic heat and volatiles and Earth's hydrosphere is reasonably well advanced, despite the fact that much of what goes on in these environments is inaccessible to us at the Earth's surface. Much of our early understanding stemmed from time series studies of crater lake systems during volcanically active periods (e.g., Giggenbach and Glover 1975; Delmelle et al. 2000; Rowe et al. 1992). Such time series data have been used to constrain numerical simulations of these systems, including reaction path

models for equilibrium gas and water chemistry (Christenson and Wood 1993), and more recently, heat-mass transport and reactive transport models of these same systems (Chiodini et al. 2003; Todesco et al. 2003; Christenson et al. 2010; Christenson and Young 2010). In the next section we briefly review results from two such models.

3.1 Gas-Groundwater Interaction

The absorption of a rising magmatic vapour into groundwater (Fig. 6) can be readily simulated with the reaction pathway algorithm REACT Bethke (1996). In this example, 10 mol of a high temperature fumarolic gas (White Island fumarole F3; Table 1) are numerically titrated over 100 steps (i.e., 0.1 mol total gas added per step) into 1 kg of the relatively dilute Silica Rapids spring water which issues from the flank of Mt Ruapehu (Table 2). Since REACT has no enthalpy constraint, temperatures are monotonically increased from 20 to 300 °C during the run (2.8 °C per step) to simulate heating that might occur through a combination of condensation of the hot vapour into the groundwater and conductive heating in the conduit region. All gases are taken into aqueous solution during the titration, i.e., there is no vapour-liquid partitioning.

System Eh and pH are plotted in Fig. 6a. The spring water has a near-neutral pH initially, and oxygen levels were set to be in equilibrium with atmosphere (~6 ppm O_2). There are rapid negative shifts in both Eh and pH in the first reaction steps which, not surprisingly, demonstrates the low buffering capacity of the dilute spring water. pH decreases to a minimum of 1.3 at ca. 250 °C, but then climbs back up to ca. 1.5 with continued heating to 300 °C. Conversely, the abrupt decline of system Eh to a minimum value of ~ +0.1 V in the first step is followed by a progressive increase to a maximum ~+0.28 V at 270 °C, before declining to +0.25 V at 300 °C. These changes correspond closely to the appearance and temperature-controlled stability of elemental sulphur in the system (Fig. 6b). Elemental sulphur precipitation initiates at the outset, and continues through to approximately 240 °C, after which it begins to redissolve. Temperature appears to be the controlling factor in sulphur stability in this system, which in turn controls the redox state of the fluid.

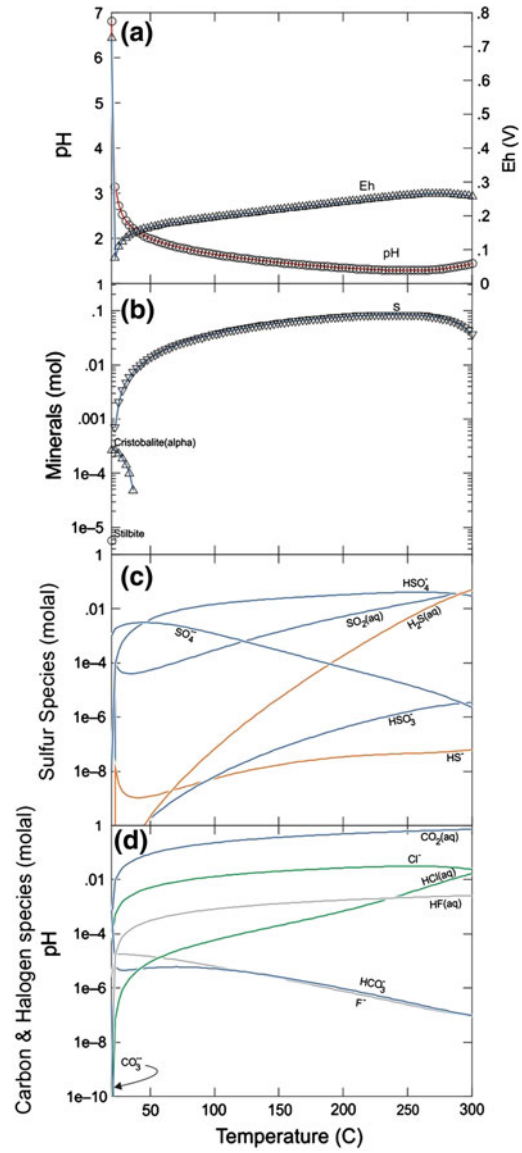

Fig. 6 Reaction path simulation for the titration of 10 mol of White Island fumarolic gas into 1 kg of Silica Rapids spring water (Mt Ruapehu), with monotonic heating from 20 to 300 °C. **a** pH and Eh variations with reaction progress (each symbol represents 1/100 of the reaction progress; **b** Minerals formed during the reaction sequence (moles); **c** Aqueous S speciation; **d** Aqueous C, F and Cl speciation with reaction progress

Table 1 White Island fumarolic #3 composition from White Island (Giggenbach and Sheppard 1989)

Date	31-8-78
T_m (°C)	540
H_2O	880,000
CO_2	84,320
S_t	18,600
N_2	1.9
HCl	4,080
HF	304
NH_3	20
He	0.68
H_2	2,100
Ar	0.86
O_2	<0.5
N_2	458
CH_4	2.2
CO	48.4

Units are μmol/mol

The generation of a strongly acidic liquid phase is perhaps the most notable aspect of this gas-water interaction. As mentioned previously, and shown in Fig. 6c, d, HCl and H_2SO_4 are the principle (strong) acids, and these are the primary hydrolysis-promoting agents involved in ensuing water-rock interaction in these environments. It is evident that temperature is ultimately a limiting factor on acidity, owing to the temperature-dependence of solvent-ion interaction where, as the dielectric constant for water decreases with temperature (Uematsu and Franck 1980), acids become increasingly associated (e.g., HCl; Ruaya and Seward 1987). It is this effect alone that is responsible for observed increases in pH above 250 °C in this comparatively simple model, and it is a trend which continues to where acids become fully associated at the point. Owing to the fact that H_2CO_3 is a weaker acid than either HCl, H_2SO_4 or even HF, it remains almost completely associated in this model environment owing to the very low pH. Whereas CO_2 is the predominant hydrolysis-promoting agent in near-neutral pH hydrothermal systems, and may in fact become buffered by the presence of calcite in such systems (Giggenbach 1981; Arnórsson 1985; Arnórsson and Gunnlaugsson 1985), in highly acidic environments such as those found in active crater lakes, CO_2 behaves as a conservative constituent, similar to any other non-reactive gas.

3.2 Gas-Lake Water-Rock Interaction

Christenson et al. (2010) simulated gas-water-rock interactions in the Ruapehu vent environment using the 1D advective reactive transport model X1t Bethke (1996). Here, we have further refined the model to examine the effects of water-rock interaction on key indicator gases in the vent hydrothermal environment. The conceptual model for this condensed vapour-water-rock interaction is shown in Fig. 7, where a column of permeable substrate (35 % porosity) measuring 10 cm^2, and 10 m in length is initially filled with Ruapehu Crater Lake water (Table 2), and is allowed to equilibrate at 50 with the reactant minerals listed in Fig. 7 (as volume %). This scenario is similar to what might be found in the vent region during periods of quiescence. We then numerically inject a 300 °C magmatic condensate proxy consisting of 0.5 molal concentrations of both H_2S(g) and SO_2(g), and 1 molal concentrations of HCl(g) and CO_2(g) under a head pressure of 0.2 MPa for 24 h into the column. A fundamental assumption of this model is that full equilibrium is established at each time step. Whereas the reality is that reaction kinetics will play an important, if not dominant, role in governing which chemical reactions prevail in these environments (see Henley this issue), our knowledge of reaction rates is not well enough advanced to rigorously account for kinetics in the modelling of such complicated systems as presented here. In our case, we consider the concept of full equilibrium as perhaps a theoretical end-point in the process. The relatively low volume percentage of the six reacting mineral phases is chosen here to simulate the actual amount of reactive surface that permeating liquid phase would interact with, taking into account the effects of armouring of pore and fracture surfaces by precipitated minerals in the reaction column.

The initial alteration mineral assemblage is of argillic nature, owing to the acidity of the starting fluid, but is uniform along the length of the

Table 2 Water compositions used in the numerical simulations

Date	Feature	Tm °C	pH	HCO_3	Li	Na	K	Ca	Mg	Cl	SO_4	B	SiO_2	H_2S	Fe	Al	As	Br	F	NH_3
20-May-11	Silica rapids	8.2	6.82	47	<0.01	13.8	3.1	26	13.0	8.0	98	<0.3	35	<0.01	<0.08	0.34	<0.015	<0.03	<0.1	0.02
15-Aug-07	Crater lake	13.5	0.95		0.54	410	65	794	692	6,304	9,074	18	284	0.04	379	562	0.53	8.8	99	15.0

Units are mg/L

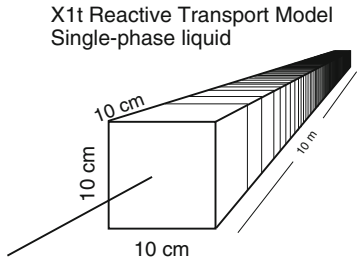

Porosity:	35%
Pressure Gradient:	0.2 Mpa
Pore Fluid:	RCL (August 4, 2007)
T (initial):	50 °C
Reactant Fluid:	1 molal SO_2, H_2S, HCl, CO_2
T (Reactant fluid):	300 °C
Reactant Minerals:	Diop(.1%), Anor(.1%), Alb(.1%), Ksp(.1%), Mt(.01%)
Duration:	1 day

Fig. 7 Reactive transport conceptual model. Flow path is 10 m long, with axis-normal dimensions of 10 cm by 10 cm. Adapted from Christenson et al. (2010)

column, and consists of (in order of decreasing abundance) jarosite, illite, pyrite, S, hematite, siderite, K-nontronite, anhydrite, kaolinite, dolomite, mesolite, Mg-saponite and quartz. Results of the advective flow model are summarised in Figs. 8 and 9. Specific discharge through the system attains a maximum at ca. 2.5 h, after which discharge declines monotonically to ca. 15 % of the peak flow by the end of the simulation (24 h; Fig. 8a). The advancing front of condensate is clearly delineated by Cl concentration (Fig. 8b), which approaches the end of the column after 24 h. Peak Cl concentrations broaden with time owing to dispersion along the pathway, whereas total C in the fluid (not shown) has a much steeper advancing front, which is governed by carbonate mineral equilibria (discussed below). Porosity abruptly declines from 35 to ca. 10 % in the first few elements (Fig. 8c). Naturally, this is reflected in permeability (Fig. 9a) which is derived as a function of porosity in X1t (the default relation for sandstone was adopted here, where $log\ k = 15\phi - 5$, with k being permeability (darcy), and ϕ the porosity of the medium). A further but smaller decrease in porosity and permeability occurs at ca. 7 m after 24 h. Interestingly, this perturbation is observed to migrate along the column during the course of the simulation,

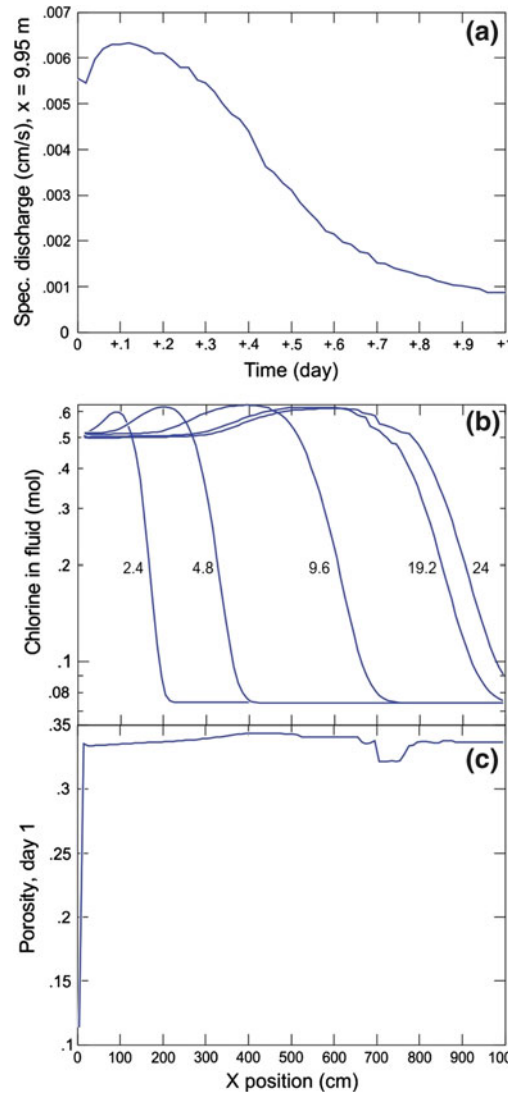

Fig. 8 Reactive transport model results. **a** Specific discharge at 9.95 m. **b** Advance of Cl front along flow path with time. **c** Porosity along flow path after 24 h

pointing to a progressing mineral front (discussed below). In contrast to the relatively rapid advance of Cl through the system, the thermal front associated with the hot condensate injection advances less than half way along the column within 24 h (Fig. 9a), pointing to decoupling of heat and mass along the flow path as heat is transferred into the host rock matrix. System Eh and pH are plotted in Fig. 9b, and reveal further evidence of chemical fronts advancing along the

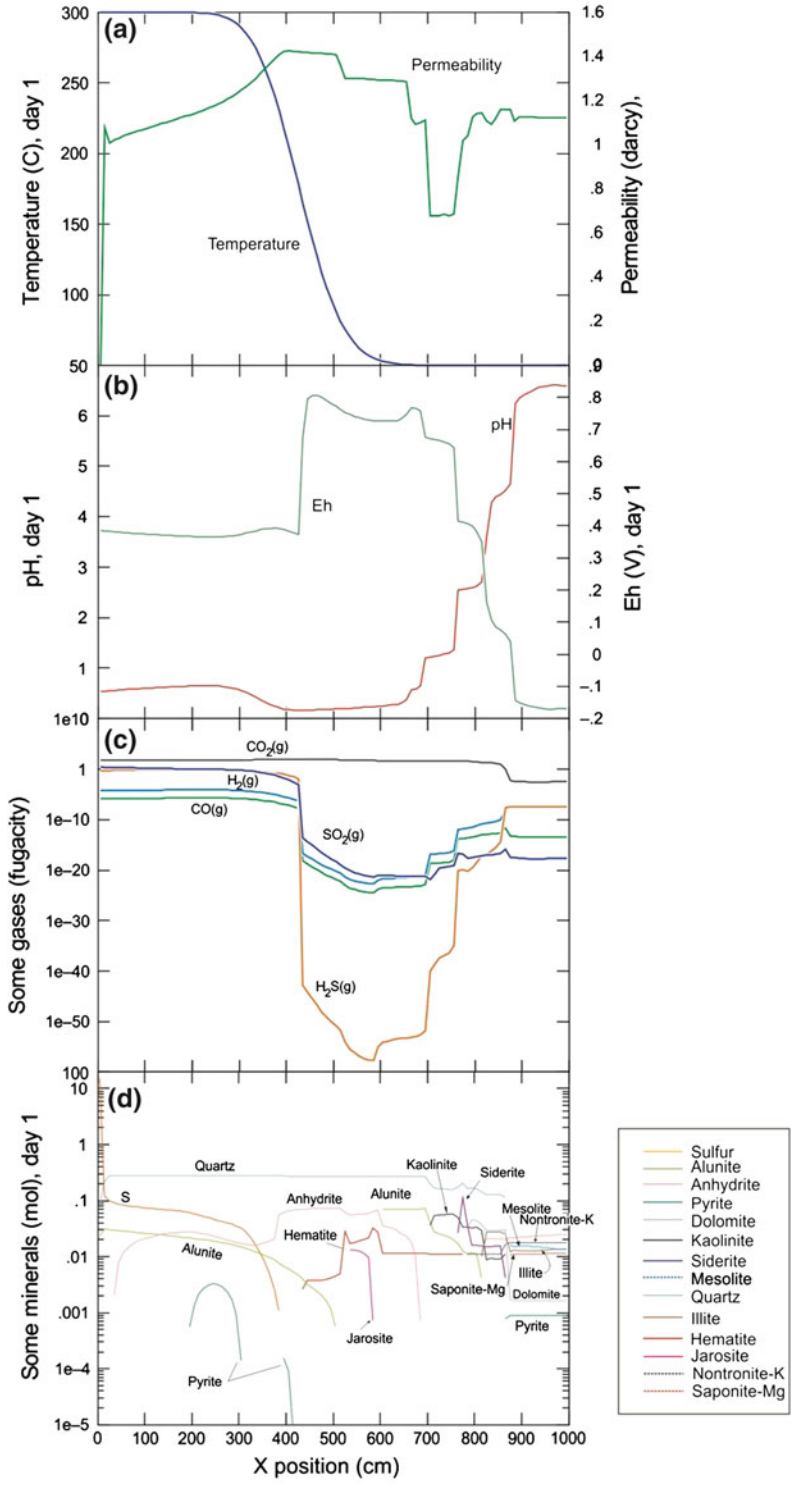

Fig. 9 Reactive transport modelling results plotted as a functions of position along flowpath. **a** Temperature and permeability. Significant drop in permeability occurs at the inlet, and another at approximately 7–8 m after 24 h, whereas the thermal front has advanced to ca. 3 m after 24 h. **b** An abrupt increase in Eh corresponds to changes in S species concentrations. Low pH front advances to ca. 7 m after 24 h. **c** S concentrations decline abruptly between ca. 4 and 7.5 m, with H_2S most strongly depleted. **d** Elemental S precipitation extends to ca. 4 m, after which its absence corresponds to the region of abruptly increased in Eh, reflecting its control over the oxidation state of the system. Carbonate and clay minerals characterise the interval from 7.5 to 10 m, and correspond to localised low permeability

flow path. The initial fluid redox state and pH are preserved only in the last metre of the column (at −0.15 and 6.4 V respectively, and are controlled by the equilibrium mineral assemblage formed from the initial interaction between lake water and reactant phases described in Fig. 7. At the inlet end, pH is strongly acidic (<1); here the injected condensate has expended the pH-buffering capacity provided by the initial equilibrium mineral assemblage.

Elemental S is the single most abundant precipitated mineral phase, and in conjunction with quartz, alunite and pyrite, is responsible for the aforementioned decline in permeability close to the source (Fig. 9d; and Christenson et al. 2010). However, consumption of H_2S and SO_2 according to Eq. (6) ultimately leads to under-saturation with respect to S along the flow path (at distances >4 m after 24 h), with an abrupt increase in system Eh thereafter (Fig. 9b). This is reflected in the increased abundance of anhydrite, and the appearance of hematite over the interval of 4–7 m. Here, pH reaches its minimum values (<1) owing primarily to declining temperature. The formation of elemental S along the flow path, and the large positive shift in redox potential in the absence of this phase are also reflected in the absolute and relative fugacities of H_2S and SO_2 (Fig. 9c). In the presence of elemental sulphur these species remain relatively constant.

Downstream of the elemental sulphur, however, H_2S is effectively absent, as reflected in log (fSO_2/fH_2S) varying from 0.4 to >30 between the two zones. Similarly, the fugacities of H_2 and CO also change abruptly across this interface, with log (fH_2/H_2O) decreasing from −5.9 to −18.2 and log (fCO/fCO_2) decreasing from −7.6 to −21.3 over the interval between 0.8 and 4.5 m. While the temperature gradient across this zone has a direct role to play in both ratios, the effect of temperature is minor compared to the presence/absence of elemental sulphur. It is noteworthy that the changes across this interval occur in the absence of any effective rock buffering capacity as described previously (Giggenbach 1987; Chiodini et al. 2001), owing to the fact that all Fe in the system occurs as Fe^{3+}.

Interestingly, gases in equilibrium with the alteration mineral assemblage occurring near the end of the flow path have log (fH_2/fH_2O) ratios of approximately −6.4. Although lower than those encountered in either of the zones upstream, the redox state of the fluid here is still considerably more oxidising than the rock buffer value of −2.8, suggesting that rocks in these environments have varying, if not fleeting capacities to buffer redox potential of the fluids moving through them. From this model, it is apparent that the presence of elemental sulphur in these systems has an important bearing on the redox state of the system, and the gases derived from them.

Reference was made earlier to the decrease in permeability observed between 7 and 8 m after 24 h, and the fact that this appears to migrate along the flow path close to the advancing Eh and pH fronts. We can see from Fig. 9d that this permeability perturbation corresponds to the presence of kaolinite, siderite and dolomite, and as mentioned previously, this corresponds to the advancing front of CO_2 through the column. Carbonate minerals have been previously identified as the main seal-forming phases at Raoul Island Christenson et al. (2007), contributing to gas over-pressuring and gas-driven, phreatic eruption activity in that system. This modelling shows that their formation is the natural consequence of acid gas injection into the more distal magmatic-hydrothermal environments, leading to the formation of highly reactive acidic fluids which interact with their enclosing rocks via hydrolysis reactions, thereby consuming hydrogen ions and leading to the downstream stabilisation and precipitation of permeability-reducing mineral phases, including carbonates.

4 Hazards Associated with Gases in Volcanic Lake Systems

4.1 Eruptions Induced by Selfsealing of Sublacustrine Gas Conduits

In volcanic lake systems fed by magmatic sources lying within hundreds of metres of the lake floor, the interaction between magmatic vapour,

ground water and rocks may lead to the formation of hydrothermal mineral seals which in themselves create significant hazards. In these cases, the very gases driving seal formation may also serve as pressure-transmitting media behind those blockages, and ultimately lead to their failure, (e.g., Phillips 1972), with consequent explosive phreatic and/or phreato-magmatic eruptions as recently observed on Raoul Island Christenson et al. (2007) and Ruapehu, Christenson et al. (2010).

Ruapehu Crater Lake, with a diameter of some 500 m and a volume of approximately 9 million m^3, sits atop the two active vents of this andesitic massif situated in Tongariro National Park. The volcano has maintained varying states of activity since Europeans first observed it the 1860s, including two lake-expelling eruptions in 1945 and 1995. A most interesting characteristic of the volcano, and one that is seemingly unaffected by large eruptive events, is its cyclic discharge of heat and volatiles through the vent-lake system (e.g., Werner et al. 2006; Christenson et al. 2010). Cycles vary between 3 and 9 months duration, with lake temperatures historically ranging between 10 and 60 °C. Phreatic eruption activity on Ruapehu most typically occurs when the lake is at or near the peak of its temperature cycles (i.e., during open vent conditions). However, three significant events have occurred in the last 25 years when the lake temperatures were at minimum values (9 °C, December, 1988; 15 °C, October, 2006, and 13 °C, September, 2007).

These eruptions occur with little or no precursory activity, and have so far proven difficult, if not impossible to forecast. The largest and most recent of these eruptions occurred in September of 2007 when some 160,000 m^3 of vent materials were ejected through the lake (Kilgour et al. 2010). The ejecta consisted of blocks comprising a variety of vent-fill lithologies (lavas, sediments and breccias), spanning a range of hydrothermal alteration intensities from fresh to intensely altered, and ranging up to 2 m diameter. Elemental sulphur was commonly observed having exuded from pore space in some of the ballistics, indicative of S having existed in a molten state (T > 119 °C) in a portion of the vent at the time of the eruption. Petrographic analysis of the intensely altered ejecta show dense, pore space accumulations of predominantly elemental S, with lesser amounts of alunite, pyrite, anhydrite and trace segregations of halite (Christenson et al. 2010), an assemblage noted previously in ejecta from earlier eruptions (Christenson and Wood 1993). This assemblage is nearly identical to that predicted from the aforementioned reactive transport modelling, and it appears to constitute an impermeable seal formed through repeated injection of magmatic volatiles through the vapour saturated conduit environment. Insights into the processes leading to these events are gained from monitoring gas emissions from the pre- and post-eruption systems.

Emissions of CO_2, SO_2 and H_2S from Ruapehu have been measured by airborne platform approximately monthly since 2003 (methodology discussed by Werner et al. 2006). Data for the period January 2006 to July 2012 are shown along with lake temperatures in Fig. 10, and this time span encompasses the two phreatic eruption events of October 2006 and September, 2007. There is a striking coherence between heat and volatile discharge in this system, indicating that gas-charged batches of magma periodically circulate into the conduit system, degas and thereby drive the thermal cycling in the lake. TOUGH2 modelling of the passage of heat and CO_2 through the vent system provides insights into the processes involved, showing early decoupling of gas from heat in the vent, with gas moving ahead of the thermal pulse, followed by a convective sweep of heat through the conduit (Christenson et al. 2010). A total of 8 heating cycles occurred between 1 January 2006 and 1 July 2012, and each has associated CO_2 maxima of varying magnitudes. C/[SO_2 + H_2S] mole ratios (hereafter C/ΣS) vary widely during this period, ranging from 3 to infinity, and are compared to the proposed so-called magmatic value of 5 for White Island (Giggenbach and Sheppard 1989). Ratios above this value may result to some extent from variability in the magmatic gas supply (i.e., varying depth of separation, as described earlier), but sulphur-budgeting arguments presented by Christenson (2000) point to

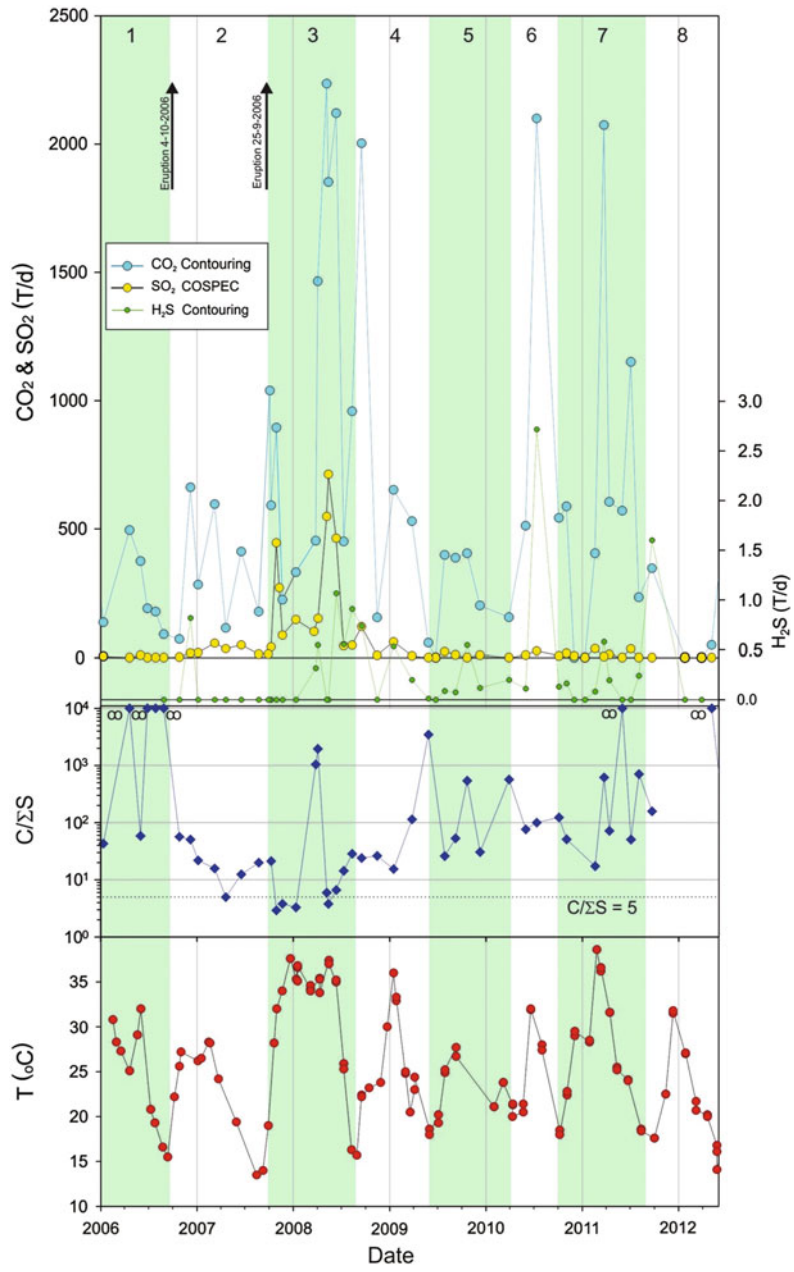

Fig. 10 Time series gas emissions data for Mt Ruapehu. Six heating cycles are portrayed (lake temperature in red), along with airborne platform data for CO_2, SO_2 and H_2S. Periods of elevated C/ΣS point to periods of S deposition (i.e., scrubbing) in the vent region. Adapted from Christenson et al. 2010

scrubbing of S in the hydrothermal system as the predominant process regulating S emission from this volcano. Hence, the period leading up to the October 2006 eruption where ratios ranged from 40 to infinity, also point to a period of extensive S scrubbing and seal formation beneath the lake.

Conditions in the vent plumbing apparently changed after the minor vent-clearing eruption in 2006, after which small but measurable levels of SO_2 were detected, suggesting that the gas stream entering the lake had equilibrated with elemental sulphur lying close to the lake floor in the hydrothermal system. CO_2 emissions throughout 2007 were erratic compared to those measured during 2006, a feature which we interpret to indicate growth and consolidation of

the seal beneath the lake floor, with consequent pressurisation of the sub-seal hydrothermal environment. CO_2 emission measured immediately after the 2007 eruption was the highest yet observed for this volcano (>1,000 T/d), and the C/ΣS ratio was ca. 20 at this time.

A conceptual model for the state of the system immediately prior to the 2007 eruption is shown in Fig. 11. The main feature here is the accumulation of a pressurised gas column behind a seal of elemental sulphur, alunite and anhydrite, infilling the interstitial pore space of what would otherwise be permeable vent breccia material. Gas emission through the northern vent of Ruapehu was very strong immediately after the eruption. This is consistent with the eruption

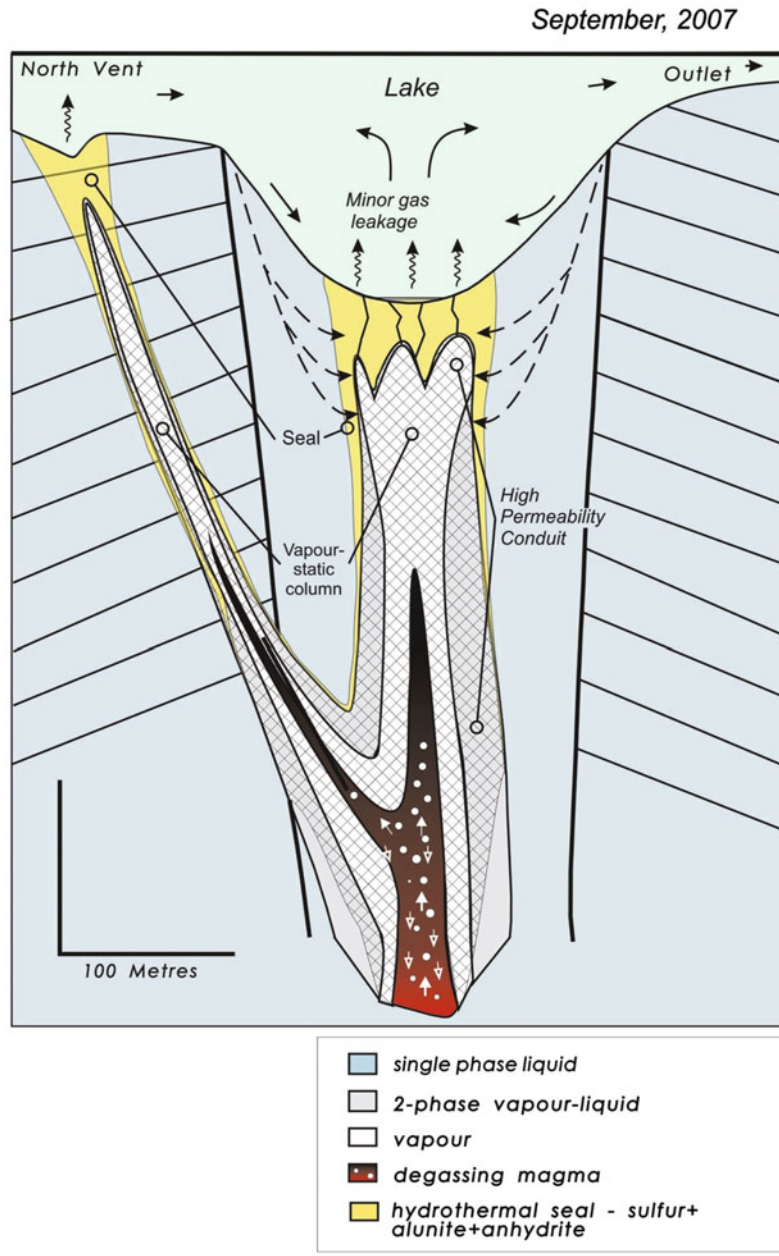

Fig. 11 Conceptual model for the sealed state of the Ruapehu vent system prior to the September 2007 eruption. Seal development reduced gas transfer through the vent, and led to increased pore pressures via formation of a compressible gas column beneath the seal. Printed with permission from Christenson et al. (2010)

having been a gas-driven event, but the strong post-eruptive degassing also points to the scale of the gas accumulation within the hydrothermal environment prior to the eruption. The elevated C/ΣS ratio immediately after the eruption is also consistent with storage of a magmatic gas in the hydrothermal environment for some time behind the seal, facilitating extensive scrubbing of H_2S and SO_2 via Eq. (6). SO_2 emission increased to ca. 500 T/d ca. one week later, and C/ΣS fell to <5, pointing to the degassing of a deeper and/or less evolved magmatic gas source through an open vent environment. A second, stronger pulse of degassing occurred in early 2008, again through the open vent, with C/ΣS ratios again close to ca. 5. Since then, C/ΣS ratios have progressively shifted upward, even during periods of unprecedented high CO_2 emission, suggesting that S scrubbing and seal formation is again occurring.

A possible mechanism by which accumulated gas pressure behind such a seal may lead to its failure is shown schematically in Fig. 12, adapted from Phillips (1972). Here the Mohr stress circles are plotted as functions of effective normal stress (typically measured in units of tensile rock strength), and are compared to a hypothetical shear failure envelope. With maximum principle stress being nearly vertical in the vicinity of the vent seal, failure of the seal will occur when the combination of effective normal stress and shear stress matches the shear strength of the of the rock, or in terms of the graph in Fig. 12, when the Mohr stress circle (denoting differential stress) intersects the shear failure envelope. This may occur through either increasing the differential stress (i.e., increasing the diameter of the stress circle), or by increasing the pore pressure within the seal which has the net effect of decreasing effective normal stress, thereby shifting the stress circle to the left towards the failure envelope. A state of critical stress is achieved when the stress circle intersects the failure envelope, and any minor perturbation of the system may trigger its failure.

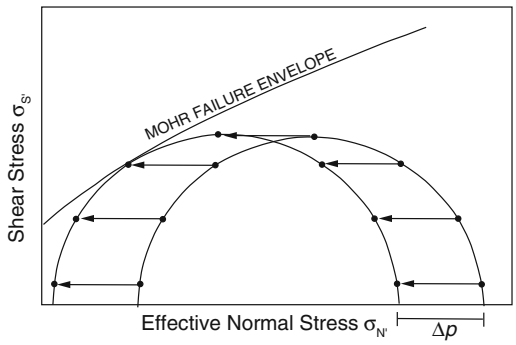

Fig. 12 Conceptual plot of effective normal stress versus shear stress. Increasing pore pressure (Δp) in the seal leads to displacement of the Mohr stress circle to the *left*, towards the failure envelope. The intersection of the stress circle and the failure envelope signifies a state of critical stress for the system. Adapted from Phillips (1972)

Christenson et al. (2010) referred to the 2007 eruption of Ruapehu as an "accidental" phreatomagmatic eruption, noting that only a very minor amount of juvenile material was present in the ejecta. Central to their model of events leading to the eruption was that a compressed gas cap had accumulated behind the seal, raising pressures in the vent to levels required for seal failure. Once decompression was initiated at the seal, a pressure transient migrated downward into the vent, eventually reaching the top of the magma conduit, thereby explaining the small amount of juvenile material observed in the ejecta.

4.2 Limnic Eruptions: Constraints from the Lake Nyos Experience

Lakes hosted in quiescent volcanic systems, i.e. those showing moderate degassing activity, are typically affected by significant inputs of salt- and CO_2-rich fluids which favour the development of vertically stratified water columns. Under these conditions, mass transfer is mostly controlled by slow diffusive mechanisms, leading to accumulation of dissolved gases at depth. As exhaustively described in other chapters of the present book, meromictic volcanic lakes having great depth and a large volume are able to store large amounts of dissolved gases, which represent a tremendous hazard in case of destabilization of water stratification, leading to a *limnic eruption* (Sabroux et al. 1987), i.e. a catastrophic release of those gases into neighbouring

environments, as occurred at Monoun and Lake Nyos in 1984 and 1986, respectively (e.g., Kling et al. 1987; Sigurdsson et al. 1987), resulting in thousands of deaths.

There is still debate on whether the initial destabilization of a stratified lake is related to external triggering, such as an earthquake, a landslide slumping into deep lake water or extreme weather conditions (Sigurdsson et al. 1987; Kling et al. 1987, 1989; Giggenbach 1990; Evans et al. 1994), or a lake rollover rather occurs "spontaneously" (Zhang 1996; Woods and Phillips 1999). Considering that the CO_2 concentration at 58 m depth in Lake Monoun in January 2003 was very close to saturation (Kusakabe et al. 2008), the second hypothesis seems plausible.

Independent of the mechanism for the origin of this natural phenomenon, the hazard for limnic eruptions in a Nyos-type lake can only be mitigated by artificial and controlled degassing of the bottom water layer. However, this solution may severely affect the shallow lacustrine environment, especially in lakes intensely populated by living organisms such as Lake Kivu (DCO). The CH_4 and CO_2-rich gas reservoir hosted in this lake Schoell et al. (1988), represent both a hazard for local population and a possible huge energy resource. According to the increase of gas accumulation rate observed over the past decades in this lake Pasche et al. (2010), artificial degassing has been considered necessary to prevent the progressive saturation of deep water layers (Hirslund 2012). Nevertheless, such an intervention may have dramatic consequences for the $\sim$2 million people living in the lake surroundings whose survival strongly depends on lake water for personal use and fishery (Pasche et al. 2009). This suggests that the hazard mitigation approaches at Lake Kivu should be carefully evaluated on the basis of further studies to evaluate different strategies aimed to mitigate the limnic eruption hazard in this area.

5 Summary and Conclusions

Clearly, volcanic lakes are dynamic environments which are highly responsive to the inputs of magmatic heat and/or volatiles. We have shown that the depth of magmatic degassing is a primary control on the compositional characteristics of the volatile stream entering the limnic environment, and this effectively controls the chemical nature of the associated lakes. Shallow magmatic degassing (with magma residing at 10s to 100s of m depth) in volcanically active systems releases heat, CO_2, SO_2, H_2S, HCl and HF gases into overlying groundwater and/or lake environments. This leads to development of a magmatic hydrothermal system which envelopes the magma conduits, and is characterised by highly acidic solutions in its core which drive hydrolysis reactions with their enclosing rocks. Lakes sitting atop such conduit systems are likewise acidic in nature, hot and they typically carry high total dissolved solids. Modelling results show that the precipitation of elemental sulphur occurs close to the conduit within the two phase liquid-vapour region, along with a suite of advanced argillic alteration minerals, which collectively fill pore space and reduce permeability. Modelling also shows that acid as fluids flow laterally away from the conduit, neutralisation (i.e., water-rock) reactions lead to the development of propyllitic mineral assemblages (including carbonates) in the presence of fluids with near-neutral pH.

Deep magmatic degassing (i.e., sourced at perhaps 10s of kms depth), on the other hand, releases primarily CO_2, N_2 and noble gases into conduits, with sulphur and halogen gases remaining largely or totally within the melt phase. With low emission rates and/or long transport pathways, such volatile streams typically decouple from their associated heat to reach the surface as cold gas emissions. CO_2 is the primary agent driving hydrolysis in these systems, and modelling shows that equilibrium is rapidly achieved with carbonate minerals, and in the presence of argillic to propylitic alteration mineral assemblages. Of course, these examples represent the extreme end members of a continuous spectrum of possible intermediate degassing depths, and potential intermediate crater lake characteristics.

Two principle hazards are associated with gases in volcanic lake environments. In the acidic systems, mineralogic seal formation resulting

from hot gas-water-rock interaction may lead to accumulation of gas behind the seal, and raise pore pressures to the point where the seal becomes critically stressed, leading to its failure and consequent phreatic eruptions. While seal formation and consequent phreatic eruptions cannot be precluded in crater lakes which receive only cold, deeply derived CO_2 discharge, an additional threat in these lakes is that the gases may become stratified in the otherwise stagnant water column. Once the water column is saturated, experience from Lake Nyos and Monoun show that even minor perturbance of the lake may lead to explosive exsolution and release of voluminous clouds of heavy, suffocating CO_2 into adjacent environs. Tropical regions, where seasonal limnic overturns typically do not occur are most at risk from these events, whereas lakes with significant heat inputs are generally safe from stratification owing to thermal instability, and consequent convection of their water columns.

References

Aeschbach-Hertig W, Hofer M, Kipfer R, Imboden DM, Wieler R (1999) Accumulation of mantle gases in a permanently stratified volcanic lake (Lac Pavin, France). Geochim Cosmochim Acta 63(19–20):3357–3372

Ahlgren I, Sorensson F, Waara T, Vrede K (1994) Nitrogen budgets in relation to microbial transformations in lakes. Ambio 23(6):367–377

Aiuppa A, Baker DR, Webster JD (2009) Halogens in volcanic systems. Chem Geol 263(1–4):1–18

Aiuppa A, Bertagnini A, Métrich N, Moretti R, Di Muro A, Liuzzo M, Tamburello G (2010) A model of degassing for Stromboli volcano. Earth Planet Sci Lett 295(1–2):195–204

Aiuppa A, Moretti R, Federico C, Giudice G, Gurrieri S, Liuzzo M, Papale P, Shinohara H, Valenza M (2007) Forecasting Etna eruptions by real-time observation of volcanic gas composition. Geology 35(12):1115–1118

Allard P (1997) Endogenous magma degassing and storage at Mount Etna. Geophys Res Lett 24(17):2219–2222

Allard P (2010) A CO_2-rich gas trigger of explosive paroxysms at Stromboli basaltic volcano. Italy J Volcanol Geotherm Res 189(3–4):363–374

Anderson AT (1975) Some baslatic and andesitic gases. Rev Geophys Space Phys 37:37–55

Arnórsson S (1985) Gas pressures in geothermal systems. Chem Geol 49(1–3):319–328

Arnórsson S, Gunnlaugsson E (1985) New gas geothermometers for geothermal exploration-calibration and application. Geochim Cosmochim Acta 49(6): 1307–1325

Asada Y, Kawamura S (1986) Aerobic hydrogen accumulation by a nitrogen-fixing cyanobacterium. Anabaena sp Appl Environ Microbiol 51(5):1063–1066

Asada Y, Miyake J (1999) Photobiological hydrogen production. J Biosci Bioeng 88(1):1–6

Bani P, Oppenheimer C, Tsanev VI, Carn SA, Cronin SJ, Crimp R, Calkins JA, Charley D, Lardy M, Roberts TR (2009) Surge in sulphur and halogen degassing from Ambrym volcano. Vanuatu Bull Volcanol 71 (10):1159–1168

Bergman B, Gallon JR, Rai AN, Stal LJ (1997) N2 fixation by non-heterocystous cyanobacteria. FEMS Microbiol Rev 19(3):139–185

Bethke CM (1996) Geochemical reaction modelling. Oxford University Press, New York, Oxford, p 397

Burton M, Allard P, Mure F, Oppenheimer C (2003) FTIR remote sensing of fractional magma degassin at Mount Etna, Sicily. In: Oppenheimer C, Pyle DM, Barclay J (eds) Volcanic degassing. Geological Society London, pp 281–293

Carmichael ISE, Ghiorso MS (1986) Oxidation-reduction relations in basic magma. Earth Planet Sci Lett 78:200–210

Carrigan CR (1983) A heat pipe model for vertical, magma-filled conduits. J Volcanol Geotherm Res 16 (3–4):279–298

Carrol MR, Webster JD (1994) Solubilities of sulfur, noble gases, nitrogen, chlorine and fluorine in magmas. In: Carrol MR, Holloway JR (eds) Volatiles in magmas. Mineralogical Society of America, pp 231–279

Cartigny P, Ader M (2003) A comment on "The nitrogen record of crust-mantle interaction and mantle convection from archean to present" by B. Marty and N. Dauphas [Earth Planet Sci Lett 206 (2003) 397–419]—discussion. Earth Planet Sci Lett 216:425–432

Chiodini G (2009) CO_2/CH_4 ratio in fumaroles a powerful tool to detect magma degassing episodes at quiescent volcanoes. Geophys Res Lett 36(2)

Chiodini G, Caliro S, Aiuppa A, Avino R, Granieri D, Moretti R, Parello F (2011) First $^{13}C/^{12}C$ isotopic characterisation of volcanic plume CO_2. Bull Volcanol 73(5):531–542

Chiodini G, Cioni R (1989) Gas geobarometry for hydrothermal systems and its application to some Italian geothermal areas. Appl Geochem 4(5):465–472

Chiodini G, Cioni R, Marini L (1993) Reactions governing the chemistry of crater fumaroles from Vulcano Island, Italy, and implications for volcanic surveillance. Appl Geochem 8(4):357–371

Chiodini G, Marini L, Russo M (2001) Geochemical evidence for the existence of high-temperature hydrothermal brines at Vesuvio volcano. Italy Geochim Cosmochim Acta 65(13):2129–2148

Chiodini G, Todesco M, Caliro S, Del Gaudio C, Macedonio G, Russo M (2003) Magma degassing as

a trigger of bradyseismic events: the case of Phlegrean Fields (Italy). Geophys Res Lett 30(8):11–17

Christenson BW (1994) Convection and stratification in Ruapehu Crater lake, New Zealand: implications for lake Nyos-type gas release eruptions. Geochem J 28:185–198

Christenson BW (2000) Geochemistry of fluids associated with the 1995–1996 eruption of Mt. Ruapehu, New Zealand: signatures and processes in the magmatic-hydrothermal system. J Volcanol Geotherm Res 97 (1–4):1–30

Christenson BW, Mroczek EK, Kennedy BM, van Soest MC, Stewart MK, Lyon G (2002) Ohaaki reservoir chemistry: characteristics of an arc-type hydrothermal system in the Taupo volcanic zone. N Z J Volcanol Geotherm Res 115(1–2):53–82

Christenson BW, Werner CA, Reyes AG, Sherburn S, Scott BJ, Miller C, Rosenberg MJ, Hurst AW, Britten K (2007) Hazards from hydrothermally sealed volcanic conduits. EOS 88(5):53–55

Christenson BW, Reyes AG, Young R, Moebis A, Sherburn S, Cole-Baker J, Britten K (2010) Cyclic processes and factors leading to phreatic eruption events: insights from the 25 September 2007 eruption through Ruapehu Crater lake. N Z J Volcanol Geotherm Res 191(1–2):15–32

Christenson BW, Wood CP (1993) Evolution of a vent-hosted hydrothermal system beneath Ruapehu Crater lake, New Zealand. Bull Volcanol 55:547–565

Christenson BW, Young RM (2010) Integrated finite difference modelling of volcanic-hydrothermal systems: the crater lake-vent system of Ruapehu, New Zealand. In: Bean CJ, Braiden AK, Lokmer I, Martini F, O'Brien GS (eds) The volume project. Volcanoes: understanding subsurface mass movement. University College Dublin, Dublin, pp 290–297

Coveney MF, Wetzel RG (1995) Biomass, production, and specific growth rate of bacterioplankton and coupling to phytoplankton in an oligotrophic lake. Limnol Oceanogr 40(7):1187–1200

Delgado-Granados H, Cárdenas González L, Piedad Sánchez N (2001) Sulfur dioxide emissions from Popocatépetl volcano (Mexico): case study of a high-emission rate, passively degassing erupting volcano. J Volcanol Geotherm Res 108(1–4):107–120

Delmelle P, Bernard A, Kusakabe M, Fischer TP, Takano B (2000) Geochemistry of the magmatic-hydrothermal system of Kawah Ijen volcano, East Java. Indonesia J Volcanol Geotherm Res 97(1–4):31–53

Evans WC, White LD, Tuttle ML, Kling GW, Tanyileke G, Michel RL (1994) Six years of change in lake Nyos, Cameroon, yield clues to the past and cautions for the future. Geochem J 28(3):139–162

Fernandez-Prini R, Alvarez JL, Harvey AH (2003) Henry's constants and vapor-liquid distribution constants for gaseous solutes in H_2O and D_2O at high temperatures. J Phys Chem Ref Data 32:903–916

Fine G, Stolper E (1986) Dissolved carbon dioxide in basaltic glasses: concentrations and speciation. Earth Planet Sci Lett 76(3–4):263–278

Fischer TP (2008) Fluxes of volatiles (H2O, CO2, N2, Cl, F) from arc volcanoes. Geochem J 42(1):21–38

Fischer TP, Hitton DR, Zimmer MM, Shaw AM, Sharp ZD, Walker JA (2002) Subduction and recycling of nitrogen along the Central American margin. Science 297(5584):1154–1157

Fischer TP, Takahata N, Sano Y, Sumino H, Hilton DR (2005) Nitrogen isotopes of the mantle: insights from mineral separates. Geophys Res Lett 32(11):1–5

Fournier RO (1999) Hydrothermal processes related to movement of fluid from plastic into brittle rock in the magmatic-epithermal environment. Econ Geol 94 (8):1193–1211

Friedman I, O'Neil JR (1977) Compilation of stable isotope fractionation factors of geochemical interest. In: Fleischer M (ed) Data of geochemistry, 6th edn. US Geol Survey, Washington D.C., p 127

Gerlach TM, McGee KA, Elias T, Sutton AJ, Doukas MP (2002) Carbon dioxide emission rate of Kīlauea volcano: implications for primary magma and the summit reservoir. J Geophys Res B: Solid Earth 107(9):1–3

Giggenbach W (1996) Chemical composition of volcanic gases. In: Scarpa R, Tilling RI (eds) Monitoring and mitigation of volcano hazards. Springer, Berlin, pp 221–256

Giggenbach W, Sheppard DS (1989) Variations in the temperature and chemistry of White Island fumarole dischargess 1972–85. In: Houghton BF, Nairn IA (ed) The 1976–82 eruption sequence at White Island volcano (Whakaari), Bay of Plenty, New Zealand. New Zealand Geological Survey, Lower Hutt, pp 119–126

Giggenbach WF (1980) Geothermal gas equilibria. Geochim Cosmochim Acta 44(12):2021–2032

Giggenbach WF (1981) Geothermal mineral equilibria. Geochim Cosmochim Acta 45(3):393–410

Giggenbach WF (1987) Redox processes governing the chemistry of fumarolic gas discharges from White Island. N Z Appl Geochem 2(2):143–161

Giggenbach WF (1990) Water and gas chemistry of lake Nyos and its bearing on the eruptive process. J Volcanol Geotherm Res 42(4):337–362

Giggenbach WF (1992) Isotopic shifts in waters from geothermal and volcanic systems along convergent plate boundaries and their origin. Earth Planet Sci Lett 113(4):495–510

Giggenbach WF, Glover RB (1975) The use of chemical indicators in the surveillance of volcanic activity affecting the crater lake on Mt. Ruapehu. N Z Bull Volcanol 39:70–81

Hanson RS, Hanson TE (1996) Methanotrophic bacteria. Microbiol Rev 60(2):439–471

Hilton DR, Fischer TP, Marry B (2002) Noble gases and volatile recycling at subduction zones. Reviews in mineralogy and geochemistry 47

Hilton DR, Porcelli D (2013) Noble gases as tracers of mantle processes. 327–353

Hirslund F (2012) An additional challenge of Lake Kivu in Central Africa-upward movement of the chemoclines. J Limnology 71(1):45–60

Hurst AW, Bibby HM, Scott BJ, McGuinness MJ (1991) The heat source of Ruapehu Crater lake; deductions from the energy and mass balances. J Volcanol Geotherm Res 46(1–2):1–20

Hysenstrand P, Blomqvist P, Pettersson A (1988) Factors determining cyanobacterial success in aquatic systems—a literature review. Arch Hydrobiol Spec Issues Adv Limnol 51:41–62

Jaupart C, Vergniolle S (1988) The generation and collapse of a foam layer at the roof of a basaltic magma chamber. J Fluid Mech 203:347–380

Jetten MSM, Strous M, Van De Pas-Schoonen KT, Schalk J, Van Dongen UGJM, Van De Graaf AA, Logemann S, Muyzer G, Van Loosdrecht MCM, Kuenen JG (1998) The anaerobic oxidation of ammonium. FEMS Microbiol Rev 22(5):421–437

Jones JG (1978) The distribution of some freshwater planktonic bacteria in two stratified eutrophic lakes. Freshw Biol 8:127–135

Kato K, Sakamoto M (1981) Vertical distribution of free-living and attached heterotrophic bacteria in lake Kizaki. Jpn J Limnol 42:154–159

Kazahaya K, Shinohara H, Saito G (1994) Excessive degassing of Izu-Oshima volcano: magma convection in a conduit. Bull Volcanol 56(3):207–216

Kilgour G, Manville V, Pasqua FD, Graettinger A, Hodgson KA, Jolly GE (2010) The 25 September 2007 eruption of Mount Ruapehu, New Zealand: directed ballistics, surtseyan jets, and ice-slurry lahars. J Volcanol Geotherm Res 191(1–2):1–14

Kilinc IA, Burnham CW (1972) Partitioning of chloride between a silicate melt and coexisting aqueous phase from 2 to 8 kilobars. Econ Geol 67(2):231–235

Kling GW, Clark MA, Compton HR (1987) The 1986 lake Nyos gas disaster in Cameroon. West Afr Sci 236 (4798):169–175

Kling GW, Tuttle ML, Evans WC (1989) The evolution of thermal structure and water chemistry in lake Nyos. J Volcanol Geotherm Res 39(2–3):151–165

Kusakabe M, Komoda Y, Takano B, Abiko T (2000) Sulfur isotopic effects in the disproportionation reaction of sulfur dioxide in hydrothermal fluids: Implications for the δ34S variations of dissolved bisulfate and elemental sulfur from active crater lakes. J Volcanol Geotherm Res 97(1–4):287–307

Kusakabe M, Ohba T, Yoshida Y, Satake H, Ohizumi T, Evans WC, Tanyileke G, Kling GW (2008) Evolution of CO_2 in lakes Monoun and Nyos, Cameroon, before and during controlled degassing. Geochem J 42 (1):93–118

Laane RWPM, Gieskes WWC, Kraay GW, Eversdijk A (1985) Oxygen consumption from natural waters by photo-oxidizing processes. Neth J Sea Res 19(2):125–128

Loeb SL, Reuter JE (1981) The epilithic periphyton community: a five-lake comparative study of community productivity, nitrogen metabolism and depth-distribution of standing crop. Verh Internat Verein Limnol 21:346–352

Lopes F, Viollier E, Thiam A, Michard G, Abril G, Groleau A, Prévot F, Carrias JF, Albéric P, Jézéquel D (2011) Biogeochemical modelling of anaerobic vs. aerobic methane oxidation in a Meromictic Crater lake (Lake Pavin, France). Appl Geochem 26(12):1919–1932

Marini L, Moretti R, Accornero M (2011) Sulfur isotopes in magmatic-hydrothermal systems, melts, and magmas. Rev Min Geochem 73:423–492

Marty B, Dauphas N (2003) The nitrogen record for crust-mantle interaction and mantle convection from Archean to Present. Earth Planet Sci Lett 206(3–4):397–410

Marty B, Humbert F (1997) Nitrogen and argon isotopes in oceanic basalts. Earth Planet Sci Lett 152:101–112

Mattey D (1991) Carbon dioxide solubility and carbon isotope fractionation in basaltic melt. Geochim Cosmochim Acta 55:3467–3473

Métrich N, Wallace PJ (2008) Volatile abundances in basaltic magmas and their degassing paths tracked by melt inclusions. In: Putirka KD, Tepley IFJ (eds) Reviews in mineralogy and geochemistry, vol 69. Mineralogical Society of America, Chantilly, pp 363–402

Naumov GB, Ryzhenko BN, Khodakovsky IL (1974) Handbook of thermodynamic data. U.S Department of Commerce, NTIS, p 328

Nelson N, Ben-Shem A (2004) The complex architecture of oxygenic photosynthesis. Nat Rev Mol Cell Biol 5 (12):971–982

Niewolak S (1974) Distribution of microorganisms in the water of Kortowskie lake. Pol Arch Hydrobiol 21:315–333

Oppenheimer C (1992) Sulphur eruptions at Volcán Poás. Costa Rica J Volcanol Geotherm Res 49(1–2):1–21

Oppenheimer C, McGonigle AJS, Allard P, Wooster MJ, Tsanev V (2004) Sulfur, heat, and magma budget of Erta 'Ale lava lake. Ethiop Geol 32(6):509–512

Oppenheimer C, Scaillet B, Martin RS (2011) Sulfur degassing from volcanoes: source conditions, surveillance, plume chemistry and earth system impacts. Rev Min Geochem 73(1):363–421

Pasche N, Alunga G, Mills K, Muvundja F, Ryves DB, Schurter M, Wehrli B, Schmid M (2010) Abrupt onset of carbonate deposition in lake Kivu during the 1960s: response to recent environmental changes. J Paleolimnol 44(4):931–946

Pasche N, Dinkel C, Müller B, Schmid M, Wuëst A, Wehrli B (2009) Physical and biogeochemical limits to internal nutrient loading of meromictic lake Kivu. Limnol Oceanogr 54(6):1863–1873

Phillips JC (1972) Hydraulic fracturing and mineralisation. J Geol Soc London 128:337–359

Pyle DM, Mather TA (2009) Halogens in igneous processes and their fluxes to the atmosphere and oceans from volcanic activity: a review. Chem Geol 263(1–4):110–121

Raghoebarsing AA, Pol A, Van De Pas-Schoonen KT, Smolders AJP, Ettwig KF, Rijpstra WIC, Schouten S, Sinninghe Damsté JS, Op Den Camp HJM, Jetten MSM, Strous M (2006) A microbial consortium couples anaerobic methane oxidation to denitrification. Nature 440(7086):918–921

Rich PH (1975) Benthic metabolism of a soft-water lake. Verh Internat Verein Limnol 19:1023–1028

Rich PH (1980) Hipolimnetic metabolism in three cape cod lakes. Am Midland Nat 104:102–109
Rowe GL, Brantley SL, Fernandez M, Fernandez JF, Borgia A, Barquero J (1992) Fluid-volcano interaction in an active stratovolcano: the crater lake system of Poás volcano. Costa Rica J Volcanol Geotherm Res 49 (1–2):23–51
Ruaya JR, Seward TM (1987) The ion-pair constant and other thermodynamic properties of HCl up to 350 °C. Geochim Cosmochim Acta 51(1):121–130
Rudd JWM, Hamilton RD, Campbell NER (1974) Measurement of microbial oxidation of methane in lake water. Limnol Oceanogr 19:519–524
Rudd JWM, Taylor CD (1980) Methane cycling in aquatic environments. Adv Aquat Microbiol 2:77–150
Saal AE, Hauri EH, Langmuir CH, Perfit MR (2002) Vapour undersaturation in primitive mid-ocean-ridge basalt and the volatile content of Earth's upper mantle. Nature 419(6906):451–455
Sabroux JC, Dubois E, Doyotte C (1987) The limnic eruption: a new geological hazard? In: Int. Scientific Congr. on Lake Nyos Disaster, Yaounde, Cameroon
Sano Y, Marty B (1995) Origin of carbon in fumarolic gas from island arcs. Chem Geol 119(1–4):265–274
Scaillet B, Pichavant M (2003) Experimental constraints on volatile abundances in arc magmas and their implications for degassing processes. Geol Soc, London, Spec Publ 213(1):23–52
Schoell M (1988) Multiple origins of methane in the earth. Chem Geol 71(1–3):1–10
Schoell M, Tietze K, Schoberth SM (1988) Origin of methane in lake Kivu (East-Central Africa). Chem Geol 71(1–3):257–265
Shinohara H, Fujimoto K (1994) Experimental study in the system albite-andalusite-quartz-NaCl–HCl–H_2O at 600 °C and 400 to 2000 bars. Geochim Cosmochim Acta 58(22):4857–4866
Shinohara H, Fukui K, Kazahaya K, Saito G (2003) Degassing process of Miyakejima volcano: implications of gas emission rate and melt inclusion data. In: De Vivo B, Bodnar B (eds) Advances in volcanology. Elsevier, Amsterdam, pp 147–161
Shinohara H, Iiyama JT, Matsuo S (1989) Partition of chlorine compounds between silicate melt and hydrothermal solutions: I. Partition of NaCl-KCl Geochim Cosmochim Acta 53(10):2617–2630
Sigurdsson H, Devine JD, Tchua FM, Presser FM, Pringle MKW, Evans WC (1987) Origin of the lethal gas burst from lake Monoun. Cameroun J Volcanol Geotherm Res 31(1–2):1–16
Silver LA, Ihinger PD, Stolper E (1990) The influence of bulk composition on the speciation of water in silicate glasses. Contrib Min Petrolo 104:142–162
Simon M (1998) Bacterioplankton dynamics in a large mesotrophic lake: II. Concentrations and turnover of dissolved amino acids. Arch Hydrobiol 144(1):1–23
Sobolev AV, Chaussidon M (1996) H_2O concentrations in primary melts from supra-subduction zones and mid-ocean ridges: implications for H_2O storage and recycling in the mantle. Earth Planet Sci Lett 137(1–4):45–55
Sparks RSJ (1978) The dynamics of bubble formation and growth in magmas: a review and analysis. J Volcanol Geotherm Res 3(1–2):1–37
Sparks RSJ (2003) Dynamics of magma degassing. Geol Soc, London, Spec Publ 213(1):5–22
Stevenson DS, Blake S (1998) Modelling the dynamics and thermodynamics of volcanic degassing. Bull Volcanol 60(4):307–317
Stumm W, Morgan JJ (1981) Aquatic chemistry. Wiley, New York
Suh CE, Sparks RSJ, Fitton JG, Ayonghe SN, Annen C, Nana R, Luckman A (2003) The 1999 and 2000 eruptions of Mount Cameroon: eruption behaviour and petrochemistry of lava. Bull Volcanol 65(4):267–281
Symonds RB, Reed MH (1993) Calculation of multicomponent chemical equilibria in gas-solid-liquid systems: calculation methods, thermochemical data, and applications to studies of high-temperature volcanic gases with examples from Mount St. Helens Am J Sci 293 (8):758–864
Symonds RB, Reed MH, Rose WI (1992) Origin, speciation, and fluxes of trace-element gases at Augustine volcano, Alaska: insights into magma degassing and fumarolic processes. Geochim Cosmochim Acta 56(2):633–657
Symonds RB, Rose WI, Reed MH (1988) Contribution of Cl- and F-bearing gases to the atmosphere by volcanoes. Nature 334(6181):415–418
Symonds RB, Rose WI, Reed MH, Lichte FE, Finnegan DL (1987) Volatilization, transport and sublimation of metallic and non-metallic elements in high temperature gases at Merapi Volcano. Indonesia. Geochim Cosmochim Acta 51(8):2083–2101
Takai Y (1970) The mechanism of methane fermentation in flooded paddy soil. Soil Sci Plant Nutr 16:238–244
Tamagnini P, Axelsson R, Lindberg P, Oxelfelt F, Wünschiers R, Lindblad P (2002) Hydrogenases and hydrogen metabolism of cyanobacteria. Microbiol Mol Biol Rev 66(1):1–20
Taran Y, Giggenbach WF (2003) Geochemistry of light hydrocarbons in subduction-related volcanic and hydrothermal fluids. In: Simmons SF, Graham I (eds) Volcanic, geothermal and ore-forming fluids: rulers and witnesses of processes with the earth. Society of Economic Geologists, Inc, Boulder, Colorado, p 343
Taran YA (1986) Gas geothermometers for hydrothermal systems. Geochem Int 23(7):111–126
Taran YA, Pokrovsky BG, Dubik YM (1989) Isotopic composition and origin of water from andesitic magmas. Dokl (Trans) Acad Sci USSR 304:440–443
Tassi F, Capecchiacci F, Cabassi J, Calabrese S, Vaselli O, Rouwet D, Pecoraino G, Chiodini G (2012) Geogenic and atmospheric sources for volatile organic compounds in fumarolic emissions from Mt. Etna and Vulcano Island (Sicily, Italy). J Geophys Res D: Atmos 117(17)
Tassi F, Vaselli O, Tedesco D, Montegrossi G, Darrah T, Cuoco E, Mapendano MY, Poreda R, Huertas AD (2009) Water and gas chemistry at Lake Kivu (DRC): geochemical evidence of vertical and horizontal

heterogeneities in a multibasin structure. Geochem, Geophy, Geosyst 10(2)
Taylor HP Jr, Sheppard SMF (1986) Isotopic fractionation and isotope systematics. Rev Min 16:227–271
Tazieff H (1989) Mechanisms of the Nyos carbon dioxide disaster and of so-called phreatic steam eruptions. J Volcanol Geotherm Res 39(2–3):109–116
Thaurer RK, Badziong W (1980) Respiration with sulfate as electron acceptor. Diversity of vacterial respiratory systems. CRC Press, Boca Raton, Fla, pp 65–85
Tison DL, Palmer FE, Staley JT (1977) Nitrogen fixation in lakes of the Lake Washington drainage basin. Water Res 11(9):843–847
Todesco M, Chiodini G, Macedonio G (2003) Monitoring and modelling hydrothermal fluid emission at La Solfatara (Phlegrean Fields, Italy). An interdisciplinary approach to the study of diffuse degassing. J Volcanol Geotherm Res 125(1–2):57–79
Todesco M, Rutqvist J, Chiodini G, Pruess K, Oldenburg CM (2004) Modeling of recent volcanic episodes at Phlegrean Fields (Italy): geochemical variations and ground deformation. Geothermics 33(4):531–547
Truesdell AH, Haizlip JR, Armannsson H, D'Amore F (1989) Origin and transport of chloride in superheated geothermal steam. Geothermics 18(1–2):295–304
Uematsu M, Franck EU (1980) Static dielectric constant of water and steam. J Phys Chem Ref Data 9:1291–1306
Valelia I (1991) Ecology of coastal ecosystems. In: Mann KH (ed) Barnes RSK. Fundamentals ofaquatic ecology Blackwell Science, Oxford, pp 57–76
Valentine DL (2002) Biogeochemistry and microbial ecology of methane oxidation in anoxic environments: a review. Antonie van Leeuwenhoek, Int J Gen Mol Microbiol 81(1–4):271–282
Varekamp JC, Ouimette AP, Herman SW, Flynn KS, Bermudez A, Delpino D (2009) Naturally acid waters from Copahue volcano. Argent Appl Geochem 24 (2):208–220
Vergniolle S, Jaupart C (1990) Dunamics of degassing at Kilauea volcano. Hawaii J Geophys Res 95 (B3):2793–2809
Wallace PJ (2005) Volatiles in subduction zone magmas: concentrations and fluxes based on melt inclusion and volcanic gas data. J Volcanol Geotherm Res 140(1–3): 217–240
Wallace PJ, Carmichael ISE (1992) Sulfur in basaltic magmas. Geochim Cosmochim Acta 56:1863–1874
Wallace PJ, Edmonds M (2011) The sulfur budget in magmas: evidence from melt inclusions, submarine glasses, and volcanic gas emissions. Rev Min Geochem 73(1):215–246
Webster JD, Mandeville CW (2007) Fluid Immiscibility in Volcanic Environments. Rev Min Geochem 65:313–362
Weissberg BG, Sarbutt J (1966) Chemistry of the hydrothermal waters of the volcanic eruption Raoul Island, November 1964. N Z J Sci 9:426–432
Werner C, Christenson BW, Hagerty M, Britten K (2006) Variability of volcanic gas emissions during a crater lake heating cycle at Ruapehu volcano. N Z J Volcanol Geotherm Res 154(3–4):291–302
Werner C, Hurst T, Scott B, Sherburn S, Christenson BW, Britten K, Cole-Baker J, Mullan B (2008) Variability of passive gas emissions, seismicity, and deformation during crater lake growth at White Island Volcano, New Zealand, 2002–2006. J Geophys Res B: Solid Earth 113(1)
Wetzel RG, Hatcher PG, Bianchi TS (1995) Natural photolysis by ultraviolet irradiance of recalcitrant dissolved organic matter to simple substrates for rapid bacterial metabolism. Limnol Oceanogr 40 (8):1369–1380
Whiticar MJ (1999) Carbon and hydrogen isotope systematics of bacterial formation and oxidation of methane. Chem Geol 161(1):291–314
Whiticar MJ, Faber E, Schoell M (1986) Biogenic methane formation in marine and freshwater environments: CO_2 reduction vs acetate fermentation–isotope evidence. Geochim Cosmochim Acta 50:693–709
Winfrey MR, Nelson DR, Klevickis SC, Zeikus JG (1977) Association of hydrogen metabolism with methanogenesis in Lake Mendota sediments. Appl Environm Microbiol 33(2):312–318
Woese CR, Kandler O, Wheelis ML (1990) Towards a natural system of organisms. Proposal for the domains archaea, bacteria and eucaria. Proc Natl Acad Sci USA 87:44576–44579
Woods AW, Phillips JC (1999) Turbulent bubble plumes and CO2-driven lake eruptions. J Volcanol Geotherm Res 92(3–4):259–270
Zehnder AJB (1978) Ecology of methane formation. In: Michel RL (ed) Water pollution microbiology. Wiley, New York
Zhang Y (1996) Dynamics of CO_2-driven lake eruptions. Nature 379(6560):57–59
Zhang Y, Zindler A (1989) Noble gas constraints on the evolution of the earth's atmosphere. J Geophys Res 94 (B10) 13(719–713):737

Hyperacidic Volcanic Lakes, Metal Sinks and Magmatic Gas Expansion in Arc Volcanoes

R.W. Henley

Abstract

Hyperacidic volcanic lakes are expressions of much larger scale magmatic gas expansion inside volcanoes from source to surface. Their temperature and acidity are sustained by the capture of heat and SO_2 (and HCl) and a suite of metals and metalloids, including Cu, Fe, As, Au, Bi, Se, Te, and Sb, from the magmatic gas. These lakes, together with high temperature fumaroles, therefore provide clues about the physics and chemistry of high temperature gas flow at the volcano scale that otherwise are inaccessible to direct observation. Understanding of the relationship between acidic volcanic lakes and these larger scale processes also has implications for modeling the flank stability of active volcanoes and how economically-valuable copper and gold deposits formed in ancient volcanoes. Such understanding may also translate to considerations of sulfur-rich environments on other planets as well as to the origin of life on earth.

Keywords

Hyperacidic crater lake · Volcanic gas · Magmatic vapor plume · Porphyry Copper · Gold

1 Introduction

Hyperacidic volcanic lakes are some of the most extreme geochemical environments in the present day earth's crust. They provide a tantalizing glimpse of the true scale of heat and mass transfer in active volcanoes and are implicated in their collapse and eruption histories, but what exactly makes them tick? What is their relationship to other volcanic phenomena, past and present, including the transport of gold, copper and other metals from intrusive suites beneath active volcanoes through to their dispersion around volcanoes via extensive geothermal systems as well as into the atmosphere via fumaroles and ash plumes?

While the dynamics and chemistry of hyperacidic lakes themselves have been detailed at lake scale in a number of major studies, these broader questions need to be addressed in the

R.W. Henley (✉)
Research School of Earth Sciences, Australian National University, Canberra, Australia
e-mail: r.143.henley@gmail.com

D. Rouwet et al. (eds.), *Volcanic Lakes*, Advances in Volcanology,
DOI 10.1007/978-3-642-36833-2_6,
© Springer-Verlag Berlin Heidelberg 2015

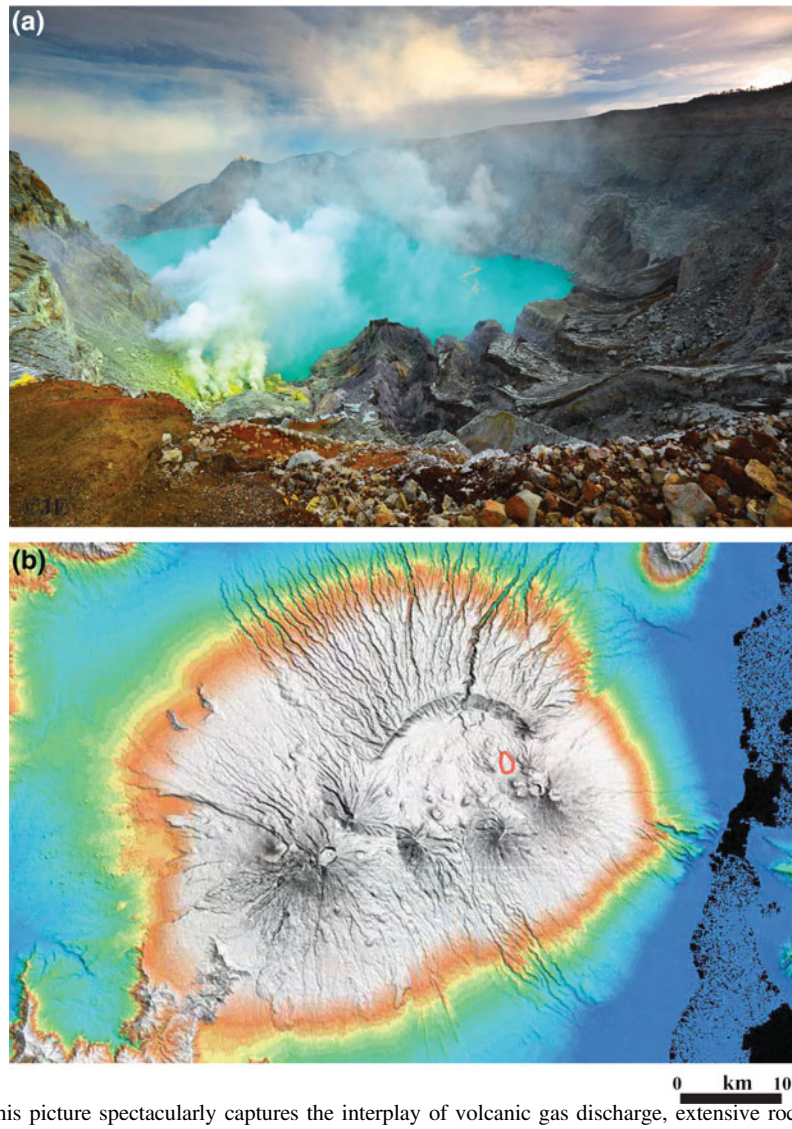

Fig. 1 *Top* This picture spectacularly captures the interplay of volcanic gas discharge, extensive rock alteration and solfatara and elemental sulfur and the scale of the hyperacidic crater lake at Kawah Ijen, Java, Indonesia. *Note* on the *left* the blue haze due to SO_2 and aerosols in the vapor plume, and the yellow–green color of the lake due to suspended silica and other particles. Copyright© Jessy Eykendorp. *Bottom* SRTM3 image of the andesitic Kawak Ijen volcanic complex showing the approximate location of the hyperacidic volcanic lake (*red outline*) in relation to the Ijen caldera and tephra cones on the rim and flank of the caldera (Image enhancement by DM Henley)

context, and at the scale, of volcanic systems. Figure 1 provides an example, for the hyperacidic Kawah Ijen crater lake in Java, Indonesia. This lake occupies one of a number of much smaller volcanoes that developed after the caldera-collapse of the original Ijen stratovolcano about 50,000 years ago (van Hinsberg et al. 2010). The surface area of the lake varies around $\sim$2 km^2, and is tiny in relation to the $\sim$700 km^2 footprint present-day Ijen volcanic system in which it is hosted.

Volcanic systems such as the suite of active vents in the Ijen volcano (Fig. 1) are characterized by the sustained discharge of major quantities of sulfur. SO_2-specific COSPEC and other remote sensing data (Williams-Jones et al. 2008) for gas and ash plumes suggest that the mass flux of sulfur from many volcanoes greatly exceeds

the mass available from simple shallow intrusive bodies (Shinohara 2008; Bani et al. 2012) suggesting that volcanic systems are open to fluxes of sulfur, water, CO_2 and other components released by sub-volcanic mantle wedge and slab dehydration processes (Stern et al. 2006; Oppenheimer et al. 2011) including via deep intrusion complexes. Kawah Ijen (Takano et al. 2004) epitomizes such sustained sulfur discharge with its sulfur-encrusted fumaroles and the lake itself, a 180 m deep, 30 million cubic meter body of hot, extremely toxic, sulfuric acid! Mineral deposits that are now exposed within now-dissected ancient volcanoes, reveal a similar picture of continuous magmatic gas streaming through volcanic systems interspersed by episodic intrusion and eruption (Henley and Berger 2013). Hunt (1977) noted that 'porphyry' copper deposits—one of the world's primary source of industrial metals—are primarily large crustal sulfur anomalies formed at a few kilometers depth beneath ancient volcanoes. They are characterized by kilometer-scale, highly fractured cylindrical regimes enriched in copper, molybdenum, gold and other metals, within an extensive volcano-scale annulus of disseminated pyrite (FeS_2). In some of them, Cu–Pb–Zn–Au–Ag skarn deposits occur as a result of aggressive replacement of carbonate rocks. These, and nearer surface sulfosalt deposits that are rich in copper and arsenic, are *sinks* of metals that progressively accumulated during the sustained streaming of magmatic gas from source to surface. As well as their economic significance, they potentially tell us a great deal about geochemical processes inside volcano-hosted hydrothermal[1] systems that otherwise remain hidden and yet may fundamentally control the history of volcanoes and the risks they represent to modern civilization.

Hyperacidic volcanic lakes, along with fumaroles high on volcanoes, are one of the surface manifestations of deeper-seated processes. The common features of these lakes are their association with solfatara,[2] their very low pH, high concentrations of oxidized and elemental sulfur, in some cases as subaqueous pools of molten sulfur. They are also enriched in a range of otherwise rare metals but, as discussed in this paper, they represent only a small component of the much larger scale hydrothermal systems that evolve inside active volcanoes. This paper focuses on how these lakes and their exotic chemistry are related to the larger scale transport of metals through active volcanoes—in other words, what is happening beneath these lakes?

2 Fumaroles, Solfatara and Hyperacidic Lakes

Geological associations—the temporal and spatial relationship to solfatara and active volcanism—lead to the widely accepted explanation that acidic volcanic lakes are a 'cold trap' for expanding magmatic gas, that, close by, is otherwise expressed as active, high temperature fumaroles and extensive rock alteration (solfatara), and by ash and gas plumes from more active volcanoes. Since the SO_2 concentration in high

[1] Terminology is always important. Here the term 'hydrothermal' refers to processes involving hot water whether liquid or gas. Vapor means a *gas* phase in equilibrium with a condensed phase whether solid, liquid or melt. In this paper, the term 'gas' is used rather than 'vapor' except where specific to a phase relationship. Miscellaneous terms that are avoided here are 'brine' (water close to saturation with salt) and 'boiling' which means phase separation due to continuous vigorous heating (as in a kettle), whereas phase separation in volcano-hosted hydrothermal systems occurs through simple processes as described in the text. The generic term *fluid* is used only in the context of fluid dynamics, i.e. how liquid, gas (or vapor) move through bodies of rock and otherwise sparingly as in convenient terms such as geothermal fluid where vapor and liquid phase properties are involved together.

[2] Although having its roots in the Italian, solfo, meaning sulphur, the term, solfatara, is used broadly to refer to volcano and geothermal regimes characterised by acidic rock alteration and steam discharges. The term, fumarole, refers specifically to vents inside solfatara. In geothermal systems, these features are associated with shallow processes (Henley and Stewart 1983). In this chapter the emphasis on is much higher enthalpy and temperature solfatara and fumaroles directly related to the discharge of volcanic gas.

temperature magmatic gas condensate from volcanoes worldwide, is around 7 wt%, lake water acidity and intense rock alteration are therefore readily ascribed to the dissolution of SO_2 (and to a lesser extent HCl since $m_{SO_2} > m_{HCl}$) into surface bodies of meteoric water with the formation of sulfuric acid and elemental sulfur (Delmelle and Bernard 2014, this issue). At Kawah Ijen the adjacent rhyolite dome is strongly degassing and is the likely source of additional inflow of acid condensate and heat into the lake (Williams-Jones et al. 2010).

The dynamics of hyperacidic lakes are well established and Takano et al. (1994), based on Yugama Lake (Kusatsu-Shirane Volcano, Japan) provide a graphic sequence of the kinds of heat and mass transfer processes that occur during the evolution of a lake system. As confined, but not closed, basins, an important aspect of these lakes is that mass and heat transfer models may be developed based on measurements of temperature profiles, outflows via spillover into drainages, estimates of evaporative heat loss and estimates of meteoric water inflow (Rouwet and Tassi 2011; Hurst et al. 2012). The value of these input-output models is that they place limits on the heat flux into such lakes due to magmatic gas. There are evident limitations relating to how constraints are placed on the enthalpy and composition of magmatic gas, and the relative heat and mass losses due to subsurface seepage away from the lakes, a critical factor in assessing risks of flank failure (Delmelle et al. 2014, this volume).

Figure 2 summarizes the range of heat flux inputs estimated for a number of hyperacidic lakes. Strict comparison of values is not appropriate given the limitations and uncertainties but they do suggest that heat fluxes[3] commonly lie in the range 100–1,000 MW_H, although values, are necessarily dependent on the scale of the lake and the eruptive stage of the host volcano (e.g., Brown et al. 1989; Hurst et al. 2012). Estimated total sulfur fluxes range from a few tens to hundreds of tonnes per day, but, as discussed below, both the thermal power and SO_2 flux estimates for these lake settings are small compared to independent estimates of the heat budgets of volcanic systems.

The overall chemistry of sulfur species ('disproportionation') in volcanic lakes are described in detail in a number of detailed analytical studies, such as Delmelle and Bernard (1994), Varekamp et al. (2000), Takano et al. (2008), van Hinsberg et al. (2010) and others reported in this volume. Kawah Ijen has been extensively studied. The lake water at Kawah Ijen, for example, has very high ionic strength dominated by sulfate ion pairs (Σ_{SO4} = ~0.7 molal[m]), chloride (~0.6 m) and fluoride (~0.07 m), and balanced by protons, H^+ (~0.3 m), aluminium (~0.2 m) and smaller concentrations of sodium (~0.04 m), iron, and magnesium (Table 1). However the focus in this paper is on the larger scale metal and metalloid flux in volcano-hosted hydrothermal systems as glimpsed through the chemistry of hyperacidic lakes, fumaroles and fossil hydrothermal systems now exposed as porphyry copper deposits. Table 1 therefore summarizes some of the available minor and metallic element data for lakes and high temperature (>800 °C) fumarole gas mixtures as indicative of magmatic gas compositions.

Very broadly the relative concentrations of minor elements (Table 1) are similar across the selection of lakes and fumaroles. Mass balance models for Kawah Ijen (van Hinsberg et al. 2010) confirm that the concentrations of many components in the lake water reflect a general process of aggressive acid dissolution of fresh rock, derived as rockfall, ash and the walls of the lake itself. These models show that lead, tin and antimony are enriched relative to this process and most likely are a consequence of input from magmatic gas. The sensitivities of the mass balance models do not rule out derivation of proportions of other metals and metalloids from magmatic gas particularly when note is taken of observed metal precipitates (Delmelle and Bernard 1994) that indicate sequestering of metals, including Cu and As, from the lake water.

[3] Heat flux is expressed as a unit of power; a megawatt (MW_H) is equivalent to an energy flow of 10^6 J of heat per second.

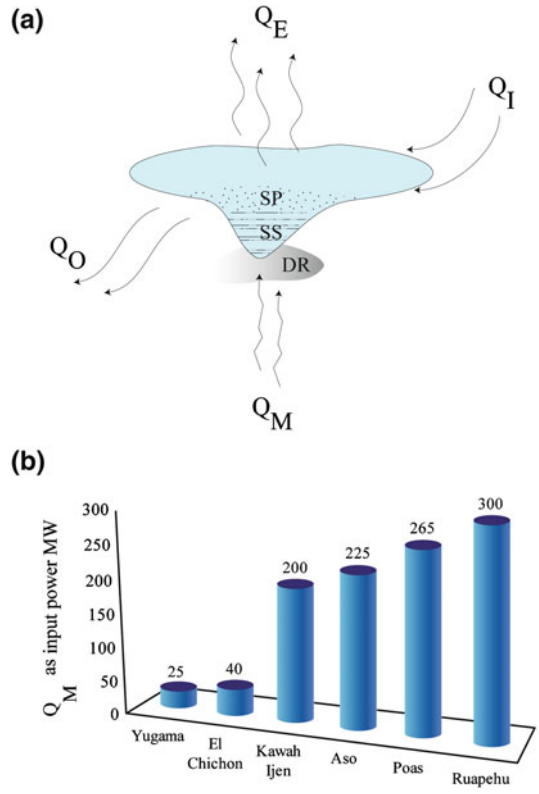

Fig. 2 **a** Simple heat balance model for a hyperacidic volcanic lake showing principal components as follows; Q_M heat input by volcanic fluid, Q_E heat output due to evaporation, Q_I heat input via meteoric and ground water, Q_O heat output through overspill and seepage underground. The simple model relates to an equivalent mass input—mass output model for dissolved components including isotopes. *DR* a dispersive regime immediately below the lake where magmatic gas, heated groundwater and lake water interact. Additional chemical sinks are shown as *SS*—the sediment layer including sulfur lakes, and *SP*—the suspended particulate load that includes submicron and larger amorphous silica and anatase(TiO_2). **b** Relative heat flows (Q_M expressed as MW_H) due to volcanic gas input to a number of well-characterized hyperacidic lakes

At Kawah Ijen, the chemistry of the adjacent fumaroles differs by only about 10 % from that of the lake with the exception of barium which, not surprisingly, precipitates as highly insoluble barite ($BaSO_4$) into lake sediments (Delmelle and Bernard 1994). Other sulfate precipitates include gypsum ($CaSO_4$, $2H_2O$) and celestite ($SrSO_4$). Particulate amorphous silica and anatase (TiO_2) are also abundant in the suspended solids and sediments in the lake, while enargite (Cu_3AsS_4), 'covellite' (CuS) and pyrite (FeS_2) actively grow within sulfur globules (Fig. 3 a–d). The importance of these data is that they provide a link to active fumaroles as well as to now extinct solfatara and crater lake environments. Figure 4 shows the range of metal and semi-metals that have been documented in sublimates from modern high temperature volcanic fumaroles (Henley and Berger 2013). Exotic lead, bismuth and thallium sulfosalts are common along with more familiar minerals including pyrite, anatase, molybdenite (MoS_2) and elemental sulfur. Native gold occurs at Kudryavy, Kurile Islands (Yudovskaya et al. 2006) and at Colima, Mexico (Taran et al. 2000), and interestingly zirconium occurs in sublimates at Kudryavy (Churakov et al. 2000) and Merapi, Java (Kavalieris 1994). Of particular interest in these fumarolic environments is the relative, but not complete, absence of copper and arsenic. Trace quantities of idaite ($\sim Cu_5FeS_6$) and covellite (CuS) occur as hypogene minerals in the, now closed, sulfur mine (an extinct fumarole) near

Table 1 Comparative analyses of trace metal concentrations in hyperacidic volcanic lakes and high temperature fumaroles

	Kawah Ijen	Kawah Ijen	Kawah Putih	Poas	El Chichon	Ruapehu	Kudryavy	St. Augustine	Colima 2
Sample	Lake	Fumarole	Lake	Lake	Lake	Lake	Fumarole	Fumarole	Fumarole
	KV99-857,858	KV99-857,858	PT-1/1		4–98		F1292	Dome-2	06.1997
Reference	1	1	2	3	4	5	6	7	8
T °C	37.1	36.9	34	44–60			940 °C	870 °C	828 °C
pH meas.	−0.1	−0.1	<0.50	−0.87 to 0.14	2.15	1.18–1.78			
Cl	22,099		12,000	18,830–114,200	2,795	4,000–7,000[a]			10,500
SO_4	66,855		11,130	34,800–180,000	755	16,300–21,400[a]			3,992
Fe	2,069			1,010–10,170			0.00	0.00	3.30
F	1,258		12.3	1,399–22,500					310
Mn	40	44	2.58	26–130	2.63		0.09	0.05	0.06
Sr	15	16	1.47		1.60		0.01	0.00	0.06
V	8			6.7–23.9	0.02		0.00	0.00	0.26
Ti	7			6–15.5			0.14	0.02	0.02
Zn	5.1	5.6	0.82	2.7–22.8	0.03	2.8–4.8	3.10	2.36	5.30
Pb	4.5	4.9	0.14	0.46–14.4	0.00		1.25	2.75	0.45
Rb	3.8	4.1	0.17		0.34		0.05	0.003	
Zr	1.9	2.1	0.04		0.00004		0.98	0.01	
Ba	1.6	0.5	0.27		0.11		0.15	0.00	0.46
As	1.6	2.0	0.86		0.06	0.2–3.3	1.20	4.17	0.43
Se	0.5	0.5			0.01		0.17	0.00	0.45
Co	0.5	0.5	0.01	0.17–0.37	0.001		0.00	0.00	0.00
Sn	0.3	0.3		2.9			0.14	0.00	
Cu	0.4	0.4	0.07	0.22–25.2	0.004	0.1–0.2	0.27	0.25	0.93
Cd	0.06	0.06	0.00	0.2–1.1	0.01		0.23	0.14	0.06
Sb	0.03	0.03			0.0010	0.0045[a]	0.08	0.26	0.04
Mo					0.00390		0.2	0.96	9.100E-02
Tl					0.00060		0.16		2.40E-02
Be			0.004	0.01–0.03	0.00014				
Bi					0.00010		0.04	0.0003	
Ag				0.05–0.37	0.00001				

Sources (1) van Hinsberg et al. (2010), (2) Sriwana et al. (2000), (3) Rowe (1991), (4) Taran et al. (2008), (5) Christenson and Wood (1993), (6) Taran et al. (1995), 7 Symonds et al. (1990), (8) Taran et al. (2001). All data are shown in mg/kg

[a] Analysis taken from a different sampling date with respect to this location

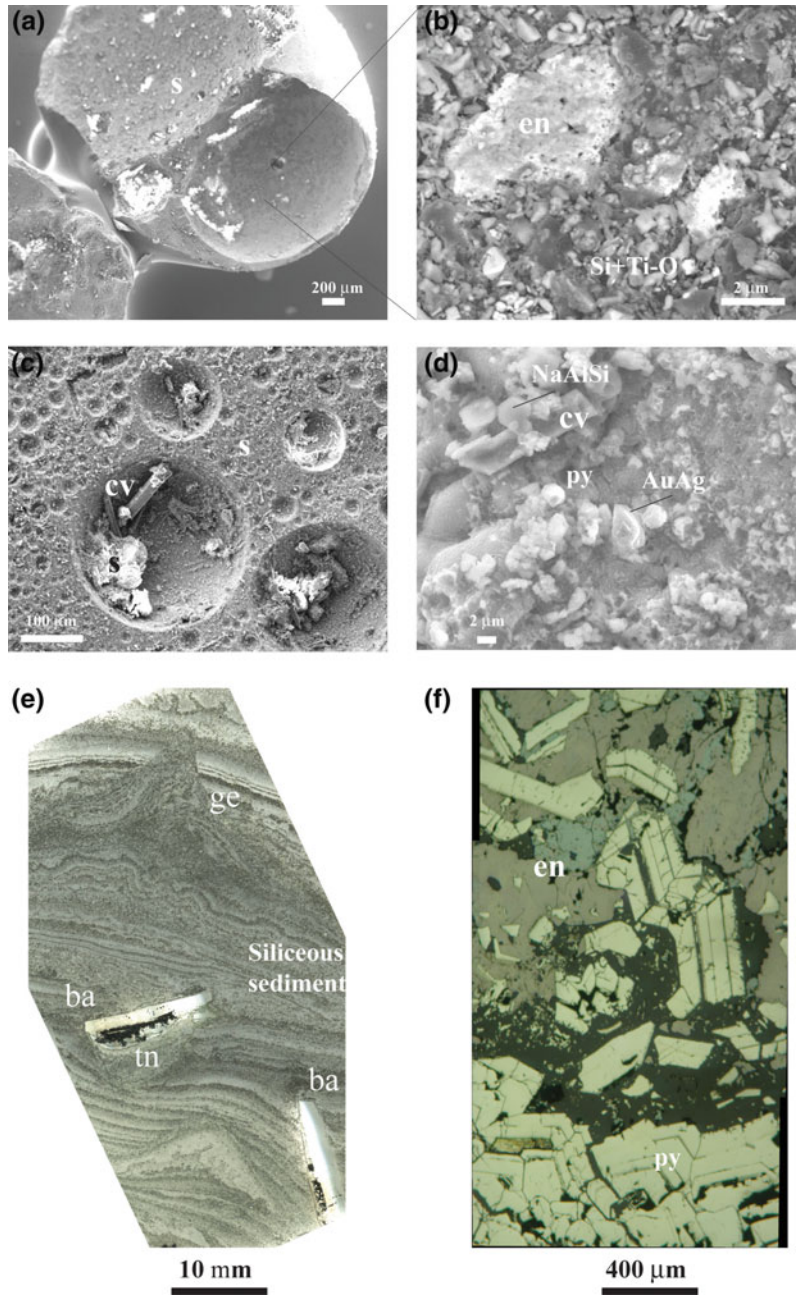

Fig. 3 Metals in sulfur from acidic volcanic lakes and submarine sulfur lakes. **a** Sulfur globule from Kawah Ijen (# KJ92) showing location of enargite (*en*) shown in (**b**). **b** Enargite growing on the inside of a sulfur globule through a coating of particulate silica, anatase (TiO_2) and sulfur. **c** Acicular CuS (nominally covellite, *cv*) and sulfur globules growing inside spherical gas cavities in floating sulfur globules, Maly Semiachik crater lake, Kamchatka (# MS93.1). **d** Acicular CuS growth overgrown by a crystalline NaAl-silicate inside sulfur from the submarine sulfur lake in the Lau basin (Kim et al. 2011). Pyrite, *py*, and native gold crystallites occur adjacent to the CuS. **e** Lepanto Cu–As–Au deposit, Lepanto, Philippines. Finely-laminated microcrystalline SiO_2–TiO_2 sediment containing isolated clasts of barite, *ba*, encrusted with tennantite (*tn* = Cu–As–S sulfosalt). This sample is interpreted as a recrystallized acid lake sediment similar to that at Kawah Ijen (Berger et al. 2014). The clasts and soft-sediment deformation structures are interpreted as drop-clasts and gas escape, *ge*, structures. **f** Sulfide-sulfosalt assemblage typical of minable-grade material within the fracture array a few hundred meters below the level of (**e**)

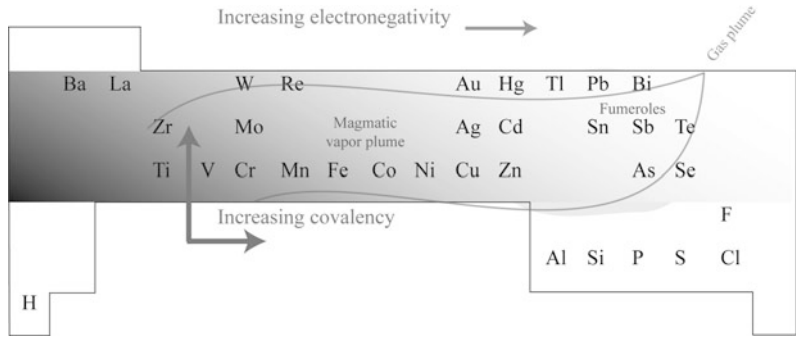

Fig. 4 Summary of elements reported in fumarole sublimates, hyperacidic lakes and ash plumes shown in terms of their position in the periodic table of the elements. The table is inverted here in order to illustrate the general fractionation from metallic elements (Cu, Fe) that are most common in the core of a magmatic vapor plume beneath an active volcano to the larger and heavier metals that characterize fumarole environments (As, Bi, Pb) and gas plumes (Cd, Tl). Silica, sulfur, chlorine, etc., are ubiquitous as ligands and as salts, sublimates and alteration minerals

the summit (6.176 m) of the quiescent Aucanquilcha volcano in northern Chile with a formation temperature interpreted from phase equilibria of about 450 °C (Clark 1970). Sulfur deposits such as these are also often seleniferous (Brown 1917). However these minor occurrences are insignificant relative to the extreme concentrations of copper—and arsenic—in deposits exposed by erosion deep into the interior of ancient volcanoes. Such deposits are extraordinarily well known and documented as a result of their economic significance as so-called 'high sulfidation' and 'porphyry' deposits. These deposits spatially and temporally track ancient volcanic arcs around the Pacific, through central Europe and many other paleo-arcs. For volcanologists though, their significance lies in providing access, through fossil equivalents, to the otherwise inaccessible hydrothermal regimes inside modern volcano-hosted hydrothermal systems (Henley and Ellis 1983, Henley and Berger 2013).

3 Copper-Arsenic-Gold Deposits Associated with Paleo-Solfatara

Figure 5 shows the mapped distribution of characteristic silica-alunite wallrock alteration that preceded and localized the formation of 'high sulfidation' enargite-gold veins at Lepanto, Philippines (Berger and Henley 2011). This deposit occurs within the Manakayan volcanic complex that also hosts a number of other vein and porphyry copper deposits, and is dated at 1.33 ± 0.15 million years BP (Arribas et al. 1995). Berger et al. (2014) recently recognized fossil acidic lake sediments (Fig. 3e) along and upstrike of the sulfosalt mineralisation (Fig. 3f). Little erosion appears to have occurred since alteration and mineralisation so that pyrite-enargite-gold deposition along the Lepanto and related fracture array occurred between depths of only 200 m and the paleo-surface, still marked by extensive silica-alunite alteration representing the paleo-solfatara around the former lake. The lake sediment, paralleling that at Kawah Ijen, is characterized by recrystallized silica with anatase, clasts of barite rimmed by sulfosalt and gas escape structures typical of soft-sediment deformation (Fig. 3e). Detailed micro-analysis of the sulfide-sulphosalt vein assemblages from Lepanto (Berger and Henley unpublished data) shows that primary sulfosalt-pyrite sublimate recrystallized post deposition with fractionation of antimony to the surface of the growing enargite-luzonite crystals. Tennantite (idealized formula $Cu_{12}As_4S_{13}$) in the Lepanto assemblages is commonly substituted by Zn, Te, Ag, Sn, Pb and V in some cases forming colusite ($Cu_{12}V(As, Sb, Sn)_3S_{16}$) and this same element suite is noted in the chemistry of the Kawah Ijen.

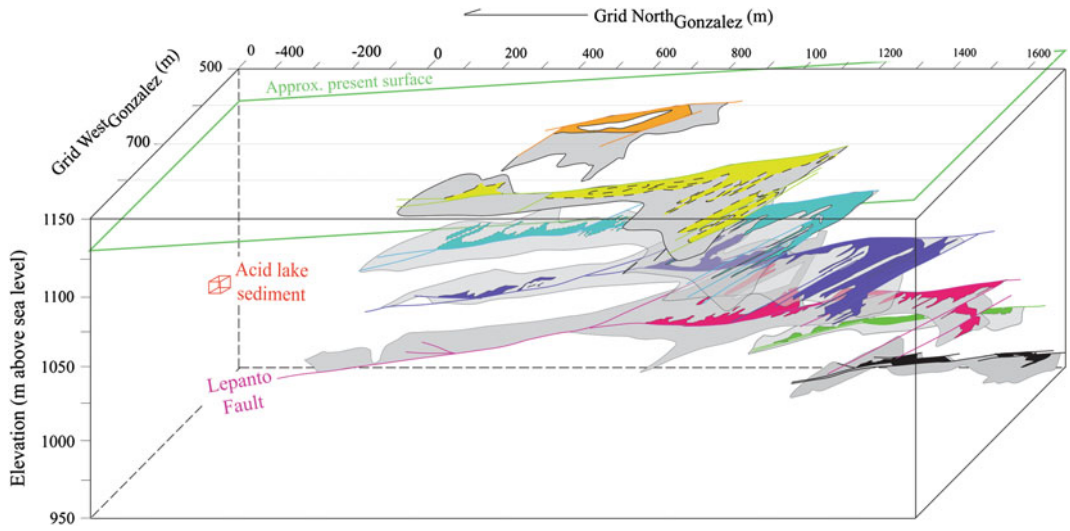

Fig. 5 Cu–As–Au–Au sulfide and sulfosalt distribution at the Lepanto deposit, Philippines. In this interpretive three-dimensional perspective view silica-alunite alteration is shown in *grey*. Pyrite-sulfosalt mineralisation occurs in veins inside this host (Berger and Henley 2011) and highlighted in a range of colors simply to help view the 3D perspective. The location of the acid lake sediment sample (Fig. 3**e**) is shown by the *red box*. This 3D compilation of level plans was prepared from the detailed underground mapping by González (1959)

Similar associations, including with native sulfur at Chinkuashih, Taiwan (Henley and Berger 2012) and surficial silica-alunite alteration blankets (Pascua, Chile-Argentina, Chouinard et al. 2005) emphasize the correlation of high sulfidation deposits with modern acid lake-solfatara environments and their direct relation to chemical processes consequent on magmatic gas expansion to the surface. Moreover, the veins mined at El Indio (Chile) formed at around 1,000 m below the paleosurface and contain evidence of fractionation of large atomic volume, heavy metals into the gas phase as arsenic-rich sulfosalts precipitated as solid sublimates and sulfosalt melts (Henley et al. 2012). This deposit may be related to the higher elevation, Tambo deposit (Deyell et al. 2004) that is characterized by solfataric alteration with abundant barite.

These occurrences may be interpreted as showing very rapid and efficient dumping of pyrite-sulfosalt sublimate assemblages during expansion of magmatic gas from a few hundred bars to surface pressures (Henley and Berger 2011) through a sequence of throttles along the fracture array that fed surface discharges. Similar processes may be considered as occurring below Kawah Ijen and other modern crater lakes and solfatara to evolve sinks for copper and arsenic and limit the observed fluxes of Cu, As, Au, Ag and other metals and metalloids at the surface.

4 Cu–Au–Mo Deposits Associated with Sub-volcanic Intrusions

The scale of high sulfidation deposits and their contained metals is trivial relative to the masses of copper deposited deeper in volcanic systems by magmatic gas as it expands from source toward surface. The 3.17 + 0.16 million year old Grasberg deposit, Irian Jaya (Indonesia), for example, may be viewed as a Cu–Au–Ag sink formed only a few kilometers below the surface of a then active volcano (Pollard et al. 2005). With inclusion of cogenetic skarn deposits in limestones adjacent to the' porphyry' mineralisation, this metal sink contains more than 30 million tonnes of copper, 2,700 million tonnes of gold and 10,700 million tonnes of silver. The giant Bingham Canyon 'porphyry' copper deposit (Utah) similarly relates to a composite volcanic system that, on the basis of stable

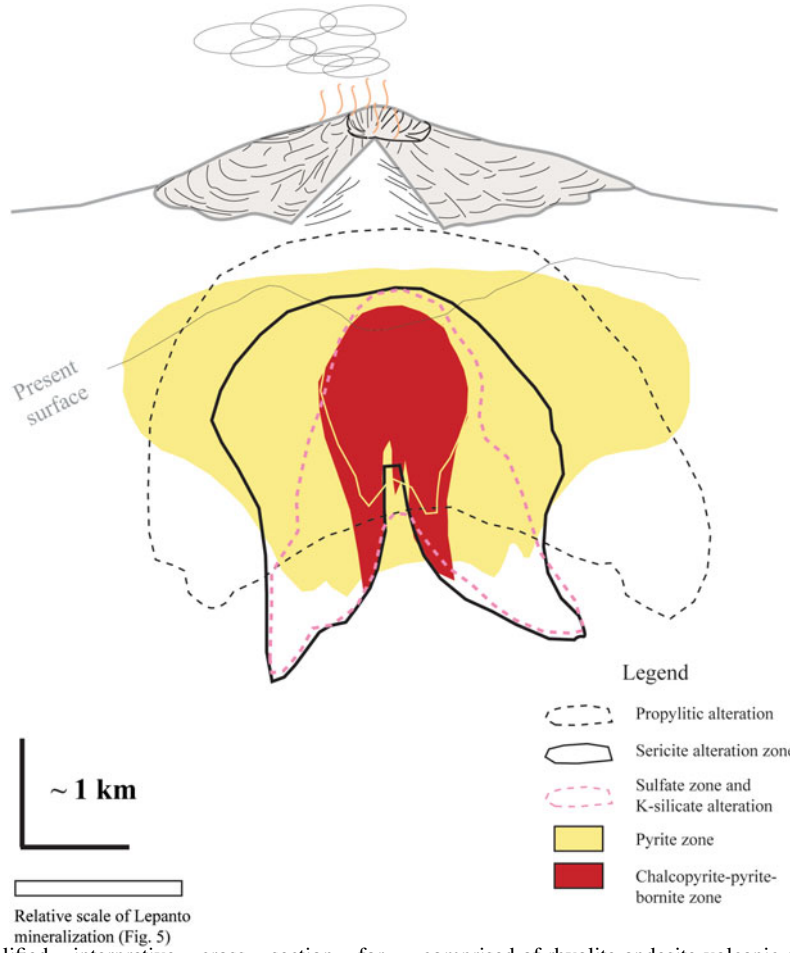

Fig. 6 Simplified interpretive cross section for the ~40 Ma El Salvador porphyry copper deposit, Chile, after Gustafson and Hunt (1975). This illustration shows the projected scales of the different zones of alteration and mineralisation associated with a paleo-volcano comprised of rhyolite-andesite volcanic and sub-volcanic intrusions (not shown). For the relative order of formation of zones, see Gustafson and Hunt: also not shown here are post-mineralisation veins, pebble dykes and an overprint of advanced argillic-supergene alteration

isotope data from alteration minerals, has even been suggested to have been topped by an acidic crater lake (Cunningham et al. 2004). Figure 6 provides another example, the 42–43 Ma porphyry copper at El Salvador, Chile, that illustrates the scales and distribution of mineralisation and alteration through the largely preserved volcanic structure (Gustafson and Hunt 1975).

The geology, geochemistry and environment of formation of porphyry copper deposits have been extensively reviewed (e.g. Sillitoe 2010). Key features interpreted from detailed mineralogical, fluid inclusion and stable isotope studies indicate that sulfide vein assemblages, at temperatures in the range 500–850 °C (e.g. Heithersay and Walshe 1995), deposited from an expanding plume of magmatic gas that interacted to varying degrees with surrounding groundwater (Henley and McNabb 1978). In the present context it is now established from deep drilling that anhydrite is ubiquitous in association with pyrite and Cu-Fe sulfides in porphyry copper deposits (Sillitoe 2005) but commonly removed by groundwater during plume collapse and later weathering. As noted above Hunt (1977) made the crucial observation that 'porphyry' deposits were, as well as economic metal accumulations at a scale of around 0.5 wt% Cu. large crustal sulfur anomalies comprising both a core of anhydrite and iron-copper sulfides and an

extensive aureole of pyrite. This provides a major insight to the processes occurring inside modern degassing volcanoes. Even more intriguing in their very detailed study of the El Salvador 'porphyry' deposit, Gustafson and Hunt (1975) noted that sulfate abundance exceeded sulfide through the deposit, and that deep veins have anhydrite and copper-iron sulfides (chalcopyrite, bornite and pyrite) occurring together. This close association of abundant oxidized sulfur (S^{VI}) and reduced sulfur (S^{II} and sometimes S^0) evolves as magmatic gas expands from source to surface at the volcano-scale, an observation that returns us to consideration of processes inside active volcanoes especially with the recognition of excess SO_2 emission in the plinean Pinatubo and other eruptions (Jakubowski et al. 2002; Luhr 2008).

5 Heat and Mass Transfer in Volcano-Hosted Hydrothermal Systems

Crater lakes, high temperature fumaroles and the extreme gas flux from erupting volcanoes all provide evidence of magmatic gas expansion from intrusive complexes and deeper sources beneath active volcanoes through to the surface. Where expanding magmatic gas interfaces with groundwater, a magmatic 'vapor' plume is established (Henley and McNabb 1978). The distal components of such dispersion plumes are more familiar in volcanic terranes as high enthalpy, near neutral pH, geothermal systems (Henley and Ellis 1977). The relationships between these key components of volcano-hosted hydrothermal systems are summarized in Fig. 7. Examples include the geothermal systems and volcanic activity of Copahue, Argentina (Varekamp et al. 2009) and Galunggung, Java (Moore et al. 2008).

6 Magmatic Gas Expansion and Dispersion

It is well established through sulfur, oxygen and deuterium isotope studies that the formation of high temperature (at quasi-magmatic

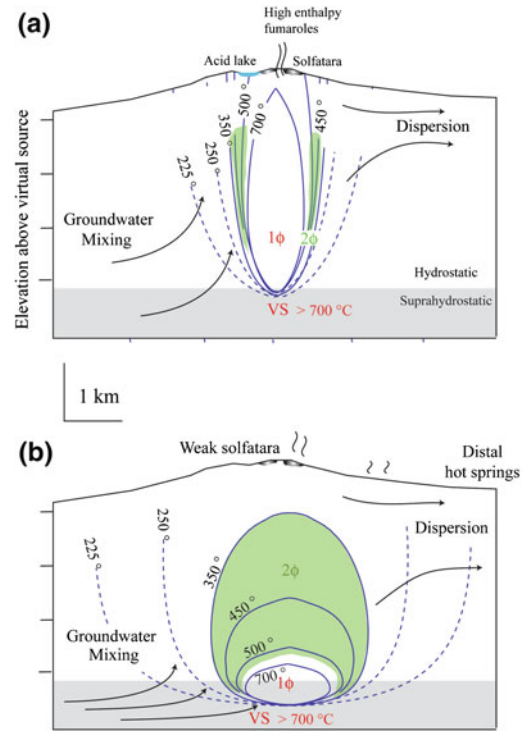

Fig. 7 Principal volcano-hosted hydrothermal system flow components associated with magmatic gas expansion as described in the text. In **a** K_p (the ratio of vertical to horizontal bulk fracture permeability) is about 5 so that a narrow plume develops through to surface discharge features including hyperacidic volcanic lakes. In **b** K_p is about 1, corresponding to the plume dimensions modeled by Henley and McNabb (1978). Major dispersion (shown by the partial streamline *flow arrows*) of the single phase (1ϕ) magmatic gas component occurs through interaction with groundwater leading to a much larger two-phase (2ϕ) plume and dispersion away from the volcano. The virtual source is a mathematical convenience representing a source of magmatic gas (Henley and McNabb 1978)

temperatures such as on Kudryavy volcano, Kurile Islands) fumaroles on the summits and flanks of volcanoes is the consequence of expansion of magmatic gas from a high pressure source regime to surface pressure. Such expansion is consequent on the maintenance of fracture permeability and internal gas pressure above that of groundwater through the volcanic system (Henley and Berger 2013). The crucial control on magmatic gas—groundwater interaction beneath volcanoes (Fig. 7 a, b) is therefore fracture permeability and, at the volcano scale, the ratio of vertical to horizontal permeability ($R_k = K_v{:}K_h$).

This ratio varies in time consequent on responses to sub-volcanic stress and mineral deposition that clogs fracture permeability (Henley and Berger 2013). Where lateral dispersion is constrained by high R_k, volcanic gas expansion occurs to higher levels within a volcanic system in contrast to low R_k systems where groundwater dispersion dilutes the magmatic input very quickly and may prevent surface indications of deep magmatic gas release (Hurwitz et al. 2003) as exemplified by the Cascade volcanoes of the Pacific Northwest (USA).

An important lesson from studies of volcano-related mineral deposits is that hydrothermal activity is continuous through the lifetime of a volcano but interspersed by episodic high level intrusive activity and eruptions. Short term variations occur at smaller scale in the near-surface regime due to local variations in rock strength, and even atmospheric pressure (Delmelle et al. 2014, this issue); a well documented example is the series of lake eruptions at Ruapehu volcano's crater lake (Christenson et al. 2010) in response to processes at the scale of around 1,000 m. Degassing of volcanoes is therefore more appropriately referred to a large scale sub-volcanic magmatic gas reservoir over a longer time period than to discrete short term intrusive events (Henley and Berger 2011, 2013). Fumarole data (Taran 2009) also suggest continuous degassing occurs through volcanic lifetimes with gases sourced from a reservoir encompassing silicate-melt systems deep below the volcano, the mantle wedge-subduction couple and intermittent, shallow intrusive activity (Wallace and Edmonds 2011; Webster and Botcharnikov 2011). Release of gas from the magmatic gas reservoir occurs across a permeability discontinuity (Cox 2005) from high to low pressure with subsequent expansion occurring through throttles in the controlling sub-volcanic fracture array resulting in a stepped gas-static pressure profile through to the surface (Henley and Berger 2011). As discussed below it is the time and space history of such pressure transients that focuses the formation of Cu–Au deposits. These deposits should, more appropriately be considered in the context of volcano scale processes as geochemical *sinks* for metals to avoid overlaying connotations of scale and economic value.

6.1 Phase Relationships

The thermal and chemical dynamics of the components of volcano-hosted hydrothermal systems are linked through simple phase and partitioning relationships. The binary system, NaCl-H_2O, may be used as a proxy[4] to trace enthalpy-pressure relations within these systems from source to surface (Fig. 8). There are an almost infinite number of pressure-enthalpy paths constrained by flow rate-permeability relations, and relative pressures of groundwater and expanding gas. Figure 8b includes a suite of illustrative pressure-enthalpy paths for heat and mass transfer processes beneath volcanoes for a magmatic gas (A) with less than 5 wt% NaCl, and with respect to the formation of high enthalpy fumaroles (B and C) and crater lakes (F).

6.2 Expansion

Nuccio et al. (1999) showed that the formation of high flux, high temperature fumaroles, such as on Kudryavy and St Augustine (Table 1), corresponds to irreversible isenthalpic expansion of magmatic gas (AB). Expansion at much lower flow rates may be isentropic with a much higher temperature drop. Low flux fumaroles may also be due to lower fracture permeability where, because conductive heat loss is relatively high (AC), the enthalpy and temperature of the expanding gas decreases relative to the initial magmatic temperature. Expansion path, AD, intersects the halite plus vapor field whose boundary (HLV) is shown in Fig. 8b. This field may have special significance to deposition of chloride-complexed metals in shallow environments as discussed below.

[4] Figure 8 charts phase boundaries and *specific* enthalpies for fluids in the NaCl–H_2O system. The CO_2 content of volcanic gases tends not to exceed a few mole percent and therefore contributes only a minor pressure effect on these systematics.

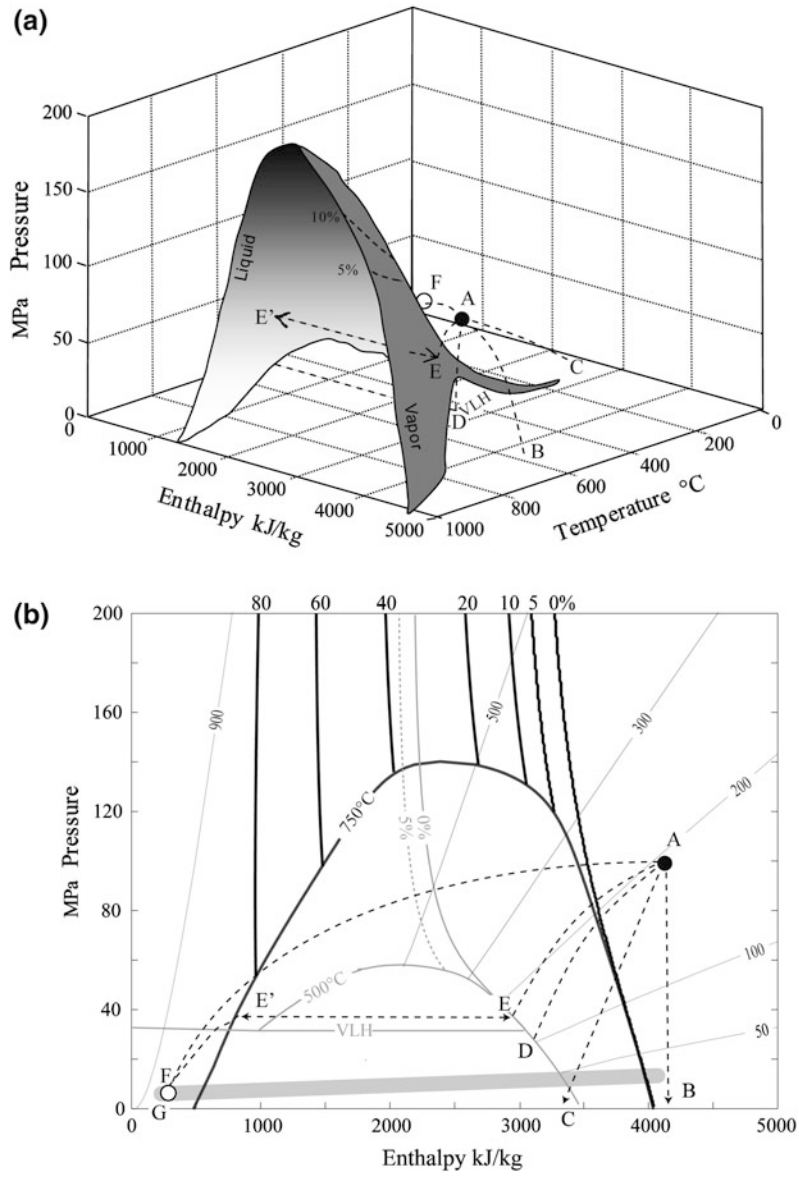

Fig. 8 Phase relations in the system NaCl–H_2O as proxy for the magmatic gas phase (<5 wt% $NaCl_{equivalent}$) and its derivatives during expansion and mixing processes (see text). Figure 8(**b**) is a projection of the 3D data onto the pressure-enthalpy plane. Note that in **b**, heat and mass transfer paths are simplified for clarity. VLH is the trace of the three phase vapor + liquid + halite triple point

6.3 Mixing

Heat transfer processes beneath volcanoes commonly include mixing with groundwater (G), or shallow meteoric water inputs near surface. They occur through pressure differentials between groundwater and the expanding magmatic gas, after and because mixing involves the addition of mass (i.e. a mass of magmatic gas plus a mass of groundwater), heat transfer paths are not linear in pressure-enthalpy space (Fig. 8b). Path AG curves over the two phase field and describes the formation of geothermal systems inside volcanoes, the temperature of the mixed liquid phase becoming limited by the boiling-point depth curve in its outflow regime.

Path AE has limited expansion, and intersects the 500 °C two-phase envelope, in this illustrative example, with consequent separation of a small liquid fraction (E'). Such paths are responsible for the development of two-phase envelopes to expanding magmatic gas plumes (Fig. 7) as

described elsewhere (Henley and McNabb 1978). Mixing in the two phase regime is constrained by the relative permeabilities to each phase and their respective volumes. In the sub-crater lake (F) environment, the high salinity liquid fraction may become isolated from the gas phase, evaporate or mix with cold groundwater. Shallow groundwater interactions (not shown in Fig. 8b) also occur in the vent regime of fumaroles with consequent relative lowering of the enthalpy of the exiting fumarole gas mixture coupled with changes in chemical and isotope composition (Botcharnikov et al. 2003). A special case is the shallow capture by ground- and meteoric water of expanding high enthalpy magmatic gas (AB), with its high SO_2 content, to form hyperacidic crater lakes (F).

6.4 Heat Flux

Economic exploitation of geothermal systems is dependent on the bulk enthalpy of the liquid phase encountered by drillholes to depths of about 4 km. Stable isotope systematics for the fluid phases in volcano-hosted hydrothermal systems confirm a mass fraction of up to about 0.25 of magmatic gas mixed with groundwater. Since the enthalpy of water-dominant magmatic gas is about 4,500 kJ/kg (M, Fig. 8a) and that of conductively heated groundwater (W) at 100 °C is about 420 kJ/kg, a consequent geothermal 'fluid' has an enthalpy of 1,440 kJ/kg such that, through isenthalpic upflow by convection through fracture arrays, it encounters boiling point-depth conditions at about 320 °C above ~1.5 km groundwater depth (~11 Mpa). Surface heat flow measurements for such systems show that exploitable systems such as this have energy fluxes of a few hundred megawatts (MW_H); Wairakei, New Zealand for example, had a pre-exploitation heat flux equivalent to about 430 MW_H corresponding to a steady state input of about 95 kg/s of water-rich magmatic gas at a depth of about 10 km (Heise et al. 2010). Corresponding power inputs for other geothermal fields in the Taupo Volcanic Zone are from a few tens to a few hundred MW_H.

For comparison, estimates of the power output of active volcanoes may be made from SO_2 flux data from atmospheric gas plumes as well as other flux data such as for CO_2 and H_2O. Table 2 provides such estimates assuming, for first order approximations mean SO_2 and H_2O contents of 2 and 98 mol % respectively; here other gases such

Table 2 Estimates of the gas phase discharge power of volcanoes at various levels of activity, based on measured SO_2 flux data

	Country	SO_2 flux t/d	H_2O flux t/day	Power (MW_H)
Etna	Italy	4,000	251,392,000	11,600
Bagana	Papua New Guinea	3,300	207,398,400	9,600
Lascar	N. Chile	2,400	150,835,200	7,000
Ruiz	Colombia	1,900	119,411,200	5,500
Sakurajima	Japan	1,900	119,411,200	5,500
Manam	PNG	920	57,820,160	2,700
Yasur	Vanuatu	900	56,563,200	2,600
Kilauea	Hawaii	800	50,278,400	2,300
Masaya	Nicaragua	790	49,649,920	2,300
San Cristobal	Nicaragua	690	43,365,120	2,000
Stromboli	Italy	730	45,879,040	2,100
Langila	Papua New Guinea	690	43,365,120	2,008
Galeras	Colombia	650	40,851,200	1,900
Fuego	Mexico	640	40,222,720	1,900
Satsuma-Iwojima	Japan	570	35,823,360	1,700
Mutnovsky	Kamchatka, Russia	200	12,569,600	600

Data sources Shinohara (2008), Mather et al. (2006). Power estimates have been rounded

as CO_2 are accommodated as H_2O-equivalent through the base (98 mol % H_2O) assuming ideal gas mixing. These crude estimates are for relatively quiescent stages of volcanic activity from 500 (Mutnovsky, Kamchatka) to over 1,100 MW (Etna, Sicily). SO_2 flux self-evidently increases with eruption magnitude and this same estimation procedure gives a thermal power output of 3.3×10^8 MW_H for the Plinean phase of the Pinatubo eruption in 1991. The equivalent and more directly estimated heat flux for the hyperacidic lakes at Kawah Ijen and Aso, Japan (Fig. 2) is $\sim$200 MW_H (Takano et al. 2004; Terada et al. 2012). If multigas sensor data for the degassing rhyolite dome immediately adjacent to Kawah Ijen (Williams-Jones et al. 2010) are added in, then the total heat flux of the Kawah Ijen gas system is about 14,000 MW_H—substantially more than the estimate for Etna. A range of assumptions are included in the Kawah Ijen estimate including the time scale for such a massive heat flux but, for perspective it is equivalent to the heat released by crystallization of about 3 m^3/s of basalt and magmatic gas flux of about 3 kg/s.

This analysis of the dynamics of magmatic gas discharge through volcano-hosted hydrothermal systems shows that hyperacidic crater lakes and fumaroles represent a small, but still significant, fraction of the continuous magmatic gas flux through a volcanic system with the remainder dispersed by groundwater mixing and outflow through the periphery of the system over distances of perhaps 10–20 km (Henley and Ellis 1983; Ingebritsen and Mariner 2010).

7 Metal Transport and Deposition in Volcano-Hosted Hydrothermal Systems

Van Hinsberg et al. (2010) showed that while a range of trace element concentrations in the filtered lake water at Kawah Ijen and altered rock material could be ascribed to aggressive acidic alteration of primary volcanic rocks, others (particularly Pb, Sn and Sb) required a separate influx coupled with the heat flux due to magmatic gas expansion into the lake. Since the thermal flux of hyperacidic volcanic lakes such as this is a fraction of the total heat flux of their host volcanic systems, the occurrence of trace metals as sulfides within them (Fig. 3) may be interpreted as indicating more substantial metal transport in the system as a whole. Evidence from equivalent fossil systems, as described above, also shows that substantial metal deposition is likely to occur into subsurface metal sinks unless very high permeability allows efficient and widespread dispersion of metals out into peripheral geothermal systems. In turn these data raise questions about how metals are transported in magmatic gases and more importantly what controls their distribution as precipitated sulfides and sulfosalts through volcano-hosted hydrothermal systems.

8 Metal Transport: Source to Sink

The wide range of metals and metalloids transported and deposited as sublimates in high temperature fumaroles is detailed in Table 1. A similar range is encountered as precipitates coating particles in ash plumes (Hinkley 1991) with Cd and Tl becoming highly enriched in this setting. In combination with the recognition of metal Fe–Cu–Au–Ag–Mo–S sinks deep within volcano-hosted hydrothermal systems, an overall pattern of increasing electronegativity and atomic volume is recognizable in the sulfide-sulfosalt assemblages as magmatic gas expands from its source reservoir to and through the surface (Vigneresse 2012, Henley and Berger 2013). This trend corresponds closely with the patterns of increasing covalency both from left to right and down series in the Periodic Table of the Elements (Fig. 4) as described by Crerar et al. (1985). Crerar et al. (1985) focused primarily in the consequences of these trends for sulfide assemblages deposited in liquid-water dominated systems ($<\sim$350 °C) where ionic species predominate, but the same trends broadly describe the overall source-to-sink distribution of metals and metalloids through much higher temperature flows in volcano-hosted hydrothermal systems.

These trends toward predominance of molecular rather than ionic species also follow from consideration of changes in the association constant, density and dielectric constant of water as temperatures increase toward magmatic conditions under relatively low pressure conditions (Liebscher 2010). The solubilities of common rock forming minerals follow these trends closely (Dolejs and Manning 2010) with much higher solubilities at high pressure relative to low pressure. The solubilities and speciation of metal and metalloids are not however so well known primarily because of difficulties of high temperature experimentation with low density, chemically aggressive gases and redox controls. However in an elegant series of solubility experiments at 150 MPa and 1,000 °C, Zajacz et al. (2011) showed, via ab initio calculations, that copper occurred as solvated cluster-like species of the form $Na(/K)CuCl_2$, $Na(/K)Cu(HS)_2$, H_2SCuHS, and $Na(/K)ClCuHS$, the relative abundance of which are determined by H_2S/total chloride and HCl/alkali chloride ratios in the gas phase. A similar range of mixed metal solvated species is likely for other metals released from magmatic systems during crystallization. For example gold may be transported as the solvated species $NaAuCl_{2(g)}$ (Zajacz et al. 2010). More covalent metals such as tungsten, and transition metals such as titanium and metalloids such as arsenic are transported as OH-species (Dolejs and Manning 2010; Pokrovski et al. 2005). The concentrations of chalcophile metals in a magmatic gas phase are also redox dependent through solubility reactions involving the fugacity of hydrogen in the gas mix.

Beyond solubility controls, the concentrations of metals and metalloids in a magmatic gas when it is released are primarily dependent upon their abundance in silicate melts, and when or if they are available as a gas phase evolves (Huber et al. 2012) to form a reservoir. This is important because it allows that metal concentrations may vary with time and, more importantly, that concentrations may not reach solubility maxima, both of which factors control their depositional profiles within volcano-hosted hydrothermal systems.

9 Metal Deposition: Sinks

As discussed above, reconstruction of the habitat of metal deposits within their sub-volcanic context, shows that substantial, but not necessarily economic, concentrations of metals occur as depositional sinks within volcano-hosted hydrothermal systems. Some metals, such as Cd and Tl do not deposit appreciably until very high in the volcanic system and in ash plumes, whilst others, such as copper, appear to deposit very efficiently deep within the core of the magmatic gas plume as gas expands into the hydrostatic regime; their ephemeral occurrence in fumaroles such as on Kudryavy and Colima volcanoes may therefore be regarded as residual components carried through to the surface in the expanding gas plume. Expansion from about 100 MPa (1,000 bars) in the upper part of the suprahydrostatic magmatic gas reservoir to 10 Mpa or less in the hydrostatic regime, for example, results in a gas phase density change from 280 to < 22 kg/m^3, a more than tenfold decrease. In essence, large cluster-like solvated species simply fly apart due to decompression of their carrier gas mixture.

As well as magmatic gas expansion itself, consequent changes in the redox state and sulfur speciation of the gas phase, phase separation and temporal changes in primary metal concentration all contribute, as described below, and lead to the eventual depth profile of metals (Sec.10) deposited through a volcanic hydrothermal system.

9.1 Magmatic Gas Expansion

One of the most important drivers for mineral deposition is the exponential decrease in water density (and therefore fugacity) due to expansion. This is amply demonstrated through the density-dependent hydrothermal solubility data for quartz (Manning 1994). For example, under magmatic conditions at about 4 km depth, the solubility of quartz is about 3,000 mg/kg but decreases to about 30 mg/kg during isenthalpic expansion to a few MPa through a fracture array to the surface. Dolejs and Manning (2010) demonstrate similar density

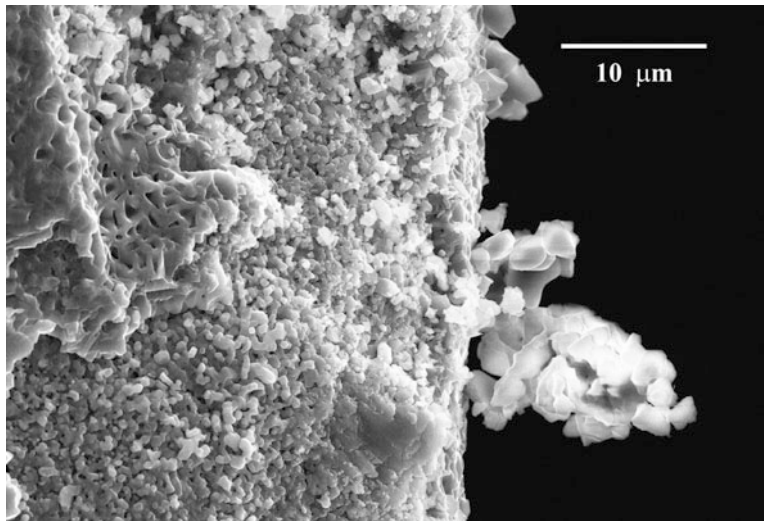

Fig. 9 'Chickenwire' textured anhydrite growth layer on plagioclase-rich rock developed by exposure to SO_2 gas at 600 °C. Here SO_2 penetration of the rock releases Ca to the surface where, exposed to SO_2, it generates supersaturation with respect to anhydrite and rapid growth of crystal clusters and a porous anhydrite layer. This experiment mimics the growth of anhydrite veins by Ca removal from wallrock leaving an aluminous selvedge. In natural systems where SO_2 is commonly aroun 5 mole percent, H_2O reacts with reduced sulfur to form H_2S in situ and the consequent concommitant rapid deposition of Cu-Fe sulfides from gas-phase metal species at a few thousand mg/kg

dependence for the solubility of a number of rock-forming minerals including rutile.

The solubility of enargite, as a principal component of high level arsenic sinks in volcano-hosted hydrothermal systems, is dependent on the gas phase species ($As(OH)_{3,g}$) as well as gas phase copper species, so that its deposition as As^{v} in enargite or As^{III} in tennantite is necessarily dependent on water fugacity (Henley and Berger 2011) as well as redox changes during expansion. Expansion into the halite-vapor field (Fig. 8b) may also be extremely important for metals transported as chloride species, since most of the chloride ligand becomes rapidly removed into halite. Decompression may also be the principle driver for characteristic potassic alteration in 'porphyry' systems (Lagache and Weissbrod 1977).

9.2 Redox State Changes in sulfur speciation

Since metal deposition in volcanic hydrothermal systems occurs primarily to form sulfide (S^{-2}) minerals, a paradox arises because sulfur in magmatic gas mixtures when released from crystallizing intrusives, is almost completely in the form of SO_2 with S in its +4 state (Henley et al. 2014). Redox changes occur in the crater lake environment to aqueous sulfate (S^{+6}) as well as thiosulfate species due to interaction with the atmosphere and may produce native sulfur (S^0) by disproportionation as at Kawah Ijen (Fig. 1).

In sub-volcanic fracture arrays where gas expansion is isolated from wallrock the redox state of sulfur is governed by homogenous gas reactions such as SO_2 disproportionation to sulfate and reduced sulfur (H_2S) as pressure and temperature decrease during expansion (Giggenbach 1987). Deep inside the gaseous core of volcanoes the very fast chemisorption reactions between SO_2 in expanding magmatic gas and Ca-Mg aluminosilicates occur to form H_2S and sulfate minerals (Henley et al. in prep; Henley et al. 2014; King et al. 2014). Figure 9 shows the rapid growth of anhydrite across the surface of plagioclase (An_{60})-rich rock at 600 °C in a flow of SO_2 gas for only 96 h. The formation of sulfate from SO_2 necessarily releases reduced sulfur to the gas phase and the removal of Ca into anhydrite leaves behind an

aluminous sodium-enriched altered rock. This is very well demonstrated in porphyry copper deposits that have been drilled below a surface regime where anhydrite has been removed by groundwater during plume collapse and subsequent erosion. Other alteration reactions, such as alkali exchange and hydration reactions, then proceed rapidly with the then destabilized primary mineral lattices in the Ca-depleted host rock.

Iron and copper carried as cluster-like gas species into the plume,at several thousand mg/kg, are captured rapidly and efficiently by the H_2S generated in situ by SO_2-aluminosilicate reactions to form Cu–Fe–S sulfides (King et al. 2014; Henley et al. 2014) co-precipitated with anhydrite. Drillcore from exploited geothermal fields peripheral to volcano-hosted hydrothermal systems, almost ubiquitously shows the conversion of 'FeO', as proxy for primary disseminated magnetite, Fe_3O_4, to form a very large annulus of pyrite, one of the signatures of 'porphyry' copper systems. Here pyrite constitutes a sink for both iron and reduced sulfur during dispersion of their magmatic gas plume source into groundwater (Henley and McNabb 1978).

9.3 Phase Separation

As described above, groundwater interaction with the margins of a magmatic gas plume results in the formation of a two-phase regime. Metal partitioning between gas and liquid phases is a function the relative phase densities and the mass fraction of liquid. Phase separation progressively sequesters NaCl and SO_2 to the liquid phase promoting 'CuS' deposition but is offset by the capture of Cu to the saline liquid phase. Partitioning of SO_2 to the small liquid fraction also involves a relative change in the redox (f_{H_2}) states of the liquid and gas fractions as well as developing a high liquid phase acidity. Whether these changes promote the deposition of Cu–Fe sulfides is unknown.

Partitioning of highly soluble acidic gases between the two phases is the determinant for developing the aggressive alteration of wallrock beneath low flux fumaroles and in equivalent Cu–As–Au deposits.

9.3.1 Hyperacidic Lakes

Phase relationships show that hyperacidic crater lakes are a consequence of high enthalpy, single phase magmatic gas flow to the surface with the gas and its contained heat captured into the cooler mass of lake water (Fig. 8b). Heat exchange with host rocks and dynamic interplays with gravity-driven groundwater and condensate flows, enable phase separation to occur marginal to the single phase gas flow into the base of these lakes. Since SO_2 is highly soluble in a liquid phase, its partitioning to the liquid fraction in a two-phase regime effectively sequesters sulfur into the acid condensate fraction and to sulfate minerals such as alunite ((Na, $K(Al_3(SO_4)_2(OH)_6)$—a phase implicated in sealing fractures and the eruption cycle at Ruapehu crater lake (Christenson et al. 2010). As shown elsewhere (Delmelle et al. 2014, this issue) density differences and two-phase permeability constraints lead to gravity separation of phases so that acid sulfate-rich liquid separated in this way recirculates into the lake system or leaks out with consequent aggressive alteration of surrounding rocks. The corollary is that the remaining lower enthalpy, gas phase is depleted in sulfur relative to less soluble gases such as CO_2, and likely is the gas-source for cooler, less acidic volcanic lakes.

Separation of halite (NaCl), rather than liquid, from gas is a variant of these mixing phenomena at very low pressures, as is evident in fumarole sampling tubes, and may occur on the margins of magmatic gas expansion below hyperacidic lakes (L) with subsequent recycling of NaCl into the flow regime. Interestingly halite and sylvite were found in ejecta from Ruapehu crater lake (Christenson and Wood 1993). For gas phase metal species, such as $NaCuCl_{2g,}$ the fast removal of NaCl during expansion (AD in Fig. 8) through a throttle self-evidently leads to fast copper deposition.

9.4 Fractionation

Henley et al. (2012) suggested, from high resolution SEM imagery, that strong fractionation of metalloids and other metals occurred during tennantite deposition from an expanding magmatic phase in the El Indio arsenic-gold deposit in Chile. This vein deposit formed at a depth of <1,000 m beneath an ancient solfatara containing low concentrations of gold and silver with abundant barite (Deyell et al. 2004). In this deposit textural evidence suggests that tennantite deposited as a sulfosalt melt (Mavrogenes et al. 2010; Henley et al. 2012) at about 15 MPa (150 bars) and >650 °C. This sulfosalt melt phase was highly aggressive to earlier deposited crystalline pyrite and enargite, and, post solidification to the recently mined sulfide-sulfosalt assemblages, contains micro-vugs containing fractionated metals including gold. A similar process is evident at Chinkuashih with solid sublimate of enargite composition forming from the expanding gas phase, subsequently crystallizing to enargite with fractionation of heavy metals, including Sb, Bi, Tl, etc. to the gas phase and their deposition along with elemental sulfur (Henley and Berger 2012). The range of heavy metals and metalloids observed in fumaroles (Fig. 4) suggest that, if arsenic-rich sulfosalts deposit as an arsenic-sink below fumaroles, similar fractionation occurs to enrich the gas phase with consequent formation of exotic Bi–Tl sublimates with other heavy metals at surface.

10 Metal Profiles

The mineral assemblages observed in fumarole sublimates and sub-surface mineral deposits in ancient systems, show no hint of equilibrium depositional relationships thereby invalidating equilibrium-constrained models for ore formation and the sequencing of sublimate minerals along fumarole sampling tubes. At best they provide a base case scenario but one that often translates into limitations on the effective modeling of processes within volcano-hosted hydrothermal systems. Henley and Berger (2000) showed that the sequencing of mineral deposition reactions could be modeled as far-from-equilibrium chemical processes triggered by, for example, gas or liquid expansion as active fractures develop in these systems. Far-from-equilibrium reactions are fast and efficient due to the consequent high initial super saturations whereas near-equilibrium deposition reactions are inevitably slow and inefficient since their reaction free energies tend to zero.

Consider the expansion of magmatic gas as a sequence of steps and assume that only a fraction of the excess metal or silica is removed in each step. Ignoring changes in temperature and in the ratio of sulfur species, the principal driver for deposition from a magmatic gas is decreasing water fugacity or density, and the consequential change in solvation number (Migdisov and Williams-Jones 2013). The mass deposited, M_z, as a function of decreasing depth, may be expressed through

$$M_z = m.\ I_{(z-1)} \cdot (d_0/d_z)^v \qquad (1)$$

where M_z is the mass deposited in depth interval, z, where water pressure is a function of depth($d_0 - d_z$), $I_{(z\ -\ 1)}$ is the mass of metal or silica remaining in the gas mixture following the prior step (z − 1), m is an expression of the efficiency of metal deposition and v is the assumed a quasi-reaction order dependence of the reaction rate (Henley and Berger 2013). As described above, fast, in situ, generation of H_2S from the dominant SO_2 of magmatic gas mixtures by aluminosilicate reactions to form anhydrite, immediately triggers the efficient, likely first order (Fig.10), capture of hard metals such as Cu and Fe and cogeneration of pyrite and Cu-Fe-sulfides with anhydrite. This is the signature reaction of porphyry copper formation. The analogous reaction with carbonate is responsible for the generation of accompanying metalliferous skarns in limestone rocks adjacent to porphyry copper deposits It is reaction kinetic profiles such as these (Fig. 10) that control the fluxes of metals observed at surface in crater lakes and high temperature fumaroles.

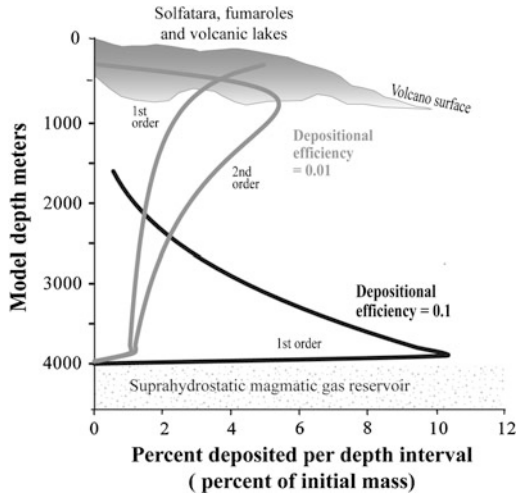

Fig.10 Depositional profiles for metals and other components based on a simple model for an expanding magmatic gas (see text) based on depositional efficiency and apparent reaction order or molecularity as calculated for a sequence of vertical steps

11 Discussion

As extreme environments, hyperacidic volcanic lakes have their own intrinsic fascination. They provide links to deep seated volcanic processes and they may be the trigger for disastrous flank collapse on active volcanoes (Delmelle et al. 2014, this issue). Their importance in earth history may go a degree further. As with other hot spring settings (Henley 1996; Nisbet and Sleep 2001) volcanic gas and geothermal discharges provide a wide variety of high surface area, nutrient-enriched environments to provide substrates for early biochemical synthesis and support of hyperthermophiles, and provide an alternative, and highly competitive, environment to those provided by submarine hydrothermal discharges. It is important in these contexts to fully understand hyperacidic and other volcanic lakes at a scale larger than the lakes themselves. To achieve this, data from modern and ancient volcano-hosted hydrothermal systems have here been joined to integrated show that large scale metal flux is a normal component of the dynamics of active volcanic systems. Observations of high SO_2 flux or 'excess' degassing from erupting volcanoes (Shinohara 2008), measurements of diffuse degassing on the slopes of quiescent volcanoes (Williams-Jones et al. 2000; Varley and Taran 2003) and the temporal and spatial distribution of metals within ancient and modern volcanoes may, through this integrative approach, be married into a single *continuous gas streaming* hypothesis for volcanic systems (Henley and Berger 2013). In this hypothesis volcanic degassing occurs throughout the history of a volcano from a magmatic gas reservoir that evolves at suprahydrostatic pressure in association with the progressive assembly of subvolcanic intrusions and magmatic gas release from them. Deeper gas flux from the mantle wedge-subduction couple and derivative mid and upper crustal intrusion complexes may also contribute to heat and gas flow in these systems. Since arc volcanoes are localized at convergent margins, the mass flux of gas to the surface is dependent on the state of stress in the sub-volcanic regime and the evolution of fracture permeability (Henley and Berger 2013)—a factor that links gas discharge and eruption frequency to regional seismicity. This hypothesis places less emphasis on the shorter term degassing of individual shallow (1–2 km) intrusions than is often assumed—intrusive activity itself being a function of stress release and fracture permeability.

Intrusive and eruptive activity release astonishing amounts of oxidized sulfur into the Earth's atmosphere (Bani et al. 2012). High SO_2 flux, with associated metals, also occurs through submarine volcanoes (Butterfield et al. 2012) and is manifest spectacularly by sulfur lakes on the sea floor. Such sulfur lakes (de Ronde et al. 2014, this issue) also contain traces of copper and gold; Fig. 3b provides an example from the Lau Basin that, as documented by Kim et al. (2011), contains the familiar element suite, Cu, As, Au, Bi, Te, and Sb, that suggests entrapment of expanding magmatic gas. These processes are mirrored elsewhere in the Solar System, including on Venus and Io (Esposito 1984; Moses et al. 2002), and doubtless, some exoplanets (Kaltenegger and Sasselov 2009). Moreover, remote observations of the surface and SO_2-rich atmosphere of Venus show enrichments of the again

familiar metal-metalloid suite, Cu, Zn, Sn, Pb, As, Sb, Bi (Brackett et al. 1995) with evidence of 'metallic snow' on the summits of Highlands volcanoes.

Where topography localizes high enthalpy gas discharge to form hyperacidic lakes in terrestrial volcanoes, a significant portion of this oxidized gas flux is captured. The lakes themselves become sinks for sulfur, as sulfate and associated species, and as elemental sulfur. Trace metals and metalloids, including copper and arsenic, and have escaped subsurface deposition, are trapped into molten sulfur and released during globule formation (Fig. 3 and Henley unpublished data) as well as disseminated through the acid sulfate lake water. These represent perhaps only the residue of the total flux of metals through the volcanic system, the bulk of the metal flux being trapped as sinks consequent on major pressure drops along the fracture arrays that feed through to surface features (Fig. 9). Dissected ancient volcanoes provide an independent record of these processes with the preservation of metal sinks (Cu–Fe–S) at paleo-depths of a few kilometers (Fig. 6) and arsenic-rich metal sinks near the paleo-surface (Fig. 5) perhaps in association with the formation of acidic lakes.[5] Hyperacidic volcanic lakes then are analogous to icebergs—the beautifully complex features that we see on surface (Fig. 1) are only a small part of much larger systems.

Acknowledgements I wish to thank Richard Arculus, Barney Berger, Bruce Christenson, Pierre Delmelle, Penny King, Gary Rowe, Tarun Whan and Jeremy Wykes for enthusiastic discussions and constructive comments. I am also grateful to Bruce for providing this opportunity to consider some of the geochemical problems posed by hyperacidic lakes. Bali-based landscape photographer, Jessy Eykendorp, very kindly gave permission for reproduction of her Kawah Ijen photograph. I thank Frank Brink for guidance in FESEM methodology. I also want to thank my wife, Meg, for patience and cheerful forbearance through 50 years of geology!

[5] Any economic value for these metal sinks, as mineral deposits, is a consequence of higher order effects such as the specific geometry of transmissive fractures and bulk strength of host rocks as they evolve in the volcano-hosted hydrothermal systems environment. Do all these sinks occur within a continuum? Much speculation has attended this question primarily as an issue for exploration geologists. There are however only a few spatial and broadly temporal locations where economic porphyry and higher level Cu–As–Au mineralisation appears to be coincident.

References

Arribas A, Hedenquist JW, Itaya T, Okada T, Concepción RA, García JS (1995) Contemporaneous formation of adjacent porphyry and epithermal Cu–Au deposits over 300 ka in Northern Luzon, Philippines. Geology 23:337–340

Bani P, Oppenheimer C, Allard P, Shinohara H, Tsanev V, Carn S, Lardy M, Garaebit E (2012) First estimate of volcanic SO_2 budget for Vanuatu island arc. J Volcanol Geoth Res 211–212:36–46

Berger BR, Henley RW (2011) Magmatic-vapor expansion and the formation of high-sulfidation gold deposits: structural controls on hydrothermal alteration and ore mineralization. Ore Geol Rev 39:75–90

Berger BR, Henley RW, Lowers HA, Pribil MJ (2014) The Lepanto Cu–Au deposit, Philippines: a fossil hyperacidic volcanic lake complex. J Volcanol Geoth Res 271:70–82

Botcharnikov RE, Shmulovich KI, Tkachenko SI, Korzhinsky MA, Rybin AV (2003) Hydrogen isotope geochemistry and heat balance of a fumarolic system: Kudriavy volcano, Kuriles. J Volcanol Geoth Res 124:45–66

Brackett RA, Fegley B, Arvidson RE (1995) Volatile transport on Venus and implications for surface geochemistry and geology. J Geophys Res 100:1553–1563

Brown CV (1917) The composition of seleniferous sulfur. Am Miner 2:116–117

Brown G, Rymer H, Dowden J, Kapadia P, Stevenson D, Barquero J, Morales LD (1989) Energy budget analysis for Poas Crater lake: implications for predicting volcanic activity. Nature 339:370–373

Butterfield DA, Nakamura K, Takano B, Lilley M, Lupton JE, Resing JA, Row KK (2012) High SO_2 flux, sulfur accumulation, and gas fractionation at an erupting submarine volcano. Geology 39:803–806

Chouinard A, Williams-Jones A, Leonardson RW, Hodgson CJ, Silva P, Téllez C, Vega J, Rojas F (2005) Geology and genesis of the multistage high-sulfidation epithermal Pascua Au–Ag–Cu deposit, Chile and Argentina. Econ Geol 100:463–490

Christenson BW, Wood CP (1993) Evolution of a vent-hosted hydrothermal system beneath Ruapehu Crater lake, New Zealand. Bull Volcanol 55:547–565

Christenson BW, Reyes AG, Young R, Moebis A, Sherburn S, Cole-Baker J, Britten K (2010) Cyclic processes and factors leading to phreatic eruption events: insights from the 25 September 2007 eruption

through Ruapehu Crater lake, New Zealand. J Volcanol Geoth Res 191:15–32
Churakov SV, Tkachenko SI, Korzhinskii MA, Bocharnikov RE, Shmulovich KI (2000) Evolution of composition of high-temperature fumarolic gases from Kudryavy Volcano, Iturup, Kuril Islands: the thermodynamic modeling. Geochem Int 38:436–451
Clark AH (1970) An occurrence of the assemblage native sulfur–covellite–"Cu5. 5xFexS6. 5x", Aucanquilcha. Chile Am Miner 55:913–918
Cox SF (2005) Coupling between deformation, fluid pressures, and fluid flow in ore-producing hydrothermal systems at depth in the crust. Econ Geol 100th Anniversary Volume: 39–75
Crerar D, Wood S, Brantley S, Bocarsly A (1985) Chemical controls on solubility of ore-forming minerals in hydrothermal solutions. Can Miner 23:333–352
Cunningham CG, Austin GW, Naeser CW, Rye RO, Ballantyne GH, Stamm RG, Barker CE (2004) Formation of a paleothermal anomaly and disseminated gold deposits associated with the Bingham Canyon porphyry Cu–Au–Mo system, Utah. Econ Geol 99:789–806
De Ronde CEJ, Chadwick WW, Ditchburn RG, Embley RW, Tunnicliffe V, Baker ET, Walker SL, Ferrini VL, Merle SM (2014). Molten sulfur lakes of intraoceanic arc volcanoes, (this volume)
Delmelle P, Bernard A (1994) Geochemistry, mineralogy, and chemical modeling of the acid crater lake of Kawah Ijen Volcano, Indonesia. Geochim Cosmochim Acta 58:2445–2460
Delmelle P, Bernard A (2014) The remarkable chemistry of sulfur in volcanic acid crater lakes: a scientific tribute to Bokuichiro Takano and Minoru Kusakabe, (this volume)
Delmelle P, Henley RW, Opfergelt S (2014) Summit acid Crater lakes and flank instability in composite volcanoes, (this volume)
Deyell CL, Bissig T, Rye RO (2004) Isotopic evidence for magmatic-dominated epithermal processes in the El Indio-Pascua Au–Cu–Ag Belt and relationship to geomorphologic setting. Soc Econ Geol Spec Publ 11:55–73
Dolejs D, Manning CE (2010) Thermodynamic model for mineral solubility in aqueous fluids: theory, calibration and application to model fluid-flow systems. Geofluids 10:20–40
Esposito LW (1984) Sulfur dioxide: episodic injection shows evidence for active Venus volcanism. Science 223:1072
Giggenbach WF (1987) Redox processes governing the chemistry of fumarolic gas discharges from White Island, New Zealand. Appl Geochem 2:143–161
González AG (1959) Geology and genesis of the Lepanto copper deposit, Mankayan, Mountain Province, Philippines. Ph.D. dissertation, Stanford University, 102 pp (Unpublished)
Gustafson LB, Hunt JP (1975) The porphyry copper deposit at El Salvador, Chile. Econ Geol 70:857–912
Heise W, Caldwell TG, Bibby HM, Bennie SL (2010) Three-dimensional electrical resistivity image of magma beneath an active continental rift, Taupo Volcanic zone New Zealand. Geophys Res Lett 37:L10301
Heithersay PS, Walshe JL (1995) Endeavour 26 North: a Porphyr Copper-Gold deposit in the Late Ordovician, Shoshonitic Goonumbla Volcanic complex, New South Wales, Australia. Econ Geol 90:1506–1532
Henley RW (1996) Chemical and physical context for life in terrestrial hydrothermal systems: chemical reactors for the early development of life and hydrothermal ecosystems. In: Bock GR, Goode JA (eds) Evolution of hydrothermal ecosystems on Earth (and Mars). Wiley, New York, pp 61–82
Henley RW, Berger BR (2000) Self-ordering and complexity in epizonal mineral deposits. Ann Rev Earth Planet Sci 28:669–719
Henley RW, Berger BR (2011) Magmatic-vapor expansion and the formation of high-sulfidation gold deposits: Chemical controls on alteration and mineralization. Ore Geol Rev 39:63–74
Henley RW, Berger BR (2012) Pyrite-sulfosalt reactions and semimetal fractionation in the Chinkuashih, Taiwan, copper-gold deposit: a 1 Ma paleo-fumarole. Geofluids 12:245–260
Henley RW, Berger BR (2013) Nature's refineries—metals and metalloids in arc volcanoes. Earth Sci Rev 125:146–170
Henley RW, Ellis AJ (1983) Geothermal systems ancient and modern: a geochemical review. Earth-Sci Rev 19:1–50
Henley RW, McNabb A (1978) Magmatic vapor plumes and groundwater interaction in porphyry copper emplacement. Econ Geol 73:1–20
Henley RW, Mavrogenes J, Tanner D (2012) Sulfosalt melts and heavy metal (As–Sb–Bi–Te–Sn–Pb–Tl) fractionation during volcanic gas expansion: the El Indio (Chile) paleo-fumarole. Geofluids 12:199–215
Henley RW, Stewart MK (1983) Chemical and isotopic changes in the hydrology of the Tauhara geothermal field due to exploitation at Wairakei. J Volcanol Geoth Res 15:285–314
Henley RW, Wykes, Jeremy, King, Penelope (2014) Sulfur In Degassing Volcanoes: thermochemistry and experiments, AGU fall meeting, San Francisco, Abstract V13D–06
Hinkley TK (1991) Distribution of metals between particulate and gaseous forms in a volcanic plume. Bull Volcanol 53:395–400
Huber C, Bachmann O, Vigneresse JL, Dufek J, Parmigiani A (2012) A physical model for metal extraction and transport in shallow magmatic systems. Geochem Geophys Geosyst 13. doi:10.1029/2012GC004042
Hunt JP (1977) Porphyry copper deposits. Geol Soc, London, Spec Publ 7:98
Hurwitz S, Kipp KL, Ingebritsen SE, Reid ME (2003) Groundwater flow, heat transport, and water table position within volcanic edifices: Implications for volcanic processes in the Cascade Range. J Geophys Res 108(B12):1–19

Hurst AW, Christenson B, Cole-Baker J (2012) Use of a weather buoy to derive improved heat and mass balance parameters for Ruapehu Crater Lake. J Volcanol Geoth Res 235–236:23–28

Ingebritsen SE, Mariner RH (2010) Hydrothermal heat discharge in the Cascade Range, Northwestern United States. J Volcanol Geoth Res 196:208–218

Jakubowski RT, Fournelle J, Welch S, Swope RJ, Camus P (2002) Evidence for magmatic vapor deposition of anhydrite prior to the 1991 climactic eruption of Mount Pinatubo, Philippines. Am Miner 87:1029–1045

Kaltenegger L, Sasselov D (2009) Detecting planetary geochemical cycles on exoplanets: atmospheric signatures and the case of SO_2. Astrophys J 708:1162

Kavalieris I (1994) High Au, Ag, Mo, Pb, V and W content of fumarolic deposits at Merapi volcano, central Java, Indonesia. J Geochem Explor 50:479–491

King, Penelope, Henley RW, Wykes, Jeremy, Renggli C, Troitzsch, Ulrike, Clark D, O'Neill H, (2014) The role of gas-silicate chemisorption reactions in modifying planetary crusts and surfaces, AGU fall meeting, San Francisco, Abstract V31A–4717

Kim J, Lee KY, Kim JH (2011) Metal-bearing molten sulfur collected from a submarine volcano: implications for vapor transport of metals in seafloor hydrothermal systems. Geology 39:351–354

Lagache M, Weisbrod A (1977) The system: two alkali feldspars-KCl-NaCl-H2O at moderate to high temperatures and low pressures. Contrib Miner Petrol 62 (1):77–101

Liebscher A (2010) Aqueous fluids at elevated pressure and temperature. Geofluids 10:3–19

Luhr JF (2008) Primary igneous anhydrite: progress since its recognition in the 1982 El Chichón trachyandesite. J Volcanol Geoth Rese 175:394–407

Manning CE (1994) The solubility of quartz in H_20 in the lower crust and upper mantle. Geochim Cosmochim Acta 58:4831–4839

Mather TA, Pyle DM, Tsanev VI, McGonigle AJS, Oppenheimer C, Allen AG (2006) A reassessment of current volcanic emissions from the Central American arc with specific examples from Nicaragua. J Volcanol Geoth Res 149:297–311

Mavrogenes J, Henley RW, Reyes AG, Berger B (2010) Sulfosalt melts: evidence of high-temperature vapor transport of metals in the formation of high-sulfidation lode gold deposits. Econ Geol 105:257–262

Migdisov AA, Williams-Jones AE (2013) A predictive model for metal transport of silver chloride by aqueous vapor in ore-forming magmatic-hydrothermal systems. Geochim Cosmochim Acta 104:123–135

Moore JN, Allis RG, Nemčok M, Powell TS, Bruton CJ, Wannamaker PE, Raharjo IB, Norman DI (2008) The evolution of volcano-hosted geothermal systems based on deep wells from Karaha-Telaga Bodas, Indonesia. Am J Sci 308:1–48

Moses JI, Zolotov MY, Fegley B (2002) Photochemistry of a volcanically driven atmosphere on Io: Sulfur and oxygen species from a Pele-type eruption. Icarus 156:76–106

Nisbet EG, Sleep NH (2001) The habitat and nature of early life. Nature 409:1083–1091

Nuccio PM, Paonita A, Sortino F (1999) Geochemical modeling of mixing between magmatic and hydrothermal gases: the case of Volcano Island, Italy. Earth Planet Sci Lett 167:321–333

Oppenheimer C, Scaillet B, Martin RS (2011) Sulfur degassing from volcanoes: source conditions, surveillance, plume chemistry and earth system impacts. Chapter 13 in Sulfur in Magmas and melts: its importance for natural and technical processes. In: Behrens H, Webster JD (eds) Reviews in mineralogy and geochemistry, vol 73, pp 363–421

Pokrovski GS, Zakirov I, Roux J, Testemale D, Hazemann J-L, Bychkov AY, Golikova GV (2005) Experimental study of arsenic speciation in vapor phase to 500 : implications for As transport and fractionation in low-density crustal fluids and volcanic gases. Geochim Cosmochim Acta 66:3453–3480

Pollard PJ, Taylor RG, Peters L (2005) Ages of intrusion, alteration, and mineralization at the Grasberg Cu–Au deposit, Papua, Indonesia. Econ Geol 100:1005–1020

Rouwet D, Tassi F (2011) Geochemical monitoring of volcanic lakes. A generalized box model for active Crater lakes. Ann Geophys 54:161–173

Rowe GL (1991) The acid crater lake system of Poás Volcano, Costa Rica: geochemistry, hydrology, and physical characteristics. Ph.D. thesis. Pennsylvania State University, Pennsylvania

Shinohara H (2008) Excess degassing from volcanoes and its role on eruptive and intrusive activity. Rev Geophys 46 RG4005. doi:10.1029/2007RG000244

Sillitoe RH (2005) Supergene oxidized and enriched porphyry copper and related deposits. In: Heddenquist JW, Thompson JFH, Goldfarb RJ (eds) Economic Geology One Hundredth Anniversary Volume, pp 723–768

Sillitoe RH (2010) Porphyry copper systems. Econ Geol 105:3–42

Stern RJ, Kohut E, Bloomer SH, Leybourne M, Fouch M, Vervoort J (2006) Subduction factory processes beneath the Guguan cross-chain, Mariana Arc: no role for sediments, are serpentinites important? Contrib Miner Petrol 151(2):202–221

Sriwana T, Van Bergen MJ, Varekamp JC, Sumarti S, Takano B, Van Os BJH, Leng MJ (2000) Geochemistry of the acid Kawah Putih lake, Patuha volcano, West Java, Indonesia. J Volcanol Geoth Res 97:77–104

Symonds RB, Rose WI, Gerlach TM, Briggs PH, Harmon RS (1990) Evaluation of gases, condensates, and SO_2 emissions from Augustine volcano, Alaska: the degassing of a Cl-rich volcanic system. Bull Volcanol 52:355–374

Takano B, Saitoh H, Takano E (1994) Geochemical implications of subaqueous molten sulfur at Yugama Crater lake, Kusatsu-Shirane volcano, Japan. Geochem J 28:199–216

Takano B, Suzuki K, Sugimori K, Ohba T, Fazlullin SM, Bernard A, Sumarti S, Sukyar R, Hirabayashi M

(2004) Bathymetric and geochemical investigation of Kawah Ijen Crater lake, East Java, Indonesia. J Volcanol Geoth Res 135:299–329

Takano B, Kuno A, Ohsawa S, Kawakami H (2008) Aqueous sulfur speciation possibly linked to sublimnic volcanic gas-water interaction during a quiescent period at Yugama Crater lake, Kusatsu-Shirane volcano, Central Japan. J Volcanol Geoth Res 178:145–168

Taran YA (2009) Geochemistry of volcanic and hydrothermal fluids and volatile budget of the Kamchatka-Kuril subduction zone. Geochim Cosmochim Acta 73:1067–1094

Taran YA, Hedenquist JW, Korzhinsky MA, Tkachenko SI, Shmulovich KI (1995) Geochemistry of magmatic gases from Kudryavy volcano, Iturup, Kuril Islands. Geochim Cosmochim Acta 59:1749–1761

Taran YA, Bernard B, Gavilanes J-C, Africano F (2000) Native gold in mineral precipitants from high temperature volcanic gases of Colima volcano, Mexico. Appl Geochem 15:337–346

Taran YA, Bernard A, Gavilanes JC, Lunezheva E, Cortes A, Armienta MA (2001) Chemistry and mineralogy of high-temperature gas discharges from Colima volcano, Mexico. Implications for magmatic gas–atmosphere interaction. J Volcanol Geoth Res 108:245–264

Taran Y, Rouwet D, Inguaggiato S, Aiuppa A (2008) Major and trace element geochemistry of neutral and acidic thermal springs at El Chichón volcano, Mexico: Implications for monitoring of the volcanic activity. J Volcanol Geoth Res 178:224–236

Terada A, Hashimoto T, Kagiyama T (2012) A water flow model of the active crater lake at Aso volcano, Japan: fluctuations of magmatic gas and groundwater fluxes from the underlying hydrothermal system. Bull Volcanol 74:641–655

van Hinsberg V, Berlo K, Sumarti S, Van Bergen M, Williams-Jones A (2010) Extreme alteration by hyperacidic brines at Kawah Ijen volcano, East Java, Indonesia: II: metasomatic imprint and element fluxes. J Volcanol Geoth Res 196:169–184

Varekamp JC, Pasternack GB, Rowe GL (2000) Volcanic lake systematics II chemical constraints. J Volcanol Geoth Res 97:161–179

Varekamp JC, Ouimette AP, Herman SW, Flynn KS, Bermudez A, Delpino D (2009) Naturally acid waters from Copahue volcano, Argentina. Appl Geochem 24:208–220

Varley NR, Taran YA (2003) Degassing processes of Popocatépetl and Volcán de Colima, Mexico. In Oppenheimer C (ed) Volcanic Degassing, vol 213. Geological Society, London Special Publication, pp 263–280

Vigneresse JL (2012) Chemical reactivity parameters (HSAB) applied to magma evolution and ore formation. Lithos. doi:10.1016/j.lithos.2012.03.014

Wallace PJ, Edmonds M (2011) The sulfur budget in magmas: evidence from melt inclusions, submarine glasses, and volcanic gas emissions. Rev Mineral Geochem 73:215–246

Webster JD, Botcharnikov RE (2011) Distribution of sulfur between melt and fluid in SOHC–Cl-bearing magmatic systems at shallow crustal pressures and temperatures. Rev Miner Geochem 73:247–283

Williams-Jones G, Stix J, Heiligmann M, Charland A, Sherwood-Lollar B, Arner N, Garzón G, Barquero J, Fernández E (2000) A model of diffuse degassing at three subduction-related volcanoes. Bull Volcanol 62:130–142

Williams-Jones G, Stix J, Hickson C (2008) The COSPEC cookbook: making SO_2 measurements at active volcanoes. IAVCEI, Meth Volcanol 1:233

Williams-Jones G, Vigouroux-Caillibot N, van Hinsberg V, Williams-Jones A (2010) Application of the multiGAS sensor to geothermal exploration and monitoring: comparison of plume and fumarole gas compositions at Kawah Ijen Volcano Indonesia. AGU Fall Meet Abstr 1:2

Yudovskaya MA, Distler VV, Chaplyygin IV, Mokhov AV, Trubkin NV, Gorbacheva SA (2006) Gaseous transport and deposition of gold in magmatic fluid: evidence from the active Kudryavy volcano, Kurile Islands. Miner Deposita 40:828–848

Zajacz Z, Seo JH, Candela PA, Piccoli PM, Heinrich CA, Guillong M (2010) Alkali metals control the release of gold from volatile-rich magmas. Earth Planet Sci Lett 297:50–56

Zajacz Z, Seo JH, Candela PA, Piccoli PM, Tossell JA (2011) The solubility of copper in high temperature magmatic vapors: a quest for the significance of various chloride and sulfide complexes. Geochim Cosmochim Acta 75:2811–2827

Isotope Fractionation and HCl Partitioning During Evaporative Degassing from Active Crater Lakes

Dmitri Rouwet and Takeshi Ohba

Abstract

This chapter provides the theoretical background and necessary practical tools to study one of the most spectacular natural features: vigorous evaporation from active crater lakes. We will give qualitative insights (lake water chemical—Cl content, and isotopic composition) rather than quantify evaporation fluxes from lakes. A major problem is that, with the current methods, we are only able to sample the lake water, while the input fluid rising into the lake (sublacustrine) and evaporation plume coming off the lake remain "inaccessible". This means that the lake behaves as a "black box", being the result of incoming and outgoing fluids of unknown chemical and isotopic composition. As visually demonstrated at many active crater lakes, evaporation is a major process. Strong evaporation from the lake surface will affect the isotopic composition of the remnant lake water, and the "steam devils" (evaporation plume) swirling over the lake. It is found that the kinetic (diffusion) isotope fractionation overshadows the equilibrium isotope fractionation effect, as a dynamic crater lake is intuitively hard to imagine as an equilibrated system. Besides a hot water mass in evaporation, water of active crater lakes is generally a hyper-saline (total salinity >100,000 mg l^{-1}) and hyper-acidic brine (pH as low as −0.5). Although "small scale" equilibrium fractionation effects, the "isotope salt effect" and "isotope acid effect" lead to isotopically heavier evaporation plumes, with respect to vapor coming off pure neutral water. Besides isotope fractionation of the water itself under such extreme lake conditions, HCl_{gas} (and HF) will partition between the liquid and vapor phases. HCl degassing

D. Rouwet (✉)
Istituto Nazionale di Geofisica e Vulcanologia,
Sezione di Bologna, Via Donato Creti 12, 40128
Bologna, Italy
e-mail: dmitri.rouwet@ingv.it

T. Ohba
Department of Chemistry, School of Science, Tokai
University, Kanagawa, Japan

D. Rouwet et al. (eds.), *Volcanic Lakes*, Advances in Volcanology,
DOI 10.1007/978-3-642-36833-2_7,
© Springer-Verlag Berlin Heidelberg 2015

is enhanced when pH is continuously lowered by the input of acidic gases (SO_2, HCl, HF), lake temperature is higher, and evaporation is physically favored by wind or lake convection. It is empirically deduced that HCl partitioning into the vapor phase is chemically controlled by the lake water temperature and density, rather than the Cl content or pH. A better quantification of the chemical and isotopic composition of evaporative gas plumes from active crater lakes will be of importance for volcano monitoring when we aim to deduce the flux and composition of the "hot magmatic end member", through chemical and isotope budget analyses. A major challenge for the future is to develop field methods to enable to sample the evaporation plume coming off lake surfaces, so we can directly determine its chemical and isotopic composition and compare them with the theoretical approach presented in this review chapter.

Keywords

Active crater lakes · Evaporation · Isotope fractionation · Isotope salt effect · Isotope acid effect · HCl partitioning · Evaporative degassing

1 Introduction

Crater lakes are windows into the depth of volcanic-hydrothermal systems. They provide the advantage to preserve eventual changes in fluid cycling with time, whereas such variations in fumarolic gases from volcano craters will be lost to the atmosphere as a "snapshot". Nevertheless, this "memory" of the crater lake can never trace back in time for periods longer than the residence time of the lake water (Varekamp 2002, 2015; Taran et al. 2013; Rouwet et al. 2014). As will turn out from this chapter: the lake water is the best we have available. But is it sufficient to close our story?

It is sometimes accepted that increases in Cl and SO_4 contents in crater lake waters directly point to enhanced degassing of the underlying magmatic-hydrothermal system (Martínez et al. 2000). This is not always true, for several reasons: (1) it has been demonstrated that crater lake water, and thus its solutes and isotopic composition, are subject to fast (re)cycling in a heat pipe mechanism (Hurst et al. 1991; Rowe et al. 1992a; Christenson and Wood 1993), implying that the measured Cl, SO_4 contents and isotopic composition are not necessarily newly derived from a fresh magma, and (2) considering the crater lake as an "open system", the interaction with the atmosphere can strongly modify the chemical and isotopic composition at any instant, especially under high-temperature (occasionally near-boiling) and extremely acidic lake water conditions (near zero pH). To partially solve these inconveniences, it is useful to track variations with time of ratios between solutes, such as SO_4/Cl and Mg/Cl ratios (Giggenbach 1975; Rowe et al. 1992b; Ohba et al. 2008; Rouwet et al. 2014). Due to the presence of a water body (i.e. the crater lake and surrounding volcano-hydrothermal system), these ratios definitely do not reveal the same information as for open-conduit degassing volcanoes: processes of scrubbing/absorption and evaporation/boiling strongly overprint the marker of direct magmatic degassing (Symonds et al. 2001), although a similar concept can be adopted, respecting particular rules for a water-dominated system, instead of magma. A steady increase in SO_4/Cl ratios of extremely acidic crater lake water often indicate enhanced loss of Cl (HCl_{gas}) during evaporation (Rowe et al. 1992b) (Fig. 1), while an increase in Mg/Cl ratios rather suggest renewed Mg-leaching from a recently crystallized magma during water-rock interaction (Giggenbach and Glover 1975; Ohba et al. 2008), and/or, again, enhanced Cl loss by evaporation.

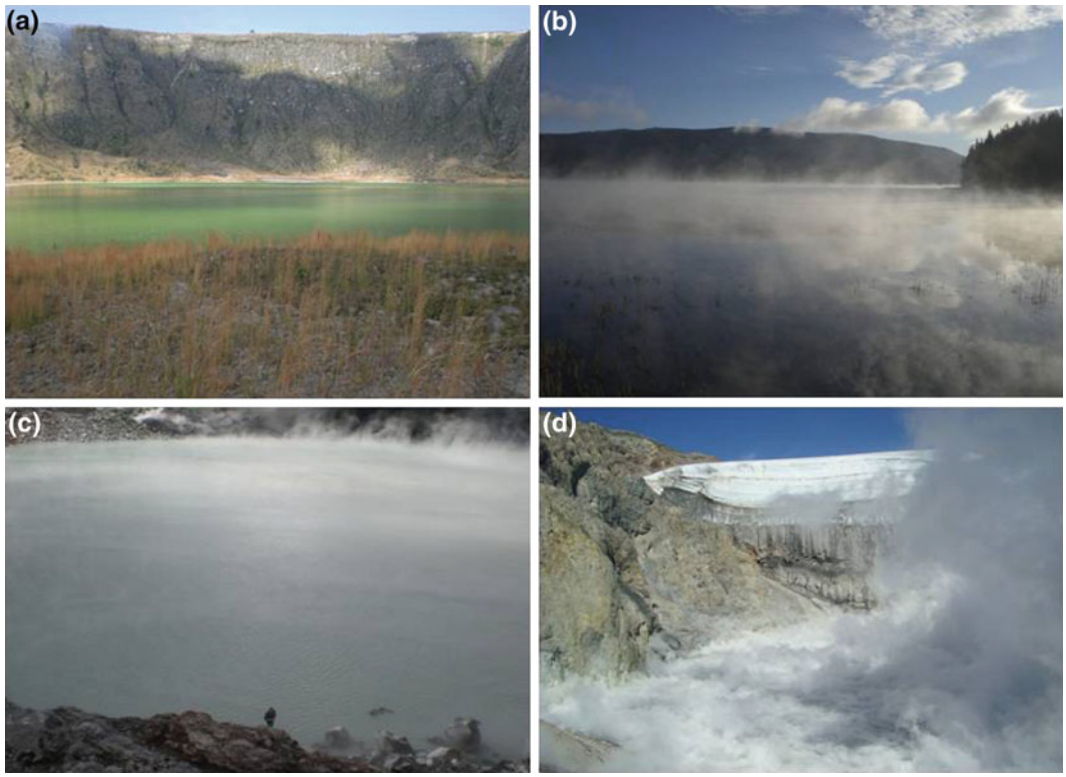

Fig. 1 Evaporation and degassing features from active crater lakes. **a** El Chichón, Mexico (November 2009; *Picture* D. Rouwet). **b** Paulina lake, Newberry Caldera, Oregon-USA (August 2010; *Picture* D. Rouwet). **c** Laguna caliente, poás volcano, Costa Rica (December 2009; *Picture* R.A. Mora-Amador). **d** Copahue, Argentina-Chile (January 2012; *Picture* A.T. Caselli)

The physical manifestation of evaporative degassing from active crater lakes strongly depends on the lake water temperature and the atmospheric conditions near the lake (Fig. 1). A more visual evaporation plume does not necessarily mean a higher evaporation rate, as the plume is better distinguished for a low relative temperature and low humidity climatic conditions: the El Chichón crater lake (Chiapas, Mexico) is of medium temperature (30 °C) and atmospheric conditions are tropical (high humidity, high ambient T) (Fig. 1a) leading to a practically invisible plume; Paulina Lake at the Newberry Caldera (Oregon, USA) has a low temperature (<20 °C) but cold ambient air is at low humidity (Fig. 1b) resulting in well defined clouds hovering over the lake; Poás' Laguna Caliente has a high temperature (49 °C) under high altitude conditions (~2,500 m asl) in a tropical climate (Fig. 1c), leading to a well visible plume; the hot lake at Copahue (>50 °C) in dry, high altitude Andean climatic conditions leads to visually vigorous plume degassing (Fig. 1d).

The ambiguous observations discussed above stress the need to review existing theoretical findings and provide practical tools to best describe the dynamic and complex systems of active crater lakes, subject to evaporative degassing. This review chapter will mainly focus on how Cl and water isotopes partition from its source (magmatic-hydrothermal system) to the atmosphere, passing a crater lake. The main focus is on evaporative degassing of acid saline crater lakes. We aim to give a partially quantitative insight into isotopic fractionation and $Cl_{liq} - HCl_{gas}$ partitioning during evaporation and boiling/steam separation, the two major processes in crater lake bearing systems.

2 The Behavior of Cl and Water Isotopes in Crater Lakes

Figure 2 shows the relationship between the two major parameters in this review chapter, Cl and δD, for waters of several peak and high activity crater lakes (Pasternack and Varekamp 1997; active crater lakes hereafter): El Chichón (Mexico; Rouwet et al. 2008), Lake Yugama (Kusatsu-Shirane volcano, Japan; Ohba et al. 2000), Kawah Ijen (Indonesia; Delmelle et al. 2000), Kawah Putih (Indonesia; Sriwana et al. 2000), Copahue (Argentina; Agusto 2011), Pinatubo (Philippines; Stimac et al. 2004), Taal (Philippines; Delmelle et al. 1998), Poás (Rouwet, Mora-Amador personal data), Rincón de la Vieja (Tassi et al. 2005), Irazú, Turrialba (ephemeral lake 2009, Rouwet, Mora-Amador personal data) (Costa Rica, the latter four). Most data sets for separate lakes show positive linear trends. This indicates: (1) mixing between a Cl-free meteoric end member and a Cl-rich, isotopically heavy "volcanic" end member, and/or (2) the occurrence of a common process which enriches the lake water in both Cl and the heavy isotope (Federico et al. 2010). Without entering in detail on the theoretical background, at this point the evaporation of a heated water body and the input of a Cl-rich "magmatic" fluid intuitively seem to be the most plausible processes to fit the observations.

Taran et al. (1989) and Giggenbach (1992) defined the "andesitic water" (AW hereafter) as the high temperature parental magmatic fluid that occasionally affects the isotopic composition of hydrothermal fluids ($\delta^{18}O$ = 7.5 ± 2.5 ‰, δD = −20 ± 10 ‰). Considering that this AW will be accompanied by a high temperature volcanic gas phase (HTVG hereafter), this fluid is also the

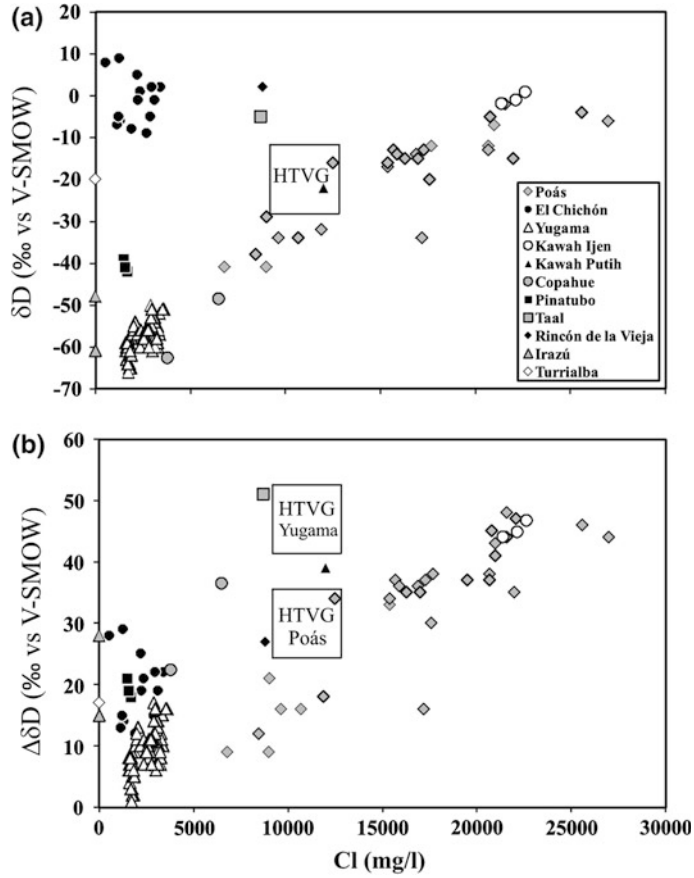

Fig. 2 **a** Cl versus δD diagram for the selected crater lake waters. HTVG = high temperature volcanic gas, with a Cl content of 11,000 mg/l and δD composition as the "andesitic water" (Taran et al. 1989; Giggenbach 1992). **b** Cl versus ΔδD diagram for selected crater lake waters. $\Delta\delta D = \delta D_L - \delta D_{lmw}$ (L = lake, lmw = local meteoric water). The HTVG area for Yugama and Poás crater lakes are presented

major, or often, the only Cl-source for active crater lakes. A proxy of the HTVG is liberated at high temperature fumaroles of actively degassing volcanoes. For 37 samples of such fumaroles at six different volcanoes (White Island, Momotombo, Poás, Satsuma-Iwojima, Kudryavy, Volcán de Fuego de Colima; Giggenbach 1975; Menyailov et al. 1986; Brantley et al. 1987; Shinohara et al. 1993; Taran et al. 1995, 2001), assuming all HCl is condensed in the liquid phase, an average Cl content of 11,000 mg/l was detected, although with a large natural range from 2,000 to 35,000 mg/l of Cl.

Plotting the HTVG-AW in Fig. 2a, no clear trend exists with the hypothetical HTVG-AW suggesting that the input of HTVG-AW is a dominating process even for the most active crater lakes. Only one crater lake consistently plots within the HTVG-range (Kawah Putih), although more data are necessary to rule out coincidence. For Lake Yugama, a direct mixing between a meteoric end-member and the HTVG-AW is plausible (Ohba et al. 2000). Higher Cl contents and δD values for Poás and Kawah Ijen waters, beyond the HTVG-AW values, suggest the input of an even more Cl-D-enriched fluid, or the additional effect of evaporation from a HTVG-AW containing fluid. Data for Copahue crater lake (two samples) fit the lower end of the Poás-Kawah Ijen trend. Single data for Taal and Rincón de la Vieja crater lakes are heavier than the HTVG-AW (Fig. 2a). Delmelle et al. (1998) suggest a seawater source for Cl in Taal crater lake, thus anomalous within the present point of view. The virtually Cl-free crater lakes of Turrialba and Irazú volcanoes result from steam condensation upon HCl scrubbing in the underlying boiling aquifer. Pinatubo and El Chichón crater lakes are Cl-poor and relatively enriched in D. For these lakes, a peculiar dynamics was discovered: the surface runoff entrance of Cl-containing waters from geyser-like springs in the crater is thought to be the only Cl-source for these lakes (Rouwet et al. 2004, 2008; Stimac et al. 2004). The large scatter of El Chichón data is the effect of (1) evaporation of a meteoric water body, (2) mixing with the geyser waters, and (3) evaporation of the resulting mixed fluid. A direct input of the HTVG-AW was excluded by Rouwet et al. (2008). The Cl content and isotopic composition of Pinatubo crater lake waters are probably due to similar processes.

As the main water source of any crater lake is meteoric precipitation, it is more appropriate to plot the difference between δD_L and δD_{lmw} ($\Delta\delta D$ is the shift in δD relative to the local meteoric water), using the δD_{lmw} for local meteoric water at each lake (Fig. 2b). This allows a direct comparison between the various lakes. The same trends as in Fig. 2a are observed, suggesting that evaporation and the eventual input of the isotopically heavy, Cl-rich "magmatic" end member (HTVG-AW) is overwhelming.

With the reasonable assumptions that the isotopic enrichment in the lake water is linearly correlated with the temperature difference between lake and air (see next section), and that the Cl content is proportional to the input of the "hot magmatic end member" (to be defined for each lake and thus not necessarily HTVG or AW), Ohba et al. (2000) introduced a simple model to quantify the above processes, expressed by the following equation:

$$\Delta\delta D = a\Delta T + bCl_L \quad (1)$$

where ΔδD is the shift in δD relative to the local meteoric water, ΔT is the difference in temperature between the lake and the air, and Cl_L is the Cl content in the lake water. The coefficients "a" and "b" are empirical for now. Dividing both sides by Cl_L yields:

$$\Delta\delta\Delta/Cl_L = a\Delta T/Cl_L + b \quad (2)$$

The coefficient "b" is the intercept of the regression line with a slope "a" and indicates the relationship between the Cl content and the isotopic shift in case no evaporation takes place (Fig. 3). On the other hand, "a" reflects the effect on the Cl content and isotopic shift in the lake water due to evaporation only (Ohba et al. 2000) (Fig. 3). This procedure was applied for the three crater lakes with the larger data sets (Poás, Yugama and El Chichón) (Fig. 3a). The calculated values for the "a" and "b" coefficients are

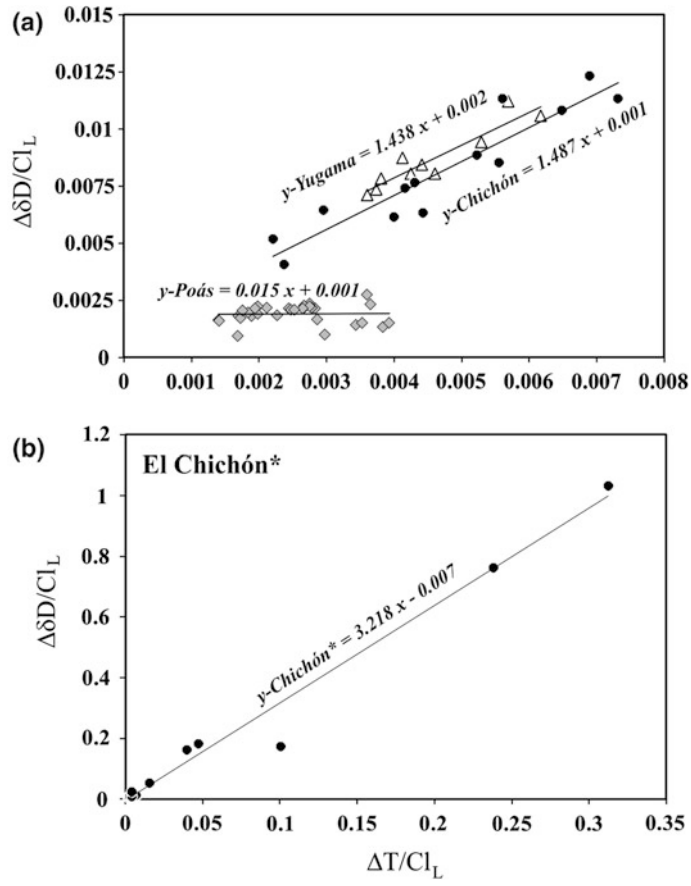

Fig. 3 **a** $\Delta T/Cl_L$ versus $\Delta\delta D/Cl_L$ diagram for Lake Yugama, Laguna Caliente (Poás) and El Chichón crater lake, as deduced by Ohba et al. (2000) as shown in Eq. (2). The linear regression lines are graphed to deduce the "a" and "b" values (following "y = ax + b", where $x = \Delta T/Cl_L$ and $y = \Delta\delta D/Cl_L$) where "a" reflects the effect on the Cl content and isotopic shift in the lake water due to evaporation only, and "b" indicates the relationship between the Cl content and isotopic shift in case no evaporation takes place. Data for El Chichón do not include the Cl-rich samples which are subject to the peculiar "lake-spring" dynamics (Rouwet et al. 2008), while b deals with the entire El Chichón data set, to demonstrate the large effect of the springs discharging into the crater lake

shown in Table 1. The percentage of enrichment due to evaporation, "% E", is obtained by (Ohba et al. 2000):

$$\%\,E = [a\Delta T / (a\Delta T + bCl_L)]100\,(\%) \quad (3)$$

It is clear that the Laguna Caliente crater lake of Poás is more affected by the input of the hot magmatic end member, with respect to Lake Yugama and the El Chichón crater lake. Despite the high temperature difference between the lake water and the atmosphere, isotopic enrichment is only accounted for by evaporation for 2–6 %, while 72–82 % and 77–82 % for Lake Yugama and El Chichón crater lake, respectively. This is demonstrated by the low slope ("a" value) in Fig. 3a. Nevertheless, at this point it is impossible to better characterize this hot magmatic end member for Poás' Laguna Caliente; it probably is a Cl-rich, isotopically heavy fluid as the residual fluid after steam separation from recycled lake water. Ohba et al. (2000) defined the parental fluid, a liquid phase or vapor phase quenched in the cooler lake water (i.e. hot magmatic end

Table 1 Numerical results of the method introduced by Ohba et al. (2000) for the data set of Poás' Laguna Caliente, Lake Yugama, and El Chichón crater lake

Lake	ΔT_{min} (°C)	ΔT_{max} (°C)	Cl_{min} (mg/l)	Cl_{max} (mg/l)	a (‰/°C)	b (‰/ppm)	% evap
Poás	9	48	6,800	27,000	0.015	0.001	2–6
Yugama	9.5	12.4	1,660	3,283	1.438	0.002	72–82
El Chichón	11	25	1,148	3,413	1.487	0.001	77–82
El Chichón*	11	33	32	3,413	3.218	−0.007	∼100

The *indicates the results for El Chichón crater lake including the Cl-rich samples, which are subject to a particular "lake-spring" dynamics (Rouwet et al. 2008)

member) for Lake Yugama as an isotopically heavy end member with a Cl content of ∼11,600 ppm and a temperature of ∼197 °C, entering from beneath the lake (Fig. 3a). At Lake Yugama in 1988 to 1996, the a and b values were evaluated to be 1.438‰/C and 0.002 ‰/ppm, respectively (Table 1). The averaged ΔT and Cl_L during the corresponding period were respectively 11.25 °C and 2,550 mg/l, resulting in the observation that 72–82 % of ΔD is due to the evaporation effect. The remaining 18–28 % of ΔD is attributed to the addition of an isotopically heavy fluid.

For the entire data set of El Chichón crater lake, an "a" value of 3.218 and a negative "b" value of −0.007 are obtained (Fig. 3b, and El Chichón* in Table 1). These outcomes confirm that no magmatic Cl-rich fluid enters El Chichón crater lake and that isotopic enrichment seems to completely result from evaporation (∼100 % in Table 1). Nevertheless, these outcomes are strongly overprinted by the geyser-lake dynamics (Rouwet et al. 2004, 2008; Taran and Rouwet 2008): instead of a hot magmatic end member entering from beneath the lake such as for Lake Yugama and Laguna Caliente, the geyser at El Chichón periodically discharges Cl-rich water into the lake. This water seems to have its particular isotopic composition of $\delta D = -10 \pm 10$ ‰ and Cl content near 2,000 mg/l (Rouwet et al. 2008). When this Cl-input ceases, the lake becomes Cl-free almost immediately. To make a comparison with Lake Yugama and Poás possible, we should take the Cl-poor samples out of the data set, as they demonstrate the El Chichón crater lake as a steam-heated pool without other external influences. The "a" and "b" values become very similar as for Lake Yugama (Table 1), resulting in an isotopic enrichment upon evaporation (77–82 %).

3 Theoretical Background Behind These Observations

3.1 Isotopic Fractionation of Water During Evaporation

Beyond the approach on what the data can teach us in the first place, what is the theoretical background of the behavior of δD and Cl in active crater lake waters? In nature, evaporation is the first step of the hydrologic cycle. It is demonstrated that quantifying the evaporation flux from water bodies is extremely difficult, especially for natural, dynamic and heated systems such as active crater lakes (Harbeck 1964; Weisman and Brutsaert 1973; Ryan et al. 1974; Sill 1983; Brown et al. 1989; Adams et al. 1990; Hurst et al. 1991, 2012, 2015; Ohba et al. 1994; Lee and Swancar 1997; Pasternack and Varekamp 1997; Sartori 2000; Taran and Rouwet 2008; Fournier et al. 2009). Moreover, with a more qualitative scope: what is this liberated vapor composed of? An adequate method to sample the "steam devils" swirling over lake surfaces (Hurst et al. 2012) remains challenging, and the isotopic composition of the evaporation plume can so far only be calculated from empirically or theoretically deduced equations. As the light isotope prefers to partition in the vapor phase we know that the evaporation plume will be isotopically lighter than the remnant lake water, but to which extend and why?

We should keep in mind that even for crater lakes topping highly active magmatic-hydrothermal systems, the major constraint in defining the isotopic composition of the lake water and its derived evaporative vapor is initially the meteoric precipitation. In physical terms, a crater lake would not even exist without abundant meteoric recharge (Pasternack and Varekamp 1997).

3.1.1 Evaporation Models Revised

Evaporation is the major water mass exchange process at the interface between two inherently non-equilibrium systems, in our case, the atmosphere and a heated crater lake disturbed by an active volcano—in an unknown way that we aim to decipher. If the atmosphere-lake interface would be in thermodynamic equilibrium, the equilibrium isotopic fractionation would be determined by well defined theoretical and experimental laws (e.g., Bigeleisen 1961; Horita and Wesolowski 1994). Horita et al. (1993a) demonstrated experimentally that an equilibrium δD was only attained after a few hours, utopia for a natural system such as a crater lake. Moreover, many authors have demonstrated that for heated pools and lakes the diffusion-controlled (kinetic) fractionation process predominates over equilibrium fractionation (Craig et al. 1963; Craig and Gordon 1965; Giggenbach and Stewart 1982; Gonfiantini 1986; Rowe 1994; Varekamp and Kreulen 2000). Besides the difference between the equilibrium and kinetic fractionation, affecting the isotopic composition of the remnant lake water and evaporation plume, the mode of steam separation strongly influences isotopic fractionation. During single-step steam separation the vapor phase separates from the liquid continuously meanwhile both phases are assumed to "travel together" and thus seek isotopic equilibrium until the vapor is liberated from the system, at a given pressure (depth) and temperature. On the contrary, during continuous steam separation the vapor phase is immediately removed from the liquid phase as it is formed, at a given pressure (depth) and temperature. More in particular for vapor separation at atmospheric pressure (i.e. evaporation), the single-step steam separation refers to steady-state evaporation from a continuously heated and replenished pool (e.g., an active crater lake unaffected by wind removal of the evaporation plume), while continuous steam separation rather implies the constant removal of the evaporating liquid phase (e.g., an active crater lake where the evaporation plume is constantly removed by wind). The latter is called Rayleigh evaporation (Giggenbach 1978; Giggenbach and Stewart 1982). It is clear that the mode of evaporation of active crater lakes is not unambiguously defined, nor constant with time.

3.1.2 From the Lake Boundary Layer into the Atmosphere: Where It All Happens

The vapor emitted from crater lakes will have its characteristic isotopic composition (δD and $\delta^{18}O$) reflecting the physical-chemical conditions of the lake surface layer and the atmospheric conditions of the boundary layer between the lake and atmosphere (Varekamp and Kreulen 2000). More in particular, the isotopic composition of the evaporation plume of a heated crater lake results from both (1) equilibrium fractionation at the thin turbulent boundary layer with a vapor pressure dependent on the lake water temperature, and (2) kinetic fractionation at the interface between the boundary layer and the open-air with a vapor pressure dependent on the atmospheric temperature and relative atmospheric humidity (Varekamp and Kreulen 2000; Cappa et al. 2003, and references herein). Figure 4 schematically shows what happens when a heated crater lake evaporates. Evaporation takes place in two interdependent steps. Right above the lake surface, a thin boundary layer forms, which is composed of saturated water vapor reigned by the lake water temperature. The isotopic composition of this vapor relates to the one of the lake by the equilibrium fractionation factor α_{eq} (Fig. 4). The value of the T-dependent α_{eq} is well constrained (Majoube 1971; Gonfiantini 1986; Horita and Wesolowski 1994; Barkan and

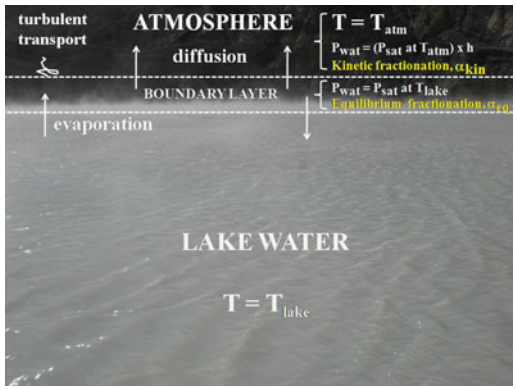

Fig. 4 Sketch of the evaporation dynamics from the lake surface, through the thin boundary layer (equilibrium isotopic fractionation effect), towards the open atmosphere by diffusion and turbulent transport (kinetic isotopic fractionation effect) [modified from Varekamp and Kreulen (2000)]

Luz 2005). Based on earlier work and on further experiments, Horita and Wesolowski (1994) reported a now generally accepted equation to estimate the δD and $\delta^{18}O$ of the vapor phase by equilibrium isotope fractionation (α_{eq}) during evaporation (α_{eq} is expressed in per mil versusV-SMOW):

$$10^3 \ln \alpha_{eq}(D) = 1158.8\left(T^3/10^9\right) - 1620.1\left(T^2/10^6\right) + 794.84\left(T/10^3\right) - 161.04 + 2.9992\left(10^9/T^3\right) \quad (4)$$

$$10^3 \ln \alpha_{eq}\left(^{18}O\right) = -7.685 + 6.7123\left(10^3/T\right) - 1.6664\left(10^6/T^2\right) + 0.35041\left(10^9/T^3\right) \quad (5)$$

Figure 5 presents the classic Craig diagram, the $\delta^{18}O$ versus δD plot, for the data compiled for the selected crater lakes. Several near linear trends are immediately evidenced. The linear evolution of the stable isotope composition of a remnant water body was established as the "Craig-Gordon model" (Craig and Gordon 1965; Gat 1981, 2008; Gonfiantini 1986; Horita et al. 2008). With respect to the Global Meteoric Water Line (GMWL in Fig. 5) the data for the warm crater lake waters plot with "flatter slopes" (Varekamp and Kreulen 2000). This was first thought as being the effect of water-rock interaction processes between the lake water and sediments, causing a positive oxygen shift, but (Rowe 1994) explained that this effect is dwarfed by kinetic evaporation processes. The flat slopes are rather created by the difference in relative kinetic isotopic fractionation (Giggenbach 1978), being larger for ^{18}O than for D, with the slope a function of h, the relative atmospheric humidity. Data confirm here that the kinetic evaporation effect by turbulent diffusion into the atmosphere (Fig. 4) dominates over the equilibrium evaporation effect at the lake boundary layer. Conceptually, the proportion of this kinetic fractionation can be described as the "concentration difference" between the open atmosphere and the boundary layer, although it consists of molecular diffusion through a laminar boundary layer and "eddy diffusion" through a turbulent zone (Craig and Gordon 1965) (Fig. 4).

As the kinetic fractionation effect on evaporating lakes is larger than the well constrained equilibrium fractionation effect (Eqs. (4) and (5), Horita and Wesolowski 1994), there is a strong need to better define the kinetic fractionation effects of oxygen and hydrogen. Only recently, experimental work by Cappa et al. (2003) and Luz et al. (2009) dealt with the question about the ratio between the kinetic fractionation factors for O and H. The total isotopic fractionation factor (α_{ev}) between the steam devils and the lake is defined as (Luz et al. 2009):

$$\alpha_{evap} = R_w/R_e \quad (6)$$

where R_w and R_e are the ratios between the heavy and the light isotopic species of water in the lake water and evaporative plume ($^1H^2H^{16}O/^1H_2^{16}O$ or $^1H_2^{18}O/^1H_2^{16}O$), respectively. If we consider the moment of observation (typically the moment of lake water sampling) as representative for a period of steady-state evaporation, the following equation counts (Luz et al. 2009):

$$\alpha_{evap(H_2O)} = \frac{R_w}{R_e} = \frac{\alpha_{kin(H_2O)}\alpha_{eq(H_2O)}(1-h)}{1-\alpha_{eq(H_2O)}h\left(\frac{R_a}{R_w}\right)} \quad (7)$$

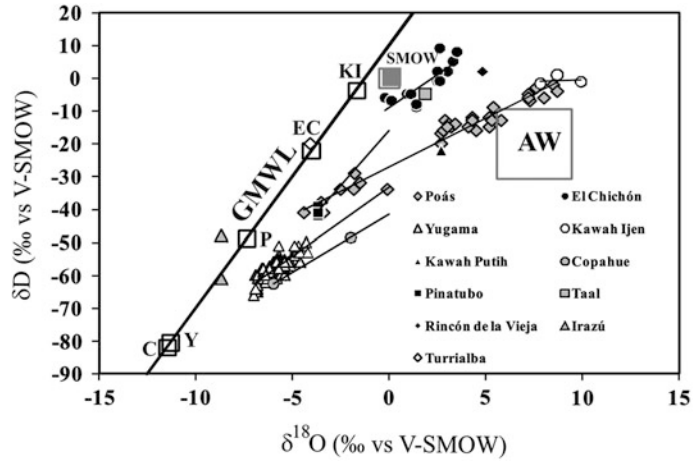

Fig. 5 Craig diagram, $\delta^{18}O$ versus δD, for the selected crater lake waters. AW = andesitic water (Taran et al. 1989; Giggenbach 1992), *SMOW* Standard Mean Ocean Water (standard), *GMWL* Global Meteoric Water Line. The black squares along the GMWL are selected meteoric end members for the various lake areas (*KI* Kawah Ijen, *EC* El Chichón, *P* Poás, *Y* Yugama, *C* Copahue). Data sets for single lakes plot along "flatter slopes" with respect to the GMWL

where $\alpha_{eq(H_2O)}$ is the equilibrium isotopic fractionation factor between liquid and vapor (for H_2O); R_a is the isotopic ratio of air moisture above the lake; $\alpha_{kin(H_2O)}$ is the kinetic isotopic fractionation factor between liquid and vapor; h is relative humidity normalized to average lake-surface temperature (vapor pressure of the air divided by saturation vapor pressure at the lake-surface temperature, Varekamp and Kreulen 2000). This normalization is necessary, as for hot lakes the lake water temperature strongly influences the air humidity in the boundary layer. Oppenheimer (1997) stressed that the directly measured lake water temperature at the lake surface is typically a few degrees higher than the actual lake surface temperature. This "skin effect" should be considered when calculating h. Similarly, Ward and Stanga (2001) demonstrated that the top 0.5 mm thick layer of the evaporating surface (the "skin") has a uniform temperature which is lower than the bulk water temperature. Moreover, evaporation is intrinsically an endothermic process, which leads to surface cooling if no heat is supplied to the surface (Cappa et al. 2003). On the other hand, for highly active crater lakes, where heat supply is high and continuous, the "skin effect" is extremely hard to quantify, which inevitably leads to large uncertainties in evaporation flux estimates (e.g., Brown et al. 1989 and later work) and isotopic fractionation effects. If the "simple" atmosphere is inherently a non-equilibrium system, the atmosphere above a hot crater lake is even further from equilibrium.

With the reasonable assumption that the lake water itself is the only source of water vapor in the air column overlying the lake, $R_a = R_e$ and $\alpha_{evap} = R_w/R_a$, and so Eq. (7) can be written in function of $\varepsilon_{kin(H_2O)}$ (Luz et al. 2009):

$$\alpha_{kin(H_2O)} = \frac{\frac{\alpha_{evap(H_2O)}}{\alpha_{eq(H_2O)}} - h}{1 - h} \tag{8}$$

where h is calculated as before, and $\alpha_{evap(H_2O)}$ from Rayleigh fractionation experiments. Earlier work on evaporating lakes in tropical areas used the slope of the evaporation trend as a major variable, hence the theoretical relation with the equilibrium and kinetic evaporation process can be expressed as (Sacks 2002; Taran and Rouwet 2008):

$$\text{slope} = \frac{h(\delta_a - \delta_i)_D + \varepsilon_{evap-D}}{h(\delta_a - \delta_i)_{18} + \varepsilon_{evap-18}} \tag{9}$$

δ_a is the isotopic composition of atmospheric moisture; δ_i is the isotopic composition of inflows to the lake (volume-weighted precipitation, ground inflow of thermal waters or sublacustrine input of fluids); ε_{evap} is the total isotopic separation factor for H and O separately, equal to:

$$\varepsilon_{evap} = 1000(1-\alpha_{eq}) + \varepsilon_{kin} \qquad (10)$$

with α_{eq} the equilibrium isotopic fractionation factor at the temperature of the air-water interface [Eqs. (4) and (5)]; and ε_{kin} the kinetic isotopic separation factor, estimated by Gonfiantini (1986) as:

$$\varepsilon_{kin} = 12.5(1-h) \quad \text{for } \delta D \qquad (11)$$

and

$$\varepsilon_{kin} = 14.2(1-h) \quad \text{for } \delta^{18}O \qquad (12)$$

D and 18 designate that the terms are for δD and $\delta^{18}O$, respectively. It is observed that for evaporating lakes in tropical areas (e.g., Indonesian crater lakes, Varekamp and Kreulen 2000), the slope of the evaporation trend is "less flat" as air humidity is higher. The flatter the slope in Fig. 5, the larger the evaporation effect.

For practical applications (e.g., isotopic budget analyses of crater lakes, see next section) it is often useful to calculate the isotopic composition of the evaporative steam coming off a lake. The following equation counts (Craig and Gordon 1965; Krabbenhoft et al. 1990; Sacks 2002):

$$\delta_E = \frac{\alpha_{eq}\delta_L - h\delta_a - \alpha_{evap}}{(1-h+0.001\varepsilon_{kin})} \qquad (13)$$

with δ_L the isotopic composition of the evaporating lake, and all other parameters as earlier defined, for H and O separately.

So far, we have assumed that the observed slope is only the result of evaporation, but how can we assure that this slope is not affected by the input of the hot magmatic end member? As for instance demonstrated by the low E % (Table 1) and the "AW-edging" trend for Poás' Laguna Caliente (Fig. 5), it is more appropriate to first calculate δ_E (Eq. 13), and weigh the proportion of evaporative loss in an isotopic balance of the particular crater lake.

3.1.3 δD Versus $\delta^{18}O$: Which One Is More Straightforward?

In this section we demonstrate why δD is practically more indicative than $\delta^{18}O$ at active crater lakes. Significant oxygen isotopic exchange can occur between water and other oxygen-bearing species:

1. Prolonged water-rock interaction processes can lead to a positive oxygen shift, due to the absorption of ^{16}O in silicate minerals (Craig 1963), which results in a misleading "flatter slope" of the evaporation trend. Nevertheless, $\delta^{18}O$ in crater lakes probably hardly reflects water-rock interaction processes, as the lake sediment is strongly altered and hence insensitive to oxygen exchange.
2. Isotopic exchange with CO_2, abundant in active crater lake systems, can lead to a negative oxygen shift. This is often observed for hydrothermal steam condensates at relatively low temperatures and high salinities. Besides isotopic exchange with CO_2, the heavy oxygen can be absorbed to clay minerals in relatively low temperature regimes (Lawrence et al. 1975; Fritz and Frape 1982; Taran et al. 1986, 1998; Vuataz and Goff 1986; Goff et al. 1995; Adams 1996).
3. Significant oxygen isotopic exchange can occur between H_2O and the most abundant species in most active crater lakes, SO_4, especially at low pH and high temperature which are typical conditions for active lakes (Lloyd 1968; Mizutani and Rafter 1969; Chiba and Sakai 1985; Delmelle et al. 1998, 2000). Under equilibrium conditions, the $\delta^{18}O_{SO_4} - \delta^{18}O_{H_2O}$ system can be used as a geothermometer: more negative $\delta^{18}O_{H_2O}$ shifts indicate lower equilibrium temperatures. For near-neutral pH conditions, oxygen exchange is extremely slow, but is faster for more acidic conditions—the case of crater lakes, combined with

intrinsically high SO_4-water. Nevertheless, SO_4-abundance and extremely dynamic fluid flushing in most active lake systems makes it impossible to quantify this SO_4−H_2O isotopic exchange effect.

Using the $\delta^{18}O$ of crater lake water to highlight evaporation is sometimes an unfortunate choice; δD certainly behaves less *capriccioso*.

3.2 The Influence of Salinity and Acidity on Isotopic Fractionation

"The isotope salt effect"

Highly acidic crater lake brines are contemporaneous surface analogs of ancient ore depositing hydrothermal fluids (Brantley et al. 1987; Hedenquist and Lowenstern 1994; Henley 2015). Besides thermal heterogeneity in time and space of active crater lakes, which was demonstrated to subtly affect the humidity and temperature of the lake boundary layer and thus evaporation, extreme salinity and acidity can also influence the isotopic fractionation. The term "isotope salt effect" was introduced in the 1950s by Taube and co-workers (Hunt and Taube 1950, 1951; Feder and Taube 1952; Taube 1954), to better understand such hydrothermal fluid circulation in ore-forming systems. The isotope salt effect infers that the liquid-vapor partitioning of water molecules is different for pure water than for saline solutions, with its effect on the isotopic composition of the vapor phase. Without a doubt, crater lake brines are subject to the isotope salt effect, an unstudied topic so far in lake research. The effect results from the "hydration of ions because the vibrational energies of water molecules in the *hydration shell* are different from those in *bulk solvent water"* (Driesner and Seward 2000). What this apparently "surreal" definition stands for at this point is open for discussion. It is clear that the isotopic composition of brines and their vapors under high-temperature and pressure (e.g., for ore-depositing brines) do not behave as boiling or evaporating pure water. Pioneering experiments on the isotope salt effect (Taube 1954; Sofer and Gat 1972; Götz and Heinzinger 1973; Bopp et al. 1977; Truesdell 1974; Graham and Sheppard 1980; O'Neil and Truesdell 1991) were revised in new experimental setups by Horita et al. (1993a, b, 1995). The isotope effect in an aqueous solution can be defined as:

$$\Gamma = \frac{a(HDO)/a(H_2O) \quad \gamma(HDO)}{X(HDO)/X(H_2O) \quad \gamma(H_2O)} \tag{14}$$

The Γ is not an isotope fractionation factor, such as in previous equations, but rather a coefficient explaining how water molecules behave in a solution. Moreover, a (activity), X (mole fraction) and γ (activity coefficient) are not measurable parameters in isotope geochemistry, a problem which should be solved. When adding a hydrogen-bearing phase A to the solution, in order to permit exchange of D-H with this phase A, we approximate a salt solution. Assuming that pure water and a salt solution isotopically equilibrate separately with the same phase A at the same temperature, and if for pure water the isotopic activity a and composition ratios are identical, Γ can be approximated as a fractionation factor in the form:

$$10^3 \ln \Gamma \approx \delta_{\text{pure water}} - \delta_{\text{salt solution}} \tag{15}$$

where δ is the isotopic composition expressed in the conventional δ-notation in per mil (and thus measurable). After experiments with varying temperatures and salinities of the salt solutions, the following equation for Γ is obtained (Horita et al. 1995):

$$10^3 \ln \Gamma = m(a + b/T) \tag{16}$$

where a (molality^{-1}) and b (K molality^{-1}) are coefficients dependent on the type of salt (NaCl, KCl, $MgCl_2$, $CaCl_2$, Na_2SO_4, or $MgSO_4$), m is the molality of the salt solution, and T (K) the temperature of the solution. Natural solutions, such as crater lake brines, are rather mixed salt solutions than single salt solutions, so:

$$10^3 \ln \Gamma_{\text{mixed salt solution}} = \sum \{m_i(a_i + b_i/T)\} \tag{17}$$

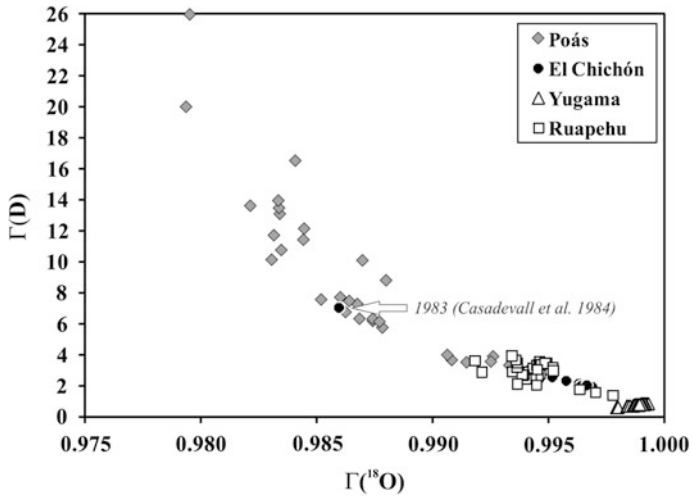

Fig. 6 Γ(D) versus Γ(^{18}O) diagram for selected data from laguna caliente (Poás, 2005–2010, DR personal data), El Chichón (Casadevall et al. 1984—*white arrow*; 1995–2011, Rouwet et al. 2008 and personal data), Yugama (1949–2005; Ohba et al. 2008 and references therein) and Ruapehu crater lakes (Christenson 2000). Calculations are based on Eqs. (18) and (19), using T_L (K) and total molalities. The isotope salt effect becomes proportionally more significant for D with respect to ^{18}O for extremely saline lakes

For each salt i. The higher Γ (or 10^3 ln Γ) the higher the salt isotope effect, as for an evaporating salt solution the vapor phase will become isotopically heavier with respect to the vapor phase from evaporating pure water, under the same P-T conditions. Or in other words, the remnant salt solution will become isotopically lighter with respect to pure water, under the same P-T conditions. Following Eqs. (16) and (17) Γ will be higher for higher molalities (m- more saline), and lower temperatures. For the most active crater lakes—subject to relatively low temperatures compared to the experimental conditions by the various authors chasing ore-fluid conditions- the lake water is a highly saline "cold" brine, and the isotope salt effect can thus be high. Nevertheless, the natural conditions of the most saline lake brines are more complicated than simple NaCl-KCl-$MgCl_2$-$CaCl_2$-Na_2SO_4-$MgSO_4$ solutions [Eq. (17)], characterized by a complicated S-speciation, secondary minerals, density differences, and HCl degassing (see next section), making a crater lake brine highly exotic and far-from-experimental. Moreover, the salt isotope effect is an equilibrium "fractionation" effect, strongly overshadowed by the kinetic isotopic fractionation effect in evaporating lakes, as earlier discussed.

For NaCl solutions (Horita et al. 1995) presented the following equations:

$$10^3 \ln \Gamma\,(\mathrm{D}) = \mathrm{m}(0.01680\ \mathrm{T} - 13.79 + 3255/\mathrm{T}) \tag{18}$$

And

$$10^3 \ln \Gamma\left(^{18}\mathrm{O}\right) = \mathrm{m}\left(-0.033 + 8.93\ \mathrm{x}\ 10^{-7}\ \mathrm{T}^2 - 2.12\ \mathrm{x}\ 10^{-9}\ \mathrm{T}^3\right) \tag{19}$$

Crater lake brines contain more than just NaCl as major salt, but if we assume m in Eqs. (18) and (19) to be equal to the total molality of all salts in solution, we are able to calculate the isotope salt effect [Γ(D) and Γ(^{18}O)] for selected data sets of active crater lakes (Poás, El Chichón, Lake Yugama and Ruapehu) (Fig. 6), without even knowing the isotopic composition of the lake water. The results are graphically presented in Fig. 6. For lower salinity lakes (Lake Yugama and El Chichón) the isotope salt effect is

proportionally more significant for ^{18}O than for D, while for highest salinity lakes (Poás, the 1983 El Chichón "magmatic" crater lake, and to some extent Ruapehu's Crater Lake) Γ(D) increases exponentially. This means that, except for extremely saline lakes (Poás), the isotope salt effect results in "flatter slopes" of the evaporation trend in the Craig diagram.

"The isotope acid effect"

In pure water hydrogen isotopes distribute among the species H_2O, H_3O^+ and OH^-. In near-neutral solutions the contents of the latter two species is too low to affect the isotopic composition, but in strongly acidic solutions, such as active crater lake waters, $H_3O^+(H^+)$ concentrations can be extremely high (remember: a presumed pH of -1 means a H_3O^+ content of 10 mol l^{-1}, considering that pH = $-\log [H_3O^+]$), and so hydrogen will be massively present as a proton. Will hydrogen distribute equally between H_2O and H_3O^+, or will fractionation due to acidity take place? For active volcanic lakes, the acidity is provided by magmatic gases, such as SO_2, H_2S, HCl and HF. Sulfate enters through scrubbing of SO_2 and H_2S in the lake water, gas and can partly leave the liquid phase as poorly soluble H_2S (Symonds et al. 2001). On the other hand, monoprotic acids (HCl, HF) will leave the acidic solution as a gas phase (see next section) which also will affect the isotopic fractionation during evaporative degassing of an active crater lake; the hydrogen isotopes are distributed among the species H_2O, H_3O^+, HX (i.e., HCl or HF) and the hydration sphere of the anion, X(H_2O) (Deines 1979). The fractionation factor of hydrogen isotope fractionation during evaporation of an acidic solution is given by:

$$\alpha_{HX} = (D/H)_v/(D/H)_s \qquad (20)$$

where $(D/H)_v$ is the D/H ratio of the total vapor, and $(D/H)_s$of the total solution. This apparently simple equation leads to a more complicated equation (Deines 1979):

where α are fractionation factors, with the subscripts meaning: W = pure water, PA = pure acid, and HS = hydration sphere; c is the concentration in solution, c' the concentration in the vapor phase; d is the degree of ionization of the acid, and n is the hydration number (for HCl, n = 1). Note the combined subscripts as well. α_{HX} depends on various isotope fractionation factors between the various species and phases and on the chemical properties of the acid. Hydrogen ^1H in the liquid phase will be distributed among the species H_2O, HX, H_3O^+ and X(H_2O), while deuterium D will be distributed among the species HDO, DX, H_2DO^+ and X(HDO). For the vapor phase ^1H will be present as H_2O or HX, while D as HDO and DX. Fortunately, the chemical properties of HCl –the gas we are most interested in for degassing crater lakes- are pretty well known.

What does this practically mean for an evaporating acidic crater lake? As is the case for saline solutions, for acidic lake waters the vapor is enriched in D with respect to neutral lake waters (remember that δD_v is isotopically lighter than δD_L), as $\alpha_{HX} > \alpha_W$. This effect becomes less strong for higher temperature lakes. Again, the isotope acid effect is an equilibrium fractionation effect, dwarfed by the kinetic isotopic fractionation effect. Despite this, we believe that the isotope acid effect should be quantified for the most acidic evaporating crater lakes (e.g., Poás, Kawah Ijen, Copahue). The evaporative degassing of HCl (HX above) from acidic crater lakes does not only affect the isotopic composition of the vapor and remnant lake water, but will also induce changes in the chemical composition of the lake water.

3.3 Liquid-Vapor Partitioning of Chlorine

Starting with a *contradictio in terminis*: chlorine is a highly volatile, but hydrophile element. In a high temperature magmatic/geothermal environment,

$$\alpha_{HX} = \frac{\{\alpha_w c'_{H_2O} + [(\alpha_{PA}\alpha_{H+W})/(2\alpha_{H+PA})](1- c'_{H_2O})\}\{2c_{H_2O} + [(1 - c_{H_2O})/(1 + d)][1 + 2d(1 + n)]\}}{[c'_{H_2O} + 1]\{c_{H_2O} + [(1- c_{H_2O})/(1 + d)][(\alpha_{H+W}/2\alpha_{H+PA})(1- d) + d(3/2\alpha_{H+W} + n\alpha_{HSW}]\}} \qquad (21)$$

chlorine tends to move as the volatile species, HCl. The tendency of HCl to partition in a vapor phase was recognized as HCl-induced corrosion of well casings in (superheated) geothermal systems (Truesdell et al. 1989). HCl is definitely not the most abundant species in volcanic gases: water vapor (90–99 %), CO_2 (1–10 %) and the sulfur species SO_2-H_2S (1–10 %) are generally present in higher concentrations (Menyailov et al. 1986; Giggenbach 1987; Shinohara et al. 1993; Taran et al. 1995). The acidity of the water of active crater lakes only depends on the absorption of SO_2-H_2S, HCl and HF. Only acid mine drainage fluids are discovered to be more acidic than e.g., Poás' Laguna Caliente and Kawah Ijen lake waters (Nordstrom et al. 2000; Rowe et al. 1992a, b; Delmelle and Bernard 1994), but the extreme acidity (pH as low as −3.6; Nordstrom et al. 2000) for mine drainage waters is purely due to the oxidation of pyrite to H_2SO_4 (the stronger acid), while Cl and F are absent in such fluids. On the other hand, for crater lake water with a pH ranging from −1 to 1, HSO_4^- is the main H^+-donor (often determined as SO_4), but HCl and HF also contribute to the H^+-activity. Besides the volatile character of HCl (and HF), even at low temperatures, the volatilization of HCl is favored by:

1. A higher abundance of H_2SO_4, and thus lower pH (Truesdell et al. 1989);
2. A higher water temperature (Truesdell et al. 1989); calculating the Cl content of the vapour in equilibrium with a 2 % HCl solution (20,000 mg/l) for a temperature ranging from 35°C to 60°C, a characteristic T range for actively degassing non disappearing crater lakes results in Cl contents in the evaporative plume of 9–26 mg/l (Washburn et al. 1928);
3. A higher content of Cl^- in the liquid phase (Truesdell et al. 1989);
4. Bubbling or boiling processes at the evaporative degassing lake surface;
5. A more efficient thermal convection of crater lake water;
6. Strong winds, to continuously remove HCl from the degassing surface;
7. Continuous recycling or new input of H_2SO_4 and Cl rich fluids at the lake bottom.

With continuous recharge or recycling of lake water from below, degassing and evaporation from a crater lake surface is an extremely dynamic, non-equilibrium process. The moment of sampling of the surface water of such a crater lake is thus only a snapshot of this dynamic degassing process. Moreover, recently it has been discovered that Cl (and F) contents can drastically decrease after multiple analyses (after several days) of the same ultra-acidic lake water sample (Copahue volcano 2012 pre-eruption; B. Capaccioni and F. Tassi, oral communication). It seems that for extremely acidic and saline solutions HCl (and HF) degassing continues even after cooling until room temperature, and the analytical results will not be representative for the physical-chemical conditions at the time of sampling. For now, this post-sampling effect is hardly quantifiable—as is the degassing process from the lake itself. This stresses the need to dilute acidic lake water sampled directly in the field (10–1,000 times), do not leave a headspace in the sampling flask, and refrigerate or, ideally, freeze the samples, to ensure no post-sampling loss of HCl(g) and HF(g).

When entering the lower temperature hydrothermal environment, chlorine will absorb in the aqueous phase rather than be lost by precipitation of intrinsically rare Cl-minerals. This opposite characteristic of chlorine converts it into an ideal tracer, transported by the water phase as a conservative element, although we know that HCl is actually not conservative at all under almost any condition.

From an experimental setup, Simonson and Palmer (1993) empirically deduced the partitioning coefficient K for HCl between the liquid and vapor phase. The partitioning coefficient K is simply dependent on the water temperature and density, rather than being expressed in function of salinity (e.g., molality or NaCl content):

$$\mathrm{LogK} = -13.4944 - 934.466/\mathrm{T} - 11.0029 \log \rho + 5.4847 \log \mathrm{T} \quad (22)$$

where K is:

$$\mathrm{K} = \mathrm{m_v}/\mathrm{m_l^2}\gamma_1^2 \quad (23)$$

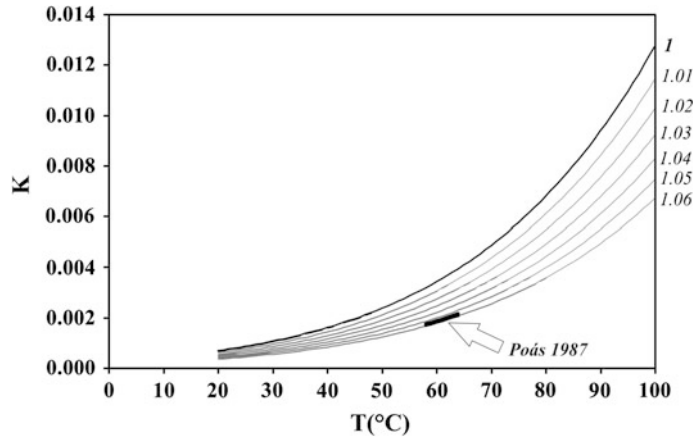

Fig. 7 T(°C) versus K diagram, where K is calculated by Eq. 22 (Simonson and Palmer 1993). The higher K, the higher the Cl-partitioning in the vapor phase. The temperature is chosen for being realistic for active crater lakes, until boiling point (complete evaporation)

With m_v and m_l the vapor phase and liquid phase molalities of HCl, respectively, and γ_l stoichiometric activity coefficients (see Simonson and Palmer 1993 for further details); ρ is the density of the liquid (g cm^{-3}) and T (K) the lake water temperature. As follows from Eq. (22), a higher temperature and lower density of the lake water favors the vapor partitioning of HCl (higher K values in Fig. 7). For the density reported for the January 1987 Laguna Caliente at Poás (1.0575 ± 0.0015 g cm^{-3}) and a T range from 58 to 64°C (Brantley et al. 1987), the calculated K ranges from 0.00175 to 0.0021(Fig. 7). Fact is that hot crater lakes are mostly saline, acidic and suspension-loaded and thus dense; these two typical characteristics for active crater lakes counterbalance each other regarding the Cl-partitioning into the vapor phase. Shinohara et al. (2015) found that the HCl from Nakadake lake (Aso volcano, Kyushu, Japan) is controlled by equilibrium evaporation. This probably results from the high HCl concentrations in the gas plume as the steep-walled Nakadake crater is protected from the wind. This equilibrium degassing counts for HCl, but not necessarily for the isotope fractionation of the water vapor in the plume.

A recent study on Cl isotope fractionation in acidic systems and fumaroles (Sharp et al. 2010), including the crater lake hosting systems of Poás and Santa Ana (El Salvador) states that the lake and the underlying hydrothermal plumbing system functions as a condenser for rising HCl-rich fumarolic vapors which leads to a strong kinetic isotope fractionation of ~10‰ (vs V-SMOC, Standard Mean Ocean Cl) in $\delta^{37}Cl$ (e.g., $\delta^{37}Cl$ for Laguna Caliente water = +0.25 to +0.50‰, while $\delta^{37}Cl$ for high-T fumaroles near the lake = 10.6 ± 1.2 ‰). The direct effect of evaporative degassing from the lake surface has not been dealt with, but experiments showed that equilibrium and kinetic isotope fractionation(for $\delta^{37}Cl$) have opposite effects (Sharp et al. 2010):

$$\text{Equilibrium fractionation}: \quad 1000 \ln \alpha_{HCl(g)-Cl-} = 1.4 \text{ to } 1.8\% \tag{24}$$

$$\text{Kinetic fractionation}: \quad 1000 \ln \alpha_{HCl(g)-Cl-} = -3.92\% \tag{25}$$

This demonstrates that multiple redissolving and consequent stripping of the light ^{35}Cl when lake water is encountered is necessary to explain the high $\delta^{37}Cl$ of high-T fumaroles. The above Eqs. (24) and (25), and the earlier idea that the kinetic isotope fractionation effect is larger than the equilibrium isotope fractionation effect (for δD and $\delta^{18}O$), only suggests that the remnant

lake water becomes isotopically heavier upon evaporative degassing. A future challenge is to focus on this fractionation effect, ideally measured in the sampled vapor plume coming off the lake (δD, $\delta^{18}O$, but also $\delta^{37}Cl$).

3.3.1 Why Not Sulfur Species?

S-species (SO_2-H_2S) are more abundant in a volcanic gas phase with respect to HCl, hence the SO_4 contents in crater lake waters will generally be higher than Cl contents. At first sight, variations in SO_4 content seem to be more indicative of eventual changes in contribution from the underlying magmatic system, entering the lake as SO_2, a commonly used trace gas in geochemical monitoring and remote sensing techniques at open-conduit degassing volcanoes (Aiuppa et al. 2002; Shinohara et al. 2015). Even more, once magmatic SO_2(g) is scrubbed by the hydrothermal system or crater lake, sulfur gases are less liberated from a hydrothermal system with respect to HCl (Symonds et al. 2001). With all these advantages, why don't we prefer to track SO_4 contents instead of the more volatile HCl species? First of all, the original proportion between SO_2 and H_2S in the entering gas phase (Giggenbach 1987) will be hardly preserved when scrubbed. Both species initially oxidize until SO_4, but SO_2 will disproportionate forming partly H_2S and partly SO_4 (Delmelle and Bernard 2015). Moreover, in acidic solutions, SO_2 and H_2S will react forming elemental sulfur, often massively precipitating as molten sulfur pools at crater lake floors, and thus lost from the solution. Sulfate minerals, such as anhydrite, gypsum and alunite can be abundant in volcanic lakes and represent another sink of SO_4 from solution. The sulfur speciation becomes even more complicated if considering polythionate ions ($S_nO_6^{2-}$ with n = 4 to 9) (Takano 1987; Delmelle and Bernard 2015). Despite HCl degassing from the most extremely acidic crater lakes, Cl often remains the best tracer available.

4 Implications for Chlorine and Isotope Budget Analyses

Mass balances equations can be expanded towards isotopic and chemical budget analyses of crater lakes by multiplying each flux term with its corresponding isotopic or chemical composition (Hurst et al. 1991; Ohba et al. 1994; Rouwet et al. 2004, 2008; Taran and Rouwet 2008; Rouwet and Tassi 2011):

$$V_L C_L = V_{L0} C_{L0} + Q_m C_m dt + Q_f C_f dt + Q_i C_i dt - Q_s C_s dt - Q_e C_e dt - Q_o C_o dt \quad (26)$$

where V_L is the estimated lake water volume at a certain period of observation, V_{L0} is the lake water volume for the previous period of observation; Q expresses a flux (kg s^{-1}) for meteoric precipitation—m, for hot fluid input from the underlying volcanic-hydrothermal system—f, for surface inflow from an external source—i, for loss by lake water seepage—s, for loss by evaporation from the lake surface—e, for loss by direct lake overflow—o; C expresses the chemical or isotopic composition of the involved end members, with respective subscripts. During volcanic surveillance, the Q_f parameter should be tracked with time, as it reflects eventual changes in the direct input (heat and chemical components) from the underlying volcano-hydrothermal system and possibly magmatic activity. Thus, Q_f. C_f will affect the thermal regime, Cl content and δD of the lake water itself, which will directly influence the evaporative degassing and related fractionation and partitioning effects. Many of the other fluxes can be measured (V_{L-L0}, Q_m, Q_i, Q_o), calculated (Q_e, Hurst et al. 2015 and references therein) or indirectly deduced by numerical simulations(Todesco et al. 2015) or chemical modeling routines (Q_s). All but two end members, the evaporation plume and the hot fluid from the volcano-hydrothermal system, can be sampled in order to determine their chemical (Cl)

and isotopic composition. If high temperature fumaroles are present near the studied crater lake, the chemical and isotopic composition can be determined and used as a proxy for C_f, converting C_e in the only unknown parameter in Eq. (26). It is clear that a better quantification of major unknowns of Eq. (26) -the isotopic composition and Cl content of the evaporation plume and entering hot magmatic end member- leads to better estimate extensive monitoring parameters such as the evaporative and input fluxes of the hot magmatic end member.

5 Conclusions and Suggestions for Future Research

An active crater lake often behaves as a kind of "open-air" large fumarole, with some memory of its recent past: (1) rising gases and fluids are absorbed in the lake water, reflected by the lake's chemical-physical properties, (2) fluids (vapor and gas) are partially released from the lake surface following "well established" chemical and physical rules. The term "well established" is often not straightforward, as a natural, dynamic and extreme system of an active crater lake does not follow the often empirically deduced rules through laboratory experiments. This disequilibrium behavior of a crater lake is for instance demonstrated by the larger kinetic isotope fractionation with respect to equilibrium isotope fractionation. Although recognized since long, only recently, this kinetic isotope fractionation is better understood (Cappa et al. 2003; Luz et al. 2009). The fact that this kinetic isotope fractionation is dominant has lead to the lack of attention for minor processes, such as the isotope salt effect and isotope acid effect, although active crater lakes are probably the best natural laboratories to study those. It is found that the more acidic and saline the lake brine is, the more D-enriched the evaporation plume will be. The observations of increasing Mg/Cl and SO_4/Cl ratios in crater lake waters—often used, however, ambiguous monitoring parameters- already suggested the loss of Cl from the lake. Acidic plumes coming off extreme lake brines (e.g., Poás, Kawah Ijen, Ruapehu, Copahue) release HCl to the vapor phase depending on the lake water temperature and density (Simonson and Palmer 1993).

A challenge for the future is to develop a sampling method for the vapor above the lake. This will permit to analyze the vapor for its chemical (HCl and HF content, pH) and isotopic composition (δD, $\delta^{18}O$, $\delta^{37}Cl$). Chlorine isotopes have been applied to crater lakes but so far followed a top down (the lake as a fumarole reservoir) instead of bottom up approach (the lake as the reservoir for evaporative degassing, Sharp et al. 2010). If these parameters can be deduced on field or in continuous, crater lake chemistry could keep up with remote sensing methods in volcano monitoring set ups. Multi-gas setups around vigorously evaporating crater lakes are promising (Di Napoli et al. 2013; Shinohara et al. 2015; Rouwet et al. 2014). Water isotopes and $\delta^{37}Cl$ provide two semi-independent tracers to track evaporative regime of a crater lake.

We should elaborate experiments, mimicking the natural situation of a crater lake, with controllable factors to better understand how evaporation and HCl degassing occurs, and how they relate to the underlying processes of magmatic heat and solute input and fluid recycling. The here reviewed literature of similar experiments provide the theoretical base for such future work (Horita et al. 1993a, b, 1995; Simonson and Palmer 1993; Horita and Wesolowski 1994; Sharp et al. 2010). Evaporating real lake samples under various conditions is probably most suitable, as crater lake brines are extremely complex solutions very hard to copy in the laboratory.

Acknowledgments The authors wish to thank R.A. Mora-Amador, C.J. Ramírez-Umaña and G. González-Ilama for additional sampling of the Poás crater lake. INGV-Palermo staff is grateful for support in analyses. We thank Cinzia Federico and Bruno Capaccioni for insightful comments as reviewers of this chapter Franco Tassi is acknowledged for efficient editorial handling.

References

Adams MC (1996) Chemistry of fluids from ascension n1, a deep geothermal well on ascension island, South Atlantic ocean. Geothermics 25:561–579

Adams E, Cosler DJ, Helfrich KR (1990) Evaporation from heated water bodies: predicting combined forced plus free convection. Water Resour Res 26:425–435

Agusto M (2011) Estudio geoquímico de los fluidos volcánicos e hidrotermales del Complejo Volcánica Copahue-Caviahue y su aplicación para tareas de seguimiento. PhD dissertation. Universidad de Buenos Aires, Argentina, pp 294

Aiuppa A, Federico C, Paonita A, Pecoraino G, Valenza M (2002) S, Cl and F degassing as an indicator of volcanic dynamics: the 2001 eruption of Mount Etna. Geophys Res Lett 29(11):1559. doi:10.1029/2002GL015032

Barkan E, Luz B (2005) High precision measurements of $^{17}O/^{16}O$ and $^{18}O/^{16}O$ of O_2 in H_2O. Rapid Commun Mass Spectrom 19:3737–3742

Bigeleisen J (1961) Statistical mechanics of isotope effects on the thermodynamic properties of condensed systems. J Chem Phys 34:1485–1493

Bopp P, Heinzinger K, Klemm A (1977) Oxygen isotopefractionation and the structure of aqueous alkali halide solutions. Z Naturforsch 324:1419–1425

Brantley SL, Borgia A, Rowe G, Fernández JF, Reynolds JR (1987) Poás volcano crater lake acts as a condenser for acid metal-rich brine. Nature 330:470–472

Brown G, Rymer H, Dowden J, Kapadia P, Stevenson D, Barquero J, Morales LD (1989) Energy budget analysis for Poás crater lake: implications for predicting volcanic activity. Nature 339:370–373

Cappa CD, Hendricks MB, DePaolo DJ, Cohen RC (2003) Isotopic fractionation of water during evaporation. J Geophys Res 108(D16):4525. doi:10.1029/2003JD003597

Casadevall TJ, De la Cruz-Reyna S, Rose Jr WI, Bagley S, Finnegan DL, Zoller WH (1984) Crater lake and post-eruption hydrothermal activity, El Chichon volcano, Mexico. J Volcanol Geotherm Res 23:169–191

Chiba H, Sakai S (1985) Oxygen isotope exchange rate between dissolved sulfate and water at hydrothermal temperatures. Geochim Cosmochim Acta 43:993–1000

Christenson BW, Wood CP (1993) Evolution of the vent-hosted hydrothermal system beneath Ruapehu crater lake, New Zealand. Bull Volcanol 55:547–565

Craig H (1963) The isotopic geochemistry of water and carbon in geothermal areas. In: Tongiorgio (ed) Nuclear geology in geothermal areas, conference proceedings (Spoleto, Italy), pp 17–53

Craig H, Gordon LI (1965) Stable isotope in oceanographic studies and paleotemperatures. V Lischi e Figli, Pisa, pp 122

Craig H, Gordon LI, Horibe Y (1963) Isotopic exchange effects in the evaporation of water. J Geophys Res 68:5079–5087

Deines P (1979) A note on hydrogen isotope fractionation involving acidic and basic solutions. Geochim Cosmochim Acta 43:1575–1577

Delmelle P, Bernard A (2015) The remarkable chemistry of sulfur in volcanic acid crater lakes: a scientific tribute to Bokuichiro Takano and Minoru Kusakabe. In: Rouwet D, Tassi F, Vandemeulebrouck J, Christenson B (eds) Volcanic Lakes. Springer, Berlin. doi:10.1007/978-3-642-36833-2_10

Delmelle P, Bernard A (1994) Geochemistry, mineralogy, and chemical modeling of the acid crater lake of Kawah Ijen volcano, Indonesia. Geochim Cosmochim Acta 58:2445–2460

Delmelle P, Kusakabe M, Bernard A, Fischer T, de Brouwer S, del Mundo E (1998) Geochemical and isotopic evidence for seawater contamination of the hydrothermal system of Taal Volcano, Luzon, the Philippines. Bull Volcanol 59:562–576

Delmelle P, Bernard A, Kusakabe M, Fischer TP, Takano B (2000) Geochemistry of the magmatic-hydrothermal system of Kawah Ijen volcano, East Java, Indonesia. J Volcanol Geotherm Res 97:31–53

Di Napoli R, Aiuppa A, Allard P (2013) First Multi-GAS based characterization of the Boiling Lake volcanic gas (Dominica, lesser antilles). Ann Geophys 56(5): S0559. doi:10.4401/ag-6277

Driesner T, Seward TM (2000) Experimental and simulation study of salt effects and pressure/density effects on oxygen and hydrogen stable isotope liquid-vapor fractionation for 4–5 molal aqueous NaCl and KCl solutions to 400 C. Geochim Cosmochim Acta 64 (10):1773–1784

Feder HM, Taube H (1952) Ionic hydration: an isotopic fractionation technique. J Chem Phys 20:1335–1336

Federico C, Capasso G, Paonita A, Favara R (2010) Effects of steam-heating processes on a stratified volcanic aquifer: stable isotopes and dissolved gases in thermal waters of Volcano Island (Aeolian archipelago). J Volcanol Geotherm Res 192:178–190

Fournier N, Witham F, Moreau-Fournier M, Bardou L (2009) Boiling Lake of Dominica, West Indies: High-temperature volcanic crater lake dynamics. J Geophys Res 114:B02203. doi:10.1029/2008JB005773

Fritz P, Frape SK (1982) Saline groundwaters in the Canadian Shield: a first overview. Chem Geol 36:179–190

Gat JR (1981) Paleoclimate conditions in theLevant as revealed by the isotopic compositionof paleowaters. Israel Meteorol Res Pap 3:13–28

Gat J (2008) The isotopic composition of evaporating waters—review of the historical evolution leading up to the Craig-Gordon model. Isot Environ Health Stud 44:5–9

Giggenbach WF (1975) Variations in the carbon, sulphur and chlorine contents of volcanic gas discharges from White Island, New Zealand. Bull Volcanol 39:15–27

Giggenbach WF (1978) The isotopic composition of waters from the El Tatio geothermal field, Northern Chile. Geochim Cosmochim Acta 42:979–988

Giggenbach WF (1987) Redox processes governing the chemistry of fumarolic gas discharges from White Island, New Zealand. Appl Geochem 2:143–161
Giggenbach WF (1992) Magma degassing and mineral deposition in hydrothermal systems along convergent plate boundaries. Econ Geol 87:1927–1944
Giggenbach WF, Glover RB (1975) The use of chemical indicators in the surveillance of volcanic activity affecting the crater lake on Mt Ruapehu, New Zealand. Bull Volcanol 39:70–81
Giggenbach WF, Stewart MK (1982) Processes controlling the isotopic composition of steam and water discharges from steam vents and steam-heated pools in geothermal areas. Geothermics 11:71–80
Goff F, McMurty GM, Roldan-Manzo A, Stimac JA, Werner C, Hilton D, van Soest MC (1995) Contrasting magma–hydrothermal activity at Sierra Negra and Alledo volcanoes, Galapagos hot spot Ecuador. EOS Trans Am Geophys Union 76(46):F702 (Abstract)
Gonfiantini R (1986) Environmental isotopes in lake studies. In: Fritz P, Fontes JCh (eds) Handbook of Environmental Isotope Geochemistry, vol 2., The Terrestrial Environment, Elsevier, Amsterdam, pp 113–168
Götz D, Heinzinger K (1973) Sauerstoffisotopieeffekte undhydratstruktur von alkalihalogenid-lösungen in H_2O und D_2O_2. Naturforschende 281:137–141
Graham CM, Sheppard SMF (1980) Experimental hydrogen isotope studies, II. Fractionations in the systems epidote-NaCl-H_20, epidote-$CaCl_2$-H_2O and epidote-seawater, and the hydrogen isotope composition of natural epidote. Earth Planet Sci Lett 48:237–251
Harbeck GE (1964) Estimated forced evaporation from cooling ponds: proceedings of the American Society of Civil Engineers. J Power Div 90(P03):1–9
Hedenquist JW, Lowenstern JB (1994) The role of magmas in the formation of hydrothermal ore deposits. Nature 370:519–527
Henley RW (2015) Hyperacidic volcanic lakes, metal sinks and magmatic gas expansion in arc volcanoes. In: Rouwet D, Tassi F, Vandemeulebrouck J, Christenson B (eds) Volcanic Lakes. Springer, Berlin. doi: 10.1007/978-3-642-36833-2_6
Horita J, Wesolowski DJ (1994) Liquid-vapor fractionation of oxygen and hydrogen isotopes of water from the freezing to the critical temperature. Geochim Cosmochim Acta 58:3425–3437
Horita J, Cole DR, Wesolowski DJ (1993a) The activity-composition relationship of oxygen and hydrogen isotopes in aqueous salt solutions: II. Vapor-liquid water equilibration of mixed salt solutions from 50 to 100°C and geochemical implications. Geochim Cosmochim Acta 57:4703–4711
Horita J, Wesolowski DJ, Cole DR (1993b) The activity-composition relationship of oxygen and hydrogen isotopes in aqueous salt solutions: I. Vapor-liquid water equilibration of single salt solutions from 50 to 100°C. Geochim Cosmochim Acta 57:2797–2817
Horita J, Cole DR, Wesolowski DJ (1995) The activity-composition relationship of oxygen and hydrogen isotopes in aqueous salt solutions: III. Vapor-liquid water equilibration of NaCl solutions to 350°C. Geochim Cosmochim Acta 59(6):1139–1151
Horita J, Rozanski K, Cohen S (2008) Isotope effects in the evaporation of water: a status report of the Craig-Gordon model. Isot Environ Health Stud 44:23–49
Hunt JP, Taube H (1950) The exchange of water between aqueous chromic ion and solvent. J Chem Phys 18:757–758
Hunt JP, Taube H (1951) The exchange of water between hydrated cations and solvent. J J Chem Phys 19:602–609
Hurst AW, Hashimoto T, Terada A (2015) Crater lake energy and mass balance. In: Rouwet D, Tassi F, Vandemeulebrouck J, Christenson B (eds) Volcanic Lakes. Springer, Berlin. doi: 10.1007/978-3-642-36833-2_13
Hurst AW, Bibby HM, Scott BJ, McGuinness MJ (1991) The heat source of Ruapehu crater lake; deductions from the energy and mass balances. J Volcanol Geotherm Res 6:1–21
Hurst T, Christenson B, Cole-Baker J (2012) Use of a weather buoy to derive improved heat and mass balance parameters for Ruapehu crater lake. J Volcanol Geotherm Res 235–236:23–28
Krabbenhoft DP, Bowser CJ, Anderson MP, Valley JW (1990) Estimating groundwaterexchange with lakes 1. The stable isotope mass balance method. Water Resour Res 26:2445–2453
Lawrence JR, Geiskes JM, Broecker WS (1975) Oxygen isotopes and cation composition of DSDP pore waters and the alteration of layer II basalts. Earth Planet Sci Lett 27:1–10
Lee TM, Swancar A (1997) Influence of evaporation, ground water, and uncertainty in the hydrologic budget of Lake Lucerne, a seepage lake in Polk County, Florida. USGS Water-Supply Papers 2439:61 p
Lloyd RM (1968) Oxygen isotope behavior in the sulfate–water system. J Geophys Res 73:6099–6110
Luz B, Barkan E, Yam R, Shemesh A (2009) Fractionation of oxygen and hydrogen isotopes in evaporating water. Geochim Cosmochim Acta 73:6697–6703
Majoube M (1971) Fractionnement en oxygene-18 et deuteriumentre l'eau et sa vapeur. J Chim Phys 197:1423–1436
Martínez M, Fernández E, Valdés J, Barboza V, Van der Laat R, Duarte E, Malavassi E, Sandoval L, Barquero J, Marino T (2000) Chemical evolution and activity of the active crater lake of Poás volcano, Costa Rica, 1993–1997. J Volcanol Geotherm Res 97:127–141
Menyailov IA, Nikitina LP, Shapar VN, Pilipenko VP (1986) Temperature increase and chemical changes of fumarolic gases at Momotombo volcano, Nicaragua, in 1982–1985: are these indicators of a possible eruption? J Geophys Res 91:12199–12214
Mizutani Y, Rafter AT (1969) Oxygen isotopic fractionation in the bisulphate ion-water system. NZ J Sci 12:54–59
Nordstrom DK, Alpers CN, Ptacek CJ, Blowes DW (2000) Negative pH and extremely acidic mine waters from Iron Mountain, California. Environ Sci Technol 34:254–258

O'Neil JR, Truesdell AH (1991) Oxygen isotope fractionation studies of solute-water interactions. In stable isotope geochemistry: a tribute to Samuel Epstein (ed HP Taylor Jr et al.) Geochem Sot, pp 17–25

Ohba T, Hirabayashi J, Nogami K (1994) Water, heat and chloride budgets of the crater lake, Yugama at Kusatsu-Shirane volcano, Japan. Geochem J 28:217–231

Ohba T, Hirabayashi J, Nogami K (2000) D/H and $^{18}O/^{16}O$ ratios of water in the crater lake at Kusatsu-Shirane volcano, Japan. J Volcanol Geotherm Res 97:329–346

Ohba T, Hirabayashi J, Nogami K (2008) Temporal changes in the chemistry of lake water within Yugama Crater, Kusatsu-Shirane volcano, Japan: Implications for the evolution of the magmatic-hydrothermal system. J Volcanol Geotherm Res 178:131–144

Oppenheimer C (1997) Ramifications of the skin effect for crater lake heat budget analysis. J Volcanol Geotherm Res 75:159–165

Pasternack GB, Varekamp JC (1997) Volcanic lake systematics 1. Physical constraints. Bull Volcanol 58:528–538

Rouwet D, Tassi F (2011) Geochemical monitoring of volcanic lakes a generalized box model for active crater lake. Ann Geophys 54(2):161–173

Rouwet D, Taran Y, Varley NR (2004) Dynamics and mass balance of El Chichón crater lake, Mexico. Geofís Int 43:427–434

Rouwet D, Taran Y, Inguaggiato S, Varley N, Santiago SJA (2008) Hydrochemical dynamics of the lake-spring system in the crater of El Chichón volcano (Chiapas, Mexico). J Volcanol Geotherm Res 178:237–248

Rouwet D, Tassi F, Mora-Amador R, Sandri L, Chiarini V (2014) Past, present and future of volcanic lake monitoring. J Volcanol Geotherm Res. doi:10.1016/j.jvolgeores.2013.12.009

Rowe GL (1994) Oxygen, hydrogen, and sulphur isotope systematics of the crater lake system of Poás Volcano, Costa Rica. Geochem J 28:264–275

Rowe GL, Brantley SL, Fernández M, Fernández JF, Borgia A, Barquero J (1992a) Fluid-volcano interaction in an active stratovolcano: the crater lake system of Poás volcano, Costa Rica. J Volcanol Geotherm Res 64:233–267

Rowe GL, Ohsawa S, Takano B, Brantley SL, Fernández JF, Barquero J (1992b) Using crater lake chemistry to predict volcanic activity at Poás volcano, Costa Rica. Bull Volcanol 54:494–503

Ryan PJ, Harleman DRF, Stolzenbach KD (1974) Surface heat loss from cooling ponds. Water Resources Res 10:930–938

Sacks LA (2002) Estimating ground-water inflow to lakes in Central Florida using the isotope mass-balance approach. US Geological Survey. Water-resources investigations report 02-4192:68 pp

Sartori E (2000) A critical review on equations employed for the calculation of the evaporation rate from free water surfaces. Sol Energy 68:77–89

Sharp ZD, Barnes JD, Fischer TP, Halick M (2010) An experimental determination of chlorine isotope fractionation in acid systems and applications to volcanic fumaroles. Geochim Cosmochim Acta 74:264–273

Shinohara H, Yoshikawa S, Miyabuchi Y (2015) Degassing activity of a volcanic crater lake: Volcanic plume measurements at the Yudamari crater lake, Aso volcano, Japan. In: Rouwet D, Tassi F, Vandemeulebrouck J, Christenson B (eds) Volcanic Lakes. Springer, Berlin. doi: 10.1007/978-3-642-36833-2_8

Shinohara H, Giggenbach WF, Kazahaya K, Hedenquist JW (1993) Geochemistry of volcanic gases and hot springs of Satsuma-Iwojima, Japan: Following Matsuo. Geochem J 27:271–285

Sill BL (1983) Free and forced convection effects on evaporation. J Hydraul Engin ASCE 109:1216–1231

Simonson JM, Palmer DA (1993) Liquid-vapor partitioning of HCl(aq) to 350 C. Geochim Cosmochim Acta 57:1–7

Sofer Z, Gat JR (1972) Activities and concentrations of oxygen-18 in concentrated aqueous salt solutions: Analytical andgeophysical implications. Earth Planet Sci Lett 15:232–238

Sriwana T, van Bergen MJ, Varekamp JC, Sumarti S, Takano B, van Os BJH, Leng MJ (2000) Geochemistry of the acid Kawah Putih lake, Patuha volcano, West Java, Indonesia. J Volcanol Geotherm Res 97:77–104

Stimac JA, Goff F, Counce D, Larocque ACL, Hilton DR, Morgenstern U (2004) The crater lake and hydrothermal system of Mount Pinatubo, Philippines: evolution in the decade after eruption. Bull Volcanol 66:149–167

Symonds RB, Gerlach TM, Reed MH (2001) Magmatic gas scrubbing: implications for volcano monitoring. J Volcanol Geotherm Res 108:303–341

Takano B (1987) Correlation of volcanic activity with sulfur oxy-anion speciation in a crater lake. Science 235:1633–1635

Taran Y, Rouwet D (2008) Estimating thermal inflow to El Chichón crater lake using the energy-budget, chemical and isotope balance approaches. J Volcanol Geotherm Res 175:472–481

Taran YA, Esikov AD, Cheshko AL (1986) Deuterium and oxygen-18 in waters of the Mutnovsky geothermal area. Geochem Int 4:458–468

Taran YA, Pokrovsky BG, Dubik YM (1989) Isotopic composition and origin of water from andesitic magmas. Dokl (Trans) Ac Sci USSR 304:440–443

Taran YA, Hedenquist JW, Korzhinsky M, Tkachenko SI, Shmulovich KI (1995) Geochemistry of magmatic gases from Kudryavy volcano, Iturup, Kuril Islands. Geochim Cosmochim Acta 59:1749–1761

Taran Y, Fischer TP, Pokrovsky B, Sano Y, Armienta MA, Macías JL (1998) Geochemistry of the volcano-hydrothermal system of El Chichón Volcano, Chiapas, Mexico. Bull Volcanol 59:436449

Taran YA, Bernard A, Gavilanes JC, Lunezheva E, Cortés A, Armienta MA (2001) Chemistry and

mineralogy of high-temperature gas discharges from Colima volcano, Mexico. Implications for magmatic gas-atmosphere interaction. J Volcanol Geotherm Res 108:245–264

Taran Y, Inguaggiato S, Cardellini C, Karpov G (2013) Posteruption chemical evolution of a volcanic caldera lake: Karymsky lake, Kamchatka. Geophys Res Lett 40:5142–5146. doi:10.1002/grl.50961

Tassi F, Vaselli O, Capaccioni B, Giolito C, Duarte E, Fernández E, Minissale A, Magro G (2005) The hydrothermal-volcanic system of Rincon de la Vieja volcano (Costa Rica): a combined (inorganic and organic) geochemical approach to understanding the origin of the fluid discharges and its possible application to volcanic surveillance. J Volcanol Geotherm Res 148:315–333

Taube H (1954) Use of oxygen isotope effects in the study of hydrationof ions. J Phys Chem 58:523–528

Todesco M, Rouwet D, Nespoli M, Bonafede M (2015) How steep is my seep? seepage in volcanic lakes, hints from numerical simulations. In: Rouwet D, Tassi F, Vandemeulebrouck J, Christenson B (eds) Volcanic Lakes. Springer, Berlin. doi: 10.1007/978-3-642-36833-2_14

Truesdell AH (1974) Oxygen isotope activities and concentrations in aqueous salt solutions at elevated temperatures: consequences for isotope geochemistry. Earth Plant Sci Lett 23:387–396

Truesdell AH, Haizlip JR, Armannsson H, D'Amore F (1989) Origin and transport of chloride in superheated geothermal steam. Geothermics 18:295–304

Varekamp JC (2015) The chemical composition and evolution of volcanic lakes. In: Rouwet D, Tassi F, Vandemeulebrouck J, Christenson B (eds) Volcanic Lakes. Springer, Berlin. doi: 10.1007/978-3-642-36833-2_4

Varekamp JC (2002) Lake contamination models for evolution towards steady state. J Limnol 62:67–72

Varekamp JC, Kreulen R (2000) The stable isotope geochemistry of volcanic lakes, with examples from Indonesia. J Volcanol Geotherm Res 97:309–327

Vuataz FD, Goff F (1986) Isotope geochemistry of thermal and nonthermal waters in the Valles caldera, Jemez Mountains, Northern New Mexico. J Geophys Res 91:1835–1853

Ward CA, Stanga D (2001) Interfacial conditions during-evaporation or condensation of water. Phys Rev E 64 (051509):U347–U354

Washburn EW, West CJ, Dorsey NE, Bichowsky FR, Klemenc A (1928) International critical tables of numerical data, physics, chemistry and technology. International research council of the national academic of science. (1st edn) McGraw-Hill Book Company, Inc, New York, p 301

Weisman RN, Brutsaert W (1973) Evaporation and cooling of a lake under unstable atmospheric conditions. Water Resour Res 9:1242–1257

Degassing Activity of a Volcanic Crater Lake: Volcanic Plume Measurements at the Yudamari Crater Lake, Aso Volcano, Japan

H. Shinohara, S. Yoshikawa, and Y. Miyabuchi

Abstract

Surface degassing is an important volatile discharge process for an active volcanic crater lake. The compositions of volcanic gases discharged from a lake surface (lake gas) were quantified by volcanic plume measurements using a Multi-GAS and alkaline-filter techniques at the Yudamari crater lake, Aso volcano, Japan. Compositions of the lake gases were quite variable and are clearly different from the gases from adjacent fumaroles. Differentiation processes of the lake gas, the lake water, and the fumarolic gases are evaluated based on their compositions. Concentrations of HCl in the lake gas and the lake water indicate that the lake gas composition is controlled by the equilibrium evaporation of the lake water at the lake temperature. Contrasting compositions of the lake gas and the lake water indicate that sulfate and elemental sulfur formation controls chemical differentiation in the lake. The composition of the hydrothermal fluids supplied to the lake is estimated based on mass balance of the lake gas and the lake water. The hydrothermal fluids have similar H_2O/S and H_2O/Cl ratios but lower CO_2/S ratios than the fumarolic gases. This composition contrast indicates that the fumarolic gases are a mixture of magmatic gases and a vapor phase separated from the hydrothermal fluids supplied to the lake.

Keywords

Lake gas · Volcanic gas composition · Multi-GAS · Aso volcano · Degassing · Evaporation · Gas solubility · Hydrothermal system

H. Shinohara (✉)
Geological Survey of Japan, AIST, Central 7, 1-1-1 Higashi, 305-8567 Tsukuba, Ibaraki, Japan
e-mail: shinohara-h@aist.go.jp

S. Yoshikawa
Aso Volcanological Laboratory, Kyoto University, Minami-Aso, Aso, Kumamoto 869-1404, Japan

Y. Miyabuchi
Kumamoto University, Kurokami 2-40-1, Kumamoto, Kumamoto 860-8555, Japan

1 Introduction

Volcanic lakes are efficient traps of volcanic volatiles supplied from depth, and a lake's water composition is considered as an indicator of the flux and composition of supplied volcanic fluids (Delmelle and Bernard 2000). Chloride and sulfates are the most abundant dissolved constituents

D. Rouwet et al. (eds.), *Volcanic Lakes*, Advances in Volcanology,
DOI 10.1007/978-3-642-36833-2_8,
© Springer-Verlag Berlin Heidelberg 2015

in volcanic lake waters, and their contents positively correlate with the acidity of the lake water, indicating that these components are supplied as acid volcanic gases to the lake (Varekamp et al. 2000). Volcanic gases are mixtures of various gas species—not only Cl and S species, but also of CO_2, H_2, and other inert gases. The concentration of inert gas species in lake waters have been rarely measured, but are likely very low because of their low solubility in water. The inert gases supplied to a lake are likely to escape from the lake surface immediately. In order to estimate the composition of the volcanic gas supplied to the lake, it is necessary to measure the composition of the gas emitted from the lake surface.

Evaporation and bubbling are major degassing processes of volcanic lakes. The stability of a volcanic lake is controlled by the energy and water budget between input by meteoric water and deep high-temperature fluids (e.g., volcanic gases) and output by lake water seepage, evaporation, radiation, and heat loss by conduction (Brown et al. 1989; Varekamp et al. 2000). Evaporation is a major energy and water sink in hot lakes that are heated by a large volcanic fluid input (Varekamp et al. 2000; Terada et al. 2012). For example, 50–90 % of the energy lost from Poás crater lake, Costa Rica, in 1985–1988 was by means of evaporation (Brown et al. 1991). Inert gas species such as CO_2 may be discharged from the lake not only by evaporation but also by bubbling through the lake; these emission rates need to be quantified separately from the energy budget estimate. Recent airborne measurements of volcanic plumes from crater lakes of Ruapehu and White Island, New Zealand, demonstrated that the crater lakes are significant sources of CO_2 degassing, similar to actively degassing volcanoes (Werner et al. 2006, 2008).

Gas emission from a lake often occurs by diffuse degassing from a large area of the lake surface. The composition of inert gas species discharged through lake degassing can be estimated by measuring the composition of bubbling gases or dissolved gases in the lake water (Inguaggiato and Rizzo 2004; Mazot et al. 2011). The composition determined by these methods, however, does not always represent the bulk composition of lake degassing, in particular when degassing activity is not homogeneous, such as when indicated by bubbling. Recently a new instrument, the Multi component gas analyzer system (Multi-GAS), was developed to estimate volcanic gas composition based on the measurements of an air-diluted volcanic gas plume composition (Shinohara 2005; Aiuppa et al. 2005). This method is also useful for measuring the composition of gases discharged from the surface of volcanic lakes. We applied this technique to estimate the composition of lake gases emitted from the Yudamari crater lake, Aso volcano, Japan. In this paper, we report the methods used for volcanic plume measurements and the results obtained and discuss the origin of the lake gases, by considering the differentiation processes in the lake as well as an underlying hydrothermal system.

2 Methods

A volcanic plume is a mixture of volcanic gas and air, and the original volcanic gas composition can be estimated by subtracting the atmospheric contribution from the plume composition. By combining the Multi-GAS and alkali-filter pack techniques, we can measure most of the major components in volcanic gases, including H_2O, CO_2, SO_2, H_2S, H_2, HCl, and HF (Shinohara et al. 2011a, b). This method was developed to estimate the composition of volcanic gases emitted from an open vent or inaccessible vents, and is also applicable to plumes originating from lake degassing.

2.1 Multi-GAS

The Multi-GAS is an instrument comprising various gas analyzers and sensors to measure concentrations of volcanic gas species in volcanic plumes, and thus to estimate the original volcanic gas composition (Aiuppa et al. 2005; Shinohara 2005). Plume measurements with Multi-GAS were begun at Aso volcano in 2003. Measurements were made in 2003 and 2004 using the Multi-GAS instrument described by Shinohara (2005), whilst an upgraded system has

been used from 2005 onwards (Shinohara et al. 2011b). The new Multi-GAS instrument has a non-dispersive infrared CO_2–H_2O analyzer (LI-840, LI-COR, Inc., Lincoln, USA), SO_2 and H_2S electrochemical sensors (KTS-512 and KHS-5TA, respectively, Komyo Rikagaku K.K., Kawasaki, Japan), and a H_2 semiconductor sensor (Model GM12s, Sensor Tech K.K., Rittou, Japan). The electrochemical SO_2 and H_2S sensors have significant cross sensitivity, and filter-type scrubbers for H_2S and SO_2 were placed in front of the KTS-512 and KHS-5TA sensors, respectively, to reduce the cross-sensitivity (Shinohara et al. 2011b). Cross-sensitivity of the H_2S sensor to SO_2 is about 0.1 %, but is variable, ranging from 0.02 to 0.2 %, depending on the condition of the scrubber (Type KP-SO2J, Komyo Rikagaku K.K., Kawasaki, Japan). Cross-sensitivity of the SO_2 sensor to H_2S is about 1 %, which is insignificant for the measurements at Aso volcano since the measured SO_2/H_2S ratios are always larger than unity. The semiconductor H_2 sensor is sensitive only to H_2, but its sensitivity is affected by H_2O concentrations. This effect is corrected for on the basis of the actual H_2O concentration measured in the plume (Shinohara et al. 2011b). The H_2S sensor was not used in 2003 and 2004, and the SO_2/H_2S concentration ratio in the plume was measured using Gas Detector Tubes (5La for SO_2 in the range 4–60 ppm and 4LT for H_2S in the range 0.2–2 ppm) manufactured by GASTECH Co (Ayase, Japan).

2.2 Alkali-filter

Relative concentrations of S, Cl, and F were measured with the alkali-filter technique (Pennisi and Le Cloarec 1998; Shinohara and Witter 2005). Each filter pack consisted of one 0.2-μm particle filter followed by two filter holders, each containing two filters impregnated with 0.2 ml of 1N KOH + 20 % glycerol solution. Sampling was performed at a flow rate of 1–2 l/min for 30–60 min. After sampling, filters in each holder were rinsed with pure water, and concentrations of F, Cl, and S were measured by ion-chromatography after oxidation with H_2O_2. Chloride and fluoride on the alkaline filters are considered as representative of HCl and HF gases trapped on the filter. S content on the filter is considered as representative of SO_2, whereas the volcanic gases contain both SO_2 and H_2S. Laboratory tests revealed that the absorption efficiencies of SO_2 and H_2S by each holder are about 100 % and 0–30 %, respectively (Shinohara et al. 2011b), and the S trapped by the second filter holder is mostly derived from H_2S, unless the first holder is saturated. For a large SO_2/H_2S ratio (e.g., >3), S content on the second filter holder is negligible; however, for a small SO_2/H_2S ratio, a significant amount of S is trapped on the second filter holder, suggesting the significant contribution of H_2S. In order to reduce the H_2S contribution, the S content is reported after correction by subtracting the S content on the second filter holder from that of the first filter holder (Shinohara et al. 2011b).

3 Yudamari Crater Lake, Aso Volcano

Yudamari crater lake, located within the summit crater of Nakadake stratocone, Aso volcano, Japan (Figs. 1 and 2), is one of the hottest and most acidic crater lakes in the world, with water temperature ranging 40–80 °C and acidity levels of pH = −1 to +1 (Ohsawa et al. 2003, 2010; Miyabuchi and Terada 2009). The high temperature and acidity indicate a large volcanic gas flux into the crater lake. Energy and material budget modeling of the Yudamari crater lake revealed that more than half of H_2O in the lake is supplied as high-temperature volcanic gases and more than half of H_2O in the lake is lost by evaporation (Saito et al. 2008; Terada et al. 2012).

The lake is inaccessible because of the steep crater wall surrounding the crater lake, which is about 300 m in diameter and 120 m deep as measured from the rim (Fig. 1). In order to study the lake, various efforts have been made to conduct measurement using a rope stretched across the lake (Terada and Yoshikawa 2009). Water and lake sediments were sampled several times by bringing sampling devices to the lake surface with the rope (Ohsawa et al. 2003, 2010; Miyabuchi

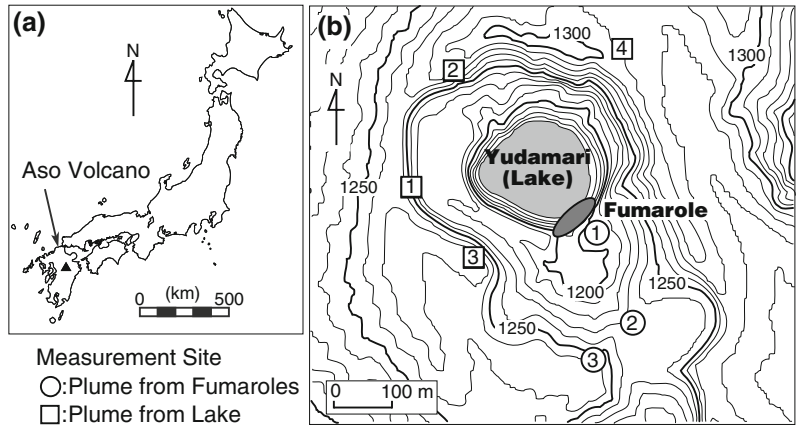

Fig. 1 Location maps. **a** The location of Aso volcano in Japan; **b** Distribution of the Yudamari crater lake and the fumarolic area at the southern wall of the summit crater of Nakadake central cone, Aso volcano. Contours are in 10-m intervals. The numbers in *circles* and *squares* indicate the locations of plume measurement targeting plumes from the fumaroles and from the lake surface, respectively

Fig. 2 A photograph of the Yudamari crater lake and the fumarolic area, taken on August 19, 2010

and Terada 2009). The instruments for continuous lake water temperature monitoring were also installed with the stretched rope (Terada et al. 2012).

The Nakadake cone is a presently active basalt to basaltic-andesitic stratocone of the Aso volcano. The activity of the Yudamari crater lake significantly changes with time and is closely correlated with the eruptive activity of the volcano (Ono et al. 1995; Sudo et al. 2006). Lake surface area and water temperature are frequently measured to monitor volcanic activity (Japan Metrological Agency Monthly Report; Terada et al. 2008; Fig. 3). The last significant eruptive activity occurred from 1988 to 1995 and was characterized by Strombolian and phreatomagmatic eruptions, and continuous ash venting (Ono and Watanabe 1985; Ono et al. 1995; Ikebe et al. 2008). After a quiet period during 1995–2003, the lake water volume decreased and the lake dried up, exposing the lake bottom. Several minor ash emissions occurred from 2003 to 2005 (Miyabuchi et al. 2008). The lake water level recovered to occupy most of the original lake area in 2006 and maintained a high level during most of the period of this study (Fig. 3). The lake water volume ranged from 2 to 8 × 10^5 m^3 during the high water level period (Saito et al. 2008;

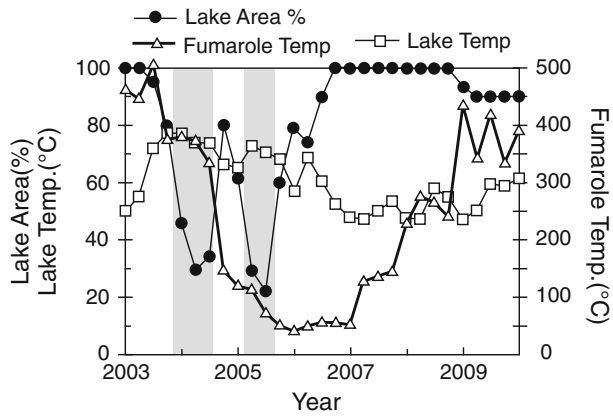

Fig. 3 Variation in lake temperature, lake area, and fumarolic area temperature (Japan Meteorological Agency, Monthly Report; http://www.seisvol.kishou.go.jp/tokyo/STOCK/monthly_v-act_doc/monthly_vact.htm). As an approximate measure, the lake area is expressed in percentage relative to the maximum size, which is defined by the steep wall of the crater. Lake water volume or water level data are available for some of the periods (Saito et al. 2008; Terada et al. 2008, 2012). Temperature of the lake surface and the fumarolic area are measured with an infrared thermometer from the western rim of the crater at about 150 m from the target

Terada et al. 2008). Magnetotelluric surveys suggest that a hydrothermal fluid reservoir is located a few hundred meters beneath the crater lake (Kanda et al. 2008).

The Nakadake cone is a persistently degassing volcano with SO_2 emission rates ranging from 200 to 400 ton/d (Japan Meteorological Agency, Monthly Report). Volcanic gases are emitted from the crater lake surface and a fumarolic area located at the southern wall of the summit crater (Figs. 1 and 2). These two gases create volcanic plumes with different appearances, particularly under dry conditions. Volcanic plumes from the lake surface are white and dense, whereas the plumes from the fumaroles are transparent with a pale-blue color (Fig. 2). This contrast is likely caused by differences in water condensation of the plume reflecting temperature difference of the source gases (Matsushima and Shinohara 2006). Low-temperature gases are emitted from the lake surface and high-temperature gases from the fumaroles.

We attempted separate quantification of the composition of the gases emitted from the Yudamari crater lake (lake gas) and the fumarolic area at the southern wall (fumarolic gas). Since both the crater lake and the fumaroles are inaccessible, plume measurement is the only way to measure their compositions. Under certain wind conditions, the plumes derived from the two sources reach different locations on the crater rim, and each plume can be measured by selecting an appropriate measurement site (Fig. 1). Cross-contamination of these gases, however, is inevitable because of the adjacent location of the sources. The effect of contamination was minimized by removing sporadic peaks with different compositions in the Multi-GAS data. The effect of contamination on the alkaline-filter data, however, could not be reduced because these data are average compositions during sampling periods of 30–60 min.

4 Results

Gas compositions were obtained as concentration ratios, which commonly have an uncertainty of about 10 % attributed to the instrumental error. The measured ratios, however, have larger and more variable errors depending on the measurement conditions, such as the plume concentrations and atmospheric conditions. Since the gas source is not a single vent both for the lake gases and the fumarolic gases, there can be some heterogeneity in composition as well as composition fluctuation. Therefore, it is quite difficult to

estimate the real error in composition determination. In some cases, multiple data sets were obtained within a day or two. Each data set was obtained by 30–60 min measurements. The multiple data agree well in many cases but also show fairly large scatters—up to 50 % in some cases (Table 1, Fig. 4). We consider these scatters as the maximum of the possible errors associated with the composition measurement.

The compositions of lake gases and fumarolic gases show large variations with time but are within distinct ranges (Fig. 4). The magnitude of the temporal variation and the compositional contrast between the two are variable for different concentration ratios. The variation of CO_2/SO_2 ratios is relatively small and the difference between the ratio between the lake gas and the fumarolic gas is also relatively small compared with other ratios (Fig. 4a). Lake gas CO_2/SO_2 ratios are always smaller than the ratios for the fumarolic gases and averages of the two gas compositions are relatively constant at about two. The CO_2/SO_2 ratios of the lake and fumarolic gases vary inversely; small lake gas ratios are commonly associated with large fumarolic gas ratios. When the two gases have similar CO_2/SO_2 ratios, such as for October 4, 2004, February 28, 2008, and October 28, 2008, the ratio is close to two, which is a median value of the variation.

Fumarolic gas SO_2/HCl ratios are relatively constant around 10, in particular excluding two data points obtained at site 2 and 3, which are likely affected by lake gas contamination (Table 1). In contrast, lake gas SO_2/HCl ratios show a large variation and are larger than that for the fumarolic gases, with two exceptions obtained during the low lake volume periods in 2003 and 2005 (Fig. 4b). HCl/HF ratios show similar variation as SO_2/HCl ratios; the HCl/HF ratios are relatively constant at $\sim$5 for fumarolic gases, and are quite variable in lake gases (Fig. 4c). Large ratios (>20) were observed during the low lake volume periods, and very low ratios (<2) were observed during the period when the lake volume was increasing. The SO_2/H_2S ratios also show a similar level of variation as the SO_2/HCl ratios; lake gas ratios are almost always larger than for fumarolic gases, and a low ratio is observed during the low lake volume period (Fig. 4d). A very large SO_2/H_2S ratio of 2,000 was measured for lake gases in 2009. Since cross-sensitivity of the H_2S-sensor to SO_2 is about 0.1 %, which corresponds to an SO_2/H_2S ratio of 1,000, this large value indicates that H_2S content in this gas was below the detection limit. Lake and fumarolic gases show similar H_2/CO_2 ratios (Fig. 4e).

Compositions of volcanic gases were estimated based on volcanic plume measurement by Fourier transform infrared spectroscopy (FT-IR) at Aso volcano (Ono et al. 1999; Hirao et al. 2001; Mori and Notsu 2008). The measurements were conducted at the south-western rim of the crater overlooking the fumarolic area at the southern crater wall, which was used as an infrared light source. These studies intended to measure fumarolic gas composition but did not explicitly try to minimize contribution of the lake gases, and the variable contributions of lake gases might have affected the measurements. Compositions reported by Mori and Notsu (2008) agree with the range for the fumarolic gas as obtained in this study, whereas the compositions reported by Hirao et al. (2001), Ono et al. (1999) are similar to those of the lake gases, suggesting that the former study measured plumes mainly from the fumarolic area, whilst he latter studies measured a mixed plume with a large contribution from the lake gases (Fig. 4). The FT-IR results obtained by Mori and Notsu (2008) on the same day of our measurement (October 15, 2003) agree well with those for the fumarolic gas obtained by this study, in particular for the CO_2/SO_2 ratio.

5 Discussion

The lake gases are separated from the lake water at the surface, and both fluids are derived from a single hydrothermal fluid. The fumarolic area is located just by the lakeshore (100 m from the center), and gases from a common magmatic source are likely supplied to the lake and the fumarole. In the following sections, we will discuss conditions of differentiation processes to explain the compositional contrast between the

Table 1 Composition of fumarolic and lake gases

Date (yy/mm/dd)	Meas. site no.	CO_2/SO_2 (mol ratio)	H_2O/SO_2	H_2/SO_2	SO_2/H_2S	SO_2/Cl	Cl/F	H_2O (μmol/mol)	CO_2	SO_2	H_2S	HCl	HF	H_2	AETS (°C)	T-S_e (°C)
Fumarolic gas																
03/10/15	3	5.0	26	–	–	6.2	8.1	–	–	–	–	–	–	–	–	–
04/10/04	2	1.8	135	–	6[a]	15	13	980,000	13,300	7,200	1,210	480	38	–	–	167
06/10/26	2	3.6	61	0.01	6	19	–	930,000	55,000	15,200	2,530	800	–	150	498	197
07/09/19	1	4.8	43	0.28	13	11	3.7	870,000	97,000	20,300	1,560	1,850	500	570	893	189
08/02/28	1	2.2	20	0.11	20	11	2.5	850,000	94,000	43,000	2,130	3,900	1,550	470	890	209
08/02/29	1	2.1	35	0.05	20	12	2.7	910,000	55,000	26,100	1,310	2,180	810	1,300	718	187
08/07/10	1	3.6	45	0.15	29	5.7	6.6	900,000	72,000	20,000	690	3,500	530	3,000	837	168
08/07/10	1	2.2	52	0.07	23	4.8	8.0	940,000	40,000	18,000	780	3,800	470	1,300	718	168
08/07/11	1	3.0	65	0.10	25	4.7	7.2	940,000	42,000	14,400	580	3,000	430	1,400	737	158
08/07/11	1	3.0	55	0.13	32	4.8	7.2	930,000	51,000	16,800	530	3,500	490	2,200	798	158
08/10/28	1	1.7	40	0.15	31	9.0	4.3	930,000	40,000	23,200	750	2,600	600	3,500	858	171
09/03/23	1	4.0	70	0.13	19	7.9	5.4	930,000	53,000	13,300	700	1,680	310	1,700	743	162
09/03/23	1	2.7	60	0.11	23	7.0	5.1	940,000	42,000	15,600	680	2,230	440	1,720	744	163
09/11/19	1	4.3	46	0.33	12	15	3.4[d]	890,000	83,000	19,300	1,610	1,540	450	6,400	905	189
09/11/19	1	3.0	44	0.36	17	12	3.5[d]	910,000	62,000	20,700	1,210	1,650	480	7,400	945	182
09/11/19	1	2.9	45	0.33	17	10	3.1[d]	910,000	59,000	20,200	1,190	1,620	480	6,700	928	181
09/11/19	1	3.4	37	0.38	15	–	-[d]	880,000	81,000	23,900	1,590	1,910	560	9,100	974	192
Lake gas																
03/10/19	3	0.8	–	–	–	3.0	33	–	–	–	–	–	–	–	–	–
04/10/04	2	1.9	66	–	70[a]	107	1.6	960,000	28,000	14,500	207	136	85	–	–	125
05/04/25	3	1.2	34	0.06	7	5.0	90	930,000	34,000	27,500	4,200	5,500	61	1,700	–	210
05/11/19	3	2.3	56	0.05	59	212	1.3	940,000	38,000	16,900	286	79	61	840	–	136
06/10/26	1	2.2	52	0.02	50	100	18	940,000	40,000	18,100	360	181	10	360	–	133
06/10/27	3	2.6	–	0.01	60	26	–	–	–	–	–	–	–	–	–	–
07/09/17	1	1.7	189	0.06	140	130	4.0	990,000	8,900	5,200	37	40	10	290	–	82
[c] 07/09/18	4	2.0	122	0.05	85	44	3.1	980,000	16,000	8,000	94	182	59	370	–	101
08/02/28	1	1.4	75	0.06	170 [b]	40	3.3	970,000	18,000	12,900	76	320	98	770	–	100

(continued)

Table 1 (continued)

Date (yy/mm/dd)	Meas. site no.	CO_2/SO_2 (mol ratio)	H_2O/SO_2	H_2/SO_2	SO_2/H_2S	SO_2/Cl	Cl/F	H_2O (μmol/mol)	CO_2	SO_2	H_2S	HCl	HF	H_2	AETS (°C)	T-S_e (°C)
08/07/11	1	0.8	66	0.05	100 [b]	79	15	970,000	11,800	14,700	147	186	12	740	–	118
08/10/28	1	1.7	180	0.05	300	90	3.4	980,000	9,300	5,500	18	61	18	270	–	71
09/03/23	1	1.0	90	0.03	2000[b]	24	4.9	980,000	10,900	10,900	5	450	92	330	–	70
09/03/24	1	1.0	100	0.01	2000	28	9.0	980,000	9,800	9,800	5	350	39	98	–	55

–Not determined

AETS Apparent Equilibrium Temperature for the following reaction: $2H_2O + H_2S = SO_2 + 3H_2$

T-S_e Saturation temperature of elemental sulfur by reaction (2) based on equilibrium constants given by Mizutani and Sugiura (1982). T-S_e of the lake gas was calculated with water vapor pressure at the lake water temperature

[a] SO_2/H_2S ratio obtained by the test tube of Komyo Rikagaku Kogyo Co

[b] Minimum estimate of the SO_2/H_2S ratio due to saturation of the SO_2 scrubber for the H_2S sensor

[c] Wind direction indicates that plumes are likely a mixture of fumarolic and lake gases

[d] The compositions on the left side are calculated with an average SO_2/Cl and Cl/F ratios of the three data sets obtained on the same day

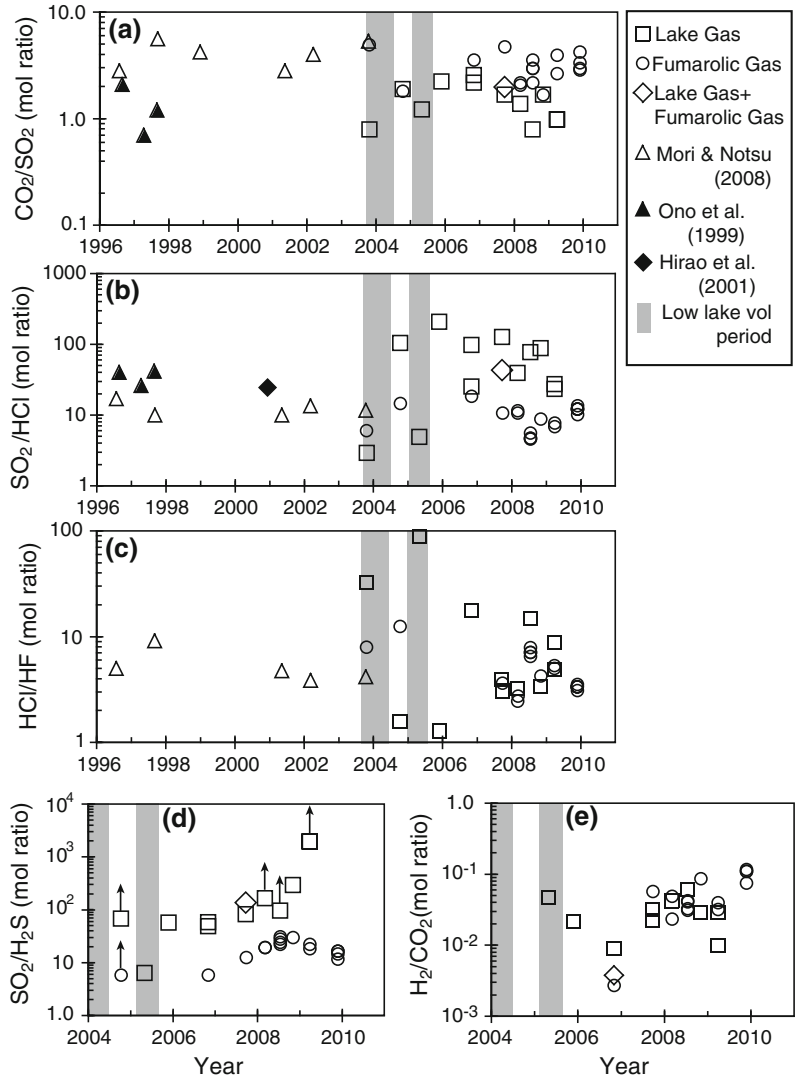

Fig. 4 Variation in gas concentration molal ratios estimated by the plume measurements. **a** CO_2/SO_2, **b** SO_2/HCl, **c** HCl/.HF, **d** SO_2/H_2S and **e** H_2/CO_2. *Circles* and *squares* are the lake gas and the fumarolic gas compositions, respectively, and a diamond represents the data from September 18, 2007, considered as a mixture of the two gas types. *Open* and *closed triangles* and *closed diamonds* indicate the compositions estimated by Fourier transform infrared spectroscopy (FT-IR) measurements in previous studies. Shadowed areas indicate the low lake volume periods. *Arrows* on **d** indicate the data obtained when the SO_2-filter was saturated, implying that the data are minimum estimates of the ratios

lake gases, the lake waters and the fumarolic gases. First, we will discuss the distribution of volcanic gas species between the lake gases and the lake waters that occurs at the surface of the lake. Then, we will estimate compositions of the hydrothermal fluids supplied to the lake. Finally, we will compare compositions of the hydrothermal fluids and the fumarolic gases to evaluate differentiation processes of these fluids.

5.1 Differentiation in the Lake

Lake gases are separated from lake waters at the lake surface. Assuming equilibrium, the distribution of gas species between the lake gas and the water can be evaluated based on solubility data. Distribution of an inert gas component i between the vapor and liquid phases can be expressed by the Henry's solubility constant (K_i),

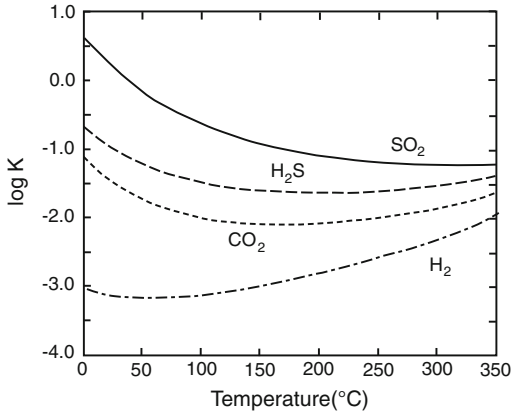

Fig. 5 Henry's law for solubility of volcanic gas species as a function of temperature (Schulte et al. 2001)

which is given as a function of temperature (Schulte et al. 2001; Fig. 5);

$$K_i = \frac{C_i^{liq}}{P_i} = \frac{X_i^{liq} \cdot N_w}{P_i \cdot X_i^{vap}} = \frac{X_i^{liq} \cdot N_w}{P_{H_2O} \cdot X_i^{lake-gas}}, \quad (1)$$

where C is molality (mol/kg) of a component indicated by the subscript in a phase indicated by the superscript; P, pressure in bars; X, mole fraction; and N_w, a constant to convert mole fraction to molality (≈1,000/18.01 = 55.5). The partial pressure of each gas component can be calculated from the lake gas composition and saturated water vapor pressure at lake water temperature. Solubility of SO_2, H_2S, CO_2, and H_2 is low, and dissolved contents of these species in the lake water will be quite low. Among these species, SO_2 is the most soluble gas component, but the SO_2 mol fraction in the lake gas is 500 times that in the lake water at 60 °C, where K_i = 0.6 and $P_{H_2O} = 0.2$. Other gas species, whose solubility is more than an order of magnitude less than that of SO_2 in the crater lake temperature range, are predominant in the lake gas.

HCl is a soluble gas species, and Cl is the most dominant component of the lake water (Ohsawa et al. 2003, 2010; Miyabuchi and Terada 2009; Terada pers. com; Table 2). As HCl dissociates in an aqueous solution, its solubility does not obey the law of Henry's solubility, but is expressed by the variation in vapor pressure as a function of temperature and concentration in the aqueous solution (Washburn 2003). By assuming the lake water as a simple HCl–H_2O system, the HCl concentration in the lake water can be calculated from the lake gas HCl/H_2O ratio at a given temperature based on a vapor pressure data set of HCl acid solution (Washburn 2003; Fig. 6). The lake water HCl concentrations calculated from the gas compositions agree well with the measured Cl concentrations in the lake water for the July–September 2007 and July 2008 datasets. This agreement indicates that the HCl and H_2O contents in the lake gases are controlled by the equilibrium evaporation of the lake waters and that the evaporation can be modeled with a simple HCl–H_2O solution in spite of the high concentration of sulfates in the lake water (Table 2). The negligible effect of the sulfate may be attributed to its smaller ionic dissociation constant compared to that of HCl.

A large difference was observed between the calculated and measured HCl concentrations in March 2009 (Fig. 6). This difference can be due to contamination of plumes coming from the fumarolic area. Since HCl/H_2O ratios of the fumarolic gases are one to two orders of magnitude larger than they are for the lake gases, even a small amount of contamination, such as a few %, can cause a significant deviation. The composition measured by the alkaline filter is an average plume composition during the 30–60 min sampling period and a small amount of cross contamination is inevitable in some cases, such as unstable wind conditions.

The lake gas compositions are controlled not only by simple gas dissolution in the lake water but also by various chemical reactions in the gas and water phases. The lake gases have high SO_2/H_2S ratios, commonly one to two orders of magnitude larger than the ratios for the fumarolic gases, except during the low lake volume period (Fig. 4d). Since SO_2 is more soluble in an aqueous phase than H_2S, these high ratios cannot be due to selective dissolution of these species into the lake water. High-temperature fumarolic gases commonly have high SO_2/H_2S ratios, and low-temperature fumarolic gases often have low SO_2/H_2S ratios (Mizutani and Sugiura 1966;

Table 2 Composition of lake water and calculated H_2O/HCl ratio in a vapor phase

Date (yy/mm/dd)	Temp (°C)	pH	Cl (mg/kg)	SO_4 (mg/kg)	F (mg/kg)	(H_2O/HCl)v[a] mol ratio	References
93/10/19	66.2	0.38	16,330	14,400		40,000	Ohsawa et al. (2003)
00/08/04	55.3	0.81	29,110	44,160	2,350	22,000	Ohsawa et al. (2003)
03/04/22	71.2	−0.72	113,600	105,600	12,000	400	Ohsawa et al. (2003)
03/08/04	90.0	−0.6	120,000	108,000	12,100	180	Ohsawa et al. (2010)
07/03/28	56.0	0.3	20,000	24,600	2,400	45,000	Ohsawa et al. (2010)
07/07/26	65.0	0.4	21,400	28,000	2,700	25,000	Ohsawa et al. (2010)
08/07/08	71.6	0.4	38,000	59,700	5,790	6,000	Miyabuchi and Terada (2009)
09/02/12	56.2	0.4	44,300	66,700	6,550	8,000	Terada pers. com.
09/03/24	60.0	−0.1	46,900	74,400	6,930	6,000	Terada pers. com.

[a] Calculated ratio in a vapor phase equilibrated with the lake water

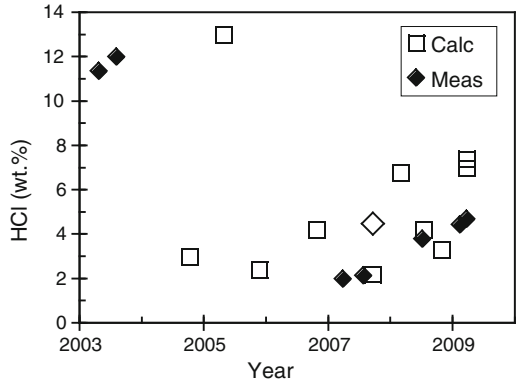

Fig. 6 Variations in HCl concentration in the lake water. *Open squares* and an *open diamond* represent HCl concentrations in the lake water calculated from the measured gas composition of the lake gas and of the mixed plume, respectively (Table 1). *Closed diamonds* show the measured HCl concentration in the lake water (Table 2; Ohsawa et al. 2003, 2010; Miyabuchi and Terada 2009; Terada pers. com.)

Giggenbach 1987). However, very high SO_2/H_2S ratios, such as those obtained for the lake gases in this study, can also be found at low-temperature fumaroles because of S deposition by the following reaction (Mizutani and Sugiura 1966; Giggenbach 1987):

$$SO_2 + 2H_2S = 2H_2O + 3S_e, \qquad (2)$$

where S_e is elemental S. When the initial ratio of SO_2/H_2S is higher than 0.5, the ratio increases by the reaction (2). Based on the temperature dependence of the equilibrium constant of reaction (2), S saturation temperatures are calculated (T-S_e in Table 1). The S saturation temperatures of the lake gases are almost always higher than the lake temperatures, implying that the lake gases are supersaturated with S_e and the high SO_2/H_2S ratios of the lake gases are likely the results of reaction (2). The higher S saturation temperatures indicate that reaction (2) does not achieve equilibrium, likely because of the short residence time of the gas species in the lake water (either as dissolved species or as bubbles). Formation of S_e through reaction (2) agrees with the S-rich lake sediments (Miyabuchi and Terada 2009). A low SO_2/H_2S ratio of the lake gas was observed in October 2003 during the low lake volume period (Fig. 4d). The low ratio might be due to poor interaction of the gas species in the lake water.

Sulfate is the predominant S species in the lake water and is likely formed by disproportionation of SO_2 through the following reactions (Giggenbach et al. 2003; Werner et al. 2008);

$$4SO_2 + 4H_2O = 3H_2SO_4 + H_2S \qquad (3)$$

or

$$3SO_2 + 2H_2O = 2H_2SO_4 + S_e. \qquad (4)$$

The sulfate formed by reaction (3) is also considered as a minor component of the lake water, which is supersaturated with H_2S in terms of reaction (2). Therefore, reaction (4) is likely the major source of sulfate in the lake.

5.2 Hydrothermal Fluids Supplied to the Lake

The composition of the hydrothermal fluids supplied to the lake can be estimated based on mass balance of the lake gases and the lake water. In recent times, the energy and material budget of the Yudamari crater lake were studied extensively (Saito et al. 2008; Terada et al. 2008, 2012; Terada and Yoshikawa 2009). Energy and water budget modeling revealed that the water discharge rate by evaporation is 2–7 times the lake water seepage (Saito et al. 2008; Terada et al. 2012). Based on these water flux ratios and compositions of the lake gases and waters, compositions of their mixture are calculated (Fig. 7). Since both lake gases and waters have variable compositions, two end member compositions are assumed both for the lake water and the lake gas (open and closed small circles; Fig. 7), and a range of compositions is calculated to cover the possible composition range of the hydrothermal fluids (shaded area; Fig. 7). The lake sediments are rich in S_e (Miyabuchi and Terada 2009). The lake water and the lake gas are not the only outputs of the lake; the S_e deposition on the lake bottom too should be considered as an output of the lake in the geochemical model since the S_e will react with neither the water nor the gases. Therefore, the S_e deposition rate should be also considered for the mass balance calculations to estimate the hydrothermal fluids composition.

The S output fluxes as the S_e, the lake gas SO_2 and the lake water sulfate can be summarized as follows. The accumulation rate of the S_e on the lake bottom was estimated based on S content in the lake sediments and a deposition rate of 250 t/d, which is comparable with the SO_2 gas flux (100–200 t/d as S) from the volcano (Miyabuchi and Terada 2009). Although both the lake gas and the fumarolic gas contribute the SO_2 emission, there is no quantitative estimate on their relative contribution. For simplicity, we assume that the lake

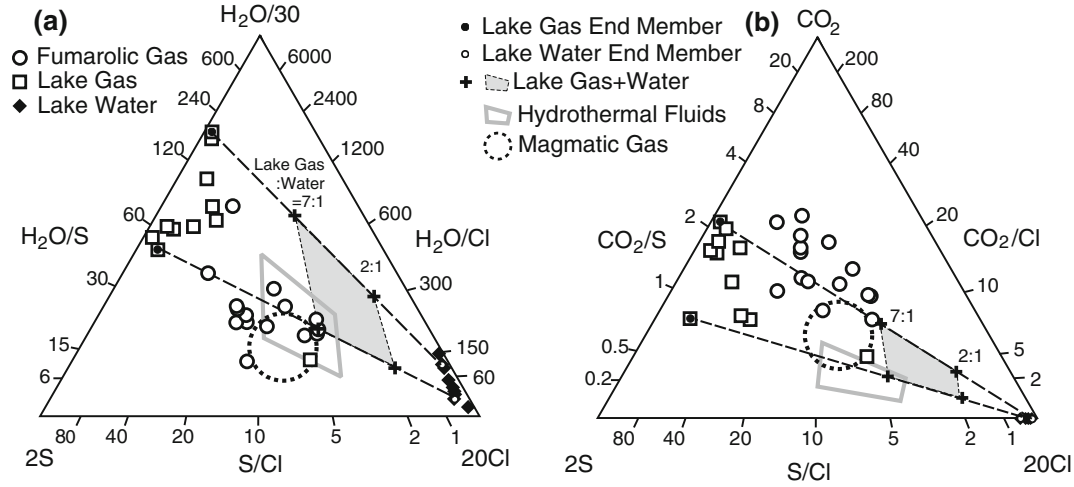

Fig. 7 Relative concentrations of **a** H_2O-S–Cl and **b** CO_2-S–Cl. *Open circles*, *open squares* and *closed diamonds* are measured compositions of the fumarolic gases, the lake gases, and the lake waters. *Dashed lines* represent the mixing line of the lake gas and the lake water end member compositions shown by the small *open* and *closed circles*, respectively. The shadowed areas indicate the estimated ranges of the lake gas and water mixture compositions with the water mixing proportion ranging from 7:1 to 2:1. The area surrounded by the *grey thick lines* shows compositions of the hydrothermal fluids estimated with an assumption that half of the sulfur in the lake fluids was deposited as elemental sulfur (see text for details). The area surrounded by the *dashed circle line* shows compositions of the magmatic gases estimated as the average of the fumarolic gases and the hydrothermal fluids. The H_2O content of the magmatic gases is estimated with an assumption that half of the H_2O in the hydrothermal fluids is derived from the meteoric water (see text for details)

gas is the major source of SO_2 with the flux of 200 t/d S. The water output flux by the lake gas (evaporation) is two to seven times larger than that by the lake water (seepage; Terada et al. 2012). Since the H_2O/S ratio of the lake water and gases are similar (Fig. 7a), the S output flux by the lake gas is also two to seven times larger than the flux by the lake water. As the lake gas S flux is 200 t/d, the S output flux by the lake water sulfate ranges from 30 to 100 t/d. The results show that the S output flux by the S_e deposition is about half (250/550–250/480) of the total S output from the lake, and S content of the hydrothermal fluids supplied to the lake is about double that of the lake gas + water mixture (the areas surrounded by the grey lines; Fig. 7). This is a crude estimate because we do not have enough data to evaluate the relative SO_2 flux of the lake gas and the fumarolic gas, and the correlation of compositions and fluxes of the lake water and lake gases. This estimate, however, indicates that the hydrothermal fluids are more S-rich than the lake gas + water mixture, and have a similar composition to the fumarolic gases on the H_2O–S–Cl plot (Fig. 7a).

The deposition of half of the S in the hydrothermal system as S_e can be an overestimate, because the reactions (2) and (4) convert only a small proportion of S species to S_e. Reaction (4) can produce S_e with only half the amount of sulfate. Efficiency of S_e formation by reaction (2) depends on the initial SO_2/H_2S ratio. If the initial SO_2/H_2S ratio is similar to that of the fumarolic gases (ten), only 15 % of the total S can be converted to S_e. In contrast, if the original SO_2/H_2S ratio of the fumarolic gases was small, such as around 0.5, a large amount of S can be formed by reaction (2) and the high ratio of the fumarolic gases can be considered as the result of reaction (2). This idea is consistent with the model that the fumarolic gases are a mixture of magmatic gases and a vapor phase formed under hydrothermal conditions as will be discussed in the next section. We need better constraints on the S_e deposition rate not only to estimate the S budget in the lake but also to model the geochemical differentiation process of the hydrothermal system.

5.3 Differentiation in a Hydrothermal System

The estimated compositions of the hydrothermal fluids are plotted near the fumarolic gases with some overlap (Fig. 7). Both compositions have wide ranges with similar H_2O/S and H_2O/Cl ratios, but the hydrothermal fluids have significantly lower CO_2/S and S/Cl ratios than do the fumarolic gases. The close occurrence of these two fluids suggests that a common magmatic gas is the source of the both fluids. The fumarolic gases can be either the source magmatic gas itself or the gas phase separated from the hydrothermal fluids in a hydrothermal system formed as a mixture of the magmatic gas and meteoric water.

The fumarolic gases are likely derived from high-temperature gases. Very high-temperatures of >500 °C were recorded by infrared thermometer measurements from the crater rim on some occasions (Fig. 3). Equilibrium temperatures calculated based on chemical and isotopic compositions also indicate that the fumarolic gases have a high-temperature origin. Apparent equilibrium temperatures (AET; Matsuo 1960; Ohba et al. 1994) for the following reaction were calculated for the fumarolic gas compositions (Table 1);

$$H_2S + 2H_2O = 3H_2 + SO_2. \quad (5)$$

The calculated AETs range from 718 to 974 °C; an exception was observed on October 26, 2006, for which an AET of 498 °C was calculated (Table 1). The AETs agree with equilibrium temperatures estimated by other studies. High temperatures, ranging from 700 to 1050 °C, were estimated with the method of Mori and Notsu (1997) based on the CO/CO_2 ratio measured by the FT-IR in 1996–2003 (Hirao et al. 2001; Mori and Notsu 2008). Tsunogai et al. (2011) measured the H_2 isotope compositions of the Aso volcanic plumes in November 2010 and estimated an isotopic equilibrium temperature of 870 °C for the H_2–H_2O isotopic exchange reaction. The similar temperature estimates, regardless of the method used or the periods, indicate that the maximum

temperature of the fumarolic gases are constant around 800–900 °C.

High-temperature emission of the fumarolic gases suggests that the fumarolic gas is a direct discharge of a magmatic gas, implying that the hydrothermal fluids are formed by differentiation of the fumarolic gas and meteoric water mixture. The composition contrast between the fumarolic gases and the hydrothermal fluids, however, disagrees with such a differentiation processes. Under acidic and high-temperature conditions, CO_2 behaves as a conservative component. In order to create the CO_2-poor hydrothermal fluids from the fumarolic gases, a CO_2-rich fluid needs to be created as the counterpart. Emission of such CO_2-rich fluids, however, is not observed around the Nakadake crater. Although diffuse emission of CO_2-rich soil gases is a candidate of such a CO_2-rich gas emission, a detailed soil gas survey concluded that soil CO_2 flux in the crater area is only 0.12 t/d (Saito et al. 2007). Therefore, the fumarolic gas needs to be the differentiation counterpart of the hydrothermal fluids. This idea is supported by the inversely correlated variation in CO_2/SO_2 ratios of the fumarolic gas and lake gas with a constant median value of about two (Fig. 4a).

The fumarolic gases have higher CO_2/S and S/Cl ratios than the hydrothermal fluids (Fig. 7b). This composition contrast is similar to the composition contrast between the lake gas and the lake water, and as that contrast is caused by vapor-liquid separation, this suggests that the composition contrast between fumarolic gases and hydrothermal fluids is also the result of vapor-liquid separation under hydrothermal conditions. Direct input of magmatic gases to the fumarolic gases, however, is also necessary because of the quite high measured and calculated equilibrium temperatures of the fumarolic gases. This idea is also supported by the fact that deviation in CO_2/SO_2 ratios of fumarolic gas and lake gas from the median value is not symmetric. Therefore, the fumarolic gases are likely a mixture of magmatic gases and a vapor phase separated from the hydrothermal fluids (Fig. 8). Because of the vapor loss to the fumarolic gases, the composition of the hydrothermal fluids also differs from the original composition of a magmatic gas-meteoric water mixture. The wide

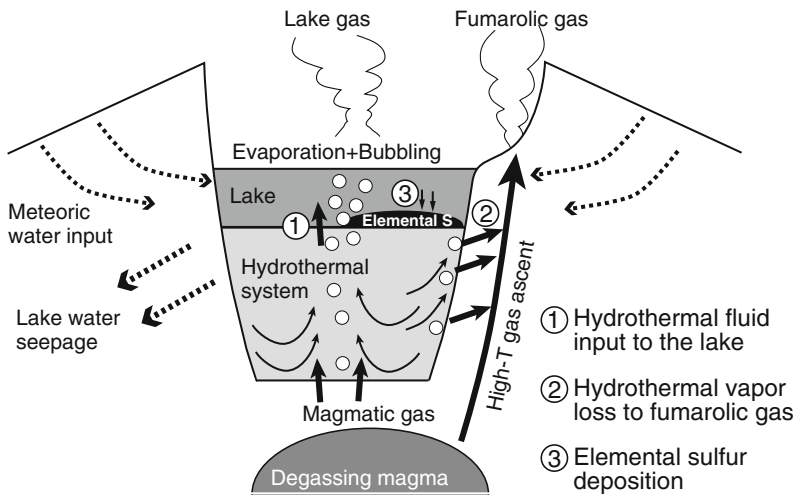

Fig. 8 A schematic diagram of a magmatic-hydrothermal system at Yudamari crater lake, Aso volcano. A hydrothermal system formed beneath the crater lake through mixing of magmatic gas and meteoric water. The hydrothermal fluids are supplied to the lake and are separated into the lake gas, the lake water and the elemental sulfur. The fumarolic gases are a mixture of the magmatic gas and a vapor phase in the hydrothermal system. The vapor phase loss to the fumarolic gases causes the hydrothermal fluids to be deficient in insoluble gas components such as CO_2

range of the fumarolic gas and the hydrothermal fluids compositions might be a result of the variable degrees and conditions of the vapor transfer to the fumarolic gases (Fig. 8).

Input of a vapor phase separated from the hydrothermal fluids results in composition shifts similar to those caused by magmatic gas scrubbing (Symonds et al. 2001). Since a crater lake and an associated hydrothermal system are effective sites for magmatic scrubbing, gas emission from a crater lake can be largely affected by this process. Werner et al. (2008) quantified CO_2/SO_2 ratios of the plumes discharged from White Island, New Zealand, by airborne measurements and observed inverse correlation with the crater lake growth; increases in the CO_2/SO_2 ratios were observed at the beginning of the crater lake formation, indicating significant magmatic gas scrubbing during this period. The simple magmatic gas scrubbing, however, will remove HCl more efficiently than SO_2, and the high HCl contents in the fumarolic gases indicate that the fumarolic gases cannot be formed simply by magmatic scrubbing.

The magmatic gases should have intermediate compositions between the fumarolic gases and the hydrothermal fluids. If the discharge rate ratio of the fumarolic gases and the hydrothermal fluids is known, we can calculate the magmatic gas composition by mass balance. Emission rates of SO_2 of the Aso volcano are regularly measured by the Japan Meteorological Agency and commonly range between 200–400 t/d, but contributions of the fumarolic gas and the lake gas are not separately quantified. Based on the energy and water budget of the lake, Terada et al. (2012) estimated that H_2O flux by the fumarolic gas is 50–100 % of the flux from the lake surface. This estimate implies that the magmatic gas compositions are similar to the average compositions of the fumarolic gases and the hydrothermal fluids (Fig. 7). Since the hydrothermal system is formed by mixing of the magmatic gases and meteoric water (Fig. 8), the magmatic gas composition is more H_2O-poor composition than the average compositions of the fumarolic gases and the hydrothermal fluids. Terada et al. (2012) estimated that the meteoric water contribution to the lake is similar to but commonly less than that by the high temperature steam. Therefore the H_2O/S ratio of the magmatic gas is likely larger than a half of the ratio for the average composition of the hydrothermal fluids and fumarolic gases (Fig. 7).

Wide ranges of compositions are estimated for the hydrothermal fluids and the source magmatic gases because of poor constraints on the material budget such as correlation of compositions and fluxes, and flux ratios of the lake gas, lake water, and fumarolic gases. Further quantification of these correlations will provide better constraints for more precise geochemical modeling. In some occasions, gas plumes from the lake surface and the fumaroles ascend as separate plumes (Fig. 2), and DOAS or SO_2-camera measurements (Mori and Burton 2006) in such occasions may enable separate quantification of discharge rates from the two sources. Such quantification of the discharge rates and compositions of the lake gases and the fumarolic gases is necessary for better estimating the magmatic gas composition and their differentiation processes.

6 Conclusions

Compositions of the lake gases and the fumarolic gases are quantified by plume measurements with Multi-GAS and alkaline-filter techniques. Compositions of both gases show large temporal variations and have distinct features; the fumarolic gases have larger CO_2/SO_2 ratios and smaller SO_2/HCl and SO_2/H_2S ratios than those of the lake gases. The HCl/H_2O ratio of the lake gas is close to that of a vapor phase in evaporation equilibrium with the lake water, implying that the lake gas and the lake water are differentiated by vapor-liquid equilibrium at lake surface conditions. Solubility of lake gas species indicates negligible gas contents in the lake water under the equilibrium conditions. Although dissolved gas contents are quite low, reactions of the gas species in the lake also control the lake gas and the lake water compositions. The large SO_2/H_2S ratios of the lake gases are attributed to S_e formation at lake temperature. A disproportionation reaction of SO_2 is the source of sulfate and

S_e in the lake and likely controls distribution of S species in the crater lake system.

Compositions of hydrothermal fluids supplied to the lake are estimated based on the compositions of the lake gases and the lake waters, and water discharge rates by lake gas evaporation and lake water seepage. The hydrothermal fluid compositions are also estimated considering formation of S_e, which contributes about 50 % of the total S in the lake fluids. The estimated hydrothermal fluids compositions have H_2O/S and H_2O/Cl ratios similar to the fumarolic gases but have slightly smaller S/Cl ratios and significantly larger CO_2/S ratios. The composition contrast between the fumarolic gases and the hydrothermal fluids and their occurrences suggest that these fluids are derived from vapor and liquid phases formed under hydrothermal conditions. Direct contribution of magmatic gases to these fluids is also suggested based on the high-temperature features of the fumarolic gases and gas-rich compositions of the lake gases. The large temporal variation in the lake gas and the fumarolic gas compositions is likely the results of changes in the mixing ratios of the magmatic gases and conditions of the hydrothermal phase separation.

Acknowledgments We wish to thank Dr. A. Terada for the unpublished lake water composition data, Drs. S. Onizawa, Toshiya Mori, Takehiko Mori, A. Namiki, Y. Sudo, N. Geshi and A. Yokoo for their discussion and assistance during the field works, Ms. M. Someya for assistance during chemical analyses, Drs. A. Aiuppa and C. Werner, for their detailed and constructive reviews, and Dr. B. Christenson for the careful editing. This work is partially supported by JSPS KAKENHI 22340130 to SH.

References

Aiuppa A, Federico C, Giudice G, Gurrieri S (2005) Chemical mapping of a fumarolic field: La Fossa Crater, Vulcano Island (Aeolian Islands, Italy). Geophys Res Lett 32:L13309. doi:10.1029/2005GL023207

Brown H, Rymer H, Dowden J, Kapadia P, Stevenson D, Barquero J, Morales LD (1989) Energy budget analysis for crater lakes: implication for predicting volcanic activity. Nature 339:370–373

Brown GC, Rymer H, Stevenson D (1991) Volcano monitoring by microgravity and energy budget analysis. J Geol Soc London 148:585–593

Delmelle P, Bernard A (2000) Volcanic lakes. In: Sigurdson H (ed) Encyclopedia of volcanoes. Academic Press, San Diego, pp 877–895

Giggenbach WF (1987) Redox processes governing the chemistry of fumarolic gas discharges from White Island, New Zealand. Appl Geochem 2:143–161

Giggenbach WF, Shinohara H, Kusakabe M, Ohba T (2003) Formation of acid volcanic brines through interaction of magmatic gases, seawater, and rock within the White Island volcanic-hydrothermal system, New Zealand. Soc Econ Geol Sp Publ 10:19–40

Hirao T, Fujimitsu Y, Nishijima J, Ehara S (2001) Remote ovservation of volcanic gases by FT-IR at Aso Volcano. Geoth Volcanol Res Rep Kyushu Univ 10:116–121

Inguaggiato S, Rizzo A (2004) Dissolved helium isotope ratios in ground-waters: a new technique based on gas-water re-equilibration and its application to Stromboli volcanic system. Appl Geochem 19:665–673

Ikebe S, Watanabe K, Miyabuchi Y (2008) The sequence and style of the 1988–1995 eruptions of Nakadake, Aso Volcano, Kyushu, Japan. Bull Volcanol Soc Jpn 53:15–33 (in Japanese with English abstract)

Japan Metrological Agency. Monthly Report (in Japanese). http://www.seisvol.kishou.go.jp/tokyo/STOCK/monthly_v-act_doc/monthly_vact.htm

Kanda W, Tanaka Y, Utsugi M, Takakura S, Hashimoto T, Inoue H (2008) A preparation zone for volcanic explosions beneath Nakadake crater, Aso volcano as inferred from electrical resistivity surveys. J Volcanol Geotherm Res 178:32–45

Matsuo S (1960) On the origin of volcanic gases. J Earth Sci Nagoya Univ 8:222–245

Matsushima N, Shinohara H (2006) Visible and invisible volcanic plumes. Geophys Res Lett 33. doi:10.1029/2006GL026506

Mazot A, Rouwet D, Taran Y, Inguaggiato S, Varley N (2011) CO_2 and He degassing at El Chichón volcano, Chiapas, Mexico: gas flux, origin and relationship with local and regional tectonics. Bull Volcanol 73:423–441

Miyabuchi Y, Terada A (2009) Subaqueous geothermal activity of acidic crater lake revealed by lacustrine sediments, Aso Volcano, Japan. J Volcanol Geotherm Res 187:140–145

Miyabuchi Y, Ikebe S, Watanabe K (2008) The July 10, 2003 and the January 14, 2004 ash emissions from a hot water pool of the Nakadake crater, Aso volcano, Japan. Bull Volcanol Soc Jpn 50:227–241 (in Japanese with English abstract)

Mizutani T, Sugiura T (1982) Variations in chemical and isotopic compositions of fumarolic gases from Showashinzan volcano, Hokkaido, Japan. Geochem J 16:63–71

Mizutani Y, Sugiura T (1966) The chemical equilibrium of the $2H_2S + SO_2 = 3S + 2H_2O$ reaction of solfataras of the Nasudake Volcano. Bull Chem Soc Japan 39:2411–2414

Mori T, Burton M (2006) The SO_2 camera: a simple, fast and cheap method for ground-based imaging of SO_2 in volcanic plumes. Geophys Res Lett 33:L24804. doi:10.1029/2006GL027916

Mori T, Notsu K (1997) Remote CO, COS, CO_2, SO_2, HCl detection and temperature estimation of volcanic gas. Geophys Res Lett 24:2047–2050

Mori T, Notsu K (2008) Temporal variation in chemical composition of the volcanic plume from Aso volcano, Japan, measured by remote FT-IR spectroscopy. Geochem J 42:133–140

Ohba T, Hirabayashi J, Nogami K (1994) Water, heat and chloride budgets of the crater lake Yugama at Kusatsu-Shirane Volcano, Japan. Geochem J 28:217–231

Ohsawa S, Sudo Y, Mawatari H, Shimoda G, Utsugi M, Amita K, Yoshikawa S, Yamada M, Iwakura K, Onda Y (2003) Some geochemical features of Yudamari Crater Lake, Aso volcano, Japan. Geotherm Res Rep Kyushu Univ 12:62–65 (in Japanese with English abstract)

Ohsawa S, Saito T, Yoshikawa S, Mawatari H, Yamada M, Amita K, Takamatsu N, Sudo Y, Kagiyama T (2010) Color change of lake water at the active crater lake of Aso volcano, Yudamari, Japan: is it in response to change in water quality induced by volcanic activity? Limnology 11:207–215

Ono A, Koya M, Fujimitsu Y, Ehara S (1999) Remote observation of volcanic gases by Fourier Transform Infrared Spectroscopy (FT-IR) at Aso Volcano. Bull Volcanol Soc Jpn 44:123–130 (in Japanese with English abstract)

Ono K, Watanabe K (1985) Geological map of volcanoes 4; geological map of Aso Volcano 1:50,000 (in Japanese). Geological Survey of Japan, Tsukuba

Ono K, Watanabe K, Hoshizumi H, Ikebe S (1995) Ash eruption of the Naka-dake crater, Aso volcano, southwestern Japan. J Volcanol Geotherm Res 66:137–148

Pennisi M, Le Cloarec MF (1998) Variation of Cl, F, and S in Mount Etna's plume, Italy, between 1992–1995. Geophys Res Lett 103:5061–5066

Saito M, Matsushima T, Matsuwo N, Shimizu H (2007) Observation of SO_2 and CO_2 fluxes in and around the active crater of Aso Nakadake Volcano. Sci Rep Dept Earth Planet Sci Kyushu Univ 22:51–52 (in Japanese with English abstract)

Saito T, Ohsawa S, Hashimoto T, Terada A, Yoshikawa S, Ohkura T (2008) Water, heat and chloride balances of the crater lake at Aso Volcano, Japan. J Geotherm Res Soc Jpn 30:107–120 (in Japanese with English abstract)

Schulte MD, Shock EL, Wood RH (2001) The temperature dependence of the standard-state thermodynamic properties of aqueous nonelectrolytes. Geochim Cosmochim Acta 65:3919–3930

Shinohara H (2005) A new technique to estimate volcanic gas composition: plume measurements with a portable multi-sensor system. J Volcanol Geotherm Res 143:319–333

Shinohara H, Witter J (2005) Volcanic gases emitted during mild Strombolian activity of Villarrica volcano. Chile. Geophys Res Lett 32:L20308. doi:10.1029/2005GL024131

Shinohara H, Hirabayashi J, Nogami K, Iguchi M (2011a) Evolution of volcanic gas composition during repeated culmination of volcanic activity at Kuchinoerabujima volcano, Japan. J Volcanol Geotherm Res 202:107–116. doi:10.1016/j.jvolgeores.2011.01.011

Shinohara H, Matsushima N, Kazahaya K, Ohwada M (2011b) Magma-hydrothermal system interaction inferred from volcanic gas measurements obtained during 2003–2008 at Meakandake volcano, Hokkaido, Japan. Bull Volcanol 73:409–421

Sudo Y, Tsuitsui T, Nakaboh M, Yoshikawa M, Yoshikawa S, Inoue H (2006) Ground deformation and magma reservoir at Aso Volcano: Location of deflation source derived from long-term geodetic surveys. Bull Volcanol Soc Jpn 51:291–309 (in Japanese with English abstract)

Symonds RB, Gerlach TM, Reed MH (2001) Magmatic gas scrubbing: implications for volcano monitoring. J Volcanol Geotherm Res 108:303–341

Terada A, Hashimoto T, Kagiyama T, Sasaki H (2008) Precise remote-monitoring technique of water volume and temperature of a crater lake in Aso volcano, Japan: implications for a sensitive window of a volcanic hydrothermal system. Earth Planet Space 60:705–710

Terada A, Yoshikawa S (2009) Development of observation techniques for inaccessible and extremely acidic crater lakes: installation of temperature telemetry buoys, dredging of lake sediments, and sampling of lake waters. J Geotherm Res Soc Japan 31:117–128 (in Japanese with English abstract)

Terada A, Hashimoto T, Kagiyama T (2012) Water flow model of active crater lake at Aso volcano, Japan: fluctuation of magmatic gas and groundwater fluxes from underlying hydrothermal systems. Bull Volcanol 74:641–655

Tsunogai U, Kamimura K, Anzai S, Nakagawa F, Komatsu DD (2011) Hydrogen isotopes in volcanic plumes: tracers for remote temperature sensing of fumaroles. Geochim Cosmochim Acta 75:4531–4546

Varekamp JC, Pasternack GB, Rowe GL Jr (2000) Volcanic lake systematics II. Chemical constraints. J Volcanol Geotherm Res 97:161–179

Washburn EW (2003) International critical tables of numerical data, physics, chemistry and technology, 1st electronic edn. Knovel, Norwich, NY, p 3414

Werner C, Christenson BW, Hagerty M, Britten K (2006) Variability of volcanic gas emissions during a crater lake heating cycle at Ruapehu Volcano, New Zealand. J Volcanol Geotherm Res 154:291–302

Werner C, Hurst T, Scott B, Sherburn S, Christenson BW, Britten K, Cole-Baker J, Mullan B (2008) Variability of passive gas emissions, seismicity, and deformation during crater lake growth at White Island Volcano, New Zealand, 2002–2006. J Geophys Res 113:B01204. doi:10.1029/2007JB005094

The Other Side of the Coin: Geochemistry of Alkaline Lakes in Volcanic Areas

Giovannella Pecoraino, Walter D'Alessandro, and Salvatore Inguaggiato

Abstract

Among surface waters, lakes in volcanic areas display the greatest range in pH values: from negative values up to about 12. The present chapter is a short review of the main features of alkaline lakes, which belong to the high-pH part of this range. They are characterised by saline or hypersaline waters, pH values higher than 9 and high Na^+, HCO_3^- and CO_3^{2-} and low Ca^{2+} concentrations. Alkaline lakes are found in quiescent or recently extinct volcanic areas where neither water vapour nor acidic magmatic gases can reach surface waters. Their occurrence depends on peculiar climatic and geological conditions that allow evaporative concentration of the water (potentially evaporation much higher than water inputs and in endorheic basins) and on geochemical factors that favour a chemical evolution towards an alkaline environment (composition of the dilute input waters characterised by a ratio between total dissolved inorganic carbon and earth-alkaline elements much higher than 1). Such initial composition, due to evaporative concentration, after the deposition of earth-alkaline carbonate minerals, will lead to the above-mentioned typical composition. Alkaline lakes also host microbial communities sometimes characterised by extremely high productivity. These microbial communities are scientifically remarkable because they comprise some interesting extremophiles, which can grow not only at very high pH and salinity conditions but also in the presence of elevated concentrations of toxic elements (e.g. As, Se, Te).

G. Pecoraino (✉) · W. D'Alessandro · S. Inguaggiato
Istituto Nazionale di Geofisica e Vulcanologia, Sezione Di Palermo, Via Ugo La Malfa 153, 90146 Palermo, Italy
e-mail: giovannella.pecoraino@ingv.it

S. Inguaggiato
Instituto de Geofísica, Universidad Nacional Autónoma de México, Coyoacán, México DF, Mexico

D. Rouwet et al. (eds.), *Volcanic Lakes*, Advances in Volcanology,
DOI 10.1007/978-3-642-36833-2_9,
© Springer-Verlag Berlin Heidelberg 2015

Keywords
Alkaline lake · Soda lake · Volcanic lake · Extremophile microbial community · Saline and hypersaline water · Endorheic basin

1 Introduction

The word "volcanic lake" is instinctively linked to a hot and acidic water body (Christenson et al., this issue). Indeed this is true in active volcanic systems where water vapour and acidic magmatic gases (mainly SO_2 and HCl) have the possibility to directly reach a lake and the dissolution of the gases will necessarily lead to high temperatures and very low pH (<0) values of the lake water (Christenson and Tassi, this issue). As widely shown in the previous chapters, such extreme conditions will consequently lead to very high salinities and unusual chemical compositions do to intense water-rock interaction processes (Varekamp, this issue).

But, if we look at the compilation of pH values in volcanic lakes made by Varekamp et al. (2000) and Marini et al. (2003) we can observe that, although clustering around a few acidic values, they span over a wide range with alkaline values being not too rare. Furthermore, it should be considered that the compilation is probably biased towards acidic values because acidic lakes are both more attractive to study and their regular survey is important for estimating the activity of the related volcanic system (Giggenbach 1990; Rowe et al. 1992; Aguilera et al. 2000; Varekamp et al. 2000; Marini et al. 2003; Taran et al. 2008).

In some active volcanic areas acidic magmatic gases do not have the possibility to reach surface water bodies. This is generally due to the presence of hydrothermal systems at depth. The most soluble of the magmatic gases (like SO_2, HCl and HF) interacting with the hydrothermal system dissolve in the liquid phase forming mainly anionic species (SO_4^{2-}, Cl^- and F^-). This process leaves the residual gas phase enriched in CO_2. The latter is also the main component of the gases released in quiescent or recently extinct volcanic areas.

The fate of the abundant upflow of CO_2 upon interaction with surface water bodies depends on their chemical and hydrological characteristics. Carbon dioxide can passively accumulate as dissolved gas in the deepest layers of the lakes leading to dangerous pressure build up that eventually could evolve in deadly massive gas releases (Kusakabe, this issue; Vaselli et al., this issue). The most known examples are the fatal episodes happened at the Cameroonian lakes Monoun and Nyos in the 1980s, which led to 37 and more than 1,700 casualties, respectively (Witham 2005; Kusakabe, this issue and references therein). The abundant geogenic CO_2 also contributes to weathering reactions within cold or thermal aquifers that release alkalis and bicarbonate to the groundwater. Such waters emerging at the surface, together with the right climatic and hydrological conditions, can possibly lead to the formation of alkaline lakes.

Alkaline or soda lakes are a peculiar type of saline lakes whose waters display pH values above 9 and whose chemical composition is characterised by Na^+ as the main cation and by the presence of high HCO_3^- and CO_3^{2-} contents. Nevertheless, sometimes the main anionic species are Cl^-, or rarely SO_4^{2-}. In the most extreme cases of evaporation (e.g., Magadi Lake, Kenya) the salinity may reach values at or near halite saturation, and the concentrations of carbonate may be very high (up to thousands of meq/l). The pH of such brines may reach 10–11 or even higher (Grant and Tindall 1986). Trona ($NaHCO_3 \cdot Na_2CO_3 \cdot 2H_2O$) and Natron ($Na_2CO_3 \cdot 10H_2O$) often precipitate in such environments. Examples of the chemical composition of alkaline lakes in volcanic areas are displayed in Table 1.

One of the most striking features of many soda lakes is their colour. Depending on the water chemistry of the individual lakes, they are likely to be green, pink, red or orange, due to massive permanent or seasonal blooms of microorganisms (Grant et al. 1990; Christenson et al., this issue). This is reflected in the extremely high primary productivity and wide variety of microbial life associated with some of these lakes.

Table 1 Location and chemical composition of some alkaline lakes

Name	Northing	Easting	Altitude (m)	pH	Na (meq/l)	K (meq/l)	Mg (meq/l)	Ca (meq/l)	F (meq/l)	Cl (meq/l)	SO_4 (meq/l)	Alk (meq/l)	SiO_2 (meq/l)	Ref.
Van lake (Turkey)	38° 39.926′	42° 54.190′	1,647	9.88	347	11.1	9.06	0.17		166	50.8	156	7	Reimer et al. (2009)
Mono lake (USA)	38° 00.422′	−119° 00.379′	2,031	10.00	1,331	45.6	2.72	0.20		518	208	593	14	Johannesson et al. (1994)
Albert lake (USA)	42° 37.727′	−120° 14.139′	1,357	9.71	1,975	33.2	0.04	0.10		1,175	37.4	699	96	Johannesson et al. (1994)
Abiyata (Ethiopia)	7° 36.300′	38° 35.976′	1,581	10.08	430	9.57	0.02	0.03	16	119	10.0	316		Gizaw (1996)
Langano (Ethiopia)	7° 35.607′	38° 45.484′	1,587	9.05	19	0.59	0.23	0.39	1	5.08	0.35	15.5		Gizaw (1996)
Magadi lake (Kenia)	−1° 55.243′	36° 16.039′	606	10.77	4,826	53.5			104	2,474	45.0	1,218	1,100	Jones et al. (1977)
Bogoria lake (Kenia)	0° 15.401′	36° 05.788′	991	9.20	1,778	16.5	0.16	1.70		255	11.4	1,550		Renaut et al. (1986)
Nau Co (China)	32° 49.305′	82° 12.224′	4,381	9.50	3,087	128	21.4	0.20		1,374	1,496	50.8		Zheng et al. (1993)
Atlacoya (Mexico)	19° 07.637′	−97° 32.486′	2,381	10.70	233	7.70	0.09	0.21		31.9	1.03	121	34	Vilaclara et al. (1993)
Cachi laguna (Bolivia)	−21° 44.054′	−67° 56.729′	4,499	10.05	4,000	910	0.24	0.30		1,610	746	2,500	432	Risacher and Fritz (1991)
Specchio di venere (Italy)	36° 48.668′	11° 59.089′	2	9.20	313	13.7	0.50	12.10		260	22.9	59		Aiuppa et al. (2007)

This review chapter highlights the geological, hydrological and climatic conditions occurring in the formation of alkaline lakes and the geochemical processes leading to high salinity and high pH waters. Some case studies in volcanic areas are discussed and finally, an overview of the rich and peculiar microbial life in alkaline lakes is given.

2 Hydrological and Geochemical Processes in Alkaline Lakes

2.1 Occurrence of Alkaline Lakes

Alkaline lakes are mostly found within closed (endorheic) basins and their occurrence depends on the combination of climatic (amount of rain waters, evaporative processes), geological/topographic and geochemical (gas-water-rock interactions) factors.

The climate provides an important function in the water balance of endorheic lakes, because it regulates the water supply coming into the basin as rain and runoff, and it determines the evaporation rate. The inflow, generally limited, must be sufficient to sustain a permanent lake. Arid and semi arid climates, where potential evaporation is always higher than the meteoric recharge, are the ideal location to form saline lakes and consequently alkaline lakes.

Geological/topographic conditions allow, or do not, the development of a closed basin (morphology of the site = closed basin, presence of springs, impermeability of shallow strata, absent or near absent outflow, etc.). Many soda lakes were formed within volcanic craters or calderas (e.g., Mono Lake, USA, and Specchio di Venere, Pantelleria Island, Italy), within a graben in areas characterised by extensional tectonics (like the lakes of African Rift Valley, e.g., Natron Lake, Kenya) or upon abrupt interruption of a riverbed by lava flows or lahars (e.g., Lake Van, Turkey Pátzcuaro Lake, Mexico). Furthermore, the presence of regional tectonic or volcano-tectonic structures favours the input to the lake of thermal waters charged with endogenous carbon dioxide, important in the evolution of alkaline lakes. The topography can also strongly influence the climate of the area creating arid conditions due to a rain shadow. A particular morphology is represented by the Lonar Lake, in India, that was formed by a high velocity meteorite impact on basaltic rocks of the Deccan traps about 50 ka ago (Wani et al. 2006; Deshmukh et al. 2011).

The chemical composition of rocks (through weathering), of groundwater, spring or surface water flowing into the lake, the presence of dissolved CO_2, and mineral precipitation-dissolution all control the final chemical composition of the lake water. According to Spencer et al. (1990), in the case of evaporative processes, water assumes a composition that is a function of the original, initial dilute composition. The evaporation induces oversaturation and the first solid phases that are precipitated are alkaline-earth carbonates. At this stage the ratio between total dissolved inorganic carbon (TDIC) and the main alkaline–earth species (Ca^{2+} and Mg^{2+}) will be the main parameters that will drive the evolution of the evaporating lake towards an alkaline composition or not (Hardie and Eugster 1970).

2.2 Water and Solute In- and Outputs

Four main types of input can generally be recognised (Volkova 1998; Jones and Deocampo 2003; Aiuppa et al. 2007; Jones et al. 2009):

1. Meteoric recharge occurs either directly to the lake surface or through the runoff along the hydrologic basin. Depending on climate, it could be a more or less important part of the water input. The solute input is generally limited for the part attaining to the direct recharge while runoff could play a significant role in dissolving previously precipitated salts along its shores.
2. Focused discharge occurs through springs from the drainage area or diffuse seeps percolating slowly through the shores. They can represent an important part of both water and solute recharge to the lake. A slow flow rate may

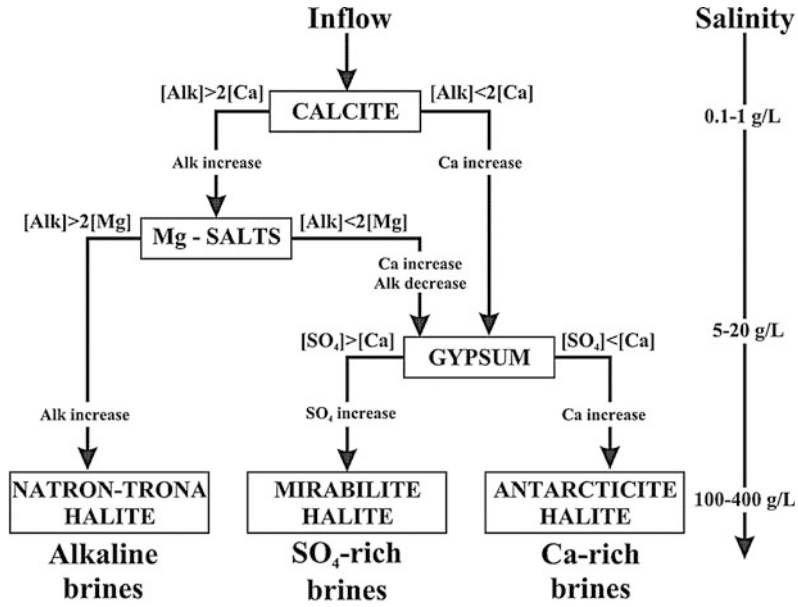

Fig. 1 Flow diagram showing both the geochemical brine evolution and mineral precipitation sequence during evaporative phenomena of lake waters. Solute constituents are indicated by *square brackets*, mineral precipitates are indicated by *boxes* (modified after Hardie and Eugster 1970; Eugster and Jones 1979)

induce an incipient evaporation of the waters before they reach the main body. In volcanic environments such input sometimes derives from geothermal systems and the water chemistry can be modified by precipitation of solid phases at the spring mouth induced by rapid changes in physico-chemical conditions (temperature drop, loss of CO_2, shifting of redox equilibria towards more oxidising conditions).

3. Rivers, generally of short length and low discharge due to the usually small area of their drainage basin can feed the lake.
4. Underground waters fill aquifers in the drainage basins. They discharge into the lake underwater through springs and seeps. Their contribution in terms of water and solute input can be variable and is often difficult to quantify depending on many geological and hydrological conditions.

As alkaline lakes are found almost always within closed basins, only three outputs can be recognized (Jones and Deocampo 2003 and references therein, Stumm 2004):

1. Evaporation accounts for the main output of the lake water, although generally without losing solutes;
2. Infiltration to the groundwater is generally limited in terms of water loss and can also be a significant solute output;
3. Precipitation of solid phases due to oversaturation of the lake waters accounts for the main loss in solutes (Fig. 1).

2.3 Geochemical Evolution

Waters undergoing evaporative concentration precipitate a sequence of minerals in order of increasing solubility. Hardie and Eugster (1970) and Eugster and Hardie (1978) introduced the basic concept of "chemical divide" to account for the evolution of solute concentration during evaporation.

The whole process is graphically shown in Fig. 1 which accounts for most natural waters. The reaching of oversaturation for a few minerals plays an important role in the water evolution. The least soluble minerals (i.e. the first to precipitate) are carbonates ($CaCO_3$ and $MgCO_3$), followed by gypsum ($CaSO_4 \cdot 2H_2O$). The mineral forming ions (both cations and anions) are removed from the water solution as they contribute to the solid phases. When the mineral precipitates, the solubility product ($K_s = [X^-]\cdot[Y^+]$) must remain constant and the more abundant constituent in solution becomes dominant with respect to the others (i.e. during

$CaCO_3$ precipitation, if Ca increases the C species decrease or vice versa). The outcome of this process is the generation of three main groups of brines: alkaline (Na^+/HCO_3^-–CO_3^{2-}–Cl^-), sulfate-rich (Na^+/SO_4^{2-}–Cl^-) and calcium-rich (Na^+–Ca^{2+}/Cl^-) brines.

As such, the final composition of the brines strongly depends on the initial composition of the dilute water. A small variation of the initial ratio of the critical components in the dilute water TDIC/Ca^{2+} and TDIC/(Ca^{2+} + Mg^{2+}) may cause drastic changes in the final brine composition. In turn, the composition of dilute inflow waters is mainly inherited from rock alteration. Therefore, there is an overall relationship between lithology and the final lake water composition. Each broad type of lithology is reflected in the composition of the dilute water which is further amplified by evaporative concentration. In a pioneering study, Garrels and Mackenzie (1967) first evidenced the strict relationship between igneous rocks and alkaline brines. High-purity igneous rocks are composed of silicate minerals being almost devoid of anionic components (Cl^-, SO_4^{2-}). The only available anion that can balance the cations derived from the weathering of pure igneous rocks is HCO_3^-, which is, in active and recently extinct volcanic areas, mainly derived from CO_2 of endogenous origin. Weathering of silicate minerals produces HCO_3^- and cations through silicate hydrolysis (Eqs. 1 and 2). The cations produced in a silicate hydrolysis reaction reflect the cations in the mineral being weathered. For instance, minerals with high Na content would tend to yield Na^+ when subjected to hydrolysis. Weathering of granitic and rhyolitic rocks (or sediments derived from them) is a common means of producing alkaline waters, as these rocks are composed primarily of K-feldspar, quartz, and Na-plagioclase, with generally little Ca (Eq. 1). Therefore, hydrolysis of granitic and rhyolitic rocks will yield HCO_3^-, Na^+, and K^+, but minor Ca^{2+} contents:

$$\mathrm{CO_2 + H_2O + \text{rhyolite (Na-plagioclase; K-feldspar; quartz)} \Rightarrow \text{clay minerals} + K^+ + Na^+ + HCO_3^-} \quad (1)$$

As a result, waters whose chemistry is controlled by silicate hydrolysis of granitic/rhyolitic rocks will have $HCO_3^- \gg Ca^{2+}$. This explains the presence of alkaline waters in granitic/rhyolitic terrains, but such waters are found also in areas dominated by andesitic/basaltic lithologies whose weathering reactions can be summarised as follows:

$$\mathrm{CO_2 + H_2O + \text{basalt (plagioclase; olivine; pyroxene)} \Rightarrow \text{clay minerals} + Ca^{2+} + Mg^{2+} + Na^+ + HCO_3^-} \quad (2)$$

In these cases, the silicates are more reactive due to their smaller grain sizes and to the presence of mafic minerals and/or volcanic glass (Jones 1966); the fast silicate weathering rates lead to a hydroxyl-neutralizing reaction

$$Ca^{2+} + HCO_3^- + OH^- \Rightarrow CaCO_3 \downarrow + H_2O \quad (3)$$

that effectively removes alkaline earths from solution, and produces alkaline waters (OH^- consumption) (Jones 1966).

Although examples of pH as high as 11–12 in soda lakes can be found in literature (Grant et al. 1990; Jones et al. 1998) these cases are rare. Pure sodium carbonate solutions have pH values of 11.3–11.5. The contact with atmospheric CO_2 and the presence of other salts, which is the real situation in the soda lakes, result in lower pH values. The sodium carbonate/bicarbonate system has its maximum buffering capacity in the pH range 9.5–10.2. Therefore, the most common pH values for soda lake waters can be expected to be found within this range, unless other buffering systems are dominating.

A useful tool to represent the compositional trend of water during evaporation is the Spencer diagram (Fig. 2): it is a Ca^{2+}, SO_4^{2-}, HCO_3^- + CO_3^{2-} (expressed in equivalent/l) ternary phase diagram in which three compositional fields, divided by compositional lines (the "chemical divides"), are indicated. The diagram shows how inflow waters evolve in composition due to evaporation and mineral precipitation. Arrows starting from the composition of the forming solid phase evidence precipitation processes. If calcite is the first mineral to precipitate (inflow water in the lower right compositional field), the water evolution always follows a trend that diverges from the calcite compositional point

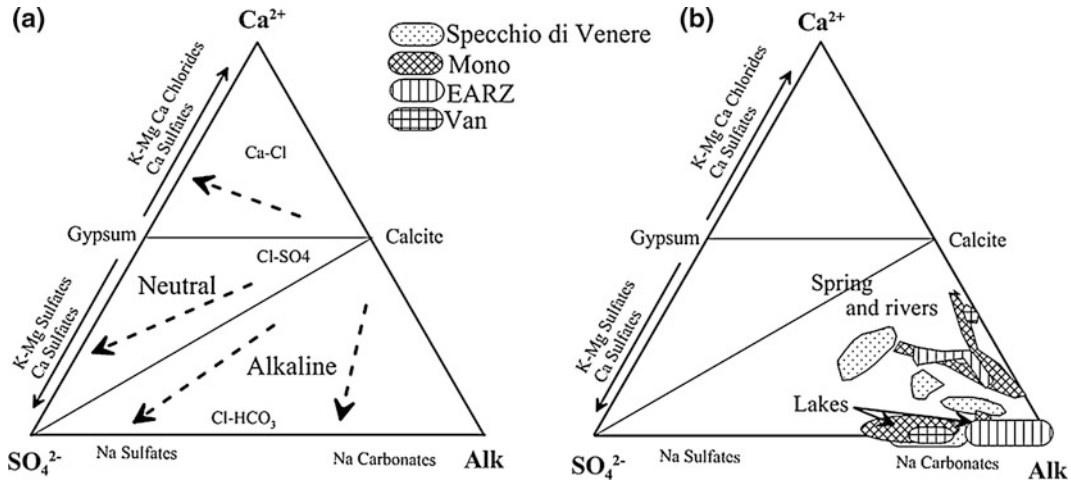

Fig. 2 **a** The spencer ternary phase diagram with compositional trends (*arrows*) of different composition evaporating waters indicated (see text for explanations); **b** some example of inflow waters (initial original composition) and lake waters (final composition) based on literature data

(Fig. 2a) becoming Ca-poor and Na, Cl, SO_4-enriched depending on the initial water composition. Waters in the Ca–Cl field evolve towards the Ca vertex as a consequence of SO_4 and HCO_3 depletion due to precipitation of calcite and gypsum. Some examples based on literature data are shown in Fig. 2b.

Due to evaporative concentration and high solubility in alkaline environments many trace elements can reach very high contents in alkaline hypersaline lakes. This could be of concern for their often high toxicity (Ochieng et al. 2007). But sometimes this could lead to elevated concentrations of elements of high economic value. For example Li and REE elements are sometimes extracted from highly concentrated brines obtained from the evaporation of the waters of alkaline lakes.

3 Geographical Distribution

Figure 3 shows the position of the alkaline lakes that were considered for the present review. As seen before among the conditions that favour the formation of an alkaline lake there is the presence of an arid or semi-arid climate, consequently there is no surprise to find them prevailingly in sub-tropical regions. These areas are the site of high atmospheric pressure feeding divergent atmospheric circulation cells. The greatest deserts are all found along this belt (Sahara, Arabian desert, central Asia deserts, Mexican and western USA deserts, Namibia, Australian desert).

The probability for a certain area to host one or more of these lakes greatly increases if the area is also endorheic and is, or was in the recent geological past affected by volcanic activity. Most of the alkaline lakes considered in this review are concentrated along the East African Rift Zone (EARZ hereafter, Lake Magadi and Lake Bogoria) (Talling et al. 1973; Melack and Kilham 1974; Jones et al. 1977; Melack 1979; Macintyre and Melack 1982; Yuretich and Cerling 1983; Renaut et al. 1986; Cerling 1996; Gizaw 1996; Grant et al. 1999; Deocampo 2005; Ochieng et al. 2007; Oduor and Schagerl 2007; Ayenew 2008; Dawson 2008; Ma et al. 2011).

The EARZ is an area of recent intense volcanic activity and also represents an endorheic area stretching about 4,000 km along the eastern part of Africa. The entire area is filled by thousands of lakes of different sizes. Despite its position close to the equator, precipitations are often rare due to a rain-shadow effect. Such

climatic and hydrologic conditions led to the formation of many saline lakes, most of which are also alkaline.

Two other areas in which many alkaline lakes are present are the south-western part of North America, e.g. Western USA (Mono Lake and Albert Lake) and Mexico (Lake Atlacoya) (Anderson 1958; Castenholz 1960; Jones 1966; Bischoff et al. 1993; Vilaclara et al. 1993; Johannesson et al. 1994; Connell and Dreiss 1995; Neumann and Dreiss 1995; Bischoff et al. 2004; Oremland et al. 2004; Baesman et al. 2009; Sahajpal et al. 2011) and the central-southern part of the Andean chain in South America (Laguna Cachi, Bolivia; Fig. 3). Both areas are within the volcanically active Ring of Fire around the Pacific Ocean. In the latter area, which comprises the territories of Bolivia, Chile and Argentina (Risacher and Fritz 1991; Risacher et al. 2003), notwithstanding the necessary hydrologic and climatic conditions, alkaline lakes are not as widespread as expected. For example, in their review on saline lakes of northern Chile, Risacher et al. (2003) state that only one of the considered 226 lakes and ponds could be classified as alkaline. The authors ascribe this to the abundance of both reduced and oxidised volcanic sulfur species. The alkalinity/calcium ratio of inflow waters is consequently lowered by the oxidation of native sulfur (reducing alkalinity) and the deposition of anhydrite or gypsum transported by strong winds (increasing Ca concentration).

Another area where climatic and hydrologic conditions favour the formation of alkaline lakes is the central part of Asia (Fig. 3) stretching from the Caspian Sea in the west to China (Tibet and Qinghai) in the east (Zheng et al. 1993; Volkova 1998; Zhang et al. 2008; Zheng and Liu 2009). Unfortunately, the literature on alkaline lakes in this area focuses on microbiology (Kompantseva et al. 2007, 2009). Despite the few notices about these lakes, the connection between the presence of alkaline lakes and recent volcanic activity of the area was highlighted by Zheng et al. (1993), at least for China.

Australia, being for its greatest part arid and composed of endorheic basins, is the host of numerous saline lakes, but the geology of the area does not create the necessary conditions for the evolution of these lakes towards alkaline conditions. On the contrary, the waters of these lakes display pH values from strongly acidic to moderately alkaline (1.7–8.6, Bowen and Benison

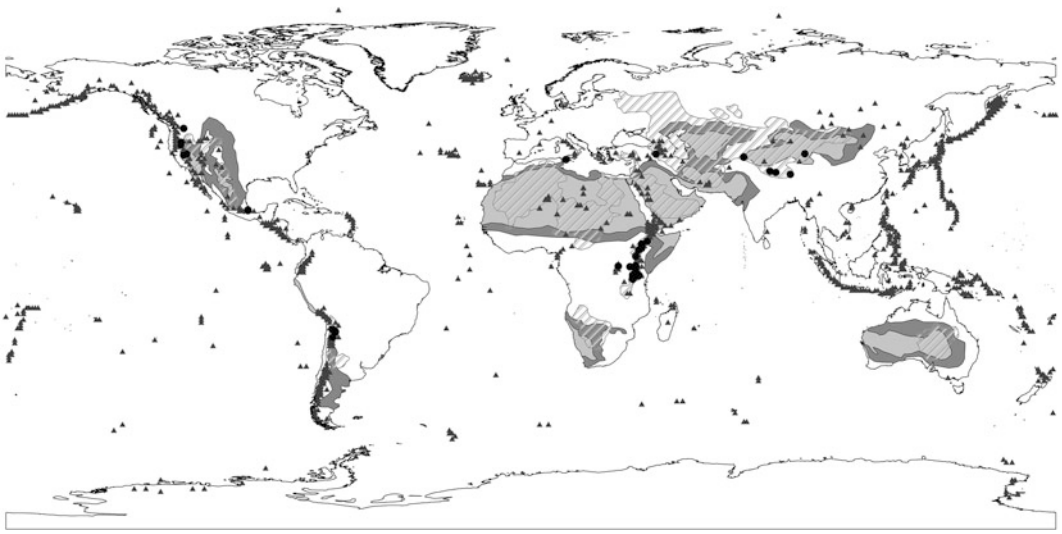

Fig. 3 Global distribution of soda lakes. Volcanoes of the ring of fire (*triangles*), soda lakes (*circles*), arid and semi-arid zones (*light gray* and *dark gray areas* respectively) and endorheic zones (*light gray shaded areas*) are indicated

2009). Most of Australia is formed by a tectonically stable Archean shield which remained above sea level exposed to weathering since the Mesozoic. As a result, the basement rocks are covered with thick zones of highly-weathered and chemically-altered regolith. In such geological framework, sulfide and Fe oxidation strongly contribute to acid formation following processes geochemically similar to those active in acid mine drainage systems (Long et al. 1992; Bowen and Benison 2009).

Even Antarctica, despite being covered for more than 99 % of its surface by a permanent ice cap, hosts some saline lakes (Green and Lyons 2009). Although some of them display pH values up to 10, no significant relation to volcanic activity or magmatic rocks has been ascertained.

4 Some Case Studies

4.1 Lake Van (Turkey)

Lake Van (Fig. 4a) is a terminal lake located on the high plateau of Eastern Anatolia (Turkey) at 1,648 m asl. This area is tectonically highly active, and earthquakes within the basin and the surrounding area of Lake Van are very frequent (Degens et al. 1984). The lake with a surface area of ca 3,600 km^2, a maximum depth of 451 m and a volume of about 600 km^3 is the largest alkaline lake and, after the drying up of Lake Aral, the third largest closed basin in the world (Landmann et al. 2011). The origin of Lake Van was ascribed to a remnant of a palaeovalley of the river Euphrates dammed about 60 ka ago by an

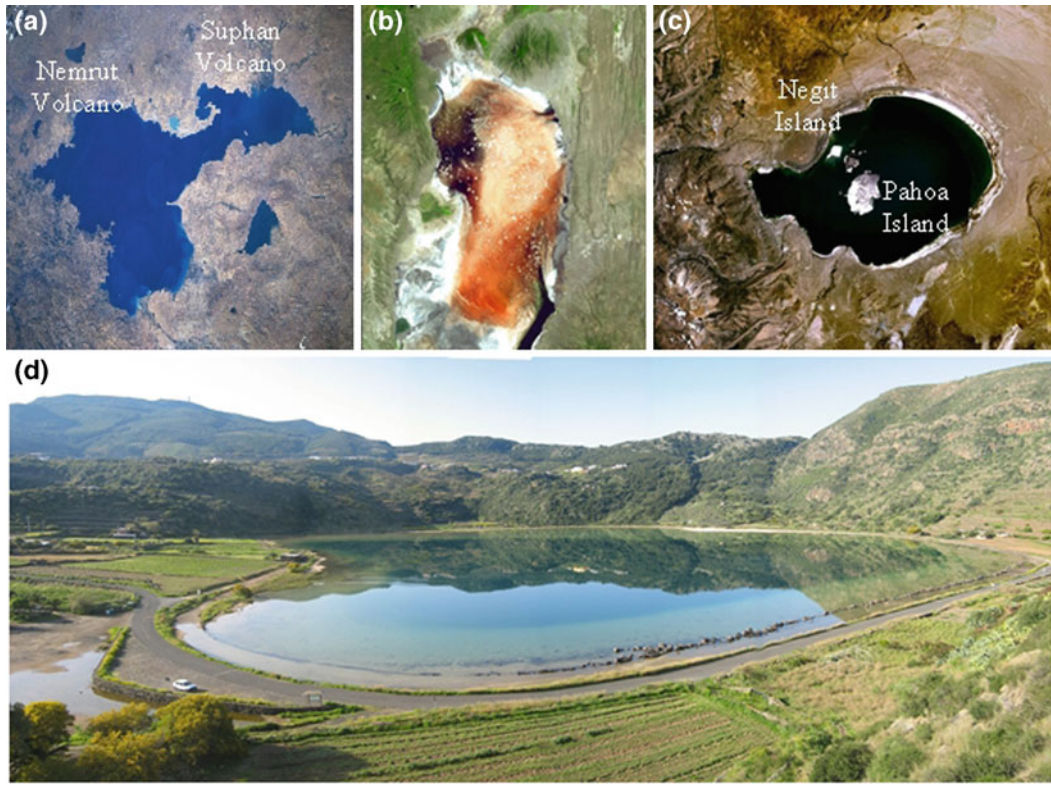

Fig. 4 Photos of selected lakes. **a** Van, Turkey. **b** Natron, Tanzania. **c** Mono, California. **d** Specchio di Venere (in Italian Mirror of Venus), Italy. *Photos* **a**, **b**, **c** from http://landsat.gsfc.nasa.gov and **d** by Walter D'Alessandro

eruption of Nemrut volcano located about 15 km west of the Lake Van (Degens and Kurtman 1978; Wong and Degens 1978; Yilmaz et al. 1998 and references there in; Utkutu 2006). Four composite volcanoes are aligned north of the lake, from WSW to ENE (Fig. 4a): Nemrut volcano (2,948 m), considered still active; Süphan volcano (4,158 m), inactive for several millennia; the older Meydan volcano (3,290 m); and Tendurek shield volcano (3,584 m) at the NE limit of the drainage area, recently active (Aydar et al. 2003). All tephra layers observed in lake cores are attributed to Nemrut volcano (Landmann et al. 1996) which erupted alkaline trachyte and basalt lavas, rhyolites and phonolites.

On the other hand, most of the drainage basin is constituted by volcanic rocks of Süphan volcano while the southern area comprises intrusive and metamorphic rocks of the Bitlis massif (Tomonaga et al. 2011). The lake has many tributaries but more than half of the runoff (highest discharge in April–May) can be attributed to Zilan, Bendimahi and Engil rivers (Reimer et al. 2009).

Christol et al. (2008) estimated a loss of 3.6 km^3 of water by evaporation and a recharge of 2.2 km^3 by rivers and 1.4 km^3 by precipitation. The lake is stratified in summer while in winter, cooling of the surface water and impact of winds induces homogeneity of water from 0 to 70 m.

Lake Van is characterised by strong seasonal oscillations in temperature, precipitation, dissolved ions and nutrient input (Kempe 1977; Huguet et al. 2011 and references therein). Salinity is around 21 g/kg and pH > 9. Sodium carbonate and sodium chloride equally contribute to the lake salinity with minor contribution of SO_4^{2-}, K^+ and Mg^{2+} (Fig. 5). Calcium results largely depleted. Water column profiles have shown an increase in salinity with depth. The lake floor is characterised by the presence of Tufa towers, huge carbonate microbialites, up to 40 m high, probably the largest on Earth reported so far (Kempe et al. 1991; López-García et al. 2005). The microbialites are externally covered by mats of coccoid cyanobacteria that appear to permineralize in situ with aragonite and inorganically

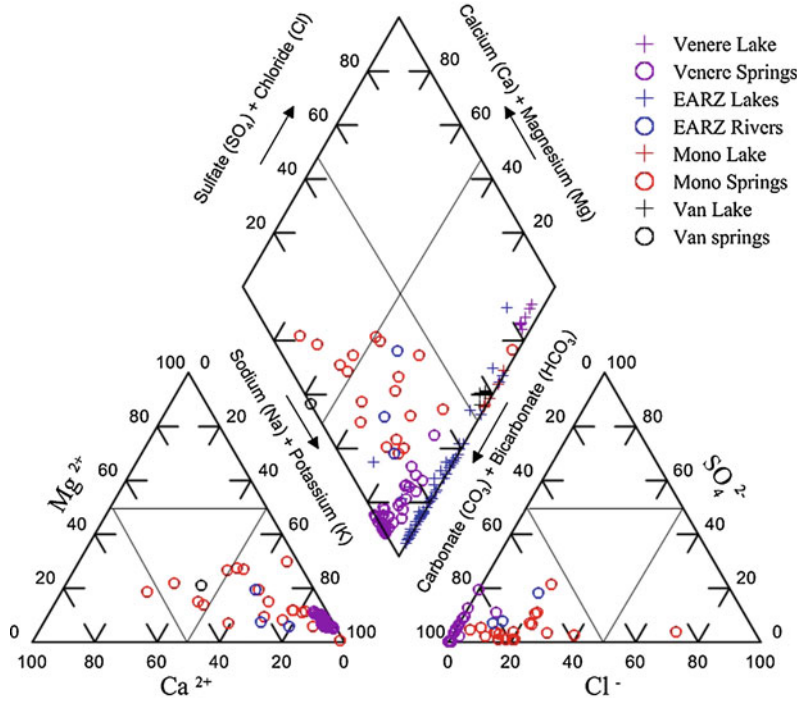

Fig. 5 Piper diagram showing the types and the main components of waters on the basis of concentration in eq/l

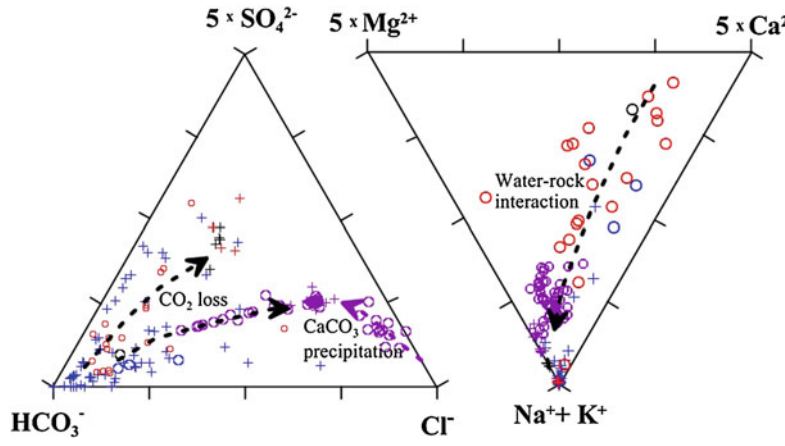

Fig. 6 Major ion *triangular plots* showing the compositional evolution of lake waters from inflow (*crosses*) to lake (*open circles*). *Arrows* indicate the water compositional trend evolution. *Symbols* as in Fig. 2b

precipitated calcite, whereas their interiors are traversed by channels transporting neutral, relatively Ca-enriched spring water flowing into the highly alkaline Ca-poor lake water. The mixing of the two water masses locally induces high calcium carbonate oversaturation and hence carbonate precipitation.

Waters flowing into the lake are predominantly bicarbonate with alkaline elements slightly exceeding alkaline earth elements (Fig. 6; Reimer et al. 2009). Furthermore, the diffuse volcanic CO_2 soil emission in this area contributes to maintain the TDIC/(Ca^{2+} + Mg^{2+}) of the rivers and springs above 1, driving the lake chemistry towards alkaline conditions.

4.2 Lake Natron (Tanzania) and the East African Rift Zone Lakes

The EARZ is the most extensive (4,000 km), NNE-SSW elongated, presently active, continental extensional zone in eastern Africa. The consequence of the extension-related fracturing was the formation of two sub parallel elongate shallow depressions, stretching from Ethiopia to Tanzania, now filled with volcanic rocks, volcano-clastic sediments, and fresh and saline lakes. The rift branch topography is characterised by half-graben basins associated with steeply-dipping border faults (Dawson 2008; Bergner et al. 2009; Corti 2009). The EARZ contains features such as snow-capped Kilimanjaro, the highest mountain on the African continent; Ngorongoro, one of the largest calderas on Earth; and active volcanoes like Nyiragongo, Nyamuragira (Tedesco et al. 2011) and Oldoinyo Lengai (Kervyn et al. 2008), which is unique for its extrusion of alkali carbonatites.

Most parts of the EARZ can be considered a closed basin with no obvious outflow where groundwater and seasonal streams flowing from the surrounding highlands collect to form (semi) permanent standing basin lakes. The EARZ lakes vary in size from large and deep lakes such as Turkana Lake (6,750 km^2 in surface and 109 m deep, Yuretich and Cerling 1983; Cerling 1996), to shallow and relatively large lakes such as Magadi Lake (100 km^2 and ~1 m depth, Jones et al. 1977), to many very small lakes.

While some of the lakes are mainly fed by rivers (Turkana, Baringo, Nakuru, Natron), others receive a considerable part of the inflow from springs often fed by hydrothermal systems (Logipi, Bogoria, Elementeita, Magadi). Sometimes, surface evaporation rates exceed the rate of water inflow allowing the dissolved minerals to concentrate into caustic alkaline brines with a pH up to 12.

Total salts vary from about 5 % in the northern lakes (Bogoria, Nakuru, Elmenteita, Sonachi) up to halite saturation (>30 %) in the southern ones (Magadi and Natron Lakes). EARZ lake waters are prevalently Na–Cl and Na–HCO_3–CO_3 (Fig. 5). The chemistry (Fig. 6) can be explained in terms of both chemical

weathering of rocks and evaporative phenomena. According to Kilham (1971), in the relatively humid areas along the rift, high temperature and rain water support the dissolution of the more soluble minerals of volcanic rocks (e.g. nepheline) and, on the contrary, in dry areas weathering is nearly absent and waters initially have a composition similar to rain water. Consequently, Na–HCO_3–CO_3 lakes develop in relatively humid basins whereas Na–Cl lakes develop in the more arid basins. Most of the alkalinity is acquired by hydrolysis of volcanic rocks (Eqs. 1–3), mainly glass and lavas, generating high concentrations of Na^+, SiO_2 and TDIC, which are reflected in the Na–CO_3 or Na–CO_3–Cl type chemical composition (Figs. 1 and 2) (Jones and Deocampo 2003). Further concentration of the lake waters (>30 %) causes the precipitation of halite, carbonates (trona and gaylussite) or silicates (Na-silicates and zeolites).

Lake Natron (Fig. 4b) is located in a closed drainage system in northern Tanzania, in the eastern branch of the East African Rift. The lake lies at 610 m asl, is 22–35 km wide and 50–75 km long, with a surface area of about 1,100 km^2. The lake is only 3–4 m deep and the evaporation rate is up to 20 mm/d (Dawson 2008). The lake is fed by four rivers: Ewaso Nyiro, Peninj, Moinik and Engare Sero. It is surrounded by escarpments and volcanoes. Pliocene to Recent volcanism resulted in basaltic and trachytic lavas to trachyandesitic and carbonatitic ashes, most recently originating from the active volcano Oldoinyo Lengai. Several mineral-rich hot springs enter on the western and eastern shores of the lake (Dawson 2008). Its waters are rich in sodium carbonate/bicarbonate, NaCl (Figs. 5 and 6) and silica, with a pH near 9.5 (Howell 1972; Dawson 2008 and references therein). The water of Lake Natron is so rich in dissolved sodium carbonate that it often feels viscous to touch.

4.3 Mono Lake (California, USA)

Mono Lake (Fig. 4c), a great endorheic and monomictic (Christenson et al., this issue) alkaline salt lake, is located on the western edge of the Great Basin in northeastern California bounded to the west by Sierra Nevada fault, to the north by the Body Hills, to the east by the Anchorite Hills and Cowtrach Mountains, and to the south by Long Valley Caldera and other rhyolitic, andesitic and basaltic volcanoes (Sahajpal et al. 2011). Mono basin itself contains young volcanic centres: Mono-Inyo craters, where the lake is located, and Paoha and Negit Islands inside the lake. The most recent eruptions in the area occurred at Paoha Island about 200 years ago (Kelleher and Cameron 1990)

Mono Lake is a terminal lake, lies at ca 1,940 m asl, is 25 km wide along its east-west axis, and has a surface area of 150–180 km^2 (depending of the evaporative status) and a maximum depth of 46 m. Snow melt from Sierra Nevada (85 %) and perennial hot and cold springs feed the lake together with a negligible amount of direct rain waters (Sahajpal et al. 2011, and references therein). Evaporation represents the main lake (and groundwater) water loss (Connell and Dreiss 1995).

The lake is fed by both alkaline and acidic (pH $\sim$ 6) springs, with different salinities in function of their origin (Neumann and Dreiss 1995). As in other closed basin lakes, changes in hydrology strongly affect the water chemistry of Mono Lake, highlighted by the salinities ranging from 20 to 100 g/l. Differences are mostly due to the sampling point (e.g. nearness to more diluted springs coming from Sierra Nevada) and evaporation processes during the hot season. Mono Lake waters are strongly alkaline (pH up to 9.8, Whiticar and Suess 1998), of Na-Cl type (Fig. 6) and the ion abundance is $Na > Cl > HCO_3 > SO_4$. Potassium is removed by ion exchange in which K^+ displaces Ca^{2+} in clays or volcanic glasses in ash layers (Connell and Dreiss 1995). Calcium is removed by precipitation of ikaite ($CaCO_3 \cdot 6H_2O$) rather then calcite, whose precipitation is inhibited by high concentration of orthophosphate (Bishoff et al. 1993).

Mixing between high-calcium groundwaters discharging into the lake and high bicarbonate lake waters causes the development of spectacular up to 3 m diameter tufa towers.

4.4 Specchio di Venere Lake (Pantelleria Island, Southern Italy)

Pantelleria Island (Fig. 4d) is a Pleistocene stratovolcano located in the NW–SE trending continental rift between North Africa and Sicily, Italy. Pantelleria represents the emerged part of a 836 m asl high volcanic structure, extending below sea-level to ~1,200 m depth. The structural setting of the island is defined by both tectonic and volcano-tectonic lineaments including regional faults and fractures with the same orientation as the rift (Boccaletti et al. 1987; Acocella et al. 2004; Mattia et al. 2007; Rotolo et al. 2007; Civile et al. 2008; Catalano et al. 2009; Civile et al. 2010). Specchio di Venere Lake (called also Venere lake or Bagno dell'Acqua) is a small alkaline saline lake located in a closed basin on the northern side of Pantelleria Island (Azzaro et al. 1983; Dongarrà et al. 1983; Duchi et al. 1994; Aiuppa et al. 2007; Cangemi et al. 2010; Pecoraino et al. 2011). Its basin is delimited in the northern part by the scarp of the Cinque Denti caldera and to the south by the slopes of domes and cones (Mt Gelfiser) which are the expression of Holocene volcanic activity.

Specchio di Venere Lake is sub-squared in shape, around 450 m long and 350 m wide, and has a maximum depth of ~12 m. The water depth and the shoreline are subject to seasonal adjustments as a function of the annual hydrological balance. In the period 1992–1996 its surface area varied between 0.136 and 0.2 km^2 (Aiuppa et al. 2007). Specchio di Venere Lake can occasionally undergo thermal and chemical stratification but due to its small water volume these are generally short lasting events and atmospheric disturbances such as strong wind are capable to totally remix its waters (Aiuppa et al. 2007). The lake is mainly fed by rainfall and by the inflow of thermal springs. The morphology of the lake floor is quite irregular. In correspondence with springs inflowing at the lake floor, in particular in the shallow south-western sector, Cangemi et al. (2010) recognise some structures related to the formation of siliceous stromatolites.

Lake water presents high Cl^- and alkali contents (Fig. 6), high electrical conductivity (up to 40 mS/cm^2) and pH values up to 9.3. The high concentrations in alkali, mainly Na^+, are the result of notable interactions between thermal waters and Na-rich peralkaline rhyolite (Pantellerite). Due to the small volume of water, change in hydrological and meteorological/rainfall inputs strongly control the composition of lake waters (Pecoraino et al. 2011).

Despite the large amount of bubbling CO_2 and the high content of HCO_3^- in inflowing springs, the TDIC in lake waters is not very high because of the intense precipitation of carbonate minerals. Lake waters are supersaturated with respect to aragonite, calcite, dolomite, accounting for the occurrence of aragonite and dolomite and sporadically calcite in lake sediments and the carbonate layers capping the exposed stromatolites (Azzaro et al. 1983; Cangemi et al. 2010).

5 Microbial Communities in Alkaline Lakes

Abundant microbial life is found in alkaline lakes up to the highest salinities. Because of the unusual characteristics of alkaline, hypersaline environments their bacterial communities have been studied for many years, in part in the quest for commercially valuable biotechnology. These studies have been summarized by Grant et al. (1990) and Oren (2002). A wealth of interesting microorganisms can be found in the soda lakes. Halophilic and alkaliphilic microorganisms are found in all three domains of life: *Archaea*, *Bacteria* and *Eucarya*. They have already made a large impact in the application of biotechnology for the manufacturing of mass-market consumer products. "Biological detergents" contain enzymes that have usually been obtained from alkaliphilic or alkalitolerant bacteria. The current proportion of total world enzyme production destined for the laundry detergents market

comfortably exceeds 25 %, and there are other possible applications in food and waste treatment industries (Grant et al. 1990).

In those cases in which the total dissolved salts concentration exceeds 250–300 g/l such as in Lake Magadi and its solar salterns and in some of the Wadi Natrun lakes, halophilic and alkaliphilic Archaea of the order Halobacteriales often impart a red colour to the brines. The occurrence of red brines is a phenomenon long known in salt production from sea water. The first descriptions may date back to about 2700 BC in the ancient Chinese literature (Oren 2002) and it has been suggested that the first Plague of Egypt (Exodus 7: 17–25), in which the water of the Nile "turned into blood", refers to such red waters. The first scientific descriptions of red bacteria in brines were made at the beginning of the 20th century, although important scientific findings about the microbiology of alkaline and hypersaline lakes were obtained since the second half of the preceding century (Oren 2002).

One of the most impressive characteristics of alkaline lakes is their extremely high primary productivity despite the extreme nature of such environments. Compared to the global mean gross primary productivity for streams and lakes (Whittaker and Likens 1972) of about 0.6 g C m^{-2} day^{-1}, alkaline lakes are characterised by productivity rates exceeding 10 g C m^{-2} day^{-1} (Talling et al. 1973; Melack and Kilham 1974). They are probably the most productive, naturally occurring aquatic environments, presumably because of the relatively high ambient temperatures, high light intensities, availability of phosphate and unlimited access to CO_2 in these carbonate-rich waters (Melack and Kilham 1974; Grant et al. 1990). They are also regarded as naturally eutrophic reservoirs and, like all eutrophic bodies of water, they feature considerable microbial diversity (Zavarzin et al. 1999). The soda lakes of the EARZ are shown to support a dense and diverse population of aerobic, organotrophic, halophilic, alkaliphilic and alkali-tolerant representatives of major bacterial and archaeal phyla (reviewed by Duckworth et al. 1996; Jones et al. 1998; Grant et al. 1999; Zavarzin et al. 1999). The primary productivity is generally due to the presence of dense populations of cyanobacteria (up to 13,000 cyanobacterial filaments per ml, Talling et al. 1973; Melack and Kilham 1974). In extreme cases, the blooms may consist almost entirely of one species, usually *Spirulina* sp. These particular cyanobacteria are the principal food of the immense flocks of flamingos that inhabit the Rift Valley.

In contrast to aerobic habitats, the anaerobic alkaline environments received less attention. But anaerobic processes have a significant role because of dissolved O_2 shortage consequence of the very high productivity of these environments (Jones et al. 1998). Lacustrine muds are black and anoxic, implying the presence of sulfides and of specific anaerobic populations of sulfate-reducing bacteria.

The nutrient cycle in soda lakes is summarised in Fig. 7 (Jones et al. 1998).

Like in other environments characterised by extreme ecological conditions also in hypersaline, closed basin soda lakes and their remnant brines microbial life coping with high concentrations of toxic elements can be found. Extreme contents of arsenic occur for example in Mono Lake (Oremland et al. 2004). Although arsenic is a well-known toxicant to eukaryotes and prokaryotes alike, some prokaryotes have evolved biochemical mechanisms to exploit arsenic oxyanions (i.e., arsenate and arsenite); they can use them either as an electron acceptor for anaerobic respiration (arsenate), or as an electron donor (arsenite) to support chemoautotrophic fixation of CO_2 into cell carbon. Despite the freshwater or marine ecosystems, these processes may assume quantitative significance with respect to the carbon cycle in arsenic-rich soda lakes (Oremland et al. 2004).

Furthermore, it was recently discovered that also Se- and Te-oxyanions are used as respiratory electron acceptors to sustain anaerobic growth of certain bacteria in the sediments of Mono Lake (Baesman et al. 2009). But most intriguing was the discovery in the same environment of "a bacterium that can grow by using arsenic instead of phosphorus" (Wolfe-Simon et al. 2011). Although some doubts have meanwhile arisen about these findings (Foster 2011) it testifies for

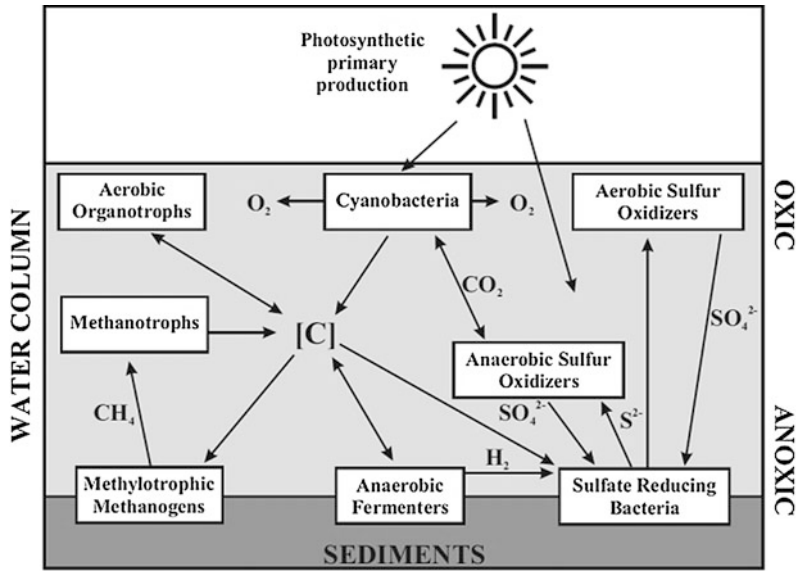

Fig. 7 Flow diagram of the nutrient cycle in soda lakes (modified after Jones et al. 1998)

the highly interesting microbial communities found in such extreme environments.

6 Summary

Alkaline lakes are a peculiar type of saline or hypersaline lakes characterised by pH values higher than 9 and whose chemical composition is characterised by Na^+ as the main cation and by the presence of high HCO_3^- and CO_3^{2-} contents, although sometimes the main anionic species could be Cl^-, or rarely SO_4^{2-}. The evolution of these lakes towards alkaline conditions is favoured by an environment in which hydrologic (endorheic) and climatic (arid or semiarid) factors cause evaporative concentration of its waters. Due to the fact that earth-alkaline carbonates are the first solid phases to reach oversaturation, the initial ratio between the total dissolved inorganic carbon (TDIC) to the main earth-alkaline elements (Ca^{2+} and Mg^{2+}) of the starting dilute waters is very important in driving the subsequent evolution of the lake waters. TDIC/(Ca^{2+}+Mg^{2+}) ratios much higher than 1 will leave the waters enriched in TDIC and devoid of Ca^{2+} and Mg^{2+} which is the typical composition of alkaline lakes. If the necessary hydrologic and climatic conditions are present, quiescent or recently extinct volcanic areas are the most favourable candidates in hosting waters that will evolve towards alkaline conditions. In these areas, where acidic magmatic gases do not have the possibility to reach the lake waters, there is an abundant input of endogenous CO_2 that will contribute to the increase of TDIC and the weathering of the volcanic silicate rocks will release to the waters prevailingly alkaline elements either because earth-alkaline elements are rare (silicic rocks) or are scarcely mobile (mafic rocks).

Alkaline lakes are also characterised by abundant and diversified microbial life. They are among the most productive, naturally occurring aquatic environments. Productivity rates exceeding 10 g C m^{-2} day^{-1} are sustained by euthrophic conditions, relatively high ambient temperatures, high light intensities and unlimited access to CO_2. Microbes living in alkaline lakes have found applications in the production of enzymes for detergents, as animal feed (*Spirulina*) and for waste treatment industries.

Due to evaporative concentration and high solubility in alkaline environments many trace elements can reach very high contents in alkaline hypersaline lakes. This could be of environmental concern in the case of toxic elements but also represent an important mineral resource (Li, B, REE).

Acknowledgments The authors would like to express special thanks to the Editor Dmitri Rouwet for his comments and advice for significantly improving and clarifying the early version of the manuscript. The authors would also like to thank the two anonymous reviewers for their constructive comments. This work was partially funded by the Italian Dipartimento della Protezione Civile under the 2004–2006 agreement with Istituto Nazionale di Geofisica e Vulcanologia (INGV-DPC Research Project V3_7—Pantelleria; Research Unit 02).

References

Acocella V, Funiciello R, Marotta E, Orsi G, de Vita S (2004) The role of extensional structures on experimental calderas and resurgence. J Volcanol Geotherm Res 129:199–217. doi:10.1016/S0377-0273(03)00240-3

Aguilera E, Chiodini G, Cioni R, Guidi M, Marini L, Raco B (2000) Water chemistry of Lake quilotoa (Ecuador) and assessment of natural hazards. J Volcanol Geotherm Res 97:271–285

Aiuppa A, D'Alessandro W, Gurrieri S, Madonia P, Parello F (2007) Hydrologic and geochemical survey of the lake specchio di venere (Pantelleria Island, Southern Italy). Environ Geol 53:903–913. doi:10.1007/s00254-007-0702-1

Anderson GC (1958) Seasonal characteristics of two saline lakes in Washington. Limnol Oceanogr 3:51–68

Aydar E, Gourgaud A, Ulusoy I, Digonnet F, Labazuy P, Sen E, Bayhan H, Kurttas T, Tolluoglu AU (2003) Morphological analysis of active mount nemrut stratovolcano, eastern Turkey: evidences and possible impact areas of future eruptions. J Volcanol Geotherm Res 123:301–312

Ayenew T (2008) The distribution and hydrogeological controls of fluoride in the groundwater of central Ethiopian rift and adjacent highlands. Environ Geol 54:1313–1324. doi:10.1007/s00254-007-0914-4

Azzaro E, Badalamenti F, Dongarrà G, Hauser S (1983) Geochemical and mineralogical studies of lake specchio di Venere, Pantelleria Island, Italy. Chem Geol 40:149–165

Baesman SM, Stolz JF, Kulp TR, Oremland RS (2009) Enrichment and isolation of *Bacillus beveridgei* sp. nov, a facultative anaerobic haloalkaliphile from Mono Lake, California, that respires oxyanions of tellurium, selenium, and arsenic. Extremophiles 13:695–705. doi:10.1007/s00792-009-0257-z

Bergner AGN, Strecker MR, Trauth MH, Deino A, Gasse F, Blisniuk P, Duhnforth M (2009) Tectonic and climatic control on evolution of rift lakes in the central Kenya rift, East Africa. Quatern Sci Rev 28:2804–2816. doi:10.1016/j.quascirev.2009.07.008

Bischoff JL, Stine S, Rosenbauer RJ, Fitzpatrick JA (1993) Ikaite precipitation by mixing of shoreline springs and lake water, mono lake, California. Geochim Cosmochim Acta 57:3855–3865

Bischoff JL, Israde-Alcantara I, Garduño-Monroy VH, Shanks WC (2004) The springs of lake patzcuaro: chemistry, salt-balance and implications for the water balance of the lake. Appl Geochem 19:1827–1835. doi:10.1016/j.apgeochem.2004.04.003

Boccaletti M, Cello G, Tortorici L (1987) Transtensional tectonics in the sicily channel. J Struct Geol 9–7:869–876

Bowen BB, Benison KC (2009) Geochemical characteristics of naturally acid and alkaline saline lakes in southern Western Australia. Appl Geoch 24:268–284. doi:10.1016/j.apgeochem.2008.11.013

Cangemi M, Bellanca A, Borin S, Hopkinson L, Mapelli F, Neri R (2010) The genesis of actively growing siliceous stromatolites: evidence from lake specchio di venere, Pantelleria Island, Italy. Chem Geol 276:318–330. doi:10.1016/j.chemgeo.2010.06.017

Catalano S, De Guidi G, Lanzafame G, Monaco C, Tortorici L (2009) Late quaternary deformation on the island on Pantelleria: new constraints for the recent tectonic evolution of the sicily channel rift (Southern Italy). J Geodyn 48:75–82. doi:10.1016/j.jog.2009.06.005

Castenholz RW (1960) seasonal changes in the attached algae of freshwater and saline lakes in the lower grand coulee, Washington. Limnol Oceanogr 5:1–28

Cerling TE (1996) Pore water chemistry of an alkaline lake: Lake Turkana. In: Johnson C, Odada EO (eds) The Limnology, Climatology, and Paleoclimatology of the East African lakes. Gordon and Breach Science Publishers/Overseas Publishers Association, Amsterdam, The Netherlands, pp 225–240

Christenson BW, Tassi F (this issue) Gas in volcanic lake environments

Christenson BW, Németh K, Rouwet D, Tassi F, Vandemeulebrouck J, Varekamp JC (this issue) Volcanic lakes

Christol A, Kuzucuoglu C, Fort M, Karabiyikoglu M, Mouralis D, Brunstein D, Dogu AF, Akkopru E, Fontugne M, Zorer H (2008) Apports de l'etude geomorphologique des terrasses fluvio-lacustresdu lac de Van (Turquie) à la connaissance des paleoenvironnements en Anatolie orientale. In: Galop D (ed) Paysages et Environnements: De la Reconstitutiondu Passé aux Modeles Prospectifs, Annales litteraires, Serie 'Environnement, societes et archeologie'. PU de Franche-Comt Besancon

Civile D, Lodolo E, Tortorici L, Lanzafame G, Brancolini G (2008) Relationships between magmatism and tectonics in a continental rift: the pantelleria Island region (sicily channel, Italy). Mar Geol 251:32–46. doi:10.1016/j.margeo.2008.01.009

Civile D, Lodolo E, Accettella D, Geletti R, Ben-Avraham Z, Deponte M, Facchin L, Ramella R, Romeo R (2010) The pantelleria graben (Sicily channel, central mediterranean): an example of intraplate 'passive' rift. Tectonophysics 490:173–183. doi:10.1016/j.tecto.2010.05.008

Connell LT, Dreiss SJ (1995) Chemical evolution of shallow groundwater along the northeast shore of

mono lake, California. Water Resour Res 31:3171–3182
Corti G (2009) Continental rift evolution: from rift initiation to incipient break-up in the main ethiopian rift, East Africa. Earth Sci Rev 96:1–53. doi:10.1016/j.earscirev.2009.06.005
Dawson JB (2008) The Gregory rift valley and neogene–recent volcanoes of Northern Tanzania. Geological Society, London, Memoirs: 33. doi: 10.1144/M33.1
Degens ET, Kurtman F (1978) The Geology of Lake Van. Publ. N 169, Mineral Research and Exploration Institute (MTA) 169 Ankara, Turkey, 158 p
Degens ET, Wong HK, Kempe S, Kurtman F (1984) A Geological study of lake van, Eastern Turkey. Geol Runds 73–2:701–734
Deocampo DM (2005) Evaporative evolution of surface waters and the role of aqueous CO_2 in magnesium silicate precipitation: lake Eyasi and Ngorongoro Crater, northern Tanzania. S Afr J Geol 108:493–504
Deshmukh KB, Pathak AP, Karuppayil MS (2011) Bacterial diversity of lonar soda lake of India. Indian J Microbiol 51(1):107–111. doi:10.1007/s12088-011-0159-5
Dongarra G, Hauser S, Alaimo R, Carapezza M, Tonani F (1983) Hot waters on pantelleria Island. Geochemical features and preliminary geothermal investigations. Geothermics 12:49–63
Duchi V, Campana ME, Minissale A, Thompson M (1994) Geochemistry of thermal fluids on the volcanic isle of pantelleria, Southern Italy. Appl Geoch 9:147–160
Duckworth AW, Grant WD, Jones BE, van Steenbergen R (1996) Phylogenetic diversity of soda lake alkaliphiles. FEMS Microbiol Ecol 19:181–191
Eugster HP, Hardie LA (1978) Saline lakes. In: Lerman A (ed) Lakes: chemistry, geology, physics. Springer, New York
Eugster HP, Jones BF (1979) Behavior of major solutes during closed-basin brine evolution. Am J Sci 279:609–631
Foster PL (2011) Comment on a bacterium that can grow by using arsenic instead of phosphorus. Science 332:1149. doi:10.1126/science1201551
Garrels RM, Mackenzie FT (1967) Origin of the chemical composition of some springs and lakes equilibrium concepts in natural water systems. Adv Chem 67:222–242
Giggenbach WF (1990) Water and gas chemistry of lake nyos and its bearing on the eruptive process. J Volcanol Geotherm Res 42:337–362
Gizaw B (1996) The origin of high bicarbonate and fluoride concentrations in waters of the main ethiopian rift valley, East African rift system. J Afr Earth Sci 22:391–402
Grant WD, Tindall BJ (1986) The alkaline saline environment. In: Herbert RA, Codd GA (eds) Microbes in extreme environments. Academic Press, London, pp 25–54
Grant S, Grant WD, Jones BE, Kato C, Li L (1999) Novel archaeal phylotypes from an East African alkaline saltern. Extremophiles 3:139–145
Grant WD, Mwatha WE, Jones BE (1990) Alkaliphiles: ecology, diversity, and applications. FEMS Microbiol Rev 75:255–270. doi:10.1111/j1574-69681990tb04099x
Green WJ, Lyons WB (2009) The Saline lakes of the mcmurdo dry valleys, Antarctica. Aquat Geochem 15:321–348. doi:10.1007/s10498-008-9052-1
Hardie LA, Eugster HP (1970) The evolution of closed-basin brines. Mineral Soc Am, Special Paper 3:273–290
Howell FC (1972) Pliocene/Pleistocene hominidae in eastern Africa: absolute and relative ages. In: Bishop WW and Miller JA (eds) Calibration of hominoid evolution. Scottish Academic Press, Edinburgh, pp 331–368
Huguet C, Fietz S, Stockhecke M, Sturm M, Anselmetti FS, Rosell-Mele A (2011) Biomarker seasonality study in lake van, Turkey. Org Geochem 42:1289–1298
Johannesson KH, Lyons WB, Bird DA (1994) Rare earth element concentrations and speciation in alkaline lakes from the western USA. Geophys Res Lett 21(9):773–776. doi:10.1029/94GL00005
Jones BE, Grant WD, Duckworth AW, Owenson GG (1998) Microbial diversity of soda lakes. Extremophiles 2:191–200
Jones BF (1966) Geochemical evolution of closed basin water in the western Great Basin. In: Rau JL (ed) Proceedings of the second symposium on salt. Geology, Geochemistry, Mining Northern Ohio Geological Society, Cleveland, pp 181–200
Jones BF, Eugster HP, Rettig SL (1977) Hydrochemistry of the lake magadi basin, Kenya. Geochim Cosmichim Acta 41:53–72
Jones BF, Deocampo DM (2003) Geochemistry of saline lakes. In: Drever JI, Holland HD, Turekian KK (eds) Freshwater geochemistry, weathering and soils. Treatise on geochemistry, vol 5, pp 393–424
Jones BF, Naftz DL, Spencer RJ, Oviatt CG (2009) Geochemical evolution of great Salt Lake, Utah, USA. Aquat Geochem 15:95–121. doi:10.1007/s10498-008-9047-y
Kelleher PC, Cameron KL (1990) The geochemistry of the mono craters-mono lake Islands volcanic complex, eastern California. J Geophys Res 95(B11):17643–17659
Kempe S (1977) Hydrographie, Warven-Chronologie und organische geochemie des Van Sees, Ost-Turkei. Geologisch-Palaontologischen Institut der Universität Hamburg, MGPIUA 47:125–228
Kempe S, Kazmierczak J, Landmann G, Konuk T, Reimer A, Lipp A (1991) Largest known microbialites discovered in Lake Van, Turkey. Nature 349:605–608
Kervyn M, Ernst GGJ, Klaudius J, Keller J, Kervyn F, Mattsson HB, Belton F, Mbede E, Jacobs P (2008)

Voluminous lava flows at Oldoinyo Lengai in 2006: chronology of events and insights into the shallow magmatic system. Bull Volcanol 70:1069–1086. doi:10.1007/s00445-007-0190-x

Kilham P (1971) The geochemical evolution of closed basin lakes. Geol Soc Am Abstr 3–7:770–772

Kompantseva EI, Bryantseva IA, Komova AV, Namsaraev BB (2007) The structure of phototrophic communities of soda lakes of the southeastern transbaikal region. Mikrobiologiya 76:243–252 (Microbiology (Engl. Transl.) 76:211–219). doi:10.1134/S0026261707020130

Kompantseva EI, Komova AV, Krauzova VI, Kolganova TV, Panteleeva AN (2009) Purple nonsulfur bacteria in weakly and moderately mineralized soda lakes of the southern transbaikal region and northeastern Mongolia. Mikrobiologiya 78:288–296 (Microbiology (Engl. Transl.) 78:246–253).doi: 10.1134/S0026261709020179

Kusakabe M (this issue) Evolution of CO_2 content in Lakes Nyos and Monoun, and sub-lacustrine CO_2-recharge system at Lake Nyos as envisaged from $CO_2/^3He$ ratios and noble gas signatures

Landmann G, Reimer A, Lemcke G, Kempe S (1996) Dating late glacial abrupt climate changes in the 14,570 year long continuous varve record of Lake van, Turkey. Palaeogeogr Palaeocl 122(1–4):107–118

Landmann G, Steinhauser G, Sterba JH, Kempe S, Bichler M (2011) Geochemical fingerprints by activation analysis of tephra layers in lake van sediments, Turkey. Appl Radiat Isot 69:929–935

Long DT, Fegan NE, McKee JD, Lyons WB, Hines ME, Macumber PG (1992) Formation of alunite, jarosite and hydrous iron oxides in a hypersaline system: lake Tyrrell, Victoria, Australia. Chem Geol 96:183–202

Lopez-Garcıa P, Kazmierczak J, Benzerara K, Kempe S, Guyot F, Moreira D (2005) Bacterial diversity and carbonate precipitation in the giant microbialites from the highly alkaline lake van, Turkey. Extremophiles 9:263–274. doi:10.1007/s00792-005-0457-0

Ma L, Lowenstein TK, Russell JM (2011) A brine evolution model and mineralogy of chemical sediments in a volcanic crater, Lake Kitagata, Uganda. Aquat Geochem 17:129–140. doi:10.1007/s10498-010-9108-x

Macintyre S, Melack JM (1982) Meromixis in an equatorial African soda lake. Limnol Oceanogr 27:595–609

Marini L, Vetuschi Zuccolini M, Saldi G (2003) The bimodal pH distribution of volcanic lake waters. J Volcanol Geotherm Res 121:83–98

Mattia M, Bonaccorso A, Guglielmino F (2007) Ground deformations in the Island of pantelleria (Italy): insights into the dynamic of the current intereruptive period. J Geoph Res 112:B11406. doi:10.1029/2006JB004781

Melack JM (1979) Photosynthesis and growth of *Spirulina platensis* (Cyanophyta) in an equatorial lake (Lake Simbi, Kenya). Limnol Oceanogr 24:753–760

Melack JM, Kilham P (1974) Photosynthetic rates of phytoplankton in East African alkaline, saline lakes. Limnol Oceanogr 19:743–755

Neumann K, Dreiss S (1995) Strontium 87/strontium 86 ratios as tracers in groundwater and surface waters in Mono Basin, California. Water Resour Res 31:3183–3193

Ochieng EZ, Lalah JO, Wandiga SO (2007) Analysis of heavy metals in water and surface sediment in five rift valley lakes in Kenya for assessment of recent increase in anthropogenic activities. Bull Environ Contam Toxicol 79:570–576. doi:10.1007/s00128-007-9286-4

Oduor SO, Schagerl M (2007) Temporal trends of ion contents and nutrients in three Kenyan rift valley saline–alkaline lakes and their influence on phytoplankton biomass. Hydrobiologia 584:59–68. doi:10.1007/s10750-007-0605-x

Oremland RS, Stolz JF, Hollibaugh JT (2004) The microbial arsenic cycle in mono lake, California. FEMS Microbiol Ecol 48:15–27

Oren A (2002) Halophilic Microorganisms and their environments cellular origin. Life in extreme habitats and astrobiology, vol 5. Springer, New York. doi: 10.1007/0-306-48053-0

Pecoraino G, Brusca L, D'Alessandro W, Longo M (2011) Geochemical surveys on specchio di venere lake, pantelleria Island, South Italy. In: 5th International limnogeological congress abs, 31 Aug–3 Sept, Konstanz, Germany, p 44

Renaut RW, Tiercelin JJ, Owen RB (1986) Mineral precipitation and diagenesis in the sediments of the lake bogoria basin, Kenya rift valley. Geol Soc London Spec Publ 25:159–175. doi:10.1144/GSLSP19860250114

Reimer A, Landmann G, Kempe S (2009) lake van, eastern Anatolia, hydrochemistry and history. Aquat Geochem 15:195–222. doi:10.1007/s10498-008-9049-9

Risacher F, Fritz B (1991) Geochemistry of Bolivian salars, Lipez, southern Altiplano. Origin of solutes and brine evolution. Geochim Cosmochim Acta 55:687–705

Risacher F, Alonso H, Salazar C (2003) The origin of brines and salts in chilean salars: a hydrochemical review. Earth-Sci Rev 63:249–293. doi:10.1016/S0012-8252(03)00037-0

Rotolo SG, La Felice S, Mangalaviti A, Landi P (2007) Geology and petrochemistry of the recent (<25 ka) silicic volcanism at pantelleria Island. Boll Soc Geol It (Ital J Geosci) 126–2:191–208

Rowe GL Jr, Ohsawa S, Takano B, Brantley SL, Fernández JF, Barquero J (1992) Using crater lake chemistry to predict volcanic activity at poas volcano, costa rica. Bull Volcanol 54:494–503

Sahajpal R, Zimmerman SRH, Datta S, Hemming NG, Hemming SR (2011) Assessing Li and other leachable geochemical proxies for paleo-salinity in lake sediments from the mono basin, CA (USA). Geochim Cosmochim Acta 75:7855–7863

Spencer RJ, Lowenstein TK, Casas E, Pengxi Z (1990) Origin of potash salts and brines in the Qaidam Basin, China. In: Spencer RJ, Chou IM (eds) Fluid-mineral interactions: a tribute to H. P. Eugster. Geochemical Society, San Antonio, pp 395–408

Stumm W (2004) Chemical Processes regulating the composition of lake waters. In: O'Sullivan PE, Reynolds CS (eds) The lakes handbook vol.1, pp 79–106

Talling JF, Wood RB, Prosser MV, Baxter RM (1973) The upper limit of photosynthetic productivity by phytoplankton: evident from Ethiopian soda lakes. Freshwat Biol 3:53–76

Taran Y, Rouwet D, Inguaggiato S, Aiuppa A (2008) Major and trace element geochemistry of neutral and acidic thermal springs at El Chichón volcano, Mexico. Implications for monitoring of the volcanic activity. J Volcanol Geotherm Res 178:224–236

Tedesco D, Vaselli O, Papale P, Carn SA, Voltaggio M, Sawyer GM, Durieux J, Kasereka M, Tassi F (2011) January 2002 volcano-tectonic eruption of Nyiragongo volcano, democratic republic of Congo. J Geophys Res 112:B09202. doi:10.1029/2006JB004762

Tomonaga Y, Brennwald MS, Kipfer R (2011) Spatial distribution and flux of terrigenic He dissolved in the sediment pore water of lake van (Turkey). Geochim Cosmochim Acta 75:2848–2864. doi:10.1016/j.gca.2011.02.038

Utkutu M (2006) Implications for the water level change triggered moderate (M ≥ 4.0) earthquakes in lake van Basin, Eastern Turkey. J Seismol 10:105–117. doi:10.1007/s10950-005-9002-y

Varekamp JC (this issue) The chemical composition and evolution of volcanic lakes

Vaselli O, Tedesco D, Cuoco E, Tassi F (this issue) Are limnic eruptions on the CO_2–CH_4-rich gas reservoir of Lake Kivu (Democratic Republic of the Congo and Rwanda) possible? Insights from physic-chemical and isotopic data

Varekamp JC, Pasternack GB, Rowe GL Jr (2000) Volcanic lake systematics: II chemical constraints. J Volcanol Geotherm Res 97:161–179

Vilaclara G, Chávez M, Lugo A, González H, Gaytán M (1993) Comparative description of crater-lakes basic chemistry in Puebla state, Mexico. Verh Internat Verein Limnol 25:435–440

Volkova NI (1998) Geochemistry of rare elements in waters and sediments of alkaline lakes in the Sasykkul depression, East Pamirs. Chem Geol 147:265–277

Wani AA, Surakasi VP, Siddharth J, Raghavan RG, Patole MS, Ranade D, Shouche YS (2006) Molecular analyses of microbial diversity associated with the lonar soda lake in India: an impact crater in a basalt area. Res Microbiol 157:928–937. doi:10.1016/j.resmic.2006.08.005

Whittaker RH, Likens GE (1972) Carbon in the biota. In: Woodwell GM, Pecan EV (eds) Carbon in the biosphere. AEC symposium series 30

Witham CS (2005) Volcanic disasters and incidents: a new database. J Volcanol Geotherm Res 148:191–233

Whiticar MJ, Suess E (1998) The cold carbonate connection between mono lake, California and the Bransfield Strait, Antarctica. Aquat Geochem 4:429–454

Wolfe-Simon F, Switzer Blum J, Kulp TR, Gordon GW, Hoeft SE, Pett-Ridge J, Stolz JF, Webb SM, Weber PK, Davies PCW, Anbar AD, Oremland RS (2011) A bacterium that can grow by using arsenic instead of phosphorus. Science 332:1163–1166. doi:10.1126/science1197258

Wong HK, Degens ET (1978) The bathymetry of Lake van, Eastern Turkey. In: Degens ET, Kurtman F (eds) Geology of lake van, Miner Res Explor Inst Ankara, Turkey

Yilmaz Y, Guner Y, Saroglu F (1998) Geology of the quaternary volcanic centres of the east Anatolia. J Volcanol Geotherm Res 85:173–210

Yuretich RF, Cerling TE (1983) Hydrogeochemistry of Lake Turkana, Kenya: mass balance and mineral reactions in an alkaline lake. Geochim Cosmochim Acta 47:1099–1109

Zavarzin GA, Zhilina TN, Kevbrin VV (1999) The alkaliphilic microbial community and its functional diversity. Microbiology, translated from Mikrobiologiya 68:503–521

Zhang Q, Kang S, Wang F, Li C, Xu Y (2008) Major ion geochemistry of nam co lake and its sources, Tibetan Plateau. Aquat Geochem 14:321–336. doi:10.1007/s10498-008-9039-y

Zheng M, Liu X (2009) Hydrochemistry of salt lakes of the Qinghai-Tibet Plateau, China. Aquat Geochem 15:293–320. doi:10.1007/s10498-008-9055-y

Zheng M, Tang J, Liu J, Zhang F (1993) Chinese saline lakes. Hydrobiologia 267:23–36

The Remarkable Chemistry of Sulfur in Hyper-Acid Crater Lakes: A Scientific Tribute to Bokuichiro Takano and Minoru Kusakabe

Pierre Delmelle and Alain Bernard

Abstract

This chapter is a tribute to Bokuichiro Takano and Minoru Kusakabe for their important contributions to our knowledge of sulfur chemistry and dynamics in hyper-acid crater lakes and geothermal lakes. Hyper-acid crater lakes are perched at the summit of active volcanoes and represent the uppermost manifestation of a shallow active magma-hydrothermal system. They act as traps for strongly acidic condensates formed as sulfur-rich magmatic gases rising from depth expand and cool in the main hydrothermal upflow zone. The remarkable sulfate content of hyper-acid crater lakes is sourced to disproportionation-hydrolysis of magmatic SO_2 in the upper part of the hydrothermal conduit. This reaction generates a strong, temperature-dependent sulfur isotopic fractionation, which typically produces high $\delta^{34}S_{SO_4}$ values. In contrast, sulfate in geothermal lakes displays much lighter sulfur isotopic compositions linked to oxidation of H_2S-rich hydrothermal discharges. Polythionates are ubiquitous in hyper-acid crater lakes and are usually attributed to aqueous interaction between SO_2 and H_2S in the lake. Fluctuations in lake polythionate concentrations have been used to infer changes in the SO_2/H_2S ratio of magmatic hydrothermal inputs. However, polythionates may also originate from hydrolysis of elemental sulfur. Elemental sulfur in hyper-acid crater lakes occurs primarily as a molten body at the hydrothermal vent-crater floor interface. The origin of this material is not entirely clear; several deposition reactions are compatible with the observed range of sulfur isotopic compositions. Sulfide and sulfosalt minerals commonly occur as

P. Delmelle (✉)
Earth and Life Institute, Environmental Sciences,
Université Catholique de Louvain, Croix du Sud 2,
bte L7.05.10, 1348 Louvain-La-Neuve, Belgium
e-mail: pierre.delmelle@uclouvain.be

A. Bernard
Earth and Environmental Sciences Department,
Université Libre de Bruxelles, Brussels, Belgium

D. Rouwet et al. (eds.), *Volcanic Lakes*, Advances in Volcanology,
DOI 10.1007/978-3-642-36833-2_10,
© Springer-Verlag Berlin Heidelberg 2015

impurities in molten sulfur from hyper-acid crater lakes. Molten sulfur is also found in some geothermal lakes. There are still plenty of research opportunities for decoding the complex cycling of sulfur between aqueous and gaseous species and elemental sulfur in hyper-acid crater lakes. In particular, efforts are needed to track intermediate sulfur species. The role that subaqueous molten sulfur plays in modulating heat and mass transfers to the overlying lake and in trapping metals transported by magmatic gases deserves further investigations.

Keywords
Hyper-acid crater lake · Sulfur chemistry · Polythionates · Hydrothermal system · Volcano monitoring

1 Introduction

On Earth, sulfur is present in vapors continuously exhaled through degassing of magma intrusions within volcanic edifices. Perched groundwater reservoirs in composite active volcanoes interact with sulfur-bearing magmatic gases to produce acid, sulfate-rich hydrothermal waters. Hyper-acid lakes hosted in summit active craters (Fig. 1a) represent the uppermost surface expression of these systems. Acid crater lakes are usually thoroughly mixed, display temperatures above those of ambient air and often exhibit extremely acidic pH values; they are termed hyper-acid crater lakes (Varekamp et al. 2000). The sulfur chemistry in such volcanic lakes is spectacular; gaseous, liquid and solid sulfur species interact with each other to produce waters that are greatly enriched in sulfate but also contain polythionates. Further, hyper-acid crater lakes host molten sulfur bodies, a very rare feature on our planet.

This chapter is a tribute to the contributions of our now-retired colleagues Bokuichiro Takano and Minoru Kusakabe to our knowledge of the remarkable sulfur chemistry in hyper-acid crater lakes. More than 25 years ago, Takano recognized for the first time the potential of using aqueous polythionates in hyper-acid crater lakes for monitoring subsurface magma-hydrothermal activity (Takano 1987). In parallel, Kusakabe investigated the sulfur isotopic chemistry in these environments and made a major breakthrough by establishing the formation conditions of dissolved sulfate (Kusakabe et al. 2000). Today, it is relatively common to apply polythionate and sulfur isotope determinations to hyper-acid crater lake studies, but it is fair to say that it is in part to Takano's and Kusakabe's efforts that we owe this approach.

Here we review the occurrence and formation of aqueous sulfur species, elemental sulfur and major sulfur minerals in hyper-acid crater lakes. Geothermal lakes, i.e., volcanic lakes very indirectly related to magmatic gases, containing acid sulfate waters and featuring subaqueous molten sulfur (Fig. 1b) are also briefly considered. We then discuss how the measurements of sulfur species in hyper-acid crater lakes can be applied to monitor volcanic activity. Future research directions are briefly proposed.

2 Overview of Sulfur Occurrence

2.1 Origin of Sulfur

Sulfur in lakes receiving hydrothermal inputs ultimately originates from vapors released from subsurface magmas. Magmatic sulfur is exsolved principally as SO_2 and H_2S in various relative proportions, depending on temperature-, pressure- and redox-controlled partition coefficients between vapor and melt, the mixing or mingling of different magma sources and the dynamics of degassing (Oppenheimer et al. 2011 and references therein). Sulfur dioxide is normally the

Fig. 1 **a** The turquoise-*green* hyper-acid crater lake of Keli Mutu volcano, Indonesia. Slicks of *yellow* sulfur spherules are visible toward the center of the lake surface and accumulate near the lake shore. **b** Oyunuma lake is part of the Noboribetsu geothermal field, Kuttara volcano, Japan. The dark color of the lake is due to elemental sulfur precipitates that contain high concentration of Fe impurities. Dark streaks of sulfur spherule slicks cover the lake surface

dominant sulfur species in magmatic gases, but H_2S is also present as revealed by high temperature fumarole compositions (e.g., Giggenbach et al. 2001). In addition, the abundance of SO_2 in the original deep magmatic vapor expanding through fracture arrays to the surface of the volcanic edifice may be modified due to secondary processes, such as cooling and re-equilibration, and interaction with rock. At high temperature (i.e., >300 °C), the following equilibrium is effective and buffers the SO_2/H_2S ratio in the gas phase (Giggenbach 1987):

$$3SO_2 + 7H_2 = H_2S + 2S^{\circ} + 6H_2O \quad (1)$$

Below 300 °C, reactions between the gas phase and the rock become significant, resulting in the consumption of SO_2, as generically expressed by:

$$SO_2 + 6(FeO)_{rock} + H_2O = H_2S + 6(FeO_{1.5})_{rock} \quad (2)$$

This equation reflects equilibrium with the major rock redox system, i.e., the assemblage of Fe^{2+}- and Fe^{3+}-containing minerals. Giggenbach (1987) emphasizes that the rock efficiency in converting SO_2 to H_2S relates to the intensity and duration of gas-rock interaction and relative flux

of high temperature SO_2-bearing magmatic vapors. Thus, H_2S-rich gases will be produced by prolonged interaction with wall rock, whereas SO_2-rich compositions will likely be maintained in the highly permeable fractures constituting the main hydrothermal conduit connected to the surface. Rocks in this part of the magma-hydrothermal system are also typically highly silicified (Delmelle et al. 2015), thus limiting the importance of reaction (2).

A small fraction of the magmatic vapor phase expanding from depth can condense in the subsurface environment. In this case, SO_2 and other acid species partitionate into the liquid phase to form hyper-acid condensates. However, complete condensation of the high-enthalpy magmatic vapor is most efficient when rapid heat transfers are allowed, for example upon entry into shallow groundwater or a hydrothermal vent-crater lake system (Henley and McNabb 1978; Henley and Berger 2011). In the waning stages of magmatic activity or if the magma intrusion is deep-seated, boiling of a liquid-dominated hydrothermal reservoir typically releases a H_2S-rich steam that may mix with shallow ground water or a lake (e.g., Henley and Ellis 1983). The results of a recent modeling study on Ruapehu Crater Lake, New Zealand, also suggest that convection dynamics within the subaqueous hydrothermal vent can lead to H_2S-rich inputs to the overlying hyper-acid crater lake (Christenson et al. 2010).

2.2 Occurrence of Aqueous Sulfur, Elemental Sulfur and Sulfate, Sulfide and Sulfosalt Minerals

2.2.1 Aqueous Sulfur Species

Dissolved sulfur in hyper-acid crater lakes and geothermal lakes occurs chiefly in the most oxidized forms, i.e., sulfate (SO_4^{2-}). At pH below 2, SO_4^{2-} is protonated into bisulfate (HSO_4^{2-}). In the following sections, we will simply refer to SO_4^{2-}. It is practically impossible to remove SO_4^{2-} from the water by inorganic oxidation; only formation of secondary minerals through precipitation or extensive water-rock interaction can do so. Hyper-acid crater lakes hosted by active craters (e.g., Kawah Ijen, Indonesia; Kusatsu-Shirane (Yugama Lake), Japan; Ruapehu; Maly Semiachik, Russia; Poás, Costa Rica) often exhibit extreme SO_4^{2-} concentrations, on a par with those reported for the most acidic mine drainages (Table 1). For example, the 3.0×10^7 m^3 crater lake of Kawah Ijen contains $\sim$77,000 mg l^{-1} of SO_4^{2-}, corresponding to a total amount of $\sim$2.1 Tg. At Poás, transient SO_4^{2-} concentrations up to $\sim$167,000 mg l^{-1} were measured in the waters during an episode of intense heating and evaporation of the lake (Rowe et al. 1992a).

Hyper-acid crater lakes are also strongly mineralized (total dissolved solid content >50,000 mg l^{-1}) and commonly display pH values below one (Table 1; Varekamp et al. 2000). These characteristics results from continuous supply of hyper-acid, sulfur-enriched liquids which form as high-enthalpy, SO_2-rich magmatic vapors expand and condense near the surface (Henley and Berger 2011; Henley and McNabb 1978). Crater lakes that sit on top of less vigorous and probably deeper subsurface magma-hydrothermal systems (e.g., Kelud, Indonesia; El Chichón, Mexico; Pinatubo, Philippines) typically show less acidic pHs and lower dissolved SO_4^{2-} concentrations (Taran et al. 1998; Varekamp et al. 2000; Table 1). Similarly, geothermal lakes (e.g., Oyunuma, Noboribetsu geothermal field; Bannoe, Uzon caldera, Russia) which receive sulfur inputs dominated by H_2S-rich steam display comparatively higher pH values and lower SO_4^{2-} concentrations (Table 1).

Polythionates (sulfur oxyanions of the type $S_xO_6^{2-}$, x = 4–6) are the most abundant aqueous sulfur species after SO_4^{2-} in hyper-acid crater lakes, occurring in concentrations of several tens to hundreds of mg l^{-1} (Table 1). To our knowledge, no $S_xO_6^{2-}$ data are available for geothermal lakes, but these sulfur compounds have been documented in a hot spring at Yellowstone National Park (e.g., Xu et al. 2000). Very few determinations exist for the other stable or metastable sulfur species, including H_2S, SO_2, polysulfides (HS_n^-), elemental sulfur (S°), sulfite (SO_3^{2-}) and thiosulfate ($S_2O_3^{2-}$), susceptible to

Table 1 pH and sulfate (SO_4^{2-}) and corresponding total polythionate ($\Sigma S_xO_6^{2-}$, x = 4–6) concentrations (mg l^{-1}) in some (hyper-)acid crater lakes and geothermal lakes

	pH	SO_4^{2-}	$\Sigma S_XO_6^{2-}$	Reference
(Hyper-)acid crater lakes				
Kawah Ijen, Indonesia	0.2/0.3	59,300/71,300	343/1157	Delmelle et al. (2000)
Kusatsu-Shirane, Yugama Lake, Japan	~1	~3,510	850	Takano and Watanuki (1990)
Poás, Costa Rica	0.2/−0.3	40,100/103,000	4,207/8	Rowe et al. (1992a)
Maly Semiachik, Russia	~1	9,700/11,000	857/350	Sugimori et al. (1995)
Ruapehu Crater Lake, New-Zealand	~0.7	20,450/16,300	192/497	Takano et al. (1994a), Christenson and Wood (1993)
El Chichón, Mexico	2.7/2.2	240/1,850		Rouwet et al. (2008)
Kelud, Indonesia	5.9	530		Bernard (unpublished data)
Voui, Vanuatu	1.6	3,780		Bani et al. (2009)
Geothermal lakes				
Oyunuma, Japan	2.5	740		Inoue and Aoki (2000)
Bannoe, Russia	4.9	90		Hollingsworth (2006)

exist in hyper-acid crater lakes and geothermal lakes. Measurements conducted at Kusatsu-Shirane, Ruapehu and Kawah Ijen hyper-acid crater lakes indicate dissolved SO_2 and H_2S concentrations in the range 10–50 and <0.2 mg l^{-1}, respectively (e.g., Takano et al. 1994a, 2004; Christenson 2000). Unsurprisingly, comparatively higher H_2S concentrations are found in geothermal lakes; for example up to 56 mg l^{-1} of H_2S was determined in the water column of Oyunuma lake (Inoue and Aoki 2000).

2.2.2 Elemental Sulfur

Elemental sulfur (S°) is commonly found in hyper-acid crater lake environments. Colloidal S° precipitated from the lake water has been reported at a few sites (Christenson and Wood 1993; Ohsawa et al. 2010). At Kawah Ijen, thick exposures of laminated S°-rich sediments suggest that the lake waters can become saturated with respect to S° for prolonged periods of time (Brouwer 1925; Delmelle et al. 2000; Takano et al. 2004). Similar crater lake sediments can be found at Dempo volcano, Indonesia (Fig. 2) and Tateyama volcano, Japan (Kusakabe and Hayashi 1986). Thermodynamic considerations corroborate the view that S° can precipitate from hyper-acid crater lake waters (e.g., Christenson and Wood 1993; Delmelle and Bernard 1994). The acid crater lake which formed immediately after the 1982 Plinian eruption of El Chichón volcano accumulated 3.8×10^7 kg of S° in less than a year, equivalent to a production rate of ~1.2 kg s^{-1} (Casadevall et al. 1984). The rate of S° deposition in the hydrothermal vent-crater lake system of Poás is estimated by Rowe et al. (1992b) to be on the order of 0.3 kg s^{-1}. Comparable values are deduced for Copahue, Argentina (Varekamp et al. 2001) and Kawah Ijen hyper-acid crater lakes (Delmelle, unpublished data).

Perhaps one of the most remarkable aspects of sulfur chemistry in hyper-acid crater lakes is the capacity of some of them to host a subaqueous molten body (or bodies) of S°. This was inferred nearly a century ago from observations of floating sulfur spherules found at Yugama Lake (Ohashi 1919). Sulfur spherules (Figs. 1a and 3a) seems to be a typical feature of hyper-acid crater lakes (e.g., Giggenbach 1974; McClelland et al. 1989; Delmelle and Bernard 1994; Pasternack and Varekamp 1994; Sriwana et al. 2000). These hollow spherules probably form as expanding volcanic gas bubbles en route to the lake surface pass through, and become coated with molten sulfur (Ohashi 1919; White et al. 1988; Delmelle et al. 2000). A few acid-sulfate geothermal lakes, for example Oyunuma (Murozomi et al. 1966) and Bannoe (Karpov and Fazlullin 1995), also

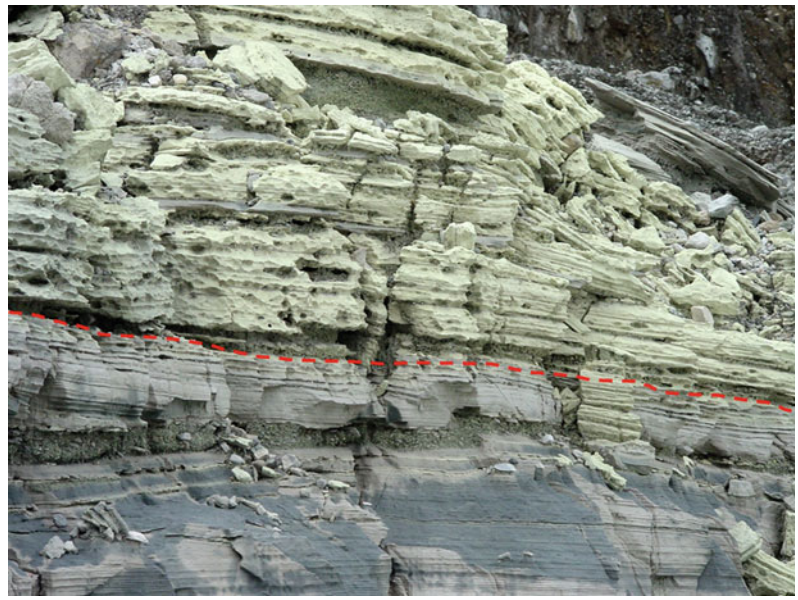

Fig. 2 Elemental sulfur sediments exposed in a cliff on the lake shore of the hyper-acid crater lake of Dempo volcano, Indonesia. Silica-rich sediments occur below (*dotted red line*) the S°-rich layers

possess a subaqueous molten sulfur pool and similarly display production of sulfur spherules (Fig. 1b).

A spectacular confirmation for occurrence of molten sulfur in hyper-acid crater lakes emerged at Poás volcano in 1989 when temporary disappearance of the lake exposed active pools of liquid sulfur at the crater floor (Oppenheimer and Stevenson 1989). Earlier discovery of molten sulfur was made at White island, when shallow boreholes sunk into the desiccated crater lake bed in 1885 penetrated 1-m-thick seams of S° (Luke 1959). Other evidence comes from the recovery of sulfur pyroclasts (Fig. 3b) ejected by phreatic eruptions through crater lakes (Bennett and Raccichini 1978; Francis et al. 1980; Delpino and Bermúdez 1996; Delmelle et al. 2000; Christenson et al. 2010). The morphology of the sulfur ejecta, as in the case of spherules, indicates formation in the liquid phase and therefore, existence of temperatures at the lake bottom above the sulfur melting point (~119.6 °C for monoclinic β-sulfur; Meyer (1976)). Direct sampling of subaqueous molten sulfur at Yugama Lake (Takano et al. 1994b), Ruapehu Crater Lake (Christenson 1994), Maly Semiachik (Takano et al. 1994b) and Bannoe (Karpov and Fazlullin 1995) suggest temperatures in the range 118−177.3 °C. The subaqueous sulfur pool at Ruapehu Crater Lake may be 50 m in diameter and at least 6 m deep (Christenson and Wood 1993). In a recent paper, Christenson et al. (2010) show that deposition of S°, along with anhydrite and alunite, in the hydrothermal vent feeding the lake causes a drastic reduction in permeability and sealing of the upper part of the vent.

A detailed mineralogical and chemical study of sulfur slicks from Yugama lake indicates the presence of homocyclic sulfur (S_x, $6 \leq x \leq 16$) and sulfane monosulfonates (HS_8SO_3H); the latter compounds are linked to H_2S dissolution in S° (Takano et al. 1994b). Moreover, impurities, mostly in the forms of minor and trace elements, in sulfur spherules and pyroclasts from hyper-acid crater lakes and geothermal lakes are ubiquitous. Iron is typically the most abundant contaminant (few tenths to a few wt %), but other metals such as As, Au, Bi, Cd, Cu, Mo, Ni, Pb, Se, Sn, Te, Tl and W are also detected, albeit in trace concentrations (Karpov and Fazlullin 1995; Kargel et al. 1999; Mason et al. 2001; Martínez et al. 2002; Takano et al. 2004). Elemental sulfur samples which display extreme As, Se and Sb enrichments (tens to thousands of times crustal abundances) probably contain sulfide and sulfosalt mineral

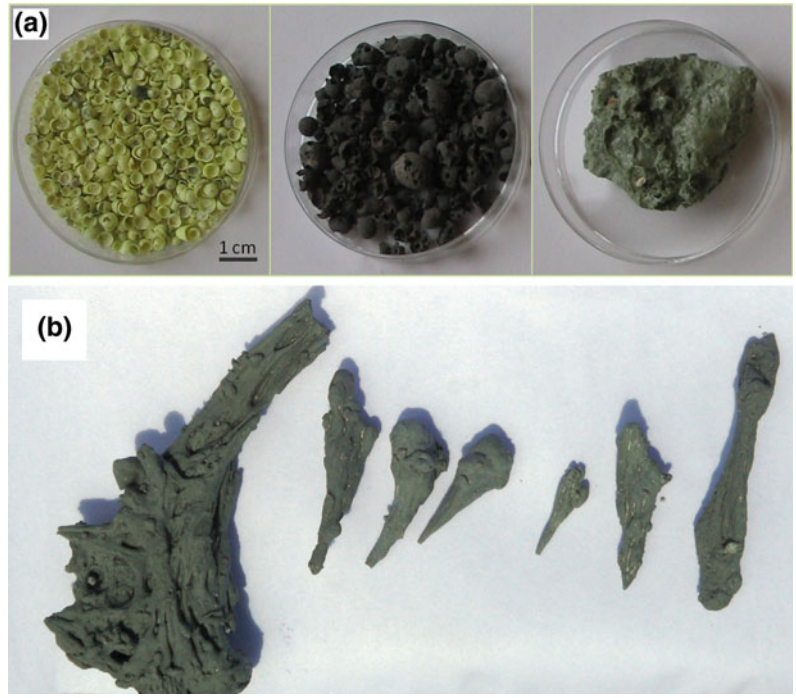

Fig. 3 **a** Sulfur spherules (*left* and *middle*) and quenched molten sulfur (*right*) collected from Kawah Ijen hyper-acid crater lake, Bannoe geothermal lake, and Kusatsu-Shirane hyper-acid crater lake, respectively. *Photo* courtesy of F. Africano. **b** Sulfur pyroclasts ejected by an eruption through the hyper-acid crater lake of Dempo volcano, Indonesia

inclusions (see Sect. 2.2.3). Kargel et al. (1999) attribute the diverse colorations, from yellow to green to black, of sulfur spherules and pyroclasts to metal impurities (Fig. 3a).

2.2.3 Sulfate, Sulfide and Sulfosalt Minerals

Sulfur in hyper-acid crater lakes may also occur as sulfate, sulfide and sulfosalt minerals. Gypsum ($CaSO_4 \cdot 2H_2O$) and alunite ($(Na, K)Al_3(SO_4)_2(OH)_6$) have been identified in the suspended sediments of Ruapehu's lake waters (Giggenbach 1974; Christenson and Wood 1993). Rowe et al. (1995) mention the presence of alunite in old lake sediments exposed in the summit crater of Poás. This mineral is ubiquitous in sediments collected from Oyunuma and Bannoe geothermal lakes (Inoue and Aoki 2000; Karpov and Fazlullin 1995). Barite is the only sulfate mineral stable in Kawah Ijen crater lake, although spectacular gypsum formation was witnessed following a recent cooling event of the lake (Fig. 4a). Gypsum also occurs as surface coatings and infill material of rocks that are intermittently exposed to the low-pH lake waters (Delmelle and Bernard 1994). Moreover, anhydrite ($CaSO_4$), gypsum and alunite occur in the ejecta produced by phreatic/phreatomagmatic eruptions through the lake (van Hinsberg et al. 2010), similar to findings at Ruapehu (Wood 1994; Christenson et al. 2010). At Kawah Ijen, massive deposition of gypsum mixed with a suite of aluminium sulfate minerals, including alunogen ($Al_2(SO_4)_3 \cdot 16H_2O$), pickeringite ($MgAl_2(SO_4)_4 \cdot 22H_2O$), tamarugite ($NaAl(SO_4)_2 \cdot 6H_2O$) and kalinite ($KAl(SO_4)_2 \cdot 11H_2O$) is observed where the hyper-acid lake water seepages escape the summit crater (Fig. 4b). Finally, an iron sulfate phase (K-jarosite, $KFe_3(OH)_6(SO_4)_2$) is suggested to have precipitated in the acid crater lake of Ambae volcano (Lake Voui), Vanuatu, during a recent unrest in 2005–2006 (Bani et al. 2009). However, this occurrence is not confirmed since the iron sulfate mineral was detected as a precipitate in the sampling bottles and not in the suspended matter collected directly from the lake.

Not only sulfate minerals, but sulfides and sulfosalts can form in hyper-acid crater lakes. Mineralogical analyses of quenched molten

sulfur materials from hyper-acid crater lakes and geothermal lakes disclose the presence of pyrite (cubic form of FeS_2) inclusions, sometimes in quantities exceeding 10 wt % (Takano et al. 1994b; Inoue and Aoki 2000). At Kawah Ijen, pyrite is the dominant sulfide mineral in sulfur spherules, but other sulfide and sulfosalt inclusions (size <20 μm), including Sb-rich enargite (Cu_3AsS_4), bismuthinite (Bi_2S_3) and rare stannite (Cu_2FeSnS_4) are also identified (Delmelle and Bernard 1994). Marcasite (orthorhombic form of FeS_2) coexists with pyrite in the quenched molten sulfur from Bannoe and Oyunuma geothermal lakes (Delmelle, unpublished data).

3 Sulfur Chemistry

3.1 Aqueous Sulfate

Various chemical reactions can lead to SO_4^{2-} generation in hyper-acid crater lakes and geothermal lakes. These include abiotic and biotic oxidation of H_2S (O'Brien and Birkner 1977; Oprime et al. 2001; reaction 3), hydrolysis of S° (Ellis and Giggenbach 1971; reaction 4), disproportionation-hydrolysis of SO_2 (Iwasaki and Ozawa 1960; Ellis and Mahon 1977; reactions 5a and 5b), disproportionation-hydrolysis of $S_xO_6^{2-}$ (Meyer and Ospina 1982; Xu et al. 2000; reaction 6) and oxidation of tetrathionate ($S_4O_6^{2-}$; Druschel et al. (2003a, 2003b); reaction 7):

$$H_2S + 2O_2 = SO_4^{2-} + 2H^+ \quad (3)$$

$$4S^\circ + 4\,H_2O = SO_4^{2-} + 3H_2S + 2H^+ \quad (4)$$

$$4SO_2 + 4H_2O = 3SO_4^{2-} + H_2S + 6H^+ \quad (5a)$$

$$3SO_2 + 3H_2O = 2SO_4^{2-} + H_2O + S^\circ + 4H^+ \quad (5b)$$

$$S_xO_6^{2-} + H_2O = SO_4^{2-} + S_{x-1}O_3^{2-} + 2H^+ \quad (6)$$

$$S_4O_6^{2-} + 3Fe^{3+} + 2.75O_2 + 4.5H_2O = 4SO_4^{2-} + 3Fe^{2+} + 9H^+ \quad (7)$$

Measurement of the sulfur isotopic composition ($\delta^{34}S$) of SO_4^{2-} has been determinant in unraveling its main formation pathway in hyper-acid crater lakes. Figure 5 highlights the existence of a broad range of $\delta^{34}S_{SO_4}$ values, but SO_4^{2-} from hyper-acid systems always displays the heaviest isotopic compositions. Oana and Ishikawa (1968) first postulated that disproportionation of SO_2 yields SO_4^{2-} distinctively enriched in the heavy sulfur isotope. Later, Kiyosu and Kurahashi (1983) concluded that this reaction explain the high $\delta^{34}S_{SO_4}$ values of acid sulfate-chloride thermal waters from Japan. Rowe et al. (1995) reached the same conclusion for Poás'crater lake waters. In 2000, Kusakabe and his colleagues published the results of an elegant experiment which unambiguously source the heavy sulfur isotope ratios of SO_4^{2-} in hyper-acid crater lakes to disproportionation of SO_2. The authors further establish the temperature dependence relationship of the equilibrium sulfur isotope fractionation, α, between SO_4^{2-} and S° associated with this reaction:

$$1000 \ln \alpha_{SO_4-S^\circ} = 6.21 \times 10^6/T^2 + 3.62 \quad (8)$$

They also emphasize that the magnitude of the isotopic exchange for the SO_4^{2-}-S° system is probably similar to that for the SO_4^{2-}-H_2S system, although a stronger dependency on temperature is expected.

Other SO_4^{2-} generation pathways in hyper-acid crater lakes fed by magmatic hydrothermal inputs are of minor importance, or simply do not occur. There is no enough dissolved H_2S in these lakes and oxidation of H_2S (reaction 3) is a negligible source of SO_4^{2-}; the latter mechanism is also incompatible with the measured heavy $\delta^{34}S_{SO4}$ values (see below). Hydrolysis of S° (reaction 4) requires relatively high temperatures (~100–350 °C) to become efficient, thus confining SO_4^{2-} production through this mechanism within the upper and hotter part of the hydrothermal vent-crater lake system. The importance of $S_xO_6^{2-}$ hydrolysis and oxidation (reactions 6 and 7, respectively) in SO_4^{2-} production in hyper-acid crater lakes is not known.

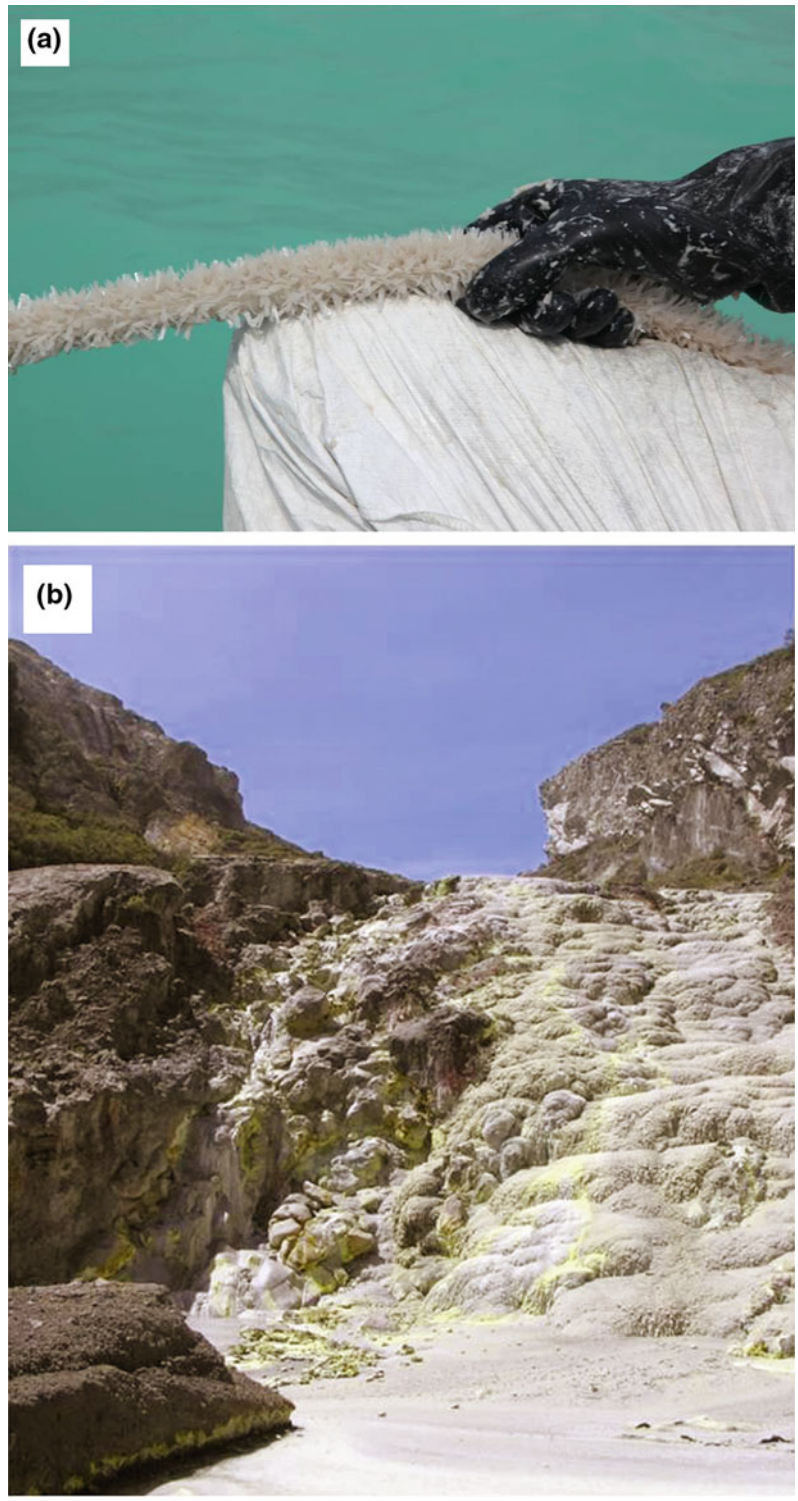

Fig. 4 **a** A nylon rope coated with macroscopic gypsum crystals after having been immersed (40 days) in the hyper-acid waters of Kawah Ijen during a cooling episode (from 37 to 30 °C)of the crater lake in August-September 2011. **b** Massive gypsum-and aluminium sulfate-containing deposits formed by intense evaporation of crater lake seepages at Kawah Ijen volcano

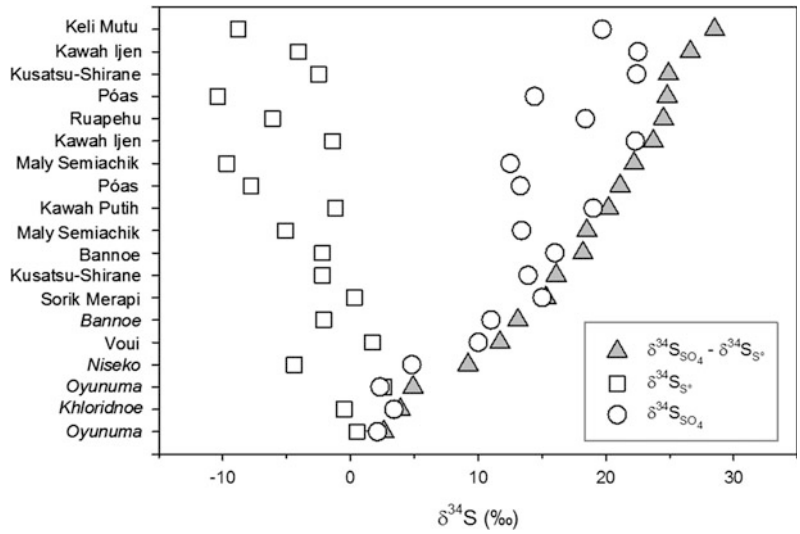

Fig. 5 Sulfur isotopic composition ($\delta^{34}S$) of dissolved SO_4^{2-} and elemental sulfur from (hyper-)acid crater lakes and *geothermal lakes*. The lakes are listed in increasing order of isotopic distance ($\Delta_{SO_4-S^\circ} = \delta^{34}S_{SO_4} - \delta^{34}S_{S^\circ}$). Data from Kusakabe et al. (2000) and Bernard (unpublished)

As illustrated in Fig. 5, acid-sulfate waters from geothermal lakes (e.g., Oyunuma; Niseko, Japan; Khloridnoe, Russia) tend to exhibit markedly lower $\delta^{34}S_{SO4}$ values as compared to hyper-acid crater lakes. This trend simply points to oxidation of H_2S in steam separated from a deep hydrothermal reservoir of near-neutral pH, reduced water as the principal pathway for SO_4^{2-} formation. Reaction (3) produces a limited sulfur isotope exchange and thus, isotopically light SO_4^{2-} (Sakai 1957; Ohmoto and Rye 1979). However, relatively high $\delta^{34}S$ values ($\sim$10 ‰, Fig. 5) are reported for SO_4^{2-} in Bannoe geothermal lake. This may indicate hydrothermal water inflows containing isotopically heavy SO_4^{2-} mobilized from old sulfate mineral deposits (e.g., alunite, anhydrite, gypsum), which themselves contain SO_2-derived SO_4^{2-} formed during a previous episode of shallow magmatic hydrothermal activity in the caldera. Conversely, the comparatively low $\delta^{34}S_{SO_4}$ measured in Lake Voui during the 2005–2006 unrest probably points to H_2S-rich hydrothermal inputs to the acid crater lake.

Oxidation of H_2S into SO_4^{2-} takes place in the near-surface environment where oxygen is available but the reaction is kinetically limited (Chen and Morris 1972). It normally proceeds through a complex chain of reactions that involve both abiotic and biotic processes. At low concentrations of oxygen, the abiotic oxidation of H_2S produces $S_2O_3^{2-}$:

$$2H_2S + 2O_2 = S_2O_3^{2-} + H_2O + 2H^+ \quad (9)$$

Thiosulfate is unstable under acid conditions and breakdown to S° and SO_3^{2-} or sulfides (e.g., Davis 1958):

$$S_2O_3^{2-} = S^\circ + SO_3^{2-} \quad (10)$$

Sulfite is then rapidly oxidized abiotically to SO_4^{2-}:

$$SO_3^{2-} + 0.5O_2 = SO_4^{2-} \quad (11)$$

Elemental sulfur generated via reaction (10) tends to accumulate because of its slow reactivity with water below 100 °C, and a catalyst or bacteria is required to proceed further. In particular, sulfur oxidizing bacteria such as *Thiobacillus thiooxidans* can utilize sulfur (enzymatic oxidation) as an energy source and converts it to SO_4^{2-} (e.g., Kelly 1982):

$$S^\circ + 1.5O_2 + H_2O \rightarrow SO_4^{2-} + 2H^+ \quad (12)$$

Thiobacillus thiooxidans is identified in several acid crater lakes and geothermal lakes (Ivanov and Karavaik 1966; Sugimori et al. 1995; Takano et al. 1997), although it is absent at pH < 1. A rate of

SO_4^{2-} production from H_2S by *Thiobacillus thiooxidans* of 8.4 g m^{-2} day^{-1} has been determined in Yugama Lake. It is nearly ten times higher in Oyunuma geothermal lake (Murozomi et al. 1966; Schoen 1969). Aerobic bacterial oxidation of S° produces a small isotopic effect (Nakai and Jensen 1964) and as a consequence, SO_4^{2-} formed through this pathway exhibits light $\delta^{34}S$ values.

3.2 Aqueous Polythionates

Complex mixtures of $S_4O_6^{2-}$, $S_5O_6^{2-}$ and $S_6O_6^{2-}$ are commonly found in hyper-acid crater lakes (e.g., Takano and Watanuki 1990; Takano et al. 1994a; Rowe et al. 1992a; Delmelle et al. 2000; Sriwana et al. 2000). The presence of $S_xO_6^{2-}$ is linked to reactions between H_2S and SO_2 gases in acidic waters (Takano 1987; Takano and Watanuki 1990), sometimes referred as a Wackenroders solution (Haff 1970), such as:

$$H_2S + 3SO_2 = S_4O_6^{2-} + 2H^+ \quad (13a)$$

$$5H_2S + 10SO_2 = 3S_5O_6^{2-} = 3S_5O_6^{2-} + 6H^+ + 2H_2O \quad (13b)$$

$$7H_2S + 11SO_2 = 3S_6O_6^{2-} = 3S_5O_6^{2-} + 6H^+ + 4H_2O \quad (13c)$$

These poorly-constrained reactions involve various unstable intermediate sulfur species that are difficult to measure. Takano et al. (1994a) suggest that $S_4O_6^{2-}$ is preferentially formed when the aqueous SO_2/H_2S molar ratio is ~3, whereas $S_5O_6^{2-}$ and $S_6O_6^{2-}$ dominate at lower ratio values of ~1 (Fig. 6). The temperature dependence of equilibrium $S_xO_6^{2-}$ distribution is not documented, but $S_xO_6^{2-}$ species are known to degrade above 100 °C (Takano and Watanuki 1990).

An alternative pathway for $S_xO_6^{2-}$ formation in hydrothermal waters has been proposed (Williamson and Rimstidt 1993; Xu and Schoonen 1995; Xu et al. 2000); it involves oxidation of $S_2O_3^{2-}$, enhanced by the catalytic action of pyrite (and possibly other metal sulfides) or Fe^{3+}. Thiosulfate may originate from the initial step of S° hydrolysis, expressed as:

$$4S^\circ + 3H_2O = S_2O_3^{2-} + 2H_2S + 2H^+ \quad (14)$$

or/and from the shortening (sulfitolysis) of $S_xO_6^{2-}$ chain length by reaction with SO_3^{2-} produced via oxidation of SO_2, according to:

$$S_{x+1}O_6^{2-} + SO_3^{2-} = S_xO_6^{2-} + S_2O_3^{2-} \quad (15)$$

Oxidation of H_2S also yields $S_2O_3^{2-}$ as an intermediate sulfur species (reaction 9). The oxidation of $S_2O_3^{2-}$ into $S_4O_6^{2-}$ can be written as:

$$2S_2O_3^{2-} + 0.5O_2 + 2H^+ = S_4O_6^{2-} + H_2O \quad (16)$$

The rate of $S_4O_6^{2-}$ formation via this reaction was shown to increase with temperature (Xu et al. 2000).

Since pyrite is a common mineral impurity in sulfur spherules from hyper-acid crater lakes and geothermal lakes, $S_xO_6^{2-}$ production through $S_2O_3^{2-}$ oxidation cannot be ruled out. At Yugama lake, Takano et al. (1994b) reported a remarkably high total $S_xO_6^{2-}$ concentration (3,900 mg l^{-1}) in the solution obtained by squeezing sulfur spherules, possibly pointing to efficient production of $S_xO_6^{2-}$ through pyrite-mediated oxidation of $S_2O_3^{2-}$. Similarly, Webster (1989) measured $S_2O_3^{2-}$ concentrations up to 10 mg l^{-1} in Ruapehu Crater Lake waters. However, the importance of a pyrite-mediated reaction pathway in hyper-acid crater lakes may be confounded by the availability of $S_2O_3^{2-}$, which is rapidly decomposed (reaction 10) under low pH and elevated temperature conditions (>150 °C; Xu et al. 2000).

Since $S_xO_6^{2-}$ anions are expected to be unstable above 100 °C (Takano and Watanuki 1990), most of $S_xO_6^{2-}$ production probably takes place in the hyper-acid crater lake itself. However, part of the $S_4O_6^{2-}$ content could be sourced to the subaqueous hydrothermal vent; kinetic data suggest that the half-life of this sulfur oxyanion below 200 °C is long enough to allow its transfer to the lake (Takano et al. 2004).

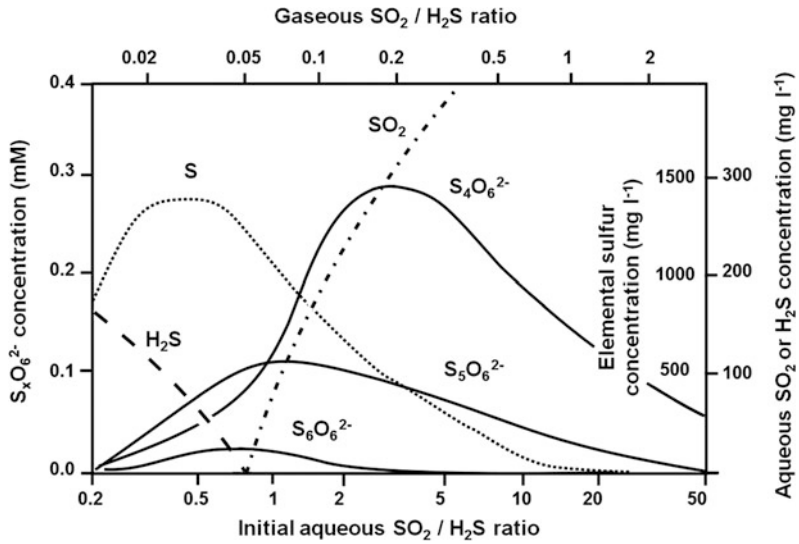

Fig. 6 Distribution of polythionates ($S_xO_6^{2-}$, x = 4–6), elemental sulfur, aqueous H_2S and SO_2 as a function of the aqueous SO_2/H_2S molar ratio (the corresponding SO_2/H_2S ratio in the gas is also shown). The concentrations of $S_xO_6^{2-}$ and aqueous SO_2 and H_2S represent values determined experimentally. Reproduced from Takano et al. (1994a) with permission from Elsevier

3.3 Elemental Sulfur

Elemental sulfur in hyper-acid crater lakes can form through several reaction pathways. In the main hydrothermal upflow zone beneath the lake, S° is readily deposited from the volcanic gas phase containing SO_2 and H_2S (Mizutani and Sugiura 1966; Giggenbach 1987):

$$SO_2 + 2H_2S = 3S^\circ + 2H_2O \qquad (17)$$

Reaction (17) is thermodynamically favored upon expansion and cooling of the magmatic gases en route to the surface. There is a positive sulfur isotopic fractionation between SO_2 and H_2S in fumarolic gases which increases as temperature decreases, but still can be several ‰ above 400 °C (Richet et al. 1977; Taylor 1986). This effect explains the light isotopic composition of fumarolic S° deposits (e.g., Sakai 1957; Delmelle et al. 2000) and is also compatible with the mildly to moderately depleted $\delta^{34}S$ values measured in sulfur spherules and pyroclasts (which correspond to 'quenched' molten sulfur) from hyper-acid crater lakes (Fig. 5). The conspicuous presence of liquid sulfur in the porosity of subsurface rocks ejected from a small gas-driven eruption through Ruapehu Crater Lake (Christenson et al. 2010) gives further credence to substantial S° deposition via reaction (17). Since this reaction consumes two moles of H_2S for one mole of SO_2, it can also explain the typically low concentration of dissolved H_2S measured in hyper-acid crater lakes.

Some hyper-acid crater lakes (e.g., Poás and Maly Semiachik) host S° with noticeably light isotopic compositions ($\delta^{34}S$ as low as −10.4‰, Fig. 5). Since SO_4^{2-} production through SO_2 disproportionation gives rise to a large sulfur isotope exchange (Sect. 3.1), strongly negative $\delta^{34}S_{S^\circ}$ values are attributed to S° formation through reaction (5b), or indirectly via reaction (5a) followed by subsequent oxidation of H_2S (reactions 9 and 10; Kusakabe et al. 2000).

A few studies (e.g., Bernard et al. 2004; Rowe 1994) posit that precipitation of S° can also result from oxidation of H_2S by Fe^{3+} in the low pH waters:

$$2Fe^{3+} + H_2S = 2Fe^{2+} + S^\circ + 2H^+ \qquad (18)$$

Ferrous iron is the stable dissolved iron species in strongly acidic conditions, and reaction (18) implies that the Fe^{2+}/Fe^{3+} ratio should

decrease with increasing lake water acidity. However, this trend has never been observed in hyper-acid crater lakes and therefore, oxidation of H_2S by Fe^{3+} is unlikely to govern S° precipitation.

Elemental sulfur deposition in hyper-acid crater lakes may also relate to $S_xO_6^{2-}$ sulfitolysis (reaction 15), and subsequent degradation of $S_2O_3^{2-}$ (reaction 10). The overall reaction is summarized by Takano (1987) as:

$$S_xO_6^{2-} + (3x-7)HSO_3^- = (2x-3)SO_4^{2-} + (2x-4)S^\circ + (x-1)H^+ + (x-3)H_2O \quad (19)$$

At Poás, Rowe (1994) argued that, over short-time periods, $S_xO_6^{2-}$ destruction through reaction (19) can lead to significant S° deposition. A similar conclusion was reached by Delmelle et al. (2000) for Kawah Ijen hyper-acid crater lake. Alternatively, S° can be a product of $S_xO_6^{2-}$ decomposition due to interaction with H_2S (Xu et al. 2000):

$$S_xO_6^{2-} + H_2S = 2S_2O_3^{2-} + (x-2)S^\circ + 2H^+ \quad (20)$$

Thus, in the presence of $S_xO_6^{2-}$, the amounts of S° and SO_4^{2-} derived from H_2S oxidation may be limited due to diversion of this species via reaction (20).

In geothermal lakes, S° originates from abiotic oxidation of H_2S (reactions 9–10 and perhaps, reaction 18) conveyed by hydrothermal steam discharges. Accordingly, S° in these lake settings tends to display less negative isotopic compositions (e.g., Oyunuma and Khloridnoe, Russia; Fig. 5) compared to those found in hyper-acid crater lakes fed by SO_2-rich magma-hydrothermal inputs. The cases of Bannoe and Niseko geothermal lakes, which display atypical $\delta^{34}S_{S^\circ}$ values, are briefly discussed later.

Molten sulfur bodies in hyper-acid crater lakes may correspond to S° deposited directly from the sulfur-bearing magmatic gas phase (reaction 17) and/or through SO_2 disproportionation (reactions 5a and 5b). Alternatively, remobilization of S°-rich lake sediments previously deposited on the crater floor (Fig. 2) may also be responsible for the formation of molten material. Interestingly, the isotopic composition determined for lacustrine S° sediments exposed in the crater of Kawah Ijen volcano falls within the range reported for the sulfur spherules and pyroclasts (Delmelle et al. 2000). Melting of S°-rich sediments may also account for the comparatively depleted $\delta^{34}S_{S^\circ}$ values of quenched molten sulfur samples from Bannoe and Niseko geothermal lakes (Fig. 5).

3.4 Sulfate, Sulfide and Sulfosalt Minerals

Sulfate minerals in hyper-acid crater lakes and geothermal lakes are restricted to the hydrous aluminum and alkaline-earth phases. As observed at a few sites, alunite can precipitate directly from the lake waters (e.g., Giggenbach 1974; Takano and Watanuki 1990; Inoue and Aoki 2000). In hyper-acid crater lakes powered by magma-hydrothermal interaction, alunite and anhydrite may form in the upper part of the hydrothermal vent due to magmatic vapor expansion (Christenson et al. 2010; Henley and Berger 2011). Such deposits can constitute a reservoir of SO_4^{2-} for the overlying crater lake when subsurface magma-hydrothermal activity fosters mineral dissolution (Christenson and Wood 1993; Takano and Watanuki 1990).

Formation of macrocrystals of gypsum in hyper-acid crater lakes is normally attributed to evaporation and enhanced saturation in the waters, although lake cooling may also prompt gypsum precipitation (Fig. 4a). Unsurprisingly, the sulfur isotopic signature of gypsum reflects that of dissolved SO_4^{2-} (Rowe 1994). Besides gypsum, various hydrated aluminum sulfate minerals may precipitate upon intense evaporation of the lake waters, as epitomized by the spectacular deposits which form on the outer flank of Kawah Ijen where lake seepages resurge (Fig. 4b; Delmelle and Bernard 2000).

Sulfides or sulfosalts have not been detected in suspended matter retrieved from hyper-acid

crater lakes, although there is suspicion that pyrite is close to saturation in Ruapehu Crater Lake (Christenson and Wood 1993; Christenson et al. 2010). Pyrite is reported to occur in lake bottom sediments at Ruapehu and Kawah Ijen. Thermodynamic calculations predict that a typical hyper-acid crater lake water becomes saturated with respect to minerals such as bornite (Cu_5FeS_4), chalcocite (Cu_2S), covellite (CuS), enargite, tennantite, bournonite ($PbCuSbS_3$), chalcopyrite ($CuFeS_2$), tetrahedrite ($(Cu, Fe)_{12}Sb_4S_{13}$), stibnite (Sb_2S_3) and orpiment (As_2S_3) when the dissolved concentration of H_2S is slightly raised (Delmelle and Bernard 1994; Pasternack and Varekamp 1994; Sriwana et al. 2000). Overall, these findings point to lack of reliable aqueous H_2S measurements in hyper-acid crater lake waters. In geothermal lake settings (e.g., Oyunuma and Bannoe), continuous supply of H_2S-rich steam maintains reducing conditions in the water column, thereby allowing readily precipitation of pyrite (Inoue and Aoki 2000).

The presence of sulfide and sulfosalt inclusions in sulfur spherules and pyroclasts from hyper-acid crater lakes is not fully understood. These minerals may precipitate in the subaqueous hydrothermal vent which hosts molten sulfur and where redox conditions are probably more reducing than in the thoroughly mixed lake water column. Interaction between magmatic gas discharges and molten sulfur may also lead to sulfide and sulfosalt formation. There is plenty of evidence that metal deposition occurs as a deep magmatic vapor expands and cools during ascent to the surface (e.g., Bernard and Le Guern 1986; Symonds and Reed 1993; Taran et al. 1995; Africano et al. 2002; Henley 2015). Fine pyrite and covellite grains and Cu-As sulfosalt inclusions in molten sulfur from a submarine volcano in the Lau Basin, southwestern Pacific Ocean, are thought to result from condensation of metal-transporting magmatic vapor (Kim et al. 2011). The same mechanism may apply to hyper-acid crater lake environments.

4 Geochemical Monitoring of Volcanic Activity at Hyper-Acid Crater Lakes Using Sulfur Compounds

4.1 Aqueous Polythionates and Sulfate

In a series of papers published between 1987 and 2008, Takano and others proposed that $S_xO_6^{2-}$ total concentration and distribution in hyper-acid crater lakes are coupled to changes in the SO_2/H_2S gas ratio of magma-hydrothermal inputs. Based on the analysis of water samples collected from Yugama Lake between 1960 and 1986, Takano (1987) and Takano and Watanuki (1990) demonstrated that phreatic activity is systematically preceded by a decrease in $S_xO_6^{2-}$ and a concomitant increase in SO_4^{2-} in the lake waters (Takano 1987; Takano and Watanuki 1990). A similar pattern was reported for Poás prior to a magmatic eruption (Rowe et al. 1992a). The inverse relationship between $S_xO_6^{2-}$ and SO_4^{2} is attributed to enhanced sulfitolysis (reaction 15) consequent on the injection of SO_2-rich gases into the lake and subsequent production of SO_3^{2-}. Takano and Watanuki (1990) also emphasized that there is a sharp increase in $S_xO_6^{2-}$ prior to onset of sulfitolysis-driven degradation. They explain this observation in terms of fresh arrival of H_2S into the lake which in turn, brings the aqueous SO_2/H_2S ratio to values optimal for $S_xO_6^{2-}$ production (Fig. 6; Takano and Watanuki 1990). Based on these findings and using times-series $S_xO_6^{2-}$ data, Takano et al. (1994a) recognize four stages of magma-hydrothermal activity at Ruapehu Crater Lake during the period 1968–1991.

Some caution is needed when interpreting $S_xO_6^{2-}$ and SO_4^{2-} in hyper-acid crater lakes in relation to changes in volcanic activity as other processes than those evoked above may alter the concentration and distribution of these species. Our understanding of the chemistry and kinetics of $S_xO_6^{2-}$ formation and destruction, which may be governed in part by complex sulfur chemistry

involving gaseous, liquid and solid sulfur species, is still fragmentary. For example, it has been shown that $S_xO_6^{2-}$ decomposition can also result from interaction with excess H_2S (reaction 20; Xu et al. 1998, 2000). The significance of $S_2O_3^{2-}$ for $S_xO_6^{2-}$ chemistry in acid waters may also have been overlooked. Further, Takano's studies imply that the concentration and distribution of $S_xO_6^{2-}$ will vary with intensity of SO_2 removal in the subsurface magma-hydrothermal system, notably through reactions (5a, 5b) and (15). Sulfur dioxide scrubbing beneath the crater lake is difficult to quantify as it encompasses various processes involving gas, water and sometimes wall rock (Symonds et al. 2001). At Yugama Lake, inter-eruptive periods are characterized by cyclic changes of total $S_xO_6^{2-}$ content (Takano et al. 2008). This pattern is thought to reflect alteration of the sulfur-bearing gas composition due to periodic fluctuations in meteoric water inputs to the magma-hydrothermal reservoir beneath the lake. Lastly, variations in lake SO_4^{2-} may also relate to dissolution/precipitation reactions involving sulfate minerals (e.g., alunite) deposited in the upper zone of the hydrothermal vent connected to the crater lake (e.g., Takano and Watanuki 1990; Christenson et al. 2010).

Another point to address when applying $S_xO_6^{2-}$ monitoring to hyper-acid crater lakes is linked to the stability of sulfoxyanions during storage. In the absence of bacteria, $S_xO_6^{2-}$ are remarkably stable under low-pH conditions (Takano et al. 1994a; Takano and Watanuki 1988, 1990), but Xu et al. (2000) pointed out that concentrations in aged samples could be overestimated due to oxidation of other intermediate sulfur species such as $S_2O_3^{2-}$.

4.2 Sulfur Isotopic Composition

Evolution of the sulfur isotopic composition of SO_4^{2-} in hyper-acid crater lakes may also provide insights into subsurface magma-hydrothermal activity. Ohsawa et al. (1993) and Kusakabe et al. (2000) analysed a 23-year dataset (1972–1995) obtained at Yugama Lake. From 1973 to 1985, $\delta^{34}S_{SO_4}$ was remarkably constant at 20–21 ‰ (a similar value was measured for one lake water sample collected in 1955), but it decreased afterwards to reach a low of ~13 ‰ in 1990, before returning to pre-1985 levels in 1995. A subsequent survey unveils similar fluctuations between 1995 and 2007 (Shimizu and Ohba 2008). This alternation of high and low $\delta^{34}S_{SO_4}$ values is thought to reflect changes in the respective contributions to the lake of SO_4^{2-} derived from SO_2 disproportionation and surface runoffs containing SO_4^{2-} produced through biotic oxidation of S° and sulfides present in the ground.

In hyper-acid crater lakes, the isotopic distance between SO_4^{2-} and S° in quenched molten sulfur often exceeds 20 ‰ ($\Delta_{SO4-S^\circ} = \delta^{34}S_{SO_4} - \delta^{34}S_{S^\circ}$, Fig. 5). Based on this observation and assuming isotopic equilibrium, Kusakabe et al. (2000) used relationship (8) to infer that SO_4^{2-} in these lakes is probably formed above 200 °C in the sublimnic hydrothermal conduit where magmatic gases condense. Thus, determination of $\Delta_{SO_4-S^\circ}$ could provide information on the temperature regime in the upper part of the magma-hydrothermal system. However, the possibility that molten sulfur bodies in hyper-acid crater lakes correspond to remobilization of old lake sediments that are not contemporaneous of SO_4^{2-} formation puts a cast on this approach. Moreover, sluggish reaction kinetics below 200 °C can yield smaller apparent isotopic fractionations (Kusakabe et al. 2000), thus limiting applicability of equation (8) at lower temperatures.

The sulfur isotopic composition of SO_4^{2-} in hyper-acid crater lakes has also been linked to the initial molar H_2S/SO_2 ratio, r_s, of the source magmatic hydrothermal inputs. Taran et al. (1996) and later Kusakabe et al. (2000) proposed the following expression:

$$\delta^{34}S_{SO_4} = \delta^{34}S_{\Sigma S} + \Delta_{SO_4-H_2S}(r_s/1 + r_s) + \Delta_{SO_4-S^\circ}1/3(1/1 + r_s) \quad (21)$$

where $\Delta_{SO_4-H_2S}$ and $\Delta_{SO_4-S^\circ}$ denote the isotopic fractionation factors at equilibrium and $\delta^{34}S_{\Sigma S}$ is the isotopic composition of total sulfur in the system. According to this expression, a decrease in r_s produces lighter $\delta^{34}S$ in SO_4^{2-}. In general, the r_s values calculated using relationship (21)

are lower than estimates obtained from $S_xO_6^{2-}$ distribution (Takano et al. 1994a; Fig. 6). This discrepancy corroborates the idea that $S_xO_6^{2-}$ are mainly formed in the crater lake itself rather than in the hydrothermal vent where higher temperatures occur.

4.3 Elemental Sulfur

Subaqueous body (or bodies) of molten sulfur in hyper-acid crater lakes and geothermal lakes may influence heat and mass transfers from a subsurface magma-hydrothermal system to the overlying lake. Hurst et al. (1991) suggested that fluctuations in the flux of hot steam and non-condensable gases to Ruapehu Crater Lake are responsible for lake temperature variations. They explained this in terms of the strong dependence of sulfur viscosity on temperature. Above 159 °C, sulfur viscosity is such that heat and mass transfers through the hydrothermal vent-hosted molten sulfur would be blocked. However, Takano et al. (1994b) challenged this idea by showing that significant heat transfer to the lake is possible through convection within the molten sulfur body, even when the viscosity of pure sulfur is maximum (i.e., viscosity = 92 Pa s^{-1} at 187 °C). Moreover, they highlighted the impact of H_2S on sulfur viscosity; dissolution of this gas in liquid sulfur alters the molecular structure, thus leading to a lower viscosity of the sulfur body and thereby, enhanced convection and associated heat transfer. A similar effect is suspected for SO_2, but the solubility of H_2S in sulfur is higher (Touro and Wiewiorowski 1966; Wiewiorowski and Touro 1966) and increases (non-linearly) in the range 120–220 °C (Fanelli 1949; Marriott et al. 2008).

While Takano et al. (1994b) dismissed a direct link between molten sulfur viscosity and temperature variations at Ruapehu Crater Lake, they acknowledged that temperature conditions at the hydrothermal conduit-crater lake interface dictates when sulfur forms a fully molten body or a partially encrusted material, which may limits heat and mass exchanges. They also argued that the mineralogy (i.e., presence or absence of sulfides), chemistry (i.e., distribution of sulfur homocycles, S_x with x = 6−8) and morphology of sulfur spherules collected at the lake surface convey information on the state of the subaqueous sulfur mass from which they derive. Notably, Takano et al. (1994a) established a positive temperature dependence of the S_7/S_8 ratio in the sulfur spherules.

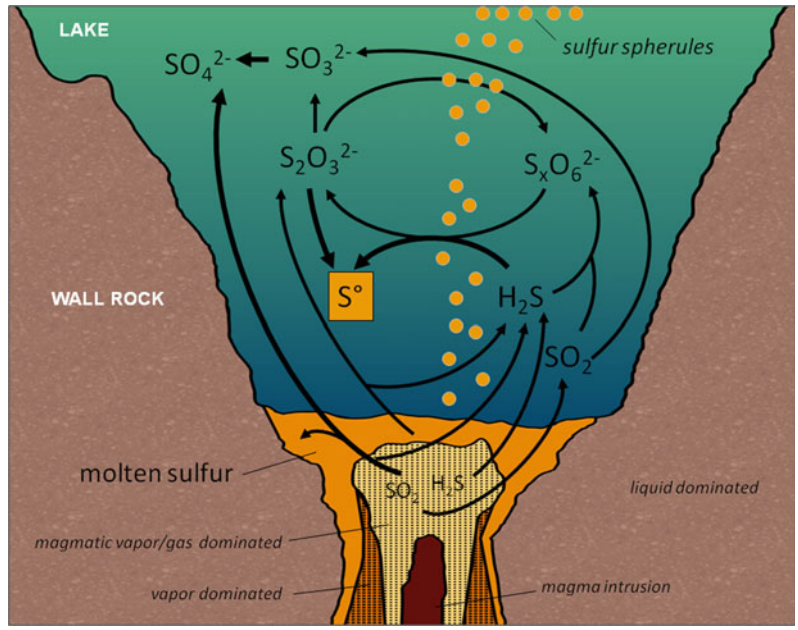

Fig. 7 Cartoon diagram illustrating the possible reactions involving the main gaseous and aqueous sulfur species and elemental sulfur in hyper-acid crater lakes. See text for details

5 Summary

A schematic diagram of major interactions involving gaseous, liquid and solid sulfur species in hyper-acid crater lakes is shown in Fig. 7.

(a) Sulfate in hyper-acid crater lakes overlying shallow magma-hydrothermal systems is mainly produced through disproportionation of magmatic SO_2 (reactions 5a and 5b) in the upper part of the hydrothermal conduit connected to the lake. Sulfur dioxide disproportionation is accompanied by a large sulfur isotopic fractionation, which produces heavy $\delta^{34}S_{SO_4}$ values. Polythionate decomposition (reactions 6 and 7) may also be a source of SO_4^{2-} in hyper-acid crater lakes. In geothermal lakes, SO_4^{2-} derives from oxidation of H_2S-rich steam inputs. Gypsum, barite and alunite may precipitate in hyper-acid crater lakes and geothermal lakes, but these phases constitute a negligible part of the SO_4^{2-} budget.

(b) Polythionates in hyper-acid crater lakes are a product of aqueous reactions between SO_2 and H_2S gases (reactions 13a–13c). The concentration and distribution of $S_xO_6^{2-}$ in hyper-acid crater lakes are thought to be controlled by SO_2/H_2S ratio in the magma-hydrothermal inputs. Sulfitolysis of $S_xO_6^{2-}$ is enhanced during episodes of strong SO_2 discharge (reaction 15), but reaction with H_2S also leads to $S_xO_6^{2-}$ decomposition (reaction 20). The role of $S_2O_3^{2-}$ oxidation in $S_xO_6^{2-}$ generation is poorly understood.

(c) Elemental sulfur deposition in hyper-acid crater lakes occurs predominantly within the subaqueous hydrothermal vent due to cooling of SO_2-, H_2S-bearing magmatic gases (reaction 17). Disproportionation of SO_2 may also generate S° (directly via reaction 5b, or indirectly via reaction 5a). Both mechanisms impart an isotopically light composition to S°. There is also evidence the hyper-acid crater lake waters can become saturated with respect to S° for prolonged periods of time. Polythionate degradation is another pathway for S° generation in these environments (reactions 19 and 20). In geothermal lakes, S° formation is sourced to abiotic oxidation of H_2S (reactions 9 and 10).

(d) Subaqueous molten sulfur in hyper-acid crater lakes probably captures a portion of the metal flux carried through to the surface by expanding magmatic gases. Metals may also precipitate as sulfide and sulfosalts in the lake waters if more reduced conditions develop.

While the combined use of chemical and isotopic measurements has provided a solid foundation for unraveling the origin of sulfur compounds occurring in hyper-acid crater lakes, important unknowns remain regarding the complex chemistry and temperature-dependent kinetics which govern the cycling of sulfur between its different redox forms in the magmatic hydrothermal-lake system. This gap in knowledge complicates interpretation of $S_xO_6^{2-}$ measurements, thereby jeopardizing geochemical monitoring efforts. Thus, more work involving on-site analyses (Druschell et al. 2003c) coupled with carefully designed laboratory experiments is needed to unravel sulfur speciation in hyper-acid crater lakes. Another rich topic for future study relates to the presence of molten sulfur in these environments. It is fundamental to better understand the ultimate origin of this material, and how a molten sulfur body influences heat and mass exchanges between the lake and the underlying hydrothermal vent. This requires improved knowledge on the impact of impurities such as SO_2, H_2S and metals on sulfur viscosity.

Acknowledgments This contribution is supported by the Belgian Fonds de la Recherche Scientifique MIS-Ulysse grant F.6001.11 to the first author. We wish to thank R.W. Henley and F. Africano for enthusiastic and constructive discussions. We are indebted to P. Ayris for helping with the drawing of Figs. 6 and 7. We warmly thank B. Christenson and Y. Taran for their constructive comments in review which greatly contributed to improve the original manuscript.

References

Africano F, Van Rompaey G, Bernard A, Le Guern F (2002) Deposition of trace elements from high temperature gases of Satsuma-Iwojima volcano. Earth Planets Space 54(3):275–286

Bani P, Oppenheimer C, Varekamp JC, Quinou T, Lardy M, Carn S (2009) Remarkable geochemical changes and degassing at Voui crater lake, Ambae volcano, Vanuatu. J Volcanol Geoth Res 188(4):347–357

Bennett FD, Raccichini SM (1978) Subaqueous sulphur lake in Volcan Poás. Nature 271:342–344

Bernard A, Le Guern F (1986) Condensation of volatile elements in high-temperature gases of Mount St. Helens. J Volcanol Geoth Res 28(1–2):91–105

Bernard A, Escobar CD, Mazot A, Gutiérrez RE (2004) The acid volcanic lake of Santa Ana volcano, El Salvador. Geol Soc Am Spec Pap 375:121–134

Brouwer AH (1925) The geology of the Netherlands East Indies. MacMillan, New York, p 160

Casadevall TJ, De La Cruz-Reyna S, Rose WI, Bagley S, Finnegan DL, Zoller WH (1984) Crater lake and post-eruption hydrothermal activity, El Chichón Volcano, Mexico. J Volcanol Geoth Res 23:169–191

Chen KY, Morris JC (1972) Kinetics of oxidation of aqueous sulfide by O_2. Environ Sci Technol 6:529–537

Christenson BW (1994) Convection and stratification in Ruapehu Crater Lake, New Zealand—implications for Lake Nyos-type gas release eruptions. Geochem J 28 (3):185–197

Christenson B (2000) Geochemistry of fluids associated with the 1995–1996 eruption of Mt. Ruapehu, New Zealand: signatures and processes in the magmatic-hydrothermal system. J Volcanol Geoth Res 97 (1–4):1–30

Christenson BW, Wood CP (1993) Evolution of a vent-hosted hydrothermal system beneath Ruapehu Crater Lake, New Zealand. Bull Volcanol 55(8):547–565

Christenson BW, Reyes AG, Young R, Moebis A, Sherburn S, Cole-Baker J, Britten K (2010) Cyclic processes and factors leading to phreatic eruption events: insights from the 25 September 2007 eruption through Ruapehu Crater Lake, New Zealand. J Volcanol Geoth Res 191(1–2):15–32

Davis RE (1958) Displacement reactions at the sulfur atom. I. An interpretation of the decomposition of acidified thiosulfate. J Am Chem Soc 80(14):3565–3569

Delmelle P, Bernard A (1994) Geochemistry, mineralogy and chemical modeling of the acid crater lake of Kawah Ijen Volcano, Indonesia. Geochim Cosmochim Acta 58(11):2445–2460

Delmelle P, Bernard A (2000) Downstream composition changes of acidic volcanic waters discharged into the Banyupahit stream, Ijen caldera, Indonesia. J Volcanol Geoth Res 97(1–4):55–75

Delmelle P, Bernard A, Kusakabe M, Fischer TP, Takano B (2000) Geochemistry of the magmatic–hydrothermal system of Kawah Ijen volcano, East Java, Indonesia. J Volcanol Geoth Res 97(1–4):31–53

Delmelle P, Henley RW, Opfergelt S, Detienne M (2015) Summiy acid crater lakes and flank instability in composite volcanoes. This volume

Delpino DH, Bermúdez AM (1996) Eruptions of pyroclastic sulfur at crater lake of Copahue volcano, Argentina. Newslett IAVCEI Comm Volcanic Lakes 8:23

Druschel GK, Hamers RJ, Banfield JF (2003a) Kinetics and mechanism of polythionate oxidation to sulfate at low pH by O_2 and Fe^{3+}. Geochim Cosmochim Acta 67 (23):4457–4469

Druschel GK, Hamers RJ, Luther GW, Banfield JF (2003b) Kinetics and mechanism of trithionate and tetrathionate oxidation at low pH by hydroxyl radicals. Aquat Geochem 9:145–164

Druschel GK, Hamers RJ, Schoonen MAA, Nordstrom DK, Ball JW, Xu Y, Cohn CA (2003c) Sulfur geochemistry of hydrothermal waters in Yellowstone National Park, Wyoming, USA. III. An anion exchange resin technique for sampling and preservation of sulfoxyanions in natural waters. Geochem Trans 4(3):12–19

Ellis AJ, Giggenbach W (1971) Hydrogen sulphide ionization and sulfphur hydrolysis in high temperature solution. Geochim Cosmochim Acta 35(3):247–260

Ellis AJ, Mahon WA (1977) Geochemistry of geothermal systems. Academic Press, New York, p 392

Fanelli R (1949) Solubility of hydrogen sulfide in sulfur. Ind Eng Chem 41:2031–2033

Francis PW, Thorpe RS, Brown GC (1980) Pyroclastic sulphur eruption at Poás Volcano, Costa Rica. Nature 283:754–756

Giggenbach WF (1974) The chemistry of crater lake, Mt Ruapehu (New Zealand) during and after the 1971 active period. NZJ Sci 17:33–45

Giggenbach WF (1987) Redox processes governing the chemistry of fumarolic gas discharges from White Island, New Zealand. Appl Geochem 2:143–161

Giggenbach WF, Tedesco D, Sulistiyo Y, Caprai A, Cioni R, Favara R, Fischer TP, Hirabayashi JI, Korzhinsky M, Martini M, Menyailov I, Shinohara H (2001) Evaluation of results from the fourth and fifth IAVCEI field workshops on volcanic gases, Vulcano island, Italy and Java, Indonesia. J Volcanol Geoth Res 108:157–172

Haff LV (1970) Oxygen-containing inorganic sulfur compounds. In: Karchmer JK (ed) The analytical chemistry of sulfur and its compounds—part I. Wiley-Interscience, New York, pp 238–239

Henley RW (2015) Hyperacidic volcanic lakes, metal sinks and continuous gas streaming in arc volcanoes. This volume

Henley RW, Berger BR (2011) Magmatic-vapor expansion and the formation of high-sulfidation gold deposits: chemical controls on alteration and mineralization. Ore Geol Rev 39(1–2):63–74

Henley RW, Ellis AJ (1983) Geothermal systems, ancient and modern: a geochemical review. Earth-Sci Rev 19:1–50

Henley RW, McNabb A (1978) Magmatic vapor plumes and groundwater interaction in porphyry copper emplacement. Econ Geol 73(1):1–20

Hollingsworth E (2006) Elemental and isotopic chemistry of the Uzon caldera: the evolution of thermal waters, gas, and mineral precipitation. M.sc. thesis, The University of Georgia

Hurst AW, Bibby HM, Scott BJ, McGuinness MJ (1991) The heat source of Ruapehu crater lake: deductions from the energy and mass balances. J Volcanol Geoth Res 46:1–20

Inoue A, Aoki M (2000) Mineralogy of Ohyunuma explosion crater lake, Hokkaido, Japan Part 1: geochemistry, hydrology, and bulk mineralogy. Clay Sci 11(2):147–168

Ivanov MV, Karavaik GI (1966) Role of microorganisms in sulphur cycle in crater lakes of Golovnin caldera. Zeitschrift Fur Allgemeine Mikrobiologie 6(1):10–22

Iwasaki I, Ozawa T (1960) Genesis of sulfate in acid hot spring. Bull Chem Soc Jpn 33(7):1018–1019

Kargel JS, Delmelle P, Nash DB (1999) Volcanogenic sulfur on Earth and Io: composition and spectroscopy. Icarus 142(1):249–280

Karpov GA, Fazlullin SM (1995) The creation and prolonged existence of the zone of molten native sulfur at the bottom of thermal lake within the volcanogenic-hydrothermal system (Uzon caldera, Kamchatka). In: Kharaka YK, Chudaev OV (eds) Water-rock interaction 8, A.A. Balkema, Rotterdam, pp 307–310

Kelly DP (1982) Biochemistry of the chemolithotrophic oxidation of inorganic sulphur. Philos Trans R Soc Lond B 298(1093):499–528

Kim J, Lee K-Y, Kim J-H (2011) Metal-bearing molten sulfur collected from a submarine volcano: implications for vapor transport of metals in seafloor hydrothermal systems. Geology 39(4):351–354

Kiyosu Y, Kurahashi M (1983) Origin of sulfur species in acid sulfate-chloride thermal waters, northeastern Japan. Geochim Cosmochim Acta 47(7):1237–1245

Kusakabe M, Hayashi N (1986) Genetic environments of the banded sulfur sediments at the Tateyama volcano, Japan. J Geophys Res 91(B12):12159–12166

Kusakabe M, Komoda Y, Takano B, Abiko T (2000) Sulfur isotopic effects in the disproportionation reaction of sulfur dioxide in hydrothermal fluids: implications for the $\delta^{34}S$ variations of dissolved bisulfate and elemental sulfur from active crater lakes. J Volcanol Geoth Res 97(1–4):287–307

Luke J (1959) History in White Island. Dept Sci Ind Res Bull 127:14–24

Marriott RA, Fitzpatrick E, Lesage KL (2008) The solubility of H_2S in liquid sulfur. Fluid Phase Equilib 269(1–2):69–72

Martínez M, Mason P, van Bergen M, Fernández E, Duarte E, Malavassi E, Barquero J, Valdés J (2002) Chemistry of sulfur globules from the acid crater lake of Poás volcano, Costa Rica. In: 11th Colima volcano international meeting, Colima, 2–6 Feb 2002

Mason RD, van Bergen M, Martínez M, Sumarti S, Valdés J, Malavassi E, Sriwana T (2001) Magmatic and hydrothermal controls on trace element output at active volcanoes as recorded by spherules of sulfur in acid crater lakes. EOS Trans Am Geophys Union Fall Meet 82(47):V42B–1019

McClelland L, Simkin T, Summers M, Nielsen E, Stein TC (1989) Global volcanism 1975–1985. Prentice-Hall, Englewood Cliffs

Meyer B (1976) Elemental sulfur. Chem Rev 76(3):367–388

Meyer B, Ospina M (1982) Raman spectrometric study of the thermal decomposition of aqueous trithionate and tetrathionate. Phosphorus, Sulfur Silicon Relat Elem 14(1):23–36

Mizutani Y, Sugiura T (1966) The chemical equilibrium of the $2H_2S + SO_2 = 3S + 2H_2O$ reaction in solfataras of the Nasudake Volcano. Bull Chem Soc Jpn 39:2411–2414

Murozomi M, Abiko T, Nakamura S (1966) Geochemical investigation of the Noboribetsu Oyunuma explosion crater lake. Bull Volcanol Soc Jpn 11:1–16

Nakai N, Jensen ML (1964) The kinetic isotope effect in the bacterial reduction and oxidation of sulfur. Geochim Cosmochim Acta 28:1893–1912

Oana S, Ishikawa H (1968) Sulfur isotopic fractionation between sulfur and sulfuric acid in the hydrothermal solution of sulfur dioxide. Geochem J 1:45–50

O'Brien DJ, Birkner FB (1977) Kinetics of oxygenation of reduced sulfur species in aqueous solution. Environ Sci Technol 11(12):1114–1120

Ohashi R (1919) On the peculiar sulphur spherules produced in a crater lake of the Volcano Shirane, in the province of Kozuke, central Japan. J Akita Min Coll 1:1–10

Ohmoto H, Rye RO (1979) Isotopes of sulfur and carbon. In: Barnes HL (ed) Geochemistry of hydrothermal ore deposits. Wiley, New York, pp 509–567

Ohsawa S, Takano B, Kusakabe M, Watanuki K (1993) Variation in volcanic activity of Kustasu-Shirane volcano as inferred from $\delta^{34}S$ in sulfate from the Yugama crater lake. Bull Volcanological Soc Jpn 38:95–99

Ohsawa S, Saito T, Yoshikawa S, Mawatari H, Yamada M, Amita K, Takamatsu N, Sudo Y, Kagiyama T (2010) Color change of lake water at the active crater lake of Aso volcano, Yudamari, Japan: is it in response to change in water quality induced by volcanic activity? Limnology 11(3):207–215

Oppenheimer C, Stevenson D (1989) Liquid sulphur lakes at Poás Volcano. Nature 342:790–793

Oppenheimer C, Scaillet B, Martin RS (2011) Sulfur degassing from volcanoes: source conditions, surveillance, plume chemistry and Earth system impacts. In: Behrens H, Webster JD (eds) Sulfur in magmas and melts: its importance for natural and technical processes. Reviews in mineralogy and geochemistry, vol 73(1), pp 363–421

Oprime M, García O, Cardoso AA (2001) Oxidation of H_2S in acid solution by Thiobacillus ferrooxidans and Thiobacillus thiooxidans. Process Biochem 37 (2):111–114

Pasternack GB, Varekamp JC (1994) The geochemistry of the Keli Mutu crater lakes, Flores, Indonesia. Geochem J 28:243–262

Richet P, Bottinga Y, Javoy M (1977) A review of hydrogen, carbon, nitrogen, oxygen, sulphur, and chlorine stable isotope fractionation among gaseous molecules. Annu Rev Earth Planet Sci 5:65–110

Rouwet D, Taran Y, Inguaggiato S, Varley N, Santiago SJA (2008) Hydrochemical dynamics of the "lake-spring" system in the crater of El Chichón volcano (Chiapas, Mexico). J Volcanol Geoth Res 178(2):237–248

Rowe GL (1994) Oxygen, hydrogen, and sulfur isotope systematics of the crater lake system of Poás Volcano, Costa Rica. Geochem J 28:263–287

Rowe GL, Ohsawa S, Takano B, Brantley SL, Fernández JF, Barquero J (1992a) Using crater lake chemistry to predict volcanic activity at Poás volcano, Costa Rica. Bull Volcanol 54:494–503

Rowe GL, Brantley SL, Fernandez M, Fernández JF, Barquero J, Borgia A (1992b) Fluid-volcano interaction in an active stratovolcano: the crater lake system of Poás volcano, Costa-Rica. J Volcanol Geoth Res 49:23–51

Rowe GL, Brantley SL, Fernández M, Borgia A (1995) The chemical and hydrologic structure of Poás Volcano, Costa Rica. J Volcanol Geoth Res 64(3–4): 233–270

Sakai H (1957) Fractionation of sulphur isotopes in nature. Geochim Cosmochim Acta 12(1–2):150–169

Schoen R (1969) Rate of sulfuric acid formation in Yellowstone National Park. Geol Soc Am Bull 80 (4):643–650

Shimizu A, Ohba T (2008) Secular variation of sulfur isotope ratio dissolved in the lake water of Yugama crater, Kusatsu-Shirane volcano, Japan. Japan geoscience union meeting, Chiba, Japan, 25–30 May 2008

Sriwana T, van Bergen MJ, Varekamp JC, Sumarti S, Takano B, van Os BJH, Leng MJ (2000) Geochemistry of the acid Kawah Putih lake, Patuha Volcano, West Java, Indonesia. J Volcanol Geoth Res 97(1–4): 77–104

Sugimori K, Takano B, Matsuo M, Suzuki K, Fazlullin SM (1995) Activity of sulfur-oxidizing bacteria in the acidic crater lake. In: Kharaka YK, Chudaev OV (eds) Water-rock interaction 8. A.A. Balkema, Rotterdam, pp 327–330

Symonds RB, Reed MH (1993) Calculation of multicomponent chemical equilibria in gas-solid- liquid systems: calculation methods, thermochemical data, and applications to studies of high-temperature volcanic gases with examples from Mount St. Helens. Am J Sci 293:758–864

Symonds RB, Gerlach TM, Reed MH (2001) Magmatic gas scrubbing: implications for volcano monitoring. J Volcanol Geoth Res 108(1–4):303–341

Takano B (1987) Correlation of volcanic activity with sulfur oxyanion speciation in crater lake. Science 235:1542–1712

Takano B, Watanuki K (1988) Quenching and liquid-chromatographic determination of polythionates in natural water. Talanta 35(11):847–854

Takano B, Watanuki K (1990) Monitoring of volcanic eruptions at Yugama crater lake by aqueous sulfur oxyanions. J Volcanol Geoth Res 40:71–87

Takano B, Ohsawa S, Glover RB (1994a) Surveillance of Ruapehu crater lake, New Zealand, by aqueous polythionates. J Volcanol Geoth Res 178:145–168

Takano B, Saitoh H, Takano E (1994b) Geochemical implications of subaqueous molten sulfur at Yugama crater lake, Kusatsu-Shirane volcano, Japan. Geochem J 28:199–216

Takano B, Koshida M, Fujiwara Y, Sugimori K, Takayanagi S (1997) Influence of sulfur-oxidizing bacteria on the budget of sulfate in Yugama crater lake, Kusatsu-Shirane volcano, Japan. Biogeochemistry 38 (3):227–253

Takano B, Suzuki K, Sugimori K, Ohba T, Fazlullin SM, Bernard A, Sumarti S, Sukhyar R, Hirabayashi M (2004) Bathymetric and geochemical investigation of Kawah Ijen Crater Lake, East Java, Indonesia. J Volcanol Geoth Res 135(4):299–329

Takano B, Kuno A, Ohsawa S, Kawakami H (2008) Aqueous sulfur speciation possibly linked to sublimnic volcanic gas-water interaction during a quiescent period at Yugama crater lake, Kusatsu-Shirane volcano, Central Japan. J Volcanol Geoth Res 178 (2):145–168

Taran YA, Hedenquist JW, Korzhinsky MA, Tcachenko SI, Shmulovich KI (1995) Geochemistry of magmatic gases from Kudryavy volcano, Iturup, Kurile Islands. Geochim Cosmochim Acta 59:1749–1761

Taran YA, Znamenskiy VS, Yurova LM (1996) Geochemical model of the hydrothermal systems of Baranskiy Volcano, Iturup, Kuril Islands. Volcanol Seismolog 17:471–496

Taran YA, Fischer TP, Pokrovsky B, Sano Y, Armienta MA, Macias JL (1998) Geochemistry of the volcano-hydrothermal system of El Chichón Volcano, Chiapas, Mexico. Bull Volcanol 59:436–449

Taylor BE (1986) Magmatic volatiles: isotopic variation of C, H and S. In: Valley JW, Taylor HP Jr, O'Neil JR (eds) Stable isotopes in high temperature geological processes. Review in mineralogy, mineralogical society of America, vol 16, pp 185−225

Touro FJ, Wiewiorowski TK (1966) Molten sulfur chemistry. II. The solubility of sulfur dioxide in molten sulfur. J Phys Chem 70:3531–3534

van Hinsberg V, Berlo K, van Bergen M, Williams-Jones A (2010) Extreme alteration by hyperacidic brines at Kawah ben volcano, East Java, Indonesia I textural and mineralogical imprint. J Volcanol Geoth Res 198 (1–2):253–263

Varekamp JC, Pasternack GB, Rowe GL (2000) Volcanic lake systematics II. Chemical constraints. J Volcanol Geoth Res 97(1–4):161–179

Varekamp JC, Ouimette AP, Herman SW, Bermudez A, Delpino D (2001) Hydrothermal element fluxes from Copahue, Argentina: A "beehive" volcano in turmoil. Geology 29(11):1059–1062

Webster JG (1989) An analytical scheme for the determination of sulfide, polysulfide, thiosulfate, sulfite and polythionate concentrations in geothermal waters. Institute of Geological & Nuclear Sciences Limited, New Zealand, Report No. CD2406

White DE, Hutchinson RA, Keith TEC (1988) The geology and remarkable thermal activity of Norris Geyser Basin, Yellowstone National Park, Wyoming. USGS professional paper 1456

Wiewiorowski TK, Touro FJ (1966) The sulfur-hydrogen sulfide system. J Phys Chem 70:234–238

Williamson MA, Rimstidt JD (1993) The rate of decomposition of the ferric-thiosulfate complex in acidic aqueous solutions. Geochim Cosmochim Acta 57 (15):3555–3561

Wood CP (1994) Mineralogy at the magma-hydrothermal system interface in andesite volcanoes, New Zealand. Geology 22(1):75–78

Xu Y, Schoonen MAA (1995) The stability of thiosulfate in the presence of pyrite in low-temperature aqueous solutions. Geochim Cosmochim Acta 59(22): 4605–4622

Xu Y, Schoonen MAA, Nordstrom DK, Cunningham KM, Ball JW (1998) Sulfur geochemistry of hydrothermal waters in Yellowstone National Park: I. The origin of thiosulfate in hot spring waters. Geochim Cosmochim Acta 62(23–24):3729–3743

Xu Y, Schoonen MAA, Nordstrom DK, Cunningham KM, Ball JW (2000) Sulfur geochemistry of hydrothermal waters in Yellowstone National Park, Wyoming, USA. II. Formation and decomposition of thiosulfate and polythionate in Cinder Pool. J Volcanol Geoth Res 97 (1–4):407–423

Molten Sulfur Lakes of Intraoceanic Arc Volcanoes

C.E.J. de Ronde, W.W. Chadwick Jr, R.G. Ditchburn, R.W. Embley, V. Tunnicliffe, E.T. Baker, S.L. Walker, V.L. Ferrini, and S.M. Merle

Abstract

Intraoceanic arcs of the world are dominated by submarine volcanoes, many of which host active hydrothermal systems. A considerable number of the morphological features common to subaerial volcanoes are also present on the submarine edifices, including summit craters. Surprisingly, some of the craters, such as at Daikoku and Nikko volcanoes of the Mariana Arc, and Macauley Cone of the Kermadec Arc, are host to lakes

Electronic supplementary material The online version of this chapter (doi:10.1007/978-3-642-36833-2_11) contains supplementary material, which is available to authorized users. Videos can also be accessed at http://www.springerimages.com/videos/978-3-642-36833-2

C.E.J. de Ronde (✉) · R.G. Ditchburn
GNS Science, P.O. Box 30-368, Lower Hutt
New Zealand
e-mail: cornel.deronde@gns.cri.nz

W.W. Chadwick Jr · S.M. Merle
CIMRS, Oregon State University, 2115 SE O.S.U. Dr, Newport, OR 97365-5258, USA

R.W. Embley
NOAA/PMEL, 2115 SE O.S.U. Dr, Newport, OR 97365-5258, USA

V. Tunnicliffe
Department of Biology/School of Earth and Ocean Sciences, University of Victoria, PO Box 3020, Victoria, BC V8W 3N5, Canada

E.T. Baker · S.L. Walker
Pacific Marine Environmental Laboratory, NOAA, 7600 Sand Point Way NE, Seattle, WA 98115-6349, USA

V.L. Ferrini
Lamont-Doherty Earth Observatory, Marine Geology and Geophysics, 61 Route 9 W, Palisades, NY 10964-8000, USA

D. Rouwet et al. (eds.), *Volcanic Lakes*, Advances in Volcanology,
DOI 10.1007/978-3-642-36833-2_11,
© Springer-Verlag Berlin Heidelberg 2015

of molten sulfur, both ancient and modern. These lakes, up to ~200 m in diameter, act as condensers of gases that derive from the underlying magmas. Volcanic vents beneath these lakes provide a steady outflow of hot gases that continuously generate molten sulfur. At Daikoku, an extraordinary lake of liquid sulfur is in constant convective and gas escape-driven motion. Smaller pools of molten sulfur occur on Nikko, and there is evidence of older, larger lakes on both this volcano and Macauley, based on the accumulation of large quantities of sulfur in the subsurface. The elemental S at these sites is produced largely by the reaction $2H_2S + SO_2 = 3S + 2H_2O$ and the disproportionation of magmatic SO_2. Anomalous concentrations of Au and Cu in the lakes are most likely transported by vapor.

Keywords
Intraoceanic arc volcanoes · Submarine crater lakes · Daikoku · Nikko · Macauley cone · Elemental sulfur · Trace elements · Sulfur isotopes

1 Introduction

The oceans cover ~72 % of the Earth's surface, obscuring most of the globally-dominant volcanism that occurs along divergent and convergent plate boundaries (Crisp 1984). As a consequence, most volcanic activity, including eruptions leading to volcano building and the discharge of associated volcanic gases, occurs out of sight on the seafloor. Only recently, with the deployment of manned submersibles and remotely operated vehicles (ROVs), have we been able to witness these processes and begun to monitor the frequency of eruptions, measure their effects, and provide insight into the realm of submarine volcanism. In some cases this volcanism has been truly spectacular, including eruptions on the seafloor witnessed for the first time in 2004 (e.g., Embley et al. 2007; Chadwick et al. 2008).

Convergent plate boundaries of the western Pacific mark a significant proportion of all intraoceanic arcs, totaling some 6,380 km in length (de Ronde et al. 2003). The Izu-Bonin/Mariana and Kermadec/Tonga arcs are prominent intraoceanic arcs within this region, with lengths of ~1,600 and ~1,530 km, respectively (Fig. 1). Each of these arcs hosts numerous volcanic centers that comprise either single or clustered edifices, cone- or caldera-type volcanoes, or groups of smaller cones. These two arcs have been the focus of regional-scale exploration for hydrothermal plumes that delineate magmatic-hydrothermal systems on the seafloor (de Ronde et al. 2001; Baker et al. 2008). Those studies initially identified hydrothermally-active sites by using a conductivity-temperature-depth-optical (CTDO) instrument package, fitted with Niskin bottles for collecting water samples, to detect and sample physical and chemical anomalies in the water column above a target volcano. Subsequent investigations by manned submersible and ROV expeditions enabled first-hand observations of volcano building (e.g., NW Rota-1 volcano, Chadwick et al. 2008, 2012; Embley et al. 2006), discharge of liquid CO_2 from seafloor vents (i.e., Eifuku volcano, Lupton et al. 2006), formation of significant seafloor massive sulfide deposits (i.e., Brothers volcano, de Ronde et al. 2005), identification of new vent-related animal communities (i.e., Tunnicliffe et al. 2010), and the remarkable discovery of seafloor crater 'lakes' of molten sulfur perched on some

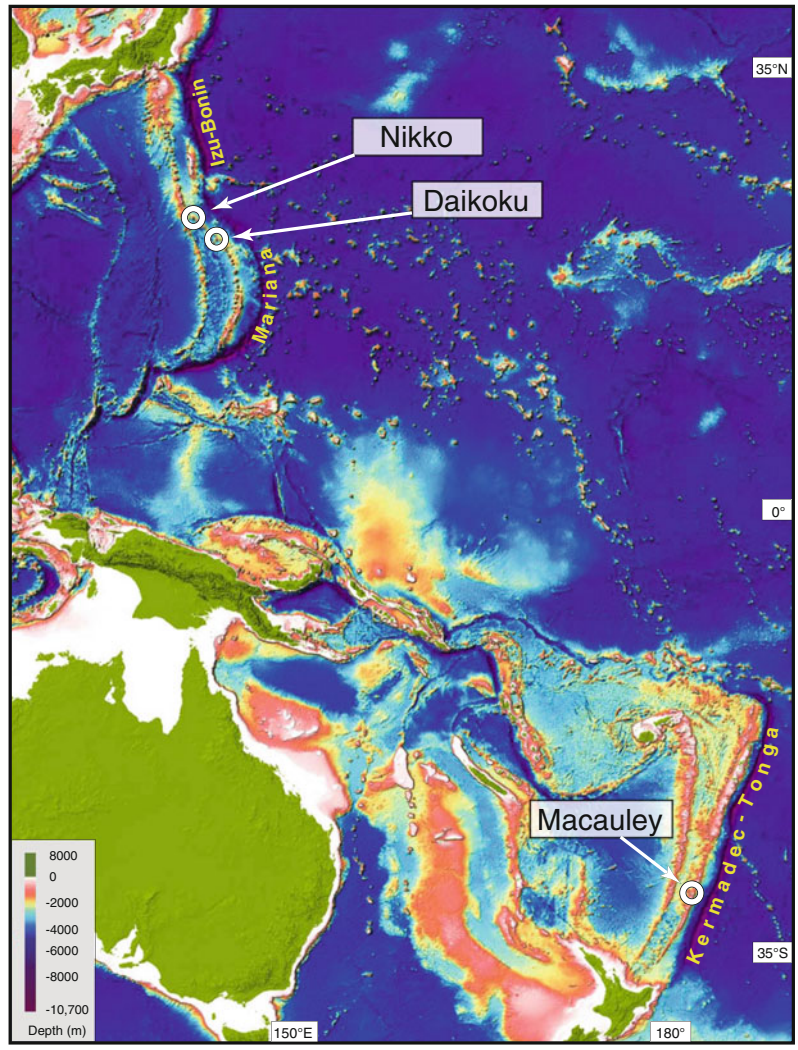

Fig. 1 Map showing the location of the submarine intraoceanic arc volcanoes Daikoku and Nikko of the northern Mariana arc, and Macauley volcano of the mid-Kermadec arc

of the volcanoes (Embley et al. 2007), which is the subject of this chapter.

Discharge of volatiles from volcanoes can be associated with eruptive activity and/or the degassing of deep-seated magma. At subaerial arc volcanoes, rock compositions range from basaltic to rhyodacitic, with volatiles dominated by H_2O, CO_2 and S (SO_2 + H_2S) (e.g., Giggenbach 1992, 1996). This is also true for submarine arc volcanoes, where high concentrations of CO_2, SO_2, and H_2S have been measured at seafloor vents (e.g., Resing et al. 2007; Lupton et al. 2008; Butterfield et al. 2011; de Ronde et al. 2011). The obvious difference between the discharge of volatiles from subaerial versus that from submarine volcanoes is the column of seawater above the latter (and the pressure it exerts), acting as a huge condenser and ensuring mixing of gas species with seawater at, or immediately below, the seafloor.

1.1 Submarine Arc Volcanoes and the Preponderance of Sulfur

Plume mapping surveys of the Mariana, Tonga and Kermadec arcs show the incidence of venting at volcanoes along these arcs is approximately 43, 30 and 77 %, respectively (Baker et al. 2005, 2008; de Ronde et al. 2001, 2007; unpublished data). The majority of venting at seafloor sites along these arcs can be described as magmatic-hydrothermal in origin, with volcanic vent fluids derived from hot, condensed magmatic gases reacting with seawater and volcanic rock as they ascend from depth into relatively shallow reaction zones immediately subseafloor.

Elemental S at these sites is produced mainly via the reaction:

$$2H_2S + SO_2 = 3S + 2H_2O \quad (1)$$

This reaction will take place where H_2S and SO_2 are present in the gas phase, where it is both kinetically and thermodynamically favorable (Mizutani and Sugiura 1966). The redox potential ($R_H = \log fH_2/fH_2O$) associated with the rock buffers quartz-fayalite-magnetite or nickel-nickel oxide is very close to that of the H_2S-SO_2 buffer at 1,000–1,200 °C, hence the importance of reaction 1 once vapors leave the melt, where these gases are assumed to be equimolar (Giggenbach 1987). The gas stream is rapidly depleted in H_2S through the formation of elemental S, according to reaction 1, whereupon disproportionation reactions involving SO_2 become more dominant.

Sulfur dioxide (SO_2) gas is a major component of high-temperature magmatic gas (Moretti and Papale 2004). It is highly soluble in water, although SO_2(aq) is thermodynamically unstable under hydrothermal conditions (i.e., <350 °C) where H_2S is the dominant form of sulfur (e.g., Giggenbach 1987; Seyfried 1987; Symonds et al. 2001). Aqueous SO_2 can undergo the following reactions (from Butterfield et al. 2011):

$$SO_2(aq) + H_2O = HSO_3^- + H^+ \quad (2)$$

$$3SO_2(aq) + 2H_2O = Se + 2H_2SO_4 \quad (3)$$

$$4SO_2(aq) + 4H_2O = H_2S + 3H_2SO_4 \quad (4)$$

Sulfur dioxide rapidly hydrates to form sulfurous acid, which in turn dissociates to yield dissolved bisulfite (reaction 2). SO_2 may also disproportionate in water to yield H_2SO_4 and either elemental sulfur (S*e*, reaction 3) or H_2S (reaction 4). Sulfur dioxide (detected as dissolved HSO_3^-), H_2SO_4, and S*e* are the dominant forms of sulfur emitted at volcanic vents such as at NW Rota-1 of the Mariana Arc (Butterfield et al. 2011), indicating that reactions 2 and 3 prevail over reaction 4 when condensed magmatic gases rapidly mix with oxygenated ambient seawater. SO_2 quenching experiments by Kusakabe et al. (2000) support the formation of elemental sulfur and H_2SO_4 (reaction 3) when SO_2-rich condensed gases are injected directly into seawater.

2 Mariana Arc

Volcanoes with magmatic-hydrothermal discharge noted along the Mariana Arc include: Seamount X, Ruby, NW Rota-1, NE Eifuku, Daikoku and Nikko volcanoes. The latter two are host to molten sulfur 'lakes' on the seafloor, both past and present. Below, we describe the physical setting of these lakes and later we detail the trace element geochemistry and isotopic composition of the sulfur.

2.1 High-Resolution Bathymetric Mapping by ROV

To better understand the physical and geological setting of the molten sulfur lakes at both Daikoku and Nikko seamounts (Fig. 1), high-resolution bathymetric mapping was conducted during the 2006 Submarine Ring of Fire expedition (Embley et al. 2007). The surveys were executed with a Kongsberg SM2000 multibeam sonar (200 kHz) mounted on the *Jason II* remotely operated vehicle (ROV) driven at an altitude of ~25 m above the seafloor while navigated by doppler

sonar (DVL). The Daikoku survey was collected during 8 h on *Jason II* dive J2-195, while the Nikko survey took 14 h during dive J2-198. Steep slopes and rough topography at both sites made the surveys challenging, particularly at times when DVL bottom-lock was lost. However, the SM2000 sonar data were feature-matched in post-processing to overcome navigational offsets that obscured bathymetric features (Roman and Singh 2007; Ferrini et al. 2007, 2008). Each SM2000 bathymetric survey is 300–500 m on a side and is roughly square in map view.

2.2 Case Study: Daikoku

Daikoku is one of over sixty submarine volcanoes that populate the Mariana arc (Fig. 1). It is hydrothermally active and in both 2003 and 2004 was emitting an intense light-backscattering plume (measured as deviations in "nephelometry transmission units"; ΔNTU), consistent with high concentrations of elemental S (Baker et al. 2001, 2008). Daikoku is elongate in an east-west direction with a large summit cone built on a flat platform, possibly an older filled caldera (Fig. 2a). The cone rises over 700 m from its base at 1,050 m, with the upper NW slope covered by unconsolidated ash and sediment. It appears to have experienced significant mass wasting, based on its dissected and eroded morphology. Daikoku has a summit crater 200 m in diameter that is breached on its northwestern side (Fig. 2b). Water column sampling mapped an optically concentrated hydrothermal plume extending from near the volcano's summit (320 m) to a depth of ~480 m, thus indicating that venting was concentrated below the summit. The concentration of elemental S in the Daikoku plume (up to 200 nM; Resing et al. 2009) was among the highest sampled anywhere along the Mariana arc.

ROV dive J2-195, spanning ~24 h, discovered a remarkable feature in a small (~20 m × 14 m) depression on the NW slope of the volcano; a small pond of molten sulfur, named "Sulfur Cauldron" (Embley et al. 2007). The high-resolution survey of Daikoku's summit shows that Sulfur Cauldron vent is located at 415 m water depth, about 250 m of NNW and 95 m deeper than the volcano summit at 320 m (Fig. 2b). The pond is elongate like the depression it occupies, and measures ~5 m long by 3 m wide (Fig. 3a, SM Videos 1–2). It has a rim projecting over the edges of the pond, reminiscent of the silica ledges formed in the hydrothermal eruption craters occupied by chloride pools, such as Champagne Pool at Wai-o-tapu, New Zealand. At the time the ROV visited the pond in 2006, the surface of the molten sulfur was ~1 m below the rim, indicative of a dynamic environment where the pond levels rise and fall (Fig. 3a). The apron surrounding the pond is conspicuous, formed as a sulfur-rich crust coated with a pavement of numerous spherules of sulfur, representing fallout of 'lapilli' from S-rich plumes (Fig. 3b). Inclusion of very fine-grained pyrite results in the sulfur in the pond being black (Fig. 3a, d). Quenching by overlying seawater makes the surface of the pond semi-brittle and semi-ductile, as shown by liquid flow patterns 'frozen' into the surface crust (a few cm thick), including the pāhoehoe-like textures shown in Fig. 3c (left-hand side) and more geometric fracture patterns shown in Fig. 3d. The pond surface is continuously being ruptured by vigorous degassing of upwelling S gases and CO_2, causing cracks to appear and resulting in undulating 'waves' rippling beneath the crust, resulting in mini 'plates' of sulfur breaking up and sometimes overturning and sliding beneath the surface (SM Videos 1–2). On occasion, the molten sulfur appeared to be circulating within the confines of the crater.

A number of S-rich crusts occur on the volcano slopes surrounding Sulfur Cauldron (Fig. 3e). Samples recovered by the ROV show individual crusts on the order of 5–10 cm thick (Fig. 3f) where even thinner layers of sulfur bind others dominated by ash (inset Fig. 3f). This suggests that the Sulfur Cauldron environs have been subjected to overflow of the pond on numerous occasions, indicative of a protracted history of discharge. A number of small (cm size) vents punctuate the apron around Sulfur

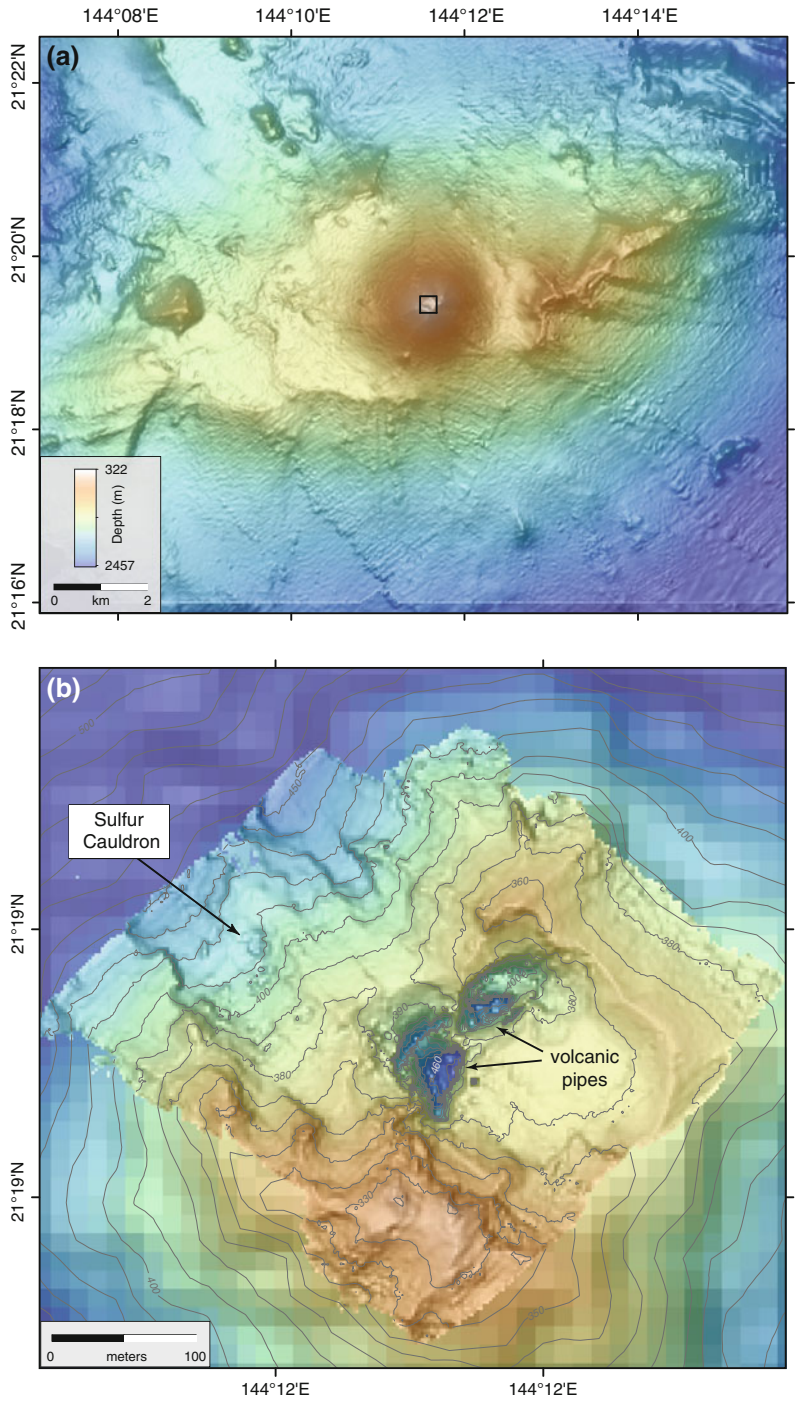

Fig. 2 **a** Bathymetric map of Daikoku volcano derived from ship-based EM300 multibeam sonar data. The *black box* outlines the location of the detailed map shown in **b**. **b** High-resolution bathymetric map of Daikoku summit (2-m grid) obtained during a 2006 SM2000 multibeam sonar survey by the ROV *Jason II*, overlain on coarser (25-m grid) EM300 bathymetry. See Fig. 3 for photographs of Sulfur Cauldron and Supplementary Material (SM) Fig. 1 for 3-D images of the volcanic pipes. A December 2014 Submarine Ring of Fire—Ironman cruise shows Daikoku was likely erupting at the time with the volcanic pipes likely destroyed and new craters formed (see: http://oceanexplorer.noaa.gov/explorations/14fire/welcome.html)

Cauldron and point to the discharge of S gases (Fig. 3a).

A broad basin-like crater ~200 m across from rim to rim, with a relatively flat bottom at a depth of 375 m lies northeast of Daikoku's summit (Fig. 2b). The crater hosts two very narrow, deep craters (or pipes) apparently explosive in origin and/or possibly lava feeder conduits. These

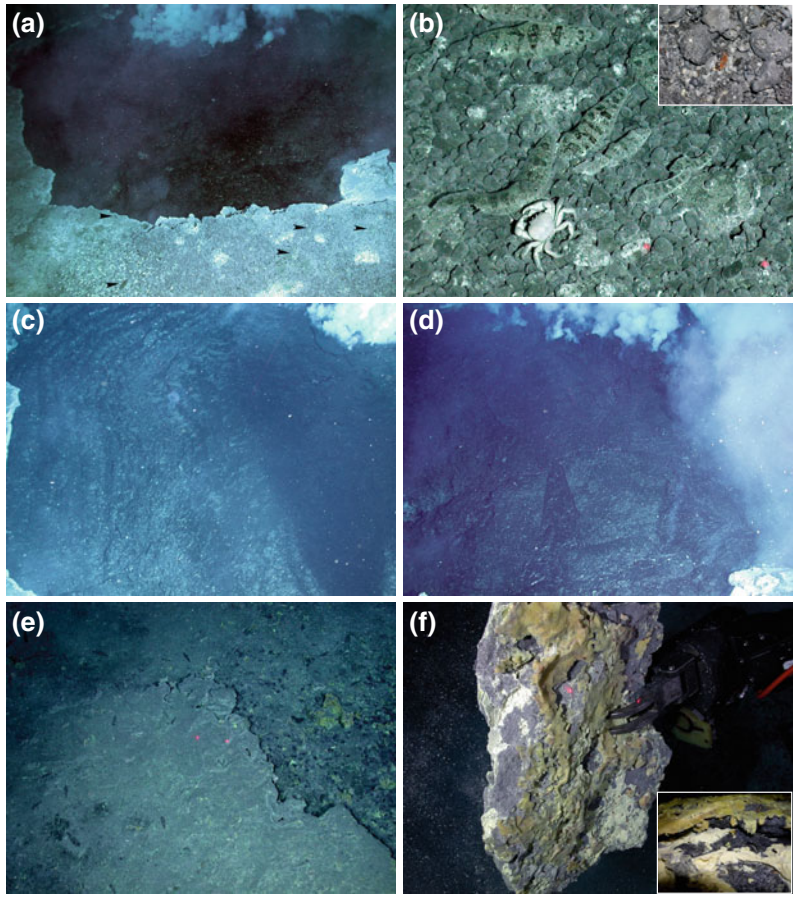

Fig. 3 **a** Sulfur Cauldron. Taken from aboard *Jason II*. A downward looking camera aboard *Medea* (a wide area survey vehicle linked to, and which hovers above *Jason II*) suggests the pond is ~5 m across when compared to the size of the ROV, and sits within a depression that is only a few m's bigger than the pond itself (see Fig. 2b). Vigorous gas discharge can be seen through a relatively hard crust at the *top* of the *photograph* against the back wall of the depression that is just out of view. *Black arrows* point to 5 of 15 well camouflaged fish in this image. **b** Close-up of the apron a few m distant from the sulfur pond (see **a**). Twelve *Thermophilus symphurus* and two *Gandalfus yunohana* on sulfur 'pebbles'; closer inspection shows the sulfur crust is also covered by numerous spherules of sulfur (*inset*). **c** Distinct ropey texture of S lake surface. **d** Brittle mini 'plates' of S crust move about on the surface of the lake, driven by gas discharge. **e** Sulfur crusts in the immediate vicinity of Sulfur Cauldron. Locally, small vents extrude molten S. **f** Surface of layered S sample intercalated with ash recovered from the same areas as that shown in **e**. *Inset* shows close-up S and ash layers. *Red* laser dots seen in **b**, **e** and **f** are 10 cm apart

craters are ~50 m in diameter although only 50 m apart, essentially vertical and cylindrical, and both likely host hydrothermal activity at their base. The 2006 high-resolution bathymetric survey imaged parts of the upper walls of the explosion craters (one down to 461 m depth, or 86 m below the rim at 375 m), but the sonar was not able to resolve the bottoms of the craters (see Supplementary Material [SM] Fig. 1). A more detailed survey inside one of the craters was accomplished during the 2004 Ring of Fire expedition with the *ROPOS* ROV. During dive R795, *ROPOS* descended 75 m down inside the NE crater to a depth of 450 m while imaging the shape of the crater in horizontal slices with its Kongsberg SM1000 obstacle-avoidance sonar.

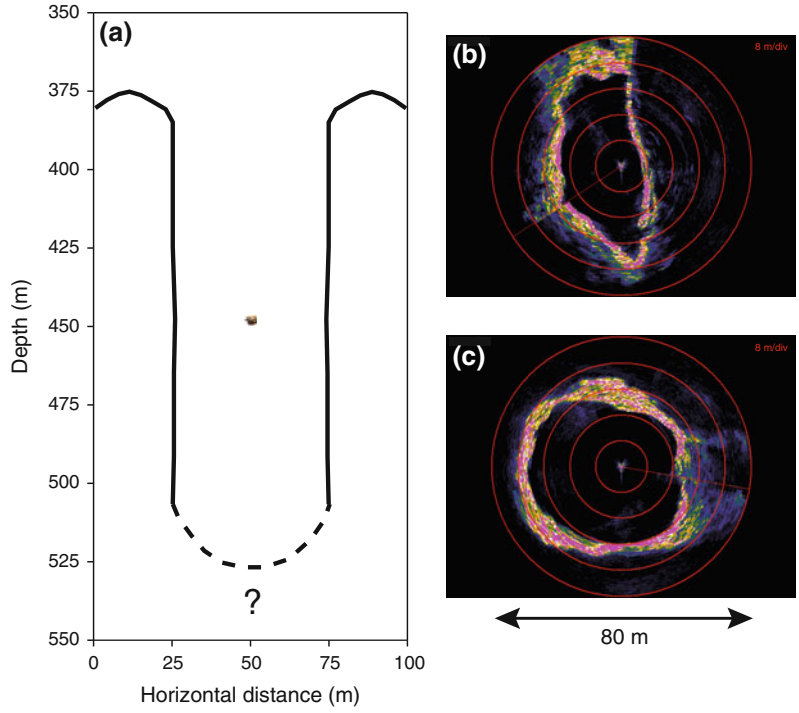

Fig. 4 **a** Diagramatic cross-section of the NE explosion crater at Daikoku, based on SM1000 sonar imaging from the *ROPOS* ROV in 2004 (see Fig. 2b). A small image of the *ROPOS* ROV shows its relative size at approximately the correct scale. The NE crater is vertical and cylindrical with a diameter of about 50 m, and is at least 135 m deep. **b** A SM1000 sonar image recorded 21 m below the rim of the NE crater showing its *lens-shaped* outline. In this map view, the ROV is at the center at a depth of 396 m, with a heading of 073° (up), and the crater walls are shown by high acoustic returns in *pink*; the *red concentric circles* are at 8-m spacing, the largest having a diameter of 80 m. C. SM1000 sonar image when the ROV was 58 m below the rim of the crater where it is more *circular* in outline (ROV depth is 433 m, heading is 140°; same scale as in **b**)

At that depth, the down-looking altimeter on *ROPOS* was still registering its maximum range of 60 m (to 510 m), meaning that this crater (pipe) was at least 135 m deep, and possibly more (Fig. 4a). The map-view outline of the NE crater is lens-shaped near the top (Fig. 4b), but almost circular with a diameter of 50 m at a depth of 60 m below the rim (Fig. 4c). The crater rim appeared to be composed of layers of sulfur-cemented ash (see SM Figs. 2a, b). Deeper in the crater, outcrops of massive lava flows were exposed in the near-vertical walls dusted by a ubiquitous "snow" of fine sulfur particles (SM Fig. 2c). While inside the crater, and near the summit of Daikoku, the visibility from the *ROPOS* video camera was only a few m due to a milky white, almost certainly sulfur-rich, particle plume (SM Fig. 2c, d). The presence of this dense plume and sulfur snow inside the crater suggests that molten sulfur ponds may exist at the bottom of the crater, or at least that it hosts vigorous sulfur-rich hydrothermal vents with a high magmatic gas component (e.g., Butterfield et al. 2011; de Ronde et al. 2011). The observation of high (0.1–1.0) ΔNTU, S-rich plumes in 2003 and 2004, and the absence of any detectable plume in 2006, suggests that venting and S emission is intermittent at Daikoku.

We believe there is likely a subterranean connection between the two deep eruptive craters (pipes) and the molten pond at Sulfur Cauldron vent located on the NW flank of Daikoku,

considering the bottom of the NE crater is more than 95 m below the depth of Sulfur Cauldron. A haze of cloudy sulfur-rich water enveloped the entire summit of Daikoku (SM Fig. 2d), suggesting that its fragmental carapace is highly permeable and that native sulfur pools and flows might be found at other sites around the top of the volcano. The chemosynthetic ecosystem at Daikoku is described in the Supplementary Material to this paper (see SM Videos 3–6).

2.3 Coffee Can Experiment

During *Jason II* dive J2-197 in 2006 we collected a sample of sulfur from Sulfur Cauldron. Our aim was to dunk our sampling device into the S lake, draw it up into the overlying seawater quenching the molten sulfur and hopefully retaining all the trace elements dissolved in the sulfur. The sampling device was a simple tin coffee can, measuring ~15.2 cm in diameter and ~15.2 cm long. We attached the can to a ~2 m long aluminum pole (SM Fig. 3a, SM Video 4) that could be held by the ROV's manipulator arm. The ROV sat near the edge of the lake with the arm of the ROV extended. The pole plus can were driven into the molten sulfur (through the surface crust) where earlier a maximum temperature of 187 °C was recorded. As the can was lifted out of Sulfur Cauldron, the 'plug' of molten sulfur in the can reacted vigorously once in contact with the ambient seawater (12.8 °C), with 'smoke' emanating from the can.

The sulfur plug was carefully extracted from the coffee can by cutting the sides of the can away with tin snips. This fragile sample was then cut longitudinally, by hand, using a hacksaw blade; the face of one side of the sample was smoothed with wet carborundum paper to provide an unmarked surface for photography. The off-cuts and unpolished piece were used for chemical and isotope analysis. The top surface of the plug is smooth and bumpy with a shiny metallic sheen, and only a few mm thick, giving way to a vesicle-rich, honeycomb- or foam-textured central core (SM Figs. 3b, c). The margins of the plug, where in contact with the can, show a ~1 cm thick outer zone of fine-grained sulfur as a result of quenching (SM Fig. 3d). A central cavity had formed towards one side of the can (SM Fig. 3e)—most likely due to the can being slightly tilted as it was pulled from Sulfur Cauldron into the overlying seawater—where the sulfur was very foamy. Elongated vesicles/cavities of variable size (which still contained H_2S prior to cutting the sample) and cracks indicate the (outwards) direction in which the gases escaped during quenching (SM Fig. 3f). A light-grey, spongy material was seen in the centre of the plug that, upon drying, became yellow and solid, but crumbled easily (see sample J2-197-22A in SM Fig. 7 later). This spongy material has a sandy matrix while its rectangular shape suggests that it had not mixed into the surrounding sulfur. The black color of the sulfur is attributed to fine-grained pyrite, as determined by X-ray diffraction analysis and wet chemical techniques (see below).

2.4 Case Study: Nikko

The summit of Nikko volcano comprises two young cones built on top of an older filled caldera, similar to Daikoku (Fig. 5a). Sitting atop the western cone is a crater 350 m wide from rim-to-rim, and 150 m wide across its floor at a depth of ~470 m. In May 2006, a high-resolution SM2000 bathymetric survey by the *Jason II* ROV mapped the interior of this crater (Fig. 5b and SM Fig. 4). The survey shows the crater is bowl-shaped with a rim that is highest on the western and southern sides and lowest on the northeastern side. There is >100 m relief between the highest point on the SW rim to the lowest point on the crater floor, although the floor is only 30 m deeper than the low saddle on the NE side of the crater (Fig. 5b). The arcuate fan NE of breached crater rim may represent sector collapse in this part of the volcano. The crater walls in the SW and SE corners are nearly vertical cliffs of intact lavas. There are two prominent, curved benches that extend outward from the base of the

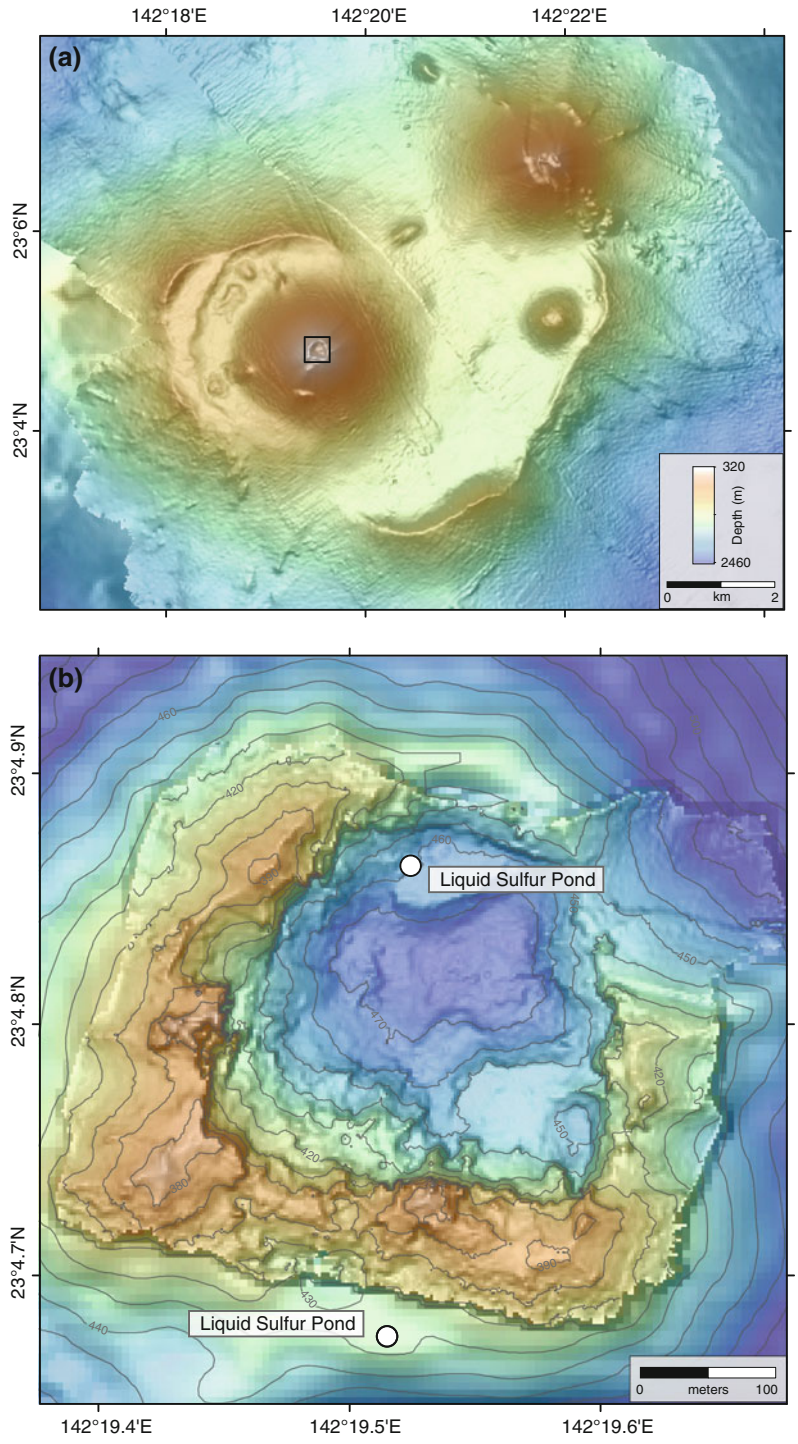

Fig. 5 **a** Bathymetric map of Nikko volcano derived from ship-based EM300 multibeam sonar data. *Black box* shows location of detailed map in **b**. **b** High-resolution (2 m grid) bathymetric map of Nikko summit derived from a SM2000 multibeam sonar survey using the *Jason II* ROV, overlain on coarser (25-m grid) EM300 bathymetry. Pools of molten S were found both inside and outside the main summit crater

crater walls, one on the north side of the crater and the other in the SE corner (Fig. 5b and SM Fig. 4). These benches appear to be formed by landslide deposits from the adjacent, inner crater walls, although they could be remnants of previous crater fill.

Hydrothermal plume layers over Nikko extended from 350 to 430 m in both 2003 and 2006. ΔNTU values were similar to those of Daikoku in 2003, but at least an order-of-magnitude higher in 2006. Water samples contained elemental S concentrations up to 250 nM, higher even than at Daikoku (Resing et al. 2009). These observations imply a substantial number of sulfur-discharging vents in the crater.

Sulfur is the most voluminous substrate seen inside the summit crater at Nikko (SM Videos 7–8). The relatively flat floor of the crater is host to some remarkable features, including pillars standing up to 1.5 m off the floor that are composed of numerous, horizontal layers of sulfur with drip-like structures protruding from some of the layers, similar in appearance to candle wax (Fig. 6a, SM Video 9). A series of these pillars were seen in the northern sector of the crater, growing upwards from the seafloor at 469 m depth, while others were seen on the floor in the central part of the crater at 470, 476 and 466 m, respectively, suggesting a sulfur lake at one time >10 m deep. The pillars are reminiscent of lava pillars, or remnants of lava lakes at mid-ocean ridges. Locally, a ~50 cm tall sulfur chimney, or spire, was also seen. The crater floor is covered in part by ubiquitous sulfur crusts that appear very thin (Fig. 6b). At the margins of the crater can be seen sections through ash and sulfur, some of the latter up to 1 m thick, consistent with an earlier, deeper sulfur lake. Overhang slabs of sulfur are also seen near the crater margins. Innumerable hydrothermal vent sites dot the crater floor, most of which are dominated by sulfur on the seafloor (Figs. 6c, d), and which also extend outside the crater.

In places, the sulfur seen on the crater floor is fragmental—the result of mechanical break-up of thick sulfur flows—with boulders of sulfur strewn over the crater floor, especially in the SE corner. These large pieces of sulfur commonly have scallop-patterned exterior surfaces, are semi-translucent and contain large crystals, a function of relatively slow cooling (cf. the coffee can sulfur). They also contain over-pressured, gas-filled inclusions/cavities that burst once the sample is at sealevel, emitting a strong smell of H_2S, and rendering large pieces into piles of small chips within minutes (Fig. 6e). Most of the crater floor and parts of its rim and upper flank is spectacularly covered by dense chemosynthetic animal communities (Fig. 6f; SM Fig. 5).

Molten sulfur has been observed at two vent sites at Nikko: (1) on the northern floor of the crater (at a depth of 462 m); and (2), outside the crater, ~100 m south of, and 40 m below, the south crater rim (at a depth of 428 m; see Fig. 5b, SM Videos 10–12). The southern site comprises a number of basketball-size pools of molten sulfur where the bubbling sulfur is black inside the pool, but yellow on the margins of the pool (Fig. 6g). White smoke (S-rich plumes) and clearer bubbles (typically CO_2) were being expelled from the pools (SM Videos 10–11). Here, a maximum temperature of 197.8 °C for the molten sulfur was recorded, similar to that measured at Daikoku (187 °C). The crater floor surrounding the small molten pool shown in Fig. 6g appeared to be 'heaving' during our observations (SM Videos 11–12), suggesting that the solid-looking edges of this pool were merely a thin crust on a much larger pond of molten sulfur. This was confirmed when the ROV *Jason II* inadvertently broke through this crust, coating the undercarriage of the vehicle with an estimated 27 kg of sulfur (Fig. 6h). The chemosynthetic ecosystem at Nikko is described in the Supplementary Material to this paper (see SM Videos 7–12).

2.5 Age of the Sulfur

Sulfur-rich sample J2-199-26R (SM Fig. 6) was collected from a thick sulfur flow in the southern molten sulfur pools area at Nikko. The sulfur layers contain Ba, ^{226}Ra, ^{228}Ra and its decay product ^{228}Th that were all recovered when pyrite (FeS_2) and barite ($BaSO_4$) were separated out from the sulfur. Sufficient barite was recovered from this and other representative sulfur samples that could be weighed and measured by gamma spectrometry (Ditchburn et al. 2012). As

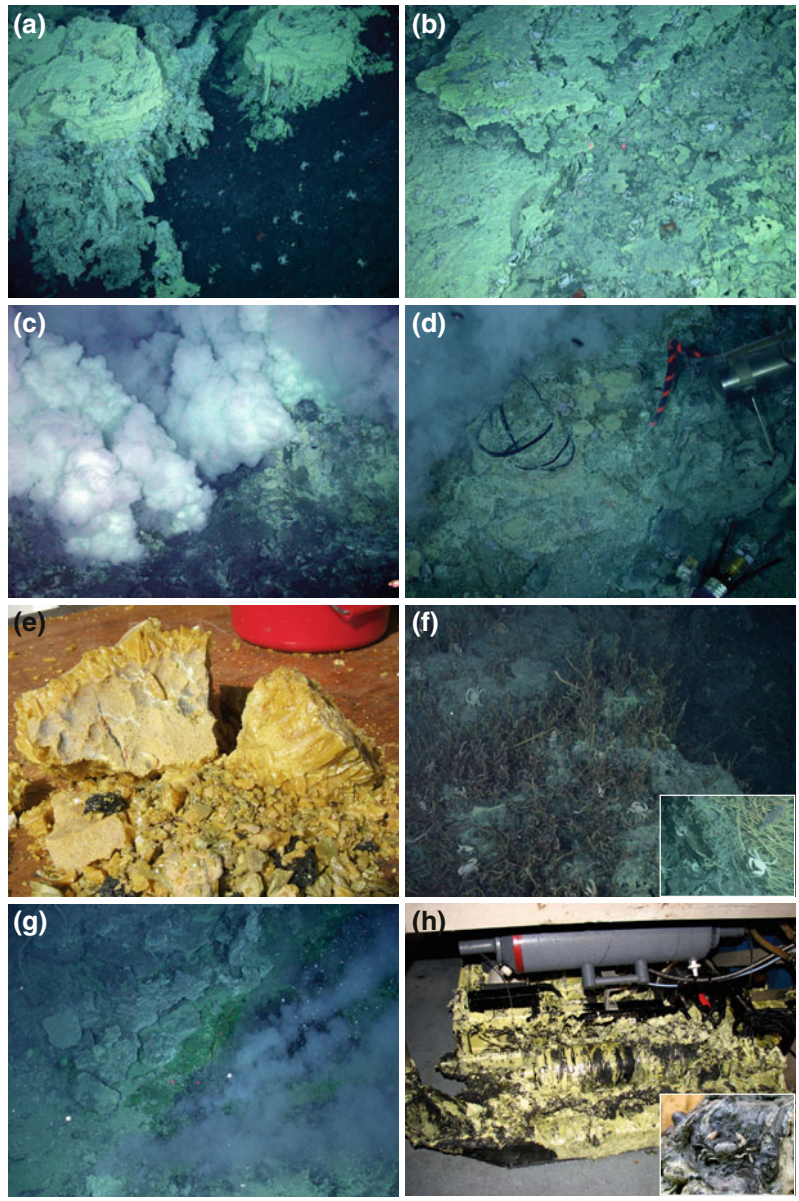

Fig. 6 **a** Oblique view of S columns inside Nikko crater. All are multi-layered with a flat top and dripping sulfur appendages. Locally, some have fallen over. They represent vestiges of an older (deeper) S lake. **b** Representative image of abundant crabs and flatfish on recent sulfur flows. **c** The whole interior of the crater was filled with S-rich smoke from vents such as this one, making visibility difficult (near Northern liquid S pond site; Fig. 5b). **d** Cable leading from an instrument (data logger) to a sensor probe that has been buried by flows of sulfur. Molten sulfur was first seen near this northern site in November 2005 with the ROV *Hyper Dolphin,* flowing from an excavated vent during water/gas sampling. **e** Large piece of semi-translucent S with scalloped shaped exterior surfaces that disintegrated within an hour of being recovered as a result of exploding, gas-rich vesicles. **f** Typical scene of dense clumps of tubeworms covering much of the crater floor at Nikko. *Inset* shows numerous bythograeid crabs foraging amongst the tubeworms. **g** Pool of molten sulfur found at the southern site (known as Naraku, or 'hell' in Japanese) at a depth of 428 m. **h** 27 kgs of extra S sample(!) when the ROV *Jason II* broke through a thin crust of S to the molten S underneath. The black streaks are very fine-grained pyrite that easily separates from the liquid sulfur when in a molten state. *Inset* shows sample J2-199-26R (see Table 2 and SM Fig. 6) covered by molten S (that also entombs a crab) as it was initially dropped into a pool of S. Laser dots shown in **b** and **g** are 10 cm apart

Table 1 Radiogenic isotopes and ages for sulfur samples from Nikko volcano

Sample no./type	FeS_2 (%)	^{226}Ra (Bq kg^{-1})	$^{228}Th/^{228}Ra$ (Bq·Bq^{-1})	Age[a] (years)
J2-199-1 Ash			0.77 ± 0.17	3.0 ± 1.0
J2-199-26 Sulfur coating[b]	6.7	465 ± 11	0.246 ± 0.054	0.74 ± 0.18
J2-199-27 Sulfur on ROV skid[c]	1.8	775 ± 23	0.214 ± 0.062	0.64 ± 0.20
J2-199-26R layered sulfur[d] zone A	48.9	52 ± 2	0.57 ± 0.19	2.0 ± 0.9
B	18.9	200 ± 6	0.98 ± 0.15	4.4 ± 1.2
C and D	7.2	283 ± 10	0.83 ± 0.16	3.3 ± 1.0
I	10.9	1,073 ± 27	0.73 ± 0.11	2.8 ± 0.6
			Mean	3.1 ± 0.5

[a] Years before time of sampling (May 2006)
[b] Molten sulfur that became coated on sample J2-199-26R
[c] Similar molten sulfur to J2-199-26, where ROV fell through sulfur crust
[d] See SM Fig. 6

the values for ^{226}Ra (Bq·kg^{-1}) and FeS_2 (wt%) are not correlated for the various samples (Table 1), barite would appear to occur within the molten sulfur independently of pyrite.

Barium and chemically similar Ra co-precipitate as a sulfate mineral (barite). The abundances of the Ra isotopes (^{228}Ra and ^{226}Ra) diminish with time because they have been physically separated from the parent isotopes that produce them (^{232}Th and ^{230}Th, respectively), and hence the decay chain is out of secular equilibrium. In the Nikko sample, the pyrite/barite fraction extracted from sample J2-199-26R was gamma counted to measure ^{228}Ra (half-life 5.75 years) and its decay product ^{228}Th (half-life 1.91 years), which had been growing from the time of mineralization. Ages were then calculated from the activity ratio $^{228}Th/^{228}Ra$ (cf. de Ronde et al. 2011; Ditchburn et al. 2012). Four sub-samples analyzed from J2-199-26R had ages at the time of sampling (May 2006) between 2.0 ± 0.9 and 4.4 ± 1.2 years, with an unweighted mean of 3.1 ± 0.5 years (Table 1). Measured ^{226}Ra concentrations in zones A to I for this sample indicate that there has been a change in barite content over a three-year period (Table 1). Unfortunately, we are unable to resolve if this was an increasing or decreasing trend due to uncertainty over which side of the sample represents the top surface.

During recovery of sample J2-199-26R by the ROV manipulator, the sample was dropped and fell into molten sulfur beneath. A thin film of streaky yellow and black sulfur immediately coated the sample (inset Fig. 6h). This film was also dated and had an age of 0.7 ± 0.2 years in May 2006. Similar material found adhering to the skid of the ROV (Fig. 6h) had a comparable age of 0.6 ± 0.2 years. Thus, if we assume that there is no age gradient through layered sulfur sample J2-199-26R, then there appears to have been two hydrothermal events fractionating Ra from Th below the Nikko summit crater; one occurred at least 3 years prior to sampling and another 0.7 years before. We believe this Ba (and Ra) was likely derived from subseafloor hydrothermal fluids entrained with ascending magmatic gases. Finally, ash-like material incorporated within molten sulfur collected from the NE sector of the crater at Nikko had an age of 3.0 ± 1.0 years, similar to layered sulfur sample J2-199-26R (Table 1).

3 Kermadec Arc

Volcanoes with known magmatic-hydrothermal discharge noted along the Kermadec Arc include: Monowai, Giggenbach, Macauley Cone, Brothers Cone, Rumble III, Rumble V, and Tangaroa (de Ronde et al. 2001, 2007).

3.1 Case Study: Macauley Cone

Macauley Cone is located inside the eastern rim of the 10 km-wide Macauley Caldera, located

immediately west of Macauley Island (Fig. 7a). The Caldera depth averages ~525 m, between a rim 500–650 m below sea level and a floor at ~1,100 m, and is thought to have formed by explosive eruption and associated caldera collapse. Macauley Cone was the target of two dives by the manned submersible *Pisces V* during the NZASRoF cruise in 2005. It is a post-caldera basaltic cone mostly composed of blocky talus, which at depths shallower than ~350 m is increasingly intercalated with black ash units. The crest of the cone is host to a NE-SW trending, elongate 80 m long by 40 m wide crater that narrows to 30 m in diameter at its base (cf. Daikoku and Fig. 4). The crater rim is continuous at 280 m although it shallows to a peak at 248 m on its southern side. The flat crater floor lies ~57 m below the rim (i.e., crater floor depth is 337 m) and is ash- and sulfur-covered.

Surveying and sampling operations at Macauley Cone included two CTDO tow-yos and two vertical casts (and three other tow-yos inside the caldera) during the 2002 NZAPLUME II cruise, two vertical casts during the 2004 NZAPLUME III cruise, and a single cast during the 2005 NZASRoF cruise. In 2002, exceptionally strong optical signals were first measured over the summit of Macauley Cone and within the summit crater. The high intensity of the plumes and their presence at several depth horizons suggested multiple sources (Fig. 7b). A plume at 250 m exceeded the full scale of the light-scattering sensor (>5.0 V) for a considerable time (56 s), the most optically intense plume (Fig. 7c) encountered anywhere along the Kermadec Arc. As at Daikoku and Nikko, plumes rich in suspended elemental sulfur particulates created exceptionally strong light scattering responses (e.g., Baker et al. 2001, 2012). A pH sensor also recorded a strong response at 250 m, consistent with the expulsion of very acidic fluids (cf. de Ronde et al. 2001; Butterfield et al. 2011; Fig. 7c).

Vigorous discharge was also observed in the water column around Macauley Cone in 2004 and 2005. In 2004, the light-backscattering plume was similar to 2002. While no pH meter was available in 2004, an oxidation-reduction-potential sensor, sensitive to reduced hydrothermal species such as H_2S and Fe^{+2} that are commonly associated with acidic discharge, detected large anomalies coincident with the optical plumes (Fig. 7c). During the 2005 NZASRoF cruise, the CTDO package was successfully lowered to within 20 m of the crater floor. The plume samples collected at this time contained some of the highest concentrations of dissolved metals (especially Fe and Mn) and particulate S and Fe among plumes sampled from any arc (de Ronde et al. 2007). Taken together, the plume surveys show that S-rich emissions have been expelled from the pit crater at Macauley Cone over a period of at least 4 years, and that this venting is associated with magmatic hydrothermal activity.

Two dives made by the submersible *Pisces V* surveyed the slopes of Macauley Cone and inside the pit crater. The flanks of the cone were covered by dense populations of mussels at depths shallower than 365 m, accompanied by predator seastars (Fig. 8a, SM Video 13). Individual layers of ash could be seen in the walls of the crater (Fig. 8b) while in places, evidence for autobrecciation of pyroclastic rock was also noted (Fig. 8c). Elsewhere inside the crater, veins related to hydraulic brecciation were seen, with clasts of wall rock floating in a matrix of finer grained volcaniclastic material (Fig. 8d, SM Video 14). Hydrothermal venting occurred at several places inside the crater (Fig. 8e) where maximum temperatures of 155 °C were recorded on the crater floor, near the north wall. Sulfur is common inside the pit crater and can occur as the matrix binding the autobreccia (Fig. 8c), thin film covering the volcanic host rock (Fig. 8d), discrete pieces within talus (background to Fig. 8e) or as layered, 'pagoda' type clumps (Fig. 8f). However, it is most commonly seen as cm-thick subhorizontal units intercalated with ash (Fig. 8g); near the crater floor it dominates the walls as a series of horizontal layers combining for over >1 m in thickness (Fig. 8h, SM Video 14). Indeed, some smooth, rounded 'blobs' of S were seen on the crater floor giving the impression they had recently been extruded in a molten state. Thus, molten S may well exist today,

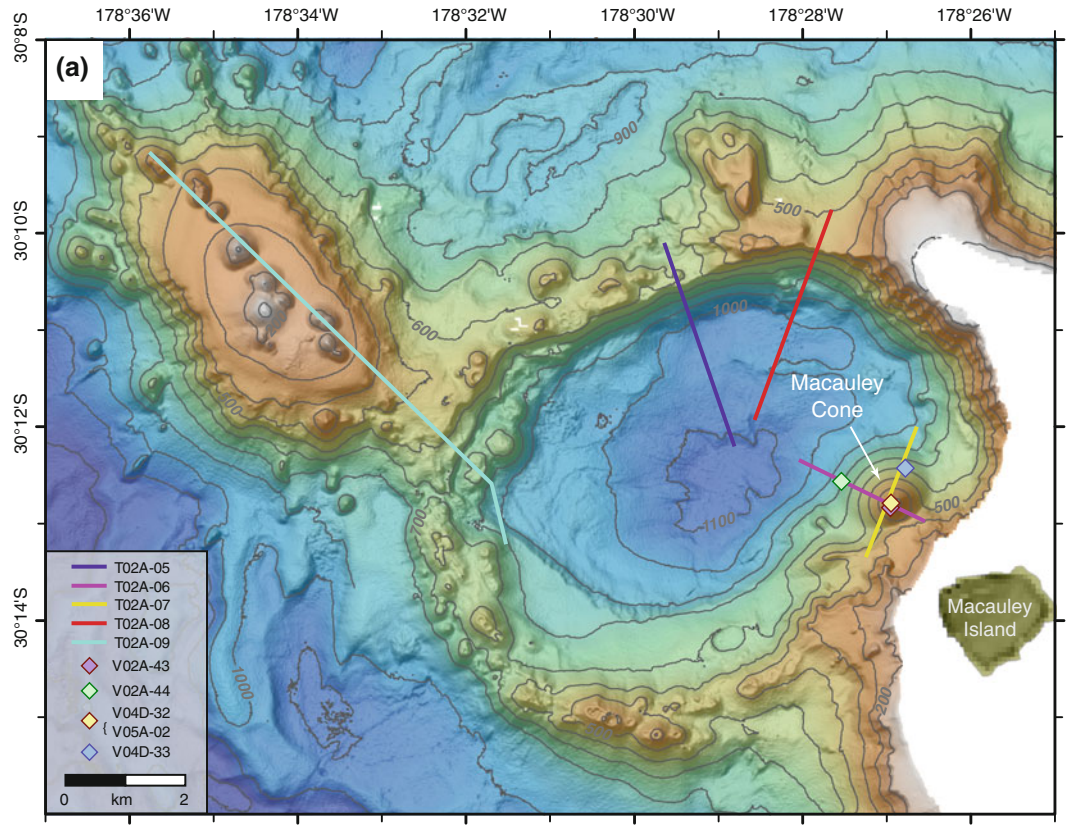
(a)
178°36'W
178°34'W
178°32'W
178°30'W
178°28'W
178°26'W
30°8'S
30°10'S
30°12'S
30°14'S
Macauley Cone
Macauley Island
T02A-05
T02A-06
T02A-07
T02A-08
T02A-09
V02A-43
V02A-44
V04D-32
V05A-02
V04D-33
0 km 2

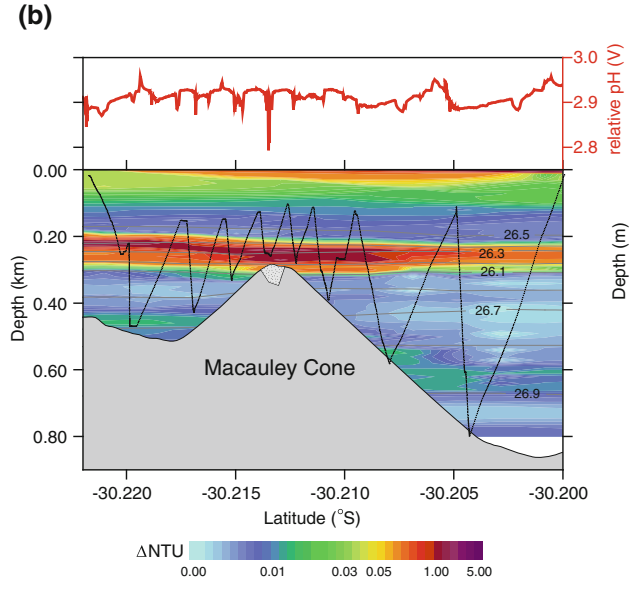
(b)
relative pH (V)
Depth (km)
Macauley Cone
26.5
26.3
26.1
26.7
26.9
Latitude (°S)
ΔNTU
0.00 0.01 0.03 0.05 1.00 5.00

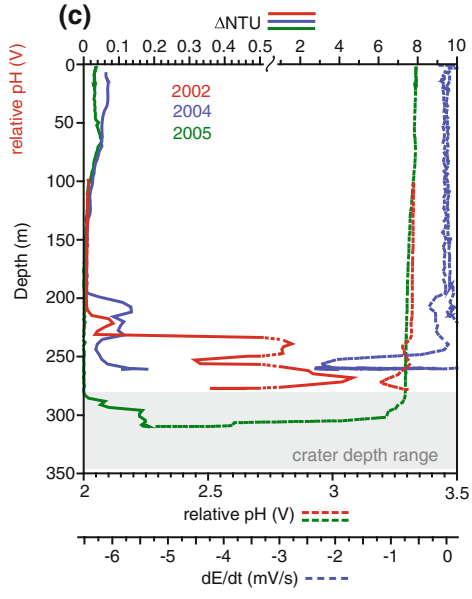
(c)
ΔNTU
2002
2004
2005
Depth (m)
crater depth range
relative pH (V)
dE/dt (mV/s)

◀ **Fig. 7** **a** Map of Macauley volcano showing a small cone located near the eastern wall of a large caldera. CTD tows (*lines*) and casts (*diamonds*) were conducted in 2002, 2004, and 2005. Mercator projection; 100 m contour interval. **b** Cross-section of Macauley cone along the path of tow T02A-06; crater width and depth approximated by the stippling at the cone summit. Plumes with high light-backscattering (ΔNTU) values emanate from the summit and form a distinct layer between ~200 and 300 m depth, with another possible deeper source occurring on the cone flank at ~500 m. Note the strong anomaly in relative pH (upper panel) as the tow passes directly over the crater of the cone. "pH" values are uncalibrated voltage levels from an in situ pH sensor. **c** Time series of ΔNTU, relative pH, and oxidation-reduction-potential (dE/dt) profiles in, and above, the crater on Macauley cone. Profiles from 2002 are from a vertical excursion during tow T02A-07 as it passed over the crater; profiles from 2004 and 2005 are from stationary vertical casts V04D-32 and V05A-02, respectively. *Note* the scale change in ΔNTU values. No pH sensor was available in 2004, but an oxidation-reduction potential sensor detected high concentrations of reduced hydrothermal species in the plumes. High values for all tracers were present each year at some depth, implying a continuing discharge that is spatially and temporally variable

immediately below the seafloor. The crosscutting of S-stained wall rock by hydraulic veins, coupled with sulfur dominating the matrix and clasts in the autobreccia, indicate a complex history of volcanic eruption, magmatic degassing, and hydrothermal fluid hydraulic fracturing. The exposed section of layered S at the base of the crater especially, combined with some sulfur 'chimneys' seen 40 m up the crater wall and images of previously-molten S 'dripping' vertically down the rock face several m above the floor are consistent with the pit crater at Macauley Cone having almost certainly been host to a relatively deep S lake in the recent past. The chemosynthetic ecosystem at Macauley Cone is described in the Supplementary Material to this paper (see SM Videos 13–14).

4 Sulfur Geochemistry

4.1 Trace Elements

Several samples of handpicked sulfur from Daikoku ($n = 10$) and Nikko ($n = 15$) volcanoes were analyzed by inductively coupled plasma source mass spectrometry (ICP-MS) and instrumental neutron activation analysis (INAA) for their trace element compositions at Activation Laboratories Ltd, Ontario, Canada. These include samples from the molten sulfur lakes at both volcanoes that contain variable pyrite content.

Element abundances, particularly Fe and Cu, are significantly greater in the sulfur lake samples of both Nikko (SM Fig. 6) and Daikoku (i.e., coffee can; SM Fig. 7) than S samples collected elsewhere at these volcanoes. Similarly, Au contents are much higher in the lake samples, ranging 112–341 ppb for Daikoku, and 37–667 for Nikko (averaging ~300 ppb for both lakes), compared to undetectable for other samples. Gold and Cu especially, but also Ag, Pb, As, Sb, Bi and some other metals correlate with Fe that represents fine-grained sulfides (mainly pyrite) contained in the samples (Fig. 9). Some elements have higher contents in the other S samples than they do from the sulfur lake samples, such as Se at Nikko (Table 2).

There are notable differences too, between trace element contents for the sulfur lake samples from the two volcanoes. For example, Nikko has average contents for Cd, Pb, As, Sb and Bi between 2.3 and 3× those of Daikoku, and almost 27× that of Zn. Higher contents of these elements in the Nikko samples could be due to micro-sulfosalt crystals (i.e., a 'nugget' effect) in the molten S of Nikko. However, most of the Nikko samples had similar contents of these elements suggesting their distribution is reasonably homogeneous. By contrast, Sulfur Cauldron at Daikoku has between 3.6 and 7× the average content of Co, Cr, Re and Ni over Nikko lake sulfur, 12× Te, 30× Ge, 33× Se and 90× Br. Iron, Cu, Ag, Au, Mn and Mo contents are similar between the two lakes. Elements such as Te, Se and Ge, when plotted against Cu, easily distinguish the lake samples from each volcano (Fig. 9).

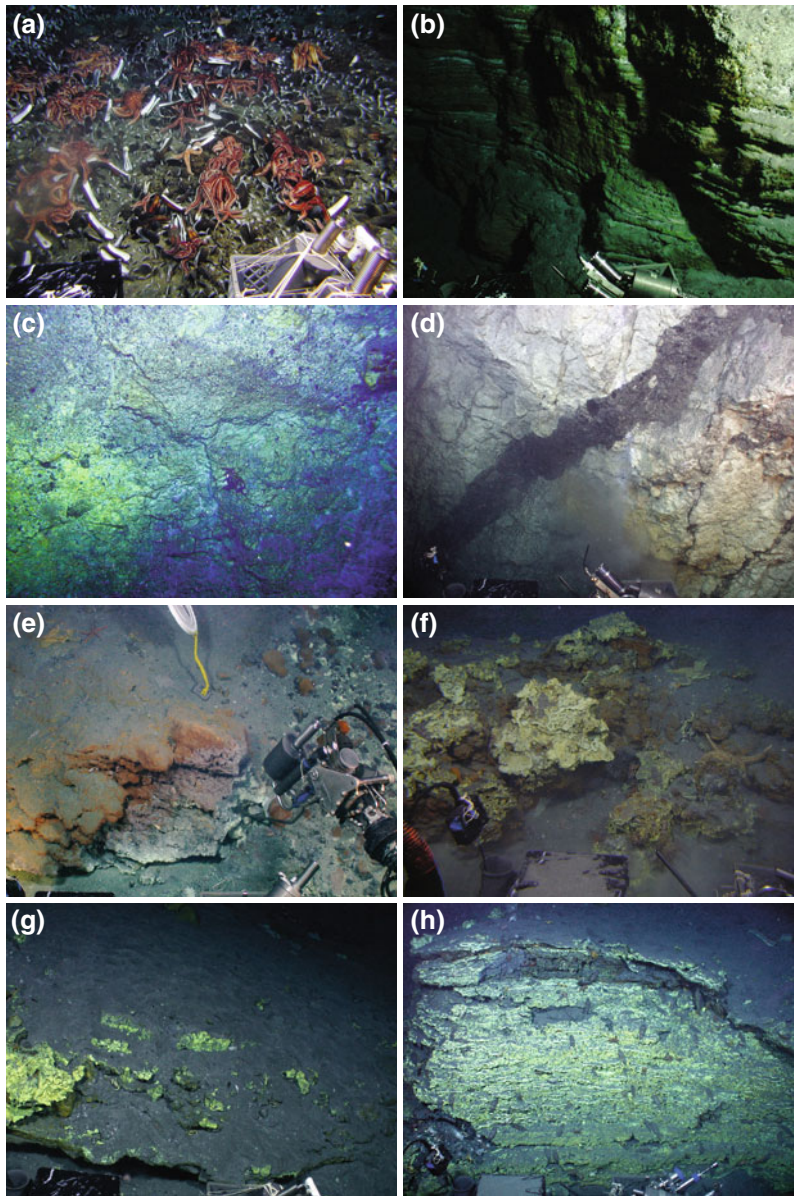

Fig. 8 **a** The upper flanks of Macauley cone were densely covered by hydrothermal vent-related mussels, together with red and yellow predator starfish. **b** The upper walls of the summit crater at Macauley cone show layers of volcanic material, mostly ash. **c** Autobrecciation of volcanic rocks is commonly seen in the walls to the pit crater, with abundant S in the matrix and as fragments in the breccia. **d** Good example of a hydraulic vein cutting earlier, S-stained rock, ~25 m up the north crater wall from the crater floor. **e** Typical example of venting seen on the floor of the pit crater (T max = 128.6 °C). Discharging hydrothermal fluids produce milky, S-rich plumes from these vents that were detected during the plume surveys (see Fig. 7). Marker #9 can be seen in the background (336 m). **f** Pagoda-like clumps (or mounds) of S that have been extruded on the seafloor. **g** In some of the individual layers of sulfur there are clear vertical striations, indicative of cooling of a horizontal lake. Photograph taken just up from the crater pit floor. **h** Vertical wall of layered sulfur clearly represents the remnants of what was once a molten lake of sulfur on the floor to the Macauley pit crater. This wall measures ~3.5–4.0 m across and ~1.5 m tall (~2 × 1 m shown in photograph). More than 20 each of tonguefish and crabs are seen to graze the face of the sulfur wall, reminiscent of those seen hovering above Sulfur Cauldron at Daikoku (see Fig. 3b)

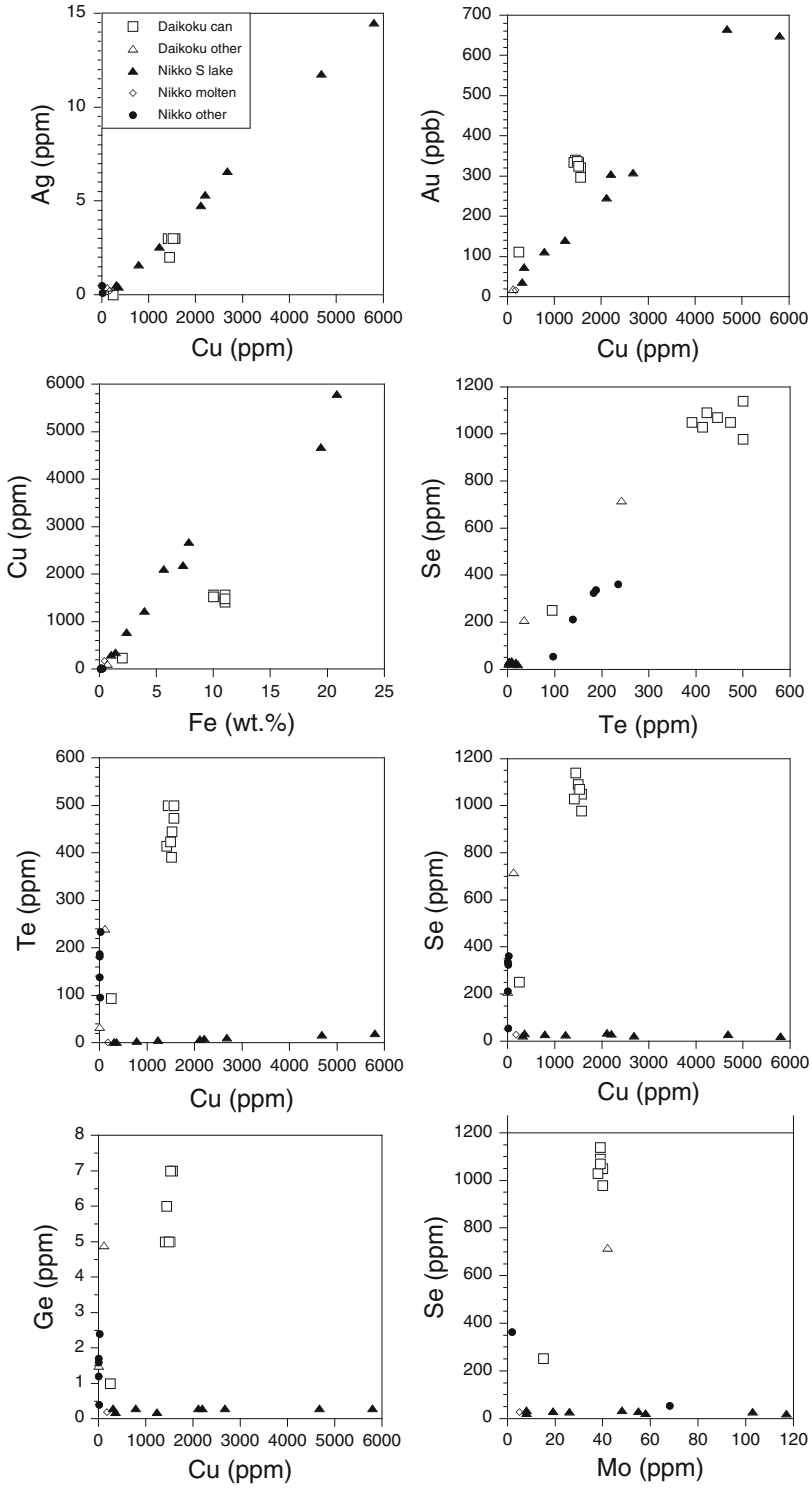
Daikoku can
Daikoku other
Nikko S lake
Nikko molten
Nikko other
Ag (ppm)
Cu (ppm)
Au (ppb)
Cu (ppm)
Cu (ppm)
Fe (wt.%)
Se (ppm)
Te (ppm)
Te (ppm)
Cu (ppm)
Se (ppm)
Cu (ppm)
Ge (ppm)
Cu (ppm)
Se (ppm)
Mo (ppm)

Fig. 9 Select variation diagrams plotting some of the trace element data given in Table 2. The first four plots clearly show strong correlations between some of the elements, notably Cu with Ag, Au and Fe, and Se with Te, with samples from both volcanoes having similar trends. By contrast, the second four plots clearly differentiate S lake samples in particular, from the two different volcanoes. 'Daikoku can' refers to the coffee can sample J2-197-22 (SM Fig. 7), 'Nikko S lake' to the laminated sample J2-199-26R from the lake margin (SM Fig. 6), 'Daikoku' and 'Nikko other' samples to clumps and chimneys of sulfur, and 'Nikko molten' to the sulfur that covered the ROV *Jason II*'s skids (see Fig. 6h)

Recovery of the coffee can full of sulfur from Sulfur Cauldron allowed us to look in detail at the distribution of elements in a molten sulfur lake. Trace element contents were determined from samples that traversed the plug of sulfur, both vertically and horizontally (see SM Figs. 3 and 7). The appearance of the sulfur is fairly homogeneous except for one sample near the centre of the can, J2-197-22A, which contains 17.4 wt% S and 2.64 wt% Fe, compared with 65 and 11 wt% for the adjacent samples, respectively (Table 2). This sample contains sandy material that has 4.7 wt% Al, 0.5 wt% Ti, 13 ppm La, 23 ppm Ce and 565 ppm Sr. In Sulfur Cauldron, low density silicates as well as pyrite will be suspended and circulated by discharging gases. Sample J2-197-22A, with its high apparent silicate content, could be aggregated material from wallrock surrounding the pond, or accumulated fractions of this material that migrated to the center of the sample upon quenching.

Small differences in the distribution of elements are noted when plotting their relative concentrations, with respect to the outermost sample, versus distance from the can wall, both in a horizontal and vertical sense (not shown). Through both profiles, elements such as Ag, Au, Cu, Fe and Pb are distributed almost identically throughout the coffee can sample. The exception is sample J2-197-22A (SM Fig. 7). All the aforementioned elements (and others) decrease sharply in their content in this zone, whereas Cr and Re contents increase (Table 2). While the center of the coffee can sample was the last to cool, it is difficult to envisage quenching of the sample causing this extreme fractionation in trace elements. Rather, it would appear that wallrock-like material occurs within the molten S lake.

$\delta^{34}S$

Sulfur and sulfide samples were analyzed for their $\delta^{34}S$ values with the aim of characterizing the magmatic signature for the sulfur lakes of Daikoku and Nikko, and to determine if processes occurring at each locality are reflected in their S isotope compositions.

On average, $\delta^{34}S$ values for sulfur and pyrite are similar at each of the sulfur lakes (Table 3). That is, average $\Delta_{sulfur\text{-}pyrite}$ is 0.2 and −0.4 ‰ for Nikko and Daikoku respectively, suggesting near-equilibrium conditions existed between the sulfur and pyrite at the time of precipitation in these lakes. The $\delta^{34}S$ values are therefore a good proxy for the isotopic composition of magmatic sulfur for these systems. It is unclear if seawater is contributing any sulfur (from sulfate) into the lakes. However, considering the isotopic composition of seawater (~21 ‰; Rees et al. 1978), even small amounts of seawater sulfate in the molten lakes would likely shift the isotopic composition of the lake sulfur values to more positive than have been measured.

$\delta^{34}S$ values for pyrite and sulfur extracted from the Sulfur Cauldron coffee can sample are, on average, more negative when compared to values from Nikko samples (Fig. 10). For example, average Daikoku $\delta^{34}S_{sulfur}$ is −8.8 ‰ compared to Nikko at −7.2 ‰, while average Daikoku $\delta^{34}S_{pyrite}$ is −9.2 ‰ compared to Nikko at −6.8 ‰. Lower $\delta^{34}S$ values are ascribed to greater magmatic influences in the system (e.g., de Ronde et al. 2005). That is, at temperatures below 400−350 °C, SO_2 will disproportionate according to reactions 3 and 4 above, generating reduced and oxidized species. This is accompanied by a kinetic isotope effect that causes the sulfide and sulfur to become enriched in ^{32}S and

Table 2 Geochemistry results for sulfur samples from Daikoku and Nikko sulfur lakes

Analyte	Fe	Cu	Ag	Au	Zn	Cd	Hg	Ge	Pb	As	Sb	Bi	Se	Te	Cr	Mn	Co	Ni	Mo	Re	Br
Unit	wt%	ppm	ppm	ppb	ppm	ppm	ppm	ppm	ppm	ppm	ppm	ppm	ppm	ppm	ppm	ppm	ppm	ppm	ppm	ppm	ppm
Detection Limit	0.01	0.2	0.05	2	0.5	0.1	1	0.1	0.5	0.5	0.1	0.1	0.1	0.1	1	1	0.1	0.5	1	0.001	0.5
Daikoku																					
J2-195-5 (S crust)	<0.01	2.2	<0.05	<2	4.6	<0.1	3	1.5	<0.5	2	<0.1	<0.1	210	34	2	6	<0.1	<0.5	<1	0.002	1.2
J2-195-11 (S chimney)	0.68	117	0.40	19	58.5	0.3	13	4.9	11.1	158	3.9	0.3	718	241	5	29	2.8	3.4	42	0.017	26.1
J2-197-22A (coffee can)	2.64	241	0.12	112	7.2	<0.1	4	1.8	29.9	119	1.9	2	252	94.2	27	116	13.5	11.2	15	0.244	28.5
J2-197-22B	11.10	1,510	3.34	335	25.7	<0.1	21	5.9	47.5	213	10.3	9.2	1,050	391	20	81	41.7	24.0	39	0.156	4.2
J2-197-22C	11.53	1,440	2.99	341	25.7	<0.1	14	6.7	41.8	244	11.7	10.9	1,140	>500	20	51	37.1	20.0	39	0.128	5.1
J2-197-22D	11.28	1,560	3.38	322	28.8	<0.1	18	7.1	46.5	254	10.9	12.5	1,050	473	23	85	40.7	22.1	40	0.123	4.5
J2-197-22E	11.00	1,410	3.16	334	26.8	<0.1	17	5.7	45.4	256	10.9	10.6	1,030	414	22	96	39.5	23.1	38	0.115	10.7
J2-197-22F	10.34	1,560	3.25	298	27.0	<0.1	15	7.1	43.1	242	10.2	11.6	979	>500	18	92	39.9	21.5	40	0.144	4.2
J2-197-22G	11.39	1,490	3.31	337	26.0	<0.1	22	5.8	46.1	270	11.6	11.6	1,090	423	18	127	38.8	22.6	39	0.129	6.0
J2-197-22H	10.89	1,520	3.35	325	32.2	0.2	14	7.2	44.1	287	12.2	12.3	1,070	445	17	85	39.5	21.8	39	0.141	8.5
Nikko																					
J2-198-3 (lump of S)	0.11	16.9	0.11	<2	44.9	0.4	6	2.4	14.6	232	4.8	0.7	363	234	2	15	0.3	<0.5	2	0.002	3.9
J2-198-4 (S spire)	0.07	2.3	<0.05	<2	2	<0.1	2	1.2	<0.5	16	0.4	<0.1	213	138	2	48	<0.1	<0.5	<1	0.002	3.5
J2-199-1 (S in ash)	0.09	2.4	<0.05	<2	9.2	<0.1	4	1.6	1.5	30	1.1	<0.1	326	182	1	49	<0.1	<0.5	<1	<0.001	5.2
J2-199-2 (lump of S)	0.10	2.3	<0.05	<2	10.8	<0.1	6	1.7	2.1	25	1.1	<0.1	337	187	<1	30	<0.1	<0.5	<1	<0.001	3.9
J2-199-12 (vugs with S)	0.25	7.5	0.49	<2	24.7	<0.1	<1	0.4	10.5	<0.5	7.9	0.5	54	95.9	33	430	0.1	1.2	68	0.034	39.1
J2-199-26R A (layered S)	20.80	5,800	14.50	650	1,150	5.9	<1	0.3	288.0	1,520	128.0	54.9	22	21	5	139	25	6.5	117	0.063	<0.5
J2-199-26R B	7.81	2,680	6.60	310	750	3.4	<1	0.3	139.0	678	60.4	27.8	23	11.9	8	27	11	3.2	58	0.019	<0.6
J2-199-26R C	1.01	311	0.55	37	113	0.5	<1	0.3	17.9	92	8.6	3.6	24	1.7	2	11	1.2	1.3	8	0.008	<0.7
J2-199-26R D	2.37	784	1.62	113	221	1.1	<1	0.3	39.3	236	22.7	8.6	31	4.1	4	87	2.9	1	19	0.008	<0.8
J2-199-26R E	19.40	4,680	11.80	667	1,580	5.7	<1	0.3	248.0	1,480	109.0	48.9	30	17.2	6	183	28	5.4	103	0.046	<0.9
J2-199-26R F	7.30	2,200	5.35	306	862	3.7	<1	0.3	111.0	684	67.8	26.5	32	9.3	4	100	9.2	2.8	55	0.025	<0.10
J2-199-26R G	1.39	358	0.45	74	167	0.7	<1	0.2	17.4	66	7.2	4.3	35	2.3	15	88	1.3	2.2	8	0.006	<0.11

(continued)

Table 2 (continued)

Analyte	Fe	Cu	Ag	Au	Zn	Cd	Hg	Ge	Pb	As	Sb	Bi	Se	Te	Cr	Mn	Co	Ni	Mo	Re	Br
J2-199-26R H	5.65	2,110	4.78	247	724	3.5	1	0.3	105.0	530	53.6	23.5	36	8	3	38	8.1	2.5	48	0.021	<0.12
J2-199-26 (broken piece)	3.92	1,230	2.58	141	417	2.3	<1	0.2	116.0	308	26.6	11.6	29	6.2	2	42	4.7	1.9	26	0.015	<0.13
J2-199-27 (molten S on skid)	0.43	172	0.24	17	44.5	0.3	<1	0.2	11.8	71	<0.1	1.9	28	1.6	3	34	0.7	1.6	5	0.005	7.4

Notes: The sulfur samples were also analysed for the following elements that were generally close to the detection limit, or too low to be used:

Li	Na	K	Rb	Cs	Be	Mg	Ca	Sr	Ba	Al	P	S	Tl
Sn	Ga	In	Sc	Ti	V	Ta	W	Th	U	Zr	Hf	Nb	Ir
Y	La	Ce	Pr	Nd	Sm	Eu	Gd	Dy	Tb	Ho	Er	Tm	Yb	Lu

All samples except J2-197-22A have 50–99.5 wt% S; J2-199-12 has 34.6 ppm W

J2-197-22A, from the centre of the coffee can (see SM Fig. 3), contains 17.4 wt% S and 4.73 wt% Al, 13 ppm La, 23 ppm Ce and 565 ppm Sr. All the other samples have <40 ppm Sr

See SM Fig. 6 for details of samples J2-199-26R A to H and see SM Fig. 7 for details of samples J2-197-22A to 22H

Table 3 $\delta^{34}S$ results for native sulfur and pyrite from Daikoku and Nikko sulfur lakes

Volcano/sample #	% Sulfur[a]	$\delta^{34}S$ in pure sulfur (‰)[b]	$\delta^{34}S$ in pyrite residue (‰)[b]	Comments
Daikoku				
J2-195-11	97.8	−8.5 ± 0.2	−8.7 ± 0.2	
J2-197-22-1	18.9	−8.6 ± 0.2		
J2-197-22-3	59.8	−8.8 ± 0.2	−9.7 ± 0.2 −9.4 ± 0.2[c]	Washed with CS_2
J2-197-22-4	69.2	−9.0 ± 0.2	−8.9 ± 0.2	
J2-197-22 pieces		−8.9 ± 0.2		Dissolved in CS_2
Nikko				
J2-199-26	93.3	−6.2 ± 0.2	−6.8 ± 0.2	Molten S coating
	98.2	−6.7 ± 0.2		ROV skid
J2-199-26R-A	51.1	−7.3 ± 0.2	−7.2 ± 0.2	
J2-199-26R-B	81.1	−7.3 ± 0.2 −7.0 ± 0.2[c]	−7.2 ± 0.2	Dissolved in CS_2
J2-199-26R-C	90.5	−7.0 ± 0.2	−6.7 ± 0.2	
J2-199-26R-D	95.1	−6.8 ± 0.2	−6.6 ± 0.2	
J2-199-26R-E	58.5	−7.2 ± 0.2	−7.1 ± 0.2	
J2-199-26R-F	82.5	−7.2 ± 0.2	−6.5 ± 0.2	
J2-199-26R-G	99.5	−7.3 ± 0.2	−6.6 ± 0.2	
J2-199-26R-H	87.7	−7.3 ± 0.2	−6.8 ± 0.2	

Notes The samples were weighed out in duplicate in tin capsules with equal amounts of VO_5 and run on a Sercon Sulphur Elemental Analyser (SEA) connected to a Europa Geo 20-20 mass spectrometer. All results are averages and standard deviations of duplicates are reported with respect to VCDT, normalized to GNS laboratory internal standard R2298 with a reported value of 8.6 ‰ for $\delta^{34}S$. The analytical precision for this instrument is 0.2 ‰ for δ^{34} S

[a] Weighing errors can limit the accuracy of the measurement, although the % S seems reliable. Average results for pure S and the black precipitate are ~100 and ~43 %, respectively. After allowing for moisture, salt, and silicate in one black precipitate, the average % S increases to 48.3 %. We believe this material is mainly pyrite (FeS_2; 53.5 % S), although one or more minerals have yet to be identified

[b] Sulfide precipitates were separated from native sulfur by dissolving the sample in hot benzene, or pyridine, to avoid any possible isotopic exchange if CS_2 had been used. The recrystallised sulfur and sulfide precipitates (mainly pyrite) were then re-submitted to the GNS Science stable isotope laboratory for further analysis

[c] Repeat analyses were done on select samples to see if there was any isotopic exchange if the reagent CS_2 were used to dissolve the S. The results are within error from those obtained when benzene or pyridine was used

the sulfate in ^{34}S. Thus, the precipitated sulfur and sulfides will have $\delta^{34}S$ values < 0 per mil, whereas the $\delta^{34}S$ values of the sulfates will be >0 per mil (Ohmoto and Rye 1979; Ohmoto and Lasaga 1982). The sulfur lake at Daikoku, therefore, would appear to have been more strongly influenced by magmatic gases than the one at Nikko.

5 Discussion

It is not intuitive to think of lakes, or ponds of liquid accumulated on the seafloor. However, this can happen for lakes of sulfur where temperatures exceed 115 °C (i.e., the melting point of S). These temperatures are a result of

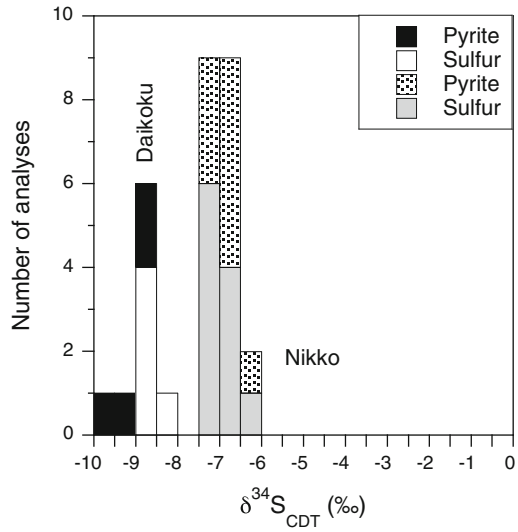

Fig. 10 Histogram of $\delta^{34}S$ values for elemental S and pyrite extracted from the molten sulfur samples from Daikoku and Nikko. All the samples from Daikoku, irrespective of elemental S or pyrite, have more negative values than those from Nikko. This suggests that Daikoku S gases have experienced a greater degree of disproportionation and/or fractionation between SO_2 and H_2S than those of Nikko, indicating a greater degree of magmatic input

hydrothermal (or gas) input and higher confining pressures at submarine arc volcanoes. That is, increasing depth equates to increasing pressure, ensuring solutions like seawater can achieve temperatures ≫100 °C (i.e., its boiling temperature at the sea surface). Similarly, with sufficient pressure, molten sulfur can reach temperatures well over 100 °C, such as the 187 °C recorded for Sulfur Cauldron. This relationship may account for the small difference in maximum temperatures recorded between Sulfur Cauldron at Daikoku (187 °C) and the molten pools of sulfur at Nikko (197.8 °C), where depths are 415 and 426 m, respectively.

Sulfur is also denser than seawater. Solid sulfur, depending on the allotrope, has a density of ~2 g cm^{-3}. Liquid sulfur is less dense, but even at 187 °C its density is ~1.76 g cm^{-3} (Espeau and Céolin 2007), notably more dense than seawater at 1.025 g cm^{-3}. Thus, even though molten sulfur is hot, its density prevents it from ascending through the water column and instead, condenses as ponds, or lakes, occupying volcanic vents on the seafloor.

Group 16 of the periodic table includes sulfur, oxygen, selenium, tellurium, and polonium, commonly referred to as the chalcogens, or ore-forming elements. Sulfur forms over 30 different allotropes (variants) in nature, with the most common allotrope being octasulfur, or cyclo-S_8, which can form large-sized crystals that are typically vivid yellow in color and somewhat translucent (see Fig. 6e). Molten sulfur assumes a dark red color above 200 °C; this color was not observed for the liquid S seen at Diakoku or Nikko, consistent with the maximum recorded temperature of 197.8 °C. A selection of sulfur samples from Daikoku and Nikko were analyzed by X-ray diffraction to determine their allotropes. Only orthorhombic S_8 could be identified. SEM images of select samples show that all the sulfur samples, including those containing pyrite, were microcrystalline in habit. Rapid cooling of molten sulfur, e.g., by quenching—as in the coffee can experiment—would result in the formation of amorphous (elastic) sulfur. However, this form is metastable at room temperature and gradually reverts to a crystalline molecular allotrope that can happen within a matter of hours to days. Not surprisingly then, no amorphous sulfur was seen in the coffee can sample.

Dissolving select sulfur samples in CS_2 to recover precipitated sulfide minerals (predominantly pyrite) for gamma spectrometry (dating), and later recrystallizing the sulfur, showed it typically to be lemon yellow in color. Two exceptions were samples from Daikoku that produced bright orange sulfur (SM Fig. 8) which trace element analysis showed contained relatively high concentrations of Se when compared to samples from Nikko (Table 2). Moreover, in the recrystallized Nikko S sample, Se and Te contents were 60 and 10 % of their original values, whereas in the recrystallized Daikoku S sample they were 100 and 50 %, respectively. This result confirms that Te-S compounds are less stable than Se-S. Finally, all the Mariana

sulfur samples were readily soluble in CS_2 showing that long chain molecules (polymers) were minor, or non-existent within the samples (Steudel and Eckert 2003).

5.1 Formation of Seafloor Sulfur Lakes

We propose that the sulfur lake at Daikoku sits atop a volcanic pipe with a direct connection to a shallow magmatic body, either a dike, sheet, or finger (cf. Reyes et al. 2003; Christenson and Wood 1993). It has been suggested that 'heat pipes' can convectively transfer heat between a magma body and the region immediately below some subaerial crater lakes (e.g., Hurst et al. 1991). In this model, the simultaneous upward movement of a vapor phase, together with the downward movement of a liquid phase from condensed vapor, would allow efficient heat transfer without overall mass transfer (Hurst et al. 1991). Also, the temperature record for Crater Lake at Mt. Ruapehu (New Zealand), for example, has shown over several years a cyclic pattern of alternate heating and cooling, with the former lasting one or two months and the latter six months to a year (Hurst et al. 1991; Christenson et al. 2010). Hurst et al. (1991, and note added in proof) and later Christenson (1994) suggested that liquid sulfur at the bottom of the lake (with temperatures of ~177 °C) acts as a partial barrier between the heat pipe and the lake, with the highly viscous sulfur blocking any upward flow of steam and gases, thus preventing heat input into the lake and resulting in a cooling phase. Only after heating from below has elevated temperatures above the high-viscosity region for sulfur (i.e., ~200 °C; see above) would gases once again pass through the sulfur barrier at the top of the heat-pipe (cf. intermittent venting and S emission at Daikoku). Modeling of the Ruapehu Crater Lake system by Christenson et al. (2010) shows that condensation of magmatic vapor into a highly porous medium of andesitic composition leads to rapid formation of an elemental sulfur–anhydrite–natroalunite mineral assemblage, and a drastic reduction in permeability due to an envelope of this assemblage (but mostly elemental S) along the margins of the 2-phase liquid–vapor region enclosing the conduit. This effectively seals the upper portion of the vent from the adjacent, hydrostatically controlled environment until the next eruption.

The combination of volcanic pipes at Daikoku (SM Figs. 1 and 4), the likelihood of liquid S occurring at their base given the discharge of S-rich plumes (SM Fig. 2c), and the probability of a subterranean connection between them and Sulfur Cauldron (Fig. 2), suggests a similar model of heat pipes transferring heat and gases to seafloor sulfur lakes. Similarly, the distribution of molten sulfur vent sites at Nikko (Fig. 5b) suggests that a subsurface connection may also exist between sites inside and outside the crater. Our study suggests that sulfur is deposited, and accumulates, in the shallow subsurface of many submarine arc volcanoes—as a consequence of the interaction of degassing magmatic SO_2 with seawater—at a number of localities, each of which are plumbed in the subsurface by conduits connected to deeper magma bodies.

At Nikko and Macauley in particular, vertical layers >1 m thick of sulfur crusts indicate that substantial sulfur flows and lakes have occurred in the past, and that this process of forming S lakes has been ongoing over a lengthy period of time at these volcanoes. Dating of barite microcrystals entrained in the molten S at Nikko showed that two hydrothermal events occurred almost 3 years apart (Table 2), though this appears to be confined to a small area, given the prolific distribution of (older) tubeworms elsewhere in the crater. While the areal extent of the S lake (or where S is known to be immediately subsurface) at Nikko is today significant (~200 m in diameter), evidence exists for lake levels to have been at least 10 m higher, indicative of a much more substantial lake in the recent past, with the requirement of deposition and accumulation of large quantities of sulfur in the subsurface. Repeated cycles of heating, melting, and remobilization of this sulfur helps form these large (and small) S crater lakes.

5.2 Origin and Transport of the S Lake Metals

The association of large Au–Cu–Ag ore deposits with convergent margins is commonly attributed to the higher content of chalcophile elements (or those that concentrate in sulfides) in the parental magmas generated at subduction zones compared with mid-ocean ridges. Limited sampling and analysis of rocks recovered from Daikoku and Nikko suggest that the former is an andesitic volcano and the latter a combination of basaltic and andesitic lavas (Blommer et al. 1989; Lin and Stern 1989). Taken as a first order approximation of composition, the aforementioned studies would suggest that andesitic magmas from Daikoku should be enriched in incompatible elements—preferentially partitioned into silicate melts rather than coexisting minerals—relative to Nikko mafic magmas. This could in turn be reflected in the S phase, assuming that Nikko sulfur was exsolved from a mafic magma and Daikoku sulfur exsolved from an andesitic magma.

Oxidized and H_2O-rich basaltic magmas of volcanic arcs carry up to 1.5 wt% S dissolved as sulfate until at very low pressures (Jugo et al. 2005). As magma differentiates towards more silicic compositions, sulfur is fractionated into immiscible sulfide-rich liquid, or sulfate-bearing phases, depending on the redox conditions (Métrich and Mandeville 2010). For example, Di Muro et al. (2008) have suggested that hydrous flushing and subsequent cooling and oxidation of basaltic andesite magma beneath Mt. Pinatubo (Philippines) injected into existing, H_2O-rich, oxidized dacitic magma that resulted in the release of S into the gas phase and the formation of low-temperature Cu-sulfides. The latter are said to have formed from hydrous, Cu-bearing fluids that coexisted with the dacitic magma. Similarly, geochemical modeling results of Crater Lake at Mt. Ruapehu are consistent with the introduction of fresh magmatic material (andesite) into the volcanic vent, initiating variations in lake chemistry that are thought to reflect the dissolution of this material and transport of metals in the vapor phase (Christenson and Wood 1993; Christenson et al. 2010). In addition, Jenner et al. (2010) suggest that the association of major Cu-Au deposits with convergent-margin magmatism results specifically from the process of magmatic evolution under oxidizing conditions. Thus, the trace element contents for the molten S samples analyzed from Daikoku and Nikko could be a reflection of magma compositions (Table 2). Trace element enrichments seen in the Daikoku coffee can sample are, with notably higher Te, Ge and Se contents, indicative of higher subseafloor temperatures, consistent with a greater *direct* magmatic input than at Nikko. This would be in keeping with more negative $\delta^{34}S$ values from the Daikoku lake sulfur than at Nikko (Fig. 10).

We believe the metals measured in the S lakes of Daikoku and Nikko likely were primarily derived from a degassing magma, transported in the vapor phase, and condensed in the lakes (cf. Kamenov et al. 2005; Kim et al. 2011; Henley and Berger 2010, 2012). For example, systematic experiments investigating the effect of sulfur ligands on metal vapor-liquid partitioning in model H_2O–S–NaCl–KCl–NaOH systems at temperatures from 350 to 500 °C show a dramatic increase in the mobility of Cu and Au in magmatic-hydrothermal vapors that are sulfur-enriched and acidic (Pokrovski et al. 2008). Copper and Au contents are similar (and anomalous) between the Daikoku and Nikko sulfur lake samples.

High CO_2 contents seen discharging through these seafloor molten S lakes and pools as streams of bubbles are also indicative of a direct injection of magmatic CO_2-rich gas into the system (e.g., Lupton et al. 2008). This might be a consequence of CO_2 being less soluble and/or less reactive than constituents such as SO_2 and H_2S and so will pass through the molten S into the ocean above. However, it has been suggested by Lowenstern (2001) that the presence of CO_2 will hasten the creation of a vapor phase causing H_2S and possibly HCl to move into the vapor and act as ligands for some metals. If true, this may reflect the different solubilities of CO_2 and SO_2

in the underlying melts, with the former exsolving at greater depths (pressures) from the magma than the latter (Lowenstern 2001).

In summary, the discovery of extraordinary lakes and pools of molten S in summit craters of submarine volcanoes attests to largely unseen processes occurring every day on the seafloor (though common on land). These S lakes act as condensers of magmatic gases exsolving from underlying magmas, transporting metals to the seafloor and acting as harbingers to the formation of hydrothermal ore deposits, especially those rich in Cu and Au.

Acknowledgments This paper was written while C de R was on sabbatical at NOAA/PMEL. A.G. Reyes, R. J. Stern and R.W. Henley are thanked for their discussion on volcanic lakes, sulfur, and magmas. K. Nakamura commented on an earlier draft of this paper. Reviews by R.J. Arculus, D. Rouwet, and B.W. Christenson improved this contribution. The captain and crew of the research tender vessels R/V Thompson (2004), R/V *Kaimikai-o-Kanaloa* (2005) and R/V Melville (2006), and the ROV (*ROPOS* and *Jason II*) pilots and engineers, are thanked for careful and safe operations while at sea. Funding for C de R was from the Foundation for Research, Science and Technology (FRST) contract #C05X0406. Funding for the Submarine Ring of Fire expeditions was from the NOAA Ocean Exploration and NOAA Vents Programs. This is PMEL contribution #3942.

References

Baker ET, Tennant DA, Feely RA, Lebon GT, Walker SL (2001) Field and laboratory studies on the effect of particle size and composition on optical backscattering measurements in hydrothermal plumes. Deep-Sea Res 48:593–604

Baker ET, Massoth GJ, Nakamura K, Embley RW, de Ronde CEJ, Arculus RJ (2005) Hydrothermal activity on near-arc sections of back-arc ridges: results from the Mariana Trough and Lau Basin. Geochem Geophys Geosyst 6:Q09001. doi:10.1029/2005GC000948

Baker ET, Embley RW, Walker SL, Resing JA, Lupton JE, Nakamura K, de Ronde CEJ, Massoth GJ (2008) Hydrothermal activity and volcano distribution along the Mariana Arc. J Geophys Res 113.B08S09. doi:10.1029/2007JB005423

Baker ET, Walker ET, Embley RW, de Ronde CEJ (2012) High-resolution hydrothermal mapping of brothers caldera, Kermadec arc. Econ Geol 107:1583–1593

Bloomer SH, Stern RJ, Fisk E, Geschwind CH (1989) Shoshonitic volcanism in the Northern Mariana arc 1. Mineralogic and major trace element characteristics. J Geophys Res 94:4469–4496

Butterfield DA, Nakamura K, Takano B, Lilley MD, Lupton JE, Resing JA, Roe KK (2011) High SO_2 flux, sulfur accumulation and gas fractionation at an erupting submarine volcano. Geology 39:803–806. doi:10.1130/G31901.1

Chadwick WW, Cashman KV Jr, Embley RW, Matsumoto H, Dziak RP, de Ronde CEJ, Lau T-K, Deardorff N, Merle SG (2008) Direct video and hydrophone observations of submarine explosive eruptions at NW Rota-1 volcano, Mariana arc. J Geophys Res 113: B08S10. doi:10.1029/2007JB005215

Chadwick WW, Dziak RP Jr, Haxell JH, Embley RW, Matsumoto H (2012) Submarine landslide triggered by volcanic eruption recorded by in-situ hydrophone. Geology 40:51–54

Christenson BW (1994) Convection and stratification in Ruapehu Crater Lake, New Zealand: implications for lake Nyos-type gas release eruptions. Geochem J 28:185–197

Christenson BW, Wood CP (1993) Evolution of a vent-hosted hydrothermal system beneath Ruapehu Crater Lake, New Zealand. Bull Volcanol 55:547–565

Christenson BW, Reyes AG, Young R, Moebis A, Sherburn S, Cole-Baker J, Britten K (2010) Cyclic processes and factors leading to phreatic eruption events: Insights from the 25 September 2007 eruption through Ruapehu Crater Lake, New Zealand. J Volcanol Geotherm Res 191:15–32

Crisp JA (1984) Rates of magma emplacement and volcanic output. J Volcanol Geotherm Res 20:177–211

de Ronde CEJ, Baker ET, Massoth GJ, Lupton JE, Wright IC, Feely RA, Greene RG (2001) Intra-oceanic subduction-related hydrothermal venting, Kermadec volcanic arc, New Zealand. Earth Planet Sci Lett 193:359–369

de Ronde CEJ, Massoth GJ, Baker ET, Lupton JE (2003) Submarine hydrothermal venting related to volcanic arcs. In: Simmons SF, Graham IG (eds) Giggenbach Memorial volume. Soc Econ Geol and Geochem Soc Special Publ 10: 91–109

de Ronde CEJ, Hannington MD, Stoffers P, Wright IC, Ditchburn RG, Reyes AG, Baker ET, Massoth GJ, Lupton JE, Walker SL, Greene RR, Soong CWR, Ishibashi J, Lebon GT, Bray CJ, Resing JA (2005) Evolution of a submarine magmatic-hydrothermal system: brothers volcano, southern Kermadec arc, New Zealand. Econ Geol 100:1097–1133

de Ronde CEJ, Baker ET, Massoth GJ, Lupton JE, Wright IC, Sparks RJ, Bannister SC, Reyners ME, Walker SL, Greene RR, Ishibashi J, Faure K, Resing JA, Lebon GT (2007) Submarine hydrothermal activity along the mid-Kermadec Arc, New Zealand: large-scale effects

on venting. Geochem Geophys Geosyst 8:Q07007. doi:10.1029/2006GC001495

de Ronde CEJ, Massoth GJ, Butterfield DA, Christenson BW, Ishibashi J, Ditchburn RG, Hannington MD, Brathwaite RL, Lupton JE, Kamenetsky VS, Graham IJ, Zellmer GF, Dziak RP, Embley RW, Dekov VM, Munnik F, Lahr J, Evans LJ, Takai K (2011) Submarine hydrothermal activity and gold-rich mineralization at Brothers volcano, Kermadec arc, New Zealand. Miner Deposita 46:541–584. doi:10.1007/s00126-011-0345-8

Di Muro A, Pallister J, Villemant B, Newhall C, Semet M, Martinez M, Mariet C (2008) Pre-1991 sulfur transfer between mafic injections and dacite magma in the Mt. Pinatubo Reservoir J Volcanol Geotherm Res 175:517–540

Ditchburn RG, de Ronde CEJ, Barry BJ (2012) Radiometric dating of volcanic massive sulfides and associated iron oxide crusts with an emphasis on ^{226}Ra/Ba and ^{228}Ra/^{226}Ra in volcanic and hydrothermal processes at intraoceanic arcs. Econ Geol 107:1635–1648

Embley RW, Chadwick WW Jr, Baker ET, Butterfield DA, Resing JA, de Ronde CEJ, Tunnicliffe V, Lupton JE, Juniper SK, Rubin KH, Stern RJ, Lebon GT, Nakamura K, Merle SG, Hein JR, Wiens DP, Tamura Y (2006) Long-term eruptive activity at a submarine arc volcano. Nature 441:494–497

Embley RW, Baker ET, Butterfield DA, Chadwick WW Jr, Lupton JE, Resing J, de Ronde CEJ, Nakamura K, Tunnicliffe V, Dower J, Merle SG (2007) Exploring the submarine ring of fire: Mariana Arc—Western Pacific. Oceanography 20:68–79

Espeau P, Céolin R (2007) Density of molten sulfur in the 334–508 K range. Thermochim Acta 459:127–129

Ferrini VL, Fornari DJ, Shank TM, Kinsey JC, Tivey MA, Soule SA, Carbotte SM, Whitcomb LL, Yoerger D, Howland J (2007) Submeter bathymetric mapping of volcanic and hydrothermal features on the East Pacific Rise crest at 9 50′ N. Geochem Geophys Geosyst 8:Q01006. doi:10.1029/2006GC001333

Ferrini VL, Tivey MK, Carbotte SM, Martinez F, Roman C (2008) Variable morphologic expression of volcanic, tectonic, and hydrothermal processes at six hydrothermal vent fields in the Lau back-arc basin. Geochem Geophys Geosyst 9:Q07022. doi:10.1029/2008GC002047

Giggenbach WF (1987) Redox processes governing the chemistry of fumarolic gas discharges from White Island, New Zealand. Appl Geochem 2:143–161

Giggenbach WF (1992) Magma degassing and mineral deposition in hydrothermal systems along convergent plate boundaries. Econ Geol 87:1927–1944

Giggenbach WF (1996) Chemical composition of volcanic gases. In: Scarpa R, Tilling RI (eds) Monitoring and mitigation of volcanic hazards. Springer, Berlin, pp 221–255

Henley RW, Berger BR (2010) Magmatic-vapor expansion and the formation of high-sulfidation gold deposits: Chemical controls on alteration and mineralization. Ore Geol Rev 39:63–74

Henley RW, Berger BR (2012) Nature's refineries—metals and metalloids in arc volcanoes. In: Rouwet D, Tassi F, Vandmeulebrouck J, Christenson B (eds) Volcanic lakes. Springer, Berlin

Hurst AW, Bibby HM, Scott BJ, McGuinness MJ (1991) The heat source of Ruapehu Crater Lake; deductions from the energy and mass balances. J Volcanol Geotherm Res 46:1–20

Jenner FE, O'Neill HSC, Arculus RJ, Mavrogenes JA (2010) The Magnetite crisis in the evolution of arc-related magmas and the initial concentration of Au, Ag and Cu. J Petrol 51:2445–2464

Jugo PJ, Luth RW, Richards JP (2005) An experimental study of the sulfur content in basaltic melts saturated with immiscible sulfide or sulfate liquids at 1300 and 1.0 GPa. J Petrology 46:783–798

Kamenov GD, Perfit MR, Jonasson IR, Mueller PA (2005) High-precision Pb isotope measurements reveal magma recharge as a mechanism for ore deposit formation: examples from Lihir Island and Conical seamount, Papua New Guinea. Chem Geol 219:131–148

Kim J, Lee K-Y, Kim J-H (2011) Metal-bearing molten sulfur collected from a submarine volcano: implications for vapor transport of metals in seafloor hydrothermal systems. Geology 39:351–354. doi:10.1130/G31665.1

Kusakabe M, Komoda Y, Takano B, Abiko T (2000) Sulfur isotopic effects in the disproportionation reaction of sulfur dioxide in hydrothermal fluids: implications for the δ^{34}S variations of dissolved bisulfate and elemental sulfur from active crater lakes. J Volcanol Geotherm Res 97:287–307

Lin P-N, Stern RJ (1989) Shoshonitic volcanism in the Northern Mariana arc 2. Large-ion lithophile and rare earth element abundances: evidence for the source of incompatible element enrichments in intraoceanic arcs. J Geophys Res 94:4497–4514

Lowenstern JB (2001) Carbon dioxide in magmas and implications for hydrothermal systems. Miner Deposita 36:490–502. doi:10.1007/s001260100185

Lupton JE, Butterfield DA, Lilley M, Evans L, Nakamura K, Chadwick WW Jr, Resing J, Embley RW, Olson E, Proskurowski G, Baker E, de Ronde CEJ, Roe KK, Lebon GT, Young C (2006) Submarine venting of liquid carbon dioxide on a Mariana arc volcano. Geochem Geophys Geosyst 7:Q08007. doi:10.1029/2005GC001152

Lupton J, Lilley M, Butterfield D, Evans L, Embley R, Massoth G, Christenson B, Nakamura K, Schmidt M (2008) Venting of a separate CO_2-rich gas phase from submarine arc volcanoes: examples from the Mariana and Tonga-Kermadec arcs. J Geophys Res 113. doi:10.1029/2007jb005467

Métrich N, Mandeville CW (2010) Sulfur in magmas. Elements 6:81–86

Mizutani Y, Sugiura T (1966) The chemical equilibrium of the $2H_2S + SO_2 = 3S + 2H_2O$ reaction in solfataras of the Nasudake volcano, Hokkaido. Japan Bull Chem Soc Japan 39:2411–2414

Moretti R, Papale P (2004) On the oxidation state and volatile behavior in multicomponent gas–melt equilibria. Chem Geol 213:265–280

Ohmoto H, Lasaga AC (1982) Kinetics of reactions between aqueous sulfates and sulfides in hydrothermal systems. Geochim Cosmochim Acta 46:1727–1745

Ohmoto H, Rye RO (1979) Isotopes of sulfur and carbon. In: Barnes HL (ed) Geochemistry of hydrothermal ore deposits, 2nd edn. Wiley, New York, pp 509–567

Pokrovski GS, Borisova AY, Harrichoury J-C (2008) The effect of sulfur on vapor-liquid fractionation of metals in hydrothermal systems. Earth Planet Sci Lett 266:45–362

Rees CE, Jenkins WJ, Monster J (1978) The sulfur isotope geochemistry of ocean water sulfate. Geochim Cosomochim Acta 42:77–382

Resing JA, Lebon G, Baker ET, Lupton JE, Embley RW, Massoth GJ, Chadwick WW Jr, de Ronde CEJ (2007) Venting of acid-sulfate fluids in a high-sulfidation setting at NW Rota-1 submarine volcano on the Mariana arc. Econ Geol 102:1047–1061

Resing JA, Baker ET, Lupton JE, Walker SL, Butterfield DA, Massoth GJ, Nakamura K (2009) Chemistry of hydrothermal plumes above submarine volcanoes of the Mariana Arc. Geochem Geophys Geosyst 10. doi:10.1029/2008GC002141

Reyes AG, Grapes R, Clemente VC (2003) Fluid–rock interaction at the magmatic–hydrothermal interface of the Mount Cagua geothermal system, Philippines. In: Simmons SF, Graham IJ (eds) Volcanic, geothermal, and ore-forming fluids: rulers and witnesses of processes within the earth vol 10. Soc Econ Geol Geochem Soc, Special Publication, pp 197–222

Roman CN, Singh H (2007) A self-consistent bathymetric mapping algorithm. J Field Robotics 24:26–51

Seyfried WE Jr (1987) Experimental and theoretical constraints on hydrothermal alteration at mid-ocean ridges. Ann Rev Earth Planet Sci 15:317–350

Steudel R, Eckert B (2003) Solid sulfur allotropes. In: Steudel R (ed) Elemental sulfur and sulfur-rich compounds I. Topics in current chemistry 230. Springer, Berlin, pp 1–80

Symonds RB, Gerlach TM, Reed MH (2001) Magmatic gas scrubbing: implications for volcano monitoring. J Volcanol Geotherm Res 108:303–341

Tunnicliffe V, Koop BF, Tyler J, So S (2010) Flatfish at seamount hydrothermal vents show strong genetic divergence between volcanic arcs. Mar Ecol 31:158–167. doi:10.1111/j.1439-0485.2010.00370.x

Summit Acid Crater Lakes and Flank Instability in Composite Volcanoes

Pierre Delmelle, Richard W. Henley, Sophie Opfergelt, and Marie Detienne

Abstract

Volcanic landslides, including flank and sector collapses, constitute a major hazard in many parts of the world. While composite volcanoes are innately unstable, the presence of a hydrothermal system maintained by a magmatic source at depth is recognized as a key factor increasing the risk of failure. This relates to the formation of hydrothermally altered rock masses within the core and upper flanks of the volcano which leads to heterogeneous distribution of rock strength properties and pore fluid pressures. Here an emphasis is placed on acid crater lakes perched high on active volcanoes. By acting as a trap for magmatic heat and gas flows, these lakes localize extreme acid attack on their surrounds, thereby creating a source of instability. We outline how acid crater lakes form in relation to magmatic hydrothermal systems hosted within composite volcanoes, and describe the associated hydrothermal alteration and its relationships to flank instability. The sustainability of a volcanic slope is partly governed by the degree of rock alteration, which in turn reflects the time-integrated flux of acidic gases (SO_2 and HCl) released from the subsurface magmatic source. Transient or longer-term changes in pore fluid pressure linked to hydrothermal system activity also readily affect the slope stability of composite volcanoes. Such fluctuations can be initiated by both magmatic and external non-magmatic processes such as major rainfall events and regional seismicity. Kawah Ijen hyper-acid crater lake, Indonesia, is used as a case study to illustrate the cascade of effects that may ensue following slope rupture linked to hydrothermal alteration.

P. Delmelle (✉) · S. Opfergelt · M. Detienne
Earth & Life Institute, Environmental Sciences,
Université catholique de Louvain, Croix du Sud 2,
bte L7.05.10, 1348 Louvain-la-Neuve, Belgium
e-mail: pierre.delmelle@uclouvain.be

R.W. Henley
Research School of Earth Sciences,
Australian National University, Canberra,
ACT, Australia

D. Rouwet et al. (eds.), *Volcanic Lakes*, Advances in Volcanology,
DOI 10.1007/978-3-642-36833-2_12,
© Springer-Verlag Berlin Heidelberg 2015

Keywords
Acid crater lakes · Magmatic gas expansion · Hydrodynamics and hydrology · Hydrothermal alteration · Volcano flank instability · Kawah ijen

1 Introduction

There is abundant evidence that most composite volcanoes have been affected by large landslides at some stages of their life cycle (e.g., Belousov et al. 1999; Carrasco-Núñez et al. 2011; Siebert 1984; Vallance et al. 1995; van Wyk de Vries and Francis 1997). These events, which can involve a sector or an entire flank of an edifice, are typically recorded by the formation of destructive debris avalanches and, in many instances, highly mobile debris flows, providing that sufficient water is present within the moving rock mass (e.g., Capra et al. 2002; Carrasco-Núñez et al. 1993; Siebert et al. 1987; Ui et al. 1986; Vallance and Scott 1997). As such, volcanic landslides represent a major threat in densely populated regions, e.g., Mombacho volcano, Nicaragua, Mount Rainier, USA (Carrasco-Núñez et al. 2011; McGuire 2003; Reid et al. 2001; Siebert 1984; Shea and van Wyk de Vries 2010; Witham 2005). A better understanding of the factors that lead to flank instability, and ultimately failure, is paramount to improving our capacity to assess volcanic hazards. Significantly, since an eruption is not necessarily needed to trigger a volcanic landslide (van Wyk de Vries and Francis 1997; Shea and van Wyk de Vries 2010), established volcano-risk monitoring may fail to include identification of collapse-prone areas, or precursor activity.

Volcanoes are inherently unstable. Their behavior and often catastrophic ruptures are oscillatory and directly related to magmatic activity, not just through eruptions but perhaps more importantly, in the long term, due to the maintenance of heat and mass transfer through to the edifice surface during quiescence (Ingebritsen and Mariner 2010). Eruptions, aided and abetted by subsequent erosion, progressively build the familiar upper level, broadly conical structures of volcanoes that are each characteristically defined by slope angle; for example, composite volcanoes tend to relatively stable slope angles of 6 to 10° on their flanks and highly unstable steeper summit regions at around 30°. Summit elevations are restricted by the internal cohesion of erupted materials and active volcanoes often have a fragile structure, which can be disturbed by eruptions, pore pressure variations, earthquakes, weather events and the progressive destabilization of the edifice by spreading and hydrothermal alteration, and importantly the positive reinforcements that may occur between them. Even perfectly symmetrical cones like Mayon volcano, Philippines, are maintained at critical conditions through tectonic stress in their basements as well as gradual load; both of which produce slip planes and related fractures (Norini and Lagmay 2005), which may also guide hydrothermal and groundwater flow within the edifice structure.

Progressive hydrothermal rock alteration is now widely recognized as a principal factor, directly or indirectly, which promotes the collapse of active composite volcanoes (e.g., López and Williams 1993; Scott et al. 1995; van Wyk de Vries and Francis 1997; Reid et al. 2001; John et al. 2008). The focus of this chapter is on slope instabilities that may be generated by the intense hydrothermal alteration found locally in the summit and flank region of composite volcanoes consequent on the sustained flux of SO_2-rich volcanic gas. In particular the collapse risk associated with alteration is increased by the formation of highly acidic crater lakes on the summits of active volcanoes (e.g., Rincón de la Vieja volcano, Costa Rica, Fig. 1) and within the flank topography (e.g., Kawah Ijen, Indonesia). How do these lakes form? What is their role in triggering large volcanic landslides?

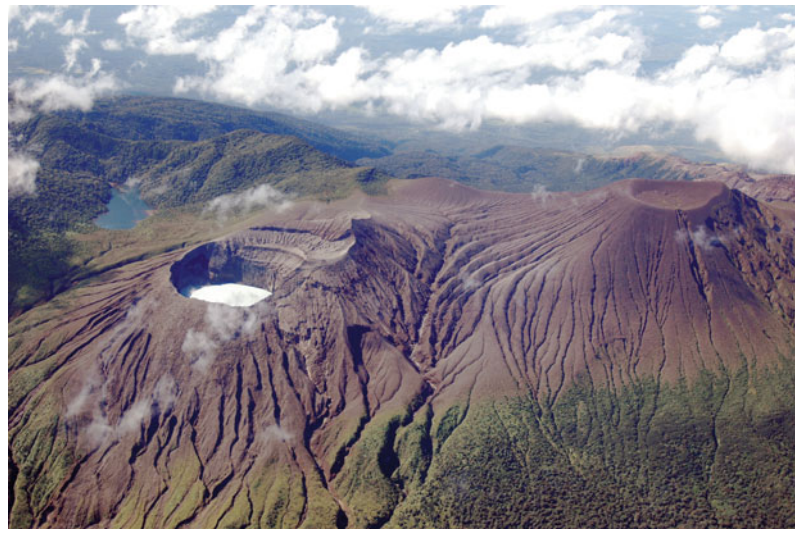

Fig. 1 View of Rincón de la Vieja volcanic complex, Costa Rica, showing the hyper-acid crater lake which is hosted in the Active Crater. Photo courtesy: OVSICORI, Costa Rica

2 Magmatic Gas Expansion and Hydrothermal Systems Inside Composite Volcanoes

Volcanic systems are defined by a history of eruption spaced by generally longer periods of repose. It is during the latter relatively quiescent stages that magmatic gases continue to discharge through solfatara on the summits and flanks of volcanoes and maintain much large scale hydrothermal systems in the core of the volcanic system (Henley 2015). This sustained flux of heat and reactive gases is responsible for rock alteration at the scale of the volcanic system and also for the more localized, intensely altered, regimes that are sometimes associated with hyper-acid lakes. These zones are a focus for flank failure and consequent events including volcanic eruptions.

2.1 Hydrodynamics at the Volcano Scale

Drilling for geothermal power and the exploration of major copper-gold resources that formed within ancient volcanoes (Henley and Ellis 1983) have provided a wide range of data that enable definition of the hydrothermal regimes and associated rock alteration inside active composite volcanoes. These systems are characterized by (i) a discrete conduit or 'chimney' of magmatic gas (Reyes et al. 1993) expanding through to high temperature fumaroles or equivalent acid lakes, and (ii) a plume of expanding magmatic gas, sustained by heat from continuing mid-crustal magmatism, that interacts with cool deep groundwater to produce the large scale, laterally extensive geothermal systems characteristic of composite volcanoes (Henley and McNabb 1978). Within a few kilometers beneath the rugged topographic surface of these systems, complexities arise due to the presence of perched groundwater systems inside the volcano superstructure, heterogeneities in the distribution of porosity, and fracture permeability and the consequent maintenance of single (gas) and two (vapor + liquid)-phase regimes.

The Karaha-Telaga Bodas magmatic-hydrothermal system associated with the active Galunggung volcano, Indonesia, has been extensively drilled and exemplifies these relations as well as the consequent distribution and evolution of alteration within these systems. Figure 2a shows the distribution of fumaroles, hot springs and drill holes across Galunggung in relation to the hyper-acid (pH $\sim$ 0.4) Telaga Bodas crater lake and the major collapse of the volcano's southeast flank, which generated a 170-km^2 debris avalanche deposit dated at

4,200 years b.p. (Moore et al. 2008). A detailed resistivity profile obtained for the upper 6 km region of Karaha-Telaga Bodas was interpreted in terms of the distribution of alteration assemblages as inferred from drill hole data (Fig. 2b). Temperatures encountered during drilling ranged up to 334 °C across the hydrothermal system, with higher temperatures (>353 °C) in drill holes close to the fumaroles beside the hyper-acid crater lake. Of particular note, is the projected pressure profile through the magmatic vapor chimney in relation to the development of a two-phase flow regime and its interaction with shallow groundwater and condensate to form the hyper-acid Telaga Bodas crater lake (Fig. 2c), which itself generates a regime of downward flowing acid sulfate water (Moore et al. 2004). Pressures and pressure profiles are complex but in conjunction with detailed mineralogical and fluid inclusion analyses, Moore et al. (2008) have provided a picture of discrete vapor-dominated flow zones, distal to the magmatic vapor chimney, and their evolution over 6,000 years, between the deep liquid phase geothermal system and shallower perched groundwater aquifers within the volcano (Fig. 2c).

2.2 Hydrology at the Acid Crater Lake Scale

The results of heat, mass and isotopic balance calculations for highly acid crater lakes (Hurst et al. 1991; Ohba et al. 1994, 2000; Rowe et al. 1995; Taran et al. 2008) confirm that they are smaller scale sub-systems within the much larger scale magmatic-hydrothermal system hosted by a volcano. These crater lakes are primarily the surface expression of the expansion and discharge of magmatic gas through to the surface and shallow interactions with its condensate and perched groundwater reservoirs. The expansion and buoyancy-directed upflow of SO_2-rich magmatic gas below such lakes is constrained by high permeability fractures (Henley and McNabb 1978; Lowell et al. 1993; Sanford et al. 1995; Berger and Henley 2011). Fractures also allow leakage from the lake through the crater floor, recirculation as dense acid waters within the subsurface main hydrothermal conduit and possibly their resurgence as springs on the flanks of the volcano. The downward and lateral dispersion of acid lake waters through structural fractures leads to rock alteration.

Evidence for the existence of lateral flows, through highly transmissive fractures, of acidic waters originating from summit crater lakes exist for several edifices. At Rincón de la Vieja, leakage from the acid lake was inferred to influence directly the chemistry of streams found on the north flank of the volcano (Kempter and Rowe 2000; Martínez et al. 2012). At Póas, Rowe et al. (1992, 1995) demonstrated a hydraulic connection between the crater lake and the Rio Agrio river on the north-east slope of the edifice. Tritium-based residence time estimates suggest that water flow from the summit crater of Poás to the Rio Agrio headwaters is hydrologically rapid (3–17 years). Similarly, the Upper Rio Agrio watershed draining the west flank of Copahue volcano, Argentina, is partly fed by a highly acid crater lake (Varekamp et al. 2001). The Ijen caldera is another example where very low-pH lake water exits a magma-hydrothermal crater lake system and feeds the Banyupahit river (Delmelle and Bernard 2000; Palmer 2009; van Hinsberg et al. 2010a). Variations in the permeability provided by fractures in the upper part of the Irazú volcanic hydrothermal system, Costa Rica, also probably explain the rapid volume changes experienced by the summit lake (Rouwet et al. 2010). The lake-hydrothermal system also feeds the Río Sucio, of which name reflects the brownish-orange color of its waters (Fig. 3).

2.3 Chemical Processes During Gas Expansion

The compositions of the hydrothermal fluids in volcano-related hydrothermal systems such as Karaha-Telaga Bodas are a consequence of the absorption of acidic magmatic gases into groundwater and subsequent pH-neutralization reactions that result in extensive rock alteration throughout the system (Henley and Ellis 1983).

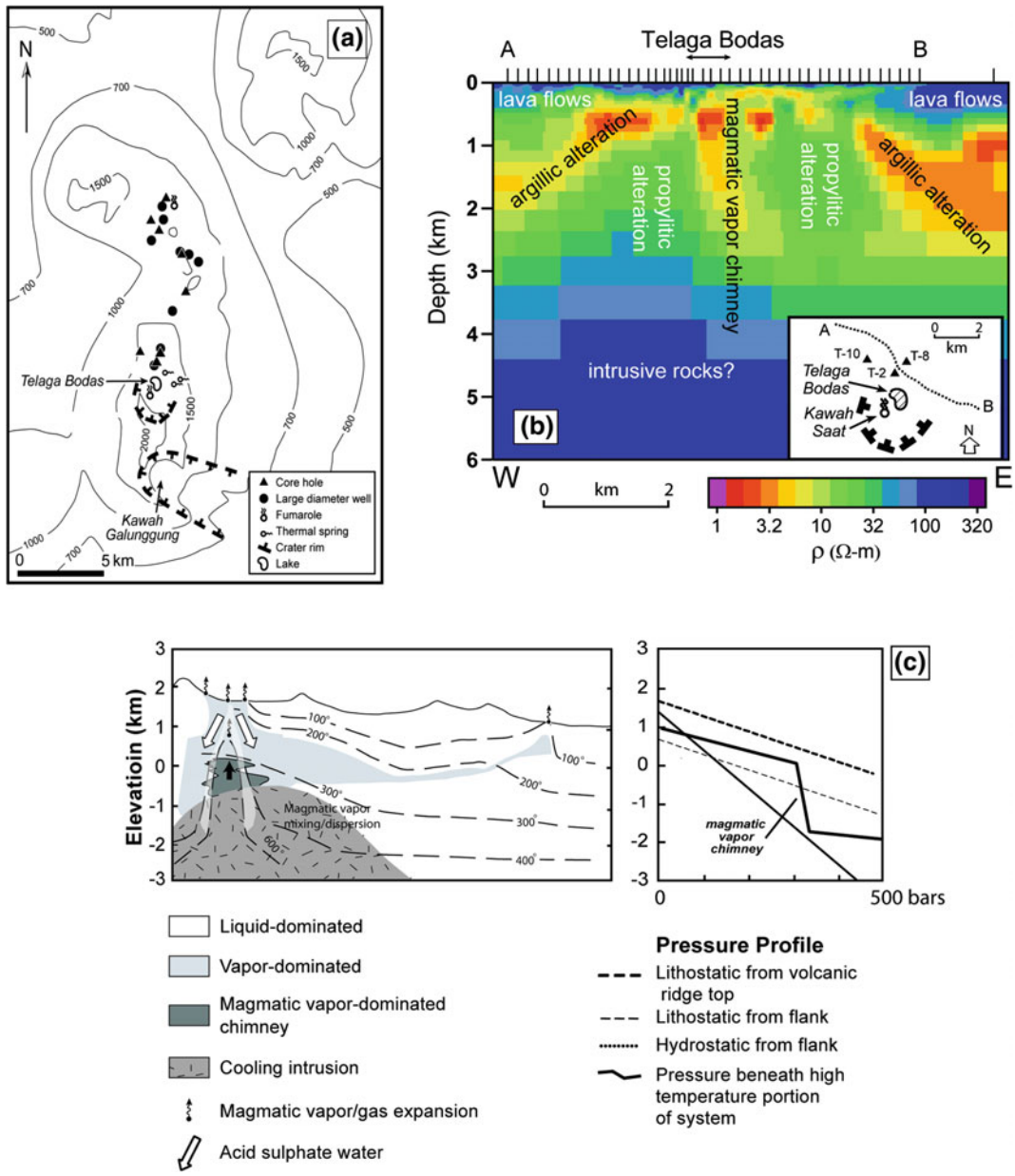

Fig. 2 Volcano-hosted hydrothermal system of Karaha-Telaga Bodas, Galunggung volcano, Indonesia. **a** Distribution of thermal features and drillholes. **b** Resistivity profile (see *inset*) showing the distribution of alteration assemblages relative to the magmatic chimney beneath Telaga-Bodas hyper-acid crater lake. **c** *Left* Generalized cross-section of the Karaha-Telaga Bodas hydrothermal system showing the magmatic vapor chimney and the surrounding, laterally extensive geothermal system; *Right* Simplified pressure profile through the magmatic vapor chimney. **a** and **b** are modified from Moore et al. (2008) and reproduced with permission of The American Journal of Science and the authors

The hydrodynamics of such large-scale magmatic-hydrothermal systems are directly related to the relative densities of liquid and vapor phases represented by the proxy system NaCl-H_2O (Henley and McNabb 1978). Low salinity gas released from crystallizing magma (M, Fig. 4a)

Fig. 3 The Río Sucio on Irazú volcano, Costa Rica. The *brownish-orange color* of the river reveals oxidation of dissolved iron originating from acid hydrothermal water inputs near the summit of the volcano. Photo courtesy: Dmitri Rouwet

expands buoyantly through available fractures into the deep groundwater regime beneath a volcano to form a single phase plume and may discharge directly at the surface, as discussed below, to form high temperature fumaroles, solfatara and acid lakes; i.e., the expressions of magmatic vapor chimneys. Flow interactions with groundwater on the margins of the gas plume results in a net decrease in enthalpy leading to a marginal two-phase regime that, with further mixing and dispersion of heat and solutes, forms large scale hydrothermal systems, such as Karaha-Telaga Bodas beneath Galunggung volcano. In volcanoes that occur in regions of very high rainfall, the expanding gas plume may intersect, and condense quantitatively into, substantial perched groundwater reservoirs, and become dispersed away from the edifice with little consequential alteration, obscuring the extent of on-going volcanism (Symonds et al. 2001; Hurwitz et al. 2003).

High temperature fumaroles at the summit of andesite-dacite volcanoes provide proxies of the single phase magmatic gas mixtures that feed into large scale hydrothermal systems. The compositions of these discharges are typically 85–95 mol% H_2O with a range of less abundant gases and a wide range of trace elements (Oppenheimer et al. 2011; Henley and Berger 2013). Carbon dioxide, SO_2 and H_2S are the next most abundant gases while volatile salt species, including (Na,K)Cl and HCl, generally make up less than about 1 mol% of the gas phase.

The complete condensation of a high temperature fumarole gas mixture results in a highly acidic liquid phase and consequent intense localized alteration of host rocks to kaolinite-alunite-silica assemblages typical of magmatic vapor chimney environments and crater lakes. For example, ignoring the formation of sulfur and intermediate oxidized sulfur species (Delmelle and Bernard 2015), it can be shown that condensation of a high temperature fumarole gas produces a sulfur-, chloride-rich liquid with pH < 0.5 (Delmelle and Bernard 1994). Evaporation of water from the surface of a hot acid lake increases solute concentrations; for the above example, condensation alone would give a lake water with $\sim$9,500 mg kg^{-1} chloride compared to the chloride concentration of Kawah Ijen, $\sim$23,000 mg kg^{-1}, and equivalently higher acidity (pH = 0.18). It is this acidity that drives intense hydrolysis of primary silicates in the host rock around volcanic gas vents (Henley and Berger 2011) and which is maintained by continuous heat and gas flow through the fracture system beneath a crater lake. Continuous input of

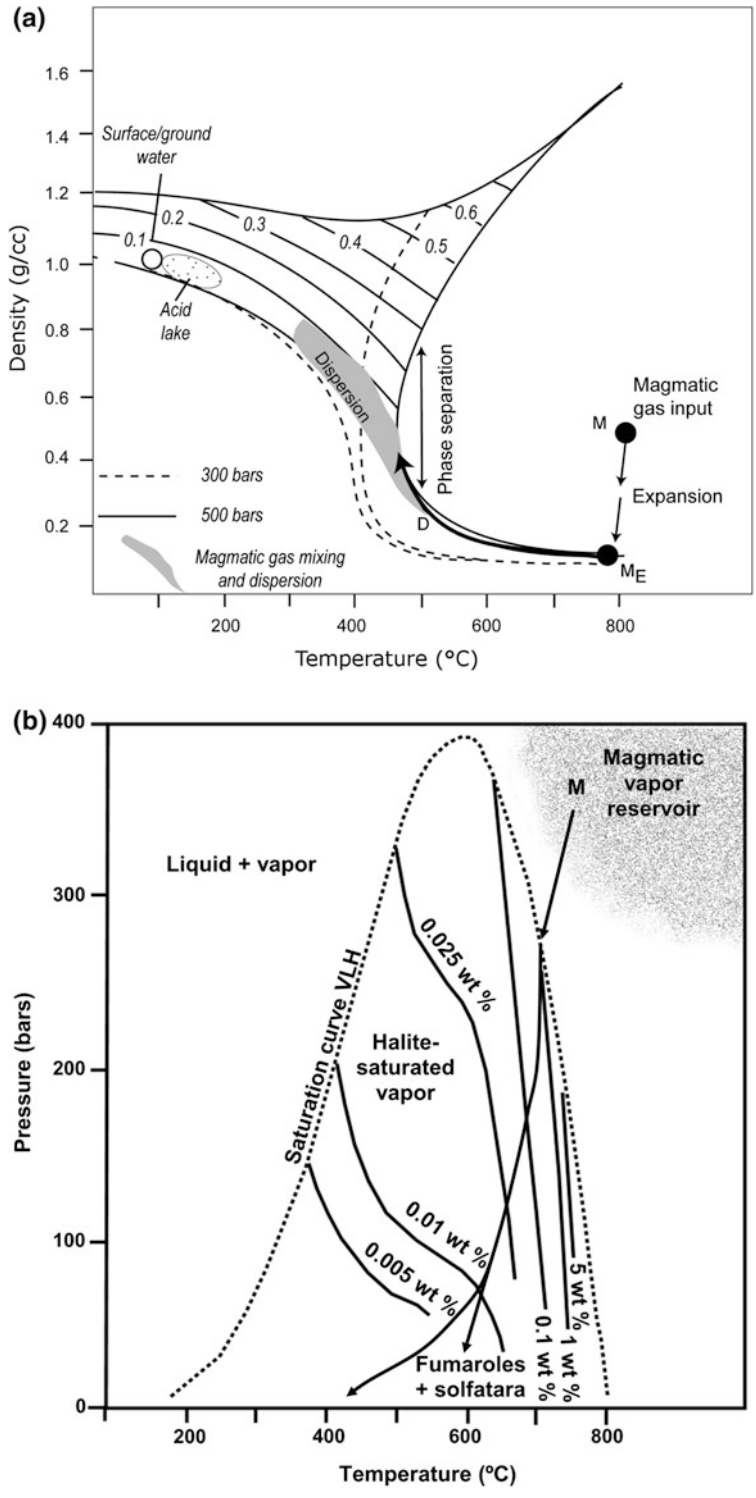

Fig. 4 **a** Density relations for liquid and vapor phase fluids in the system NaCl-H_2O, after Henley and McNabb (1978). A water-rich gas mixture released from the underlying magma system at lithostatic pressure is throttled via fractures to feed an overlying magmatic-hydrothermal system at M_E. Heat loss and mixing result in condensation of a small liquid fraction with strong partitioning of SO_2 into this liquid phase. Further expansion occurs beneath and into the base of a crater lake resulting in hyper-acidity and sulfur deposition. The pressure gradient in the expanding magmatic gas and two-phase regimes are close to vaporstatic and greater than that of the surrounding groundwater. **b** Phase diagram in the system NaCl-H_2O in relation to isenthalpic expansion of a magmatic gas. Reproduced and modified from Henley and Berger (2011) with permission of Ore Geology Reviews

SO_2 combined with surface evaporation is responsible for the elevated dissolved sulfate concentration of hyper-acid lakes. Accumulation of molten sulfur bodies and sulfur-rich lacustrine sediments in turn becomes prima facia evidence of the flux of pristine volcanic gas through vents.

The hydrology beneath crater lakes is necessarily complex because of the density-driven interactions between cooled lake water and upflowing gas expanding through available fractures (Fig. 4a). On a single fracture, fingers of dense hyper-acidic lake water mix and exchange heat with magmatic gas in sublake fracture arrays resulting in reflux of components into the buoyant vapor discharge into the lake. Figure 4b shows the phase relations for an expanding magmatic gas at low pressures in the upper few kilometers of a magmatic gas plume. Since a small temperature drop is associated with isenthalpic expansion, the overall buoyancy of the plume is preserved when a small liquid fraction condenses; this is a consequence of the conservation of the volumetric dominance of the low density vapor. Much of the SO_2 and HCl react directly with aluminosilicate minerals in host rocks with consequent intense alteration and development of anhydrite-sulfide veins; these are well exposed in large scale porphyry copper-gold deposits that formed beneath paleo-volcanoes (Henley and Berger 2013). Under low pressure conditions expansion of the primary magmatic gas occurs into the halite-vapor field without the formation of a liquid fraction. Sulfur dioxide released directly to the surface environment ultimately is adsorbed quantitatively into the lake water and is responsible, as shown above, for its hyper-acidity and the intensity of alteration of wall rocks and fracture arrays below and marginal to the lake where fluid leakage occurs on the flank of volcanoes.

3 Hydrothermal Alteration Inside Composite Volcanoes

The range of alteration minerals and their apparent temperatures of formation in magmatic hydrothermal systems associated with active composite volcanoes have been detailed based on geothermal drilling to 4,000 m (Reyes 1990). A prime example is the quiescent Alto Peak volcano (Reyes et al. 1993). These data emphasize the occurrence of narrow zones of intense clay-dominated, mostly kaolinite and dickite $\pm$ pyrophyllite assemblages due to leaching and alteration associated directly with magmatic gas expansion to depths of at least 2,500 m (Reyes 1991). Elemental sulfur and sulfate minerals, including natroalunite, alunite, jarosite and anhydrite, also typically form during interaction of the host rocks with hydrothermal acid sulfate waters (e.g., Stoffregen 1987; Moore et al. 2004). These alteration mineral assemblages contrast with the much lower intensity alteration due to weak, mainly carbonic acid and cation-exchange reactions (Henley et al. 1984) within liquid-dominated geothermal systems through which magmatic components are widely dispersed. In this latter regime, clay minerals range from smectites (<180 °C) through mixed layer illite-chlorite clays to illites and chlorites (>200 °C).

The alteration mineralogy beneath and around volcano-hosted acid crater lakes has been documented at Mt. Ruapehu, New Zealand, Kawah Ijen and Póas (Rowe and Brantley 1993; Delmelle and Bernard 1994; Wood 1994; Christenson et al. 2010; van Hinsberg et al. 2010b). In general, rocks directly in contact with the low pH sulfate-chloride lake waters that prevail in these environments are converted into a silica-enriched residual rock (Fig. 5), regardless of the primary mineralogy, bulk composition and texture. At Kawah Ijen, this material contains >85 wt% SiO_2 (Delmelle and Bernard 1994) and although silica is supersaturated in the lake waters, the silicified residue is believed to be formed solely by incongruent rock dissolution; i.e., addition of silica by precipitation is not involved (Delmelle and Bernard 1994; van den Boorn 2008). Gypsum is often found as a surface coating and infill of cracks in rocks which have been in contact with the acid lake waters, but the presence of this sulfate mineral seems to reflect the effect of evaporation on its saturation in the lake water (Delmelle and Bernard 1994; Christenson et al. 2010).

Fig. 5 Silicified rock retrieved from Kawah Ijen hyper-acid crater lake, Indonesia

Insights into rock alteration in the hydrothermal conduit connected to a lake come from examination of ejecta produced during phreato and phreatomagmatic eruptions. The ejected materials have often been reported to be highly vesicular, with vesicles/vugs partially to completely filled with hydrothermal alteration minerals consisting of assemblages of silica polymorphs (cristobalite and opal), gypsum, anhydrite, alunite, natroalunite, elemental sulfur and pyrite (Giggenbach 1974; Christenson and Wood 1993, 1994; Christenson et al. 2010; van Hinsberg et al. 2010b). At Mt. Ruapehu, rock ejecta sourced to deeper levels in the subsurface magma-hydrothermal system consisted of cristobalite, anhydrite, halite and magnetite. Rocks from an actively degassing fumarolic area adjoining Kawah Ijen hyper-acid crater lake were completely altered to homogeneous masses of amorphous silica (van Hinsberg et al. 2010b). Unsurprisingly, the alteration mineral assemblages found in the phreatomagmatic products from White Island, New Zealand, and Papandayan, Indonesia, two composite volcanoes with active magma-hydrothermal systems, exhibit similar alteration mineral assemblages as those described above (Wood 1994; Mazot et al. 2008).

The clay minerals (kaolinite-dickite + pyrophyllite) which are normally part of an advanced argillic alteration assemblages (Hemley et al. 1969; Stoffregen 1987) have been rarely observed in the materials erupted through acid crater lake systems. This may simply reflect the fact that the rocks brought to the surface during phreatomagmatic explosions were eroded from the main hydrothermal conduit where extremely low pH and high sulfur activity impede clay mineral formation. However, both kaolinite and pyrophyllite were found in ejected lake muds from Mt. Ruapehu (Wood 1994; Christenson et al. 2010). In common with other magmatic hydrothermal systems, pervasive argillic alteration probably forms an envelope at the periphery of the high upflow core that discharges magmatic gas condensates into summit crater lakes. The vertical and lateral extent of the silicified and advanced argillic alteration beneath acid crater lakes is not known, but studies of ancient volcano-hydrothermal systems provide some clues. At Mt. Shimokura, Japan, advanced argillic alteration was inferred to extend to nearly 2,000 m-depth, although it was not present in the first ~250 m (Ohba and Kitade 2005). Strongly hydrothermally altered rocks linked to shallow magma-hydrothermal activity at the summit of

Citlaltépetl volcano are exposed in a vertical extent of more than 675 m (Zimbelman et al. 2005).

4 Hydrothermal Alteration and Flank Instability at Composite Volcanoes

Many studies emphasize that the presence of large masses of hydrothermally altered rocks within a volcanic edifice may promote flank instability (López and Williams 1993; Scott et al. 1995; van Wyk de Vries and Francis 1997; Reid et al. 2001; John et al. 2008). Increased slope instability results from the development of lower rock shear strengths, which thereby provide sliding planes or surfaces for rupture. According to the Mohr-Coulomb failure criterion, slippage along any internal plane in the rock should occur when the shear stress along that plane reaches the critical value τ_c:

$$\tau_c = \mathrm{c} + \sigma_n \tan \phi \qquad (1)$$

where σ_n is the effective normal stress on the rupture plane in the rock, c the cohesive strength of the rock and ϕ the angle of internal friction of the sliding rock material (Jaeger and Cook 1976). Laboratory tests can simulate the material behavior at a maximum depth of ~100 m (i.e., σ_n = 2 MPa). However, sector and large flank collapses usually are sourced to deeper failure levels within the volcanic edifice. The non-linearity of Eq. (1) becomes apparent when higher pressure measurements are performed (e.g., see Figs. 32 and 33 in Voight et al. 2002). This reflects that ϕ decreases with depth, while c increases. Slippage condition can also be conveniently expressed by the factor of safety, F, i.e., the quotient of shear strength of the material and the shear stress required for static equilibrium (Voight et al. 2002). A value of F = 1 represents a condition of incipient failure, while higher values indicate stability. Thus, a decrease in rock shear strength due to hydrothermal alteration reduces F and can trigger failure. A similar effect is expected when shear increases due to transient seismicity or incremental loading of the edifice.

In their seminal work, Hubbert and Rubey (1959) emphasized the importance of considering pore fluid pressure, λ, in the assessment of slope stability. Day (1996) later expanded this idea in the volcanic context. These authors demonstrated that the critical angle of a slope, θ_c, necessary for sliding of a large 'wet' rock mass to occur on a slope flank depends on the pore fluid pressure, λ (expressed as a fraction of the lithostatic pressure) and the angle of internal friction, ϕ, of the sliding material according to:

$$\tan \theta_c = (1 - \lambda) \tan \phi \qquad (2)$$

In Eq. (2), c is assumed to be negligible, i.e., the cohesive strength on the slide surface is zero. This assumption is valid when failure involves a pre-existing fracture or immediately after fracture initiation and subsequent slippage (Hubbert and Rubey 1959; Day 1996).

The evolution of θ_c as a function of λ and ϕ is illustrated in Fig. 6. Clearly, the sustainability of a volcanic slope is strongly dictated by ϕ and hence, by the degree of alteration of the rock. This stems from the observation that altered rocks, in particular when clays dominate the alteration mineral assemblages, exhibit lower

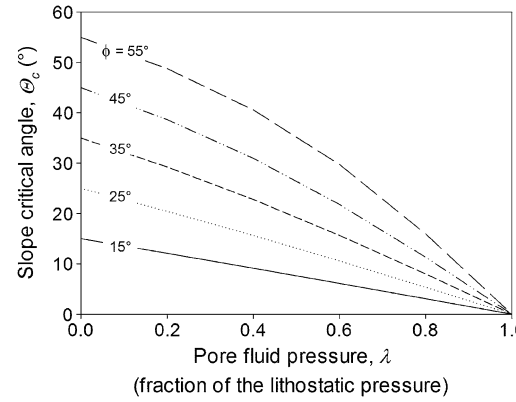

Fig. 6 Dependence of the critical angle of a slope, θ_c, on pore fluid pressure, λ (expressed as a fraction of the lithostatic pressure) for different values of the angle of friction, ϕ, of the sliding rock mass. See Sect. 4 for explanation

values of ϕ than the unaltered materials. Igneous rocks typically have ϕ in the range ~35–40° (Hoek and Bray 1977; Watters et al. 2000), but the hydrothermally altered rocks from Mount Rainier and Mount Hood, USA, displayed ϕ values as low as 24° (Watters et al. 2000). Similar low values were found for the advanced argillic altered rocks from the summit area of Citlaltépetl volcano (Zimbelman et al. 2004). At Teide stratovolcano, Tenerife, ϕ values in the range 16–33° were determined for alunite-, kaolinite-rich hydrothermally altered rocks collected from a fumarolic field (del Potro and Hurlimann 2009). Even lower ϕ measurements (3–14°) were reported for a clay-rich material entrained in the avalanche debris produced by the 26 December 1997 sector collapse at Soufrière Hills volcano, Montserrat (Voight et al. 2002). Interestingly, the altered rocks from Teide which contain kaolinite had lower ϕ values than the ones where alunite dominated (ϕ = 16–25° and 27–33°, respectively; del Potro and Hurlimann 2009). This may suggest that the type, rather than the degree or amount, of alteration governs ϕ. It should also be noted that altered rocks that still contain crystals are likely to have higher ϕ values than altered aphyric rocks with similar bulk clay content (Hoek and Bray 1977).

Figure 6 also highlights the impact of λ on θ_c for a given degree of rock alteration, i.e., a prescribed value of ϕ. The development of high pore fluid pressures within the upper part of the host edifice in response to gas flow, or to the other mechanisms, will depend strongly on the permeability of the rocks (Day 1996; Reid 2004) and therefore, is also tied to the intensity of rock alteration. The variety of materials (lava, pyroclasts, debris avalanche/flow deposits, etc.) that comprise the volcano leads to a highly heterogeneous permeability field in the subsurface. Mean permeability values ranging between 10^{-11} and 10^{-16} m^2 are reported for hydrothermal systems (Lowell et al. 1993) and references therein. However, the formation of clay minerals and deposition of silica during alteration can result in gradual closing of fracture permeability (e.g., Berger and Henley 2011; Lowell et al. 1993). In addition to clay and silica deposition, precipitates of elemental sulfur and sulfate minerals can also play a role in the development of self-sealed fractures. For example, Christenson et al. (2010) showed that the hydrothermal vent beneath Mt. Ruapehu's crater lake can be chocked by elemental sulfur and alunite. A recent geophysical survey of the summit area of Kawah Ijen volcano also revealed that the shallow magma-hydrothermal system effectively sealed itself within the upper volcanic edifice (Mauri 2010), possibly a consequence of the same alteration/deposition mechanisms. Further, lateral transport of acidic steam-heated waters at shallow level along the upper volcano slopes can produce layers of clayey materials which form a low-permeability carapace within the flanks of the edifice (Moore et al. 2004, 2008). Such a low permeability carapace can enclose the expanding magmatic gas plume in the core of the volcano and allows the development of elevated pore fluid pressure throughout the edifice.

Day (1996) argued that the rapid or gradual development of high λ within the materials of a volcano is the primary factor leading to slope failure. The pressurization of faults, joints and more permeable layers within the volcanic edifice allows shear rupture to occur at lower stress differences than was possible previously. A variety of mechanisms can produce elevated values of, and large increase in, λ values within a volcano. These relate to the thermal and mechanical effects of shallow or deep magmatic intrusions, intrusion degassing, discharges of highly pressurized fluids from depth and deformation associated with faulting (Day 1996; Reid 2004).

From the above considerations, one can see that the permeability of rocks within a volcano-hosted magma-hydrothermal system changes over time and space due to the interplay of mineral deposition and dissolution and rock hydrofracturing processes (Lowell et al. 1993; Day 1996; Reid et al. 2010). Hence, λ and ϕ are coupled in altered rocks. Therefore, the risk of volcanic slope failure, as simply expressed by Eq. (2), appears to be strongly determined by the extent of alteration, consequent on magmatic SO_2 (and HCl) flux through the volcano. Based

on these concepts and using high resolution airborne magnetic and electromagnetic data (Finn et al. 2001) at Mt. Rainier volcano, USA, Reid et al. (2001) performed a three-dimensional analyses of the edifice stability and concluded that '… flank collapse (>0.1 km^3) is promoted by voluminous, weak, hydrothermally altered rock situated high on steep slopes'. The large masses of highly altered rocks were inferred to have thicknesses greater than 200 m and some considerably thicker, and increase where these rocks are exposed on the flank of the volcano. Similarly, potential failure volumes at Citlaltéptel volcano, Mexico, were estimated to range between 0.04–0.5 km^3 (Zimbelman et al. 2004).

Alteration scenarios similar to Mt Rainier occur in other volcanoes and are implicated in their flank collapse histories (e.g., Nevado del Ruíz, Columbia; López and Williams 1993). In some cases volcanic landslides may be tied to extreme weather events (e.g., Casita, Nicaragua; Scott et al. 2005) as well as to seismicity, and environmental changes. These second order processes show that the variation of risk level with respect to mechanical slope rupture during the life of a volcano is related to small perturbations including renewed magmatic activity and related changes in internal gas pressure (e.g., Newhall et al. 2001). In other words, θ_c represents a critical phase state subject to rapid and catastrophic changes due to small perturbations (Lighthill 1986). Roughly translated, flank collapse may be predicable within limits but catastrophic failure may be triggered by very small independent 'Black Swan' events such as monsoon conditions or stress perturbations due to distant earthquakes in a manner not dissimilar to modern financial markets (Taleb 2010).

5 Kawah Ijen Volcano Case Study

Kawah Ijen is a ~700 m high volcanic cone built on the western flank of Gunung Merapi volcano (elevation ~2,799 m above sea level), inside the Ijen caldera rim. It consists of alternating layers of ash, scoria and lava flow deposits representing basalt to andesitic compositions. Kawah Ijen hosts a $\sim 3.0 \times 10^7$ m^3 lake of hyper-acid water (pH < 0.5) from which leakage occurs into local drainage systems including the Banyupahit river (Delmelle and Bernard 2000; Delmelle et al. 2000; Takano et al. 2004; Mauri 2010). The onset of lake development is unknown but historical reports indicate its existence in 1789 (Hengeveld 1920).

Figure 7 is a topographic profile through the volcanic complex; key features with regard to the risk of flank collapse are the rugged topography and steep slopes, and the presence of an active magma at depths of a minimum of 400 m below the lake (Mauri 2010). High temperature magmatic gas sources both the summit crater lake and associated fumaroles. A magmatic gas flow regime develops beneath the lake as a consequence of the larger scale heat and mass transfer through the volcanic complex (Fig. 7). Vapor volumetrically dominates pressure in this sub-lake regime and flow and counter-flow of acid condensate occurs as discussed above as a result of the density differential of the two phases. It is leakage from the plume that sustains gaseous SO_2 (and HCl) flows into the lake and consequent hyper-acidity and sulfur accumulation. This relationship implies pressure steps in the hydrologic profile similar to those defined by drilling at the Karaha-Telega-Bodas volcanic complex (Sect. 2.1). In order to develop a first order model of the hydrology of this magmatic hydrothermal system, we note that there is a pressure balance between expanding magmatic gas and the perched acidic lake. The latter is related to a groundwater flow regime through Gunung Merapi and the slopes below Kawah Ijen.

Leakages through the flanks of the acid lake inevitably build a substantial body of highly altered rock within the upper part of the volcano. Here alteration grades outward from a simple unconsolidated assemblage of silica and alunite to progressively less altered kaolinitic assemblages localized by fractures (Sect. 3). It has been proposed that the formation of silicified rocks due to intense leaching and dissolution beneath hyper-acid crater lakes weakens the interior of the volcano, increasing the risk of flank sliding

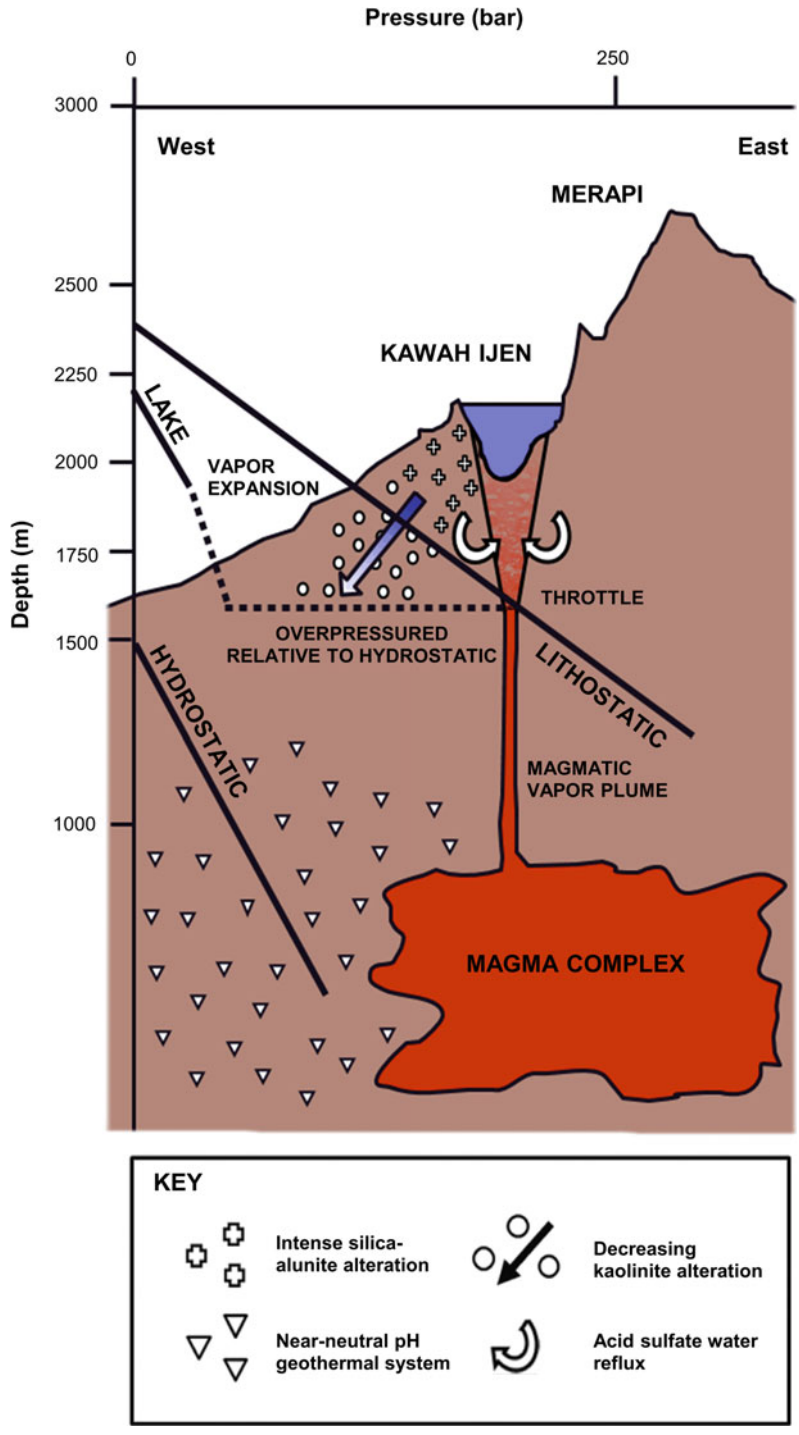

Fig. 7 Simple model of the pressure profile through Kawah Ijen volcano. See Sect. 5 for explanation

(Rowe et al. 1992, 1995; Varekamp et al. 2001). Contradicting this hypothesis, strength tests show that silicified rocks are strong (Watters et al. 2000) and therefore promote stability rather than instability. However, Berger and Henley (2011) and Henley and Berger (2011) have shown that

silicification occurs progressively so that at inception clay and poorly crystallized or amorphous silica occur in the evolving alteration assemblage, only much later recrystallizing to a silicified state. Therefore, it is the unconsolidated silica-clay-filled fractures which probably define potential zones of flank failure (Sect. 4). A large landslide generated by this instability would first lead to catastrophic drainage of the Ijen lake with the formation of highly corrosive and devastating debris flows. The pressure release which would ensue could trigger a phreatic eruption, which in turn could destabilize the western flank of Gunung Merapi (e.g., the 1888 eruption of Bandai-san, Siebert 1984). Ultimately, such cascade of events could produce a major phreato-magmatic eruption.

6 Summary

Volcanic edifices are inevitably unstable due to their growth by tephra accumulation and lava flow. Flank stabilities are maintained in a critical state balanced between growth and slope failure. The relative risk of landslide is heightened in volcanoes which host an active magma-hydrothermal system primarily because of the fracture-focused and time-integrated flux of acidic gases (SO_2 and HCl) as they expand from a magmatic source to the surface with the formation of low pH condensate. These are focused in the flanks and summits of active volcanoes where topographic evolution results in the formation of acid or hyper-acid crater lakes and associated solfatara. Localization of intense silica-clay alteration in these focal regimes produces critical instabilities due to heterogeneous distribution of rock strength properties and pore fluid pressures—a coupled relationship between the flux of acidic gases and permeability in the system.

Such instabilities are easily perturbed by changes in pore fluid pressure due to increased internal permeability consequent on progressive changes in internal stress, or to blockage of fracture permeability by rock alteration, inside the volcanic edifice. Transient fluctuations also occur due to seismicity or enhanced groundwater infiltration associated with extreme weather events. The generation of instabilities in such volcanic systems is a major source of risk and includes simple topographic collapses that change the groundwater regime relative to pressure within the magmatic vapor plume or local vapor-rich zones, and crater lakes as sources of extreme hyper-acidic attack on the host rock sequence. Each of these second order sources of risk has the potential to trigger extreme events due to cascades of energy release; thus reduction of confining pressure due to surficial slip and catastrophic release of acid lake water (resulting in a hot acidic debris flow), in turn releases pressure on the underlying magmatic system that may then trigger a Plinian eruption as large as Mt St Helens in 1980 (Vinciguerra et al. 2005) and Mt Pinatubo in 1991 (Newhall et al. 2002).

Acknowledgments This work was supported by the Belgian Fonds de la Recherche Scientifique (FNRS) MIS-Ulysse grant F.6001.11 to P.D., Postdoctoral Researcher grant 1.7.048.09.F to S.O. and Doctoral studentship to M. D. R.W.H. thanks the Australian Research Council for continued support of studies of magmatic hydrothermal systems. J. Moore kindly provided original graphics for the Telega-Bodas hydrothermal system and constructive comments on an early draft of this chapter. We are very grateful to P. Ayris for producing some of the diagrams. We thank R. del Potro for his critical and useful comments in review.

References

Belousov A, Belousova M, Voight B (1999) Multiple edifice failures, debris avalanches and associated eruptions in the Holocene history of Shiveluch volcano, Kamchatka, Russia. Bull Volcanol 61 (5):324–342

Berger BR, Henley RW (2011) Magmatic-vapor expansion and the formation of high-sulfidation gold deposits: structural controls on hydrothermal alteration and ore mineralization. Ore Geol Rev 39(1–2):75–90

Capra L, Macías JL, Scott KM, Abrams M, Garduño-Monroy VH (2002) Debris avalanches and debris flows transformed from collapses in the Trans-Mexican Volcanic Belt, Mexico—behavior, and implications for hazard assessment. J Volcanol Geotherm Res 113(1–2):81–110

Carrasco-Núñez G, Vallance JW, Rose WI (1993) A voluminous avalanche-induced lahar from Citlaltépetl volcano, Mexico—implications for hazard assessment. J Volcanol Geotherm Res 59(1–2):35–46

Carrasco-Núñez G, Siebert L, Capra L (2011) Hazards from volcanic avalanches. In: Veress B, Szigethy J (eds) Horizons in Earth Science Research, Nova, p 199–227

Christenson BW, Wood CP (1993) Evolution of a vent-hosted hydrothermal system beneath Ruapehu crater lake, New Zealand. Bull Volcanol 55(8):547–565

Christenson BW, Reyes AG, Young R, Moebis A, Sherburn S, Cole-Baker J, Britten K (2010) Cyclic processes and factors leading to phreatic eruption events: insights from the 25 September 2007 eruption through Ruapehu crater lake, New Zealand. J Volcanol Geotherm Res 191(1–2):15–32

Day SJ (1996) Hydrothermal pore fluid pressure and the stability of porous, permeable volcanoes. In: McGuire WJ, Jones AP, Neuberg J (eds) Volcano instability on the Earth and other planets. Geological Society, Special Publications, London, pp 77–93

del Potro R, Hurlimann M (2009) The decrease in the shear strength of volcanic materials with argillic hydrothermal alteration, insights from the summit region of Teide stratovolcano, Tenerife. Eng Geol 104 (1–2):135–143

Delmelle P, Bernard A (1994) Geochemistry, mineralogy and chemical modeling of the acid crater lake of Kawah Ijen Volcano, Indonesia. Geochim Cosmochim Acta 58(11):2445–2460

Delmelle P, Bernard A (2000) Downstream composition changes of acidic volcanic waters discharged into the Banyupahit stream, Ijen caldera, Indonesia. J Volcanol Geotherm Res 97(1–4):55–75

Delmelle P, Bernard A (2015) The remarkable chemistry of sulfur in volcanic acid crater lakes: a scientific tribute to Bokuichiro Takano and Minoru Kusakabe. This volume

Delmelle P, Bernard A, Kusakabe M, Fischer TP, Takano B (2000) Geochemistry of the magmatic–hydrothermal system of Kawah Ijen volcano, East Java, Indonesia. J Volcanol Geotherm Res 97(1–4):31–53

Finn CA, Sisson TW, Deszcz-Pan M (2001) Aerogeophysical measurements of collapse-prone hydrothermally altered zones at Mount Rainier volcano. Nature 409(6820):600–603

Giggenbach WF (1974) The chemistry of crater lake, Mt Ruapehu (New Zealand) during and after the 1971 active period. NZJ Sci 17:33–45

Hemley JJ, Hostetle PB, Gude AJ, Mountjoy WT (1969) Some stability relations of alunite. Econ Geol 64 (6):599–612

Hengeveld GJN (1920) De mogelijkheid en de plaats van den bouw van een nieuwe sluis bij het kratermeer Kawah Idjen. Mededelingen en rapporten van het departement der burgelijke openbare werken; Geologische onderzoekingen ten behoeve van's lands waterstaat-, gewestelijke- en gemeentewerken in Nederlandsch-Indie. Weltevreden:93–118

Henley RW (2015) Hyperacidic volcanic lakes, metal sinks and continuous gas streaming in arc volcanoes. This volume

Henley RW, Berger BR (2011) Magmatic-vapor expansion and the formation of high-sulfidation gold deposits: chemical controls on alteration and mineralization. Ore Geol Rev 39(1–2):63–74

Henley RW, Berger BR (2013) Nature's refineries: metals and metalloids in arc volcanoes. Earth Sci Rev 125:146–170

Henley RW, Ellis AJ (1983) Geothermal systems, ancient and modern: a geochemical review. Earth Sci Rev 19:1–50

Henley RW, McNabb A (1978) Magmatic vapor plumes and groundwater interaction in porphyry copper emplacement. Econ Geol 73(1):1–20

Henley RW, Truesdell AH, Barton PB, Whitney JA (1984) Fluid-mineral equilibria in hydrothermal systems. In: Roberston JM (ed) Reviews in Economic Geology. Society of Economic Geologists, Socorro

Hoek E, Bray JW (1977) Rock slope engineering. The Institution of Mining and Metallurgy, Taylor & Francis, London

Hubbert MK, Rubey WW (1959) Role of fluid pressure in mechanics of overthrust faulting. I. Mechanics of fluid-filled porous solids and its application to overthrust faulting. Geol Soc Am Bull 70(2):115–166

Hurst AW, Bibby HM, Scott BJ, McGuinness MJ (1991) The heat source of Ruapehu crater lake; deductions from the energy and mass balances. J Volcanol Geotherm Res 46:1–20

Hurwitz S, Kipp KL, Ingebritsen SE, Reid ME (2003) Groundwater flow, heat transport, and water table position within volcanic edifices: implications for volcanic processes in the Cascade Range. J Geophys Res Solid Earth 108(B12):2557. doi:10.1029/2003JB002565

Ingebritsen SE, Mariner RH (2010) Hydrothermal heat discharge in the Cascade Range, northwestern United States. J Volcanol Geotherm Res 196(3–4):208–218

Jaeger JC, Cook NGW (1976) Fundamentals of rock mechanics. Science paperbacks

John DA, Sisson TW, Breit GN, Rye RO, Vallance JW (2008) Characteristics, extent and origin of hydrothermal alteration at Mount Rainier Volcano, Cascades Arc, USA: implications for debris-flow hazards and mineral deposits. J Volcanol Geotherm Res 175(3):289–314

Kempter KA, Rowe GL (2000) Leakage of Active crater lake brine through the north flank at Rincon de la Vieja volcano, northwest Costa Rica, and implications for crater collapse. J Volcanol Geotherm Res 97(1–4): 143–159

Lighthill J (1986) The recently recognized failure of predictability in newtonian dynamics. Proc Roy Soc Lond Ser Math Phys Eng Sci 407(1832):35–50

López DL, Williams SN (1993) Catastrophic volcanic collapse—relation to hydrothermal processes. Science 260(5115):1794–1796

Lowell RP, Vancappellen P, Germanovich LN (1993) Silica precipitation in fractures and the evolution of permeability in hydrothermal upflow zones. Science 260(5105):192–194

Martínez M, Fernández E, Sáenz W, van Bergen MJ, Ayres G, Pacheco JF, Brenes J, Avard G, Malavassi E (2012) Connections between hyper-acid crater lakes and flank springs: new evidence from Rincón de la Vieja volcano (Costa Rica). EGU General Assembly 2012, Vienna

Mauri G (2010) Multi-scale analysis of multiparameter geophysical and geochemical data from active volcanic systems, PhD thesis, Simon Fraser University, Vancouver

Mazot A, Bernard A, Fischer T, Inguaggiato S, Sutawidjaja IS (2008) Chemical evolution of thermal waters and changes in the hydrothermal system of Papandayan volcano (West Java, Indonesia) after the November 2002 eruption. J Volcanol Geotherm Res 178(2):276–286

McGuire WJ (2003) Volcano instability and lateral collapse. Revista 1:33–45

Moore JN, Christenson BW, Allis RG, Browne PRL, Lutz SJ (2004) The mineralogical consequences and behavior of descending acid-sulfate waters: an example from the Karaha—Telaga Bodas geothermal system, Indonesia. Can Mineral 42:1483–1499

Moore JN, Allis RG, Nemcok M, Powell TS, Bruton CJ, Wannamaker PE, Raharjo IB, Norman DI (2008) The evolution of volcano-hosted geothermal systems based on deep wells from Karaha-Telaga Bodas, Indonesia. Am J Sci 308(1):1–48

Newhall CG, Albano SE, Matsumoto N, Sandoval T (2001) Roles of groundwater in volcanic unrest. J Geol Soc Philippines 56:69–84

Newhall CG, Power JA, Punongbayan RS (2002) Pinatubo eruption—"to make grow". Science 295 (5558):1241–1242

Norini G, Lagmay AMF (2005) Deformed symmetrical volcanoes. Geology 33(7):605–608

Ohba T, Kitade Y (2005) Subvolcanic hydrothermal systems: implications from hydrothermal minerals in hydrovolcanic ash. J Volcanol Geotherm Res 145 (3–4):249–262

Ohba T, Hirabayashi JI, Nogami K (1994) Water, heat and chloride budget of the crater lake Yugama at Kusatsu-Shirane volcano, Japan. Geochem J 28:217–231

Ohba T, Hirabayashi J, Nogami K (2000) D/H and O-18/O-16 ratios of water in the crater lake at Kusatsu-Shirane volcano, Japan. J Volcanol Geotherm Res 97 (1–4):329–346

Oppenheimer C, Scaillet B, Martin RS (2011) Sulfur degassing from volcanoes: source conditions, surveillance, plume Chemistry and Earth system impacts. Rev Mineral Geochem 73(1):363–421

Palmer SCJ (2009) Hydrogeochemistry of the upper Banyu Pahit River valley, Kawah Ijen volcano, Indonesia, MSc thesis, McGill University, Montreal

Reid ME (2004) Massive collapse of volcano edifices triggered by hydrothermal pressurization. Geology 32 (5):373–376

Reid ME, Sisson TW, Brien DL (2001) Volcano collapse promoted by hydrothermal alteration and edifice shape, Mount Rainier, Washington. Geology 29(9):779–782

Reid ME, Keith TEC, Kayen RE, Iverson NR, Iverson RM, Brien DL (2010) Volcano collapse promoted by progressive strength reduction: new data from Mount St. Helens. Bull Volcanol 72(6):761–766

Reyes AG (1990) Petrology of Philippine geothermal systems and the application of alteration mineralogy to their assessment. J Volcanol Geotherm Res 43(1–4):279–309

Reyes AG (1991) Mineralogy, distribution and origin of acid alteration in Philippine geothermal systems. Geological Survey of Japan Report, Tsukuba

Reyes AG, Giggenbach WF, Saleras JRM, Salonga ND, Vergara MC (1993) Petrology and geochemistry of Alto Peak, a vapor-cored hydrothermal system, Leyte Province, Philippines. Geothermics 22:479–519

Rouwet D, Mora-Amador RA, Ramírez-Umaña CJ, González G (2010) Seepage of "aggressive" fluids reduce volcano flank stability: the Irazú and Turrialba case, Costa Rica. IAVCEI commission on volcanic lakes 7 workshop, Costa Rica

Rowe GL, Brantley SL (1993) Estimation of the dissolution rates of andesitic glass, plagioclase and pyroxene in a flank aquifer of Poás Volcano, Costa Rica. Chem Geol 105(1–3):71–87

Rowe GL, Brantley SL, Fernández M, Fernández JF, Barquero J, Borgia A (1992) Fluid-volcano interaction in an active stratovolcano: the crater lake system of Poás volcano, Costa-Rica. J Volcanol Geotherm Res 49:23–51

Rowe GL, Brantley SL, Fernández M, Borgia A (1995) The chemical and hydrologic structure of Poás Volcano, Costa Rica. J Volcanol Geotherm Res 64 (3–4):233–270

Sanford WE, Konikow LF, Rowe GL, Brantley SL (1995) Groundwater transport of crater-lake brine at Poás volcano, Costa Rica. J Volcanol Geotherm Res 64(3–4):269–293

Scott KM, Vallance JW, Pringle PT (1995) Sedimentology, behavior, and hazards of debris flows at Mount Rainier. USGS Professional Paper, Washington 1547

Scott KM, Vallance JW, Kerle N, Macias JL, Strauch W, Devoli G (2005) Catastrophic precipitation-triggered lahar at Casita volcano, Nicaragua: occurrence, bulking and transformation. Earth Surf Proc Land 30 (1):59–79

Shea T, van Wyk de Vries B (2010) Collapsing volcanoes: the sleeping giants' threat. Geol Today 26 (2):72–77

Siebert L (1984) Large volcanic debris avalanches—characteristics of source areas, deposits, and associated eruptions. J Volcanol Geotherm Res 22(3–4):163–197

Siebert L, Glicken H, Ui T (1987) Volcanic hazards from Bezymianny- and Bandaï-type eruptions. Bull Volcanol 49:435–459

Stoffregen R (1987) Genesis of acid-sulfate alteration and Au-Cu-Ag mineralization at Summitville, Colorado. Econom Geol 82(6):1575–1591

Symonds RB, Gerlach TM, Reed MH (2001) Magmatic gas scrubbing: implications for volcano monitoring. J Volcanol Geotherm Res 108(1–4):303–341

Takano B, Suzuki K, Sugimori K, Ohba T, Fazlullin SM, Bernard A, Sumarti S, Sukhyar R, Hirabayashi M (2004) Bathymetric and geochemical investigation of Kawah Ijen crater lake, East Java, Indonesia. J Volcanol Geotherm Res 135(4):299–329

Taleb NN (2010) The black swan: the impact of the highly improbable. Random house trade paperbacks

Taran Y, Rouwet D, Inguaggiato S, Aiuppa A (2008) Major and trace element geochemistry of neutral and acidic thermal springs at El Chichón volcano, Mexico implications for monitoring of the volcanic activity. J Volcanol Geotherm Res 178(2): 224–236

Ui T, Yamamoto H, Suzukikamata K (1986) Characterization of debris avalanche deposits in Japan. J Volcanol Geotherm Res 29(1–4):231–243

Vallance JW, Scott KM (1997) The Osceola Mudflow from Mount Rainier: sedimentology and hazard implications of a huge clay-rich debris flow. Geol Soc Am Bull 109(2):143–163

Vallance JW, Siebert L, Rose WI, Giron JR, Banks NG (1995) Edifice collapse and related hazards in Guatemala. J Volcanol Geotherm Res 66(1–4):337–355

van den Boorn SHJM (2008) Silicon isotopes and the origin of Archaean cherts, PhD thesis, University of Utrecht, Utrecht

van Hinsberg V, Berlo K, Sumarti S, van Bergen M, Williams-Jones A (2010a) Extreme alteration by hyperacidic brines at Kawah Ijen volcano, East Java, Indonesia: II metasomatic imprint and element fluxes. J Volcanol Geotherm Res 196(3–4):169–184

van Hinsberg V, Berlo K, van Bergen M, Williams-Jones A (2010b) Extreme alteration by hyperacidic brines at Kawah ben volcano, East Java, Indonesia I Textural and mineralogical imprint. J Volcanol Geotherm Res 198(1–2):253–263

van Wyk de Vries B, Francis PW (1997) Catastrophic collapse at stratovolcanoes induced by gradual volcano spreading. Nature 387(6631):387–390

Varekamp JC, Ouimette AP, Herman SW, Bermúdez A, Delpino D (2001) Hydrothermal element fluxes from Copahue, Argentina: a "beehive" volcano in turmoil. Geology 29(11):1059–1062

Vinciguerra S, Elsworth D, Malone S (2005) The 1980 pressure response and flank failure of Mount St. Helens (USA) inferred from seismic scaling exponents. J Volcanol Geotherm Res 144:155–168

Voight B, Komorowski J-C, Norton GE, Belousov AB, Belousova MG, Boudon G, Fransis PW, Franz W, Heinrich P, Sparks RSJ, Young SR (2002) The 26 December (boxing day) 1997 sector collapse and debris avalanche at Soufrière Hills Volcano, Montserrat. In: Druitt TH, Kokelaar BP (eds) The eruption of Soufrière Hills Volcano, Montserrat, from 1995 to 1999. Memoirs, Geological Society, London, pp 363–407

Watters RJ, Zimbelman DR, Bowman SD, Crowley JK (2000) Rock mass strength assessment and significance to edifice stability, Mount Rainier and Mount Hood, cascade range volcanoes. Pure Appl Geophys 157(6–8):957–976

Witham CS (2005) Volcanic disasters and incidents: a new database. J Volcanol Geotherm Res 148(3–4):191

Wood CP (1994) Mineralogy at the magma-hydrothermal system interface in andesite volcanoes, New Zealand. Geology 22(1):75–78

Zimbelman DR, Watters RJ, Firth IR, Breit GN, Carrasco-Núñez G (2004) Stratovolcano stability assessment methods and results from Citlaltepetl, Mexico. Bull Volcanol 66(1):66–79

Zimbelman DR, Rye RO, Breit GN (2005) Origin of secondary sulfate minerals on active andesitic stratovolcanoes. Chem Geol 215(1–4):37–60

Crater Lake Energy and Mass Balance

Tony Hurst, Takeshi Hashimoto, and Akihiko Terada

Abstract

The volume and temperature of a Crater Lake in an active volcano depends on the balance between the input of volcanic fluids and gases, with their thermal energy, and the evaporation and other processes by which the lake loses energy. The general situation is that we can measure the bulk properties of the lake, and want to determine the mass and energy that is entering the bottom of the lake from the volcano. This chapter describes the processes likely to be significantly affecting such a lake, and how to estimate their effect. Evaporation is the dominant cooling process for hot lakes, and we compare proposed equations to select those most suitable for the volcanic lake situation. Several case studies are included to show how heat and energy balance calculations can be used in actual situations.

Keywords

Crater Lake · Energy balance · Mass balance · Water/steam input · Radiation · Evaporation · Ruapehu · Yudamari · Boiling Lake

1 Introduction

A substantial fraction of the craters produced by volcanic eruptions fill with water to form a Crater Lake, especially in areas with humid climates. This chapter will discuss the situation if this occurs while the volcano is still active, and the lake is significantly heated by the volcanic activity. The temperature of such a lake then provides an indication of the energy input from the volcano below, and this is often one of the best indications of the state of the volcano and the current hazard from it.

T. Hurst (✉)
Institute of Geological and Nuclear Sciences,
Lower Hutt, New Zealand
e-mail: t.hurst@gns.cri.nz

T. Hashimoto
Institute of Seismology and Volcanology,
Faculty of Science, Hokkaido University,
Sapporo, Japan

A. Terada
Volcanic Fluid Research center,
Tokyo University of Technology, Gunma, Japan

D. Rouwet et al. (eds.), *Volcanic Lakes*, Advances in Volcanology,
DOI 10.1007/978-3-642-36833-2_13,
© Springer-Verlag Berlin Heidelberg 2015

Hot Crater Lakes, the kind being considered here, are heated by the input of steam (the gas phase of water) and hot liquid water. The large amount of heat released by the condensation of steam, shown by its high enthalpy (heat content per unit mass) means that this is usually the main energy source. Hot gases entering the lake also contribute heat. Solar radiation heats Crater Lakes, just like any other water body.

Three main processes tend to cool Crater Lakes. The hotter they are, the more water will evaporate. Evaporation reduces the energy in the lake, as well as the volume. Because of the latent heat transferred to the atmosphere in the evaporation process, this tends to lower the lake temperature, as does the second process, the heating of the air immediately above it by the lake. The third main cooling effect is from the input of cold water and snow. This comes from direct precipitation, from surface streams or, and by subsurface groundwater flows. There are other minor cooling effects, such as long-wave radiation, that are also discussed in later sections.

The main reason why energy and mass balance studies are made on hot Crater Lakes is to improve our understanding of the volcano underneath. We cannot see what it is doing, but the changing state of the lake above can often give better estimates of the volcanic output, in terms of mass and energy, than we can get for volcanoes without Crater Lakes. When the total output of the volcano is into a lake, it is usually easier to quantify it than it is to estimate the mass and energy from open vents and fumaroles. Increases in heat output, or sudden decreases that indicate a blockage in the vent, can be deduced from the lake temperature. However, it is still often difficult to use this information to deduce what the volcano will do next.

Another reason to study this aspect of Crater Lakes is to forecast the state of the lake, often to see how this affects hazards. Overflowing Crater Lakes have produced many dangerous lahars, including the 24 December 1953 lahar from Mt. Ruapehu, New Zealand, in which 151 people were killed when a bridge was destroyed as an express train was crossing it (O'Shea 1954).

One of the first accounts of the factors affecting a Crater Lake in an active volcano was given by Friedlaender (1898), who described how in Ruapehu Crater Lake, when the heating effect of hot water, steam and gases was opposed by the cooling effect of snow from the surrounding glaciers, the final result was a warm lake. Dibble (1972, 1974) studied this same lake and was able to use the approximately monthly readings of lake temperature, level and chemistry to produce a quantitative model to calculate the heat and mass flows into the bottom of the lake. Another early study was that of Robson and Willmore (1955). They looked at a number of West Indian soufrières, or fumarolic areas, but their study included the Crater Lake of Soufrière St Vincent. Similarly Sugawa (1960) developed an approximate relationship between lake temperature and evaporation for the hot lake Oyunuma in Hokkaido, Japan, to enable the underground inflow to be better calculated.

2 Mass and Energy Balance Model

Both the total energy of the Crater Lake, and the mass of each component, are controlled by conservation laws. As an example, if for a particular period we know how much water is entering or leaving the lake by every mechanism except for the input from the volcano, and we know the total change in mass, then we can calculate what mass of water has come from the volcano for that period. Similarly, we might be able to calculate the volcanic energy input, using the change in lake temperature.

The first equation is the water mass balance, which states that the change in mass of the lake equals the water inflow minus the water outflow. This is usually expressed as

$$\dot{M} = \frac{dM}{dt} = \dot{M}_{volc} + \dot{M}_{precip} - \dot{M}_{evap} - \dot{M}_{out} \quad (1)$$

where

M is the lake mass and $\dot{M}$ or dM/dt is its rate of change in kg/s

$\dot{M}_{volc}$ is the input rate of steam and hot water into the lake from the volcano

$\dot{M}_{precip}$ is the input rate of water and snow from precipitation (direct and indirect)

$\dot{M}_{evap}$ is the rate at which water is lost by evaporation

$\dot{M}_{out}$ is the rate of water outflow, both surface and underground seepage

Then there is the energy balance, which can be written as

$$\dot{E} = \frac{dE}{dt} = \dot{E}_{volc} - \dot{E}_{precip} - \dot{E}_{evap} - \dot{E}_{out} + \dot{E}_{solar} - \dot{E}_{long} + \dot{E}_{cond} - \dot{E}_{sens} \quad (2)$$

where E is the thermal energy in the lake, and dE/dt is its rate of change in W

$\dot{E}_{volc}$ is the power input from steam and hot water into the lake from below

$\dot{E}_{precip}$ is the rate at which energy is needed to heat incoming precipitation

$\dot{E}_{evap}$ is the rate of energy loss by evaporation

$\dot{E}_{out}$ is the rate of energy loss as a result of water outflow

The four terms above represent changes in energy related to mass flows, while the four terms below represent energy change with no change in mass.

$\dot{E}_{solar}$ is the solar radiation power entering the lake

$\dot{E}_{long}$ is the net long-wave radiation loss from the lake

$\dot{E}_{sens}$ is the rate of energy loss at the lake surface by heating the atmosphere (sensible heat)

$\dot{E}_{cond}$ is the net rate of energy gained by conduction from the lake surrounds

Figure 1 shows these flows schematically.

Some of these mass and energy flows can be calculated, but, for a single set of observations at a given time, there will always be more unknowns than the two that can be calculated from two equations. The number of unknowns can be reduced if we know the enthalpies (the thermodynamic energy) associated with some flows. The energy related to a particular mass flow depends on the enthalpy of the fluid involved, the enthalpy being a measure of the heat energy of the fluid per unit mass. Enthalpies can be found in Steam Tables for water and steam. Note however that enthalpies are not absolute, but relative to a certain temperature. This reference temperature also applies to our calculations of total thermal energy. Commonly 0 °C is used as the reference temperature (e.g. Hurst and Dibble 1981), but in some cases another temperature is used. For instance, Stevenson (1992) used enthalpies relative to the ambient air temperature, a selection which is particularly suited for tropical lakes with a constant warm atmosphere. In this case the enthalpy associated with rain and water flow into the lake is zero. On the other hand Pasternack and Varekamp (1997) used the lake temperature as the reference temperature, and so had to explicitly allow for the energy required to heat incoming precipitation.

An increase in the energy/mass ratio is equivalent to an increase in temperature. In other words, in a state with water mass M and total energy E, and an average lake temperature of T, then

$$T - T_{ref} = E/cM \quad \text{in } ^\circ\text{C} \quad (3)$$

where T_{ref} is the enthalpy reference temperature and c is the specific heat of water.

And if a later state has mass $M + \Delta M$ and total energy $E + \Delta E$, then its temperature T^* will be such that

$$T^* - T_{ref} = (E + \Delta E)/c(M + \Delta M) \quad \text{in } ^\circ\text{C} \quad (4)$$

Often only the surface temperature of a Crater Lake is monitored, which could mean that changes in the surface temperature do not adequately reflect the overall change in lake temperature. Since we are discussing lakes with significant heat input, usually at their deepest point, which will produce strong convective overturning, it is often safe to assume that active Crater Lakes will be fairly mixed and of approximately constant temperature. The temperature profile of Ruapehu

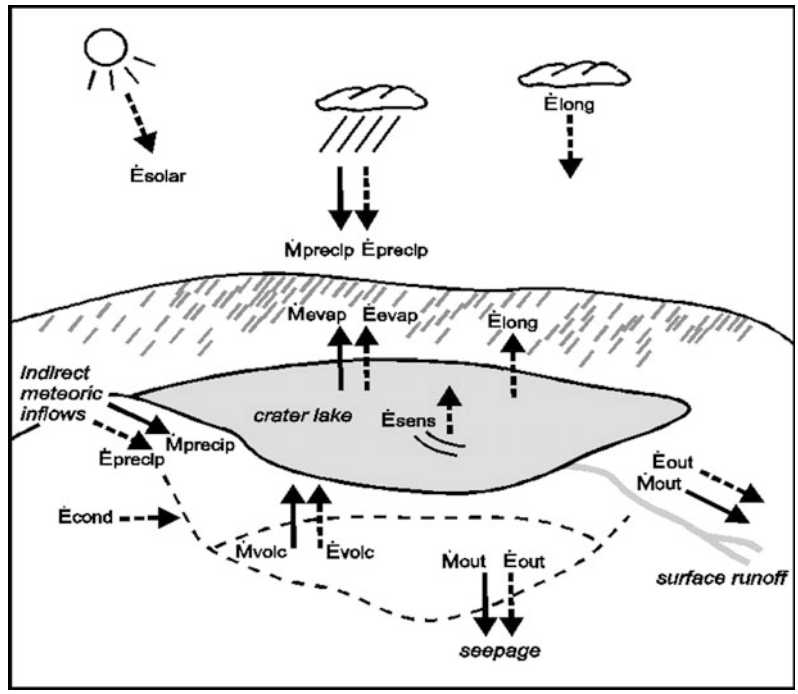

Fig. 1 Heat and mass flows affecting a Crater Lake

Crater Lake in 1966 by Dibble (1974) could be seen as an exception, with a rapid increase in temperature below 100 m depth towards the maximum depth of 297 m, but this was in a very small vent, and the volume affected was a very small part of the lake.

Before describing how the model is operated, we will discuss each of the mass flows, and then all the energy balance that affect the thermodynamic state of a Crater Lake.

3 Mass Balance

$\dot{M}_{volc}$ is the net input of water in both liquid and steam states from the volcano. Since it is primarily an input under the lake, it will usually be the unknown quantity which has to be deduced from the equations, particularly from the mass balance equation once the other mass terms are estimated.

Different lakes vary in the extent to which we can estimate $\dot{M}_{precip}$, the precipitation entering the lake. Firstly, there are variations in how accurately the local precipitation is measured. Only a few volcanoes, such as Poás in Costa Rica, have weather stations close enough to represent the actual conditions at the Crater Lake. Then there are often doubts as to the effective catchment area of the lake, and there can be a considerable delay between the precipitation and the water entering the lake. For the lake Yugama at Kusatsu-Shirane volcano in Japan, Ohba et al. (1994) were able to calculate an effective catchment size 2.5 times bigger than the lake area for the autumn rain period in September–October 1990. The effective catchment would be less in winter, when snow would lie around the lake rather than flow in. The extreme case is volcanoes with surrounding permanent snowfields such as Ruapehu, where the amount of water-equivalent in the snowfield can build up or reduce significantly over a number of years. In such cases, the effective catchment area will only be slightly larger than the lake if cold conditions cause very little snowmelt, but will be very large in a warmer period with a lot of snowmelt.

Generally it is easier to match precipitation over a longer period, say annually, to the apparent water input to the lake, rather than expect daily

values to match. This component can never be negative, and this is often a useful constraint on the maximum possible value of $\dot{M}_{volc}$.

The water loss due to evaporation ($\dot{M}_{evap}$) depends on the surface area and temperature of the lake, as well as on the atmospheric temperature, humidity and wind speed. The equations relating evaporation to these factors will be discussed in Sect. 4.3.

The water outflow ($\dot{M}_{out}$) includes both visible outflow, when a stream or river drains the lake, and invisible underground seepage. For very few lakes can this be measured directly, so it is often estimated indirectly by calculating the dilution of chemical constituents in the lake, as discussed in the next section.

During heavy rain it is common for a surface layer of cold fresh water to develop on a Crater Lake, because even though the main part of the lake is warmer, if it has a high salt concentration it will have a higher density than the cold water. This is often seen as a downwards spike in the lake temperature measured near the surface. If this happens for a lake with a surface outflow, some of the precipitation is likely to flow out without mixing with the rest of the lake, and hence will not be counted in the water balance.

3.1 Dilution

Active Crater Lakes have a range of ionic species present in the water. The concentrations of many of these will be dependent on solubility or on secondary reactions. However, there are generally some species whose concentrations are not so affected, and these can be used to improve the estimates of the mass flows by giving an indication of the extent to which the lake fluid is being diluted by outflow being replaced by precipitation or other inflow.

One useful species is chloride ion, as it is unusual for any metal chloride to reach its solubility limit in a Crater Lake. Incoming volcanic gases commonly contain chloride as HCl gas, so it is common for chloride concentrations to increase, but chloride concentrations can only normally decrease when the lake water has been diluted by outflow and seepage being replaced by fresh (usually meteoric) water. Rouwet et al. (2004, 2008) used chloride and mass balances to analyse the state of the Crater Lake in El Chichón volcano, where the chloride content appeared to be coming from a "buried Crater Lake" hydrothermal system.

Giggenbach (1974) introduced the use of Mg^{2+} for Crater Lake dilution studies on the Crater Lakes of andesite volcanoes. Here the only normal source of magnesium ions is the hot interaction of andesite with liquid-phase water. The magnesium concentration will therefore normally only increase at times of significant volcanic activity. At all other times, the concentration should only be affected by dilution as it is not precipitated in most Crater Lake conditions. The total amount of Mg^{++} will be constant if there is no outflow from the lake. However, if over a period the total outflow of water is M_{out}, then the total quantity of Mg^{++} will be reduced by a factor $M(M + Mout)$, where M is the mass of water in the lake when it is full. In most cases the outflow is compensated for by inflows which keep the lake volume roughly constant, so we will see a steady decline in the Mg^{++} concentration which can be used to derive the total outflow over a period. As long as the decrease in Mg^{++} in any period is less than about 5 %, the linear formula above is still accurate enough, but for large decreases one should use integration to calculate the dilution effect, as in Stevenson (1992).

The Cl^{-} and Mg^{++} concentrations should only change slowly, except for rapid increases during periods of volcanic activity. Other rapid variations in these concentrations are probably the result of imperfect mixing in the lake, and the amount of variation gives an indication of whether this is a problem for the modelling in a particular lake.

As more chemical species are routinely analysed, ions might be useful for constraining mass and energy balances. A related technique is the use of stable isotope concentrations, based on the preferential evaporation of light isotopes, tending to increase the concentration of heavy isotopes such as ^{18}O and ^{2}H in the lake. This is discussed in other chapters of this book.

4 Energy Balance

4.1 Water/Steam Input

$\dot{E}_{volc}$ is the rate of heat input to the lake from volcanic fluids. Normally this is mainly H_2O, in the steam and water phases, with minor amounts of other gases. Pasternack and Varekamp (1997) used a molar ratio of H_2O:CO_2:SO_2 = 93:5:2 for their modelling study, which is similar to results obtained by Giggenbach (1974) for White Island. This means that nearly all the heat comes from the water component, and especially from the steam phase of this, because of the large latent heat of vaporization of water.

For instance, with the gas molar ratios mentioned above and an initial temperature of 250 °C, if the water is in the liquid phase due to a pressure over 4 MPa, the contributions to the total enthalpy (with reference to 0 °C) are H_2O 1.0 MJ/kg, CO_2 0.01 MJ/kg and SO_2 0.003 MJ/kg, but if the pressure was less so the H_2O was entirely present as steam it would contribute 2.8 MJ/kg.

Pasternack and Varekamp (1997) assumed that for Crater Lakes with high gas fluxes, the initial gas temperature would be close to that of liquid magma, e.g. 800 °C, for high-output volcanoes. This would give total enthalpy contributions of H_2O 4.1 MJ/kg, CO_2 0.03 MJ/kg and SO_2 0.01 MJ/kg. So we can expect that likely enthalpies range from about 1.0 MJ/kg for lakes heated by hot water up to about 4.1 MJ/kg for those where the full energy from magmatic steam is available. Note that the actual enthalpies will be slightly smaller if all enthalpies are referenced to a temperature above 0 °C.

4.2 Radiation

Crater Lakes receive short-wave radiant energy from the sun ($\dot{E}_{solar}$), just like any other lakes. The energy at the top of the atmosphere depends on the latitude and season, but the fraction of this that makes it to the lake depends on the average weather conditions, especially the average cloud cover. Henderson-Sellers (1986) reviewed the energy flows that affect ordinary (non-volcanic) lakes, and included a detailed discussion of solar radiation.

For volcanic lakes, for which solar energy is a minor component of the total energy, it is probably adequate to use a formula or tables (e.g. p. 323 of Linacre 1992) for the seasonal variation of the extra-terrestrial or clear-sky insolation, and either annual or monthly estimates of the effect of cloud cover. An alternative is to use the satellite data which is now available, for example at the NASA Surface meteorology and Solar Energy site: http://eosweb.larc.nasa.gov/sse which provides estimates of the average solar radiation for each 1° by 1° area of the Earth's surface. An albedo of 0.06, means that 6 % of the short-wave radiation is reflected by the lake (Henderson-Sellers 1986).

There is also long-wave radiation, both emitted from the lake and arriving at the lake from other sources (low temperature radiation sources produce predominantly long-wavelength radiation, whereas the much hotter sun produces mainly short-wavelength radiation). The relevant equation is the Stefan-Boltzmann law for the radiated power per unit area. The power lost by each square metre of the lake (Φ_{ro}) is

$$\Phi_{ro} = \varepsilon_w \sigma T_s^4 \quad \text{in W m}^{-2} \tag{5}$$

where

- σ is the Stefan-Boltzmann coefficient 5.67×10^{-8} W m^{-2} K^{-4},
- ε_w is the lake emissivity,
- T_s is the water surface temperature of the lake (°K)

The water surface temperature will normally be slightly (typically 1–2 °C) less than the temperature measured within the water near the surface (Oppenheimer 1997). This difference also affects evaporation and sensible heat transfer.

A similar formula gives the incoming long-wave radiation from the atmosphere, with an input power per square metre of (Φ_{ri})

$$\Phi_{ri} = \varepsilon_a \sigma T_a^4 \quad \text{in W m}^{-2} \tag{6}$$

which involves the effective air temperature (T_a), an indication of the average temperature of the parts of the atmosphere radiating energy towards

the lake. Low clouds during a warm day will give a high effective temperature, whereas a clear night will give a very low effective temperature. Henderson-Sellers (1986) gives 0.97 for ε_w, while ε_a is about 0.8. This reference also gives details on how to calculate T_a, but for a Crater Lake with temperature significantly above its surroundings, the incoming long-wave radiation is usually only a very minor component in the energy balance.

$\dot{E}_{long}$ is the net long-wave radiation loss, namely

$$\dot{E}_{long} = A(\Phi_{ro} - \Phi_{ri}) = \sigma A\left(\varepsilon_w T_s^4 - \varepsilon_a T_a^4\right) \text{ in W} \quad (7)$$

where A is the lake area in square metres.

4.3 Evaporation

Normally the largest component of the heat loss for volcanic Crater Lakes is the cooling effect of evaporation ($\dot{E}_{evap}$), with the next largest being the closely related transfer of sensible heat to the air above the lake (sensible heat is a term used to distinguish the heat transfer process from the latent heat associated with evaporation).

However, although the general factors involved in evaporation have been known for two centuries since the time of John Dalton (1760–1844), there is still no consensus as to an appropriate formula for a warm lake of significant size. It is normal to distinguish free convection, which is the convection with no external wind, produced when the water temperature is higher than ambient, from forced convection, which is convection produced by wind blowing across the water surface. One contentious topic is the extent to which these processes interact for a lake that is significantly warmer than its surroundings.

In this section, we will consider a number of evaporation formulae, and compare their results for a typical volcanic lake.

The first equation considered is that of Ryan et al. (1974). They used the basic formulation traceable back to Stelling (1882) in which the evaporative heat flux, $\Phi_{e,}$ is given by

$$\Phi_e = (a + bW_z)(e_s - e_a) \quad \text{in W/m}^2 \quad (8)$$

where

a and b	are parameters to be derived
W_z	is the wind velocity at height z (often 2 m above the lake surface), in m s^{-1}
e_s	is the saturation vapour pressure at the water surface temperature, in mbar
e_a	is the actual vapour pressure in the ambient air, in mbar

To calculate $\dot{E}_{evap}$, Φ_e is simply multiplied by the lake area.

The saturation vapour pressure of water at any temperature is found in Steam Tables, giving e_s directly, while e_a is the saturation vapour pressure at the ambient air temperature multiplied by the relative humidity.

In other words, a is the free convection term, and b the forced convection term, and they are simply added. Ryan et al. (1974) provided a theoretical justification for an a that contained a term in $(T_s - T_a)^{1/3}$, and then used measurements of various lakes to fit the constant b to the actual results. Their final expression for the heat loss due to evaporation was

$$\Phi_e = (\lambda(T_{sv} - T_{av})^{1/3} + 3.2W_2)(e_s - e_2) \text{ in W/m}^2 \quad (9)$$

with $\lambda = 2.7$, while W_2 and e_2 are wind speed and vapour pressure measured at a height of 2 m above the lake. However, although this formula is often quoted with λ as the constant 2.7, λ is derived from a formula for gas transfer, and varies significantly with temperature, decreasing about 10 % for a 20 °C rise in average air temperature. The second constant is empirical, based on matching observed evaporation under various conditions.

The temperatures T_{sv} and T_{av} are virtual surface and air temperatures, derived from the actual surface and air temperatures by the formula

$$T^*_{xv} = T^*_x/(1 - 0.378e_x/P_a) \quad \text{in Kelvin for } x = s \text{ or } a \tag{10}$$

where P_a is the atmospheric pressure and e_x the water vapour pressure (for T_{sv}, the saturation vapour pressure, for T_{av}, at the average humidity), and T^* is temperature in absolute units. These virtual temperatures allow for the extra buoyancy of water vapour compared to air. The effect for warm lakes is to make $T_{sv}-T_{av}$ significantly higher than T_s-T_a. Note that there is no explicit consideration in this formula for the effect of the lake on the properties of the air passing over it, either by a lake size term or in any other fashion.

Whereas Ryan et al. (1974) started with empirical formulae that had been shown to be applicable for ordinary (non-heated) lakes and adapted then for heated lakes, Weisman and Brutsaert (1973) (herein referred to as W & B) developed a new theory for the interaction of a normal stable air mass meeting a relatively warm lake, taking into account the change in the properties of the air as it passes over the lake. As they stated "The present problem is formulated for unstable conditions over the water; the water vapour stratification creates buoyancy in the air, and turbulent transfer, amplified by buoyant convection, is considerably larger than it is when it results from forced convection only."

As part of their analysis, W & B derived two dimensionless parameters A_* and B_*, the first representing the fractional change in temperature, and the second the change in surface specific humidity, at the lake edge.

$$A_* = -[(T_s - T_a)/T_a]\left(kgz_o/u_*^2\right), \tag{11a}$$

$$B_* = -0.61(e_s - e_a)\left(kgz_o/u_*^2\right), \tag{11b}$$

where k is the von Kármán constant (typically 0.41), g is the local acceleration due to gravity, z_o is the roughness length (2×10^{-4} m, or 0.2 mm is the value used by W & B) and u_* is the friction velocity, which can be regarded as the wind velocity at the elevation of the roughness length. These terms are related to the microscopic scale at which the water and air exchange mass and heat. For a logarithmic wind profile with a velocity at 2 m high of 1 m/s, u_* will be 0.05 m/s. W & B solved the dimensionless version of the equations to get the total average vapour flux as a function of lake width traversed by the wind (the fetch), and found that this could be fitted by the equation

$$\Phi_e = ax^{-n}\rho L\, u_*(e_s - e_a) \quad \text{in W m}^{-2} \tag{12}$$

If the fetch, the distance wind travels across the lake, is X_o metres, then $x = X_o/z_o$.

The constants a and n are obtained from the numerical solution of turbulent diffusion equations, and the second part of this equation converts the dimensionless flux back into actual values. This equation effectively incorporates both free and forced convection, because as the wind velocity decreases there is an increase in the ax^{-n} term, indicating an increasing importance of the free convection component. This can be seen in Fig. 2.5 of Stevenson (1992), where for a lake temperature of 50 °C, the evaporation appears to be constant for wind velocities up to 3 m/s.

A disadvantage of W & B is that the complexity of the equations meant that they only supplied numerical solutions for some cases. In particular, since the vapour flux is proportional to u_*, the equation cannot actually deal with the pure free convection when there is no wind. This means that there was still a need for a straightforward equation that would give a reasonable estimate of the convection from a lake.

Sill (1983) looked at cases where both free and forced convection were significant, such as with light winds across warm lakes, and concluded that forced convection actually disrupted free convection. He suggested that once the forced convection became nearly comparable with free convection (which he suggested was when the ratio Free:Forced was 1.37:1), a different equation should be used that reflected this disruption, with the contribution from free convection reducing from this point. This idea was further developed by Adams et al. (1990), who also considered that that the Ryan et al. (1974) formula (Eq. 9) over-predicted the amount of evaporation when both free and forced

convection were significant. They suggested taking the square root of the sum of squares, rather than simple addition, which significantly lowers the total evaporation, and also noted that the free evaporation coefficient λ of Eq. 9) should be reduced for temperatures above about 20 −30 °C. As with Ryan et al. (1974), Adams et al. (1990) included studies using atmospheric measurements that were made on rafts, in which the temperature and humidity would have been influenced by the lake. This was seen in Table 2 of Adams et al. (1990), where the evaporation coefficient for forced convection was significantly higher when the air measurements were made on lakes compared to when they were on land. They compared their revised evaporation formula with two cases where energy and mass balances had been done for artificially heated ponds. At the East Mesa site, the best fit was with a forced convection term that varied with lake surface area (A) according to ($A^{-0.05}$), based on Harbecks (1962) studies of reservoirs, which were more or less in thermal equilibrium with their surroundings. Their formula is

$$\Phi_e = \left[\left(2.7(T_{sv} - T_{av})^{1/3}\right)^2 + \left(5.1A^{-0.05}W_2\right)^2\right]^{1/2} \times (e_s - e_a) \quad \text{in W m}^{-2} \tag{13}$$

where A is the lake area in hectares. Note that these coefficients actually give higher heat losses than Ryan et al. (1974) for high wind velocities, for ponds and lakes smaller than about 1 km^2. However, for the high-temperature ponds at Savannah River, they found the best-fitting formula was one with a significantly lower forced convection, but with no fetch dependence

$$\Phi_e = \left[\left(2.2(T_{sv} - T_{av})^{1/3}\right)^2 + (3.2W_2)^2\right]^{1/2} \times (e_s - e_a) \quad \text{in W m}^{-2} \tag{14}$$

In both these equations, the free convection is the term that contains the virtual temperature difference $T_{sv} - T_{av}$, while the forced component contains W_2, the wind velocity 2 m above the lake.

Sartori (2000) made a comparison of a large number of equations applying to forced evaporation, and found several equations which all gave good results for small ponds, in which the air properties did not change significantly as it went across the pond. He concluded that for turbulent flow (the inevitable condition for a lake warmer than its surroundings) the fetch-dependent term proportional to $X_o^{-0.2}$ suggested by theory also best fitted the measurements for larger water bodies, and proposed the equation

$$\Phi_e = L\left(0.00407u^{0.8}X_o^{-0.2} - 0.01107X_o^{-1}\right) \times (e_s - e_a)/P_a \quad \text{in W/m}^2 \tag{15}$$

where L is the latent heat of evaporation of water (2.4 MJ/kg at 40 °C), X_o is the fetch in metres, and P_a is the atmospheric pressure, in the same units as e_s and e_a. For a Crater Lake of reasonable size, the 0.01107 X_o^{-1} term can be disregarded.

This is used to replace the forced convection component in Adams et al. (1990), still using the square root of sum of squares to combine free and forced convection.

$$\Phi_e = \left[\left(2.2(T_{sv} - T_{av})^{1/3}(e_s - e_a)\right)^2 + \left(L\left(0.00407u^{0.8}X_o^{-0.2}\right)(e_s - e_a)/P_a\right)^2\right]^{1/2} \quad \text{in W m}^{-2} \tag{16}$$

Figure 2 shows how the various formulae predict the evaporative heat flux as a function of wind velocity for a lake the size of Ruapehu Crater Lake (200,000 m^2) at a temperature of 40 °C.

The graph shows there are three formulae which give fairly similar results in this case, W & B, the Adams et al. (1990) formula without fetch dependence and Sartori (2000). Since the typical heated Crater Lake clearly affects the temperature and humidity of the air crossing it, we should use a formula which tries to incorporate this, such as the Sartori (2000) formula Eq. 16. The advantage of this over W & B is that it is an explicit formula that can be calculated for any conditions,

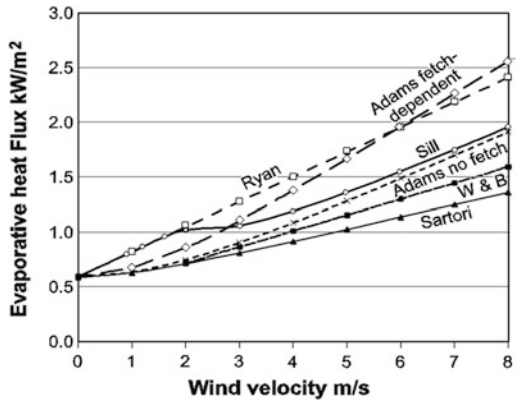

Fig. 2 Comparison of evaporative heat flux as a function of wind velocity for different evaporation equations

whereas W & B only provide solutions for certain ranges of the normalised variables.

One of the reasons why we have differing formula is probably the difference between the temperature and humidity of the average air above the warm lake compared to the incident air. The early evaporation studies mainly looked at lakes in equilibrium with their surroundings, for which this effect would have been less important. W & B produced a theoretical study based on a neutral comparatively dry air mass encountering a warm wet surface, whereas all the other equations obtain forced convection by empirical means. It is reasonable to assume that the empirical formula that agree with W & B are also using incident air conditions, whereas the two formula that give higher evaporation under apparently the same conditions have in fact been derived by looking at cases in which air properties are measured above the lakes.

We would recommend that Eq. 16 from Sartori (2000) should be used whenever the ambient air conditions are measured upwind of the lake, or estimated as if the lake is not there. If the air conditions are measured on the lake, then one of the equations from Adams et al. (1990), such as Eq. 14 is likely to be more appropriate. All the formula in this section are for heat flux, so for the total evaporative loss ($\dot{E}_{evap}$) they have to be multiplied by the lake area A.

4.4 Thermal Conduction to Atmosphere

The energy loss by thermal conduction between the lake surface and the atmosphere, also known as the sensible heat loss (P_{sens}) is closely related to the heat loss by evaporation, as they both involve the close contact between the lake surface and the atmosphere.

The terminology can be confusing here. The microscopic process taking place in the boundary layer is conduction of heat from water to air. Then convection takes this heat up into the air column. Hence some authors say the process is conductive heat loss, and others convective. By using the term sensible heat to distinguish it from the latent heat involved in evaporation, we avoid confusion over what process we are talking about.

For the sensible heat component, Ryan et al. (1974) used the ratio of the heat loss due to sensible heat to that due to evaporation that was derived by Bowen (1926), with Bowen's Ratio (the ratio of sensible heat loss to evaporative heat loss) given by

$$\dot{E}_{sens}/\dot{E}_{evap} = 0.61(T_w - T_a) / (e_s - e_2). \quad (17)$$

Other authors (e.g. Stevenson 1992) have pointed out that the constant (0.61) is actually proportional to pressure, so should be modified for pressures differing from atmospheric. Sartori (2000) provides an equation suitable for high elevation lakes where the atmospheric pressure is lower than normal

$$\dot{E}_{sens}/\dot{E}_{evap} = 0.61(T_w - T_a) / (e_s - e_2) * P_a/P_0 \quad (18)$$

where P_a is the actual atmospheric pressure, and P_0 is the standard atmospheric pressure.

In other words, having decided how to calculate $\dot{E}_{evap}$, Eq. 18 should be used to calculate $\dot{E}_{sens}/\dot{E}_{evap}$ and then we use

$$\dot{E}_{sens} = \dot{E}_{evap}\left(\dot{E}_{sens}/\dot{E}_{evap}\right) \quad \text{in W} \quad (19)$$

to get the sensible heat loss.

Fig. 3 Night photo showing incandescent area adjacent to the Crater Lake of Poas Volcano, Costa Rica. Photographed by Elicier Duarte OVSICORI-UNA on 8 September 2011

4.5 Thermal Conduction Between Lake and Surroundings

This term $(\dot{E}_{cond})$ is the net energy gain from thermal conduction from the bed of the lake, possibly supplemented by small-scale convection, and is usually very small. However there are cases where it is significant, one being Poás volcano, where in September 2011 there was an area of incandescence very close to the lake, as shown in Fig. 3. The high thermal gradient in such situations will produce thermal conduction, and possibly also set up local convection in groundwater. It is unlikely that such an energy flux can be accurately estimated, so emphasising that calculations are much easier for the case in which all the volcanic activity is under the lake.

4.6 Energy Loss Associated with Precipitation or Outflow

As mentioned earlier, the calculation of the total thermal energy in the lake uses enthalpies that are relative to a particular temperature. In the calculations of energy balance, an increase in the enthalpy/mass is equivalent to an increase in temperature.

So for any mass flow at a temperature different from the enthalpy reference temperature, we must also account for its enthalpy. In other words, if the enthalpy reference temperature is 0 °C, then lake inflow at that temperature, as is common with snow-covered volcanoes, carries zero energy $(\dot{E}_{precip} = 0)$. However with a warm lake, its mass will lower the energy/mass ratio, indicating it will lower the lake temperature. Snowfall will have a negative enthalpy, even for a reference temperature of 0 °C, because it requires energy to melt it.

On the other hand, water flowing or seeping out will take away enthalpy at a rate $\dot{E}_{out}$ depending on the lake temperature, but the energy/mass ratio and hence temperature will stay the same. Other choices of the enthalpy reference temperature will change the calculations, but should always give the same results.

5 Applications and Case Studies

The purpose of calculating the heat and mass balances for the Crater Lakes of active volcanoes is usually to better understand the sub-lake processes. We can only make reasonable estimates of the mass and heat coming from the volcano if

we have removed other effects such as precipitation and evaporation. The extent to which we can do this varies from volcano to volcano, some examples follow to give an idea of the way in which the conservation equations can be used.

5.1 Effective Steam Enthalpy at Ruapehu Crater Lake

One of the main conclusions of Hurst et al. (1991) was that for Ruapehu Crater Lake, the ratio of energy input to mass input, the effective steam enthalpy, was much greater than the actual enthalpy of steam at any state likely to be entering the lake. This was done by adjusting the input steam enthalpy and looking to see what enthalpy was required to avoid any significant non-negative melt flow. The conclusion that the effective steam enthalpy had to be at least 6 MJ/kg, more than even the value for magmatic temperatures, led to the conclusion that much of the energy entering the lake must be by means of a heat pipe, in which steam ascends and water descends in the vent, transferring energy but not net mass.

After the eruptions of 1995 and 1996, which ejected the whole lake, Ruapehu Crater Lake slowly refilled. For the period from when the lake reached a reasonable size at the beginning of 2003, until just before it overflowed in March 2007, there was no surface outflow, and therefore the net volume change could be calculated without any need to use dilution measurements to calculate outflows. This minimised errors in the melt flow calculation. Figure 4 shows that the heat-pipe was still in operation, as a 3 MJ/kg enthalpy produces significant negative melt flows. It is difficult to distinguish between the effects of 6 MJ/kg (about 50 % energy conveyed by heat-pipe) and 9 MJ/kg (about 67 % energy conveyed by heat-pipe), even in a period where both lake temperature and lake height/volume were being directly measured and there was no outflow.

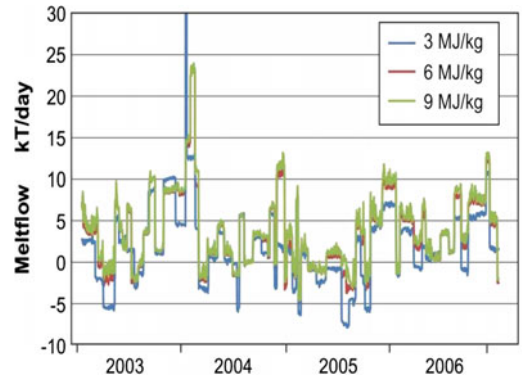

Fig. 4 Time series plot of calculated melt flow (which should be non-negative) into Ruapehu Crater Lake for different effective steam enthalpies

5.2 Boiling Dry

Pasternack and Varekamp (1997) discussed the permanence of Crater Lakes with high heat fluxes. They concluded that lakes with sufficient heat flux to maintain a surface temperature over about 45–50 °C are likely to boil dry and disappear. They also concluded that small lakes were particularly likely to disappear, although this was based on a catchment size only twice the lake size, and small lakes with larger catchments would be more stable.

5.3 Boiling Lake, Dominica

Fournier et al. (2009) discussed the Boiling Lake in Dominica, a very high temperature Crater Lake that falls well outside the region considered by Pasternack and Varekamp (1997) to be stable. However, rather than being unstable by evaporating away, it is normally full, but occasionally the lake level suddenly drops, but with a drop in the lake temperature, and a cessation of the gas flow and convection. Then the lake refills and heats up to its normal state. Fournier et al. (2009) explained this behaviour by a model in which the lake water level is only maintained above the local water table by the gas flux, so being

potentially unstable to gravitational collapse. The model for this instability is one originally proposed by Witham et al. (2006) for lava lakes. The energy and mass balance calculations by Fournier et al. (2009) showed clearly that the ratio of energy input to steam input was greater than any reasonable steam enthalpy, indicating that some energy was being brought in by lake water cycling down and being heated, before returning to the lake.

Since their model involved the lake level being maintained by water being brought up with the gas input, Fournier et al. (2009) proposed the concept of another conduit under the lake, in which water could flow downwards. They carried out experiments similar to that of Witham et al. (2006), and found that if this conduit was large, the lake would no longer be stable at a level above the water table. At a particular intermediate size, they could reproduce the behaviour of Boiling Lake, and the system was stable against small fluctuations. The key to this model was that there was one region in which steam bubbles were pushing water up, but in another region water was able to descend without being affected by steam bubbles, they did not necessarily be separate identifiable conduits. Fournier et al. (2009) suggested that the up flow might be in discrete cracks under the lake, with the down flow in regions of distributed permeability around the cracks.

Another feature of the modelling of Boiling Lake by Fournier et al. (2009) was that they tried to calculate the effects of the otherwise unknown amount of seepage from Boiling Lake by comparing the mass and energy balances from two periods of steady state, one with normal rainfall and the other during a period of heavy rain.

5.4 Yudamari, Mt Aso

The First Crater of Nakadake is the currently active crater of Aso volcano, Kyushu, Japan. It contains a hot Crater Lake, locally referred to as Yudamari, with a diameter greater than 200 m, and strongly acid water (pH of 0–1). In recent years, when there have been no significant eruptions, the lake temperature has normally been in the 60–70 °C range. Large amounts of volcanic gas (typically 200–400 t/d of SO_2) have been continuously emitted from lake surface and fumaroles located on the inner crater wall.

Terada et al. (2008) calculated the heat discharge across the lake surface, using the evaporation equation of Ryan et al. (1974), and found that it was almost constant, with a value of approximately 220 MW during the recent non-eruptive period. This rate is not far short of the values for Ruapehu Crater Lake (Hurst et al. 1991) and Poás (Brown et al. 1989), which are two of the highest thermal input Crater Lakes in the world. Although Aso volcano is in an area of high rainfall, with typically 1,000–2,000 mm of rain falling in the June–July rainy season, precipitation cannot explain the maintenance of the lake, because the volume of water lost from the lake surface caused by an evaporation rate of 60–80 kg/s is an order of magnitude greater than the volume of water gained through precipitation. This suggests that the lake water is obtained mainly via inflows at the lake bottom.

Yudamari Crater Lake shows interesting variations in water level and temperature. A numerical model employed by Terada et al. (2012) revealed that seasonal changes in mass fluxes (75–132 kg/s) and enthalpy (1,840–3,030 kJ/kg) for the fluid supplied to the lake. The relation between the enthalpy and mass flux indicates that the fluid input at the lake bottom originates as a mixture of groundwater and high-temperature steam. The groundwater flux exhibits a seasonal increase lagging behind the rainy season by 2 months. The fluctuation pattern in the flux of the high-temperature steam is related to the amplitude of volcanic tremors, suggesting that heating of the hydrothermal system drives the tremors.

Historical documents record the repeated appearance and disappearance of Yudamari Crater Lake over the past 1,500 years, which indicates that the long-term heat discharge activity has occurred concomitantly with short-term fluctuations in the fluid supply, including eruptions.

6 Concluding Remarks

This chapter has applied the basic conservation equations of energy and mass of water. With so many variables, it may seem that it is something of a forlorn hope to estimate the volcanic input to a Crater Lake. However, in many cases some of the flows are known to be minor and can be disregarded. At other volcanoes, seasonal variations in temperature and precipitation can be used to separate different effects. If the surroundings of the lake are below freezing in winter, there will be very little indirect precipitation, and measuring the snowfall beside the lake might give a good estimate of the direct precipitation. If there is a well-defined rainy season, as with Yudamari, the seasonal effect of this on the lake can be used to get an indication of how significant the precipitation component is for the water balance.

At other volcanoes, it might be the volcanic activity that varies. At a volcano that seems quiescent, one could measure the fastest rate at which the lake cools and by assuming zero volcanic input at these times, obtain a minimum estimate of the heat loss. The examples given above are just a few of the cases in which the use of Crater Lake heat and mass balances has given valuable information about the state of the underlying volcano.

References

Adams E, Cosler D, Helfrich K (1990) Evaporation from heated water bodies: predicting combined forced plus free convection. Water Resour Res 26(3):423–435

Bowen IS (1926) The ratio of heat losses by conduction and by evaporation from air water surface. Phys Rev 27:779–787

Brown G, Rymer H, Dowden J, Kapadia P, Stevenson D, Barquero J, Morales LD (1989) Energy budget analysis for Poás Crater Lake: implications for predicting volcanic activity. Nature 339:370–373

Dibble RR (1972) Seismic and related phenomena at active volcanoes in New Zealand, Hawaii and Italy. Ph.D. thesis. Victoria University of Wellington, Wellington

Dibble RR (1974) Volcanic seismology and accompanying activity of Ruapehu Volcano, New Zealand. In: Civetta L, Gasparini P, Luongo G, Rapolla A (eds) Physical volcanology. Elsevier, Amsterdam, pp 49–85

Fournier N, Witham F, Moreau-Fournier M, Bardou L (2009) Boiling lake of Dominica, West Indies: high-temperature volcanic Crater Lake dynamics. J Geophys Res 114:B02203. doi:10.1029/2008JB005773

Friedlaender B (1898) Some notes on the volcanoes of the Taupo district. Trans N Z Inst 31:498–510

Giggenbach WF (1974) The chemistry of Crater Lake, Mt Ruapehu (New Zealand) during and after the 1971 active period. N Z J Sci 17:33–45

Harbeck EG (1962) A practical field technique for measuring reservoir evaporation using mass transfer theory. US Geol Surv Prof Pap 272-E:101–105

Henderson-Sellers B (1986) Calculating the surface energy balance for lake and reservoir modeling: a review. Rev Geophys 24:625–649

Hurst AW, Dibble RR (1981) Bathymetry, heat output and convection in Ruapehu Crater Lake, New Zealand. J Volcanol Geotherm Res 9:215–236

Hurst AW, Bibby HM, Scott BJ, McGuinness MJ (1991) The heat source of Ruapehu Crater Lake; deductions from the energy and mass balances. J Volcanol Geotherm Res 46:1–20

Linacre E (1992) Climate data and resources: a reference and guide. Routledge, London

Ohba T, Hirabayashi J, Nogami K (1994) Water, heat and chloride budgets of the Crater Lake, Yugama at Kusatsu-Shirane volcano, Japan. Geochem J 28:217–231

Oppenheimer C (1997) Ramifications of the skin effect for Crater Lake heat budget analysis. J Volcanol Geotherm Res 75:159–165

O'Shea BE (1954) Ruapehu and the Tangiwai disaster. N Z J Sci Technol B36:174–189

Pasternack GB, Varekamp JC (1997) Volcanic lake systematics I: physical constraints. Bull Volcanol 58:528–538

Robson GR, Willmore PL (1955) Some heat measurements in West Indian soufrières. Bull Volcanol 17:13–39

Rouwet D, Taran YA, Varley NR (2004) Dynamics and mass balance of El Chichón Crater Lake, Mexico. Geofís Int 43(3):427–434

Rouwet D, Taran Y, Inguaggiato S, Varley N, Santiago JA (2008) Hydrochemical dynamics of the "lake–spring" system in the crater of El Chichón volcano (Chiapas, Mexico). J Volcanol Geotherm Res 178:237–248. doi:10.1016/j.jvolgeores.2008.06.026

Ryan PJ, Harleman DRE, Stolzenbach KD (1974) Surface heat loss from cooling ponds. Water Resour Res 10:930–938

Sartori E (2000) A critical review on equations employed for the calculation of the evaporation rate from free water surfaces. Sol Energy 68(1):77–89

Sill BL (1983) Free and forced convection effects on evaporation. J Hydraul Eng 109:1216–1231

Stelling E (1882) Über die Abhängigkeit der Verdunstung des Wassers von seiner Temperatur und von der Feuchtigkeit und Bewegung der Luft [1881], no 3. Repertorium für Meteorologie, Kaiserliche Akademie der Wissenschaften (Meteorologicheskii Sbornik, Imperatorskoj Akademii Nauk) St Petersburg 8, pp 1–49

Stevenson D (1992) Heat transfer in active volcanoes: models of Crater Lake systems. Ph.D. thesis, The Open University

Sugawa A (1960) Evaporation from the water surface of high temperature. Geophys Bull Hokkaido Univ 7:63–70

Terada A, Hashimoto T, Kagiyama T, Sasaki H (2008) Precise remote-monitoring technique of water volume and temperature of a Crater Lake in Aso volcano, Japan: implication for a sensitive window of volcanic hydrothermal system. Earth Planets Space 60:705–710

Terada A, Hashimoto T, Kagiyama T (2012) A water flow model of the active Crater Lake at Aso Volcano, Japan: fluctuations of magmatic gas and groundwater fluxes from the underlying hydrothermal system. Bull Volcanol 74:641–655. doi:10.1007/s00445-011-0550-4

Weisman RN, Brutsaert W (1973) Evaporation and cooling of a lake under unstable atmospheric conditions. Water Resour Res 9:1242–1257

Witham F, Woods AW, Gladstone C (2006) An analogue experimental model of depth fluctuations in lava lakes. Bull Volcanol 69:51–56

How Steep Is My Seep? Seepage in Volcanic Lakes, Hints from Numerical Simulations

Micol Todesco, Dmitri Rouwet, Massimo Nespoli, and Maurizio Bonafede

Abstract

The existence and survival of volcanic lakes require the accomplishment of a delicate balance between meteoric recharge, evaporation, and water loss by infiltration within the volcanic edifice, commonly referred to as seepage. A deep-seated, volcanic component may participate to a variable extent to the lake's evolution, depending on volcanic activity. In this work, we apply a numerical model of hydrothermal fluid circulation to study the interaction between the hot volcanic gases and the shallow lake water. We focus on the conceptual model developed for Poás volcano (Costa Rica), where a shallow magma intrusion drives the hydrothermal activity underneath and around the crater lake. Numerical simulations are carried out to assess the role of relevant system properties, including rock permeability, reservoir conditions, lake geometry, and meteoric recharge. Our results suggest that vertical seepage can be severely hindered by the ascent of volcanic gases, whereas horizontal infiltration through the vertical lake walls may ensure a long-term water loss. Our simulations also show that the permeability distribution, especially around the lake, determines the overall pattern of circulation affecting the development and spatial distribution of hot springs and fumaroles, and ultimately controlling the evolution of the lake.

Electronic supplementary material The online version of this chapter (doi:10.1007/978-3-642-36833-2_14) contains supplementary material, which is available to authorized users. Videos can also be accessed at http://www.springerimages.com/videos/978-3-642-36833-2

M. Todesco · D. Rouwet (✉) · M. Nespoli
Istituto Nazionale di Geofisica e Vulcanologia, Sezione di Bologna, Bologna, Italy
e-mail: dmitri.rouwet@ingv.it

M. Todesco
e-mail: micol.todesco@ingv.it

M. Nespoli · M. Bonafede
Università degli, Studi di Bologna, Bologna, Italy

D. Rouwet et al. (eds.), *Volcanic Lakes*, Advances in Volcanology,
DOI 10.1007/978-3-642-36833-2_14,
© Springer-Verlag Berlin Heidelberg 2015

Keywords
Active crater lake · Numerical simulations · Seepage · TOUGH2 modeling · Hydrothermal circulation

1 Introduction

Volcanic lakes are very special geological features. They form when meteoric water fills a volcanic crater, and their temperature and chemical composition testify to a variable contribution from the volcanic system. As a result, volcanic lakes are very transient features, whose major characteristics (such as size, temperature, chemical composition of lake water) commonly undergo significant variations through time. Their existence requires the accomplishment of a delicate balance between processes that feed the lake, such as meteoric precipitation or the condensation of volcanic vapor, and processes that drain the lake, such as runoff, seepage (i.e., infiltration into the volcanic edifice), boiling and evaporation (Hurst et al. this issue). Mass and energy balances of the lakes therefore depend on atmospheric conditions, as well as on the input from the volcanic system. In some cases, hot vents of volcanic fluids are evident near or within volcanic lakes. As a result, the evolution of the lake can be related to the state of activity of the volcano, and can therefore provide useful hints to the assessment of volcanic hazard. For this reason, monitoring of lake conditions is often carried out in surveillance programs (Rowe et al. 1992; Rouwet et al. 2004; Rouwet and Tassi 2011; Terada and Sudo 2012; Terada et al. 2012). However, the interpretation of monitoring data are not always straightforward and volcanic activity may occur regardless of the lake conditions. At Ruapehu, New Zealand, phreatic or phreatomagmatic activity took place both during cold and quiet periods or, more commonly, when the lake was hot (Christenson et al. 2010). In other cases lake conditions remain constant for some period of time. To fully exploit the observations carried out at crater lakes, we need to assess the mass and energy balances that govern their evolution. Several authors addressed this problem (Brown et al. 1989; Hurst et al. 1991, this issue; Ohba et al. 1994; Rouwet et al. 2004, 2008; Taran and Rouwet 2008; Fournier et al. 2009; Rouwet and Tassi 2011), however some terms of these balances cannot be measured directly, such as the input of volcanic gases, or the amount of water that lost by seepage.

Numerical modeling of the hydrothermal fluid circulation underneath the lake may provide useful clues to understand the mechanisms that drive the evolution of volcanic lakes. In this work, we present the results of numerical simulations of a hydrothermal system that feeds a volcanic lake. The conceptual model we used to set up our simulations is based on the Poás volcanic system (Costa Rica), and on its crater lake, Laguna Caliente. This volcanic system is well known, and long-term monitoring has shown that the crater lake is particularly active, and well represents the main features of volcanic lakes, in general. Our main focus is the fluid flow underneath the lake, and in particular the interaction between meteoric recharge and hydrothermal fluids. At this time, our description of the lake evolution is rather crude, and this prevent a direct comparison between modeling results and monitoring data. Nevertheless, we could assess some general features, and the conclusions that we draw here may be applied to other crater lakes. In the following we describe the numerical simulations that we performed, first considering a steady lake, with fixed temperature and water level, and then some preliminary results describing the evolution of the lake, as well as of the hydrothermal system.

2 Laguna Caliente Crater Lake

Laguna Caliente is a hot, acidic lake that was formed within the active crater of the Poás volcano (Fig. 1). This complex stratovolcano belongs to

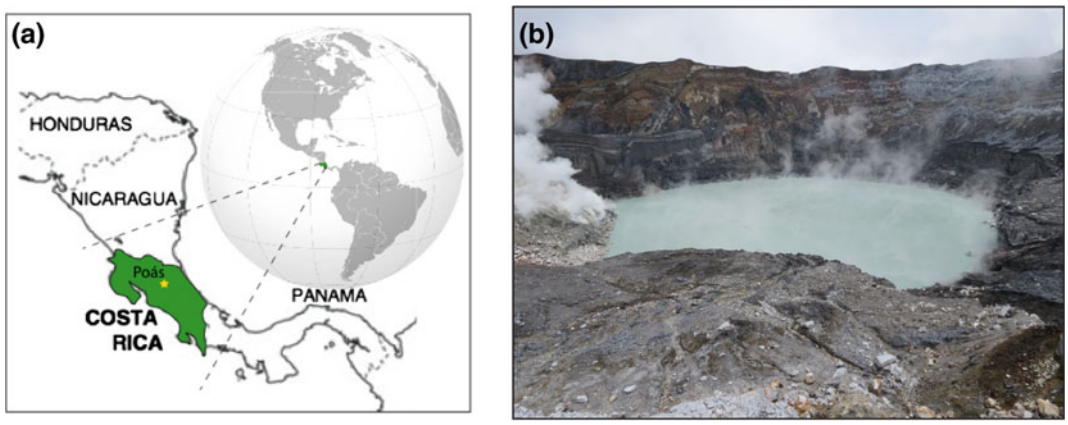

Fig. 1 The Poás volcano in Costa Rica (**a**) and the Laguna Caliente crater lake (**b**) (May 2012 *picture by* D. Rouwet)

the Cordillera Volcánica Central, Costa Rica, and is located ca. 35 km to the northwest of the capital San José. The summit area comprises three cones, one of which hosts another lake, the cold Laguna Botos. The active crater (Main Crater, 2,300 m asl) is 800 m wide and hosts the Laguna Caliente lake and a lava dome. The lava dome was extruded in 1954, during the last magmatic eruptive period (1952–1955) that involved Surtseyan and Strombolian events, alternated with numerous phreatic explosion within Laguna Caliente (Casertano et al. 1987; Rowe et al. 1992, 1995; Marti´nez et al. 2000). The activity within the crater is driven by a shallow magma body, whose presence was inferred based on geophysical data (Brown et al. 1989; Rymer et al. 2000, 2009; Fournier et al. 2004). The crater is subject to persistent but highly variable hydrothermal activity that feeds within the dome and periodically triggers phreatic activity within the lake. The temperature of the fumaroles may reach 1000 °C during periods of volcanic unrest, and drop to boiling temperature during quiet times (Brown et al. 1989; Vaselli et al. 2003). The hydrothermal system also includes hot springs, along the northwest flank of the volcano, at ca. 3 km from the active crater. These springs formed along a lava-lahar stratigraphic contact that represents a preferential hydraulic pathway. Although data on chemistry and flow rates of these springs are missing, their presence is known to drive a fraction of the hot hydrothermal brines from the crater region down to the volcano's flank (Rowe et al. 1992, 1995; Sanford et al. 1995). Lake conditions and water level have changed through time: during periods of unrest the water temperature can reach 80 °C, enhancing evaporation. Complete lake desiccation occurred several times and preceded the onset of the 1910 and 1953 eruptive episodes, and periods of enhanced activity in the 1980–1990s (Oppenheimer and Stevenson 1989). During quiet times, the lake temperature may drop to 20 °C (near ambient temperature), and the water level can rise to 50 m (Rowe et al. 1992). The lake evolution certainly depends on meteoric recharge as well, and is affected by the abundant precipitation that characterizes the region. Rainfall data are available for the Poás summit area, and are supplied by the ICE Hydromet station #084063 (data courtesy by R.A. Mora-Amador), located 2 km south of the active crater, at an elevation of 2,560 m asl. This is the rain gauge nearest to the crater area and besides the one with the longest time record (Rowe et al. 1992). Precipitation ranges from 120 mm/month in the dry season (December–April) to 420 mm/month during the wet season (May–November). In the period 2005–2010 the yearly average rainfall ranged from 3,800 mm in 2006 (1.2×10^{-4} kg/m^{2}s) to 5,600 mm in 2009 (1.8×10^{-4} kg/m^{2}s). The monthly average precipitation ranged from 1.5×10^{-5} kg/m^{2}s (April 2006) to 4.3×10^{-4} kg/m^{2}s (October 2008). Considering a catchment area corresponding to the crater surface area (7.1×10^5 m^2), these values

correspond to an average meteoric recharge ranging from 10 to 300 kg/s.

3 Numerical Simulations

To study the interaction between the lake and the hydrothermal system, we performed a set of TOUGH2 numerical simulations. TOUGH2 (Pruess et al. 1999) is a well assessed porous media flow model, capable of describing the coupled flow of heat and fluids through heterogeneous porous media. The model describes the water phase transitions and accounts for the presence of non-condensible gas components, such as air, or carbon dioxide. Here we applied the TOUGH2/EOS3 module, describing the presence of water and air. Figure 2 illustrates the computational domain and boundary conditions of our model. The domain is two-dimensional and axisymmetric, and describes the shallowest portion of the volcano that hosts the lake inside a steep-walled basin. The domain extends laterally for 1 km and reaches a maximum depth of 250 m. Atmospheric conditions (air saturated, 0.1 MPa and 15 °C) are prescribed along the upper and lateral boundary, which are open to heat and fluid flows. The bottom boundary is impermeable and adiabatic, except underneath the lake, where the boundary is open over a hot, pressurized, dry-gas hydrothermal reservoir, whose existence is related to the presence of shallow intrusive bodies (Brown et al. 1989; Rymer et al. 2000, 2009; Fournier et al. 2004). Pressure and temperature of the reservoir are fixed at 350 °C and 2.4 MPa. These values correspond to the temperature inferred for the shallower portion of the intrusive body (Rowe et al. 1995) and to the hydrostatic pressure at the corresponding depth. The extent of this feeding zone along the bottom boundary was chosen assuming that both the lake formation and the ascent of hydrothermal fluids take place within the remnants of an old volcanic conduit. Where not otherwise specified, our simulations describe a system where the lake is a steady state feature, with a constant temperature and water level. Although this is generally not the case, these conditions occur, every now and then, even in an active environment as the Poás volcano (for instance between 1995 and 2005, Rymer et al. 2009). The simulation of a steady state lake, at first, will highlight those aspects of the system that do not depend on the lake evolution, and will provide a sound basis to address the more complex, transient behavior. Steady state lake conditions are simulated by imposing fixed, open boundary conditions along the crater bottom and walls. This portion of the upper boundary is set as water saturated (single-phase, liquid), with at a fixed temperature of 25 °C, corresponding to the lake temperature during quiet periods, and a fixed, hydrostatic pressure computed assuming a lake depth of 50 m. A few simulations include a rough description of the lake and are performed to account for evolving lake conditions. Further details on how we described the lake evolutions are provided below. The properties of the rock are listed in Fig. 2. Where not otherwise specified, they are uniform over the domain. In a few cases, we modified the properties of the rocks by introducing a lava layer (also shown in Fig. 2), or by assigning a lower permeability along the bottom of the lake. All simulations are run to an arbitrary final time of 100 years.

3.1 Steady State Lake Conditions

3.1.1 The Reference Case

The first simulations are carried out considering a stationary lake, whose water level and temperature do not change through time. This occurs occasionally at volcanic lakes, implying that the system has achieved a balance between the water gained by meteoric recharge, or by the inflow of hydrothermal fluids, and the water lost by evaporation or seepage. For some lakes (e.g. Lago Albano, Italy; pre-2007 Kelud; Indonesia), the lake volume is held constant by direct lake overflow (Funiciello et al. 2003; Bernard and Mazot 2004). Here we assume the lake conditions observed at Poás from 1995 to 2005, when the water level was 50 m and the water

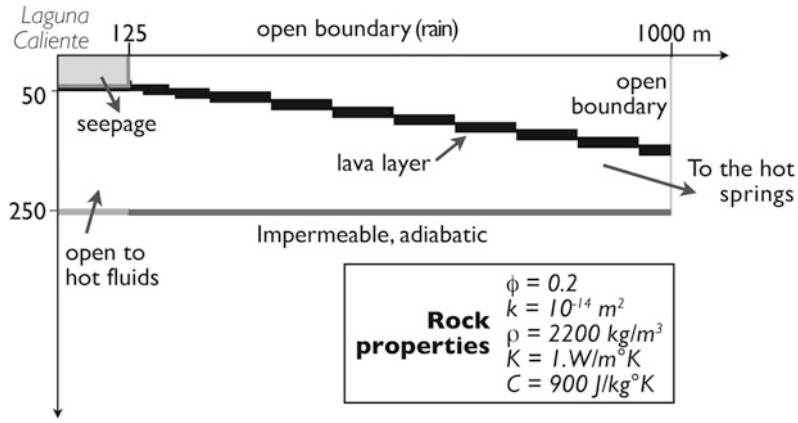

Fig. 2 The computational domain and boundary conditions. The domain is axisymmetric, and subdivided into 2,288 elements, with a constant thickness of 5 m and radial dimension ranging from 5 to 100 m. The domain is initially still, and entirely saturated with air at atmospheric pressure and temperature. *Top and lateral boundary* are set at fixed atmospheric conditions and are open to heat and fluid flow. The *bottom boundary* is impermeable and adiabatic except than for the small sector underneath the lake, which is open to the hydrothermal fluids. Uniform rock properties, as listed in the box, apply to most of the simulation (Φ = porosity; k = permeability; ρ = density; K = thermal conductivity; C = specific heat). The presence of a lava layer extending from the base of lake to the *outer boundary* has been considered in a few simulations (see text for discussion)

temperature was ca. 25 °C. The lake boundaries are open to heat and fluids, they are fully water saturated, and set at the lake temperature. The pressure is fixed to the hydrostatic pressure at each given point. Figure 3 describes the evolution of a reference case. As the simulation begins, the lake water infiltrates downward while the hot, pressurized hydrothermal vapor enters the system through the open portion of the bottom boundary. As the vapor rises, it cools and a fraction of it condenses. A small rim of liquid water forms along the outer edge of the rising plume, mostly composed by a two-phase mixture. The rising hydrothermal fluids and the downward seeping water merge after 3 years at a depth of 150 m below the lake surface. In the following years, the ascent of the hydrothermal fluids continues, heating up the region underneath the lake to temperatures above 150 °C. With time, the dry gas region at the base of the domain enlarges, while the hot, two-phase region shrinks underneath the lake, and expands laterally. Liquid water continues its downward percolation, and flows around the edge of the hot plume, joining the hydrothermal condensates. When this liquid water reaches the impervious base of the domain, it forms a thermal aquifer that slowly propagates toward the outer boundary of the domain. When the hot fluids reach the bottom of the lake, the seepage becomes progressively hindered: infiltration still takes place, but mostly horizontally, through the vertical wall. When the simulation stops after 100 years, the thermal aquifer along the bottom boundary has stretched outward and is characterized by a considerable thermal gradient. Despite the rather large rock permeability, the fluid flow in this case is not enhanced by a slope, and by the end of the simulation the thermal water has not reached the outer boundary. In other words, under the simulated conditions no springs are expected to form along the volcano's flank. In this particular case, the persistent water infiltration through the vertical wall of the crater prevents the formation of fumaroles nearby the lake, and keep the rising gases confined at greater depths.

The simulation results allow to quantify the temporal evolution of water seepage through the base and the wall of the lake and the inflow of the hydrothermal fluids into the lake. Figure 4 describes the evolution of the seepage through time, highlighting the contributions through the

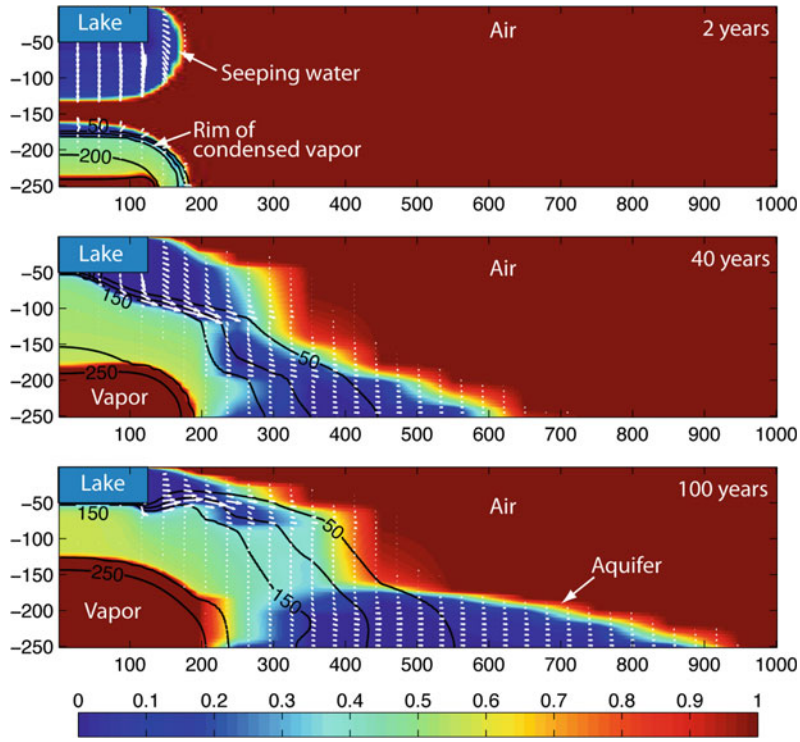

Fig. 3 Distribution of volumetric gas fraction (*color*) and temperature (*contours*) at three different times for the reference simulation. *Blue* indicates liquid water while *red* indicates gas, which can either be air or water vapor. Contour lines every 50°C. *White arrows* show the flow pattern of liquid water

vertical and horizontal lake boundaries. Under the rock properties and conditions considered here, the total seepage is characterized by an overall declining trend which is faster during the first 10 years of simulation, and more gentle on the long term. This trend reflects the two main phenomena taking place in the simulation: the progressive infiltration of lake water through the initially unsaturated volcanic rocks; and the ascent of the hot hydrothermal fluids. At the beginning of the simulation most of the water is lost through the base of the lake, thanks to the larger pressure gradient, and a saturation front propagates downward. As the initially dry rock becomes liquid saturated, the corresponding pressure increases, and the pressure gradient across the lake bottom quickly drops, strongly affecting the vertical seepage (dash-dotted line in Fig. 4). The downward propagation of infiltrated water is further delayed by the ascent of hydrothermal fluids, that tend to shift the water motion outward. After 39 years, the hydrothermal fluids reach the bottom of the lake, initially only near the symmetry axis and progressively all along the lake bottom. As a result, the water infiltration is progressively hindered until, after 90 years more of simulation, it disappears completely. The horizontal seepage through the vertical crater wall is also shown in Fig. 4 (dotted line). This component is initially less important, but unlike the vertical component, it undergoes only a minor decline when the rock surrounding the crater becomes liquid-saturated. Being substantially unaffected by the arrival of hydrothermal fluids, the horizontal seepage quickly becomes the dominant component and, on the long term, it ensures that the total seepage (solid line) never vanishes. Figure 4 also shows the time (dot) at which the total amount of infiltrated water equals the amount of water inside the lake. Under the conditions considered here, and in absence of meteoric recharge, the lake would completely drain within 12 years. Given that the yearly average precipitation is higher than the simulated seepage rate, we can assume that meteoric recharge would easily replace the water loss by infiltration, ensuring the lake survival.

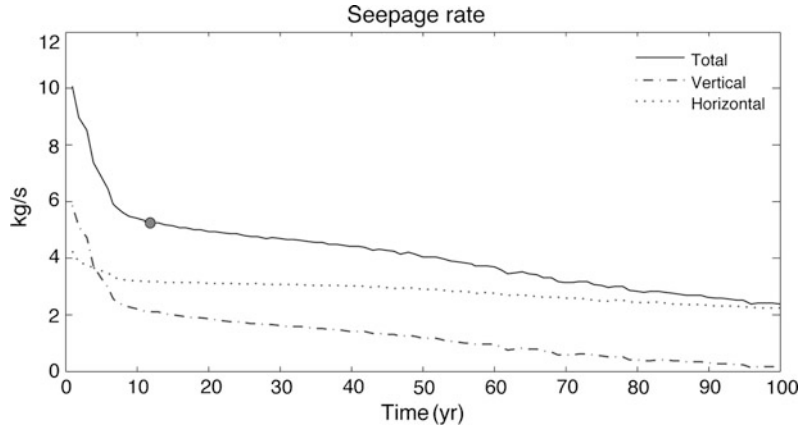

Fig. 4 Temporal evolution of the liquid water outflow (seepage) through the lake boundaries. The *dotted line* shows the horizontal outflow through the vertical boundary, and the *dash-dotted line* the outflow through the base of the lake. The *filled circle* indicates the time at which the lake would drain completely, in absence of a meteoric recharge

When the hot fluids reach the base of the lake, heat and fluids enter the lake and are expected to alter its conditions. The simulated inflow of hot vapor begins after 39 years and increases progressively to a maximum value of 0.12 kg/s that is reached at the end of the simulation. It is worth pointing out that, under such circumstances, the model assumption of constant lake properties does not hold anymore. The entire simulation is shown here for the sake of completeness.

Numerical simulations published elsewhere showed that the evolution of seepage rate is controlled by several features, including the conditions of the hydrothermal reservoir, the water level in the lake, and the permeability of the volcanic rocks (Todesco et al. 2012). The pressure and temperature of the hydrothermal source, in particular, determine the phase of the hydrothermal fluid (vapor or liquid) and the flow rate at which they rise through the volcanic edifice. Temperatures below 200 °C result in the discharge of liquid water, that tends to propagate radially away from the source and is much less efficient in hindering the lake seepage. The hotter the reservoir, the higher the amount of vapor that reaches the base of the lake, and the lower seepage rates achieved on the long term. Source pressure has an even stronger effect on the seepage evolution, with larger values causing a more effective fluid ascent, and a prompt decline in seepage rate. The water level inside the lake was shown to mostly affect the horizontal infiltration, with deeper lakes being able to discharge more water than shallow ones. For the considered range of water levels (10–50 m), the vertical seepage through the bottom of the lake is not substantially affected by the lake level. Higher seepage rates are favored by a good rock permeability: the long term seepage, in particular, is sensitive to the permeability of the vertical boundary of the lake, as seepage through the lake bottom is in any case hindered by the ascent of the hot hydrothermal fluids.

3.1.2 Heterogeneous Rock Permeability

The reference simulation was run under the assumption of a uniform permeability distribution. Stratovolcanoes, however, are by definition made of alternating lava and tephra which are expected to have different hydraulic properties. In the case of Poás volcano, the presence of an inclined, permeable lava layer is known to convey part of the hot fluids from the crater area toward lower elevations, where the hot springs formed along the northwestern flank of the volcano (Rowe et al. 1992, 1995). The presence of a preferential pathway certainly alters the pattern of fluid circulation and the resulting seepage rate.

Similarly, the presence of an impervious rock layer is expected to affect the interaction between meteoric waters and hydrothermal fluids. The simulations presented in this section all include the presence of an inclined lava layer that extends from the lake bottom to the outer boundary of the domain (Fig. 2), and is characterized by a different permeability than the surrounding rocks. Figure 5 shows the phase distribution after 3 and 100 years for the reference case and for two extreme cases of either a very permeable (10^{-12} m^2) and very impervious (10^{-16} m^2) lava layer. The presence of an impervious layer clearly prevents vertical seepage (Fig. 5a): infiltration only occurs through the vertical wall and it remains confined above the lava layer to the end of simulation (Fig. 5b). A thermal aquifer still forms at the base of the domain, but it is only fed by the condensed water vapor from the hydrothermal reservoir. When the lava layer is more permeable than the surroundings, it promotes the outward expansion of the lake water. Liquid water quickly propagates along the permeable layer, and when the lava becomes entirely saturated, the liquid water percolates downward, entering the lower portion of the domain. This turns out to be a very effective way to convey the liquid water to the deeper portion of the domain, which becomes entirely water saturated by the end of the simulation (Fig. 5b). This extreme liquid saturation affects the thermal plume, which is smaller and richer in gas, and the final temperature distribution, which is lower than in the previous cases. The simulation with a permeable lava layer is the only one in which the water actually reaches the outer portion of the domain. The presence of a layer with different permeability affects the seepage rate. Figure 6 shows that the presence of a permeable lava layer strongly influences the seepage rate which, in this case, is more than 4 times higher than in the reference case. The total seepage is mostly due to the horizontal infiltration through the vertical wall of the crater, and is characterized by a minor increment after ca. 40 years of simulation. This unusual trend is also due to the presence of a permeable lava, which extends along the bottom of the lake. The

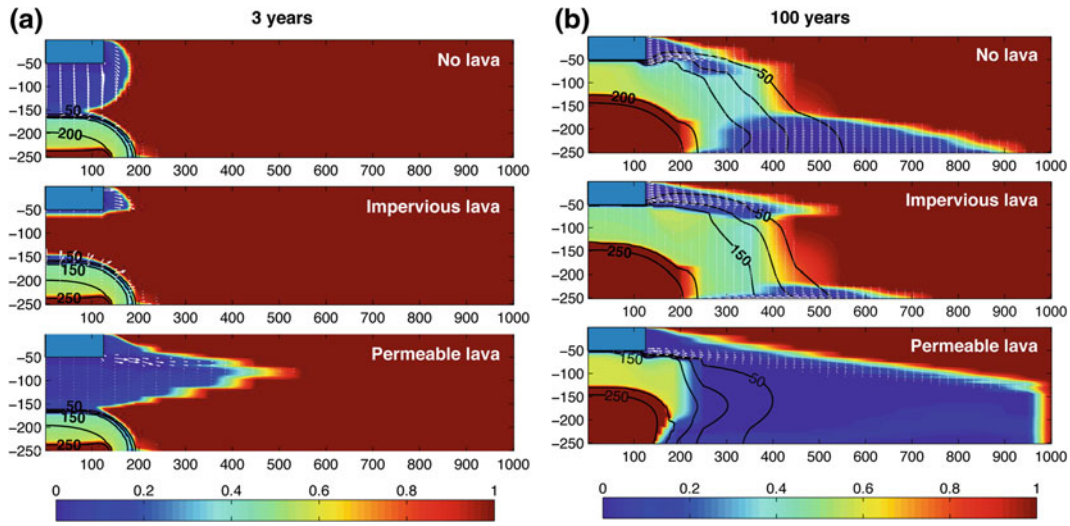

Fig. 5 **a** Volumetric gas fraction (*colors*) and temperature (°C, *contours*) after 3 years of simulation for the simulations with homogeneous domain (10^{-14} m^2), with an impervious (10^{-16} m^2) lava layer, and with a permeable (10^{-12} m^2) lava layer, respectively. *White arrows* indicate the flow pattern of liquid water. The position and size of the lava layer is shown in Fig. 2. **b** Volumetric gas fraction (*colors*) and temperature (°C, *contours*) after 100 years of simulation for the simulations with homogeneous domain, with an impervious lava layer, and with a permeable lava layer, respectively. *White arrows* indicate the flow pattern of liquid water. The position and size of the lava layer is shown in Fig. 2

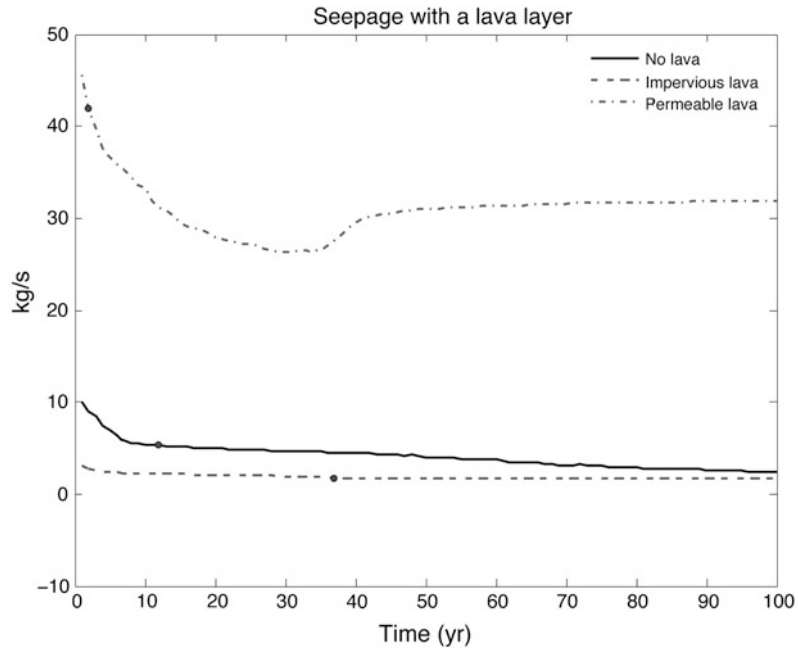

Fig. 6 Total seepage rate versus time for the three simulations with homogeneous properties (*solid*), with an impervious layer (*dashed*), and with a permeable layer (*dot dashed*). The three *dots* show the times at which the total infiltration would drain the lake in the three simulations

horizontal flow along the base of the lake is enhanced by the higher permeability and when the hot plume reaches the bottom of the lake, a fraction of steam enters the lake (ca. 0.05 kg/s), while some part condenses and propagates outward, along the permeable layer. The outflow of these condensates adds to the seepage from the lake, and is responsible for the seepage increase that is observed after ca. 40 years of simulation. The presence of an impervious layer mostly affects the vertical seepage, and keeps the total infiltration to the (low) values of the horizontal flow through the vertical wall of the crater.

3.2 Evolving Lake Conditions

The simulations described above are run considering the lake as a boundary condition set at constant temperature and pressure. These conditions imply that the lake does not change during the simulation, keeping a constant water level and temperature. Even though there are periods during which the lake conditions may not change significantly, the water level, composition, and temperature are known to evolve through time, in response to seasonal changes, a variable volcanic input, evaporation, or even because of changes in the hydraulic properties of the rocks.

A complete description of all the processes that characterize the evolution of the lake is beyond the aim of the present work. At this time, we are interested in evaluating if and how variable lake conditions affect the dynamics of subsurface flows, and in particular the temporal evolution of water seepage. To this purpose, we performed a set of TOUGH2 simulations that include a rough description of the lake. In our theoretical exercise, the lake is described by grid elements that are entirely occupied by water. We introduced a fake porous medium to represent the lake with the TOUGH2 porous-media flow simulator, with a porosity equal to 1 and a permeability of 10^{-10} m^2, high enough to ensure the onset of convection when the lake is heated, but small enough to ensure numerical stability. The thermal properties of this fake material are set equal to the water properties at atmospheric conditions. According to this crude approximation, the lake itself is treated as a porous medium, i.e., the flow within the lake is computed according to Darcy's law, and is therefore driven

by pressure gradients and buoyancy, under the assumption of steadiness and negligible inertial forces. As a consequence, the description of heat and fluid flow within the lake is certainly not realistic and cannot be considered a proper representation of the lake dynamics, or of its response to changes in the volcanic system. On the other hand, the simulated lake reacts to heat and fluid flow from the surroundings, and therefore its temperature and water level change through time, even if at a different rate than in reality. This rough approach enables us to study a system where lake conditions evolve through time and see how this affects the entire hydrothermal circulation.

3.2.1 The Reference Case with Evolving Lake

As a first test, we run the reference simulation again, this time including the simulation of the lake (Fig. 7). Initially, the lake is filled with cold water. As time goes by, seepage takes place and the water level in the lake drops. Since no meteoric recharge is simulated in this case, the lake quickly drains. Contrary to what happens in the reference case, here the amount of water available for infiltration is limited by the finite volume of the lake. As the water level drops, the downward propagation of the wetting front is somewhat slower than in the reference case (Fig. 3). The lower amount of liquid water that infiltrates underneath the lake is less effective in counteracting the ascent of hydrothermal fluids, which reach the lake after only 20 years. At this time, hot vapor enters and fills the crater that hosted the lake. After 40 years of simulation, the lake is completely dry, while the region underneath the lake is hotter and richer in gas than in the reference simulation. Hot steam rises along the vertical wall of the crater, while a small amount of liquid water survives around the plume and along the bottom of the domain (Fig. 7). Interestingly, some fraction of the hot steam that rises along the lake basin wall, condenses near the surface and flows back

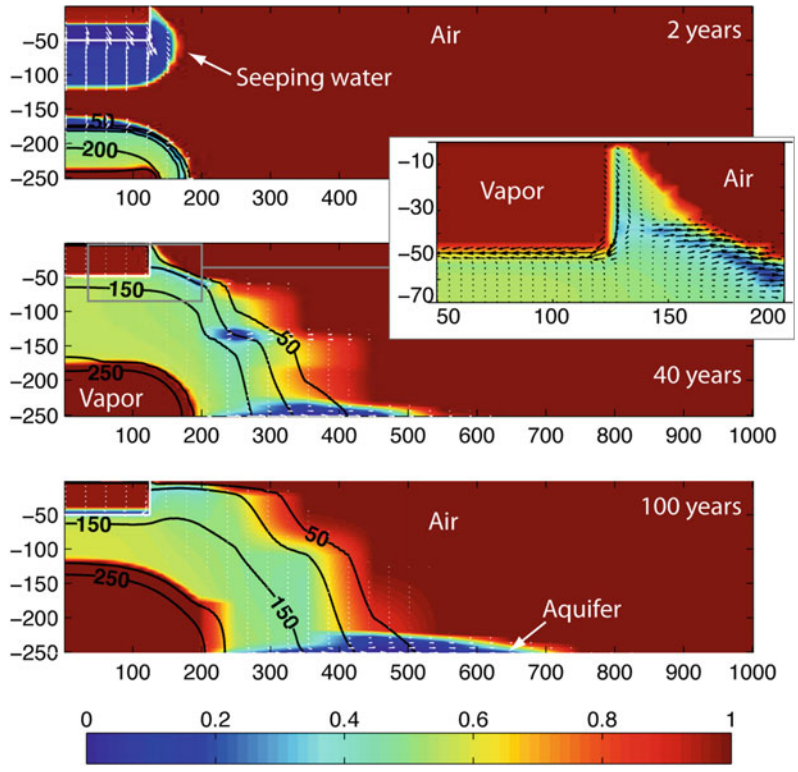

Fig. 7 Distribution of volumetric gas fraction (*color*) and temperature (*contours*) at three different times for the reference case including the simulation of the lake. *Blue* indicates liquid water while *red* indicates gas, which can either be air or water vapor. *White arrows* show the flow pattern of liquid water. The *inset* shows the distribution of gas fraction and liquid flow at the edge of the crater. *Arrows* are shown in *black* to enhance visibility

downward (Fig. 7, inset) into the crater where a shallow lake forms by the end of the simulation. The lower amount of liquid water available to the system is reflected by the thermal aquifer along the base of the domain that is thinner and colder, with respect to the one in the reference case.

The seepage rate that corresponds to this evolution is shown in Fig. 8. A comparison with Fig. 4 shows that the seepage rate is initially higher, but quickly reaches negligible values as the lake drains. The horizontal component, in particular, that in the reference case was responsible for the long-term seepage (Fig. 4), here disappears as the water level drops, contributing to the fast decline of the total seepage rate. The slight seepage increase, observed after 26 years, is due to the horizontal flow of condensates that enter the lake through its base, when the plume reaches it, and then flow outwards through the vertical wall of the crater. Water vapor also enters the lake, with a maximum inflow rate of 1.2 kg/s that is reached at the end of the simulation.

It is worth noting that, despite our rough lake representation, the seepage that drains the lake is controlled by the infiltration through the porous rocks, and is appropriately described. Water evaporation (not included into the model) would further contribute to the quick disappearance of the lake. The survival of the lake therefore depends on the choice of rock permeability, and/or on the availability of an effective meteoric recharge. In the following simulations, both these aspects are considered: a lower permeability along the lake boundaries, and abundant precipitation.

3.2.2 Evolving Lake and Meteoric Recharge

This simulation is similar to the previous one, but it incorporates a meteoric recharge. The average precipitation is simulated by placing water sources along the upper boundary of the domain. The assigned flow rate is 1.5×10^{-4} l/m^2 s (i.e., an average yearly precipitation of ca. 4,700 mm), which is within the range of variation observed for the yearly precipitation at Poás. As in the previous case, at the beginning of the simulation the lake level drops, as the water infiltrates into the volcanic edifice. After 2 years of simulation, the infiltration of rain water creates a wetting front that propagates downward, along the top of the domain (Fig. 9a). After about 10 years of simulation (not shown), the lake reaches a minimum depth of ca. 15 m and a minor temperature gradient (a few °C) drives a small convective cell near the symmetry axis. The combined effect of convection and meteoric recharge mitigate the

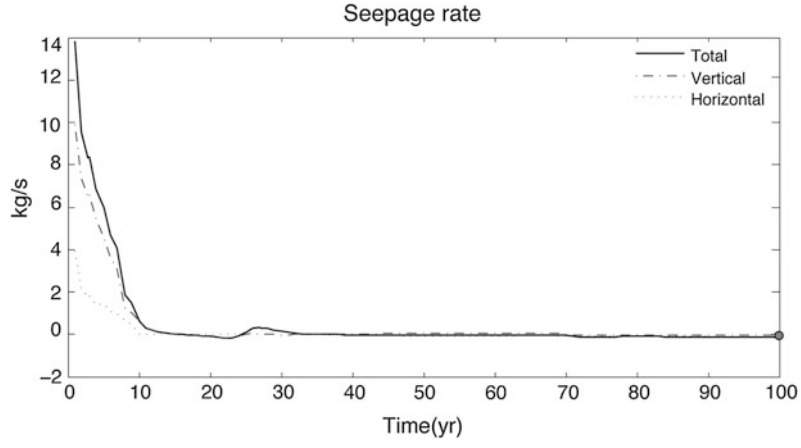

Fig. 8 Temporal evolution of the liquid water outflow (seepage) through the lake boundaries, with evolving lake conditions. The *dotted line* shows the horizontal outflow through the vertical boundary, and the *dash-dotted* line the outflow through the base of the lake. The *filled circle* indicates the time at which the lake would drain completely, in absence of a meteoric recharge

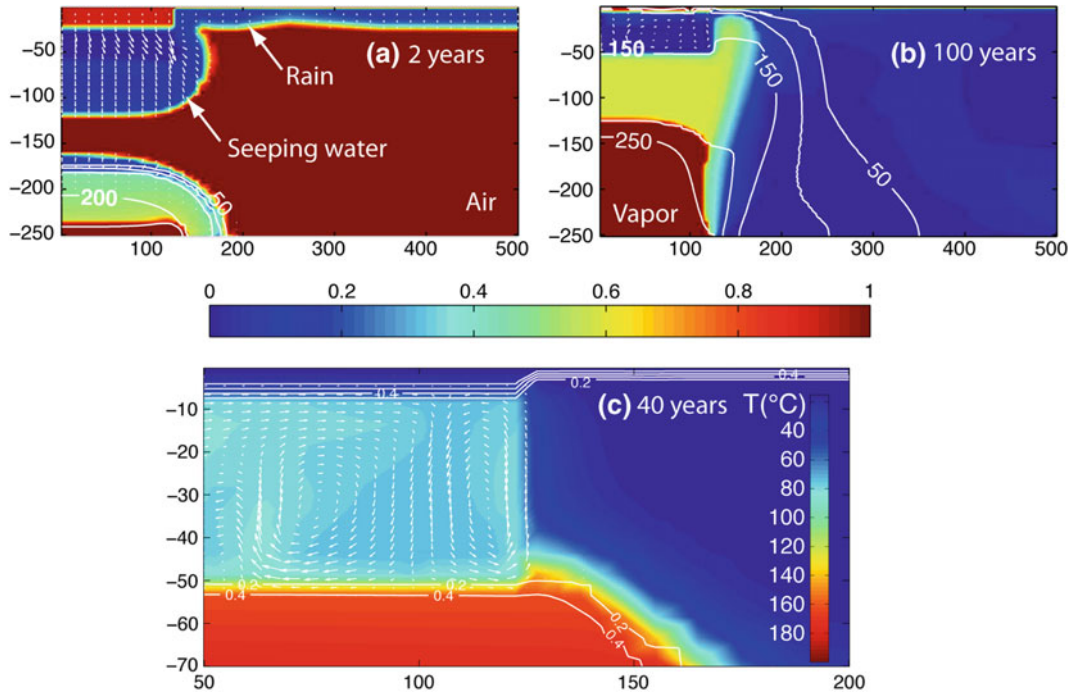

Fig. 9 Distribution of volumetric gas fraction (*color*) and temperature (*contours*) after 2 years (**a**) and 100 years (**b**) of simulation. *Blue* indicates liquid water while *red* indicates gas, which can either be air or water vapor. Temperature (°C) distribution (*color*) after 40 years of simulation (**c**). Contours refer to the volumetric gas fraction. *White* arrows in all graphs show the flow pattern of liquid water. The simulation is similar to the reference case, but includes the description of the lake and of meteoric recharge

water loss by seepage, and the lake level starts to rise again. In the next decades (not shown), the thermal disturbance associated with the ascending hydrothermal fluids affects the water circulation within the lake (~20 years), and the lake level returns near its original value (~30 years). The seepage rate at this time is reduced by the arrival of the hydrothermal fluids, while the condensed steam adds to the volume of the lake. At the end of the simulation (Fig. 9b), the entire volcanic edifice is saturated by meteoric water which keeps the hydrothermal fluids confined within the axial region. Here, a wide dry-gas zone develops above the hydrothermal reservoir and is capped by a gas-rich, two-phase region underneath the lake. The presence of a continuous meteoric recharge ensures the survival of the lake, which becomes heated and stirred by vigorous convection. After 40 years of simulation, water temperature reaches 80 °C (Fig. 9c). It is important to note that at temperatures above 50 °C evaporation is not negligible: the loss of liquid water due to evaporation at these temperatures can be estimated to about 90 l/s (Fournier et al. 2009). Considering an average meteoric recharge of ca. 20 l/s and the volume of the lake, complete evaporation at these conditions would occur in about 1 year.

The seepage rate under these conditions (not shown here) is similar to the one observed for the previous case (Fig. 8). In this case, however, a larger amount of water is available, thanks to the meteoric recharge, and the initial drop in seepage rate is more gentle. The seepage continues with a rate of ca. 1 kg/s until the hydrothermal fluids reach the lake and enter through its bottom, after

ca. 30 years. The overall declining trend is characterized by small fluctuations, associated with the convection of lake water.

3.2.3 The Permeability of the Lake Basin Walls

This simulation was carried out without meteoric precipitation, but imposing a low permeability to the lake boundaries. Various reasons can explain a low permeability at the bottom of volcanic lakes, including the presence of fine deposits, the occurrence of widespread mineral alteration, or thanks to the presence of molten sulphur, when temperature at depth is above 120 °C (Takano et al. 1994). Figure 10 shows the system evolution when a permeability of 10^{-16} m^2 is assigned to the lake boundaries. The time frames are chosen as in Fig. 7. A comparison between the two figures highlights how seepage is reduced by the lower permeability. Lake water infiltrates through the rock, but after 10 years of simulation (not shown here), the water front is still within 30 m from the bottom of the lake, and does not fully saturate the infiltrated rocks (the maximum fraction of liquid water is 0.6). The ascent of hydrothermal fluids is not hindered by an important infiltration front and the thermal plume reaches the bottom of the lake after only 15 years of simulation (Fig. 10, inset). At this time, the lake water undergoes a considerable heating, and is stirred by a vigorous convection. The hydrothermal vapor that condenses along the plume edges is driven outward and upward by the ascent of the hydrothermal fluids. After 40 years, these condensates accumulate along the lake walls (Fig. 10), without a significant contribution from the lake water. At the end of the simulation, both temperature and pressure are increased within the lake (>100 °C). A thin, thermal aquifer forms along the bottom boundary of the domain, in this case without the contribution of lake water.

3.2.4 The Birth of the Lake

This simulation begins with an empty lake basin, and describes the development of the volcanic lake due to the combined contribution of

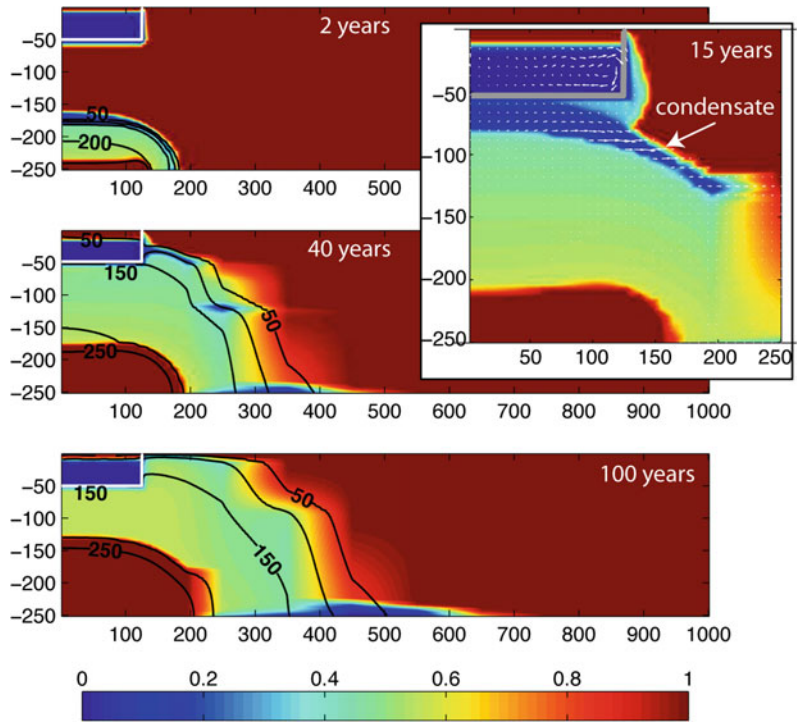

Fig. 10 Distribution of volumetric gas fraction (*color*) and temperature (*contours*) at four different times. The simulation describes an evolving lake, which is confined by a layer of lower permeability (10^{-16} m^2) along its boundaries (*white line*). The *inset* shows a zoom on the crater area at the time when the hot thermal plume reaches the bottom of the lake

hydrothermal fluids and meteoric recharge. The crater is initially filled by air at atmospheric pressure and temperature. Low permeability (10^{-16} m^2) is assigned to its walls and floor, as in the previous case. Rain water enters through the upper boundary of the domain at a constant flow rate of 1.5×10^{-4} l/m^2 s. Meteoric water infiltrates through the unsaturated shallow rocks around the crater, and begins to accumulate at the bottom of the crater; at the same time, hydrothermal fluids ascend toward the lake. After 10 years of simulation (Fig. 11a), the lake depth is less than 5 m, and only minor infiltration takes place through its floor. After 25 years, the hydrothermal fluids have reached the lake, and cause an increase in temperature and water level (Fig. 11b): the lake depth at this time has reached ca. 30 m and a thin plume of warm water (50 °C) rises along the symmetry axis. Convection continues through time, and contributes to an efficient heating of the lake (Fig. 11c). Despite the high lake temperature at the end of the simulation, only minor boiling takes place, due to the high pressure within the lake, and the gas fraction inside the lake at this time is higher than 0.1 (Fig. 11d). As in the previous case, the fluid flow through the lake boundary is severely hindered by the low permeability assigned. Minor seepage (less than 2 kg/s) occurs at the beginning of the simulation and ceases after 10 years (not shown),

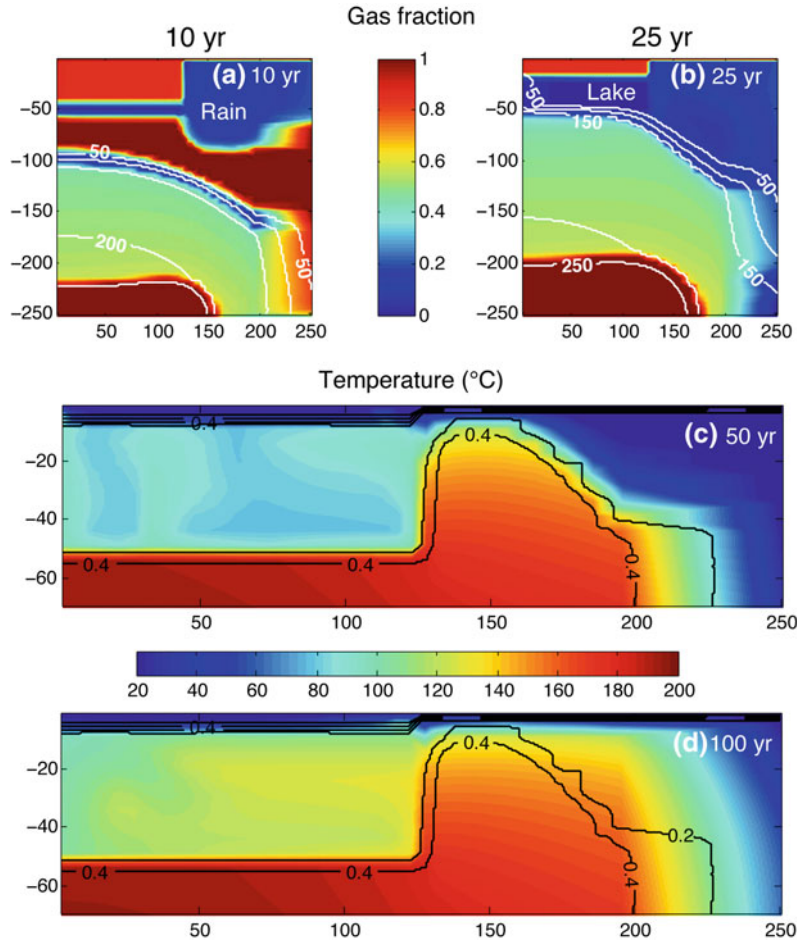

Fig. 11 Distribution of gas fraction and temperature (°C) at different times. The simulation describes an empty crater fed by both meteoric recharge and by hydrothermal fluids. Plots at 10 and 25 years show the gas fraction in *color* and temperature as *contour lines*; plots at 50 and 100 years show the temperature in *color*, and the gas fraction as *contour lines*

when it is overcome by the inflow of hydrothermal fluids. It is worth reminding that these solutions neglect the effects of evaporation, which would effectively reduce the amount of liquid water available in the lake.

4 Discussion and Conclusions

This work addresses the interaction between a volcanic lake and the underlying hydrothermal system. Numerical modeling (TOUGH2) was applied to study the infiltration of lake water (seepage) and its relations with the rising hydrothermal fluids. Our preliminary approach is based on some crude assumptions and simplifications of the natural system. Nevertheless, our results provide some interesting hints for the study of these complicated systems. Previous work focused on the role of the hydrothermal source, and showed how the system evolution is controlled by the conditions assigned to the reservoir (Todesco et al. 2012): high pressure and temperature severely hinder the water seepage, and favor the development of a hot, vapor-rich environment. On the contrary, low reservoir pressure and temperature are associated with significant water infiltration and lead to a colder, water saturated system.

Here, we focus on the role of rock permeability and of its distribution within the system, keeping the reservoir conditions unchanged. We also consider the effects of meteoric precipitation and of evolving lake conditions. A first set of simulations describe the seepage rate under steady lake conditions, where water level and temperature of the lake are held constant throughout the simulation. In the reference case, carried out with uniform rock permeability, lake water infiltrates both downward, through the lake bottom, and laterally, across the basin walls. The vertical seepage drops quickly, when the ascending fluids merge with the downward infiltration front, and the overall pressure profile becomes unfavorable to the downward flow. The horizontal component, on the other hand, is not affected by the hydrothermal plume, and never vanishes, ensuring some amount of seepage toward the end of the simulation. Results also show the development of a thermal aquifer along the bottom boundary of the domain, formed partially by hydrothermal condensates, and partially by infiltrated meteoric waters.

More complex results are obtained by considering a heterogeneous permeability distribution. The presence of an inclined layer with different hydraulic properties controls the propagation of infiltrated water within the volcanic edifice and the interaction between the meteoric and the hydrothermal components. Under the steady lake conditions considered here, a permeable layer favors the mixing and a full water saturation for a large portion of the system. The development of thermal springs along the flank of the volcano is favored, but the temperatures are buffered by the large fraction of cold, shallow water. Seepage rate greatly increases under these conditions. If, on the other hand, the inclined layer is less permeable than the surrounding rocks, it provides an effective separation between the shallow water and the hydrothermal fluids. A thermal aquifer still forms along the bottom of the domain, but without a meteoric contribution it does not reach the outer boundary of the domain. Seepage is only possible through the vertical wall of the lake basin and leads to the development of a small perched aquifer, whereas most of the system remains unsaturated.

When the lake is included in the simulation, the amount of meteoric water available to the system is limited by the size of the lake and, in some simulation, by the simulated precipitation. As discussed above, our model does not adequately represent the lake dynamics, and we did not incorporate the effects of evaporation. Therefore, we did not aim at an accurate assessment of the mass and energy balance of the lake. Nevertheless, our simulations describe the evolution of a system where the lake conditions are not steady, and where only a finite amount of water is available. A first consequence is that the system is more efficiently heated, especially near

the surface and along the crater wall. The simulations also show that the lake drains easily because of seepage, if the lake is surrounded by permeable rocks and precipitation is not accounted for. A lake confined by low permeability boundaries has greater chances of survival. Under these conditions, higher temperature and gas fraction are reached around the lake, favoring the onset of fumarolic activity. Rain water also favors the survival of the lake. An average meteoric recharge quickly saturates the entire volcanic edifice, buffering the temperature and limiting the expansion of the hydrothermal plume, especially at the base of the system.

Our simulations suggest that seepage and interaction with the hydrothermal fluids are controlled by the permeability of the lake boundaries. The vertical crater walls, in particular, determine the long term seepage and the system conditions around the crater.

The overall permeability distribution controls the degree of interaction between the meteoric and hydrothermal component and the development of hot springs. Shallow heating and fumarolic activity only develop when water seepage is limited, i.e., when reservoir pressure is high, the water level in the lake is low, or the permeability around the lake is limited.

Further studies are required to better assess the evolution of the system. The presence and geometry of isolated fractures may completely alter the distribution of temperature and fluid phases, by controlling the propagation of high-temperature fluids. Finally, the comparison between the available data sets and numerical results requires a better description of the lake and its dynamics and evolution. This will allow to fully exploit the available monitoring data and will provide a better description of the natural system.

References

Bernard A, Mazot A (2004) Geochemical evolution of the young crater lake of Kelud volcano in Indonesia. In: Wanty, Seal II (eds) Water-rock interaction, pp 87–90

Brown G, Rymer H, Dowden J, Kapadia P, Stevenson D, Barquero J, Morales LD (1989) Energy budget analysis for Poás Crater lake—implications for predicting volcanic activity. Nature 339:370–373

Casertano L, Borgia A, Cigolini C, Morales LD, Montero W, Gomez M, Fernández JF (1987) An integrated dynamic model for the volcanic activity at Poás volcano, Costa Rica. Bull Volcanol 49:588–598

Christenson BW, Reyes AG, Young R, Moebis A, Sherburn S, Cole-Baker J, Britten K (2010) Cyclic processes and factors leading to phreatic eruption events: insights from the 25 September 2007 eruption through Ruapehu Crater lake, New Zealand. J Volcanol Geotherm Res 191:15–32. doi:10.1016/j.jvolgeores.2010.01.008

Fournier N, Rymer H, Williams-Jones G, Brenes J (2004) High-resolution gravity survey: investigation of subsurface structures at Poás volcano. Costa Rica Geophys Res Lett 31:L15602

Fournier N, Witham F, Moreau-Fournier M, Bardou L (2009) Boiling lake of Dominica, West Indies: high-temperature volcanic crater lake dynamics. J Geophys Res 114:B02203

Funiciello R, Giordano G, De Rita D (2003) The Albano Maar lake (Colli Albani volcano, Italy): recent volcanic activity and evidence of pre-roman age catastrophic lahar events. J Volcanol Geotherm Res 123:43–61

Hurst AW, Bibby HM, Scott BJ, McGuinness MJ (1991) The heat source of Ruapehu Crater lake; deductions from the energy and mass balances. J Volcanol Geotherm Res 46:1–20

Hurst T, Hashimoto T, Terada A (this issue) Crater lake energy and mass balance

Martínez M, Fernández E, Valdés J, Barboza V, Van de Laat R, Duarte E, Malavassi E, Sandoval L, Barquero J, Marino T (2000) Chemical evolution and volcanic activity of the active crater lake of Poás volcano, Costa Rica, 1993–1997. J Volcanol Geotherm Res 97:127–141

Ohba T, Hirabayashi J-I, Nogami K (1994) Water, heat and chlorine budgets of the crater lake, Yugama at Kusatsu-Shirane volcano, Japan. Geochem J 28:217–231

Oppenheimer C, Stevenson D (1989) Liquid sulphur lakes at Poás volcano. Nat News 342:790–793

Pruess K, Oldenburg C, Moridis G (1999) TOUGH2 user's guide, version 2.0. Paper LBNL-43134

Rouwet D, Taran YA, Varley NR (2004) Dynamics and mass balance of El Chichón Crater lake. Mex Geofís Intern 43:427

Rouwet D, Taran Y, Inguaggiato S, Varley N, Santiago SJA (2008) Hydrochemical dynamics of the "lake-spring" system in the crater of El Chichón volcano (Chiapas, Mexico). J Volcanol Geotherm Res 178:237–248

Rouwet D, Tassi F (2011) Geochemical monitoring of volcanic lakes. A generalized box model for active crater lakes. Ann Geophys. doi:10.4401/ag-5035

Rowe G, Brantley SL, Fernández J, Borgia A (1995) The chemical and hydrologic structure of Poa´ s volcano, Costa Rica. J Volcanol Geotherm Res 64:233–267

Rowe GL Jr, Brantley SL, Fernández M, Fernández JF, Borgia A, Barquero J (1992) Fluid-volcano interaction in an active stratovolcano: the crater lake system of Poás volcano, Costa Rica. J Volcanol Geotherm Res 49:23–51

Rymer H, Cassidy J, Locke CA, Barboza M, Barquero J, Brenes J, Van der Laat R (2000) Geophysical studies of the recent 15-year eruptive cycle at Poas volcano, Costa Rica. J Volcanol Geotherm Res 97:425–442

Rymer H, Locke CA, Borgia A, Martínez M, Brenes J, Van der Laat R, Williams-Jones G (2009) Long term fluctuations in volcanic activity: implications for future environmental impact. Terra Nova 21:304–309

Sanford WE, Konikow LF, Rowe Jr GL, Brantley SL (1995) Groundwater transport of crater-lake brine at Poás volcano, Costa Rica. J Volcanol Geoth Res 64:269–293

Takano B, Saitoh H, Takano E (1994) Geochemical implications of subaqueous molten sulfur at Yugama Crater lake, Kusatsu-Shirane volcano, Japan. Geochem J 28:199–216

Taran Y, Rouwet D (2008) Estimating thermal inflow to El Chichón crater lake using the energy-budget, chemical and isotope balance approaches. J Volcanol Geotherm Res 175:472–481

Terada A, Hashimoto T, Kagiyama T (2012) A water flow model of the active crater lake at Aso volcano, Japan: fluctuations of magmatic gas and groundwater fluxes from the underlying hydrothermal system. Bull Volcanol 1–15

Terada A, Sudo Y (2012) Thermal activity within the western-slope geothermal zone of Aso volcano, Japan: development of a new thermal area. Geothermics 42:56–64

Todesco M, Rouwet D, Nespoli M, Mora-Amador RA (2012) To seep or not to seep? Some considerations regarding water infiltration in volcanic lakes. In: Proceedings, TOUGH symposium 2013

Vaselli O, Tassi F, Minissale A et al (2003) Fumarole migration and fluid geochemistry at Poás volcano (Costa Rica) from 1998 to 2001. Geol Soc London Spec Publ 213:247–262. doi:10.1144/GSL.SP.2003.213.01.15

CO_2 Degassing from Volcanic Lakes

Agnes Mazot and Alain Bernard

Abstract

Measurements of CO_2 flux emitted at the surface of volcanic lakes have been performed using the so-called floating accumulation chamber method. Two statistical methods are used to process data: the graphical statistical and stochastic simulation methods. The results of graphical statistical approach allow the quantification of two degassing processes acting at the lake surface: one corresponding to CO_2 fluxes resulting from rising bubbles and the second corresponding to equilibrium diffusion of dissolved CO_2 at the water-air surface. The sequential Gaussian simulation method has been used for mapping the CO_2 flux and estimating the total CO_2 emission rate at the surface of volcanic lakes. The study of two volcanic lakes is presented in this chapter: Kelud, Indonesia and El Chichón, Mexico. Before a lava dome appeared in the middle of Kelud Lake on the 4th November 2007, the lake contained near neutral waters with a pH of 6. The total CO_2 emission rate estimated by stochastic simulation ranged from 105 t day^{-1} for 2001 to 35 t day^{-1} for 2006. In early July 2007, the total flux for the lake area was estimated at 307 t day^{-1}, showing that CO_2 flux monitoring at the surface of volcanic lakes is a powerful tool in the improvement of early warning systems of volcanic eruptions. A significant change in CO_2 flux was not detected for El Chichón lake during the period of survey (2007–2008) but the mapping of the CO_2 flux on the lake area highlighted lineaments reflecting structures controlled by the main local and regional tectonic patterns.

A. Mazot (✉)
GNS Science, Department of Volcanology,
Wairakei Research Center, 114 Karetoto Road,
Taupo 3377, New Zealand
e-mail: A.Mazot@gns.cri.nz

A. Bernard
Laboratoire de Volcanologie, Université Libre de
Bruxelles, CP 160/02, 50 Avenue F. Roosevelt,
1050 Brussels, Belgium

D. Rouwet et al. (eds.), *Volcanic Lakes*, Advances in Volcanology,
DOI 10.1007/978-3-642-36833-2_15,
© Springer-Verlag Berlin Heidelberg 2015

Keywords
CO_2 flux · Volcanic lakes · Floating accumulation chamber · El Chichón · Kelud

1 Introduction

Volcanic lakes are surface manifestations of complex processes occurring in the hydrothermal system. The lake chemistry is affected by the water-rock interaction, dilution by meteoric water, evaporation, drainage and recirculation of water from the lake into the hydrothermal system below the lake. Hence, the physical and chemical characteristics of these lakes are variable because they reflect the state of magma degassing and the importance of the water-rock interactions in the hydrothermal system. Acidic magmatic gases, such as SO_2, HCl and HF, are highly soluble in water and are easily absorbed in hydrothermal systems and/or volcanic lakes (Symonds et al. 2001). CO_2 is the most abundant volcanic gas species after H_2O but, depending on the pH, a large amount of CO_2 can react with water to give other species such as HCO_3^-. So CO_2 flux is related to the capacity of CO_2 absorption in water and so, to a lesser extent, to the pH. In acidic water (pH < 4) CO_2 can pass through crater lakes without being absorbed and so can increase the CO_2 flux from the lake to the atmosphere.

Degassing through the surface of a volcanic lake occurs by bubbling (convective/advective degassing), evaporation and diffusion through the water/air interface. Bubbling at the bottom of Kelud lake, Indonesia, was highlighted by a hydro acoustic monitoring station set up for recording in continuous the underwater noise level (Vandemeulebrouck et al. 2000). Three separated frequency bands were determined from this station with one acoustic level corresponding to bubbling at the bottom of the lake. These measurements provided information on the evolution in CO_2 degassing in the lake as well as in the hydrothermal system.

The first measurements of the diffuse degassing from lakes by using the floating accumulation chamber method were performed by Kling et al. (1991) to study biogenic CO_2 production from an Arctic lake. Bernard et al. (2004), Bernard and Mazot (2004) and Mazot and Taran (2009) were the first to apply this method to volcanic lakes of Santa Ana in El Salvador, Kelud in Indonesia and El Chichón in Mexico (Mazot et al. 2011a, b).

In this chapter we present an overview of the floating accumulation chamber method for the measurements of CO_2 flux at the surface of volcanic lakes, as well as the statistical processing of the data. Estimates of total CO_2 emission from volcanic lakes worldwide is presented in this chapter as well as case studies of CO_2 degassing from El Chichón, Mexico and Kelud, Indonesia.

2 CO_2 Flux Measurement at the Surface of Volcanic Lakes and Data Processing

2.1 CO_2 Flux Measurement Techniques

Different CO_2 flux measurement techniques have been used to estimate gas exchange at the water-air interface (Frankignoulle et al. 1996; Upstill-Goddard et al. 1990; McGillis et al. 2001; Zappa el al. 2003; Whanninkhof et al. 1985; Clark et al. 1994). Direct methods include floating chamber (Frankignoulle et al. 1996), the eddy correlation or eddy covariance (McGillis et al. 2001) and the gradient flux techniques (Zappa et al. 2003). Other indirect methods have been used and consist in the measurement of rate of evasion from waters of an added tracer SF_6 (Upstill-Goddard et al. 1990; Frankignoulle et al. 1996) or SF_6–^3He (Clark et al. 1994) or measurements based on the surface ocean invasion rate of natural or bomb-derived $^{14}CO_2$ (Broecker et al. 1985).

Using the floating chamber method has two main advantages over the other techniques: it is easy to use and is a low cost technique. Furthermore, the fact that the lakes consist of flat and perfectly homogeneous surfaces makes the CO_2

flux measurements easier than on volcanic soils. The only disadvantage is that the floating chamber method cannot be used at wind speed higher than 8–10 m s^{-1} (Kremer et al. 2003).

2.2 Floating Chamber Method

CO_2 flux measurements have been performed according to the accumulation chamber method (Chiodini et al. 1998), modified in order to work on a volcanic lake by using a floating accumulation chamber (Fig. 1). The CO_2 flux measurements are usually done by means of LICOR LI-8100-103 non-dispersive infrared CO_2 analyzer or by using a West Systems instrument with a LICOR LI-800 or a Dräger Polytron non-dispersive infrared CO_2 detector. CO_2 gas liberated at the lake surface passes through the chamber and the infra-red sensor, consequently it returns to the chamber where it accumulates with the new CO_2 entering the chamber. The flux is derived by obtaining the increase of the CO_2 concentration with time (ppmvol s^{-1}). Each measurement takes about 40–60 s. In order to convert volumetric concentrations to mass concentrations (g m^{-2} day^{-1}), atmospheric pressure, temperature and total volume (sum of the chamber, IRGA connection tube, and the floating device) are taken in account. The fieldwork is usually undertaken under dry and stable meteorological conditions.

The reliability of the floating chamber method with other methods (i.e., Eddy Covariance, SF_6 tracer technique) has been validated in small lakes and reservoirs (Matthews et al. 2003; Guérin et al. 2007; Cole et al. 2010), coastal water bodies (Frankignoulle 1988; Borges et al. 2004a) and ocean (Kremer et al. 2003; Calleja et al. 2009). The floating chamber method evaluation agrees with those of many other studies. Usually the fluxes measured with the floating chamber method are generally overestimated particularly in low-wind speed (Kremer et al. 2003; Matthews et al. 2003; Vachon et al. 2010). In Guérin et al. (2007) the difference in the flux measurements between the floating chamber and Eddy Covariance methods was negligible. In Borges et al. (2004a, b), the discrepancy in the fluxes based on the floating chamber method with other direct methods was within 10–30 %.

One important recommendation when measuring CO_2 flux is to record the wind speed as wind-induced wave action strongly enhances gas transfer at the surface of lakes (Barbier 2010; Zhao and Xie 2010).

2.3 Method of Analysis of CO_2 Flux Data

2.3.1 The Graphical Statistical Approach (GSA)

The computation of the CO_2 flux data, based on a graphical statistical approach (Chiodini et al. 1998, 2001; Cardellini et al. 2003) permits the differentiation among different degassing mechanisms of

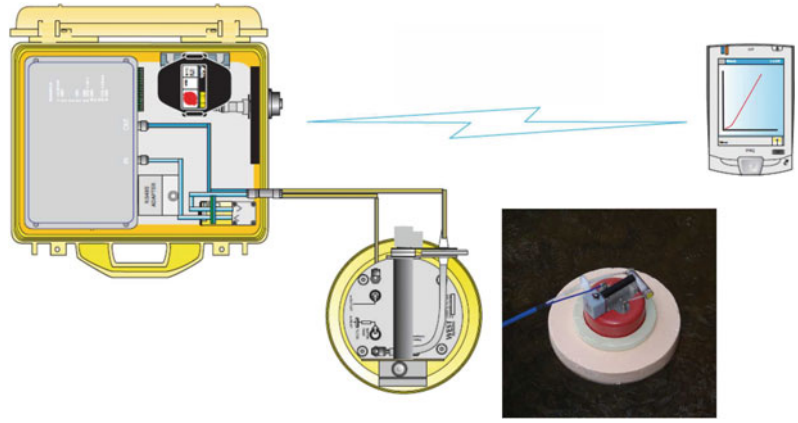

Fig. 1 Schema of the CO_2 flux system measurement (WestSystems 2006) and picture of the modified accumulation chamber

CO_2, in our case degassing by bubbling and by diffusion through volcanic lakes. According to the GSA approach (Sinclair 1974), the histogram must be transferred to a log probability plot. This plot indicates that the CO_2 flux data are separated into two or more different populations recognizable by the inflection point on the curve (Fig. 2). The multiple-population percentages must be checked and validated by combining the populations in the different proportions at various levels of log F_{CO_2}. The checking procedure uses the following relationship: $P_M = f_A P_A + f_B P_B + f_X P_X \ldots$, where P_M is the probability of the "mixture", P_A, P_B, Px… are cumulative probabilities of population A, B, X… from the plot at a specified x value; f_A, f_B, f_X… are the proportions of populations A and B. Afterwards, parameters of the individual partitioned populations can be estimated. To estimate the arithmetic mean value of CO_2 flux and the central 90 % confidence interval of the mean in the original data units (in g m^{-2} d^{-1}) for each population, we used, according to Chiodini et al. (1998), the Sichel's t estimator (David 1977).

2.3.2 Sequential Gaussian Simulation

The mapping of degassing areas and the estimation of the total CO_2 emission from the lake with associated uncertainty is performed by means of sequential Gaussian simulation (sGs, Deutsch and Journel 1998). The basic idea of the sGs is to generate a set of equiprobable representations (100 realizations for our study) of the spatial distribution of the simulated values, reproducing the statistical (histogram) and spatial (variogram) characteristics of the original data. The measured CO_2 fluxes in randomly distributed points on the surface were interpolated by a distribution over a grid of square cells covering

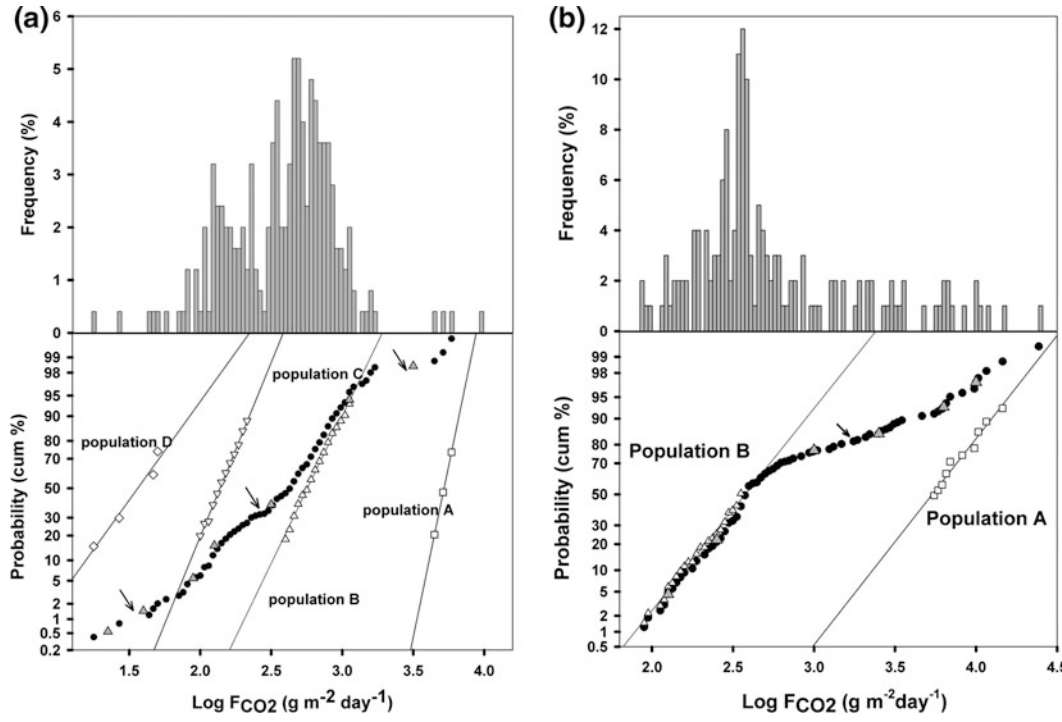

Fig. 2 Histograms and probability plots of CO_2 flux data (*black circles*) for Kelud (**a**) and El Chichón (**b**) lakes. Populations *A* (*open squares*), *B* (*open triangles down*), *C* (*open triangles up*) and *D* (*open diamonds*) are shown as *straight lines*. The inflection point is indicated by an *arrow* and corresponds to the percentage of each population. The "mixture" is represented by *gray triangles*

the study area using the exponential variogram model (Deutsch and Journel 1998). Then, 100–500 simulations of the CO_2 fluxes with the obtained distribution are performed. For each simulation, the CO_2 flux estimated at each cell is multiplied by the cell area and added to the other CO_2 fluxes estimated at the neighbouring cells of the grid to obtain a total CO_2 output. Following Goovaerts (2001), the differences among all simulated maps are used to compute the uncertainty of the flux estimation.

The sGs of CO_2 flux data proceeds in different steps, as follows (1) declustering if the data are spatially clustered; (2) normal score transform of the data as CO_2 flux data are generally positively skewed (high flux values measured); (3) processing of an experimental variogram and its model; (4) checking for bivariate normality of the normal score data. (5) Sequential simulation of the score normal data; and (6) backtransform of the simulated values into the original unit (g m^{-2} day^{-1}).

3 Degassing Mechanisms of CO_2 at the Surface of the Volcanic Lakes

By computing the CO_2 flux data following the GSA method described above, the resulting data histograms and logarithmic probability plots usually show at least two log normally distributed populations, indicating two different mechanisms of CO_2 degassing at the lake surface (Fig. 2, Table 1). The mechanisms of CO_2 degassing at the surface of volcanic lake (Mazot and Taran 2009) are usually governed by bubbling (higher F_{CO_2} values) and by diffusion of CO_2 through the water-air interface (lower F_{CO_2} values).

To evaluate CO_2 degassing by diffusion, the flux (F) between water and air can be calculated using the thin boundary layer model (Fig. 3; Liss and Slater 1974). This model considers a thin water film between the water layer and the atmosphere. The flux by diffusion is calculated by an empirical equation similar to the Fick's 1st law equation (e.g. McGillis and Wanninkhof 2006);

$$F\left(g\ m^{-2}day^{-1}\right) = k_{CO_2} \times \left(C_w - C_{w/a}\right) \times 240 \quad (1)$$

where k_{CO_2} is the gas transfer velocity (in cm h^{-1}) for CO_2, C_w and $C_{w/a}$ refer to the concentration of CO_2 in water, and in the water film at the water-air interface, respectively, and 240 is the conversion factor between mg cm^{-2} h^{-1} and g m^{-2} day^{-1}.

The flux of CO_2 from the water to the atmosphere is driven by the difference in fugacity (or pressure) between surface water and air rather than by concentration differences across the interface:

$$\begin{aligned} F &= k_{CO_2} \times K_0 (f_{CO_2w} - f_{CO_2a}) \\ &= k_{CO_2} \times \left(K_w f_{CO_2w} - K_{w/a} f_{CO_2a}\right) \end{aligned} \quad (2)$$

where K_0 is the solubility (mol kg^{-1} atm^{-1}), f_{CO_2w} and f_{CO_2a} (μatm) are the fugacity of CO_2 in surface water and air, respectively. $K_{w/a}$ is the solubility at the water-air interface and K_w is the solubility in water. The product of K_0 and f_{CO_2a})

Table 1 Proportions of each population with a mean CO_2 flux and the 90 % confidence interval obtained by statistical graphical approach for Kelud (2002; Mazot 2005) and Chichón (Mazot et al. 2011a, b)

Study Area	Populations of CO_2 flux	Proportion (%)	Mean CO_2 flux (g m^{-2} day^{-1})	90 % confidence interval (g m^{-2} day^{-1})
Kelud 2002	A	1	9,072	7,301–14,295
	B	73	945	882–1,027
	C	25	209	196–226
	D	1	87	75–115
El Chichón, March 2007	A	17	6,702	5,154–10,429
	B	83	464	442–490

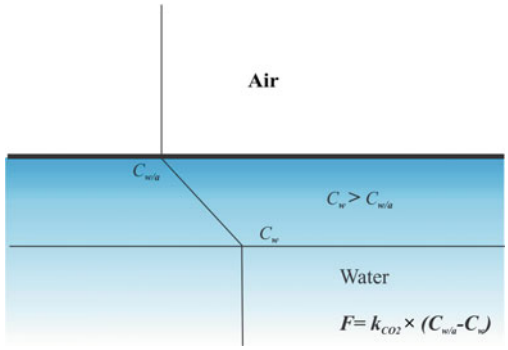

Fig. 3 Thin boundary layer model (modified from Liss and Slater 1974). Concentration profile through the layer. The *vertical lines* give the concentrations in air and bulk water and the *diagonal line* is the concentration change through the water boundary layer

is the thermodynamic driving force of the flux. If surface water f_{CO2} levels are greater than that of atmosphere, the flux is out (positive flux); if it less, the net flux is into the water (negative flux). The issues with using f_{CO_2} instead of C_w are more apparent when determining the effect of near surface processes on water-air CO_2 fluxes. Use of f_{CO_2} can lead to physically incorrect interpretations of the concentration gradient across the water film unless the temperature at the top and bottom of the layer and the temperature dependence of the dissociation constants and solubility are known. Proper use of C_w avoids many of the ambiguities in calculating water-air CO_2 fluxes. Various models have been used to evaluate F_{CO_2} at the water-air interface, the only difference is the estimation of the gas transfer velocity k_{CO_2}. This coefficient depends on the diffusion rate and the wind speed or water agitation and cannot be measured in situ. However the wind speed can be easily measured and so k_{CO_2} can be formulated using this parameter (e.g., Liss and Merlivat 1986; Zhao and Xie 2010).

As an example, F_{CO_2} calculation on the surface of volcanic lake of El Chichón, Mexico, is described in detail in this paper. The value of k_{CO_2} was calculated using the relationships among wind speed, wind wave and k_{CO_2} derived from theoretical studies on air-sea exchange (Zhao and Xie 2010) as follows;

$$k_{CO_2} = 6.81 \times \left(0.0538 \times u_1^3\right)^{0.63} \times [Sc_{CO_2}/600]^{-1/2} \quad (3)$$

where u_1 is the wind speed at 1 m height, Sc is the Schmidt Number, defined as the kinematic viscosity of water at the measured temperature divided by the diffusivity of the gas at that temperature. The transfer velocity k_{CO_2} can be corrected here to a common Schmidt number of 600, corresponding to the value for dissolved atmospheric CO_2 in fresh water at 20 °C (Liss and Merlivat 1986). The Sc_{CO_2} is a function of temperature as (Wanninkhof 1992);

$$Sc_{CO_2} = 1911.1 - 118.11 \times t + 3.4527 \times t^2 - 0.04132 \times t^3 \quad (4)$$

where t is the temperature (in ºC).

The Sc_{CO_2} at 30 °C is 360. At an average windspeed u_1 of 2 m s^{-1} (Atlas del Agua de la Republica Mexicana 1976), k_{CO_2} is calculated as 5.2. The Cw obtained after the analyses of water sampled at three different locations in the lake are 0.26, 0.29 and 0.53 mg cm^{-3} (at 30 °C, Capasso and Inguaggiato 1998). The Cw/a is assumed to be the same as the concentration of CO_2 in the air-saturated water (10^{-5} mg cm^{-3}). From Eq. 1, k_{CO_2} of 5.2 and Cw of 0.26–0.53 (mg cm^{-3}), we estimated the CO_2 flux by diffusion ranging from 320 to 663 (g m^{-2} day^{-1}) that is in the range of the mean value of F_{CO_2} (464 g m^{-2} day^{-1}) calculated using GSA method (Table 1).

4 Total CO_2 Output from Volcanic Lakes

The estimation of the total CO_2 emission from volcanic lakes with associated uncertainty are performed by the sequential Gaussian simulation described above. From 100 to 500 sGs can be performed using variogram models (i.e., exponential model) and simulation grids of different spacing depending on the size of the lake and on the length between measurement points. Figure 4 shows the CO_2 flux map of Kelud volcano (Indonesia) for 2002 based on 100 simulations, over a grid of square cells (7×7 m^2) covering the

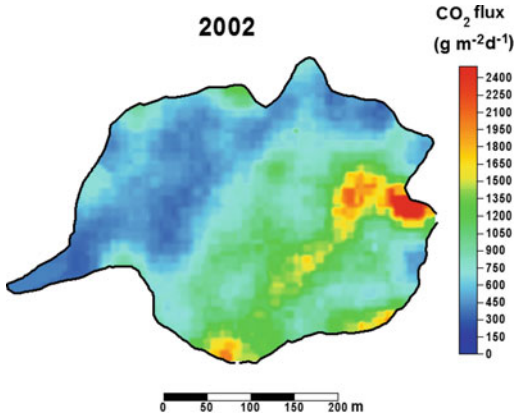

Fig. 4 CO_2 flux map for Kelud Lake, 2002 as a mean of 100 sequential Gaussian simulations (see text for explanation)

study area (103,600 m^2). From the simulations the estimated average CO_2 output was 86 t day^{-1} (σ = 2.26 t day^{-1}).

Figure 5 shows the CO_2 emission for volcanic lakes studied in the world depending on their areas. These lakes were grouped in acid (red circles), alkaline (green circles) and neutral (blue circles) lakes (Pérez et al. 2011). Following Pérez et al. (2011), acidic lakes show higher CO_2 emission rates (614 t km^{-2} day^{-1}) than neutral (201 t km^{-2} day^{-1}) and alkaline (5.5 t km^{-2} day^{-1}) lakes. Alkaline lakes contain small amounts of dissolved CO_2 mostly present as HCO_3^- and CO_3^{2-}. By using the areas of each group of volcanic lakes and the total number of volcanic lakes in the world, Pérez et al. (2011) estimated a total CO_2 emission rate of 104 Mt $year^{-1}$.

5 Mapping CO_2 Flux and Highlighting Structures

Fluid release from active volcanoes is mostly structurally controlled, with fractures acting as the main transport pathways of gases and waters. CO_2 flux surveys often reveal lineaments of high gas fluxes and faults related to the regional tectonic structures (e.g. Baubron et al. 1990; Williams-Jones et al. 2000; Aiuppa et al. 2004; Werner and Cardellini 2006; Toutain et al. 2009). El Chichón volcano is located in the central region of the Strike-Slip Fault Province of the Sierra de Chiapas (Meneses-Rocha 2001), dominated by NW-SE and E-W trending sinistral strike-slip faults. The Chiapas Volcanic Arc, situated between the Central American Volcanic Arc and the Transmexican Volcanic Belt, extends some 150 km in the northern highlands of central Chiapas. El Chichón volcano is the youngest and only active volcano in this arc (370 ka BP, Layer et al. 2009) and is located ~100 km NNW from its main volcanic centres. The transcurrent faults cutting the Jurassic to Tertiary carbonate-evaporite basement beneath El Chichón, such as the sinistral E-W San Juán strike-slip fault, are probably western prolongations of the Motagua-Polochic fault system (García-Palomo et al. 2004). The southeastern end of El Chichón is underlain by a series of N45 ° E normal faults (Chapultenango Fault System; Fig. 6), creating a half-graben geometry (García- Palomo et al. 2004). El Chichón is situated on top of the head of a N10°W oriented synclinal structure, the Buena Vista Syncline, flanked to the east by the 7.5 km-wide 12–20° NW plunging Caimba anticline and to the west by the N–S trending 7 km-wide La Unión anticline (Fig. 6).

The 1982 eruption of El Chichón volcano ejected 1.1 km^3 of anhydrite-bearing trachyandesite pyroclastic material to form a new 1 km-wide and 200 m-deep crater (Rose et al. 1984). Currently, intense hydrothermal activity, consisting of fumaroles (mainly at the boiling point), steaming ground, a geyser-like spring and an acidic (pH ≈ 2.3) and warm lake (~30 °C) occurs in the summit crater (Fig. 1B). With the low pH of the lake, CO_2 is mainly present as a gaseous phase and partially dissolved in water. So, at this range of pH, the other carbonate species HCO_3^- and CO_3^{2-} are not present in the water for which we were sure to measure the whole CO_2 input into the lake from the hydrothermal system. The El Chichón lake area changed with the lake water level between March 2007 and April 2008, mostly related to the activity of the Soap Pool geyser-like springs feeding the crater lake (Rouwet et al. 2008). The CO_2 flux anomalies on

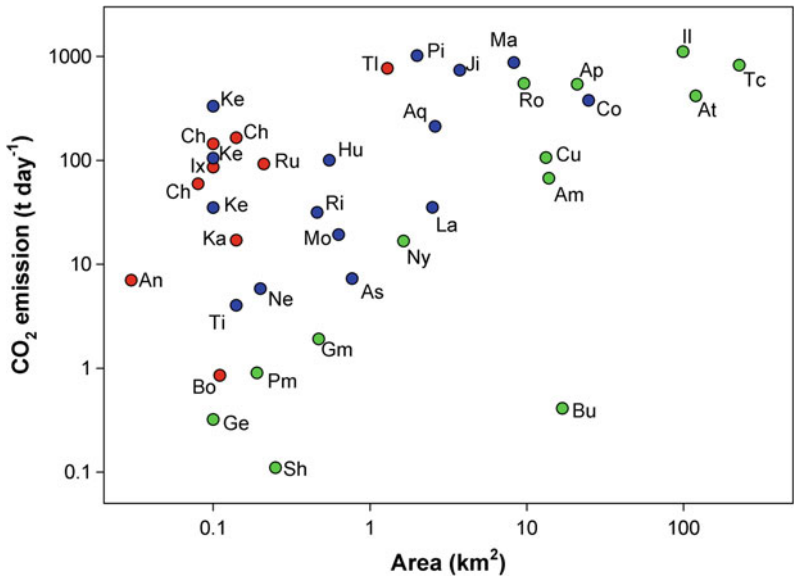

Fig. 5 Comparison of CO_2 flux among volcanic lakes in the world. Lakes were grouped in acid (*red circles*), alkaline (*green circles*) and neutral (*blue circles*) lakes. Am: Amatitlan (Pérez et al. 2011); An: Santa-Ana (Bernard et al. 2004); Ap: Apoyo (Pérez et al. 2011); Aq: Apoyeque (Pérez et al. 2011); As: Asososca Managua (Pérez et al. 2011); At: Atitlan (Pérez et al. 2011); Bo: Laguna de Botos (Pérez et al. 2011); Bu: Lago de Buhi (Pérez et al. 2011); Ch: El Chichón (Mazot et al. 2011a, b); Co: Coatepeque (Pérez et al. 2011); Cu: Cuicocha (Padrón et al. 2008); Ge: Germundeer (Pérez et al. 2011); Gm: Grande Lago di Monticchio (Mazot et al. 2011a, b); Hu: Laguna de Hule (Pérez et al. 2011); Il: Ilopango (López et al. 2004); Ix: Ixpaco (Pérez et al. 2011); Ji: Jiloa (Pérez et al. 2011); Ka: Katanuma crater lake (Pérez et al. 2011); Ke: Kelud (Mazot 2005; this study); La: Laacher See (Pérez et al. 2011); Ma: Laguna de Masaya (Pérez et al. 2011); Mo: Monoun (Pérez et al. 2011); Ne: Nejapa (Pérez et al. 2011); Ny: Nyos (Pérez et al. 2011); Pi: Pinatubo crater lake (Pérez et al. 2011); Pm: Piccolo Lago di Monticchio (Mazot et al. 2011a, b); Ri: Laguna Rio Cuarto (Pérez et al. 2011); Ro: Rotomahana (this study); Ru: Ruapehu (this study); Sh: Shalkermehren (Pérez et al. 2011); Ti: Tiscapa (Pérez et al. 2011); Tc: Taal caldera (Pérez et al. 2011); Tl: Taal crater lake (Pérez et al. 2011)

the lake surface are likely due to the subaqueous fumaroles discharging into the lake (Taran and Rouwet 2008). The CO_2 flux maps show that the high CO_2 flux spots are located near the eastern lake shore, the northeastern lake shore and the northwestern shore (Fig. 7). The CO_2 flux surveys also revealed three cross-cutting faults in the crater area: an E–W fault, probably coinciding with the San Juán sinistral strikeslip fault system; a NW–SE fault coinciding with the regional orientation of extension, the orientation of the CVA and the orientation of distribution of the dome at El Chichón; and a NE-SW structure which could be related to the Chapultenango half-graben structure to the southeast of El Chichón (Mazot et al. 2011a, b).

6 Temporal Variation of CO_2 Flux

Temporal variations in CO_2 fluxes can be related to changes in the volcanic activity and may be important for the mitigation of volcanic risk (Hernández et al. 2001; Notsu et al. 2005). Kelud volcano is one of the most active and most dangerous stratovolcano in Indonesia. In the past six centuries Kelud eruptions lead to destructive lahars, as in the 1919 eruption (5,160 victims). Before the 1990 eruption an artificial drainage system was constructed in order to maintain a constant volume of the lake (2×10^6 m^3) and to control the lahars. The presence of a lake with near-neutral pH water (pH ≈ 6) and with a

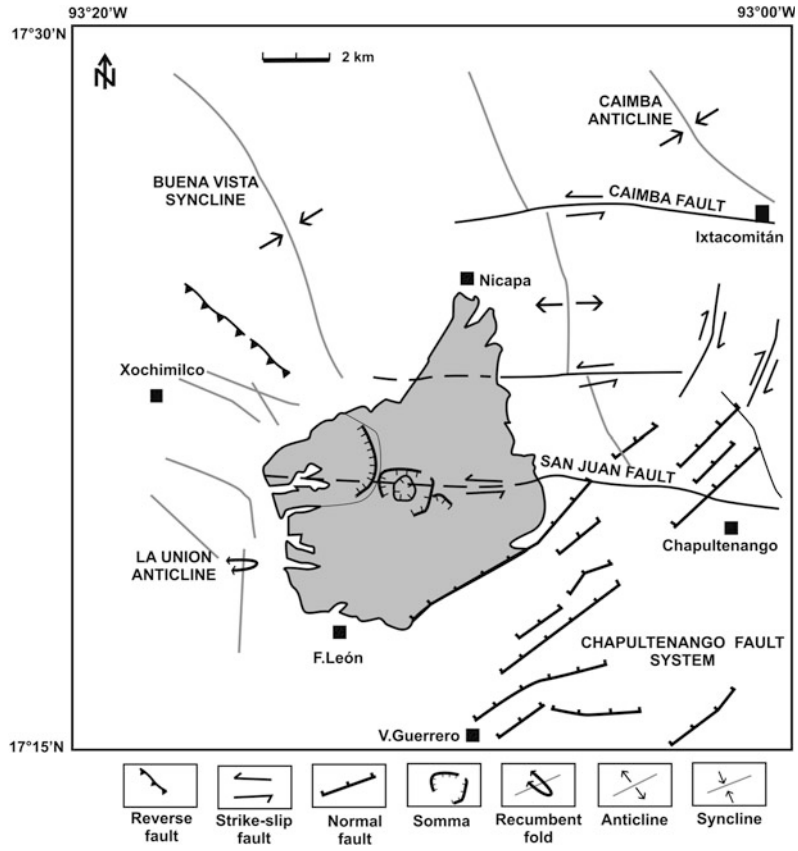

Fig. 6 Structural map of the El Chichón volcano showing main structural features. The *grey area* delimits El Chichón volcano. Modified from Garcia- Palomo et al. (2004)

temperature of about 33 °C represented an unusual site for geochemical monitoring as the majority of the other volcanic lakes characterized by similar volcanic activity contain highly acidic waters (Varekamp et al. 2000). In 1996 and 2001 two significant changes in temperature were registered without any eruption. In August 2007, CO_2 flux increased and was followed by a progressive increase in lake water temperature. On 4th of November 2007 a dome appeared at the surface of the lake and continued growing through until April 2008 (Bernard et al. 2008).

From 2001 to 2007, measurements of CO_2 emitted from the surface of the lake were performed by using the floating accumulation chamber method (Mazot 2005). The results of the graphical statistical approach showed the different degassing processes acting at the lake surface: one corresponding to CO_2 fluxes resulting from rising bubbles and the other corresponding to equilibrium diffusion of dissolved CO_2 at the water-air surface (Fig. 2). Total CO_2 emission rate estimated by sGs ranges from 105 t day^{-1} for 2001 to 29 t day^{-1} for 2006 (Table 2). In August 2007 the mean CO_2 emission increased up to 330 t day^{-1}(Bernard et al. 2008) (Fig. 8). CO_2 flux was the first parameter to be recorded one month before the increase in lake water temperature and two months before the increase in seismic activity. This demonstrates the utility of monitoring CO_2 flux on volcanic lakes as an early warning sign of volcanic unrest.

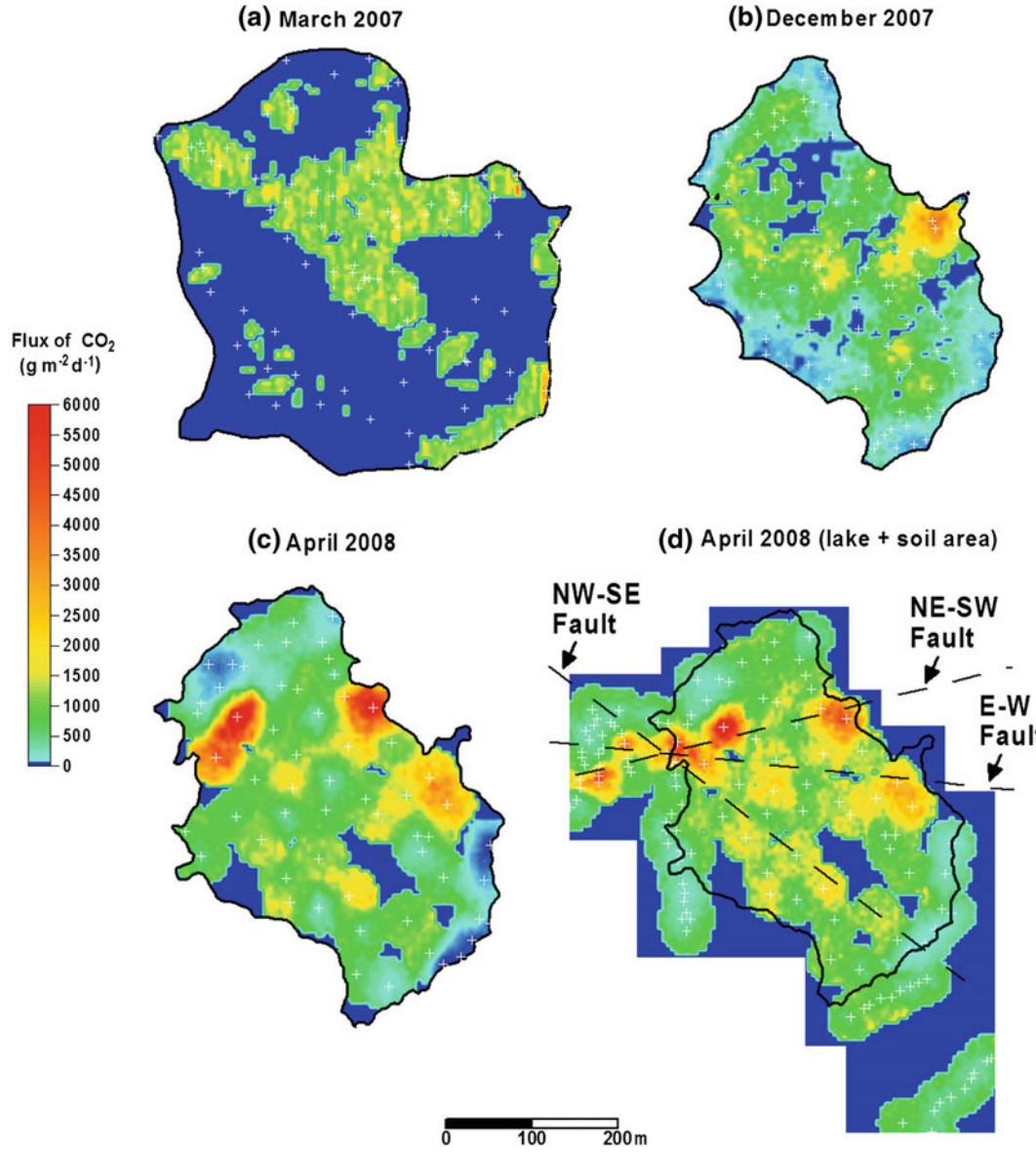

Fig. 7 CO_2 flux maps obtained by the 100 sequential Gaussian simulations for El Chichón (see text for explanation). The *black contour* is the shape of the lake at the dates of the survey. The areas of the lake for **a** March 2007, **b** December 2007 and **c**, **d** April 2008 are 138,075, 81,500 and 96,400 m^2, respectively. The *white crosses* indicate the CO_2 flux measurement sites. The *black dashes* are structures suggested from distribution of the high CO_2 flux area: (1) E–W, (2) NW–SE and (3) NE–SW (modified from Mazot et al. 2011a)

Table 2 Total CO_2 emission, deviation standard, mean CO_2 flux obtained by the sequential gaussian simulation for Kelud volcano and total CO_2 emission for the lake area

Date	Simulated area (m^2)	Total CO_2 emission (t day^{-1})	Standard deviation (t day^{-1})	Total CO_2 emission (t day^{-1}) for lake area (103,600 m^2)
2001	65,709	67	0.84	105
2002	103,292	86	2.26	87
2003	102,851	67	2.34	68
2004	102,459	35	0.61	35
2005	91,287	29	0.44	32
2006	82,075	28	0.34	35
2007 (July)	90,650	269	6.77	307

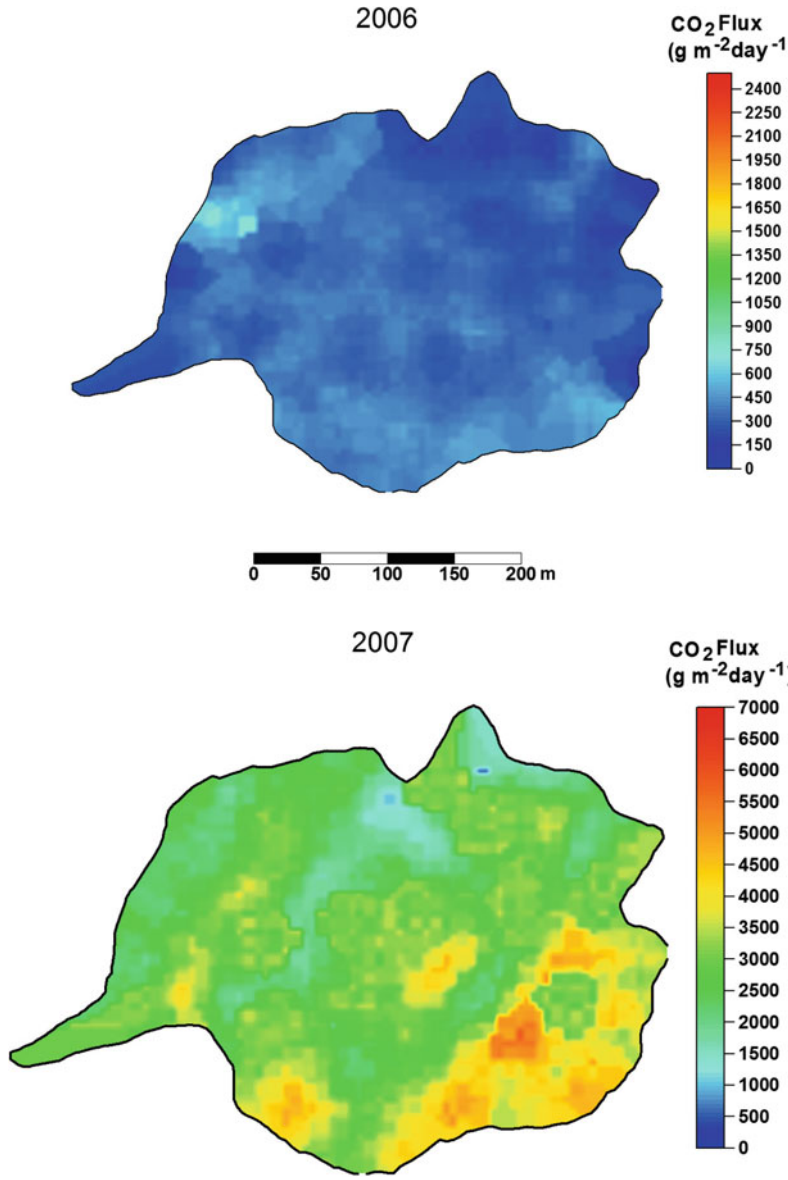

Fig. 8 CO_2 flux maps obtained by the 100 sequential Gaussian simulations for Kelud, 2006 and 2007. See the difference in the colour scale between 2006 and 2007 maps

7 Conclusion and Perspectives

CO_2 degassing from volcanic lakes is readily quantified by use of the floating accumulation chamber method, a technique first used in 2001 on Kelud volcano. Since then, this method has been proven reliable in the estimation of total CO_2 emission rate from volcanic lakes worldwide (Pérez et al. 2011). Geostatistical methods used for processing the CO_2 flux data (i.e., Graphical Statistical Approach, Sequential Gaussian Simulation) have provided valuable insights in the degassing processes at the surface of volcanic lakes (bubbling and CO_2 diffusion at the interface lake-atmosphere). Furthermore, mapping CO_2 flux on volcanic lakes can help to better understand the underlying volcanic/hydrothermal system as in highlighting structures and estimating total CO_2 emission rate for acquiring data baseline and monitoring volcanic activity level.

Other techniques of CO_2 flux measurement on volcanic lakes have been developed since a few years. For instance, echo sounding method has been used on volcanic lakes for bathymetry purpose but recently this method has been used for quantifying CO_2 flux. Four months before Kelud eruption in 2007, a detailed echo sounding survey of the volcanic lake coupled to floating accumulation chamber measurements detected abnormally high CO_2 emissions (Caudron et al. 2012). It constituted the earliest sign of the volcanic unrest; well before any other monitored parameter.

Acknowledgments Thoughtful reviews by Takeshi Ohba and Salvatore Ingguagiato were most helpful in improving the manuscript.

References

Aiuppa A, Caleca A, Federico C, Gurrieri S, Valenza M (2004) Diffuse degassing of carbon dioxide at Somma-Vesuvius volcanic complex (southern Italy) and its relation with regional tectonics. J Volcanol Geotherm Res 133:55–79

Atlas del Agua de la Republica Mexicana (1976) Secretaria de recursos hidraulicos. Atlas del Agua de la Republica Mexicana, Mexico, Mexico

Barbier B (2010) Heat transfer and geochemical characteristic of the hydrothermal system of Rinjani volano (Lombok, Indonesia). Ph.D. thesis, Universite Libre deBruxelles, Brussels, Belgium (in French)

Bernard A, Escobar CD, Mazot A, Guttiérrez RE (2004) The acid crater lake of Santa Ana volcano, El Salvador. Geol Soc Am Special Paper 375:121–133

Bernard A, Mazot A (2004) Geochemical evolution of the young crater lake of Kelud volcano in Indonesia. In: Proceedings of the 11th international symposium on water–rock interaction, Saratoga Springs, New York, USA 1, pp 87–90

Bernard A, Solikhin A, Syahbana D, Kunrat S, Barbier B, Hallet V (2008) Kelud eruption. BGVN 33(03):2–7

Baubron JC, Allard P, Toutain JP (1990) Diffuse volcanic emissions of carbon dioxide from Vulcano Island, Italy. Nature 344:51–53

Borges AV, Delille B, Schiettecatte L-S, Gazeau F, Abril G, Frankignoulle M (2004a) Gas transfer velocities of CO_2 in three European estuaries (Randers Fjord, Scheldt and Thames). Limnol Oceanogr 49:1630–1641

Borges AV, Vanderborght J-P, Schiettecatte L-S, Gazeau F, Ferron-Smith S, Delille B, Frankignoulle M (2004b) Variability of the gas transfer velocity of CO_2 in a macrotidal estuary (the Scheldt). Estuaries 27 (4):593–603

Broecker WS, Peng TH, Ostlund T, Stuiver M (1985) The distribution of bomb radiocarbon in the ocean. J Geophys Res 90:6953–6970

Calleja ML, Duarte CM, Prairie YT, Agusti S, Herndl GJ (2009) Evidence for surface organic matter modulation of air-sea CO_2 gas exchange. Biogeosciences 6:1105–1114

Capasso G, Inguaggiato S (1998) A simple method for the determination of dissolved gases in natural waters. an application to thermal waters from Vulcano Island. Appl Geochem 13:631–642

Cardellini C, Chiodini G, Frondini F (2003) Application of stochastic simulation to CO_2 flux from soil: mapping and quantification of gas release. J Geophys Res 108:2425. doi:10. 1029/2002JB002165

Caudron C, Mazot A, Bernard A (2012) Carbon dioxide dynamics in Kelud volcanic lake. J Geophys Res 117: B05102. doi:10.1029/2011JB008806

Chiodini G, Cioni R, Guidi M, Raco B, Marini L (1998) Soil CO_2 flux measurements in volcanic and geothermal areas. Appl Geochem 13:543–552

Chiodini G, Frondini F, Cardellini C, Granieri D, Marini L, Ventura G (2001) CO_2 degassing and energy release at Solfatara volcano. J Geophys Res 106 (B8):16213–16221

Clark JF, Wanninkhof R, Schlosser P, Simpson HJ (1994) Gas exchange in the tidal Hudson River using a dual tracer technique. Tellus 46B:274–285

Cole JJ, Bade DL, Bastviken D, Pace ML, Van de Bogert M (2010) Multiple approaches to estimating air-water gas exchange in small lakes. Limnol Oceanogr: Methods 8:285–293

David M (1977) Geostatistical ore reserve estimation. Elsevier, New York

Deutsch CV, Journel AG (1998) GSLIB: Geostatistical software library and users guide, 2nd edn. Oxford University Press, New York, p 369

Frankignoulle M (1988) Field measurements of air-sea CO_2 exchange. Limnol Oceanogr 33:313–322

Frankignoulle M, Gattuso J-P, Biondo R, Bourge I, Copin-Montégut G, Pichon M (1996) Carbon fluxes in coral reefs.II Eulerian study of inorganic carbon dynamics and measurement of air-sea CO_2 exchanges. Mar Eco Pro Series 145:123–132

García-Palomo A, Macias JL, Espíndola JM (2004) Strike-slip faults and K-alkaline volcanism at El Chichón volcano, southeastern Mexico. J Volcanol Geotherm Res 136:247–268

Guérin F, Abril G, Serça D, Delon D, Richard S, Delmas R, Tremblay A, Varfalvy L (2007) Gas transfer velocities of CO_2 and CH_4 in a tropical reservoir and its river downstream. J Mar Syst 66:161–172

Goovaerts P (2001) Geostatistical modelling of uncertainty in soil science. Geoderma 103(3):26

Hernández PA, Salazar JM, Shimoike Y, Mori T, Notsu K, Pérez N (2001) Diffuse emission of CO_2 from Miyakejima volcano, Japan. Chemical Geol 177:175–185

Kling GW, Kipphut GW, Miller MC (1991) Arctic lakes and streams as gas conduits to the atmosphere: implications for tundra carbon budgets. Science 251:298–301

Kremer JN, Nixon SW, Buckley B, Roques P (2003) Technical note: conditions for using the floating chamber method to estimate ai-water gas exchange. Estuaries 26:985–990

Layer PW, García-Palomo A, Jones D, Macías JL, Arce JL, Mora JC (2009) El Chichón volcanic complex, Chiapas, México: stages of evolution based on field mapping and $^{40}Ar/^{39}Ar$ geochronology. Geofís Int 48:33–54

Liss PS, Merlivat L (1986) Air-sea gas exchange rates: introduction and synthesis. In: Buat Ménart P (ed) The role of air-sea exchange in geochemical cycling. Series C: mathematical and physical sciences. Reidel, D. Publishing Company, Dordrecht, Holland, pp 113–127

Liss PS, Slater PG (1974) Flux of gases across the air–sea interface. Nature 247:181–184

López D, Ransom L, Pérez NM, Hernández PA, Monterrosa J, Notsu K (2004) Dynamics of diffuse degassing at Ilopango caldera, El Salvador, Central America. In: Rose WI, Bommer JJ, Sandoval C (eds) Natural hazards in El Salvador. Geological Society of America, Special Paper, 375:191–202

Matthews CJD, Saint-Luis VL, Hesslein RH (2003) Comparison of three techniques used to measure diffusive gas exchange from sheltered aquatic surfaces. Environ Sci Technol 37:772–780

Mazot A (2005) CO_2 degassing and fluid geochemistry at Papandayan and Kelud volcanoes, Java Island, Indonesia (in French). Ph.D. thesis, Universite Libre de Bruxelles, Brussels

Mazot A, Rouwet D, Taran Y, Inguaggiato S, Varley N (2011a) CO_2 and He degassing at El Chichón volcano, Chiapas, Mexico: gas flux, origin and relationship with local and regional tectonics. In: Inguaggiato S, Shinohara H, and Fischer T (eds) Geochemistry of volcanic fluids: a special issue in honor of Yuri A. Taran. Bull Volcanol 73(4):423–442

Mazot A, Taran Y (2009) CO_2 flux from the volcanic lake of El Chichón (Mexico). Geofís Int 48:73–83

Mazot A, Vaselli O, Nisi B (2011b) Estimation of CO_2 flux from Lakes Monticchio, Mt Vulture, Southern Italy. Geophys Res Abs 13, EGU2011-9543

McGillis WR, Edson JB, Ware JD, Dacey JWH, Hare JE, Fairall CW, Wanninkhof R (2001) Carbon dioxide flux techniques performed during GasEx-98. Mar Chem 75:267–280

McGillis WR, Wanninkhof R (2006) Aqueous CO_2 gradients for air–sea flux estimates. Mar Chem 98:100–108

Meneses-Rocha JJ (2001) Tectonic evolution of the Ixtapa Graben, an example of a strike-slip basin of southeastern Mexico: implications for regional petroleum systems. In: Bartolini C, Buffler RT, Cantú-Chapa A (eds) The western Gulf of Mexico Basin: tectonics, sedimentary basins, and petroleum systems. AAPG Memoir 75. AAPG, Tulsa, pp 183–216

Notsu K, Sugiyama K, Hosoe M, Uemura A, Shimoike Y, Tsunomori F, Sumino H, Yamamoto J, Mori T, Hernández PA (2005) Diffuse CO_2 efflux from Iwojima volcano, Izu-Ogasawara arc, Japan. J Volcanol Geotherm Res 139:147–161

Padrón E, Hernández PA, Toulkeridis T, Pérez NM, Marrero R, Melían G, Virgili G, Notsu K (2008) Diffuse CO_2 emission rate from Pululahua and the lake-filled Cuicocha calderas, Ecuador. J Volcanol Geotherm Res 176:163–169

Pérez NM, Hernández PA, Padilla G, Nolasco D, Barrancos J, Melían G, Padrón E, Dionis S, Calvo D, Rodríguez F, Notsu K, Mori T, Kusakabe M, Arpa MC, Reniva P, Ibarra M (2011) Global CO_2 emission from volcanic lakes. Geology 39:235–238

Rose BW, Bornhorst TJ, Halsor SP, Capaul WA, Plumley PS, De La Cruz Rayna S, Mena M, Mota R (1984) Volcan El Chichón, Mexico: Pre-1982 S-rich eruptive activity. J Volcanol Geotherm Res 23:147–167

Rouwet D, Taran Y, Inguaggiato S, Varley N, JA SS (2008) Hydrochemical dynamics of the "lake-spring" system in the crater of El Chichón volcano (Chiapas, Mexico). J Volcanol Geotherm Res 178:237–248

Sinclair AJ (1974) Selection of threshold values in geochemical data using probability graphs. J Geochem Explor 3:129–149

Symonds RB, Gerlach TM, Reed MH (2001) Magmatic gas scrubbing: implications for volcano monitoring. J Volcanol Geotherm Res 108:303–341

Taran Y, Rouwet D (2008) Estimating thermal inflow to El Chichón crater lake using the energy-budget, chemical and isotope balance approaches. J Volcanol Geotherm Res 175:472–481

Toutain JP, Sortino F, Baubron JC, Richon O, Surono SS, Nonell A (2009) Structure and CO_2 budget of Merapi

volcano during intereruptive periods. Bull Volcanol 71:815–826

Upstill-Goddard RC, Watson AJ, Liss PS, Liddicoat MI (1990) Gas transfer velocities in lakes measured with SF_6. Tellus 42B:364–377

Vachon D, Prairie YT, Cole JJ (2010) The relationship between near-surface turbulence and gas transfer velocity in freshwater systems and its implications for floating chamber measurements of gas exchange. Limnol Oceanogr 55(4):1723–1732

Vandemeulebrouck J, Sabroux J-C, Halbwachs M, Surono N, Poussielgue N, Grangeon J, Tabbagh J (2000) Hydroacoustic noise precursors of the 1990 eruption of Kelut volcano, Indonesia. J Volcanol Geotherm Res 97:443–456

Varekamp JC, Pasternack GB, Rowe GL (2000) Volcanic lake systematics II. Chemical constraints. J Volcanol Geotherm Res 97:161–179

Wanninkhof J (1992) Relationship between wind speed and gas exchange over the ocean. J Geophys Res C5:7373–7382

Wanninkhof R, Ledwell JR, Broecker WS (1985) Gas exchange wind speed relationship measured with sulphur hexafluoride on a lake. Science 227:1224–1226

Werner C, Cardellini C (2006) Comparison of carbon dioxide emissions with fluid upflow, chemistry, and geologic structures at the Rotorua geothermal system, New Zealand. Geothermics 35:221–238

WestSystems (2006) Portable diffuse flux meter LI820 carbon dioxide handbook, p 92

Williams-Jones G, Stix J, Heiligmann M, Charland A, Sherwood Lollar B, Arner N, Garzón G, Baquero J, Renández E (2000) A model of diffuse degassing at three subduction-related volcanoes. Bull Volcanol 62:130–142

Zappa C, Raymond PA, Terray EA, McGillis WR (2003) Variation in surface turbulence and the gas transfer velocity over a tidal cycle in a macro-tidal estuary. Estuaries 26:1401–1415

Zhao D, Xie L (2010) A practical bi-parameter formula of gas transfer velocity depending on wave states. J Ocean 66:663–671

Quantitative Hydrogeology of Volcanic Lakes: Examples from the Central Italy Volcanic Lake District

R. Mazza, S. Taviani, G. Capelli, A.A. De Benedetti, and G. Giordano

Abstract

Volcanic lakes are surface expressions of the hydrogeology of volcanic complexes. Hydrogeological analysis of volcanic complexes is important both in terms of management of the water resource and from the point of view of associated geothermal and volcanic processes. In particular volcanic lakes are the site of possible mixing between superficial fluids (water) and endogenous fluids (gas and/or magma). The Tyrrhenian volcanic domain hosts several volcanic lakes, which, depending on their origin, can be classed as crater lakes or caldera lakes. The presence of large cities (like Rome), and intense industrial and agricultural activities have significantly modified the "natural" equilibrium and groundwater resources have been significantly depleted during the last 20–30 years. In many areas the situation has turned "critical", involving both the lowering of groundwater and lake levels. In this chapter, we present the results of quantitative hydrogeological analysis of two volcanic lakes in the surroundings of the densely urbanized hinterland of Roma capital city (Italy): the Bracciano caldera lake basin (Sabatini volcanic complex) and the Albano crater lake basin (Colli Albani volcano). The groundwater flow systems have been analyzed and the hydrogeological water balances defined. A focus has been put on the areas with larger aquifer depletion. The methodologies applied to the lake water balances include GIS analyses supported by geostatistics.

Keywords

Crater and Caldera lakes · Hydrogeology · Management · Aquifer

1 Introduction

Volcanic lakes represent the outcropping of the groundwater table associated with the hosting volcano. Volcanic lakes can be classified as crater lakes or caldera lakes depending on the

R. Mazza · S. Taviani (✉) · G. Capelli · A.A. De Benedetti · G. Giordano
Dipartimento di Scienze, Università di Roma TRE, Largo S. Leonardo Murialdo 1, 00146 Rome, Italy
e-mail: sara.taviani@uniroma3.it

D. Rouwet et al. (eds.), *Volcanic Lakes*, Advances in Volcanology,
DOI 10.1007/978-3-642-36833-2_16,
© Springer-Verlag Berlin Heidelberg 2015

origin of the morphology that hosts the lake. Crater lakes are hosted by conical depressions excavated during explosive events (either magmatic or phreatomagmatic) and may be hundreds of meters across, and more rarely larger than 1 km (Cas and Wright 1987). Their shape depends on the explosive mechanism, and on their age, in terms of both crater wall retreat and amount of crater filling. Generally in young crater lakes the basin aspect ratio (lake radius/lake depth) is low. Caldera lakes, instead, form inside depressions due to collapse of the roof of the magma reservoir caused by withdrawal of large volumes of magma. Generally diameters of caldera lakes are several kilometers up to tens of kilometers across. Caldera lake geometry is controlled by caldera-faults, with collapse heights usually in the order of hundreds to one thousand of meters (Geyer and Marti 2008). The resulting caldera lake basins are rather cylindrical with a high aspect ratio. The different origins and structural settings affect also the hydrogeology of crater versus caldera lakes. In particular, caldera lakes are always the expression of the main volcanic aquifer, whereas crater lakes may be associated with perched aquifers or even be hydrogeologically isolated. Since early human history, areas around volcanoes have supported communities taking advantage of the abundance of high quality water resources. Central volcanoes usually form individual hydrogeological units as they are rather simple, conical edifices, made of permeable to highly permeable rocks. The basal aquicludes may show complex geometries due to caldera collapses and volcanotectonics. The presence of caldera and/or crater lakes at the summit of volcanoes enhances the effective infiltration and uncovers the top of the hydrogeological system. Another specific and very important characteristic of volcanic hydrogeological systems is the abundance of vertical structures like dikes, conduits, diatremes, caldera and volcano tectonic faults, which potentially allow exchanges across aquifers at different depths (Ayenew and Becht 2008; Jutzeler et al. 2011). Crater Lake, in Oregon, USA, is an example of a very deep caldera lake, with a maximum depth of 594 m and a surface area of 54 km^2. Long term monitoring of Crater Lake has been used to develop a baseline of information about the natural dynamics and complexity of the lake (Larson et al. 2003).

In active or young volcanoes, the influence of the upraise of deep-seated fluids from geothermal and magmatic systems allows the formation of shallow hydrothermal systems, which are particularly relevant for groundwater movement. Furthermore, in case of an eruption, ground and surface waters may efficiently interact with magma giving rise to highly hazardous phreatomagmatic (thermo-hydraulic) explosions (e.g. Buettner et al. 1999; Mastin 2007; Pardo et al. 2009; Rouwet ad Morrissey 2014, this issue).

Crater and caldera lakes are natural piezometers of the volcanic hydrogeology, and therefore excellent sites for monitoring the availability of groundwater, their physical-chemical characteristics, the potential for geothermal energy exploitation and hazard arising from phreatomagmatism.

Quantitative analysis of volcanic lakes involves the knowledge of the volcanic hydrogeological system, of the basin in- and out-flows, and the vertical exchanges with deeper systems. Ayenew and Becht (2008) presented a comparative assessment of the water balance and hydrology of selected Ethiopian and Kenyan rift lakes. In highly populated areas associated with crater lakes worldwide, the human pressure on the hydrogeological system can be extreme, becoming, in fact, the most important element in the hydrogeological balance.

The Tyrrhenian volcanic domain (Fig. 1) is an excellent area to approach the complex interplay between natural and human-induced factors affecting Quaternary volcanic lakes and associated hydrogeological systems (Capelli et al. 2005), and serves to explore the implications of these factors for groundwater management, geothermal potential, and volcanic hazards. The Tyrrhenian volcanic domain hosts several volcanic lakes (Mattei et al. 2010), distinguished in crater lakes (e.g. the Albano Lake) and caldera lakes (e.g. the Bracciano Lake). Mosello et al. (2004) discussed the chemical composition of Bolsena Lake waters, and compared them with those of other volcanic lakes in Latium

Fig. 1 Digital elevation model of Central Italy, with the indication of all the 10 crater and caldera lakes. *VL* Vulsini *1* Bolsena, *2* Mezzano; *Vc* Vicani, *3* Vico; *Sa* Sabatini *4* Bracciano, *5* Martignano, *6* Monterosi; *CA* Colli Albani, *7* Albano, *8* Nemi; *Rm* Roccamonfina; *CF* Campi Flegrei, *11* Averno, *12* Grande. *V* Vesuvio; *Vu* Vulture, *9* Monticchio (Lago Grande), *10* Monticchio (Lago Piccolo)

(Bracciano, Albano, Nemi and Vico). The volcanic domain is densely populated, with many cities and towns forming the hinterland to Rome capital city. At the same time there are many areas of intense industrial and agricultural activities. Groundwater resources have been significantly depleted in the last 20–30 years (Capelli et al. 2002; Mazza et al. 2009). Recent studies have successfully applied an original method to define the state of stress of the volcanic aquifers under human exploitation in central Italy (Capelli et al. 2005). A stressed aquifer can be described in terms of thickness, piezometric drawdown (by comparing the year 1970 with the year 2000 piezometries), the spatial distribution and relative amount of human withdrawal for different uses (potable, agricultural and industrial). "Critical areas" in the volcanic aquifers of Central Italy, i.e. areas with a high hydric stress, are those where the total withdrawal for hectare is equal or more than 1,600 m^3/year (Capelli et al. 2005).

In this chapter, we present the results of quantitative hydrogeological analysis of two volcanic lakes: the Bracciano caldera lake (North of Rome) and Albano crater lake (South of Rome). These two case histories allow to show two different groundwater flow systems, where the interplay between the structure of the lake basin and the related volcanic aquifer are discussed. The hydrogeological balance is approached by taking into account both natural and human factors, with a focus on the relationships between lake level and ground-water table variations.

2 Geological Setting

The Central Italian Volcanic Lake District (CIVOLD) is located between 42°36' N (Bolsena Lake) and 40°50' N (Averno Lake) (Figs. 1, 2 and Table 1). These volcanic lakes are hosted by the Pleistocene–Holocene volcanoes that form the NW-trending, K-alkaline, peri-Tyrrhenian volcanic belt. The volcanic belt is composed of several main volcanic complexes forming the Roman Magmatic Province (Mattei et al. 2010, and references therein). The locations of volcanoes are related to cross-cutting NW-trending and NE-trending extensional structures. The erupted

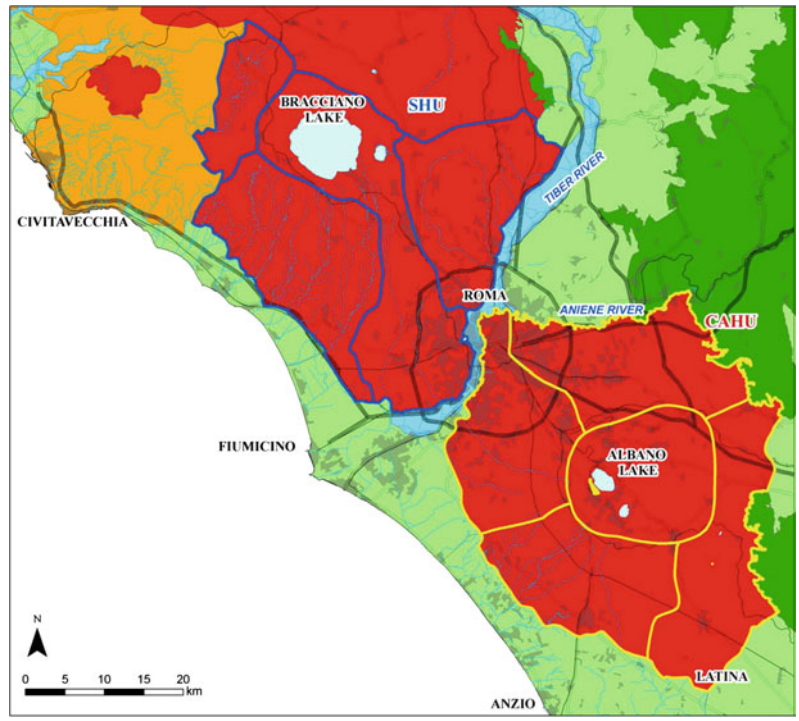

Fig. 2 Map of the Sabatini Hydrogeologic Unit (SHU) and Colli Albani Hydrogeologic Unit (CAHU)

volumes are in the order of several hundreds of cubic kilometers for each volcanic complex and several thousands of cubic kilometers for the entire volcanic belt. All main volcanoes are associated with two types of calderas: caldera complexes and summit calderas. Caldera complexes are associated with the paroxysmal eruption of tens to hundreds of cubic kilometers of ignimbrites that induce caldera collapses with diameters between 10 and 20 km. Ignimbrites form layered successions of tens to hundreds of meters thick and are distributed radially around the calderas, forming vast and gently sloping plateaus, thousands of square kilometers wide. The caldera complexes of the CIVOLD are, from north to south, the Bolsena-Latera (Vulsini, Barberi et al. 1994), the Bracciano-Sacrofano (Sabatini, De Rita et al. 1983, 1996), the Vulcano Laziale (the early edifice of the Colli Albani volcano, Giordano et al. 2006, 2010) and, in the Neapolitan area, the Campi Flegrei (Scandone et al. 1991; Orsi et al. 1996). Caldera lakes are present today only at Bolsena and Bracciano; the other calderas are filled by both lacustrine sediments and post-caldera volcanic deposits. Stratovolcanoes, from north to south, are Vico (Sollevanti 1983; Bear et al. 2009a, b), Faete (the intracaldera edifice of the Colli Albani volcano, Giordano et al. 2006, 2010), Roccamonfina, Ventotene (Pontinan islands, Bellucci et al. 1997; De Rita et al. 2001), Ischia and Procida (Scandone et al. 1991; Orsi et al. 1996), Somma-Vesuvius (Santacroce 1987; Bianco et al. 1998) and Vulture (Principe 2006). These stratovolcanoes also consist of erupted ignimbrites and can host small summit collapse calderas. Vico hosts the only caldera lake at the summit of a stratovolcano. In all volcanic complexes, phreatomagmatic activity has occurred forming large and deep maar craters. Some of the most recent maars still host lakes at present (Table 1). Many other maar lakes had dried due to sedimentation or, in historical times, were dried out by the construction of artificial outlets (Castellani and Dragoni 1997; De Benedetti and Funiciello 2007). The formation of maars testifies the presence of significant aquifers within and below the volcanoes. In many cases the groundwater comes from a

Table 1 Characteristics of Central Italy volcanic lakes

Volcanic district	Lake	Type	Max width (m)	Max length (m)	Max depth (m)	Elevation (m asl)	Caldera/crater forming events	Minimum age (ky)	Emissary-type	References
Vulsini	Bolsena	Caldera	1,391	1,207	151	294	Montefiascone ig., Orvieto ig., Basal ig. (Nenfri)	370	Natural	Innocenti and Trigila (1987)
	Mezzano	Crater	827	750	31	452	Hydromagmatic final er.	145–100	Natural	
Vico	Vico	Caldera	5,078	4,850	49.5	510	Carbognano Fm., Ronciglione Fm., Sutri Fm. (Tufo rosso a scorie nere), Farine Fm.	138	Natural	Bear et al. (2009a, b)
Sabatini	Bracciano	Caldera	9,310	9,090	165	164	Tufo di Bracciano ig.—Tufo Rosso a scorie nere ig.	400–150	Natural	De Rita et al. (1993)
	Martignano	Crater	1,925	1,547	60	207	1st Martignano hydromagmatic unit	>86	Artificial	Sottili et al. (2012)
	Monterosi	Crater	660	574	7	237	Monterosi center hydromagmatic deposits	>83 < 150	No	De Rita et al. (1993)
Colli Albani	Albano	Crater	3,422	2,333	165	293	Montagnaccio, Coste dei Laghi, Corona del Lago, Cantone, Peperino Albano, Villa Doria, Albalonga units	<70	Artificial	De Benedetti et al. (2008)
	Nemi	Crater	1,846	1,291	37	316	Nemi unit	<200	Artificial	Giordano & the CARG team (2010)
Vulture	Monticchio (Lago Grande)	Crater	830	574	38	656	Subsintemi di Lago Grande e Lago Piccolo	<140	No	Principe (2006)
	Monticchio (Lago Piccolo)	Crater	493	384	35	658				
Campi Flegrei	Averno	Crater	971	747	35	2	Averno er.	5–3,5		Giacomelli and Scandone (2007)
	Lago grande	Crater	225	175		10	Astroni er.	5–3,5		

geothermal system, as in the case of the Albano and Nemi maars in the Colli Albani (De Benedetti et al. 2008, 2010) and Monterosi in the Sabatini complex (De Rita et al. 1989).

3 Climatic Framework

The CIVOLD is located in the "Middle Tyrrhenian" climatic region. Most of the lakes occupy the highest part of the volcanic edifice; due to their sub-littoral geographical location, they experience a maritime climate with generally mild winters and hot summers (Ambrosetti and Barbanti 2002). Values of average annual precipitation range from 800 to 1,200 mm and values of average annual temperature from 11.5 to 15.3°C, surveyed at the main hydrologic stations located near the lakes (the last 50 years as the reference period).

4 Quantitative Hydrogeology

4.1 Methodology

4.1.1 The Importance of the Geological-Structural Model

Volcanic morphologies, the 3D architecture of volcanic deposits and volcano-tectonics strongly control the groundwater flow system. Pasternack and Varekamp (1997) analyzed the general physical factors that contribute to lake formation, and introduced a physicochemical classification scheme for volcanic lakes. According to their classification, Bracciano and Albano lakes belong to the low-activity/no-activity groups, due to their low temperature and low values of total dissolved solids.

The geological-structural differences between the Bracciano caldera lake and the Albano crater lake are reflected in different hydrogeological models. Bracciano lake, located inside a caldera structure, is in contact with the main volcanic aquifer; it occupies an area of around 56 km^2. Its aspect ratio ranges from 27.8 (considering the maximum depth of 164 m) to 50.8 (considering the mean depth of 88.6 m). Albano lake is located inside a crater and relates to a perched aquifer; it occupies an area of around 5 km^2 (Fig. 2; Table 1). It has an aspect ratio ranging from 8.7 (considering the maximum depth of 165 m) to 17.5 (considering the mean depth of 80 m). The hydrogeological system of Bracciano and Albano lakes could be considered similar to many caldera and crater lakes around the world.

Faults, dykes and volcanic conduits can represent either preferential vertical flow paths or flow barriers, depending on the type of permeability developed. Volcanic products are characterized by a high heterogeneity in terms of permeability and geometry, therefore a volcanic succession may not be considered either homogeneous or isotropic at the local scale; however at a larger scale the volcanic succession may be associated with an "equivalent hydraulic conductivity" (Matheron 1967). The geological-structural model helps to define the number of aquifers present in the system, the aquifer characteristics (confined or unconfined), the aquifer productivity, and the watershed boundaries.

Although Bracciano and Albano lakes can be considered as low-activity/no-activity lakes, both lakes are located in active geothermal areas characterized by upwelling of deep fluids which mix with the shallow groundwater. One striking indication of this phenomenon is the diffuse thermal anomaly of the shallow aquifers. In Fig. 3, the map of groundwater temperature reports measurements in wells collected from 2002 to 2009 and measurements in springs (Capelli et al. 2012). Temperatures in 611 wells range from 5.6 to 37.3 °C, with 96 wells in which temperature exceed 20 °C. Temperature and total dissolved solids (TDS) have been measured in a total of 138 springs; 21 springs are considered as mineral (TDS > 750 mg/L), 6 as thermal (T °C > 20 °C), 15 as thermomineral (TDS > 750 mg/L and T > 20 °C), and 96 as meteoric water. The lowest values are located in the area near Albano lake, whereas the highest values are in the northwest area, near Bracciano lake (Vicarello area) where temperatures of springs reach 48 °C and TDS around 1,500 mg/L. High values of temperature

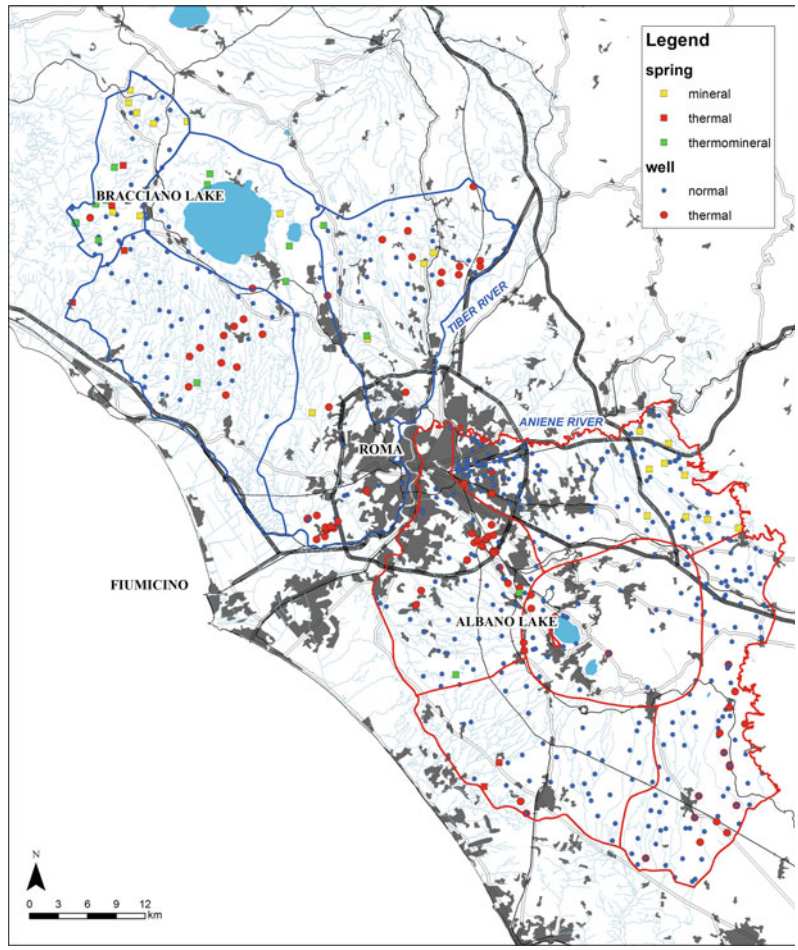

Fig. 3 Bracciano and Albano groundwater temperature, measured in wells and springs, see text for explanation (Capelli et al. 2012)

and TDS in aquifers have been explained as due to the influence of deeper geothermal aquifers (Duchi et al. 1991; Chiodini and Frondini 2001).

4.1.2 Mass Conservation and Hydrological Balance

The lake water balance is part of the total water balance of the hydrogeological basin. The lake is "contained" by a volcanic depression and the amount of lake water in- and out-flows are strongly controlled by the hydrogeological setting. The first step in calculating the water balance is to quantify volumes of water exchanged between the atmosphere and lithosphere (Fig. 4). It is therefore necessary to deal with volumetric units (the groundwater basin) and with transient conditions. Many authors have focused on the understanding of lake water balance (Hurst et al. 1991; Rowe et al. 1992; Ohba et al. 1994; Pasternack and Varekamp 1997; Rouwet et al. 2004, 2008; Rouwet and Tassi 2011). The influence of the surrounding terrain, regional hydrogeology and lake geometry on the overall lake water budget has been studied in some detail (Krabbenhoft et al. 1990; Anderson and Cheng 1993; Cheng and Anderson 1994; Kratz et al. 1997; Winter 1999; Townley and Trefry 2000). Demlie et al. (2007) presented a comprehensive conventional hydrological and hydrogeological study conducted in two crater lakes in Ethiopia. Particular emphasis was given to the estimate of the water balance and assessment of groundwater and surface water interactions.

The Bracciano caldera lake belongs to the Sabatini Hydrogeological Unit (SHU), and the

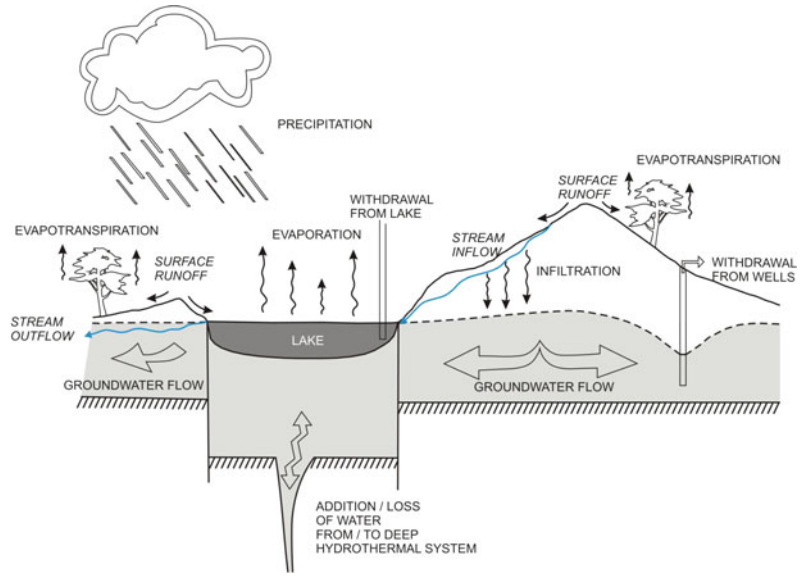

Fig. 4 Idealized sketch of main factors involved in water balance of volcanic lakes

Albano crater lake belongs to the Colli Albani Hydrogeological Unit (CAHU) (Fig. 2). Table 2 describes the natural factors contributing to the water balance calculated for the two units, expressed in mm/y and m^3/s. It is seen that the amount of water that feeds the aquifer, i.e. the Recharge, represents around 30 % of the Precipitation, for both areas. In the central Italy climatic context Evapotranspiration represents about 50 % of Precipitation. The effects of human pressure are expressed by the voices related to different withdrawals; the total withdrawal constitutes 79 % of the Recharge in the CAHU and 41 % of the Recharge in the SHU. The human stress on the groundwater system is evident and has to be considered as an influent factor in strongly urbanized areas.

Focusing on the lake, the volume of water and the lake level are related to the equilibrium between the sources and sinks of water with time. The quantification of the water balance of a lake requires defining the inflow and outflow components of the hydrogeological cycle (Fig. 4; Table 3). It can be mathematically represented as:

Change in storage = Inflow−Outflow and the water balance components for the lakes are given by:

$$P + SR + G_i + S_i - E - G_o - S_o - W \pm \Delta S = 0 \quad (1)$$

where P is the Precipitation on the lake, SR the Surface Runoff from the hydrologic basin, G_i the Groundwater inflow, S_i is the Stream base flow, E the lake water Evaporation, G_o the Groundwater outflow, S_o is the flow from the lake to the outlet (if present), W the withdrawal from the lake, and ΔS is the change in storage/net flux of the unmeasured groundwater component including errors that might be incorporated in estimating the other water balance components. These components are expressed in m^3/s (Eq. 1). Rouwet and Tassi (2011) proposed a generalized box model for active crater lakes, emphasizing the importance of estimation of the influx of "volcanic" fluids with the purpose of geochemical monitoring. In the cases of low-activity/no-activity lakes as Bracciano and Albano, this quantity is very low and at first approximation can be neglected.

4.1.3 Use of Geographic Information System (GIS) to Evaluate the Hydrogeological Balance

The use of GIS facilitates evaluation of the hydrogeological balance at high spatial and temporal resolution. The methodology includes: analysis of the spatial and temporal variability of the rain and temperature at a monthly scale and

Table 2 Distributed water balance for Albano area (Capelli et al. 2005) and Bracciano area and lake hydrogeologic balance from numerical groundwater model simulation for Albano lake (Capelli et al. 2005) and for Bracciano lake

Distributed balance methodology calculated for the hydrogeologic basin area (CAHU and SHU)				
Area (km^2)	Factor	mm/y	m^3/s	% of precipitation
Colli Albani volcanic unit (1,982)	Precipitation	731	45.94	**100**
	Evapotranspiration	346	21.75	**47.3**
	Surface runoff	138	8.63	**18.7**
	Recharge	247	15.52	**33.8**
	Baseflow measured	62	3.90	**8.5**
	Agricultural withdrawal	*46*	*2.89*	*6.3*
	industrial withdrawal	*75*	*4.71*	*10.3*
	Potable public withdrawal	*53*	*3.33*	*7.3*
	Total withdrawal	175	11.00	**23.9**
Sabatini volcanic unit (1,109)	Precipitation	664	23.35	**100**
	Evapotranspiration	334	11.75	**50.3**
	Surface runoff	114	4.01	**17.2**
	Recharge	216	7.60	**32.5**
	Baseflow measured	10	0.35	**1.5**
	Agricultural withdrawal	*37*	*1.30*	*5.6*
	Industrial withdrawal	*31*	*1.09*	*4.7*
	Potable public withdrawal	*17*	*0.60*	*2.6*
	Total withdrawal	86	3.02	**13.0**

Taviani S (2011) Application of the Modflow groundwater numerical model to hydrogeological volcanic units. Unpublished Ph.D. Thesis, Rome, Italy

Table 3 Lake water balance of Bracciano and Albano lakes (Capelli et al. 2005)

Lake balance			
Area	Factor	mm/y	Mm^3/y
Albano (5.7 km^2) hydrologic basin 10.7 km^2	P (precipitation)	731	4.17
	SR (surface runoff)	127	0.63
	Si (stream inflow)	–	–
	E (evaporation)	1,051	5.99
	W (withdrawal)	–	–
Change in lake storage = (precipitation + surface runoff + stream inflow + Gw inflow) − (evaporation + Gw outflow + withdrawal)[a]			−193 mm/y −1.19 Mm^3/y
Bracciano (56.7 km^2) hydrologic basin 150 km^2	P (precipitation)	664	37.65
	SR (surface runoff)	88	8.21
	Si (stream inflow)	17	1.58
	E (evaporation)	968	54.89
	W (withdrawal)	167	9.47
Change in lake storage = (precipitation + surface runoff +stream inflow + Gw inflow) − (evaporation + Gw outflow + withdrawal)[a]			−366 mm/y −16.91 Mm^3/y

[a] Gw inflow and Gw outflow unknown

Taviani S (2011) Application of the Modflow groundwater numerical model to hydrogeological volcanic units. Unpublished PhD Thesis, Rome, Italy

grid resolution, consideration of runoff and evapotranspiration effects due to morphological, lithological and of land-use conditions, at a high spatial resolution, comparison of the distribution of withdrawal in relation to the recharge distribution, quick update of data streams, and the possibility to summarize information at the single hydrogeological basin scale.

The recharge has been calculated using a method of spatial variable balance as reported by Capelli et al. (2005) on a raster map (250 × 250 m cells) with each cell representing the corresponding calculated recharge. The maximum size of computational cells must be comparable with the minimum size of considered cartographic elements (land use, lithological associations, morphology, Available Water Capacity (AWC), etc.). The timescale should allow to consider seasonal variability and, ultimately, distribution and intensity of meteorological events. The experimental data currently available made a monthly, and in some case even daily approach necessary. It is always advisable to obtain the Recharge as the sum of monthly or daily contributions, in order to take into account variability of regional and climate factors during several years.

$$R(\text{year}) = \Sigma(P_{\text{month}} - EVR_{\text{month}} - SR_{\text{month}}) \quad (2)$$

The annual Recharge in each cell is the difference between Precipitation, real Evapotranspiration and Surface Runoff (in mm/y and in m^3/s, Eq. 2 and Table 2).

Values of Table 2, taken from Capelli et al. 2005, have been calculated as yearly mean values, taking into consideration the reference period 1997–2001. The GIS platform, schematized in Table 4 (Taviani S (2011) Application of the Modflow groundwater numerical model to hydrogeological volcanic units. Unpublished PhD Thesis, Rome, Italy) accounts for:

- Climate spatial and temporal distribution (temperature, rainfall, solar radiation, wind speed, humidity). Starting from daily data of precipitation, maximum and minimum temperature registered in the gauging stations, a monthly aggregation (for precipitation) and a mean value of maximum and minimum temperature have been considered. Data have been processed using kriging FAI-K interpolation (Chilès and Delfiner 1999) and a grid with distributed values of monthly precipitation (mm) has been obtained. With the same approach, grids of maximum and minimum temperature (°C) have been obtained, considering kriging FAI-K with the Digital Elevation Model (DEM) as external drift (topography);
- A polygon shape file containing information on vegetation cover and land use was included. Considering Corine land cover (Regione Lazio 1994) and color orthophotos a map of Unit of Land Hydro-exigency (ULH) has been built. By assigning to each class of ULH a monthly value of the Kc crop coefficient (Capelli et al. 2005) a grid of Kc (adimensional, from 0 to 1.1) has been obtained;
- From the analysis of "stone gradient" (Capelli et al. 2005), elaborated from the geological map at 1:25000 scale and from the thickness of soil and soil characteristics, the AWC has been evaluated as a grid in mm. The AWC is the amount of water available in the soils for the crops growth;
- A grid representing distributed values of Kennessy coefficient, Ck (Kennessey 1930) was obtained by the overlap of information layers taken from the geology, aquifer lithology (rock permeability), the morphology (slope from Digital Elevation Model, exposure, presence of drainage and the vegetal covering, ULH).

Surface runoff (Eq. 3 and Tables 2 and 4) is expressed as the sum of the monthly difference between precipitation and evapotranspiration, multiplied by the average annual runoff coefficient (Kennessey coefficient, Ck):

$$SR(\text{year}) = \Sigma(P_{\text{month}} - EVR_{\text{month}}) * Ck \quad (3)$$

Experimental data on surface runoff have been collected (Gasparri A (1987) Idrologia e idrogeologia dell'apparato vulcanico dei monti della Tolfa e del piccolo bacino rappresentativo del

Table 4 Scheme for calculating the distributed value of recharge

Starting data	Kind of aggregation/other informations	Data processing	Unit of measurement and maximum and minimum value	Output	Time variable
Daily precipitations	Monthly cumulate precipitation	Kriging, FAI-k	mm	P distributed value of monthly precipitation (grid)	Yes
Maximum daily temperatures	Tmax monthly mean of the maximum daily temperatures	Kriging FAI-k, with external drift	°C	Tmax distributed value of the monthly mean of the maximum daily temperatures (grid)	Yes
Minimum daily temperatures	Tmin monthly mean of the minimum daily temperatures	Kriging FAI-k, with external drift	°C	Tmin distributed value of the monthly mean of the minimum daily temperatures (grid)	Yes
Mean daily temperatures (obtained by the mean of the minimum and maximum daily temperature values)	Tmean monthly mean of the medium daily temperatures	Kriging FAI-k, with external drift	°C	Tmean distributed value of the monthly mean of the medium daily temperatures (grid)	Yes
Corine land cover (shape polygon)		Building a specific legend correlate to fotointerpretation areas		ULH (Unit of Land Hydro exigency) mapping units with homogeneous need of water (shape polygon)	Yes
Colors ortophotos—scale 1:10000 of the regione Lazio flight of year 2000		Fotointerpretation of colors ortophotos			
Topographic map 1:10000		Draw perimeters of the ULH			
H = thickness of soil (m)—from geology map (1:25000) shape polygon	Value necessary in the estimation of the evapotranspiration	AWC = H*(1−P)*120 F available water capacity	mm, from 0 to 235	Distributed value of the AWC (grid)	No
P = gradient of stone (%)					
120 = mean unitary value of the reference AWC for the considered soils (mm/y)					
F = correction factor for vulcanic soils					
ULH		A monthly value of kc is associated to every ULH class	From 0 to 1,1	Kc—distributed monthly value of the crop coefficients (grid)	Yes
Hydraulic conductivity (geology)		Assigning a percent value to each component	From 0 to 1	Ck—distributed value of the Kennessey coefficient (grid)	Almost no
Topography slope (DEM)					
Vegetal covering (UTI)					
RA solar radiation, it has an unic monthly value for the entire area	EVR (evapotraspiration)	EVR = ETR (if there isn't deficit)	If P + Ui > ETR	$ETP = 0{,}0023\ (Tmean + 17{,}8)\ (Tmax - Tmin)^{0{,}5}\ RA$	
			ETR = ETP*kc		
DF deficit		EVR = P + Ui (if there is deficit)	If P + Ui < ETR		
Uim = (P − ETR + Ui)m − 1; if Uim > AWC ≥ Uim = AWC; if Uim < AWC ≥ Uim = Uim and DF = (Ui − ETR + P)m					
Surface runoff	SR (year) = Σ (Pmonth−EVRmonth)*Ck				
Recharge	R (year) = Σ (Pmonth − EVR month − SRmonth)				

Taviani S (2011) Application of the Modflow groundwater numerical model to hydrogeological volcanic units. Unpublished PhD Thesis, Rome, Italy

Cinque Bottini. Unpublished master's thesis, Università degli Studi di Roma "La Sapienza", Roma; Tarantino L (1991) Bacino "Cinque Bottini" (Allumierre): bilancio idrologico del periodo maggio 1986–aprile 1987. Unpublished master's thesis, Università degli Studi di Roma "La Sapienza", Roma) in an adjacent basin to the study area, similar to CAHU and SHU, from a geologic point of view. Calibrated instruments were installed for flow measurement on a closed section of a watercourse. Results from experimental data were compared to the surface runoff calculated above and a similarity is found. The effective infiltration is the portion of rain that contributes to aquifer recharge. In the case of aquifers where contributions of surface water and groundwater from adjacent areas can be considered as negligible, the effective infiltration corresponds to the amount of renewable resource, and thus available for the maintenance of underground and surface outflow/inflow basis of the waterways and for human activities.

The total amount of human withdrawal was estimated in different ways depending on the type of withdrawal:

- Water supply for potable use was estimated by the PRGA document (AA.VV. 2004). In the case of PRGA, it was possible to consider the amount of withdrawal for several wells distributed in the study area and feeding public aqueducts of the towns around lakes. A problem concerning PRGA is the reliability of data since no official version of this plan exists and all the information is not from validated versions provided by Regional Administrator;
- Value of monthly average withdrawal from Lake Bracciano, are known from the Water Agency database;
- Water supply for industrial and irrigation use was estimated by an evaluation of the water required for the time window considered. The estimation of industrial and agriculture abstraction was made by the evaluation of water requirement, according to a distributed grid (considering a cell value of 100 m) based on different information, such as land use, climate and information on population and on the economical activities as given by the National Statistic Institute (ISTAT 1991).

5 Case Studies: Bracciano Caldera Lake and Albano Crater Lake

The two case studies regard the Bracciano caldera lake in the Sabatini volcanic complex and the Albano crater lake in the Colli Albani volcano; they are representative of caldera lakes and crater lakes, respectively. These lakes are important because the Sabatini and the Colli Albani volcanoes are located just north and south of Rome, respectively: their water resources have been used since Roman times for the potable, agricultural and industrial needs of the Roman metropolitan area. In Table 1 the main physical and morphometric parameters of the two lakes are reported, along with those of the other volcanic lakes in the CIVOLD. Their catchment areas are very different, i.e. small for Albano and much larger for Bracciano. Primary inflows to the Bracciano lake and the Albano lake are precipitation, surface runoff and groundwater inflow. Primary outflows at present are evaporation and lake water seepage. Both lakes have outlets currently dry because of drops in lake levels since the 1990s.

5.1 Albano Crater Lake

The Albano lake is located in the central area of the Colli Albani volcano, inside a maar located on the edge of a larger caldera structure. Albano lake has an artificial 1.5 km long tunnel-outlet dug through the crater wall by Romans (around 394 BC) in order to delimit the lake level (Funiciello et al. 2003, De Benedetti et al. 2008). Albano lake is the upper part of the hydrogeological system. It is hydrogeologically related to

the main regional volcanic aquifer. The Colli Albani Hydrogeological Unit (CAHU, 1,982 km^2, Fig. 2) is bounded to the west and southwest by the Tyrrhenian sea, and to the north and northeast by the Tiber and Aniene rivers. The potential aquifer productivity for the whole CAHU, is around 450 Mm^3/year (>15 m^3/s) (Capelli and Mazza 2005). Based on the stratigraphic and structural characteristics of the complex and observed aquifer water levels, the CAHU can be divided in five hydrogeological basins. The Albano lake is part of the central hydrogeological basin (Mazza and Capelli 2010) (Figs. 2 and 5), called Faete basin (244 km^2), which is composed of scoria, lava and phreatomagmatic deposits and is characterized by the presence of several crater and caldera structures acting as closed topographic depressions, such is the Albano crater. Figure 6 shows a hydrogeological cross section that illustrates the conceptual model for the Albano lake and associated hydrogeological unit. A semi-confined volcanic aquifer, which drains the upper Faete basin to the west, feeds Albano lake laterally and from below. A shallow unconfined aquifer is also present (Fig. 6); this shallow aquifer is associated with a small hydrogeological basin of 12 km^2 (Fig. 5). Focusing on the lake, the outflow from Albano lake measured in the historic outlet tunnel was on average around 80 l/s (2.53 Mm^3/year) in the period before the 1990s. Such steady conditions characterized most of the 20th century and probably before, when human withdrawal was minimal. However, the outlet tunnel is currently dry as a result of drops in lake level, which started in 1990 and accelerated in 1996 (Fig. 7). An hydrogeological conceptual model has been constructed for the hydrogeological unit associated with Albano lake. The geology in the model was simplified to four layers representing the main hydrogeological units. The lake cross-cuts the upper layer modeled with low permeability to represent the uppermost phreatomagmatic deposits, which host the shallow unconfined aquifer (Fig. 6). The underlying layers, with intermediate to high permeability represent scoria cones and lava of the Faete stratovolcano (Fig. 6). The contact with pre-volcanic units (Fig. 6), which are very low permeability deposits, constitute the bottom boundary of the model. The conduit of the Albano crater is a vertical structure

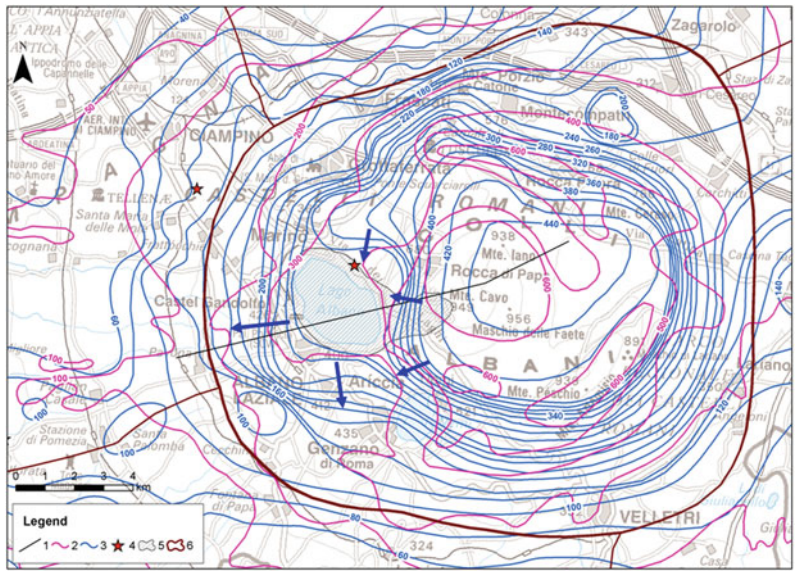

Fig. 5 Groundwater piezometric map of the Albano area. *1* trace of hydrogeological cross section, *2* isopiezometric line—1980 (m asl) (Boni et al. 1988), *3* isopiezometric line—2006 (m asl), *4* gas emission, *5* lake hydrologic basin, *6* faete hydrogeological basin. *Blue arrows* indicate the groundwater flow direction. (Capelli et al. 2005)

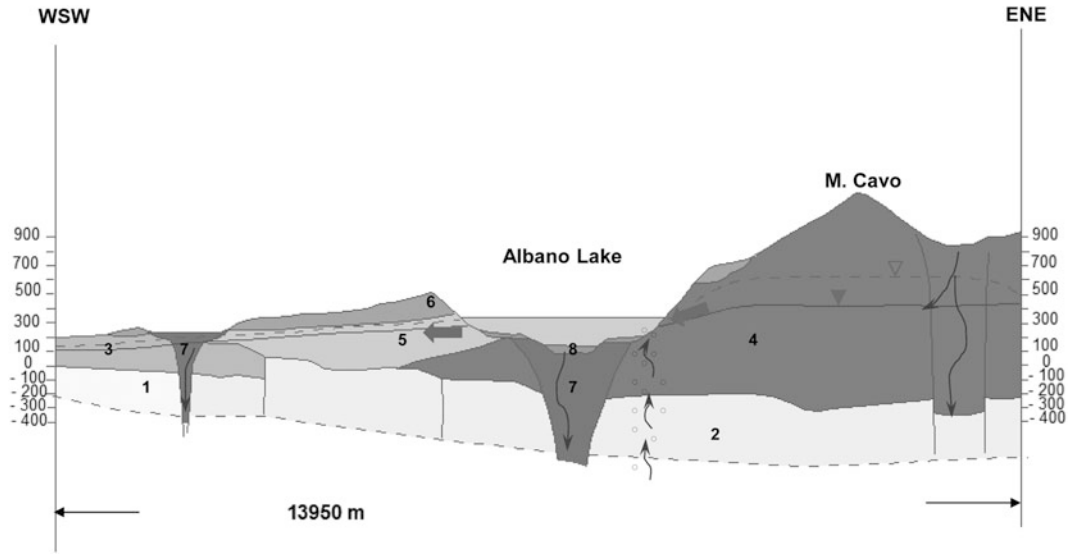

Fig. 6 Hydrogeological cross section of Albano area. *1* undefined prevolcanic units, very low permeability; *2* undefined volcanic units, low-intermediate permeability, *3* ignimbrites, very high permeability, *4* pyroclastic deposits and scoria cones, very high permeability, *5* pyroclastic deposits and ash fallout deposits, intermediate-low permeability, *6* phreatomagmatic units, low permeability, *7* crater deposits, undefined permeability, *8* lakebed deposits, very low permeability. Faults are indicated. Continuous line represent the water table elevation of 2006 whereas the dotted line the 1980 one. *Thick arrows* indicate the groundwater flow direction. Thin *upward arrows* indicate gas upwelling, fine *downward arrows* indicate possible way of deep groundwater feed

excavated in correspondence to a previous caldera fault. Toward the west, the pre-caldera ignimbrites have a very high permeability. Two different water-level scenarios (based on several well and on stream flow measurements, Mazza et al. 2009) were considered. The comparison of the modern groundwater piezometric map, surveyed in 2006 (Mazza et al. 2009) to an older map from 1980 (Boni et al. 1988) shows that dramatic changes have occurred in the highest area around Monte Cavo, where the groundwater table elevation was around 600 m asl in 1980, and dropped to around 440 m asl in 2006. The lowering of the water table elevation is also visible in the northern area. The groundwater flow is from the highest area located to the east, i.e. from the summit of the intracaldera stratovolcano of Mt Cavo, toward the west where it feeds Albano lake. The lake water, in turn, feeds aquifers to the northwest, west and southwest. In Fig. 7 the

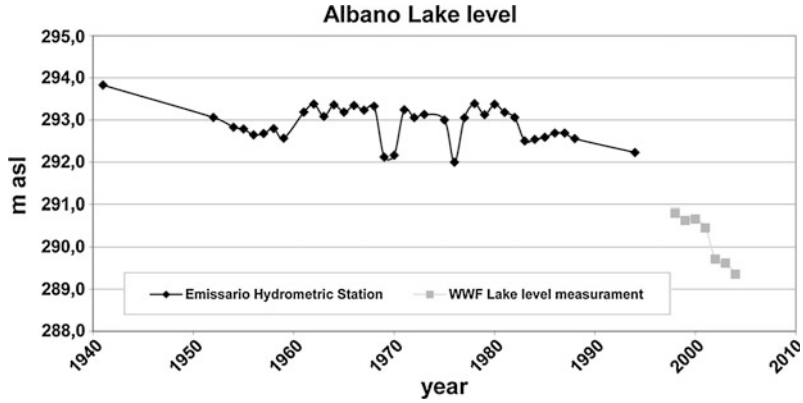

Fig. 7 Time series water level of Albano lake, based on monthly measurements from National Survey Agency, from 1951 until 1995. From 1999 to 2004 lake level measurement from WWF report information (Papa 2009)

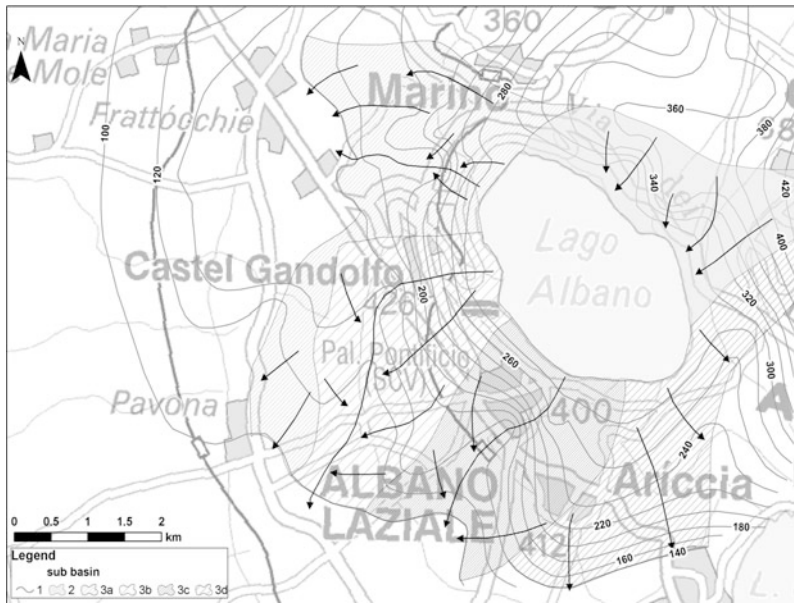

Fig. 8 Groundwater piezometric map of the Albano area, 1998 *1* isopiezometric line, *2* lake inflow basin, *3* outflow from lake basins *a* northern part, *b*, *c* and *d* more and more to the south. *Arrows* indicated the groundwater flow direction

yearly average lake level for the period from 1941 to 1994 is reported (National Survey Agency of the "Emissario" Hydrometric Station). After 1994 the hydrometric Station was no longer active because of the drop in lake level below the tunnel outlet. From 1999 to 2004 World Wildlife Found (Papa 2009) reports the lake levels. A definite lake drawdown trend of more then 3 m in the last 20 years is noted. The elevation drop is from 293 m asl in January 1988 to 289 m asl in January 2004. Since the outlet tunnel has become dry, Albano lake is currently a seepage lake, with groundwater inflows from the northeast. The outflows are distributed along a wider perimeter from the north to the east (Fig. 8). The distribution pattern is related to the varying transmissivity (i.e. permeability × thickness of the aquifer) across the lake (Fig. 6).

5.2 Bracciano Caldera Lake

The Bracciano lake is part of the Sabatini volcanic district which forms a main Hydrogeologic Unit (SHU, Fig. 2), bounded to the south and to the east by the Tiber river and to the west by the outcropping of pre-volcanic clay and silt deposits. To the north the interfingering between Sabatini volcanic deposits and the Vico stratovolcano does not allow delineation of a structural hydrogeological boundary. The SHU hosts one main regional unconfined volcanic aquifer which drains southward. The potential aquifer productivity for the whole SHU is around 227 Mm^3/y (~7,200 l/s, Capelli et al. 2005). Based on the stratigraphic and structural characteristics and measured groundwater levels, the SHU can be divided into four hydrogeological basins. The Bracciano caldera lake itself is part of the northern Bracciano hydrogeological basin (380 km^2) (Fig. 9), which is composed of ignimbrite deposits, tuffs, lava and scoria cones. Bracciano lake is located inside a caldera and occupies the majority of this basin. Along the northern caldera wall, the recharging aquifer is characterized by a high hydraulic gradient, which connects the rather flat isopiezometric top that characterizes the northern slopes of the volcano down to the lake level. This high gradient is interpreted as due to the presence of a shallow pre-volcanic basal

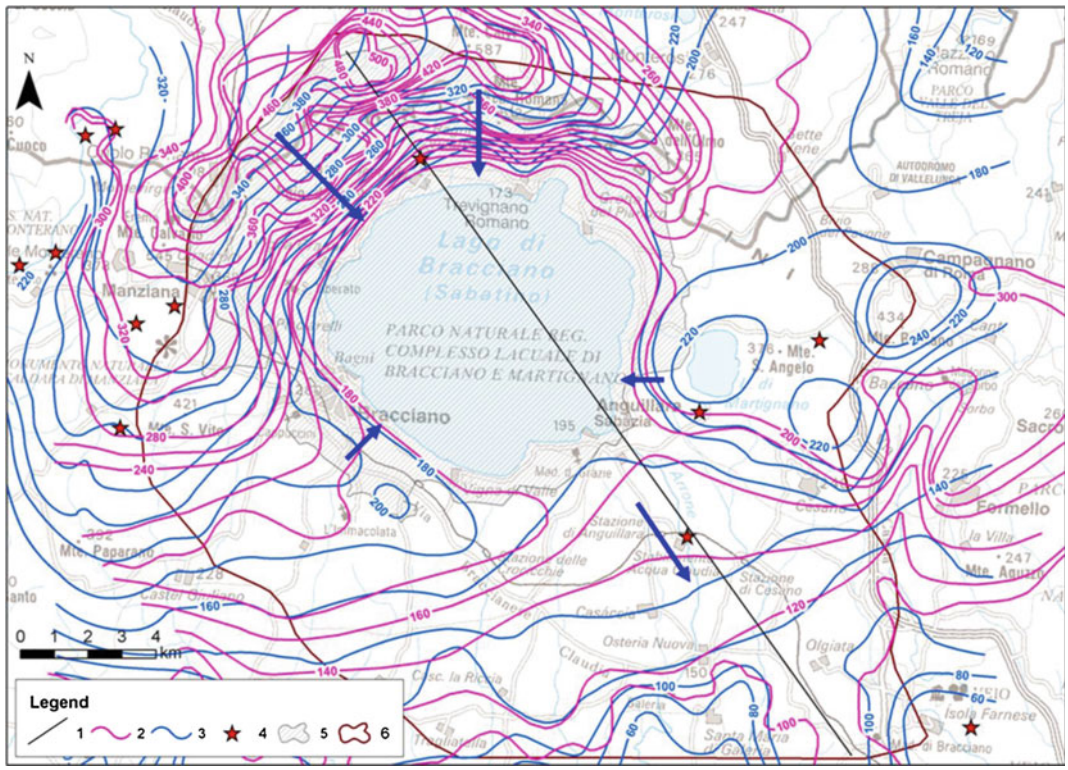

Fig. 9 Groundwater piezometric map of the Bracciano area *1* trace of hydrogeological cross section, *2* isopiezometric line—1967 (m asl) (Camponeschi and Lombardi 1968), *3* isopiezometric line—2009 (m asl) (Taviani S 2011), *4* gas emission, *5* lake hydrologic basin, *6* Bracciano hydrogeological basin. *Blue arrows* indicate the groundwater flow direction

aquiclude along the northern slope of the volcano and its downthrowing along caldera faults (Figs. 9 and 10). Groundwater flow feeding Bracciano lake is from the highest topographic areas located to the northwest and the southeast. The northeast and west sides of the lake are also characterized by a minor inflow from groundwater to the lake. Instead, the lake water feeds the main regional volcanic aquifer toward the southeast. The Bracciano lake has a natural effluent, the Arrone river. In the past when the system was under less stress, the outflow from Bracciano lake was around 1,000 l/s, measured in the Arrone river near the lake outlet (31.5 Mm^3/year). The Arrone river is currently dry in the highest part of its channel, while it only becomes perennial 4 km downstream from the lake. The lake level started to drop in 1970 and became definitively lower then the Arrone outlet elevation in 1989 (Fig. 10). A hydrogeological conceptual model was built for the Bracciano hydrogeological unit for management purposes. The geology was simplified in two-layers representing the main hydrogeological units. Based on geological characteristics, zones with a different hydraulic conductivity are identified for each layer. The lake cross-cuts the upper layer modeled with permeability representing the uppermost ignimbrites and tuff (zones 3, 4 5 and 6 in the cross section shown in Fig. 10). At depth, pre-volcanic units of very low permeability (zone 1 in Fig. 10) constitute the model bottom. The Pre-volcanic unit is characterized by the presence of several preferential-flow conduits and vertical structures which correspond to faults (collapse caldera and regional faults). These structures could allow the addition of water to the lake or to

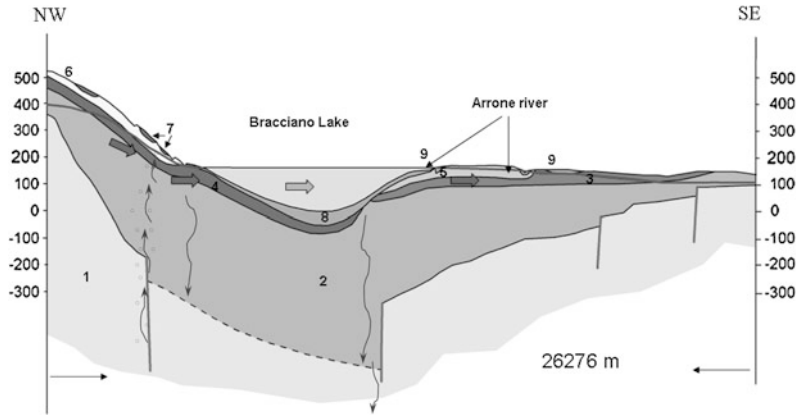

Fig. 10 Hydrogeologic cross section of Bracciano lake area *1* undefined pre-volcanic deposits, very low permeability; *2* undefined volcanic units, low-intermediate permeability; *3* tuff deposits, intermediate-high permeability; *4* tuff deposits, intermediate-high permeability *5* highly porous tuff deposits, very high permeability; *6* pyroclastic fall deposits, very high permeability; *7* lavas and scoria cones, intermediate-low permeability; *8* lake-bed deposits, low permeability; *9* alluvium sediments, permeability very variable. Faults are indicated. *Continuou line* represent the water table elevation of 2009. *Thick arrows* indicate the groundwater flow direction. *Thin upward arrows* indicate gas upwelling, fine *downward arrows* indicate possible way of deep groundwater feed

the SHU or loss of water to the deep geothermal aquifers. Two different piezometric scenarios were considered (based on several well measurement and stream flow measurement, Camponeschi and Lombardi 1968; Taviani S (2011) Application of the Modflow groundwater numerical model to hydrogeological volcanic units. Unpublished PhD Thesis, Rome, Italy). In the case of a caldera lake, the focus is on an extended area (contrary to the crater lake case). The piezometric map (Fig. 9) compares the water table elevation in 2009 (Taviani S (2011) Application of the Modflow groundwater numerical model to hydrogeological volcanic units. Unpublished PhD Thesis, Rome, Italy) with the one in 1967 (Camponeschi and Lombardi 1968). The main elevation changes are observed in the highest hills to the northwest of the lake, where the water table elevation was around 500 m asl in 1967 and decreased to around 380 m asl in 2009. The same drop is not evident in the southern area. In Fig. 11 the yearly Bracciano lake level is reported. From 1951 to 1996 information was given by the National Survey Agency of the "Anguillara Sabazia" Hydrometric Station. After 1996 the Hydrometric Station was no longer active. From 2001 to 2010 the "Castello Vici-ACEA" Hydrometric Station reported lake levels. An irrelevant drop can be noted, from 162.63 m asl in January 1951 to 162.37 m asl in January 2010, corresponding to a water loss of around 28 Mm^3. In spite of such minimal lake level variation, a significant modification of the lake hydrogeological outflow is observed at the Arrone River. This river has been the active outflow for the Bracciano lake till the 1970s, with a flow-rate of about 1,000 l/s, making the second largest outflows of the lake balance after evaporation. Presently, the river inlet is dry and groundwater is drained 2 km downstream, with a largely reduced water flow rate (150 l/s; Taviani S (2011) Application of the Modflow groundwater numerical model to hydrogeological volcanic units. Unpublished PhD Thesis, Rome, Italy; Capelli et al. 2012), as the river is now solely linked to the groundwater supply, and not directly recharged by the lake.

The Bracciano lake is characterized by a surface runoff groundwater inflow distributed around the lake from southwest to east, mainly

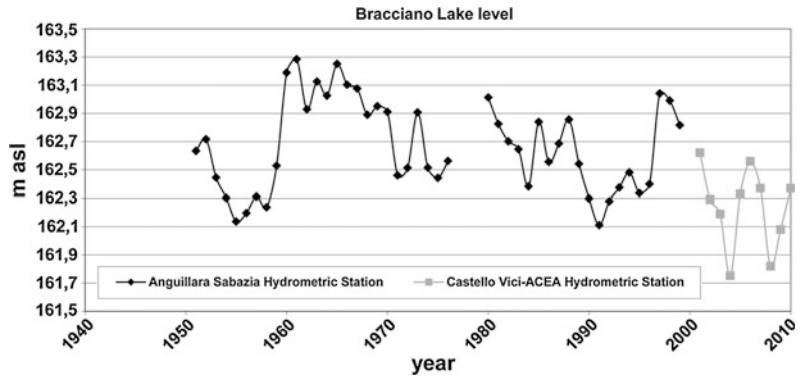

Fig. 11 Time series water level of Bracciano lake, based on monthly measurements from national hydrographic service (Servizio Idrografico), from 1966 until 2010

from the northwest side. The outflow is concentrated in the southeast part and drains toward the city of Rome (Fig. 9).

5.3 Hydrogeological Balance

To quantitatively evaluate the water balance of the lake basin (Eq. 1), it is necessary to know climatic variables, such as precipitation and evaporation (which depends on air temperature and humidity), the surface runoff, the stream in- and outflow and the groundwater in- and outflow, as well as lake withdrawal, i.e. the human pressure on the lake balance.

Table 2 presents the hydrogeological basin water balance factors (Capelli et al. 2005), where all factor values are the total fluxes of the hydrogeological balance for the CAHU and SHU units.

In the case of CAHU, the recharge and total withdrawal are respectively the 33.5 and 23.8 % of the precipitation, attesting to a "stressed" groundwater condition. In the case of the SHU, values of recharge and total withdrawal are respectively 31 and 13.3 % of the precipitation. The Bracciano area could be considered slightly less stressed than the Albano area (Table 2).

Considering groundwater-surface water as a single resource (Feinstein 2012), focusing on the lake water balance, Eq. 1 can be considered. Results for the lake water balance are given in Table 3. The information obtained is the difference between the in- and outflow. For Albano the change in lake storage is around −193 mm/year. The strong decreasing trend of Albano lake level shows that there is an insufficient amount of net groundwater flow in order to stabilize the imbalance in such a way that the present drawdown of the lake level is substantial (Fig. 7).

In the case of Bracciano lake, a change in lake storage of −366 mm/y is compensated by net groundwater flow as testified by the very little drop in the lake level (Fig. 11).

6 Discussion and Conclusions

6.1 Implications for Water Management

Volcanic lakes are natural piezometers of volcanic aquifers. In some active volcanoes, crater lakes are dominated by contamination from deep seated fluids, and monitoring of the lake levels and the physical-chemical characteristics of the lake water are useful for volcanic hazard assessment (e.g. Carapezza et al. 2010a, b; Chiodini et al. 2012). Many volcanic lakes and related hydrogeological units around the world are exceptional water resources and, consequently, are sites of intense urbanization. For this reason many volcanic lakes represent the major water resource utilized for civil and agricultural and industrial purposes (e.g. Capelli et al. 2005; Pardo et al. 2009). The evaluation of the hydrogeological balance and particularly of groundwater withdrawal is therefore an essential tool for the water resource management. In order to evaluate the influence of withdrawal on the

hydrogeological balance, the Recharge (Eq. 2 and Table 2) should be defined (Castany 1967). This evaluation starts from the analysis of the hydrogeological water balance; depending on the hydrogeological conditions (K, porosity, etc.) that will give indications on the relationship between a lake level variation and a dV/dt in the aquifer.

Hydrogeological water balances were calculated for the cases of Albano and Bracciano lakes. The calculation of the hydrogeological balance for both the related CAHU and SHU basins quantifies very high withdrawal outflow values that are higher than the natural inflows (Table 2); increasing withdrawals have brought to strong and continuing drawdown of both the groundwater table (at a basin scale) and of lake levels (at more local scale). This could be seen in the CAHU case, where the aquifer of the Albano Lake has been strongly affected by withdrawal in the past 30 years and lake level has dropped by around 4 m.

While there is an obvious correlation between the aquifer depletion and the dramatic increase in groundwater withdrawal, all the in- and outflows that contribute to the basin and lake budgets must be considered from the Regional Water Authorities to define groundwater protection policies.

Recent studies have successfully applied an original method able to define the state of stress of the volcanic aquifers under human exploitation in Central Italy (Capelli et al. 2005). A stressed aquifer can be described in terms of thickness, piezometric drawdown (by comparing the year 1970 with the year 2000 piezometries), relative amount of withdrawal for different uses (potable, agricultural and industrial) and the spatial distribution of withdrawal. "Critical areas" in the volcanic aquifers of Central Italy, i.e. areas with a high hydric stress, are those where the total withdrawal for hectare is equal or more than 1,600 m^3/year (Capelli et al. 2005).

It is essential to analyze the real land use (e.g. the type of plantations and/or farming present in a studied area) and to evaluate the water required from different plants to grow instead of just considering the farmer declared groundwater withdrawal (often farmers declared smaller numbers of water withdrawal than those utilized in reality, for the obvious reason to save money). Groundwater databases generally only reveal part of the situation relative to water availability. In the CIVOLD, the loss of water is often linked to "transfers" of large water volumes from one hydro-structure to another along dedicated aqueducts. This transfer is regulated by the administrative need to satisfy public potable request, or for agricultural or industrial purposes.

In the region around Rome the Latium Regional Government has implemented water resources policies that consider these factors in order to protect volcanic aquifers (Regione Lazio 2004). Because hydrogeological systems are highly dynamic environments, groundwater and surface water should be monitored continuously. A comprehensive GIS database could become the starting point for the analysis. Starting from the achieved studies a groundwater numerical model should be constructed, calibrated and validated, to obtain a management tool capable of considering the in- and outflows that control the health of the lakes. Different stress conditions can be simulated through the use of groundwater numerical models (increased rates of withdrawal, decreased recharge rates, changing runoff rates, etc.). Well monitoring, spring and stream flow monitoring (expression of groundwater/surface water interaction) are needed to delineate the water table elevation of the basin and to define basin boundaries, which form the basis for management.

6.2 Implications for Geothermal Systems

Volcanic hydrogeology in active or quiescent volcanoes is usually linked to geothermal resources. The presence of vertical permeable pathways for deep-seated fluids allow the transfer of fluids and heat between shallow and deep levels. The CIVOLD is the site of one of the

most important geothermal areas on Earth (Barberi et al. 1994). Volcanic lakes and associated hydrogeological units are therefore essential for geothermal prospection as they provide evidence for local thermal and chemical anomalies (Carapezza et al. 2010b; Chiodini et al. 2012). One largely unexplored issue is the potential for the vertical recharge of the deep geothermal system from the shallow volcanic hydrogeological system. Volcanotectonic structures, conduits and dykes that are associated at depth with volcanic lakes may effectively promote both the upward flow of buoyant deep-seated fluids and the downward seepage of groundwater (Figs. 6 and 10). The calculation of hydrogeological balances such as those for Bracciano and Albano lakes can, in principle, give information on the rates and volumes of vertical flows (considering density effects). Uncertainties in the computations of the balance's parameters and in the calculations are estimated at around 5 and 10 %, respectively. Consequently, it is not possible to estimate possible outflows from the hydrogeological units to the deep geothermal aquifers which are typically smaller then the above errors. On the other hand, field evidence clearly shows that vertical discontinuities allow ascent of endogenous fluids (gas-water) which give rise at the surface to gaseous manifestations or thermo-mineral springs. As the fluid movements are from zones with higher pressure potential and higher hydraulic head towards zones of lower pressure and head, it is true that the upward or downward direction of circulation of gases and fluids along fractures may change depending on the physical conditions at each site. In volcanic contexts fluid pressures are controlled by gravity, temperatures, and by the partial pressures of volatile species. It is not possible to exclude that geothermal activity contributes appreciably to the recharge of volcanic hydrogeological units. Future research will undoubtedly lean heavily towards isotope chemical analyses. Furthermore, environmental decision-makers should consider each factor of the balance when dealing with potential exploitation of geothermal resources connected to the shallow hydrogeological system.

6.3 Implications of Hydrogeology of Volcanic Lakes on Phreatomagmatism

Mild to moderate explosive activity in many volcanic settings is commonly associated with phreatomagmatism, i.e. the explosive interaction of the rising magma with either surface- or ground-water (see Morrisey et al. 2000; Rouwet and Morrissey, this issue). This has been the case for the most recent activity at Colli Albano (Giordano et al. 2002; Anzidei et al. 2008; De Benedetti et al. 2008) and at Sabatini volcanic fields (Funiciello and Giordano 2008; Sottili et al. 2009). Phreatomagmatic activity can dramatically enhance volcanic hazards associated with moderate eruptions because of the generation of powerful lateral blasts and base surges. These hazardous phenomena may reach the coast where emergent volcanism is close to inhabited islands or to the mainland (e.g. the 1911 and 1965 eruptions at Taal caused 1,335 and 200 casualties respectively; Moore et al. 1966). While both experimental and field-based studies of phreatomagmatic eruptions and deposits have increased our understanding of the fundamental eruptive, transportational and sedimentary processes (Kokelaar 1983; Sheridan and Wohletz 1983; Sohn and Chough 1992; White 1996; Zimanowski et al. 1997; Giordano et al. 2008; Dellino et al. 2011), natural conditions for efficient magma-water interaction are still poorly known, mostly due to the absence of a clear understanding of the hydrogeology associated with volcanic domains. For example, it is experimentally proven that an efficient explosive interaction, i.e. the conversion of thermal energy into explosive mechanical energy, occurs at a magma: water mass ratios between 3:1 and 10:1 (Sheridan and Wohletz 1983; Zimanowski et al. 1997). However, all experiments describe magma-water interaction in terms of mass ratios, whereas the natural eruptions involve transient discharge ratios over finite conduit/vent areas at discharge rates comparable with strombolian to violent strombolian and small sub-plinian eruptions. The quantification of the hydrogeology of volcanic systems in terms of saturation levels, aquifer thickness and transmissivity, as well as lake

bathymetry, volumes and shape (e.g. Anzidei et al. 2008) is therefore essential to map the hazard associated with the potential of phreatomagmatism. Eventhough at Albano the probability of an eruption is presently minimal, the area is quiescent, so this hazard cannot be discounted (Carapezza et al. 2010a). In any case, in other active volcanic areas the hydrogeology is rarely quantified and used for hazard assessment, whereas we believe that groundwater settings should be carefully assessed for monitoring and modeling purposes.

References

AA.VV. (2004) Aggiornamento del Piano Regolatore Generale degli Acquedotti. Regione Lazio

Ambrosetti W, Barbanti L (2002) Physical limnology of Italian lakes 1 relationship between morphometry and heat content. J Limnol 61(2):147–157

Anderson MP, Cheng X (1993) Long- and short-term transience in a groundwater/lake system in Wisconsin, USA. J Hydrol 145:1–18

Anzidei M, Carapezza ML, Esposito A, Giordano G, Tarchini L, Lelli M (2008) The Albano Maar lake high resolution bathymetry and dissolved CO_2 budget (Colli Albani District, Italy): constrains to hazard evaluation. J Volcanol Geotherm Res 151:258–268. doi:10.1016/j.volgeores.2007.11.024

Ayenew T, Becht R (2008) Comparative assessment of the water balance and hydrology of selected Ethiopian and Kenyan rift lakes. Lakes Reservoirs Res Manage 13(10):181–196

Barberi F, Buonasorte G, Cioni R, Fiordelisi A, Foresi L, Iaccarino S, Laurenzi MA, Sbrana A, Vernia L, Villa I (1994) Plio-Pleistocene geological evolution of the geothermal area of Tuscany and Latium. Mem Desc Carta Geol Ital 49:77–134

Bear AN, Giordano G, Giampaolo C, Cas RAF (2009a) Volcanological constraints on the post emplacement zeolitisation of ignimbrites and geoarchaeological implications for etruscan tomb construction (6th–3rd century BC) in the Tufo Rosso a Scorie Nere, Vico Caldera Central Italy. J Volcanol Geotherm Res 183 (3–4):183–200

Bear AN, Cas RAF, Giordano G (2009b) Variations in eruptive style and depositional processes associated with explosive, phonolitic composition, caldera-forming eruptions: The 151 ka sutri eruption, Vico Caldera, Central Italy. J Volcanol Geotherm Res 184(3–4):1–24

Bellucci F, Grimaldi M, Lirer L, Rapolla A (1997) Structure and geological evolution of the island of Ponza, Italy: inferences from geological and gravimetric data. J Volcanol Geotherm Res 79:87–96

Bianco F, Castellano M, Milano G, Ventura G, Vilardo G (1998) The somma-vesuvius stress field induced by regional tectonics: evidences from seismological and mesostructural data. J Volcanol Geotherm Res 82:199–218

Boni C, Bono P, Capelli G (1988) Carta Idrogeologica del Territorio della Regione Lazio (Scala 1:250.000) Regione Lazio, Assessorato alla Programmazione, Ufficio Parchi e Riserve Naturali -Università degli Studi "La Sapienza"-Dipartimento di Scienze della Terra, Roma

Buettner M, Daily W, Ramírez A, Bussod G (1999) Electrical resistance tomography of unsaturated flow and transport in Yucca Mountain. Proc SAGEEP 1999:341–347

Camponeschi B, Lombardi L (1968) Idrogeologia dell'area vulcanica Sabatina. Mem Soc Geol It 8:25–55

Capelli G, Mazza R (2005) Water criticality in the Colli Albani (Rome, Italy). Giorn Geol Appl 1:261–271

Capelli G, Mazza R, Giordano G, Cecili A, De Rita D, Salvati R (2002) The colli albani volcano (Rome—Italy): equilibrium breakdown of a hydrogeological units as a result of unplanned and un controlled overexploitation. Hydrogeology 4:63–70

Capelli G, Mazza R, Gazzetti C (eds) (2005) Strumenti e strategie per la tutela e l'uso compatibile della risorsa idrica nel Lazio -Gli acquiferi vulcanici. Quaderni di tecniche di protezione ambientale. Protezione delle acque sotterranee. vol 78, Pitagora Editrice, Bologna 216 pp

Capelli G, Mastrorillo L, Mazza R, Petitta M, Baldoni T, Banzato F, Cascone D, Di Salvo C, La Vigna F, Taviani S, Teoli P (2012) Carta Idrogeologica del Territorio della Regione Lazio scala 1:100.000)—Regione Lazio—SELCA Firenze

Carapezza ML, Barberi F, Tarchini L, Ranaldi M, Ricci T (2010a) Volcanic hazard of Colli Albani. In: Funiciello R, Giordano G (eds) The Colli Albani volcano. Special Publication of IAVCEI, 3. The Geological Society, London, 000–000

Carapezza ML, Lelli M, Tarchini L (2010b) Geochemistry of the Albano crater lake. In: Funiciello R, Giordano G (eds) The Colli Albani Volcano. Geolocial Society London, Special Publication of IAVCEI, vol 3 pp 279–297

Cas RAF, Wright JV (1987) Volcanic successions: modern and ancient. Chapman & Hall, London 528

Castany G (1967) Introduction à l'étude des courbes de tarissements. Chronique d'Hydrogéol 10

Castellani V, Dragoni W (1997) Ancient tunnels: from Roman outlets back to the early Greek civilization. Proc XII Inter Conf Speleol La Chaux-de-Fonds Switz 3(2):365–368

Cheng X, Anderson MP (1994) Simulating the influence of lake position on groundwater fluxes. Water Resour 30:2041–2049

Chilès JP, Delfiner P (1999) Geostatistics. Modelling Spatial Uncertainty. Wiley Series in Probability Statistics

Chiodini G, Frondini F (2001) Carbon dioxide degassing from the Albani Hills volcanic region, Central Italy. Chem Geol 177:67–83

Chiodini G, Tassi F, Caliro S, Chiarabba C, Vaselli O, Rouwet D (2012) Time-dependent CO_2 variations in Lake Albano associated with seismic activity. Bull Volcanol 74:861–871. doi:10.1007/s00445-011-0573-x

De Benedetti AA, Funiciello R (2007) Geological aspects. In: Stoch F (ed) Volcanic lakes - Fire, water and life. Italian Habitats, vol 17. Museo Friulano di Storia Naturale, Udine, Italy, pp 11–27

De Benedetti AA, Funiciello R, Giordano G, Caprilli E, Diano G (2008) Volcanology, history and miths of the Albano maar. In: Cashman K, Giordano G (eds) Volcanoes and human history. J Volcanol Geotherm Res 176:387–406. doi: 10.1016/j.jvolgeores.2008.04

De Benedetti AA, Caprilli E, Rossetti F, Giordano G (2010) Metamorphic, metasomatic and intrusive xenoliths of the Colli Albani volcano and their significance for the reconstruction of the volcano plumbing system. In: Funiciello R, Giordano G (eds) The Colli Albani volcano. Geol Soc, Special Publication IAVCEI 3:153–176

De Rita D, Funiciello R, Rossi U, Sposato A (1983) Structure and evolution of the Sacrofano Baccano caldera Sabatini volcanic complex, Rome. J Volcanol Geotherm Res 17:219–236

De Rita D, Di Filippo M, Sposato A (1989) Geological map of the Sabatini volcanic complex. CNR- Pro Fin Geodinamica Sta Salomone, Roma

De Rita D, Funiciello R, Corda L, Sposato A, Rossi U (1993) Volcanic Units. In: M.D. Filippo (ed) Sabatini Volcanic Complex. Quad Ric Sci CNR Roma, Italy, 114, 11: pp 33–79

De Rita D, Di Filippo M, Rosa C (1996) Structural evolution of the Bracciano volcanotectonic depression, Sabatini volcanic district, Italy In: Mc Giure WJ, Jones AP, Neuberg J (eds) Volcano instability on the Earth and Other Planets, Geol Soc, Special Publication 110: 225–236

De Rita D, Giordano G, Cecili A (2001) A model for submarine rhyolite dome growth: Ponza island (central Italy). J Volcanol Geotherm Res 107:221–239

Dellino P, De Astis G, La Volpe L, Mele D, Sulpizio R (2011) Quantitative hazard assessment of phreatomagmatic eruptions at Vulcano (Aeolian Islands, Southern Italy) as obtained by combining stratigraphy, event statistics and physical modelling. J Volcanol Geotherm Res doi: 10.1016/j.jvolgeores.2010.06.009

Demlie M, Ayenew T, Wohnlich S (2007) Comprehensive hydrological and hydrogeological study of topographically closed lakes in highland Ethiopia: the case of Hayq and Ardibo. J Hydrol 339:145–158

Duchi V, Paolier M, Pizzetti A (1991) Geochemical study on natural gas and water discharges in the southern Latium (Italy), circulation, evolution of fluids and geothermal potential in the region. J Volcanol Geotherm Res 47:221–235

Feinstein (2012) Since "Groundwater and surface water—A single resource": some U.S. Geological survey advances in modeling groundwater/surface-water interactions. Acque Sotterranee—Italian J Ground Water AS01001:009–024

Funiciello R, Giordano G (2008) La Carta Geologica di Roma alla scala 1:10:000: Litostratigrafia e organizzazione stratigrafica. In: Funiciello R, Praturlon A, Giordano G (eds) La geologia di Roma: dal centro storico alla periferia. Mem Descr Carta Geol It 80:39–86

Funiciello R, Giordano G, de Rita D (2003) The Albano maar lake (Colli Albani Volcano, Italy): recent volcanic activity and evidence of pre-roman age catastrophic lahar events. J Volcanol Geotherm Res 123:43–61

Geyer A, Marti J (2008) The new worldwide collapse caldera database (CCDB): a tool for studying and understanding caldera processes. J Volcanol Geotherm Res 175:334–354

Giacomelli L, Scandone S (2007) Vulcani di Italia. Liguori, Napoli, Italy, pp 488

Giordano G, the CARG Team (2010) Stratigraphy and volcano-tectonic structures of the Colli Albani volcanic field. In: Funiciello R, Giordano G (eds) The Colli Albani volcano. Geol Soc, Special Publication IAVCEI 3:43–97

Giordano G, De Rita D, Cas R, Rodani S (2002) Valley Pond and Ignimbrite veneer deposits in small volume phreatomagmatic basic ignimbrite, Lago Albano Maar, Colli Albani volcano, Italy: influence of topography. J Volcanol Geotherm Res 118:131–144

Giordano G, De Benedetti AA, Diana A, Diano G, Gaudioso F, Marasco F, Miceli M, Mollo S, Cas RAF, Funiciello R (2006) The Colli Albani caldera (Roma, Italy): stratigraphy, structure and petrology. In: Cas RAF, Giordano G (eds), Explosive Mafic Volcanism. J Volcanol Geotherm Res 155:49–80

Giordano G, Porreca M, Musacchio P, Mattei M (2008) The Holocene Secche di Lazzaro phreatomagmatic succession (Stromboli, Italy): evidence of pyroclastic density current origin deduced by facies analysis and AMS flow directions. Bull Volcanol 70:1221–1236. doi:10.1007/s00445-008-0198-x

Hurst AW, Bibby HM, Scott BJ, McGuinness MJ (1991) The heat source of Ruapehu Crater Lake; deductions from the energy and mass balances. J Volcanol Geotherm Res 6:1–21

Innocenti F, Trigila R (eds) (1987) Vulsini Volcanoes. Per Mineral 56:238

ISTAT (1991) Censimento decennale dell'agricoltura e dell'industria e dei servizi. ISTAT

Jutzeler M, Varley N, Roach M (2011) Geophysical characterization of hydrothermal systems and intrusive bodies, El Chichón volcano (Mexico). J Geophys Res 116.doi:10.1029/2010JB007992

Kennessey B (1930) Lefolyasi téniezok és retenciok. Vizugy, Koziemènyek (in Hungarian)

Kokelaar BP (1983) The mechanism of surtseyan volcanism. J Geol Soc London 140:939–944

Krabbenhoft DP, Bowser CJ, Anderson MP, Valley JW (1990) Estimating groundwater exchange with lakes. 2. Calibration of a three dimensional, solute transport model to stable isotope plume. Wat Resource Res 26:2455–2462

Kratz TK, Webster KE, Bowser CJ, Magnuson JJ, Benson BJ (1997) The influence of landscape position on lakes in northern Wisconsin. Freshw Biol 37:209–217

Larson G, Collier R, Buktenica M (2003) Two decades of research at crater lake. Research brief for resource managers. USGS, May 15

Mastin LG (2007) Generation of fine hydromagmatic ash by growth and disintegration of glassy rinds. J Geophys Res 112:B02203. doi:10.1029/2005JB003883

Matheron G (1967) Elements Pour une Theorie des Milieux Poreux. Masson, Paris

Mattei M, Conticelli S, Giordano G (2010) The Tyrrhenian margin geological setting: from the Apennine orogeny to the K-rich volcanism. In: Funiciello R, Giordano G (eds) The Colli Albani Volcano. Geol Soc, Special Publication IAVCEI 3:7–27

Mazza R, Capelli G (2010) Hydrogeology of the Colli Albani volcano. In: Funiciello R, Giordano G (eds) The Colli Albani volcano, Geol Soc London, Special Publication IAVCEI 3:189–214

Mazza R, Capelli G, Taviani S, Teoli P, Gazzetti C, Rosa C, La Vigna F (2009) L'unità idrogeologica dei Colli Albani: modellazione numerica degli acquiferi per un piano di uso compatibile della risorsa. Atti Conv Lincei "La crisi dei sistemi idrici: approvvigionamento agro-industriale e civile" (22 marzo 2007—Roma). Accademia Nazionale dei Lincei pp 253–269

Moore JG, Nakamura K, Alcaraz A (1966) The 1965 eruption of Taal volcano. Science 151(3713):955–960

Mosello S, Arisci S, Bruni P (2004) Lake Bolsena (Central Italy): an updating study on its water chemistry. J Limnol, 63(1):1–12

Ohba T, Hirabayashi J, Nogami K (1994) Water, heat and chloride budgets of the crater lake, Yugama at Kusatsu-Shirane volcano, Japan. Geochem J 28:217–231

Orsi G, De Vita S, di Vito M (1996) The restless, resurgent Campi Flegrei nested caldera (Italy): constraints on its evolution and configuration. J Volcanol Geotherm Res 74:179–214

Papa F (2009) Situazione e crisi idrica nei Castelli Romani http://www.wwf.it/UserFiles/File/

Pardo N, Macías JL, Giordano G, Cianfarra P, Bellatreccia F, Avellán DR (2009) The ~1245 yr BP Asososca maar eruption: the youngest event along the Nejapa-Miraflores volcanic fault, western Managua Nicaragua. J Volcanol Geotherm Res 184(3–4):292–312

Pasternack GB, Varekamp JC (1997) Volcanic lake systematic I physical constraints. Bull Volcanol 58:528–538

Principe C (2006) La geologia del Monte Vulture. Regione Basilicata. Grafiche Finiguerra, Lavello, 217 pp

Regione Lazio (1994) Carta dell'uso del suolo della regione lazio—classificazione corine land cover 94, scala 1:100.000. Regione Lazio, SIRA

Regione Lazio (2004) Misure di salvaguardia degli acquiferi vulcanici dei Colli Albani e dei Monti Sabatini. Boll Uff Reg Lazio suppl. ord 4 a (Boll Uff2 20-01-2004)

Rouwet D, Morrissey MM (2014) Mechanism of crater lake breaching eruptions

Rouwet D, Tassi F (2011) Geochemical monitoring of volcanic lakes. A generalized box model for active crater lakes. Ann Geophys 54(2). doi: 10.4401/ag-5035

Rouwet D, Taran Y, Varley NR (2004) Dynamics and mass balance of El Chichón crater lake, Mexico. Geofís Int 43:427–434

Rouwet D, Taran Y, Inguaggiato S, Varley N, Santiago SJA (2008) Hydrochemical dynamics of the "lake-spring" system in the crater of El Chichón volcano (Chiapas, Mexico). J Volcanol Geotherm Res 178:237–248

Rowe GL, Brantley SL, Fernández M, Fernández JF, Borgia A, Barquero J (1992) Fluid-volcano interaction in an active stratovolcano: the Crater Lake system of Poás Volcano, Costa Rica. J Volcanol Geotherm Res 64:233–267

Santacroce R (1987) Somma-Vesuvius CNR, Quaderni de La Ricerca Scientifica 114 Prog Fin Geodinamica Monografie finali 8:251 pp

Scandone R, Bellucci F, Lirer L, Rolandi G (1991) The structure of the companion plain and the activity of neapolitan volcanoes. J Volcanol Geotherm Res 48:1–31

Sheridan MF, Wohletz KH (1983) Hydrovolcanism: Basic considerations and review. J Volcanol Geotherm Res 17:1–29

Sohn YK, Chough SK (1992) The Ilchulbong tuff cone, Cheju Island, South Korea: Depositional processes and evolution of an emergent, Surtseyan type tuff cone. Sediment 39:523–544. doi:10.1111/j.1365-3091.1992.tb02135.x

Sollevanti F (1983) Geologic, volcanologic and tectonic setting of the Vico-Cimino area, Italy. J Volcanol Geotherm Res 17:203–217

Sottili G, Palladino DM, Gaeta M, Masotta M (2012) Origins and energetics of maar volcanoes: examples from the ultrapotassic Sabatini Volcanic District (Roman Province, Central Italy). Bull Volcanol 74:163–186

Sottili G, Taddeucci J, Palladino DM, Gaeta M, Scarlato P, Ventura G (2009) Sub-surface dynamics and eruptive styles of maars in the Colli Albani Volcanic District, Central Italy. J Volcanol Geotherm Res 180:189–202

Taviani (2011) Application of the Modflow groundwater numerical model to hydrogeological volcanic units. Unpublished Ph.D. Thesis, Rome, Italy

Townley LR, Trefry MG (2000) Surface water—groundwater interaction near shallow circular lakes: flow geometry in three dimensions. Wat Resour Res 36:935–949

White JDL (1996) Impure coolants and interaction dynamics of phreatomagmatic eruptions. J Volcanol Geotherm Res 74:155–170

Winter TC (1999) Relation of streams, lakes, and wetlands to groundwater flow systems. Hydrogeol J 7:28–45

Zimanowski B, Büttner R, Lorenz V, Häfele HG (1997) Fragmentation of basaltic melt in the course of explosion volcanism. J Geophys Res 102:803–814

Volcanic Lake Sediments as Sensitive Archives of Climate and Environmental Change

Aldo Marchetto, Daniel Ariztegui, Achim Brauer, Andrea Lami, Anna Maria Mercuri, Laura Sadori, Luigi Vigliotti, Sabine Wulf, and Piero Guilizzoni

Abstract

In efforts to understand the natural variability of the Earth climate system and the potential for future climate and environmental (e.g., biodiversity) changes, palaeodata play a key role by extending the baseline of environmental and climatic observations. Lake sediments, and particularly sediment archives of volcanic lakes, help to decipher natural climate variability at seasonal to millennial scales, and help identifying causal mechanisms. Their importance includes their potential to provide precise and accurate inter-archive correlations (e.g., based on tephrochronology) and to record cyclicity and high frequency climate signals. We present a few examples of commonly used techniques and proxy-records to investigate past climatic variability and its influence to the history of the lakes and of their biota. This paper is rather a presentation of potentials and limits of palaeolimnological and limnogeological research on crater lakes, than a pervasive review of palaeolimnological studies on crater lakes. We show the importance of seismic stratigraphy for the selection of coring sites, and discuss problems in core chronology. Then we give examples of physical and chemical proxies, including magnetism, microfacies and oxygen and carbon stable isotopes from crater lake deposits mainly located in central and southern Europe. Finally, we present

A. Marchetto (✉) · A. Lami · P. Guilizzoni
CNR ISE Institute of Ecosystem Study, Largo Tonolli 50, 28922 Verbania Pallanza, Italy
e-mail: a.marchetto@ise.cnr.it

D. Ariztegui
University of Geneva, Section of Earth and Environmental Sciences, Rue des Maraichers, 13, 1205 Geneva, Switzerland

A. Brauer · S. Wulf
GFZ German Research Center for Geosciences, Section 5.2 Climate Dynamics and Landscape Evolution, 14473 Potsdam, Germany

A.M. Mercuri
Department of Biology, University of Modena and Reggio Emilia, viale Caduti in Guerra 127, 41121 Modena, Italy

L. Sadori
Department of Environmental Biology, University "La Sapienza", Piazzale Aldo Moro 5, 00185 Rome, Italy

L. Vigliotti
CNR ISMAR, Institute of Marine Sciences, Via P. Gobetti 101, 40129 Bologna, Italy

D. Rouwet et al. (eds.), *Volcanic Lakes*, Advances in Volcanology,
DOI 10.1007/978-3-642-36833-2_17,
© Springer-Verlag Berlin Heidelberg 2015

the use of air-transported (pollens) and lacustrine biological remains. The continuing need to develop new approaches and methods stimulated us to mention, as an example, the potential of the studies of subsurface biosphere, and the effects of microbiological metabolism on mineral diagenesis in sediments.

Keywords

Paleolimnology · Volcanic lake sediments · Seismic sequence stratigraphy · Dating sediment cores · Oxygen and carbon isotopes · Magnetism · Palynology · Climate and environmental change

1 Introduction

Lacustrine sediments are among the most complete and detailed natural archives, documenting —typically in greater detail than their marine counterparts—the temporal evolution of chemical, physical and biological features of a lake, its catchment and the prevalent climate of the region (Oldfield 2005).

According to Frey (1988), palaeolimnology sets lacustrine sediment studies in a broader context in which the trajectory of the effects of humans and natural changes on lakes requires long-term records of chemical and biological factors, on time scales ranging from the most recent (Holocene) to early geological times (e.g., Permian, Cretaceous, middle Pleistocene). Palaeolimnology studies the origin and the geomorphological history of lake basins and the response of their biocoenoses (plant and animal communities) to variations, for example, in nutrient levels (Guilizzoni et al. 2011), temperature (Battarbee 2000), water levels (Piovano et al. 2002; Giraudi et al. 2011), wind conditions (Brauer et al. 2008), dissolved substances which have occurred throughout time (Meyer 2003), as well as a wide spectrum of other impacts (Smol 2008). The stratigraphic study of sediment cores can provide information linked to local stressors, but also to global phenomena, both on long time scale, such as phases of glaciation (Ramrath et al. 1999; Tzedakis et al. 2001), and on shorter time scales (e.g., ENSO, von Gunten et al. 2012).

Volcanic lakes are particularly interesting for palaeolimnological research. In many regions, such as a large part of Europe and North America, most lakes are formed as a result of glacial activity, and are consequently younger than the last glaciation, or strongly influenced by it. Crater and maar lakes, on the other hand, are located in volcanic areas that are often less influenced by the events related to glaciation (e.g., Eifel Volcanic Field, central and southern Italy, southern France, East Africa, central Mexico, southern Patagonia), and they are "small enough to core easily and old enough to have had a respectable history" (Hutchinson et al. 1970). Volcanic lakes can be very deep and they often lack major in- and outlets which enhance the preservation of the structure of lake bottom sediments often triggering the formation of varves.

Some volcanic lakes are relatively young (less than 10,000 years), but most studies deal with ancient lakes, allowing a number of studies to go back in time up to more than 100,000 years BP, such as for example the dried out lake Valle di Castiglione (Follieri et al. 1988) and Lago Grande di Monticchio (Brauer et al. 2007), both in Italy, or Lac Ribains in France (de Beaulieu and Reille 1992; Rioual et al. 2007). Some palaeolimnological studies on volcanic lakes aim to identify the effect of recent human impact on lake biota, such as fish stocking (Skov et al. 2010) and atmospheric deposition of pollutants in ancient (Schettler and Romer 1988) as well as recent times (Ruíz-Fernández et al. 2007). The

relatively small catchment areas of volcanic lakes make them ideal sites to study atmospheric processes and deposition of pollen and other natural air-transported proxies. Human induced changes in land use in the small and sometimes apparently undisturbed catchments of crater and maar lakes should be taken into account, as some of these lakes are strongly affected, even during the Bronze Age (Guilizzoni et al. 2002).

It should be noted that palaeolimnological studies dealing on lake biota or in-lake biogeochemical processes can be strongly influenced by the volcanic nature of the lake itself. For example, endogenous fluids can carry warmer water to the deepest part of the lake, directly affecting the biota, or dissolved carbon dioxide, altering water pH, such as in the case of Lago di Albano and Lago di Bracciano (Carapezza et al. 2010). Furthermore, these lakes can be subject to rapid and pronounced variations in water level (Funiciello et al. 2003) that can also affect lake biota and sediment deposition. Finally, submerged aquifer sources can also carry chemicals to the lake, strongly affecting the biogeochemical cycling of other compounds: for example high Fe concentration can alter the phosphorus concentration by the precipitation of insoluble compounds (Michard et al. 1994).

2 Seismic Sequence Stratigraphy

Most palaeolimnological studies rely on results from a single core that is considered as representative of a uniform, continuous sediment unit throughout a basin. Limnogeology, as envisioned by Kerry Kelts in the early 1980s, refers to a broader approach to study lake systems driven by the progress in ocean research in the context of marine geology, including the study of complex systems and their interactions (Kelts 1987). Modern profiling with various-scale seismic resolution is a good example of a limnogeological approach, since it can provide valuable lithological and geometric information prior to coring (e.g., Ariztegui et al. 2001a), allowing the identification and three dimensional mapping of sediment packages.

Seismic sequence stratigraphy has been widely applied for marine geophysical surveying, and has also been applied in a comprehensive way to lacustrine basins. In analogy to marine studies, when applied to lake systems, seismic stratigraphy can yield unique evidence on lake level fluctuations and rapid changes in the sedimentary system and facies (Mullins et al. 1996). Such changes are commonly due to climatic factors and, furthermore, the responses in lakes are likely to be much faster and more relevant than for ocean margins (Ariztegui et al. 2001a).

Studies of seismic profiling in lakes provide valuable information on the thickness, structure, tectonics, and extent of sedimentary patterns prior to coring. They offer direct support to sediment coring programs in order to select optimal sites for coring long sediment sequences with continuous palaeoclimate records. Seismic profiles allow to identify undisturbed sediment packages that can be used to retrieve continuous cores. They can also be used to correlate distinctive seismic packages among core networks and map the extent of lake level changes (Gilli et al. 2005; Anselmetti et al. 2009). Furthermore, without seismic stratigraphy, it may be difficult to recognize unconformities, slumps, or gaps in spatially limited core sections.

Mapping different seismic facies in volcanic lakes is ideal to distinguish sedimentary packages (Niessen et al. 1993). A succession of high-amplitude, parallel reflections, for example, defines layering within a distinct unit. Strong petrophysical signatures are useful to correlate reflections among coring-sites. Gas-rich zones are not penetrated by the seismic signal and appear seismically transparent. Seismic profiles are important to describe the irregular bottom structure of complex volcanic lakes, such as in the case of Yellowstone Lake (Morgan et al. 2003). Differences in the seismic thickness of sedimentary packages can be exploited in a targeted coring campaign. Thinned or eroded

sequences can be cored for maximum age-depth recovery, whereas thicker units may provide higher resolution, or the timing and history of recurring events (Anselmetti et al. 2009).

In Lago Albano (central Italy), for example, the interpretation of high-resolution profiles allows the identification of major lake level changes and is critical for the correlation of different sedimentary cores (Niessen et al. 1993; Chondrogianni et al. 2004). Additionally, seismic information from across the basin provides a unique means to choose the best site for core retrieval in an area of the lake containing parallel reflections. This approach allows the recovery of the entire Holocene and Pleistocene sequence that can be further correlated with geochemical and biological proxies, and can be extended throughout the basin using the geometries determined by seismic profiling (Ariztegui et al. 2001b). Seismic information also allows to discard cores retrieved from the deepest part of the basin, where thick mass-flows or turbidites are detected.

An intensive and multiple seismic survey of Laguna Potrok Aike, southernmost Patagonia, Argentina, has provided critical information prior to the undertaking of a deep drilling program that has recovered ca. 50,000 years of continuous sediments (Anselmetti et al. 2009). Several seismic campaigns were carried out on the lake, as site surveys prior to the drilling, in order to determine (a) the sedimentary architecture of the lacustrine infill; (b) the prevalent geometries to reconstruct lake-level changes; and (c) to confirm the maar origin of the basin (Anselmetti et al. 2009; Gebhardt et al. 2011). While the high-resolution seismic profile was instrumental to reconstruct the most recent lake-level changes (Fig. 1), the air-gun and refraction surveys provide fundamental evidence about the total sedimentary infill and the geometry of the maar (Fig. 2). Thus, Laguna Potrok Aike seismic survey is an excellent example of the use of different seismic arrays and techniques to answer scientific questions pertaining to volcanic lakes and to solve a maximum of uncertainties prior to deep drilling.

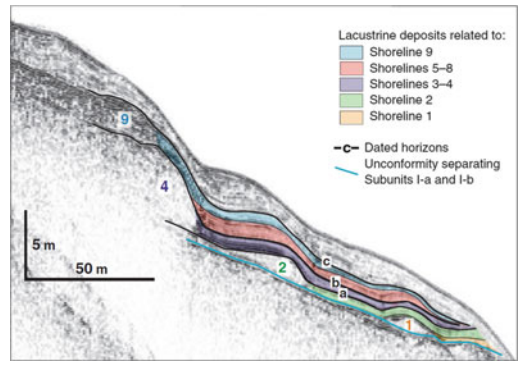

Fig. 1 High-resolution seismic profile from Laguna Potrok Aike with interpreted and numbered palaeoshorelines and identified seismic stratigraphic horizons (a–c). These lacustrine horizons can be linked seismically to palaeoshorelines (a = 2, b = 4, c = 9) allowing determination of palaeo-lake levels (modified from Anselmetti et al. 2009)

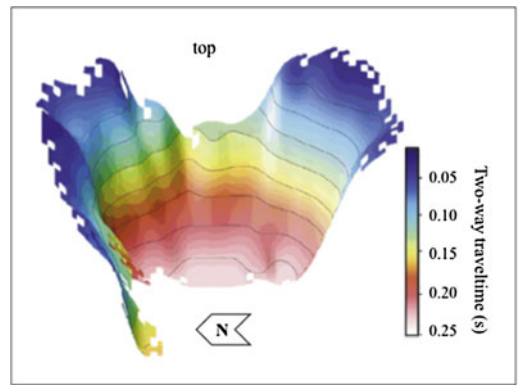

Fig. 2 3D view of the Potrok Aike crater reconstructed using refraction seismic. Depths are given in two-way travel times (modified from Gebhardt et al. 2011)

3 Dating Volcanic Lake Sediment Cores

Dating sedimentary deposits of volcanic lakes ideally follows a multiple dating approach (Fig. 3) encompassing several independent methods including radiometric, incremental and relative dating methods. The most commonly applied method in palaeolimnology is radiocarbon dating of carbon-bearing materials reaching

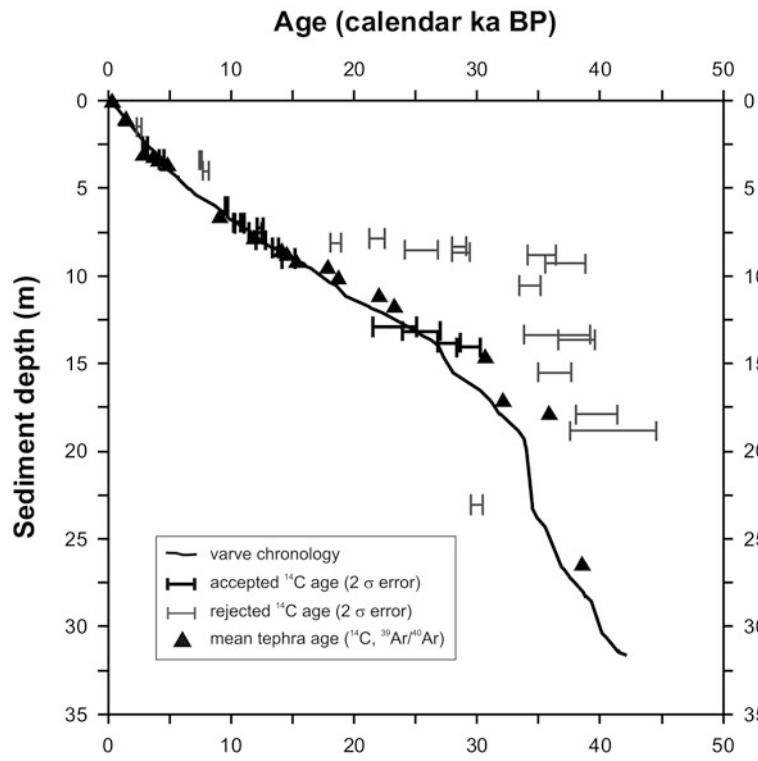

Fig. 3 Comparison of radiocarbon dates, varve chronology and tephrochronology of lake sediments from Lago Grande di Monticchio (southern Italy) for the last ca 40,000 cal years BP (modified after Wulf et al. 2004). ^{14}C dates obtained on bulk sediments and aquatic plant remains (*gray bars*) giving too old ages are rejected, while dates of terrestrial plant material (*black bars*) fit both the varve based age model and the tephrochronology

back in time to ca 40,000 years BP (Lowe and Walker 1997). Accelerator mass spectrometry (AMS) techniques allow dating of small samples (≤1 mg), but there are many inherent sources of errors related to ^{14}C dating in addition to the measurement uncertainty provided in the dating protocols, such as contamination with 'old' or 'young' carbon. Depending on the dated material, the resulting ages may vary significantly (Oldfield et al. 1997) which often is ignored in the error discussion. A particular problem might appear in dating sediments from volcanic lakes, where juvenile volcanic CO_2 rising from sublacustrine springs can be assimilated by submerged macrophytes resulting in too old dates (Hajdas et al. 1998). This problem can be avoided by dating exclusively terrestrial macrofossils, which are, however, rare in sediments taken from the central and deepest parts of volcanic lakes.

A crucial issue of ^{14}C dating is calibration into calendar year time scales. For the dendrocalibration period back to ca 12,500 calibrated (cal) years BP, a robust calibration curve is available (Reimer et al. 2009), but periods of constant radiocarbon ages, the so-called ^{14}C-plateaus, cannot be finely resolved and require additional increment dating, as counting fine annual laminations (varves).

Depending on local climate and lake morphology, varves tend to be rarely formed and preserved in lake sediments. However the typically deep, funnel-shaped maar and crater lake basins favour anoxic deep-water conditions, ideal for the formation and preservation of varves that can be used to establish precise chronologies (Zolitschka 2006). A wide range of different annual laminations, including siliciclastic, organic and evaporitic varves (Brauer 2004) might form, depending on the climate regime and catchment geology. Where they exist, varve counting of undisturbed sediments can be carried out on cleaned surfaces of split cores, photographs, X-radiographs and large-scale thin sections. Micro-facies analyses of thin sections provide crucial information on the seasonal deposition required for reliable recognition of

sub-layer boundaries. Typical errors of varve chronologies include missing varves, as a result of erosion and sediment distortion, and counting uncertainties due to poor varve preservation. In the case of sediment sections without any varve preservation, age interpolations have to be carried out based on detailed sedimentation rate determinations in adjacent varved intervals (Zolitschka and Negendank 1996). The most recent decades of varve chronologies can be verified by complementary ^{137}Cs and ^{210}Pb dating (Lami et al. 1994; Alvisi et al. 1996) or historical documented marker layers like, for example, extreme floods or land-use changes. If varves are not preserved in sub-recent sediments, the established varve chronology is considered "floating" and must be anchored to the absolute time scale using isochronous markers such as tephra layers (Brauer et al. 2000).

Explosive volcanic eruptions produce huge amounts of ash material (tephra) which is distributed over large areas and deposited in terrestrial and aquatic environments. A tephra layer from a single, well-defined eruption can be unequivocally identified on the basis of geochemical 'fingerprinting' of volcanic glass using electron microprobe (major elements) and Laser-Ablation-ICP-MS techniques (trace elements) (Lowe 2011). The tephra layer can then be used as an isochronous time marker in sediment archives. The dating of tephra deposits in their proximal settings uses radiometric (^{14}C on buried and intercalated organic material) and radioisotopic techniques (i.e., K/Ar, Ar/Ar, U/Th on phenocrystals or volcanic glass), and the datum obtained can be imported to correlate tephras deposited in other archives.

Volcanic lakes are ideal for recording tephra events due to both the vicinity to active explosive volcanoes and the preservation of tephra layers in largely undisturbed and possibly varved sediments (e.g., Lago Albano, Calanchi et al. 1996; Lago di Mezzano, Ramrath et al. 1999). Combining varve counting and tephra analysis, exceptionally long stratigraphies can be developed for crater and maar lakes in favourable wind position to volcanic sources like, for example, Lago Grande di Monticchio (Wulf et al. 2004), San Gregorio Magno Basin (Munno and Petrosino 2007) and Sulmona Basin (Giaccio et al. 2009) in southern and central Italy.

Varve chronology has demonstrated to be particularly suitable for determining the duration of certain climatic intervals ranging from entire interglacials (Brauer et al. 2007) to short-term climate oscillations (Prasad et al. 2006) and the precise timing of abrupt climate changes (Brauer et al. 2008).

In palaeoclimate research, there is an increasing need to establish a network of key sediment archives from different regions and environments to obtain a more comprehensive picture of past changes. The precise correlation of various well-dated sediment records needs specific synchronisation techniques based on relative dating like biostratigraphy (Litt et al. 2009), palaeomagnetic data (see below) and tephrochronology (Lowe 2011).

4 Micro-Facies as Climate Proxy

Varved lake sediments are key terrestrial archives that provide detailed evidence on past environmental variations in response to climatic change or human impacts (Lamoureux 2001; Zolitschka 2006). While traditional geochemical, physical and biological analyses on discrete bulk samples allow, at best, reconstructions of past changes at decadal to sub-decadal resolution, varve thickness and integrated micro-facies analyses reveal information related to environmental and climatic changes at annual to seasonal scales (Brauer 2004). Microscopic analyses of varve sub-layers on large scale thin sections provide semi-quantitative information on both lake internal processes: for example, diatom blooms and endogenic mineral formation (calcite), as well as catchment processes through composition and structure of detrital matter transported into the lake. In addition, early diagenetic authigenic mineral formation (e.g., pyrite, vivianite) and sedimentological processes like mixing through bioturbation or degassing and internal reworking (slumping) can be traced at great detail. Recently developed µ-XRF element scanning methods provide

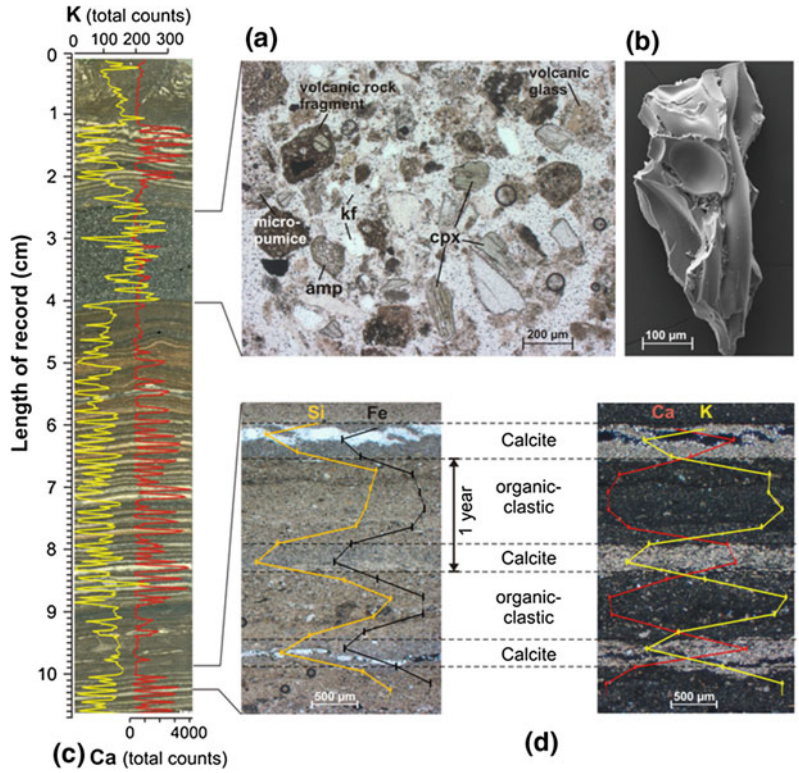

Fig. 4 Microscopic photographs of a varved sediment section from the Lago Grande di Monticchio containing a *tephra layer* from Vesuvius (southern Italy, ca. 35 ka). a Transmitted light photography of tephra components showing juvenile clasts (volcanic glass shards, micro-pumices), rock fragments and phenocrystals (*kf* K-feldspar, *cpx* clinopyroxene, *amp* amphibole). b SEM picture of a typical cuspate shaped volcanic glass shard used for microprobe analysis. c Large-scale thin section (polarized light) showing the elemental distribution of potassium (*yellow line*) and calcium (*red line*) obtained by µ-XRF measurements. Note that the tephra layer in this record (a) is identified by relatively high potassium concentrations. d Transmitted light (*left*) and polarized light (*right*) photographs of individual varves from the lower part of the sediment section. Varves are made up of alternating sublayers of autochthonous calcite precipitates (*summer layer*) and organic-clastic material (*autumn/winter layer*) which are reflected in high calcium concentrations and increased silica, iron and potassium intensities, respectively. *Photo courtesy* K. Wutke, GFZ Potsdam, Germany

complementary geochemical data at comparable sub-millimetre resolution leading to a significant extension of the proxy database and to an improved interpretation of sediment records. In particular, element scanning with vacuum µ-XRF analytical devices on impregnated sediment slabs that have been prepared for thin section fabrication allows precise linking of microscopic observations and high-resolution element data (Brauer et al. 2009). This novel integrative analytical approach allows detailed element profiling across individual varves and precise detection of tephra layers (Fig. 4), as well as other allochthonous sedimentation events like flood layers. Moreover, the detection limits, especially of abrupt climate changes and short to long-term changes in seasonality (Mingram et al. 2004), has significantly improved. Understanding the mechanisms and dynamics of abrupt and high-amplitude climate shifts in the past is crucial for assessing the probability of such events in the future. The onset of the last major climatic oscillation, the Younger Dryas cold phase, is exceptionally well documented in varved sediments from Meerfelder Maar (Eifel, Germany). Here, analysis of the micro-facies at sub-annual

resolution, combined with high-resolution element scanning, allows for the identification of the transition from a calm, anoxic lake environment to a seasonally well-mixed and turbulent lake, indicating an abrupt increase in storminess during the autumn to spring seasons (Brauer et al. 2008).

Another key challenge in palaeoclimate research is to decipher changes in seasonality and understanding the driving mechanisms. This is particularly important for strongly seasonal climate regimes like the Asian monsoon systems. Micro-facies analyses and integrated μ-XRF scanning of varved sediments from the Sihailongwan Maar in northeastern China reveal long-term changes in seasonal dynamics controlled by the Southeast Asian monsoon. It is demonstrated that the warm early Holocene is characterized by a more pronounced inter-annual variability compared to the mid- and late Holocene (Mingram et al. 2004), indicating an intensified monsoon as a result of increased northern hemisphere summer insolation.

A future challenge of micro-facies analyses is to integrate comparably precise combinations with biological proxies into the present databases, mainly including sedimentological and geochemical data.

5 Oxygen and Carbon Stable Isotopes

Authigenic carbonates are often a major component of maar lake sediments and they provide material to develop a chemostratigraphy of the sequence with an excellent temporal resolution (Leng and Marshall 2004). Both $\delta^{13}C_{(carbonate)}$ and $\delta^{18}O_{(carbonate)}$ are excellent sources of information concerning lake productivity as well as changes in source of precipitation and hydrological conditions (Nelson and Smith 1966). In addition, the carbon stable isotope composition of the bulk organic matter, $\delta^{13}C_{(OM)}$, can be used to reconstruct changes in both sources of organic matter (Meyers 1994) and lake productivity (Schelske and Hodell 1995).

Changes of water temperature (mean summer) of the Late Glacial transition of Lago Albano (Italy), for example, are estimated using the $\delta^{18}O_{(carbonate)}$ compositions of authigenically precipitated calcite and valves of benthic ostracods (Chondrogianni et al. 2004). These calculated temperatures, however, are generally too high and in conflict with other ecological evidence in the same record. Although diagenetical overgrowths of calcite could not be excluded, an additional source could distort the original isotopic signal. It is proposed that the $\delta^{18}O_{(carbonate)}$ oscillations of authigenic calcite are not simply due to variations in water temperature, but additionally reflect changes in the $\delta^{18}O$ composition of precipitation and consequently of lake water.

To test the above hypothesis, lake-water temperature is also estimated using the oxygen isotopic composition in amorphous silica ($\delta^{18}O_{(opal)}$). These $\delta^{18}O_{(opal)}$ values reveal maximum water temperature changes of 8 °C between oxic and anoxic intervals, with abrupt changes of 4–6 °C occurring within 40–100 years. The trends in $\delta^{18}O_{(opal)}$ generally co-vary with the values of authigenic calcite, but are again in conflict with the ecological data, confirming the assumption of hydrologic variations overprinting the temperature effect, including changes in groundwater hydrology related to climate, human activities and volcanic activity (Telford and Lamb 1999; Funiciello et al. 2003). Changes in $\delta^{18}O$ composition of local precipitation may also occur, due to variations of ambient air temperatures and/or modifications in atmospheric circulation that shift the source of moisture (Fig. 5).

Another example of the application of stable isotopes to lacustrine sediments is Sacred Lake, a closed crater lake occupying a basaltic explosion crater in the humid mountain rain forest of Mount Kenya, East Africa. In this record the carbon isotopic compositions of the bulk organic matter along with those of specific organic compounds (e.g., n-alkanes, phenols) are used to reconstruct past changes in climate and carbon cycling (Street-Perrot et al. 2004).

Organic carbon isotopes are also used to characterize the Late Glacial and Holocene varved sediments of Holzmaar, Germany. They provide an outstanding record of lacustrine

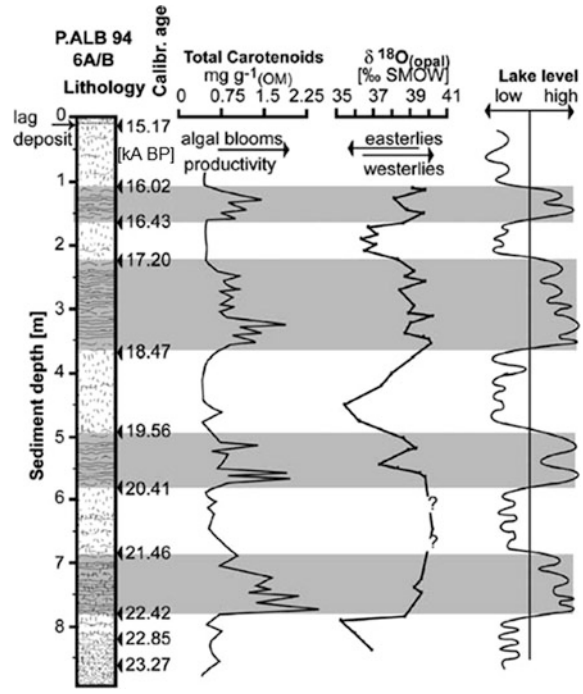

Fig. 5 Multi-proxy palaeoenvironmental records from Lago Albano: lithology, concentration of total carotenoids and $\delta^{18}O_{(opal)}$ as well as interpreted lake level fluctuations from a sediment core encompassing the last deglaciation (modified from Chondrogianni et al. 2004)

palaeoproductivity as well as palaeoenvironmental and palaeoclimatic information (Lücke et al. 2003).

Combined with proxies of lake response and of human activity in the catchments, isotope analysis can help to disentangle the effect on lakes and landscapes of climatic variability and societal development partially stimulated by climate variability itself (Wick et al. 2002; Ryves et al. 2011).

6 Magnetism

Since the application of rock magnetism to environmental disciplines (Thompson and Oldfield 1986), a number of studies demonstrate that the mineral magnetic-palaeoclimatic-environmental linkage reflects the control exerted by climate over magnetic mineral concentration and composition. The supply of magnetic minerals is dominated by catchment sources, but is influenced by weathering and erosion which are mainly under direct climatic control. Environmental magnetism is based on the sensitivity of iron compounds to physical-chemical changes, as iron oxides are among the most sensitive minerals to chemical and thermal transformations of the environment.

Magnetic susceptibility is the main magnetic proxy used for palaeoclimatic reconstruction in volcanic lake sediments. The morphology and depth of these lakes usually allow a rapid and continuous accumulation of sediments, and the drainage input is composed of volcanic sediments that contain a significant amount of iron oxides. Their mineralogy is then able to register the direction of the Earth magnetic field, a key issue for the chronology of the sediment by using the palaeosecular variation record (PSV).

In fact, PSV provides a detailed chronology independent of ^{14}C dating, for the last 10,000–100,000 years or more, and the palaeomagnetic record of volcanic lake sediments are used as a reference for the PSV in different continents. Barton and McElhinny (1981) obtained a master curve by stacking the declination and inclination results of three volcanic lakes for southeast Australia. Several volcanic lakes from Mexico are investigated to retrieve a palaeosecular

variation record used for the age model of sediment cores (Chaparro et al. 2008).

The palaeomagnetic data from Lago Grande di Monticchio and Lago di Mezzano, in Italy, record secular variations reaching back 102 and 31 ka BP, respectively (Brandt et al. 1999). The comparison of biogenic and minerogenic sediment accumulation rates, reconstructed for a time window between 34 and 14 ka from both lakes, suggest synchronous periods with increased minerogenic deposition with enhanced erosion and runoff related to the existing hydrological and climatic conditions. Additional data from the late Pleistocene-Holocene sediments of Holzmaar, Germany, record large variations in magnetic mineral concentration through time. The relative contribution of magnetic components, as expressed by magnetic susceptibility, points to a correlation with sediment accumulation rate and non-arboreal pollen content that has been interpreted as representative of cooler conditions (Stockhausen and Zolitschka 1999).

A multi-proxy approach, well supported by palaeomagnetic and rock magnetic data, was used to study the record of cores collected in Lago Albano and Lago di Nemi (Italy, Rolph et al. 1996) as well as in Lac du Bouchet (France, Williams et al. 1996), spanning 30 and 300 ka, respectively. The magnetic signature of the Late-Glacial sediments of Lago Albano exhibits several intervals with low magnetic content, larger grain size and increasing contribution by antiferromagnetic minerals (Rolph et al. 1996, 2004; Vigliotti et al. 2010) (Fig. 6). The correlation with indicators of biological productivity suggests that these intervals were deposited under anoxic conditions driven by bacterial degradation of organic matter in coincidence with increasing lake level that witness short-term warmer climatic conditions occurring during the Late Glacial. The relevant change in magnetic parameters in the varved sediment indicates that these oscillations took place within few decades. Late-Holocene sediments are characterized by higher magnetic susceptibility than catchment rocks, pointing out to the presence of bacterial magnetite (Rolph et al. 1996, 2004; Vigliotti et al. 2010). The reliability of the palaeomagnetic

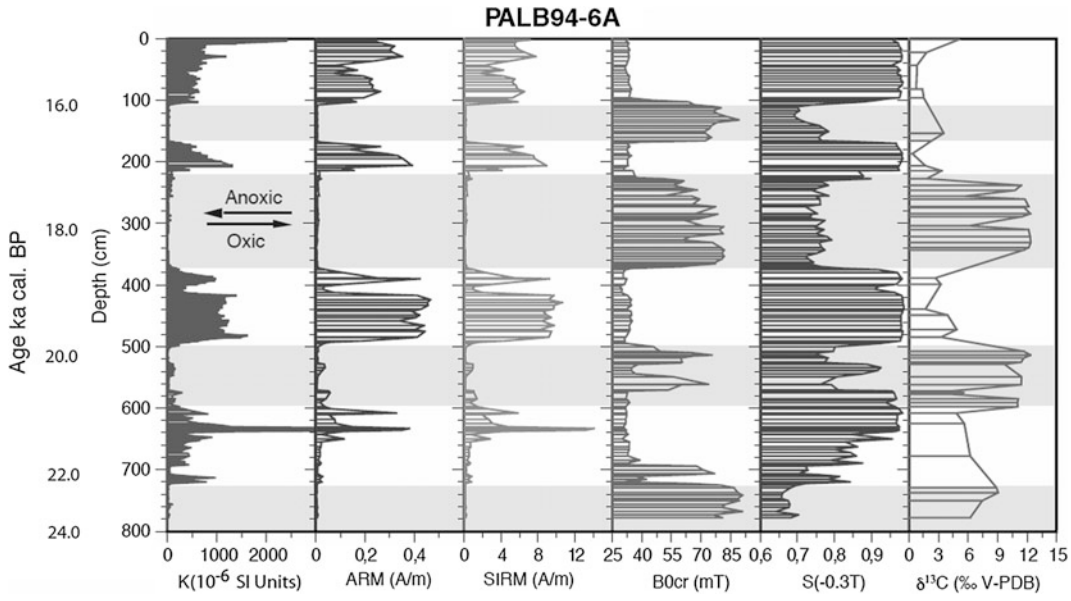

Fig. 6 Stratigraphic variation of bulk magnetic parameters (sediment core PALB94-6A from Lago Albano). *k* low-frequency magnetic susceptibility, *ARM* anhysteretic remanent magnetization, *SIRM* saturation high-field isothermal remanent magnetisation, *B0cr* back field remnant coercivity of the remanence, S(−0.3T): ratio: IRM–0.3T/SIRM, $\delta^{13}C$: deviation of isotopic concentration of ^{13}C (from Vigliotti et al. 2010)

record is also confirmed by Vigliotti (2006), who reports for the neighboring Lago di Nemi, a significant correlation of the PSV record with records obtained from historical lava flows from Etna and Vesuvius volcanoes.

The sediments from Lac du Bouchet are characterized by a detrital magnetic fraction with a composition dominated by titanomagnetite. During interglacials, dilution due to augmented input of catchment materials and diagenetic dissolution resulting from eutrophic conditions causes a decrease in magnetic susceptibility, reflecting climatic variability and strongly correlate with marine $\delta^{18}O$ isotope stages and sub-stages during the last 140 ka (Thouveny et al. 1996). The results from the adjacent Lac de Saint-Front yield a similar trend (Vlag et al. 1996). However, detailed studies of Eemian sediments from both lakes and from Lac Ribains indicate that local processes control the detrital and biogenic input and that variations in ferrimagnetic concentration cannot be interpreted by rock-magnetic results only (Stockhausen and Thouveny 1999).

As already observed by Dearing (1999), magnetic parameters correlate with both glacial-interglacial cycles and arboreal pollen concentration, indicating the role exerted by climate and vegetation on the delivery of the detrital particles to the lake sediments.

In spite of the active diagenesis observed at Lac du Bouchet and Lac de Saint-Front, the palaeomagnetic record is interpreted as representative of relative palaeointensity (Vlag et al. 1996; Williams et al. 1996) with minimum values occurring during the Laschamp, Blake and Iceland Basin geomagnetic excursions.

Maar lake sediments studied in equatorial-tropical Africa also suggest close relationships between climate and magnetic mineral assemblages. For example, Late Quaternary deposits from Lake Magadi (Kenya) yield a magnetic signature indicating the occurrence of dry conditions during the Younger Dryas that led to the separation of Lake Magadi from Lake Natron (Williamson et al. 1993). Mineral-magnetic proxies of erosion/oxidation cycles are observed in the sediments of Lake Tritrivakely (Madagascar): the mineral-magnetic properties are strongly controlled by erosional processes and high-coercivity ferric (oxyhydr)oxides characterize the period of low lake level, corresponding to dry periods, whereas they completely lack the siderite-rich laminated sediments deposited during periods of permanent and stratified water bodies (Williamson et al. 1998). In Lake Massoko (Tanzania), the comparison of sedimentary magnetic signature with catchment material shows three intervals corresponding to humid conditions (high lake level) characterized by increasing pedogenic processes and runoff during the last 45 ka (Williamson et al. 1999).

7 Palynological Studies

Pollen analysis is a central topic in palaeoecological reconstructions. After the pioneering work carried out in central Italy by Frank (1969) and Hutchinson et al. (1970), the first important palynological studies on volcanic lake sediments were undertaken in the late-1980s in Spain (Olot region, Pérez-Obiol 1988), France (Lac Ribains, de Beaulieu and Reille 1992) and Italy (Valle di Castiglione, Follieri et al. 1988). The results from these studies were very promising, as crater and maar lakes have well-defined catchments and little surface inflow, so sediment deposition is rarely disturbed by erosional phenomena. Sedimentation in these lakes is, therefore, fairly uniform, and laminated sediments are often present.

The aim of most palynological studies is to identify pollen evidence of terrestrial vegetation changes, comparing them to climate-driven modifications of lake hydrology and chemistry for the same area. Pollen analysis is intrinsically informative of the plant landscape in the region surrounding the lake. Differences in pollen productivity and dispersal, methods of pollination, past vegetation settings and human disturbance are variables that must be taken into consideration as major factors influencing trends of pollen curves (Faegri et al. 1989). Woodland cover and composition, wetlands, open areas, human environments including cultivated lands, pastures and settlement areas, may be reconstructed based on the observation of pollen percentages, and on

objective inferences based on pollen concentration and influx. The pollen influx value is closely related to the abundance of a species around the site where its pollen is found (Berglund and Ralska-Jasiewiczowa 1986), but the calculation of influx requires a robust chronology. A decline in pollen concentration and influx is often interpreted as a signal of increased erosion in the catchment, generally as a result of forest reduction or clearance (Sadori et al. 2011).

At present, palynology of volcanic lakes has spread worldwide (e.g., in Oceania, Lancashire et al. 2002; in Asia, Mingram et al. 2004; in Africa, Ryner et al. 2007; in Europe, Litt et al. 2009 and in South America, Rull et al. 2010), spanning time intervals ranging from the Eocene to the last centuries.

Central and southern Italy is probably the area most covered by palinological studies covering the whole Holocene. From North to South, studied lakes, existing or drained, are: Lago di Mezzano (Sadori et al. 2004), Lagaccione (Magri 1999), Lago di Vico (Magri and Sadori 1999), Stracciacappa (Giardini 2007), Valle di Castiglione (Follieri et al. 1988), Lago Albano and Lago di Nemi (Lowe et al. 1996; Mercuri et al. 2002), Lago di Averno (Grüger and Thulin 1998), and Lago Grande di Monticchio (Watts et al. 1996; Allen and Huntley 2009). For this reason, we use this area as an example in the following discussion.

In Italy, as and in other Mediterranean countries (Wick et al. 2002) and in Africa (Ssemmanda et al. 2005), it can be difficult to discern between natural changes and human impacts. Figure 7 shows the example of two volcanic lakes (Lago Albano and Lago di Mezzano) that record similar vegetation changes at the end of the last Glacial and during the present interglacial (Mercuri and Sadori 2012). Humans have impacted these lakes since the Middle Bronze Age, as documented by archaeological remains of settlements along their shores. Chronologies of the cores have been assessed by several studies (e.g., Ramrath et al. 2000; Rolph et al. 2004) and a stratigraphical marker, the Avellino tephra layer is available in both sediment cores. New studies on the Avellino tephra, dated at 4,200–4,100 years BP in the previous two studies, suggest a younger age for this eruption (3,945 cal. years BP, Sulpizio et al. 2008; Sevink et al. 2011). We take the tephra occurrence as a stratigraphical marker useful for

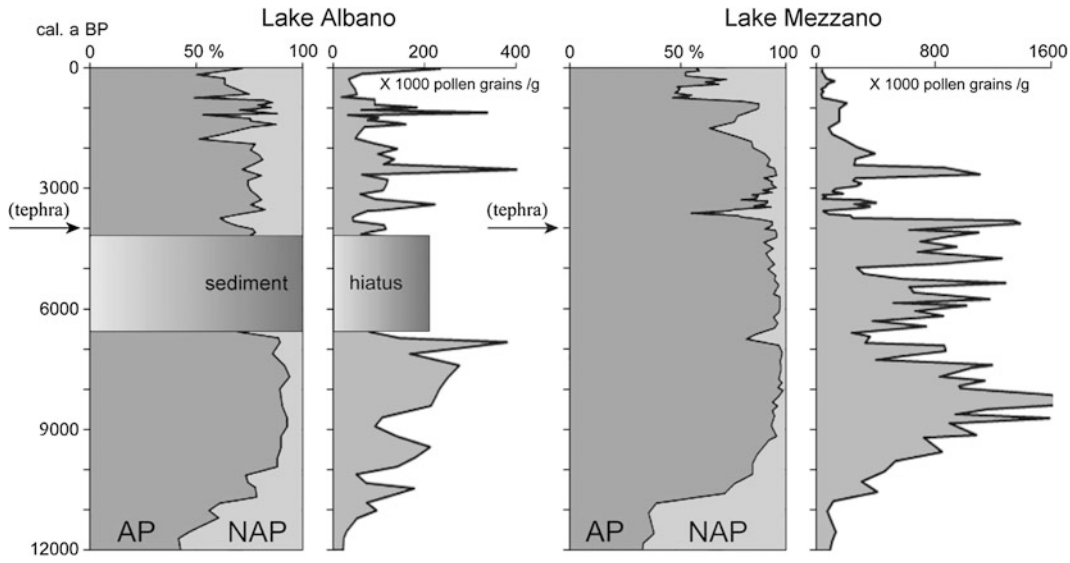

Fig. 7 Pollen records from Lago Albano (Mercuri et al. 2002) and Lago di Mezzano (Sadori unpublished). Pollen percentage (*AP* arboreal pollen, *NAP* non arboreal pollen) and concentration diagrams of Holocene age. The Avellino *tephra layer* is also indicated

core correlation. Few centuries after tephra deposition, a sudden forest change is inferred, indicating drier conditions. It is suggested that climate was the first agent of the shift toward aridity, actually visible in many Mediterranean pollen diagrams at ~4,000 cal. years BP. This is testified by some palynological evidences, such as arboreal pollen concentration that decreased by ca. 80 % in Lago di Mezzano and 60 % in Lago Albano, without any sign of increased fires. Aridity probably pushed human populations to settle along the lake shores, leaving signs of pile dwellings and causing strong modifications in an already open landscape (Sadori et al. 2004).

Since ~3,600 cal. years BP, signs of human activities are evident, such as the cultivation of cereals and legumes, increase in other anthropogenic indicators including *Olea*, forest clearance of selected taxa, fire and grazing activities. Some of these effects are also evident in Lago di Nemi and Lago di Vico. Then, between 2,900 and 2,700 cal. years BP, cultivated trees (*Juglans, Olea* and *Castanea*) spread simultaneously, together with cereals and weeds, suggesting that pre-Roman Iron Age populations had a significant impact on landscape (Follieri et al. 1988; Mercuri et al. 2002). At Lago di Vico, after the forest clearing which occurred during the Bronze Age, the cultivation of trees matches an enhanced forest cover. Finally, a '*Cannabis*-phase', i.e. a hemp pollen peak which followed the peaks of cultivated trees, marked Roman times at Lago Albano and Lago di Nemi, while the 'chestnut landscape' definitively spread at around 700 years BP (Mercuri et al. 2012).

These examples show how the combined interpretation of pollen percentage and influx data can be a robust tool for disentangling climate change and human impact (Sadori et al. 2011). To better identify the relationships between human activity, changes in landscape and in climate and lake response, pollen analysis can be included in multi-proxy analyses of chemical sedimentary parameters (e.g., isotopes) and non terrestrial biotic remains (Guilizzoni et al. 2000; Ryner et al. 2007).

8 Non-terrestrial Biological Records

A number of organisms living in lakes can leave identifiable remains that are used for palaeolimnological studies. A non-exhaustive list includes diatom frustules, algal and bacterial pigments, chrysophyte and dinoflagellate cysts, plant macrofossils, remains of Cladocera and of chironomid larvae, ostracods shells and sponge spicules.

Diatom frustules are the most used remains because they occur frequently, are well preserved, and allow taxonomic identification to species level. The distribution of most species is affected by water pH, salinity, nutrient level and habitat features. In volcanic lakes, diatom analysis is frequently combined with pollen analysis to infer regional climate variability and the consequent lake responses, or to verify and complement the climatic signal with an independent proxy. The presence and abundance of diatom species are used to infer past variability in pH (Lancashire et al. 2002), lake depth (Bradbury 2000; Mayr et al. 2005; Ryner et al. 2007), nutrient levels (Bradbury 2000; Mayr et al. 2005; Stebich et al. 2005), salinity (Gasse et al. 1995; Ryner et al. 2007; Ryves et al. 2011) and the length of winter ice cover (Stebich et al. 2005).

Chironomid head capsules are the second most used biological proxy: their distribution in lakes is influenced by chemical and physical factors, and their presence and abundance is used to infer past lake depth (Manca et al. 1996; Engels et al. 2011), nutrient level (Hoffmann 1993a; Manca et al. 1996; Engels et al. 2011), temperature (Hoffmann 1993a) or salinity (Ryner et al. 2007; Ryves et al. 2011).

Algal pigments are a promising proxy, allowing detailed reconstruction of phytoplankton development and primary productivity. They are surprisingly well preserved in sediments of tens of thousands of years old, although they tend to be degraded compared to the original pool (Leavitt 1993). Promisingly, pigments are used in the palaeolimnology of volcanic lakes (Guilizzoni et al. 2002; Skov et al. 2010).

Other macrofaunal remains, such as ostracod shells (Belis and Ariztegui 2004; Ryner et al. 2007; Gouramanis et al. 2010) or Cladocera head shields, ephippia, or resting eggs (Hofmann 1993b; Manca et al. 1996; Skov et al. 2010), can also be used for inferring past lake depth, salinity or nutrient status.

Alongside these mainly descriptive studies, quantitative inferences of past environmental condition from biotic assemblages are also performed in volcanic lakes: a transfer function, calibrated using data from a set of 30–100 lakes covering an environmental gradient is used along the core to shed light on past lake conditions (Birks 1998).

Specific data sets are developed for volcanic lakes, for example to deduce lake water conductivity from diatom assemblages (Mills and Ryves 2012). However, other regional data sets, not specifically based on volcanic lakes (Gasse and Tokaia 1983; Battarbee et al. 1998), have been used to infer nutrient status (Ryves et al. 1996; Rioual et al. 2007), pH (Barker et al. 2003), salinity (Rioual et al. 2007; Ryves et al. 2011) and lake level and hydrological changes (Rioual et al. 2007) from diatoms, salinity from chironomids (Ryves et al. 2011), ostracods (Gouramanis et al. 2010), and diatoms (Rioual et al. 2007; Ryves et al. 2011) and lake productivity from algal pigments (Guilizzoni et al. 2002).

Combining several biological indicators in a multi-proxy approach can provide a more detailed picture of past lake development. This was first used by Hutchinson et al. (1970) on Lago di Monterosi (Italy), and later by Guilizzoni et al. (2000) on Lago Albano, by Ryner et al. (2007) on Lake Emakat (Empakaai Crater, Tanzania) or by Ryves et al. (2011) on lakes Kasenda and Wandakara (Uganda), to understand the effect of climate variability and human impact on lake ecosystems.

As an example, the multi-proxy study on Lago Albano is summarized in Fig. 8. This study reported strong evidence for aperiodic oscillations in lake biota throughout the period ca. 28–17 ka BP, which can be interpreted as responses to climate forcing through its impact on lake levels and changing aquatic productivity. Productivity peaks can be inferred by the increase in algal pigment concentrations, the abundance of diatoms typical of eutrophic lakes, the presence of sulphur photosynthetic bacteria requiring an anoxic hypolimnion and the high number of animal remains. Chironomid species composition confirms that in these periods lake water was warmer and lake level higher.

9 Subsurface Biosphere

Most published studies in earth sciences dealing with the fast evolving field of geomicrobiology have been carried out in the marine realm. Their results point out the complexity of the chemical reactions associated with microbes that are mostly centered upon changes in redox conditions. These reactions often take place at lithological and geochemical boundaries and result in the formation of diagenetic minerals. The study of these complex interactions is often referred to as the "deep biosphere" and show that the Earth's biosphere extends far below the surface of our planet, including sediments and rocks of the deep ocean. Many microbes in this subsurface biosphere grow extraordinarily slow and under extreme conditions (Konhauser 2007). Studying them is critical in order to obtain a basic understanding of the physiological capabilities and biogeochemical consequences of sub-seafloor life. The source of energy for microbial growing is vast and the exact mechanisms behind them often remain elusive (Konhauser 2007; Inagaki 2010).

In recent years, similar geomicrobiological investigations into lacustrine basins have shown a substantial microbial impact on lake sediments (Jiang et al. 2007). Their study tends to be logistically easier than in their oceanic counterparts, providing analogues to certain marine environments and the ability to investigate a wide range of processes involving extremophiles (Mapelli et al., this issue).

Studies on the subsurface biosphere aim to constrain the physico-chemical conditions of microbially mediated precipitation/dissolution

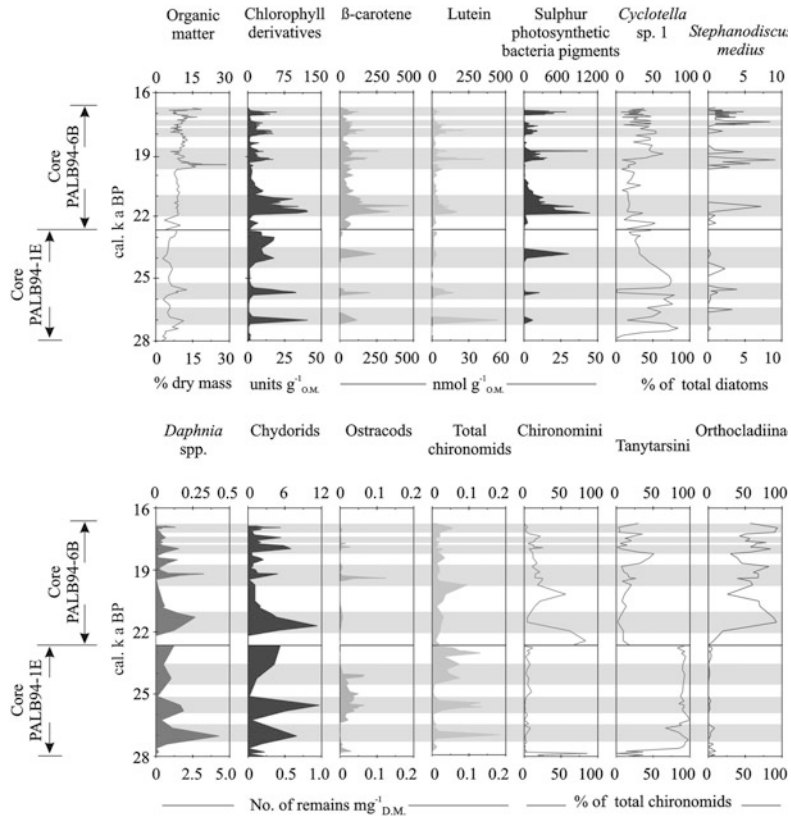

Fig. 8 Biological multi-proxy records at the base of Lago Albano cores PALB94-1E and PALB94-6B. *Dashed grey areas*, based on wide peaks that appear in most proxies, reflect high productivity (indicated by *algal pigments and diatoms*) and higher lake water level intervals. Note the different x-axis scales between the two for cores (from Guilizzoni et al. 2000, with permission)

reactions in the sediments deposited under contrasting and often extreme- environmental conditions (Inagaki 2010). These investigations include living microbial communities in the proximity of fluid/gas seeps and within the sediments to characterize the subsurface biosphere, emphasizing integrated studies of microbiology, geochemistry (pore waters), and mineral authigenesis/diagenesis. Authigenic minerals can be used as signatures of the prevalent conditions during their formation (Manning et al. 1991; Nealson and Stahl 1997).

Standard microbiological methods have been adapted to lake study to detect living microbial communities (e.g., DAPI: 4′,6-diamidino-2-phenylindole, microbial cell count, scanning electron microscopy, etc.). Molecular tools are also used to unambiguously identify the diversity and specific composition of microbial (bacterial and archean) communities. The micro-biota can be further investigated by analyzing the 16S rRNA gene clone library. The results of these investigations allow testing whether microbial communities directly contribute to precipitation and diagenesis of authigenic minerals as well as elemental recycling (Vuillemin et al. 2013).

A 100-m long core taken in Laguna Potrok Aike is used for a detailed geomicrobiological study and sampled in order to address a knowledge gap, related to the lacustrine subsurface biosphere (Vuillemin et al. 2010). The presence of adenosine-5'-triphosphate (ATP) is used as an indication of living organisms within the sediments, as it is not known to form abiotically, and it can be easily detected with high sensitivity and high specificity using an enzymatic assay:

$$\mathrm{ATP} + \mathrm{Luciferin} + \mathrm{O_2} \rightarrow \mathrm{AMP} + \mathrm{Oxyluciferin} + \mathrm{PPi} + \mathrm{CO_2} + \mathrm{Light}$$

Light is emitted as a result of the reaction, which is detected by a photomultiplier.

The microbial activity in Laguna Potrok Aike sediments provides information on ongoing organic matter mineralization processes, and helps to understand the influence of microbes during early diagenesis (Vuillemin et al. 2013). This procedure could be easily and routinely applied, adding microbiological information, complementary to several standard lacustrine proxies, such as the stable isotope composition of authigenic carbonates and, organic matter, although the sampling protocol should avoid contamination.

10 Conclusions

Sedimentary records from volcanic lakes have the potential for detailed reconstruction of the natural and anthropogenic variability. A number of geographical areas are studied, such as Africa for understanding monsoon history, Mexico for the Southern Oscillation and Australia for phenomena not related to the continental mass of the northern hemisphere. The resulting data are crucial for testing Earth system models (Lenton and Kageyama 2012). In particular, we focussed on central and southern Italy, which represents a tantalizing challenge for palaeoclimatologists, since it is a critical area for understanding the pattern and periodicities of Mediterranean climate, and is affected by impacts of human activities over long timescales.

The combination of a broad range of physical, chemical and biological proxies is required to synthesise and compare lacustrine archives in order to decipher both the pattern and amplitude of climatic forcing and the response of aquatic ecosystems.

Volcanic lakes are interesting study sites to understand small scale climate variability using changes in pollen profiles and rock magnetic properties, whereas the lake response and human disturbance is reflected by limnic biota.

New techniques are continuously improving the ability to utilize lake sediments to deduce past lake conditions. For example, the subsurface biosphere studies, applied to a maar lake in Patagonia, provide information about diagenetic processes and organic matter mineralization processes occurring in the sediments, filling the gap in the knowledge of the role of microbial metabolism in these processes.

Acknowledgments We are grateful to J.P. Smol and two anonymous reviewers for their comments that improved the quality of this manuscript, and to Dmitri Rouwet for inviting us to join this editorial project.

References

Allen JRM, Huntley B (2009) Last interglacial palaeovegetation, palaeoenvironments and chronology: a new record from lago grande di Monticchio, southern Italy. Quat Sci Rev 28:15–16

Alvisi F, Frignani M (1996) ^{210}Pb-derived sediment accumulation rates for the central Adriatic Sea and the crater lakes Albano and Nemi (central Italy). Mem Inst Ital Idrobiol 55:303–320

Anselmetti FS, Ariztegui D, De Batist M, Gebhardt C, Haberzettl T, Niessen F, Ohlendorf C, Zolitschka B (2009) Environmental history of southern Patagonia unravelled by the seismic stratigraphy of Laguna Potrok Aike. Sedimentology 56:873–892

Ariztegui D, Anselmetti FS, Kelts K, Seltzer G, D'Agostino K (2001a) Identifying paleoenvironmental change across South and North America using high-resolution seismic stratigraphy in lakes. In: Markgraf V (ed) interhemispheric climate linkages. Academic Press, San Diego, pp 227–240

Ariztegui D, Chondrogianni C, Lami A, Guilizzoni P, Lafargue E (2001b) Lacustrine organic matter and the Holocene paleoenvironmental record of Lake Albano (central Italy). J Paleolimnol 26:283–292

Barker P, Williamson D, Gasse F, Gibert E (2003) Climatic and volcanic forcing revealed in a 50,000-year diatom record from Lake Massoko, Tanzania. Quat Res 60:368–376

Barton CE, McElhinny MW (1981) A 10 000 yr geomagnetic variation record from three Australian maars. Geophys J Roy Astron Soc 67:465–485

Battarbee RW (2000) Palaeolimnological approaches to climate change, with special regard to the biological record. Quat Sci Rev 19:107–124

Battarbee RW, Juggins S, Gasse F, Anderson NJ, Bennion H, Cameron NG (1998) European diatom database (EDDI). An information system for palaeoenvironmental reconstruction. In: Proceedings of european climate science conference, pp 1–10

Belis C, Ariztegui D (2004) The influence of biological and environmental factors on the stable isotopic composition of ostracods—the late pleistocene record from Lake Albano, Central Italy. J Limnol 63:219–232

Berglund BE, Ralska-Jasiewiczowa M (eds) (1986) Handbook of Holocene Palaeoecology and Palaeohydrology. Wiley, Chichester-Toronto

Birks HJB (1998) Numerical tools in palaeolimnology—progress, potentialities, and problems. J Paleolimnol 20:307–332

Bradbury JP (2000) Limnologic history of Lago de Patzcuaro, Michoacan, Mexico for the past 48,000 years: impacts of climate and man. Palaeogeogr Palaeoclimatol Palaeoecol 163:69–95

Brandt U, Nowaczyk NR, Ramrath A, Brauer A, Mingram J, Wulf S, Negendank JFW (1999) Palaeomagnetism of Holocene and Late Pleistocene sediments from Lago di Mezzano and Lago Grande di Monticchio (Italy). Quat Sci Rev 18:961–976

Brauer A (2004) Annually laminated lake sediments and their palaeoclimatic relevance. In: Fischer H, Kumke T, Lohmann G, Miller H, Negendank J (eds) The climate in historical times. towards a synthesis of Holocene proxy data and climate models. Springer, Berlin

Brauer A, Endres C, Negendank JFW, Zolitschka B (2000) Lateglacial and Holocene AMS radiocarbon and varve chronology from the annually laminated sediment record of Lake Meerfelder Maar, Germany. Radiocarbon 42:355–368

Brauer A, Allen JRM, Mingram J, Dulski P, Wulf S, Huntley B (2007) Evidence for last interglacial chronology and environmental change from Southern Europe. Proc Natl Acad Sci USA 104:450–455. doi 10.1073/pnas.0603321104

Brauer A, Haug GH, Dulski P, Sigman DM, Negendank JFW (2008) An abrupt wind shift in Western Europe at the onset of the Younger Dryas cold period. Nat Geosci 1:520–523

Brauer A, Dulski P, Mangili C, Mingram J, Liu J (2009) The potential of varves in high-resolution paleolimnological studies. PAGES Newslett 17:96–98

Calanchi N, Dinelli E, Lucchini F, Mordenti A (1996) Chemostratigraphy of late quaternary sediments from Lake Albano and central Adriatic Sea cores (PALICLAS Project). Mem Inst Ital Idrobiol 55:247–264

Carapezza ML, Lelli M, Tarchini L (2010) Geochemistry of the Albano crater lake. In: Funiciello R, Giordano G (eds) The Colli Albani Volcano. Special Publications of IAVCEI, Geological Society, London, pp 107–139

Chaparro MAE, Böhnel HN, Byrne R, Nowaczyk NR, Molina-Garza RS, Jungjae PJ (2008) Paleomagnetic secular variation and rock-magnetic studies of Holocene sediments from a maar lake (Hoya de San Nicolas) in Central Mexico. Geophys J Int 175:462–476

Chondrogianni C, Ariztegui D, Rolph T, Juggins S, Shemesh A, Rietti-Shati M, Guilizzoni P, Lami A, Niessen F, McKenzie JA, Oldfield F (2004) Millennial to interdecadal climate variability in the Mediterranean during the LGM—the lake Albano record. Quat Int 122:31–41

Dearing JA (1999) Holocene environmental change from magnetic proxies in lake sediments. In: Maher BA, Thompson R (eds) Quaternary climates, environments and magnetism. Cambridge University Press, Cambridge

de Beaulieu JL, Reille M (1992) Long Pleistocene pollen sequences from the Velay Plateau (Massif Central, France). I. Ribains maar. Veg Hist Archaeobot 1:242–243

Engels S, Bohncke SJP, Heiri O, Schreber K, Sirocko F (2011) The lacustrine sediment record of Oberwinkler Maar (Eifel, Germany): chironomid and macroremain-based inferences of environmental changes during Oxygen Isotope stage 3. Boreas 37:414–425

Faegri K, Kaland PE, Krzywinski K (1989) Textbook of pollen Analysis. Wiley, New York

Follieri M, Magri D, Sadori L (1988) 250,000-year pollen record from Valle di Castiglione (Roma). Pollen Spores 30:329–356

Frank AHE (1969) Pollen stratigraphy of the Lake of Vico (Central Italy). Palaeogeogr Palaeoclimatol Paleoecol 6:67–85

Frey DG (1988) What is paleolimnology? J Paleolimnol 1:5–8

Funiciello R, Giordano G, De Rita D (2003) The Albano maar lake (Colli Albani Volcano, Italy): recent volcanic activity and evidence of pre-roman age catastrophic lahar events. J Volcanol Geoth Res 123:43–61

Gasse F, Tekaia F (1983) Transfer functions for estimating paleocological conditions (pH) from East African diatoms. Hydrobiologia 103:85–90

Gasse F, Juggins S, Khelifa LB (1995) Diatom-based transfer-functions for inferring past hydrochemical characteristics of African lakes. Palaeogeogr Palaeocl Palaeoecol 117:31–54

Gebhardt CA, De Batist M, Niessen F, Anselmetti FS, Ariztegui D, Kopsch C, Ohlendorf C, Zolitschka B (2011) Deciphering lake and maar geometries from seismic refraction and reflection surveys in Laguna Potrok Aike (southern Patagonia, Argentina). J Volcanol Geoth Res 201:357–363

Giaccio B, Messina P, Sposato A, Voltaggio M, Zanchetta G, Galadini F, Gori S, Santacroce R (2009) Tephra layers from Holocene lake sediments of the Sulmona Basin, central Italy: implications for volcanic activity in Peninsular Italy and tephrostratigraphy in the central Mediterranean area. Quat Sci Rev 28:2710–2733

Giardini M (2007) Late quaternary vegetation history at Stracciacappa (Rome, central Italy). Veg Hist Archaeobot 16:301–316

Gilli A, Anselmetti F, Ariztegui D, Beres M, McKenzie JA, Markgraf V (2005) Seismic stratigraphy, buried beach ridges and contourite drifts: the late quaternary history of the closed Lago Cardiel basin, Argentina (49 °S). Sedimentology 52:1–23

Giraudi C, Magny M, Zanchetta G, Drysdale R (2011) The Holocene climatic evolution of the Mediterranean Italy: a review of the continental geological data. Holocene 21:105–115

Gouramanis C, Wilkins D, De Deckker P (2010) 6000 years of environmental changes recorded in Blue Lake, South Australia, based on ostracod ecology and valve chemistry. Palaeogeogr Palaeocl Palaeoecol 297:223–237

Grüger E, Thulin B (1998) First results of biostratigraphical investigations of Lago d'Averno near Naples relating to the period 800 BC–800 AD. Quat Int 47 (48):35–40

Guilizzoni P, Marchetto A, Lami A, Oldfield F, Manca M, Belis CA, Nocentini AM, Comoli P, Jones VJ, Juggins S, Chondrogianni C, Ariztegui D, Lowe JJ, Ryves DB, Battarbee RW, Rolph TC, Massaferro J (2000) Evidence for short-lived oscillations in the biological records from the sediments of Lago Albano (Central Italy) spanning the period ca. 28 to 17 kyr BP. J Paleolimnol 23:117–127

Guilizzoni P, Lami A, Marchetto A, Jones V, Manca M, Bettinetti R (2002) Palaeoproductivity and environmental changes during the Holocene in central Italy as recorded in two crater lakes (Albano and Nemi). Quat Int 88:57–68

Guilizzoni P, Marchetto A, Lami A, Gerli S, Musazzi S (2011) Use of sedimentary pigments to infer past phosphorus concentration in lakes. J Paleolimnol 45:433–445

Hajdas I, Bonani G, Zolitschka B, Brauer A, Negendank JFW (1998) ^{14}C ages of terrestrial macrofossils from Lago Grande di Monticchio (Italy). Radiocarbon 40:803–807

Hofmann W (1993a) Late-Glacial/Holocene changes of the climatic and trophic conditions in three Eifel maar lakes, as indicated by faunal remains. I. Cladocera. Paleolimnology of european maar lakes. Lecture notes in earth sciences, vol 49. pp 393–420

Hofmann W (1993b) Late-Glacial/Holocene changes of the climatic and trophic conditions in three Eifel maar lakes, as indicated by faunal remains. II. Chironomidae (Diptera). Paleolimnology of european maar lakes. Lecture notes in earth sciences, vol 49. pp 421–473

Hutchinson GE, Bonatti E, Cowgill UM, Goulden CE, Leventhal EA, Mallet ME, Margaritora F, Patrick R, Racek A, Roback SA, Stella E, Ward-Perkins JB, Wellman TR (1970) Ianula: an account of the history and development of the Lago di Monterosi, Latium, Italy. Trans Am Philos Soc 69:1–178

Inagaki F (2010) Deep subseafloor microbial communities. In Encyclopedia of life sciences. Wiley, Chichester

Jiang HC, Dong HL, Yu BS, Liu XQ, Li YL, Ji SS, Zhang CLL (2007) Microbial response to salinity change in Lake Chaka, a hypersaline lake on Tibetan plateau. Environ Microbiol 9(10):2603–2621

Kelts K (1987) Limnogeological research in Switzerland. Ann Bull Swiss Commission Oceanogr Limn. 1–6

Konhauser K (2007) Introduction to geomicrobiology. Blackwell Publishing Company, Maldon

Lami A, Niessen F, Guilizzoni P, Masaferro J, Belis CA (1994) Palaeolimnological studies of the eutrophication of volcanic Lake Albano (Central Italy). J Paleolimnol 10:181–197

Lamoureux SF (2001) Varve chronology techniques. In: Last WM, Smol JP (eds). Developments in paleoenvironmental research (DPER), tracking environmental change using lake sediments: physical and chemical techniques, vol 2. Kluwer, Dordrecht

Lancashire AK, Flenley JR, Harper M (2002) Late Glacial beech forest: an 18000–5000-BP pollen record from Auckland, New Zealand. Global Planet Change 33:315–327

Leavitt PR (1993) A review of factors that regulate carotenoid and chlorophyll deposition and fossil pigment abundance. J Paleolimnol 9:109–127

Leng MJ, Marshall JD (2004) Isotopes in quaternary paleoenvironmental reconstruction. Quat Sci Rev 23:811–831

Lenton T, Kageyama M (2012) Earth System Models: how well do Earth system model simulate the dynamics of global change? PAGES News 20(1):8–9

Litt T, Schölzel C, Kühl N, Brauer A (2009) Vegetation and climate history in the Westeifel Volcanic Field (Germany) during the past 11,000 years based on annually laminated lacustrine maar sediments. Boreas 38:679–690

Lowe D (2011) Tephrochronology and its application: a review. Quat Geochronol 6:107–153

Lowe JJ, Walker MJC (1997) Reconstructing quaternary environments. Longman, London

Lowe J, Accorsi CA, Bandini Mazzanti M, Bishop A, van der Kaars S, Forlani L, Mercuri AM, Rivalenti C, Torri P, Watson C (1996) Pollen stratigraphy of sediment sequences from lakes Albano and Nemi, (near Rome) and from the central Adriatic, spanning the interval from oxygen isotope stage 2 to the present day. Mem Inst Ital Idrobiol 55:71–98

Lucke A, Schleser GH, Zolitschka B, Negendank JFW (2003) A Lateglacial and Holocene organic carbon isotope record of lacustrine palaeoproductivity and climatic change derived from varved lake sediments of Lake Holzmaar, Germany. Quat Sci Rev 22:569–580

Magri D (1999) Late quaternary vegetation history at Lagaccione near Lago di Bolsena (central Italy). Rev Palaeobot Palynol 106:171–208

Magri D, Sadori L (1999) Late Pleistocene and Holocene pollen stratigraphy at Lago di Vico (central Italy). Veg Hist Archaeobot 8:247–260

Manca M, Nocentini AM, Belis CA, Comoli P, Corbella L (1996) Invertebrate fossil remains as indicators of late Quaternary environmental changes in Latium crater lakes (L. Albano and L. Nemi). Mem Inst Ital Idrobiol 55:149–176

Manning PG, Murphy TP, Prepas EE (1991) Intensive formation of vivianite in the bottom sediments of mesotrophic Narrow Lake, Alberta. Can Mineral 29:77–85

Mayr C, Fey M, Haberzettl T, Janssen S, Lucke A, Maidana NI, Ohlendorf C, Schabitz F, Schleser GH, Struck U, Wille M, Zolitschka B (2005) Palaeoenvironmental changes in southern Patagonia during the last millennium recorded in lake sediments from Laguna Azul (Argentina). Palaeogeogr Palaeocl Palaeoecol 228:203–227

Mercuri AM, Sadori L (2012) Climate changes and human settlements since the Bronze Age period in central Italy. Rend Online Soc Geol Ital 18:26–28

Mercuri AM, Accorsi CA, Bandini Mazzanti M (2002) The long history of *Cannabis* and its cultivation by the Romans in central Italy, shown by pollen records from

Lago di Albano and Lago di Nemi. Veg Hist Archaeobot 11:263–276
Mercuri AM, Bandini Mazzanti M, Torri P, Vigliotti L, Bosi G, Florenzano A, Olmi L, Massamba N'siala I (2012) A marine/terrestrial integration for mid-late Holocene vegetation history and the development of the cultural landscape in the Po Valley as a result of human impact and climate change. Veg Hist Archaeobot 21:4–5. doi: 10.1007/s00334-012-0352-4
Meyers PA (1994) Preservation of elemental and isotopic source identification of sedimentary organic matter. Chem Geol 114:289–302
Meyers PA (2003) Applications of organic geochemistry to paleolimnological reconstructions: a summary of examples from the Laurentian Great Lakes. Org Geochem 34:261–289
Michard G, Viollier E, Jezequel D, Sarazin G (1994) Geochemical study of a crater lake: Pavin Lake, France—Identification, location and quantification of the chemical reactions in the lake. Chem Geol 115:103–115
Mills K, Ryves DB (2012) Diatom-based models for inferring past water chemistry in western Ugandan crater lakes. J Paleolimnol 48:383–399. doi:10.1007/s10933-012-9609-2
Mingram J, Allen JRM, Brüchmann C, Liu J, Luo X, Negendank JFW, Nowaczyk N, Schettler G (2004) Maar- and crater lakes of the Long Gang Volcanic Field (N.E. China)—overview, laminated sediments, and vegetation history of the last 900 years. Quat Int 123–125:135–147
Morgan LA, Shanks WC, Lovalvo DA, Johnson SY, Stephenson WJ, Pierce KL, Harlan SS, Finn CA, Lee G, Webring M, Schulz B, Dühn J, Sweeney R, Balistrieri L (2003) Exploration and discovery in Yellowstone Lake: results from high-resolution sonar imaging, seismic reflection profiling, and submersible studies. J Volcanol Geoth Res 122:221–242
Mullins HT, Hinchey EJ, Wellner RW, Stephens DB, Anderson WT, Dwyer TR, Hine AC (1996) Seismic stratigraphy of the Finger Lakes: a continued record of Heinrich event H-1 and Laurentide ice sheet instability. Geol Soc Am Spec Pap 311:1–35
Munno R, Petrosino P (2007) The late quaternary tephrostratigraphical record of the San Gregorio Magno basin (southern Italy). J Quat Sci 22:247–266
Nealson KH, Stahl DA (1997) Microorganisms and biogeochemical cycles: what can we learn from layered microbial communities? Rev Mineral 35:5–34
Nelson CS, Smith AM (1966) Stable oxygen and carbon isotope compositional fields for skeletal and diagenetic components in New Zealand Cenozoic non-tropical carbonate sediments and limestones: a synthesis and review. NZ J Geol Geophys 39:93–107
Niessen F, Lami A, Guilizzoni P (1993) Climatic and tectonic effects on sedimentation in central Italian volcano lakes (Latium)—implications from high resolution seismic profiles. Lect Notes Earth Sci 49:129–148
Oldfield F (2005) Environmental change—key issues and alternative approaches. Cambridge University Press, Cambridge
Oldfield F, Crooks P, Harkness D, Petterson G (1997) AMS radiocarbon dating of organic fractions from varved lake sediments: an empirical test of reliability. J Paleolimnol 18:87–91
Pérez-Obiol R (1988) Histoire Tardiglaciaire et Holocène de la végétation de la région volcanique d'Olot (NE Péninsule Ibérique). Pollen Spores 30:189–202
Piovano EL, Ariztegui D, Moreira SD (2002) Recent environmental changes in Laguna Mar Chiquita (central Argentina): a sedimentary model for a highly variable saline lake. Sedimentology 49:1371–1384
Prasad S, Brauer A, Rein B, Negendank JFW (2006) Rapid climate change during the early Holocene in western Europe and Greenland. Holocene 16:153–158
Ramrath A, Zolitschka B, Wulf S, Negendank JFW (1999) Late Pleistocene climatic variations as recorded in two Italian maar lakes (Lago di Mezzano, Lago Grande di Monticchio). Quat Sci Rev 18:977–992
Ramrath A, Sadori L, Negendank JFW (2000) Sediments from Lago di Mezzano, central Italy: a record of Late Glacial/Holocene climatic variations and anthropogenic impact. Holocene 10:87–95
Reimer PJ, Baillie MGL, Bard E, Bayliss A, Beck JW, Blackwell PG, Bronk Ramsey C, Buck CE, Burr GS, Edwards RL, Friedrich M, Grootes PM, Guilderson TP, Hajdas I, Heaton TJ, Hogg AG, Hughen KA, Kaiser KF, Kromer B, McCormac FG, Manning SW, Reimer RW, Richards DA, Southon JR, Talamo S, Turney CSM, van der Pflicht J, Weyhenmeyer CE (2009) INTCAL09 and MARINE09 radiocarbon age calibration curves, 0–50,000 years cal BP. Radiocarbon 51:1111–1150
Rioual P, Andrieu-Ponel V, de Beaulieu JL, Reille M, Svobodova H, Battarbee RW (2007) Diatom responses to limnological and climatic changes at Ribains Maar (French Massif Central) during the eemian and early wurm. Quat Sci Rev 26:1557–1609
Rolph TC, Oldfield F, van der Post KD (1996) Palaeomagnetism and rock-magnetism results from Lake Albano and the central Adriatic Sea (Italy). Mem Inst Ital Idrobiol 55:265–283
Rolph TC, Vigliotti L, Oldfield F (2004) Mineral magnetism and geomagnetic secular variation of marine and lacustrine sediments from central Italy: timing and nature of local and regional Holocene environmental change. Quat Sci Rev 23:1699–1722
Ruiz-Fernández AC, Hillaire-Marcel C, Páez-Osuna F, Ghaleb B, Caballero M (2007) ^{210}Pb chronology and trace metal geochemistry at Los Tuxtlas, Mexico, as evidenced by a sedimentary record from the Lago Verde crater lake. Quat Res 67:181–192
Rull V, Cañellas-Boltà N, Sáez A, Giralt S, Pla S, Margalef O (2010) Paleoecology of Easter Island: evidence and uncertainties. Earth Sci Rev 99:50–60
Ryner M, Gasse F, Rumes B, Verschuren D (2007) Climatic and hydrological instability in semi-arid equatorial East Africa during the late Glacial to Holocene transition: a multi-proxy reconstruction of aquatic ecosystem response in northern Tanzania. Palaeogeogr Palaeocl Palaeoecol 248:440–458

Ryves DB, Jones VJ, Guilizzoni P, Lami A, Marchetto A, Battarbee RW, Bettinetti R, Devoy EC (1996) Late Pleistocene and Holocene environmental changes at Lake Albano and Lake Nemi (Central Italy) as indicated by algal remains. Mem Inst Ital Idrobiol 55:119–148

Ryves DB, Mills K, Bennike O, Brodersen KP, Lamb AL, Leng MJ, Russell JM, Ssemmanda I (2011) Environmental change over the last millennium recorded in two contrasting crater lakes in western Uganda, eastern Africa (Lakes Kasenda and Wandakara). Quat Sci Rev 30:555–569

Sadori L, Giraudi C, Petitti P, Ramrath A (2004) Human impact at Lago di Mezzano (central Italy) during the Bronze Age: a multidisciplinary approach. Quat Int 113:5–17

Sadori L, Jahns S, Peyron O (2011) Mid-Holocene vegetation history of the central Mediterranean. Holocene 21:117–129

Schelske CL, Hodell DA (1995) Using carbon isotopes of bulk sedimentary organic matter to reconstruct the history of nutrient loading and eutrophication in Lake Erie. Limnol Oceanogr 40:918–929

Schettler G, Romer D (1988) Anthropogenic influences on Pb/Al and lead isotope signature in annually layered Holocene Maar lake sediments. Appl Geochem 13:787–797

Sevink J, van Bergen MJ, van der Plicht J, Feiken H, Anastasia C, Huizinga A (2011) Robust date for the Bronze Age Avellino eruption (Somma-Vesuvius): 3945 ± 10 calBP (1995 ± 10 calBC). Quat Sci Rev 30:1035–1046

Skov T, Buchaca T, Amsinck SL, Landkildehus F, Odgaard BV, Azevedo J, Goncalves V, Raposeiro PM, Andersen TJ, Jeppesen E (2010) Using invertebrate remains and pigments in the sediment to infer changes in trophic structure after fish introduction in Lake Fogo: a crater lake in the Azores. Hydrobiologia 654:13–25

Smol JP (2008) Pollution of Lakes and Rivers: a paleoenvironmental perspective, 2nd edn. Wiley-Blackwell Publishing, Oxford

Ssemmanda I, Ryves DB, Bennike O, Appleby PG (2005) Vegetation history in western Uganda during the last 1200 years: a sediment-based reconstruction from two crater lakes. Holocene 15:119–132

Stebich M, Bruchmann C, Kulbe T, Negendank JFW (2005) Vegetation history, human impact and climate change during the last 700 years recorded in annually laminated sediments of Lac Pavin, France. Rev Palaeobot Palynol 133:115–133

Stockhausen H, Thouveny N (1999) Rock-magnetic properties of Eemian maar lake sediments from Massif Central, France: a climatic signature? Earth Planet Sci Lett 173:299–313

Stockhausen H, Zolitschka B (1999) Environmental changes since 13,000 cal BP reflected in magnetic and sedimentological properties of sediments from Lake Holzmaar (Germany). Quat Sci Rev 18:913–925

Street-Perrot FA, Ficken KJ, Huang Y, Eglington G (2004) Late quaternary changes in carbon cycling in Mount Kenya, East Africa: and overview of the $\delta^{13}C$ record in lacustrine organic matter. Quat Sci Rev 23:861–879

Sulpizio R, Bonasia R, Dellino P, Di Vito MA, La Volpe L, Mele D, Zanchetta G, Sadori L (2008) Discriminating the long distance dispersal of fine ash from sustained columns or near ground ash clouds: The example of the Pomici di Avellino eruption (Somma-Vesuvius, Italy). J Volcanol Geoth Res 17:263–276

Telford RJ, Lamb HF (1999) Groundwater-mediated response to Holocene climatic change recorded by the diatom stratigraphy of an Ethiopian crater lake. Quat Res 52:63–75

Thompson R, Oldfield F (1986) Environmental magnetism. Allen and Unwin, Oxford

Thouveny N, de Beaulieu JL, Bonifay E, Creer KM, Guiot J, Icole M, Johnsen S, Jouzel J, Reille M, Williams T, Williamson D (1996) Climate variation in Europe over the past 140 kyr deduced from rock magnetism. Nature 371:503–506

Tzedakis PC, Andrieu V, de Beaulieu J-L, Birks HJB, Crowhurst S, Follieri M, Hooghiemstra H, Magri D, Reille M, Sadori L, Shackleton NJ, Wijmstra TA (2001) Establishing a terrestrial chronological framework as a basis for biostratigraphical comparisons. Quat Sci Rev 20:1583–1592

Vigliotti L (2006) Secular variation record of the earth magnetic field in Italy during the Holocene: constraints for the construction of a master curve. Geoph J Int 165:414–429

Vigliotti L, Ariztegui D, Guilizzoni P, Lami A (2010) Reconstructing natural and human-induced environmental change in central Italy since the late Pleistocene—the multi-proxy records from maar lakes Albano and Nemi. In: Funiciello R, Giordano G (eds) The Colli Albani Volcano, Special Publications of IAVCEI 3. Geological Society of London, London, pp 245–257

Vlag P, Thouveny N, Rochette P, Williamson D, Ben-Atig F (1996) Evidence for a geomagnetic excursion recorded in the sediments of Lac St. Front. A link with the Laschamp excursion? J Geophys Res 101:28211–28230

von Gunten L, Grosjean M, Kamenik C, Fujak M, Urrutia R (2012) Calibrating biogeochemical and physical climate proxies from non-varved lake sediments with meteorological data: methods and case studies. J Paleolimnol 47:583–600

Vuillemin A, Ariztegui D, PASADO Scientific Team (2013) Geomicrobiological investigations in lake sediments over the last 1500 years. Quat Sci Rev 71:119–130. doi:10.1016/j.quascirev.2012.04.011

Vuillemin A, Ariztegui D, Vasconcelos C, PASADO Scientific Drilling Party (2010) Establishing sampling procedures in lake cores for subsurface biosphere studies: assessing in situ microbial activity. Sci Drilling 10:35–39. doi: 10.2204/iodp.sd.10.04.2010

Watts WA, Allen JRM, Huntley B, Fritz SC (1996) Vegetation history and climate of the last 15,000 years at Laghi di Monticchio, southern Italy. Quat Sci Rev 15:113–132

Wick L, Lemcke G, Sturm (2002) Evidence of Lateglacial and Holocene climatic change and human impact in eastern Anatolia: high-resolution pollen, charcoal, isotopic and geochemical records from the laminated sediments of Lake Van, Turkey. Holocene 13:665–675

Williams T, Thouveny N, Creer K (1996) Paleomagnetic significance of the 300 kyr mineral magnetic record from the sediments of Lac du Bouchet, France. Quat Sci Rev 15:223–235

Williamson D, Taieb M, Damnati B, Icole M, Thouveny N (1993) Equatorial extension of the Younger Dryas event: rock-magnetic evidence from Lake Magadi. Global Planet Change 7:235–242

Williamson D, Jelinowska A, Kissel C, Tucholka P, Gibert E, Gasse F, Massault M, Taieb M, van Campo E, Wieckowski K (1998) Mineral-magnetic proxies of erosion/oxidation cycles in tropical maar lake sediments (Lake Tritrivakely, Madagascar): paleoenvironmental implications. Earth Planet Sci Lett 155:205–219

Williamson D, Jackson MJ, Banerjee SK, Marvin J, Merdaci O, Thouveny N, Decobert M, Gibert-Massault E, Massault M, Mazaudier D, Taieb M (1999) Magnetic signatures of hydrological change in a tropical maar-lake (Lake Massoko, Tanzania): Preliminary results. Phys Chem Earth A 24:799–803

Wulf S, Kraml M, Brauer A, Keller J, Negendank JWF (2004) Tephrochronology of the 100 ka lacustrine sediment record of Lago Grande di Monticchio (southern Italy). Quat Int 122:7–30

Zolitschka B (2006) Varved lake sediments. In: Elias SA (ed) Encyclopedia of quaternary science. Elsevier, Amsterdam

Zolitschka B, Negendank JFW (1996) Sedimentology, dating and palaeoclimatic interpretation of a 76.3 ka record from Lago Grande di Monticchio, southern Italy. Quat Sci Rev 15:101–112

The Comparative Limnology of Lakes Nyos and Monoun, Cameroon

George W. Kling, William C. Evans, and Gregory Z. Tanyileke

Abstract

Lakes Nyos and Monoun are known for the dangerous accumulation of CO_2 dissolved in stagnant bottom water, but the shallow waters that conceal this hazard are dilute and undergo seasonal changes similar to other deep crater lakes in the tropics. Here we discuss these changes with reference to climatic and water-column data collected at both lakes during the years following the gas release disasters in the mid-1980s. The small annual range in mean daily air temperatures leads to an equally small annual range of surface water temperatures ($\Delta T \sim 6$–7 °C), reducing deep convective mixing of the water column. Weak mixing aids the establishment of meromixis, a requisite condition for the gradual buildup of CO_2 in bottom waters and perhaps the unusual condition that most explains the rarity of such lakes. Within the mixolimnion, a seasonal thermocline forms each spring and shallow diel thermoclines may be sufficiently strong to isolate surface water and allow primary production to reduce P_{CO2} below 300 μatm, inducing a net influx of CO_2 from the atmosphere. Surface water O_2 and pH typically reach maxima at this time, with occasional O_2 oversaturation. Mixing to the chemocline occurs in both lakes during the winter dry season, primarily due to low humidity and cool night time air temperature. An additional period of variable mixing, occasionally reaching the chemocline in Lake Monoun, occurs during the summer

G.W. Kling (✉)
Department of Ecology and Evolutionary Biology,
University of Michigan, Ann Arbor, MI 48109, USA
e-mail: gwk@umich.edu

W.C. Evans
U.S. Geological Survey, Menlo Park,
CA 94025, USA
e-mail: wcevans@usgs.gov

G.Z. Tanyileke
Institute for Geological and Mining Research,
Yaounde, Cameroon
e-mail: gtanyileke@yahoo.co.uk

D. Rouwet et al. (eds.), *Volcanic Lakes*, Advances in Volcanology,
DOI 10.1007/978-3-642-36833-2_18,
© Springer-Verlag Berlin Heidelberg 2015

monsoon season in response to increased frequency of major storms. The mixolimnion encompassed the upper ~40–50 m of Lake Nyos and upper ~15–20 m of Lake Monoun prior to the installation of degassing pipes in 2001 and 2003, respectively. Degassing caused chemoclines to deepen rapidly. Piping of anoxic, high-TDS bottom water to the lake surface has had a complex effect on the mixolimnion. Algal growth stimulated by increased nutrients (N and P) initially stimulated photosynthesis and raised surface water O_2 in Lake Nyos, but O_2 removal through oxidation of iron was also enhanced and appeared to dominate at Lake Monoun. Depth-integrated O_2 contents decreased in both lakes as did water transparency. No dangerous instabilities in water-column structure were detected over the course of degassing. While Nyos-type lakes are extremely rare, other crater lakes can pose dangers from gas releases and monitoring is warranted.

Keywords

Nyos · Monoun · Crater lakes · Volcanic gas hazards · Cameroon Volcanic Line · Tropical limnology

1 Introduction

Cameroon contains a large number of volcanic lakes, but limnological studies prior to the 1980s were fairly limited in scope (e.g., Hassert 1912; Green 1972; Green et al. 1974). Kling (1987a, b, 1988) conducted a comprehensive study of 34 volcanic lakes and several other Cameroonian lakes not known to occupy volcanic craters. This work helped delineate the impacts of climate, morphometry, sheltering, water transparency and conductivity, and other factors on tropical lake dynamics such as stratification and mixing, thermocline depth, and oxygen profiles. The research was timely because it was conducted during the years when the disastrous gas releases occurred at Lake Monoun (1984) and Lake Nyos (1986), although pre-release data collection was limited to a sample of surface water from Lake Nyos in 1985 (Kling 1987a, 1988).

The Lake Monoun gas release was described by Sigurdsson et al. (1987), and the Lake Nyos release was described by Tuttle et al. (1987), Kling et al. (1987), Tietze (1987), Freeth (1992) and several papers in Le Guern and Sigvaldason (1989, 1990). Numerous studies conducted at lakes Nyos and Monoun in the years after the gas releases focused on the evolution of the deep water layers and on the natural recharge rate of CO_2 near lake bottom (Nojiri et al. 1990, 1993; Evans et al. 1993). These studies were important for understanding the cause of the gas releases and the likelihood of recurrence. The demonstration that dangerous amounts of gas remained in the lakes after the disasters, and that the recharge rate of CO_2 was high enough to substantially increase the risk of recurrence on a decadal timescale, provided stimulus for the installation of pipes to safely remove the gas. The rates of gas removal and changes in gas content of the lakes have since been monitored (e.g., Kling et al. 2005; Kusakabe et al. 2008). However, even though degassing is well underway at Lake Nyos and essentially complete at Lake Monoun, there has been little published on how the degassing has affected the surface water limnology of these lakes.

This chapter discusses comparative limnological aspects of Lakes Nyos and Monoun with an emphasis on the characteristics and behavior of the "mixolimnion", the dilute water layer overlying denser gas-rich water at depth (herein called bottom water). The mixolimnion exhibits diel and seasonal responses to climatic forcing at

the lake surface, and at least episodically is affected by some mixing with bottom water. The mixolimnion is important because it keeps pressure on deeper layers and allows the gas concentrations to build up. Conditions in the mixolimnion that affect its chemical composition and physical structure have a bearing on whole-lake stability and thus on the hazard of uncontrolled gas release. We restrict our detailed discussion to Lakes Nyos and Monoun, but in a final section we discuss other lakes that share characteristics with Nyos and Monoun where the comparison has relevance to gas release hazards.

2 Methods

Methods of water sampling, chemical analyses, and many results are presented in Tuttle et al. (1987), Kling et al. (1989, 2005), and Evans et al. (1993, 1994). Dissolved organic carbon (DOC) and total dissolved nitrogen (TDN) were filtered through Whatman GFF filters (nominal pore size 0.6 µm), acidified to pH ~ 2–3, and stored dark at 4 °C until measurement on a Shimadzu TOC V analyzer. Total dissolved phosphorus (TDP) was measured on similarly filtered, treated, and stored water using a persulfate digestion and subsequent analysis of soluble reactive phosphate using a molybdenum blue method on an Alpkem autoanalyzer. Particulate C and N were filtered on to GFF filters and analyzed in a Perkin-Elmer 2400 CHN elemental analyzer. Underwater light extinction was measured using a Secchi disk and a Licor LI-1000 meter with a LI-193 spherical quantum sensor (PAR, 400–700 nm) following methods and calculations in Kling (1988). Profiles of temperature were measured using a recently calibrated Seabird SBE 19 CTD (0.01 °C accuracy, 0.001 °C precision, conductivity 10 µS/cm accuracy) with a SBE 18 pH sensor. Continuous measurements of lake temperature were made from an anchored raft near the center of the main lake basins using thermistor strings containing YSI 46030 precision resistors (0.1 °C interchangeability, thermometric drift < 0.01 °C over 100 months, 2.5 s time constant) connected to a Campbell Scientific CR23x datalogger recording every 60 s and averaging into 30 min intervals. At these same time intervals using the CR23x datalogger, a meteorological station on the raft measured air temperature and relative humidity (Campbell HMP45C, accuracy 0.2 °C and 2 % RH), wind speed and direction (MetOne 041A windset, accuracy 0.2 m/s, threshold 0.45 m/s), and downwelling solar radiation (Licor LI-200 pyranometer, 400–1,100 nm, accuracy 3 %); sensor heights were ~1.5–2 m above mean water level.

3 Results and Discussion

3.1 Climate

The overall climate affecting Lakes Nyos and Monoun is similar and is driven by seasonal movements of the Inter-Tropical Convergence Zone (ITCZ). In this part of Cameroon the ITCZ movement creates a dry season with virtually no rain in December–February and a monsoon season with heavy rains in June–September. Data from the floating climate stations on both lakes show similar patterns of the coolest air temperatures and lowest humidity during the dry season, the warmest air temperatures coming out of the dry season at the end of February and into March, and the highest humidity during the summer monsoon (Figs. 1 and 2). The lowest maximum daily temperatures occur in June, offset several months from the period of lowest minimum temperatures in late December through early February. This time of lowest minimum temperatures is also the calmest time of the year with wind speeds rarely exceeding 5 m/s, and incoming solar radiation at a minimum due to atmospheric dust from the Harmattan winds (Figs. 1 and 2). Air temperature at both lakes shows no trend since late 1989 when measurements first began (data prior to 2000 not shown), and none of the climate variables measured shows a significant trend over time.

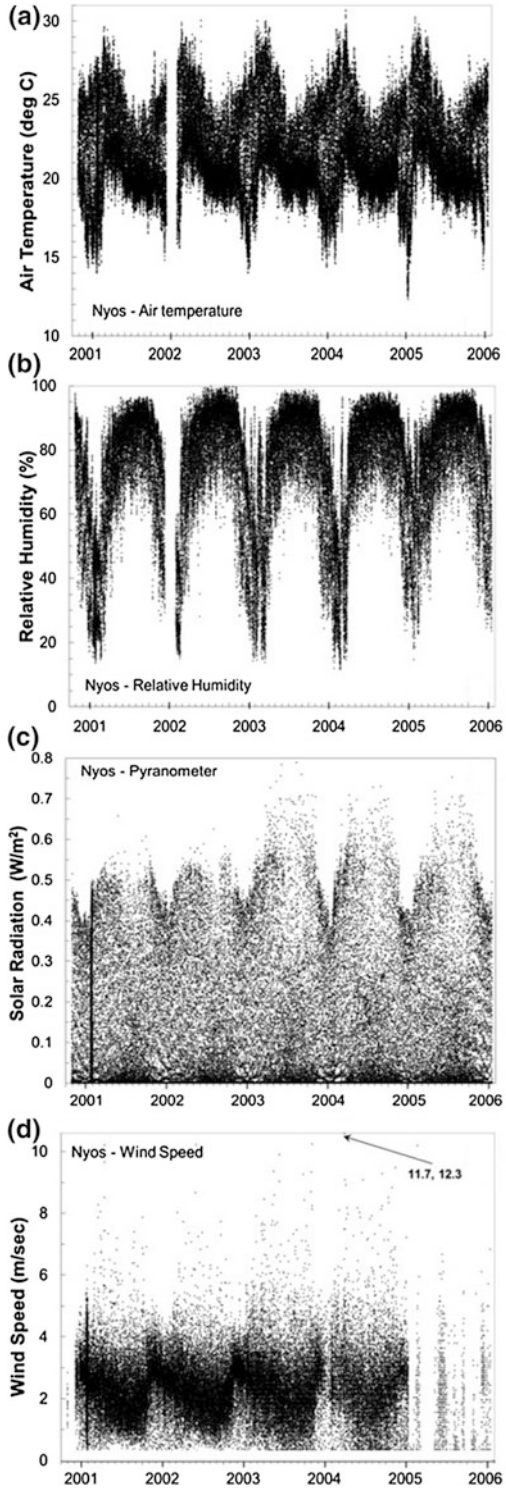

Fig. 1 Selected climatic variables recorded at 30 min intervals on an anchored raft at Lake Nyos

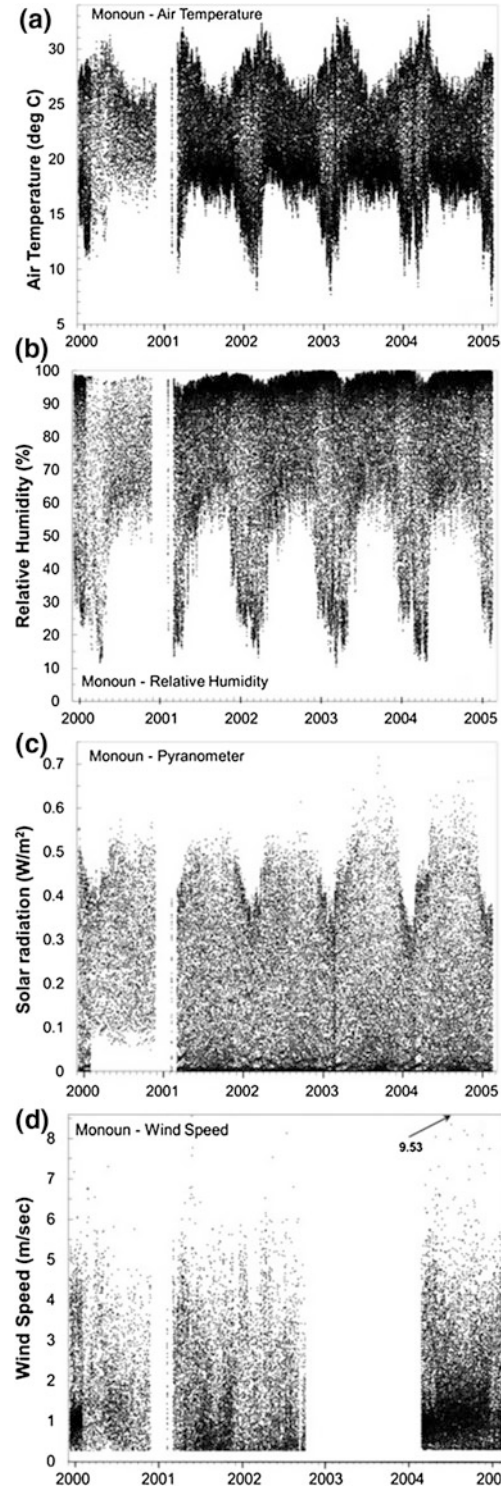

Fig. 2 Selected climatic variables recorded at 30 min intervals on an anchored raft at Lake Monoun

3.2 Lake Morphology and Hydrology

Almost all of Cameroon's volcanic lakes, including Nyos and Monoun, occupy maar craters (Kling 1988; Lockwood and Rubin 1989; Aka et al. 2008). These craters are typically flat bottomed rather than conical, and many are quite deep in relation to their diameters (Kling 1988). At 210 m, Lake Nyos is the deepest of the Cameroonian lakes, but it is only 42 m deeper than Lake Manengouba-Female. Several of the lakes match or exceed the depth of Lake Monoun at 100 m. Both Lakes Nyos and Monoun have a surface area that is much larger than the diameter of the main crater containing the gassy water. Lake Nyos contains a small basin ~48 m deep at its northern end near the point of outflow, and a shallow arm in the southern end near the inflow stream. Lake Monoun contains a small crater ~50 m deep just west of the main crater and a relatively shallow arm further west near the outlet (Sigurdsson et al. 1987).

Unlike many volcanic summit crater lakes, the maar lakes of Cameroon are generally not fully ringed by high rims. Ejecta ramparts extend only part way around Lakes Nyos and Monoun (Sigurdsson et al. 1987; Lockwood and Rubin 1989). Granitic bedrock forms part of the rim around Lake Nyos, but both these lakes have low-elevation rims on two sides that reduce sheltering from the wind. Both maars erupted through existing surface stream drainages, and the lakes capture the inflow from drainage basins several km^2 larger than the actual lake surface area. Riverine inflow and outflow is perennial at Lake Monoun. Only the inflow is perennial at Lake Nyos, and surface outflow only occurs during the rainy season. From 1987–2004 the outflow over the spillway began on average in early July, and ended by early December (Fig. 3). Annual differences in climate can cause outflow to begin as early as April or as late as August. Seepage from Lake Nyos, which is perched on a mountain-side, feeds large discharge springs just downslope. In combination with lack of rain in the dry season and evaporation from the lake surface, this seepage causes lake level to drop below the spillway each year (Tuttle et al. 1992; Evans et al. 1994). The magnitude of lake-level drop

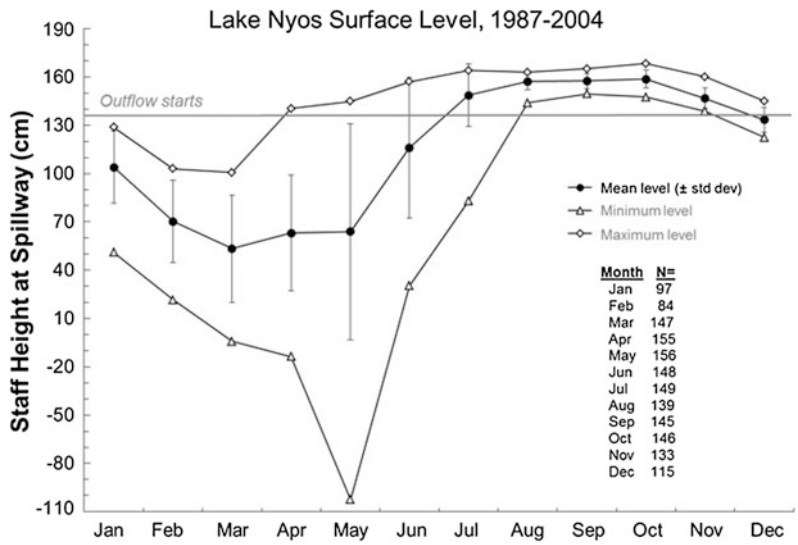

Fig. 3 Staff height (cm) at the spillway of Lake Nyos representing lake level measured over the period 1987–2004. Each point is a mean value for one month calculated using all years of data. The average across all years (*circles*) is shown with *error bars* representing standard deviation of the total number (N) of measurements across all years by month. The range in lake level is taken as the minimum (*triangles*) and maximum (*diamonds*) value of the monthly mean lake level across all years

below the spillway has reached 238 cm but varies from year to year (Fig. 3). Interannual variation in lake level is much less during the outflow period from August into December.

Shallow inflows of dilute groundwater constitute a significant part of the water budget at Lake Nyos (Tuttle et al. 1992). Inflow and outflow of shallow groundwater have not been investigated at Lake Monoun, but may not be significant given the low gradient in topography for many km upstream and downstream of the lake. Inflow of groundwater that is rich in dissolved CO_2 and higher in Total Dissolved Solids (TDS) than surface water or shallow groundwater occurs at or near the bottom of both lakes, and is the ultimate source of gas for the associated hazard. Discrete inflow vents have never been sampled or even precisely located, but the characteristics of this inflowing water have become better constrained over time through the observed changes in bottom water temperature and chemistry (Kling et al. 1989; Evans et al. 1993; Nojiri et al. 1993; Kusakabe et al. 2000; Schmid et al. 2003; Kusakabe 2015).

3.3 Water-Column Structure

The overall density structure in lakes which are permanently stratified (meromictic) includes an upper zone called the mixolimnion which experiences seasonal stratification and turnover, and a lower zone called the monimolimnion which stays permanently stratified. The separation between these two layers is usually called the main chemocline or pycnocline. The upper layer is chemically dilute while lower layers can accumulate salts or gases. In the upper layer there is a thermocline, which is deeper in Lake Nyos than in Lake Monoun due to the greater surface area and water clarity at Nyos (Kling 1988). Profiles of dissolved CO_2, CH_4, and dissolved salts (usually plotted as conductivity) show increasing concentrations with depth below the chemocline. In addition, the shape of the depth profiles evolved during the years following the gas releases. The patterns of change have been presented elsewhere (e.g., Kling et al. 2005; Kusakabe et al. 2008 and updated in Kusakabe 2015). The most important and ominous change was a clear increase in dissolved CO_2 over time in both lakes.

Temperature also increases with depth below the chemocline, and this in part offsets the strength of stratification due to dissolved CO_2 and TDS because warmer temperature reduces water density. The opposing effects of temperature and dissolved substances could allow double-diffusive convection to govern transport within the water column (e.g., Nojiri et al. 1993), and this phenomenon was observed over a limited depth interval in 2002 in Lake Nyos (Schmid et al. 2004). Water-column heat and mass fluxes otherwise appear to be slow and diffusion controlled (e.g., Kantha and Freeth 1996; McCord and Schladow 1998; Kusakabe et al. 2000). The inflow of high-TDS water near lake bottom may actually be the main driver of net upward transport in these lakes, consistent with modeling results (Schmid et al. 2006) and observed profile development (Kusakabe 2015).

This basic two-component model of the water column accounts for the depth profiles of most dissolved gases and ions, but complexities arise regarding Fe and CH_4. Transport of these species involves solid and gaseous phases that can sink or rise at much different rates than dissolved substances. The lakes are essentially traps for Fe, which is present as ferrous iron in anoxic bottom water (Kling et al. 1989). Any mixing or diffusion of dissolved salts up into overlying oxygenated water converts the iron into ferric oxy-hydroxide particles, which then sink instead of being flushed from the lake. The precipitated iron is then reduced and redissolved in anoxic bottom water. The occurrence of this process over many years of stratification explains why Fe constitutes ≥40 % of the cations in bottom water of Lake Nyos and ≥80 % in Lake Monoun. The Fe cycling was discussed in detail by Teutsch et al. (2009).

Along with iron precipitates, particulate organic matter also settles down into bottom water where it donates electrons to reduce ferric

to ferrous iron and serves as a carbon or electron source to promote production of CH_4. Evans et al. (1993) showed that the CH_4 in Lake Nyos was produced at least in part from surficial organic matter based on its high ^{14}C content (41 % modern C) relative to that of the CO_2 (1–2 % modern C). In the years after the gas releases, CH_4 concentrations in both lakes increased much faster than did CO_2 concentrations, also showing lacustrine production of CH_4. The greatest increase occurred just above lake bottom, but CH_4 increases were substantial even at depths where CO_2 and TDS concentrations remained nearly constant (Kling et al. 2005). Either some distributed CH_4 production occurs within the water column, which contains <1 mg/L SO_4 throughout (mean = 0.19 mg/L ± 0.18 S.D., N = 34), or the CH_4 is transported in the lake independently of dissolved species as a separate gas phase. Probably the settling organic matter supports methanogenesis even in the upper water column on anoxic microsites (e.g., Karl and Tilbrook 1994; Cabassi et al. 2013).

Evidence of a separate, gas-phase transport for CH_4 came from trapping bubbles of CH_4-rich gas (47 %) in an inverted funnel suspended at the chemocline in Lake Nyos (Kling et al. 2005). In addition, depth sounders sometimes return images that are interpreted as rising gas bubbles (Sabroux 2001, pers. comm.). Gas saturation apparently is reached at the sediment-water interface or possibly on particles in the water column, at least in local areas, allowing the bubbles to form. Even though CH_4 constitutes only ~2 % (on a molar basis) of the total dissolved gas at the bottom of these lakes, it would make up ~50 % of the gas bubbles because of its much lower solubility (Wilhelm et al. 1977).

3.4 Lake Stability

Dissolved CO_2 is a greater factor than TDS in the increased density of bottom water that leads to stratification in these lakes. However, as the water-column stability imparted by dissolved CO_2 increases, it becomes metastable when saturation is reached because gas bubbles can form. The presence of bubbles greatly reduces bulk water density and the gas rises rapidly and destroys the water column stability. This loss of density structure and lake stability can lead to spontaneous lake mixing and amplification of gas exsolution to the point of creating massive, dangerous gas releases.

Because of this non-linear effect of CO_2 on water density, standard formulas for calculating the energy required to overcome lake stratification are inapplicable to gas-rich lakes. An alternate parameter, E^*, was developed to evaluate lake stability and the potential danger of massive gas bursts (Kling et al. 1994). E* decreases as the pressure of dissolved gas (CO_2 + CH_4 + N_2) approaches hydrostatic (gas saturation), especially in situations with high (i.e., dangerous) gas pressures. Profiles showing low E* indicate low lake stability in gas-rich zones below the chemoclines in Nyos and Monoun, even though density gradients and conventional water-column stability might be large. Increases in E* stability due to controlled degassing were predicted and later observed (Kling et al. 2005).

3.5 The Mixolimnion

3.5.1 Seasonal Patterns at Nyos

Temperature variations in the mixolimnion and their relation to climate have been discussed by numerous authors (e.g., Kling et al. 2005; Schmid et al. 2006) and are shown in Fig. 4 for several annual cycles. Surface water shows a seasonal variation of ~6 °C with a period of pronounced warming in the spring months March–May following increases in air temperatures (Fig. 1). The onset of the summer rainy season brings some cooling of the surface layer, but subsurface layers continue to warm. During this period there is heat loss from surface water to the atmosphere, and downward heat transfer from the surface to lower layers by mixing. As the strength of the thermocline decreases, there is more heat transfer to greater depths; for example,

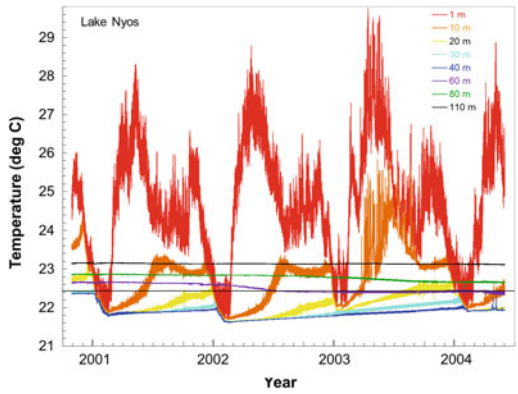

Fig. 4 Lake Nyos water temperatures at fixed depths (relative to mean lake level) recorded at 30 min intervals

water at 10 m depth warms most rapidly in June as surface water cools, and water at 20 m depth warms later, in August through October, as temperatures at 10 m depth decline (Fig. 4). The near-constant temperature at 60 m depth, immediately below the chemocline, during the pre-degassing period indicates no significant upward heat transfer across this boundary.

Early fall (September–November) brings a slight increase in the shallow water temperature gradient, perhaps due to the declining frequency of major storms, but the low humidity increases evaporation and the coldest night-time temperatures of the year cause a rapid cooling of surface water in December–February (Fig. 4). The cooling over this period gradually deepens the upper mixing layer until it eventually reaches the chemocline before springtime warming begins again. Thus, the annual pattern of mixolimnion dynamics can be divided into three main parts: a period of strong stratification in spring, a period of weak stratification in summer, and a period of deep mixing in winter.

Temperature and conductivity profiles with depth (CTD) typical of each of the three periods are shown in Fig. 5, and they can be compared to the annual cycle shown in Fig. 4. The April profile (Fig. 5a) shows the strong spring-time stratification, with the sharp seasonal thermocline beginning at about 8 m depth. The temperature gradient is fairly small between 20 and 40 m depth, where the chemocline begins as seen in the specific conductance profile. Temperatures begin to increase at the chemocline and continue to warm all the way to lake bottom. The early November profile (Fig. 5b) was actually collected at the end of the rainy season, but it shows the cumulative effect of the preceding months of wet and windy weather. Thermal stratification is much weaker than in April but persists as is shown by a relatively uniform temperature gradient from the surface down to about 40 m depth. The late January 2001 profile (Fig. 5c), the last to be collected prior to the start of degassing, reflects the deep mixing of wintertime. Water temperature is nearly uniform from 5 to 42 m depth. The weak thermocline in the upper few meters reflects daytime solar heat inputs and disappears most nights, as seen in Fig. 4.

Specific conductance profiles help to understand mixing dynamics in the mixolimnion. The January profile (Fig. 5c) shows the uniformity of specific conductance from 0 to 40 m during deep wintertime mixing. This uniformity mostly persists during the height of springtime stratification, even when the thermocline prevents mixing between the over- and under-lying water masses (Fig. 5a). A gradient in specific conductance (above 30 m depth) is only seen in the November profile (Fig. 5b).

Superimposing the specific conductance profiles from all three dates highlights the subtle differences in structure and shows that water in the uppermost $\sim$25 m was significantly diluted in November relative to the earlier or later dates (Fig. 6). The November chemocline was also slightly less sharp than on the other dates. The surface dilution likely reflects the effects of the preceding months of the rainy season and some wind-driven eddy mixing down to $\sim$25 m, as discussed above. The slight weakening of the chemocline is more interesting. Based on the annual patterns shown in Fig. 4, a profile collected in November would follow an 8-month period of stratification in the mixolimnion since the preceding winter mixing. The weakening of the chemocline seen in Fig. 6 documents some limited mixing across this boundary that must have occurred during the preceding 8 months. Downward mixing of surface water appears to stop at 25 m depth, but the violent storms of

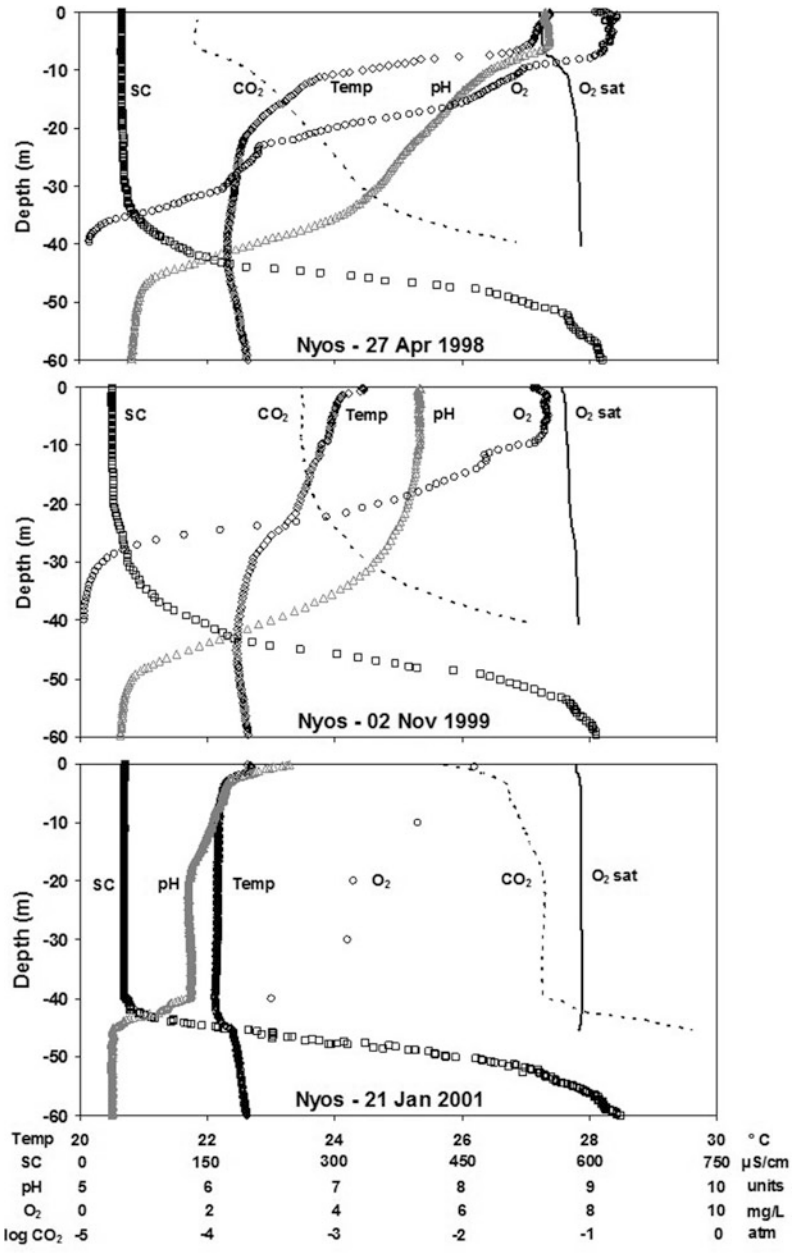

Fig. 5 Profiles of the upper 60 m of Lake Nyos obtained by CTD equipped with pH and O_2 probes. "Temp" (*diamonds*) is temperature in °C, "SC" (*squares*) is specific conductance in µS/cm, pH (*triangles*) in log units, O_2 (*circles*) in mg/L. *Dotted line* shows the log of Henry's law CO_2 pressure (in atm) estimated from pH and our observation that for SC <200 µS/cm, HCO_3 (mg/L) = 6.68 + 0.530 × SC (µS/cm) (N = 44; R^2 = 0.94). Solid "O_2 sat" line is the calculated concentration of oxygen in water (mg/L) at the measured temperature in equilibrium with the atmosphere at lake surface elevation. **a** Profiles in April 1998. **b** Profiles in November 1999. **c** Profiles in January 2001 (O_2 determined on water samples retrieved to lake surface)

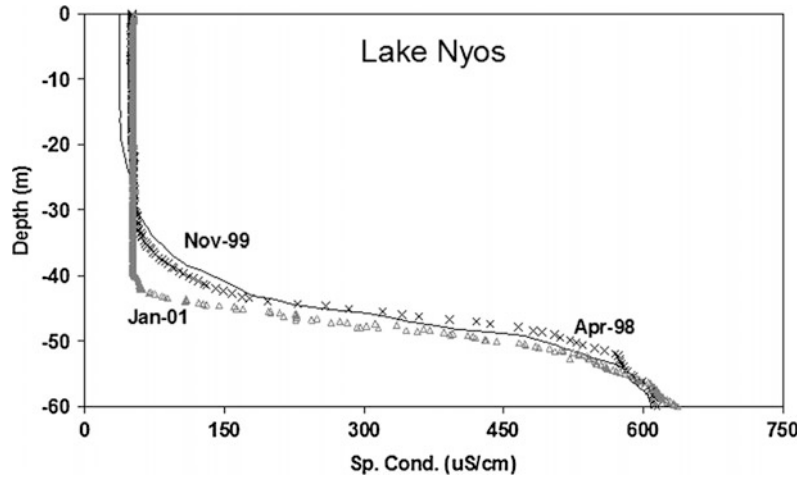

Fig. 6 Lake Nyos specific conductance profiles in April 1998 (*crosses*), November 1999 (*solid line*), and January 2001 (*triangles*)

summer could still potentially transfer energy to the chemocline depth and promote some mixing through shear or wave breaking on internal seiches.

The concentrations of O_2 and CO_2 also reflect mixing processes, but unlike the major ionic species that behave nearly conservatively, these gases have independent sources and sinks such as photosynthesis and respiration plus exchange with the atmosphere. Thus their profiles differ from those of specific conductance. Our CTD casts did not directly measure CO_2, but it can be estimated from pH and specific conductance as discussed by Kusakabe et al. (2008).

As expected for a lake with anoxic bottom water, O_2 profiles show decreasing concentrations with depth and always drop below detection at the top of the chemocline. Dissolved CO_2 profiles show increasing concentrations with depth; pH profiles show the mirror image with decreasing values from the surface down to the chemocline as seen clearly in Figs. 5a and b.

In April, both O_2 and pH profiles show a conspicuous jump to higher values in surface waters above the thermocline (Fig. 5a). In fact, O_2 concentrations in this layer reach 120 % of saturation with respect to the overlying atmosphere. Similar O_2 oversaturation has been observed during spring months in other years. These high O_2 concentrations, and the corresponding decrease in CO_2 (increased pH) are clearly caused by photosynthetic activity in the surface waters (as discussed below). The strong springtime thermocline allows these conditions to develop by effectively isolating the surface water from the underlying CO_2 source and O_2 sink.

By November, thermal stratification has greatly weakened and O_2 concentrations in the surface water have dropped to just below saturation (Fig. 5b). Both the O_2 and pH profiles have become fairly smooth curves exhibiting little correlation to the temperature profile. Deep mixing in winter reduces surface O_2 concentrations below saturation but does not completely eliminate the gradient in either O_2 or pH throughout the mixolimnion, at least during the CTD cast in late January (Fig. 5c). This reduction in O_2 is likely due to upward mixing of anoxic water from beneath the chemocline as the thermocline deepens in winter. Therefore, while some deep mixing to the chemocline might occur nightly (as indicated in Fig. 4), the complete homogenization of the mixolimnion implied by the temperature and specific conductance profiles (Fig. 5c) is a less frequent event.

The January O_2 profile (Fig. 5c) was derived from measurements in water samples retrieved to the surface and protected from atmospheric contact. The pH was also determined on these samples, and alkalinity was determined within several hours after collection, allowing the CO_2

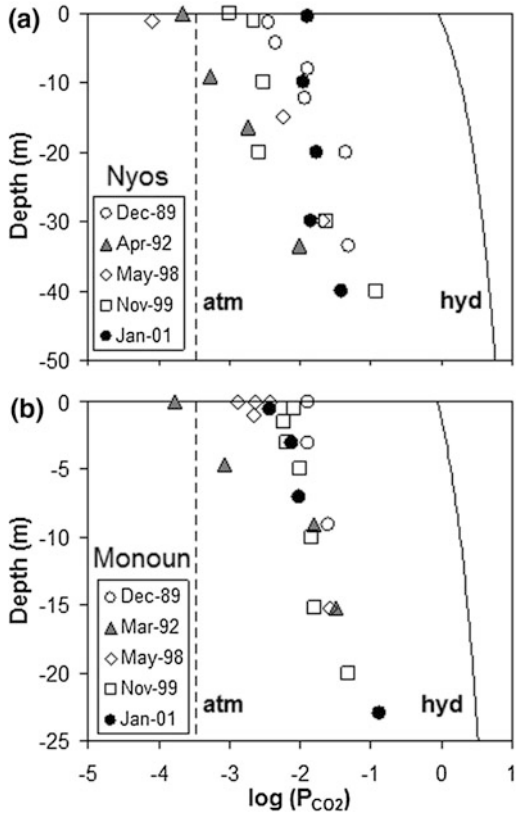

Fig. 7 Calculated P_{CO2} values for different depths and dates. The "*atm*" *line* shows the expected P_{CO2} of water in equilibrium with the atmosphere at lake surface conditions. The "*hyd*" *curve* shows hydrostatic pressure, the maximum P_{CO2} that could exist in a stable solution. **a** Lake Nyos. **b** Lake Monoun

partial pressure to be accurately calculated. The CO_2 pressures for these and similarly processed samples from other dates are shown in Fig. 7.

The P_{CO2} values show a large seasonal range at the lake surface, from about 10,000 µatm to <100 µatm. The highest surface P_{CO2} was found in January 2001, near the time of the profile in Fig. 5c when surface pH was low and deep mixing had brought some gas-rich bottom water into the surface water. The lowest P_{CO2} was found in early May 1998, just days after the profile in Fig. 5a.

The April and May surface P_{CO2} values are well below saturation with respect to the overlying atmosphere (atmospheric saturation ~330 µatm at lake elevation using 390 ppmv in the atmosphere). The strong springtime temperature stratification that traps photosynthetically-produced O_2 above the thermocline also blocks upward transport of CO_2 into surface waters so effectively that invasion of CO_2 from the atmosphere must occur to support photosynthesis. That this lake, made famous by the enormous amount of CO_2 stored in bottom waters, should at times be a net sink for atmospheric CO_2 is remarkable and highlights the role of limnological processes in concealing the hazard at depth.

3.5.2 Seasonal Patterns at Monoun

Annual cycles of temperature variations in the mixolimnion of Lake Monoun (Fig. 8) are similar to those of Lake Nyos, although the upper mixing layer in Monoun is shallower. Both lakes show a period of springtime warming, and the onset of the summer rainy season in late June brings cooling of the surface layer. However, in contrast to Lake Nyos, summertime mixing can involve the entire mixolimnion as seen for example in the small temperature gradients near the surface and the abrupt temperature drop at 15 m depth during August 2000. This deeper mixing in late summer to early fall has also been observed in crater lake Barombi Mbo in southwestern Cameroon, and may play a role in the timing of the Nyos and Monoun gas releases which both occurred in August (Kling 1987). Weak temperature stratification continues through the summer and fall until the lowest temperatures of the upper water

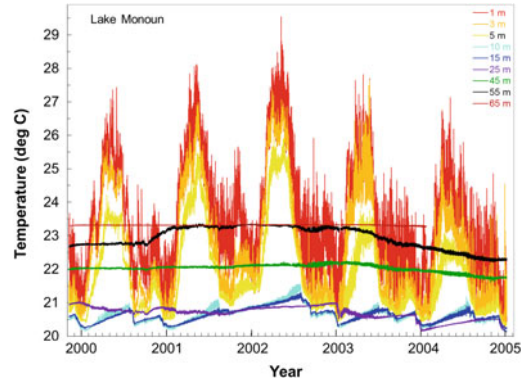

Fig. 8 Lake Monoun water temperatures at fixed depths (relative to mean lake level) recorded at 30 min intervals

column are reached typically in late December and January. These lowest water temperatures are due to low humidity and cold nighttime air temperatures, the same factors affecting Lake Nyos surface water temperature at this time of year. Thus, the annual cycle of the mixolimnion at Lake Monoun can be divided into two main periods: a period of strong stratification in late-winter and spring, and a period of deep mixing or very weak stratification in summer to early winter.

The period of weak thermal stratification is typified by the November profile (Fig. 9a) showing a thermocline at about 2 m depth. The water column is nearly isothermal below the thermocline down to the top of the chemocline at ~17 m depth, although there is still some chemical structure to the water column as seen by the conductivity profile. The May profile (Fig. 9b) shows a stronger and deeper thermocline, and the temperature gradient continues down to the chemocline where it reverses and temperatures get warmer all the way to lake bottom (Kling et al. 2005).

Annual changes in chemistry at Lake Monoun are in general similar to those at Lake Nyos. For example, the strong springtime thermocline allows the pH in overlying water to shift to higher values (Fig. 9b) because the effect of photosynthetic production of O_2 is restricted to the surface water layer where there is sufficient light and nutrients. Based on limited available data, it appears that the volumetric photosynthetic production of O_2 in surface water from 0–3 m depth is similar at Lake Monoun and Lake Nyos. The mean O_2 production (light-dark bottle method) in Monoun was 0.14 mg O_2/L/h (± 0.04 S.D., N = 1 date and 3 depths) and at Nyos it was 0.11 mg O_2/L/h (± 0.08 S.D., N = 3 dates and 10 depths). Oxygen oversaturation in Monoun

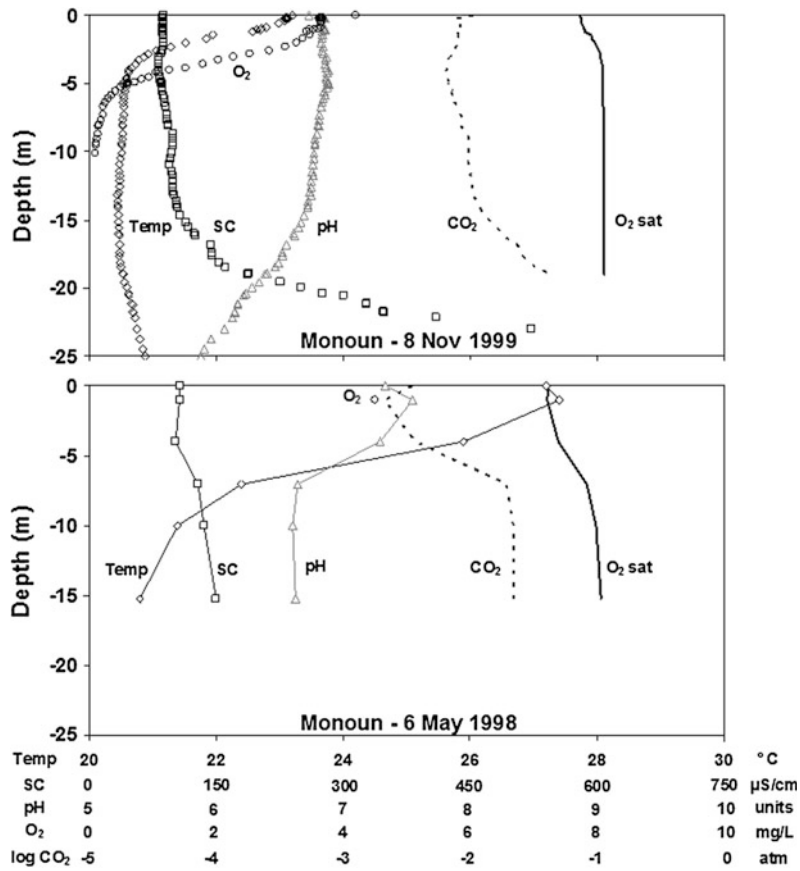

Fig. 9 Profiles of the upper 25 m of Lake Monoun (see Fig. 5 caption for more details). **a** Obtained in November 1999 by CTD equipped with pH and O_2 probes. **b** Determined on samples retrieved to lake surface in May 1998

surface water was observed in April 1992, when the O_2 concentration at the lake surface reached 115 % of saturation. Surface water temperatures and thermocline strength at that time were comparable to those shown for May 1998 (Fig. 9b). Profiles of CO_2 show the drawdown that occurs in surface waters during the spring thermal stratification due to photosynthetic uptake (Fig. 9b). Undersaturation in CO_2 observed in March 1992 (Fig. 7b) coincided with O_2 oversaturation and a rise in surface water pH to 8.67.

Unlike Lake Nyos, where some dissolved O_2 can be detected below the thermocline and occasionally as deep as the top of the chemocline (e.g., Fig. 5c), water below the thermocline in Lake Monoun is normally anoxic and we have never detected O_2 at depths >10 m (e.g., Fig. 9a). This likely reflects a greater oxygen demand in Lake Monoun relative to Lake Nyos, for example by bacteria using the high DOC concentrations as a substrate for respiration or by greater demand for oxidation of Fe(II). Mixing across the chemocline may be more important at Lake Monoun because of its much shallower chemocline depth. Water below the chemocline is extremely rich in ferrous iron, and thus any input of this water would create a huge oxygen demand in the overlying water.

3.5.3 Short-Term Variability at Both Lakes

The most obvious short-term change is the regular diel variation in surface water temperature, which produces the high-frequency signal at 1 m depth in Figs. 4 and 8. The diurnal range in temperature is commonly about 1 °C in both lakes, but occasionally reaches 2 °C in Lake Nyos and 3 °C in Lake Monoun with its shallow thermocline and lower light transparency.

Diurnal variations in specific conductance are near the detection limit, but changes in dissolved O_2 and CO_2 can be large during daylight hours as photosynthesis proceeds. The three CO_2 values for surface water at Lake Monoun in May 1998 (from right to left in Fig. 7b) were measured at one-hour intervals beginning at 09:45 on a morning with full sun and no wind. The progressive decline in CO_2 over two hours is significant in comparison to the seasonal variability.

3.6 Chemocline Evolution

The chemocline represents the plane of greatest resistance to vertical mixing in the lakes, and its depth constrains the total amount of gas that may accumulate in bottom waters. Thus an understanding of the controls on chemocline depth and its evolution are important for the process of controlled degassing and the cycle of gas buildup and release in the lakes. The mixing of bottom water up to the surface during the gas releases disrupted pre-existing chemoclines in both Lake Nyos and Monoun. After the events, the chemocline redeveloped, deepening and strengthening in both lakes during the years after the gas releases (e.g., Kusakabe et al. 2008).

In Nyos, this redevelopment began soon after the 21 August 1986 gas release. Water samples collected just two weeks later in early September show the largest gradient in TDS between 2.6 and 5.4 m depth (Tuttle et al. 1987; Kling et al. 1987), and by October a sharp chemocline had developed at 7 m depth (Kanari 1989). By December of 1988 the chemocline had deepened to 30 m (Kusakabe et al. 2008), and it reached 47 m depth by November 1993 and remained near this depth for many years (Kling et al. 2005). In Lake Monoun a similar deepening occurred from a chemocline depth of 8 m in October 1986 to 17 m in 1993 and to 23 m in 1999 (Kusakabe et al. 2008). Profiles of conductivity between 1999 and 2003 suggest only a slight deepening ($\sim$1 m) over that time period (Kling et al. 2005).

The specific conductance of surface water in both lakes as a function of time is shown in Fig. 10, as is the range in specific conductance of the main inflows based on rainy season and dry season samples at each lake. One pre-release surface sample at Lake Nyos was collected in 1985 (Kling et al. 1987a), and it shows that specific conductance increased during the gas release by more than a factor of five and remained at this high level for several months. The overlying water became more dilute in

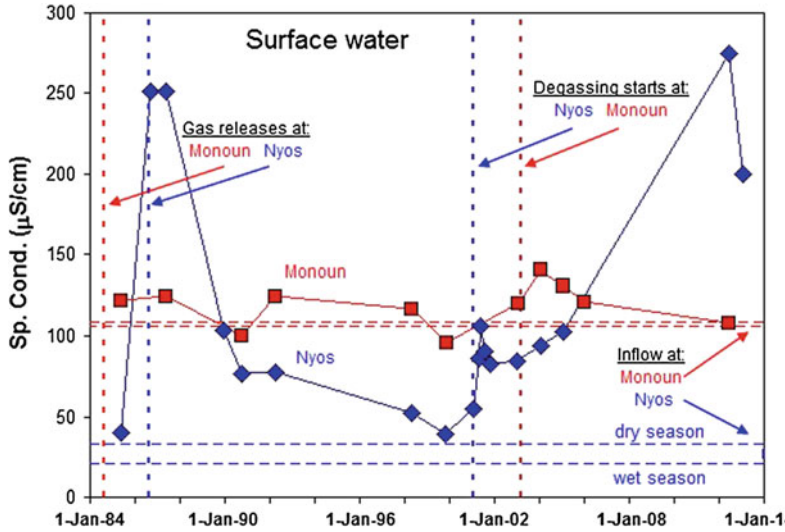

Fig. 10 Specific conductance of surface water through time at Lake Nyos (*blue diamonds*) and Lake Monoun (*red squares*). *Dashed horizontal lines* show the specific conductance range in the main inflows, based on rainy and dry season samples (highest in dry season). *Dashed vertical lines* show timing of gas releases and of initial pipe installation

subsequent years as the chemocline deepened, and prior to the start of degassing the surface waters were similar to the pre-release value. The specific conductance of surface water has always been slightly higher than in the inflow stream, and the difference is more significant considering that the inflow stream is more dilute at high flow during the rainy season. This effect probably reflects some bottom water mixing across the chemocline both before and after the gas release. High-conductivity water input to the deepest levels of the lake (e.g., Kusakabe 2015) would require some throughput to the surface unless a matching level of seepage occurred below the chemocline.

At Lake Monoun, the specific conductance of surface water prior to the start of degassing was always near to that of the inflow. This likely reflects the greater impact of the Panke River on the relatively small lake. Specific conductance was probably elevated for a brief period following the gas release, but that period had passed before the first measurement of specific conductance ten months later (Kling 1987a). In summary, the CTD profiles, the time course of conductivity (Kling et al. 2005), and the time series of specific conductance in surface water all indicate that chemocline depth and the chemistry of the mixolimnion had stabilized in both lakes prior to the onset of degassing. One indication of this stabilization is the fact that the profiles of TDS and gas measured at Lake Nyos in January 2001 show that the temperature of surface water would have to drop to <20 °C to achieve a density great enough to sink and penetrate the chemocline. Such temperatures do not occur anywhere in our multi-year record. A similar situation applies to Lake Monoun.

A numerical model presented by Schmid et al. (2006) reproduced fairly well the chemocline deepening that was observed prior to the onset of degassing at Lake Nyos, but the predicted final chemocline depth (without degassing) of 60–70 m is deeper than the stable depth of ~50 m observed prior to degassing (Fig. 6). Either the "equilibrium" mixing depth was not reached by 2001, or one-dimensional models cannot completely account for some factors that might influence chemocline depth, such as bathymetry effects and the depth distribution of groundwater inflows and outflows.

Groundwater inflow and outflow are known to be important to the water budget at Lake Nyos (Tuttle et al. 1992; Evans et al. 1994). Such flows may affect chemocline depth by altering the

density gradient in the lake. For example, the density gradient is strengthened by addition of CO_2 and high-TDS water beneath the chemocline or by addition of dilute water above the chemocline, and surface stirring processes may not be able to mix water as deeply against the stronger gradient, and the chemocline would rise. Similarly, outflow of gas-rich, dense water from 60 m depth could deepen the chemocline, but outflow of dilute water from 40 m depth would not. However, groundwater inflow and seepage are unlikely to influence chemocline depth at Lake Monoun where the surrounding terrain is relatively flat and there is only a small gradient in groundwater head. In terms of bathymetry, both lakes have a surface area that is much larger than the diameter of the main crater containing the gassy water. The lip of the main crater is at ~40 m depth in Lake Nyos and ~20 m depth in Lake Monoun. The submerged lip effectively reduces the fetch and thus the transfer of mixing energy from the wind to the crater area compared to the entire surface area of the lake.

The chemocline depth before the 1984 (Monoun) and 1986 (Nyos) gas releases is difficult to predict. In this monograph, Kusakabe (2015) proposes that the pre-release chemoclines in both lakes were very deep, near 55 m in Lake Monoun and 110 m in Lake Nyos. On the basis of depths of mixing recorded in other tropical lakes (Kling 1988) it is unlikely that surface mixing would help to establish a chemocline at such great depths. However, it is possible that chemoclines could form at any depth depending on the vertical distribution of inputs of dense, gas-charged groundwater, and that a gradient zone would exist above a deep chemocline up to the depth of typical seasonal mixing such as observed at 50–60 m depth in Lake Nyos.

3.7 Effects of Degassing

The intent of installing pipes is to remove the gas from these lakes, but the pipes actually function as circulators that bring bottom water to the lake surface where the gas can escape to the atmosphere. Complete degassing of a lake requires that all of the gas-rich water below the chemocline be brought up and discharged onto the lake surface. The stability of stratification must be maintained throughout the degassing process in order to keep the remaining gas trapped in solution and prevent a spontaneous release. Initial concerns that the density stratification in the lake would be destroyed by (1) the sinking of degassed but still salt-laden and dense water released at the surface from the pipes, (2) the lateral flow of water to the pipe intake creating sheer and turbulence, or (3) density currents formed by cooling of the pipe during exsolution of gas, all proved groundless. Several modeling studies concluded that disruption of lake stability from sinking of dense water released at the surface was unlikely (McCord and Schladow 1998; Kusakabe et al. 2000), and temperature monitoring near the pipe intake during the initial tests of degassing at Lake Monoun in 1992 (Halbwachs et al. 2004) showed no evidence that the second and third processes occurred. In fact, during degassing there was remarkable preservation of water column structure (Halbwachs et al. 2004; Kling et al. 2005; Kusakabe et al. 2008). Entire water layers have been removed sequentially as overlying layers have lowered, analogous to the removal of cards from the bottom of a deck.

The main effects of degassing on the upper water column are (1) changes in thermal structure, (2) a redistribution of salts from bottom to surface waters and a deepening of the chemocline in each lake, (3) increases in dissolved nutrients (especially N and P) from bottom waters, which stimulated algal growth and oxygen generation, (4) consumption of oxygen in surface waters due to the oxidation of reduced iron brought from depth to the surface, and (5) a reduction in light penetration. As expected, the specific conductance of surface water in both lakes increased with the onset of degassing (Fig. 10). The effect is less pronounced at Lake Monoun and quickly diminished with time because of greater flushing and dilution from the Panke River compared to the inlet stream of Lake Nyos. In contrast, the specific conductance of surface water at Lake Nyos has remained elevated over time, in part due to the installation of

two more degassing pipes in 2010. The surface water conductivity reached a peak in June 2012 of ~280 μS/cm, higher than the values just after the gas release in 1986 (Fig. 10), and then decreased to ~200 μS/cm in January 2013.

3.7.1 Changes in Thermal Structure

The main changes in thermal structure of both lakes during the first 1–3 years of degassing were noticed near the depths of the upper chemoclines. The upper water column temperatures are dominated by seasonal and annual changes in climate (Figs. 4 and 8). Independent of these natural variations, at Nyos the water temperatures at the 60 and 80 m thermistor depths, around the 23 °C isotherm, started to decrease ~1 year after degassing started in early 2001 (Fig. 4; Kling et al. 2005). Cooling at 60 m began in April 2002 and at 80 m in September 2002, and temperatures decreased by ~0.2 °C at both depths by early 2004 (Fig. 4). Because TDS at these depths did not change initially, and only gradually decreased over time (Kling et al. 2005; see discussion below), Schmid et al. (2004) proposed that double-diffusive convection observed at these depths in 2002 was responsible for the cooling.

At Lake Monoun similar decreases in water temperatures at the 45 and 55 m thermistor depths occurred within ~1 month of the start of degassing in early 2003 and continued through 2004 (Fig. 8; Kling et al. 2005). Surface water temperatures down to 25 m were slightly cooler in 2003 and 2004 compared to prior years, and deeper mixing of these cooler waters may have contributed to the declining temperatures at 45 and 55 m (Fig. 8). However, in the case of Monoun and as discussed in detail in the next section, deep-water removal from the degassing pipe was likely the main cause of chemocline lowering resulting in cooling temperatures at mid-depth.

3.7.2 TDS Redistribution and Chemocline Deepening

During the degassing operation deepening of the chemocline occurred in both lakes by a combination of processes. First, the chemocline is lowered as water beneath it is piped to the surface. Second, increases in surface water conductivity reduce the density gradient across the chemocline and allow for deeper mixing. For example, in Lake Nyos average surface water conductivity increased from 61 μS/cm in January 2001 to 87 μS/cm in January 2004, during which time the chemocline was lowered by ~13 m (Kling et al. 2005). Because the deep chemocline around 180 m depth in Lake Nyos was only lowered by 3–4 m during this same time period (Halbwachs et al. 2004; Kling et al. 2005), most of the drop in the upper chemocline must have been due to deeper mixing. Despite the combined effects of double diffusive convection and increased TDS in surface water to weaken the chemocline, it remained above 60 m depth until after January 2004 (Kling et al. 2005) indicating that the lower water column was still strongly stratified and stable during the degassing.

In Lake Monoun, measurements in 2004 showed that the inflowing Panke River (106.5 μS/cm) and the pipe discharge (~2,300 μS/cm) mixed to form surface water with a specific conductance of 140.4 μS/cm in the main crater near the pipe platform. Surface-water values in the neighboring middle basin and in the shallow western arm of the lake were similar, 139.0 and 138.8 μS/cm, respectively, showing uniform horizontal mixing across the lake surface. From the start of degassing in January 2003 until January 2004 the main chemoclines at 25 and 55 m were each lowered by ~7 m (Kling et al. 2005). The fact that both chemoclines were lowered the same amount indicates that chemocline subsidence was caused more by deep-water removal than by enhanced mixing and erosion at the surface. In early 2003 the depth of surface mixing clearly reached the 25 m thermistor (Fig. 8). As 2003 progressed and especially into early 2004, the temperatures at 45 and 55 m depth cooled in response to deep water removal.

3.7.3 Nutrients and Oxygen

Total dissolved phosphorus (TDP) concentrations in January of 2005 were less than 0.1 μM in the surface waters of Nyos and Monoun, but

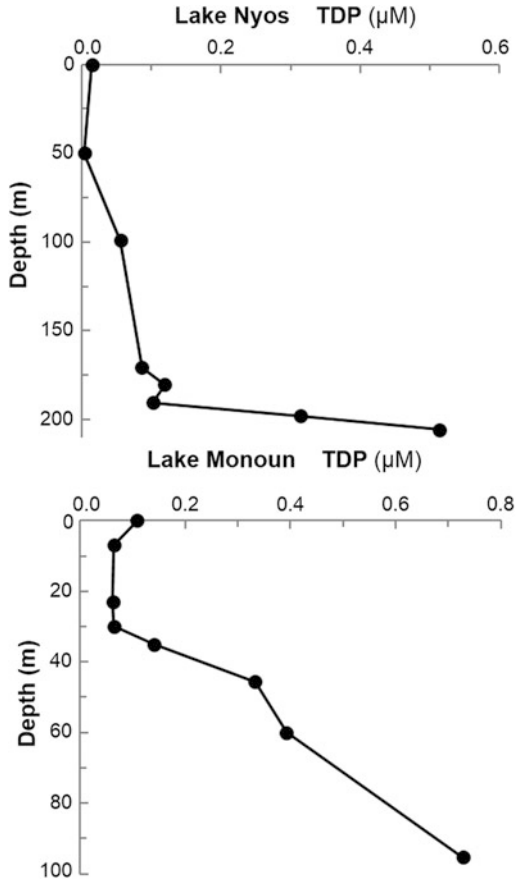

Fig. 11 TDP concentrations in Lakes Nyos and Monoun in January 2005

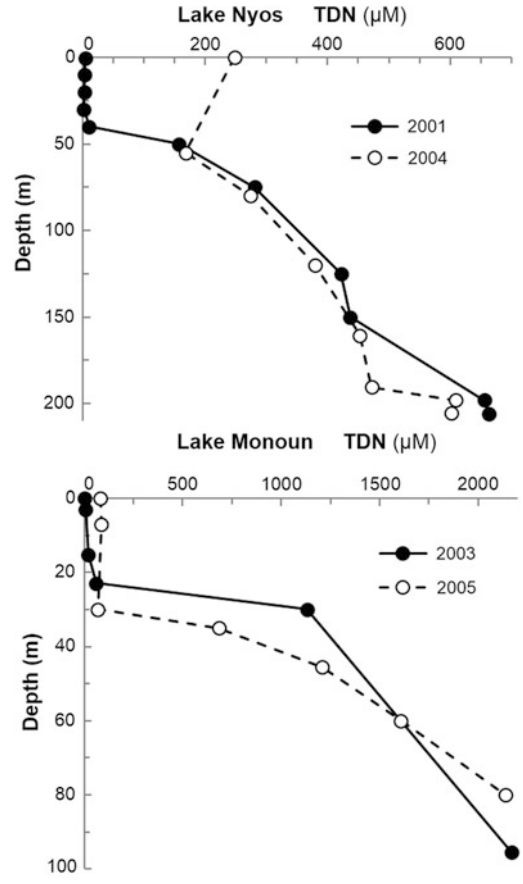

Fig. 12 TDN concentrations in Lake Nyos in January 2001 and January 2004 and Lake Monoun in January 2003 and January 2005

were at least 10-fold greater near lake bottom (Fig. 11). Differences in surface and bottom water concentrations of total dissolved nitrogen (TDN) were also striking, and pumping of nutrient-rich bottom water to the surface during degassing increased TDN in surface waters over time (Fig. 12). For example, in Lake Monoun in January 2003 before degassing, the average TDN concentration in surface waters (0–7 m) was 21 μM, and one year after degassing started the average concentration increased to 85 μM. In Lake Nyos prior to degassing in January 2001 the average TDN concentration in surface waters was 4 μM (0–40 m) and in 2004 it had increased to 208 μM (Fig. 12).

These increases in surface-water dissolved N and P concentrations would be expected to increase phytoplankton growth rates and increase the production of dissolved oxygen. The dissolved O_2 concentrations are a net of production and consumption, and the degassing pipes also brought water with high dissolved ferrous iron to the surface. The Fe(II) rapidly oxidizes at surface conditions to form reddish hydroxy-oxide precipitates, and the oxidation process consumes oxygen according to:

$$Fe^{2+} + 1/4O_2 + H^+ = Fe^{3+} + 1/2H_2O$$
$$Fe^{3+} + 3H_2O = Fe(OH)_3 + 3H^+$$

where each mole of O_2 consumed can produce 8 H^+, converting 8 HCO_3^- to 8 $CO_{2\ (aq)}$ + 8 H_2O.

At Lake Nyos in October 2001, after degassing had started, dissolved O_2 in surface water was the highest ever measured at the lake, at

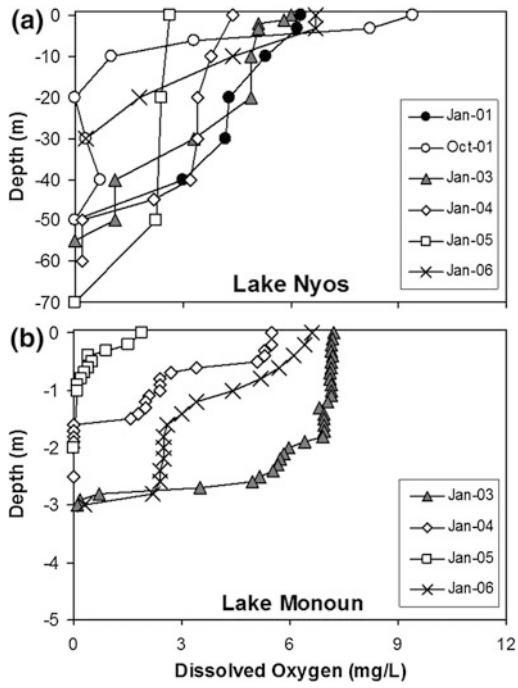

Fig. 13 Dissolved oxygen for different depths and dates after the start of degassing. **a** In January 2001 at Lake Nyos. **b** In January 2003 at Lake Monoun

times exceeding 150 % of saturation (Fig. 13). We interpret this high O_2 concentration to result from photosynthetic production that was stimulated by increased dissolved nutrients brought to the surface from the degassing pipe. At this time the surface water had turned a greenish color from an algal bloom. Dissolved oxygen concentrations dropped quickly with depth however, reaching a low value at just 10 m. Such a sharp drop was abnormal compared to pre-degassing profiles (e.g., Fig. 5). In addition, although we have no post-degassing data on phytoplankton biomass, profiles in both Nyos and Monoun indicate that chlorophyll *a* and total particulate carbon concentrations were highest in the near-surface waters (Fig. 14). Particulate C produced at the surface settled through the water column and concentrations often increased again at depth approaching the pycnocline, but there was little chlorophyll content at depth (Fig. 14). In addition, particulate C:N molar ratios in both Nyos and Monoun in surface waters were similar to ratios expected in phytoplankton (mean C: N = 8.6 ± 3.5 in Nyos and 11.7 ± 3.5 S.D. in Monoun; expected value of 8.3, Sterner et al. 2008). Thus we assume that the phytoplankton bloom responsible for the high surface O_2 buildup was limited to the very upper water column, and the rapid decline in oxygen with depth was likely due to respiration of the organic matter produced by the algal bloom. Overall, the lake contained less total O_2 on this date than ever before.

Oxygen profiles for January sampling from successive years can be compared without considering seasonal effects. In general the profiles are similar to the January 2001 profile, obtained just prior to degassing, and indicate that the overall effect of degassing on lake productivity (as estimated by the oxygen-change method) was fairly small. The situation at Lake Monoun was much different. All profiles measured after the start of degassing show greatly reduced O_2 relative to the January 2003 profile, collected just prior to degassing (Fig. 13b). The 2005 profile shows O_2 dropping to low levels within the upper 0.5 m of the water column. Bottom water in Lake Monoun is richer in ferrous iron, relative to Lake Nyos, and oxidation of this iron was apparently a major factor in the large reduction in dissolved O_2.

3.7.4 Light Penetration

Pumping of bottom water to the surface decreased water clarity and light penetration in both lakes. This decrease was due to a combination of increased iron hydroxide floc, increased dissolved organic carbon concentrations, and likely increases in algal biomass due to nutrient additions to surface waters. The average Secchi depth in Lake Nyos prior to degassing from 1989–2001 was 4.09 m and has been reduced to an average of 1.73 m since degassing began (Table 1). Within the period of degassing the light penetration has tended to decrease, in part due to the addition of two more degassing pipes in 2010. The shallowest Secchi depths recorded in Nyos are 0.21 m in June 2012 and 0.34 m in January 2013. The highest light extinction coefficient (K) measured in Nyos prior to degassing

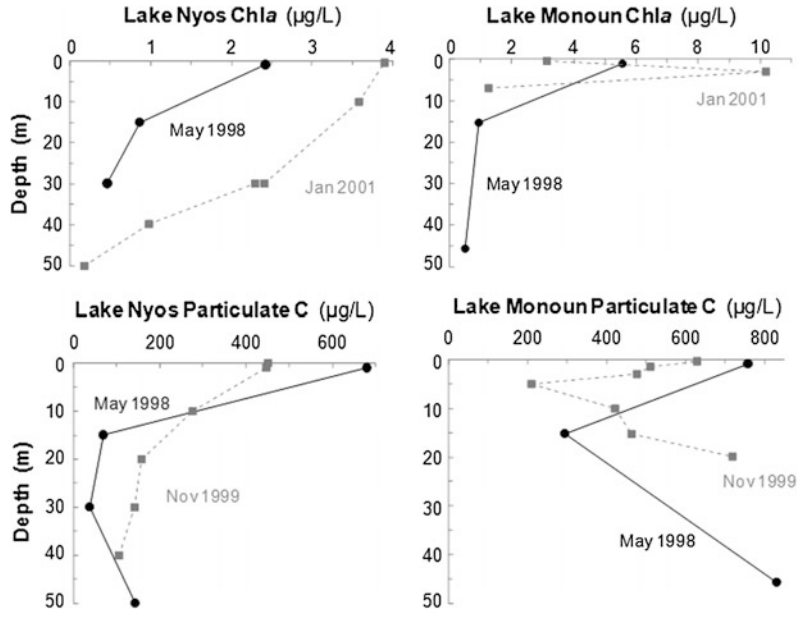

Fig. 14 Chlorophyll *a* (*top*) and particulate carbon concentrations (*bottom*) in Lakes Nyos and Monoun in May 1998, November 1999, and January 2001

Table 1 Changes in Secchi depths (m) in Lakes Nyos and Monoun prior to, during, and after degassing

Lake Monoun Secchi depth (m)			
Pre-degassing		*During degassing*	*Post degassing*
Dec 1989–Jan 2003		*Jan 2005-Jan 2006*	*Jun 2012–Jan 2013*
Mean	1.49	0.41	1.37
SD	0.26	0.17	0.29
Range	0.90–1.85	0.27–0.70	1.16–1.57
N	10	5	2
Lake Nyos Secchi depth (m)			
Pre-degassing		*During degassing*	
Dec 1989-Jan 2001		*Jan 2001–Jan 2013*	
Mean	4.09	1.73	
SD	1.27	1.16	
Range	2.90–6.20	0.21–3.64	
N	8	9	

SD is the standard deviation of the mean, range gives the minimum and maximum values, and *N* is the number of unique sampling dates or locations

was 0.33 m^{-1} in December 1989, and the lowest is 0.73 m^{-1} in January 2005 during the degassing (no measurements available after that time). In Lake Monoun the water transparency has also decreased from a mean Secchi depth of 1.49 m before degassing to 0.41 m during the piping operations. However, after the degassing operation ceased in late 2008, the Secchi depth increased to 1.57 m in June 2012 and 1.16 in January 2013. The light extinction coefficient was 1.23 m^{-1} prior to and 5.23 m^{-1} during the degassing.

Dissolved organic carbon (DOC) is often the most important light-absorbing component in lake water. Bottom water concentrations of DOC are high in Lakes Monoun (5,200 µM at 95.4 m

depth in January 2003) and Nyos (3,400 μM at 205.5 m depth in January 2001). In Monoun the mean DOC value in 0–15 m water was 240 μM and 320 μM in January 2001 and January 2003, respectively. Surface water concentrations increased to 460 μM in the upper 7 m of Monoun in January 2004 one year after degassing started. In Lake Nyos, the DOC concentration was 60 μM in surface waters (mean of 0–40 m), and after degassing started the concentrations in the upper mixing layer (mean of 0–50 m) increased to 80 μM in January 2003 and to 210 μM in January 2004. Thus at least part of the decrease in water transparency in these lakes results from colored DOC being brought to the surface during degassing.

3.8 After Degassing Completion

At the end of the degassing process, gas-rich high-TDS water will occupy only the bottom few meters of the lake. The entire overlying water column will likely consist of a nearly homogeneous mixture of degassed water from depth and the original surface water, modified by inflows and outflows. Modeling indicates that this thick layer could mix every year or every few years down to within a few meters of the lake bottom (Schmid et al. 2006), and this would serve to flush some gas from the lake and prevent a gas buildup. Without any pipes in place however, the inflowing gassy water would likely begin to refill the main crater and raise the chemocline depth over time, but how rapidly this occurs and how much gas is ultimately stored in the lake is linked in part to the equilibrium position and strength of the chemocline. The design and urgency of future mitigation efforts would in part depend on this information.

It is unclear whether either lake would return to the same water column structure and gas content that existed prior to the gas releases. There is some evidence that the rate of gas input to bottom waters of Lake Nyos changes over time (Evans et al. 1993; Kusakabe et al. 2000) and it is conceivable that pre-release lake structure and gas content reflected inflow rates much different from those observed during the relatively short period of observation.

3.9 Global Implications

Although the gas releases from Lakes Nyos and Monoun helped fuel a global study of volcanic crater lakes, the two Cameroonian lakes ~100 km apart appear to be unique. They constitute the "bursting bicarbonate volcanic lake" category in the classification scheme of Pasternack and Varekamp (1997).

Several attributes of Lakes Nyos and Monoun likely contribute to the dangerous gas buildup, and may explain why more lakes are not gas-charged (Kling 1987b; Kling et al. 2005). The lakes must be deep enough to contain gas at high pressures, and large enough to hold substantial amounts of CO_2 in solution. The lakes must be strongly stratified and maintain that stratification for multiple years to allow the buildup of gases. Such strong stratification is aided in Nyos and Monoun by submerged steep-walled main craters that inhibit penetration of wind-driven mixing and by the small seasonal cooling of the tropical climate that may limit deep convective mixing. Finally, there must be a strong local source of CO_2, which occurs in Cameroon in the form of low-temperature, CO_2-charged soda springs that are widespread along the Cameroon Volcanic Line (Tanyileke et al. 1996).

Still, the global absence of known analogues among crater lakes remains a bit curious because CO_2 sources are common in many volcanic regions, CO_2 of presumed magmatic origin is now known to vent into many crater lakes (e.g., Mazot and Taran 2009), and a recent estimate of the global emission of CO_2 through volcanic lakes is surprisingly large (Pérez et al. 2011). In addition, many crater lakes are deep and steep-walled. However, meromictic lakes are relatively rare, even in the tropics, and the unlikely combination of a deep meromictic lake and a gas source feeding directly into the bottom waters, is probably the main factor limiting the occurrence of lethal gas-charged lakes worldwide.

The characteristics of the CO_2 source are also important for the scarcity of Nyos and Monoun analogues. For example, if the inflowing CO_2 is in gas phase, then bubbles can create plumes that convey the gas to the lake surface where it is lost to the atmosphere, especially if the gas inflow is located in a relatively shallow part of the lake. Examples include Lake Quilotoa (Aguilera et al. 2000), the Laacher See (Aeschbach-Hertig et al. 1996), and Ruapehu (Christenson 1994). At low inflow rates, gas bubbles could dissolve completely and raise the CO_2 concentration of bottom water, but the correspondingly small density increase might then be insufficient to prevent mixing and flushing of the CO_2 to the atmosphere during seasonal cooling and lake turnover. A gas supply rate sufficient to enhance perennial density stratification, but not large enough to produce a buoyant plume, may be an unlikely occurrence.

The bubble plume is avoided if the CO_2 gas first dissolves in groundwater, which then flows into and gradually fills up the deeper part of the lake over time, the process thought to occur at Lakes Nyos and Monoun (Kling et al. 1987; Nojiri et al. 1993). Buoyancy remains an issue because CO_2-rich groundwaters that are substantially warmer and thus less dense than ambient lake water should rise in the lake to their point of neutral buoyancy and would not become trapped near lake bottom. Nyos-type lakes require the coincidence of a strong magmatic gas source that is also depleted in heat. However, the density increase in cold groundwater that absorbs CO_2 will also reduce its tendency to move upward into a lake basin. External hydraulic head can drive the upflow of CO_2-rich water into Lakes Nyos and Monoun, but not at summit crater lakes or lakes that are perched above the local water table.

The source strength of CO_2, heat from magma, and other factors like water table depth or climate can change over time, and conditions may be right for gas buildup in a crater lake for only a small window of its existence. Several Italian crater lakes are located in areas of strong CO_2 emission (Chiodini and Frondini 2001), and magmatic gas components have been found in lake waters (Carapezza et al. 2008; Caracausi et al. 2009; Cabassi et al. 2013). The lakes currently pose no hazard of a catastrophic release, but unusual events that might have involved gas releases are recorded in ancient Roman writings (Cioni et al. 2003). Results of a multi-year study of Lake Albano indicate that an anomalous spike in CO_2 input accompanied a seismic swarm in 1989 (Chiodini et al. 2012). Carapezza et al. (2008) suggest that a prolonged warm spell without winter-time mixing might allow initiation of stable stratification and gas buildup in this lake, the reverse of a proposed weakening of stratification in Cameroonian lakes due to an unusually cool period in the mid-1980s (Kling 1987b).

Lake Kivu in eastern Africa is often considered the closest analogue to Nyos and Monoun even though it does not occupy a volcanic crater. This huge rift lake certainly contains a vast quantity of dissolved CO_2 in stratified water layers at depth, and the associated hazard was recognized soon after the disasters in Cameroon (Kling et al. 1987; Tuttle et al. 1990; Tietze 1992). The lake consists of several basins, of which Kabuno Bay appears to present the greatest hazard of an uncontrolled gas release (Tassi et al. 2009). Methane constitutes a larger fraction of the dissolved gas, relative to the Cameroonian lakes, and will become a greater factor in the hazard if it continues to increase at present rates (Pasche et al. 2011). Experience at Lakes Nyos and Monoun continues to inform plans to remove the gas from Lake Kivu, especially the procedure for safe discharge of the degassed water (Kling et al. 2006; Hirslund 2012).

Gas releases have been invoked at other lakes, such as in Lake Voui based on an observed color change (Bani et al. 2009), in Lake Quilotoa based on historical records (Aguilera et al. 2000), and in Lake Kivu based on unusual sediment layers (Haberyan and Hecky 1987). A confirmed gas release from a crater lake atop Mount Chiginagak volcano in 2005 differed in many respects from the Cameroonian disasters but showed some

similarities. As elaborated by Schaefer et al. (2008), this 105 m deep meltwater lake formed quickly in response to renewed upflow of heat and gas into a snow- and ice-filled crater. Water eventually burst through a cavity in the glacial ice impounding the upper ~45 m of the lake and cascaded down the steep slopes into the valley below. The rapid depressurization and agitation released sulfur-rich gas, likely as an aerosol, which flowed as a cloud down the valley.

The Chiginagak region is remote and uninhabited, but vegetation bleached and killed by the acidic cloud preserved a record of its 29 km^2 area and height (Schaefer et al. 2008), which indicate a volume comparable to the Lake Nyos gas cloud (~0.2–1 km^3). The huge size of the cloud suggests that the drop in lake level may have induced additional gas to exsolve from the lake water remaining in the crater or even vent rapidly from the underlying volcanic conduit. This latter process is a concern at other crater lakes where rim failure could cause a large drop in lake level and thus pressure on underlying gas stores, even if the lake itself does not contain large amounts of gas. At Lake Nyos where a fragile dam impounds the upper 40 m of water (Lockwood et al. 1988), a significant amount of gas may be contained in the sediments and would remain a concern after the lake itself is degassed (Freeth 1994). Thus the current effort to strengthen the natural dam to prevent flooding (Aka and Yokoyama 2013) has a double benefit.

4 Conclusions

The water columns of Lakes Nyos and Monoun evolved over time into structures consisting of dilute surface waters and high-TDS bottom waters separated by a sharp chemocline. The strength of this boundary allowed climate, inflows and outflows, and biological processes to completely control short-term and seasonal patterns in surface waters; impacts from the underlying bottom waters were almost imperceptible. Piping of bottom water onto the lake surface during degassing has caused complex but predictable changes to surface waters and has led to expected deepening and in Monoun weakening of the chemocline. The likely evolution of lake structure after degassing is somewhat uncertain but could trend back toward dangerous gas accumulation.

Nyos-type lakes can form only when several conditions are simultaneously met: great depth, large volume, CO_2 input, and persistent stratification to allow CO_2 buildup beneath one or more chemoclines. Nyos-type lakes are rare because most lakes apparently fail to meet one of these necessary conditions. Over geologic time however, it seems unlikely that Lakes Nyos and Monoun would be the only crater lakes to cycle through gas buildup and massive release. As conditions change, perhaps even subtly, deep crater lakes could turn into Nyos-type lakes and become dangerous (see Pasternack and Varekamp 1997; Aguilera et al. 2000). Thus some program of occasional monitoring is worthwhile, especially for those lakes in regions of volcanic activity or known to have magmatic CO_2 inputs.

Gas release hazards can exist at lakes much different from Lakes Nyos, Monoun, or even Kivu. For example, crater lakes at active volcanoes might be warm and acidic but have such a strong input of gas that buildup can outpace convective flushing to the atmosphere, especially if salts or suspended solids contribute to any density gradient in the water column. Although gas pressure might never become sufficient to drive a Nyos-type overturn and violent gas burst, depressurization of lake water through crater breaching could allow dangerous amounts of gas, including sulfur gases, to be rapidly released.

Acknowledgments Funding and support came from U.S.AID-OFDA grant AOTA-00-99-00223-00, the Cameroonian Government (MINRESI-IRGM), the U.S. and Japanese Embassies in Cameroon, the U.S. Geological Survey, the Japanese SATREPS project of JST-JICA, and the Japan Society for the Promotion of Science. We thank Karen Riseng, Ibrahim Issa, Aka Festus, Nia Paul, Chris Wallace, Mark Brahce, Amanda Field, Sara Fortin, Susanna Michael, Mark Huebner, and Keisuke Nagao for field or laboratory help. Aka Festus, Minoru Kusakabe, and an anonymous reviewer provided helpful comments on the draft.

References

Aeschbach-Hertig W, Kipfer R, Hofer M, Imboden DM, Wieler R, Signer P (1996) Quantification of gas fluxes from the subcontinental mantle: the example of Laacher See, a maar lake in Germany. Geochim Cosmochim Acta 60:31–41

Aguilera E, Chiodini G, Cioni R, Guidi M, Marini L, Raco B (2000) Water chemistry of Lake Quilotoa (Ecuador) and assessment of natural hazards. J Volcanol Geotherm Res 97:271–285

Aka FT, Yokoyama T (2013) Current status of the debate about the age of Lake Nyos dam (Cameroon) and its bearing on potential flood hazards. Nat Hazards 65:875–885

Aka FT, Yokoyama T, Kusakabe M, Nakamura E, Tanyileke G, Ateba B, Ngako V, Nnange J, Hell J (2008) U-series dating of Lake Nyos maar basalts, Cameroon (West Africa): implications for potential hazards on the Lake Nyos dam. J Volcanol Geotherm Res 176:212–224

Bani P, Oppenheimer C, Varekamp JC, Quinou T, Lardy M, Carn S (2009) Remarkable geochemical changes and degassing at Voui crater lake, Ambae volcano, Vanuatu. J Volcano Geotherm Res 188:347–357

Cabassi J, Tassi F, Vaselli O, Fiebig J, Nocentini M, Capecchiacci F, Rouwet D, Bicocchi G (2013) Biogeochemical processes involving dissolved CO_2 and CH_4 at Albano, Averno, and Monticchio meromictic volcanic lakes (Central–Southern Italy). Bull Volcanol 75:683. doi:10.1007/s00445-012-0683-0

Caracausi A, Mario Nuccio P, Favara R, Nicolosi M, Paternoster M (2009) Gas hazard assessment at the Monticchio crater lakes of Mt. Vulture, a volcano in Southern Italy. Terra Nova 21:83–87

Carapezza ML, Lelli M, Tarchini L (2008) Geochemistry of the Albano and Nemi crater lakes in the volcanic district of Alban Hills (Rome, Italy). J Volcanol Geotherm Res 178:297–304

Christenson BW (1994) Convection and stratification in Ruapehu Crater Lake, New Zealand: implications for Lake Nyos-type gas release eruptions. Geochem J 28:185–197

Chiodini G, Frondini F (2001) Carbon dioxide degassing from the Albani Hills volcanic region, Central Italy. Chem Geol 177:67–83

Chiodini G, Tassi F, Caliro S, Chiarabba C, Vaselli O, Rouwet D (2012) Time-dependent CO_2 variations in Lake Albano associated with seismic activity. Bull Volcanol 74:861–871

Cioni R, Guidi M, Raco B, Marini L, Gambardella B (2003) Water chemistry of Lake Albano (Italy). J Volcanol Geotherm Res 120:179–195

Evans WC, Kling GW, Tuttle ML, Tanyileke G, White LD (1993) Gas buildup in Lake Nyos Cameroon: the recharge process and its consequences. Appl Geochem 8:207–221

Evans WC, White LD, Tuttle ML, Kling GW, Tanyileke G, Michel RL (1994) Six years of change at Lake Nyos, Cameroon, yield clues to the past and cautions for the future. Geochem J 28:139–162

Freeth SJ (1992) The Lake Nyos gas disaster. In: Freeth SJ, Ofoegbu CO, Onuoha KM (eds) Natural hazards in West and Central Africa. Vieweg, Braunschweig, pp 63–82

Freeth SJ (1994) Lake Nyos: can another disaster be avoided. Geochem J 28:163–172

Green J (1972) Ecological studies on crater lakes in West Cameroon. the zooplankton of Barombi Mbo, Mboandong, Lake Kotto and Lake Soden. J Zool Lond 166:283–301

Green J, Corbet SA, Betney E (1974) Ecological studies on crater lakes in West Cameroon. Debundsha Lake. J Zool Lond 173:199–223

Haberyan KA, Hecky RE (1987) The late Pleistocene and Holocene stratigraphy and paleolimnology of lakes Kivu and Tanganyika. Palaeogeogr Palaeoclimatol Palaeoecol 61:169–197

Halbwachs M, Sabroux J-C, Grangeon J, Kayser G, Tochon-Danguy J-C, Felix A, Béard J-C, Villevieille A, Vitter G, Richon P, Wüest A, Hell J (2004) Degassing the "Killer Lakes" Nyos and Monoun, Cameroon. EOS 85(281):285

Hassert K (1912) Seenstudien in Nord-Kamerun. Z Ges Erdk Berl 1912:7–41,135-144,203-216

Hirslund F (2012) An additional challenge of Lake Kivu in Central Africa—upward movement of the chemoclines. J Limnol 71:45–60

Kanari S (1989) An inference on the process of gas outburst from Lake Nyos, Cameroon. J Volcanol Geotherm Res 39:135–149

Kantha LH, Freeth SJ (1996) A numerical simulation of the evolution of temperature and stratification in Lake Nyos since the 1986 disaster. J Geophys Res 101 (B4):8187–8203

Karl DM, Tilbrook D (1994) Production and transport of methane in oceanic particulate organic matter. Nature 368:732–734

Kling GW (1987a) The comparative limnology of lakes in Cameroon, West Africa. PhD thesis, Duke University

Kling GW (1987b) Seasonal mixing and catastrophic degassing in tropical lakes, Cameroon, West Africa. Science 237:1022–1024

Kling GW (1988) Comparative transparency, depth of mixing, and stability of stratification in lakes of Cameroon, West Africa. Limnol Oceanogr 33:27–40

Kling GW, Clark MA, Compton HR, Devine JD, Evans WC, Humphrey AM, Koenigsberg EJ, Lockwood JP, Tuttle ML, Wagner GN (1987) The 1986 Lake Nyos gas disaster in Cameroon, West Africa. Science 236:169–175

Kling GW, Tuttle ML, Evans WC (1989) The evolution of thermal structure and water chemistry in Lake Nyos. J Volcanol Geotherm Res 39:151–165

Kling GW, Evans WC, Tuttle ML, Tanyileke G (1994) Degassing of Lake Nyos. Nature 368:405–406

Kling GW, Evans WC, Tanyileke G, Kusakabe M, Ohba T, Yoshida Y, Hell JV (2005) Degassing Lakes Nyos and Monoun—defusing certain disaster. Proc National Acad Sci 102:14185–14190

Kling, GW, MacIntyre S, Steenfelt J, Hirslund F (2006) Lake Kivu gas extraction: report on lake stability. Report produced for the World Bank and the Government of Rwanda, p 104

Kusakabe M (2015) Evolution of CO_2 content in Lakes Nyos and Monoun, and sub-lacustrine CO_2-recharge system at Lake Nyos as envisaged from C/^{3}He ratios and noble gas signatures. doi:10.1007/978-3-642-36833-2

Kusakabe M, Tanyileke GZ, McCord SA, Schladow SG (2000) Recent pH and CO_2 profiles at Lakes Nyos and Monoun, Cameroon: implications for the degassing strategy and its numerical simulation. J Volcanol Geotherm Res 97:241–260

Kusakabe M, Ohba T, Issa Yoshida Y, Satake H, Ohizumi T, Evans WC, Tanyileke G, Kling GW (2008) Evolution of CO_2 in Lakes Monoun and Nyos, Cameroon, before and during controlled degassing. Geochem J 42:93–118

Le Guern F, Sigvaldason GE (1989) The Lake Nyos event and natural CO_2 degassing I. J Volcanol Geotherm Res 39:95–275

Le Guern F, Sigvaldason GE (1990) The Lake Nyos event and natural CO_2 degassing II. J Volcanol Geotherm Res 42:307–401

Lockwood JP, Rubin M (1989) Origin and age of the Lake Nyos maar, Cameroon. J Volcanol Geotherm Res 39:117–124

Lockwood JP, Costa JE, Tuttle ML, Nni J, Tebor SG (1988) The potential for catastrophic dam failure at Lake Nyos maar, Cameroon. Bull Volcanol 50:340–349

Mazot A, Taran Y (2009) CO_2 flux from the volcanic lake of El Chichón (Mexico). Geofis Int 48:73–83

McCord SA, Schladow SG (1998) Numerical simulations of degassing scenarios for CO_2-rich Lake Nyos, Cameroon. J Geophys Res 103(B6), 12355−12364

Nojiri Y, Kusakabe M, Hirabayashi J, Sato H, Sano Y, Shinohara H, Njine T, Tanyileke G (1990) Gas discharge at Lake Nyos. Nature 346:322–323

Nojiri Y, Kusakabe M, Tietze K, Hirabayashi J, Sato H, Sano Y, Shinohara H, Njine T, Tanyileke G (1993) An estimate of CO2 flux in Lake Nyos, Cameroon. Limnol Oceanogr 38:739–752

Pasche N, Schmid M, Vazquez F, Schubert CJ, Wüest A, Kessler JD, Pack MA, Reeburgh WS, Bürgmann H (2011) Methane sources and sinks in Lake Kivu. J Geophys Res 116:G03006. doi:10.1029/2011JG001690

Pasternack GB, Varekamp JC (1997) Volcanic lake systematics I; physical constraints. Bull Volcanol 58:528–538

Pérez NM, Hernández PA, Padilla G, Nolasco D, Barrancos J, Melían G, Padrón E, Dionis S, Calvo D, Rodríguez F, Notsu K, Mori T, Kusakabe M, Carmencita Arpa M, Reniva P, Ibarra M (2011) Global CO_2 emission from volcanic lakes. Geology 39:235–238

Schmid M, Lorke A, Wüest A, Halbwachs M, Tanyileke G (2003) Development and sensitivity analysis of a model for assessing stratification and safety of Lake Nyos during artificial degassing. Ocean Dyn 53:288–301

Schmid M, Lorke A, Dinkel C, Tanyileke G, Wüest A (2004) Double-diffusive convection in Lake Nyos, Cameroon. Deep-Sea Res I 51:1097–1111

Schmid M, Halbwachs M, Wüest A (2006) Simulation of CO_2 concentrations, temperature, and stratification in Lake Nyos for different degassing scenarios. Geochem Geophys Geosyst 7:Q06019. doi:10.1029/2005GC001164

Schaefer JR, Scott WE, Evans WC, Jorgenson J, McGimsey RG, Wang B (2008) The 2005 catastrophic acid crater lake drainage, lahar, and acidic aerosol formation at Mount Chiginagak volcano, Alaska, USA: field observations and preliminary water and vegetation chemistry results. Geochem Geophys Geosyst 9:Q07018. doi:10.1029/2007GC001900

Sigurdsson H, Devine JD, Tchoua FM, Presser TS, Pringle MKW, Evans WC (1987) Origin of the lethal gas burst from Lake Monoun, Cameroon. J Volcanol Geotherm Res 31:1–16

Sterner RW, Andersen T, Elser JJ, Hessen DO, Hood JM, McCauley E, Urabe J (2008) Scale-dependent carbon: nitrogen:phosphorus seston stoichiometry in marine and freshwaters. Limnol Oceanogr 53:1169–1180

Tanyileke GZ, Kusakabe M, Evans WC (1996) Chemical and isotopic characteristics of fluids along the Cameroon volcanic line, Cameroon. J Afr Earth Sci 22:433–441

Tassi F, Vaselli O, Tedesco D, Montegrossi G, Darrah T, Cuoco E, Mapendano MY, Poreda R, Delgado Huertas A (2009) Water and gas chemistry at Lake Kivu (DRC): geochemical evidence of vertical and horizontal heterogeneities in a multibasin structure. Geochem Geophys Geosyst 10:Q02005. doi:10.1029/2008GC002191

Teutsch N, Schmid M, Müller B, Halliday AN, Bürgmann H, Wehrli B (2009) Large iron isotope fractionation at the oxic-anoxic boundary in Lake Nyos. Earth Planet Sci Lett 285:52–60

Tietze K (1987) Results of the German-Cameroon research expedition to Lake Nyos (Cameroon) October/November 1986. Interim-Report, Bundesanstalt für Geowissenschaften und Rohstoffe Archive no. 100470, 84p

Tietze K (1992) Cyclic gas bursts: are they a 'usual' feature of Lake Nyos and other gas-bearing lakes? In: Freeth SJ, Ofoegbu CO, Onuoha KM (eds) Natural hazards in West and Central Africa. Vieweg, Braunschweig, pp 97–107

Tuttle ML, Clark MA, Compton HR, Devine JD, Evans WC, Humphrey AM, Kling GW, Koenigsberg EJ, Lockwood JP, Wagner GN (1987) The 21 August

1986 Lake Nyos gas disaster, Cameroon. US Geol Surv Open-File Rep 87–97:58

Tuttle ML, Briggs PH, Evans WC, Kling GW, Lockwood JP (1992) Influence of mafic minerals on water chemistry and water column stability of Lake Nyos, Cameroon. In: Kharaka Y, Maest A (eds.) Water-rock interaction, Vol. 1, A.A. Balkema, Rotterdam, pp 449–452

Tuttle ML, Lockwood JP, Evans WC (1990) Natural hazards associated with Lake Kivu and adjoining areas of the Birunga Volcanic Field, Rwanda and Zaire, Central Africa. US Geol Surv Open-File Rep 90–691:47

Wilhelm E, Battino R, Wilcock RJ (1977) Low-pressure solubility of gases in liquid water. Chem Rev 77:219–262

Evolution of CO_2 Content in Lakes Nyos and Monoun, and Sub-lacustrine CO_2-Recharge System at Lake Nyos as Envisaged from $CO_2/^3He$ Ratios and Noble Gas Signatures

Minoru Kusakabe

Abstract

Lakes Nyos and Monoun in Cameroon are known as "killer lakes" because they killed ~1,800 people in the mid-80s after a gas explosion or limnic eruption, a sudden release of carbon dioxide accumulated in deep waters. This event attracted the interest of the international scientific community, not only for the sake of disaster mitigation but also for its volcanological significance. Follow-up studies indicated that the CO_2 concentration in deep water increased at an alarming rate at both lakes, and that a future gas explosion was likely to occur. To avoid recurrence of the explosion, artificial degassing of the lakes was set up using pipes based on the gas self-lift principle. This chapter compiles the results of the geochemical monitoring of the two lakes for the last 25 years. Pre- and syn-degassing evolution of CO_2 profiles was translated into the temporal changes of CO_2 content in the lakes, and thus estimate CO_2 recharge and removal rates. Degassing went on smoothly, and more than 90 % of the maximum amount of CO_2 was removed from Lake Monoun by 2011, reaching safe levels. Since the lake has lost its gas self-lift capability, degassing will no longer continue. At Lake Nyos, degassing is on-going and 33 % of the maximum amount of CO_2 has now been removed. A model of spontaneous gas exsolution is proposed. This idea is based on the temporal variation of CO_2 profiles at Lake Monoun between 1986 and 2003. During this period the profiles evolved rather steadily, i.e., the deep CO_2-rich layer thickened while its CO_2 concentration remained constant. This suggests that the recharge fluid coming from depth had a CO_2 concentration similar to that of the bottom water, and that it pushed the deepest water upward, resulting in CO_2 saturation at the top of the CO_2-rich layer, which led to the 1984 limnic eruption. A similar situation

M. Kusakabe (✉)
Department of Biology and Environmental Chemistry, University of Toyama, 3190 Gofuku, Toyama-shi 980-8555, Japan
e-mail: kusakabe@sci.u-toyama.ac.jp

D. Rouwet et al. (eds.), *Volcanic Lakes*, Advances in Volcanology,
DOI 10.1007/978-3-642-36833-2_19,
© Springer-Verlag Berlin Heidelberg 2015

was observed at Lake Nyos just before the degassing operation started in 2001, i.e., the deep, CO_2-rich layer thickened while its CO_2 concentration remained unchanged at about 350 mmol/kg, which is still far below CO_2 saturation. In this lake, pre-degassing deep water had low $CO_2/^3He$ ratios ($\sim 0.5 \times 10^{10}$), whereas the recharge fluid was characterized by relatively high $CO_2/^3He$ ratios ($\sim 1.7 \times 10^{10}$). This suggests that the behavior of CO_2 and He in the lake was decoupled. The recharge fluid is likely produced by mixing of magmatic fluids, which are characterized by relatively high $^3He/^4He$, $^{40}Ar/^{36}Ar$, $^{20}Ne/^{22}Ne$ and $^{21}Ne/^{22}Ne$ ratios, with groundwater having air isotopic signatures.

Keywords

Lake Nyos · Lake Monoun · Evolution of CO_2 content · Spontaneous exsolution of gas · Artificial degassing · CO_2–He decoupling · Sub-lacustrine fluid reservoir

1 Introduction

Volatiles in the deep interior of the Earth are brought to the surface by volcanic activity. In terms of the present-day global carbon cycle, CO_2 discharge from subaerial volcanism and passive CO_2 discharge from the flanks or craters of volcanoes are the major non-anthropogenic contributors to atmospheric CO_2 (e.g., Kerrick 2001; Gerlach 2011). Lakes Nyos and Monoun in Cameroon, West Africa, are volcanic lakes situated along the Cameroon Volcanic Line (Fig. 1), and are typical sites of passive CO_2 degassing. Although currently no active volcanism is found near the lakes, magmatic CO_2 is continuously discharged from depth, trapped and accumulated in deep waters of the lakes (e.g., Kusakabe and Sano 1992). Excessive accumulation of such CO_2 in these lakes resulted in sudden outbursts of dissolved gases in mid-80 s, inducing the gas disasters that claimed altogether close to 1,800 lives (Sigurdsson et al. 1987; Sigvaldason 1989). A term "limnic eruption" was coined by J.-C. Sabroux to describe the gas outburst from a lake (Halbwachs et al. 2004), and will be used in this article.

After the 1986 Lake Nyos gas disaster, a UNESCO-sponsored international conference on the disaster was held in Yaounde in 1987, and the initial phase of scientific studies on the geological, geochemical, limnological, medical, and socio-anthropological aspects of the Nyos and Monoun events was presented. Some of them were published in the special issue of Journal of Volcanology and Geothermal Research, edited by Sigvaldason (1989). Follow-up studies of Lakes Nyos and Monoun clearly indicated that CO_2 content in the lakes was increasing at an alarming rate, which is unusual as a geological phenomenon (Evans et al. 1993; Kusakabe et al. 2000, 2008; Kling et al. 2005). It was then considered that recurrence of a limnic eruption in the near future was highly probable, and artificial removal of dissolved gases from the lakes was strongly recommended. To achieve this goal, the Nyos-Monoun Degassing Program (NMDP) was set up in 1996.

The present chapter describes (1) the pre-degassing chemical evolution of the lakes, (2) the rate of CO_2 recharge to the lakes, (3) the syn-degassing chemical evolution of the lake water, including the latest situation of dissolved CO_2

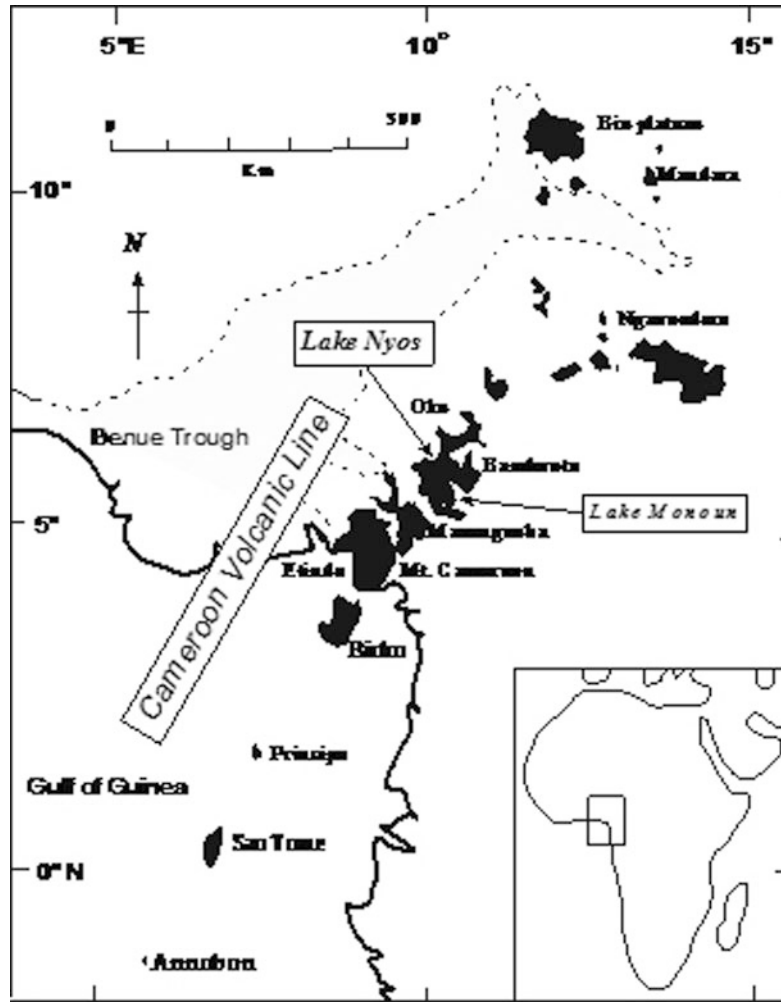

Fig. 1 A map showing locations of Lakes Nyos and Monoun along the Cameroon volcanic line (CVL). CVL is a 1,600 km long, SW-NE trending chain of Cenozoic volcanic centers starting from Annobon Island in the Atlantic Ocean to Biu Plateau-Mandara Mountains in northern Cameroon. The map was revised from Aka et al. (2004)

and future prospect, (4) discussions on the sub-lacustrine CO_2-recharge system as envisaged by $C/^3He$ ratios and noble gas signatures. A new Japanese-Cameroonian project for mitigation of a future gas disaster in Cameroon will be briefly mentioned.

2 A Brief History of the Degassing Operation

The ways of controlled removal of gas from the lakes were discussed among the scientists working on the lakes (e.g., Freeth et al. 1990). The idea to use a degassing pipe, based on the gas self-lift principle, was proposed soon after the Nyos event (Tietze 1987; Freeth et al. 1990), because it was believed that degassing by this method would not cause unfavorable instability of the lakes' water column. After careful physical examination of degassing procedures, experimental degassing at Lake Monoun (Halbwachs et al. 1993) and Lake Nyos (Halbwachs and Sabroux 2001) was carried out. On this basis, a permanent degassing apparatus was installed at Lake Nyos in 2001, and at Lake Monoun in 2003 under NMDP, funded by the U.S. Office of Foreign Disaster Assistance (OFDA, USAID), and later by the French Embassy in Yaounde and the Cameroonian and French Governments. The technical details of the degassing systems were described in Halbwachs et al. (2004). According

to this method, deep CO_2-rich water was discharged from the mouth of the degassing pipe where the exsolved gas was released into the atmosphere. High-density polyethylene pipes with an internal diameter of 102 mm for Lake Monoun and 140 mm for Lake Nyos were used. Since the depth of Lakes Monoun and Nyos at the deepest point is 100 m and 210 m, respectively, the intake depth of the pipe was set at 73 m at Lake Monoun and 203 m at Lake Nyos (Halbwachs et al. 2004). The gas/water volume ratios of the discharged fluid were 9 and 3, and the water flow rates were 70 and 50 L/s for Lakes Nyos and Monoun, respectively. Driven by the gas self-lift principle we were able to see beautiful fountains in the remote African lakes (Fig. 2a, b). The intake depth of the Monoun pipes was deepened from 73 to 93 m (Issa, pers. commun.) in January 2006 when two additional pipes were installed (Fig. 2c). Also two degassing pipes were added at Lake Nyos (Fig. 2d) in late 2011 and early 2012 using a fund from EU to increase the degassing rate, and the water intake depth was deepened to 207–209 m, only a few meters above the lake bottom. The color of the lake surface turned red due to suspension of iron hydroxide precipitates that formed by the oxidation of Fe^{2+}-rich deep water upon contact with atmospheric oxygen. The red coloration became intense after three pipes started working in March 2012 at Lake Nyos.

The degassed water was sprayed onto the lake surface. A concern that since the degassed water was cooler, therefore denser, than the surface water due to adiabatic expansion it might resink deep enough to destabilize the water column and trigger another man-made limnic eruption was published (Freeth 1994). Numerical modeling on the behavior of such sprayed water showed that discharged deep water would not sink to the depth where CO_2 still remained undegassed, and thus destabilization of the water column would not occur (McCord and Schladow 1998; Kusakabe et al. 2000; Halbwachs and Sabroux 2001). This conclusion was supported by later observations of the lakes' chemical structure. The observations indicated that stable stratification has been maintained during the controlled degassing and that the CO_2 profiles subsided gradually without being disturbed by the degassing operation at both lakes (Kling et al. 2005; Kusakabe et al. 2008).

The controlled degassing went on successfully at both lakes. The three pipes drastically accelerated the rate of gas removal from Lake Monoun, resulting in considerable deepening of the level of gas-rich water in a short period of time as shown in Kusakabe et al. (2008) and later in this chapter. At Lake Nyos, the gas removal rate by a single pipe was too low and insufficient to reduce the gas content to a safe level within several years (Kling et al. 2005; Kusakabe et al. 2008). However, the two additional degassing pipes are expected to increase the gas removal rate and to help attain a safe level in the near future. Numerical models have been developed to simulate the conditions under which a limnic eruption can take place (Kantha and Freeth 1996; McCord and Schladow 1998; Schmid et al. 2003, 2006). Such conditions need to be checked by detailed regular field observation to elaborate the models.

3 Chemical Evolution and Rate of CO_2 Recharge of Lakes Nyos and Monoun Prior to Controlled-Degassing

The first paper on the 1984 Lake Monoun gas disaster (Sigurdsson et al. 1987) reported high concentration of dissolved CO_2, HCO_3^- and Fe^{2+} in the lake, and concluded that the gas accumulation was attributed to long-term exhalation of volcanic CO_2 from vents within the crater. This paper had a lot of implications for the cause(s) of the 1986 Lake Nyos gas disaster and could be a guideline for the Lake Nyos disaster studies, but unfortunately it was published just *after* the Lake Nyos limnic eruption, resulting in some chaotic situation on the interpretation of the cause(s) of the limnic eruption at the International Conference on the Lake Nyos Gas Disaster held in Yaounde in 1987 (Sigvaldason 1989). Many scientific surveys were conducted after the Nyos event, some of which reported chemical and isotopic compositions of Lake Nyos water

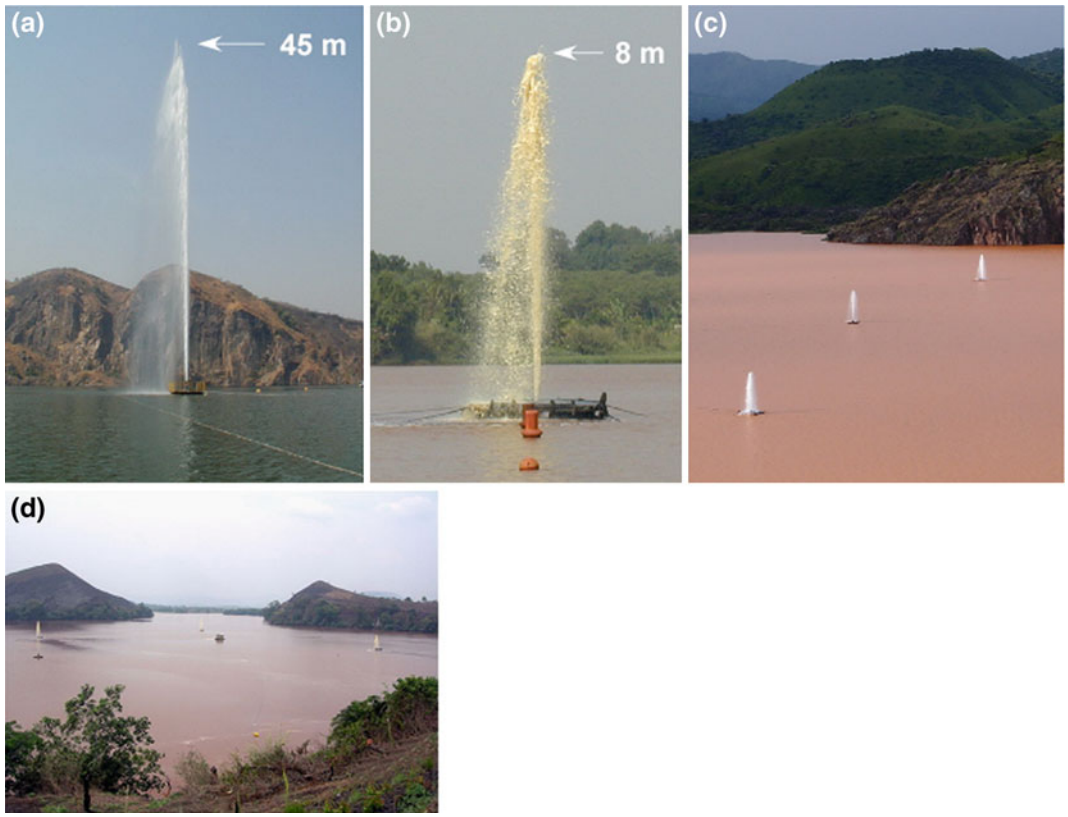

Fig. 2 Photographs showing degassing operation at Lakes Nyos and Monoun. **a** A 45 m high fountain at Lake Nyos in February 2001 (*photo* by Y. Yoshida). **b** A 8 m high fountain at Lake Monoun in January 2001 (*photo* by Y. Yoshida). **c** 3 degassing pipes in operation at Lake Nyos in March 2012 (*photo* by M. Kusakabe). **d** 3 degassing pipes in operation at Lake Monoun, February 2006 (*photo* kindly supplied by Jean-Christophe Beard). The lakes turned red during degassing with 3 pipes

(see papers published in the special issue "The Lake Nyos event and natural CO_2 Degassing I and II" (Le Guern and Sigvaldasson eds., J Volcanol Geotherm Res vol. 39–42, 1989–1990). At the 1987 Yaounde conference, there was a sharp confrontation between a group of scientists who believed that the lake played a key role in accumulating CO_2 (limnic eruption hypothesis) and another group of scientists (e.g., Barberi et al. 1989; Tazieff 1989) who believed that the cause of the Nyos catastrophe was a volcanic eruption near the lake bottom (phreatic eruption hypothesis). This confrontation resulted in a compromise of the resolutions of the Yaounde Conference (Sigvaldason 1989). However, the follow-up studies after the disaster clearly indicated steady supply and accumulation of magmatic CO_2 in the lake, strongly favoring the limnic eruption hypothesis.

The first scientific reports on the 1986 Lake Nyos gas disaster were published by Freeth and Kay (1987), Kling et al. (1987) and Tietze (1987). Of these, Kling et al. (1987) was most comprehensive as results of the geological survey of the region, geochemistry of water and gas from the lake, and pathology of hospitalized people and victims were included. They concluded that (i) the gas released was CO_2 that had been stored in the lake's hypolimnion, (ii) the victims died of CO_2 asphyxiation, (iii) CO_2 was derived from magmatic sources, and (iv) there was no direct volcanic activity involved. Kusakabe et al. (1989) reached similar conclusions on the basis of water chemistry and carbon

and noble gas isotopic compositions of gases dissolved in Lakes Nyos and Monoun. They noted that H_2S concentration in the released gas should have been far below the lethal level. The same authors also reported the first petrochemical data of ejecta around Lakes Nyos and Monoun, which indicated that the lavas were transitional to slightly alkaline in nature.

The temporal variation of the chemical structure of Lakes Nyos and Monoun since the limnic eruption at both lakes was reported by Kusakabe et al. (2008). This paper presented a most comprehensive data set of chemical composition, conductivity, temperature, pH and CO_2 profiles measured almost every 2–3 years since 1986 until 2006, allowing evaluation of the evolution of CO_2 in the lakes before and during controlled degassing. The chemical structure of the lakes is best represented by a conductivity profile (Fig. 3). Both lakes have a similar chemical structure which represents four layers. At Lake Monoun layer I is the shallowest, well-mixed, low conductivity water. A sharp chemocline separates layer I and layer II at 23 m (January 2003 situation), the latter extending down to 51 m depth, where the second chemocline develops. A well-mixed layer III continues down to ca. 85 m. Below this depth, conductivity increases steadily toward the bottom (layer IV) (Fig. 3a). Lake Nyos has basically the same structure as Lake Monoun: layer I is the shallowest, well mixed, low conductivity water. A sharp chemocline at about 50 m depth separates layer I and layer II that extends down to about 180 m depth. A lower chemocline develops around this depth, below which a well-mixed layer III continues down to ~203 m. Below this depth, conductivity sharply increases toward the bottom (layer IV) (Fig. 3b).

Pre-degassing temperature variation at Lake Monoun (from October 1986 to January 2003) and at Lake Nyos (from November 1986 to January 2001) are shown in Fig. 4a, b, respectively. I refer to Kusakabe et al. (2008) for the 1986 and 1988 data source. The temperature profiles at Lake Monoun show minima at 5-21 m (layer I), followed by (1) an increasing trend to about 23 °C down to the lower chemocline at 50–63 m depths (layer II), (2) constant values down to around 90 m (layer III),and (3) a second increase to >24 °C toward the bottom (layer IV). It is worth noting that the temperature of the layer III water increased significantly between 1986 and 1999, and at the same time the layer III (thermally homogeneous zone) thickened forming a "shoulder" at a depth of 51 m. The thickening suggests that warmer water was added to layers III and IV, and the profiles were pushed

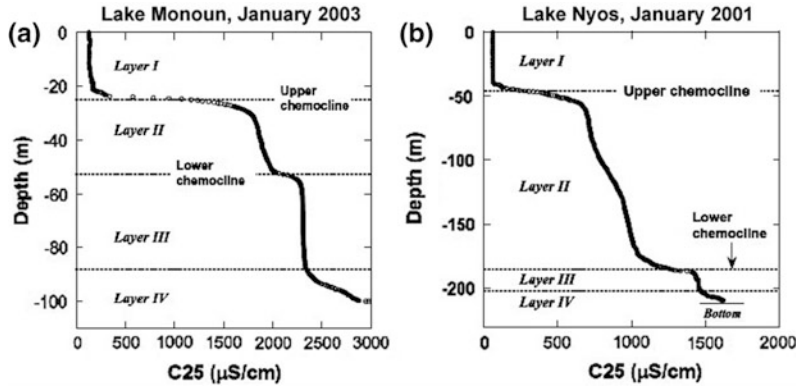

Fig. 3 Conductivity profiles at Lake Monoun in January 2003 (**a**) and Lake Nyos in January 2001 (**b**). Chemical structure of the lakes, basically similar to each other, can be divided into 4 layers. Layers I, II and III are bordered by the *upper* and *lower* chemoclines. Layer IV is the deepest water characterized by increasing conductivity toward the *bottom*. In the diagrams C25 stands for conductivity normalized to values at 25 °C. The figures were reproduced from Figs. 1 and 7 of Kusakabe et al. (2008)

upward. A simple heat balance indicates that the heat accumulated in layers III and IV during 15 years (from October 1986 to January 2003) is 7.8×10^{12} J or a heat supply rate of 5.1×10^{11} J/year (~0.02 MW) on the average. Incremental upward movement of the lower chemocline (Fig. 4a) indicates addition of water to layer III and IV, most likely from the bottom. If 4.1×10^8 tons of water having temperature of 27 °C was added, it would account for the heat accumulation during the period. Diffusive and conductive heat loss to layer II and above was not taken into consideration in this simple heat balance calculation, thus giving a minimum heat supply. Note that the rate of heat and water supply to layer III and IV initially appears high judging from the change in the temperature profiles (Fig. 4a).

Similar to Lake Monoun, the temperature of Lake Nyos bottom water kept increasing after the limnic eruption (Fig. 4b), indicating heat input to the lake. The heat input to layer III and IV was reported to decrease from an initially high value of 0.93 MW (August 1986–May 1987) through 0.43 MW (November 1986–December 1988, Nojiri et al. 1993) to 0.32 MW (May 1987-September 1990, Evans et al. 1993).

Pre-degassing conductivity variation over time at Lakes Monoun and Nyos is given in Fig. 5. As previously stated, Lake Monoun water is divided into four layers separated by chemoclines (Fig. 5a). The conductivity profile has a "shoulder" just below the lower chemocline between layers II and III. As shown in Fig. 5a, the shoulder got shallower and sharper and layer III expanded with time and with increasing conductivity. Almost vertical conductivity profiles in layer III indicate well-mixing in the layer. Rise of the shoulder indicates addition of recharge water from the bottom, which is consistent with the changes in temperature (Fig. 4a). By combining the conductivity profiles from October 1986 to January 2003 (15 years) with the bathymetry used in Kling et al. (2005) we calculated an overall increase of 2.7×10^3 tons of Total Dissolved Solids (TDS) in layers III and IV. This is translated into an average input rate of 1.7×10^2 tons/year of TDS. The sharp conductivity rise toward the bottom in layer IV may be related to dissolution and reduction of particles containing ferric compounds to release Fe^{2+} and HCO_3^- when contacted with sediments that are rich in organic material. Concentration of Fe^{2+}, HCO_3^- and NH_4^+ increased significantly with depth only in layer IV whereas the other ions such as Na^+, K^+, Mg^{2+}, Ca^{2+} showed steady increase with depth.

At Lake Nyos, shallow water in November 1986 had a higher conductivity (Fig. 5b), indicating that deep, saline water that was brought to the surface during the limnic eruption still remained. The upper chemocline in October 1986 deepened with time down to 47 m in 1993 and 50 m in 2001. Conductivity profiles at mid-depths (70–160 m) stayed almost unchanged for 15 years after the eruption, suggesting that

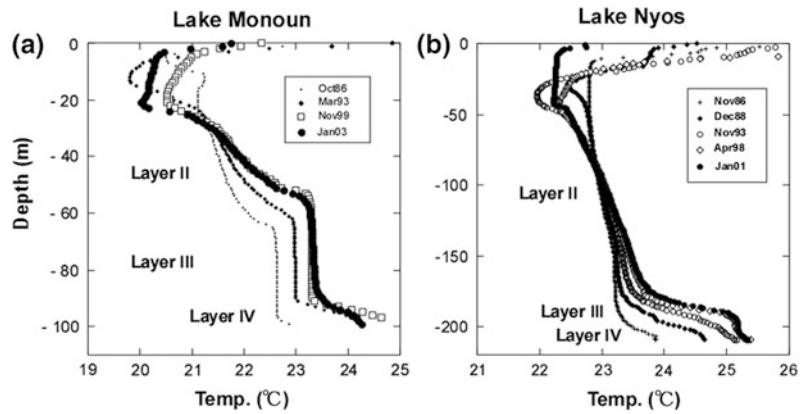

Fig. 4 Variation with time in pre-degassing temperature profiles at Lakes Monoun (**a**) and Nyos (**b**). The figures were reproduced from Figs. 4a and 9a of Kusakabe et al. (2008)

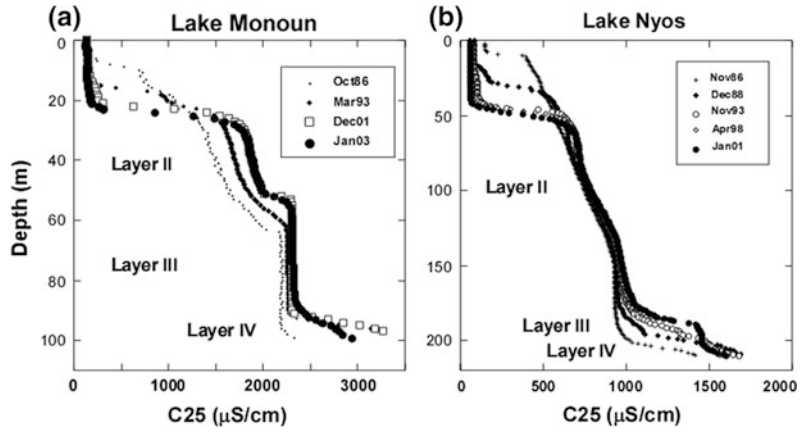

Fig. 5 Variation with time in pre-degassing conductivity profiles at Lakes Monoun (**a**) and Nyos (**b**). The figures were reproduced from Figs. 4b and 9b of Kusakabe et al. (2008)

transport of dissolved chemical species through layer II was limited. The conductivity of layer III and IV water (170–210 m) increased notably with time (Fig. 5b). In January 2001 the conductivity profile between 185 m and 202 m became steep, with the associated reduction of earlier high conductivity in layer IV, indicating initiation of mixing in the deepest zone. This tendency had started in 1998, although the 1998 profile hides behind the 2001 profile in Fig. 5b. From the depth of 205 m to the bottom, conductivity increased sharply towards a maximum. This trend is the same as observed at bottom water of Lake Monoun. The pre-degassing increase of the conductivity in layer III and IV from November 1986 to January 2001 (14 years) corresponds to an increase of 7,700 tons of TDS, with the average input being 540 ton/yr. Initially, the input rate was relatively high (more than double of the average rate) and afterwards decreased as shown by the close spacing of the conductivity profiles (Fig. 5b). This temporal trend was similar to that of water temperature.

Pre-degassing $CO_{2(aq)}$ variations with time at Lakes Monoun and Nyos are shown in Fig. 6. The determination of $CO_{2(aq)}$ concentration was made in two ways: (1) the syringe method, and (2) the pH method (Kusakabe et al. 2000). At Lake Monoun (Fig. 6a), there were no measured data in 1986. The 1986 profile, estimated from the later CO_2-conductivity relationships, shows the lowest $CO_{2(aq)}$ concentrations in the deep water, around 130 mmol/kg in layers III and IV and the CO_2 shoulder at a depth of ~63 m. The $CO_{2(aq)}$ profiles changed with time, especially from 1986 to 1993. The thickness of layers III and IV expanded with time, supporting the hypothesis that the CO_2-rich recharge fluid was added from the bottom. In January 2003, the CO_2 shoulder at 58 m depth (157 mmol/kg) was very close to the CO_2 saturation concentration at 50 m depth (Duan and Sun 2003). Considering that the rate at which the shoulder rose is about 1 m/year, saturation at 58 m depth could be reached in less than 10 years. Formation of CO_2 bubbles, able to induce a limnic eruption, could have occurred in a very near future after 2003 at Lake Monoun if no degassing operation had been undertaken.

Figure 6b shows the temporal variation of $CO_{2(aq)}$ profiles between November 1986 and January 2001 at Lake Nyos. General features of Fig. 6b are summarized as: (1) $CO_{2(aq)}$ concentration was lowest in early days, (2) there was little change with time in mid-depths (~50–150 m), (3) the greatest change took place at a depth of >170 m where $CO_{2(aq)}$ concentration at a given depth increased significantly with time, and (4) $CO_{2(aq)}$ concentration at the bottom-most water is almost constant, near 350 mmol/kg since 1999. The change in the bottom waters is likely caused by the gradual addition of recharge fluid having a CO_2 concentration of 350 mmol/kg.

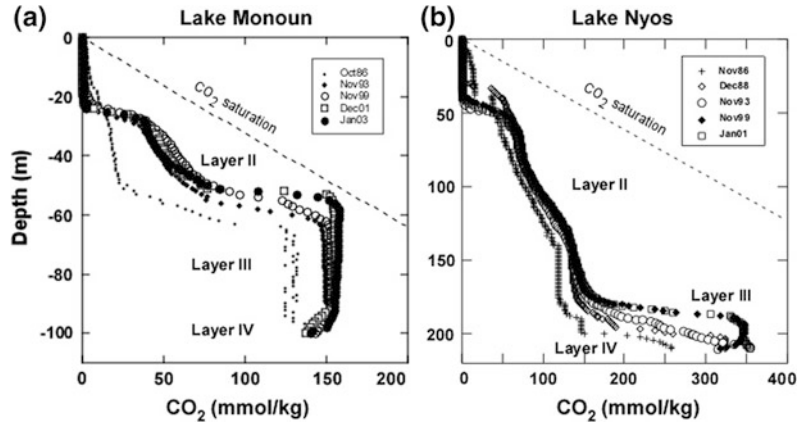

Fig. 6 Variation with time in pre-degassing $CO_{2(aq)}$ profiles over time at Lakes Monoun (**a**) and Nyos (**b**). The figures were reproduced from Fig. 4d and Fig. 9d of Kusakabe et al. (2008)

The CO_2 content of the lake was calculated by integrating the $CO_{2(aq)}$ profiles over the water column below layer II using the bathymetry used in Kling et al. (2005), assuming that the horizontal distribution of CO_2 is uniform, and that CO_2 loss through the upper chemocline was negligible. The CO_2 accumulation rate can be regarded as the CO_2 recharge rate. Accumulation of CO_2 in layer II and in deeper layers is tabulated in Table 1 for Lakes Monoun and Nyos. Considering that there were no measured CO_2 data for Lake Monoun in 1986 and that the $CO_{2(aq)}$ profile in October 1986 was estimated in an indirect way (Kusakabe et al. 2008), the overall rate of CO_2 accumulation below the surface chemocline was calculated using the 1993–2003 profiles. The change in CO_2 content below layer II in the main basin for the pre-degassing period of 1993 to 2003 was 77 Mmol, with a CO_2 recharge rate of 8.4 Mmol/year. Almost the same recharge rate of 8.2 Mmol/yr was reported by Kling et al. (2005) using their own data obtained between 1992 and 2003 for Lake Monoun. At Lake Nyos the CO_2 content below layer II steadily increased until January 2001, when permanent degassing started. The increase in the CO_2 content can be translated into the CO_2 recharge rate, which was 0.12 Gmol CO_2/year between November 1986 and January 2001 (Table 1. Again, this rate is in good agreement with the value of 0.13 GmolCO_2/yr given by Kling et al. (2005).

4 Evolution of CO_2 Content During Degassing and Future Prospect

The $CO_{2(aq)}$ profiles at both lakes during degassing are shown in Fig. 7. Generally speaking, degassing went smoothly, as the $CO_{2(aq)}$ profiles subsided steadily, although minor technical problems of the system happened during the early stage of degassing, resulting in a temporary cessation of degassing. The shape of the profiles did not change with ongoing degassing, showing that only bottom water and dissolved CO_2 were removed without causing any effect on the stratification of the lakes. At Lake Monoun (Fig. 7a) the highest $CO_{2(aq)}$ concentration decreased to 88 mmol/kg at the bottom and thickness of layer III was reduced to ~10 m in 2009. The highest $CO_{2(aq)}$ concentration at the bottom was further reduced to 70 mmol/kg in 2011 (Kusakabe et al. 2011), when two of the degassing pipes stopped working completely and one was issuing weak bubbly flow from its mouth. Thus, it can be said that the degassing pipes at Lake Monoun have lost their gas self-lift capability. At Lake Nyos (Fig. 7b) the $CO_{2(aq)}$ profiles subsided steadily until January 2011, resulting in very thin layer III by that time. As two more degassing pipes with a greater diameter (25.7 cm I.D.) were installed in December 2011-March 2012 (Issa, pers. commun.), the degassing

Table 1 Change with time in CO_2 content at Lakes Monoun and Nyos during the last 20 years

Date	Time after eruption (year)	Total CO_2 (giga mol)	CO_2 below layer II (giga mol)	CO_2 accumulation rate (giga-mol/yr)	CO_2 removal rate (giga-mol/yr)
Lake Monoun: pre-degassing					
October 1986	2.17	*0.38*	*0.38*	–	–
November 1993	9.25	0.53	0.53	–	–
April 1996	11.67	*0.59*	*0.59*	–	–
November 1999	15.25	0.60	0.60	–	–
December 2001	17.33	0.61	0.61	–	–
January 2003	18.42	0.61	0.61	0.0084 (1993–2003)	–
Lake Monoun: during-degassing					
January 2004	19.42	0.53	0.52	–	–
January 2005	20.42	0.42	0.42	–	–
June 2006	21.92	0.43	0.42	–	–
January 2007	22.42	0.22	0.21	–	–
December 2007	23.33	0.11	0.08	–	0.098 (2003–2007)
January 2009	24.42	0.07	0.05	–	–
January 2011	26.42	0.04	0.04	–	0.005 (2009–2011)
Lake Nyos: pre-degassing					
November 1986	0.17	*13.1*	*12.9*	–	–
December 1988	2.33	*13.3*	*13.3*	–	–
November 1993	7.25	13.6	13.6	–	–
April 1998	11.67	14.1	14.0	–	–
November 1999	13.25	14.4	14.0	–	–
January 2001	14.42	14.8	14.6	0.12 (1986–2001)	–
Lake Nyos: during-degassing					
December 2001	15.33	14.2	14.0	–	–
January 2003	16.42	13.1	13.1	–	–
January 2004	17.42	13.2	13.0	–	–
January 2005	18.42	12.3	12.6	–	–
January 2006	19.42	11.8	11.7	–	–
January 2007	20.42	*11.6*	*11.4*	–	–
January 2009	22.42	*11.2*	*11.1*	–	–
January 2011	24.42	*10.0*	*9.7*	–	0.46 (2001–2011)

Note 1 The values for October 1986 at Lake Monoun were estimated using the CO_2/C25 versus C25 relationship (Kusakabe et al. 2008)

Note 2 Italicized figures were obtained with the pH-CO_2 method

Note 3 Errors were less than 5 % of the figures accepting the assumptions involved in different analytical methods of CO_{2aq} (Kusakabe et al. 2008)

Note 4 CO_2 removal rate was calculated using the CO_2 content below layer II during the period shown in brancket

Note 5 Data after 2007 were taken from Kusakabe et al. (2011)

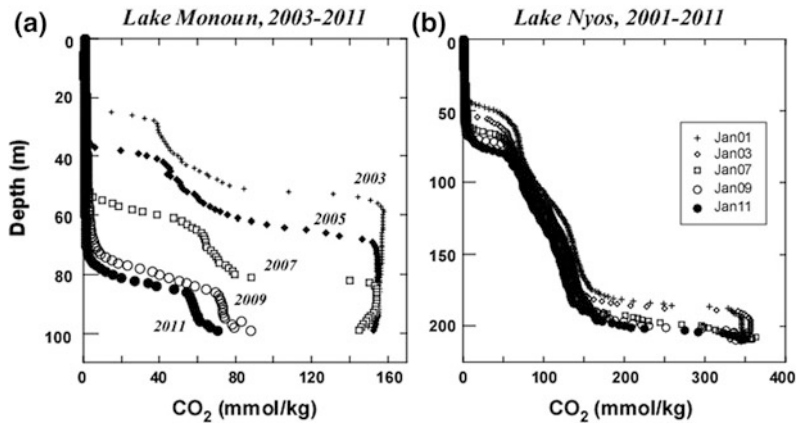

Fig. 7 **a** Temporal change of $CO_{2(aq)}$ profile during controlled degassing at Lakes Manoun (January 2003–January 2011) (**a**), and that for Lake Nyos (January 2001–January 2011) (**b**). Note that the $CO_{2(aq)}$ profile of January 2003 at Lake Monoun and that of January 2001 are shown as the last pre-degassing profiles as the starting point of degassing. The 2009 and 2011 data were taken from Kusakabe et al. (2011)

rate will be greatly enhanced. We can expect that most of the CO_2-rich bottom water will disappear from Lake Nyos in several years.

Using the $CO_{2(aq)}$ profiles and bathymetry of the lakes, the amount of $CO_{2(aq)}$ dissolved below the surface chemocline (layers II, III and IV) was calculated as a function of time since the limnic eruption at both lakes (Fig. 8). The amount of dissolved CO_2 in Lake Monoun (Fig. 8a) increased steadily with a rate of 8.4 Mmol/year before the degassing operation. It reached a maximum value of 610 Mmol in January 2003, shortly before the degassing operation started. The degassing was effective, and the amount of dissolved CO_2 kept decreasing with a mean rate of 98 Mmol/yr between January 2003 and December 2007. This rate is approximately 12 times greater than the natural recharge rate as shown by a sharp slope of Fig. 8a. The installation of two additional pipes in April 2006 accelerated the gas removal rate. In January 2009, gas self-lifting almost stopped, although very weak flow of bubbly water from one of the three pipes was still observed. In January 2011 the highest $CO_{2(aq)}$ concentration was reduced to 70 mmol/kg with the total amount of dissolved $CO_{2(aq)}$ of 37 Mmol, or only 6 % of the maximum value observed in 2003 (Kusakabe et al. 2011). It can be said that Lake Monoun has been made safe as the deep water lost its gas self-lift capability. However, tailing-off of the CO_2 content after 2008 (Fig. 8a) implies that re-buildup of CO_2 is inevitable at Lake Monoun if natural recharge of CO_2 continues with the previously estimated rate. It is imperative to continue to monitor the lakes' situation and to remove CO_2 from the bottom water in order to avoid the gas re-buildup and to make the lake constantly safe.

Evolution of CO_2 content over time since 1986 at Lake Nyos is shown in Fig. 8b. The gas removal rate by a single pipe was about four times greater than the rate of natural recharge of 0.12 Gmol/year. Currently 33 % of the maximum amount of gas has been removed. With this removal rate, however, it would take another 20 years or more to remove all the gas from the lake. Fortunately, two additional degassing pipes were installed in early 2011, using a fund from the EU. Since pipes with a greater diameter (25.7 cm) were used and the water intake depth was deepened for the additional pipes, this should greatly accelerate the rate of gas removal. We hope most of the remaining gas is removed during the next years. At Lake Nyos, as at Lake Monoun, a system to pump up CO_2-rich bottom water needs to be set up after the current degassing system has lost the gas self-lifting capability. It has been suggested that CO_2 will be

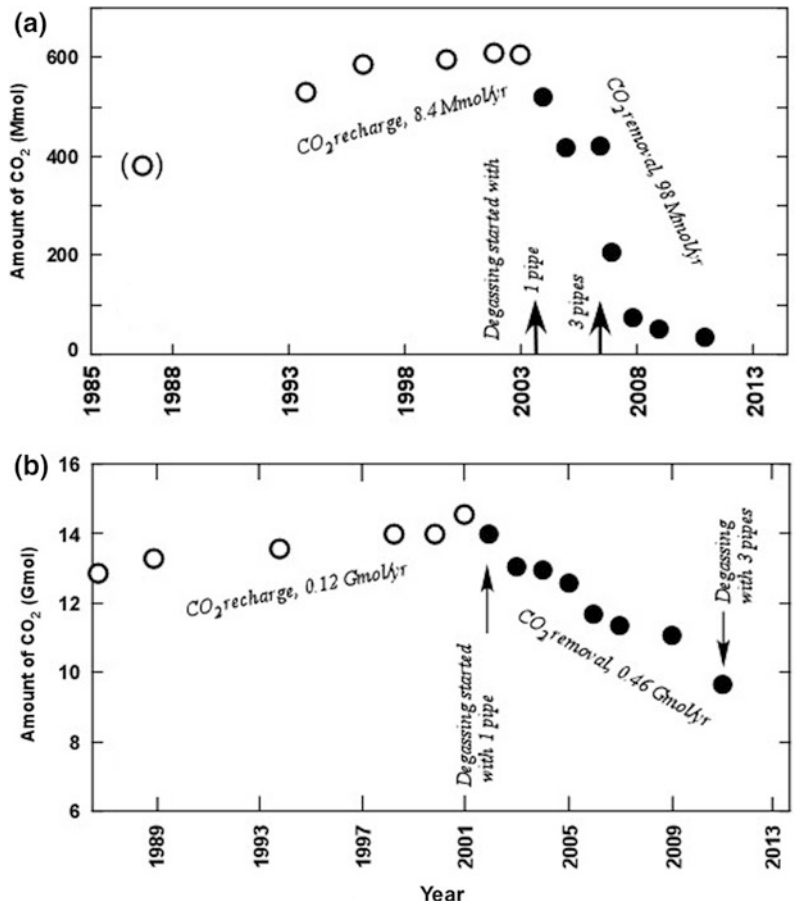

Fig. 8 Change in CO_2 content with time at Lake Monoun (**a**) and at Lake Nyos (**b**) since the limnic eruption. *Open* and *closed circles* indicate the CO_2 content before and during controlled degassing, respectively. The data point in parenthesis (Lake Monoun in 1986) was not included in calculation of the CO_2 recharge rate. The degassing slowed down after 2007 at Lake Monoun. The 2009 and 2011 data points were taken from Kusakabe et al. (2011)

continuously supplied to the lake for a long time in the future on the basis of a geochemical study on the generation of CO_2 in the Nyos mantle (Aka 2015, this volume).

5 Models and Triggers of the Limnic Eruption

Many ideas have been put forward to explain why the limnic eruption occurred. Sigurdsson et al. (1987) proposed that a landslide slumped into deep lake water, pushing up CO_2-rich water and inducing the 1984 limnic eruption at Lake Monoun. The same idea was also suggested for the 1986 Lake Nyos event (Kling et al. 1987, 1989). Tietze (1987) suggested super-saturation of dissolved CO_2 just below the shallow chemocline (~8 m depth) to be the main cause of the eruption. The strong density stratification of this layer worked as a trap for rising gases, inhibiting them from penetrating this density gap. The super-saturation led to the exsolution of gases to form a fountain. This process was self-intensified and deeper water was steadily degassed in turn. Since the water from the fountain was cooler than the surface water, it sank around the fountain, forming a cylindrical "density wall". This wall limited lake-wide exsolution of gases, leaving CO_2 dissolved in deep water (>150 m?) intact during the eruption. Assuming that Lake Nyos was isothermal and fully saturated with CO_2, Kanari (1989) presented a fluid-dynamics model to explain how the limnic eruption proceeded. In his model degassing started from the bottom but it was confined in a limited area at the surface. Circulation of the water was confined in small cells that stacked at

various depths. The stratification within the lake was little destroyed according to his model. Kanari estimated (1) the released gas volume to be 0.68 km^3 as the difference between the saturation and CO_2 profile observed in 1986 by Kusakabe et al. (1989), (2) the maximum height of the gas cloud to be 110 m, and (3) the speed of gas cloud running down the valley to be 19 m/s.

Obviously, any degassing model depends on the knowledge of pre-eruption distribution of CO_2 in the lake. Evans et al. (1994) proposed a revised model of a linear pre-eruption relationship between CO_2 and TDS at Lake Nyos on the basis of water chemistry, CTD measurements, gas analysis and tritium profiles obtained between 1987 and 1992. An almost linear relationship between tritium and TDS was interpreted to reflect the destruction of the pre-existing gradient in the mid-depth during the eruption, suggesting that CO_2 exsolved from deep water. In their model, the surface chemocline was placed at ~50 m depth, similar to the chemocline depth observed in January 2001 (14 years after the limnic eruption, and just prior to the initiation of artificial degassing (Fig. 5b). Some trigger (a combination of seasonal decline in stability, landslide and/or seiche) pushed water upward at a layer around the chemocline to the CO_2 saturation depth. Then, bubble formation followed and relatively quiet degassing continued. Local reduction in hydrostatic pressure beneath the release area created a rising column of shallow, slightly gassy water. This was followed by mixing with pre-release surface water (low TDS) to form the surface water that was observed soon after the limnic eruption. The base of the column was deepened slowly, bringing CO_2-rich, more saline deep water upward. When the base of the column reached the deeper chemocline below which CO_2 and TDS concentrations were much higher, gas release became more violent and created wave damage along the lake shore such as flattening of vegetation and passing of water over 80 m high promontory in the southern part of the lake. The duration of this violent fountaining was short (<1 min). The amount of CO_2 released was estimated at 6.3 Gmol. This scenario is consistent with the survivors' testimonies.

Giggenbach (1990) proposed that the gas release at Lake Nyos was triggered by a climatic factor. The descent of a parcel of unusually cold rain water (18.5 °C) pushed initially CO_2-rich shallow water upward. Uplift of the CO_2-rich water above saturation depth induced bubble formation which accelerated upward movement by reduction of density, leading to formation of a convecting water flow that entrained deeper, more CO_2-enriched water, and finally to the limnic eruption. Degassed less dense waters were accumulated at the surface, making deeper CO_2-rich water (>100 m) difficult to reach the surface, terminating the eruption. Thus deep water CO_2 was left almost intact. The amount of CO_2 released was estimated at 5.4 Gmol.

In contrast to the previous models for the cause of the limnic eruption, *spontaneous* exsolution of dissolved gases has been suggested by Kusakabe et al. (2008). They paid attention to the pre-degassing evolution of dissolved CO_2 at Lake Monoun (see Fig. 6a) which indicated that the $CO_{2(aq)}$ profiles evolved with time and that CO_2-rich layers below the surface chemocline thickened due to continuous recharge of CO_2-charged fluid from beneath. Note that $CO_{2(aq)}$ concentration in water below the surface chemocline (layer III) was constant at ~157 mmol/kg. In January 2003, just prior to the initiation of degassing operation, the $CO_{2(aq)}$ concentration immediately below the surface chemocline was very close to saturation. If no degassing operation was undertaken, saturation of $CO_{2(aq)}$ would have been attained at that depth, and bubble formation would have followed by additional input of the recharge fluid. Thus, at Lake Monoun another limnic eruption could have occurred *spontaneously* within several years after 2001. In other words, it is implied that no external forcing was needed to induce the limnic eruption.

The above scenario gives a clue to estimate the pre-eruptive CO_2 profile at Lake Nyos. It is conceivable that it was similar to Monoun's 2001–2003 profiles in shape (see Fig. 6a). It is interesting to note that the CO_2 profile for the deep layer of Lake Nyos (>180 m in 1999 and 2001; Fig. 6b) was developing in a way similar to

that observed at Lake Monoun. Thickness of CO_2-rich water close to the bottom kept increasing from after the 1986 eruption till 2001 due to addition of the recharge fluid from beneath. The $CO_{2(aq)}$ concentration below 195 m reached 350 mmol/kg in 1999. This concentration stayed unchanged until January 2005 down to the bottom (Kusakabe et al. 2008). This observation suggests that $CO_{2(aq)}$ concentration of the recharge fluid is constant at ~350 mmol/kg. If no degassing was made, the thickness of bottom CO_2-rich water would have kept increasing and the top level of the CO_2-rich layer could have eventually reached saturation at some shallow depth. This speculation is schematically presented in Fig. 9. In this case, the pre-eruption profile, shown as "Before 1986", has a shoulder that touches the saturation curve at a depth of ~110 m. The limnic eruption would take place spontaneously, releasing the dissolved gases to the atmosphere, to give a profile shown as "November 1986" in Fig. 9 (process 1). Observed evolution of CO_2 content between November 1986 and January 2001 is shown as "process 2" in Fig. 9.

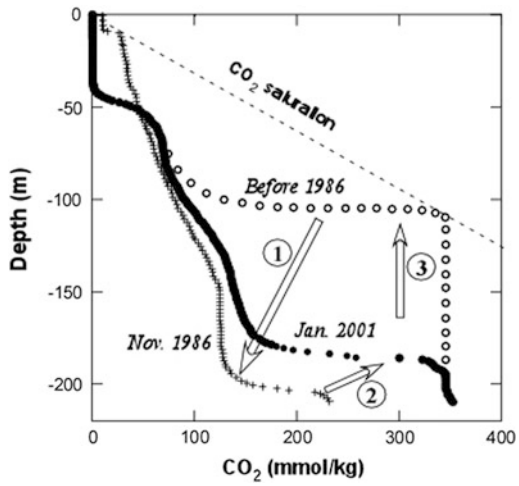

Fig. 9 A model of spontaneous limnic eruption at Lake Nyos. An assumed pre-eruption CO_2 profile is shown by *small open circles* as "Before 1986". After the eruption the CO_2 profile turned to the post-eruption profile shown as "Nov. 1986" (process 1). It evolved to the January 2001 profile in 15 years (process 2). If natural recharge continues, the January 2001 profile may "recover" the pre-eruption situation (process 3)

If no degassing is undertaken and if natural recharge of CO_2 continues as before, the $CO_{2(aq)}$ profile would shift upward following "process 3". If this conceptual model is correct, the difference between the pre- and post-eruption profiles integrated over the lake volume gives the amount of gas released at the time of the eruption, which is calculated to be ~14 Gmol or 0.31 km^3. This value is greater than the estimate (0.14 km^3 STP) by Evans et al. (1994) by a factor of ~2, but significantly smaller than an early estimate of 0.7–1 km^3 at STP (Tuttle et al. 1987; Kanari 1989; Faivre Pierret et al. 1992). The estimated amount of CO_2 released obviously depends on the assumptions involved. As long as the lake receives natural recharge of CO_2, limnic eruptions can occur repetitively (Tietze 1992), but may not be regular as described in a model calculation by Chau et al. (1996) considering a possible variation in the rate of natural recharge of CO_2. However, if the conceptual model shown in Fig. 9 is correct, it would take ~110 years to attain the pre-eruption CO_2 level shown by the "Before 1986" curve starting from the curve "November 1986" assuming a constant CO_2 recharge rate of 0.12 Gmol/year (process 3).

6 Sublacustrine CO_2-Recharge System as Envisaged from C/^{3}He Ratios and Noble Gas Signatures

The isotopic signatures of carbon of dissolved CO_2 and helium reveal that gases recharging Nyos and Monoun lakes are mainly of magmatic origin (e.g., Kusakabe and Sano 1992). The initial report on the Lake Nyos disaster by Kling et al. (1987) included a $^3He/^4He$ ratio of 6 R_{atm} (where $R_{atm}$is the atmospheric ratio of 1.40 × 10^{-6}) for Lake Nyos. Later the $^3He/^4He$ ratios of 5.39–5.75 R_{atm} (corrected for air contamination) for Lake Nyos and 3.56 R_{atm} for Lake Monoun were reported by Sano et al. (1987). The $\delta^{13}C$ values, expressed relative to VPDB, were −3.3 to −3.4 ‰ for Lake Nyos and −6.8 ‰ for Lake Monoun (Kling et al. 1987; Kusakabe and Sano 1992). Nagao et al. (2010) reported more

precise data using samples that were perfectly air-contamination free. The $^3He/^4He$ ratios in gases in Lake Nyos are lower than the typical mantle values of 7–9 R_{atm} that are for depleted mantle producing MORBs (Graham 2002). The reasons why $^3He/^4He$ ratios of Lake Nyos are lower than the mantle values are related to the sub-lithospheric structure beneath the Cameroon Volcanic Line (CVL). The CVL is a linear chain of Cenozoic volcanoes stretching for 1,600 km from the Gulf of Guinea into the continental part of central Africa, straddling oceanic and continental lithosphere (Fig. 1). Halliday et al. (1988) reported variations in radiogenic isotopic ratios (Pb, Nd, and Sr) of volcanic rocks along the CVL, where $^{206}Pb/^{204}Pb$ and $^{208}Pb/^{204}Pb$ ratios were found the highest at the oceanic and continental boundary. Barfod et al. (1999) and Aka et al. (2001, 2004) published a detailed study of noble gases in CO_2-rich gases, basalts and xenoliths from CVL volcanic rocks, showing a symmetrical distribution of $^3He/^4He$ ratios along the CVL. The lowest $^3He/^4He$ ratios($\sim$2 R_{atm}) were found at Etinde, a small volcano next to Mt. Cameroon, which is located at the oceanic and continental boundary. $^3He/^4He$ ratios became close to the MORB values (7–9 R_{atm}) as we go away from the oceanic and continental boundary toward both ends (Aka et al. 2004). This symmetric isotopic variation has been explained to reflect geochemical characteristics of the mantle, or continental lithosphere underneath the boundary which is of a HIMU character (Halliday et al. 1988). The mineral separates from rocks around Lake Nyos (clinopyroxene and amphibole in xenolith) have $^3He/^4He$ ratios of 6.7–7.0 R_{atm} (Aka et al. 2004), slightly lower than the typical MORB values, implying a small degree of the HIMU character of the magma source beneath Lake Nyos. Deep water of the lake has even lower value of 5.7 R_{atm} as stated above. This low ratio may mean that He in deep water was originally derived from magma generated from a slightly HIMU mantle and acquired radiogenic He on the way from the source magma to the sublacustrine fluid reservoir during passage of the magmatic fluid through granitic basement rocks.

A detailed study on noble gases dissolved in Lakes Nyos and Monoun was recently published by Nagao et al. (2010). Although supply of magmatic fluids to the lakes has been indicated in earlier studies on the basis of $^3He/^4He$ and $^4He/^{20}Ne$ ratios (e.g., Kling et al. 1987; Sano et al. 1987, 1990), Nagao et al. (2010) reported distribution of isotopic ratios of not only He but also Ne, Ar, Kr, Xe and C in waters collected at closely separated depths. They stressed the importance of samples that were free from air-contamination, because noble gas concentration, especially that of Ar and Ne, is so low in gases exsolved from CO_2-rich waters compared to air that any sample exposed to the atmosphere during sampling or storage in an improper way is no good for analysis. They collected samples from Lake Nyos in January 2001 using the "Flute de Pan" which had been deployed by the French scientific team. The Flute de Pan consisted of 11 plastic hoses with outside diameter of 15 mm, each having a different intake depth (83–210 m). CO_2-rich gas spouting out of the hose was introduced in a bucket filled with surface water of the lake, and then the bubbles were introduced into a glass bottle using an inverted funnel. Although contamination of air dissolved in the water was still suspected to some extent especially for heavy noble gases, this sampling method was found promising. In the December 2001 sampling, a plastic hose method, essentially the same as the Flute de Pan method, was adopted. A single plastic hose (12 mm I.D.) was deployed initially to the bottom, followed by pulling it upward step by step to a desired depth of the lake. The sampling depth was measured with a calibrated wire attached to the hose. After water inside the hose was completely replaced by water at the target depth, exsolved CO_2 gas was directly allowed to pass through a sampling bottle made of uranium glass that has low He diffusivity. With this method Nagao et al. (2010) were able to collect perfectly air-contamination free samples judging from measured $^{40}Ar/^{36}Ar$ ratios. This method was later modified to measure the total gas concentration on site (Tassi et al. 2009; Yoshida et al. 2010).

Figure 10a, b illustrates the profiles of He, Ne, Ar, Kr and Xe in water, measured in 2001, at Lake Nyos and Lake Monoun, respectively. Except for He, they show roughly constant concentrations with respect to depth below 80 m (Lake Nyos) and 50 m (Lake Monoun). The Ne, Ar, Kr and Xe concentrations are up to several times lower than those in air saturated water (ASW). Note, however, that the He concentration in lake water is more than 3 orders of magnitude higher than in ASW. Depth profiles of $^{3}He/^{4}He$ ratio for Lakes Nyos and Monoun are presented in Fig. 11. The data published by earlier workers (Kling et al. 1987; Sano et al. 1987, 1990; Kusakabe and Sano 1992) are in the same range. Roughly speaking the $^{3}He/^{4}He$ ratios are almost constant in the depth range of 80–210 m at Lake Nyos and 40–100 m at Lake Monoun, although

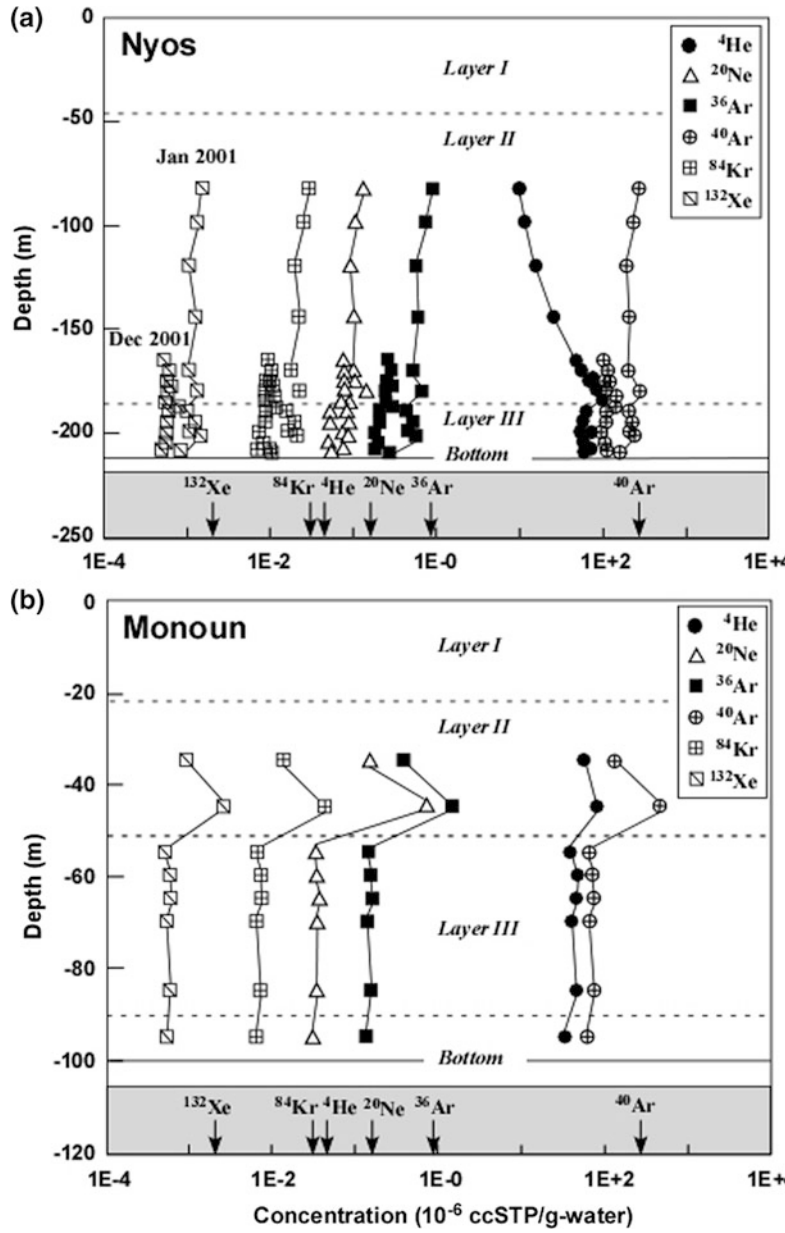

Fig. 10 **a** Depth profiles of ^{4}He, ^{20}Ne, ^{36}Ar, ^{40}Ar, ^{84}Kr and ^{132}Xe concentrations in water (10^{-6}ccSTP/g-water) measured at Lake Nyos in January 2001 and December 2001. **b** Noble gas profiles at Lake Monoun in December 2001. Noble gas concentrations in air saturated water (ASW) at 30 °C are shown by *arrows* for comparison in the *gray box* at the *bottom* of each figure. The figures were revised from Figs. 1b and 2b of Nagao et al. (2010)

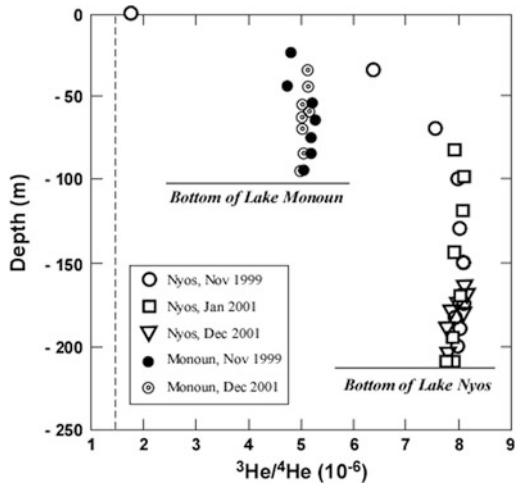

Fig. 11 $^3He/^4He$ ratios as a function of depth at Lakes Nyosand Monoun in 1999 and 2001. They are almost constant below the surface chemocline, i.e., −22 m at Lake Monoun and −51 m at Lake Nyos. The figure was revised from Fig. 4a of Nagao et al. (2010)

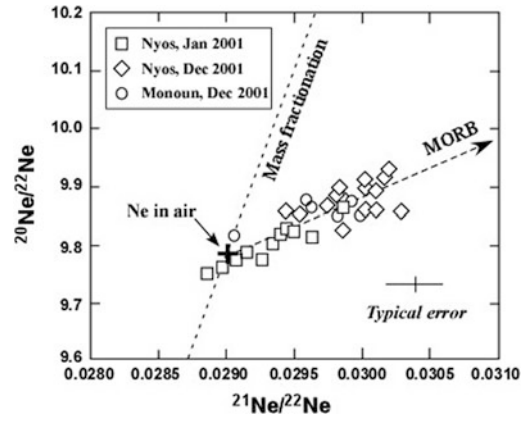

Fig. 12 Plot of $^{20}Ne/^{22}Ne$ versus $^{21}Ne/^{22}Ne$ ratios for samples collected in January and December 2001 from Lakes Nyos and Monoun. A thick cross stands for the isotopic ratios of atmospheric Ne. The "mass fractionation line" indicates Ne isotopic ratios for mass fractionated atmospheric Ne. A *dashed line* heading to MORB represents a *mixing line* between atmospheric Ne and Ne in MORB or upper mantle (Ballentine et al. 2005). The figure was revised from Fig. 5 of Nagao et al. (2010)

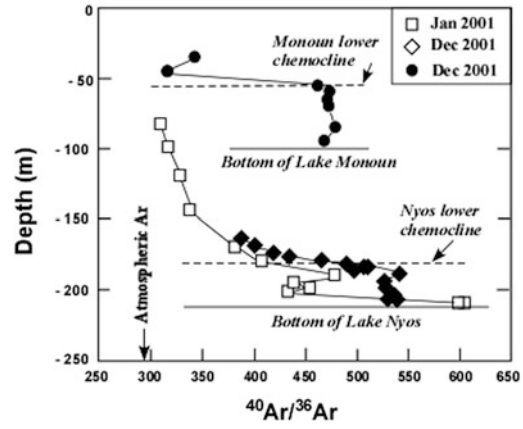

Fig. 13 $^{40}Ar/^{36}Ar$ profiles in Lakes Nyos and Monoun measured in 2001. A zigzag pattern was evident in January 2001 but less evident in December 2001. The ratio approaches the atmospheric value shown by an *arrow*($^{40}Ar/^{36}Ar$ = 296) as we go shallower. The figure was reproduced from Fig. 6 of Nagao et al. (2010)

the ratio tends to decrease slightly toward the bottom at Lake Nyos. The $^3He/^4He$ ratio approaches to the atmospheric value in waters shallower than 80 m and 40 m for Lakes Nyos and Monoun, respectively. High $^4He/^{20}Ne$ ratios up to ~1,500 (not shown here) support magmatic gas input to the lake as inferred by high $^3He/^4He$ ratios.

Neon isotopic ratios are presented in Fig. 12. Compared to the atmospheric Ne, small excess in both $^{20}Ne/^{22}Ne$ and $^{21}Ne/^{22}Ne$ ratios is observed. Most data points of both lakes lie on the MORB line connecting the atmospheric Ne and mantle Ne that was reported by Ballentine et al. (2005). The data clearly indicate the presence of mantle Ne in the lakes, and are consistent with the conclusion by Barfod et al. (1999) that the CVL mantle contains MORB-like Ne.

Argon isotopic ratios are presented in Fig. 13. It shows that $^{40}Ar/^{36}Ar$ ratios for all samples are higher than the atmospheric value of 296, but much lower than the estimated value of >1,650 for Ar in upper mantle beneath the CVL (Barfod et al. 1999). This means that magmatic fluids containing mantle Ar mixed with atmospheric Ar on the way to the surface such as in a sub-lacustrine fluid reservoir. This is consistent with the conclusion derived from the Ne signature (Fig. 12). At Lake Nyos, the highest $^{40}Ar/^{36}Ar$ ratio of about 600 was found at the bottom (210 m). The $^{40}Ar/^{36}Ar$ profile in January 2001 decreased gradually toward the surface approaching to the atmospheric ratio of 296, but

it showed a zigzag pattern below the lower chemocline at ~180 m with a second maximum value of 480 at 190 m. The zigzag $^{40}Ar/^{36}Ar$ profile disappeared in December 2001 with uniform ratios around 530 below 190 m. This may have resulted from vertical mixing in the depth range caused by the degassing operation, because water was pumped out by the degassing pipe with the intake depth of 203 m. Tendency of such homogenization was also observed in the water temperature and electric conductivity at the corresponding depths (Kusakabe et al. 2008), although they were less clear than the noble gas profiles. At Lake Monoun, the $^{40}Ar/^{36}Ar$ ratios were in a narrow range at about 470 between 60 and 100 m (bottom) (Fig. 13). The ratios are lower than those in deep waters of Lake Nyos, indicating that contribution of atmospheric Ar to the magma-derived gases at Lake Monoun is greater than that at Lake Nyos.

Characteristic features of noble gases observed at Lake Nyos can be summarized as follows (Nagao et al. 2010). (1) Helium in the lake water derived originally from the mantle where $^3He/^4He$ ratios of 9-10 × 10^{-6} are found in mantle xenoliths (Aka et al. 2004), but on its way to the surface approximately 20 % of radiogenic ^4He that accumulated in crustal rocks was admixed to give the ratios of ~8 × 10^{-6}, probably in sub-lacustrine region. (2) The observed $^{40}Ar/^{36}Ar$ ratios of 450–550 is also explained by the addition of atmospheric Ar ($^{40}Ar/^{36}Ar$ = 296) to the mantle derived Ar ($^{40}Ar/^{36}Ar$ > 1,650, Barfod et al. 1999) on the way to the lakes. The most likely source of Ar to reduce the mantle $^{40}Ar/^{36}Ar$ ratio is groundwater that carries atmospheric Ar. (3) Ne in the lakes may be a mixture of atmospheric Ne and a small amount of MORB-like Ne from the mantle. The observed He, Ne and Ar isotopic ratios in lake waters can be best explained by mixing between two noble gas reservoirs, i.e., air dissolved ground water and the mantle. It is conceivable that the mantle-derived gases meet radiogenic ^4He from crustal rocks, and atmospheric Ar and Ne carried by groundwater, and are finally homogenized in the sub-lacustrine reservoir.

As stated previously, the greatest chemical change took place at depth deeper than 180 m at Lake Nyos. The CO_2 profiles in the depth range of 160 and 210 m are enlarged in Fig. 14a, which shows that the increase of CO_2 concentration in deep water of Lake Nyos after the limnic eruption in 1986 resulted in thickening of CO_2-rich water and in formation of the clear lower chemocline at the top of the CO_2-rich water. The ^3He concentration observed in 2001 in the same depth range (Fig. 14b) was compared with the

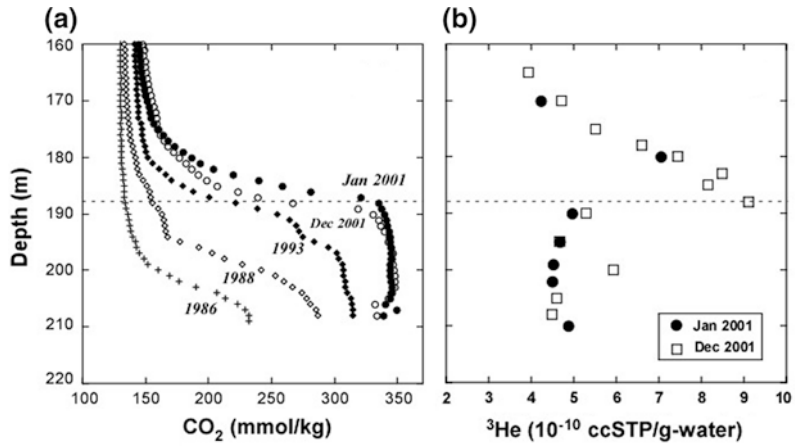

Fig. 14 **a** CO_2 profiles in deep water of Lake Nyos in the depth range of 160–210 m where the greatest change took place during 1986 and 2001. **b** ^3He profile in the same depth range observed in January 2001 and December 2001. Note a sharp maximum of ^3He concentration at 188 m. *Dashed line* indicates the chemocline bordering layers II and III in 2001

CO_2 profiles. The ^{3}He profile was obtained from the ^{4}He profile (Fig. 10) and ^{3}He/^{4}He profile (Fig. 11). It should be noted that the ^{3}He concentrations below 160 m in January 2001 and December 2001 show a sharp maximum at around 188 m with a concentration up to 9.1×10^{-10} ccSTP/g-water (December 2001). The ^{4}He concentrations have a pattern very similar to those of ^{3}He in the same depth range because of almost constant ^{3}He/^{4}He ratios (Fig. 11), although the ^{4}He concentrations are not graphically shown. Between 190 and 210 m the ^{3}He concentrations are nearly constant at $\sim 5 \times 10^{-10}$ ccSTP/g-water. The ^{3}He concentrations gradually decrease in shallower water (layer II). The observed depth profiles of ^{3}He (Fig. 14b), ^{40}Ar/^{36}Ar (Fig. 13) and ^{4}He/^{20}Ne ratios (not shown) in Lake Nyos, which showed a maximum at around the lower chemocline ($\sim$190 m in depth), were interpreted by Nagao et al. (2010) to suggest that fluids from the sub-lacustrine reservoir are supplied not from the bottom but mainly from the side wall of the lake at that depth, because it would be easier for the sub-lacustrine fluids to find their way to the lake through the periphery where sediments would be less thick and coarser than those in the central part of the lake. This interpretation is interesting and is different from a widely disseminated view that the fluids are supplied from the lake bottom to the lakes, although the point of issue of the recharge fluids has not been located and further examination of this view is required.

The C/^{3}He ratios of volcanic fluids have been widely used to constrain the magma sources. The C/^{3}He ratios of MORB glasses have shown to be fairly constant at 2.0 (±0.5) $\times 10^9$, suggesting that the source region of MORB in the upper mantle has little variation in C/^{3}He ratio (Marty and Jambon 1987). The ratios for volcanic gases from subduction volcanism, however, have been found significantly greater than the MORB values, i.e., 7×10^9–30×10^9. These high ratios, coupled with δ^{13}C values, indicate existence of recycled carbon (marine carbonates, slab carbonates and/or organic materials) in subduction zone magmas (Sano and Williams, 1996, and references therein).

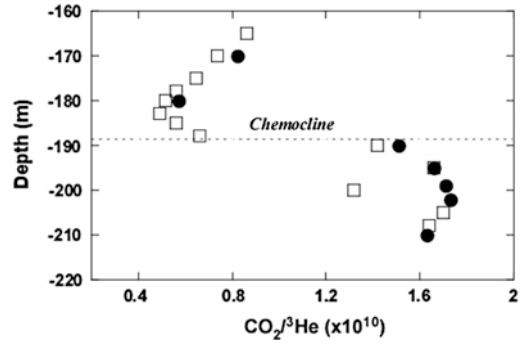

Fig. 15 CO_2/^{3}He ratios observed in the depth range of 160-210 m at Lake Nyos in January 2001 (*solid circles*) and December 2001 (*open squares*). There is a clear difference in the ratios above and below the deep chemocline, showing "decoupling" of CO_2 and ^{3}He

Figure 15 shows the C/^{3}He ratios in the depth range between 160 and 210 m calculated from the CO_2 and ^{3}He concentrations. The C/^{3}He ratios range from 0.5×10^{10} to 1.7×10^{10}. These values are higher than the mantle values of $\sim 2 \times 10^9$, consistent with the earlier notes based on Ne and Ar isotopes that the mantle beneath Lake Nyos is not a typical MORB-source mantle. It is interesting to note that the C/^{3}He ratios in waters below the lower chemocline are significantly high at around 1.6×10^{10}, and they sharply decrease to 0.5×10^{10} above the lower chemocline. Thus, the behavior of CO_2 and ^{3}He can be said *decoupled* below and above the chemocline. The cause(s) of the decoupling may be explained by under plating of the recharge fluids from the bottom that are characterized by different C/^{3}He ratios. It is possible that the ratio was low before the limnic eruption and high after the limnic eruption. At the time of the limnic eruption, the lake was not completely mixed, suggesting the deep water still contained a large fraction of "pre-eruption" water (Giggenbach 1990; Tietze 1992; Evans et al. 1994) which may have been proportionally higher in He and lower in CO_2 concentrations with the CO_2/^{3}He ratio of $\sim 0.5 \times 10^{10}$. The recharge fluids entering the lake after the eruption may have the ratio of $\sim 1.6 \times 10^{10}$. This interpretation implies that the CO_2/^{3}He ratio in the recharge fluids may vary with time and the ratios have changed from low

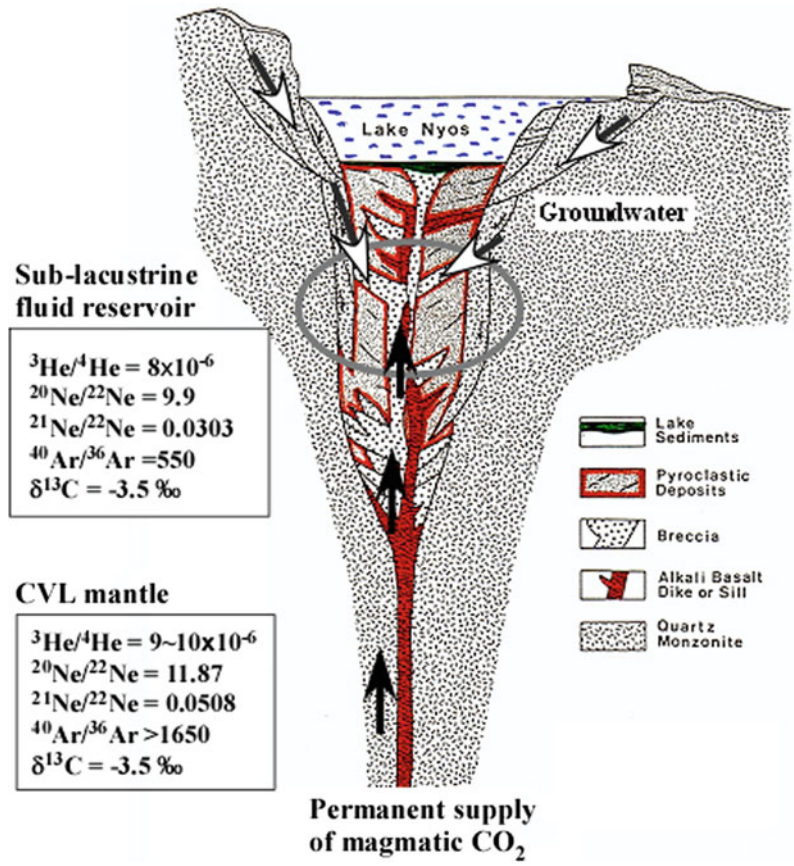

Fig. 16 Schematic presentation of the sub-lacustrine fluid reservoir which is encircled by *gray line*. The geological cross section of Lake Nyos was taken from Lockwood and Rubin (1989). *Arrow* with white head indicates the flow of groundwater, and that with *black* head indicates magmatic fluid coming from magma underneath. Noble gas and carbon isotopic ratios of respective reservoirs are shown

to high values with time, reflecting increased contribution of atmospheric noble gases carried by groundwater into the recharge fluids. A gradual change with time in $CO_2/^3He$ ratio has been observed in fumarolic gases from Mammoth Mountain in the Long Valley caldera, California, where "tree-kill" took place due to anomalous CO_2 discharge of magmatic origin from soils (Farrar et al. 1995; Sorey et al. 1998). The $CO_2/^3He$ ratios changed from $\sim 0.3 \times 10^{10}$ to 1.6×10^{10} in about 10 years. The change was caused by a decreasing trend of He concentrations and $^3He/^4He$ ratios, since CO_2 concentration was kept almost constant. These observations indicate that the above geochemical parameters ($CO_2/^3He$ ratio, He concentration, etc.) that carry information about magmatic fluids can change within a geologically very short period of time, i.e., an order of 10 years, at a single volcanic system. Thus, it is conceivable that the decoupling of CO_2 and ^3He observed at Lake Nyos after the limnic eruption was caused by addition of "recent" recharge fluids that were characterized by relatively high CO_2 and low ^3He concentrations. From the foregoing discussions based on noble gas signatures and $C/^3He$ ratios, we can envisage the sub-lacustrine CO_2-recharge system at Lake Nyos as shown in Fig. 16.

7 New Japan-Cameroon Joint Project for Mitigation of a Future Gas Disaster in Cameroon

Regular monitoring of Lakes Nyos and Monoun has shown that the amount of dissolved CO_2 has been greatly reduced due to successful artificial degassing. Since the supply of CO_2 to the lakes from underlying magma is supposed to be

semi-permanent, the regular monitoring of the lakes needs to be continued in order to observe how much gas has been removed and to evaluate any change in the supply rate of CO_2. The lake monitoring has been mainly led by foreign scientific teams, e.g., Japan and USA, supported by Cameroonian scientists and technicians. The Nyos and Monoun disasters have been a trauma for most Cameroonians, therefore, removal of the trauma is essential for them. Unfortunately, the scientific base in Cameroon has been insufficient to perform regular lake monitoring and other scientific tasks by themselves. In order to solve this problem, a new project called Science and Technology Research Partnership for Sustainable Development (SATREPS) has been introduced to Cameroon. The SATREPS is a program for joint research cooperation between Japan and developing countries for resolving global issues, e.g., environment, energy, natural disaster prevention and infectious diseases control. It is sponsored by Japan Science and Technology Agency (JST) and Japan International Cooperation Agency (JICA), and was launched in 2008. The JST and JICA are the organizations under the Ministry of Education, Culture, Sports, Science and Technology of Japan, and the Ministry of Foreign Affairs of Japan, respectively. Our "SATREPS-Cameroon" is one of the projects under the SATREPS, and is entitled "Magmatic fluid supply into Lakes Nyos and Monoun, and mitigation of natural disasters through capacity building in Cameroon". It started in April 2011 and will continue until March 2016. The goal of the project is to mitigate natural disasters in Cameroon through capacity building, specifically for the issues related to the Lakes Nyos and Monoun gas disasters. To accomplish the goal, the following sub-projects have been set up as joint research between Japan and Cameroon: (1) clarification of the CO_2 recharge system beneath Lakes Nyos and Monoun, (2) the hydrological regime around the lakes, (3) eruptive history of volcanoes along Cameroon Volcanic Line (CVL), (4) CO_2 distribution in Lakes Nyos, Monoun and other lakes along CVL, (5) setup of experimental system for removing CO_2-rich deep water to prevent gas re-building in Lake Monoun, and (6) continuation of geochemical monitoring of Lakes Nyos and Monoun. The capacity building includes education of young Cameroonian scientists and students in Japan and donation of some scientific equipment that is necessary for continuous monitoring of the lakes. After the SATREPS-Cameroon project is over, it is expected the trauma in Cameroonians' mind be removed through their scientific accomplishment without foreign support any longer.

8 Conclusions

Lakes Nyos and Monoun are, unfortunately, a site of accumulation of strong passive magmatic CO_2 degassing. The changes with time in physico-chemical parameters such as temperature, conductivity, chemical composition and CO_2 content have been found unusually rapid as a geological phenomenon, as revealed by regular geochemical monitoring of the lakes that has continued for the last 25 years. Such rapid changes have given an opportunity for the international scientific community to acquire experience of the phenomenon and to take necessary measures to avoid re-buildup of magmatic gas in the lakes. The artificial degassing operation at both lakes advanced satisfactorily. The CO_2 content of Lake Monoun was reduced to 6 % of the maximum value, and the lake has lost its gas self-lift capability, or no more degassing is expected. A similar situation will be reached at Lake Nyos in the near future because recent installation of additional degassing pipes greatly enhanced the rate of degassing. The lake is expected to lose gas self-lift capability in the next few years. Since natural recharge of magmatic gas would continue, it is necessary to adopt a strategic intervention to stop gas re-buildup.

The scientific knowledge we have accumulated, current situation and future prospect of the lakes need to be informed to Cameroonian people, especially to the local residents, because they do not know what happened at the time of gas disaster and are still afraid of its recurrence. It is also important to decide the guideline for

declaration of the safety of the lakes. Of course, there is no "absolute safety" in natural disasters, but once the gas concentration is reduced to a level where water has lost the gas self-lift capability, there would be no immediate threat for a limnic eruption to occur. For the sake of safety, regular monitoring of the lakes should be continued in order to observe if there is any change in the amount of dissolved gas and in the recharge rate of sub-lacustrine fluids to the lakes. The safety declaration should be given by the Cameroonian Government after they are fully convinced by scientific evidence that has been and will be obtained by Cameroonian scientists.

Acknowledgments The author would like to thank for financial support for my regular monitoring of Lakes Nyos and Monoun mainly from the Grant-in Aid for Scientific Research from the Japan Society for the Promotion of Science (1986-2007) and partly from OFDA (2000) and SATREPS (2011). Thanks also go to J.V. Hell, director of the Institute of Research for Geology and Mining (IRGM), Cameroon, and the IRGM staff for supporting our field work. The field work was done together with my colleagues, namely, Y. Yoshida, T. Ohba, K. Nagao, Issa, G. Tanyileke, and many others to whom I owe. Photos used in Fig. 2 were supplied by Y. Yoshida and J.-C. Beard. The early version of the manuscript was improved by valuable comments by Issa, F. Tassi and D. Rouwet. The English was improved by J. Runzo.

References

Aka FT (2015) Depth of melt segregation below the Nyos maar-diatreme volcano (Cameroon, West Africa): major-trace element evidence and their bearing on the origin of CO_2 in Lake Nyos (this volume)

Aka FT, Kusakabe M, Nagao K, Tanyileke GT (2001) Noble gas isotopic compositions and water/gas chemistry of soda springs from the islands of Bioko, Sao Tome and Annobon, along with Cameroon volcanic line, West Africa. Appl Geochem 16:323–338

Aka FT, Nagao K, Kusakabe M, Sumino H, Tanyileke G, Ateba B, Hell J (2004) Symmetrical helium isotope distribution on the Cameroon volcanic line, West Africa. Chem Geol 203:205–223

Barberi F, Chelini W, Marinelli G, Martini M (1989) The gas cloud of Lake Nyos (Cameroon, 1986): results of the Italian technical mission. J Volcanol Geotherm Res 39:125–134

Barfod DN, Ballentine CJ, Halliday AN, Fitton JG (1999) Noble gases in the Cameroon line and the He, Ne, and Ar isotopic compositions of high μ (HIMU) mantle. J Geophys Res 104:29509–29527

Ballentine CJ, Marty B, Sherwood Lollar B, Cassidy M (2005) Neon isotopes constrain convection and volatile origin in the Earth's mantle. Nature 433:33–38

Chau HF, Kwok PK, Mak L (1996) A model of gas buildup and release in crater lakes. J Geophys Res 101 (B12):28253–28263

Duan Z, Sun R (2003) An improved model calculating CO_2 solubility in pure water and aqueous NaCl solutions from 273 to 533 K and from 0 to 2000 bar. Chem Geol 193:257–271

Evans WC, Kling GW, Tuttle ML, Tanyileke G, White LD (1993) Gas buildup in Lake Nyos, Cameroon: the recharge process and its consequences. Appl Geochem 8:207–221

Evans WC, White LD, Tuttle ML, Kling GW, Tanyileke G, Michel RL (1994) Six years of change at Lake Nyos, Cameroon, yield clues to the past and cautions for the future. Geochem J 28:139–162

Faivre Pierret RX, Berne P, Roussel C, Le Guern F (1992) The Lake Nyos disaster: model calculations for the flow of carbon dioxide. J Volcanol Geotherm Res 51:161–170

Farrar CD, Sorey ML, Evans WC, Howle JF, Kerr BD, Kennedy BM, King CY, Southon JR (1995) Forest-killing diffuse CO_2 emission at Mammoth Mountain as a sign of magmatic unrest. Nature 376:675–678

Freeth SJ, Kay RLF (1987) The Lake Nyos gas disaster. Nature 325:104–105

FreethSJ Kling GW, Kusakabe M, Maley J, Tchoua FM, Tietze K (1990) Conclusions from Lake Nyos disaster. Nature 348:201

Freeth SJ (1994) Lake Nyos: can another disaster be avoided? Geochem J 28:163–172

Gerlach T (2011) Volcanic versus anthropogenic carbon dioxide. EOS 92(24)

Giggenbach WF (1990) Water and gas chemistry of Lake Nyos and its bearing on the eruptive process. J Volcanol Geotherm Res 42:337–362

Graham D (2002) Noble gas isotope geochemistry of mid-oceanic ridge and ocean island basalts: characterization of mantle source reservoirs. Noble Gases in Geochemistry and Cosmochemistry. In: Porcelli D, Ballentine CJ, Wieler R (eds) Reviews in mineralogy and geochemistry, vol 47. Social Mineral Society America, Washington, D.C, pp 247–317

Halbwachs M, GrangeonJ Sabroux J-C, Villevielle A (1993) Purge par auto-siphon du gaz carbonique dissous dans le lac Monoun (Cameroun): premiers resultants experimentaux. C. R. Acad. Sci., Paris, t. 316. Serie II:483–489

Halbwachs M, Sabroux JC (2001) Removing CO_2 from Lake Nyos in Cameroon. Science 292:436

Halbwachs M, Sabroux J-C, Grangeon J, Kayser G, Tochon-Danguy J-C, Felix A, Beard J-C, Villevieille A, Vitter G, Richon B, Wuest A, Hell J (2004) Degassing the "Killer Lakes" Nyos and Monoun, Cameroon EOS 85(30):281–288

Halliday AN, Dickin AP, Fallick AE, Fitton JG (1988) Mantle dynamics: A Nd, Sr, Pb and O isotopic study of the Cameroon line volcanic chain. J Petrol 29:181–211

Kanari S (1989) An inference on process of gas outburst from lake Nyos, Cameroon. J Volcanol Geotherm Res 39:135–149

Kantha LH, Freeth SJ (1996) A numerical simulation of the evolution of temperature and CO_2 stratification in Lake Nyos since the 1986 disaster. J Geophys Res 101 (B4):8187–8203

Kerrick DM (2001) Present and past nonanthropogenic CO_2 degassing from the solid Earth. Revi Geophys 39:565–585

Kling GW, Clark MA, Compton HR, Devine JD, Evans WC, Humphrey AM, Koenigsberg EJ, Lockwood JP, Tuttle ML, Wagner GN (1987) The 1986 Lake Nyos gas disaster in Cameroon, West Africa. Science 236:169–175

Kling GW, Evans WC, Tanyileke G, Kusakabe M, Ohba T, Yoshida Y, Hell JV (2005) Degassing Lakes Nyos and Monoun: defusing certain disaster. Proc Nat Acad Sci USA 102:14185–14190

Kling GW, Tuttle ML, Evans WC (1989) The evolution of thermal structure and water chemistry in Lake Nyos. J Volcanol Geotherm Res 39:151–156

Kusakabe M, Ohsumi T, Aramaki S (1989) The Lake Nyos gas disaster: chemical and isotopic evidence in waters and dissolved gases from three Cameroonian crater lakes, Nyos, Monoun and Wum. J Volcanol Geotherm Res 39:157–185

Kusakabe M, Sano Y (1992) Origin of gases in Lake Nyos, Cameroon. In: Freeth SJ, Ofoegb CO, Onohua KM (eds) Natural hazards in West and Central Africa. International monograph series on interdisciplinary earth science research and applications, Friedrich Vieweg & SohnVerlag, Braunschweig, Wiesbaden, pp 83–95

Kusakabe M, Tanyileke G, McCord SA, Schladow SG (2000) Recent pH and CO_2 profiles at Lakes Nyos and Monoun, Cameroon: implications for the degassing strategy and its numerical simulation. J Volcanol Geotherm Res 97:241–260

Kusakabe M, Ohba T, Issa, Yoshida Y, Satake H, Ohizumi T, Evans WC, Tanyileke G, Kling GW (2008) Evolution of CO_2 in Lakes Monoun and Nyos, Cameroon, before and during controlled degassing. Geochem J 42:93–118

Kusakabe M, Ohba T, Yoshida Y, Anazawa K, Kaneko K, Ueda A, Miyabuchi Y (2011) Lake Nyos disaster (Cameroon): latest situation. Abstract ID: SE52-A002. The 8th annual meeting of Asia Oceania geosciences society (AOGS2011), Taipei, Taiwan, 8–12 Aug 2011

Lockwood JP, Rubin M (1989) Origin and age of the Lake Nyos maar, Cameroon. J Volcanol Geotherm Res 39:117–124

Marty B, Jambon A (1987) $C/^3He$ in volatile fluxes from the solid Earth: implications for carbon geodynamics. Earth Planet Sci Lett 83:16–26

McCord SA, Schladow SG (1998) Numerical simulations of degassing scenarios for CO_2-rich Lake Nyos, Cameroon. J Geophys Res 103:12355–12364

Nagao K, Kusakabe M, Yoshida Y, Tanyileke G (2010) Noble gases in Lakes Nyos and Monoun, Cameroon. Geochem J 44:519–554

Nojiri Y, Kusakabe M, Tietze K, Hirabayashi J, Sato H, Sano Y, Shinohara H, Njine T, Tanyileke G (1993) An estimate of CO_2 flux in Lake Nyos, Cameroon. Limnol Oceanogr 38:739–752

Sano Y, Wakita H, Ohsumi T, Kusakabe M (1987) Helium isotope evidence for magmatic gases in Lake Nyos, Cameroon. Geophys Res Lett 14:1039–1041

Sano Y, Kusakabe M, Hirabayashi J, Nojiri Y, Shinohara H, Njine T, Tanyileke G (1990) Helium and carbon fluxes in Lake Nyos, Cameroon: constraint on next gas burst. Earth Planet Sci Lett 99:303–314

Sano Y, Williams SN (1996) Fluxes of mantle and subducted carbon along convergent plate boundaries. Geophys Res Lett 23:2749–2752

Schmid M, Lorke A, Wuest A, Halbwachs M, Tanyileke G (2003) Development and sensitivity analysis of a model for assessing stratification and safety of Lake Nyos during artificial degassing. Ocean Dyn 53:288–301

SchmidM, Halbwachs M, Wuest A (2006) Simulation of CO_2 concentrations, temperature, and stratification in Lake Nyos for different degassing scenarios. Geochem Geophys Geosyst. doi:10.1029/2005GC001164

Sigurdsson H, Devine JD, Tchoua M, Pressor TS, Pringle MKW, Evans WC (1987) Origin of the lethal gas burst from Lake Monoun, Cameroun. J Volcanol Geotherm Res 31:1–16

Sigvaldason GE (1989) Interanational conference on Lake Nyos disaster, Yaounde, Cameroon, 15–20 March 1987: conclusions and recommendations of the conference. J Volcanol Geotherm Res 39:97–107

Sorey ML, Evans WC, Kennedy BM, Farrar CD, Hainsworth LJ, Hausback B (1998) Carbon dioxide and helium emissions from a reservoir of magmatic gas beneath Mammoth Mountain, California. J Geophys Res 103:15303–15323

Tassi F, Vaselli O, Tedesco D, Montegrossi G, Darrah T, Cuoco E, Mapendano MY, Poreda R, Delgado Huertas A (2009) Water and gas chemistry at Lake Kivu (DRC): geochemical evidence of vertical and horizontal heterogeneities in a multibasin structure.

Geochem Geophys Geosyst (G3) 10(1). doi:10.1029/2008GC002191 (2009)
Tazieff H (1989) Mechanisms of the Nyos carbon dioxide disaster and of so-called phreatic steam eruptions. J Volcanol Geotherm Res 39:109–116
Tietze K (1987) The Lake Nyos gas catastrophe in Cameroon: cause, sequence of events, consequences. Proc XXII Congress IAHR, Lausanne, pp 93–98
Tietze K (1992) Cyclic gas bursts: are they a 'usual' feature of Lake Nyos and other gas-bearing lakes? In: Freeth SJ, Ofoegb CO, Onohua KM (eds) Natural hazards in West and Central Africa. International monograph series on interdisciplinary earth science research and applications, Friedrich Vieweg & Sohn-Verlag, Braunschweig, Wiesbaden, pp 97–107
Tuttle ML, Clark MA, Compton HR, Devine JD, Evans WC, Humphrey AM, Kling GW, Koenigsberg EJ, Lockwood JP, Wagner GN (1987) The 21 August 1986 Lake Nyos gas disaster, Cameroon. US geology survey open-file report, vol 87–97, 58 p
Yoshida Y, Issa Kusakabe M, Satake H, Ohba T (2010) An efficient method for measuring CO_2 concentration in gassy lakes: Application to Lakes Nyos and Monoun, Cameroon. Geochem J 44:441–448

Modelling Air Dispersion of CO_2 from Limnic Eruptions

Antonio Costa and Giovanni Chiodini

Abstract

Limnic eruptions, like the August 1986 Lake Nyos event, can release huge amounts of dense CO_2 that, under the control of local topography and wind, can travel up to distal areas suffocating wildlife, livestock and humans. We present a computational approach, based on shallow layer equations, used to simulate the dispersion of dense CO_2 clouds and assess the associated gas hazard. Examples of application of such an approach to hazard assessment of gas accumulations generated by persistent CO_2 emissions in Italy, and simulation results of the CO_2 air dispersion from the limnic eruption of the 21 August 1986 at Nyos are also discussed. The method presented can be a useful tool to evaluate gas hazard both for persistent gas emissions and for the most hazardous gas-driven limnic eruptions.

Keywords

Dense gas dispersion · Computational model · Gas hazards · Carbon dioxide · Lake Nyos

1 Introduction

The most tragic historically reported event of a gas lake overturn, i.e. limnic eruption, occurred at Lake Nyos (Cameroon, West Africa, Fig. 1) in the evening of 21 August 1986 (Kling et al. 1987). The gas burst killed over 1,700 people and more than 3,000 cattle and animals (Baxter and Kapila 1989; Kling 1987). At Lake Nyos, the liberated CO_2 has a magmatic origin, entering at the lake bottom from the HCO_3-dominated regional aquifer (Evans et al. 1994; Klinget al., this monograph). The CO_2 accumulation in the water at the bottom of lake Nyos has been monitored since 1986 (Kusakabe et al. 2008). In order to control and decrease the pressure of dissolved gases in bottom water of the lake, a degassing pipe was installed in 2001 (Kling et al. 2005; Kusakabe this issue). It is generally accepted that the 1986 dramatic event has a limnic rather than a magmatic-volcanic origin although the exact trigger mechanism is not well

A. Costa (✉)
Istituto Nazionale di Geofisica e Vulcanologia, Sezione di Bologna, Bologna, Italy
e-mail: antonio.costa@ingv.it

G. Chiodini
Istituto Nazionale di Geofisica e Vulcanologia, Sezione di Napoli, Napoli, Italy

D. Rouwet et al. (eds.), *Volcanic Lakes*, Advances in Volcanology,
DOI 10.1007/978-3-642-36833-2_20,
© Springer-Verlag Berlin Heidelberg 2015

Fig. 1 Photo of a view from the southwest of Lake Nyos, taken on 29 August 1986, 8 days after the major limnic eruption. Area impacted by water waves is evident as discoloured layer near the lake shore. Courtesy of the U.S. Geological Survey

known (Evans et al. 1994). However, the physical mechanism of such a lake overturn has been studied and modelled in a few articles (e.g., Zhang 1996; Rice 2000; Zhang and Kling 2006; Mott and Woods 2010), but it remains unclear how the expelled dense gas cloud moved through time and space after its release at the lake surface. Although modelling of denser than air gases is routine in industry for major incident planning at sites where large amounts of gases are stored (e.g. Britter 1989), very few studies have been carried out to describe the atmospheric dispersion of dense CO_2 cloud released from natural Earth degassing (e.g., Pierret et al. 1992; Costa et al. 2008; Chiodini et al. 2010a). In order to know the impact of the CO_2 cloud at the different locations where fatalities occurred it is necessary to know the evolution of the CO_2 concentration in air. At 5 % air CO_2 concentration (dangerous threshold), the breathing increases to twice the normal rate, humans are affected by a weak narcotic effect and headache. In these conditions the time exposure to avoid discomfort or the development of adverse health symptoms is a few minutes. For instance, the short time exposure limit for a CO_2 concentration of 3 %, has been fixed at 15 min by the (National Institute of Occupational Safety and Health 1997). At 10 % air CO_2 concentration (very dangerous threshold) humans are affected by respiratory distress with loss of consciousness in 10–15 min. Finally CO_2 air concentrations >15 % (lethal threshold) are intolerable for humans and cause a rapid death.

In order to simulate dispersion of the heavy gas from a limnic eruption and assess the consequent hazard, here we describe a model based on a shallow layer approach (Britter 1989; Hankin and Britter 1999a, b, c; Costa et al. 2008; Folch et al. 2009). This approach, that uses depth-averaged variables to describe the flow behaviour of dense gas over complex topography, represents a good compromise between the complexity of Computational Fluid Dynamics (CFD) models and the simpler integral models.

We first briefly review applications of the model to persistent gas emissions in Central and South Italy, i.e. Caldara di Manziana, Lazio (Costa et al. 2008) and Mefite d'Ansanto, Campania (Chiodini et al. 2010a). Then we report in detail a new application of the numerical model for the CO_2 cloud dispersion from the gas driven 1986 lake eruption at Lake Nyos (Chiodini et al. 2010b). Reconstruction of the parameters controlling the gas cloud dispersion is based mainly on available semi-quantitative data on the event.

2 Dense Gas Transport Model Based on Shallow Layer Approach

The dispersion of a gas cloud with a density greater than that of air and released from a given source is governed by gravity and by effects of lateral eddies, which increase the mixing with

surrounding air at the edges of the cloud, decreasing its density. During the initial dispersion phase, negative buoyancy controls the gas dynamics and gas moves as a gravity current (gravitational phase) following the ground surface (e.g., Simpson 1997). In contrast, when the density contrast is less important, gas dynamics is basically controlled by the wind and the atmospheric turbulence (passive dispersion phase). In the last case, simulations can be carried out using simplified approaches (e.g., Costa et al. 2005; Granieri et al. 2013).

In theory, gas dispersion can be studied by solving the transport equations for mass, momentum and energy. However, in practice, because the demanding computational requests, different simplified models that partially describe the physics are commonly used. These models range from simpler analytical to more complex CFD models. A compromise between the complexity of CFD models and the simpler integral models is given by the shallow layer approach using depth-averaged variables to describe the flow behavior (Hankin and Britter 1999a, b, c; Venetsanos et al. 2003). These models are able to describe gravity driven flows of dense gas over a complex topography. They are valid in the limit $H/L \ll 1$, being H the generic undisturbed fluid height and L the characteristic wavelength scale in the flow direction.

The TWODEE-2 model (Costa et al. 2008; Folch et al. 2009) is based on depth-averaged equations obtained by integrating mass, density and momentum balance equations over the fluid depth, from the bottom up to the free surface. This approach is able to describe the cloud as a function of time and of the two-dimensional ground positions in terms of four variables: cloud depth, two depth-averaged horizontal velocities, and depth-averaged cloud concentration. Thermodynamic effects such as condensation are not included at present but further development could account for them by introducing an additional equation for gas enthalpy.

2.1 Depth Averaged Variables

As real gas clouds do not have a definite upper surface it is necessary to define the cloud depth, h, in terms of the vertical concentration distribution $\rho(z)$:

$$\int_{z=0}^{h} g(\rho(z) - \rho_a)dz \equiv \alpha \int_{z=0}^{\infty} g(\rho(z) - \rho_a)dz \quad (1)$$

where α is an empirical constant with a value of about 0.95 (Hankin and Britter 1999a), g is the gravity acceleration, and ρ_a is the air density.

The actual vertical concentration profile is not uniform as for liquids, but it is rather characterized by an exponential decay (Hankin and Britter 1999a, b, c):

$$\rho(z) - \rho_a = (\bar{\rho} - \rho_a)\frac{2}{S_1}\exp\left(-\frac{2}{S_1}\frac{z}{h}\right) \quad (2)$$

where S_1 an empirical parameter, and $\bar{\rho}$ is the gas depth average density defined as:

$$h(\bar{\rho} - \rho_a) \equiv \int_{z=0}^{\infty} (\rho(z) - \rho_a)dz \quad (3)$$

The depth-averaged velocities ($\bar{u}$, $\bar{v}$) are given by the following relationships

$$\begin{aligned} h(\bar{\rho} - \rho_a)\bar{u} &\equiv \int_{z=0}^{\infty} (\rho(z) - \rho_a)u(z)dz \\ h(\bar{\rho} - \rho_a)\bar{v} &\equiv \int_{z=0}^{\infty} (\rho(z) - \rho_a)v(z)dz \end{aligned} \quad (4)$$

where $u(z)$, and $v(z)$ denote the vertical velocity distributions.

Concentration profile, $c(z)$, can be evaluated as:

$$c(z) = c_b + \frac{\rho(z) - \rho_a}{\rho_g - \rho_a}(10^6 - c_b) \quad (5)$$

where c is expressed in parts per million (ppm), c_b is the background concentration, and ρ_g denotes the density of unmixed dense gas (Costa et al. 2008; Folch et al. 2009).

2.2 Depth Averaged Equations

Keeping in mind the limitations of such an approach, governing equations can be expressed in terms of the variables introduced above, i.e., the cloud depth, h, the gas depth average density, $\bar{\rho}$, and the depth-averaged velocities $\bar{u}$ and $\bar{v}$ (Hankin and Britter 1999a). The first equation stating the conservation of volume of the cloud can be written as:

$$\frac{\partial h}{\partial t} + \frac{\partial h\bar{u}}{\partial x} + \frac{\partial h\bar{v}}{\partial y} = u_{entr} \tag{6}$$

As the density $\bar{\rho}$ is allowed to change as a function of space and time, an equation similar to (6) expressing the conservation of mass has to be considered (Hankin and Britter 1999a; Costa et al. 2008):

$$\frac{\partial h(\bar{\rho}-\rho_a)}{\partial t} + \frac{\partial h(\bar{\rho}-\rho_a)\bar{u}}{\partial x} + \frac{\partial h(\bar{\rho}-\rho_a)\bar{v}}{\partial y} = \rho_a u_{entr} \tag{7}$$

Finally two equations, describing the balance of forces for a dense gas (accounting for the entrained air; Hankin and Britter 1999a) under the assumption of a hydrostatic pressure distribution, can be written as:

$$\begin{aligned}&\frac{\partial h\bar{\rho}\bar{u}}{\partial t} + \frac{\partial h\bar{\rho}\bar{u}^2}{\partial x} + \frac{\partial h\bar{\rho}\bar{u}\bar{v}}{\partial y} + \frac{1}{2}S_1\frac{\partial_g(\bar{\rho}-\rho_a)h^2}{\partial x} \\ &\quad + S_1 g(\bar{\rho}-\rho_a)h\frac{\partial e}{\partial x} \\ &\quad + \frac{1}{2}\rho C_D\bar{u}|\bar{\mathbf{u}}| \\ &\quad + V_x + k\rho_a\left(\frac{\partial}{\partial t} + u_a\frac{\partial}{\partial x} + v_a\frac{\partial}{\partial y}\right) \\ &\quad \times [h(\bar{u}-u_a)] = u_{entr}\rho_a u_a\end{aligned} \tag{8}$$

$$\begin{aligned}&\frac{\partial h\bar{\rho}\bar{v}}{\partial t} + \frac{\partial h\bar{\rho}\bar{v}^2}{\partial y} + \frac{\partial h\bar{\rho}\bar{u}\bar{v}}{\partial x} + \frac{1}{2}S_1\frac{\partial_g(\bar{\rho}-\rho_a)h^2}{\partial y} \\ &\quad + S_1 g(\bar{\rho}-\rho_a)h\frac{\partial e}{\partial y} \\ &\quad + \frac{1}{2}\rho C_D\bar{v}|\bar{\mathbf{u}}| + V_y \\ &\quad + k\rho_a\left(\frac{\partial}{\partial t} + u_a\frac{\partial}{\partial x} + v_a\frac{\partial}{\partial y}\right) \\ &\quad \times [h(\bar{v}-v_a)] = u_{entr}\rho_a v_a\end{aligned} \tag{9}$$

Here t denotes time, x and y the horizontal coordinates, u_{entr} the entrainment rate of air, $e = e(x, y)$ is the terrain elevation, u_a and v_a represent air velocity (wind), V_x and V_y indicate the components of turbulent shear stress exerted on the cloud, C_D is a skin friction coefficient, and k is a semi-empirical parameter. The model TWODEE-2 is based on the numerical solution of the above equations by using the Flux Corrected Transport (FCT) scheme of Zalesak (1979). This scheme combines the low numerical diffusion of high order schemes with the absence of numerical oscillations typical of low order schemes. FCT calculates the fluxes between adjacent elements using a weighted average of flux as computed by a low order scheme and a high order scheme. The weighting is done in such a manner as to use the high order scheme unless doing so would result in the creation of numerical overshoots not predicted by the low order scheme. For a more detailed description of the equations see Hankin and Britter (1999a); for the numerical parameters and further details about the code see Folch et al. (2009).

In TWODEE-2 wind can be described using different options. The first one consists of assuming a wind described by the classical similarity theory. Thus the wind velocity profile is expressed in terms of the roughness length, z_0, the friction velocity, u_*, and the Monin-Obukhov length L:

$$U_a(z) = \frac{u_*}{K}\left[\ln\left(\frac{z}{z_0}\right) - \psi_m\left(\frac{z}{L}\right)\right] \tag{10}$$

where K is the von Karman constant (K = 0.4) and ψ_m is the classical stability function for momentum (e.g., Jacobson 1999). The second option, more appropriate for large computational domain and complex terrains, consists of coupling the gas dispersion model with a zero-divergence wind field that incorporates local terrain effects (Douglas and Kessler 1990; Folch et al. 2009).

In summary, basic input data needed by TWODEE-2 consist of source position, source gas flux, Digital Elevation Model (DEM) of the terrain, and wind field (Folch et al. 2009).

3 Application Examples for Hazard Assessment of CO_2 from Natural Persistent Gas Emissions

3.1 Persistent Gas Emissions: Italian Case Studies

Italy is one of the regions of the world characterized by intense and widespread processes of Earth degassing. High temperature gases are released by crater plumes and fumaroles in volcanic environments, whereas numerous low temperature gas manifestations rich in carbon dioxide (CO_2) are located in a large area, mainly in the western sector of central and southern Italy (Fig. 2). The origin of this anomaly is still a debated matter. According to Chiodini et al. (2004) the most probable source of the gas is the degassing of a mantle anomalously rich in fluids because contaminated by crustal material. Low temperature gas emissions occur from different types of manifestations such as vents, diffuse soil degassing, mud volcanoes, CO_2 rich groundwater. Many gas emissions have occasionally caused animal and human fatalities and have permanently damaged ecosystems and plant life, making environments inhospitable for life. One of the most relevant gas hazards in the area is due to the toxicity of CO_2, which is the main constituent of the gas emissions. Several accidents have also been recorded in Italy (Chiodini et al. 2008). Few examples include: Mefite d'Ansanto (Campania) where three people were killed during the 1990s and historical chronicles describe the death of many others during the 17th century; Tivoli springs, near Rome, where the gas emitted by the CO_2 saturated water killed several boys during the 1970s; Colli Albani (Rome), where gas emissions caused death by asphyxiation of 29 cows in September 1999, five sheep in March 2000 and a man in December 2000; Veiano (Lazio) where gas emissions killed two hunters in 1991; Mt Amiata (Siena) where in November 2003 a hunter was killed by the CO_2 discharged by one of the many emissions of the area; and many others.

Here we summarize the application of TWODEE-2 for the gas hazard at Caldara di Manziana, Latium region (Costa et al. 2008), and at Mefite d'Ansanto, Campania region (Chiodini et al. 2010a).

Caldara di Manziana (CdM) is a sub-circular structure of $\sim$0.25 km^2 affected by an intense degassing of CO_2 located $\sim$20 km NW of Rome, genetically related to the alkali-potassic volcanism which characterized Central Italy. The emission occurs both as focused vents from water pools, the main of which sustains a 0.5 m high water column, as well as soil diffuse degassing from the crater floor (Fig. 3a). A detailed map of the diffuse CO_2 degassing (after a survey carried out from 12 to 14 June 2006) and specific gas flux rates from vents were used by Costa et al. (2008) to constrain TWODEE-2 simulations. Furthermore, in February 2007, two automatic stations were used to measure, respectively, meteorological data and CO_2 concentration in air. Using the measured CO_2 fluxes and meteorological data as input, TWODEE-2 simulations satisfactorily reproduced measured concentrations (see Fig. 3b) within a factor of 2, similarly to other experiments that used the same model (Hankin and Britter 1999c). In particular the model predicted that the CO_2 concentration at 0.1 m height reaches maximum values of about 7 % near to the main vents. These values indicate that dangerous concentrations can be reached near the soil defining a potentially lethal region for small-size animals. At 1.5 m height, which was considered the inhalation height for humans,

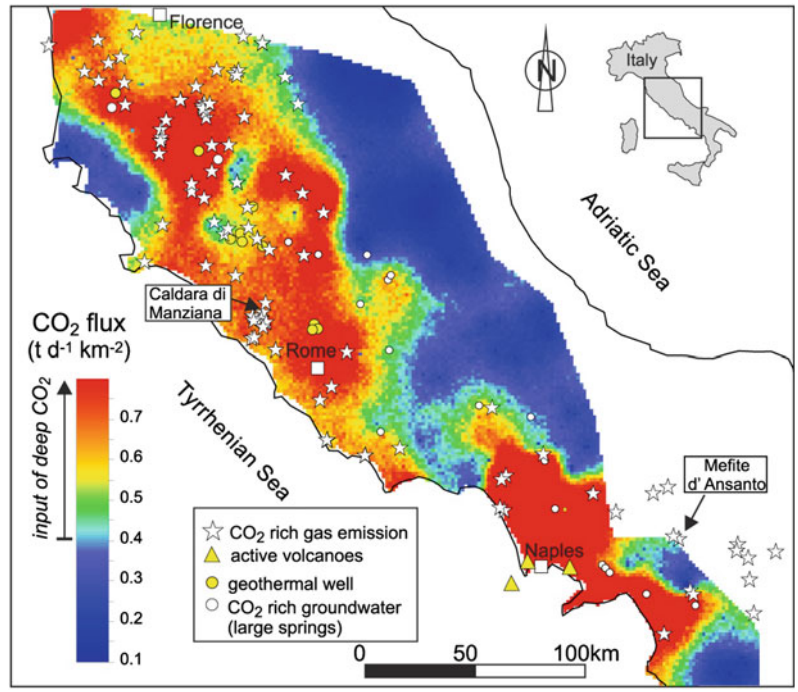

Fig. 2 Map of Earth degassing in central and southern Italy based on the CO_2 dissolved in the groundwater of regional aquifers (modified after Chiodini et al. 2004). Locations of the two gas sources discussed here, CdM and MdA are also reported

the model found a maximum CO_2 concentration of about 3 %, well below the dangerous threshold for humans (Fig. 3c). These results generally agree with the fact that in the area accidents to humans were never recorded, whereas sometimes small size animals were killed by the gas. TWODEE-2 was also used to establish what CO_2 flux would be able to produce lethal conditions for humans at CdM. For example, an increase of the soil CO_2 flux of a factor of five would cause lethal CO_2 concentration at 1.5 m height in the area (see Fig. 3d).

Mefite d'Ansanto (MdA) represents the largest natural emission of low temperature CO_2-rich gases from non-volcanic environment ever measured on Earth (Chiodini et al. 2010a). For low wind conditions, the gas flows along a narrow natural channel producing a persistent gas river which has already killed many peoples and animals (Fig. 4a). In order to estimate the gas flux over the cross-section A-A′ of the channel showed in Fig. 4a, fifty-five measurements of gas concentration and gas stream velocity were made from the ground surface to 3 m height, at a 0.5 m vertical interval, along eight 1.5 m-spaced profiles. A total gas flux of ~2,000 ton per day was estimated by coupling the field measurements with the results of the TWODEE-2 model (Chiodini et al. 2010a). The model was also used to assess the gas hazard of the area. Several simulations were performed varying wind speed and direction in order to reproduce any different meteorological condition that can occur in the area. The most dangerous conditions occur up to wind velocity of ~2 m/s. Such low wind conditions occur very frequently during the summer, whereas they are less frequent during the winter. Furthermore, in accordance to historical chronicles (Chiodini et al. 2010a), simulations showed that winds blowing from the north tend to enhance gas concentration in the topographic depression producing the most hazardous conditions. The maximum heights at which CO_2 concentrations of 5, 10 and 15 % can be reached were also computed (Fig. 4).

3.2 Limnic Eruptions: The Nyos Case

Lake Nyos, Cameroon, is situated on the northeastern ends of the SW-NE lineament of Cameroon Volcanic Line (e.g., Aka this monograph).

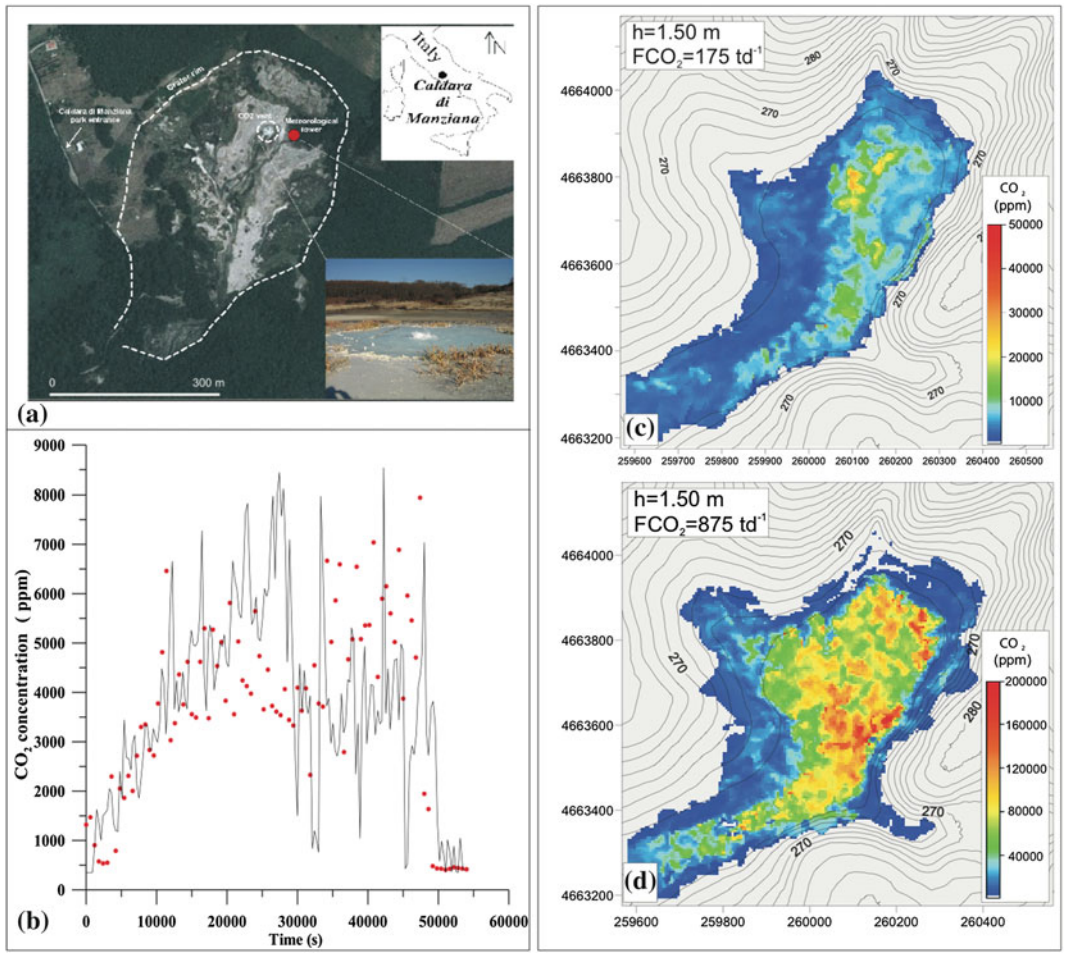

Fig. 3 Aerial photograph of Caldara di Manziana showing the position of the meteorological station and the main CO_2 vent (**a**). Comparison between the measured (*red dots*) and simulated (*black lines*) CO_2 concentrations during the experiment carried out on 5 and 6 February 2007 (**b**). Gas concentration maps at heights of 1.50 m assuming very low wind stable conditions for a total flux was equal to the measured one (**c**) and five times the measured one (**d**). After Costa et al. (2008)

In the early evening of 21 August 1986, heavy rains and thunderstorms occurred in the Nyos area (Tuttle et al. 1987; Giggenbach 1992). By about 9.30 PM meteorological calmness returned and the air temperature was cool (~15 °C; Kling 1987). Shortly after, a rumbling sound could be heard, with a duration of 15–20 s. Although not completely reliable (Baxter and Kapila 1989), witnesses described that a white cloud rose from the lake, and a large water wave was directed towards the south coast. The gas cloud would have probably reached ~100 m in height. The water surge associated with the lake overturn was probably about 25 m large, as inferred by vegetation damages. On the south-western shore, a water fountain probably frothed over an 80 m high rock promontory. Towards the north, a 6 m high water surge spilled over the 100 m wide-40 m high natural dam, limiting the lake with a northern canyon continuously fed by seeping lake water at the base of the dam (Aka et al. 2008; Aka this monograph). After the event, the lake level had dropped by ~1 m implying a loss of water volume of ~1.8×10^6 m^3. The gas

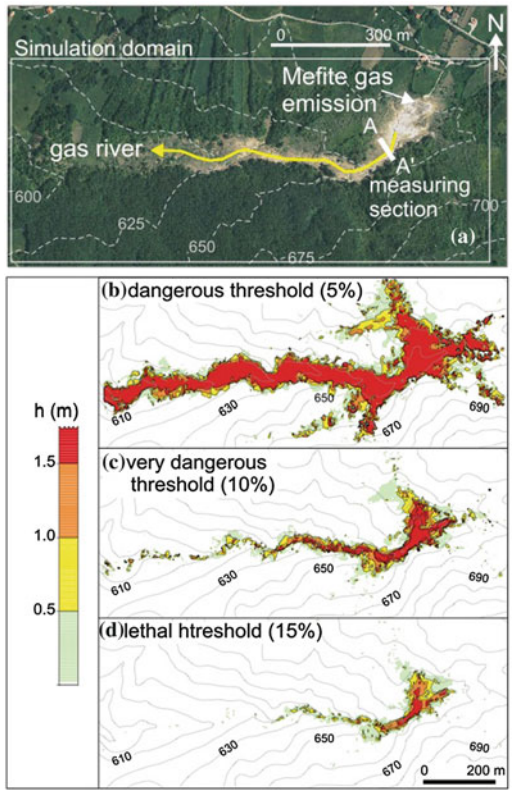

Fig. 4 Aerial photograph of the Mefite gas emission and the associated gas river (**a**). Maximum elevation of selected CO_2 thresholds (**b**–**d**) simulated by Chiodini et al. (2010a) using TWODEE-2 code. After Chiodini et al. (2010a)

cloud was estimated to have travelled distances of between 10 km (Tuttle et al. 1987; Kling et al. 1987) and 20 km (Le Guern et al. 1992) north of the lake. These estimations are consistent with the fact that deaths in humans and cattle occurred for at least 15 km along two main valleys towards the north (Baxter and Kapila 1989). A concentration of CO_2 of at least 10–15 % is sufficient to send people rapidly unconscious and over 30 % to kill them (Baxter and Kapila 1989). The head of the flowing cloud probably maintained high concentrations of CO_2 because it would have been continuously recharged from the faster moving tail of the cloud. This characteristic could explain the lethality of the cloud to greater than expected distances. It is yet not well established how fast the cloud moved, as the event occurred in the evening. Most people were going to bed and lost consciousness very rapidly (Baxter and Kapila 1989). The vegetation around Lake Nyos could have slowed down the cloud, or have formed stagnant ponds of higher CO_2 concentrations in enclosed spaces. Plants appeared unaffected after the event. The area impacted by the gas cloud was about 29 km^2.

In lake overturn models, the critical amplitude of the vertical water movement necessary to initiate degassing has to be defined (Mott and Woods 2010). No particular trigger mechanism is generally accepted and several trigger scenarios have been proposed: (1) an internal wave (by wind stress or a travelling internal pressure field), (2) a seismic shock, though not evidenced, (3) a landslide into the lake, (4) a strong wind shift, (5) slight cooling of the surface water combined with a seasonal wind shift, (6) a minor volcanic eruption. However, it is accepted that any disturbance of the metastable system, or a combination of the above mechanisms could have been responsible to trigger the Lake Nyos gas burst. It is worth noting that 2 years earlier a similar but smaller gas burst took place at Lake Monoun (~100 km S-SE of Lake Nyos) on 15 August 1984 (Kusakabe et al. 2000; Kusakabe this issue). From other limnological research in the area it appears that August-September is the time of minimum stability of some Cameroon lakes, the period when the anoxic bottom waters favour to mix with the surface waters (Kling 1987). The weakened stratification of Lake Monoun and Nyos was probably due to the lower mean air temperatures and effective insolation, and distinctly wetter summers in 1984–1986, resulting in cooler denser surface waters, favouring lake overturn (Kling 1987). During this timeframe when the lake was vulnerable to overturn, bottom waters probably did not need to be supersaturated with CO_2 to have caused the eruption. Assuming conditions of supersaturation a maximum volume of released CO_2 of 1 km^3 was estimated.

The degassing pipe installed in Lake Nyos in 2001 has facilitated controlled venting of CO_2 to the atmosphere (e.g. Kling et al. 2005; Kusakabe this monograph). However, breakthrough of the northern dam could cause a sudden drop in lake level by 40 m, followed by decompression and

inevitably a new gas burst (Aka and Yokoyama 2012). The released water mass (10^8 m^3) would flow down as a lahar into the northern canyon, directed to Nigeria, 100 km further downstream. Although not as eminent and alarming as previously thought (Aka and Yokoyama 2012), such a dam break event may possibly have severe socio-political implications.

Here we describe simulations obtained using the TWODEE-2 code to reproduce the gas cloud dispersion from Lake Nyos over the surroundings area on 21 August 1986, constraining the model with all available semi-quantitative observations and previous estimations of the gas source conditions. The obtained results highlight the potential of codes like TWODEE-2 of investigating the impact of different degassing scenarios in order to mitigate the associated gas hazard.

3.3 Input Data

3.3.1 Gas Source

Simulation results are strongly affected by the total amount of gas released and by the duration of the event. The total amount of CO_2 released in the event was estimated from 0.15 to 1 km^3, while the duration of the gas emission from 2 to 4 h (Tuttle et al. 1987; Kanari 1989; Evans et al. 1994). Chiodini et al. (2010b) considered four different scenarios in order to cover this wide range of CO_2 fluxes. Scenario I is based on Evans et al. (1994) results. It consists of a total volume release of CO_2 of 0.15 km^3 (0.29 Gg in mass) for a duration of about 2 h emitted with a constant rate of 4.3×10^5 kg $m^{-2}d^{-1}$ from a square cell of 90 m × 90 m. Scenario II is based on the work of Kanari (1989) assuming a total volume release of CO_2 of 0.68 km^3 (1.33 Gg in mass) for a duration of about 4 h emitted with a constant rate of 1.4×10^5 kg $m^{-2}d^{-1}$ from a square cell of 235 m × 235 m. Senarios III and IV are both based on the study of Tuttle et al. (1987) considering a total volume release of CO_2 of 1 km^3 (1.95 Gg in mass) released from a square cell of 235 m × 235 m in about 2 h (with a rate of 4.2×10^5 kg $m^{-2}d^{-1}$) for Scenario III and in 4 h (at a rate of 1.7×10^5 kg $m^{-2}d^{-1}$) for Scenario IV. Total gas volume and mass, gas fluxes, event duration and references of each scenario are summarized in the Table 1.

3.3.2 Digital Elevation Model and Land Use

For the four scenarios considered in Table 1 the 90 m × 90 m SRTM DEM (Jarvis et al. 2008), available at http://srtm.csi.cgiar.org, was used for the entire computational domain (Fig. 5). Another information needed by the model is the roughness length z_0. In principle such information could be provided at each point of the computational grid considering different land use properties of the domain. However, considering all other sources of uncertainties to be more relevant, simulations were performed assuming an average value of z_0 = 0.1 m which corresponds to terrain covered by low crops with occasional large obstacles.

For all four scenarios the topography was interpolated at a resolution of 50 m × 50 m that

Table 1 Definition of the scenarios considered by Chiodini et al. (2010b)

Scenario	Gas ejection duration (hour)	Gas volume (km^3)	Gas mass (Gg)	Gas mass flux (10^5 × kg $m^{-2}d^{-1}$)	Gas source extension (m × m)	References
I	2	0.15	0.29	4.3	90 × 90	Evans et al. (1994)
II	4	0.68	1.33	1.4	235 × 235	Kanari (1989)
III	2	1	1.95	4.2	235 × 235	Tuttle et al. (1987)
IV	4	1	1.95	1.7	235 × 235	Tuttle et al. (1987)

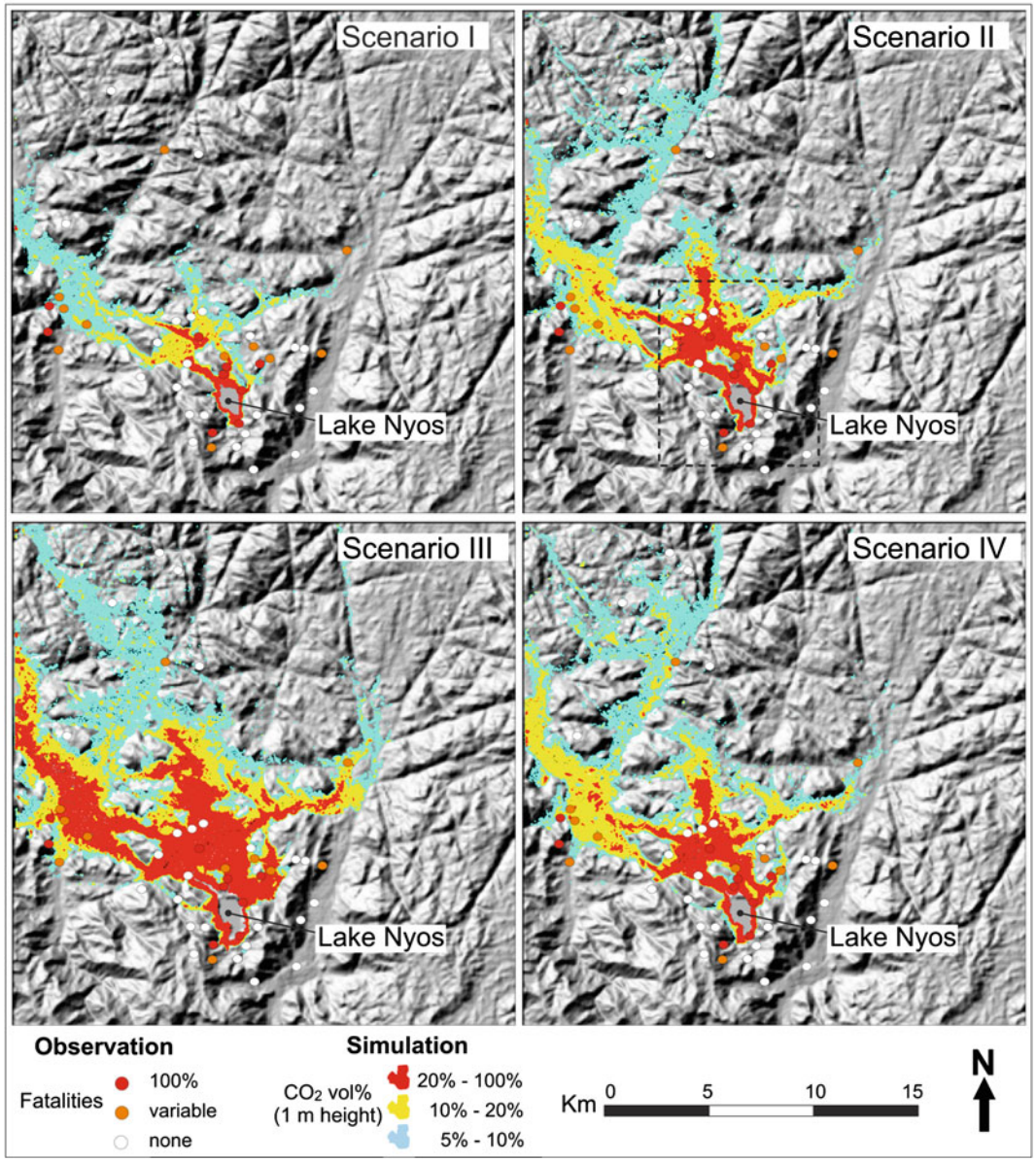

Fig. 5 Maximum CO_2 concentration reached at 1 m height at any location during the simulations for the four considered scenarios for the August 1986 limnic gas burst of Lake Nyos. Total gas volume and mass, gas fluxes, event duration and references of each scenario are summarized in the Table 1

was used as computational grid spacing for the simulations. Furthermore scenario II, that appeared to be the more realistic, was run at higher resolution (50 m × 50 m) using a more detailed DEM has been derived from the topographic map (20 m × 20 m) and a finer computational grid spacing on a sub-region of the larger domain (Fig. 6).

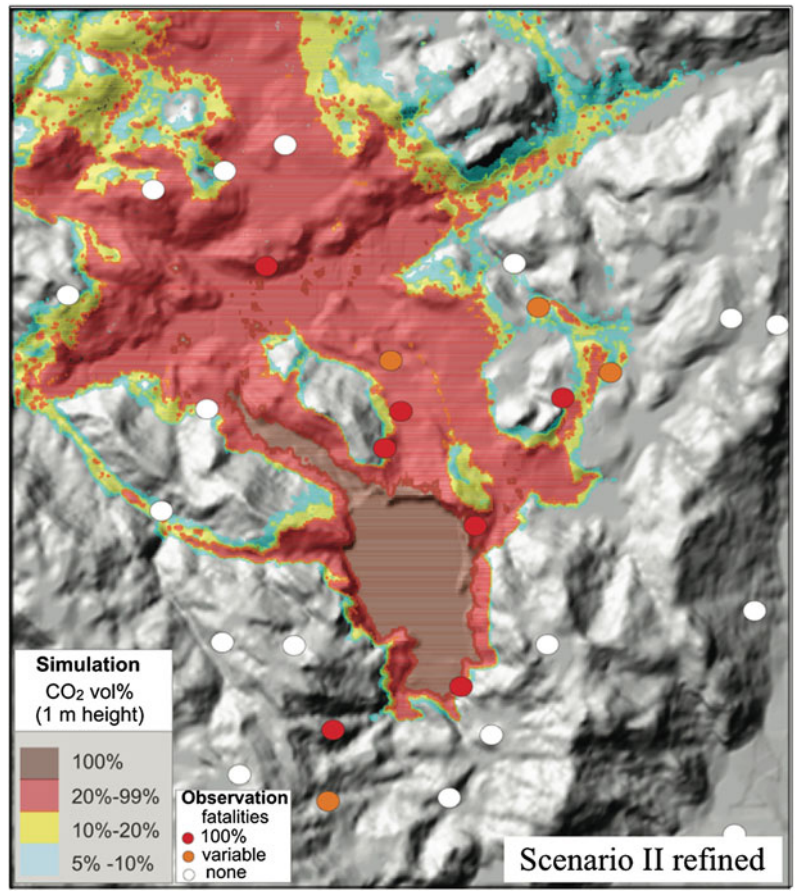

Fig. 6 Maximum CO_2 concentration at 1 m height for the area enclosed by the *dashed line* in Fig. 5 for the Scenario II (flux from Kanari 1989) obtained performing the simulation with a refined DEM

3.3.3 Wind

Concerning the wind field, there are no wind measurements available at Lake Nyos during the degassing event of 21 August 1986. Only qualitative eyewitness descriptions report very low wind conditions. It is worth nothing that, although for wind of ~10 m/s dispersion patterns are not strongly affected by terrain features, for low wind conditions, i.e. ~1 m/s or less, impacted areas are substantially affected by local topography (Hankin 2004a, b).

As input for TWODEE2 simulations surface wind data from the NCEP/NCAR Reanalysis-1 database (Kalnay et al. 1996), covering the entire globe with a relatively coarse mesh (2.5° × 2.5°) 4-times daily, were used. As a reference wind value the closest point of the global reanalysis mesh (lat = 5; lon = 10) at 18:00 UTC of 21 August 1986, having wind components of V_x = −0.5 m/s and V_y = 0.8 ms at 10 m height, was used. Obviously the actual wind field could be different from this reference value. A better approach, object of ongoing studies, consists of reconstructing the local wind field on a refined grid for the duration of the gas cloud dispersion using a mesoscale meteorological model initialized using the high resolution meteorological reanalysis data of the region (e.g., ECMWF ERA-interim reanalysis available at http://apps.ecmwf.int/datasets/data/interim_full_daily).

4 Results

In Fig. 5 we show the maximum CO_2 concentrations reached at 1 m height for the four scenarios considered by Chiodini et al. (2010b). We used three different colours to highlight the areas where the maximum simulated concentration exceeded 20 % in volume (in red), was between

10 and 20 % (in yellow), and between 5 and 10 % (in cyan). Even the lowest concentration limit can cause death if exposure is over an extended period of time (National Institute of Occupational Safety and Health 1997) that is likely as most of people were sleeping. Comparison of maximum gas concentration maps with the locations where fatalities occurred (Le Guern et al. 1992) shows a qualitative agreement. However, in order to avoid providing a wrong sense of precision, we need to keep in mind the limitations associated with the definition of the locations and numbers of dead reported in Figs. 5 and 6 after Le Guern et al. (1992). In fact many humans were probably rapidly buried before outsiders got there and the cows were clearly not counted although they were more reliable indicators of where the fatal concentrations were (Baxter and Kapila 1989). In general the scenarios that better fit the observations are those, which involve the highest CO_2 releases (0.68–1 km^3, scenarios II, III, IV). A poor description of the local wind field is likely to be the reason why any simulation seems producing high concentrations in the localities southern than Lake Nyos where some fatalities occurred. As a higher DEM resolution improve the accuracy in delimiting area reached by lethal concentrations can be seen in Fig. 6 that reports the maps of maximum CO_2 concentration at 1 m height obtained performing the simulation with a refined DEM for the area enclosed by the dashed line in Fig. 5 for the Scenario II (flux from Kanari 1989). Channelling of gas into the valleys is also highlighted

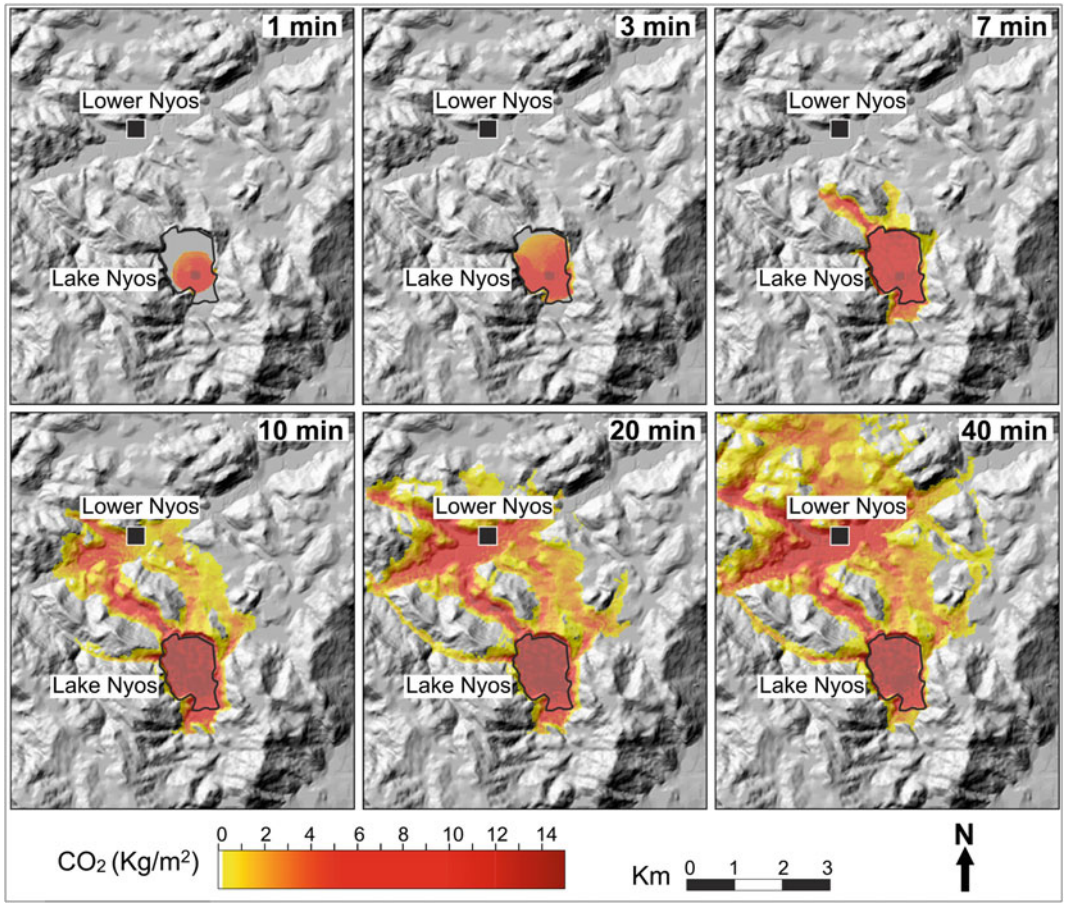

Fig. 7 Temporal evolution of the cloud dispersion over the topography around Lake Nyos

from Fig. 7 that shows the temporal evolution of the CO_2 cloud. The simulation was performed assuming the scenario II-refined (Kanari 1989) as the reference. In particular snapshots of CO_2 load (kg/m^2) during the first 40 min of the event were reported. From the simulations it is clear that the dispersion process was rapid and strongly controlled by the topography. Results indicate that CO_2 cloud reached the village of Lower Nyos, where ~1,000 fatalities occurred, in about 10 min.

4.1 Towards a Probabilistic Hazard Map for Nyos-Type Lakes

Results of our preliminary study reproducing the dispersion of the gas cloud at Nyos show that such a modelling approach can become useful to create hazards maps for lakes like Nyos, where the potential for a limnic eruption is not negligible (e.g., Lake Albano, Italy). Considering a statistical set of the main input parameters (e.g., source position, gas flux, DEM and wind) probabilistic hazard map scan be obtained from the simulations of distribution and evolution of critical gas concentrations in the area of interest which account for uncertainty and natural variability associated to the controlling quantities, such as seasonal and daily wind variability, and plausible gas flux values (e.g., up to the maximum value corresponding to the saturation for the lake volume and depth).The performance of the shallow-layer approach, representing a good compromise between a full description of the involved physics and the need to decrease the computational requests, allows one to produce such maps even in a modern powerful PC, and for the situations the gas flux is monitored and measured, to produce forecast of gas concentrations in the area of interest.

5 Conclusion

Limnic eruptions, like the event of August 1986 at Lake Nyos, Cameroon, can release in the atmospheric surface layer huge amounts of CO_2 able to suffocate wildlife, livestock and humans. Here we presented a computational method used to simulate the dispersion of dense CO_2 clouds and assess the associated gas hazard. The approach is based on shallow layer equations. We reviewed the applications of such an approach to hazard assessment of gas accumulations generated by persistent CO_2 emissions in Italy. Then we described the results obtained from simulations of the CO_2 air dispersion from the gas driven lake eruption of the 21 August 1986 at Nyos. The simulations regarded various scenarios different for the total amount of the gas released and for the duration of the event. A strong effect of the topography is evident in any application: the gas flows along the different valleys following the complex topography of the area. The scenarios involving large amount of gas are those that better reproduce the observations, as in this case the simulations reproduce lethal CO_2 concentrations in most of the sites where fatalities did occur. The approach resulted a useful tool to evaluate gas hazard both for persistent gas emission and for the most hazardous gas driven limnic eruptions.

Acknowledgments The authors are grateful to Dmitri Rouwet for discussion and comments on an earlier version of the manuscript. We thank two anonymous reviewers for their comments that improved the quality of the paper.

References

Aka FT (this monograph) Depth of melt segregation below the Nyos maar-diatreme volcano (Cameroon, West Africa): major-trace element evidence and their bearing on the origin of CO_2 in Lake Nyos

Aka FT, Yokoyama T, Kusakabe M, Nakamura E, Tanyileke G, Ateba B, Ngako V, Nnange J, Hell J (2008) U-series dating of Lake Nyos maar basalts, Cameroon (West Africa): implications for potential hazards on the Lake Nyos dam. J Volcanol Geotherm Res 176:212–224. doi:10.1016/j.jvolgeores.2008.04.009

Aka FT, Yokoyama T (2012) Current status of the debate about the age of Lake Nyos dam (Cameroon) and its bearing on potential flood hazards. Nat Hazards 65:875–885. doi:10.1007/s11069-012-0401-4

Baxter PJ, Kapila M (1989) Acute health impact of the gas release at Lake Nyos. Cameroon 1986. In: Le

Guern F, Sigvaldason G (eds) The Lake Nyos event and natural CO_2 degassing. J Volcanol Geotherm Res 39:265–275

Britter RE (1989) Atmospheric dispersion of dense gases. Annu Rev Fluid Mech 2:317–344

Chiodini G, Cardellini C, Amato A, Boschi E, Caliro S, Frondini F, Ventura G (2004) Carbon dioxide Earth degassing and seismogenesis in central and southern Italy. Geophys Res Lett 31(7). doi:L0761510.1029/2004GL019480

Chiodini G, Valenza M, Cardellini C, Frigeri A (2008) A new web-based catalog of earth degassing sites in Italy. EOS Trans AGU 89(37):341–342

Chiodini G, Granieri D, Avino R, Caliro S, Costa A, Minopoli C, Vilardo G (2010a) Non-volcanic CO_2 Earth degassing: case of Mefite d'Ansanto (Southern Apennines), Italy. Geophys Res Lett 37:L11303. doi:10.1029/2010GL042858

Chiodini G, Costa A, Rouwet D, Tassi F (2010b) Modeling CO_2 air dispersion from gas driven lake eruptions. Abstract V23A-2384, AGU Fall Meeting

Costa A, Macedonio G, Chiodini G (2005) Numerical model of gas dispersion emitted from volcanic sources. Annu Geophys 48(4/5):805–815

Costa A, Chiodini G, Granieri D, Folch A, Hankin RKS, Caliro S, Avino R, Cardellini C (2008) A shallow-layer model for heavy gas dispersion from natural sources: application and hazard assessment at Caldara di Manziana, Italy. Geochem Geophys Geosyst 9: Q03002. doi:10.1029/2007GC001762

Douglas S, Kessler R (1990) User's manual for the diagnostic wind model. In: Carr L (ed) User's guide for the urban airshed model, vol 3. EPA-450/4-90-007C, San Rafael, CA

Evans WC, White LD, Tuttle ML, Kling GW, Tanyileke G, Michel RL (1994) Six years of change at Lake Nyos, Cameroon, yield clues to the past and cautions for the future. Geochem J 28:139–162

Folch A, Costa A, Hankin RKS (2009) A shallow layer model for dense gas dispersion on complex topography. Comput Geosci 35:667–674. doi:10.1016/j.cageo.2007.12.017

Giggenbach WF (1992) Water and gas chemistry of Lake Nyos and its bearing on the eruptive process. J Volcanol Geotherm Res 42:337–362

Granieri D, Costa A, Macedonio G, Chiodini G, Bisson M (2013) Carbon dioxide in the city of Naples: contribution and effects of the volcanic source. J Volcanol Geotherm Res (in press)

Hankin RKS, Britter RE (1999a) TWODEE: the health and safety laboratory's shallow layer model for heavy gas dispersion. Part 1. Mathematical basis and physical assumptions. J Hazard Mater A66:211–226

Hankin RKS, Britter RE (1999b) TWODEE: the health and safety laboratory's shallow layer model for heavy gas dispersion. Part 2. Outline and validation of the computational scheme. J Hazard Mater A66:227–237

Hankin RKS, Britter RE (1999c) TWODEE: the health and safety laboratory's shallow layer model for heavy gas dispersion. Part 3. Experimental validation (Thorney island). J Hazard Mater A66:239–261

Hankin RKS (2004a) Major hazard risk assessment over non-flat terrain. Part I: continuous releases. Atmos Environ 28:695–705

Hankin RKS (2004b) Major Hazard risk assessment over non-flat terrain. Part II: instantaneous releases. Atmos Environ 28:707–714

Jacobson M (1999) Fundamentals of atmospheric modelling, 1st edn. Cambridge University Press, New York

Jarvis A, Reuter HI, Nelson A, Guevara E (2008) Hole-filled seamless SRTM data V4. International centre for tropical agriculture (CIAT). Available from http://srtm.csi.cgiar.org

Kalnay E, Kanamitsu M, Kister R, Collins W, Deaven D, Gandin L, Iredell M, Saha SGW, Woollen J, Zhu Y, Chelliah M, Ebisuzaki M, Higgins W, Janowiak J, Mo K, Ropelewski, C, Wang J, Leetmaa A, Reynolds R, Jenne R, Joseph D (1996) The NCEP/NCAR 40-years reanalysis project. Bull Am Meteorol Soc 77:437–470. Data available at http://www.cdc.noaa.gov/cdc/reanalysis/

Kanari S (1989) An inference on process of gas outburst from Lake Nyos, Cameroon. J VolcanolGeotherm Res 39:135–149

Kling GW (1987) Seasonal mixing and catastrophic degassing of tropical lakes, Cameroon, West Africa. Science 237:1022–1024

Kling GW, Evans WC, Tanyileke GZ (this monograph) The comparative limnology of Lakes Nyos and Monoun, Cameroon

Kling GW, Clark MA, Compton HR, Devine JD, Evans WC, Humphrey AM, Koenigsberg EJ, Lockwood JP, Tuttle ML, Wagner GN (1987) The 1986 Lake Nyos gas disaster in Cameroon, West Africa. Science 236:169–175

Kling GW, Evans WC, Tanyileke G, Kusakabe M, Ohba T, Yoshida Y, Hell JV (2005) Degassing Lakes Nyos and Monoun: defusing certain disaster. Proc Natl Acad Sci 102(40):14158–14190

Kusakabe M (this monograph) Evolution of CO_2 content in Lakes Nyos and Monoun, and sub-lacustrine CO_2-recharge system at Lake Nyos as envisaged from C/^{3}He ratios in noble gas signatures

Kusakabe M, Ohba T, Issa, Yoshida Y, Satake H, Ohizumi T, Evans WC, Tanyileke G, Kling GW (2008) Evolution of CO_2 in Lakes Monoun and Nyos, Cameroon, before and during controlled degassing. Geochem J 42:93–118

Kusakabe M, Tanyileke G, McCord SA, Schladow SG (2000) Recent pH and CO_2 profiles at Lakes Nyos and Monoun, Cameroon: implications for the degassing strategy and its numerical simulation. J Volcanol Geotherm Res 97:241–260

Le Guern F, Shanklin E, Teboff S (1992) Witness accounts of the catastrophic event of August 1986 at

Lake Nyos (Cameroon). J Volcanol Geotherm Res 51:171–184

Mott RW, Woods AW (2010) A model of overturn of CO_2 laden lakes triggered by bottom mixing. J Volcanol Geotherm Res 192:151–158. doi:10.1016/j.jvolgeores.2010.02.009

National Institute of Occupational Safety and Health (NIOSH) (1997) Pocket guide to chemical hazard, Rep. 97-140, Washington, DC

Pierret RXF, Berne P, Roussel C, Le Guern F (1992) The Lake Nyos disaster: model calculations for the flow of carbon dioxide. J Volcanol Geotherm Res 51:161–170

Rice A (2000) Rollover in volcanic crater lakes: a possible cause for Lake Nyos type disasters. J Volcanol Geotherm Res 97:233–239

Simpson JE (1997) Gravity currents in the environment and the laboratory, 2nd edn. Cambridge University Press, Cambridge

Tuttle ML, Clark MA, Compton HR, Devine JD, Evans WC, Humphrey AM, Kling GW, Koenigsberg EJ, Lockwood JP, Wagner GN (1987) The 21 August (1986) Lake Nyos gas disaster, Cameroon. US Geol Surv Open-File Rept 87-97, 58 p

Venetsanos A, Bartzis J, Wurtz J, Papailiou D (2003) DISPLAY-2: a two-dimensional shallow layer model for dense gas dispersion including complex features. J Hazard Mater A99:111–144

Zalesak ST (1979) Fully multidimensional flux-corrected transport algorithms for fluids. J Comput Phys 31:335–362

Zhang Y (1996) Dynamics of CO_2-driven lake eruptions. Nature 379:57–59

Zhang Y, Kling GW (2006) Dynamics of lake eruptions and possible ocean eruptions. Annu Rev Earth Planet Sci 34:32–293

Depth of Melt Segregation Below the Nyos Maar-Diatreme Volcano (Cameroon, West Africa): Major-Trace Element Evidence and Their Bearing on the Origin of CO_2 in Lake Nyos

Festus Tongwa Aka

Abstract

The Nyos maar-diatreme volcano on the Oku Volcanic Group (OVG) in NW Cameroon carries yet the most infamous maar lake in the world because the lake exploded in 1986 releasing CO_2 that killed ~1,750 people and over 3,000 livestock. A process of safely getting rid of accumulated gas from the lake started in 2001. Even though ~33 % of it has been removed, gas continues to seep into the lake from the mantle, so the lake still poses a thread. Available data on basaltic lava from the maar-diatreme volcano and other volcanoes of the OVG are used here to determine the depth and location where the magmas are produced, and to make inferences on the generation of CO_2 in the Nyos mantle. Fractionation-corrected major element data agree well with experimental data on mantle peridotite and suggest that Lake Nyos magmas formed at pressures of 2–3 GPa in the garnet stability field. This inference is corroborated by trace element models that indicate small degree (1–2 %) partial melting in the presence of residual garnet (2–3 %). The basalts have elevated High Field Strength Element (HFSE) ratios (Zr/Hf = 48.5 ± 1.2 and Ti/Eu = 5,606 ± 224) which cannot be explained by any reasonable fractional crystallization model. A viable mechanism would be melting of a mantle that was previously spiked by percolating carbonatitic melts. It is suggested that small degree partial melting of this metasomatised mantle produces the lavas with super chondritic HFSE ratios, and is generating the CO_2 that seeps into and accumulates in the lake, and which asphyxiated people and animals during the 1986 gas disaster. This finding requires that current efforts to degas Lake

F.T. Aka (✉)
Institute of Geological and Mining Research (IRGM), P.O. Box 4110, Yaoundé, Cameroon
e-mail: akatongwa@yahoo.com

F.T. Aka
Division of Scientific Policy and Planning (DPSP), Ministry of Scientific Research and Innovation (MINRESI), P.O. Box 1457, Yaoundé, Cameroon

D. Rouwet et al. (eds.), *Volcanic Lakes*, Advances in Volcanology,
DOI 10.1007/978-3-642-36833-2_21,
© Springer-Verlag Berlin Heidelberg 2015

Nyos should take into account the fact that CO_2 will continue to seep into the lake for a yet undetermined but long time in the future. A viable solution would be to avoid renewed stratification of the lake, by (somehow) safely and permanently bringing bottom gas-charged waters to the surface to release gas, even after the gas currently stocked in the lake has been completely removed.

Keywords
Lake Nyos maar · Oku volcanic group (OVG) · Mantle · Carbonatitic metasomatism · Depth and degree of melting · Carbon dioxide · Crystal fractionation

1 Introduction

Monogenetic maar-diatreme volcanism is the second most important type of volcanism on continents and islands, after intermediate, basic and ultrabasic scoria cones (Lorenz 1985, 1986; Wohletz and Heiken 1992). Amongst other places, it has been described in the following fields that are young and have similar life-spans: the Campo de Calatrava volcanic field in Spain (Martín-Serrano et al. 2009), the Eifel volcanic field of Germany (Lorenz 2003), the Massif Central Region in France (Camus et al. 1973), the Colli Albani Volcanic District in Italy (Sottili et al. 2009), the Auckland volcanic field in New Zealand (Németh et al. 2012), the Newer Volcanic Province of Southeastern Australia (Price et al. 2003), the Kamchatka Peninsula in Russia (Belousov 2005), maars in the Ventura and Santa Domingo volcanic fields of Mexico (Aranda-Gómez et al. 1992; Aranda-Gómez and Luhr 1996; Pier et al. 1992), the Cameroon Volcanic Line (CVL) in West Central Africa (Lockwood and Rubin 1989), and in some other volcanic environments. Maar-diatreme volcanoes form when magma interacts explosively on its approach to the Earth's surface with ground water (phreatomagmatism) leading to brittle fragmentation of the magma and the surrounding country rocks (Lorenz 1986; Zimanoswski 1998; White and Ross 2011; Morrissey and Rouwet, this issue). They typically consist of a feeder dyke, a root zone, the crater, and the surrounding tephra rings (White and Ross 2011). The thermohydraulic explosions result in deeply incised craters (maars). Some of these may remain dry as in the Pali Aike volcanic field (Mazzarini and D'Orazio 2003; Haller and Németh 2006), the Crater Elegante and Joya Honda in Mexico (Martin and Németh 2006; Aranda-Gómez and Luhr 1996). Some may be subsequently filled with surface, mineral and/or CO_2-rich spring water to form maar lakes as in Potrok Aike, Argentina (Gebhardt et al. 2011, 2012), Eifel (Schmincke 2007), Nyos and Monoun on the CVL (Sigurdsson et al. 1987; Lockwood and Rubin 1989). Still others may be filled with lava as La Brena in Mexico (Aranda-Gómez et al. 1992; Pier et al. 1992).

Until the last three decades or so, research on volcanic hazards like tephra falls, pyroclastic flows and surges, lahars, earthquakes, lava flows, ballistic projectiles, and volcanic gases associated with explosive (e.g., phreatomagmatic) volcanism (Blong 1984; Lorenz 2007) made little or no mention of catastrophic lethal release of CO_2 accumulated in monogenetic maar crater lakes. However, in 1979, 142 people were killed by CO_2 that resulted from a phreatic eruption at Dieng volcano in Indonesia (Allard et al. 1989). Release of CO_2 from maar Lakes Monoun (1984) and Nyos (1986) asphyxiated about 1,750 people and over 3,000 livestock in the western Cameroon highlands (Sigurdsson et al. 1987; Le Guern and Sigvaldason 1989). These two lakes are located along the CVL (Fig. 1). It has been suggested that, as in Lakes Nyos and Monoun, the destruction of all animal life found in borings

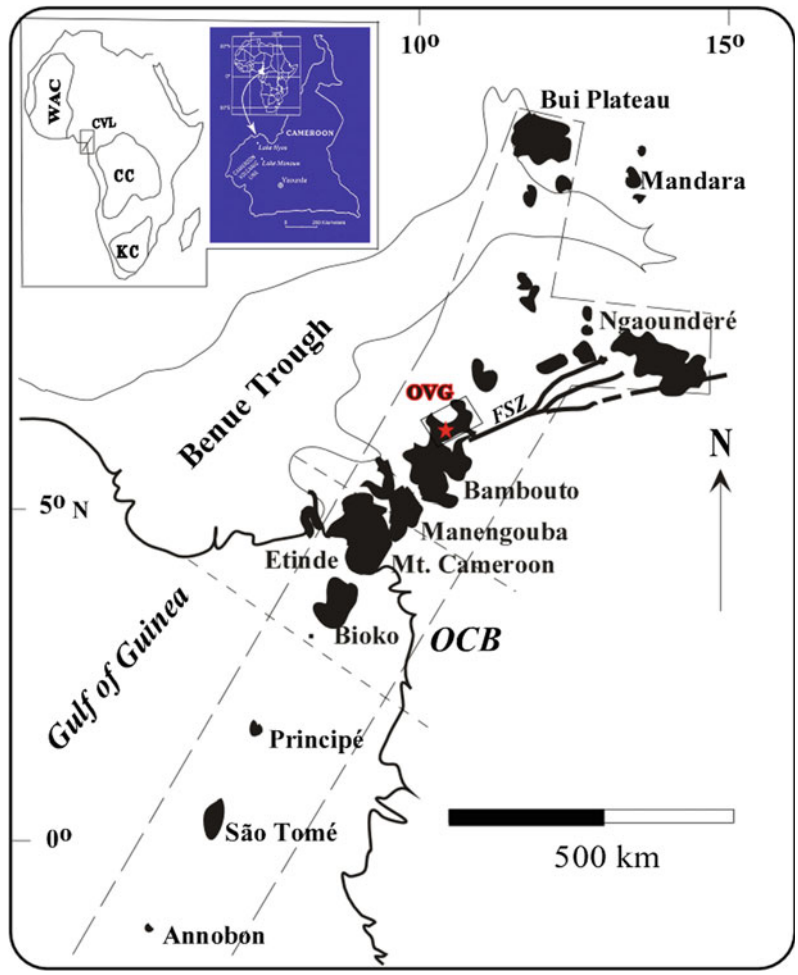

Fig. 1 Map showing the Cameroon Volcanic Line (CVL) with the location of Lake Nyos (*red star*) in the Oku Volcanic Group (OVG —box). *Insets* show Cameroon and the CVL within the main tectonic units of Africa (*WAC* West African craton; *CC* Congo craton; *KC* Kalahari craton; *FSZ* Foumban shear zone; *OCB* Ocean Continent Boundary)

and paleontological digs in a paleo-maar at Sénèze (French Massif Central) might have resulted from asphyxiation by CO_2 released from the maar (Couthures 1989). Lake Kivu in East Africa has been found to contain huge, dominantly methane gas concentrations (Tietze 1980; Lorke et al. 2004; Vaselli et al., this issue). Apart from Nyos and Monoun in Cameroon, and Dieng in Indonesia, Hule and Río Cuarto in Costa Rica (Tassi et al. 2009; Alvarado et al. 2011) are the only other maar lakes that we are aware of from where emanating gas has asphyxiated animals. In addition therefore to its role in unraveling natural resources like diamond (kimberlite pipes) and in bringing up mantle xenoliths that provide snapshots of the lithospheric mantle, and thus the evolution of the Earth at the time of their eruption (Pearson et al. 2003), it is seen that like in the above cases, monogenetic maar–diatreme volcanism set the stage for previously unrecognized secondary volcanic hazards. Occurrence of the Lake Nyos event has sparked investigations of the risk of similar catastrophic degassing from lakes in France (Aeschbach-Hertig et al. 1999), Germany (Camus et al. 1993; Aeschbach-Hertig et al. 1996), Costa Rica (Tassi et al. 2009; Alvarado et al. 2011), Southwest Cameroon (Lake Barombi Mbo, Cornen et al. 1992), and other places.

Geochemical monitoring of Lake Nyos shows that the bottom CO_2 content has increased steadily while the mid-depth content has remained almost constant (Kusakabe et al. 2008; Kusakabe, this issue). This is interpreted (Kusakabe personal

communication) as indirect evidence that the CO_2-rich fluid is added (underplated below the deep chemocline) from below the lake. Recent lake noble gas data suggest that the fluid may be supplied at about 190 m depth (the lake is 210 m deep) at the edge of the diatreme where the highest helium concentration was observed (Nagao et al. 2010). Note that the lake bottom is covered by sediments, the low permeability of which may restrict any direct inflow of the fluid. Helium and carbon isotopic studies show that the CO_2 that enters Lake Nyos from below is magmatic (Kusakabe et al. 2008; Nagao et al. 2010). Unlike in typical temperate lakes where mixing of the epilimnion and hypolimnion occurs during the year (Walther 2005), deep equatorial lakes like Monoun and Nyos do not mix seasonally (Kling 1988). The CO_2 that enters Lake Nyos from below therefore stagnates and can be released catastrophically as in 1986.

Attention has so far been focused mainly on artificially getting rid of the gas from the lake in order to preempt another catastrophe (see below). A magmatic origin for the CO_2 means that it comes from the Lake Nyos mantle, so it must have a genetic relationship with the petrogenetic processes generating magma below the volcano. The most that isotopic studies of the gas itself can do is say whether it is magmatic or not. The question arises as to whether a study of the solid products like scoria, lava, xenoliths and the fluids trapped in them, of these petrogenetic processes, may hold further clues on (i) why the mantle below Lake Nyos is so rich in CO_2, (ii) the relationship between magmatic volatiles trapped in the solid products and phreatomagmatic fragmentation. Fortunately, the phreatomagmatic process that formed Lake Nyos was interspaced with magmatic phases materialized on the field by lava flows, scoria, and base surge deposits (Fig. 2a–c) thus offering an opportunity to address the above questions.

Here, we first make a brief review of the current state of knowledge on hazards around Lakes Monoun and Nyos. Data compiled on the major and trace elements previously analyzed in the lavas of the Lake Nyos maar and other volcanoes of the Oku Volcanic Group (OVG) are then screened for alteration, crustal contamination and fractionation effects, before being used to probe the Nyos mantle for depth and location of melting, degree of melting, its mineralogy, and its enrichment process. Implications of this on the origin of CO_2 in the lake and on the current degassing process are discussed.

2 Regional Context

The Lake Nyos maar-diatreme volcano is located within the OVG in northwestern Cameroon, West Central Africa. It is found in the northeastern corner of the ~700 km-long continental sector of the CVL (Fig. 1). The OVG lies within the Bamenda-Wum-Nkambe- Ndu-Oku range. Mount Oku is the highest peak on this range (3,011 m a.s.l.). Mount Cameroon is the only currently active member (Suh et al. 2003; Yokoyama et al. 2007; Favalli et al. 2011; Mathieu et al. 2011) of the 12 volcanic centers that constitute the 1,600 km-long CVL from the South Atlantic basin island of Annobon and seamounts in the Gulf of Guinea, to continental Africa (Fitton 1987; Lee et al. 1994; Marzoli et al. 2000; Aka et al. 2001a, 2004; Rankenburg et al. 2005). The OVG experienced both silicic and basic volcanism that has yielded ages from 31–12.5 Ma (Kamgang et al. 2007 and Refs. therein). The most recent volcanic activity in the group must have been explosive as shown by little- weathered cinder/scoria cones, and phreatomagmatic explosion craters of Lakes Oku, Elum, Nyi, Wum, Enep and Nyos, all of which cut through Pre-Cambrian (Pan African) basement complex (Freeth and Rex 2000). Lake Nyos occupies a maximum area of $\sim 1.58 \times 10^6$ m^2, is 210 m deep, with a maximum volume of 1.794×10^8 m^3 (Kling et al. 2005). Both Lakes Nyos and Monoun lie near the Foumban shear zone (Fig. 1), a NE-SW trending fault complex that is seismically active (Tabot et al. 1992). Details about the geology of Lake Nyos can be found in Schenker and Dietrich (1986), Lockwood et al. (1988) and Freeth and Rex (2000).

Fig. 2 **a** Section of the eastern wall of Lake Nyos forming products—scoria, lava and surge deposits lying on basement granite. The lava (**b**) and surge (**c**) contain abundant mantle xenoliths (1) mantled by juvenile host basalts (2) contaminated by crustal fragments (*whitish parts* in 2), sometimes all embedded in the surge (3). **d** CO_2 monitoring station. **e** Lake Nyos degassing pipes (viewed from south) installed in 2001, 2010 and 2012. **f** Northern end of Lake Nyos showing the natural dam (*outlined*). **g** Pot holes and cracks that lither the spillway on the dam. The man in the hole is 1.63 m tall. **h** Downstream face of the dam showing front of back erosion (erosion from outside of the lake) of surge material lying on basement granite. **i** Giant blocks (*outlined*) that fall from the downstream face of the dam

3 Hazards Associated with Lakes Nyos and Monoun

Lake Monoun was the site of a catastrophic gas explosion in 1984, which killed 37 people. Two years after, in August 1986, Lake Nyos also exploded releasing $\sim 3 \times 10^6$ m^3 CO_2 that asphyxiated $\sim$1,750 people and over 3,000 cattle. Lake monitoring studies (Kusakabe et al. 2000; Halbwachs et al. 2004; Kling et al. 2005) showed that the killer gas in both lakes was magmatic CO_2, and that gas concentrations in them were increasing, thus increasing the potential for other gas releases. To preempt similar catastrophes, the Government of Cameroon created the Nyos-Monoun Degassing Project (NMDP) with an international scientific committee, for degassing the lakes and general hazard mitigation around them. The two main goals of NMDP are to install a continuously operating CO_2 monitoring system near populated areas close to the each lake, and to install pipes in the lakes that will safely siphon gas-rich bottom waters to the surface thus liberating the CO_2 from lake bottom to the atmosphere (Kusakabe, this issue). Carbon dioxide is denser than air and turns to hug the ground level.

Carbon dioxide early warning systems were installed at both lakes. The stations contain infrared CO_2 detectors that continuously monitor CO_2 concentrations in the atmosphere (Fig. 2d). Air contains $\sim$0.03 % CO_2. When its concentration reaches $\sim$5 %, it will extinguish a flame and is dangerous to both animals and people. The warning system sounds a siren when the CO_2 concentration in the air reaches 0.5 %, i.e. $\sim$10 times higher than the normal air value. The siren sounds repeatedly until the gas concentration drops below a dangerous level. The local people have been told to, on hearing the siren, move away from the lakes to higher ground, notify other people not to go towards the lake, and inform the nearest authorities as soon as possible. Three degassing columns installed in Lake Monoun from 2003 have removed all the gas from this lake, so it is now void of accumulated gas (Kusakabe et al. 2008; Kusakabe, this issue). Over 30 % of the gas contained in Lake Nyos has been removed by three degassing pipes installed in 2001, 2010 and 2011, and currently operating in the lake (Fig. 2e). It is anticipated that Lake Nyos should also be void of accumulated gas in the next 1–2 years.

The northern border of Lake Nyos is confined by a 40 m-high natural dam made up of unconsolidated pyroclastic deposits and affected by many joints (Fig. 2f–g). Lockwood et al. (1989) have ^{14}C-dated a piece of wood collected from the base of the dam at 400 years BP, and suggest this as the formation age of the Nyos maar. Since the original width of the pyroclastic cone is estimated to have been several hundred meters wide, the back erosion rate, i.e. erosion of the cone from outside of the lake, rather than erosion by lake water from within (Fig. 2h–i) may be as high as 1.5 m/y considering the 45 m present width of the dam. Lockwood et al. (1988) calculate that if the dam were to fail from back erosion, a devastating flood could occur that will sweep areas along the Katsina-Ala valley to as far north of the lake as Nigeria, affecting over 10,000 people (UNEP/OCHA 2005). Whole rock K–Ar dates for basalts collected from the dam range from 110 to 450 ka (Freeth 1988; Freeth and Rex 2000; Aka et al. 2001b; Aka and Yokoyama 2012), much older than the ^{14}C age. The inconsistency in the estimates of the dam age has implications on the evaluation of the flood hazard. To solve this problem, Aka et al. (2008) applied the U–Th–Ra disequilibrium technique on basaltic lava samples from the dam and lake surroundings. They found both ($^{230}Th/^{238}U$) and ($^{226}Ra/^{230}Th$) disequilibria in the samples. ^{230}Th and ^{226}Ra enrichments indicate strongly that the Lake Nyos maar, thus the dam, is younger than 350 ka, believed to be the limit of the U–Th disequilibrium age, or even younger than 10 ka, believed to be the limit of the Th–Ra disequilibrium age (Ivanovich and Harmon 1992). Using the measured ($^{230}Th/^{238}U$) activity ratio of the samples, and assuming that the initial ($^{226}Ra/^{230}Th$) ratio in them is similar to the ($^{226}Ra/^{230}Th$) ratio of basalts erupting on Mount Cameroon today (Yokoyama et al. 2007), these

authors argued that Lake Nyos is older than 5 ka but younger than 10 ka. Aka et al. (2008) and Aka and Yokoyama (2012) concluded that the general stability of the Lake Nyos dam is a cause for concern, but in the absence of an external trigger, collapse of the dam from erosion alone is not alarmingly imminent. Work is on-going on a one-year European Union funded project to reinforce the dam.

4 Data

4.1 Samples

Data for 35 samples were compiled for this paper. There are 18 samples for Lake Nyos, with twelve from Aka et al. (2008), three from Aka (2000), one from Sato et al. (1990) and two from Schenker and Dietrich (1986). For comparison, we have included available data from other volcanoes of the OVG. There are 17 samples in this group, six from Aka (2000: with one each for Lakes Wum, Nyi and Enep, and three for Lake Elum), seven samples from Sato et al. (1990: simply named 'Oku' with no further precision), three samples for Jakiri from Marzoli et al. (2000), and one sample for 'Oku' from Fitton (1987). Only data was compiled for which the analytical methods were clearly described and judged consistent, as revealed by internal consistency of the data, had MgO > 4 wt%, and loss on ignition <1. Analytical techniques and details on the petrography of the samples can be found in the data sources cited.

4.2 Major Elements

For consistency, all compiled analyses were recalculated to 100 % volatile-free with total iron as Fe_2O_3* (Fe_2O_3 = Fe_2O_3* × 0.15). Major element compositions (wt%) for the data set are: SiO_2, 49.73–44.60; TiO_2, 3.34–1.39; Al_2O_3, 15.15–14.23; Fe_2O_3*, 13.55–11.93; MnO, 0.22–0.15; MgO, 10.07–6.41; CaO, 9.31–8.04; Na_2O, 4.46–2.53; K_2O, 1.94–0.37, and P_2O_3, 0.94–0.14. The most primitive sample has Mg-number (molar percent Mg/(Mg + Fe^{2+}) of 64.8, in a range down to 50.9. The most evolved (SiO_2-rich) basalts so far reported on the OVG are the two tholeiites from Lake Nyos described in Aka et al. (2008). Recent more detailed field studies show that these rocks that were initially thought to be limited to the dam area are indeed more widespread in tephra deposits around the lake, and range in size from fine ash in the tephra to blocks of up to 50 cm in diameter. They may represent rocks torn by thermohydraulic explosions during lake formation from the feeder dike in the root zone or upper levels of the underlying diatreme. Work continues on their characterization. On the TAS diagram of Le Bas et al. (1986) (Fig. 3), the Lake Nyos and other OVG data are compared to 347 high quality literature data (MgO > 4 wt%) from other CVL volcanoes. The OVG data, including Lake Nyos, plot in the basanite-basalt-hawaiite junction, similar to other CVL data. The two Lake Nyos tholeiites plot in the field of the East African Rift System (EARS). Apart from these tholeiites with ~16 % hypersthene in their norm, similar to the 22–17 % hypersthene for northern CVL tholeiites, all other 16 Nyos samples are Ne-normative, with 12–3 % nephelene in their norm. Five other samples from the OVG suit (Fitton 1987; Sato et al. 1990; Marzoli et al. 2000) have between 13 and <1 % hypersthene in their norm.

The variation of selected major elements with MgO is shown in Fig. 4, and suggests a role for fractionation of olivine and limited fractionation of clinopyroxene and plagioclase feldspar. Figure 4a–d shows the back-calculated liquidus compositions that are discussed later. There are weak positive correlations between MgO and both SiO_2 and Al_2O_3, and a weak positive correlation between MgO and CaO/Al_2O_3 (Fig. 4e). However, in most cases, the data define fields without coherent trends.

4.3 Trace Elements

Key compatible trace elements in mantle phases, like Ni, Sc and Co vary in Lake Nyos and OVG samples from 272 to 29, 24 to 17 and 84 to

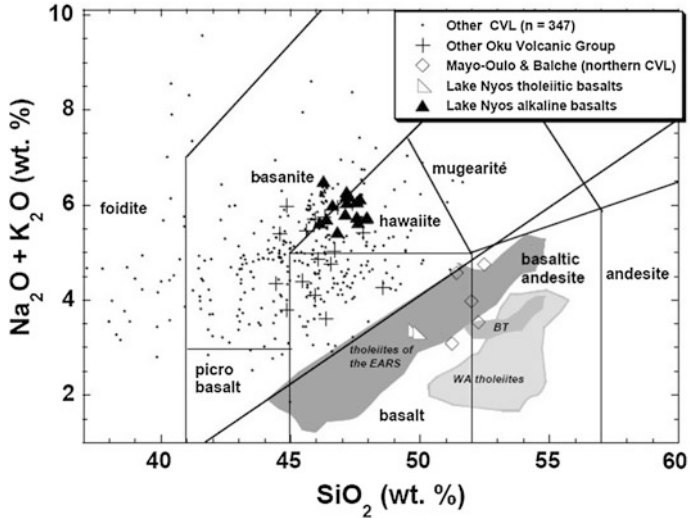

Fig. 3 TAS diagram (Le Bas et al. 1986) for Lake Nyos and OVG compared to other CVL samples. Lake Nyos alkaline basalts have similar SiO_2 with other OVG but plot at slightly higher total alkalis (wt% $Na_2O + K_2O$: total range of 6.50–3.31). Also plotted are the other tholeiites from Mayo-Oulo and Balche reported north of the CVL by Ngounouno et al. (2001) and Bea et al. (1990). Fields for tholeiites from the East African Rift System (EARS), the Benue Trough (BT) and West Africa (WA) are shaded. Data sources are: BT (Coulon et al. 1996), EARS (Georock data base) and WA (Bertrand 1991). Other sources are given in Sect. 4.1 of text. The alkaline/tholeiite divide from MacDonald and Katsura (1964). All analyses have MgO > 4 wt%, and were recalculated to 100 % volatile-free with all iron as Fe_2O_3* ($Fe_2O_3 = Fe_2O_3* \times 0.15$). Note that the Lake Nyos tholeiites plot in the field of the EARS

15 ppm, respectively. These ranges are lower than expected for primary mantle melts, for example, Ni abundances >380 ppm (Frey et al. 1978). Chromium and V range in the Lake Nyos and OVG samples 426–46 and from 259–144 ppm, respectively. MgO displays a good correlation ($r^2 = 0.71$) with Ni, an indication of olivine fractionation. The CaO/Na_2O ratio does not correlate with V. Alkaline basalts of the OVG have incompatible trace element patterns akin to ocean island basalts (OIB). They are enriched in large ion lithophile elements (LILE), with a mean Ba concentration of 627 ± 18 ppm, i.e. 90 times the primitive mantle value of Sun and McDonough (1989). This is slightly higher than in Mount Cameroon (520 ± 40). Light rare earth elements (LREE) are highly fractionated from heavy rare earth elements (HREE). For example, when normalized to primitive mantle and compared to other continental CVL volcanoes, La/Yb ratios are Etindé (68 ± 6), Mount Cameroon (29 ± 1), Biu (27 ± 9), Bambouto (19.2 ± 6), and Lake Nyos (15.3 ± 0.5) (see Fig. 1 for location of volcanic centers). The Lake Nyos basalts show a pronounced K trough (K/K* ~ 0.80: where K/K*, Ba/Ba* etc. are defined as $b^* = b/\sqrt{(a \cdot c)}$ with b = Ba, K, Pb, Eu, and a and c their neighboring elements on a primitive mantle-normalized trace element variation diagram like Fig. 3b in Aka et al. (2008).

5 Alteration, Crustal Contamination and Primary Melt Composition

5.1 Alteration and Crustal Contamination

To use the data for estimating the depth of melt segregation and degree of melting, it must first be evaluated for the effects of (meteoric) alteration that can influence element mobility, and also for shallow level magma chamber processes like crustal contamination and crystal fractionation.

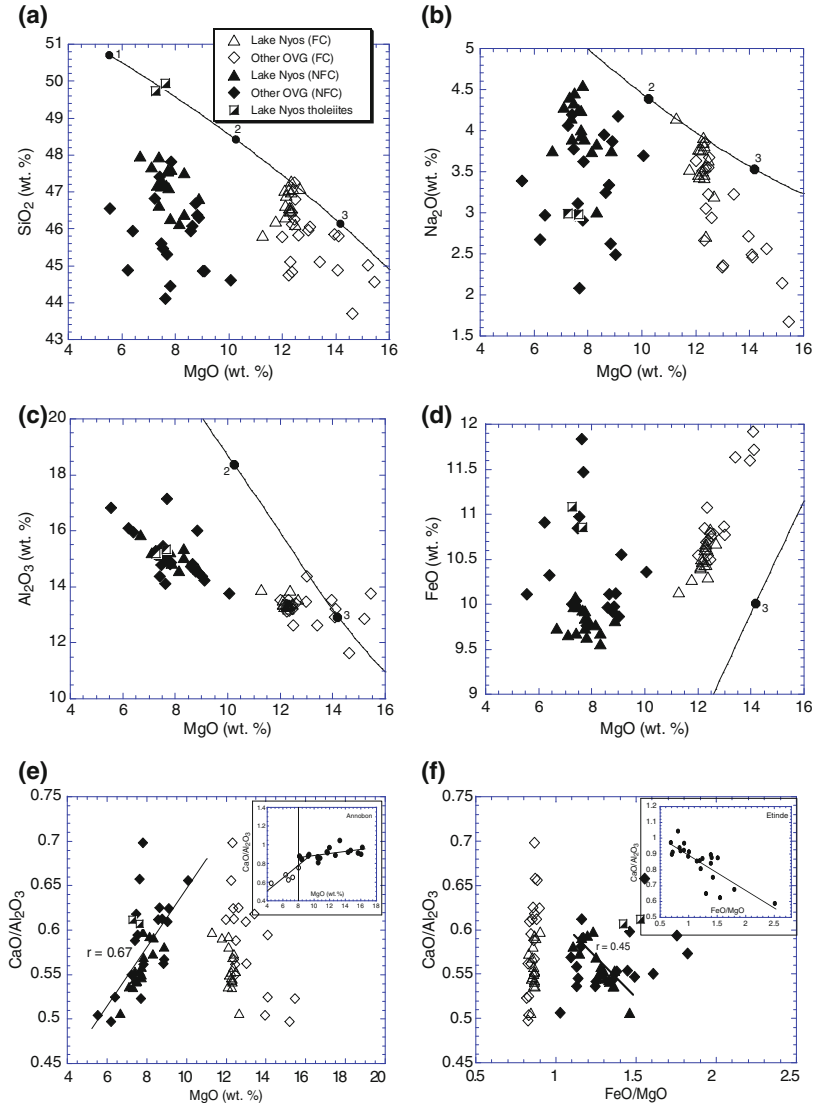

Fig. 4 MgO versus SiO_2, Na_2O, Al_2O_3, and FeO (wt%, **a**–**d**) variations in Lake Nyos and other basalts from the OVG. Filled symbols represent the raw data (references in Sect. 4.1 of text) while open symbols represent data corrected to a Mg number value of 68 by incremental addition of equilibrium olivine (see text). The curves (in **a**–**d**) labeled with pressure (in GPa) are the near-solidus garnet lherzolite melt compositions from the Herzberg and Zhang (1996) algorithms. The SiO_2 pressure curve (in **a**) was calculated as explained in the text. The variations of MgO versus CaO/Al_2O_3 (**e**) and FeO/MgO versus CaO/Al_2O_3 (**f**) ratios are also shown. *Inset* in (**e**) shows the MgO versus CaO/Al_2O_3 ratio in Annobon samples, while the *inset* in (**f**) shows the FeO/MgO versus CaO/Al_2O_3 ratios in Etindé samples. More explanations in the text

We have used the LILE/HFSE, i.e. mobile/immobile element ratios, to check element mobility. Figure 5a is a Ba versus Nb plot for 33 samples. Due to their relatively low Ba (113–133 ppm) and Nb (5–6 ppm) abundances, the two Nyos tholeiites are not plotted on this diagram. The Ba/Nb ratio in Lake Nyos and OVG alkaline basalts varies from 15.16–6.63, with a mean of 10.50 ± 1.51 (Fig. 5a). The mean ratio is well within the primitive mantle window of 10.03–9.80 (Hoffmann 1988; Sun and McDonough 1989). Figure 5a shows four

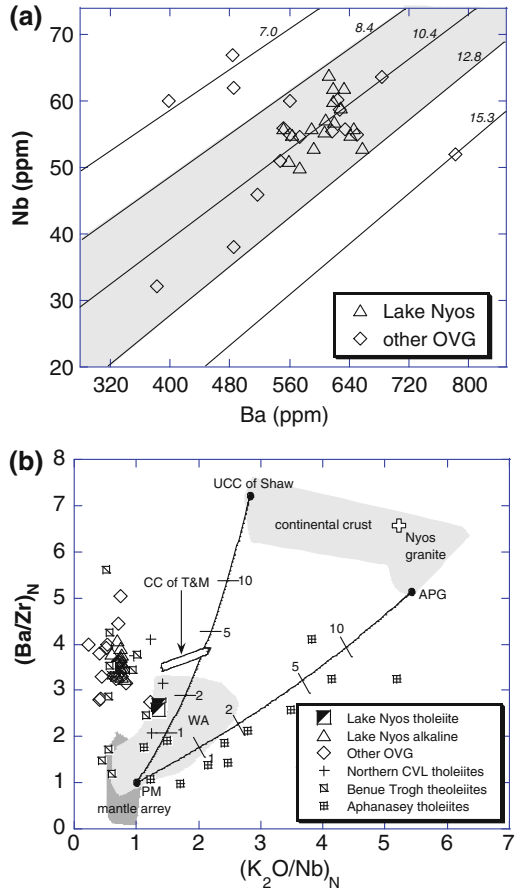

Fig. 5 **a** Ba versus Nb diagram for Lake Nyos and other Oku Volcanic Group alkaline basalts. Lines of equal Ba/Nb ratio are labeled. The zone occupied by samples unlikely to have suffered severe element mobility, i.e., having similar Ba/Nb ratios as in primitive mantle (see text) is shaded. These samples are used for quantitative constrains on the degree of melting and depth of melt segregation. **b** Primitive mantle (Sun and McDonough 1989)-normalized K_2O/Nb versus Ba/Zr ratios for Lake Nyos and other basalts from the OVG, tholeiites from northern CVL and the Benue Trough, compared to oceanic basalts (mantle array), the continental crust, crustally contaminated tholeiites from Aphanasey Nikitin Rise (Indian ocean, Borisova et al. 2001) and West African (WA) tholeiites (Bertrand 1991). CC of T&M stands for the continental crust of Taylor and McClennan (1995). Bulk mixing lines in (**b**) were calculated with primitive mantle (PM) as one end-member and the upper continental crust of Shaw et al. (1986) and average Phenerozic granite (APG) of Condie (1993) as other end-members. Numbers on the *lines* show the percentage of crustal material added. Lake Nyos granite is from Schenker and Dietrich (1986). MORB array defined by Georoc data base (http://georoc.mpch-mainz.gwdg.de/georoc/Start.asp). Other data sources used for delineating the zone of the continental crust are given in the text

outliers. Three samples from Jakkiri (Marzoli et al. 2000) have very low (down to 6.3) Ba/Nb ratios that may suggest mobility of Ba during alteration. One other sample from 'Oku' has a high value of 15.16 that may be due to crustal contamination. Such samples will be eliminated in further discussion.

Both the alkaline and tholeiitic basalts of Lake Nyos are incompatible element (e.g. Ba)- enriched. For example, Ba/Ba* varies from 1.7 to 1.3 in the alkaline basalts and from 2.0 to 1.8 in the tholeiites. However, in the tholeiites, this enrichment is accompanied by Pb-enrichment (Pb/Pb* = 0.9 compared to 0.4 in the alkaline basalts), seen as Pb peaks in the spider diagrams (see Table 2 and Fig. 3b of Aka et al. 2008). This results in their low ($\sim$11) Ce/Pb ratios, compared to the mean Ce/Pb ratio of 30.10 ± 4.18 in the alkaline basalts. They also have low (3.2–2.7) Nb/U ratios compared to the basalts (5.29 ± 0.33). Bulk continental crust has Ce/Pb and Nb/U ratios of 4.13 and 12.09, respectively (Taylor and McClennan 1995). These data suggest that the tholeiites might have suffered crustal contamination. We have modeled the crustal contamination process using the K_2O/Nb and Ba/Zr ratios (Fig. 5b). Primitive mantle- normalized K_2O/Nb and Ba/Zr ratios ($(K_2O/Nb)_N$ and $(Ba/Zr)_N$, respectively) range from a high of 9.7 for average Archean granite (Condie 1993) to a low of 2.4 for the lower continental crustal estimate of Taylor and McLennan (1985). $(Ba/Zr)_N$ ratios range from 9.6 for global subducting sediment (GLOSS of Planck and Langmuir 1998) to 5 for average Proterozoic granite (Condie 1993). When compared to asthenospheric and lithospheric mantle, $(K_2O/Nb)_N$ ratios in the crustal samples are an order of magnitude higher, meanwhile $(Ba/Zr)_N$ ratios are >2 times higher than in oceanic island basalts. K_2O/Nb and Ba/Zr ratios for samples not affected by element mobility, would therefore be sensitive indicators of crustal contamination of a mantle-derived melt. $(K_2O/Nb)_N$ ratios range in the Lake Nyos alkaline basalts from 0.81 to 0.71, with a mean (0.75 ± 0.04), that is within the range of oceanic basalts (Hoffmann 1988), despite their having erupted in a continental setting. $(Ba/Zr)_N$ ratios in the samples have a mean of 3.66 ± 0.20.

This shows that they have not suffered crustal contamination. Conversely, $(K_2O/Nb)_N$ ratios in the tholeiites and one sample from 'Oku' are, with 1.4 ± 0.02, higher than in oceanic basalts. A $(K_2O/Nb)_N$ versus $(Ba/Zr)_N$ two-component mixing model with the primitive mantle of Sun and McDonough (1989) as an end-member and the upper continental crust of Shaw et al. (1986) as another end member shows that the Lake Nyos tholeiites and the 'Oku' sample plot along a trajectory that would suggest admixture of between 1 and 2 % upper continental crustal material (Fig. 5b). It is suggested that such crustal contamination would result in the Ba and Pb peaks seen on the spider diagrams of the tholeiites (see Fig. 3b of Aka et al. 2008). We are checking this suggestion using isotopes. These three samples are henceforth not considered in the petrogenetic models.

5.2 Primary Melt Composition

Crystal fractionation will reduce the mafic nature of magma and hinder its use for fingerprinting the mantle source. Many criteria are often considered for the identification of primitive, or at least primary magmas (Frey et al. 1978). (i) The lavas should carry mantle xenoliths. Lake Nyos and other OVG alkaline basalts certify this criterion because they contain abundant mainly lherzolite (e.g. Fig. 2c) mantle and also upper crustal xenoliths (Aka et al. 2004; Temdjim et al. 2004; Touret et al. 2010). Field evidence does not show any reaction rims between these xenoliths and their host lavas. This suggests that the magmas travelled quickly, probably in a matter of days, through the lithosphere and crust and were probably not modified by secondary crystal fractionation and assimilation processes in shallow magma chambers. (ii), the magma should have high concentrations of compatible trace elements such as Ni (300–400 ppm), Co, and Sc, which have mineral/melt partition coefficients far exceeding unity for most upper mantle phases. Mineral/melt partition coefficients of compatible trace elements are strongly temperature- and composition- dependent (Mysen 1979; Righter et al. 2006). If however, one ignores this compositional dependence, then 1–25 % equilibrium partial melting of the Lake Nyos spinel lherzolite with (wt%) 75, 6, 17 and 2, respectively, of olivine (ol), orthopyroxene (opx), clinopyroxene (cpx) and spinel (sp), having Ni, Co and Sc concentrations (ppm) of 2,239; 123 and 18, respectively (Tietchou, personal communication), should produce a melt that ranges (ppm) in Ni from 235 to 300, in Co from 35.7 to 43.1, and in Sc from 15.6 to 16.3 (using partition coefficients set 1 of Ottonello et al. 1984). The Lake Nyos and OVG samples used here have maximum Ni contents of 272 ppm, suggesting they are not primary magmas. (iii), Basaltic magma derived from the least refractory (least depleted) upper mantle peridotite should have a Mg no. value ($=100 \times Mg/(Mg + Fe^{2+})$) of ≈88–89. For a $K_{D(ol/melt)}^{(Fe/Mg)} = 0.3$ (Roeder and Emslie 1970) and 30 % partial melting, such a source should produce a melt with a Mg no. value of ≈68–75 (Frey et al. 1978). The measured Mg no. values for the Lake Nyos and OVG samples that range from 64.8 to 50.9, are lower than expected for basaltic magmas derived from refractory upper mantle peridotite. This suggests that they suffered some degree of mineral fractionation within the upper mantle before incorporating mantle xenoliths., This is illustrated in Fig. 6, where the MgO content of the samples is plotted against their Ni content, together with model partial melting and olivine fractionation curves calculated according to Hart and Davis (1978). One sample from the suit intersects the mantle melting curve at a Ni content of ≈272 ppm, still lower than would be expected when in equilibrium with mantle peridotite. The other Lake Nyos and OVG data do not intersect the melting curve (even at 0.5 % mantle melting—not shown in Fig. 6). This model is therefore inappropriate in estimating the MgO of the Nyos unfractionated (primary) magma.

The effect of fractionation in the samples was compensated by normalization, assuming that olivine was the only fractionating phase. This was done by adding olivine to each composition while maintaining a constant $K_{D(ol/melt)}^{(Fe/Mg)}$ of 0.3 (Roeder and Emslie 1970), until the liquidus phase had olivine of Fo_{88}, corresponding to Mg no. value of 68. The assumption of olivine as the

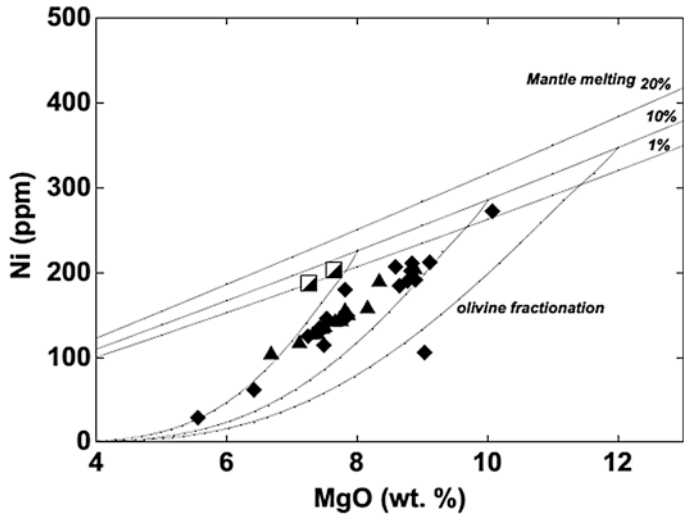

Fig. 6 MgO—Ni diagram for Lake Nyos and OVG lavas compared to modeled trends due to mantle partial melting and fractional crystallization (Hart and Davis 1978). The *diagonal lines* are for 1, 10 and 20 % partial melting respectively and the *curves* show olivine fractionation trends. The Lake Nyos and OVG data does not intersect the *melting curve* (even at 0.5 % mantle melting—not shown). Triangles, half-filled squares and diamonds represent Lake Nyosalkaline basalts, tholeiites and other OVG samples respectively

major fractionating phase is supported by the following arguments from the data set. (i) The good correlation between MgO and Ni. (ii) The not so good correlation between MgO and CaO/Al_2O_3 (Fig. 4e). This suggests that only limited clinopyroxene has fractionated in the Lake Nyos and OVG samples, compared for example to a clear decrease (abrupt slope change) in CaO/Al_2O_3 at ~8 wt% MgO for Annobon (Fig. 4e inset) that would correspond to the appearance of clinopyroxene phenocrysts, abundant in samples from this volcanic center (Loitard et al. 1982). The limited role of clinopyroxene is further shown by the lack of a coherent trend between FeO/MgO and CaO/Al_2O_3 for the whole OVG dataset (Fig. 4f). Compare this to the good correlation (r = 0.89) in Etindé samples (Fig. 4f inset) that have abundant clinopyroxene phenocrysts (Nkambou et al. 1995). Samples that fractionate clinopyroxene would be expected to lie along a V–CaO/Na_2O (clinopyroxene fractionation) trajectory because V has a clinopyroxene/melt partition coefficient of ~4 (Hart and Dunn 1993; Jenner et al. 1993). This is not observed. (iii) The lack of a pronounced positive Eu abnormally in the samples (E/E* values of 1.12–1.06), coupled with the good negative correlation (r = 0.72, Fig. 4c) between MgO and Al_2O_3, do not support plagioclase feldspar as a major fractionating phase. (vi) The near absence of clinopyroxene and plagioclase as phenocrysts phases in the OVG samples (see Refs. in Sect. 4.1).

The amount of olivine required in this calculation to reach a liquidus composition with Fo_{88} ranged from 9 to 15 % for Lake Nyos samples and from 10 to 23 % for other OVG samples. Trace element concentrations were recalculated to account for the added olivine. This was done assuming Rayleigh fractionation and employed the formula: $C_o = C_L/F^{(D-1)}$, where C_o and C_L are the pre- and post-fractionation concentrations, respectively, D is mineral/melt partition coefficient and F is the amount of liquid remaining after fractionation.

The screening above reduced the number of samples from 35 to 26, with 14 from the Lake Nyos area and 12 from other OVG volcanoes. These are used below to fingerprint the petrogenetic processes in the mantle underlying these volcanoes.

6 Depth and Location of Melting

6.1 Major Element Evidence

Experimental studies on mantle peridotite have demonstrated that the principal control on the major element (e.g. SiO_2, Al_2O_3, FeO, CaO, Na_2O) chemistry of MORBs is the pressure of melting (Langmuir et al. 1992; Hirose and Kushiro 1993). The pressure (depth) of melting of the Lake Nyos and OVG basalts was estimated using algorithms derived by Herzberg and Zhang (1996) over a range of pressures in melting experiments on a quasi primitive peridotite KLB-1. Herzberg and Zhang (1996) do not give an algorithm for SiO_2, but state that it is fairly constant between 45 and 47 %.The fractionation-corrected SiO_2 contents of all (26) samples lie in the range 45.0–47.1 %, so the SiO_2 pressure was calculated using the regression equation of Haase (1996) from data of the melting experiments of the three depleted mantle peridotites KLB-1, PHN1611 and Tinaquillo (see Haase 1996 for references). The SiO_2 pressures calculated in this way are similar to those obtained using the equation of Scarrow and Cox (1995). Pressures were estimated for individual samples. The trajectories of the estimated pressures over a range of 1–4 GPa are plotted in Fig. 4a–d, together with the fractionation-corrected and the raw data. There is generally good agreement, especially for SiO_2, Al_2O_3, and Na_2O, where the fractionation-corrected data intersects the pressure trajectory (Fig. 4). It will be argued below that the Lake Nyos source contains hydrous phases. The Herzberg and Zhang (1996) experiments were conducted on fertile peridotites. Given the source differences, the agreement between the fractionation-corrected data and the melting trajectories is satisfactory, and supports the view that the depth of melting is the main control on the major element composition. The mean (n = 14, see Fig. 7 inset) pressure values (in GPa) for Lake Nyos are 2.8 (SiO_2), 2.5 (MgO), 2.9 (Al_2O_3), 3.2 (FeO) and 2.7 (Na_2O). These pressures were converted to depths for individual samples using a density of 3,300 kg/m^3, and are plotted in Fig. 7. There is still considerable debate (see Walter et al. 2002) on the depth at which garnet transforms to spinel. Experimental studies by Robinson and Wood (1998) show that garnet is completely broken down at 85 km. The 60–80 km depth spinel-garnet transition zone adopted in Fig. 7 is from Shen and Forsyth (1995). The results on Fig. 7 show that melts in the Lake Nyos and other OVG source mantle formed and

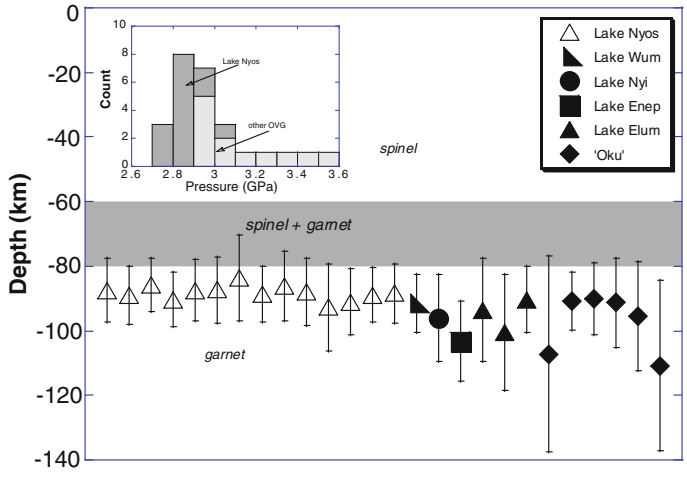

Fig. 7 Depth of melt segregation from the mantle source for individual samples from Lake Nyos and other OVG volcanoes. Depths were obtained by converting the pressures (insert histogram) using a density of 3,300 kg/m^3. The pressures were estimated as explained in the caption of Fig. 4 and text. The spinel-garnet transition zone is after Shen and Forsyth (1995)

segregated over a 80–100 km depth range, within the garnet stability field. These estimated pressures correspond to source potential temperatures of 1,300–1,400 °C (Albarède 1992).

6.2 Trace Element Evidence

Further constrains can be placed on the melting dynamics of the Lake Nyos and other OVG lavas using their trace element contents. We chose the Zr/Nb and La/Yb ratios to constrain the source mineralogy and enrichment because (i) the Zr/Nb ratio is not affected significantly by fractional crystallization of mantle phases, so it can distinguish the effects of partial melting from those of fractional crystallization, and also the enrichment level of the source mantle, and (ii) the La/Yb ratio can distinguish melting between spinel and garnet- lherzolite sources because Yb (a HREE) is compatible in garnet but not in clinopyroxene. The Lake Nyos and OVG data is modelled on a Zr/Nb versus La/Yb diagram (Fig. 8, see caption for parameters used for modelling). It is seen that the samples are clearly displaced from the spinel lherzolite melting trend and plot within the garnet melting trajectories. The tight range in the Zr/Nb (5.07–4.61) and the elevated La/Yb (20.22–22.49) ratios of these samples argue against significantly variable degrees of melting below these volcanoes, and make it hard to avoid the conclusion that the melts were generated in the presence of (2–3 %) garnet by small (1–2 %) degree partial melting of the mantle source. This conclusion is supported by the major element systematics, and also by the observation (Aka et al. 2008) of ^{230}Th and ^{226}Ra excesses in these samples, that can only be generated in the presence of garnet (Beattie 1993).

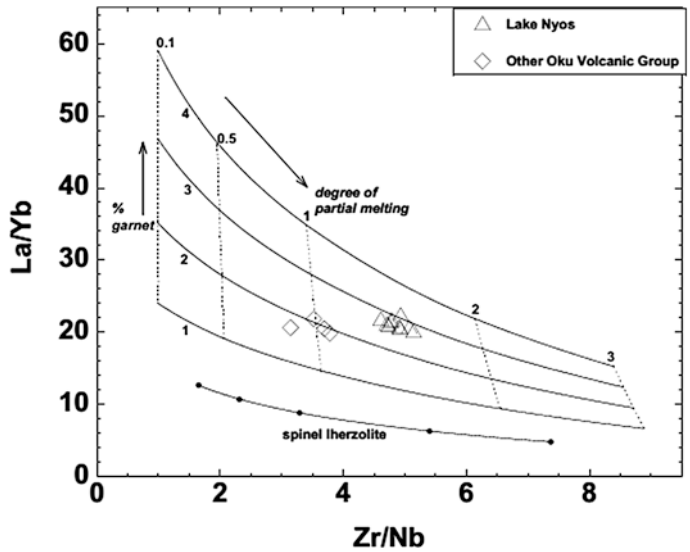

Fig. 8 Variation of fractionation-corrected Zr/Nb versus La/Yb ratios in Lake Nyos and other OVG alkaline basalts, compared with a non-modal fractional (Shaw 1970) melting grid with primitive mantle ratios (Sun and McDonough 1989) as source. The garnet mode in the source is assumed to vary from 1–4 % (shown as *sub-horizontal continuous lines*). Melt increments (*sub-vertical dashed lines*) are shown for 0.1, 0.5, 1, 2 and 3 % melting. A spinel lherzolite melting curve is also shown for the same melt increments. Phase proportions and melt reaction coefficients for spinel lherzolite (sp lherz) from Kinzler (1997), garnet lherzolite (gt lherz) from Walter (1998) and garnet-amphibole-phlogopite lherzolite (gt-amp-phlo lherz, used for Fig. 10) from Gurenko et al. (2006). For sp lherz: ol = 0.53, 0.06; opx = 0.27, 0.28; cpx = 0.17, 0.55; sp = 0.03, 0.11. For gt lherz: ol = 0.6, 0.03; opx = 0.2, 0.16; cpx = 0.1, 0.72; gt = 0.1, 0.09. For gt-amp-phlo lherz: ol = 0.6, 0.1; opx = 0.2, 0.18; cpx = 0.1, 0.3; gt = 0.05, amp = 0.04, 0.1; phlo = 0.01, 0.04. Mineral/melt partition coefficients are from compilations of Halliday et al. (1995), White (2005), and Salters (1996)

7 Implications of the Data on the Origin of CO_2 in Lake Nyos

Speculation on the significance of the data on the origin of CO_2 in Lake Nyos is based on the following observations. (i) the occurrence of many soda springs on the floor of, and around the lake. These springs are today copiously discharging gas with lethal amounts (over 99 % by volume) of CO_2. Any animals like the bird in Fig. 9 or cattle grazing nearby that dare to come too close to the springs to have a drink are asphyxiated. Herdsmen put makeshift barriers round this 'Fulani spring' to prevent cattle getting too close. (ii) Judging from the $\delta^{13}C-CO_2$ (-3.5 ± 0.2 ‰) and the $^3He/^4He$ ratio of associated helium (5.7 times the atmospheric ratio), the CO_2 in Lake Nyos is clearly magmatic (Aka et al. 2001a) even though the helium ratio is lower than in the MORB source (Graham et al. 1992). (iii) As mentioned earlier, Lake Nyos alkaline basalts have trace element patterns akin to OIB. They have a mean Nb/U ratio that falls well within the relatively constant asthenosphere-derived OIB window. On the other hand, they show a marked K depletion in their spidergrams. Barium that is also a mobile element like K does not show a similar depletion (see Fig. 3b of Aka et al. 2008), so the K depletion cannot be due to removal by weathering. The samples also show a negative (albeit weak) correlation ($r = 0.62$) when their La/Yb ratios are plotted against their Pb/Pb* ratios. These characteristics can be interpreted to result from the presence of a buffering residual K-rich phase (e.g. amphibole and/or phlogopite) during partial melting in the mantle source. Amphibole and phlogopite are indeed present in peridotite xenoliths hosted by these basalts (Aka et al. 2004; Temdjim et al. 2004; Teitchou et al.

Fig. 9 **a** A bird (*arrow*) asphyxiated by CO_2 exolving from the Nyos 'Fulani' spring. Note the reddish color of the spring **b** and lake water (northern part with dam and spill way) **c** that is due to oxidation of Fe^{2+} to Fe^{3+} (Kusakabe this volume). Photos were taken in September 1991 (**a**), December 2011 (**b**) by FT Aka and in September 2012 (**c**) by Romaric Ntchantcho

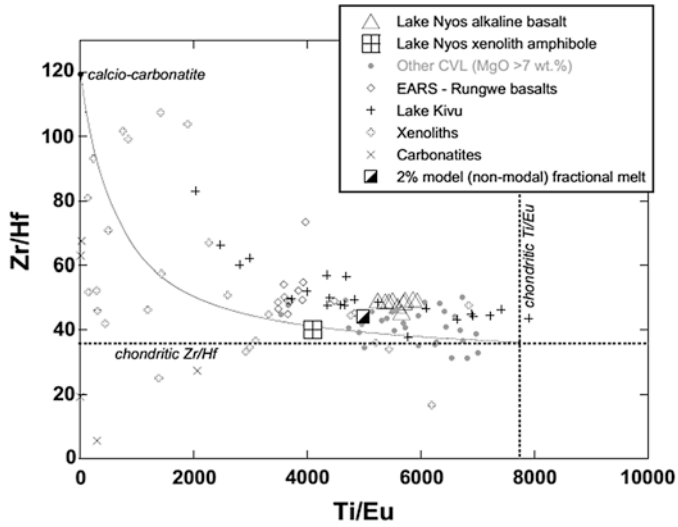

Fig. 10 Variation of fractionation-corrected Ti/Eu versus Zr/Hf ratios in Lake Nyos basalts compared to other mafic lavas from Rungwe and Lake Kivu (East African Rift System) which are considered to have suffered metasomatism, carbonatite-metasomatised peridotite xenoliths from Ethiopia, Tanzania, Australia and Italy. Also shown are data for mafic (MgO > 7 wt%) lavas from other CVL volcanoes (literature), a Lake Nyos xenolith amphibole (Teitchou, pers. comm.), typical carbonatites, and a mixing curve between primitive mantle and calsio-carbonatite (see Sect. 7 of text for Refs.). Ti/Eu and Zr/Hf fractionation in the Lake Nyos basalts is similar to that produced by low degree (2 %) partial melting of a garnet-amphibole- phlogopite lherzolite source. The model melt composition was calculated assuming non-modal fractional melting (Shaw 1970). Mineral-melt partition coefficients, phase proportions and melt reaction coefficients used are given in Fig. 8 caption

2011). Since amphibole and phlogopite are not primary mantle minerals, they are believed to precipitate in the mantle from percolating metasomatising melts or fluids (Greenough 1988; Green and Wallace 1988; Hawkesworth et al. 1990), and are restricted to the cold conductive mantle lithosphere because temperatures in the hot convective mantle are too high for their stability (Class and Goldstein 1997). Observation (iii) above would therefore imply some sort of interaction between melts from the convective and conductive mantle below Lake Nyos. Such asthenosphere-lithosphere interaction has been advocated as a viable petrogenetic model for some CVL volcanoes like Bambouto (Marzoli et al. 2000), Bui (Rankenburg et al. 2005) and more recently Mount Cameroon (Yokoyama et al. 2007). More detailed verification of such a model for the OVG system is underway.

The Zr/Hf and Ti/Eu ratios of Lake Nyos basalts are plotted in Fig. 10. With mean Zr/Hf and Ti/Eu ratios of 48.5 ± 1.2 and 5606 ± 224, respectively, the Lake Nyos samples show a shift with respect to chondritic values (Sun and McDonough 1989) of ~30 % to higher Zr/Hf and lower Ti/Eu ratios. Fractional crystallization cannot produce the shifts observed in these samples. For example up to 50 % fractional crystallization of a 'basaltic' assemblage consisting of (wt%) 0.2 ol, 0.3 cpx and 0.5 plagioclase will increase the Zr/Hf ratio by less than 5 % (using $D^{Zr,Hf}_{p\lg/melt}$ of 0.001 (Zr) and 0.051 (Hf), with the other partitioning data as in footnote of Fig. 8). With $D^{Ti,Eu}_{gt/melt} = 0.98$ and $D^{Zr,Hf}_{gt/melt} = 0.87$, melting of a dry garnet-bearing source cannot account for the observed fractionations as much as melting of an amphibole ($D^{Ti,Eu}_{amp/melt} = 1.83$, $D^{Zr,Hf}_{amp/melt} = 0.83$) and phlogopite ($D^{Ti,Eu}_{ph\log/melt} = 31.6$, $D^{Zr,Hf}_{ph\log/melt} = 1.37$)-bearing mantle source would do (Fig. 10). Also plotted in Fig. 10 are mafic lavas from Rungwe—Tanzania and Lake Kivu, which are interpreted to derive from a source peridotite that has suffered metasomatism (Marcelot et al. 1989; Furman 1995), carbonatite-metasomatised peridotite

xenoliths from Mega-Ethiopia (Bedini et al. 1997), Tanzania (Rudnick et al. 1993), Australia (Yaxley et al. 1991, 1998) and Italy (Downes et al. 2002), as well as typical carbonatites (Nelson et al. 1988; Hoernle et al. 2002). Carbonatite metasomatism produces CO_2 as a by-product (see equations in Yaxley et al. 1991 and Kogarko et al. 2001). Experimental studies by Green and Wallace (1988) suggest that up to 50 % of a (percolating) metasomatizing carbonatite melt may be lost as a CO_2-rich fluid. It is seen in Fig. 10 that an amphibole in a Lake Nyos xenolith has Ti/Eu and Zr/Hf ratios that plot exactly on the primitive mantle-carbonatite mixing line, while Lake Nyos basalts plot together with a model melt formed by 2 % (non-modal fractional, Shaw 1970) melting of a garnet, amphibole and phlogopite-containing source. The simplest interpretation of this is that the amphibole was added to the garnet lherzolite source by carbonatitic fluids, and the basalts were produced by (low degree) melting of the metasomatized source. We argue that decarbonation reactions of the carbonatitic metasomatism are actively taking place in the Lake Nyos mantle today. They would be responsible for producing the magmatic CO_2 that is draining through the underlying fractured diatreme and via mineral springs into the bottom of the lake. It is this that asphyxiated people and animals during the 1986 gas disaster. This conclusion requires that current efforts to degas Lake Nyos should take into account the fact that CO_2 will continue to seep into the lake for a yet undetermined but long time in the future. A possible solution will be to avoid stratification by (somehow) safely and permanently bringing bottom waters to the surface to release any newly accumulated gas.

7.1 Timing of the Enrichment Event

The radiogenic helium isotope signatures of the OCB zone (e.g. Mount Etindé, Fig. 1) compared to the OVG are thought to result from Lower Neocomian U + Th enrichment by melts from the St. Helena hotspot when it underlay this portion of the CVL lithospheric mantle in the Mesozoic (Halliday et al. 1990; Aka et al. 2004). Only four (Rb–Sr), two (Sm–Nd) and one (U–Pb) isotopic data are available for the OVG in samples with MgO > 4 wt%. In these 22–23 Ma samples, ($^{87}Sr/^{86}Sr$) ranges from 0.70380–0.70333, ($^{143}Nd/^{144}Nd$) from 0.51260–0.51283, ($^{206}Pb/^{204}Pb$) is 18.77, ($^{207}Pb/^{204}Pb$) is 15.56, and ($^{208}Pb/^{204}Pb$) is 38.70. The ($^{206}Pb/^{204}Pb$) ratio in Etindé is 20.52 (Halliday et al. 1990). The less radiogenic lead of the OVG compared to Etindé may suggest either that the Mesozoic event did not affect the CVL mantle as far inland as the OVG, or that the OVG suffered a more local but later enrichment event. These scenarios are being investigated.

8 Conclusions

The available dataset for 35 samples of basaltic lavas from the Lake Nyos maar- diatreme volcano and other volcanoes of the Oku Volcanic Group of the Cameroon Volcanic Line includes that of two samples from Lake Nyos, preliminarily identified as tholeiitic basalts. These rocks are more widespread in the Lake Nyos tephra deposits than previously thought. They may be remnants of magma that got stalled (diatreme) at crustal levels below Lake Nyos. More detailed studies of these rocks are needed'. The whole dataset was screened for alteration, crustal contamination and the effects of crystal fractionation. The results indicate that the tholeiites and 25 % of the samples may have suffered 1–2 % crustal contamination, and/or between 15 % (Lake Nyos) and 23 % (other OVG) fractionation of olivine. Clinopyroxene and plagioclase feldspar are not major fractionating phases in the studied lavas of the OVG volcanoes. The subset of screened data (26 samples) has major and trace element characteristics that indicate 1–2 % partial melting of a (2.3 %) garnet peridotite at ~90 km depth. The data show that polybaric melt pooling from the mantle source is not a viable petrogenetic process in the OVG. Trace element systematics suggest that the Lake Nyos mantle has been spiked by carbonatitic melts, akin to that generating melts in the East African Rift System. Melting of this metasomatised mantle is releasing

the CO_2 that seeps into and accumulates in the lake. Current degassing efforts should consider the fact that CO_2 will continue to exsolve into Lake Nyos from the mantle for an undetermined but long time in the future.

Acknowledgments Compilation of the Cameroon Volcanic Line and other data used in this paper was made when I was on a 'mis à la disposition' of Okayama University Institute for Study of the Earth's Interior (ISEI) in Misasa, Japan, from the Institute for Geological and Mining Research (IRGM, Cameroon). My stay in ISEI was supported by a JSPS grant to Minoru Kusakabe for 'Asia-Africa Science Platform Program (Geochemistry of Lake Nyos gas disaster, Cameroon Volcanic Line-Rift Valley volcanoes and the underlying mantle), and also by a COE-21 (Center of Excellence in the 21st Century in Japan) grant to Eizo Nakamura. Assistance from colleagues and collaborators of IRGM and ISEI is acknowledged. Some of the pictures shown in Figs. 2 and 9 were taken during many trips to Lake Nyos within the framework of (1) the Lakes Nyos and Monoun Degassing Project funded by the Government of Cameroon, USAID and the French Cooperation; (2) SATREPS-IRGM project headed by Prof. Takeshi Ohba of Tokai University (Japan) and funded by the Government of Cameroon, the Japan International Cooperation Agency (JICA) and the Japan Science and Technology Agency (JST); (3) the Lake Nyos dam reinforcement project funded by the Government of Cameroon and the European Union. We acknowledge the leadership of MINRESI, through IRGM that coordinates all these projects. Discussions with T. Yokoyama and review comments from Dmitri Rouwet, Karoly Németh and Tanya Furman helped in improving the paper. I stayed at the Misasa Onsen Hospital for part of the time that I was in Misasa, but was able to continue to work. I commend Y. Nakano (COE-21 administrative officer), all the nurses and doctors through Yukari Tanabe and Morio Yasuo respectively, for the assistance that they gave me.

References

Aeschbach-Hertig W, Hofer M, Kipfer R, Imboden DM, Wieler R (1999) Accumulation of mantle gases in a permanently stratified volcanic lake (Lac Pavin, France). Geochim Cosmochim Acta 63:3357–3372

Aeschbach-Hertig W, Kipfer R, Hofer M, Imboden DM, Wieler R, Signer P (1996) Quantification of gas fluxes from the subcontinental mantle: the example of Laacher See, a maar lake in Germany. Geochim Cosmochim Acta 60:31–41

Aka FT (2000) Noble gas systematics and K–Ar chronology: implications on the geotectonic evolution of the Cameroon Volcanic Line, West Africa. Ph.D. thesis, University Okayama, Japan, p 175

Aka FT, Kusakabe M, Nagao K, Tanyileke G (2001a) Noble gas isotopic compositions and water/gas chemistry of soda springs from the islands of Bioko, São Tomé and Annobon, along the Cameroon Volcanic Line, West Africa. Appl Geochem 16:323–338

Aka FT, Kusakabe M, Nagao K (2001b) New K–Ar ages for Lake Nyos maar, Cameroon: implications for hazard evaluation. J Geosci Soc Cam 1:25–26

Aka FT, Nagao K, Kusakabe M, Sumino H, Tanyileke G, Ateba B, Hell J (2004) Symmetrical helium isotope distribution on the Cameroon Volcanic Line, West Africa. Chem Geol 203:205–223

Aka FT, Yokoyama T, Kusakabe M, Nakamura E, Tanyileke G, Ateba B, Ngako V, Nnange JM, Hell JV (2008) U-series dating of Lake Nyos maar basalts, Cameroon (West Africa); implications for potential hazards on the Lake Nyos dam. J Volcanol Geotherm Res 176:212–224

Aka FT, Yokoyama T (2012) Current status of the debate about the age of Lake Nyos dam (Cameroon) and its bearing on potential flood hazards. Nat Haz. doi:10.1007/s11069-012-0401-4

Albarède F (1992) How deep do common basaltic magmas form and differentiate? J Geophys Res 97:10997–11009

Allard P, Dajlevic D, Delarue C (1989) Origin of CO_2 emanation from the 1979 Dieng eruption, Indonesia: implications for the 1986 Nyos catastrophe. J Volcanol Geotherm Res 39:195–205

Alvarado GE, Gerardo JS, Flavia MS, Pablo R, de Hurtado Mendoza L (2011) The formation and evolution of Hule and Río Cuarto maars, Costa Rica. J Volcanol Geotherm Res 201:342–356

Aranda-Gómez JJ, Luhr JF (1996) Origin of the Joya Honda maar, San Luís Potosí, México. J Volcanol Geotherm Res 74:1–18

Aranda-Gómez JJ, Luhr JF, Pier JG (1992) The La-Brena-El-Jaguey-Maar Complex, Durango, Mexico: I. Geological evolution. Bull Volcanol 54(5):393–404

Bea A, Cocheme JJ, Trompette R, Affaton P, Soba D, Sougy J (1990) Graben d'âge paléozoïque inférieur et volcanism tholéiitigues associé dans la région de Garoua au North-Cameroun. J Afr Earth Sci 10:657–667

Beattie P (1993) The generation of uranium series disequilibria by partial melting of spinel peridotite: constraints from partitioning studies. Earth Planet Sci Lett 117:379–391

Bedini RM, Bodinier JL, Dautria JM, Morten L (1997) Evolution of LILE-enriched small melt fractions in the lithospheric mantle: a case study from the East African Rift. Earth Planet Sci Lett 153:67–83

Belousov AB (2005) Distribution and eruptive mechanism of maars in the Kamchatka Peninsula. Dokl Earth Sci 406(1):24–27

Bertrand H (1991) The mesozaoic tholeiitic province of Northwest Africa: a volcano-tectonic record of the early opening of Central Atlantic. In: Kampunzu AB, Lubala RT (eds) Magmatism in extensional structural settings: the Phanerozoic African plate. Springer, Berlin, pp 147–188

Blong RJ (1984) Volcanic hazards—a sourcebook on the effects of eruptions. Academic Press, Sydney

Boriscova AYu, Belyatsky BV, Portnyagin MV, Sushcheskaya NM (2001) Petrogenesis of olvine-phyric basalts from the Aphanasey Nikitin Rise: evidence for contamination by cratonic lower continental crust. J Petrol 42(2):277–319

Camus G, Goér de Herve A, Kieffer G, Mergoil J, Vincent PM (1973) Mise au point sur le dynamisme et la chronologie des volcans holocénes de la région de Besse-en-Chandesse (Massif Central Francais). Contre Rendu de l'Académie de Science Paris 277D:629–632

Camus G, Michard G, Olive P, Boivin P, Desgranges P, Jézéquel D, Meybeck M, Peyrus JC, Vinson JM, Viollier E, Kornprobst J (1993) Risques d'éruption gazeuse carbonique en Auvergne. Bulletin de Société Géologique de France 164:767–781

Class C, Goldstein SL (1997) Plume-lithosphere interactions in the ocean basin: constrains from the source mineralogy. Earth Planet Sci Lett 150:245–260

Condie KC (1993) Chemical composition and evolution of the upper continental crust: contrasting results from surface samples and shales. Chem Geol 104:1–37

Cornen G, Bandetb Y, Giressec P, Maleyd J (1992) The nature and chronostratigraphy of Quaternary pyroclastic accumulations from Lake Barombi Mbo (West-Cameroon). J Volcanol Geotherm Res 51:357–374

Coulon C, Vidal P, Dupuy C, Baudin P, Popoff M, Maluski H, Hermitte D (1996) The Mesozoic to early Cenozoic magmatism of the Benue Trough (Nigeria): geochemical evidence for the involvement of the St Helena plume. J Petrol 37:1341–1358

Couthures J (1989) The Sénèze maar (French Massif-Central): Hypothesis regarding a catastroph occurring about 1.5 million years ago. J Volcanol Geotherm Res 39:207–210

Downes H, Kostoula T, Jones AP, Beard AD, Thirlwall MF, Bodinier JL (2002) Geochemistry and Sr–Nd isotope compositions of mantle xenoliths from the Monte Vulture carbonatite-melilitite volcano, central Italy. Contrib Mineral Petrol 144:78–92

Favalli M, Tarquini S, Papale P, Fornaciai A, Boschi E (2011) Lava flow hazard and risk at Mt. Cameroon volcano. Bull Volcanol. doi:10.1007/s00445-011-0540-6

Fitton JG (1987) The Cameroon line, West Africa: a comparison between oceanic and continental alkaline volcanism. In: Fitton, JG, Upton B (eds) Alkaline igneous rocks, vol 30. Geological Society, London, Special Publications, London, pp 273–291

Freeth SJ, Rex DC (2000) Constraints on the age of Lake Nyos, Cameroon. J Volcanol Geotherm Res 97:261–269

Freeth SJ (1988) When the Lake Nyos dam fails there will be serious flooding in Cameroon and Nigeria—but when will it fail? EOS Trans Am Geophy Union 69 (32):776–777

Frey FA, Green DH, Roy SD (1978) Integrated models of basalt petrogenesis: a study of quartz tholeiites to olivine melilitites from south eastern Australia utilizing geochemical and experimental petrological data. J Petrol 19:463–513

Furman T (1995) Melting of metasomatised subcontinental lithosphere: undersaturated mafic lavas from Rungwe, Tanzania. Contrib Mineral Petrol 122:97–115

Gebhardt AC, De Batist M, Niessen F, Anselmetti FS, Ariztegui D, Haberzettl T, Kopsch C, Ohlendorf C, Zolitschka B (2011) Deciphering lake and maar geometries from seismic refraction and reflection surveys in Laguna Potrok Aike (Southern Patagonia, Argentina). J Volcanol Geotherm Res 201(1–4):357–363

Gebhardt AC, Ohlendorf C, Niessen F, De Batist M, Anselmetti FS, Ariztegui D, Kliem P, Wastegard S, Zolitschka B (2012) Seismic evidence of up to 200 m lake-level change in Southern Patagonia since marine isotope stage 4. Sedimentology 59(3):1087–1100

Graham DW, Jenkins WJ, Schilling JG, Thompson G, Kurz MD, Humphris SE (1992) Helium isotope geochemistry of mid-ocean ridge basalts from the South Atlantic. Earth Planet Sci Lett 110:133–147

Green DH, Wallace ME (1988) Mantle metasomatism by ephemeral carbonatite melts. Nature 336:459–462

Greenough JD (1988) Minor phases in the Earth's mantle: evidence from trace and minor element patterns in primitive alkaline magmas. Chem Geol 69:177–192

Gurenko AA, Hoernle KA, Hauff F, Schmincke HU, Han D, Miura YN, Kaneoka I (2006) Major, trace element and Nd–Sr–Pb–O–He–Ar isotope signatures of shield stage lavas from the central and western Canary Islands: insights into mantle and crustal processes. Chem Geol 233:75–112

Haase K (1996) The relationship between the age of the lithosphere and the composition of oceanic magmas: constraints on partial melting, mantle sources and the thermal structure of the plates. Earth Planet Sci Lett 144:75–92

Halliday AN, Davidson JP, Holden P, DeWolf C, Lee DC, Fitton JG (1990) Trace-element fractionation in plumes and the origin of HIMU mantle beneath the Cameroon line. Nature 347:523–528

Halliday AN, Lee DC, Tommasini S, Gareth RD, Paslick CR, Fitton JG, Dodie EJ (1995) Incompatible trace elements in OIB and MORB and source enrichment in the sub-oceanic mantle. Earth Planet Sci Lett 133:379–395

Halbwachs M, Sabroux JC, Grangeon J, Kayser G, Tochon-Danguy JC, Alain F, Beard JC, Villevieille A, Vitter G, Richon P, Wüest A, Hell J (2004) Degassing the 'Killer Lakes' Nyos and Monoun, Cameroon. EOS Trans Am Geoph Union 85(30):281–288

Haller MJ, Németh K (2006) Architecture and pyroclastic succession of a small Quaternary (?) maar in the Pali Aike Volkanic field, Santa Cruz, Argentina. Zeitschrift der Deutschen Geologischen Gesellschaft 157(3):467–476

Hart SR, Davis KE (1978) Nickel partitioning between olivine and silicate melt. Earth Planet Sci Lett 40:203–219

Hart SR, Dunn T (1993) Experimental cpx/melt partitioning for 24 trace elements. Contrib Mineral Petrol 113:1–8

Hawkesworth CJ, Kempton PD, Rogers NW, Ellam RM, van Calsteren PW (1990) Continental mantle lithosphere and shallow level enrichment processes in the Earth's mantle. Earth Planet Sci Lett 96:256–268

Herzberg C, Zhang J (1996) Melting experiments on anhydrous peridotite KLB-1: compositions of magmas in the upper mantle and transition zone. J Geophy Res 101:8271–8295

Hirose K, Kushiro I (1993) Partial melting of dry peridotites at high pressures: determination of compositions of melts segregated from peridotite using aggregates of diamonds. Earth Planet Sci Lett 114:477–489

Hoernle K, Tilton G, Le Bas M, Duggen S, Garbe-Schonberg D (2002) Geochemistry of oceanic carbonatites compared with continental carbonatites: mantle recycling of oceanic crustal carbonate. Contrib Mineral Petrol 142:520–542

Hofmann AW (1988) Chemical differentiation of the Earth: the relationship between mantle, continental crust and oceanic crust. Earth Planet Sci Lett 90:297–314

Ivanovich M, Harmon SR (1992) Uranium-series disequilibrium: applications to Earth, Marine and Environmental Sciences. Oxford University Press, Oxford, p 910

Jenner GA, Foley SF, Jackson SE, Green TH, Fryer BJ, Longerich HP (1993) Determination of partition coefficients for trace elements in high pressure-temperature experimental run products by laser ablation microprobe-inductively coupled plasma mass spectrometry (LAM-ICP-MS). Geochim Cosmochim Acta 57:5099–5103

Kamgang P, Njonfang E, Chazot G, Tchoua F (2007) Geochemistry and geochronology of felsic lavas of the Bamenda Mountains (Cameroon Volcanic Line). Contre Rendu Geosci 339:659–666

Kinzler RJ (1997) Melting of mantle peridotite at pressures approaching the spinel to garnet transition: application to mid-ocean ridge basalt petrogenesis. J Geophy Res 102:853–874

Kling GW (1988) Comparative transparency, depth of mixing, and stability of stratification in lakes of Cameroon, West Africa. Limnol Oceanogr 33(1):27–40

Kling GW, Evans WC, Tanyileke G, Kusakabe M, Ohba T, Yoshida Y, Hell JV (2005) Degassing Lakes Nyos and Monoun: Defusing certain disaster. Proc Nat Acad Sci 102(40):14185–14190

Kogarko LN, Kurat G, Ntaflos T (2001) Carbonate metasomatism of the oceanic mantle beneath Fernando de Noronha Island, Brazil. Contrib Mineral Petrol 140:577–587

Kusakabe M, Ohba T, Issa, Yoshida Y, Satake H, Ohizumi T, Evans WC, Tanyileke G, Kling GW (2008) Evolution of CO_2 in Lakes Monoun and Nyos, Cameroon, before and during controlled degassing. Geochem J 42:93–118

Kusakabe M, Sano Y (1992) Origin of gases in Lake Nyos, Cameroon. In: Freeth SJ, Ofoegb CO, Onohua KM (eds) Natural hazards in West and Central Africa. International monograph series on interdisciplinary earth science research and applications. Friedrich Vieweg & Sohn Verlag, Braunschweig, Wiesbaden, pp 83–95

Kusakabe M, Tanyileke G, McCord SA, Schladow SG (2000) Recent pH and CO_2 profiles at Lakes Nyos and Monoun, Cameroon: implications for the degassing strategy and its numerical simulation. J Volcanol Geotherm Res 97:241–260

Kusakabe M (this volume) Evolution of CO_2 content in Lakes Nyos and Monoun, and sub-lacustrine CO_2-recharge system at Lake Nyos as envisaged from $CO_2/^3He$ ratios and noble gas signatures. In: D. Rouwet et al. (eds) Volcanic Lakes. Springer, Berlin

Langmuir CH, Klein EM, Plank T (1992) Petrology systematics of mid-ocean ridge basalts: constraints on melt generation beneath ocean ridges. In: Phipps Morgan J, Blackman DK, Sinton JM (eds) Mantle flow and Mmelt generation at mid-ocean ridges, vol 71. American Geophysical Union Monograph, pp 183–280

Lee DC, Halliday AN, Fitton JG, Poli G (1994) Isotopic variation with distance and time in the volcanic Islands of the Cameroon line: evidence for a mantle plume origin. Earth Planet Sci Lett 123:119–138

Le Bas MJ, Le Maitre RW, Streckeisen A, Zanettin B (1986) Chemical classification of volcanic rocks based on the total alkali-silica diagram. J Petrol 27:745–750

Le Guern F, Sigvaldason GE (1989) (eds) The Lake Nyos event and natural CO_2 degassing, 1. J Volcanol Geotherm Res 39:95–275

Lockwood JP, Rubin M (1989) Origin and age of Lake Nyos maar, Cameroon. J Volcanol Geotherm Res 39:117–124

Lockwood JP, Costa JE, Tuttle ML, Tebor SG (1988) The potential for catastrophic dam failure at Lake Nyos maar, Cameroon. Bull Volcanol 50:340–349

Liotard JM, Dupuy C, Dostal J, Cornen G (1982) Geochemistry of the volcanic Island of Annobon, Gulf of Guinea. Chem Geol 35:115–128

Lorke A, Tietze K, Halbwachs M, Wüest A (2004) Response of Lake Kivu stratification to lava inflow and climate warming. Limnol Oceanogr 49(3):778–783

Lorenz V (2003) Maar-diatreme volcanoes, their formation, and their setting in hard-rock and soft-rock environments. Geolines 15:72–83

Lorenz V (2007) Syn- and posteruptive hazards of maar-diatreme volcanoes. J Volcanol Geotherm Res 159(1–3):285–312

Lorenz V (1985) Maars and diatremes of phreatomagmatic origin: a review. Trans Geol Soc South Africa 88:459–470

Lorenz CA (1986) On the growth of maars and diatremes and its relevance to the formation of tuff rings. Bull Volcanol 48:265–274

MacDonald GA, Katsura T (1964) Chemical composition of Hawaiian lavas. J Petrol 5:83–113

Marcelot G, Dupuy C, Dostal J, Rancon JP, Pouclet A (1989) Geochemistry of mafic volcanic rocks from the Lake Kivu (Zaire and Rwanda) section of the western branch of the African Rift. J Volcanol Geotherm Res 39:73–88

Martín-Serrano A, Vegas J, García-Cortés A, Galán L, Gallardo-Millán JL, Martín-Alfageme S, Rubio FM, Ibarra PI, Granda A, Pérez-González AJL (2009) Morphotectonic setting of maar lakes in the Campo de Calatrava Volcanic Field (Central Spain, SW Europe). Sediment Geol 222:52–63

Martin U, Németh K (2006) Eruptive mechanism of phreatomagmatic volcanoes from the Pinacate Volcanic Field: comparison between Crater Elegante and Cerro Colorado, Mexico. Zeitschrift der Deutschen

Gesellschaft für Geowissenschaften (ZDGG) 157 (3):451–466
Marzoli A, Piccirillo EM, Renne PR, Bellieni G, Iacumin M, Nyobe JB, Aka Tongwa F (2000) The Cameroon volcanic line revisited: petrogenesis of continental basaltic magmas from lithospheric and asthenosphric mantle sources. J Petrol 41:87–109
Mathieu L, Kervyn M, Ernst GGJ (2011) Field evidence for flank instability, basal spreading and volcano-tectonic interactions at Mt Cameroon. Bull Volcanol, West Africa. doi:10.1007/s00445-011-0458-z
Mazzarini F, D'Orazio M (2003) Spatial distribution of cones and satellite-detected lineaments in the Pali Aike Volcanic Field (southernmost Patagonia): insights into the tectonic setting of a Neogene rift system. J Volcanol Geotherm Res 125(3–4):291–305
Morrissey and Rouwet this issue
Mysen B (1979) Nickel partitioning between olivine and silicate melt; Henry's law revisited. Am Mineral 64:1107–1114
Nagao K, Kusakabe M, Yoshida Y, Tanyileke G (2010) Noble gases in Lakes Nyos and Monoun, Cameroon. Geochem J 44:519–543
Nelson DR, Chivas AR, Chappell BW, McCulloch MT (1988) Geochemical and isotopic systematics in carbonatites and implications for the evolution of ocean-island sources. Geochim Cosmochim Acta 52:1–17
Németh K, Agustin-Flores J, Briggs R, Cronin SJ, Kereszturi G, Landsay A (2012) Monogenetic volcanism of the South Auckland and Auckland Volcanic Fields. In: IAVCEI—CMV/CVS—IAS 4IMC conference Auckland, New Zealand
Ngounouno I, Deruelle B, Guiraud R, Vicat JP (2001) Magmatismes tholéiitique et alkalin des demi-grabens crétacés de Mayo Oulo-Léré et de Babouri-Figuil (North du Cameroun – Sud du Tchad) en domaine d'extension continentale. Contre Rendu Geoscience 333:201–207
Nkambou C, Deruelle B, Danielle V (1995) Petrology of Mt. Etindé nephelinite series. J Petrol 36(2):373–393
Ottonello G, Ernst WG, Joron JK (1984) Rare earth and transition element geochemistry of peridotite rocks: I. peridotites from the western Alps. J Petrol 25:434–472
Pearson DG, Canil D, Shirey SB (2003) Mantle samples included in volcanic rocks: xenoliths and diamonds. Treatise Geochemistry V2:171–275
Pier JG, Luhr JF, Podosek FA, Aranda-Gómez JJ (1992) The La Brena—El Jaguey Maar Complex, Durango, Mexico: 1. Petrology and geochemistry. Bull Volcanol 54:405–428
Plank T, Langmuir CH (1998) The chemical composition of subducting sediment and its consequences for the crust and mantle. Chem Geol 145:325–394
Price RC, Nicholas IA, Grey CM (2003) Cainozoic igneous activity. In: Birch WD (ed) Geology of Victoria, Special Publication 23. Geological Society of Australia, pp 361–375
Rankenburg K, Lassiter JC, Brey G (2005) The role of continental crust and lithospheric mantle in the genesis of Cameroon Volcanic Line lavas: constraints from isotopic variations in lavas and megacrysts from Biu and Jos plateaux. J Petrol 46(1):169–190
Righter K, Leeman WP, Hervig RL (2006) Partitioning of Ni, Co and V between spinel- structured oxides and silicate melts: importance of spinel composition. Chem Geol 227:1–25
Roeder PL, Emslie RL (1970) Olivine-liquid equilibrium. Contrib Mineral Petrol 29:275–289
Robinson JAC, Wood BJ (1998) The depth of the spinel to garnet transition at the peridotite solidus. Earth Planet Sci Lett 164:277–284
Rudnick RL, McDonough WF, Chappel BW (1993) Carbonatite metasomatism in the northern Tanzanian mantle: petrographic and geochemical characteristics. Earth Planet Sci Lett 114:463–475
Salters VJM (1996) The generation of mid-ocean ridge basalts from the Hf and Nd isotope perspective. Earth Planet Sci Lett 141:109–123
Sato H, Aramaki S, Kusakabe M, Hirabayashi JI, Sano Y, Nojiri Y, Tchoua F (1990) Geochemical difference of basalts between polygenetic and monogenetic volcanoes in the central part of the Cameroon Volcanic Line. Geochem J 24:357–370
Scarrow JH, Cox KG (1995) Basalts generated by decompressive adiabatic melting of a mantle plume—a case study from the Ise of Skye, NW Scotland. J Petrol 36:3–22
Schmincke HU (2007) The quaternary volcanic fields of the east and west Eifel (Germany). In: Ritter J, Christensen U (eds) Mantle plumes. Springer, Berlin, pp 241–322
Schenker F, Dietrich V (1986) The Lake Nyos gas catastrophe (Cameroon). A magmatological interpretation. Scweiz Mineralogie ünd Petrographie Mitt 66:343–384
Shaw DM (1970) Trace element fractionation during anatexis. Geochim Cosmochim Acta 34:237–243
Shaw DM, Cramer JJ, Higgines MD, Truscott MG (1986) Composition of the Canadian Precambrian shield and the continental crust of the Earth, Special Publication 24. Geological Society, London, pp 275–282
Shen Y, Forsyth DW (1995) Geochemical constraints on initial and final depth of melting beneath mid-ocean ridges. J Geophys Res 100:2211–2237
Sigurdsson H, Devine ID, Tchoua FM, Presser TS, Pringle MK, Evans WC (1987) Origin of the lethal gas burst from Lake Monoun, Cameroon. J Volcanol Geotherm Res 31:1–16
Sottili G, Taddeucci J, Palladino DM, Gaeta M, Scarlato P, Ventura G (2009) Sub-surface dynamics and eruptive styles of maars in the Colli Albani Volcanic District, Central Italy. J Volcanol Geotherm Res 180:189–202
Suh CE, Sparks RSJ, Fitton JG, Ayonghe SN (2003) The 1999 and 2000 eruptions of Mount Cameroon: eruption behavior and petrochemistry of lava. Bull Volcanol 65:267–281
Sun SS, McDonough WF (1989) Chemical and isotopic systematics of oceanic basalts: implications for mantle composition and processes. In: Saunders AD, Norry MJ (eds) Magmatism in the ocean basins, Special Publication 42. Geological Society, London, pp 313–345

Tabot CT, Fairehead JD, Stuart GW, Ateba B, Ntepe N (1992) Seismicity of the Cameroon Volcanic Line, 192-1990. Tectonophysics 212:303–320

Tassi F, Vaselli O, Fernández E, Duarte E, Martínez M, Delgado Huertas A, Bergamaschi F (2009) Morphological and geochemical features of crater lakes in Costa Rica: an overview. J Limnol 68(2):193–205

Taylor SR, McLennan SM (1995) The chemical evolution of the continental crust. Rev Geophy 33:241–265

Temdjim R, Boivin P, Chazot G, Robin C, Rouleau E (2004) L`hétérogénité du manteau supérieur a l`aplomb du volcan de Nyos (Cameroun) révélée par les enclaves ultrabasiques. C R Geosci 336:1239–1244

Teitchou MI, Grégoire M, Temdjim R, Ghogogu RT, Ngwa C, Aka FT (2011) Mineralogical and geochemical fingerprints of mantle metasomatism beneath Nyos volcano (Cameroon VolcanicLine). Geological Society of America Special Papers 478, 193–210

Tietze K (1980) The unique methane gas deposit in Lake Kivu (Central Africa)—stratification, dynamics, genesis and development. In: Proceedings of the first annual symposium on unconventional gas recovery, Society of Petroleum Engineers (SPE) of the American Institute of Mining, Metallurgical, and Petroleum Engineers (AIME) and United States Department of Energy (DOE), Pittsburgh, SPE/DOE 8957, pp 275–287

Touret J, Grégoire M, Teitchou MI (2010) Was the lethal eruption of Lake Nyos related to a double CO_2/H_2O density inversion? C R Geosci 342:19–26

UNEP/OCHA Joint Environment Unit (2005) Lake Nyos dam assessment, Cameroon. http://www.reliefweb.int/library/documents/2005/ocha-cmr

Vaselli et al. (this issue) Are limnic eruptions in the CO_2–CH_4-rich gas reservoir of Lake Kivu (Democratic Republic of the Congo and Rwanda) possible? Insights from physico-chemical and isotopic data. In: In: D. Rouwet et al. (eds) Volcanic Lakes. Springer, Berlin

Walter MJ (1998) Melting of garnet peridotite and the origin of komatiite and depleted lithosphere. J Petrol 39:29–60

Walter MJ, Katsura T, Kubo A, Shinmei T, Nishikawam O, Ito E, Lesher C, Funakoshi K (2002) Spinel–garnet lherzolite transition in the system CaO-MgO-Al_2O_3-SiO_2 revisited: An in situ X-ray study. Geochim Cosmochim Acta 66(12):2109–2121

White W (2005) Geochemistry. www.geo.cornell.edu/geology/clsses/geo455/Chapters.HTML

White JDL, Ross PS (2011) Maar-diatreme volcanoes: a review. J Volcanol Geotherm Res 201(1–4):1–29

Walther JV (2005) Essentials of geochemistry. Jones and Bartlett Publishers, Boston, p 704

Wohletz K, Heiken G (1992) Volcanology and geothermal energy. University of California Press, Berkeley, p 432

Yaxley GM, Crawford AJ, Green DH (1991) Evidence for carbonatite metasomatism in spinel peridotite xenoliths from western Victoria, Australia. Earth Planet Sci Lett 107:305–317

Yaxley GM, Green DH, Kamenetsky V (1998) Carbonatite metasomatism in the southeastern Australian lithosphere. J Petrol 39(11–12):1917–1930

Yokoyama T, Aka FT, Kusakabe M, Nakamura E (2007) Plume-lithosphere interaction beneath Mt. Cameroon volcano, West Africa: Constraints from ^{238}U-^{230}Th-^{226}Ra and Sr–Nd–Pb isotopic systematics. Geochim Cosmochim Acta 71:1835–1854

Zimanoswski B (1998) Phreatomagmatic explosions. In: Freundt A, Rosi M (eds) From magma to tephra. Developments in Volcanology, vol 4. Amsterdam, pp 25–54

Are Limnic Eruptions in the CO_2–CH_4-Rich Gas Reservoir of Lake Kivu (Democratic Republic of the Congo and Rwanda) Possible? Insights from Physico-Chemical and Isotopic Data

Orlando Vaselli, Dario Tedesco, Emilio Cuoco, and Franco Tassi

Abstract

An overturn of Lake Kivu was seriously considered after the January 2002 Nyiragongo volcanic eruption, which erupted 20×10^6 m^3 of lava from a NS-oriented fissure on the southern flank of the Congolese volcano. Part of this silica-undersaturated magma produced a lava flow that entered Lake Kivu down to a depth of 70–100 m. The possibility of a rollover comes from the fact that Lake Kivu is meromictic and below ≈250 m a CO_2–CH_4-rich gas reservoir is present. Thus, the riparian population (≈2,500,000 people) is endangered by a possible limnic eruption. During last 30 years several vertical profiles carried out by several researchers have evidenced a relatively pronounced vertical physico-chemical and isotopical variation. Nevertheless, saturation of CO_2 and CH_4 appears to be far from critical values, indicating that presently the hydrostatic pressure cannot presently be overcome. Recent studies have suggested an increase in dissolved gases (particular CH_4) at depth and the uprising of the chemocline, a limnic eruption could possibly occur within 80–200 years from now. More studies are needed to follow up the lake evolution with time. Simulations will shed light on possible internal and external factors able to provoke the release a

O. Vaselli · F. Tassi (✉)
Department of Earth Sciences, Via G. La Pira 4, 50121 Florence, Italy
e-mail: franco.tassi@unifi.it

O. Vaselli · F. Tassi
CNR-IGG, Institute of Geosciences and Earth Resources, Via G. La Pira 4, 50121 Florence, Italy

D. Tedesco
Analysis and Prevention of Natural Hazards in DRC —UNOPS, Goma, DRC

D. Tedesco · E. Cuoco
Department of Environmental Sciences, 2nd University of Naples, Via Vivaldi 43, 81100 Caserta, Italy

D. Rouwet et al. (eds.), *Volcanic Lakes*, Advances in Volcanology,
DOI 10.1007/978-3-642-36833-2_22,
© Springer-Verlag Berlin Heidelberg 2015

suffocating and, possibly, inflammable killer cloud. In this paper, we investigate using recent historical eruptive events of Nyiragongo volcano, we discuss the possibility that a limnic eruption may occur in a near future, although the stability of Lake Kivu is presently high: only exceptionally high magnitude events appear to be able to destabilize the 560 × 10^9 m^3 water volume contained in its basin.

Keywords
Lake Kivu · Limnic eruptions · CO_2–CH_4-rich gas reservoir · Physical-chemical limnology · Energy resource · Hazard assessment

1 Introduction

Lake Kivu (1°24′S–2°30′S and 28°50′E and 29°23′E) lies between the territories of the Democratic Republic of the Congo (DRC) and Rwanda (Fig. 1). The lake water, at an altitude of 1,460 a.s.l., covers a surface of about 2,400 km^2 (1,370 km^2 of which are in the Congolese territory) with a catchment area of about 7,000 km^2. The maximum length of Lake Liku is 84 km and the maximum width is 50 km. Lake Kivu belongs to the western branch of the East African Rift

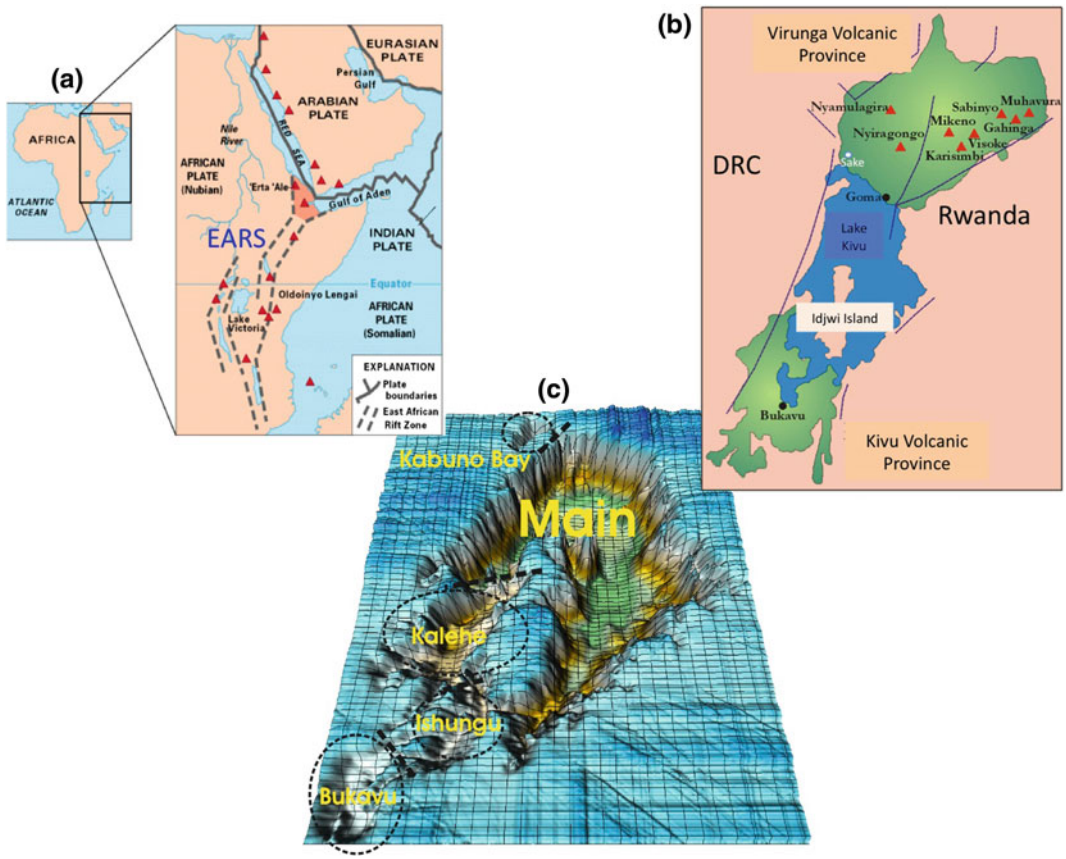

Fig. 1 Schematic geodynamical (**a**) and volcanological (**b**) setting and bathymetry of lake Kivu with the five sub-basins (**c**)

System (EARS) (Fig. 1a) and is part of the Virunga Volcanic Province (Ebinger and Furnam 2002/2003) (Fig. 1b) where silica-undersaturated, ultra-alkaline and alkalic-mafic magma predominate. The two active Virunga volcanoes, Nyiragongo and Nyamuragira (Fig. 1b), are located north of Lake Kivu. The erupted Nyiragongo lavas have an unusual composition with the lowest recorded viscosity among terrestrial magmas (Chakrabarti et al. 2009 and references therein).

Lake Kivu is an important water resource among the African Great Lakes, having an estimate water volume of 560×10^9 m^3. Its depth is remarkable, the mean depth being 240 m, while the deepest point is 485 m. Lake Kivu drains to the south into the Ruzizi River, which feeds Lake Tanganyika.

One of most striking peculiarities of Lake Kivu is the presence of a large CO_2–CH_4-rich gas reservoir at depth >250 m (e.g. Damas 1937; Schmitz and Kufferth 1955; Capart 1960) and for this reason in the past limnologists and geoscientists were attracted by the singularity of the physico-chemical composition of the lake water (e.g. Degens et al. 1973; Tietze 1978). An estimated 300 km^3 of carbon dioxide and 55–60 km^3 of methane are dissolved and trapped at significant depth in the lake (e.g. Kling et al. 2006).

In January 2002, the sudden eruption of Nyiragongo produced more than 20×10^6 m^3 of fresh magma that fed several lava flows and one of them entered the lake down to a depth of ≈70 m (e.g. Tedesco et al. 2007). This event promptly recalled the disastrous limnic eruption at Lake Nyos (Cameroon) in 1986. Here, about 1,800 people were suffocated by a CO_2-rich cloud released from the deepest part of this lake (Tietze 1987; Kling et al. 1989; Evans et al. 1993; Evans and Kling, this issue; Kusakabe, this issue). The magnitude and the number of people possibly involved in a gas outburst at Lake Kivu would be much higher. Moreover, the scenario generated by the presence of an inflammable gas such as methane can hardly be constrained.

In this chapter, we report the main compositional features of the deep water strata of Lake Kivu with the aim to (i) outline the peculiar chemical and isotopic stratification and its physico-chemical properties, (ii) highlight the scenarios related to a possible overturn of the lake and (iii) estimate the current hazard from the lava flow constrained from previous eruptive events and (iv) suggest future studies for the monitoring of Lake Kivu.

2 The Lake Kivu: Structure, Limnology and Geochemical Features

About 1,300 mm of rainwater represent the annual precipitation in the region. Rainfall is higher along the western side with respect to the eastern side of Lake Kivu (Villanueva et al. 2008). The average surface water lake temperature is about 24 °C (Snoeks 1994). Lake Kivu, characterized by a Main basin and four sub-basins, can be classified as a damming lake, resulting by the intense volcanic activity of the numerous central edifices and parasitic centers that form the Virunga Volcanic Province (Capaccioni et al. 2002, 2003; Chakrabarti et al. 2009). The Great Valley was thus dammed to the north, interrupting the northward flow of the pre-existing rivers (Holzförster and Schmidt 2007 and references therein). Presently, the lake waters are drained to the south by the River Ruzizi, which enters the Lake Tanganyika at a rate of ~100 L/s. The central part is occupied by the world's tenth-largest inland island (Idjwi) that is home of more than 150,000 people. Totally, the 1,200 km long lake shoreline, that stretches no more than 50 m away from it (Van den Bossche and Bernacsek 1990; Verheyen et al. 2003), hosts several settlements, e.g. Bukavu, Kabare, Kalehe, Sake and Goma in DRC and Gisenyi, Kibuye and Cyangugu in Rwanda, with an estimated population of more than 2,500,000 people.

A permanent water stratification at Lake Kivu was highlighted by many authors (e.g. Tassi et al. 2009 and references therein). According to Coulter et al. (1984) and Snoeks (1994), Lake Kivu is a meromictic lake with a large methane and carbon dioxide reservoir at depth. The anoxic layer (monimolimnion) is located below 60 m and methane-saturated waters are occurring in the

deepest part of the lake (Coulter et al. 1984; Van den Bossche and Bernacsek 1990; Isumbisho et al. 2004; Sarmento et al. 2006). Despite the fact that most of the East African Valley lakes is characterized by a relatively deep pelagic zone, abundantly colonized by small fishes (Coulter et al. 1984; Lowe-McConnell 1993), Lake Kivu is also distinguishably different in this respect since fish diversity is relatively poor with only 26 endemic species (Hanek et al. 1991; Snoeks 1994; Villanueva et al. 2008). Exotic fishes were introduced, i.e. *Oreochromis macrochir* (Boulenger) and *Tilapia rendalli* (Boulenger) (Chapman et al. 1996; De Vos et al. 2001) and *Limnothrisssa miodon* (Boulenger) and *Stolothrissa tanganyicae* (Regan) (Spliethoff et al. 1983; Van den Bossche and Bernacsek 1990), to increase biodiversity and productivity of the lake (Welcomme 1988).

The presence of large amounts of dissolved gases in the deep waters of Lake Kivu was recognized for the first time in 1935 (Damas 1937). However, it is about 20 years later that Lake Kivu was recognized to contain a *lake of gas* at depth (Peeters 1957; Kiss 1959, 1966; Borginiez 1960; Capart 1960; Kufferath 1960; Burke and Muller 1963; Schmitz and Kufferath 1955). This "*lake in the lake*" is mainly composed by a reservoir of CO_2 and CH_4, the latter being considered exploitable for renewable energy (e.g. Tietze 2000) since a recharge of gas in the lake was estimated to be comprised between 125 and 250,000,000 m^3 per year (e.g. Halbwachs 2003).

A systematic study on the definition of the vertical chemical stratification with depth in Lake Kivu began in the early seventies. Several authors, and particularly those belonging to the *Degens Group*, produced several scientific articles where the peculiar features of the Kivu deepwater structure were highlighted (Degens et al. 1972, 1973; Degens and Kulbiki 1973; Deuser et al. 1973; Hecky and Degens 1973; Wong and Von Herzen 1974; Jannash 1975; Krumbein 1975; Degens and Ittekkot 1982). In 1974 and 1975 the vertical stratification of Lake Kivu was also stressed by Tietze (1978), when 23 profiles were measured at different locations. In 2004, Schmid et al. (2005) provided four more temperature and salinity profiles between Idjwi Island and Goma. From these profiles average profiles, giving the density and other parameters at a 1 m vertical resolution, were calculated. More recently, Hirslund (2012) assessed that the chemoclines at the Lake Kivu are moving upwards with a vertical flow rates varying from ~0.05 below 390 m to ~1.39 below ~140 m (km^3 $year^{-1}$).

In Fig. 2, the variations of pressure, temperature, electrical conductivity (EC) and density with depth for the Main Basin of Lake Kivu are reported (Tietze 1978). At about 250 m a sharp increase in temperature, EC and density is

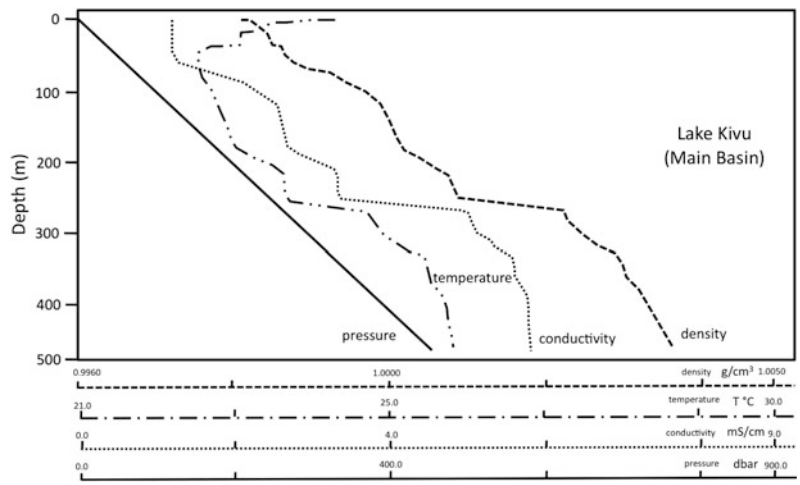

Fig. 2 Density, temperature, electrical conductivity and pressure vertical profile in the MAIN Kivu (modified after Tietze 1978)

observed, which marks the presence of the CO_2–CH_4(+H_2S) dissolved gases, which are stored at depth due to the hydrostatic pressure. Unless EC and density, which show a more or less progressive increase with depth, temperature is characterized by a relatively dramatic decrease down to 50 m and consequently manifests a slow, though continuous, increment up to 250 m (Fig. 2). At the lake bottom, a temperature of about 26 °C is recorded. Remarkably, pH values strongly vary from the surface to the bottom of the lake, being decreasing from about ≈9 down to 6.5 (e.g. Tassi et al. 2009). The variability of the physical parameters and the pH values also reflects the distribution of the main and trace solutes with the depth. The total sum of anions and cations increases from about 15–75 meq/L (Fig. 3a, b). It is worthy to observe that HCO_3 (Fig. 3c) and Na (Fig. 3d) do represent a large percentage of the anions and cations, respectively. Their distribution with depth, similarly to that of some of the trace elements (Fig. 3e, f) analyzed by Tassi et al. (2009), intimately mimic that of the physical parameters (Fig. 2).

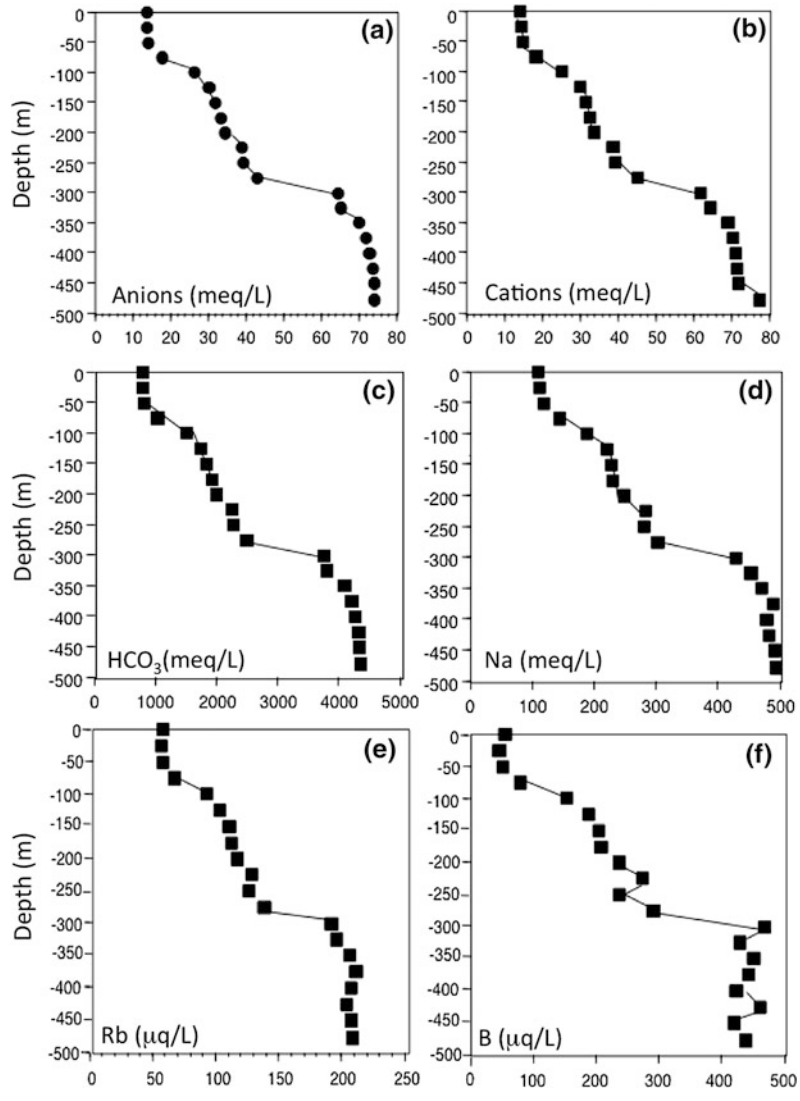

Fig. 3 Vertical distribution of anions (**a**) and cations (**b**) (in meq/L), HCO_3 (**c**) and Na (**d**) in mg/L and Rb (**e**) and B (**f**) in µg/L from the main basin. Data from Tassi et al. (2009)

The physical and chemical data of Fig. 2 are referred to the Main Kivu, i.e. the largest and deepest portion of Lake Kivu. The Rwandan-Congolese lake can however be divided into five sub-basins (Main, Kabuno Bay, Kalehe, Ishung and Bukavu; Fig. 1c), which are topographically separated by relatively shallow sills (Degens et al. 1973; Tietze 1978; Botz et al. 1988; Spigel and Coulter 1996; Lahmeyer-Osae 1998; Tassi et al. 2009). In Tassi et al. (2009), the five sub-basins were sampled vertically for water and dissolved gas chemical and isotopic analysis by descending a Rilsan® tube (impermeable to water and gas diffusion) at the maximum depths for each basin. The geochemical and isotopic compositions highlighted that distinct features characterize the five sub-basins, likely due to three processes: (i) water-mineral equilibrium, (ii) biological cycle and (iii) deep fluid inputs. Bukavu Basin does not show any vertical chemical stratification due to either the relatively low depth (≈80 m) or the absence of deep gas/water inputs, as testified by its flat morphology, likely due to the dismantling of the Southern Kivu volcanic (extinct) edifices. Chemical and isotopic variations were recorded for the four basins.

A general agreement exists on the origin of carbon dioxide, which is mainly related to the discharge of scrubbed magmatic fluids at depth (e.g. Tassi et al. 2009 and references therein), whereas methane is basically formed by methanogenic microbial activity (e.g. Schoell et al. 1988).

A debate on the Lake Kivu water data unchained when Tietze (1978) assessed that, despite the importance of the data provided by the *Degens Group*, several errors were recognized, mainly due to the equipment used to determine the vertical profile of CO_2 and, particularly of CH_4. On the other hand, Tassi et al. (2009) stated that the vertical distribution of the molar concentrations of dissolved CO_2 and CH_4 were consistent with those of Tietze (1978) and Schmid et al. (2005) up to a depth ≤250 m. Below 250 m, the concentrations of both species were recognized by Tassi et al. (2009) to be significantly lower, especially with respect to those reported by Schmid et al. (2005) (Fig. 4a).

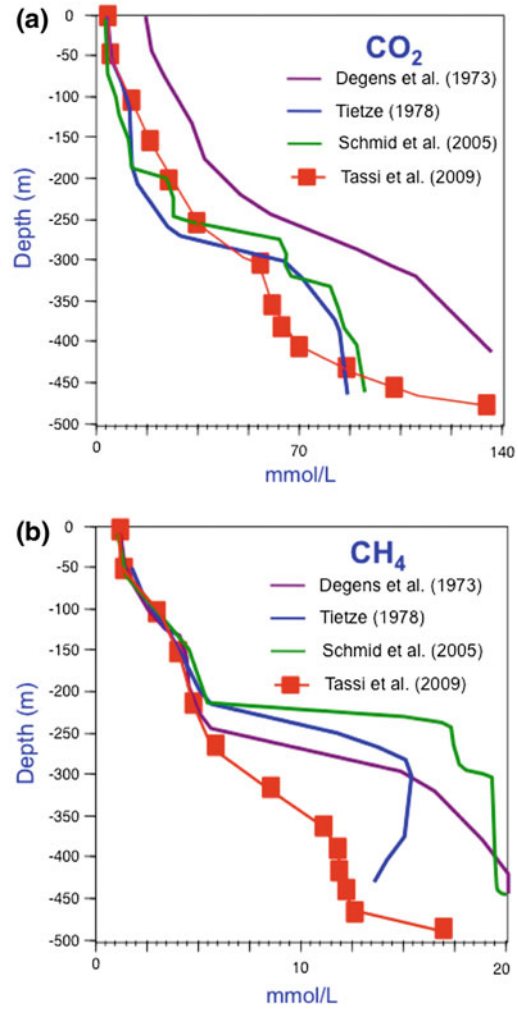

Fig. 4 Vertical distribution of CO_2 (**a**) and CH_4 (**b**) from the main basin, according to different authors. Modified after Tassi et al. (2009)

Tietze (2000) suggested that imprecision and inaccuracy of the sampling and analytical techniques by various authors (e.g. Schmitz and Kufferath 1955; Degens et al. 1973; Tietze 1978; Tietze et al. 1980; TECHNIP and BRGM 1986) were responsible for these differences. Nevertheless, Tassi et al. (2009) concluded that the observations reported in Tietze (2000) cannot be accepted as the only cause of these compositional differences, because they do not explain the general agreement of most authors among the measured CO_2 and CH_4 vertical profiles of water strata above the gas reservoir.

The differences in methane concentrations measured in 1974 (Tietze et al. 1978) and in 2004 (Schmid et al. 2005) were interpreted as due to the progressive increase in nutrient input to the lake related to the fast-growing human population in its catchment area, and thus the increase in the biomass population (Pasche et al. 2011). This process would have led to a more efficient CO_2–CH_4 conversion (Schmid et al. 2005). Tassi et al. (2009) claimed that the reasonable hypothesis proposed by Tietze (1978) and Schmid et al. (2005) is however not able to motivate the significant differences among the CO_2 concentration profiles measured in the Main Kivu by various scientific teams in the Main Basin (Fig. 4a). Furthermore, the CH_4 concentrations measured by Degens et al. (1973) were even higher than those measured more than 30 years later (Fig. 4b). Tietze (1978) and Schmid et al. (2005) concluded that these differences can possibly be attributed to a spatial variability able to affect methanogenic bacterial communities in terms of amount and types. This statement is supported by the significant differences recognized in various areas of the lake of the phytoplankton biomass in the epilimnion, the latter showing strong seasonal variations (Sarmento et al. 2006). If so, a different mechanism must be invoked to account for the differences among the CO_2 vertical profiles measured in the last decades. Carbon dioxide originates from mantle degassing (e.g. Schoell et al. 1988; Schmid et al. 2005), thus its spatial distribution might depend on the location of the sub-lacustrine discharges. Nevertheless, a direct relationship between the distribution of dissolved CO_2 anomalies and the location of the sub-lacustrine discharges is not expected, as the effects of horizontal mixing in open lakes, such as the Main Basin, controlled by processes governed by a complex combination of chemical-physical parameters, are difficult to predict (e.g. Murthy 1976; Imbonden and Wüest 1995; Peeters et al. 1996).

To solve the problem of the vertical distribution of the two main (CO_2 and CH_4) and other gas components in Lake Kivu, a joint measurement involving the different scientific groups should be planned in order to: (i) directly compare the different methodologies adopted for defining the stratigraphical variations; (ii) avoid differences that might be expected when comparing chemical profiles obtained in different periods of the year; (iii) adopt recent techniques that imply the utilization of new CO_2 and CH_4 sensors.

3 The Kabuno Sub-basin

Most studies in Lake Kivu focused on the Main Basin since the 2002 lava flow descended into the lake at a depth of 70 m, less attention was paid to the sub-basin of Kabuno (about 150 m deep), despite the fact that is has a strong chemical stratification with a shallow (25 m deep) CO_2-rich layer. No significant methane concentrations were found in the Kabuno basin. This is also highlighted by the variation with depth of the sum of anions and cations with the depth. Basically, the concentrations of these two parameters at 150 m are similar to or even higher (Fig. 5a, b) than those measured in the Main Basin at the depth of 485 m (Fig. 3a, b). When comparing the contents of HCO_3 (Fig. 5c) and Na (Fig. 5d), as well as those of selected trace elements (Fig. 5e, f), the general picture is that Kabuno acquired a higher salinity and gas content with respect to all the other sub-basins that form Lake Kivu. Significant differences between the Main and Kabuno basins are also evidenced when considering the oxygen and hydrogen isotopic values, those of Kabuno are consistently lower than those of the Main Basin (Fig. 6).

To explain the peculiar geochemical features of Kabuno, separated by a shallow (ca. 7 m) threshold from the Main Basin, Tassi et al. (2009) hypothesized a high-rate of a sub-lacustrine CO_2-rich mantle-derived discharge into Lake Kivu, likely preventing the conditions for the presence of methanogenic bacteria, as instead occurs in the remaining part of the lake. Nevertheless, a decoupling between the carbon (in CO_2) and helium isotopes was observed since the $\delta^{13}C$–CO_2 values have a more negative signature (<−10 and ‰) than that of the Main Basin (Fig. 7a). The $\delta^{13}C$-TDIC values at Kabuno

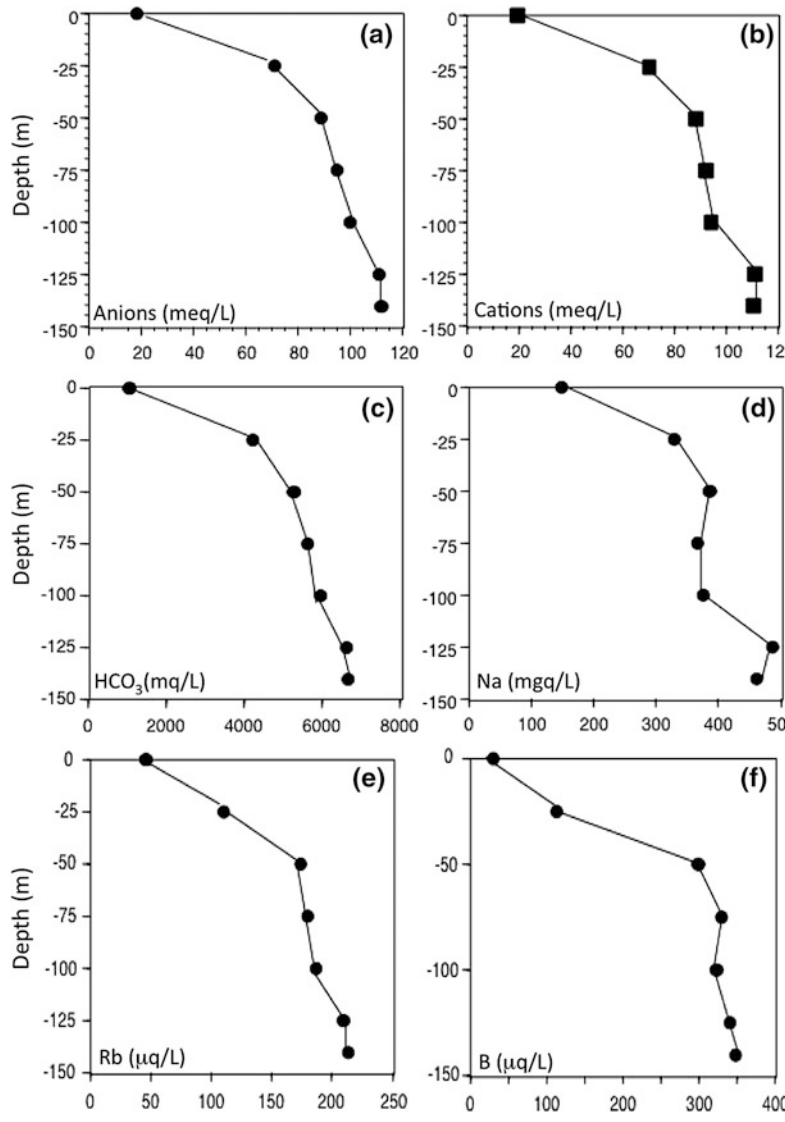

Fig. 5 Vertical distribution of anions (**a**) and cations (**b**) (in meq/L), HCO_3 (**c**) and Na (**d**) in mg/L and Rb (**e**) and B (**f**) in µg/L from the Kabuno basin. Data from Tassi et al. (2009)

below 25 m are as negative as those of the Main Basin at depths >300 m where they tend to achieve the same negative values (Fig. 7b). Contrarily, the helium isotopes, corrected with respect to the relative amount of neon in the samples, assuming that Ne is essentially all of atmospheric origin (Poreda and Craig 1989), show values up to 6 (as R/Ra) and thus, higher than those recorded in the Main Basin (R/Ra ≈ 3) (Fig. 7c), where a contribution of crustal helium is present (Tedesco et al. 2010). This apparent contradiction between the carbon and helium isotopes in the Main and Kabuno basins can possibly be explained with a different system feeding the Kabuno Basin with respect to that of the Main Basin. Alternatively, the presence of organic-rich terrains and/or ground waters interacting with the deep fluids may be responsible of the lighter carbon isotopic composition observed in the Kabuno Basin.

This decoupling between the helium and carbon isotopes may also be related to the different vulcanological settings of the Main and Kabuno basins, the first one being located in the

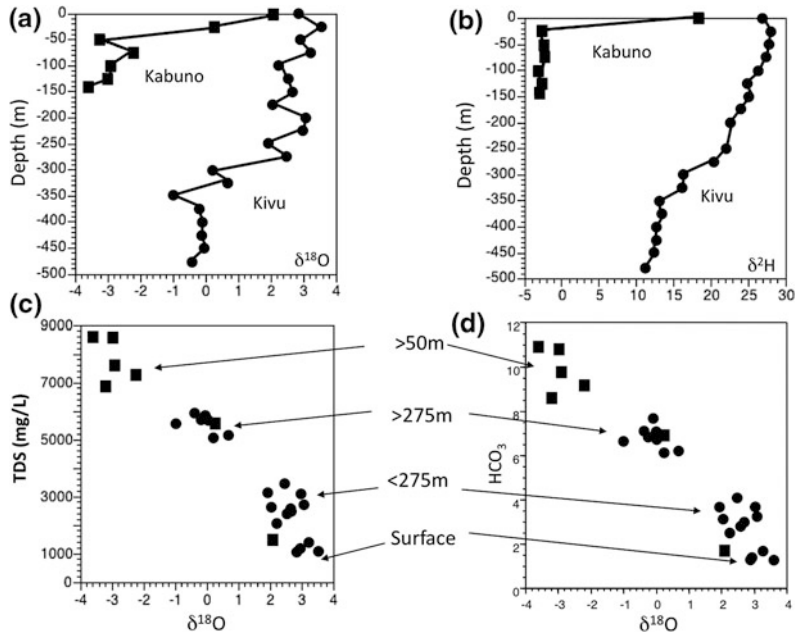

Fig. 6 Vertical distribution of $\delta^{18}O$ (**a**) and $\delta^{2}H$-H_2O (**b**) and Total Dissolved Solids (TDS) versus $\delta^{18}O$ (**c**) and HCO_3 versus $\delta^{18}O$ (**d**) in the main and Kabuno basins. Data from Tassi et al. (2009)

Nyiragongo realm, while the second one in that of Nyamuragira. Interestingly, the inland manifestations, inside and near the town of Sake (Fig. 1b) that lies in the geological domain of Nyamuragira, show the same isotopic features as those observed in the Kabuno Basin, i.e. negative $\delta^{13}C$–CO_2 and high R/Ra values, also comparable to those of the fumarolic gas discharges at the Nyiragongo crater and surrounding areas (Vaselli et al. 2002, 2003; Smets et al. 2010a; Tedesco et al. 2010) (Fig. 8). The gas discharges in the Main Basin seem to be more affected by an "infra-cratonic component" (Minissale et al. 2000), which is physically represented by some gas manifestations originating in the Archaean terrains on the eastern side of the rift (e.g. Rambo thermal springs, Tedesco et al. 2010), diluting the mantle component (Fig. 8). Consequently, a tentative conceptual model for the northern part of the Lake Kivu is shown in Fig. 9.

According to the concentrations of the dissolved gases at the Kabuno Basin (Tassi et al. 2009), the pressure of each gas components is plotted versus depth in Fig. 10. In order to overcome the hydrostatic pressure, an increase of the pressure at depth of about 2 bars or a displacement of about 18 m of the gas reservoir located at 50 m are required. As a consequence, Kabuno Bay may represent the most hazardous source of gas outburst since its gas reservoir is not only dominated by mantle-derived gases, but it is also physically isolated from mixing currents that moderate gas accumulation in the other basins of the lake.

4 The Lake Kivu: Energy Resource Versus Limnic Eruption

Despite the clear evidence that Lake Kivu is a resource related to the possibility of using the large reservoir of methane stored at depth as a clean energy fuel, most scientists (e.g. Hallbwachs et al. 2002 and references therein) have pointed out the hazard related to the presence of the mixed gases stored within the lake. The main reason of this warning is chiefly related to the presence next to the lake of the two active volcanoes, Nyiragongo and Nyamuragira (Fig. 1). The experience of the January 2002 eruption of Nyiragongo has alarmed the scientific community since the lava flow that reached the depth of 70 m inside the lake was not able to trigger a

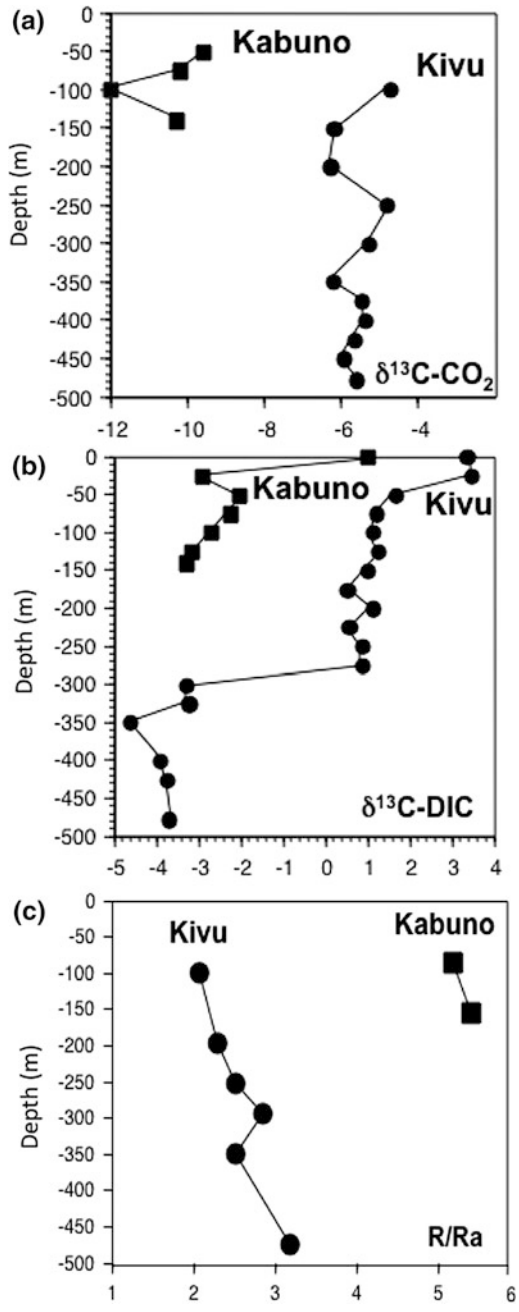

Fig. 7 Vertical distribution of **a** $\delta^{13}C$–CO_2 and **b** $\delta^{13}C$-DIC (Dissolved Inorganic Carbon) and **c** helium isotopes (expressed as Rc/Ra, where *R* is the measured $^3He/^4He$, while *Ra* is that in the air, i.e. 1.39×10^{-6}). The helium isotopic ratios (R) were corrected with respect to the relative amount of neon in the samples, assuming that Ne is essentially all of atmospheric origin (Poreda and Craig 1989). Data from Tassi et al. (2009)

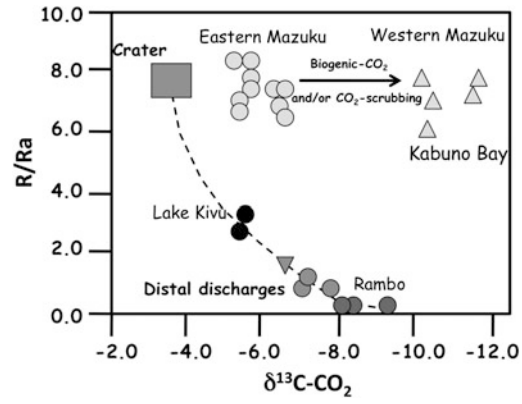

Fig. 8 Helium isotopes versus $\delta^{13}C$-CO_2 in the main gas manifestations in the Virunga Province. The helium isotopic ratios (R) were corrected with respect to the relative amount of neon in the samples, assuming that Ne is essentially all of atmospheric origin (Poreda and Craig 1989). Gas samples are from the fumarolic crater discharges of Nyiragongo volcano, the dry gas vents in the eastern and western part of the lake Kivu shoreline, the bottom of lake Kivu and the distal discharges including those gases seeping from the Archaean basement (i.e. Rambo). Modified after Tedesco et al. (2010)

thermally driven gas outburst induced by the presence of the large CO_2 and CH_4-rich gas reservoir located below the depth of about 250 m. According to Lorke et al. (2004), no gas outbursts are expected at Kivu from future eruptions with similar or comparable dimensions of that occurred in 2002. However, on the basis of sediment cores, Haberyan and Hecky (1987) have indicated a posteriori the probable occurrence of previous large-scale limnic eruptions since in at least five layers of the past 5,000 years, common microfossils were missing in the lake-bottom sediments and huge amount of external debris were present. These layers were later explained to be the result of a large-scale wave (possibly produced by a gas outburst) that favored a large influx of terrigeneous sediments and external organic matter (Haberyan and Hecky 1987) on its way back to the lake. This observation appears to be supported by Al-Mutlaq et al. (2008) who recognized in a sediment core of Lake Kivu a sapropelic horizon reflecting lake water turnover with ventilation or hydrothermal activity. Nevertheless, the present

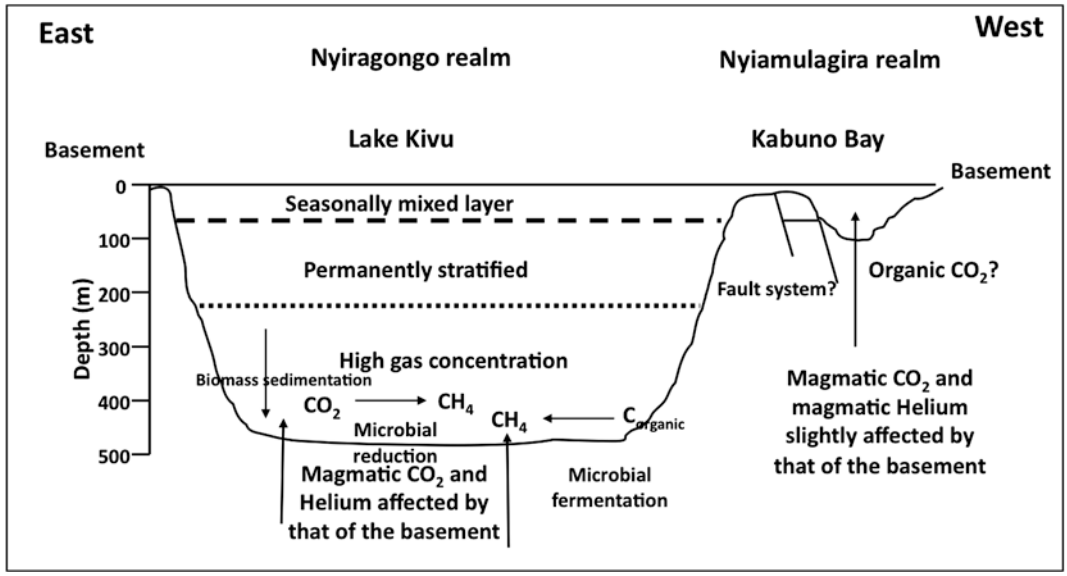

Fig. 9 Schematic conceptual model of lake Kivu. See text for explanations

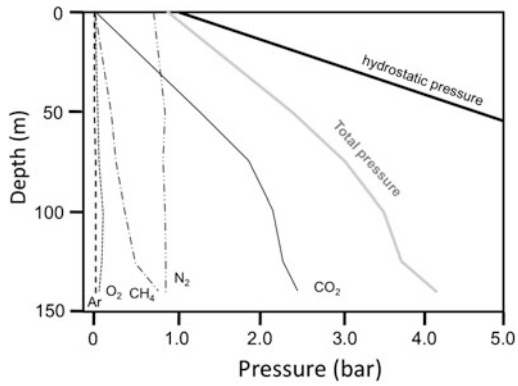

Fig. 10 Relative and total pressure (in bar) of the main dissolved gas in the Kabuno sub-basins. Data from Tassi et al. (2009)

gas concentrations in the lake would require an energy input particularly high to trigger a gas outburst (Schmid et al. 2010), unless a volcanic eruption will be occurring inside the lake (Tedesco et al. 2002; Schmid et al. 2002, 2003). The situation appears to be relatively different for the Kabuno Basin where the amount of CO_2 is close to the saturation, although constrained in a relatively thin layer when compared with the Main Basin (Tietze 1978; Tassi et al. 2009).

If the mainly effusive volcanic activity of Nyiragongo and Nyamuragira has to be taken into account, it is necessary to understand the relationships with time between volcanic activity and the lake. The best way to proceed is to apply the main rule in geology, where "*the past is the key to understand and possibly forecast the future*". Lake Kivu is considered a "killer lake" along with the Cameroonian lakes of Monoun and Nyos (e.g. Kling 2010). The peculiarity of Lake Kivu resides in the fact that the presence of CO_2 is accompanied by CH_4. As previously mentioned, most scientists agree that lava flows entering the lake and interacting with the gas reservoir is a major hazard along with a possible eruption occurring directly within the lake. In this section we analyze, according to historical activities, how the hypothesis of lava flows reaching the bottom of the lake cannot be ruled out.

In Smets et al. (2010b) the effusive activity of Nyiragongo and Nyamuragira volcanoes in the last hundreds years is reported. While Nyiragongo only erupted twice in the last two centuries (1977, e.g. Durieux 2002/2003; Tedesco et al. 2002, 2007; Komorowski et al. 2002/2003), more than 28 eruptions have occurred at

Nyamuragira (the most active volcano in the African continent) since 1938, both from the central crater and/or peripheral craters, some of them close the northern shoreline of Lake Kivu (Smets et al. 2010b).

During the last century, several eruptions from the two Congolese volcanoes have produced lava flows that ended their path within the lake at both Main and Kabuno basins. In particular, two major historical lava flows of Nyamuragira entered the Kabuno Basin (1938/1940 and 1948). These events can be regarded as the most appropriate examples to understand the dynamics within this part of the lake. The eruptive event that occurred from January 1938 to June 1940 is considered the longest one in the region of the last century. Two lava flows hit the Kabuno Basin and penetrated the waters during the first weeks of the eruption. Despite the fact that this event lasted for three and a half years, producing a gigantic amount of lava that reached the lake, most probably at its bottom,[1] Apparently, all activities around the lake continued and tea and coffee plantations did not suffer any specific damage. Similarly, the population of the area was not affected by direct volcanic hazard. The only exception was created by two lava flows that cut off the main road from Sake to Goma for a long time. Consequently, the use of boats became necessary for transportation of goods. This latter aspect points out that no degassing occurred from the Kabuno Basin. Again in 1948, a lava flow, lasting only four and half months, reached the Kabuno basin waters during the first week of the eruption. Also in this case no specific events related to a thermally driven limnic eruption were recorded.

Now the question is: why did these two events not produce, as it could be expected, a sudden degassing and overturn of the Kabuno Basin? First of all, it is necessary to take into account several parameters that may play a specific role in this process and, as highlighted by many authors (e.g. Kivu Research Conference, 13–15 January 2010, Gisenyi, Rwanda), a comparison between Lake Kivu and Lake Nyos in terms of those processes that could have led to a limnic eruption becomes of fundamental importance. Nevertheless, this approach does not appear to be correct for the Main nor for Kabuno basins. First of all, a comparison between the Main Basin and Kabuno basins and secondly, between them and Lake Nyos, should be considered, as follows: (1) the dimensions, the water volume and the amount of the deep-seated gas; (2) the volume of lava entering the lake; (3) the temperature and the rheological properties of lava flow when entering the lake.

Lake Kivu is almost one hundred times bigger than Lake Nyos with a water volume ratio of 550/0.179 (in km^3; Kling et al. 2006). The Kabuno Basin is only slightly bigger than Lake Nyos. It seems clear that an event such a lava flow, generally quiet small, entering the lake does not apply to Nyos. In the past, most lava flows that hit the northern shoreline of lake Kivu did likely not reached the lake bottom (485 m). Contrarily, lava flows in the Kabuno Basin, whose the maximum depth is of 148 m, have a higher probability to enter the gas reservoir. We can speculate that the 1938/1940 and 1948 Nyamuragira lava flows did not cause a limnic event because the size of the lava flows compared to the water volume of the lake was relatively small. Moreover, the temperature of the lava was likely lower than at the emission vent, having flown for several kilometers before reaching the lake. The relatively fast (quenching) temperature and flow speed decreased once the lava hit the late waters.

The Lake Nyos limnic event was probably generated by a landslide of huge proportions that moved down from an almost vertical cliff within the lake (e.g. Freeth et al. 1990). The fast conversion from potential to kinetic energy of the water mass was significant along with the dispersion speed of the landslide. When comparing the landslide event with a lava flow, it is clear that the two events are completely different. The lava flow is generally slow, with little kinetic energy and its volume by unit of time entering

[1] Witnesses (Dario Merlo Kassouku's father and son) living in the area have described the entrance of the lava into the Kabuno sub-basin without any specific degassing, explosions or lake over-turning.

the lake is extremely small, i.e. several orders of magnitudes lower than that of the landslide at Lake Nyos. The only parameter that could play a favorable role for the lava flow is the temperature. We believe that when the lava flow hit the lake, as witnessed in the January 2002 event, its temperature was immediately quenched by the cold lake waters. This means that the progression at depth by the lava flow is mainly controlled by gravity. During the same event, it was witnessed that the front of the lava was rapidly frozen, favoring the formation of a carapace that partially protected the feeding lava and forming a sort of vertical lava tunnel and/or pillow lavas. However, while the first lava was almost completely frozen the subsequent arriving and warmer lava was simply mechanically pushing the former one at depth. This process does not likely seem to be adequate to deeply change, vertically and/or horizontally, the chemical and physical equilibriums in the lake. As a consequence, the Kabuno and/or Main basins can unlikely be affected by the simple emission of lava flows.

Capaccioni et al. (2002/2003 have highlighted that the southern flank of the Nyiragongo volcano is dominated by several tens of NE-SW- and NS-oriented eccentric cones and their volcanic activity was apparently controlled by the distance of the present lake shoreline. Among the hydrovolcanic cones, mainly located in proximity of the lake, two different types of opening settings can be recognized: (1) sub-aereal, mostly characterized by phreatic eruptions; (2) sub-aqueous, with no-explosive or mildly explosive sub-aqueous effusions, the latter being related to high stand conditions of the Lake Kivu levels. At distances roughly in excess of 2 km from the lake shoreline the adventive cones tend to become cinder or spatter cones or effusive vents, while no hydrovolcanic cones are recorded. Capaccioni et al. (2002/2003) concluded that the phreatic/hydromagmatic activity is mainly located in the very first 2 km from the lake shoreline, whereas pure magmatic activities are at distances >2 km. The absence of a documented relatively shallow aquifer at distance >2 km from the Lake Kivu shoreline may explain this lateral zoning. Deeper ground waters should not give rise to efficient magma/water interaction because resting below the fragmentation level of the rising magma. Furthermore, the past occurrence of a diffuse hydrovolcanism coincides with the highest concentration of CO_2-rich gas discharges (Vaselli et al. 2002/2003).

If a sub-lacustrine or near-shore event should occur, a main lake degassing suddenly liberating most of the gases contained in the deep layers of the lake is more probable. To have such an event we need to have an active part of the rift within the lake or close to the shoreline.

As previously mentioned, the peripheral volcanic activity is widespread all around the volcano Nyiragongo and as near as the current shores of Lake Kivu. Only one single cone, namely “l’Ile aux Cochons” is located within the lake, less than one hundred meter from the shore, next to the peninsula (sedimentary realm) that borders the Kabuno Basin (Fig. 1). It is worth to mention that the northern shoreline of Lake Kivu is NW-SE-oriented and from the shoreline to the lake there are several EW-oriented blocked terrains, possibly originated from tectonic movements, i.e. orthogonal to the NS direction of the main rift. Such a tectonic setting is also reflected in the helium and carbon (in CO_2) isotopic values, which tend to show different values from the shoreline dry gas manifestations with respect to those of the Nyiragongo crater. Tedesco et al. (2010) interpreted these dry gas leaks as belonging to a very deep reservoir, mantle-wise, more than surficial magmatic reservoir(s) such as those of Nyiragongo.

The bathymetry of the lake provides some interesting features that were, in the wake of the 2002 eruption of Mt Nyiragongo, interpreted as volcanic craters (e.g. Schmid et al. 2004). Nevertheless, we can speculate that prior to the onset of the volcanic activity by Nyiragongo and Nyamuragira volcanoes, the whole region might have had a landscape resembling those of Rwanda, the land of the thousands hills, and those morphological reliefs could instead be related to sedimentary heights. However, more data are necessary to support one of the two hypotheses since, in the former case, eruptive sub-lacustrine events are unlikely representing a

real danger, whereas in the latter speculation an overturn of the lake might efficiently triggered.

It is clear that several questions marks should still be solved, such as the events that have brought to the formation of the 5 horizons in the sediment records of Lake Kivu and attributed by Haberyan and Hecky (1987) to limnic eruptions. Whatever the scenario of a possible limnic event is, it is evident that the scientific community needs to acquire more geological, physical and geochemical data and address new projects with the financial support of public agencies. This may avoid a sort of "mediatic terrorism" related to interviews or articles whose effects are just those to produce anxiety and misunderstandings to local inhabitants and regional, national and international authorities.

It is our strong belief that joint multidisciplinary projects, data sharing and better interactive connections among scientists and between them and the local and international authorities are necessary to create a solid structure addressed to the mitigation of the multiple geological hazards that may affect the Nyiragongo and Nyamuragira surrounding areas.

5 Conclusions

After the January 2002 eruption of Nyiragongo volcano, when one of the many lava flows entered the Lake Kivu, potential gas outbursts (limnic eruption) were seriously considered by the scientific community. Several scenarios are taken into account: lake overturn induced by (1) a large amount of lava reaching the lake bottom in both the Main and Kabuno basins, (2) increase of the gas discharge at the lake bottom and (3) volcanic and seismic activities inside the lake basin.

The relative saturation of the dissolved gases achieves the highest values at the depth of about 270 m where that of CO_2 and CH_4 is of 8 and 43 %, respectively, relative to the hydrostatic pressure (e.g. Deuser et al. 1973; Tietze et al. 1980; Lorke et al. 2004). According to Tietze et al. (1980), the dissolved gases remain in the deep waters because the seasonal convective mixing of the surface boundary layer only occurs until 50 m depth. The water is anoxic below this mixolimnion and CO_2 (mainly of mantle origin and entering the lake by groundwater inflow) and CH_4 (produced by anaerobic bacteria) increment their concentrations with depth.

Sedimentary records of previous limnic eruptions were highlighted by Haberyan and Hecky (1987) and Al-Mutlaq et al. (2008) and Boyle et al. (2009) suggested that a limnic eruption in the foreseeable future is trustworthy, possibly in the range 80–200 years. This estimation was partly defined on the basis of the acceleration of gas accumulation over the last decades (e.g. Schmid et al. 2004; Pasche et al. 2009, 2010; Wüest et al. (2009). According to Hirslund (2012), chemoclines at the Lake Kivu are moving upwards. This situation may be considered as an increasing risk of a future limnic eruption since the upward movement is likely due to inflows in the deeper parts of the lake from water sources with different salinities and densities Hirslund (2012).

Nevertheless, despite the many physical and chemical peculiarities of Lake Kivu and its geodynamical and volcanological setting, it is important to remark that its stability is presently high and only in the case of large internal and external events able to strongly impact the gas reservoir, no impending risks can be invoked. Increased temperatures of about 0.5 °C in the upper part of the lake, recorded within the last 30 years, are related to climate variability (Lorke et al. 2004) and the double-diffusive structure (Schmid et al. 2010) appears to be well preserved (Hirslund 2012). As a consequence, major projects on Lake Kivu are expected to focus on the acquisition of vertical physico-chemical and isotopes profiles in different sites of the lake, with particular reference to the Kabuno Basin.

Lava flows as those occurred in historical times can apparently be discarded as potential triggers for limnic events: temperature, kinetic energy and the involved mass of lava are likely too low to deeply modify the chemical and physical equilibrium currently present within the lake. This seems to be corroborated by the most formidable eruptive episode occurred 740 ± 110 years BP

(Tuttle et al. 1990), namely Buyinga lava flow. This eruption is considered one of the most important eruption occurred in the Virunga Volcanic Province in terms of erupted volume and very fast emplacement, burying the area where the towns of Goma (DRC) and Gisenyi (Rwanda) are presently settled. However, no effects on the Lake Kivu were apparently recorded. This is supported by the fact that the most recent anomalous organic-rich layers recognized by Haberyan and Hecky (1987) in the Lake Kive sediments, and attributed to a limnic eruption, were dated at about 2,000 years BP.

Geophysical and GPS data of the lake, monitoring of the vertical profile, particularly in the Main and Kabuno basins, and simulations of possible scenarios in case of lava fronts entering the lake as well as eruptive sub-lacustrine and sub-areal events in and close to the Lake Kivu shoreline are of paramount importance.

Acknowledgments Many thanks are due to D. Rouwet and A. Caracausi for their useful corrections and suggestions that greatly improved an early version of the manuscript.

References

Al-Mutlaq KF, Standley LJ, Simoneit BRT (2008) Composition and sources of extractable organic matter from a sediment core in lake Kivu, East African rift valley. Appl Geochem 23:1023–1040

Borginiez G (1960) Données pour la Mise en Valeur du Gisement de Méthane du Lac Kivu. Académie Royale des Sciences d'Outre-Mer, Classe des Sciences Techniques, Mémoires in −8°, Nouvelle série XIII(1), Brussels:110 pp

Botz R, Stoffers P, Faber E, Tietze K (1988) Isotope geochemistry of carbonate sediments from lake Kivu (East-Central Africa). Chem Geol 69:299–308

Boyle J, Hirslund F, Morkel P, Schmid M, Tietze K, Wüest A (2009) Management prescriptions for the development of lake Kivu gas resources. Document prepared for the Ministry of Infrastructure, Rwanda and Ministry of Hydrocarbons, D.R. Congo

Burke K, Mueller G (1963) Dissolved gases in East African lakes. Nature 198:568–569

Capaccioni B, Vaselli O, Santo AP, Yalire MM (2002/2003) Monogenic and polygenic volcanoes in the area between the Nyiragongo summit crater and the lake Kivu shoreline. Acta Vulcanol 14–15:129–136

Capart A (1960) Le Lac Kava. Les Naturalistes Belge 41:397–417

Chakrabarti R, Basu AR, Santo AP, Tedesco D, Vaselli O (2009) Isotopic and geochemical evidence for a heterogeneous mantle plume origin of the virunga volcanics, Western rift, East African rift system. Chem Geol 259:273–289

Chapman LJ, Chapman CA, Ogutu-Ohwayo R, Chandler M, Kaufman L, Keiter AE (1996) Refugia for endangered species from an introduced predator in Lake Nabugabo, Uganda. Conserv Biol 10:554–561

Coulter GW, Allanson BR, Bruton MN, Greenwood PH, Hart RC, Jackson PBN, Ribbink AJ (1984) Unique qualities and special problems of the African great lakes. Environ Biol Fishes 17:161–183

Damas H (1937) La stratification thermique et chimique des lacs Kivu, Edourd et Ndalaga (Congo Belge). Verhandlungen der Internationalen Vereinigung für Theoretische und Angewandte Limnologie 8:51–68

De Vos L, Snoeks J, Thys van den Audenaerde DK (2001) An annotated checklist of the 742 fishes of Rwanda (East-Central Africa) with historical data on introductions of commercially important species. J East Afr Nat Hist 90:41–68

Degens ET, Von Herzen RP, Wong HK, Deuser WG, Jannach HW (1973) Lake Kivu: Structure, chemistry and biology of an East African Rift Lake. Geol Rundsch 62:245–277

Degens ET, Ittekkot V (1982) In situ metal-staining of biological membranes in sediments. Nature 298:262–264

Degens ET, Kulbicki G (1973) Hydrothermal origin of metals in some East African rift lakes. Miner Deposita 8:388–404

Degens ET, Okada H, Honjo S, Hathaway JC (1972) Microcrystalline sphalerite in resin globules suspended in lake Kivu, East Africa. Miner Deposita 7:1–12

Deuser WG, Degens ET, Harvey GR, Rubin M (1973) Methane in lake kivu: new data bearing on its origin. Science 181:51–54

Durieux J (2002/2003) Nyiragongo: the January 10th 1977 Eruption. Acta Vulcanol 14/15:145–148

Ebinger C, Furman T (2002/2003) Geodynamical setting of the Virunga volcanic province, East Africa. Acta Vulcanol 15:9–16

Evans WC, Kling GW, Tuttle ML, Tanyileke G, White LD (1993) Gas buildup in lake Nyos, Cameroon: the recharge process and its consequences. Appl Geochem 8:207–221

Freeth SJ, Kling GW, Kusakabe M, Maley J, Tchoua FM, Tietze K (1990) Conclusions from the lake Nyos disaster. Nature 348:201

Haberyan KA, Hecky RE (1987) The late pleistocene and holocene stratigraphy and paleolimnology of lakes Kivu and Tanganyika. Palaeogeogr Palaeoclim Palaeoecol 61:169–197

Halbwachs M (2003) The exploitation of methane in lake Kivu: pilot station project. Data environment, 70 pp

Halbwachs M, Tietze K, Lorke A, Mudaheranwa C (2002) Investigations in lake Kivu (East Central Africa) after the Nyiragongo eruption of January 2002. Specific study on the impact of the sub-water lava inflow on the lake stability. Report for Solidarites, Aide Humanitarie d'Urgence, Paris (France), 49 pp

Hanek G, Leendertse K, Farhani B (1991) Socio-economic investigations of lake Kivu fisheries. UNDP/FAO Regional Project for Inland Fisheries Planning (IFIP), RAF/87/099-TD/23/91 (En), 55 pp

Hecky RE, Degens ET (1973) Late pleistocene- holocene chemical stratigraphy and paleolim- nology of the rift lakes of Central Africa. Woods Hole Oceanographic Institution technical report, pp 73–28

Hirslund F (2012) An additional challenge of lake Kivu in Central Africa—upward movement of the chemo-clines. J Limnol 71:45–60

Holzförster F, Schmidt U (2007) Anatomy of a river drainage reversal in the Neogene Kivu-Nile Rift. Quaternary Sci Rev 26:1771–1789

Imboden DM, Wüest A (1995) Mixing mechanisms in lakes. In: Lerman A, Imboden D, Gat J (eds) Physics and chemistry of lakes, Springer, New York, 83–138 pp

Isumbisho P, Kaningini B, Descy J-P, Baras E (2004) Seasonal and diel variations in the diet of the young stages of Limnothrissa miodon in lake Kivu, Eastern Africa. J Trop Ecol 20:1–11

Jannash AW (1975) Methane oxydation in lake Kivu. Limnol Oceanogr 20:860–864

Kiss R (1966) Le Lac Kivu. Chronique de l'IRSAC I (1):20–28

Kiss R (1959) Analyse quantitative du zooplancton du lac Kivu. Fol Scient Afr Centr 5:78–80

Kling GW (2010) Lethal gas burst from lakes. Kivu Research Conference, Gisenyi, 13–15 January 2010

Kling GW, Tuttle ML, Evans WC (1989) The safety of Cameroon lakes. Nature 337:215

Kling G, MacIntyre S, Steenfelt JS, Hirslund F (2006) Lake Kivu gas extraction—report on lake stability. World Bank, 102 pp

Komorowski J-C, Tedesco D, Kasareka M, Allard P, Papale P, Vaselli O, Durieux J, Baxter P, Halbwachs M, Akumbe M, Baluku B, Briole P, Ciraba H, Dupin J-C, Etoy O, Garcin D, Hamaguchi H, Houlié N, Kavotha KS, Lemarchand A, Lochwood J, Lukaya N, Mavonga G, De Michele M, Mpore S, Mukambilwa K, Munyololo F, Newhall C, Ruch J, Yalire MM, Wafula M (2002/2003) The January 2002 flank eruption of Nyiragongo volcano (Democratic Republic of Congo): chronology, evidence for a tectonic rift trigger, and impact of lava flows on the city of Goma. Acta Vulcanol 14–15:27–62

Krumbein WE (1975) Biogenic monohydrocalcite spherules in lake sediments of lake Kivu (Africa) and the solar lake (Sinai). Sedimentology 22:631–634

Kufferath J (1960) Le Méthane du Lac Kivu. Les naturalistes Belge 41:418–426

Lahmeyer-Osae (1998) Bathymetric survey of lake Kivu. Final report, Republic of Rwanda, Ministry of Public Work, Directory of Energy and Hydrocarbons, Kigali, 18 pp

Lorke A, Tietze K, Halbwachs M, Wüest A (2004) Response of lake Kivu stratification to lava inflow and climate warming. Limnol Oceanogr 49:778–783

Lowe-McConnell RH (1993) Fish faunas of the African great lakes: origins, diversity, and vulnerability. Cons Biol 7:634–643

Minissale A, Vaselli O, Chandrasekharam D, Magro G, Tassi F, Casiglia A (2000) Origin and evolution of "intracratonic" thermal fluids from central-western peninsular India. Earth Planet Sci Lett 181:377–394

Murthy CR (1976) Horizontal diffusion characteristics in lake Ontario. Phys Oceanogr 6:76–84

Pasche N, Alunga G, Mills K, Muvundja F, Ryves DB, Schurter M, Wehrli B, Schmid M (2010) Abrupt onset of carbonate deposition in lake Kivu during the 1960s: response to recent environmental change. J Paleolimnol 44:931–946. doi:10.1017/s10933-010-9465-x

Pasche N, Dinkel C, Müller B, Schmid M, Wüest A, Wehrli B (2009) Physical and biogeochemical limits to internal nutrient loading of meromictic lake Kivu. Limnol Oceanogr 54:1863–1873

Pasche N, Schmid M, Vazquez F, Schubert CJ, Wüest A, Kessler JD, Pack MA, Reeburgh WS, Bürgmann H (2011) Methane sources and sinks in Lake Kivu. J Geopyhs Res 116, G03006. doi:10.1029/2011JG001690

Peeters F, Wüest A, Piepke G, Imboden DM (1996) Horizontal mixing in lakes. J Geophys Res 101:18361–18375

Peeters L (1957) Contribution à l'Étude de la Genèse du Lac Kivu. Bull Soc Belg, Études Géogr 26:155–168

Poreda RJ, Craig H (1989) Helium isotope ratios in circum-Pacific volcanic arcs. Nature 338:473–478

Sarmento H, Isumbisho P, Descy JP (2006) Phytoplankton ecology of lake Kivu (Eastern Africa). J Plankton Res 28:815–8829

Schmid M, Busbridge M, Wüest A (2010) Double-diffusive convection in lake Kivu. Limnol Oceanogr 55:225–238

Schmid M, Halbwachs M, Wehrli B (2004) Report on the scientific expeditions to lake Kivu on November 2003 and February 2004: an investigation on physical and chemical properties of lake Kivu as a base for gas outburst risk assessment. UN-OCHA, 17 pp

Schmid M, Halbwachs M, Wehrli B, Wüest A (2005) Weak mixing in lake Kivu: new insights indicate increasing risk of uncontrolled gas eruption. Geochem Geophys Geosys 6. doi:10.1029/2004GC000892

Schmid M, Tietze M, Halbwachs M, Lorke A, McGinnis D, Wüest A (2002) How hazardous is the gas accumulation in lake Kivu? Arguments for a risk assessment in light of the Nyiragongo volcano eruption of 2002. Acta Vulcanol 14–15:115–122

Schmitz DM, Kufferath J (1955) Problèmes posées par la Présence de Gaz dissous dans les Eaux profondes du Lac Kivu. Acad Royales Sci Colon, Bull Séances, nouvelle Série 1:326–356

Schoell M, Tietze K, Schoberth S (1988) Origin of the methane in lake Kivu (East-Central Africa). Chem Geol 71:257–265

Smets B, Tedesco D, Kervin F, Kies A, Vaselli O, Yalire MM (2010a) Dry gas vents ("mazuku") in goma region

(North-Kivu, Democratic Republic of Congo): formation and risk assessment. J Afric Earth Sci 58:787–798

Smets B, Wauthier C, d'Oreye N (2010b) A new map of the lava flow field of Nyamulagira (D.R. Congo) from satellite imagery. J Afric Earth Sci 58:778–786

Snoeks J (1994) The haplochromines (Teleostei, Cichlidae) of lake Kivu (East Africa): a taxonomic revision with notes on their ecology. Ann Mus Royal Afr Centr Sc Zool 270:221 pp

Spigel RH, Coulter GW (1996) Comparison of hydrology and physical limnology of the East African great lakes: Tanganyika, Malawi, Victoria, Kivu and Turkana (with reference to some North American great lakes). In: TC Johnson, EO Odada (eds) The limnology, climatology and paleoclimatology of the East African lakes, Toronto, Gordon and Breach, pp 103–139

Spliethoff PC, De Iongh HH, Frank VG (1983) Success of the introduction of the freshwater clupeid Limnothrissa miodon (Boulenger) in Lake Kivu. Fish Management 14:17–31

Tassi F, Vaselli O, Tedesco D, Montegrossi G, Darrah T, Cuoco E, Mapendano MY, Poreda R, Delgado Huertas A (2009) Water and gas chemistry at lake Kivu (DRC): geochemical evidence of vertical and horizontal heterogeneities in a multi-basin structure. Geochem Geophys Geosyst 10(2). doi:10.1029/2008GC002191

TECHNIP, BRGM (1986) Etudes gaz methane. Programme 1: Mesures sur le gisement de gaz au Cap Rubona. Final Report n° 5840 Y 01, République Rwandaise, Ministére des Travaux Publics et de l'Energie, Kigali, Rwanda, 53 pp

Tedesco D, Papale P, Vaselli O, Durieux J (2002) The January 17th, 2002 eruption of Nyiragongo, Democratic Republic of Congo. Report UN-OCHA Consultant Volcanologists Team, 52 pp

Tedesco D, Tassi F, Vaselli O, Poreda R, Darrah T (2010) Gas isotopic signatures (He, C and Ar) in the lake Kivu region (western branch of the East African rift system): geodynamic and volcanological implications. J Geophys Res 115:B01205. doi:10.1029/2008JB006227

Tedesco D, Vaselli O, Papale P, Carn SA, Voltaggio M, Sawyer GM, Durieux J, Kasereka M, Tassi F (2007) January 2002 volcano-tectonic eruption of Nyiragongo volcano, Democratic Republic of Congo. J Geophys Res 112:B09202. doi:10.1029/2006

Tietze K (1978) Geophysikalische Untersuchung des Kivusees und seiner ungewöhnlichen Methangaslagerstätte Schichtung, Dynamik und Gasgehalt des Seewassers, Kiel (Germany), VIII, 149 pp

Tietze K (1987) Results of the German-Cameroon research expedition to lake Nyos (Cameroon) October/November 1986. Interim-Report, Bundesanstalt für Geowissenschaften und Rohstoffe Archive no. 100470, 84 pp

Tietze K (2000) Lake Kivu gas development and promotion-related issues: safe and environmentally sound exploitation, Republic of Rwanda; Ministry of Energy, Water And Natural Resources, Kigali, 110 pp

Tietze K, Geyh M, Müller H, Schröder L, Stahl W, Wehner H (1980) The genesis of the methane in lake Kivu (Central Africa). Geol Rund 69:452–472

Tuttle ML, Lockwood JP, Evans WC (1990) Natural hazards associated with lake Kivu and adjoining areas of the Virunga Volcanic Field, Rwanda and Zaïre, Central Africa. Final Report, USGS Open File Report 90–691:40 pp

Van den Bossche JP, Bernacsek GM (1990) Source book for the inland fishery resources of Africa, Volume 1, CIFA Technical Paper No.18.1, FAO, Rome, 240 pp

Vaselli O, Capaccioni B, Tedesco D, Tassi F, Yalire MM, Kasareka MC (2002/2003) The "Evil's Winds" (Mazukus) at Nyiragongo volcano (Democratic Republic of Congo). Acta Vulcanol 14–15:123–128

Verheyen E, Salzburger W, Snoeks J, Meyer A (2003) Origin of the superflock of cichlid fishes from lake Victoria, East Africa. Science 300:325–328

Villanueva MCS, Isumbisho M, Kaningini B, Moreau J, Micha J-C (2008) Modeling trophic interactions in lake Kivu: what roles do exotics play? Ecol Model 212:422–438

Welcomme RL (1988) International transfers of inland fish species. FAO Fisheries Technical Papers 294, 318 pp

Wong HK, Von Herzen RP (1974) A geophysical study of lake Kivu, East Africa. Geophys J Royal Astr Soc 37:371–389

Wüest A, Jarc L, Schmid, M (2009) Modelling the reinjection of deep-water after methane extraction in Lake Kivu. EAWAG and BTC for the Governments of Rwanda and DR Congo, 141 pp

Microbial Life in Volcanic Lakes

Francesca Mapelli, Ramona Marasco, Eleonora Rolli, Daniele Daffonchio, Stuart Donachie, and Sara Borin

Abstract

Lakes in the craters of active volcanoes and their related streams are often characterised by conditions considered extreme for life, such as high temperatures, low pH and very high concentrations of dissolved metals and minerals. Such lakes tend to be transient features whose geochemistry can change markedly over short time periods. They might also vanish completely during eruption episodes or by drainage through the crater wall or floor. These lakes and their effluent streams and springs host taxonomically and metabolically diverse microorganisms belonging in the *Archaea*, *Bacteria*, and *Eucarya*. In volcanic ecosystems the relation between geosphere and biosphere is particularly tight; microbial community diversity is shaped by the geochemical parameters of the lake, and by the activities of microbes interacting with the water and sediments. Sampling these lakes is often challenging, and few have even been sampled once, especially in a microbiological context. Developments in high-throughput cultivation procedures, single-cell selection techniques, and massive increases in DNA sequencing throughput, should encourage efforts to define which microbes inhabit these features and how they interact with each other and the volcano. The study of microbial communities in volcanic lake systems sheds light on possible origins of life on early Earth, or on extraterrestrial systems. Other potential outcomes

F. Mapelli · R. Marasco · E. Rolli · D. Daffonchio · S. Borin (✉)
Department of Food Science and Microbiology, Università degli Studi di Milano, Via Celoria 2, 20133 Milan, Italy
e-mail: sara.borin@unimi.it

S. Donachie (✉)
Department of Microbiology, University of Hawai'i at Mānoa, 2538 McCarthy Mall, Honolulu, HI 96822, USA
e-mail: donachie@hawaii.edu

D. Rouwet et al. (eds.), *Volcanic Lakes*, Advances in Volcanology,
DOI 10.1007/978-3-642-36833-2_23,
© Springer-Verlag Berlin Heidelberg 2015

include the development of microbial inocula to promote plant growth in altered or degraded soils, bioremediation of contaminated waste or land, and the discovery of enzymes or other proteins with industrial or medical applications.

Keywords
Volcanic lake · Microbial communities · Extremophiles · Microbial diversity

1 Introduction

If asked to define a lake, most people would probably describe a body of fresh water surrounded by land. Some might attempt to distinguish a lake from a pond. Few, however, would consider the origin or nature of the lake basin, or of the water therein. In all likelihood, most people view lakes as permanent features that only affect them in terms of recreation, commerce, and biological productivity. In such terms, lakes in the craters of extinct or dormant volcanoes probably differ little from most lakes on Earth, in that their hydrological conditions may largely reflect only the surrounding air temperature, amount and nature of meteoric water, inflowing streams or rivers, and host rock chemistry (Donachie et al. 2004). In short, volcanic or geothermal forces no longer drive their circulation and chemistry, or affect their flora and fauna composition; these are the neutral dilute volcanic lakes defined by Pasternack and Varekamp (1997). Lakes in the craters of active volcanoes present very different physical and chemical characteristics, with conditions spanning broad ranges defined largely by the proximity of magma, and origin and nature of the adjacent rock and water (Pasternack and Varekamp 1997; Takano et al. 1997; Martínez et al. 2000, 2002; Jóhannesson et al. 2007). Visitors to such lakes may be surprised to find life in what are, to humans, extreme conditions. In this respect, organisms that thrive in conditions markedly different from what we might consider 'normal' are defined by the generic term 'extremophile', and their presence in such environments should be expected (MacElroy 1974). Evidence for active microbial communities in volcanic systems emerged from geochemical studies, resulting in hypotheses describing microbial roles in the oxidation/reduction of particular chemical species. Studies of elemental and isotopic profiles along with direct measurements of microbial activity provided evidence for microbial participation in the stoichiometry of crater lake waters and sediments, and their importance in these systems (Takano et al. 1997; Wendt-Potthoff and Koschorreck 2002; Koschorreck et al. 2008; Parker et al. 2008).

Microbiologists until recently rarely visited such lakes (Takano et al. 1997; Donachie et al. 2002; Gaidos et al. 2004, 2008; Löhr et al. 2006a; Urbieta et al. 2012). Sampling strategies cannot always include boats, for obvious reasons, while remote sample-return vehicles have not been deployed, nor have automatic devices to collect samples at regular intervals as at hydrothermal vents (Reysenbach et al. 2000). As with other hydrothermal systems, however, the chemical composition of water in a crater lake depends on its interactions with the host rock and gas emissions. This chemistry, plus heat, generally shapes microbial community structure, so it is difficult to predict a universal microbiology for such features. One common trait of crater lakes and volcanic hot spring water is low pH, such that strong acids interact with the rock and mobilize potentially toxic metals. Here we focus on microbial diversity in volcanic acidic lakes, which represent one of the most common naturally acidic aquatic habitats on Earth (Löhr et al. 2006a). Little is known about the evolution and diversity of microbial communities in volcanic lakes, however, a fact that might be attributed to the lakes often being remote and difficult to

access. To simply establish that life is present in a lake in the crater of an active volcano requires overcoming significant logistic challenges (Woelfl and Whitton 2000; Gaidos et al. 2004, 2008; Thorsteinsson et al. 2008). The hypotheses to be tested will determine the methodology, but we should bear in mind that any sample may be the last before the lake vanishes.

2 Methods to Study Environmental Microbes

Defining which microorganisms are in a habitat has long challenged microbiologists. Indeed, we may yet be unable to say with certainty what is the absolute taxonomic diversity in a microbial community, regardless of the methods employed (Curtis et al. 2002). With the benefit of hindsight, supported by advances in technology, we can see how naïve we might have been when describing taxonomic diversity decades ago. For example, from the nineteenth and well into the twentieth centuries we were able only to determine which bacteria were in a sample by inoculating subsamples to nutrient media. Tweaking the concentrations of a medium's components, the gas atmosphere, adjusting the pH, or modifying the light regime, encouraged the growth of metabolically and taxonomically different bacteria. In essence, we 'knew' which microbes were in a sample by growing them on or in such media. However, after more than a century of offering what might seem 'infinite' media and incubation conditions, it became clear to microbiologists that they could not cultivate representatives of all species from most samples. This was underscored in the 1980s by a then new technique, the analysis of nucleotide sequences of specific genes in DNA extracted from the environment and amplified in polymerase chain reactions (PCR); this approach detected bacteria (*Archaea* and *Bacteria*) for which no cultivated representatives then existed (Stahl et al. 1984; Ward et al. 1990). Advances in microscopy also showed the number of bacteria we might cultivate ranges from far less than 1 to ~50 % of those counted by microscopy, depending on the sample type (Staley and Konopka 1985; Donachie 1996; Wilson et al. 1997; Handelsman 2004). It should be noted here that these statistics refer only to the number of cells present, and not the number of 'species' or any other taxonomic unit we might define (Donachie et al. 2007). Such observations, however, encouraged use of terms such as 'nonculturable' or 'unculturable' to describe those cells we could not grow (Xu et al. 1982; Colwell and Grimes 2000). These terms have taken on almost meme-like status. However, we might note that Amann et al. (1995) observed, perhaps wryly, "With the availability of innovative techniques, many more microorganisms will become culturable. […] After all, nature can cultivate all extant microorganisms."

That analysis of ribosomal gene sequences in environmental samples detected bacteria that had never been cultivated led many microbiologists to justify using only those techniques, now termed 'molecular approaches', in studies of taxonomic diversity (Schmidt et al. 1991; Barton et al. 2004; Valenzuela-Encinas et al. 2008). Such a single-method approach has been shown not to describe microbial diversity in toto; cultivation and molecular approaches detect very different bacteria in the same sample (Suzuki et al. 1997; Bowman et al. 1999; Kaiser et al. 2001; Donachie et al. 2002, 2004, 2007; Munson et al. 2002; Shawkey et al. 2005). Whatever might be the merits of one approach over another, the utility of both cultivation-based and molecular techniques in microbial diversity studies has been significantly enhanced with the development of high-throughput culturing methods and high-throughput DNA sequencing (Connon and Giovannoni 2002; Zengler et al. 2002; Donachie et al. 2007; Kalyuzhnaya et al. 2008; Kircher and Kelso 2010). The apparent unculturable nature of some microorganisms is surely in part attributable to the medium composition or growth conditions provided not suiting them. Conditions in extreme environments such as volcanic features render it difficult to exactly reproduce the correct concentrations of nutrients and growth factors in the laboratory (Rodríguez-Valera 2002). Characterizing geochemical and physical parameters is thus essential if one is to reproduce in situ conditions

in artificial systems, and highlights the importance of a multidisciplinary approach in microbiological studies of these environments (Fig. 1). In addition to extrinsic factors, microbes might also require intrinsic factors such as syntrophic interactions, a mutual relationship based on nutrient exchange, or quorum-sensing, intercellular communication mediated by small molecules only when a certain population density is attained.

2.1 Cultivation Approaches

Cultivating bacteria from environmental samples as a scientific objective dates back to the nineteenth century (Certes 1884). Detailed reviews of the myriad requirements and often creative techniques used in the pursuit of a 'pure culture' can be found throughout the literature. Today, data from molecular methods can be of use in developing media and incubation conditions to isolate new taxa (Palleroni 1997; Giovannoni and Stengl 2007). It remains statistically prohibitive to cater to all species that may occupy a particular habitat, but given sufficient information about the habitat and with supporting molecular data we can target specific genera or metabolic groups (Huber et al. 1995; Teske et al. 1996; Tyson et al. 2005). Although the exact concentration of every component in a volcanic habitat might be difficult to faithfully reproduce from scratch in the laboratory, anyone collecting samples from such sites should be able to collect enough material to provide the base of many culture media (Rodríguez-Valera 2002). We can thus address in part the need for specific components or combinations thereof found only in the native sample.

New cell selection and cultivation strategies have attempted to overcome the limitations of diluting samples to extinction, a procedure that statistically provides a suspension of the most abundant species, while diluting out those which are less abundant but perhaps more competitive (Fröhlich and König 2000). A drawback is that the least abundant taxa are unlikely to be present in the most dilute samples; they might also be outcompeted when inoculated to media with other species. Recent 'high-throughput' and 'gel microdroplet' techniques operate on the same principle of dilution to provide single to a few cells that are inoculated to media in microplates. These have enabled significant expansion of the number of

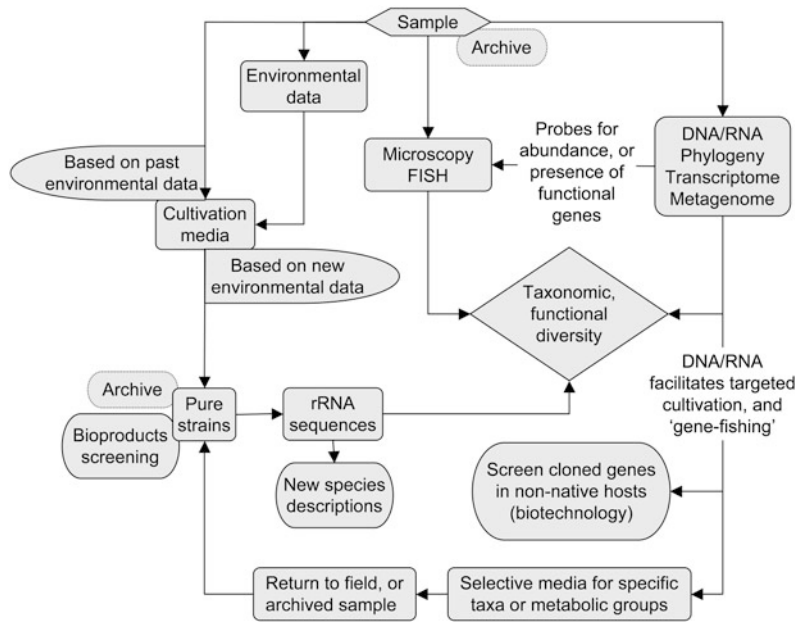

Fig. 1 Schematic representation of approaches used by microbiologists to investigate diversity, function and potential applications of microbes in environmental samples

samples that can be processed in a given time (Connon and Giovannoni 2002; Zengler et al. 2002). However, they do not allow direct selection of any particular cell type, and given there are perhaps billions of cells in a liter of most naturally occurring waters they would still require an unfeasibly high number of microplates to sample all cells per liter. And that is before one provides different media, temperatures, or any other such parameter. All is not lost, though. Cell sorting by flow cytometry can target specific cell types, but does not isolate single microbial cells that one directly observes. To collect single cells that one can see, and pass those cells from a sample to downstream analyses, or to media wherein they may grow free of competition from other taxa, a range of microfluidic, and laser microdissection and catapulting systems offer various capabilities (Krüger et al. 2002; Ho et al. 2005; Baret et al. 2009; Chen et al. 2009; Kang et al. 2011). Cells historically termed 'unculturable' will numerically dominate hundreds or even thousands of selected cells, but today's laser systems are combined with imaging capabilities that enable us to move beyond random selection. By establishing a library of cell images we might attempt to isolate visually distinctive cells that we have previously related to specific taxa through rRNA gene sequencing after whole genome amplification (sensu Morris et al. 2004; cf. Fig. 1); their phylogeny and physiology can thus be predicted and in subsequent selections they can be transferred to tailored growth media in microplates within which they can grow free of competition from more rapidly growing or antagonistic taxa (sensu Kovac and Voldman 2007). Laser-mediated methods have proved themselves in isolating novel microbes (Huber et al. 1995).

2.2 Cultivation-Independent Approaches

Molecular approaches were first used in microbial ecology about three decades ago, based on the study of the nucleotide sequences of specific genes. They revolutionized the field and quickly became the most widely used methods to investigate microbial diversity in any sample. The most widely used methods are based on examination of so-called "molecular chronometers". These are ribosomal, or rRNA genes, e.g., 16S rRNA genes in *Archaea* and *Bacteria*, and 18S rRNA genes in the *Eucarya*, that encode for the production of ribosomes (Kimura 1968, 1983; Stackebrandt et al. 1985). The slow rate at which these genes' nucleotide sequences have mutated over evolutionary time renders them valuable in classification. Such sequences also form the basis of the reclassification of all life into the three currently recognized domains, *Archaea*, *Bacteria* and *Eucarya* (Woese 1987). Moreover, functional genes encoding proteins involved in specific metabolisms such as nitrogen fixation or sulphate reduction can be used as proxies for particular bacterial groups (Moisander et al. 2006; Wagner et al. 1998). Many DNA-based methods developed since the 1990s provide data on both taxonomic and metagenomic diversity in microbial communities. Furthermore, "-omics" approaches including metatranscriptomics and metaproteomics allow one to determine which proteins microbial communities in the environment express. Further advances now see these techniques being used at the single cell level, permitting evaluation of the role and spatial topology of each community member (Kang et al. 2011). Information about the presence and spatial distribution of specific populations can also be obtained through microscopic analyses that target specific phylogenetic groups. Among these, techniques such as fluorescence in situ hybridization (FISH) have been instrumental in both significant discoveries and routine counting of specific microbial groups (Amann et al. 1990; Karner et al. 2001). Enhanced FISH-based techniques including substrate-tracking autoradiography (STAR-FISH) and catalyzed reporter deposition (CARD-FISH) have been applied to the study of microbial communities in water, e.g., warm monomictic crater lake Alchichica (Mexico), and a subglacial volcanic lake beneath Iceland's Vatnajökull ice cap (Ouverney and Fuhrman 1999, 2000; Gaidos et al. 2008).

Molecular- or PCR-based approaches do have limiting factors, including the amount and quality

of DNA that can be extracted from the sample, and the amount of that DNA which can be sequenced in a given time at an acceptable cost. The latter is now a minor issue given that today's DNA sequencers can process, relatively cheaply, billions of nucleotides in a few hours. Molecular approaches today appear to offer the possibility of quickly detecting all genes, and thus all bacteria in a sample, as long as one can guarantee extracting all DNA from all cells. Just over a decade ago a multi-capillary Sanger-type sequencer was considered 'high-throughput.' Such a machine's performance pales into insignificance compared to that offered by today's platforms, which can complete millions of reads in an afternoon. Such performance revealed "unexpected" taxonomic diversity in the deep-sea (Sogin et al. 2006), while metagenomic analyses also showed an equally remarkable functional diversity (DeLong et al. 2006). These techniques have not yet been widely used in volcanic habitats, although Gaidos et al. (2008) showed the metagenome in anoxic water of a sub-glacial volcanic lake comprised an oligarchic microbial consortium suited to the lake's geochemical context. Further advances in sequencing technology, along with miniaturization and reduced cost per nucleotide sequenced, promise greater insights, with some caveats, of course (Kunin et al. 2010; Niedringhaus et al. 2011).

3 Microbial Diversity in Volcanic Lakes

3.1 Cultivated Microbes

Reports of microbes cultivated from crater lakes in active volcanoes are few and far between. Indeed, most of the effort to determine which microbes are in these lakes appears to have been based on molecular approaches. It also seems we might know more of the diversity, physiology and abundance of microbes, both cultivated and uncultivated, at submarine volcanic features than we do in their analogous terrestrial features (Karl et al. 1989; Donachie et al. 2003, 2004; Nakagawa and Takai 2008). In this respect, myriad reports of microbes in features related to volcanoes such as geothermal springs and effluent streams appear throughout the literature (Sonne-Hansen and Ahring 1997; Hugenholtz et al. 1998; D'Imperio et al. 2008). Through just a handful of papers, however, one can appreciate what challenging environments acidic crater lakes are for microorganisms.

Takano et al. (1997) elegantly describe how sulfur-oxidizing bacteria affect the sulfate budget of the Yugama crater lake (pH 1–1.5), part of the andesitic Kusatsu-Shirane strato-volcano, Japan, noting also how pH controls distributions within the crater of two *Thiobacillus* species, *T. thiooxidans* and *T. ferrooxydans*. Members of the *Thiobacillus,* subsequently reclassified as *Acidithiobacillus*, are known to colonize extremely acidic environments characterized by high levels of reduced sulfur, which they oxidize (Kelly and Wood 2000). In the Yugama crater lake a molten sulfur pool at a then active subaqueous fumarolic vent was discharged into the water column, while sulfur particles dispersed throughout the lake as aqueous sulfur dioxide and hydrogen sulfide reacted (Takano et al. 1994b); hydrogen sulfide, polythionates, and elemental sulfur were consumed by bacteria, while reduced sulfur compounds were converted by these bacteria to sulfuric acid. An acidophilic diatom, *Pinnularia braunii* var. *amphicephala*, on the floor of a stream in the crater was identified by microscopy, showing that eukaryotes also colonize crater lake environments.

The first report of microbial communities in acidic waters of the White Island andesitic stratovolcano applied both cultivation and molecular methods (Donachie et al. 2002). The water here is a dilute mix of sulfuric and hydrochloric acids containing dissolved andesite rock and other components. Sub-samples of water emanating from a hot spring in the crater floor were inoculated to a range of media (pH 1.29 to ~8) to cater to expected metabolic groups, and incubated at one of five temperatures between 30 and 60 °C for up to one year. Four pure cultures affiliated with the heterotrophic and acidophilic mesophile, *Acidiphilium* sp. (*Alphaproteobacteria*), which requires only low concentrations of organics and

cannot use sulfur or Fe^{2+} (Harrison 1981); with *Nocardia* sp., and *Nocardioides* sp. (*Actinobacteria*), and with *Cyanidium caldarium* (*Eucarya*, Rhodophyta), a photoautroph (Doemel and Brock 1971). The success of the *Eucarya* in volcanic crater lakes is likely controlled by temperature, even if they can tolerate the extremely low pH (Tansey and Brock 1972). For example, *Cyanidium caldarium* was absent from the lake in the White Island volcano, where pH was ~0 but temperature was 58 °C, yet it was isolated from slightly cooler 'soil' just meters from the lake (Fig. 2) (Donachie et al. unpubl.). This photosynthetic eukaryote does not grow above 56 °C (Kleinschmidt and McMahon 1970).

A crater lake whose microbiology was investigated in austral summer 2007 by both cultivation and molecular approaches is the summit lake on Simba volcano (Demergasso et al. 2010), also referred to as Lake (cf. Laguna) Aguas Calientes (Escudero et al. 2007; Cabriol et al. 2009). This is an unusual lake because of its high altitude (5,870 m) and concomitantly high UV radiation exposure, yet rather moderate pH for a crater lake. Although water and sediment samples were inoculated to enrichment media, no growth was detected in the incubation period, while several bacteria from just two phyla were cultivated from nearby Salar Aguas Calientes and Laguna Lejía. In November of 2006, *Bacteria* were cultivated from the same lake, but their diversity was limited to just a couple of *Gammaproteobacteria* (*Pseudomonas* spp.) and a *Firmicutes* (*Staphylococcus epidermidis*). *S. epidermidis* is probably not part of the autochthonous microbiota since it is generally found on the human skin and membranes, and is a frequent contaminant in laboratory tests (Queck and Otto 2008). Molecular methods showed a higher phylogenetic diversity, revealing the presence of taxa reported from other high altitude lakes rather than acidic lakes per se, and belonging in the *Bacteria* and *Archaea* (Demergasso et al. 2010). This work demonstrates the value of coupling cultivation-dependent and molecular methods.

Wendt-Potthoff and Koschorrek (2002) determined the abundances of various physiological groups of bacteria along the Rio Agrio on the Copahue volcano (Argentina), an andesitic stratovolcano, and its recipient lake, Caviahue. Iron- and sulfur-oxidizers, and sulphate-reducers were enumerated in enrichment media used in other acidic environments. The presence of fermentative bacteria was determined by gas production at pH

Fig. 2 Sampling at White Island, New Zealand. Acidic gases require use of respirators. The water's green coloration is due to elemental sulfur. (*Photo* SPD)

2.0. All metabolic groups were detected, although abundance was low, and the authors posited that distribution varies with rate of water flow, sediment texture, and light availability rather than solely with pH. Lavalle et al. (2005) worked along the same river, but also sampled from the crater lake (Laguna del Volcán) itself. In a targeted approach with specific media, acidophilic, chemolithotrophic and ferrous-oxidizing bacteria were cultivated only from the river, where the pH ranged from 2 to 4. These bacteria were assigned to the iron-sulphur oxidizer *Acidithiobacillus ferroxidans*. A broader microbiological survey of the same system reported that the lake's pH ranges from 0.2 to 1.1 (Chiacchiarini et al. 2010); these authors used diverse media and incubation conditions and cultivated bacteria that use inorganic reduced sulphur compounds as energy sources, and CO_2 (chemolithoautotrophs) or organic compounds (chemolithoheterotrophs) as carbon sources. Among these were *Bacteria* (e.g., *Leptospirillum ferrooxidans*, *Acidithiobacillus ferrooxidans*, *Acidithiobacillus thiooxidans*) and *Archaea* (*Acidianus*, *Sulfolobus*), plus yeasts and filamentous fungi from sites that extended from a 70 °C, pH ~1.0 hot spring (el Vertedero) emerging from the mountain, just below the lake, and along the Upper and Lower Rio Agrio, and from Caviahue Lake. Temperature along this water course drops to ~8 °C and pH increases to 4.2. An unidentified extremely acidotolerant (pH < 2) filamentous fungus was cultivated, as were over a dozen yeasts from at least three genera (*Cryptococcus*, *Rhodotorula*, *Sporidiobolus*). That no microbes were cultivated from the Laguna del Volcán by both Lavalle et al. (2005) and Chiacchiarini et al. (2010), although water samples were inoculated to media, is consistent with observations elsewhere that bacterial growth does not proceed in crater lakes when the pH is <1 (Satake and Saijo 1974; Takano et al. 1994a).

A discussion of microbes in the environment should not overlook the potential for viral infections. Just as the role of viruses in marine biogeochemical cycling has been reassessed in the last couple of decades, so too might we find that viruses are instrumental in controlling populations of thermophiles and acidophiles in volcanic settings (Short and Suttle 2002; Rice et al. 2001; Snyder et al. 2003). Almost 30 years ago, Janekovic et al. (1983) described a family of viruses that infect *Thermoproteus tenax*, a thermophilic *Archaea* found in hot springs. Multiple viruses in *Sulfolobus*, which inhabit high temperature hydrothermal environments, are now known (Zillig et al. 1996; Arnold et al. 2000). Geslin et al. (2003) reported the first virus in an hyperthermophilic archaeon, *Pyrococcus abyssi* from marine hydrothermal vents. An attempt about 10 years ago to isolate phage from water in Ruapehu crater (pH ~2, 45–55 °C) found neither phage nor DNA that could be amplified (Hugh Morgan, pers. comm.).

3.2 Microbial Diversity in Volcanic Systems by Molecular Methods

Molecular 'fingerprinting' methods are routinely applied in microbial ecology to compare phylogenetic diversity in microbial communities. Such diversity in volcanic environments has to date been largely investigated by denaturing gradient gel electrophoresis (DGGE) of ribosomal (rRNA) gene fragments (Muyzer et al. 1993; Löhr et al. 2006a, b; Wendt-Potthoff and Koschorreck 2002). Gene fragments with different nucleotide sequences in different species are visualized in DGGE as different 'bands' (Fig. 3). The DGGE profile, or community fingerprint, of different samples can be statistically analyzed for comparative purposes. Determining the nucleotide sequence of the rRNA gene fragment in each band permits tentative assignment of the original bacterium to a taxonomic group. More recently, 'chip-based' techniques have been developed, such that specific RNA probes on a microarray can detect their complementary genes, allowing detection of potentially thousands of species in a single experiment (De Santis et al. 2003). In this respect, an acidophilic bacterial microarray was developed and tested in habitats such as Spain's Rio Tinto, where the extremely acidic conditions are similar to those in some volcanic lakes (Garrido et al. 2008).

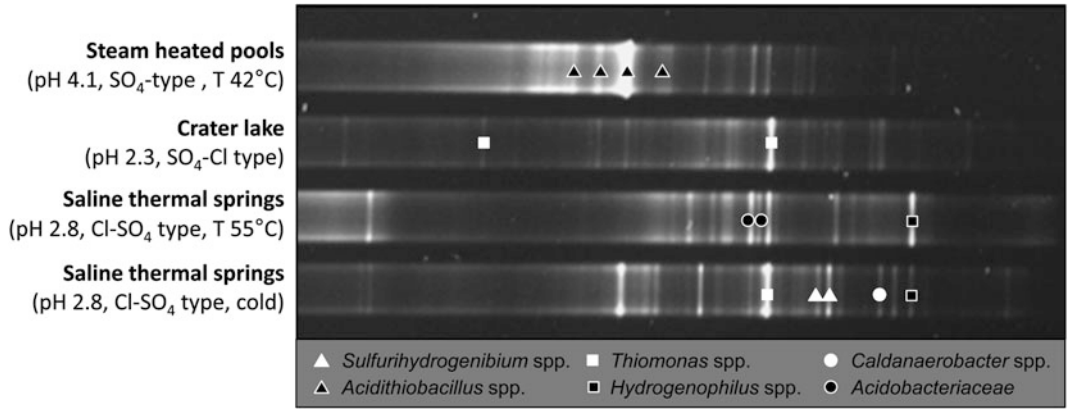

Fig. 3 DGGE gel of amplified 16S rRNA genes from El Chichón crater lake and associated thermal springs. Bands in each lane represent a different bacterial species. Symbols show which band corresponds to a particular *Bacteria* genus or family

In addition to the cultivation-based data described above for White Island, cloned 16S rRNA gene fragments from the acid stream affiliated with *Pandoraea* and *Ralstonia* (*Burkholderiaceae*, *Betaproteobacteria*), *Rhodovulum* (*Rhodobacteraceae*, *Alphaproteobacteria*), *Acidosphaera* (*Acetobacteraceae*, *Alphaproteobacteria*), and the photoautotrophic *Chlorobium vibrioforme* (Chlorobi) (Donachie et al. 2002). No DNA was detected in water collected from the pH ~0, 58 °C lake (Donachie et al. unpubl.).

The largest known acidic crater lake is Kawah Item, Indonesia, whose pH 0.3 water is clearly extreme compared to that of more typical lakes and rivers (Geller and Schultze 2009). As the river Banyupahit-Banyuputih flows from Kawah Ijen, its pH increases from 0.39 to 7.62. Microbial diversity in the lake and river investigated by DGGE detected no *Bacteria* or *Eucarya* in the lake, although they were detected along the effluent rivers (Löhr et al. 2006a). No attempts were made to cultivate microbes, nor were other sequencing strategies with larger sample sizes conducted. *Bacteria* sequences detected by DGGE in the highest pH river water affiliated with *Betaproteobacteria*, *Gammaproteobacteria* and Flavobacteria; in the most acidic sample, only a sequence affiliated with the *Pseudomonadaceae* family was detected. None of the *Bacteria* detected were known acidophiles, and *Eucarya* were absent from low pH waters in both the Kawah Ijen lake and the upper reaches of the river Banyupahit-Banyuputih. However, *Eucarya* diversity was high in water at pH ≥2.66, and included both algae and diatoms (Löhr et al. 2006b). *Archaea* sequences were detected at all sites, but taxonomic diversity was generally low and reached minima in the most acidic sites. *Archaea* typical of acidic environments were not detected (Löhr et al. 2006b).

Microbial communities in the Copahue-Caviahue system of Argentina have also been studied (Urbieta et al. 2012; Löhr et al. 2006a). Here, extremely acidic water (pH 0.2–1.1) flows from L. Copahue in the Copahue volcano into the Río Agrio. The river can be divided into the Upper Río Agrio (URA) that flows into L. Caviahue (pH 2.1–3.7), and its effluent Lower Río Agrio (LRA). Bacterial abundance in water from the Upper Río Agrio and in L. Caviahue determined by microscopy was $\sim 2 \times 10^5$ cells ml^{-1}, of the order of that reported in acid mine lakes, the anthropogenic homologue of volcanic lakes (Wendt-Potthoff and Koschorreck 2002). A more recent study by CARD-FISH detected 10× more cells in the Upper Rio Agrio (Urbieta et al. 2012). Measurements of microbial activity such as oxygen consumption, and iron oxidation and reduction at three points along the URA, one of which was immediately before the inflow to L.

Caviahue, showed a gradient of microbial abundance and activity. Iron- and sulphur-oxidizing bacteria and iron-reducing bacteria were previously reported, as one might expect given the abundances of iron and sulphur in this type of ecosystem (Wendt-Potthoff and Koschorreck 2002). FISH detected acidophilic bacteria with a potential for iron and sulphur metabolism, such as *Sulfobacillus*, *Leptospirillum*, *Acidithiobacillus* and *Acidimicrobium*, in the hot spring of Copahue village (Giaveno et al. 2009a). *Acidithiobacillus ferroxidans*, *Acidithiobacillus thiooxidans* and members of the genus *Leptospirillum* and the *Archaea* genus *Sulfolobus* were cultivated from different parts of the Copahue-Caviahue system in a study to isolate microbes that may bioleach ores and recover precious metals (Chiacchiarini et al. 2010). Bacterial diversity in four water samples from the Upper Río Agrio was also recently reported on the basis of 16S rRNA gene clone libraries and CARD-FISH (Urbieta et al. 2012). Sampling sites were characterized by increasing pH (1–2) and temperature (6.7–59 °C). CARD-FISH revealed *Archaea* were the most abundant members of the community, albeit not diverse since most sequences affiliated with just one species, the chemolithoautotrophic, iron-oxidizing, *Ferroplasma acidiphilum*. Members of the *Ferroplasma* genus are key players in the sulphur cycle through oxidation of sulphides and regeneration of Fe^{3+}, the primary oxidant of pyrite at low pH (Urbieta et al. 2012). In contrast to what one might expect in an 'ecological dogma' context, that more extreme conditions exert a stronger selective pressure that results in a less complex community, a *Bacteria* 16S rRNA gene clone library from the sample with the lowest pH (1) and highest temperature (59 °C) contained the most phylogenetically diverse community. Moreover, a 'less extreme' habitat, that characterized by pH 2 and 15.9 °C, showed the lowest diversity indices. *Bacteria* clones in URA waters affiliated with *Alpha-, Beta-* and *Gammaproteobacteria*, and the phyla *Actinobacteria*, *Firmicutes* and *Nitrospirae*, the latter represented only by the genus *Leptospirillum*, typically found in acid environments with high concentrations of reduced iron and sulphur. The distribution of *Acidithiobacillus ferrooxidans*, a known iron-sulfur oxidizing bacterium, along the URA correlated with the iron content of the water and pH value, confirming previous cultivation-dependent experiments (Chiacchiarini et al. 2010). Clone libraries also contained an *Acidiphilium* sp., an important observation given they may scavenge organic molecules that would otherwise be toxic to chemolithoautotrophs such as *Acidithiobacillus ferrooxidans* (Johnson 1995; Urbieta et al. 2012). Sulphur-oxidizing species affiliating with *Acidithiobacillus thiooxidans* and *Acidithiobacillus albertensis* were also detected in the URA; these species, along with *Sulfobacillus* spp., are typically found in natural or man-made acidic habitats, e.g., the Río Tinto in the Iberian Pyritic Belt, or in acid mine drainage.

As with studies of the Upper Río Agrio, a DGGE survey of the El Chichón crater lake (Mexico) revealed the presence of chemolithoautotrophic bacteria able to synthesize organic carbon from carbon dioxide (Fig. 3). *Alpha-, Beta-* and *Gammaproteobacteria* along with *Aquificae*, *Firmicutes* and *Acidobacteria* were detected in acidic, sulphate-rich waters of the lake (Peiffer et al. 2011; Mapelli, pers. comm.). The presence of *Sulfurihydrogenibium*, *Acidithiobacillus*, *Thiomonas* and *Hydrogenophilus,* members of which are involved in sulphur and iron cycling, and hydrogen oxidation, reflects the chemical composition of El Chichón's lake and thermal springs.

Volcanic lakes present unique challenges for both microbes and microbiologists. After a few decades of cultivation- and microscopy-based studies, plus a decade or so of molecular methods, it seems we might conclude the microbial flora in the few lakes studied is limited to a handful of microbial eukaryotes, and some *Archaea* and *Bacteria* (Schleper et al. 1995; Donachie et al. 2002). On the other hand, these lakes have been so rarely investigated in microbiological terms that we should reserve judgment until more extensive data are available.

4 Potential Applications of Microbiological Studies of Volcanic Lakes

Interest in microbial diversity in crater lakes is both scientific and economic in nature. For example, knowledge of ecological processes in natural and artificial acidic systems provides leads for established and novel biotechnological applications (Antranikian et al. 2005; Liu and Zhang 2008). Such studies may allow improvement of or development of new applications, such as in biomining, and the development of strategies to restore waters and ecosystems affected by acidification. Applications of biological resources from volcanic systems extend to reclaiming or scavenging metals from contaminated substrates or toxic mixtures. For example, Chiacchiarini et al. (2010) showed a putative *Acidothiobacillus ferrooxidans* from the Upper Rio Agrio could reduce chromium and zinc concentrations in municipal sludge to below permitted levels; consortia of bacteria from Copahue–Caviahue could also extract more gold from a sulphide concentrate than could pure cultures of *Acidothiobacillus ferrooxidans* DSM 11477 *and Leptospirillum ferrooxidans* ATCC 29047^{T} (Giaveno et al. 2009b). These type strains and related species have long been the focus of bioleaching studies (Porro et al. 1989; Donati et al. 1996).

An innovative application of microbiological research in volcanic systems is that of Plant Growth Promoting (PGP) bacteria, those that help sustain plant growth in extreme geochemical settings. Associations with microbes are an acknowledged evolutionary strategy in plants that may improve the bioavailability of nutrients and protect against pathogens. Plant-microbe associations can also enhance a plant's survival against abiotic stresses such as extreme pH or presence of toxic compounds. Only certain pioneer plants can tolerate the severe environmental conditions that typify soils affected by volcanic activity, such as high temperature, anomalous gas fluxes through soils and sediments, low pH, and presence of potentially toxic elements in aerosols and water. A PGP bacterial activity that may be widespread and important to plants colonizing volcanic systems is the detoxification of phytotoxic compounds, such as heavy metals. PGP bacteria isolated from pioneer plants in volcanic areas have potential in the formulation of 'biofertilizers' able to sustain plant growth in altered and degraded soils. Potential PGP bacteria associated with a pioneer plant growing in a hot, acidic stream emanating from the crater lake of El Chichón volcano (Mexico) have been isolated and characterized (Fig. 4). PGP bacteria can be isolated from the root interior or the adhering soil, the so-called "rhizosphere", of pioneer plants and screened in vitro for known PGP activities and resistance to abiotic stressors. To develop an effective 'biofertilizer' it is essential to determine if the bacteria are rhizocompetent, i.e., able to colonize the plant root. Rhizocompetence can be evaluated by engineering the cells to express a 'green fluorescent protein'. Such bacteria can be used in root colonization experiments on model plants and observed in root sections by epifluorescence microscopy. The most efficient or rhizocompetent bacteria strains in vitro and in vivo are tested in field trials on plants growing in suboptimal conditions. Microbial inocula such as these, with detoxification or growth stimulation activity, can enhance a plant's tolerance of stress, and promote rhizoremediation, phytoremediation and phytostabilization techniques (Ma et al. 2011; Regvar et al. 2006). The cultivation of microbes from volcanic systems, or the application of genetic information from these and uncultivated taxa, may well contribute to socially acceptable, environmentally friendly practices in land restoration.

Volcanic activity has always been part of Earth's history, so investigating microbial life in volcanic crater lakes and their effluent rivers may provide clues to the origin of life on Earth, and how life has adapted over time to extreme conditions. Astrobiology is a multidisciplinary field focusing on the origin, evolution and pattern of life on Earth and extraterrestrial bodies. The only incidence in the solar system of life as we know it is on Earth. We thus define conditions required

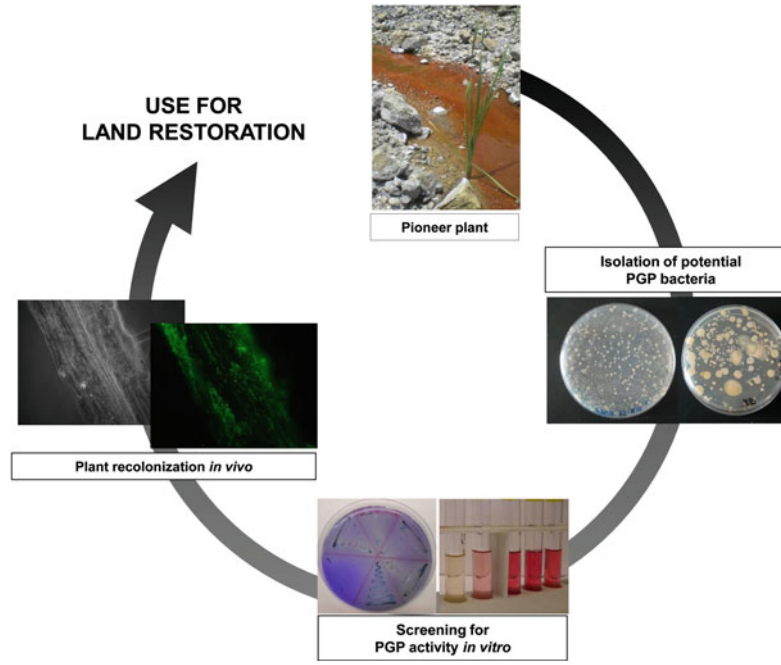

Fig. 4 Extremophilic bacteria can be isolated from pioneer plants, studied under laboratory and in vivo conditions, and may be used in environmental biotechnology, e.g., for land clean-up and restoration.

for the development of life according to observations here, and especially in volcanic systems where extreme pH, temperature and chemistry are considered analogs of both early Earth and extraterrestrial habitats. Geochemical features such as pH, and sulphur and iron species in crater lakes, appear to be the principal forces shaping the composition of autochthonous microbial communities. Iron in particular plays a fundamental role in the biogeochemistry of many volcanic ecosystems, and was probably important on the early Earth (Weber et al. 2006). Signatures of acidic aqueous systems with iron- and sulfur-based redox cycles have been found on the Martian surface (Bibring et al. 2007). For example, jarosite, an iron oxide mineral found on the surface of Mars by the 'Opportunity' rover (Klingelhofer et al. 2004) can be produced from pyrite by *Acidithiobacillus ferrivorans* cultivated from iron bioweathered soil (Borin et al. 2009), and from El Chichón crater lake (Mapelli, pers. obs.). *Acidithiobacillus* spp. and other extremophiles have been proposed as biomarkers for life detection strategies on planetary bodies (Gómez and Parro 2012). Moreover, some of the most extreme crater lakes, such as those in the Chilean Altiplano, are eminently suited to investigations of microbial physiology and community dynamics in rapidly changing and extreme environments (Demergasso et al. 2010). Considerable technical challenges await those who choose to work on the microbiology of volcanic crater lakes, but the field will surely yield both exciting methodological developments and scientific discoveries.

References

Amann RI, Krumholz L, Stahl DA (1990) Fluorescent oligonucleotide probing of whole cells for determinative, phylogenetic and environmental studies in microbiology. J Bacteriol 172:762–770

Amann RI, Ludwig W, Schleifer K-H (1995) Phylogenetic identification and in situ detection of individual microbial cells without cultivation. Microbiol Rev 59:143–169

Arnold HP, Zillig W, Ziese U, Holz I, Crosby M, Utterback T, Weidmann JF, Kristjanson JK, Klenk HP, Nelson KE, Fraser CM (2000) A novel lipothrixvirus, SIFV, of the extremely thermophilic crenarchaeon *Sulfolobus*. Virology 267:252–266

Antranikian G, Vorgias CE, Bertoldo C (2005) Extreme environments as a resource for microorganisms and novel biocatalysts. Adv Biochem Eng Biotechnol 96:219–262

Baret J-C, Miller OJ, Taly V, Ryckelynck M, El-Harrak A, Frenz L, Rick C, Samuels ML, Hutchison JB, Agresti JJ, Link DR, Weitz DA, Griffiths AD (2009) Fluorescence-activated droplet sorting (FADS): efficient microfluidic cell sorting based on enzymatic activity. Lab Chip 9:1850–1858

Barton HA, Taylor MR, Pace NR (2004) Molecular phylogenetic analysis of a bacterial community in an oligotrophic cave environment. Geomicrobiol J 21:11–20

Bibring J-P, Arvidson RE, Gendrin A, Gondet B, Langevin Y, Le Mouelic S et al (2007) Coupled ferric oxides and sulfates on the martian surface. Science 317:1206–1210

Borin S, Ventura S, Tambone F, Mapelli F, Schubotz F, Brusetti L, Scaglia B, D'Acqui LP, Solheim B, Turicchia S, Marasco R, Hinrichs KU, Baldi F, Adani F, Daffonchio D (2009) Rock weathering creates oasis of life in a high Arctic desert. Environ Microbiol 12:293–303

Bowman JP, Rea SM, Brown MV, McCammon SA, Smith MC, McMeekin TA (1999) Community structure and psychrophily in Antarctic microbial ecosystems. In: Bell CR, Brylinsky M, Johnson-Green M (eds) Microbial biosystems: new frontiers. Proceedings of the 8th International Symposium on Microbial Ecology, vol 1. Atlantic Canada Society for Microbial Ecology, Kentville, Nova Scotia, Canada, pp 287–292

Cabrol NA, Grin EA, Chong G, Minkley E, Hock AN, Yu Y, Bebout L, Fleming E, Häder DP, Demergasso C, Gibson J, Escudero L, Dorador C, Lim D, Woosley C, Morris RL, Tambley C, Gaete V, Galvez ME, Smith E, Ukstins Peate I, Salazar S, Dawidowicz G, Majerowicz J (2009) The high-lakes project. J Geophys Res 114 G00D06. doi:10.1029/2008JG000818

Certes A (1884) Sur la culture, a l'abri des germes atmospheriques, des eaux et des sediments rapportes par les expeditions der Travailleur et du Talisman. Compt Rend Acad Sci 98:690–693

Chen CH, Cho SH, Tsai F, Erten A, Lo YH (2009) Microfluidic cell sorter with integrated piezoelectric actuator. Biomed Microdevices 11:1223–1231

Chiacchiarini P, Lavalle L, Giaveno A, Donati E (2010) First assessment of acidophilic microorganisms from geothermal Copahue-Caviahue system. Hydrometallurgy 104:334–341

Colwell RR, Grimes DJ (2000) Semantics and strategies. In: Colwell RR, Grimes DJ (eds) Nonculturable microorganisms in the environment. ASM Press, Washington, DC, pp 1–6

Connon SA, Giovannoni SJ (2002) High-throughput methods for culturing microorganisms in very-low-nutrient media yield diverse new marine isolates. Appl Environ Microbiol 68:3878–3885

Curtis TP, Sloan WT, Scannell JW (2002) Estimating prokaryotic diversity and its limits. Proc Natl Acad Sci USA 99:10494–10499

DeLong EF, Preston CM, Mincer T, Rich V, Hallam SJ, Frigaard NU et al (2006) Community genomics among stratified microbial assemblages in the ocean's interior. Science 311:496–503

Demergasso C, Dorador C, Meneses D, Blamey J, Cabrol N, Escudero L, Chong G (2010) Prokaryotic diversity pattern in high-altitude ecosystems of the Chilean Altiplano. J Geophys Res 115 G00D09. doi:10.1029/2008JG000836

D'Imperio S, Lehr CR, Oduro H, Druschel G, Kuhl M, McDermott TR (2008) The relative importance of H_2 and H_2S as energy sources for primary production in geothermal springs. Appl Environ Microbiol 74:5802–5808

Doemel WN, Brock TD (1971) The physiological ecology of *Cyanidium caldarium*. Microbiology 67:17–32

Donachie SP (1996) A seasonal study of marine bacteria in Admiralty Bay (Antarctica). Proc NIPR Symp Polar Biol 9:111–124

Donachie SP, Christenson B, Kunkel DD, Malahoff A, Alam M (2002) Microbial community in acidic hydrothermal waters of volcanically active White Island, New Zealand. Extremophiles 6:419–425

Donachie SP, Hou S, Gregory TS, Malahoff A, Alam M (2003) *Idiomarina loihiensis*, sp. *nov*., a new halophilic γ-*Proteobacterium* isolated from the Lō'ihi submarine volcano, Hawai'i. Int J Syst Evol Microbiol 53:1873–1879

Donachie SP, Hou S, Lee K-S, Riley CW, Pikina A, Belisle C, Kempe S, Gregory TS, Bossuyt A, Boerema J, Liu J, Freitas TA, Malahoff A, Alam M (2004) The Hawaiian Archipelago: a microbial diversity hotspot. Microb Ecol 48:509–520

Donachie SP, Foster JS, Brown MV (2007) Culture clash: challenging the dogma of microbial diversity. ISME J 1:97–102

Donati E, Curutchet G, Pogliani C, Tedesco P (1996) Bioleaching of covellite using pure and mixed cultures of *Thiobacillus ferrooxidans* and *Thiobacillus thiooxidans*. Process Biochem 31:129–134

DeSantis TZ, Dubosarskiy I, Murray SR, Andersen GL (2003) Comprehensive aligned sequence construction for automated design of effective probes (CASCADE-P) using 16S rDNA. Bioinformatics 19:1461–1468

Escudero L, Chong G, Demergasso C, Farías ME, Cabrol NA, Grin E, Minkley E Jr, Yu Y (2007) Investigating microbial diversity and UV radiation impact at the high-altitude Lake Aguas Calientes, Chile. Proc SPIE 6694:66940Z

Fröhlich J, König H (2000) New techniques for isolation of single prokaryotic cells. FEMS Microbiol Rev 24:567–572

Gaidos E, Lanoil B, Thorsteinsson T, Graham A, Skidmore M, Han S-K, Rust T, Popp B (2004) A viable microbial community in a subglacial volcanic crater lake, Iceland. Astrobiology 4:327–344

Gaidos E, Marteinsson V, Thorsteinsson T, Johannesson T, Rafnsson AR, Stefansson A, Glazer B, Lanoil B, Skidmore M, Han S, Miller M, Rusch A, Foo W (2008) An oligarchic microbial assemblage in the anoxic bottom waters of a volcanic subglacial lake. ISME J 3:486–497

Garrido P, González-Toril E, García-Moyano A, Moreno-Paz M, Amils R, Parro V (2008) An oligonucleotide prokaryotic acidophile microarray: its validation and its use to monitor seasonal variations in extreme acidic environments with total environmental RNA. Environ Microbiol 10:836–850

Geller W, Schultze M (2009) Acidification. In: Likens GE (ed) Encyclopedia of Inland Waters. Elsevier, Oxford, pp 1–12

Geslin C, Le Romancer M, Erauso G, Gaillard M, Perrot G, Prieur D (2003) PAV1, the first virus-like particle isolated from a hyperthermophilic euryarchaeote, *Pyrococcus abyssi*. J Bacteriol 185:3888–3894

Giaveno A, Huergo J, Lavalle L, Sand W, Donati E (2009a) Molecular and morphological characterization of cultures from the extreme environmental area of Copahue Volcano-Argentina. Adv Mat Res 71–73:93–96

Giaveno A, Chiacchiarini P, Cordero C, Lavalle L, Huergo J, Donati E (2009b) Oxidative capacity of native strains from Copahue geothermal system in the pretreatment of a gold sulfide ore. Adv Mat Res 71–73:473–476

Giovannoni S, Stingl U (2007) Opinion: the importance of culturing bacterioplankton in the 'omics' age. Nat Rev Microbiol 5:820–826

Gómez F, Parro V (2012) Applications of extremophiles in astrobiology: habitability and life detection strategies. In: Stan-Lotter H, Fendrihan S (eds) Adaption of microbial life to environmental extremes. Springer, Wien, pp 199–229

Handelsman J (2004) Metagenomics: application of genomics to uncultured microorganisms. Microbiol Mol Biol Rev 68:669–685

Harrison AP (1981) *Acidiphilium cryptum*, gen. nov., sp. nov., heterotrophic bacterium from acidic mineral environments. Int J Syst Bact 31:327–332

Ho CT, Lin RZ, Chang HY, Liu CH (2005) Micromachined electrochemical T-switches for cell sorting applications. Lab Chip 5:1248–1258

Huber R, Burggraf S, Mayer T, Barns SM, Rossnagel P, Stetter KO (1995) Isolation of a hyperthermophilic archaeum predicted by in situ RNA analysis. Nature 376:57–58

Hugenholtz P, Pitulle C, Hershberger KL, Pace NR (1998) Novel division level bacterial diversity in a Yellowstone hot spring. J Bacteriol 180:366–376

Janekovic D, Wunderl S, Holz I, Zillig W, Gierl A, Neumann H (1983) TTV1, TTV2 and TTV3, a family of viruses of the extremely thermophilic, anaerobic, sulfur-reducing archaebacterium *Thermoproteus tenax*. Mol Gen Genet 192:39–45

Jóhannesson T, Thorsteinsson T, Stefánsson A, Gaidos EJ, Einarsson B (2007) Circulation and thermodynamics in a subglacial geothermal lake under the Western Skaftá cauldron of the Vatnajökull ice cap, Iceland. Geophys Res Lett 34:L19502

Johnson D (1995) Selective solid media for isolating and enumerating acidophilic bacteria. J Microbiol Meth 23:205–218

Kaiser O, Pühler A, Selbitschka W (2001) Phylogenetic analysis of microbial diversity in the rhizoplane of Oilseed Rape (*Brassica napus* cv. Westar) employing cultivation-dependent and cultivation-independent approaches. Microb Ecol 42:136–149

Kalyuzhnaya MG, Lapidus A, Ivanova N, Copeland AC, McHardy AC, Szeto E, Salamov A, Grigoriev IV, Suciu D, Levine SR, Markowitz VM, Rigoutsos I, Tringe SG, Bruce DC, Richardson PM, Lidstrom ME, Chistoserdova L (2008) High-resolution metagenomics targets specific functional types in complex microbial communities. Nat Biotechnol 26:1029–1034

Kang Y, Norris MH, Zarzycki-Siek J, Nierman WC, Donachie SP, Hoang TT (2011) Transcript amplification from single bacterium for transcriptome analysis. Genome Res 21:925–935

Karl DM, Brittain AM, Tilbrook BD (1989) Hydrothermal and microbial processes at Loihi Seamount, a mid-plate hot-spot volcano. Deep Sea Res 36:1655–1673

Karner M, DeLong EF, Karl DM (2001) Archaeal dominance in the mesopelagic zone of the Pacific Ocean. Nature 409:507–510

Kelly DP, Wood AP (2000) Reclassification of some species of *Thiobacillus* to the newly designated genera *Acidithiobacillus* gen. nov., *Halothiobacillus* gen. nov. and *Thermithiobacillus* gen. nov. Int J Syst Evol Microbiol 50:511–516

Kimura M (1968) Evolutionary rate at the molecular level. Nature 217:624–626

Kimura N (1983) The neutral theory of molecular evolution. Cambridge University Press, New York, p 384

Kircher M, Kelso J (2010) High-throughput DNA sequencing—concepts and limitations. BioEssays 32:524–536

Kleinschmidt MG, McMahon VA (1970) Effect of growth temperature on the lipid composition of *Cyanidium caldarium*. Plant Physiol 46:286–289

Klingelhofer G, Morris RV, Bernhardt B, Schroder C, Rodionov CS, de Souza PA Jr et al (2004) Jarosite and hematite at meridiani planum from opportunity's mössbauer spectrometer. Science 306:1740–1745

Koschorreck M, Wendt-Potthoff K, Scharf B, Richnow HH (2008) Methanogenesis in the sediment of the acidic Lake Caviahue in Argentina. J Volcanol Geoth Res 178:197–204

Kovac JR, Voldman J (2007) Intuitive, image-based cell sorting using opto-fluidic cell sorting. Anal Chem 79:9321–9330

Krüger J, Singh K, O'Neill A, Jackson C, Morrison A, O'Brien P (2002) Development of a microfluidic device for fluorescence activated cell sorting. J Micromech Microeng 12:486–494

Kunin V, Engelbrektson A, Ochman H, Hugenholtz P (2010) Wrinkles in the rare biosphere: pyrosequencing

errors can lead to artificial inflation of diversity estimates. Appl Environ Microbiol 12:118–123

Lavalle L, Chiacchiarini P, Pogliani C, Donati E (2005) Isolation and characterization of acidophilic bacteria from Patagonia, Argentina. Process Biochem 40:1095–1099

Liu B, Zhang X (2008) Deep-sea thermophilic *Geobacillus* bacteriophage GVE2 transcriptional profile and proteomic characterization of virions. Appl Microbiol Biotechnol 80:697–707

Löhr AJ, Laverman AM, Braster M, van Straalen NM, Röling WFM (2006a) Microbial communities in the world's largest acidic volcanic lake, Kawah Ijen in Indonesia, and in the Banyupahit river originating from it. Microb Ecol 52:609–618

Löhr AJ, Sluik R, Olaveson MM, Ivorra N, Van Gestel CAM, Van Straalen NM (2006b) Macroinvertebrate and algal communities in an extremely acidic river and the Kawah Ijen crater lake (pH < 0.3), Indonesia. Arch Hydrobiol 165:1–21

Ma Y, Prasad MNV, Rajkumar M, Freitas K (2011) Plant growth promoting rhizobacteria and endophytes accelerate phytoremediation of metalliferous soils. Biotechnol Adv 29:248–258

Macelroy RD (1974) Some comments on the evolution of extremophiles. Biosystems 6:74–75

Martínez M, Fernández E, Valdés J, Barboza V, van der Laat R, Malavassi E, Sandoval L, Barquero J, Marino T (2000) Chemical evolution and volcanic activity of the active crater lake of Poás volcano, Costa Rica, 1993–1997. J Volcanol Geoth Res 97:127–141

Martínez M, Mason P, van Bergen M, Fernández E, Duarte E, Malavassi E, Barquero J and Valdés J (2002) Chemistry of sulphur globules from the acid crater lake of Poás Volcano, Costa Rica. In: Proceedings of Colima volcano international meeting, 2002, Colima

Moisander PH, Shiue L, Steward GF, Jenkins BD, Bebout BM (2006) Application of a *nif*H oligonucleotide microarray for profiling diversity of N_2-fixing microorganisms in marine microbial mats. Environ Microbiol 8:1721–1735

Morris RM, Rappe MS, Urbach E, Connon SA, Giovannoni SJ (2004) Prevalence of the Chloroflexi related SAR202 bacterioplankton cluster throughout the mesopelagic zone and deep ocean. Appl Environ Microbiol 70:2836–2842

Munson MA, Pitt-Ford T, Chong B, Weightman A, Wade WG (2002) Molecular and cultural analysis of the microflora associated with endodontic infections. J Dent Res 81:761–766

Muyzer G, De Waal EC, Uitterlinden AG (1993) Profiling of complex microbial populations by denaturing gradient gel electrophoresis analysis of polymerase chain reaction-amplified genes coding for 16S rRNA. Appl Environ Microbiol 59:695–700

Nakagawa S, Takai K (2008) Deep-sea vent chemoautotrophs: diversity, biochemistry and ecological significance. FEMS Microbiol Ecol 65:1–14

Niedringhaus TP, Milanova D, Kerby MB, Snyder MP, Barron AE (2011) Landscape of next-generation sequencing technologies. Anal Chem 83:4327–4341

Ouverney CC, Fuhrman JA (1999) Combined microautoradiography-16S rRNA probe technique for the determination of radioisotope uptake by specific microbial cell types in situ. Appl Environ Microbiol 65:1746–1752

Ouverney CC, Fuhrman JA (2000) Marine planktonic *Archaea* take up amino acids. Appl Environ Microbiol 66:4829–4833

Palleroni NJ (1997) Prokaryotic diversity and the importance of culturing. Antonie von Leeuwenhoek 72:3–19

Parker SR, Gammons CH, Pedrozo FL, Wood SA (2008) Diel changes in metal concentrations in a geogenically acidic river: rio agrio, Argentina. J Volcanol Geoth Res 178:213–223

Pasternack GB, Varekamp JC (1997) Volcanic lake systematics I. Physical constraints. Bull Volcanol 58:528–538

Peiffer L, Taran YA, Lounejeva E, Solís-Pichardo G, Rouwet D, Bernard-Romero RA (2011) Tracing thermal aquifers of El Chichón volcano–hydrothermal system (México) with $^{87}Sr/^{86}Sr$, Ca/Sr and REE. J Volcanol Geoth Res 205:55–66

Porro S, Boiardi JL, Tedesco PH (1989) Bioleaching improvement at pH 1.4 using selected strains of *Thiobacillus ferrooxidans*. Biorecovery 1:145–154

Queck SY, Otto M (2008) *Staphylococcus epidermidis* and other coagulase-negative Staphylococci. In: Lindsay J (ed) *Staphylococcus: Molecular Genetics*. Caister Academic Press, Norfolk, pp 227–254

Regvar M, Vogel-Mikuš K, Kugonič N, Turk B, Batič F (2006) Vegetational and mycorrhizal successions at a metal polluted site: indications for the direction of phytostabilisation? Environ Poll 144:976–984

Reysenbach AL, Longnecker K, Kirshtein J (2000) Novel bacterial and archaeal lineages from an in situ growth chamber deployed at a Mid-Atlantic Ridge hydrothermal vent. Appl Environ Microbiol 66:3798–3806

Rice G, Stedman K, Snyder J, Wiedenheft B, Willits D, Brumfield S, McDermott T, Young MJ (2001) Viruses from extreme thermal environments. Proc Natl Acad Sci USA 98:13341–13345

Rodríguez-Valera F (2002) Approaches to prokaryotic biodiversity: a population genetics perspective. Environ Microbiol 4:628–633

Satake K, Saijo Y (1974) Carbon dioxide content and metabolic activity of microorganisms in some acid lakes in Japan. Limnol Oceanogr 19:331–338

Schleper C, Pühler G, Kühlmorgen B, Zillig W (1995) Life at extremely low pH. Nature 375:741–742

Schmidt TM, DeLong EF, Pace NR (1991) Analysis of a marine picoplankton community by 16S rRNA gene cloning and sequencing. J Bacteriol 173:4371–4378

Shawkey MD, Mills KL, Dale C, Hill GE (2005) Microbial diversity of wild bird feathers revealed through cultured-based and culture-independent techniques. Microb Ecol 50:40–47

Short SM, Suttle CA (2002) Sequence analysis of marine virus communities reveals that groups of related algal viruses are widely distributed in nature. Appl Environ Microbiol 68:1290–1296

Snyder JC, Stedman K, Rice G, Wiedenheft B, Spuhler J, Young MJ (2003) Viruses of hyperthermophilic *Archaea*. Res Microbiol 154:474–482

Sogin ML, Morrison HG, Huber JA, Mark Welch D, Huse SM, Neal PR et al (2006) Microbial diversity in the deep sea and the underexplored 'rare biosphere'. Proc Natl Acad Sci USA 103:12115–12120

Sonne-Hansen J, Ahring BK (1997) Anaerobic microbiology of an alkaline Icelandic hot spring. FEMS Microbiol Ecol 23:31–38

Stackebrandt E, Ludwig W, Fox GE (1985) 16S ribosomal RNA oligonucleotide cataloguing. In: Gottschalk G (ed) Methods in microbiology. Academic Press, London, pp 75–107

Stahl DA, Lane DJ, Olsen GJ, Pace NR (1984) Analysis of hydrothermal vent-associated symbionts by ribosomal RNA sequences. Science 224:409–411

Staley JT, Konopka A (1985) Measurement of in situ activities of non-photosynthetic microorganisms in aquatic and terrestrial habitats. Annu Rev Microbiol 39:321–346

Suzuki MT, Rappé MS, Haimberger ZW, Winfield H, Adair N, Ströbel J, Giovannoni SJ (1997) Bacterial diversity among SSU rRNA gene clones and cellular isolates from the same seawater sample. Appl Environ Microbiol 63:983–989

Takano B, Ohsawa S, Glover RB (1994a) Surveillance of Ruapehu Crater Lake, New Zealand, by aqueous polythionates. J Volcanol Geoth Res 60:29–57

Takano B, Saitoh H, Takano E (1994b) Geochemical implications of subaqueous molten at Yugama crater lake, Kusatsu-Shirane volcano, Japan. Geochem J 28:199–216

Takano B, Koshida M, Fujiwara Y, Sugimori K, Takayanagi S (1997) Influence of sulfur-oxidizing bacteria on the budget of sulfate in Yugama crater lake, Kusatsu-Shirane volcano, Japan. Biogeochemistry 38:227–253

Tansey MR, Brock TD (1972) The upper temperature limit for eukaryotic organisms. Proc Natl Acad Sci USA 69:2426–2428

Teske A, Sigalevich P, Cohen Y, Muyzer G (1996) Molecular identification of bacteria from a coculture by denaturing gradient gel electrophoresis of 16S ribosomal DNA fragments as a tool for isolation in pure cultures. Appl Environ Microbiol 62:4210–4215

Thorsteinsson T, Elefsen SO, Gaidos E, Lanoil B, Jóhannesson T, Kjartansson V, Marteinsson VP, Stefánsson A, Thorsteinsson T (2008) A hot water drill with built-in sterilization: design, testing and performance. Jökull 57:71–82

Tyson GW, Lo I, Baker BJ, Allenn EE, Hugenholtz P, Banfield JF (2005) Genome-directed isolation of the key nitrogen fixer *Leptospirillum ferrodiazotrophum* sp. nov. from an acidophilic microbial community. Appl Environ Microbiol 71:6319–6324

Urbieta MS, González Toril E, Aguilera A, Giaveno MA, Donati E (2012) First prokaryotic biodiversity assessment using molecular techniques of an Acidic River in Neuquén, Argentina. Microb Ecol. doi:10.1007/s00248-011-9997-2

Valenzuela-Encinas C, Neria-González I, Alcántara-Hernández RJ, Enríquez-Aragón JA, Estrada-Alvarado I, Hernández-Rodríguez C, Dendooven L, Marsch R (2008) Phylogenetic analysis of the archaeal community in an alkaline-saline soil of the former lake Texcoco (Mexico). Extremophiles 12:247–254

Wagner M, Roger AJ, Flax JL, Brusseau GA, Stahl DA (1998) Phylogeny of dissimilatory sulfite reductases supports an early origin of sulfate respiration. J Bacteriol 180:2975–2982

Ward DM, Weller R, Bateson MM (1990) 16S rRNA sequences reveal numerous uncultured microorganisms in a natural community. Nature 345:63–65

Weber KA, Achenbach LA, Coates JD (2006) Microorganisms pumping iron: anaerobic microbial iron oxidation and reduction. Nat Rev Microbiol 4:752–764

Wendt-Potthoff K, Koschorreck M (2002) Functional groups and activities of bacteria in a highly acidic volcanic mountain stream and lake in Patagonia, Argentina. Microb Ecol 43:92–106

Wilson MJ, Weightman AJ, Wade WG (1997) Applications of molecular ecology in the characterisation of uncultured microorganisms associated with human disease. Rev Med Microbiol 8:91–101

Woelfl S, Whitton BA (2000) Sampling, preservation and quantification of biological samples from highly acidic environments (pH ≤ 3). Hydrobiologia 433:173–180

Woese CR (1987) Bacterial evolution. Microbiol Rev 51:221–271

Xu H-S, Roberts N, Singleton FL, Atwell RW, Grimes DJ, Colwell RR (1982) Survival and viability of nonculturable *Escherichia coli* and *Vibrio cholerae* in the estuarine and marine environment. Microb Ecol 8:313–323

Zengler K, Toledo G, Rappé M, Elkins J, Mathur EJ, Short JM, Keller M (2002) Cultivating the uncultured. Proc Natl Acad Sci USA 99:15681–15686

Zillig W, Prangishvili D, Schleper C, Elferink M, Holz I, Albers S, Janekovic D, Goetz D (1996) Viruses, plasmids and other genetic elements of thermophilic and hyperthermophilic *Archaea*. FEMS Microbiol Rev 18:225–236

A View on Volcanic Lakes

(See Figs. A.1, A.2, A.3, A.4, A.5, A.6, A.7, A.8, A.9, A.10, A.11, A.12, A.13–A.14, A.15, A.16, A.17, A.18 and A.19)

Fig. A.1 Lake Nyos, Cameroon (5 June 2012) (picture by Yutaka Yoshida). Degassing fountains are removing CO_2-rich bottom waters. Lake surface turned *red* by iron oxide as a result of oxidation of iron dissolved in bottom water when moved to the lake water

D. Rouwet et al. (eds.), *Volcanic Lakes*, Advances in Volcanology,
DOI 10.1007/978-3-642-36833-2,
© Springer-Verlag Berlin Heidelberg 2015

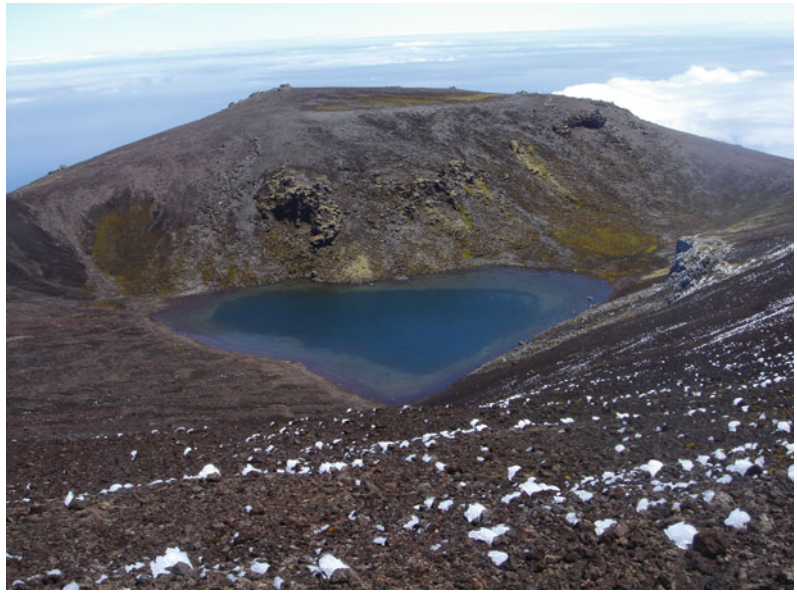

Fig. A.2 Summit crater lake, Queen Mary's Peak, Tristan da Cunha, British Overseas Territory (10 November 2009) (Picture by Anna Hicks). Tristan da Cunha is a large active volcano in the South Atlantic Ocean. The island is home to the most remote community in the world, with a population of just 260 people. The lake is not ephemeral—it is been permanent since records began (1816) but likely a considerably long time before this. There has been some extremely minor hydrothermal activity near the summit, but no eruption has centered on this area (that we know of) for the last 5,000 years. Tristan da Cunha is active though, last erupting in 1961, and with an offshore eruption in 2004. During this last, event the population was temporarily evacuated to the UK

Fig. A.3 El Chichón volcano, Chiapas, Mexico, seen from the north (March 2007) (Picture by Martin Jutzeler). This crater lake was formed almost immediately after the renowned March-April 1982 Plinian eruptions. The lake has varied dynamically in volume but has never disappeared since its formation. Until 2014, the March 2007 lake showed its largest volume ever. The fast lake volume variations are due to the alternations in discharge from a boiling geyser-like spring feeding the crater lake with water and solutes from the northern shores

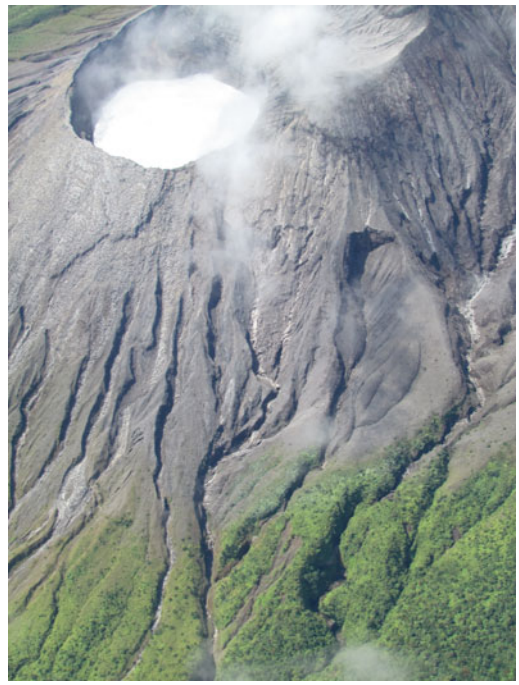

Fig. A.4 Rincón de la Vieja volcano, Costa Rica, seen from the northwest (picture by Raúl Mora-Amador). This highly acidic crater lake is often disrupted by cycles of phreatic eruptions. The current cycle started in 2011. Phreatic eruptions can expel lake water, flushing over the unstable north flank creating small lahars

Fig. A.5 Öskjuvatn (Askja lake), Askja volcano, Iceland (9 August 2011) (picture by Dave McGarvie). A young volcanic lake formed by caldera collapse. Its formation started in 1875 during an explosive rhyolite eruption, and in the years after the eruption a deep depression was formed. The lake gradually filled and by the 1920s was full. It is fed purely by precipitation (i.e. not by major streams or rivers). With a depth of about 420 m, it is Iceland's deepest lake. The crater on the right with the pale-colored water is Víti ('hell') which is considered to be a vent from the 1875 eruption which escaped the caldera collapse. It contains warm sulfurous water. The prominent lava flow on the left is Bátshraun ('boat lava'), so named because people left a boat by the lake and when they returned the next year (1921) the boat had been buried beneath this new lava flow

Fig. A.6 Lagoa do Fogo, Aqua de Pau volcano, São Miguel, Azores-Portugal (10 August 2007) (picture by Andreas Dill). Situated on the largest of the Azores islands, the lake is easy accessible, even by car. You can climb the volcano from the north, visiting the fumaroles and hot springs at the slopes. Or by a steep walk from the beaches in the south. Scenic hikes from the east are ending at the crater floor. Chances are high that you will find the lake heavily clouded and even invisible in the mist. The photo was made on one rare occasion of splendid sights over the lake and the central island mountains

Fig. A.7 Kawah Ijen volcano, Java, Indonesia (May 2010) (picture by Raphaël De Plaen, used with permission by Corentin Caudron). The Kawah Ijen crater lake is the largest natural, acidic surface water reservoir on Earth. The picture was taken during an echo sounding campaign on the lake

Fig. A.8 Rinjani volcano, Lombok, Indonesia (13 May 2010) (picture by Julie Oppenheimer, used with permission by Corentin Caudron). An eruption from the cone on the peninsula entering the lake, before starting CTD profiles and CO_2 measurements on the lake

Fig. A.9 Lake Toba, Sumatra, Indonesia (18 January 2008) (picture by Craig Chesner). Resurgent doming at the Toba Caldera, Sumatra, Indonesia. The 100 × 30 km Toba Caldera in northern Sumatra, Indonesia formed from a super-eruption 74,000 years ago. Two resurgent domes (Samosir Island and the Uluan peninsula) now dominate the landscape within the steep-walled caldera. In this view looking east, the Uluan peninsula, consisting of welded tuffs (Oldest Toba Tuff, ~800 ka) capped by non-welded tuffs (Youngest Toba Tuff, 74 ka), is seen between the fault bounded Latung Strait (middle foreground) and the steep caldera wall in the background. The photograph was taken from Samosir Island (foreground), about 600 m above lake level, where welded Youngest Toba Tuff is overlain by a veneer of lake sediments. Ages of these lake sediments suggest that Samosir emerged from Lake Toba just 30,000 years ago, attesting to the dynamic nature of Earth's largest Quaternary resurgent caldera (Chesner and Luhr 2010)

Fig. A.10 Zao volcano, Honshu, Japan (July 2006) (picture by Jacques-Marie Bardintzeff). Zao volcano is 1841 m high and lies close to Yamagata (Tohoku Province), not so far north from Tokyo. Its crater (named Okama) is filled by a beautiful acid (pH = 1.3) lake, 300 m in diameter. This lake has a *nice green* color that changes from jade to emerald according to the sunlight. Last eruption (phreatic) occurred in 1939–1940 (copyright JM Bardintzeff)

Fig. A.11 Lake Karymsky, Caldera Akademia Nauk, Kamchatka, Russia (September 2006) (picture by Alexander Morawitz), seen from the east shore. The 1996 eruption of Caldera Akademia Nauk causes the lake water to boil and throw masses of boiling water into the shore vegetation because of tsunamis. The result is here visible: dead wood of boiled pines. In the back you can observe Karymsky volcano

Fig. A.12 Gorely volcano, Kamchatka, Russia (October 2011) (picture by Emanuela Bagnato). Gorely volcano is located in Southern Kamchatka, about 75 km SW of Petropavlovsk-Kamchatsky. It is the most active volcano in southern Kamchatka. The volcano structure of Gorely consists of a caldera (13 × 12 km) with three merged cones and seven superimposed summit craters. In 2008 there were plates of sulfur on the summit lake surface and intense steaming

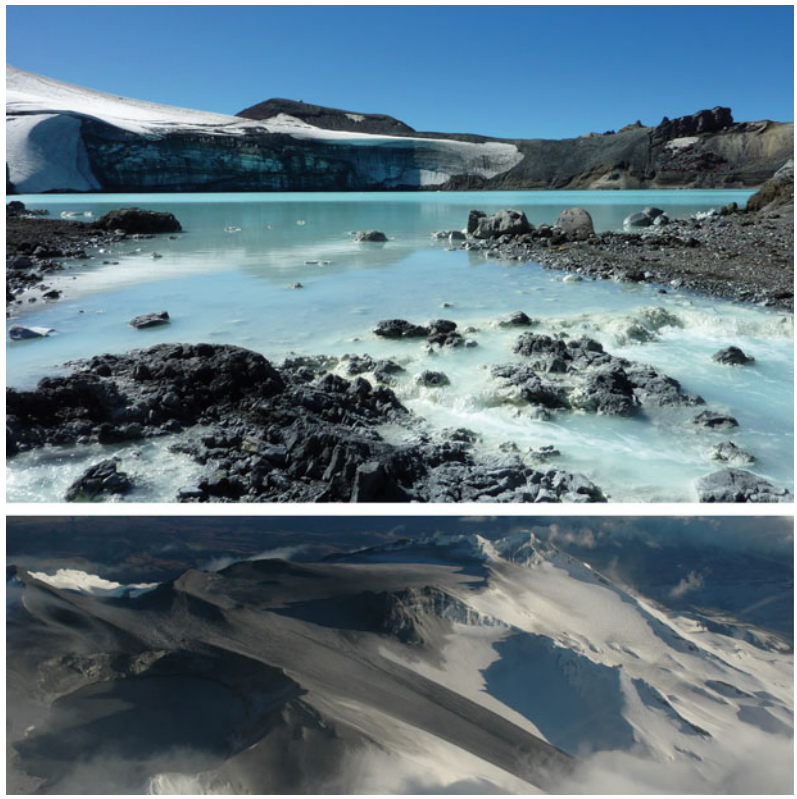

Fig. A.13–14 Crater Lake, Ruapehu volcano, New Zealand (April 2010) (pictures by Bruce Christenson). Ruapehu Crater Lake. View across the outlet for the lake, which serves as the headwaters for the Whangaehu Stream. The lake is acidic (pH ~1), and exhibits temperature cycling ranging between ca. 10 and 50 °C. The photo was taken during a bathymetric survey which measured a maximum depth of 109 m over the central vent area. Eruptive activity in 1995–1996 totally expelled the lake (~9 million cubic metres), and it took some 10 years to refill to its former outlet level

Fig. A.15 Lake Letas, Garet volcano, Gaua, Vanuatu (19 June 2010) (picture by Bernard Fountaine). "During a visit to some volcanoes of Vanuatu, we are four members of LAVE-Belgium team guided by the plume of Mt Garet on the way to Gaua Island. On 19 June 2010, we start climbing the caldera where Lake Letas is located, to observe the volcanic activity. From our canoe, lake water samples were collect. The field trip was made possible thanks to the kindness and assistance of Esline Garaebiti (manager) and A. Worwor (technician) of VGO (Vanuatu Geohazards Observatory) as well as of my friend Thierry, always ready for a volcano trip." (by Bernard Fountaine)

Fig. A.16 Main Crater Lake, Taal volcano, Philippines (March 2012) (picture by Takeshi Hashimoto, used with permission by Tony Hurst). The Main Crater Lake of Taal is located on Taal volcano Island, in Lake Taal, about 50 km south of Manila on Luzon Island in the Philippines. The lake is about 1 km in diameter, and has an average temperature of 29 °C. The lake level and temperature are monitored by the local observatory of PHIVOLCS. There have been many recorded eruptions of Taal volcano, with the largest in 1,754, while there were over 1,000 fatalities from a Plinian eruption in 1911. The most recent activity was phreatic from Mount Tabaro on Taal volcano Island in 1977, while the most recent activity in Main Crater Lake was geysering during 1999–2000

Fig. A.17 Licancabur volcano, Chile/Bolovia (17 April 2010) (picture by Richard Sanderson). The lake is apparently located on the Chilean side however. It is not clear if the lake has a particular name other than 'Lago Licancabur'. It is sometimes credited as being the world's highest lake but there are some reports of higher ones on Ojos del Salado (another volcano) and in the Himalayas. It has been scuba-dived in so it has the unofficial record for altitude diving

Fig. A.18 Azufral volcano, Colombia (12 July 2009) (picture by Hugo Murcia). This picture was taken during a field trip with Sofia Navarro from the Geological Survey of Colombia and Ian Coulson from the University of Regina, Canada. On this trip to the lake we were collecting water as well as taking physical and chemical parameters. 6 days later, on July 18, a hydrothermal eruption occurred and we understood that going down to the lake was more dangerous than we had initially thought. In the picture, the *white area* is the evidence of repeated and sudden eruptions as a result of hydrothermalism. Currently there is public access to the lake and researchers continue visiting the lake for scientific purposes

Fig. A.19 Mount Katmai (Katmai volcano), Alaska, USA (9 June 2012) (picture by Dave McGarvie). Formed in 1912, the collapse of Mount Katmai to form this crater (now filled with water) is considered to be the result of magma extraction from beneath the area to feed the eruption taking place 9–10 km away at Novarupta, which was the site of the largest volcanic eruption of the 20th century. The exact link between Mount Katmai volcano and the Novarupta vent is not known with certainty, and remains one of volcanology's most recent mysteries. At Mount Katmai the collapse was not accompanied by substantial eruptive activity, but instead by phreatic activity. A small dacitic dome was erupted, which is now covered by ~250 m of water. In this photograph the ice-free area is created by upwelling water (heated by hydrothermal vents on the crater floor). The *faint green patches* are thought to represent precipitation from hot-warm mineral-rich fluids rising from these hydrothermal vents

Reference

Chesner CA, Luhr JF (2010) A melt inclusion study of the Toba Tuffs, Sumatra, Indonesia. J Volcanol Geotherm Res 197:259–278